

NASA

Scientific and Technical Reports for 1968

A Selected Listing

NATIONAL AERONAUTICS AND SPACE ADMINISTRATION

PUBLISHED BY UNITED STATES GOVERNMENT NATIONAL AERONAUTICS AND SPACE ADMINISTRATION SCIENTIFIC AND TECHNICAL INFORMATION DIVISION

NASA Scientific and Technical Reports for 1968—A Selected Listing (NASA SP-7033) is prepared by the NASA Scientific and Technical Information Facility operated for the National Aeronautics and Space Administration by the Technical Information Services Company.

NASA SP-7033

NASA

Scientific and Technical

Reports for 1968

A Selected Listing



Scientific and Technical Information Division OFFICE OF TECHNOLOGY UTILIZATION MAY 1969 NATIONAL AERONAUTICS AND SPACE ADMINISTRATION Washington, D.C.

For sale by the Superintendent of Documents, U.S. Government Printing Office Washington, D.C. 20402 - Price \$4.00

Introduction

WHAT NASA SCIENTIFIC AND TECHNICAL REPORTS FOR 1968 IS

NASA Scientific and Technical Reports for 1968. A Selective Listing (NASA SP-7033) combines in a single publication a selective listing of NASA reports that were announced during 1968 in *Scientific and Technical Aerospace Reports (STAR)*, NASA's semimonthly announcement journal for the aerospace sciences. The documents listed were issued as part of the following NASA report series: *Special Publications* (NASA SP-), *Technical Reports* (NASA TR-), *Technical Notes* (NASA TN D-), *Technical Memorandums* (NASA TM X-), *Technical Translations* (NASA TT F-), and *Contractor Reports* (NASA CR-). The listing does not include references to journal articles that were published as a result of NASA-sponsored activities.

As in the case of the similar publication for 1967 (NASA SP-7029), the present volume has been limited to reports which were printed and widely distributed. Access to material thus omitted from this listing continues to be available through *STAR* and its Indexes.

HOW NASA SCIENTIFIC AND TECHNICAL REPORTS FOR 1968 IS ORGANIZED

The arrangement of this publication is the same as that of *STAR*. The first section contains the bibliographic citations and abstracts arranged by *STAR* subject categories. The second section contains five indexes (subject, personal author, corporate source, report/accession number, and accession/report number.)

AVAILABILITY OF DOCUMENTS

Documents listed are available on initial distribution without charge to:

- 1. NASA Offices, Centers, contractors, subcontractors, grantees, and consultants;
- 2. Other U.S. Government agencies and their contractors;
- 3. Libraries in the United States that have arrangements with NASA to maintain collections of NASA documents for public use;
- 4. Other organizations in the United States having a need for NASA documents in work related to the aerospace program; and
- 5. Foreign government or academic organizations that have established appropriate reciprocal arrangements with NASA.
- NASA documents that have been microfiched⁽¹⁾ (identified by the # sign in the citation) are available on microfiche without charge at any time to the same organizations, described above, that are eligible to receive full-sized copy on initial distribution.

HOW TO OBTAIN MICROFICHE

If you are registered with NASA and eligible to receive reports as described above, send the completed *Document Request* (Facility Form 492) to:

NASA Scientific and Technical Information Facility

College Park, Maryland 20740

If you are not registered with NASA and wish to receive information concerning registration, request *Registration Form—Technical Publications* (Facility Form 713) from the NASA Scientific and Technical Information Facility at the address given above. Others may obtain microfiche copies by purchase as described in the following paragraphs.

(1) A microfiche is a transparent sheet of film, 105×48 mm in size, capable of containing up to 72 pages of information reduced to micro images (not to exceed 20:1 reduction).

P. O. Box 33

PUBLIC SALE OF DOCUMENTS

All documents listed with a Clearinghouse for Federal Scientific and Technical Information (CFSTI) availability statement or a Superintendent of Documents, U.S. Government Printing Office (GPO) availability statement in the citation may be purchased from the U.S. Government sales agency cited, at the address given below.

Publications with a CFSTI availability statement are sold in hard copy (HC) and in microfiche copy (MF) by:

> Clearinghouse for Federal Scientific and Technical Information (CFSTI) Springfield, Virginia 22151

The following unit price has been established by CFSTI: \$3 for hard copy, \$0.65 for microfiche.

Publications with a GPO availability statement in the citation are sold in hard copy by:

Superintendent of Documents, U.S. Government Printing Office

(GPO) Washington, D.C. 20402.

NASA documents available from GPO are also available from CFSTI at the GPO price given in the citation.

COSATI SUBJECT CATEGORY CODE

In the citation of each document is a code, e.g., CSCL 25A, that indicates the subject category assigned to it from the *COSATI Subject Category List* (first edition, December 1964) published by the Committee on Scientific and Technical Information of the Federal Council for Science and Technology.

INDEXING VOCABULARY

The Preliminary Edition of the NASA Thesaurus (December 1967) (NASA SP-7030) is used as the authority for the indexing vocabulary that appears in the subject index. The NASA Thesaurus should be consulted in examining the current indexing vocabulary, including associated cross-reference structure. Only the subject terms that have been selected to describe the documents abstracted in this publication appear in the subject index. Copies of the NASA Thesaurus may be obtained from the Clearinghouse for Federal Scientific and Technical Information or the Superintendent of Documents, U.S. Government Printing Office at \$8.50 for the three-volume set.

TABLE OF CONTENTS

Subject Categories

	Abstracts in the journal are grouped under the following categories:	page:
01	AERODYNAMICS Includes aerodynamics of bodies, combinations, internal flow in ducts and turbomachinery; wings, rotors, and control surfaces. For applications see: 02 Aircraft and 31 Space Vehicles. For related information see also: 12 Fluid Mechanics; and 33 Thermodynamics and Combustion.	1
02	AIRCRAFT Includes fixed-wing airplanes, helicopters, gliders, balloons, ornithopters, etc; and specific types of complete aircraft (e.g., ground effect machines, STOL, and VTOL); flight tests; operating problems (e.g., sonic boom); safety and safety devices; economics; and stability	
	and control. For basic research see: 01 Aerodynamics. For related information see also: 31 Space Vehicles; and 32 Structural Mechanics.	17
03	AUXILIARY SYSTEMS Includes fuel cells, energy conversion cells, and solar cells; auxiliary gas turbines; hydraulic, pneumatic and electrical systems; actuators; and inverters. For related information see also: 09 Electronic Equipment; 22 Nuclear Engineering; and 28 Propulsion Systems.	29
04	BIOSCIENCES Includes aerospace medicine, exobiology, radiation effects on biological systems; physiological and psychological factors. For related information see also: 05 Biotechnology.	39
05	BIOTECHNOLOGY Includes life support systems, human engineering; protective clothing and equipment; crew training and evaluation, and piloting. For related information see also: 04 Biosciences.	43
06	CHEMISTRY Includes chemical analysis and identification (e.g., spectroscopy). For applications see: 17 Materials, Metallic; 18 Materials, Nonmetallic; and 27 Propellants.	51
07	COMMUNICATIONS Includes communications equipment and techniques; noise; radio and communications blackout; modulation telemetry; tracking radar and optical observation; and wave propagation. For basic research see: 23 Physics, General; and 21 Navigation.	53
08	COMPUTERS Includes computer operation and programming; and data processing. For basic research see: 19 Mathematics.	59

09	ELECTRONIC EQUIPMENT Includes electronic test equipment and maintainability; component parts, e.g., electron tubes, tunnel diodes, transistors; integrated circuitry; microminiaturization. For basic research see: 10 Electronics. For related information see also: 07 Communications and 21 Navigation.	63
10	ELECTRONICS Includes circuit theory; and feedback and control theory. For applications see: 09 Electronic Equipment. For related information see: Specific Physics Categories.	. 67
11	FACILITIES, RESEARCH AND SUPPORT Includes airports; lunar and planetary bases including associated vehicles; ground support systems; related logistics; simulators; test facilities (e.g., rocket engine test stands, shock tubes, and wind tunnels); test ranges; and tracking stations.	69
12	FLUID MECHANICS Includes boundary-layer flow; compressible flow; gas dynamics; hydrodynamics; and turbulence. For related information see also: 01 Aerodynamics; and 33 Thermodynamics and Combustion.	75
13	GEOPHYSICS Includes aeronomy; upper and lower atmosphere studies; oceanography; cartography; and geodesy. For related information see also: 20 Meteorology; 29 Space Radiation; and 30 Space Sciences.	85
14	INSTRUMENTATION AND PHOTOGRAPHY Includes design, installation, and testing of instrumentation systems; gyroscopes; measuring instruments and gages; recorders; transducers; aerial photography; and telescopes and cameras.	89
15	MACHINE ELEMENTS AND PROCESSES Includes bearings, seals, pumps, and other mechanical equipment; lubrication, friction, and wear; manufacturing processes and quality control; reliability; drafting; and materials fabrication, handling, and inspection.	97
16	MASERS Includes applications of masers and lasers. For basic research see: 26 Physics, Solid-State.	105
17	MATERIALS, METALLIC Includes cermets; corrosion; physical and mechanical properties of materials; metallurgy; and applications as structural materials. For basic research see : 06 Chemistry. For related information see also: 18 Materials, Nonmetallic; and 32 Structural Mechanics.	107
18	MATERIALS, NONMETALLIC Includes corrosion; physical and mechanical properties of materials (e.g., plastics); and elastomers, hydraulic fluids, etc. For basic research see: 06 Chemistry. For related information see also: 17 Materials, Metallic; 27 Propellants; and 32 Structural Mechanics.	117
19	MATHEMATICS Includes calculation methods and theory; and numerical analysis. For applications see: 08 Computers.	119

20	METEOROLOGY Includes climatology; weather forecasting; and visibility studies. For	
	related information see also: 13 Geophysics; and 30 Space Sciences.	125
21	NAVIGATION	
	Includes guidance; autopilots; star and planet tracking; inertial platforms; and air traffic control. For related information see also: 07 Communications.	127
22	NUCLEAR ENGINEERING	145
	Includes nuclear reactors and nuclear heat sources used for propulsion and auxiliary power. For basic research see: 24 Physics, Atomic, Molecular, and Nuclear. For related information see also: 03 Auxiliary Systems; and 28 Propulsion Systems.	133
23	PHYSICS, GENERAL	
	Includes acoustics, cryogenics, mechanics, and optics. For astrophysics see: 30 Space Sciences. For geophysics and related information see also: 13 Geophysics, 20 Meteorology, and 29 Space Radiation.	143
24	PHYSICS, ATOMIC, MOLECULAR, AND NUCLEAR	
	Includes atomic, molecular and nuclear physics. For applications see: 22 Nuclear	
	Engineering. For related information see also: 29 Space Radiation.	147
25	PHYSICS, PLASMA	
	Includes magnetohydrodynamics. For applications see: 28 Propulsion Systems.	153
26	PHYSICS, SOLID-STATE Includes semiconductor theory; and superconductivity. For applications see: 16 Masers. For related information see also: 10 Electronics.	159
27	PROPELLANTS	
	Includes fuels; igniters; and oxidizers. For basic research see: 06 Chemistry; and 33 Thermodynamics and Combustion. For related information see also: 28 Propulsion Systems.	163
28	PROPULSION SYSTEMS	
	Includes air breathing, electric, liquid, solid, and magnetohydrodynamic propulsion. For nuclear propulsion see: 22 Nuclear Engineering. For basic research see: 23 Physics, General; and 33 Thermodynamics and Combustion. For applications see: 31 Space Vehicles. For related information see also: 27 Propellants.	165
29	SPACE RADIATION	
	Includes cosmic radiation; solar flares; solar radiation; and Van Allen radiation belts. For related information see also: 13 Geophysics; and 24 Physics, Atomic, Molecular, and Nuclear.	173
30	SPACE SCIENCES	
	Includes astronomy and astrophysics; cosmology; lunar and planetary flight and exploration; and theoretical analysis of orbits and trajectories. For related information see also: 11 Facilities, Research and Support; and 31 Space Vehicles.	175

31 SPACE VEHICLES

Includes launch vehicles; manned space capsules; clustered and multistage rockets; satellites; sounding rockets and probes; and operating problems. For basic research see: 30 Space Sciences. For related information see also: 28 Propulsion Systems; and 32 Structural Mechanics.	191
32 STRUCTURAL MECHANICS	
Includes structural element design and weight analysis; fatigue; thermal stress;	
impact phenomena; vibration; flutter; inflatable structures; and structural tests. For related information see also: 17 Materials, Metallic; and 18 Materials, Nonmetallic.	203
33 THERMODYNAMICS AND COMBUSTION	
Includes ablation, cooling, heating, heat transfer, thermal balance, and other	
thermal effects; and combustion theory. For related information see also: 12 Fluid Mechanics; and 27 Propellants.	217
34 GENERAL Includes reports of a broad nature related to industrial applications and technology, and to basic research; defense aspects; law and related legal matters; and legislative hearings and documents.	229
SUBJECT INDEX I-1	
PERSONAL AUTHOR INDEX I-119	
CORPORATE SOURCE INDEX I-171	
REPORT/ACCESSION NUMBER INDEX I-197	
ACCESSION/REPORT NUMBER INDEX	

TYPICAL CITATION AND ABSTRACT

NASA SPONSORED	↓↓	AVAILABLE O MICROFICH
NASA ACCESSION NUMBER	 N68-37900*# Astro Research Corp., Santa Barbara, Calif. LARGE LOW-FREQUENCY ORBITING RADIO TELESCOPE Hans U. Schuerch and John M. Hedgepeth Washington NASA 	CORPORAT SOURC
TITLE	Oct. 1968	PUBLICATIO DAT
AUTHOR	Contract NAS7-426) (NASA-CR-1201; ARC-R-282) CFSTI: HC \$3.00/MF \$0.65	SALES AGENC
CONTRACT OR GRANT	CSCL 22B Studies have been performed of the feasibility of a large	AND PRIC
REPORT NUMBER	(1500-meter) orbiting paraboloidal antenna for use in low-frequency (< 10 MHz) radio astronomy. Such a radio telescope would be extremely useful in a variety of scientific astronomical studies. A conceptual configuration has been evolved which consists of a tenuous conductive paraboloidal network which is deployed and stiffened by centrifugal forces due to spin about the axis of symmetry. Meridional tension forces are produced in the net by means of an extremely long deployable mast which runs along the axis of symmetry and forms the backbone of the structure. The entire configuration is deployed from a package suitable for launch on such vehicles as the Titan III. Results of the various theoretical and experimental analyses which have led to this baseline concept are summarized. Author	COD



NASA Scientific and Technical Reports for 1968

a selected listing

MAY 1969

01

AERODYNAMICS

Includes aerodynamics of bodies, combinations, internal flow in ducts and turbomachinery; wings, rotors, and control surfaces. For applications see: 02 Aircraft and 31 Space Vehicles. For related information see also: 12 Fluid Mechanics; and 33 Thermodynamics and Combustion.

N68-10060* National Aeronautics and Space Administration. Langley Research Center, Langley Station, Va.

A MOVING-BELT GROUND PLANE FOR WIND-TUNNEL GROUND SIMULATION AND RESULTS FOR TWO JET-FLAP CONFIGURATIONS

Thomas R. Turner Washington NASA Nov. 1967 39 p refs (NASA-TN-D-4228) CFSTI: \$3.00 CSCL 14B

A moving-belt ground plane designed to eliminate the ground boundary layer for tests in ground proximity has been installed in a 17-foot (5.18-meter) wind-tunnel test section at the Langley Research Center. The test station was calibrated with this moving belt installed, and the effects of ground proximity on the characteristics of a swept and an unswept full-span blowing-flap configuration have been investigated. The results indicate that the moving belt satisfactorily removes the boundary layer on the ground plane. The lift loss of models at small distances from the ground and high lifts is considerably less with the belt moving at stream velocity (boundary layer removed) than with the belt at zero velocity. For configurations with full-span lift devices, the data indicate that the moving-belt ground plane is not needed for ratios of wing height (in spans) to lift coefficient greater than about 0.050, but is desirable for smaller ratios. Author

N68-10093*# National Aeronautics and Space Administration. Langley Research Center, Langley Station, Va.

WIND-TUNNEL INVESTIGATION OF A 3/8-SCALE AUTOMOBILE MODEL OVER A MOVING-BELT GROUND PLANE

Thomas R. Turner Washington, NASA Nov. 1967 36 p refs (NASA-TN-D-4229) CFSTI: HC\$3.00/MF\$0.65 CSCL 01A

An investigation of the effect of ground-plane boundary layer in wind-tunnel testing of a model automobile over a fixed ground plane has been made by using the endless moving-belt ground plane in the 17-foot test section of the Langley 300-MPH 7- by 10-foot tunnel. A 3/8-scale automobile model was tested with the ground-plane belt at free-stream velocity (i.e., with the boundary layer eliminated) as well as at a reduced velocity and zero velocity (i.e., with boundary layers). The results indicate that the boundary layer on the ground plane tends to increase the lift but has negligible effect on other components. The lift increment due to ground-plane boundary layer was smaller than that due to crosswinds or configuration changes such as a flush fairing on the underbody. Author

N68-10380* National Aeronautics and Space Administration. Langley Research Center, Langley Station, Va.

FREE-FLIGHT AERODYNAMIC CHARACTERISTICS OF A SLENDER CONE BETWEEN MACH NUMBERS OF 7 AND 8 Joseph H. Judd Washington NASA Nov. 1967 42 p refs (NASA-TN-D-4245) CSCL 01A

A free-flight test of a 3.56° half-angle cone configuration was made by use of the rocket test technique. The cone model was accelerated to a Mach number of 8 and a Reynolds number based on nominal body length of 25×10⁶. Data are presented during the decelerating flight to a Mach number of 7 and a Reynolds number based on body length of 2.5×10^6 as the slowly spinning cone was disturbed in pitch by pulse rockets. The cone model demonstrated a good aerodynamic efficiency, having a lift-drag ratio of 2.77 at a Mach number of 7.3 and at an angle of incidence of 9°. During the decelerating flight a relatively steady value of the roll resonance parameter, spproximately 0.8, was maintained. The measured variation of axial-force coefficient with resultant-force coefficient in the transverse plane agreed with estimated values obtained by using Newtonian theory and classical hypersonic similarity, although the estimated values obtained by using similarity were slightly lower. Author

N68-10529*# National Aeronautics and Space Administration. Lewis Research Center, Cleveland, Ohio.

USE OF SIMILARITY PARAMETERS FOR EXAMINATION OF GEOMETRY CHARACTERISTICS OF HIGH-EXPANSION-RATIO AXIAL-FLOW TURBINES

Arthur J. Glassman and Warner L. Stewart Washington NASA Nov. 1967 35 $p\ refs$

(NASA-TN-D-4248) CFSTI: HC\$3.00/MF\$0.65 CSCL 10A

The similarity parameters are discussed with respect to turbine stage and overall characteristics. Interrelations among the number of stages, the stage diameter variation, the turbine expansion ratio, and the stage-similarity-parameter variation are explored. The highest overall efficiency in a multistage turbine is attained when the stage similarity parameters are maintained approximately constant near the stage optimum values. A turbine with a constant mean diameter cannot meet this requirement, especially for a high-expansion-ratio application. Appropriate proportioning of stage work and stage diameter as a function of stage-exit volume flow is used to estimate geometry characteristics for a constant stage-parameter design. More stages are required for the constant stage-parameter design than for the constant mean-diameter design. For the high-expansion-ratio cases, the rate of increase of stage diameter may become so severe as to exceed practical limitations. A limit imposed on the stagewise increase in diameter resulted in a reduction in the overall diameter variation but in a further increase in the number of stages. The turbine geometry characteristics were obtained for a nuclear rocket, a mercury Rankine cycle, and alkali-metal Rankine cycle applications. Author

N68-11036*# National Aeronautics and Space Administration. Langley Research Center, Langley Station, Va.

WIND-TUNNEL INVESTIGATION OF A DEFLECTED-SLIP-STREAM CRUISE-FAN V/STOL AIRCRAFT WING

William A. Newsom, Jr. Washington Dec. 1967 54 p refs (NASA-TN-D-4262) CFSTI: HC\$3.00/MF\$0.65 CSCL 01A

An investigation was made of a wing with ducted fans mounted so that the slipstream would spread over most of the span of the wing. The wing was equipped with a double slotted flap and the ducts could be mounted at various positions on the leading edge. Tests were made for three different duct exit configurations over a range of angles of attack and fan thrust for various flap angles. The greatest amount of circulation lift was induced on the wing when the two ducts were mounted at the 1/4- and 3/4-semispan stations and when the slipstream from the ducts was divided with one-third of it going over the wing and two-thirds of it beneath the wing. The investigation also showed that chordwise fences on the upper surface of the flaps were effective in improving the turning effectiveness of the flaps and increasing the lift induced on the wing by the duct exit flow. The efficiency of the subject powered lift system was such that the model had a desirably low thrust required curve throughout the transition speed range. In this speed range the thrust required closely approximated that required as calculated from momentum relations based on the idealized assumption of an elliptical distribution of lift across the entire span of the wing. A slipstream deflection angle for hovering flight of 88° with a thrust loss of only 8% was obtained with the subject model. Author

N68-11253*# National Aeronautics and Space Administration. Langley Research Center, Langley Station, Va.

EFFECT OF THRUST AND ALTITUDE IN STEEP APPROACHES ON GROUND TRACK NOISE

John A. Zalovcik Washington Nov. 1967 13 p refs

(NASA-TN-D-4241) CFSTI: HC\$3.00/MF\$0.65 CSCL 01B

A brief analysis was made of measurements of sound pressure level taken during approaches of a four-engine medium-range turbojet transport to determine the variation of sound pressure level with thrust and altitude for various glide slope angles. The sound pressure level data were obtained at four ground stations during 3° approaches with several flap deflections which provided variations in airplane drag and hence in the required thrust. The thrust required for stabilized flight on the 3° glide slope was computed from lift-drag polars available for the airplane for the three flap deflections. By using the measured height of the aircraft above the four ground stations, the computed thrust, and the measured sound pressure level, the variation of sound pressure level with aircraft height and thrust for stabilized flight on 3° to 7° glide slopes was derived. The results of the analysis indicated that by increasing the glide slope from 3° to 6°, the value of the sound pressure level could be reduced 11.5 to 14.0 dB, depending on the ground station location. Of this reduction, about 7.5 dB would be due to reduction in thrust and the remainder (4 to 6.5 dB), to increase in altitude. Values of sound pressure level computed on the basis of this analysis at one ground station for several steep approach profiles flown showed good agreement with sound pressure level measurements made during the steep approaches. Author

N68-11640* National Aeronautics and Space Administration. Manned Spacecraft Center, Houston, Tex.

AERODYNAMIC STABILITY CHARACTERISTICS OF THE APOLLO LAUNCH ESCAPE VEHICLE (LEV) WITH CANARD SUFACES DEPLOYED

William C. Moseley, Jr. and Bass Redd Washington Dec. 1967 108 p refs

(NASA-TN-D-4280) CFSTI: \$3.00 CSCL 22B

A series of wind-tunnel studies was made to determine both static and dynamic stability characteristics of the Apollo launch escape vehicle, with canard surfaces in the deployed (open) position. This configuration is known as the post-abort vehicle. Results indicate that these canard surfaces are effective in producing a desired destabilizing increment in pitching moment. Positive damping was generally indicated. Author

N68-11936*# National Aeronautics and Space Administration. Ames Research Center, Moffett Field, Calif.

BALLISTIC-RANGE TESTS OF A DRAG-RING CONFIGURA-TION AT MACH NUMBERS AROUND 2

Charles E. De Rose Washington Dec. 1967 23 p ref

(NASA-TN-D-4291) CFSTI: HC\$3.00/MF\$0.65 CSCL 01A

Free-flight measurements of an unusual configuration proposed as a Mars atmospheric probe were made in the Ames Pressurized Ballistic Range. The configuration consisted of a cone-cylinder centerbody supported within a large conical-sector flare (called a drag ring) with a wide gap between the two components. Tests were made in air at a nominal Mach number of 2 and a Reynolds number, based on the drag-ring diameter of 50,000. All experimental data are compared with values obtained at a Mach number of 20 and with Newtonian theory to check the effect of a large change in flight velocity. A limited investigation was undertaken in the Pressurized Ballistic Range at Ames Research Center to study the drag, lift, and static and dynamic stability of this shape in air at a Mach number of approximately 2, and to photograph the flow around the free-flying model. The results of this investigation are reported here. Author

N68-11958*# National Aeronautics and Space Administration. Langley Research Center, Langley Station, Va.

EXPERIMENTAL PRESSURE DISTRIBUTIONS AND AERODYNAMIC CHARACTERISTICS OF A LOW-FINENESS-RATIO CYLINDER AT A MACH NUMBER OF 10.5 AND ANGLES OF ATTACK FROM 0° TO 90°

Thomas A. Blackstock and Philip E. Everhart Washington Dec. 1967 29 p refs

(NASA-TM-X-1487) CFSTI: HC\$3.00/MF\$0.65 CSCL 01A

An investigation was made in the continuous-flow hypersonic tunnel to measure the surface pressures and the force and moment characteristics of a fuel capsule designed for use on the Nimbus B weather satellite. The capsule, a fineness-ratio-2 cylinder with a recessed face, was tested at angles of attack from 0° to 90° at a Reynolds number of 0.8×10^6 based on free-stream conditions and cylinder length. At angles of attack from 37° to 90°, forces and moments were also measured on a corresponding cylinder

with a flat face. Pressures on the recessed face reached a maximum at angles of attack from 40° to 50°. Significant end effects on the pressure were concentrated within 1/2 diameter of the end of the cylinder. Analysis of the results indicated that normal force can be predicted within 15 percent by modified Newtonian theory. Agreement between experiment and theory for axial force was good near angles of attack of 0° and 90°, but the calculated results were generally somewhat low at other attitudes. The high pressure induced by the lip of the recess also produced a moderate increase in axial force, but had little effect on normal force. The recessed sover the values for the flat-faced cylinder were noted. Author

N68-14747*# National Aeronautics and Space Administration. Lewis Research Center, Cleveland, Ohio.

COMPUTER PROGRAM FOR DESIGN OF TWO DIMENSIONAL SUPERSONIC NOZZLE WITH SHARP EDGED THROAT

Michael R. Vanco and Louis J. Goldman, Washington, Jan. 1968 19 p. refs

(NASA-TM-X-1502) CFSTI: HC \$3.00/MF \$0.65 CSCL 10A

The FORTRAN IV computer program for the design of a two-dimensional supersonic nozzle with a sharp-edged throat is presented along with the equations used. The nozzle, which has uniform parallel flow at the exit, is designed on the basis of two-dimensional isentropic flow of a perfect gas. The program requires as input the exit Mach number and the specific-heat ratio. The output yields the nozzle contour for the supersonic portion. Input and output for a sample case are included. Author

N68-15743*# National Aeronautics and Space Administration. Lewis Research Center, Cleveland, Ohio.

COLD-AIR INVESTIGATION OF A TURBINE FOR HIGH-TEMFERATURE-ENGINE APPLICATION. 3: OVERALL STAGE PERFORMANCE

Warren J. Whitney, Edward M. Szanca, Bernard Bider, and Daniel E. Monroe Washington Feb. 1968 23 p refs

(NASA-TN-D-4389) CFSTI: HC\$3.00/MF\$0.65 CSCL 10A

An experimental investigation was made to determine the performance of a 30-inch (0.762-m) single-stage turbine, designed for high-engine temperature application. The characterizing features for this application, pertinent to the turbine aerodynamic performance, are thick blade profiles, blunt leading and trailing edges, and low solidity. The turbine developed equivalent design specific work output at equivalent design speed with an efficiency of 0.923, which was the highest efficiency obtained over the range of conditions investigated. The equivalent mass flow, 40.64 pounds per second (18.434 kg/sec), is 1.8 percent greater than the design mass flow. It was concluded that the compromising of the airfoil shapes, which was necessary because of cooling considerations, did not impair the turbine performance. The design mean radius velocity diagram is compared with that calculated from the experimental results obtained at equivalent design speed and equivalent design specific work output. The comparison indicates that an overexpansion occurred across the stator and that the reaction across the rotor was reduced. This effect was attributed to an excessive passage area allowance at the rotor outlet which resulted from an assumed design efficiency which was lower than the experimentally obtained efficiency. Author

N68-15778*# National Aeronautics and Space Administration. Ames Research Center, Moffett Field, Calif.

COMPARISON OF EXPERIMENTAL AND THEORETICAL SHOCK SHAPES AND PRESSURE DISTRIBUTIONS ON FLAT-FACED CYLINDERS AT MACH 10.5

Mamoru Inouye, Joseph G. Marvin, and A. Richard Sinclair Washington NASA Feb. 1968 21 p refs

(NASA-TN-D-4397) CFSTI: HC\$3.00/MF\$0.65 CSCL 01A

Shock-wave shapes and surface pressures were measured on flat-faced cylinders with shoulder to base radius ratios of 0.0, 0.05, 0.15, 0.25, and 0.5. The measured values were compared with one- and two-strip numerical solutions obtained by the method of integral relations. The two-strip solutions predicted adequately both the shock shapes and surface pressures. The one-strip solutions predicted adequately the shock shapes but underestimated the surface pressures. The shock-wave standoff distances decreased linearly with increasing shoulder radius. The computed stagnation-point velocity gradients increased with increasing shoulder radius, but not linearly. Author

N68-16299*# National Aeronautics and Space Administration. Langley Research Center, Langley Station, Va.

WIND TUNNEL INVESTIGATION OF THREE PROPOSED LAUNCH VEHICLES AT MACH NUMBERS FROM 2.30 TO 4.63

A. B. Blair, Jr. and Melvin M. Carmel Washington Feb. 1968 66 p

(NASA-TM-X-1498) CFSTI: HC\$3.00/MF\$0.65 CSCL 01A

A wind tunnel investigation has been made to determine the aerodynamic characteristics of three 1/12.4-scale models of proposed multi-stage launch vehicles. Tests of the second stage alone were made of the models. The investigation included tests of models both with and without fins and auxiliary boosters. The results of the investigation indicated approximately linear variations of the aerodynamic coefficients with angle of attack and sideslip over the range of the tests. The first-stage fins were effective in providing stabilizing increments of pitching and yawing moment although the increments decreased with increasing Mach number The rolling moment due to sideslip appeared to be reasonably small over the range of the tests.

N68-16480*# National Aeronautics and Space Administration. Langley Research Center, Langley Station, Va. SUPERSONIC AERODYNAMIC CHARACTERISTICS OF A MODEL OF AN AIR TO-GROUND MISSILE Clyde Hayes Washington Feb. 1968 40 p

(NASA-TM-X-1491) CFSTI: HC\$3.00/MF\$0.65 CSCL 01A

An investigation was conducted to determine the aerodynamic characteristics of a model of an air-to-ground missile simulating both the boost- and glide-phase configurations. The results include the effects of fin size and sweep angle as well as the effects of the size and deflection of the control wings. The investigation was conducted for model roll angels of 0° and 45° at Mach numbers of 1.60 and 2.00 at a Reynolds number of 8.41×10⁶ based on the body length. The results of the investigation indicated that the body-fin combination was generally stable about the assumed moment center for the range of fin size and fin sweep angle of the tests, although at Mach number 2.00 and at a sweep angle of 65° regions of instability were indicated for angles of attack above about 9°. The addition of the control wings had little effect on the longitudinal stability but did produce a substantial increase in normal-force curve slope and in axial force. Deflection of the control wings was effective in providing increments of side force and normal force with essentially no effect on pitching or yawing moments. The presence of wing slots, which simulated slots into which the wings fold, had no effect on the aerodynamic characteristics of the model. Author

N68-17555*# National Aeronautics and Space Administration. Ames Research Center, Moffett Field, Calif.

INVISCID HYPERSONIC FLOW OVER A BLUNT BODY WITH HIGH RATES OF MASS AND HEAT TRANSFER E. Dale Martin Washington Mar. 1968 54 p refs

(NASA-TN-D-4252) CFSTI: HC\$3.00/MF\$0.65 CSCL 01A

A study of steady hypersonic flow over a blunt body with a very high rate of continuous mass transfer from the body surface,

with heat conduction, is presented. An approximate analysis is made of the inviscid flow over a sphere with large mass flux. Lighthill's well-known constant-density inviscid blunt-body flow solution was previously extended by Vinokur and Sanders and by Cresci and Libby to include inviscid flow at a high rate out of the body surface. The present analysis further extends Cresci and Libby's solution to include the effects of the boundary shock wave, a thin viscous region dominated by viscous-compressive stresses (rather than viscous shear) and the associated heat conduction in the gas adjacent to the body surface. These effects are important to consider when there is a significant source of translational nonequilibrium at the body surface (such as absorption of intense radiation and the accompanying large heat conduction). Author

N68-17880*# National Aeronautics and Space Administration. Langley Research Center, Langley Station, Va.

EFFECTS OF LEE-SURFACE VOLUME ADDITION ON LONGITUDINAL AERODYNAMICS OF A HIGH-LIFT-DRAG-RATIO WING-BODY CONFIGURATION AT MACH 6.0

David R. Stone and George C. Ashby, Jr. Washington Mar. 1968 30 $\,p$ refs

(NASA-TN-D-4361) CFSTI: HC\$3.00/MF\$0.65 CSCL 01A

An aerodynamic investigation of the addition of volume to the leeward surface of a basic high-wing configuration has been made with volume additions varying from 9 percent to 92 percent of the basic wing-body volume. The free-stream Reynolds number based on body length was 9.5×10^6 . For a given volume addition, the experimental results show that span-height ratio, cross-sectional shape, and longitudinal contour had only secondary effects on the maximum lift-drag ratio. Calculations using shock theory indicate the effects of these parameters are overshadowed by the interaction between the volume-addition shock and the wing-body shock. The results indicate that a practical design practice would be to place the forebody volume addition at the wing apex, and the amount of afterbody volume added would thus be limited by the center-of-gravity location and the associated pitch characteristics of the vehicle. For a constant afterbody length, the maximum lift-drag-ratio variation with volume addition was found to be correlated by the parameter comprised of the product of the forebody slope and the percent volume added. Author

N68-17896*# National Aeronautics and Space Administration. Langley Research Center, Langley Station, Va.

PRESSURE DISTRIBUTIONS AND AERODYNAMIC CHARACTERISTICS OF 90° AND 15° BLUNTED CONES IN NITROGEN AND HELIUM AT MACH 20

Theodore R. Creel, Jr., Charles G. Miller, III, Dal V. Maddalon, and Ralph D. Watson Washington Mar. 1968 37 p refs

(NASA-TN-D-4314) CFSTI: HC\$3.00/MF\$0.65 CSCL 01A

An experimental investigation to determine the pressure distributions and force and moment characteristics on a 9° semiapex angle spherically blunted cone was conducted in nitrogen in the Langley hotshot tunnel. Pressure distributions were obtained in the Langley 22-inch helium tunnel on 9° semiapex angle spherically blunted and flat-faced cones and on a 15° semiapex angle spherically blunted cone. The results of this investigation indicated that pressure distributions on the 9° and 15° semiapex angle spherically blunted cones at zero angle of attack were underpredicted by ideal gas inviscid theory, but a theory accounting for viscous effects predicted the pressure distribution on the 9° spherically blunted cone in nitrogen. Blast-wave-type correlation parameters were observed to yield a fair correlation of pressure distributions obtained on the most windward meridian for angles of attack of 5° to 40° when an effective cone angle was used. Newtonian theory adequately predicted the radial pressure distributions on the windward side of the 9° and 15° semiapex angle spherically blunted cones. The shock shapes of the 9° and 15° cones were correlated by using blast-wave-type correlating parameters. Force and moment coefficients for the 9° spherically blunted cone in nitrogen were in good agreement with those of other investigations using air and nitrogen as test gases. Author

N68-17899*# National Aeronautics and Space Administration. Langley Research Center, Langley Station, Va.

A REAL-GAS STUDY OF LOW-DENSITY WEDGE-INDUCED LAMINAR SEPARATION ON A HIGHLY COOLED BLUNT FLAT PLATE AT M $\infty=12$

John B. Anders and C. L. W. Edwards Washington Mar. 1968 40 p refs

(NASA-TN-D-4320) CFSTI: HC\$3.00/MF\$0.65 CSCL 01A

A study has been made of real-gas wedge-induced laminar separation. A series of experimental tests on a blunt flat plate with a trailing-edge flap was made at a free-stream Mach number of 12 and a free-stream Reynolds number of 10^4 /ft (3.3×10^4 /m). The tests were conducted for stagnation enthalpies ranging from 1465 Btu/lbm (3.41 MJ/kg) to 2030 Btu/lbm (4.73 MJ/kg). A calculation technique is developed to predict the chordwise extent of wedge-induced laminar separation and agrees reasonably well with the present real-gas experimental data. The computed effect of free-stream Reynolds number and total enthalpy on the extent of separation is demonstrated. Sample calculations are shown for equilibrium and frozen flow for a range of total enthalpies.

N68-18189*# National Aeronautics and Space Administration. Lewis Research Center, Cleveland, Ohio.

WIND TUNNEL INVESTIGATION OF TECHNIQUES FOR REDUCING COWL DRAG OF AN AXISYMMETRIC EXTERNAL-COMPRESSION INLET AT MACH 2.49

James E. Calogeras and Edward T. Meleason Washington Mar. 1968 33 p refs

(NASA-TM-X-1516) CFSTI: HC\$3.00/MF\$0.65 CSCL 01A

A wind-tunnel investigation was made at Mach 2.49 to determine the effectiveness of two techniques for cowl-drag reduction on an axisymmetric external-compression inlet. The first method involved reducing the external cowl-lip angle from 25° to values of 15° and 6°. Use of the flatter cowls deliberately violated the criterion for internal cowl-lip shock attachment to affect a tradeoff between cowl pressure drag and induced additive drag. Results showed an increase in external drag over that associated with the 25° cowl, and inlet performance was significantly reduced with use of the flatter cowls. The second method-used a low-external-angle visor with the 25° cowl. An air gap existed between the cowl and the visor base to aid in starting the inlet, and several gap sizes were investigated. With the smallest air gap tested, external drag was reduced by 54 percent with only a small loss in performance. With a larger air gap sized to permit self-start at Mach 2.5, external drag was reduced by 35 percent; this reduction however was accompanied by some loss in overall inlet performance associated with flow expansion into the visor gap. Author

N68-18720*# National Aeronautics and Space Administration. Langley Research Center, Langley Station, Va.

COMPARISON OF THE MACH 3.0 AERODYNAMIC CHARACTERISTICS OF TENSION STRING, TENSION SHELL, AND 120° CONICAL SHAPES

James Wayne Sawyer Washington Mar. 1968 30 p refs (NASA-TN-D-4360) CFSTI: HC\$3.00/MF\$0.65 CSCL 01A

An investigation was conducted at a Mach number of 3.0 to determine aerodynamic characteristics of three decelerator shapes based on the tension string structural concept. The shapes were tested at angles of attack up to 12° and at free-stream Reynolds numbers, based on maximum body diameter, of approximately 1.0 \times 10⁶ and 3.0 \times 10⁶. A comparison was made between the aerodynamic characteristics thus obtained and published results for a 120° cone and comparable tension shell configurations. The results showed that the tension string shapes were more susceptible to flow separation than the tension string shapes, but the aerodynamic coefficients of the tension as much as were the aerodynamic characteristics of the tension shell shapes. The

aerodynamic coefficients, static stability, and aerodynamic centers of the tension string shapes showed little sensitivity to variation in body length and nose radius and, in general, approximated those of the cone. Author

N68-19063*# National Aeronautics and Space Administration. Langley Research Center, Langley Station, Va.

EFFECT OF TWO-DIMENSIONAL MULTIPLE SINE-WAVE PROTRUSIONS OF THE PRESSURE AND HEAT-TRANSFER DISTRIBUTIONS FOR A FLAT PLATE AT MACH 6

Aubrey M. Cary, Jr. and E. Leon Morrisette Washington Mar. 1968 57 p refs

(NASA-TN-D-4437) CFSTI: HC\$3.00/MF\$0.65 CSCL 01A

Surface pressure and heat transfer were measured and oil-flow patterns were observed on two-dimensional, shallow, multiple sine-wave protrusions embedded in a flat surface. The maximum laminar heating on multiple waves was found to correlate empirically with results from previous investigations. The maximum turbulent heating for a series of waves decreased rapidly from wave to wave. Tests with single waves and with the first wave of the multiple-wave model indicated that the maximum turbulent heating on single waves increased almost linearly with decreasing width-height ratio of the wave. The method used to predict the maximum turbulent heating gave fair results when there was no boundary-layer separation prior to the wave. Author

N68-19180*# National Aeronautics and Space Administration. Ames Research Center, Moffett Field, Calif.

ANALOG STUDY OF THE LONGITUDINAL RESPONSE OF A SWEPT-WING TRANSPORT AIRPLANE TO WIND SHEAR AND SUSTAINED GUSTS DURING LANDING APPROACH C. Thomas Snyder Washington Apr. 1968 20 p refs

(NASA-TN-D-4477) CFSTI: HC\$3.00/MF\$0.65 CSCL 01B

Analog-computed time histories and altitude-ground track plots indicate the longitudinal responses of the airplane to varying wind conditions. Controls-fixed runs first demonstrated the differences in responses of an airplane to horizontal gusts and to vertical gusts. Airplane static stability, lift-curve slope, lift-drag ratio, and airplane size were varied while the airplane, with controls fixed, was subjected to wind shear and sustained gusts. Controlled responses showed the effect of maintaining constant pitch attitude or constant airspeed during flight in a wind shear region, into a downdraft, and into a combined wind shear and downdraft. Realistic combinations of downdraft and shear (of decreasing head wind) were found that could significantly steepen descent with little initial attitude change. In fact, the initial changes in attitude and airspeed might induce the pilot to steepen the flight path further. Author

N68-19189*# National Aeronautics and Space Administration. Ames Research Center, Moffett Field, Calif.

LARGE-SCALE WIND-TUNNEL TESTS OF AN AIRPLANE MODEL WITH TWO PROPELLERS AND ROTATING CYLINDER FLAPS

James A. Weiberg and Berl Gamse Washington Mar. 1968 49 p refs

(NASA-TN-D-4489) CFSTI: HC \$3.00/MF \$0.65 CSCL 01A

Wind-tunnel tests were made of a model of a twin turbo-propeller airplane with rotating cylinder flaps. The model had a straight untapered wing of aspect ratio 3.57 equipped with end plates. Cylinder rotation provided a lift coefficient increment of 2.0 and a maximum lift coefficient of 4.0 with 60° flap deflection and zero propeller thrust. A maximum lift coefficient of 9.1 was obtained with a thrust coefficient of 4. The cylinder rotational speed required varied with flap deflection and was independent of angle of attack and slipstream velocity. For a flap deflection of 60° and a free-stream velocity of 40 knots, the cylinder power required was approximately 0.7 horsepower per foot of cylinder length. Author N68-19206*# National Aeronautics and Space Administration. Langley Research Center, Langley Station, Va.

PRELIMINARY STUDY OF DRAG REDUCTION FOR COASTING MISSILES AT MACH NUMBERS FROM 1.57 TO 4.63

Dennis E. Fuller and Donald L. Wassum Washington Apr. 1968 66 p

(NASA-TM-X-1537) CFSTI: HC\$3.00/MF\$0.65 CSCL 16D

An investigation of various body alterations aimed at reducing the drag of a missile during power-off flight was made. Tests were made for conical afterbody closures of two lengths (with and without slots), afterbody perforations, and afterbody scoops. The investigation was made at Mach numbers from 1.57 to 4.63, angles of attack from about -4° to 4° , and a Reynolds number of 9.84×10⁶ per meter. The results indicated that a conical afterbody closure with a closure-length-body-diameter ratio of about 2.9 effected sizable reductions in drag and increases in lift-drag ratio for the test Mach number range; for the lower test Mach numbers an afterbody closure with a closure-length-body-diameter ratio of about 1.4 provided an increase in drag and a decrease in lift-drag ratio. A reduction in the ratio of a slot area to cone area for the long afterbody closure led to progressive decreases in drag coefficient with corresponding increases in lift-drag ratio. Afterbody perforations provided a means of obtaining moderate drag reductions throughout the test Mach number range. Author

N68-19237*# National Aeronautics and Space Administration. Lewis Research Center, Cleveland, Ohio.

EFFECT OF BOATTAIL JUNCTURE SHAPE ON PRESSURE DRAG COEFFICIENTS OF ISOLATED AFTERBODIES George D. Shrewsbury Washington Mar. 1968 34 p refs

(NASA-TM-X-1517) CFSTI: HC\$3.00/MF\$0.65 CSCL 01A

A variety of afterbodies were tested on a sting-supported model of a closed-inlet nacelle. Jet effects were simulated with a cylinder positioned downstream of the afterbody base. Axial-force coefficients were obtained for a 7° conical boattail and various 15° boattailed afterbodies on which the boattail juncture with the cylindrical portion of the nacelle had been smoothed with different radii of curvature. Data were obtained over a Mach number range of 0.56 to 1.00 at angles of attack from 0 to 8° The results indicate that increasing the boattail radius of curvature generally delays the occurrence of the transonic drag rise. Author

N68-19341*# National Aeronautics and Space Administration. Flight Research Center, Edwards, Calif.

A METHOD FOR THE SURFACE INSTALLATION AND FAIRING OF STATIC-PRESSURE ORIFICES ON A LARGE SUPERSONIC-CRUISE AIRPLANE

Norman V. Taillon Washington Mar. 1968 12 p

(NASA-TM-X-1530) CFSTI: HC\$3.00/MF\$0.65 CSCL 01C

A method for installing and fairing static-pressure orifices on the wing surface of a supersonic airplane without penetrating the skin is described. Orifice discs were fixed to pressure tubes which were, in turn, attached to the ferrous skin by welded straps. The assembly was faired over with a temperature-resistant aerodynamic smoothing compound hand-milled flush with the orifices. Some deviation from the mold line is inherent in the method; however, analytical estimates indicate that the effect on local aerodynamic pressures is negligible for this installation. The smoothing compound has been found to be operationally suitable at a Mach number of 3.

N68-19954*# National Aeronautics and Space Administration. Langley Research Center, Langley Station, Va. AN INVESTIGATION OF EXTREMELY FLEXIBLE LIFTING ROTORS

Matthew M. Winston Washington Apr. 1968 28 p refs

(NASA-TN-D-4465) CFSTI: HC\$3.00/MF\$0.65 CSCL 01A

This investigation includes analytical and experimental studies of rotors with very low structural stiffness and single-surface, deformable airfoils. The analytical study focused on the planform and tip-mass requirements necessary to prevent luffing (fabric instability) of a completely flexible blade and included consideration of the

aeroelastic characteristics of flexible blades having chordwise stiffeners spaced along the blade. The experimental investigation focused on determining the hovering characteristics of a 30-foot-(9.144-meter-) diameter flexible rotor. The results of the analytical study indicate that very careful planform design and judicious choice of tip mass are required to prevent luffing on a completely flexible blade. Tip-mass requirements with the attendant increase in overall rotor weight indicate that large rotors of this type are not assured the performance benefits of low disk loadings that were initially expected. Although partial stiffening of the blade chord makes planform and tip-mass design requirements less critical. both types of flexible rotors may operate at disk loadings higher than initially expected, since rotor size-weight relationships may be dictated by requirements for aeroelastic stability. The experimental study indicates that low hovering efficiencies and high power consumption resulted from blade deformations and excessive twist; however, the aerodynamically-induced camber developed during operation provided high mean lift coefficients. Author

N68-20330*# National Aeronautics and Space Administration. Lewis Research Center, Cleveland, Ohio.

PERFORMANCE OF ANNULAR PLUG AND EXPANSION-DEFLECTION NOZZLES INCLUDING EXTERNAL FLOW EF-FECTS AT TRANSONIC MACH NUMBERS

Robert A. Wasko Washington Apr. 1968 33 p

(NASA-TN-D-4462) CFSTI: HC\$3.00/MF\$0.65 CSCL 21H

Experiments covered the Mach number range from 0.56 to 2.0 and included the effects of base bleed as well as variations in plug length and nozzle internal expansion. The full-length plug nozzle performed nearly constant and with optimum quiescence. while the expansion-deflection (ED) nozzle performed only similar to a conical convergent-divergent (CD) nozzle. Thus, the plug nozzle was altitude compensating, while the ED nozzle was not. Plug nozzle efficiency ranged from 98.4% at a pressure ratio of 68 (corresponding to sea-level altitude) to 99% at the design pressure ratio of 290. ED and CD nozzle efficiencies were, respectively, 92.3 and 92.6% at sea level, and 97.6 and 97.8% at the design point. Truncation of the plug nozzles with internal expansion to a nominal 21, 10, and 0% of full plug length resulted in decreased nozzle performance that varied from 96.4, 95.3, and 94.9% at sea level to 98.3, 97.0, and 96.8%, respectively, at the design point. Base bleed improved the truncated plug nozzles with internal expansion. However, ED nozzle performance improved only at pressure ratios above design. Elimination of internal expansion and external plug surface caused poor nozzle performance. Maximum performance loss due to external flow effects was 2.5% of the ideal thrust and occurred below Mach 1.0. Secondary flow reduced the performance loss to as little as 1.75% of ideal thrust. K W

N68-20370*# National Aeronautics and Space Administration. Ames Research Center, Moffett Field, Calif.

LARGE-SCALE WIND-TUNNEL INVESTIGATION OF AN AIRPLANE MODEL WITH A TILT WING OF ASPECT RATIO 8.4, AND FOUR PROPELLERS, IN THE PRESENCE OF A GROUND PLANE

Stanley O. Dickinson, V. Robert Page, and Wallace H. Deckert Washington Apr. 1968 80 p refs

(NASA-TN-D-4493) CFSTI: HC\$3.00/MF\$0.65 CSCL 01A

Aerodynamic characteristics of a large-scale model of a tilt-wing V/STOL transport aircraft are presented. The investigation was conducted in Ames 40- by 80-foot wind tunnel at various heights above a fixed ground plane. Free-stream Reynolds number varied from 0 to 2.9 million. Model configurations included wing tilt angles from 0° to 90°, trailing-edge flap deflections from 0° to 60°, and partial-span wing leading-edge slats. Results show ground proximity decreased lift up to 20 percent (depending on wing tilt angle), decreased drag, and increased nose-down pitching moment.

N68-21374*# National Aeronautics and Space Administration. Lewis Research Center, Cleveland, Ohio.

COMPUTER PROGRAM FOR CALCULATING VELOCITIES AND STREAMLINES ON A BLADE-TO-BLADE STREAM SURFACE OF A TURBOMACHINE

Theodore Katsanis Washington Apr. 1968 100 p refs (NASA-TN-D-4525) CFSTI: HC\$3.00/MF\$0.65 CSCL 10A

A FORTRAN IV computer program was written that gives the solution of the two-dimensional, subsonic, compressible (or incompressible), nonviscous flow problem for a rotating or stationary circular cascade of blades on a blade-to-blade surface of revolution. The flow may be axial, radial, or mixed. There may be a change in stream channel thickness in the through-flow direction. The computer program requires the basic cascade geometry, the meridional stream channel coordinates, fluid total conditions, weight flow, and inlet and outlet flow angles. The output includes streamline coordinates, velocity magnitude and direction throughout the passage, and the blade surface velocities. The method is based on the stream function with the solution of the simultaneous, nonlinear, finite-difference equations being obtained by two major levels of iteration. The inner iteration consists of the solution of simultaneous linear equations by successive overrelaxation, using an estimated optimum overrelaxation factor. The outer iteration then changes the coefficients of the simultaneous equations to Author compensate for compressibility.

N68-21579*# National Aeronautics and Space Administration. Langley Research Center, Langley Station, Va.

INTERFERENCE EFFECTS OF CANARD CONTROLS ON THE LONGITUDINAL AERODYNAMIC CHARACTERISTICS OF A WINGED BODY AT MACH 10

Cuyler W. Brooks, Jr. (M.S. Thesis-Virginia Univ.) Washington Apr. 1968 73 p refs

(NASA-TN-D-4436) CFSTI: HC\$3.00/MF\$0.65 CSCL 01A

An experimental investigation of the interference effects of canard controls on two hypersonic winged configurations was made at a Mach number of 10 in the Langley 15-inch hypersonic flow apparatus. The effect of variations in canard size and shape, body length, wing planform, and wing vertical position was determined. The results indicate that the canard control induces a broad pattern of interference in which the average flow angle over the wing and body surfaces downstream of the canard varies significantly from the free-stream value. The magnitude of the interference increases with increasing canard deflection and, in general, with increasing angle of attack. The most significant configuration parameters (aside from canard deflection) are wing position and canard size. The low-wing configurations are affected considerably less by interference than the high-wing configurations, especially at higher angles of attack. As would be expected, the larger canard causes larger disturbances in the flow than does the Author smaller canard.

N68-21681*# National Aeronautics and Space Administration. Langley Research Center, Langley Station, Va.

EXPERIMENTAL PRESSURE DISTRIBUTIONS ON A BLUNT LIFTING-ENTRY BODY AT MACH 3.71

W. Douglas Morris and Lana M. Couch Washington Apr. 1968 53 p refs

(NASA-TN-D-4494) CFSTI: \$3.00 CSCL 01A

An experimental investigation was conducted to determine the pressure distribution on a blunted 15° half-cone-wedge lifting-entry body. The tests were conducted at a Mach number of 3.71 and Reynolds numbers per foot of 2.81×10^{6} and 4.68×10^{6} (Reynolds numbers per meter of 9.22×10^{6} and 15.35×10^{6}). The angle-of-attack range was from -40° to 40° , and the angle-of-sideslip range was from -10° to 10° . A modified Newtonian method was compared with the data and, in general, found to predict the trends as well as the magnitude over the angle-of-attack and angle-of-sideslip ranges. Author N68-21692*# National Aeronautics and Space Administration. Lewis Research Center, Cleveland, Ohio.

COMPARATIVE STUDY OF MIXED- AND ISOLATED-FLOW METHODS FOR COOLED-TURBINE PERFORMANCE ANALYSES

Warren J. Whitney Washington Apr. 1968 39 p refs

(NASA-TM-X-1572) CFSTI: HC\$3.00/MF\$0.65 CSCL 01A

The two methods are described and then compared by using two simplified example turbines, one being a two-stage impulse type and the other a two-stage reaction turbine. The agreement in efficiency predicted by the two methods is within ± 0.01 for total coolant fractions up to 0.156 and within ± 0.22 . Author

N68-21703*# National Aeronautics and Space Administration. Lewis Research Center, Cleveland, Ohio.

AN EXPERIMENTAL INVESTIGATION OF THE RESTART AREA RATIO OF A MACH 3.0 AXISYMMETRIC MIXED COMPRESSION INLET

Glenn A. Mitchell and Robert W. Cubbison Washington Apr. 1968 25 p refs

(NASA-TM-X-1547) CFSTI: HC\$3.00/MF\$0.65 CSCL 01A

Restart area ratios were obtained for the test inlet from Mach number 2.5 to 3.0 and compared to ratios from other inlets. All inlets restarted with throat areas smaller than required by theory to pass the flow through a simple normal shock at the cowl lip. Details of the unstarted inlet flow field were obtained at Mach 3. The unstarted inlet flow field was characterized by a separated region on the centerbody causing an oblique shock ahead of the throat. The size of the separated region was controlled by the inlet throat area, and the separation terminated at the throat station. The restart throat area was smaller than predicted because of the higher pressure recovery produced by the multiple shock structure. Author

N68-21940*# National Aeronautics and Space Administration. Langley Research Center, Cleveland, Ohio.

AERODYNAMIC CHARACTERISTICS IN PITCH OF A MODIFIED-HALF-RING-WING-BODY COMBINATION AT MACH 2.16 TO 3.70

Odell A. Morris and Milton Lamb Washington Apr. 1968 40 p refs

(NASA-TM-X-1551) CFSTI: HC\$3.00/MF\$0.65 CSCL 01A

An investigation has been conducted at Mach numbers from 2.16 to 3.70 to determine the aerodynamic characteristics in pitch of a modified-half-ring-wing model. The investigation also included tests of a swept-wing model. Both models had a wide flat body and could be fitted with various forebody and afterbody sections. Results of the investigation indicated that favorable interference-lift effects were obtained for both wing-body models at zero angle of attack, the largest effects occurring for the modified-half-ring-wing model. The maximum lift-drag ratios, however, were obtained with the swept-wing model since it produced greater lift-curve slopes than the modified-half-ring-wing model. The changes in forebody and afterbody shapes investigated for both models produced no significant changes in maximum lift-drag ratios, as compared with the ratios for the basic symmetrical body Author shape.

N68-21941*# National Aeronautics and Space Administration. Ames Research Center, Moffett Field, Calif.

A METHOD FOR PREDICTING SHOCK SHAPES AND PRESSURE DISTRIBUTIONS FOR A WIDE VARIETY OF BLUNT BODIES AT ZERO ANGLE OF ATTACK George E. Kaattari Washington Apr. 1968 41 p refs (NASA-TN-D-4539) CFSTI: HC\$3.00/MF\$0.65 CSCL 01A

A method is presented for determining shock envelopes and pressure distributions for a variety of blunt bodies at zero angle of attack. Correlation functions obtained from exact solutions are used to relate the shock standoff distance, at the stagnation and sonic points, to the body geometry. These functions were obtained for a perfect gas but may be applied for real gases in equilibrium flows. The method is restricted to cases where the bow shock is detached from the body and the flow over the forward face is subsonic. Results given by the method are shown to be in good agreement with experimental values.

N68-21950*# National Aeronautics and Space Administration. Marshall Space Flight Center, Huntsville, Ala. ANALYTICAL AND EXPERIMENTAL STUDY OF DYNAMIC

CHARACTERISTICS OF TURBOPUMPS H. Ohashi Washington Apr. 1968 115 p refs

(NASA-TN-D-4298) CFSTI: HC\$3.00/MF\$0.65 CSCL 13K

The response of pressure rise of turbopumps to fluctuating flow rate was studied analytically and experimentally. Unsteady flow around a two-dimensional, linear cascade of airfoils was solved and the frequency response of the deflection angle of the cascade was calculated for the periodically oscillating inlet condition. Based on the unsteady cascade theory, the dynamic characteristics of turbopumps were analyzed. For the evaluation of an approximate response, a simplified model theory was also developed, which enables the calculation to be made without entering into the details of the pump design. An experimental investigation was made to determine the dynamic characteristics of a centrifugal pump. The test showed that the analytical calculation was close to the experimental result. The limiting fluctuating frequency under which the dynamic characteristics agree with the quasi-static ones, was determined from the test result. The time constant of the response of pressure rise to a step-like change of flow rate was also derived. Author

N68-22002*# National Aeronautics and Space Administration. Langley Research Center, Langley Station, Va.

EFFECTS OF SIMULATED WING DAMAGE ON THE AERODYNAMIC CHARACTERISTICS OF A SWEPT-WING AIRPLANE MODEL

Clyde Hayes Washington Apr. 1968 70 p

(NASA-TM-X-1550) CFSTI: HC\$3.00/MF\$0.65 CSCL 01A

An investigation was conducted to determine the effects of simulated wing damage on the aerodynamic characteristics of a swept-wing airplane model. Wing damage was simulated by removal of either a leading-edge portion or a trailing-edge portion of one wing panel or by removal of an entire wing panel. The investigation was conducted at Mach numbers from 1.70 to 2.86 at a constant Reynolds number of 2.25×10^{6} per foot (7.38 $\times 10^{6}$ per meter). The results of the investigation indicated that removing the leading- or trailing-edge portion of the wing or removing the entire wing panel led to a decrease in both lift-curve slope and maximum lift-drag ratio. At the lower Mach numbers, removal of the trailing edge caused a rolling moment slightly larger than that caused by removal of the leading edge. At the higher Mach numbers, however, the effect on rolling moment due to removal of the trailing edge was less than that caused by removal of the leading edge even though a larger area of the wing was removed. Except when the entire wing panel was removed, the roll induced by wing asymmetry could be offset by sideslip within reasonable Author limits of angle of attack and sideslip.

N68-22475*# Therm Advanced Research, Inc., Ithaca, N. Y. INVISCID FLOW FIELD INDUCED BY A ROTOR IN GROUND EFFECT

Michael D. Greenberg and Alvin L. Kaskel Washington NASA May 1968 54 p refs (Contract NAS1-6349) (NASA-CR-1027) CFSTI: \$3.00 CSCL 01A

The inviscid flow field induced by a rotor in ground effect is calculated based upon an actuator disk model of the rotor, for the case of a constant circulation distribution over the blade radius. The governing nonlinear integral equations are solved by a systematic iterative scheme which is similar to the Newton-Raphson method for the solution of nonlinear algebraic equations. Numerical results are presented for both the ground-effect case and the out-of-ground-effect limit. Author

N68-24617# National Aeronautics and Space Administration. Langley Research Center, Langley Station, Va.

APPROXIMATION OF THE SPANWISE DISTRIBUTION OF WIND-TUNNEL-BOUNDARY INTERFERENCE ON LIFT OF WINGS IN RECTANGULAR PERFORATED-WALL TEST SECTIONS

Ray H. Wright and Benferd L. Schilling Washington May 1968 39 p refs

(NASA-TR-R-285) CFSTI: HC\$3.00/MF\$0.65

An approximation method was developed for calculating the spanwise distribution of wind-tunnel-boundary upwash interference on lift of wings in rectangular perforated-wall test sections. This method is applied to square test sections with an assumed effective permeability constant of 0.6. A problem of considerable difficulty in practical application of the method presented is the estimation of an effective permeability constant. Because of the variation of the upwash interference with Mach number and of the influence of boundary layer on the effective permeability factor, the boundary interference in a perforated-wall wind-tunnel test section at high subsonic Mach numbers is likely to be of the nature of that in an open-throat tunnel.

N68-25093*# National Aeronautics and Space Administration. Langley Research Center, Langley Station, Va.

CALCULATION OF AXISYMMETRIC SUPERSONIC FLOW PAST BLUNT BODIES WITH SONIC CORNERS, INCLUDING A PROGRAM DESCRIPTION AND LISTING Jerry C. South, Jr. Washington May 1968 63 p refs

(NASA-TN-D-4563) CFSTI: HC\$3.00/MF\$0.65 CSCL 01A

A program for the approximate calculation of supersonic flow of an ideal gas past blunt bodies with sonic corners is described. Numerical solutions are obtained for the system of differential equations derived from the one-strip integral (Belotserkovskii) method. Aerodynamic results of interest include the surface pressure and velocity distributions, the shape and location of the detached bow shock wave, and the forebody pressure drag coefficient. Comparison of the calculations with experimental data is given, with particular emphasis on spherically blunted cones of large apex angle. For this configuration, a simple method is suggested for estimating angle-of-attack pressure distributions. Other shapes included are a circular disk and a spherical cap convex or concave to the stream. The program operation and listing in FORTRAN IV language are given in the appendixes.

N68-25916*# National Aeronautics and Space Administration. Ames Research Center, Moffett Field, Calif.

DYNAMIC RESPONSE OF A FAMILY OF AXISYMMETRIC HAMMERHEAD MODELS TO UNSTEADY AERODYNAMIC LOADING

Robert C. Robinson, Phillip R. Wilcox, Bruno J. Gambucci, and Robert E. George Washington Jun. 1968 42 $\,p\,$ refs

(NASA-TN-D-4504) CFSTI: HC\$3.00/MF\$0.65 CSCL 01A

The effects of boattail angle and diameter ratio on the unsteady aerodynamic loading on hammerhead launch vehicles were studied in wind-tunnel tests of 13 related dynamic models using the partial-mode model technique. The test Mach numbers ranged from 0.80 to 2.50 and the Reynolds numbers from 3.2×10^6 to 4.5×10^6 based on maximum diameter of the models. It was found that the unsteady aerodynamic loading was the result of two phenomena: buffeting due to separated flow and dynamic instability due to fluctuations between separated and attached flow. Author

N68-25919*# National Aeronautics and Space Administration. Ames Research Center, Moffett Field, Calif.

AERODYNAMIC CHARACTERISTICS OF A LARGE-SCALE MODEL WITH UNSWEPT WING AND AUGMENTED JET FLAP

David G. Koenig, Victor R. Corsiglia, and Jospeh P. Morelli (Army Aeron. Res. Lab.) Washington Jun. 1968 90 p refs

(NASA-TN-D-4610) CFSTI: HC\$3.00/MF\$0.65 CSCL 01A

An investigation was made to determine the aerodynamic characteristics of a complete model equipped with an augmented jet flap. The augmented jet flap is a jet flap with the primary jet thrust increased by means of an ejector system installed in the wing trailing-edge flap. The flap was installed on the inboard part of the wing, and blown ailerons were installed on the outboard part. Tests were made with and without the horizontal tail at zero airspeed and at a dynamic pressure of 8 psf corresponding to a Reynolds number of 3.0×106. The measured thrust of the augmented jet flap was about 1.42 times that of the measured primary jet for flap deflections of 60° and 70° and 1.25 times the isentropic jet thrust. This ratio did not significantly decrease at forward speed. A maximum life coefficient of 6 was measured for a jet coefficient of 1.30 when the model was equipped with full-span leading-edge slats. Symmetrical aileron deflection and flap boundary-layer control were effective in producing lift increments at model attitudes below that for wing stall. With the horizontal tail installed, the variation of pitching moment with angle of attack was stable up to and including wing stall. Comparisons with jet flap test results on the basis of the same static thrust output of the systems indicated that the present augmented-jet flap configuration produced slightly higher lift increments and had more forward center-of-pressure locations. For the same isotropic primary thrust, the augmented jet flap produced 50 percent more jet force and 22 percent more lift than the jet flap. Author

N68-28220*# National Aeronautics and Space Administration. Ames Research Center, Moffett Field, Calif. TRANSITION AND FLOW REATTACHMENT BEHIND AN APOLLO-LIKE BODY AT MACH NUMBERS TO 9 Robert L. Kruse Washington Jul. 1968 31 p refs

(NASA-TN-D-4645) CFSTI: HC\$3.00/MF\$0.65 CSCL 01A

Transition from laminar to turbulent flow in the near wake of a bluff body has been studied in the Ames Pressurized Ballistic Range. The location of transition and the reattachment of the separated flow have been determined from shadowgraphs and have been correlated on the basis of Mach number, Reynolds number, and angle of attack. The Mach numbers ranged from 1 to 9, the Reynolds numbers (based on body diameter) from 0.25×106 , to 5×106 , and the angles of attack from 0° to 25°. Author

N68-28268*# National Aeronautics and Space Administration. Ames Research Center, Moffett Field, Calif.

AN INVESTIGATION OF FULL-SCALE HELICOPTER ROTORS AT HIGH ADVANCE RATIOS AND ADVANCING TIP MACH NUMBERS

John L. McCloud III, James C. Biggers, and Robert H. Stroub Washington Jul. 1968 135 p

(NASA-TN-D-4632) CFSTI: HC\$3.00/MF\$0.65 CSCL 01A

Five full-scale rotors were investigated at various advance ratios and advancing tip Mach numbers in the Ames 40- by 80-foot wind tunnel. The primary differences between rotors were twist, articulation, and tip airfoil section. Four of the rotors incorporated the NACA 0012 airfoil section over the entire blade length. The fifty rotor had tapering thickness and incorporated leading-edge camber over the outer 20% of the blade radius. The fully articulated rotor with zero twist blades was tested at advance ratios from 0.30 to 1.05. The other rotors were investigated in the 0.30 to 0.50 advance-ratio range. The teetering rotor with tapered tip blades was tested at advancing blade tip Mach numbers up to 1.00. Force, moment, power, and control-setting data were obtained for a wide range of lift and propulsive forces, and are presented without discussion. Author

N68-28447*# National Aeronautics and Space Administration. Langley Research Center, Langley Station, Va.

WIND-TUNNEL INVESTIGATION OF THE STATIC AERODYNAMIC CHARACTERISTICS OF A MULTILOBE GLIDING PARACHUTE

George M. Ware and Charles E. Libbey Washington Jul. 1968 23 p refs

(NASA-TN-D-4672) CFSTI: HC\$3.00/MF\$0.65 CSCL 01B

An investigation has been conducted in the Langley full scale tunnel to determine the performance and static stability and control characteristics of a five-lobe gliding parachute. The model was completely void of any rigid structural members and utilized only the tension forces produced by aerodynamic loading to maintain the shape of the canopy. The configuration consisted of a five-lobe canopy, roughly rectangular in inflated planform with an airfoil-type leading edge. The tests were made over an angle-of-attack range from the lowest angle attained before wing collapse, which was about 22.5° to 90°, which corresponded approximately to the vertical-descent condition. Results indicate that maximum lift occurred at an angle of attack of about 25°. The model was longitudinally stable and could be trimmed at angles of attack from the minimum angle of the tests to 30°. In the angle-of-attack range from 30° to 75°, the model had no stable trim conditions but was reable and could be trimmed at angles of attack from 75° to 90°. The stable trim angle-of-attack ranges gave values of lift-drag ratio of 2.2 to about 1.5 in the lower angle range and values near 0 in the higher angle range. The model was directionally stable and had positive effective dihedral at the lower angles of attack, but was directionally unstable and had negative effective dihedral over much of the range of angles of attack above 30°. Similarly, the model had satisfactory static lateral-control characteristics at angles of attack up to about 45°; however, because of a reversal in the direction of the vawing moment with control deflection, the model had unsatisfactory control characteristics at the higher angles of attack. Author

N68-28795*# National Aeronautics and Space Administration. Lewis Research Center, Cleveland, Ohio.

PERFORMANCE OF CENTERBODY VORTEX GENERATORS IN AN AXISYMMETRIC MIXED-COMPRESSION INLET AT MACH NUMBERS FROM 2.0 TO 3.0

Glenn A. Mitchell and Ronald W. Davis Washington Jul. 1968 34 p refs

(NASA-TN-D-4675) CFSTI: HC\$3.00/MF\$0.65 CSCL 01A

Three vortex generator configurations were installed aft of the inlet throat on the centerbody of a Mach 3.0 mixed compression inlet. The three were about equal in improving diffuser pressure recovery and all produced significant, although unequal, reductions in distortion. Only the most densely spaced configuration generated vortices that dissipated before reaching the compressor face. Vortex generators effectively energized the normally retarded flow adjacent to the centerbody even during supercritical operation where they were immersed in supersonic flow. Generators were also effective at inlet angles of attack to at least 5°. Author N68-28817*# National Aeronautics and Space Administration. Langley Research Center, Langley Station, Va.

A THEORETICAL STUDY OF THE EFFECT OF PIVOT LOCATION ON THE AERODYNAMIC-CENTER MOVEMENT OF VARIABLE-SWEEP WINGS IN INCOMPRESSIBLE FLOW John E. Lamar Washington Jul 1968 29 p refs

(NASA-TN-D-4635) CFSTI: HC\$3.00/MF\$0.65 CSCL 01A

Theoretical studies of aerodynamic center movement have been conducted for a series of variable sweep wings in incompressible flow, which have unbroken leading and trailing edges and a skewed tip in the high sweep positions. Some comparisons of theoretical results with experimental results are made to validate the theoretical method. The low sweep outer panels and corresponding pivot locations, selected to be used with each high sweep wing having the same tip skew angle, are determined from two parameters: the ratio of low to high sweep wing span and the fraction of high-sweep normal chord at which the pivot is specified to be located. These studies indicate that for a given low sweep of the outer panel, the spanwise location of the pivot required to give a zero aerodynamic center movement in going from high sweep to low sweep of the outer panel seems to be essentially linearly related to the ratio of low to high sweep wing span in such a way that as the value of the span increase parameter becomes larger the pivot must move outboard. Furthermore, the lower the sweep of the outer panel, the farther outboard the pivot location must be. Author

N68-28830*# National Aeronautics and Space Administration. Langley Research Center, Langley Station, Va. WIND-TUNNEL STUDY TO EXPLORE THE USE OF SLOT

SPOILERS TO MODULATE THE FLAP-INDUCED LIFT OF A WING

Joseph W. Sickle and Robert C. Henry Washington Jul. 1968 16 p refs

(NASA-TN-D-4664) CFSTI: HC\$3.00/MF\$0.65 CSCL 01A

This report presents the results of a preliminary study to explore a proposed new concept for achieving direct lift control on an airplane. The concept employs variable-width slot type spoilers to modulate the lift increment produced by a deflected flap. The study utilized a constant chord airfoil model wing modified to provide various size slots on both the wing and flap sections. Each configuration was tested through an angle-of-attack range of -2° to 16° in a low speed tunnel with a 12 foot octagonal test section. The tests were conducted at a Reynolds number of approximately 410,000. The results indicate that the use of a variable width slot is effective in controlling the lift increment obtained from flap deflection and that there is relatively little change in drag coefficient associated with slot width changes. Author

N68-28868*# National Aeronautics and Space Administration. Langley Research Center, Langley Station, Va.

A MODIFIED MULTHOPP APPROACH FOR PREDICTING LIFTING PRESSURES AND CAMBER SHAPE FOR COMPOSITE PLANFORMS IN SUBSONIC FLOW John E. Lamar Washington Jul. 1968 80 p refs

(NASA-TN-D-4427) CFSTI: HC\$3.00/MF\$0.65 CSCL 01A

A modified version is presented of Multhopp's subsonic lifting surface theory which has been programed in two parts for the IBM 7094 electronic data processing system or Control Data 6400 computer system along with a discussion of the character of its results. The first part is used to find both basic and additional loadings over a given planform with known mean camber surface and the second part is used to determine the required mean camber surface for a given planform and set of loadings. For the loading program, various aerodynamic characteristics are determined on both simple and composite planforms when the spanwise loading is symmetrical. Studies are conducted to determine when these answers are most valid, and some results for delta, sweptback and

tapered, double delta, and variable sweep wings are compared with other theoreis and experiments to determine the accuracy of this method. Application of this method is then made in predicting the aerodynamic effects of changing the outer panel sweep of a variable sweep wing, of increasing the Mach number in the subsonic regime, and of incorporating twist and chamber in a wing. The first two applications also have experimental data presented for comparison. Comparisons are made for a two- and three-dimensional case to aid in the evaluation of the present method. One application is made for a highly sweptback and tapered planform. Author

N68-29405*# National Aeronautics and Space Administration. Langley Research Center, Langley Station, Va.

EXPERIMENTAL INVESTIGATION OF LAMINAR-FLOW SEPARATION ON A FLAT PLATE INDUCED BY DEFLECTED TRAILING-EDGE FLAP AT MACH 19

William D. Harvey Washington Aug. 1968 55 p refs

(NASA-TN-D-4671) CFSTI HC\$3.00/MF\$0.65 CSCL 01A

An experimental investigation to determine the pressure and heat-transfer distributions on a flat plate in laminar flow with deflected trailing-edge flap was conducted at a nominal free-stream Mach number of 19 and at Reynolds numbers per foot (per 30.48 cm) of 7.6 \times 104 to 26 \times 104. Model-geometry variables included flap width, flap length, and leading-edge bluntness. Neither the addition of end plates nor an increase in the width of the model without end plates resulted in true two-dimensional flow. The separated flow was found to be three-dimensional and significantly affected by variations in flap length and width for the sharp-leading-edge model. Separation length and maximum flap pressure apparently approach some maximum value for a given flap-deflection angle when the flap length is increased. Large decreases in separation length occurred with decreasing flap width even though the maximum flap pressure remained approximately constant. Blunting the leading edge reduced both the length of the separated region and the pressure rise through separation to plateau. For the flow over approximately the forward half of the flap, reasonably good agreement was obtained between the measured heating distributions and calculations obtained by using the measured pressure and the calculated value of Stanton number at the hinge line for the sharp plate; however, the predictions obtained for the blunt plate by this method were higher than the actual results when the flow was unseparated. Author

N68-29952*# National Aeronautics and Space Administration. Langley Research Center, Langley Station, Va.

HYPERSONIC AERODYNAMIC CHARACTERISTICS OF LOW-WAVE-DRAG ELLIPTICAL-BODY-TAIL COMBINA-TIONS AS AFFECTED BY CHANGES IN STABILIZER CON-FIGURATION

Charles H. Fox, Jr. and Bernard Spencer, Jr. Washington Aug. 1968 44 p refs

(NASA-TM-X-1620) CFSTI: HC\$3.00/MF\$0.65 CSCL 01A

This investigation represents the initial portion of a study to determine methods of providing stability from hypersonic through low subsonic speeds for vehicles with high hypersonic lift drag ratios. The results of this investigation indicate that the maximum untrimmed lift drag ratio is reduced approximately 15 percent due to the outboard stabilizers for either fineness ratio body. The resultant aerodynamic performance is, however, relatively insensitive to changes in the outboard stabilizer dihedral angle for any given configuration tested. For a moment reference location selected as 55 percent of the body length, the outboard stabilizers set at positive dihedral angles provide positive pitching moment at zero angle of attack, less out of trim pitching moment at maximum lift drag ratio, and resultantly less increase in stability variation with increasing angle of attack as compared with outboard stabilizers set at negative dihedral angles. In addition, the directional-stability parameter at maximum lift drag ratio varies nonlinearly with outboard stabilizer dihedral angle with a maximum stabilizing effect indicated in the dihedral angle region from 30° to 60° for positive dihedrals. Author

N68-29955*# National Aeronautics and Space Administration. Langley Research Center, Langley Station, Va.

EFFECT OF HINGE-LINE BLEED ON HEAT TRANSFER AND PRESSURE DISTRIBUTION OVER A WEDGE-FLAP COMBINATION AT MACH 10.4

H. Harris Hamilton and J. David Dearing Washington Aug. 1968 46 ${\bf p}$ refs

(NASA-TN-D-4686) CFSTI: HC\$3.00/MF\$0.65 CSCL 01A

An experimental investigation has been conducted to determine the effect of boundary layer bleed on the heat transfer and pressure distributions over a wedge-flap combination with a gap between the wedge and flap. The model was tested, with the wedge at angles of attack of 6.83° and 12.83° and the flap deflected up to 30°, at a nominal free-stream Mach number of 10.4 and free stream Reynolds numbers (based on distance to the flap hinge line) of 0.8×106 and 3.6×106. At the lower free-stream Reynolds number, the boundary layer was laminar over the entire model. The pressure and heat transfer over the forward portion of the flap increased slightly as the gap size increased. At the higher free stream Reynolds number, the boundary layer was transitional at the hinge line for an angle of attack of 6.83° and was fully turbulent for an angle of attack of 12.83°. Under these conditions, the largest flap deflection of the tests did not separate the boundary layer even with the gap sealed, and increasing the gap size had very little effect on either the pressure or heat-transfer distributions. The turbulent heat transfer rate for deflected flap was predicted reasonably well by the Spalding and Chi turbulent theory by using boundary layer edge properties calculated from oblique shock theory and by assuming that the turbulent boundary layer originated at the flap hinge line. Author

N68-29994*# National Aeronautics and Space Administration. Lewis Research Center, Cleveland, Ohio.

EFFECT OF VARIABLE STATOR AREA ON PERFORMANCE OF A SINGLE-STAGE TURBINE SUITABLE FOR AIR COOLING. 1: STATOR OVERALL PERFORMANCE WITH 130-PERCENT DESIGN AREA

Edward M. Szanca, Frank P. Behning, and Harold J. Schum Washington Aug. 1968 22 $\,p$ refs

(NASA-TM-X-1632) CFSTI: HC\$3.00/MF\$0.65 CSCL 01A

The turbine is being investigated at stator area settings of 70, 100, and 130 percent of design. This report presents the overall stator performance at the open setting and compares the results with those obtained from design tests. Results are presented in terms of weight flow, outlet flow angle, blade surface static pressure and velocity distributions, as well as inner and outer wall static pressures as obtained over a stator pressure ratio range. Author

N68-30030*# National Aeronautics and Space Administration. Langley Research Center, Langley Station, Va.

AERODYNAMIC CHARACTERISTICS OF TWO BLUNT, HALF-CONE WEDGE ENTRY CONFIGURATIONS AT MACH NUMBERS FROM 2.30 TO 4.63

Gerald V. Foster Washington Aug. 1968 35 p

(NASA-TM-X-1621) CFSTI: HC\$3.00/MF\$0.65 CSCL 01A

An investigation has been conducted in the Langley Unitary Plan wind tunnel to determine the aerodynamic characteristics in combined pitch and sideslip for two blunt, half-cone-wedge entry vehicles at Mach numbers from 2.30 to 4.63. The vehicles differed primarily in length. The results of the investigation indicated that both configurations were longitudinally stable although the drag level was greater for the short configuration. Both configurations exhibited positive directional stability and a positive dihedral effect throughout the ranges of angle of attack and Mach number; however, the parameters for the long configuration varied considerable with angle of attack. Author

N68-30033*# National Aeronautics and Space Administration. Lewis Research Center, Cleveland, Ohio.

OVERALL PERFORMANCE IN ARGON OF A 6-INCH **RADIAL-BLADED CENTRIFUGAL COMPRESSOR**

Edward R. Tysl, Calvin L. Ball, Carl Weigel, and Laurence J. Heidelberg Washington Aug. 1968 28 p refs

(NASA-TM-X-1622) CFSTI: HC\$3.00/MF\$0.65 CSCL 01A

Overall and impeller performance is presented as a function of equivalent weight flow. At the design equivalent weight flow of 1.52 pounds per second (0.69 kg/sec) and design equivalent tip speed of 989 feet per second (301.5 m/sec) the compressor developed an overall total pressure ratio of 2.3 with an adiabatic efficiency of 76.5 percent. Peak efficiency at design speed was 78.0 percent and occurred at an equivalent weight flow of 1.35 pounds per second (0.61 kg/sec). Author

N68-30128*# National Aeronautics and Space Administration. Lewis Research Center, Cleveland, Ohio.

DILUTION-JET MIXING STUDY FOR GAS-TURBINE COMBUSTORS

Carl T. Norgren and Francis M. Humenik Aug. 1968 45 p refs (NASA-TN-D-4695; E-4213) CFSTI: HC \$3.00/MF \$0.65 CSCL 01A

An experimental mixing study was undertaken to evaluate various dilution-jet entries. Thirteen geometries including four geometric variations on rectangular diluent jets with flush openings, attached scoops immersed in the diluent air stream, attached chutes immersed in the hot air stream, and a single geometry incorporating flush circular holes were investigated. Diluent and hot streams with a velocity ratio from 0.55 to 2.20 (diluent stream Mach range 0.082 to 0.232) were introduced into the rectangular configuration exhausting directly to the atmosphere. The mixed-stream exhaust temperature was in the order of 750° to 975°R. Test conditions were representative to scaled engine operation by geometric, velocity, and Reynolds number similarity. Author

N68-30595*# National Aeronautics and Space Administration. Langley Research Center, Langley Station, Va.

A WIND TUNNEL INVESTIGATION OF JET-WAKE EFFECT OF A HIGH-BYPASS ENGINE ON WING-NACELLE INTERFERENCE DRAG OF A SUBSONIC TRANSPORT James C. Patterson, Jr. Washington Aug. 1968 43 p refs (NASA-TN-D-4693) CFSTI: HC\$3.00/MF\$0.65 CSCL 01A

An experimental wind-tunnel investigation was conducted recently to determine the aerodynamic interference associated with underwing fan-jet engine-pylon installations including the effect of a jet wake from a powered high bypass fan-jet engine. Tests were made on a semispan model of a typical transport airplane configuration. These tests were conducted over a Mach number range of 0.70 to 0.84, at angles of attack from 0° to 4°, and over a Reynolds number range of 6.67 imes 10⁶ to 7.38 imes 10⁶ based on the mean geometric chord of 58.30 centimeters. The data indicate that the interference drag for the type of underwing engine-pylon installation investigated may be favorable as a result of a reduction in induced drag associated with an inboard end-plate effect of the nacelle-pylon. The addition of engine power has a strong influence on aerodynamic interference. The longitudinal and vertical position of the engine relative to the wing also has a pronounced effect on interference drag. The greatest favorable interference was obtained during this investigation with the engine in the most forward longitudinal and lowest vertical test position. An increase in Mach number above the design speed has an adverse influence on the aerodynamic interference. Author

N68-31445*# National Aeronautics and Space Administration. Manned Spacecraft Center, Houston, Tex.

AERODYNAMIC STABILITY CHARACTERISTICS OF THE APOLLO COMMAND MODULE

William C. Moseley, Jr., Ralph E. Graham, and Jack E. Hughes Washington Aug. 1968 171 p refs

(NASA-TN-D-4688) CFSTI: HC\$3.00/MF\$0.65 CSCL 01A

Results from wind-tunnel tests conducted during the design and development of the Apollo command module are presented. Investigations were made to develop static and dynamic stability data for the basic configuration of the command module. Parametric studies were conducted to determine the effects of varying certain. geometric dimensions of the basic command module configuration. Studies of modifications designed to provide an increased lift-to-drag ratio were also conducted. Representative samples, from an extensive series of tests of alterations designed to eliminate an apex-forward trim condition, are included. Author

N68-31484*# National Aeronautics and Space Administration. Langley Research Center, Langley Station, Va.

DESIGN OF BODIES TO PRODUCE SPECIFIED **SONIC-BOOM SIGNATURES**

Raymond L Barger Washington Aug. 1968 10 p refs

(NASA-TN-D-4704) CFSTI: HC\$3.00/MF\$0.65 CSCL 01B

A mathematical procedure is described for calculating the shape of a body of revolution that will generate a specified signature at a given Mach number and lateral spacing from the body. The applicability of the method is contingent on the requirement that the signature be physically obtainable. Results of a wind-tunnel study with three sample bodies support qualitatively the validity of the theory Author

N68-31515*# National Aeronautics and Space Administration. Langley Research Center, Langley Station, Va.

A MODIFIED MULTIHOPP APPROACH FOR PREDICTING LIFTING PRESSURES AND CAMBER SHAPE FOR COMPOSITE PLANFORMS IN SUBSONIC FLOW John E. Lamar [1968] 143 p

(NASA-TN-D-4427, Sup.) CFSTI: HC \$3.00/MF \$0.65 CSCL

This supplement contains information about the two main computer programs (Langley computer program A0313, loading program, and Langley computer program A0457, mean camber program) used to obtain the results presented in NASA Technical Note D-4427 along with two supplementary programs (Langley computer program A1590, aspect ratio program, and Langley computer program A1591, pivot determining program) used in obtaining input data for them. In part I of this supplement, the input and some output variables for each of the two main programs (A0313 and A0457) are presented and pertinent comments made. Further, sample listings of input and output data are shown and the entire computer program listings provided. In part II of this supplement, a discussion of the two supplementary programs is presented with a list of input data required, and sample input and output listings as well as program listings are given. Author

N68-31551*# National Aeronautics and Space Administration. Langley Research Center, Langley Station, Va.

SUPERSONIC AERODYNAMICS OF LARGE-ANGLE CONES James F. Campbell and Dorothy T. Howell Washington Aug. 1968 71 p refs

(NASA-TN-D-4719) CFSTI: HC\$3.00/MF\$0.65 CSCL 01A

An investigation has been made to determine the supersonic aerodynamics of a series of conical bodies with semiapex angles from 40° to 90° (disk). The tests were performed at Mach numbers from 2.30 to 4.63, at angles of attack from -4° to 24°, and at a Reynolds number based on model (base) diameter of 0.8 \times 106 These data were compared with those predicted by exact cone theory, modified Newtonian theory, and an integral relations method. Results of this study indicated that all the configurations are statically stable with the center of gravity located at the model base.

As the cone semiapex angle is increased, axial force increases, the rate of increase being largest between 40° and 50° cone configurations. Experimental values of axial force at an angle of attack of 0° are adequately predicted for all cone semiapex angles by utilizing a combination of exact theory and an integral relations method. As the cone semiapex angle is increased, normal force decreases, normal force being zero for the flat disk. Shock standoff distance varies almost linearly with cone semiapex angle and the inverse of Mach number squared; these trends are adequately predicted by an integral relations method.

N68-31990*# National Aeronautics and Space Administration. Langley Research Center, Langley Station, Va.

APPLICATION OF THE LEADING-EDGE-SUCTION ANALOGY OF VORTEX LIFT TO THE DRAG DUE TO LIFT OF SHARP-EDGE DELTA WINGS

Edward C. Polhamus Washington Aug. 1968 14 p refs (NASA-TN-D-4739) CF\$TI: HC\$3.00/MF\$0.65 CSCL 01A

A study has been made of the application of the leading-edge-suction analogy of vortex lift to the prediction of the drag due to lift on thin sharp-edge delta wings in incompressible flow. The study included comparisons with experimental results over a range of aspect ratios from 0.25 to 2.0. The results indicated that the drag due to lift can be predicted accurately by the zero-leading-edge-suction assumption, provided the vortex lift is accounted for by the leading-edge-suction-analogy method of NASA Technical Note D-3767. It was also found that because of the vortex lift, the drag due to lift for wings of extremely low aspect ratio can be less than that for optimum potential flow. Author

N68-33043*# Bell Aerosystems Co., Buffalo, N. Y.

A GENERALIZED EXPERIMENTAL INVESTIGATION OF HOT GAS RECIRCULATION AND INGESTION FOR JET VTOLAIRCRAFT

Patrick E. Ryan, Richard J. Heim, and Wayne J. Cosgrove Washington NASA Sep. 1968 150 p refs

(Contract NAS1-6706)

(NASA-CR-1147) CFSTI: HC\$3.00/MF\$0.65 CSCL 21E

Results of a small scale experimental investigation into the engine inlet temperature rise and flow field caused by the recirculating hot exhaust gases from various simulated V/STOL jet engine arrangements in static proximity to ground are presented. Experimental data were obtained to evaluate the recirculating flow field and engine inlet temperature rise caused by hot exhaust jets impinging on the ground. The effect of engine spacing, height, exhaust deflection angle, exhaust nozzle geometry, and wing planform are included.

N68-33081*# National Aeronautics and Space Administration. Ames Research Center, Moffett Field, Calif.

A COMPUTER PROGRAM FOR SYSTEMATICALLY ANALYZING FREE-FLIGHT DATA TO DETERMINE THE AERODYNAMICS OF AXISYMMETRIC BODIES

Gerald N. Malcolm and Gary T. Chapman Washington Sep. 1968 39 p refs

(NASA-TN-D-4766) CFSTI: HC\$3.00/MF\$0.65 CSCL 01A

The computer program analyzes free-flight motions to deduce coefficients of drag, lift, and static and dynamic stability from any set of free flight data complete enough to define the trajectory and angle history. Nonlinear behavior can be accurately assessed from the results of the data reduction program, and available methods are discussed. To demonstrate the effectiveness of the data reduction method, free flight tests of the AGARD standard hypersonic ballistic correlation model HB-2 were conducted. The results for lift and static and dynamic stability at a Mach number of 2 agreed well with conventional wind tunnel results. Significant differences were found in the drag data because of different base pressures believed due to sting effects in the wind tunnel tests. N68-33374*# National Aeronautics and Space Administration. Lewis Research Center, Cleveland, Ohio.

EXPERIMENTAL INVESTIGATION OF THE DYNAMIC RESPONSE OF A SUPERSONIC INLET TO EXTERNAL AND INTERNAL DISTURBANCES

Joseph F. Wasserbauer and Daniel L. Whipple Washington Sep. 1968 28 p refs

(NASA-TM-X-1648) CFSTI: HC\$3.00/MF\$0.65 CSCL 01A

The terminal shock position and static-pressure responses of an inlet were measured at a Mach number of 3.0 in the 10-by 10-foot supersonic wind tunnel. Internal and external disturbances were investigated over frequency ranges of 0.3 to 200 and 0.1 to 12 Hz, respectively. For an internal disturbance, the dynamic response of the terminal shock and static pressure near the inlet throat exhibited a lag characteristic to about 40 Hz but encountered resonant conditions at about 85 and 180 Hz. For the external disturbance, the dynamic response of the terminal shock and static pressure near the inlet throat exhibited a lead characteristic. Author

N68-33451*# Rice Univ., Houston, Tex.

CONICAL BODIES OF GIVEN LENGTH AND VOLUME HAVING MAXIMUM LIFT-TO-DRAG RATIO AT HYPERSONIC SPEEDS. VARIATIONAL METHODS

Ho-Yi Huang Washington NASA Aug. 1968 29 p refs (Grant NGR-44-006-063)

(NASA-CR-1156; Rept.-36) CFSTI: HC \$3.00/MF \$0.65 CSCL 01A

An investigation of the lift-to-drag ratio attainable by a slender, conical body flying at hypersonic speeds is presented under the assumptions that the pressure distribution is modified Newtonian and the surface-averaged friction coefficient is constant. Length and volume are given, and the values of the free-stream dynamic pressure, the factor modifying the Newtonian pressure distribution, and the surface-averaged friction coefficient are known a priori. The indirect methods of the calculus of variations are employed, and numerical solutions are found using an IBM 7040 computer. It is found that a one-parameter family of external solutions exists, the parameter being the dimensionless area S^* . It is also noted that the geometry of the optimum contour and the maximum value of the modified lift-to-drag ratio E^* are uniquely related to the dimensionless area S^* .

N68-33765* # Nielsen Engineering and Research, Inc., Palo Alto, Calif.

INVESTIGATION OF METHODS FOR PREDICTING THE AERODYNAMIC CHARACTERISTICS OF TWO-LOBED PARAWINGS

M. R. Mendenhall, S. B. Spangler, and J. N. Nielsen Washington NASA Sep. 1968 125 p refs

(Contract NAS1-6615)

(NASA-CR-1166) CFSTI: HC\$3.00/MF\$0.65 CSCL01A

The present study seeks to develop accurate methods for predicting the longitudinal aerodynamic characteristics of two-lobed conical parawings with leading-edge booms for high aspect ratios and high slackness. For prediction purposes, the assumption was made that the booms and canopy can be considered separately. The canopy was then considered to nave a known shape for purposes of determining its aerodynamic performance. Various theoretical methods were studied for determining canopy aerodynamic characteristics, including profile drag. Force increments due to the leading-edge booms were studied both analytically and empirically. Comparisons were made between theory and data for rigid wings of known shape with no leading-edge booms to check the canopy prediction methods. Comparisons were also made for flexible wings of triangular and NASA planforms with leading-edge booms for overall evaluation of the methods. The canopy shape assumption was checked by comparison with earlier slender-body results, and the aerodynamic performance was found to be insensitive to small shape differences. Author

N68-33836*# National Aeronautics and Space Administration. Langley Research Center, Langley Station, Va.

AERODYNAMIC CHARACTERISTICS OF SEVERAL HYPERSONIC BOOST-GLIDE-TYPE CONFIGURATIONS AT MACH NUMBERS FROM 2.30 TO 4.63

Ernald B. Graves and Melvin M. Carmel Washington Sep. 1968 27 p refs

(NASA-TM-X-1601) CFSTI: HC\$3.00/MF\$0.65 CSCL01A

Two all-wing and three wing-body configurations were tested through an angle-of-attack range from about -4° to 33° and an angle-of-sideslip range from -4° to 8° at a Reynolds number of 3×10^6 per foot (9.84 × 10⁶ per meter). The results of the investigation indicate that the wing-body configurations produced higher values of maximum lift-drag ratio than those produced by the all-wing models. The high wing-body configurations tend to have a self-trimming capability as opposed to that for the low wing-body configurations. Each of the configurations produced a positive dihedral effect that increased with increasing angle of attack and decreased with increasing Mach number. The high wing-body models produced decreasing values of directional stability with increase in angle of attack, whereas the low wing-body provided increasing values of directional stability with increase in angle of attack Author

N68-35141*# National Aeronautics and Space Administration. Langley Research Center, Langley Station, Va.

EFFECTS OF SEVERAL RAMP-FAIRING, UMBILICAL, AND PAD CONFIGURATIONS ON AERODYNAMIC HEATING TO APOLLO COMMAND MODULE AT MACH 8

James L. Hunt and Robert A. Jones Washington Sep. 1968 70 p refs

(NASA-TM-X-1640) CFSTI: HC\$3.00/MF\$0.65 CSCL 01A

Test were made at angles of attack of 18°, 22°, and 26° and free-stream Reynolds numbers, based on model diamuter, of 0.76 \times 106 and 1.48 \times 106. For the ramp-fairing-umbilical configurations tested, the area of high interference heating on the body at the windward base of the leeward umbilical was reduced substantially below that which occurred for the configuration having a protruding leeward shear pad and a flush-face umbilical: however, no significant reduction in the peak interference heating factor was observed. The presence of a simulated wire bundle case on the windward face of the protruding leeward umbilical appeared to reduce the peak heating on the body at the base of the umbilical. The highest heating rates on the Apollo configurations tested occurred in the interference regions of the shear and compression pads. The magnitude of these interference heating rates was 3 to 4.5 times the stagnation-point value for an angle of attack of 22° and a free-stream Reynolds number of 0.76 \times 10⁶ based on model diameter. The placement of a recessed umbilical just downstream of the leading edge on the windward afterbody produced interference heating factors of 1.26 and 1.48 just downstream of the umbilical for Reynolds numbers of 0.76 imes 10⁶, respectively. These heating factors were about 74 percent lower than the lowest peak factors obtained with any of the protruding leeward umbilical configurations. Author

N68-35173*# National Aeronautics and Space Administration. Flight Research Center, Edwards, Calif.

FLOW-FIELD INVESTIGATIONS ON THE X-15 AIRPLANE AND MODEL UP TO HYPERSONIC SPEEDS

L. J. McLain and Murray Palitz Washington Sep. 1968 33 p refs

(NASA-TN-D-4813) CFSTI: HC\$3.00/MF\$0.65 CSCL 01B

Flight measured impact pressures and local Mach numbers near the surface of the rear lower fuselage centerline, wing lower surface, and upper vertical tail of the X-15 airplane are presented and compared with calculated results and wind tunnel data. In addition, wind tunnel derived total pressures in the rear lower fuselage flow field are presented. The flight measurements are presented over a free stream Mach number range of 1 to 5.7 and an angle of attack range of 0° to 20°. The wind tunnel measurements cover a Mach number range of 4.0 to 8.0. The calculated predictions of Moeckel Love and Inouye Lomax at an angle of attack of 0° gave reasonable estimates of the flight measured flow field parameters in the three local flow regions. Flight measured impact pressures near the rear lower fuselage were somewhat lower than wind tunnel measurements, whereas the flight and wind tunnel measurements for the vertical tail and wing lower surface showed good agreement. Author

N68-35497*# National Aeronautics and Space Administration. Langley Research Center, Langley Station, Va.

HEAT TRANSFER AND PRESSURE DISTRIBUTIONS ON SPHERICALLY BLUNTED 25° HALF-ANGLE CONE AT MACH 8 AND ANGLES OF ATTACK UP TO 90°

Dennis M. Bushnell, Robert A. Jones, and Jarrett K. Huffman Washington Oct. 1968 41 p refs

(NASA-TN-D-4792) CFSTI: HC\$3.00/MF\$0.65 CSCL01A

Local heat transfer and pressure distributions were measured over the conical portion of the cone. The investigation was conducted at at Mach number of 8.00 and Reynolds numbers of 0.37×10^6 and 1.65×10^6 based on free stream conditions and model base diameter. The pressure data are generally in good agreement with the semiempirical theory over the entire angle-of-attack range. The heat-transfer data for angles of attack up to 45° are in agreement with predictions using the small-cross-flow theory; whereas, the data at higher angles of attack are fairly well represented by the swept-cylinder theory based on the local cone diameter. Author

N68-35523*# Fairchild Hiller Corp., Farmingdale, N. Y. EFFECT ON BLUNTNESS ON HYPERSONIC TWO-DIMENSIONAL INLET TYPE FLOWS

Robert J. Sanator, John L. Boccio, and Dan Shamshins Washington NASA Oct. 1968 105 p refs

(Contract NAS7-416)

(NASA-CR-1145) CSCL01A

Tests were performed on two geometric configurations—a flat plate and an isentropic compression ramp—each accommodating leading edges of three different radii. The nominal test Mach numbers were 7.3 and 10.55, with corresponding free-stream unit Reynolds number ranges of 0.25 to 2.0×10^6 per foot, and 0.75 to 2.0×10^6 per foot, respectively. Results generated during the test phases of this program are compared with theoretical analyses and reflect blunt leading edge effects on inviscid flow profiles, surface pressure phenomena and viscous layer growth along the models, with and without incident shock wave-boundary layer interactions.

N68-35617*# National Aeronautics and Space Administration. Langley Research Center, Langley Station, Va.

SUBSONIC LONGITUDINAL AERODYNAMIC MEASURE-MENTS ON A TRANSPORT MODEL IN TWO SLOTTED TUN-NELS DIFFERING IN SIZE

Arvo A. Luoma, Richard J. Re, and Donald L. Loving Washington Oct. 1968 47 $\,p\,$ refs

(NASA-TM-X-1660) CFSTI: HC\$3.00/MF\$0.65 CSCL01A

An investigation of the static longitudinal aerodynamic characteristics of the same 5-foot-span (1.5-meter) model of a large subsonic cargo-type transport was made in the Langley 8-foot transonic pressure tunnel and in the Langley 16-foot transonic tunnel at Mach numbers from 0.700 to 0.825. The Reynolds numbers, the test conditions, and the data-reduction procedures were the same in the two investigations. The agreement in the data obtained was generally satisfactory. The greatest differences in the comparisons usually occurred at lift coefficients beyond the cruise lift where probably unequal effects of flow separation, particularly at supercritical speeds, may be expected. The results indicate that a model having a wing span which is large relative to the width of the test section can be tested in a slotted wind tunnel at subsonic speeds and that the results of such tests can be used with

confidence provided the test techniques and data-reduction methods used adhere to acceptable standards developed for such tests. Author

N68-36081*# National Aeronautics and Space Administration. Langley Research Center, Langley Station, Va.

AERODYNAMIC CHARACTERISTICS OF A FIVE JET VTOL CONFIGURATION IN THE TRANSITION SPEED RANGE

Richard J. Margason and Garl L. Gentry, Jr. Washington Oct. 1968 189, p refs

(NASA-TN-D-4812) CFSTI: HC\$3.00/MF\$0.65 CSCL 01A

A wind tunnel investigation was conducted of a powered model of a VTOL fighter airplane configuration, having three lift engines in the forward fuselage and two deflected lift cruise engines in the aft fuselage, to determine the aerodynamic characteristics of the model in the transition speed range. The jet induced interference showed that the expected increase in lift loss and nose up pitching moment with increasing forward speed was rather small because of the counteracting effects of the front and rear jets. A substantial part of the nose up interference pitching moment was found to be due to the engine inlet mass flow for this engine arrangement. These results showed that increasing angle of attack had very little effect on interference lift and drag but that significant increases in interference pitching moment can occur if the horizontal tail is on or below the wing chord plane. Further investigation of tail height showed that the jet induced downwash was highest for the low tail position but that the jet induced longitudinal instability was mild for the three tail positions used in the tests. The effects of ground proximity were found to be relatively small for this configuration. Author

N68-36112*# National Aeronautics and Space Administration. Langley Research Center, Langley Station, Va.

EFFECT OF LARGE SIDESLIP ANGLES ON STABILITY CHARACTERISTICS OF A T-TAIL TRANSPORT CONFIGURATION

Edward J. Ray Washington Oct. 1968 48 p refs

(NASA-TM-X-1665) CFSTI: HC\$3.00/MF\$0.65 CSCL01A

An investigation has been made to determine the effects of large sideslip angles on the static stability characteristics of a typical T-tail transport configuration. In addition, damping-in-roll derivatives were determined for the basic T-tail arrangement over an angle-of-attack range extending from about 0° to 36°. The effects of large sideslip variations on the pitching-moment characteristics were also ascertained for selected configurations. The study was made in the Langley high-speed 7- by 10-foot tunnel at a Mach number of 0.30 and a corresponding Reynolds number of 1.20 imes106. In order to assess this assumed linearity and to determine the lateral-directional characteristics over large sideslip ranges, several of the configurations were positioned at fixed angles of attack (range of 0° to 11°) and varied through sideslip angles extending from -22° to 22°. These tests indicated significant nonlinearities in the variation of yawing-moment coefficient with sideslip angle at relatively low angles of attack. Two aft nacelle locations were investigated and it was determined from this limited study that the static directional stability characteristics could be substantially influenced at moderate angles of attack and sideslip by the position of the nacelles on the rearward portion of the fuselage. Author

N68-36132*# National Aeronautics and Space Administration. Lewis Research Center, Cleveland, Ohio.

PERFORMANCE OF A COLLAPSIBLE PLUG NOZZLE HAVING EITHER TWO-POSITION CYLINDRICAL OR VARIABLE ANGLE FLOATING SHROUDS AT MACH NUMBERS FROM 0 TO 2.0 Robert A. Wasko and Douglas E. Harrington Washington Oct. 1968 44 p refs

(NASA-TM-X-1657) CFSTI: HC\$3.00/MF\$0.65 CSCL01A

An experimental study was made concerning the effects of two types of shroud geometry on the performance of a collapsible plug nozzle. Shroud geometries considered were a two position cylindrical shroud and a variable angle floating shroud. Quiescent performance was obtained at nozzle pressure ratios from 2 to 15, and external flow effects were obtained at Mach numbers from 0.56 to 1.97. At subsonic cruise, the performance of the two position shroud was nearly comparable to that of the floating shroud. However, the two position shroud had better performance for subsonic acceleration whereas the floating shroud had better performance at supersonic Mach numbers. Maximum external flow effects occurred at Mach 1.2 for both shroud configurations. Author

N68-36133*# National Aeronautics and Space Administration. Lewis Research Center, Cleveland, Ohio.

EFFECT OF MODEL FOREBODY SHAPE ON PERFORATED TUNNEL WALL INTERFERENCE

Glen A. Mitchell Washington Oct. 1968 47 p refs

(NASA-TM-X-1656) CFSTI: HC\$3.00/MF\$0.65 CSCL01A

A 0.73-percent blockage cylindrical body was tested in the 8- by 6-foot supersonic wind tunnel with several forebody shapes to determine the magnitude of wall interference effects on model pressure distributions. The test section Mach number was varied from 0.4 to 2.0, and the distribution of wall porosity was adjusted. The forebody shape variations included cones with half angles of 15° and 42°, and a tangent ogive with a length to diameter ratio of 3. Results were compared to data on a 10° conical forebody from a previous test.

N68-36134*# National Aeronautics and Space Administration. Lewis Research Center, Cleveland, Ohio.

BLOCKAGE EFFECTS OF CONE-CYLINDER BODIES ON PERFORATED WIND TUNNEL WALL INTERFERENCE Glenn A. Mitchell Washington Oct. 1968 63 p refs

(NASA-TM-X-1655) CFSTI: HC\$3.00/MF\$0.65 CSCL01A

A variety of cone-cylinder models were tested in the 8by 6-foot supersonic wind tunnel at speeds from Mach 0.5 to 2.0 to evaluate the effect of wall reflected disturbances on model pressure distribution. In all cases, a 10° half-angle conical forebody was used; and the cylinder diameter was varied from 4 inches (10.16 cm) to 16 inches (40.64 cm). There were additional variations in model position within the test section and also in tunnel wall porosity. Author

N68-36193*# National Aeronautics and Space Administration. Langley Research Center, Langley Station, Va.

AERODYNAMIC CHARACTERISTICS OF BODIES OF REVOLUTION AT MACH NUMBERS FROM 1.50 to 2.86 AND ANGLES OF ATTACK TO 180°

Lloyd S. Jernell Washington Oct. 1968 40 p ref (NASA-TM-X-1658) CFSTI: HC\$3.00/MF\$0.65 CSCL01A

An investigation has been conducted in the Langley Unitary Plan wind tunnel to determine the aerodynamic characteristics of a series of cylinder, cone-cylinder, and ogive-cylinder bodies with various nose and afterbody fineness ratios for angles of attack from 0° to 180° and Mach numbers from 1.50 to 2.86. The data indicated that with the center of gravity located at 50 percent of the body length, none of the test configurations were statically stable at angles of attack near 0° or 180°. The magnitude of the normal force was primarily dependent upon the magnitude of the planform area. Generally, the more rearward the planform-area centroid, the more rearward the center of pressure. Author N68-36334*# National Aeronautics and Space Administration. Langley Research Center, Langley Station, Va.

A HOVERING INVESTIGATION OF AN EXTREMELY FLEXIBLE LIFTING ROTOR

Matthew M. Winston Washington Oct. 1968 54 p refs (NASA-TN-D-4820) CFSTI: HC\$3.00/MF\$0.65 CSCL01A

A hovering investigation of an extremely flexible rotor was conducted to determine the effects of rotor-tip configuration and operating conditions on performance and to obtain a comparison with a conventional rotor. The results show the manner in which luffing (fabric instability) restricted the envelope of tip speed and collective pitch angles within which the rotor could be operated. In the range where the rotor could be operated, variations in tip speed altered the blade camber and resulted in substantial variations with tip speed in hovering performance, particularly at the higher thrust conditions. The results suggest the existence of optimum combinations of tip body mass, tip center of gravity, and tip stabilizer incidence for each value of tip speed since these variables determine the amount and distribution of blade camber and twist. The hovering efficiency of this rotor was poor in comparison with a conventional rotor. Because of the large amount of aerodynamically induced camber, however, the rotor attained very high mean lift Author coefficients.

N68-36509*# National Aeronautics and Space Administration. Langley Research Center, Langley Station, Va.

EFFECTS OF NOSE SHAPE AND FIN GEOMETRY ON STATIC STABILITY OF A HIGH-FINENESS-RATIO SOUNDING ROCKET

Dennis E. Fuller Washington Oct. 1968 29 p refs

(NASA-TM-X-1661) CFSTI: HC\$3.00/MF\$0.65 CSCL 01A

Tests were conducted in the Langley 4- by 4-foot supersonic pressure tunnel to determine the effects of variations in nose shape and fin geometry on the static stability of two sounding rocket models having length-diameter ratios of 18.20 and 23.77. Tests were made at a Mach number of 2.01 for angles of attack from about -4° to 24° and for angles of sideslip from about -5° to 9°. The Reynolds number was 9.8 \times 10 6 per meter. The results indicated that significant changes in nose shape and fin geometry had little effect in improving the pitching-moment nonlinearities of the high-fineness-ratio rockets. The fins of higher aspect ratio tended to improve the directional stability and to delay the induced rolling moments to higher angles of attack.

N68-37054*# National Aeronautics and Space Administration. Langley Research Center, Langley Station, Va.

EFFECT ON BASE DRAG OF RECESSING THE BASES OF CONICAL AFTERBODIES AT SUBSONIC AND TRANSONIC SPEEDS

William B. Compton, III Washington Oct. 1968 50 p refs (NASA-TN-D-4821) CFSTI: HC\$3.00/MF\$0.65 CSCL 01A

An investigation was conducted to determine the effect on base drag of recessing the bases of truncated conical afterbodies. The drag of a flat base was compared with the drag of recessed bases of equal size for afterbodies having boattail angles of 0°, 3°, 5°, and 10° and having ratios of boattail length to maximum diameter of 1.0 and 1.5. For each boattail, the amount of base concavity was varied in several steps from a flat base to an open base. A fully conical afterbody with a boattail angle of 10° was tested also. The tests were run at an angle of attack of 0° and through a Mach number range of 0.3 to 1.3. The Reynolds number based on model length was in the range of 8×10^6 to 16×10^6 depending on the Mach number. In addition, boundary layer profiles and afterbody drag coefficient plots are included. Results indicate that recessing the base gives an increase in base pressure coefficient of 0.01 to 0.03, depending on the boattail, and hence a reduction in base drag. For a given boattail, base drag decreases with increasing base concavity up to a certain point, but, beyond this point, further concaving the base has little or no effect. The ratio

of the amount of base concavity to base radius necessary to achieve maximum base drag reduction depends on the boattail angle and length. Author

N68-37065*# National Aeronautics and Space Administration. Langley Research Center, Langley Station, Va.

EFFECTS OF FLEXIBILITY ON LIFT AND PITCHING-MOMENT CHARACTERISTICS OF A SERIES OF LOW-ASPECT-RATIO WING-BODY COMBINATIONS AT TRANSONIC SPEEDS

Robert V. Doggett, Jr. and A. Gerald Rainey Washington Oct. 1968 49 p refs

(NASA-TN-D-4655) CFSTI: HC\$3.00/MF\$0.65 CSCL 01A

Measurements of lift and pitching moment were made on a series of low aspect ratio wing-body combinations of different stiffnesses in the Mach number range from 0.70 to 1.10 and at angles of attack up to 30°. The configurations consisted of three different delta wings in combination with a single conical-cylindrical body. The three delta wings differed in leading-edge-sweep angle, aspect ratio, and area. Both rigid and flexible models were tested at Reynolds numbers per meter of 10.5×10^6 and 5.9×10^6 . The experimental results indicated that there is no appreciable effect of vehicle flexibility on the lift characteristics for the models tested. The pitching moment characteristics were affected by flexibility; in general, increasing flexibility produced an appreciable deterioration of the static longitudinal stability characteristics. The linear theory showed good agreement with the experimental results in values of the lift curve slope at the zero lift condition. One of the nonlinear theories showed fair agreement with the experimentally determined lift characteristics for all three configurations. None of the analytical methods used were completely adequate for the prediction of the lift and pitching moment characteristics throughout the entire angle of attack range of the investigation. Author

N68-37238*# National Aeronautics and Space Administration. Langley Research Center, Langley Station, Va.

FLOW FIELD PROPERTIES NEAR AN ARROW WING-BODY MODEL AT MACH NUMBERS OF 1.60, 2.36, AND 2.96

Robert L. Weirich and Walter A. Vahl Washington Oct. 1968 136 p refs

(NASA-TN-D-4809) CFSTI: HC\$3.00/MF\$0.65 CSCL 01A

A wind-tunnel investigation was conducted at supersonic Mach numbers to determine the flow-field properties near an arrow-wing-body model at several stations which were considered to be potential locations for engine air inlets. The tests were conducted at Mach numbers of 1.60, 2.36, and 2.96 at a Reynolds number of 9.84 \times 10⁶ based on a 1-meter length. The model angle-of-attack range was 0° to 9° and the model angles of sideslip were 0° , 5° , and -5° . The local flow parameters Mach number, upwash and sidewash angles, and ratio of local to free-stream total pressure-were measured by pressure-instrumented 15° half-angle conical probes. These local flow characteristics are presented as contour plots for the locations which were surveyed. The results of this investigation indicate that several locations are potentially suitable as inlet locations. Below the wing-body, the Mach numbers are less than the free-stream value and the flow is reasonably uniform except in the region of the wing-body juncture. Locations below the fuselage and below the wing appear suitable for inlets. Above the plane of the wing, the Mach number is generally greater than the free-stream value. However, near the fuselage the flow is uniform except at high angles of attack, and this region appears suitable as an inlet location. Author

N68-37255*# Air Vehicle Corp., La Jolla, Calif.

NONLINEAR LIFT AND PRESSURE DISTRIBUTION OF SLENDER CONICAL BODIES WITH STRAKES AT LOW SPEEDS

E. S. Levinsky and M. H. Y. Wei Washington NASA Oct. 1968 64 p refs

(Contract NAS2-3523)

(NASA-CR-1202) CFSTI: HC \$3.00/MF \$0.65 CSCL 01A

Nonlinear vortex lift and pressure distributions were obtained analytically for conical bodies of circular and elliptical cross-section with small span sharp-edged conical wings or strakes of arbitrary dihedral angle. The analytical approach, which is an extension of the Mangler and Smith theory for slender flat triangular wings, made use of a generalized conformal transformation to map this class of wing-bodies of high volumetric efficiency into a vertical slit. A single pair of spiral vortex sheets was assumed to originate from the leading edge of each strake. The shape and strength of the spiral vortex sheet were determined as part of the calculation procedure. The nonlinear theory was evaluated by comparing with low-speed wind tunnel force and pressure data obtained on a series of related models. Both theory and experiment indicated relatively large increases in lift with even the smallest strake sizes considered, viz., 10% of the body radius. Good correlation between theory and experiment was obtained over the complete angle of attack range for cones with strakes of 50% of the body radius or greater. For these configurations, the lift was approximately twice the linear theory value at angles of attack equal to twice the strake semi-apex angle. Author

N68-37365*# National Aeronautics and Space Administration. Ames Research Center, Moffett Field, Calif.

WIND TUNNEL INVESTIGATION OF THE LOW SPEED HIGH LIFT AERODYNAMICS OF A ONE-FIFTH SCALE VARIABLE SWEEP SUPERSONIC TRANSPORT Anthony M. Cook Washington Oct. 1968 126 p refs

(NASA-TN-D-4844) CFSTI: HC\$3.00/MF\$0.65 CSCL01A

Low-speed aerodynamic characteristics of a large-scale variable-sweep supersonic transport model were determined in a 40 by 80-foot wind tunnel. Included are data for the model both in and out of ground effect. The results are presented as six-component aerodynamic force and moment data obtained at various angles of attack and sideslip. The investigation was made at a free-stream dynamic pressure of 25 pounds per square foot, corresponding to a Reynolds number of 11 million, based upon the mean aerodynamic chord of the fully swept wing. The majority of testing was directed toward the optimization of high-lift configurations and the investigation of longitudinal stability and control characteristics for the take-off and landing configurations. Data concerning low-speed flight at highter wing sweeps of 30°, 42°, and 72° are also presented. It is shown that the model maintained acceptable levels of longitudinal stability up to 13° angle of attack at high lift in both the landing and take-off configurations. The model also exhibited lateral and directional stability up to high angles of sideslip. Author

N68-37854*# National Aeronautics and Space Administration. Langley Research Center, Langley Station, Va.

AERODYNAMIC CHARACTERISTICS OF A PARASOL-WING BODY COMBINATION UTILIZING FAVORABLE LIFT INTERFERENCE AT MACH NUMBERS FROM 3.00 TO 4.63 Odell A. Morris and Robert J. Mack Washington Oct. 1968 38 p 9 refs

(NASA-TN-D-4855) CFSTI: HC\$3.00/MF\$0.65 CSCL 01A

An investigation has been conducted in the Langley Unitary Plan wind tunnel at Mach numbers from 3.00 to 4.63 to determine the longitudinal aerodynamic characteristics of a parasol-wing-body model. The model has a swept wing with a curved leading edge and a body with circular cross sections and a Von Karman forebody shape. Variations in wing position and forebody shape were also studied. Results of the investigation show that large favorable lift interferences were obtained at zero angle of attack for all configurations with the largest interference values being measured at Mach numbers from 4.00 to 4.63 in tests of low, single strut configuration. Variation in wing vertical position from a high to a low position improved the interference lift increments at the higher Mach numbers (4.00 to 4.63) with a corresponding increase in the maximum values of the lift-drag ratio. Variations in forebody shape from the basic body resulted in only small changes in the maximum values of the lift-drag ratio. Theoretical calculations of the lift-drag curve for the basic configuration at a Mach number of 3.00 showed good agreement with the experimental data. Author

Includes fixed-wing airplanes, helicopters, gliders, balloons, ornithopters, etc; and specific types of complete aircraft (e.g., ground effect machines, STOL, and VTOL); flight tests; operating problems (e.g., sonic boom); safety and safety devices; economics; and stability and control. For basic research see: 01 Aerodynamics. For related information see also: 31 Space Vehicles; and 32 Structural Mechanics.

N68-10047*# Honeywell, Inc., Minneapolis, Minn. DEVELOPMENT AND FLIGHT TESTING OF A FLUIDIC CONTROL SYSTEM

D. L. Rodgers Washington NASA Oct. 1967 146 p (Contract NAS4-763)

(NASA-CR-913; Rept.-20175-FR2) CFSTI: HC \$3.00/MF \$0.65 CSCL 01D

A three-axis fluidic automatic flight control system was developed, installed, and flight tested in an Aero Commander 680 FP aircraft. The results of the analytical studies, system design work, and flight testing are presented in this report Author

N68-11147*# National Aeronautics and Space Administration. Flight Research Center, Edwards, Calif.

WIND-TUNNEL INVESTIGATION OF THE FLOW FIELD BENEATH THE FUSELAGE OF THE X-15 AIRPLANE AT MACH NUMBERS FROM 4 TO 8

Earl J. Montoya and Murray Palitz Washington Nov. 1967 92 p refs

(NASA-TM-X-1469) CFSTI: HC\$3.00/MF\$0.65 CSCL 01C

Wind-tunnel data were obtained on the local flow field beneath the fuselage of a model of the X-15 airplane approximately 5 to 8 fuselage diameters aft of the model nose from the model surface to the bow shock. Multiple-tube rakes, model surface pressure orifices, and a cone probe were used to survey the flow field. Test results were obtained at free-stream Mach numbers from 4 to 8 and estimate the survey and the survey of the surve

8 and angles of attack from -3° to 20° and were compared with theory and flight data. Results indicate that Mach number, impact pressure, and flow-angularity gradients exist between the vehicle's surface and the bow shock. These gradients generally become larger with both increased angle of attack and Mach number. Good agreement with theoretical results at zero angle of attack was obtained. Mass flow through a proposed hypersonic ramjet engine inlet positioned beneath the X-15 was determined by using both a two-dimensional oblique-shock-wave assumption and wind-tunnel results. The two-dimensional oblique-shock assumption predicted a larger inlet mass flow than was obtained from the wind-tunnel data. Author

N68-11174*# LTV Aerospace Corp., Dallas, Tex. ADDITIONAL STUDIES ON THE FEASIBILITY OF V/STOL CONCEPTS FOR SHORT-HAUL TRANSPORT AIRCRAFT K. R. Marsh Washington NASA Dec. 1967 46 p refs (Contract NAS2-3036)

(NASA-CR-670(01)) CFSTI: HC\$3.00/MF\$0.65 CSCL 01C

Various V/STOL short haul transport aircraft design proposals were reevaluated in terms of size, range, noise levels, and other operating characteristics. Among the conclusions reported are: (1) Operation at nonoptimum cruise conditions would require revisions in the proposed aircraft designs. (2) Matching of propeller takeoff RPM and engine takeoff RPM would be economically advantageous and would provide reductions in far field noise characteristics. Matching resulted in increased cruise speeds for turboprop STOL aircraft; but for turboprop VTOL aircraft, reduced propeller takeoff tip speed and the increased engine takeoff RPM lowered hover performance, necessitating increases in engine size. (3) Existing noise prediction methods do not yield accurate propeller-driven aircraft noise predictions. E.C.

N68-11519*# National Aeronautics and Space Administration. Langley Research Center, Langley Station, Va.

EFFECT OF GROUND PROXIMITY ON THE LONGITUDINAL, LATERAL, AND CONTROL AERODYNAMIC CHARACTERIS-TICS OF A TILT-WING FOUR-PROPELLER V/STOL MODEL Kenneth W. Goodson Washington Dec, 1967 112 p refs (NASA-TN-D-4237) CFSTI: HC\$3.00/MF\$0.65 CSCL 01C

A wind tunnel investigation of a four propeller tilt wing V/STOL configuration was conducted to determine the longitudinal, lateral, and control aerodynamic characteristics in ground proximity. The tests were made utilizing the moving-belt ground plane. The investigation showed that reductions in lift and drag occurred on the tilt-wing configuration when in ground proximity. Smoke-flow observations showed that ground proximity caused the slipstream to be deflected forward of the model. At certain ground heights and wing-tile-flap-deflection angles, these self-generated disturbances became quite erratic. For some wing-flap angle combinations, the unsteady flow caused erratic vawing moments at 0° sideslip. Smoke flow observations also showed that the ground-height-to-chord ratio at which the onset of flow recirculation occurred was proportional to the ratio of disk loading to free-stream dynamic pressure. The extent of the recirculation in front of the wing was dependent upon the wing tile angle at a given flap deflection and ground height. Ground proximity reduced the aileron yaw control by about 50 percent for the design condition ($\delta_{a_{L}}$ =50°; $\delta_{a_{1}}$ is the left-wing aileron deflection) at the lowest ground height of the tests. Increasing the aileron deflection to $\delta_{a_1} = -70^\circ$ and deflection a 0.10-chord upper-surface spoiler increased the control yawing moment to about 70 percent of original out-of-ground-effect value obtained with $\delta_{a_L}=-50^\circ$. Ground proximity also considerably reduced the adverse rolling moment due to aileron deflection for yaw control. Author

N68-11545*# National Aeronautics and Space Administration. Flight Research Center, Edwards, Calif.

AN ANALYSIS OF THE LIMIT-CYCLE AND STRUCTURAL-RESONANCE CHARACTERISTICS OF THE X-15 STABILITY AUGMENTATION SYSTEM

Lawrence W. Taylor, Jr. and John W. Smith Washington Dec. 1967 52 p refs

(NASA-TN-D-4287) CFSTI: HC \$3.00/MF \$0.65 CSCL 01D

During the early flights of the X-15 airplane, two problems associated with the stability augmentation system were encountered: limit cycles, primarily in roll, and control-surface resonance. The limit cycles were usually only an annoyance to the pilot, but at flight conditions with the largest control power, the nature of the limit cycles changed abruptly to large-amplitude oscillations that could have caused complete loss of control. The

frequency and amplitude of the airplane-system limit cycles were calculated by using the describing-function technique together with a nonlinear mathematical model to represent the control system and the airplane. These calculated characteristics compared well with experimental results from flight, ground tests, and simulations. The calculations were repeated for two different electronic filters, the original and a subsequent, improved design, that were incorporated in the stability augmentation system. The calculated limit-cycle characteristics for the final filter did not agree as well with experimental results as did the characteristics calculated for the original filter.

N68-11627*# National Aeronautics and Space Administration. Ames Research Center, Moffett Field, Calif.

LARGE-SCALE WIND-TUNNEL INVESTIGATION OF A MODEL WITH AN EXTERNAL JET-AUGMENTED FLAP

Jerry V. Kirk, David H. Hickey, and Kiyoshi Aoyagi Washington Dec. 1967 35 p refs

(NASA-TN-D-4278) CFSTI: HC\$3.00/MF\$0.65 CSCL 01C

An investigation has been conducted in the Ames 40- by 80-Foot Wind Tunnel of a large-scale model powered by turbojet engines. The wing had 38.5° sweep of the leading edge, an aspect ratio of 5.38, a taper ratio of 0.23, and a dihedral of 3° The wings airfoil section was an NACA 65-412. The trailing-edge flaps extended from 8 to 63 percent semispar. A small auxiliary flap spanned the main flap. The exhaust from the engines was directed against the flaps to augment lift. Longitudinal aerodynamic characteristics for various combinations of main and auxiliary flap deflections are shown for thrust coefficients from 0 to approximately 1.4. Limited longitudinal and lateral-directional characteristics are shown for a simulated engine-out condition. Results also demonstrate the feasibility of using the small auxiliary flap as a means of providing direct-lift flight-path control.

N68-11638*# National Aeronautics and Space Administration. Langley Research Center, Langley Station, Va.

FLIGHT INVESTIGATION OF PERFORMANCE CHARAC-TERISTICS DURING LANDING APPROACH OF A LARGE POWERED-LIFT JET TRANSPORT

Albert W. Hall, Kalman J. Grunwald, and Perry L. Deal Washington Dec. 1967 27 $\,p\,$ refs

(NASA-TN-D-4261) CFSTI: HC\$3.00/MF\$0.65 CSCL 01D

A flight investigation has been conducted to determine low-speed performance characteristics of an airplane employing a powered-lift system. The airplane used during this investigation was a modified jet transport which was equipped to provide engine compressor air for boundary-layer control over the wing trailing-edge flaps. It was found that for powered-lift aircraft the approach speeds should be based on a given percentage of the power-on stall speeds, but not less than a fixed margin above the stall speeds. These criteria provided adequate maneuver capability for all configurations during instrument approaches. These approach speeds fell slightly below the speeds for maximum lift-drag ratio for all configurations, but this speed-thrust instability caused no objectionable characteristics. Problems encountered during this program which should be considered for operational powered-lift aircraft design were uncomfortable airplane approach attitudes and insufficient thrust margin at low approach speeds and maximum landing weights. Automatic speed control was found to be very effective in reducing pilot workload during instrument approaches. Author

N68-11772*# National Aeronautics and Space Administration. Ames Research Center, Moffett Field, Calif.

PREDICTION OF AIRCRAFT SONIC BOOM CHARACTERIS-TICS FROM EXPERIMENTAL NEAR FIELD RESULTS

Raymond M. Hicks and Joel P. Mendoza Washington Nov. 1967 14 p refs

(NASA-TM-X-1477) CFSTI: HC\$3.00/MF\$0.65 CSCL 01B

Near field pressure signature data measured in a wind tunnel were used for predicting aircraft sonic boom characteristics. With the data plus the theoretical concepts of Whitham, an experimental area function F(y) could be determined. Evaluation of the area function for the configuration in turn allows an assessment of the sonic boom pressure signature at any distance ratio greater than that used for the original measurement of the near field data. On the basis of limited tests of a 12-inch model of the XB-70 airplane, good correlations of wind tunnel to wind tunnel and wind tunnel to flight pressure signature results were obtained. A near field signature measured at a distance ratio of 1.0 and a Mach number of 1.8 was used to predict the over-pressure characteristics of the XB-70 configuration. The prediction was accurate at a near field distance ratio of 4.5, and a far field distance ratio of 290. Author

N68-13517*# Boeing Co., Renton, Wash.

STUDY OF AIRCRAFT IN SHORT HAUL TRANSPORTA-TION SYSTEMS

Washington NASA Jan. 1968 74 p (Contract NAS2-3862)

(NASA-CR-986) CFSTI: HC\$3.00/MF\$0.65 CSCL01C

The intercity operation of advanced short-haul transport aircraft were evaluated in several assumed transportation systems in the 1985 period. Three separate areas of the country, the Northeast, West Coast, and the Gulf Coast–Florida areas, were used in assessing the suitability of aircraft ranging from vertical takeoff and landing, through short takeoff and landing, to conventional takeoff and landing types. The figures of merit considered in comparing the relative suitability of the concepts included direct operating costs versus range, vehicle profitability on a systems wide basis, and the extent and magnitude of the noise generated by each concept. The sensitivity of mission performance to changes in the aircraft characteristics and system operations is determined and key problem areas where additional research may improve the aircraft transportation systems are identified. R.N.A.

N68-14090* National Aeronautics and Space Administration. Langley Research Center, Langley Station, Va.

MEASUREMENTS OF GROUND EFFECT ON A LOW-ASPECT-RATIO OGEE-WING AIRPLANE MODEL AND CALCULATIONS OF LANDING-FLARE TRAJECTORIES Vernard E. Lockwood and W. Pelham Phillips Washington Jan.

1968 39 p refs

(NASA-TN-D-4329) CFSTI: \$3.00 CSCL 01B

An investigation has been made to determine the ground effect on a 0.15-scale model of a fighter-type airplane having an ogee-wing planform. The characteristics in close proximity to the ground were determined by utilizing the moving-belt facility of the Langley 300-MPH 7- by 10-foot tunnel with and without ground-plane boundary-layer removal. Trim characteristics were determined for the model with and without landing gear. An analytical study showing the effect of airplane size on landing trajectories is also included. No significant differences in the aerodynamic characteristics were indicated with ground-plane boundary layer present or removed. The increases in lift-curve slope and longitudinal stability and the reduction in induced drag usually encountered by an airplane entering ground effect were noted. A landing-flare motion analysis using the experimentally determined data has indicated the descent rate at touchdown for a large low-aspect-ratio wing airplane of the supersonic transport size would be less than for a small airplane during a constant pitch attitude approach due to the longer time spent in ground effect. The descent rates encountered at touchdown were excessive for normal operational landings. Author

N68-14903* National Aeronautics and Space Administration. Langley Research Center, Langley Station, Va.

EFFECTS OF PAVEMENT TEXTURE ON WET-RUNWAY BRAKING PERFORMANCE Trafford J. W. Leland, Thomas J. Yager, and Upshur T. Joyner Washington Jan. 1968 37 p refs

(NASA-TN-D-4323) CFSTI: \$3.00 CSCL 01B

An extensive test program was conducted at the Langley landing-loads track to investigate the effect on braking of tire tread pattern and tread materials for a variety of runway surfaces. Some of the tire test results were excerpted from this program and are presented to show the importance of runway surface texture in determining braking friction coefficient levels on wet runways. A technique for measuring the average texture depth of a given surface is suggested, and a limited correlation is shown between the texture depth measurements of four runway surfaces and the average friction coefficients developed by a smooth tire when braking on these wet surfaces. Surface wear due to traffic and weathering is shown to have a marked influence on the braking friction coefficient levels attained on wet runways.

N68-15894*# National Aeronautics and Space Administration. Langley Research Center, Langley Station, Va.

STATIC AND DYNAMIC LONGITUDINAL STABILITY DERIVATIVES OF A POWERED 0.18-SCALE MODEL OF A FAN-IN-WING VTOL AIRCRAFT

Joseph R. Chambers and Sue B. Grafton Washington Feb. 1968 66 p refs

(NASA-TN-D-4322) CFSTI: HC\$3.00/MF\$0.65 CSCL 01C

An investigation was conducted to determine the static and dynamic longitudinal stability derivatives of a powered fan-in-wing V/STOL aircraft model for trimmed level flight at an angle of attack of 0°. The model had a lift fan located in each wing panel and a smaller fan located in the nose for pitch control. The investigation covered a range of values of thrust condition and oscillatory frequencies for the model with the horizontal tail both on and off. The results of the investigation indicate that the model was statically unstable with respect to angle of attack and was statically stable with respect to velocity for the lower speeds for fan-powered flight; these trends tended to reverse as the transition to conventional wingborne flight progressed. The model had positive damping in pitch (negative values of the damping-in-pitch parameter) throughout the ranges of test conditions investigated. Author

N68-15941*# National Aeronautics and Space Administration. Langley Research Center, Langley Station, Va.

CALCULATION OF THE DYNAMIC LONGITUDINAL STABILITY OF A TILT-WING V/STOL AIRCRAFT AND CORRELATION WITH MODEL FLIGHT TESTS

Joseph R. Chambers and Sue B. Grafton Washington Feb. 1968 63 p refs

(NASA-TN-D-4344) CFSTI: HC\$3.00/MF\$0.65 CSCL 01C

An analytical study has been conducted to determine the important factors influencing the dynamic longitudinal stability characteristics of a typical tilt-wing V/STOL aircraft. Calculations have been made for the initial condition of steady level flight at wing incidences corresponding to speeds ranging from hovering to conventional forward flight. The results of the calculations have been compared with qualitative measurements of dynamic stability obtained during free-flight tests of a 1/9-scale model of the aircraft. The results of the investigation indicated that the control-fixed motions of the aircraft without artificial stabilization in hovering flight would be dominated by an unstable oscillation similar to that displayed by most helicopters. As the transition to conventional forward flight progressed, stability characteristics were encountered in which aperiodic divergent modes of motion, as well as unstable oscillations, were present. These results also indicated that the unstable oscillation occurring in the hovering and low-speed flight regions can be stabilized by the addition of a combination of pitch-rate and pitch-attitude stabilization, but that angle-of-attack stability must be increased if the aperiodic divergent modes of motion are to be made stable. Author

N68-16522*# National Aeronautics and Space Administration. Langley Research Center, Langley Station, Va.

AN ANALYSIS OF VGH DATA FROM ONE TYPE OF FOUR-ENGINE TURBOJET TRANSPORT AIRPLANE DURING COMMERCIAL OPERATIONS

Paul A. Hunter Washington Feb. 1968 48 p refs

(NASA-TN-D-4330) CFSTI: HC\$3.00/MF\$0.65 CSCL 01C

An analysis of VGH records collected on one type of four-engine turbojet transport during routine commercial operations on two airlines has provided information on acceleration, turbulence, and airspeed operating practices. The data cover operations of two airplanes by one airline on eastern United States and Caribbean routes and of one airplane operated by a second airline on routes which ranged along the east coast of the United States, across the Caribbean Sea and along the west coast of South America. For the two airplanes operated by the same airline, the results were very similar in regard to the gust-velocity experiences and the accelerations caused by gusts, operational maneuvers, check-flight maneuvers, and landing impact. The results indicated that the acceleration experiences, the gust velocity experiences, and the airspeed operating practices were not significantly different for the airplanes operated by the two airlines. In general, the airspeeds in rough air (gust velocity \geq 2 fps (0.6 m/sec)) were approximately equal to the airspeeds in smooth air. The results indicated, however, that the airspeeds in heavy turbulence (gust velocities higher than 20 fps (6.1 m/sec)) were generally lower than the average operating speeds. Author

N68-17023*# National Aeronautics and Space Administration, Langley Research Center, Langley Station, Va.

WIND-TUNNEL INVESTIGATION OF LATERAL AERODY-NAMIC CHARACTERISTICS OF A POWERED FOUR-DUCT-PROPELLER VTOL MODEL IN TRANSITION

Kenneth P. Spreemann Washington Feb. 1968 76 p refs

(NASA-TN-D-4343) CFSTI: HC\$3.00/MF\$0.65 CSCL01C

An investigation to determine the lateral and directional aerodynamic characteristics of a powered four-duct-propeller 1/5-scale model of a VTOL airplane was conducted in the 17-foot test section of the Langley 300-mph 7- by 10-foot tunnel. The model was tested through a sideslip-angle range at angles of attack of 0°, 8°, and 12° and with duct deflection angles from -5° to 90° at various thrust coefficients from hovering to conventional forward flight. The initial cruise configuration had neutral directional stability in the power-off-low-angle-of-attack conditions (0° and 8°) and became stable at the high-angle-of-attack condition (12°). A larger vertical tail having a higher aspect ratio than was used on the initial configuration provided a slightly stable model in the power-off condition; however, in the power-on condition, the model became unstable in the lower transition-speed range regardless of tail geometry. Tail-wing fairings of various sizes and shapes significantly increased the directional stability. Directional deflection of the elevons (vanes) in the ducts provided large control increments in roll and yaw through the transition-speed range; however, the total requirements for trim and control will necessitate the use of both elevon deflection and differential propeller thrust throughout the transition-speed range. Author

N68-17055*# National Aeronautics and Space Administration, Langley Research Center, Langley Station, Va.

SUBSONIC AND TRANSONIC FLUTTER AND FLOW INVESTIGATIONS OF THE T-TAIL OF A LARGE MULTIJET CARGO AIRPLANE

Maynard C. Sandford, Charles L. Ruhlin, and E. Carson Yates, Jr. Washington Feb. 1968 41 p refs

(126-14-02-03-23)

(NASA-TN-D-4316) CFSTI: HC\$3.00/MF\$0.65 CSCL01C

Flutter and flow studies of the T tail of a large multijet cargo airplane have been conducted in the Langley transonic dynamics tunnel at Mach numbers up to 1.08. The tail and aft fuselage of the model employed were geometrically, dynamically,

and elastically scaled, whereas only the mass and stiffness characteristics of the forward fuselage, wings, and nacelles were simulated. The flutter studies included variations in fin-spar stiffness. stabilizer-pitch-actuator stiffness, rotational stiffnesses of elevators and rudder, as well as small variations in stabilizer juncture and included the use of vortex generators and fences, as well as modifications to the bullet-fairing shape. The results indicated that for a configuration with a weaker than design fin spar, the antisymmetric flutter boundary had a transonic dip amounting to a 41% reduction in dynamic pressure from the low speed value, the minimum occurring near Mach number 0.7. For the design configurations, no flutter occurred within the Mach number and dynamic-pressure ranges investigated. Separated flow over the fin and stabilizer was alleviated by the use of vortex generators, but flow over the aft portion of the bullet fairing remained separated. Author

N68-17391*# National Aeronautics and Space Administration. Ames Research Center, Moffett Field, Culif.

A PILOTED SIMULATOR STUDY 6.5 TAKEOFF PERFORMANCE AND HANDLING QUALITIES OF A DOUBLE DELTA SUPERSONIC TRANSPORT

C. Thomas Snyder and Charles T. Jackson, Jr. Washington Feb. 1968 49 p refs

(NASA-TN-D-4396) CFSTI: HC\$3.00/MF\$0.65 CSCL 14B

The takeoff characteristics of a generalized double-delta supersonic transport configuration were investigated in a fixed-cockpit simulator equipped with an external visual display. The objectives were to investigate performance and handling qualities, identify possible problem areas, and assist in the evaluation of certification requirements to be used during the development of the SST. The unaugmented SST exhibited: (1) excellent performance during normal takeoffs, (2) a greater probability of nacelle or tail scrapes than the SJT, indicating a need for more time for the rotation maneuver, a longer landing gear on the design tested, or higher lift-off speeds, (3) initial climb characteristics which were acceptable but unpleasant, due to a tendency toward pitch "wandering," aggravated by negative speed-drag stability, (4) good lateral-directional and engine-out characteristics, and (5) a performance sensitivity to lift-off speed abuse during marginal-thrust takeoffs, which indicated the need for review of the present airworthiness criterion regarding one-engine-inoperative first-segment climb. Author

N68-18250*# National Aeronautics and Space Administration. Langley Research Center, Langley Station, Va.

LOW-SUBSONIC FLIGHT AND FORCE INVESTIGATION OF A SUPERSONIC TRANSPORT MODEL WITH A DOUBLE-DELTA WING

Delma C. Freeman, Jr. Washington Mar. 1968 47 p refs (NASA-TN-D-4179) CFSTI: HC\$3.00/MF\$0.65 CSCL 01C

An investigation has been conducted in the Langley full-scale tunnel to determine the low-speed static and dynamic longitudinal and lateral stability characteristics of a 1/20-scale model of a double-delta supersonic commercial air transport configuration. The results of the investigation showed that the dynamic longitudinal stability and control characteristics of the model were generally satisfactory over the test angle-of-attack range except from about 20° to 25° where neutral or negative static longitudinal stability made flying difficult. The Dutch roll oscillation was well damped throughout most of the test angle-of-attack range but the damping decreased rapidly above an angle of attack of about 20°. The use of a roll-rate damper to provide artificial stabilization in roll generally gave satisfactory Dutch roll characteristics over the test angle-of-attack range. The directional stability was satisfactory at low angles of attack but deteriorated rapidly at the high angles of attack and the model diverged in yaw against full corrective control near an angle of attack of 28°. The lateral control characteristics were satisfactory over the test angle-of-attack range. Author

N68-18771*# National Aeronautics and Space Administration. Ames Research Center, Moffett Field, Calif.

LARGE-SCALE WIND-TUNNEL TESTS OF A DEFLECTED SLIPSTREAM STOL MODEL WITH WINGS OF VARIOUS ASPECT RATIOS

V. Robert Page, Stanley O. Dickinson, and Wallace H. Deckert Washington Mar. 1968 56 p refs

(NASA-TN-D-4448) CFSTI: HC\$3.00/MF\$0.65 CSCL 01B

A wind-tunnel investigation was conducted to determine the longitudinal force characteristics of a large-scale model representative of a propeller-driven STOL transport aircraft. Longitudinal characteristics were obtained for a wing of aspect ratio of 5.7 that was fully immersed in the propeller slipstream and for wings of greater span (up to aspect ratio 8.1) that were only partially immersed in the propeller slipstream. Test configurations included: three wing spans, full-span leading-edge slats, full-span triple-slotted trailing-edge flaps deflected from 0° to 100°, two directions of propeller rotation, and spanwise variation of propeller thrust. Test results show that lift coefficient increased and drag coefficient decreased as the wing tips were extended outboard. Leading-edge slats controlled the progression of flow separation and extended the angle of attack for maximum lift approximately 10° For each wing span tested descent capability could be improved by spanwise variation of propeller thrust. However, the spanwise variation of propeller thrust was most effective on the short span Author wina.

N68-19065*# National Aeronautics and Space Administration. Ames Research Center, Moffett Field, Calif.

WING SURFACE PRESSURE DATA FROM LARGE-SCALE WIND-TUNNEL TESTS OF A PROPELLER-DRIVEN STOL MODEL

V. Robert Page and Paul T. Soderman Washington Mar. 1968 65 p ref

(NASA-TM-X-1527) CFSTI: HC\$3.00/MF\$0.65 CSCL 01C

The model tested is representative of a propeller-driven STOL transport aircraft. The variables include the effect of: trailing-edge flap deflection (0° to 100°), spanwise variation of propeller thrust, wing leading-edge slats, and propeller thrust and rotation on the three wing spans tested. Wing pressure distribution data and integrated chordwise normal-force coefficients are tabulated. Author

N68-19184*# National Aeronautics and Space Administration. Langley Research Center, Langley Station, Va.

FLIGHT INVESTIGATION TO DETERMINE THE EFFECT OF LONGITUDINAL CHARACTERISTICS ON LOW-SPEED INSTRUMENT OPERATION

Daniel J. Di Carlo, James R. Kelly, and Robert W. Sommer Washington Mar. 1968 22 p refs

(NASA-TN-D-4364) CFSTI: HC\$3.00/MF\$0.65 CSCL 01D

A flight investigation using a variable-stability helicopter was conducted under instrument flight rules (IFR) to determine the effects of gross changes in longitudinal static stability characteristics on handling qualities for V/STOL operation. Various combinations of angle-of-attack stability, speed stability, pitch-rate damping, and longitudinal control sensitivity were evaluated by means of a simulated instrument task which was selected as being representative of low-speed instrument flight. Neutral to slightly stable angle-of-attack stability was found to be most satisfactory, regardless of the level of pitch-rate damping. Low unstable values of angle-of-attack stability were tolerable when sufficient pitch-rate damping was provided. Combinations of angle-of-attack stability and pitch-rate damping which provide minimum satisfactory handling qualities are in general agreement with current specifications for low values of angle-of-attack stability. Variations in the longitudinal control sensitivity had little effect on pilot rating over a wide range of values centered about the optimum tested. Author

N68-19620*# National Aeronautics and Space Administration. Langley Research Center, Langley Station, Va.

REVIEW OF CAUSES AND ALLEVIATION OF LOW TIRE TRACTION ON WET RUNWAYS

Walter B. Horne, Thomas J. Yager, and Glenn R. Taylor Washington Apr. 1968 37 p refs

(NASA-TN-D-4406) CFSTI: HC\$3.00/MF\$0.65 CSCL 01B

Three main factors which cause loss of tire traction on wet runways, namely, dynamic hydroplaning, viscous hydroplaning, and tire tread rubber reversion are reviewed. Consideration is given to the interaction of certain variables such as pavement surface texture, runway water depth, tire tread design, vertical tire load, and tire inflation pressure with these factors. A method for measuring average texture depth of a runway surface is described and appears promising as a means of classifying runway surfaces as to their slipperiness when wet. Finally, two promising methods for increasing tire traction on wet runways are discussed; namely, air jets placed in front of tires and pavement grooving. Author

N68-21112*# National Aeronautics and Space Administration. Ames Research Center, Moffett Field, Calif.

PROPOSED ANALYTICAL MODEL FOR THE FINAL STAGES OF LANDING A TRANSPORT AIRPLANE Maurice D. White Washington Apr. 1968 14 p rei

(NASA-TN-D-4438) CFSTI: HC\$3.00/MF\$0.65 CSCL 01C

Methods for defining the certifying landing distances and approach speeds of transport airplanes are currently being reviewed. Revisions are being sought that would make the requirements and demonstration procedures account more realistically for operational practices and variables. As an aid in this task, a simple model is proposed for describing the final airborne stages of landing a transport airplane manually. The model separates the maneuver into three distinct phases, an initial flare, a float, and a touchdown. Methods are indicated for estimating the speed changes or lift increments associated with each phase. Assumptions regarding thrust management in the maneuver are shown to be important. The considerations that affect these assumptions are discussed and indicate how the thrust would probably be managed in normal operations. Limited flight data are described which confirm the main elements of the model. Additional refinement of the model is desirable to make it useful in the development of more rational rules for certifying landing characteristics. Author

N68-21413*# National Aeronautics and Space Administration, Washington, D. C.

SONIC BOOM RESEARCH

A. R. Seebass, ed. 1967 115 p refs Proc. of NASA Conf. on Res. on the Generation and Propagation of Sonic Booms, Washington, 12 Apr. 1967

(NASA-SP-147) GPO: HC\$0.50; CFSTI: MF\$0.65 CSCL 01B

CONTENTS:

1. BRIEF REVIEW OF THE BASIC THEORY W. D. Hayes (Princeton Univ.) p 3-7 refs (See N68-21414 11-02)

2. EXPERIMENTAL AND ANALYTIC RESEARCH ON SONIC BOOM GENERATION AT NASA H. W. Carlson (NASA. Langley Res. Center) p 9–23 refs (See N68-21415 11-02)

3. SONIC BOOM FLIGHT RESEARCH: SOME EFFECTS OF AIRPLANE OPERATIONS AND THE ATMOSPHERE ON SONIC BOOM SIGNATURES D. J. Maglieri (NASA. Langley Res. Center) p 25–48 refs (See N68-21416 11-02)

4. SOME EFFECTS OF THE ATMOSPHERE ON SONIC BOOM E. J. Kane (Boeing Co.) p 49-63 refs (See N68-21417 11-02)

5. SONIC BOOM EFFECTS ON PEOPLE AND STRUCTURES H. H. Hubbard and W. H. Mayes (NASA. Langley Res. Center) p 65-76 refs (See N68-21418 11-02) N68-21834*# National Aeronautics and Space Administration. Flight Research Center, Edwards, Calif.

PRELIMINARY MEASURED AND PREDICTED XB-70 ENGINE NOISE

Paul L. Lasagna and Norman J. Mc Leod Washington Apr. 1968 21 p refs

(NASA-TM-X-1565) CFSTI: HC\$3.00/MF\$0.65 CSCL01C

Noise measurements on the ground were made during takeoffs, a landing, and a flyby of the XB-70 airplane. Noise predictions made by using the SAE method differed from the measured levels. The substitution of standard-day atmosphere for actual atmosphere improved the comparison of the measured and predicted noise spectra. Further investigation is needed to determine the reasons for the difference between the measured and the predicted levels. Perceived noise levels of the XB-70 were approximately 7 PNdB to 10 PNdB higher than the maximum overall sound-pressure levels in decibels.

N68-22033*# National Aeronautics and Space Administration. Langley Research Center, Langley Station, Va.

AN INVESTIGATION OF THE HELICOPTER HEIGHT VELOCITY DIAGRAM SHOWING EFFECTS OF DENSITY ALTITUDE AND GROSS WEIGHT

Robert J. Pegg Washington May 1968 33 p refs

(NASA-TN-D-4536) CFSTI: HC\$3.00/MF\$0.65 CSCL 01C

Within the limitations of the available data, this report is intended to provide a method by which experimentally determined helicopter height-velocity diagrams may be modified to show the effects of density altitude and gross weight. Variations in the established height-velocity diagram can be predicted for changes in density altitude and gross weight by using a generalized nondimensional curve. This generalized curve is based on semiempirical functions derived from flight-test data. During the flight testing of new helicopter designs, this semiempirical method can be used advantageously to predict changes in autorotation characteristics. This method can also predict the approximate shape of the height-velocity diagram while preliminary designs of a helicopter are being made. To illustrate the use of the semiempirical procedure, a detailed numerical example is given. The step-by-step calculations show the use of the curves and equations. Author

N68-22291*# National Aeronautics and Space Administration. Langley Research Center, Langley Station, Va.

SUMMARY OF VGH DATA COLLECTED ON ONE TYPE OF TWIN-ENGINE JET AIRPLANE DURING AIRLINE OPERATIONS

Paul A. Hunter and Marian E. Brazziel Washington May 1968 32 p refs

(NASA-TN-D-4529) CFSTI: HC\$3.00/MF\$0.65 CSCL 01C

A VGH data sample collected on two identical twin-engine turbojet airplanes during routine airline operations has been analyzed to determine the operational experiences of the airplanes. The results indicate that the gust and maneuver accelerations are comparable to corresponding results for turboprop airplanes. Accelerations due to oscillatory motions were of low amplitude, were experienced infrequently, and are considered insignificant in regard to the total airplane acceleration experience. The results indicate that the gust velocity experience for the twin-engine jet airplane is significantly lower than the experience for two types of turboprop airplanes and is comparable to that for a four-engine turboiet transport. Placard-speed exceedances were relatively infrequent and were generally less than 6 knots beyond the overspeed warning bell. The results indicate that, in general, airspeed reduction was practiced during the more severe turbulence. The landing-impact accelerations, which were quite severe during the initial airplane operation, were reduced to a level comparable to that of several other two- and three-engine jet transports after a modification of the landing gear. Author

N68-22886*# National Aeronautics and Space Administration. Lewis Research Center, Cleveland, Ohio. METHOD OF CALCULATING THE NORMAL MODES AND

FREQUENCIES OF A BRANCHED TIMOSHENKO BEAM Francis J. Shaker Washington May 1968 41 p refs

(NASA-TN-D-4560) CFSTI: HC\$3.00/MF\$0.65 CSCL 20K

The method is essentially a modified Stodola method and requires an iteration procedure to determine the normal modes and frequencies of the system. In this method, an arbitrary deflection, consistent with the boundary condition, is assumed. Also, because of the presence of the spring-mass system, the frequency is not a constant factor in the governing equations and must also be assumed. Knowing the deflection and frequency, the corresponding shears, moments, slopes, and new deflection can be determined by integrating the governing differential equations of the system. The new deflection is then adjusted to satisfy the boundary conditions, and a new frequency is subsequently calculated. The process is then repeated, and the frequency is used as the criterion for convergence. Although the method can be applied for any type of boundary conditions, particular attention was given to those boundary conditions of interest in launch-vehicle dynamics, namely, the free-free beam and the cantilevered-free beam. Author

N68-23456*# National Aeronautics and Space Administration, Washington, D. C.

HELICOPTERS—CALCULATION AND DESIGN. VOLUME 2: VIBRATIONS AND DYNAMIC STABILITY

M. L. Mil' et al May 1968 484 p refs Transl. into ENGLISH of the book "Vertolety. Raschet i Proyektirovaniye. 2. Kolebaniya i Dinamicheskaya Prochnost" Moscow, Mashinostr. Press, 1967 p 1–470

(NASA-TT-F-519) CFSTI: HC\$3.00/MF\$0.65 CSCL01C

This volume contains theory and problems of vibration, stress calculations for helicopters in flight, and particularly stress calculations for rotor blades. Covered are methods for calculating structural fatigue and vibrational amplitudes. The problem of coupled vibrations of rotor and fuselage is examined. The self-excitation phenomenon of ground resonance is discussed in detail for helicopters on the ground, during takeoff and landing, and during cruising flight. Theory and calculation methods are presented for analyzing bearing loads of major helicopter components under various operating conditions. K.W.

N68-23895*# National Aeronautics and Space Administration. Lewis Research Center, Cleveland, Ohio.

TANKAGE SYSTEMS FOR A METHANE-FUELED SUPERSONIC TRANSPORT

Joseph D. Eisenberg and Rene E. Chambellan Washington May 1968 21 p refs

(NASA-TM-X-1591) CFSTI: HC\$3.00/MF\$0.65 CSCL 01C

The use of liquid-methane fuel promises economic improvement, but its cryogenic nature causes on-board storage problems. Should the fuel be loaded in a saturated condition, much fuel will flash off due to pressure reductions during climb. Pressurized tanks or subcooled fuel will solve this problem. Subcooled fuels require a pressurizing gas. Low solubility gases have low availability and must be salvaged. Bladders or stand-pipes to reduce the contact area may be used with soluble or condensible pressurizers. Analytical studies indicate that these methods, when used separately or in combination, offer potential solutions to the tankage problem. Author

N68-23901*# National Aeronautics and Space Administration. Flight Research Center, Edwards, Calif.

A REVIEW OF TRANSPORT HANDLING-QUALITIES CRITERIA IN TERMS OF PRELIMINARY XB-70 FLIGHT EXPERIENCE

Bruce G. Powers Washington May 1968 33 p refs (NASA-TM-X-1584) CFSTI: HC\$3.00/MF\$0.65 CSCL 01C

A preliminary flight evaluation of handling qualities of the unaugmented XB-70 airplane was made during the initial flight test and envelope-expansion program. The evaluations consisted of pilot ratings and comments on the longitudinal and lateral-directional characteristics. The pilot ratings were compared with several current handling-qualities criteria for transport aircraft to establish the applicability of these criteria to this class of airplane. The results of the study show that for the longitudinal mode fair correlation was obtained between the XB-70 handling qualities and specific criteria boundaries based on the short-period frequency and damping. It appears that a combination of many handling-qualities factors on the XB-70 airplane obscured the effects of any single handling-qualities parameter. These factors include excessive yaw due to aileron input, restricted sideslip limits, poor pitch and roll control harmony, and poor attitude and heading information. Author

N68-24245*# National Aeronautics and Space Administration. Langley Research Center, Langley Station, Va.

FLIGHT TEST OF A 40-FOOT NOMINAL DIAMETER DISK GAP BAND PARACHUTE DEPLOYED AT A MACH NUMBER OF 1.91 AND A DYNAMIC PRESSURE OF 11.6 POUNDS PER SQUARE FOOT

John S. Preisser and Clinton V. Eckstrom Washington May 1968 38 p refs Film supplement number L-1000 to this report is available on loan from NASA. Langley Res. Center

(NASA-TM-X-1575) CFSTI: HC \$3.00/MF \$3.00/MF \$0.65 CSCL 01C

A 40-foot nominal-diameter disk-gap-band parachute was flight tested. The test parachute was elected by a deployment mortar from an instrumented payload at an altitude of 140,000 feet. The payload was at a Mach number of 1.91 and the dynamic pressure was 11.6 pounds per square foot at the time the parachute deployment mortar was fired. The parachute reached suspension line stretch in 0.43 second with a resultant snatch force loading of 1990 pounds. The maximum parachute opening load of 6500 pounds came 0.61 second later at a total elapsed time from mortar firing of 1.04 seconds. The first full inflation occurred at 1.12 seconds and stable inflation was achieved at approximately 1.60 seconds. The parachute had an average axial-force coefficient of 0.53 during the deceleration period. During the steady-state descent portion of the flight test, the average effective drag coefficient was also 0.53 and pitch-yaw oscillations of the canopy averaged less than 10° in the altitude region above 100,000 feet. Examination of the recovered parachute revealed that it was not damaged during the flight test. Author

N68-24476*# National Aeronautics and Space Administration. Langley Research Center, Langley Station, Va.

TRENDS IN REPEATED LOADS ON TRANSPORT AIRPLANES

Thomas L. Coleman Washington May 1968 refs Presented at Symp. on Fatigue Design Procedures, Munich, 16–18 Jun. 1965 (NASA-TN-D-4586) CFSTI: HC\$3.00 /MF\$0.65 CSCL 01C

Statistical loads data collected on piston- and turbine-powered transport airplanes during routine feeder-line, short-haul, and long-haul airline service from 1947 to 1965 are summarized. The data presented pertain to the repeated loads resulting from atmospheric turbulence, maneuvers, airplane oscillatory motions, landing contact, and ground operations. The data for several categories of airplanes are compared to show the trends in the loads with the evolution of the transports. The data are presented in terms of the normal accelerations measured near the center of gravity of the airplanes. It is shown that the distributions of repeated loads for various types of transports exhibit much less variation when expressed in terms of number of occurrences per flight rather than in terms of occurrence per flight mile.

N68-24498*# National Aeronautics and Space Administration. Flight Research Center, Edwards, Calif.

PRELIMINARY FLIGHT EVALUATION OF THE STABILITY AND CONTROL DERIVATIVES AND DYNAMIC CHARACTERISTICS OF THE UNAUGMENTED XB-70-1 AIRPLANE INCLUDING COMPARISONS WITH PREDICTIONS

Chester W. Wolowicz, Larry W. Strutz, Glenn B. Gilyard, and Neil W. Matheny Washington May 1968 77 p refs

(NASA-TN-D-4578) CFSTI: HC\$3.00/MF\$0.65 CSCL 01C

Stability and control characteristics of the XB-70-1 airplane were evaluated from data obtained during the early phases of the flight-test program at Mach numbers extending to 2.56 and altitudes to 64,700 feet (19,700 meters). Flight-determined stability and control derivatives and dynamic characteristics for three wing-tip configurations were found generally to be in fair agreement with predictions based on wind-tunnel tests and theoretical estimates of structural flexibility effects. The results show the short-period and Dutch roll modes of the unaugmented aircraft to be positively damped for the flight conditions evaluated. The airplane exhibited negative (adverse) values of the aileron-yaw parameter $C_{n\delta_n}$ at Mach numbers above about 0.90, although proverse values were predicted. Positive values were obtained at subsonic speeds, but the flight-measured values were less than predicted. The flight-determined effective dihedral was negative for fully deflected wing tips (65°) and higher than predicted. The combination of negative effective dihedral and adverse aileron yaw was conducive to divergent pilot-induced oscillation tendencies. Flight tests showed a marked reduction in directional stability beyond approximately 2° of sideslip. This nonlinearity was found in wind-tunnel studies to be the result of canard interference. Author

N68-24499* # National . Aeronautics and Space Administration. Langley Research Center, Langley Station, Va.

A SUMMARY OF ROTOR-HUB BENDING MOMENTS ENCOUNTERED BY A HIGH PERFORMANCE HINGELESS-ROTOR HELICOPTER DURING NAP-OF-THE-EARTH MANEUVERS

William J. Snyder Washington May 1968 31 p refs (NASA-TN-D-4574) CFSTI: HC\$3.00/MF\$0.65

A brief investigation was recently undertaken to study the flying qualities and structural loads of a hingeless-rotor helicopter, the XH-51N, during nap-of-the-earth maneuvers. This investigation was part of Langley's continuing flight research with hingeless-rotor helicopters. The series of nap-of-the-earth maneuvers was devised primarily to simulate military helicopter operation in a hostile environment where remaining undetected is a necessity. Most of the maneuvers employed are abrupt turns, starts, and stops which require a helicopter with very good maneuverability to perform them effectively. Previous investigations have shown that the cyclic loads of the hingeless rotor can be very high during these abrupt types of maneuvers. Time histories of the rotor-hub bending moments measured during the investigation show that during the abrupt maneuvers a rapid buildup in the cyclic bending moments occurs. This buildup, in most cases, exceeds the assigned endurance limit of the rotor hub to such an extent that the service life of the hub is significantly shortened. These results indicate that any operational hingeless-rotor helicopter utilized for nap-of-the-earth flying must be carefully evaluated with respect to the service life of the rotor system. Author

N68-24662# National Aeronautics and Space Administration. Langley Research Center, Langley Station, Va.

A SUMMARY OF RESULTS ON SONIC-BOOM PRESSURE SIGNATURE VARIATIONS ASSOCIATED WITH ATMOSPHERIC CONDITIONS

I. E. Garrick and D. J. Maglieri Washington May 1968 28 p refs

(NASA-TN-D-4588) CFSTI: HC\$3.00/MF\$0.65 CSCL 01C

This report reviews the most pertinent information obtained in recent years relating to atmospheric effects on the sonic boom and, in particular, includes some results of various flight programs. These atmospheric effects are complex, and a statistical approach appears necessary. The statistics of peak pressures follows approximately a log normal distribution, a result that is indicated by existing theory for pure (sinusoidal) sound. A tabular summary of the flight data gives the standard deviations of pressure peaks relative to nominal calculated values of the mean. Information is included on observed variations of sonic-boom signatures for different types and sizes of airplanes. Measurements indicate that wavelike spatial patterns exist in which peaked and rounded waves may alternate and vary with time. Such variations are shown to be induced by the atmosphere rather than by effects of airplane unsteady motion. The spectral content of some ideal and some measured pressure signatures is exhibited and discussed with reference to peakedness or roundness of the wave. Author

N68-25313# National Aeronautics and Space Administration. Langley Research Center, Langley Station, Va.

INVESTIGATION OF THE EFFECT OF WHEEL BRAKING ON SIDE-FORCE CAPABILITY OF A PNEUMATIC TIRE Thomas A. Byrdsong Washington June 1968 24 p refs (NASA-TN-D-4602) CFSTI: HC\$3.00/MF\$0.65 CSCL 01B

An experimental investigation was made to determine the effects of wheel braking on the side force capability of a pneumatic tire. Data were obtained from tests of a smooth-tread pneumatic tire with an inflation pressure of 30 pounds per square inch at ground speeds of 10, 20, and 30 miles per hour at wheel yaw angles of 4° and 8° on both wet and dry paved surfaces. The results indicate that a considerable amount of side-force capability is available during wheel braking force. For additional wheel braking, the side force decreases rapidly to zero at full skid.

N68-25817*# Colorado Univ., Boulder. OPTIMUM MANEUVEGS OF HYPERVELOCITY VEHICLES A. Busemann, N. X. Vinh, and G. F. Kelley Washington, D. C.

A. Busemann, N. A. Vinn, and G. F. Keney Washington, D. C. NASA Jun. 1968 67 p refs (Grant NGR-06-003-033)

(NASA-CR-1078) CFSTI: HC\$3.00 /MF\$0.65 CSCL 01B

This report presents the analytical solutions of the problem of optimum maneuvering of a glide vehicle flying at hypervelocity regime. The investigation is based on the approximation of Allen and Eggers, namely along the fundamental part of a reentry or ascent trajectory the aerodynamic forces greatly exceed the components of the force of gravity in the directions tangent and normal to the flight path. The problem consists of finding an optimal control law for the lift program such that the final velocity or the final altitude is maximized. As applications, the problem can be viewed as bringing the vehicle to the best condition for interception, or penetration, or making an evasive maneuver. If the range is not constrained, the solutions are obtained in closed forms. If the lift control is bounded, then bounded control is optimal whenever it is reached. The switching sequences for different cases are discussed and it is shown that there are at most two switchings. When the range is also prescribed the problem consists of integrating a second order nonlinear system. Using Poincaré's series expansions technique, an approximate solution is obtained for the case of optimizing the final velocity with a slightly constrained range. Author

N68-26691*# Dynamic Science Corp., Monrovia, Calif. A STUDY OF AIRCRAFT FIRE HAZARDS RELATED TO NATURAL ELECTRICAL PHENOMENA Final Report, Jun. 1966-Jul. 1967

Frank L. Kester, Melvin Gerstein, and J. A. Plumer (GE, Pittsfield, Mass.) Washington NASA Jun. 1968 128 p refs Prepared jointly with GE, High Voltage Lab., Pittsfield, Mass. (Contract NASw-1416)

(NASA-CR-1076; SN-9000) CFSTI: HC \$3.00/MF \$0.65 CSCL 01B

The problems of natural electrical phenomena as a fire hazard to aircraft are evaluated. Assessment of the hazard is made over the range of low level electrical discharges, such as static sparks, to high level discharges, such as lightning strikes to aircraft. In addition, some fundamental work is presented on the problem of flame propagation in aircraft fuel vent systems. This study consists of a laboratory investigation in five parts: (1) a study of the ignition energies and flame propagation rates of kerosene-air and JP-6-air foams, (2) a study of the rate of flame propagation of n-heptane. n-octane, n-nonane, and n-decane in aircraft vent ducts, (3) a study of the damage to aluminum, titanium, and stainless steel aircraft skin materials by lightning strikes, (4) a study of fuel ignition by lightning strikes to aircraft skins, and (5) a study of lightning induced flame propagation in an aircraft vent system. Author

N68-26930*# Consultants in Engineering Science (CONESCO), Watertown, Mass.

PROCEDURES FOR ESTIMATING THE EFFECTS OF DESIGN AND OPERATIONAL CHARACTERISTICS OF JET AIRCRAFT ON GROUND NOISE

Robert Lee, James Farrell, George Henry, and Albert Lowe Washington NASA Jun. 1968 166 p refs

(Contract NAS1-5724)

(NASA-CR-1053) CFSTI: HC\$3.00/MF\$0.65 CSCL01B

Procedures have been developed for estimating the effects of design and operational characteristics of jet aircraft on ground noise; this has been done for various engine-cycle parameters, aircraft-design characteristics, and aircraft-flight characteristics; parametric plots have been prepared to show how these different inter-related factors influence noise; and, when possible, assessments have been made of the accuracies and limitations of the graphs, nomographs, and equations that have been developed. One important general conclusion that can be drawn from all this effort is that it is feasible to develop simplified analytic procedures for relating aircraft design and flight characteristics to ground noise, and that such techniques can be extremely useful for providing design guidance and for showing how various flight paths influence ground noise. The report includes the following: Noise prediction procedures for jets and compressors. An analytical investigation of noise as a function of engine-cycle parameters for jet and fan engines. Several simplified calculational methods for determining PNdb including (a) jet and compressor noise PNdb from overall sound-pressure level, (b) PNdb of the combined jet and compressor noise from individual PNdb values, and (c) variation of PNdb with distance for jet, compressor, and jet combined with compressor noise. An analytical study of ground noise as a function of design and flight characteristics. Author

N68-28153*# National Aeronautics and Space Administration. Langley Research Center, Langley Station, Va.

A STUDY OF THE OPTIMUM VALUES OF SEVERAL PARAMETERS AFFECTING LONGITUDINAL HANDLING QUALITIES OF VTOL AIRCRAFT

James R. Kelly and John F. Garren, Jr. Washington Jul. 1968 11 p refs

(NASA-TN-D-4624) CFSTI: HC\$3.00/MF\$0.65 CSCL01D

Because of the many factors which influence handling qualities, a disparity often exists between the absolute pilot rating results obtained from various investigations. In this paper, longitudinal handling qualities data from three published studies have been analyzed and compared in terms of pilot rating trends associated with changes in each of several important parameters. Optimum values or points of diminishing returns for each of these parameters (pitch-rate damping, angle-of-attack stability, speed stability, and longitudinal control sensitivity) appear to be largely independent of changes in other parameters and operating conditions covered. Author

N68-28277*# National Aeronautics and Space Administration. Langley Research Center, Langley Station, Va.

HOT-GAS INGESTION INVESTIGATION OF LARGE-SCALE

H. Clyde Mc Lemore and Charles C. Smith, Jr. Washington Jun. 1968 258 p refs

(NASA-TN-D-4609) CFSTI: HC\$3.00/MF\$0.65 CSCL 01C

An investigation to study the problem of hot-gas ingestion was conducted in the Langley full-scale tunnel and outdoors on large-scale jet VTOL fighter-type aircraft configurations. The investigation included several rectangular and in-line exhaust-nozzle arrangements, inlet positions, and wing positions for a range of forward and side-wind conditions. The exhaust-gas source was a turbojet engine operating at a nozzle pressure ratio of about 1.8 and a nozzle temperature of 1200°F (649°C). The ingestion of hot-engine exhaust gases into the inlets was found to be very dependent upon the aircraft configuration and upon the wind speed. An in-line arrangement of engine exhaust nozzles resulted in virtually no hot-gas ingestion, whereas a rectangular arrangement of nozzles resulted in an inlet air temperature rise above ambient of 100°F to 200°F for many test conditions. The ingestion of hot exhaust gases was greatest at wind speeds from zero to 20 knots. and there was virtually no hot-gas ingestion than the side inlets, and the low-wing configuration was found to result in lower inlet air temperatures than did the high-wing configuration. Deflecting the jet exhaust 25° rearward with the vectoring nozzles generally eliminated the ingestion of hot exhaust gases. Author

N68-28831*# National Aeronautics and Space Administration. Lewis Research Center, Cleveland, Ohio. AIRPLANE SIZE AND STAGING EFFECTS ON SST CRUISE

SONIC BOOM John B. Whitlow, Jr. Washington Jul. 1968 53 p refs

(NASA-TN-D-4677) CFSTI: HC\$3.00/MF\$0.65 CSCL 01B

An analytical study was made to determine the performance requirements and economic penalities involved in reducing the cruise sonic boom of various sizes of a domestic-range SST. No attempt was made to reduce the climb sonic boom since climb might possibly be scheduled over sparsely populated areas. For airplanes in the 200-passenger category, it was found that cruise at nonoptimum altitudes allows reductions up to 10 per-cent in initial cruise boom at the expense of a 10-percent increase in DOC. By size and weight reductions, cruise boom can be reduced almost 40 percent at the expense of a five-fold increase in DOC. A similar study of a two-stage vehicle with stage separation just prior to cruise revealed that a boom reduction of only about 5 percent is possible with this concept, relative to unstaged airplanes of the same payload capacity.

N68-29372*# National Aeronautics and Space Administration. Langley Research Center, Langley Station, Va.

SIMULATION STUDIES OF THE SUPERSONIC TRANSPORT IN THE PRESENT DAY AIR TRAFFIC CONTROL SYSTEM Richard H. Sawyer, Milton D. McLaughlin, and Norman S. Silsby

Washington Jul. 1968 78 p refs

(NASA-TN-D-4638) CFSTI: HC\$3.00/MF\$0.65 CSCL 17G

The problems for the supersonic transport (SST) encountered in operations in a simulated present day air traffic control (ATC) system have been studied in real time by using an SST aircraft flight simulator and ATC simulation facilities. Airline crews operated the SST flight simulator, and experienced air traffic controllers operated the ATC simulation facilities. Design study configurations of the SST were used in the tests. The test program consisted of departures and arrivals under weather conditions which required operation by FAA instrument flight rules in the New York and San Francisco terminal areas. The investigation showed that on established departure and arrival routes the SST was required in many instances to make substantial changes in heading at low supersonic speeds. For departures, such turns were detrimental to performance: straight-line route segments from 120 to 170 nautical miles long for SST supersonic acceleration were considered to be highly desirable. On the basis of fuel allowances, terminal area maneuvering in the New York area consumed on the average up to 40 percent of the en route contingency fuel in departures and up to 38.6 percent in arrivals. Crew workload associated with ATC communications and navigation was not, in general, enough higher than that for subsonic jet transport operations to elicit adverse comments from the pilots. Author

N68-29406*# National Aeronautics and Space Administration. Langley Research Center, Langley Station, Va. NOISE REDUCTION BY MEANS OF INLET-GUIDE-VANE CHOKING IN AN AXIAL-FLOW COMPRESSOR David Chestnutt Washington Jul. 1968 32 p refs (NASA-TN-D-4682) CFSTI: HC\$3.00/MF\$0.65 CSCL 10A

Studies have been made to evaluate noise-reduction benefits obtainable by alteration of the inlet guide vanes of a specially designed 25-pound/second (11.32-kilogram/second) three-stage transonic axial-flow research air compressor. Particular attention has been given to the use of inlet guide vanes to choke the flow aerodynamically for the purpose of preventing noise radiation out of the inlet. Choking was obtained in the inlet guide vanes either by increasing the thickness of each inlet guide vane or by turning the inlet guide vanes to reduce the air passage area and increase the airflow. When the vane thickness was increased, there were no compressor-efficiency losses. When the vanes were turned, there was an average compressor-efficiency loss of 8 percent. The results indicate that inlet guide vanes with variable thickness hold the most promise for maximum noise reductions without compromising compressor performance. However, for both methods of obtaining choked flow, there were pressure-ratio losses of 7 to 8 percent. The corresponding noise reductions obtained in both choked-flow modes were 25 to 30 decibels in the overall sound pressure level and 36 decibels in the first-rotor-blade passage-frequency sound pressure level. Author

N68-29887*# National Aeronautics and Space Administration. Lewis Research Center, Cleveland, Ohio.

SOUND MEASUREMENTS ON A FULL-SCALE JET-ENGINE INLET-NOISE-SUPPRESSOR COWLING

L. Jack Smith, Loren W. Acker, and Charles E. Feiler Washington Jul. 1968 27 p refs

(NASA-TN-D-4639) CFSTI: HC\$3.00/MF\$0.65 CSCL 21E

Several prototype suppressors were ground tested on a jet engine. Broadband resonant absorbers were used as the acoustic absorption treatment. Inlet geometries included both acoustically treated struts and a circumferential splitter ring. Results of calculations on far field noise data showed a maximum total sound power reduction of 10.2 decibels and simulated flyover noise reductions up to 10.5 perceoved noise decibels. Strut geometries were best for sideline noise reduction, but the splitter configuration, with the most treated surface areas, achieved the greatest sound power reduction. A mathematical model of sound power attenuation correlated with the data. Author

N68-31956*# National Aeronautics and Space Administration. Manned Spacecraft Center, Houston, Tex.

EXPERIMENTAL VERIFICATION OF SCALE FACTORS FOR PARAWING OPENING CHARACTERISTICS David L. Eichblatt, Robert H. Moore, and Richard L. Barton Washington Aug. 1968 30 p refs

(NASA-TN-D-4665) CFSTI: HC\$3.00/MF\$0.65 CSCL 01C The verification of an analytical scaling technique by experimental drop tests under controlled conditions is presented in which the opening characteristics of a full-scale flexible parawing are predicted from the results of model testing. The scaling method is derived from a comparison of similar forces (in the equation of motion) on a scale model with a keel length of 4 feet and a full scale of 8 feet. Initial velocities of 17 to 40 feet per second were used in the test program. Test results within the scope of the program indicate that the models can be used to predict full-scale deployment characteristics.

N68-33669*# National Aeronautics and Space Administration. Langley Research Center, Langley Station, Va.

EFFECT OF SPEED BRAKES ON THE SUPERSONIC AERODYNAMIC CHARACTERISTICS OF A VARIABLE SWEEP TACTICAL FIGHTER MODEL AT MACH NUMBERS FROM 1.60 TO 2.50

Celia S. Richardson Washington Sep. 1968 35 p refs (NASA-TN-D-4773) CFSTI: HC\$3.00/MF\$0.65 CSCL01B

An investigation has been made in a wind tunnel to determine the effect of various speed-brake configurations on the aerodynamic characteristics of a current multimission tactical fighter model. The speed-brake configurations, which included upgapped and gapped brakes with variations in area, location, planform, and deflection angle, were tested at Mach numbers from 1.60 to 2.50 for a wing-leading-edge sweep angle of 72.5°. Tests were made through an angle-of-attack range from about -4° to 28° and at angles of sideslip from about -6° to 11° . The test Reynolds number was 3.0×10⁶ per meter). The results indicated the drag values of a gapped and an ungapped brake configuration were about the same; even though the gapped speed brakes were somewhat smaller than the ungapped brakes. The ungapped speed brakes generally increased the directional stability of the model. The gapped speed brakes generally reduced the directional stability of the model particularly at the higher test Mach numbers. Author

N68-33879*# National Aeronautics and Space Administration. Langley Research Center, Langley Station, Va.

FREE-FLIGHT AND WIND-TUNNEL STUDIES OF DEPLOYMENT OF A DYNAMICALLY AND ELASTICALLY SCALED INFLATABLE PARAWING MODEL

Alice T. Ferris and H. Neale Kelly Washington Sep. 1968 44 p refs

(NASA-TN-D-4724) CFSTI: HC\$3.00/MF\$0.65 CSCL 01A

The deployment characteristics of a 1/8-size dynamically and elastically scaled model of an inflatable parawing suitable for the recovery of an Apollo-type spacecraft were investigated in free flight and in the Langley transonic dynamics tunnel using a model which was mounted to permit limited angular freedom. The deployments were of a passive type; that is, there was no powered reel-in or reel-out of the suspension lines. However, a braking system was used to attenuate the dynamic loads in the suspension lines. The deployment technique was developed in an initial series of wind-tunnel tests. By utilizing the equipment and technique evolved from the wind-tunnel studies, successful free-flight deployments were accomplished and the transient loads associated with the deployments were measured. These results were compared with the results of subsequent wind-tunnel tests. The general behavior of the parawing during deployment in the wind tunnel and during free flight was similar and loads measured in the wind tunnel can be used to give a preliminary indication of those that will be encountered in free-flight deployments. Thus, it was concluded that the wind tunnel can serve as a useful tool in the development of a deployment technique for an inflatable parawing. Author

N68-34907*# National Aeronautics and Space Administration, Washington, D. C.

SECOND CONFERENCE ON SONIC BOOM RESEARCH Ira R. Schwartz ed. 1968 218 p refs Conf. held at Washington, D.C., 9–10 May 1968; Sponsored by NASA

(NASA-SP-180) CFSTI: HC\$3.00/MF\$0.65 CSCL01A

CONTENTS:

1. ATMOSPHERIC EFFECTS ON THE SONIC BOOM I. E. Garrick (NASA. Langley Res. Center) p 3–17 refs (See N68-34908 22-02)

2. SONIC BOOM GROUND PRESSURE MEASUREMENTS FOR FLIGHTS AT ALTITUDES IN EXCESS OF 70,000 FEET AND AT MACH NUMBERS UP TO 3.0 D. J. Maglieri (NASA. Langley Res. Center) p 19–27 refs (See N68-34909 22-02)

3. LABORATORY SONIC BOOM RESEARCH AND PREDICTION TECHNIQUES H. W. Carlson (NASA. Langley Res. Center) p 29–36 ref (See N68-34910 22-02)

4. CONFIGURATION DESIGN FOR SPECIFIED PRESSURE SIGNATURE CHARACTERISTICS F. E. McLean (NASA. Langley Res. Center) p 37-45 refs (See N68-34911 22-02)

5. EVALUATION OF CERTAIN MINIMUM BOOM CONCEPTS H. L. Runyan and H. R. Henderson (NASA. Langley Res. Center) p 47–55 refs (See N68-34912 22-02)

6. CURRENT RESEARCH IN SONIC BOOM L. W. Hunton (NASA. Ames Res. Center) p 57-66 refs (See N68-34913 22-02)

7. PRELIMINARY INVESTIGATION OF FLOW FIELD ANALYSIS ON DIGITAL COMPUTERS WITH GRAPHIC DISPLAY H. Lomax (NASA. Ames Res. Center) p 67-71 (See N68-34914 22-02)

8. REPORT ON SONIC BOOM STUDIES: PART 1: ANALYSIS OF CONFIGURATIONS A. Ferri and A. Ismail (New York Univ.) p 73–88 refs (See N68-34915 22-02)

9. REPORT ON SONIC BOOM STUDIES: PART 2: INCIDENCE OF N-WAVES ON STRUCTURES L. Ting and Y. S. Pan (New York Univ.) p 89–98 refs (See N68-34916 22-01)

10. REDUCTION OF SONIC BOOM ATTRIBUTED TO LIFT E. L. Resler, Jr. (Cornell Univ.) p 99–106 refs (See N68-34917 22-02)

11. THE APPROACH TO FAR-FIELD SONIC BOOM F. K. Moore and L. F. Henderson (Cornell Univ.) p 107–115 refs (See N68-34918 22-02)

12. NONLINEAF EFFECTS ON SONIC BOOM INTENSITY M. T. Landahl, I. L. Ryhming, and L. Hilding (Aeron. Res. Inst. of Sweden) p 117-124 refs (See N68-34919 22-02)

13. THE FEASIBILITY OF LARGE SONIC BOOM REDUCTIONS A. Busemann (Colo. Univ.) p 125–128 ref (See N68-34920 22-02)

14. REVIEW OF SECOND-ORDER WAVE STRUCTURE D. A. Caughey and W. D. Hayes (Princeton Univ.) p 129–132 refs (See N68-34921 22-12)

15. MULTIPOLES, WAVEFORMS, AND ATMOSPHERIC EFFECTS A. R. George and A. R. Seebass (Cornell Univ.) p 133-144 refs (See N68-34922 22-02)

16. UNIFORM RAY THEORY APPLIED TO SONIC BOOM PROBLEMS M. B. Friedman and M. K. Myers (Co. Univ.) p 145–149 (See N68-34923 22-02)

17. THE ARAP SONIC BOOM COMPUTER PROGRAM W. D. Hayer (Princeton Univ.) and R. C. Haefeli (Aeron. Res. Asso. of Princeton) p 151–158 refs (See N68-34924 22-02)

18. GEOMETRIC ACOUSTICS AND WAVE THEORY W. D. Hayes (Princeton Univ.) P 159-164 refs (See N68-34925 22-12)

19. SIMILARITY RULES FOR NONLINEAR ACOUSTIC PROPAGATION THROUGH A CAUSTIC W. D. Hayes (Princeton Univ.) p 165–171 refs (See N68-34926 22-12)

N68-35177*# Boeing Co., Morton, Pa. Vertol Div.

SUPPLEMENT TO FEASIBILITY OF V/STOL CONCEPTS FOR SHORT-HAUL TRANSPORT AIRCRAFT Bernard L. Fry Washington NASA Sep. 1968 63 p refs (Contract NAS2-3142)

(NASA-CR-743(1); D8-0375, V. 3) CFSTI: HC \$3.00/MF \$0.65 CSCL 01C

Examination of the aircraft designed to the ground rules of the original study showed the considerable influence on aircraft size, and therefore cost, of such parameters as flight profile and fixed equipment assumptions. A revised set of ground rules was developed with respect to range, payload, reserves, flight profile, etc., and tilt wing and lift fan aircraft were designed to these ground rules. More economical aircraft than those designed to the original rules have resulted. One of the tradeoffs made in the original study investigated the effect of advanced propulsion technology. This report investigates the effect of advanced airframe and propulsion technology and shows that weight savings of more than 20 percent may be possible relative to 1970 aircraft designed to identical ground rules.

N68-35595*# Litchford Systems, Northport, N. Y. ANALYSIS OF CUMULATIVE ERRORS ASSOCIATED WITH CATEGORY 2 AND 3 OPERATIONS WITH REQUIREMENTS FOR ADDITIONAL RESEARCH

G. B. Litchford Washington NASA Sep. 1968 29 p refs (Contract NASw-1441)

(NASA-CR-1188) CFSTI: HC\$3.00/MF\$0.65 CSCL01B

The results are presented of a study and investigation of conventional and unconventional terminal flight paths for CTOL aircraft in connection with low visibility landing problems. The interrelationships of the geometry of possible approach paths, visual and electronic guidance equipments, and numerous aircraft piloting problems are reviewed. Pilot display requirements for optimizing these interrelationships under typical airline operating conditions are described as well as the flight path dispersions expected at the transition from instrument to visual flight guidance. Areas requiring improved simulation, flight validation, or other means of establishing statistically significant data for these critical operations are identified. The ILS standards will be examined to identify errors that affect the transition from instrument to visual flight. Author

N68-36073*# National Aeronautics and Space Administration. Flight Research Center, Edwards, Calif.

LANDING LOADS AND ACCELERATIONS OF THE XB-70-1 AIRPLANE

Ronald J. Wilson and James M. McKay Washington Oct. 1968 29 p refs

(NASA-TN-D-4836) CFSTI: HC\$3.00/MF\$0.65 CSCL01C

Data are presented on landing contact conditions for the first 48 landings of the XB-70-1 airplane. Landing weights varied from 419,800 pounds to 274,600 pounds. Vertical velocities at touchdown ranged from 5.26 feet/second to 1.49 feet/second. Maximum indicated airspeed was 195.0 knots, with a minimum of 167.3 knots. Landing contact conditions of the XB-70-1 are compared with those of a modern turbolet transport. The mean vertical velocity at touchdown for the XB-70-1 was 3.21 feet/second, which was 1.59 feet/second higher than that reported for the turbojet transport. A mean indicated airspeed of 180.5 knots was 47.7 knots greater than that reported for the transport. The maximum XB-70-1 roll angle (3.0) and rolling velocity (3.28 deg/sec) at touchdown were less than the values (4.3° and 8.7 deg/sec. respectively) for the transport. The measured main dear maximum vertical reaction generally compared favorably with predicted values. The nose gear initial maximum vertical reactions were generally less than the predicted values. The mean acceleration measured at the pilot's station was 1.39g due to main gear impact and 1.54g due to nose gear impact. Author

N68-36074*# National Aeronautics and Space Administration. Lewis Research Center, Cleveland, Ohio.

COMPARATIVE STUDY OF FUSELAGE TANKS FOR LIQUID METHANE FUELED SUPERSONIC AIRCRAFT

Rene E. Chambellan and William A. Bevevino Washington Oct. 1968 18 p refs

(NASA-TN-D-4837) CFSTI: HC\$3.00/MF\$0.65 CSCL01C Three designs of flight-weight nonintegral tanks, capable

of gage pressures of 15 or 30 psi (10.8 or 20.7 N/cm²), were studied. Two void spaces representative of a forward and an aft fuselage segment were selected. Ratios of tank weight to contained fuel weight range from 0.0110 to 0.0482 and volumetric efficiencies range from 75 to 95.4 percent. Tanks studied are thin walled pressure vessels of titanium or nonmetallic fabric constrained to an envelope by structural elements internal to the tank. Author

N68-37066*# National Aeronautics and Space Administration. Langley Research Center, Langley Station, Va.

EFFECTS OF VARIATIONS IN NOSE AND WINDSHIELD GEOMETRY ON SUPERSONIC AERODYNAMIC CHARACTERISTICS OF A VARIABLE-SWEEP TACTICAL FIGHTER MODEL

Celia S. Richardson Washington Oct. 1968 55 p refs (NASA-TM-X-1664) CFSTI: HC\$3.00/MF\$0.65 CSCL 01C

An investigation was made in the low Mach number test section of the Langley Unitary Plan wind tunnel to determine the effects of various nose and windshield shapes on the aerodynamic characteristics of a current multimission tactical fighter model. Tests were performed for a wing leading edge sweep of 72.5° at Mach numbers of 1.6, 2.16, and 2.50, at angles of attack from about -2° to 20°, and at angles of sideslip of about 0° and 4°. The Reynolds number per foot was $3.0 \times 10^{\circ}$. The data indicate that each of the forebody modifications, which resulted in forebodies somewhat longer than the basic forebody, generally caused a slight increase in minimum drag and a reduction in directional stability. Author

N68-37075*# National Aeronautics and Space Administration. Langley Research Center, Langley Station, Va.

EFFECTS OF REDUCED AIRSPEED FOR LANDING APPROACH ON FLYING QUALITIES OF A LARGE JET TRANSPORT EQUIPPED WITH POWERED LIFT

Harold L. Crane, Robert W. Sommer, and Frederick M. Healy Washington Oct. 1968 91 p refs

(NASA-TN-D-4804) CFSTI: HC\$3.00/MF\$0.65 CSCL 01B

A flight research program was conducted to determine the effects of reduced landing approach speeds on the flying qualities of a typical large jet transport for simulated instrument approaches. The reduced approach speeds were made possible by a powered lift system which blew air over the upper surface of the wing flaps. The effects of reduced approach speeds on flying qualities and flying-qualities requirements are discussed. It was found that a 25 percent reduction in landing approach speed would not necessarily result in new requirements for satisfactory flying qualities. However, such items as pitch response and trim characteristics, Dutch roll damping, and lateral directional coupling are likely to be more difficult to maintain at satisfactory levels. Author

N68-37932*# Southampton Univ. (England). HELICOPTER NOISE-A BLADE SLAP. PART 1: REVIEW AND THEORETICAL STUDY

John W. Leverton Washington NASA Oct. 1968 58 p refs (Grant NGR-52-025-002)

(NASA-CR-1221) CFSTI: HC\$3.00/MF\$0.65 CSCL01C

This report reviews previous work on the topic of blade

slap and the various mechanisms for its generation. It is concluded that blade/tip vortex interaction is the most likely noise producing mechanism. A theoretical approach to the problem leading to the development of a Blade Slap Factor (BSF), which will give an indication of the severity of blade slap likely on any helicopter. is also included. A comparison between some subjective assessments of the blade slap noise and the BSF is also given. Author

N68-37941*# National Aeronautics and Space Administration. Lewis Research Center, Cleveland, Ohio.

WIND TUNNEL INVESTIGATION OF AIRFRAME INSTALLATION EFFECTS ON UNDERWING ENGINE NACELLES AT MACH NUMBERS FROM 0.56 TO 1.46

Bernard J. Blaha and Daniel C. Mikkelson Washington Nov. 1968 83 p refs

(NASA-TM-X-1683) CFSTI: HC\$3.00/MF\$0.65 CSCL01C

A 1/20 scale model of the F-106B with simulated underwing engine nacelles was tested in the 8- by 6-foot supersonic wind tunnel. Pressures and boattail drag coefficients were obtained on cone-cylinder and bulged nacelles with 15° conical boattail afterbodies and jet boundary simulators. Data were obtained with and without inlet airflow through the nacelles at attack angles from 0° to 8°. Effects of nacelle strut geometry, local elevon geometry, and elevon deflection were also investigated. The installed boattail pressure drag coefficient was lower than isolated nacelle values at all Mach numbers, and transonic drag rise was delayed to Mach 0.975. Author

Includes fuel cells, energy conversion cells, and solar cells; auxiliary gas turbines; hydraulic, pneumatic and electrical systems; actuators; and inverters. For related information see also: 09 Electronic Equipment; 22 Nuclear Engineering; and 28 Propulsion Systems.

N68-10103*# National Aeronautics and Space Administration. Lewis Research Center, Cleveland, Ohio.

AUTOMATED DATA COLLECTION SYSTEM APPLIED TO HALL EFFECT AND RESISTIVITY MEASUREMENTS Ralph D. Thomas Washington NASA Nov. 1967 26 p refs

(NASA-TM-X-1464) CFSTI: HC\$3.00/MF\$0.65 CSCL 14B

A description of the instrumentation and theory of operation of a fully programmable automated Hall effect and resistivity apparatus is presented. The apparatus has the capability of controlling all operational conditions over a wide range of temperatures and logging data in the form of both typewritten copy and computer-compatible punched paper tape. Application of the system for measuring both thin film and bulk samples of cadmium sulfide and bulk samples of n-type and p-type silicon in the temperature region between 4.2° and 400°K is discussed. Also discussed are a simple yet highly reliable technique for obtaining ohmic contacts to the samples, the systematic procedure followed for each measurement run, the data program and computer recording format, and samples of the computer results. Extension of the system to include measurement of materials of high resistivity was achieved by operating a high-input-impedance electrometer between the sample leads and the input scanner. A sample holder was designed to accept either thin-film samples on substrates up to 1-inch (2.54 cm) square or bridge-shaped bulk samples. A complete Dewar system was assembled for controlling the temperature and sample environment at temperatures between 4.2° and 400°K. The system accuracy and specifically the accuracy of the reduced Hall effect and resistivity measurements are discussed. Calibration procedures for the thermocouples and gaussmeter are outlined. Author

N68-11920*# National Aeronautics and Space Administration. Lewis Research Center, Cleveland, Ohio.

EXPERIMENTAL PERFORMANCE EVALUATION OF A 6.02-INCH (15.29-CM) RADIAL-INFLOW TURBINE WITH AN EXIT DIFFUSER

Samuel M. Futral, Jr. and Donald E. Holeski Washington Dec. 1967 17 p refs

(NASA-TM-X-1480) CFSTI: HC\$3.00/MF\$0.65 CSCL 10A

The evaluation used argon as the working fluid and covered a range of speeds and pressure ratios. Turbine inlet conditions were fixed at values corresponding to design Reynolds number for design equivalent speed and design pressure ratio operation. Results of the investigation indicated that, at design equivalent speed and pressure ratio, the turbine static efficiencies before and after diffusion were 0.825 and 0.865, respectively. The results also indicated a decrease in total efficiency of approximately 2 percent across the diffuser with the leaving loss accounting for less than 1 percentage point in the efficiency. The ratio of diffuser static pressure recovery to the diffuser inlet impact pressure was approximately 0.6. This recovery is about 71 percent of the isentropic incompressible value for the same area ratio. Author **N68-14630*** National Aeronautics and Space Administration. Lewis Research Center, Cleveland, Ohio.

PARAMETRIC ANALYSIS OF RADIOISOTOPE-THERMO-ELECTRIC GENERATORS

James J. Ward, William J. Bifano, and Larry S. Blair Washington Oct. 1967 22 $\,p\,$ ref

(NASA-TM-X-1453) CFSTI: \$3.00 CSCL 10B

A parametric analysis of a radioisotope-thermoelectric power generator is presented. A cylindrical heat-source geometry was assumed with either lead telluride or silicon-germanium thermoelectric elements located around the lateral surface of the fuel block. The heat source was treated parametrically by using the effective-volume power density of the heat source as a variable. Generator efficiency and specific weight were determined for fuel-block length-to-diameter ratios from 0.5 to 10.0, effective-volume power densities from 0.5 to 10.0 watts per cubic centimeter (W/cc), thermoelectric element hot-junction temperatures of 811°K for lead telluride and 1089° and 1255°K for silicon-germanium, and generator electrical output powers from 100 to 1000 watts. The results indicate that a substantial specific weight advantage is gained by employing silicon-germanium thermoelectric elements rather than lead telluride. In all cases, however, minimum specific weight is achieved at the lowest output power level, that is, 100 watts electric (We). For silicon-germanium generators having an output power of 100 We, the minimum specific weights are 120 and 88 lb/kWe (54.5 and 40 kg/kWe) for hot-junction temperatures of 1089° and 1255°K, respectively, with corresponding generator efficiencies of 4.1 and 5.8 percent. Author

N68-14639*# National Aeronautics and Space Administration. Lewis Research Center, Cleveland, Ohio.

PERFORMANCE EVALUATION OF A TWO STAGE AXIAL-FLOW TURBINE FOR TWO VALUES OF TIP CLEARANCE

Milton G. Kofskey and William J. Nusbaum Washington Jan. 1968 20 p refs

(NASA-TN-D-4388) CFSTI: HC\$3.00/MF\$0.65 CSCL 10A

An experimental investigation was made of a two-stage turbine designed to drive an alternator for a 10-kilowatt-shaft-output space power system. Performance results were obtained for the turbine operating with the rotor top clearance of 0.031 inch (0.079 cm) recommended for preliminary hot operation of the turbine. These results are compared with the results obtained with the design tip clearance of 0.013 inch (0.033 cm). Tests were made with cold argon as the working fluid over a speed range from 0 to 120 percent of design equivalent speed and at pressure ratios ranging from 1.08 to 1.55. The results of the investigation indicated that the static and total efficiencies were 0.785 and 0.792, respectively, for a tip clearance of 0.031 inch (0.079 cm). These values represent a 4-percentage-point decrease in turbine deficiency when the tip clearance is increased. The results based on

two tip clearances indicated that the subject turbine, which was designed with high rotor reaction, was very sensitive to changes in tip clearance. There was a 3.7-percent decrease in turbine specific work for an increase in tip clearance of 1.0 percent of passage height. This decrease is substantially greater than the 1.75-percent decrease in turbine work obtained for a reference turbine of impulse design. Author

N68-15943*# National Aeronautics and Space Administration. Lewis Research Center, Cleveland, Ohio.

ANALYTICAL DETERMINATION OF RADIAL INFLOW TURBINE DESIGN GEOMETRY FOR MAXIMUM EFFICIENCY Harold E. Rohlik Washington Feb. 1968 32 p refs (NASA-TN-D-4384) CFSTI: HC\$3.00/MF\$0.65 CSCL 10A

Radial turbine performance was examined analytically in order to determine optimum design geometry for various applications as characterized by specific speed. Five specific losses were calculated for various combinations of stator-exit flow angle, outlet- to inlet-diameter ratio, and the ratio of stator blade height to rotor-exit diameter. The losses considered were stator loss, rotor loss, tip-clearance loss, windage, and exit kinetic energy. Resulting static efficiencies ranged from 0.23 to 0.87 for a specific-speed range of 15 to 173 (0.12 to 1.34). Turbine pressure ratio had no appreciable effect on optimum geometry except in the case of stator blade height. Curves of blade-jet speed ratio, stator-exit flow angle, tip-diameter ratio, and the ratio of stator blade height to rotor-inlet diameter are presented for maximum static efficiency over a wide range of specific speed. These curves permit the systematic selection of optimum turbine size and shape for a variety of turbine applications. An exit diffuser of 0.6 effectiveness was examined for its effect on overall performance. The gain in static efficiency was appreciable except at very high specific speeds where a lower diffuser effectiveness or a different type of turbine would be required. Author

N68-16228*# National Aeronautics and Space Administration. Lewis Research Center, Cleveland, Ohio.

PERFORMANCE IN AIR OF 4-INCH-(10.16-CM-) MEAN-DIAMETER SINGLE STAGE AXIAL-FLOW TURBINE FOR REYNOLDS NUMBERS FROM 4,900 TO 188,000

Hugh A Klassen and Robert Y Wong Washington Feb. 1968 25 p refs

(NASA-TN-D-4383) CFSTI: HC\$3.00/MF\$0.65 CSCL 10A

A 4-inch mean-diameter turbine was investigated in air over a range of absolute inlet total pressures from 1.0 to 35.0 psia which corresponds to a Reynolds number range of 4900 to 188 000. Results were compared with those obtained for a reference 4-inch mean-diameter turbine with higher peak suction surface velocities on the stator and rotor and with higher rotor surface diffusion. Peak efficiency for the subject turbine increased from 0.40 at the lowest Reynolds number to 0.63 at the highest. The turbine had higher peak efficiencies than the reference turbine over the entire Reynolds number range. Stator- and rotor-outlet flow separation reported for the reference turbine was absent in the subject turbine except for the lowest Reynolds number of 4900. where the rotor-relative-outlet flow angle was 14° greater than design. Rotor losses were smaller than those used in the turbine design. The stator over-expansion caused by these low losses resulted in negative rotor reaction. Stator, rotor, and exit losses were computed for a blade-jet speed ratio of 0.32 and an overall staticto static-pressure ratio of 2.5. Author

N68-16321*# Douglas Aircraft Co., Inc., Newport Beach, Calif. Astropower Lab.

INORGANIC SEPARATOR FOR A HIGH TEMPERATURE SILVER-ZINC BATTERY

F. C. Arrance, R. Greve, and A. Rosa Washington NASA Feb. 1968 177 $p\ refs$

(Contract NAS3-7639)

(NASA-CR-965; SM-48461-F) CFSTI: HC \$3.00/MF \$0.65 CSCL 10C

The design, development and testing of a multiplate five amperehour cell are described. The fabrication of the various cell components in accordance with the cell design is discussed, and the testing and evaluation of each is described with emphasis on electrode configuration and performance. Graphs are given to illustrate results of cycling tests performed on the various cells at 30 ma/cm² at 25° and 100°C. Among the results from the evaluation and performance of the zinc cells constructed with inorganic separators are: (1) The 5-Ah silver-zinc cells of this type are capable of long cycle life at both 25° and 100°C. (2) The cells can be operated using KOH concentrations ranging from 30% to 45% without substantially effecting operating characteristics or cell life. (3) The inorganic separator proved its effectiveness in preventing electrode species migration, its inertness to reaction with the silver electrode, and its applicability to practical high energy density cell designs. B.S.D.

N68-16439*# General Electric Co., Cincinnati, Ohio. Space Power and Propulsion Section.

TWO-STAGE POTASSIUM TEST TURBINE. VOLUME 2: FLUID DYNAMIC DESIGN AND PERFORMANCE

R. J. Rossbach and G. C. Wesling Washington NASA Feb. 1968 240 p refs

(Contract NAS5-1143)

(NASA-CR-922) CFSTI: HC\$3.00/MF\$0.65 CSCL 10A

The design, fabrication and test of a two-stage turbine suitable for operation in wet potassium vapor at temperatures of 1400 to 1600°F are reported. The test turbine consisted of stages three and four of a five-stage 500 KW turbine and had a design flow capacity of 2.8 pounds per second at 1600°F turbine inlet temperature. One principal objective of the program was to establish accurate fluid flow design methods for potassium turbines operating in the wet vapor region. The fluid flow design methods were verified when performance data measured during tests with potassium vapor agreed within five percent with values calculated prior to the tests.

N68-16469*# National Aeronautics and Space Administration. Lewis Research Center, Cleveland, Ohio.

AERODYNAMIC EVALUATION OF TWO-STAGE AXIAL FLOW TURBINE DESIGNED FOR BRAYTON-CYCLE SPACE POWER SYSTEM

Milton G. Kofskey and William J. Nusbaum Washington Feb. 1968 30 p refs

(NASA-TN-D-4382) CFSTI: HC\$3.00/MF\$0.65 CSCL 10B

An experimental investigation was conducted of a two-stage turbine designed to drive an alternator for a 10-kilowatt-shaft-ouput space power system. First-stage and two-stage performance results are described for operation at approximately design Reynolds number at equivalent design speed and pressure ratio with argon as the working fluid. Tests were made at speeds ranging from 1 to 120 percent of equivalent design speed and at pressure ratios from 1.02 to 1.65. The results of the investigation indicated that, for two-stage operation, the static and total efficiencies, based on turbine-inlet and rotor-exit conditions, were 0.825 and 0.845, respectively, which compare favorably with design. The equivalent mass flow, however, was 4 percent lower than design and was attributed to the flow areas in the blade rows being smaller than design. At this point the first- and second-stage total efficiencies were 0.864 and 0.805 or approximately 2 points higher and 4 points lower than design, respectively. Two-stage performance based on turbine-inlet and collector-exit tions indicated static and total efficiencies of 0.826 and 0.835, respectively. These results, which indicate a drop in total efficiency within the collector of approximately 1 point with no change in static efficiency, compare closely with design. Author

N68-16631*# National Aeronautics and Space Administration. Lewis Research Center, Cleveland, Ohio.

PARAMETRIC MASS ANALYSIS AND COMPARISON OF TWO TYPES OF REACTANT COOLING-AND-STORAGE UNITS FOR A LUNAR-BASED HYDROGEN-OXYGEN REGENERATIVE FUEL-CELL SYSTEM

Norman H. Hagedorn Washington Feb. 1968 34 p refs

(NASA-TN-D-4386) CFSTI: HC\$3.00/MF\$0.65 CSCL 13A

This study was to determine the effect of prestorage reactant cooling on the mass of a lunar-based hydrogen-oxygen regenerative fuel cell system. Consideration was given to cooling by radiators and by refrigerator-radiator combinations. Parametric mass analyses were performed for components of each cooling-and-storage unit and for the residual reactant in each tank. The combined radiative-plus-refrigerative unit has a minimum mass when the reactant is cooled to subcritical temperatures. The mass of the purely radiative unit minimizes when the reactant is cooled to within 0.5°K of the radiator sink temperature. All cooling which occurs above these optimum temperatures decreases, but does not minimize, the mass of these units. Decreasing the final storage pressure leads to considerable mass increases when the reactants are stored at supercritical temperatures. There exists an optimum allowable heat leak into the storage tanks which minimizes the total mass of the unit. For the combined unit there exists an optimum heat-rejection temperature which minimizes the sum of the masses of the solar cells and the radiator required by the Author refrigerator.

N68-17075*# General Electric Co., Cincinnati, Ohio.

TWO-STAGE POTASSIUM TEST TURBINE. VOLUME 2: MECHANICAL DESIGN AND DEVELOPMENT

H. E. Nichols and R. W. Fink Washington NASA Feb. 1968 227 p refs

(Contract NAS5-1143)

(NASA-CR-923) CFSTI: HC\$3.00/MF\$0.65 CSCL 10A

This report is one of a series describing the design and development of a two-stage, Rankine cycle turbine for operation with potassium vapor. This volume presents the turbine mechanical design and describes a three-phase development test program comprising stem and air testing, potassium vapor performance testing, and a 2000-hour endurance test with turbine inlet potassium vapor at 1500°F. As part of the endurance testing, four each of TZM and TZC molybdenum blades were inserted in the second stage to observe any effects of corrosion and/or erosion. The average weight changes of the rotor blades during the endurance test were: Stage 1 (U-700), -0.304%; Stage 2 (U-700), -0.019%; Stage 2 (TYM), -0.105%; and Stage 2 (TYC), -0.102%. The testing demonstrated minimal deterioration of the turbine parts in 2100 hours of vapor operation and the feasibility of long-time operation of a potassium turbine of the design described herein. Author

N68-17110*# National Aeronautics and Space Administration. Lewis Research Center, Cleveland, Ohio.

REDUCTION OF APPARENT-POWER REQUIREMENT OF PHASE-CONTROLLED PARASITICALLY LOADED TURBO-ALTERNATOR BY MULTIPLE PARASITIC LOADS Leonard J. Gilbert Washington Feb. 1968 35 p refs

(NASA-TN-D-4302) CFSTI: HC\$3.00/MF\$0.65 CSCL 10B

Alternator output is improved when a phase-controlled parasitically loaded turbo-alternator has multiple sequentially actuated parasitic loads. Phase-controlled currents produce some unwanted effects. Included among these effects is an increase in the apparent-power (volt-ampere) requirement of the alternator. Phase control also produces strong harmonic components in the alternator current. The effects derive from the nonsinusoidal and reactive character of the parasitic load. The results of the analysis give the alternator apparent power and the toal harmonic content of the alternator current as a function of parasitic load. One means of reducing the unwanted effects is to subdivide the parasitic load. The analysis shows this reduction as a function of the number of divisions of the parasitic load. For the model of the circuit analysis, an undivided parasitic load produces a total harmonic content of 32 percent in the alternator current when used with a basic 0.8 lagging power factor load. But when the parasitic load is divided into two loads, the total harmonic content is reduced to 18 percent. With the same basic 0.8 lagging power factor load, the apparent power with an undivided parasitic load is 7.6 percent greater than the apparent power without a parasitic load. However, when the parasitic load is divided, this difference is only 3 percent. Additional division of the original parasitic load reduces the undesirable effects further. The amount of improvement at each division decreases appreciably with increasing number of loads.

N68-18044*# General Electric Co., Cincinnati, Ohio. TWO-STAGE POTASSIUM TEST TURBINE. VOLUME 3: TEST FACILITIES

S. E. Eckard Washington NASA Feb. 1968 199 p refs (Contract NAS5-1143)

(NASA-CR-924, V. 3) CFSTI+HC\$3.00/MF\$0.65 CSCL 10A

A detailed description of the two phase potassium test facility is presented. Pertinent information on operating procedures and problems is disclosed. The potassium containment piping and component hardware in the test facility were fabricated of Type 316 stainless steel. The facility was designed to produce potassium vapor up to 1600°F at 3.5 lb/sec flowrate. Maximum obtainable vapor temperature was 1587°F. The test facility was designed for Rankine cycle testing of a two-stage potassium vapor turbine. More than 2000 hours of turbine testing were completed at 1500°F turbine inlet temperature. Also thermodynamic properties of potassium vapor through a large convergent-divergent nozzle prior to turbine testing. Author

N68-18501*# National Aeronautics and Space Administration. Lewis Research Center, Cleveland, Ohio.

EXPERIMENTAL PERFORMANCE EVALUATION OF AN 8.5 INCH (21.59 CM) MEAN-DIAMETER AXIAL FLOW TURBINE AT REYNOLDS NUMBERS FROM 18,000 TO 177,000

William J. Nusbaum and Milton G. Kofskey Washington Mar. 1968 21 p refs

(NASA-TN-D-4432) CFSTI: HC\$3.00/MF\$0.65 CSCL 10A

An experimental investigation of an 8.5-inch- (21.59-cm-) mean-diameter, two-stage, axial-flow turbine was conducted to determine the effect of a change in Reynolds number on the performance of a turbine of this type and size. The investigation was conducted with cold argon over a range of inlet pressures from about 1.0 to 9.0 psia (0.68 to 6.2 N/cm² abs) with corresponding Reynolds numbers from 18,000 to 177,000. At each value of turbine-inlet pressure, data were taken at design equivalent speed and various pressure ratios. Results of the investigation indicated that at design equivalent speed and pressure ratio an increase in Reynolds number resulted in a 5.8 percent increase in mass flow over the range of Reynolds number covered. The total efficiency at design equivalent speed and pressure ratio increased from 0.82 to 0.88 with an increase in Reynolds number over the same range. The corresponding static efficiency increased from 0.80 to 0.86. The variation in loss with change in Reynolds number agreed well with a theoretical variation, wherein 0.7 of the loss was attributed to viscous losses and the remaining 0.3 was attributed to other losses which are independent of Reynolds number. Author

N68-18702*# National Aeronautics and Space Administration. Lewis Research Center, Cleveland, Ohio.

DYNAMIC CHARACTERISTICS OF PARASITIC LOADING SPEED CONTROLLER FOR 10 KILOWATT BRAYTON CYCLE TURBOALTERNATOR

Raymond L. E. Fischer and Darryl J. Droba Washington Mar. 1968 18 p refs

(NASA-TM-X-1456) CFSTI: HC\$3.00/MF\$0.65 CSCL 10B

An investigation was conducted to determine the operating characteristics of a static parasitic-loading speed controller, including the transient and off-design characteristics, when operating with an air driven turboalternator. The speed controller was designed to be used with the turboalternator in a 400 hertz Brayton cycle power conversion system. The speed controller begins to deliver power to the parasitic load when the turboalternator output frequency increases above the rated frequency of 400 hertz, and it delivers maximum power to the load when the frequency reaches 406 hertz. With this controller, the system speed was maintained within 2 percent for voltage variations from 140 to 92 volts and step load changes of 10 kilowatts, with an alternator output of 10.5 kilowatts.

N68-18998*# National Aeronautics and Space Administration. Lewis Research Center, Cleveland, Ohio.

ANALYSIS OF THE MAXIMUM PERFORMANCE OF A PARABOLOIDAL SOLAR COLLECTION SYSTEM FOR SPACE POWER

Gabriel N. Kaykaty Washington Mar. 1968 19 p refs (NASA-TN-D-4415) CFSTI: HC\$3.00/MF\$0.65 CSCL 10B

An analytical study was performed to investigate the effects and interactions of the concentrator surface errors and rim angle, collection system orientation error, and cavity receiver operating temperature on the maximum thermal efficiency of a paraboloid collection system operating in the vicinity of the earth. The ranges investigated were: standard deviation of surface error (0 to 18 min), orientation error (0 to 30 min), receiver temperature (2000° to 4000°R or 1110° to 2200°K), and concentrator rim angle (45 to 60 deg). Results indicate that the surface error, orientation error, and receiver operating temperature each decidedly affect the collection efficiency and that these effects are interdependent. It is shown that surface and orientation error became increasingly important with increasing receiver operating temperature. A variation in rim angle, on the other hand, produces only a slight variation in collection efficiency and does not materially modify the effects of the other three parameters. This information can be applied to the more comprehensive design optimization of a solar power system with regard to such factors as weight, size, and manufacturing simplicity. Author

N68-20276*# National Aeronautics and Space Administration. Lewis Research Center, Cleveland, Ohio.

ANALYTICAL INVESTIGATION OF SUPERSONIC TURBOMACHINERY BLADING. 2: ANALYSIS OF IMPULSE TURBINE-BLADE SECTIONS

Louis J. Goldman Washington Apr. 1968 23 p refs

(NASA-TN-D-4422) CFSTI: HC\$3.00/MF\$0.65 CSCL 10A

The geometric characteristics of supersonic impulse turbine-blade sections were investigated. The blade sections were designed to produce vortex flow conditions within the blade passage. The effects of the lower- and upper-surface Mach numbers M₁ and M_u, inlet flow angle β_i , and specific-heat ratio γ on the geometric characteristics were studied over an inlet Mach number range of 1.5 to 5.0. Blade design limitations imposed by consideration of supersonic starting and flow separation problems as well as restriction of the axial velocity to subsonic values were also investigated over the same Mach number range. The results indicated that the lower-surface Mach number level M1 and the inlet flow angle β_i had a significant effect on blade shapes, whereas the upper-surface Mach number Mu did not. For similar surface Mach numbers the effect of specific-heat ratio γ on blade shape was small. Increasing M₁ or decreasing β_1 resulted in thinner blades. The blade solidities σ were affected significantly by all the design parameters. Increasing M₁ resulted in an increase in σ , while increasing either M_u or β_i caused σ to decrease. For similar surface Mach numbers, increasing γ tends to increase σ . Although the design limitation considered herein places severe restrictions on the freedom on choice of the design parameters, it was still possible to obtain blades of reasonable shape and solidities that meet these restrictions. Author

N68-20344*# National Aeronautics and Space Administration. Lewis Research Center, Cleveland, Ohio.

DISCHARGE CHARACTERISTICS OF SOME COPPER OXIDE-MAGNESIUM THERMAL CELLS

Lawrence H. Thaller Washington Apr. 1968 23 p refs

(NASA-TN-D-4306) CFSTI: HC\$3.00/MF\$0.65 CSCL 10A

Primary thermal cells were discharged at 450°C for periods ranging from 24 to 290 hours. These cells employed magnesium (99.8 percent) as the anode material. The cathode material was the wire form of cupric oxide, which is about 80-mole-percent cupric oxide with the remainder cuprous oxide. The electrolytes consisted of 59-mole-percent lithium chloride with the remaining 41-mole-percent mixtures of potassium chloride and cesium chloride ranging from pure potassium chloride to pure cesium chloride. The average capacity of the cells was 15 ampere-hours $(5.4 \times 10^4 \text{C})$. The service life was limited by self-discharge arising from internal chemical reactions and short circuits. In this work, several features of cell design were altered in order to reduce self-discharge. A woven glass fabric separator was successful in eliminating the internal short circuits. Self-discharge from internal chemical reaction was reduced by increasing the electrode spacing and by adding CsCl to the electrolyte. The former increased the distance that electrode materials had to diffuse before reaction, and the latter reduced the diffusion coefficient. With these improvements, the rate of self-discharge was reduced from 200 milliamperes to less than 1 milliampere with a corresponding increase in cell resistance from 0.2 to 2.0 ohms. Service lives up to 12 days were achieved. Author

N68-20363*# National Aeronautics and Space Administration. Lewis Research Center, Cleveland, Ohio.

INVESTIGATION OF THE USE OF THE LUNAR SURFACE LAYER TO STORE ENERGY FOR GENERATING POWER DURING THE LUNAR NIGHT

Gerald J. Barna and Roy L. Johnson Washington Apr. 1968 19 p

(NASA-TM-X-1560) CFSTI: HC\$3.00/MF\$0.65 CSCL 10A

A solar concentrator and a surface heat exchanger with a coating having a high ratio of solar absorptivity to thermal emissivity were used to increase the thermal input to the storage bed during the lunar day. A Rankine cycle system was selected as the conversion device; the boiling temperature of the cycle varied from 560° to 760°R. To cover a range of possibilities, dry sand in a vacuum, pumicite, basalt lava, and basalt rock were considered. For a powerplant conversion efficiency of 0.135, the required specific storage bed area for basalt rock was approximately 37.2 m²/kW_e for a boiling temperature of 560°R, more than 2 times as large for basalt lava, more than 6 times as large for pumicite, and about 40 times as large for dry sand. Raising the cycle boiling temperature was studied for basalt rock and basalt lava. Throughout the study assumptions favorable to the thermal energy storage device were used. It was concluded that the possibility of developing an attractive thermal energy storage device using this concept does not appear promising. K.W.

N68-20432*# National Aeronautics and Space Administration. Lewis Research Center, Cleveland, Ohio.

A 23.4 SQUARE-FOOT (2.17-SQ-M) CADMIUM SULFIDE THIN-FILM SOLAR CELL ARRAY

Henry W. Brandhort, Jr. and Adolph E. Spakowski Washington Apr. 1968 11 p refs

(NASA-TM-X-1519) CFSTI: HC\$3.00/MF\$0.65 CSCL 10A

A large film solar cell array was built to explore the construction problems associated with the assembly of flexible,

large-area solar cells. The array contains 378 cells, is 7 feet long and 3.35 feet wide, and weighs 1.76 pounds. The array is extended vertically from a storage drum by self-extending booms. In air mass 1 sunlight at 25°C the array output was 43.8 watts per pound of cells. The overall array had an efficiency of 3.55 percent and a cell packing factor of 0.94. Efficiencies of cells used in the array ranged betweed 3.0 and 5.5 percent, and no cell selection was made during assembly. Cell series connections had a resistance of less than 0.5 milliohm and a tensile strength to rupture of 70 pounds. The demonstration model has been extended and retracted over 500 times with no damage to either cells or connections.

N68-21562*# National Aeronautics and Space Administration. Lewis Research Center, Cleveland, Ohio.

CRITICAL ELECTRICAL ASPECTS OF ALTERNATING-CUR-RENT POWER SOURCE FOR CENTAUR SPACE VEHICLE Maurice F. Baddour and John P. Quitter Washington Apr. 1968 36 p

(NASA-TM-X-1569) CFSTI: HC\$3.00/MF\$0.65 CSCL 10B

A solid-state inverter is used on Centaur to supply high-quality three-phase electric power to the guidance, autopilot, and propellant utilization systems. (Centaur is a high-energy, cryogenic-fueled second-stage vehicle.) The results of a test program to evaluate the design and performance of this inverter are described. The scope of the program is concerned primarily with measurements on internal parts of the inverter while it was subjected to extreme service conditions. Detailed data are presented on electrical and thermal design margins. Special attention is directed toward transient susceptibility and the effect of source impedance variations. Significant wave shapes are shown, and their implications are examined. Test failures and critical weaknesses in the system are analyzed, and design improvements are proposed. These improvements were incorporated into the inverter and verified by test. Subsequent flight performance has been excellent, and the inverter has provided three-phase electric power of high quality at 400 hertz to the Atlas-Centaur launch vehicle on 14 flights. Author

N68-21651*# National Aeronautics and Space Administration. Lewis Research Center, Cleveland, Ohio.

A BREADBOARD FLUERIC-CONTROLLED PNEUMATIC STEPPING MOTOR SYSTEM

William S. Griffin Washington Apr. 1968 67 p refs

(NASA-TN-D-4495) CFSTI: HC\$3.00/MF\$0.65 CSCL 13G

This report describes flueric circuitry used to drive a novel pneumatic stepping motor. The design and breadboard implementation of the circuitry are presented along with some of the techniques used for interconnection of digital fluid jet amplifiers. The experimental performance of a breadboard flueric-drivecircuitry-stepping-motor actuator system is evaluated. Finally, a comparison is made between the resultant pneumatic stepping-motor system and the more conventional pneumatic piston-in-cylinder actuator. The principal conclusions of the work are: (1) The flueric-drive-circuitry-stepping-motor combination constitutes a reliable, fast, open-loop digital stepping actuator system which has high resolution and output stiffness. The breadboard flueric-drive-circuitry-stepping-motor system could be stepped at 173 steps per second in either direction and cyclicly reversed, without missing steps, at 115 steps per second. The step size of the shaft output motion was 0.25° and a maximum static output torque of 70 inch-pounds force (788.9 cm-N) was obtained. (2) The flueric-drive-circuitry-stepping-motor actuator system consumes more flow than a conventional electropneumatic piston-in-cylinder actuator designed to do the same job. Author

N68-21766*# National Aeronautics and Space Administration. Lewis Research Center, Cleveland, Ohio.

ELECTRICAL PERFORMANCE OF A RHENIUM-NIOBIUM CYLINDRICAL THERMIONIC CONVERTER

Richard M. Williams and William J. Bifano Washington Apr. 1968 23 p refs

(NASA-TN-D-4533) CSCL 10A

The electrical performance of a cylindrical rhenium-niobium thermionic converter was measured by a pulse technique for the following temperatures: emitter, 1873° to 2073° K; collector, 850° to 1050° K; and cesium reservoir, 590° to 670° K. The peak output power densities at 1873° , 1973° , and 2073° K were 7.0, 9.4, and 11.4 W/cm^2 at 0.4, 0.5, and 0.6 V, respectively. The corresponding collector temperatures were about 900° , 940° , and 950° K, and the cesium reservoir temperatures were 595° , 606° , and 611° K. The Rason–Warner correlation was used to estimate a 5.0 ± 0.1 V work function for the vapor-deposited rhenium emitter.

N68-21835*# National Aeronautics and Space Administration. Lewis Research Center, Cleveland, Ohio.

DESIGN AND PERFORMANCE OF FLUERIC ANALOG-TO-PULSE-FREQUENCY-CONVERTER

Miles O. Dustin Washington Apr. 1968 29 p refs

(NASA-TN-D-4497) CFSTI: HC \$3.00/MF \$0.65 CSCL 13G

A flueric circuit which converts an analog pressure signal to pulse frequency is described, and design considerations are discussed. The performance characteristics of a breadboard model are also included. The breadboard model was constructed to commercial flueric amplifiers and one specially developed amplifier. The circuit uses a three-amplifier, flueric oscillator having a pulsed output whose frequency is a function of input pressure level. The frequency of the oscillator varies continuously from 0 to 180 pulses per second when the input pressure changes from 5.2 psig $(36 \times 10^3 \text{ N/m}^2 \text{ gage})$ to 3.1 psig $(21 \times 10^3 \text{ N/m}^2 \text{ gage})$. The complete converter system will operate from 0 to 160 pulses per second when the input pressure to the converter is varied over a range of 2 psi (13.8×103 N/m2). The converter system has flat saturation characteristics. The oscillator circuit will recover from a step change in input pressure within one output pulse. The flueric amplifiers use supply pressures of 20 psig (138×10³ N/m² gage) or less. The analog-to-pulse-frequency converter will be used to drive a pneumatic stepping actuator system developed for positioning nuclear reactor control drums. Author

N68-22257*# National Aeronautics and Space Administration Lewis Research Center, Cleveland, Ohio.

EXPERIMENTAL INVESTIGATION OF REACTOR-LOOP TRANSIENTS DURING STARTUP OF A SIMULATED SNAP-8 SYSTEM

Pierre A. Thollot, Henry B. Block, and Kent S. Jefferies Washington May 1968 46 p refs

(NASA-TN-D-4546) CFSTI: HC\$3.00/MF\$0.65 CSCL 10B

Experimental investigations of primary-loop transients during the startup of a Rankine-cycle space-power system were conducted in the SNAP-8 Simulator Facility at Lewis. Of particular significance to these studies was the fact that both a realistic reactor simulator and a flight-weight mercury boiler were used in the primary loop. Furthermore, the system tested used the same liquid metals and operated at similar temperatures, pressures, and flow rates as those of the SNAP-8 system. During startup, the electric heater power input was automatically controlled so that the transient behavior of a real reactor could be duplicated. With the exception of this automic power control, all other variables were manually controlled to predefined values. In order to evaluate the relative merits of the wide variety of startup modes studied, a method of judging the results of each run was derived based on the reactor simulator exit temperature excursion. A comparison of this criterion with individual nuclear-system constraints showed excellent Author agreement.

N68-22258*# National Aeronautics and Space Administration. Langley Research Center, Langley Station, Hampton, Va. THE GEOMETRIC PROPERTIES OF AN EXPANDABLE WHIRLING-MEMBRANE SOLAR-ENERGY CONCENTRATOR John M. Jerke and Atwood R. Heath, Jr. Washington May 1968 36 p refs

(NASA-TN-D-4532) CFSTI: HC\$3.00/MF\$0.65 CSCL 10A

The whirling-membrane concept of solar-concentrator fabrication has been proposed for use with spacecraft-power-conversion devices because of its compact-packaging potential. Three membranes of 0.01-millimeter-thick aluminized plastic were constructed and attached to metal hubs for which the ratios of the hub radius to the membrane radius were 0.20, 0.35, and 0.50. The resulting models that had design focal lengths of 132.1 centimeters and design diameters of 3.05 meters were rotated at 71 radians per second in a vacuum chamber at pressures below 133 newtons per meter². The accuracy with which each membrane achieved the design paraboloidal shape was measured by an optical-ray-trace technique. The membrane with the metal hub of largest diameter gave the best concentration of energy. For this model, the focal length was 130.5 centimeters or 1 percent less than the design value. A geometric efficiency of 1.00 was obtained at a concentration ratio of 23. Membrane surface mean errors varied from -0.6° to 0.4° in the radial direction and were essentially zero in the circumferential direction. The random error has a standard deviation of 0.5° in the radial direction over most of the membrane and 0.25° in the circumferential direction. Location of supporting cables relative to the metal hub was found to be an important factor in the design of a whirling-membrane concentrator. Author

N68-22842*# Bendix Corp., Davenport, Iowa. DEVELOPMENT OF A LIQUID SHROUD CRYOGENIC SUPERCRITICAL PRESSURE STORAGE SYSTEM Washington NASA May 1968 66 p refs

(Contract NAS9-4634)

(NASA-CR-1048; Rept.-3734A-67) CFSTI: HC \$3.00/MF \$0.65 CSCL 13A

The concept of insulating a cryogenic fluid by the vaporization of a secondary cryogenic refrigerant is not new. This technique has been used for several years in ground equipment and laboratory type liquid helium dewars. However, little effort has previously been expended in applying this technique to flight-type equipment. Fuel cell reactants supply systems, environmental control systems, and propellant pressurization systems to be utilized aboard future spacecraft will all require improved state-of-the-art advances in the handling and storage of cryogenic fluids. The concept of shroud cooling of a cryogenic storage system is discussed in this report to determine the potential weight savings and improved thermal performance for certain applications. In addition, vapor cooling of a discrete radiation shield for more effective insulation is discussed. The cryogenic shroud system fabricated and tested in this program is described. The feasibility of this cryogenic storage system for specific flight applications has been successfully demonstrated by this program. Author

N68-23476*# General Electric Co., Schenectady, N. Y. CHARACTERISTICS OF A VARIABLE SPACED PLANAR THERMIONIC CONVERTER WITH A TUNGSTEN EMITTER AND A NIOBIUM COLLECTOR

V. C. Wilson and J. Lawrence Washington NASA May 1968 105 p refs

(Contract NAS3-8511)

(NASA-CR-1033) CFSTI: HC\$3.00/MF\$0.65 CSCL 10A

A parallel plane, variable spaced, thermionic converter was built with a polycrystalline tungsten emitter and a polycrystalline niobium collector. Current-voltage characteristics were obtained for a range of emitter temperatures from 1673 to 2153°K; collector temperatures from 873 to 1173°K; cesium reservoir temperatures from 583 to 683°K, and spacings from 1.0 to 20.0 mils. Over fifty families of curves consisting of over 190 load lines were obtained. Description of the converter processing procedure, test facility and experimental techniques is included. The output characteristics are compared with those of three converters with nickel collectors. Author **N68-24461 *#** National Aeronautics and Space Administration. Lewis Research Center, Cleveland, Ohio.

CAVITATING PERFORMANCE OF TWO LOW-AREA-RATIO WATER JET PUMPS HAVING THROAT LENGTHS OF 7.25 DIAMETERS

Nelson L. Sanger Washington May 1968 39 p refs

(NASA-TN-D-4592) CFSTI: HC\$3.00/MF\$0.65 CSCL 10B

Cavitation performance of two jet pumps was evaluated in a closed-loop facility using room-temperature, deaerated water. Objectives of the investigation were to study the cavitation performance of jet pumps having low ratios of nozzle to throat area and to examine methods of cavitation prediction in jet pumps. Experimental performance was obtained with two nozzles operated separately in one test section. Each nozzle was operated at three spacings of the nozzle exit from the throat entrance. At each nozzle spacing, tests were conducted at four values of secondary-to primary-flow ratio, while secondary (pumped fluid) inlet pressure was varied. Extensive amounts of cavitation were observed before performance was affected. However, when the head ratio deteriorated, it did so quite sharply. For the test section considered in this investigation, a nozzle spacing of approximately one throat diameter best satisfied the two major performance requirements of high efficiency and cavitation resistance. The design of the secondary inlet region was important to jet pump cavitation performance. Smooth hydrodynamic streamlining of this region and a thin nozzle wall at the nozzle exit would reduce cavitation Author susceptibility.

N68-24596*# Pratt and Whitney Aircraft, East Hartford, Conn. RESEARCH AND DEVELOPMENT OF HIGH-PERFORMANCE AXIAL-FLOW TURBOMACHINERY. VOLUME 1: DESIGN OF TURBINE-COMPRESSOR

P. Bolan, R. Cohen, and W. K. Gilroy Washington NASA May 1968 157 p refs

(Contract NAS3-4179)

(NASA-CR-800) CSCL 10A

An evaluation of candidate Brayton-cycle turbomachinery configurations was conducted. As part of this program, a turbine-compressor incorporating a single-stage axial-flow turbine driving a six-stage axial-flow compressor supported on gas bearings was designed. The gas bearing rotor support system was successfully tested in a gas bearing dynamic simulator. A backup gas bearing system was designed and various experimental investigations were conducted to verify certain areas of the turbine-compressor design in addition to the gas bearing testing. Author

N68-24597^{*}# Pratt and Whitney Aircraft, Philadelphia, Pa. RESEARCH AND DEVELOPMENT OF HIGH-PERFORMANCE AXIAL-FLOW TURBOMACHINERY. VOLUME 3: DESIGN OF BACKUP GAS BEARINGS

J. T. Mc Cabe, W. Shapiro, and T. Y. Chu Washington NASA May 1968 265 p refs

(Contract NAS3-4179)

(NASA-CR-802) CFSTI: HC\$3.00/MF\$0.65 CSCL 10A

An evaluation of candidate Brayton-cycle turbomachinery configurations was conducted. As part of this program, a turbine-compressor incorporating a single-stage axial-flow turbine driving a six-stage axial-flow compressor supported on gas bearings. A backup gas bearing system was designed. The design activities included steady-state analysis and time transient rotor support system studies. A satisfactory backup gas bearing system was designed. Author

N68-24757*# National Aeronautics and Space Administration. Lewis Research Center, Cleveland, Ohio.

INJECTION START OF A BRAYTON CYCLE TURBOCOM-PRESSOR OPERATING ON GAS BEARINGS IN A CLOSED LOOP

Robert Y. Wong, Robert C. Evans, Donald J. Spackman, and Charles H. Winzig Washington May 1968 30 p refs (NASA-TM-X-1590) CFSTI: HC\$3.00/MF\$0.65 CSCL 10B

A Brayton cycle turbocompressor was experimentally investigated to determine whether the gas bearings could withstand the transients associated with a space start using gas injection. Of the two injection methods studied, constant flow injection and bottle injections, the constant flow injection method imposed a lower thrust load on the turbocompressor during injection. It was also observed that the turbocompressor unit was able to withstand the transients during start, shutdown, and accidental compressor surge. A compressor bypass valve proved to be capable of effecting emergency shutdown without causing severe vibrations. Author

N68-25059*# National Aeronautics and Space Administration. Lewis Research Center, Cleveland, Ohio.

THERMAL PERFORMANCE OF A RHENIUM NIOBIUM CYLINDRICAL THERMIONIC CONVERTER

R. M. Williams and W. J. Bifano Washington May 1968 26 p refs

(NASA-TN-D-4582) CFSTI: HC\$3.00/MF\$0.65 CSCL 10A

Efficiency and steady state performance were measured for a cylindrical thermionic converter having a rhenium emitter and a niobium collector. Measurements were made at the cesium-reservoir temperatures at which peak output power was obtained from emitter temperatures in the range from 1873° to 2073°K and collector temperatures in the range from 850° to 1050°K. Increasing the emitter temperature from 1873° to 2073°K resulted in increasing the maximum electrode efficiency from 0.127 to 0.144. The output power at maximum efficiency increased from 5.7 to 9.2 W/cm². For fixed emitter temperatures, the emitter-to-collector heat flux increased linearly with current at the rate of 2.10 W/A.

N68-25304*# National Aeronautics and Space Administration. Manned Spacecraft Center, Houston, Tex.

TRANSIENT THERMODYNAMIC ANALYSIS OF A FUEL-CELL SYSTEM

William Emile Simon Washington, D. C. Jun. 1968 89 p refs (NASA-TN-D-4601) CFSTI: HC \$3.00/MF \$0.65 CSCL 10A

This report presents a transient thermodynamic analysis of a fuel-cell system exclusive of cryogenic supply system and external heat dissipation system. The results of a simplified analysis and of a more general analysis are compared, and the results of the more general analysis are compared with performance test data. The analysis is oriented toward a particular application, but the methods employed are sufficiently general to allow application of these concepts to most fluid-loop systems involving heat and mass transfer. Author

N68-25829*# National Aeronautics and Space Administration. Lewis Research Center, Cleveland, Ohio.

ANALYSIS AND SELECTION OF DESIGN CONDITIONS FOR A RADIOISOTOPE BRAYTON-CYCLE SPACE POWERPLANT

John L. Klann, Leonard Soffer, Gerald J. Barna, Gabriel N. Kaykaty, Paul T, Kerwin et al Darl D. Bien Washington Jun. 1968 83 p refs

(NASA-TN-D-4600) CFSTI: \$3.00/MF\$0.65 CSCL 18E

Selections were made for a conceptual plutonium 238 module for electric powers in the range from 2 to 10 kilowatts. Based on the selections, component and system efficiency and weight were estimated for powers of 2, 6, and 10 kilowatts. Author

N68-28101*# National Aeronautics and Space Administration. Lewis Research Center, Cleveland, Ohio.

EVALUATION OF ALTERNATING-CURRENT LINE-VOLTAGE REGULATORS IN AUXILIARY ELECTRIC POWER SYSTEMS Richard R. Secunde and James E. Vrancik Washington Jul. 1968 19 p refs

(NASA-TN-D-4627) CFSTI: HC\$3.00/MF\$0.65 CSCL 09E

The operation of ferroresonant and feedback alternating-current line-voltage regulators in a 15-kilowatt auxiliary power system was experimentally evaluated. Input current harmonics, transient response, input-output voltage harmonic isolation, and efficiency were measured and are discussed. Author

N63-28280*# National Aeronautics and Space Administration. Lewis Research Center, Cleveland, Ohio.

ANALYSIS OF RADIATOR CHARACTERISTICS OF A SINGLE-LOOP 100-KILOWATT BRAYTON SPACE POWER SYSTEM USING A PURE GAS AND A GAS-SOLID SUSPENSION

Robert Pfeffer (City Coll. of the City of New York), Salvatore Rossetti (City Coll. of the City of New York), and Seymour Lieblein Washington Jul. 1968 68 p refs

(NASA-TN-D-4659) CFSTI: HC\$3.00/MF\$0.65 CSCL 22B

Results are presented for an exploratory comparative analysis of radiator geometric characteristics based on a simplified radiator model with either a pure gas or a graphite-gas suspension working fluid. Radiator variables investigated were gas-flow Reynolds number, pressure-drop fraction, and suspension-particle loading ratio. For the pure gases, type of gas and Reynolds number had a pronounced effect on tube and panel geometry, but Reynolds number and pressure drop fraction had a relatively small effect on planform area for fixed overall cycle loss pressure ratio. Only moderate reductions in radiator planform area (10 to 17 percent) were indicated with the use of graphite-gas suspensions. Author

N68-28310*# National Aeronautics and Space Administration. Lewis Research Center, Cleveland, Ohio.

A RADIATOR CONCEPT BASED ON CAPILLARY RETENTION OF LIQUID

Alex Vary Washington Jul. 1968 45 p refs

(NASA-TN-D-4370) CFSTI: HC\$3.00/MF\$0.65 CSCL 13A

A preliminary study was made to define problem areas and potential advantages of a radiator for extraterrestrial applications in which a heat exchange liquid is circulated through a capillary medium. An evaluation of surface energy, heat transfer, hydraulic, geometric, and meteoroid penetration factors in a capillary radiator operating under extraterrestrial conditions is presented to indicate feasibility in a potential application. Author

N68-28420*# National Aeronautics and Space Administration. Manned Spacecraft Center, Houston, Tex.

CRYOGENIC STORAGE SYSTEMS FOR EARTH-ORBITAL AND MARS-FLYBY MISSIONS

Robert K. Allgeier, Thomas L. Davies, and Robert R. Rice Washington Jul. 1968 42 p refs

(NASA-TN-D-4619) CFSTI: HC\$3.00/MF\$0.65 CSCL 22B

A study program was undertaken to assess cryogenic gas requirements and storage methods for four design reference missions with respect to present thermal performance. Developed data indicate that anticipated improvements in static insulation techniques will not suffice to meet long-term cryogenic gas storage requirements unless vessel environmental temperatures are lowered, and the data indicate that there is need for further research on refrigeration techniques. Parametric curves and data are presented to make possible the rapid determination of cryogenic expendable requirements, Dewar sizes, and thermal protection schemes for application similar to the design reference systems. Author

N68-28870*# National Aeronautics and Space Administration. Lewis Research Center, Cleveland, Ohio.

AERODYNAMIC PERFORMANCE OF A 4.59-INCH MODIFIED RADIAL-INFLOW TURBINE FOR A SINGLE-SHAFT BRAYTON CYCLE SPACE POWER SYSTEM

Charles A. Wasserbauer and Milton G. Kofskey Washington Jul. 1968 19 p refs

(NASA-TM-X-1615) CFSTI: HC\$3.00/MF\$0.65 CSCL 10B

The turbine was modified to include a stator with 60 percent design throat area to be consistent with the single shaft system requirements. Tests were conducted with argon at an inlet temperature of 560°R and an inlet pressure of 6.0 psia. Performance results are presented in terms of equivalent specific work, torque, mass flow, and efficiency for a range of speeds from 0 to 110 percent of design. Author

N68-29460*# General Electric Co., Cincinnati, Ohio. Space Power and Propulsion Section.

DEVELOPMENT OF ELECTRICAL SWITCHGEAR FOR SPACE NUCLEAR ELECTRICAL SYSTEMS

A. H. Powell, ed. Washington NASA Jul 1968 119 p (Contract NAS3-6467)

(NASA-CR-1026; R67SD3012) CFSTI: HC \$3.00/MF \$0.65 CSCL 10B

High capacity circuit breakers and contactors are needed for future large spacecraft systems with 500 to 1000 KWe power supplies. Based on the latest experience on utility and industrial systems, a vacuum interrupter appears to be the simplest means of obtaining suitable performance in a space environment. The feasibility of power interruption in a vacuum capsule in a space environment of 1000°F ambient temperature had been previously investigated, and with this background, preflight prototype single pole breakers and contactors have now been designed, built, and extensively tested. The breaker, rated 1000 volts, 600 amperes, 2000 cps, for main system protection, and the contactor, rated 10,000 volts, 10 amperes, for propulsion engine switching, have been mechanically and electrically tested. Overall performance has been determined in a preliminary way, and successful completion of 1000-hour endurance test in the 1000°F and 10-6 (or lower) torr pressure has given confirmation of the feasibility of the vacuum switchgear for large space systems. Author

N68-29960*# National Aeronautics and Space Administration. Lewis Research Center, Cleveland, Ohio.

EXPERIMENTAL EVALUATION OF A VOLTAGE REGULATOR-EXCITER FOR A 15 KILOVOLT-AMPERE BRAYTON CYCLE ALTERNATOR

Gary Bollenbacher, Richard A. Edkin, and Dennis A. Perz Washington Aug. 1968 31 $\,p$ refs

(NASA-TN-D-4697) CFSTI: HC\$3.00/MF\$0.65 CSCL 10A

A voltage regulator-exciter for a 15 kVA, 120/208 volts, 400 hertz alternator was experimentally evaluated. Emphasis was placed on the effect of the voltage regulator-exciter on the alternator performance. Specific items tested include the voltage regulator-exciter output capacity, its regulating capability, its effect on alternator waveshape, and its performance during transient and startup conditions. Author

N68-30002*# National Aeronautics and Space Administration. Lewis Research Center, Cleveland, Ohio.

PERFORMANCE CHARACTERISTICS OF 15 kVA HOMOPOLAR INDUCTOR ALTERNATOR FOR 400 Hz BRAYTON-CYCLE SPACE-POWER SYSTEM

Richard A. Edkin, Martin É. Valgora, and Dennis A. Perz Washington Aug. 1968 40 p refs

(NASA-TN-D-4698) CFSTI: HC\$3.00/MF\$0.65 CSCL 10A

The measured performance of a 15 kVA homopolar inductor is presented and compared with design goals. Test results include alternator saturation, voltage unbalance, harmonic analysis, short circuits, machine reactances, and time constants. The following overall performance was obtained: maximum continuous output, 22.5 kVA: peak efficiency, 0.918 at 11.25 kVA; and efficiency at rated 15 kVA output, 0.915. Author N68-30241*# National Aeronautics and Space Administration. Lewis Research Center, Cleveland, Ohio.

COLD-AIR INVESTIGATION OF EFFECTS OF PARTIAL ADMISSION ON PERFORMANCE OF 3.75-INCH MEAN-DIAMETER SINGLE STAGE AXIAL-FLOW TURBINE Hugh A. Klassen Aug. 1968 22 p ref

(NASA-TN-D-4700; E-4407) CFSTI: HC \$3.00/MF \$0.65 CSCL 21E

Total to static efficiency is described as a function of percentage of admission and blade-jet speed ratio. At design blade-jet speed ratio, efficiency decreased from 0.68 to 0.56 as percentage of admission was reduced from 100 to 11.76. Partial admission efficiency losses are divided into rotor pumping and windage losses and all other losses. Author

N68-30506*# National Aeronautics and Space Administration. Lewis Research Center, Cleveland, Ohio.

EFFECT OF A VARIABLE STATOR AREA ON PERFORMANCE OF A SINGLE-STAGE TURBINE SUITABLE FOR AIR COOLING. 2: STATOR DETAILED LOSSES WITH 130 PERCENT DESIGN AREA

Thomas P. Moffitt, Herman W. Prust, Jr., and Bernard Bider Washington Aug. 1968 21 $\ensuremath{\mathsf{p}}$ refs

(NASA-TM-X-1635) CFSTI: HC\$3.00/MF\$0.65 CSCL 21E

The turbine is being investigated at stator area settings of 70, 100, and 130 percent of design. The experimental and analytically predicted results are presented for the stator having open (130 percent) area setting and compares these results with similar results obtained for the design (100 percent) area setting. The final results are presented in terms of kinetic energy loss coefficients as a function of velocity level. The experimental losses were close to those predicted analytically and indicate a stator efficiency of about 96 percent.

N68-30751*# National Aeronautics and Space Administration. Lewis Research Center, Cleveland, Ohio.

PRELIMINARY ANALYSIS OF A TITANIUM ALLOY HONEYCOMB SOLAR ABSORBER HAVING BLACKENED WALLS

William J. Bifano Washington Aug. 1968 27 p refs (NASA-TN-D-4727) CFSTI: HC\$3.00/MF\$0.65 CSCL 18N

A titanium alloy hexagonal honeycomb with blackened walls is considered as an absorber of collimated solar solar energy. Circular cylindrical geometry is assumed for the analysis as an approximation of the hexoganal cell structure. The apparent hemispherical emittance of such an absorber positioned over a black surface is calculated. Results are presented for cell length-to-diameter ratios of from 1 to 7 and cell diameters of 0.25, 0.5, and 1.0 in. (0.635, 1.27, and 2.54 cm, respectively). The collimated incident solar flux is assumed sufficient to attain base surface temperatures of 1860° and 2060° R (1033 and 1144 K). The corresponding weight per unit area of such an absorber is also calculated. Author

N68-33062*# AiResearch Mfg. Co., Los Angeles, Calif. RECUPERATOR FOR SOLAR BRAYTON CYCLE SYSTEM A. F. Anderson Washington NASA Aug. 1968 222 p refs (Contract NAS3-2793)

(NASA-CR-1150) CFSTI: HC\$3.00/MF\$0.65 CSCL 10B Results are presented of analytical and test work conducted on a recuperator to be utilized in a closed Brayton cycle space power system that uses solar energy as a heat source and argon as the working fluid. The initial phase of the work was a parametric design study to determine the optimum recuperator operating conditions for the Brayton cycle. The study was followed by analysis and testing for the final design configuration. The final phase of this program included fabrication and testing of a recuperator. Author N68-34234*# National Aeronautics and Space Administration, Lewis Research Center, Cleveland, Ohio.

EFFECT OF AMOUNT OF ELECTROLYTE, DRAIN RATE AND ELECTRODE GEOMETRY ON PERFORMANCE OF COPPER OXIDE-MAGNESIUM THERMAL CELLS Lawrence H. Thaller Washington Sep. 1968 15 p refs

(NASA-TN-D-4790) CFSTI: HC\$3.00/MF\$0.65 CSCL 10C

Studies continued on the performance of Mg/LiCl-KCl/Cu, O-CuO thermal cells operating at 450°C. The measure of performance used is the parameter X, the depth of discharge at which the approximate 0.25-V drop in open circuit voltage occurs. This parameter was evaluated as a function of three factors which influence mass transport, namely, the amount of electrolyte, the rate of discharge, and the electrode shape and spacing. The amount of electrolyte per unit of cell capacity had little effect on X. In tests on horizontal- and vertical-type cells, X was inversely related to current density, with a stronger dependence on current density for cells with poorer mass transport characteristics. An increase in current density and decrease in operating temperature promoted premature failure (low cathode utilization). Author

N68-35467*# National Aeronautics and Space Administration. Lewis Research Center, Cleveland, Ohio.

THERMAL RADIATIVE AND ELECTRICAL PROPERTIES OF A CADMIUM SULFIDE SOLAR CELL AT LOW SOLAR INTENSITIES AND TEMPERATURES

John R. Jack and Ernie W. Spisz Washington Oct. 1968 18 p refs

(NASA-TN-D-4818) CFSTI: HC\$3.00/MF\$0.65 CSCL 10A

A typical thin film cadmium sulfide solar cell was investigated in a solar space environment simulator facility. The solar radiation intensity was varied from 0.028 to 1.07 solar constants. The associated solar cell temperature ranged from 155° to 325°K. The results showed that the absorptance –emittance ratio was approximately constant at 0.43 over the temperature range of 200° to 325°K. Below 200°K the absorptance–emittance ratio increased rapidly to 0.70 at a temperature of 155°K. Author

N68-35536*# National Aeronautics and Space Administration. Lewis Research Center, Cleveland, Ohio.

EFFECT OF VARIABLE STATOR AREA ON PERFORMANCE OF A SINGLE-STAGE TURBINE SUITABLE FOR AIR COOLING. 3: TURBINE PERFORMANCE WITH 130-PERCENT DESIGN STATOR AREA

Harold J. Schum, Thomas P. Moffitt, and Frank P. Behning Washington Oct. 1968 24 p refs

(NASA-TM-X-1663) CFSTI: HC\$3.00/MF\$0.65 CSCL 21E

The performance changes resulting from adjusting the stator area of an experimental 30-inch (0.762-m) single stage turbine, with blading designed to incorporate physical features associated with turbines for high engine temperature application, are being investigated. The performance of the turbine with design stator area has been previously reported. The performance of this same turbine, modified so the stator area was increased to 130% of the design by reorienting the stagger angle of the blades, is presented herein. When results of these two turbine configurations were compared, it was found that when the stator area was increased by 30%, the choking equivalent work output of operating point corresponding to equivalent design speed and an equivalent work output of 17.00 Btu per pound (39,572 J/kg) showed that the efficiency decreased from 0.923 to 0.897 for the subject opened turbine. This decrease in efficiency is primarily attributable to the incidence angle relative to the motor, which was calculated to be changed about 28° from design. Author

N68-37162*# National Aeronautics and Space Administration. Lewis Research Center, Cleveland, Ohio.

PREDICTION OF WINDAGE POWER LOSS IN ALTERNATORS

James E. Vrancik Washington Oct. 1968 21 p refs

(NASA-TN-D-4849) CFSTI: HC\$3.00/MF\$0.65 CSCL 10A

The purpose of this report is to develop a method of predicting the windage loss of rotating electrical machines operating in various gases under different pressures and temperatures. An equation was developed for a cylindrical rotor and modified by empirical relations to take into account the effects of the salient poles and shrouds of the homopolar inductor alternator. The effect of the gap length is briefly studied. The windage loss for a shrouded homopolar inductor alternator was calculated by these equations and compared to the experimental results obtained at the NASA Lewis Research Center. The agreement was within ± 10 percent for a range of pressure from standard atmospheric to 40 psia (2.75×10^5 N/m²). Author

N68-37217*# National Aeronautics and Space Administration. Lewis Research Center, Cleveland, Ohio.

LENGTH OF WINDING ON A TORUS IN TWO IDEAL MODELS

Janis M. Niedra Washington Oct. 1968 16 p

(NASA-TM-X-1674) CFSTI: HC\$3.00/MF\$0.65 CSCL 09A

An analysis of the relation of the total number of turns on a torus to the length of winding is presented for two models. One model is based on the assumption of circular turns; the other assumes close packed windings. Results are presented for ratios of major to minor radii of the torus of 1.25 to 10 and for fractional filling of the winding window from 0 to 1.0. The curves presented enable the winding length for a particular number of turns to be easily determined.

N68-37263*# National Aeronautics and Space Administration. Lewis Research Center, Cleveland Ohio.

EXPERIMENTAL PERFORMANCE OF A 5-INCH (13 cm) AXIAL-FLOW TURBINE OVER A RANGE OF REYNOLDS NUMBER

Samuel M. Futral, Jr. and Donald E. Holeski Washington Oct. 1968 20 p refs

(NASA-TM-X-1679) CFSTI: HC\$3.00/MF\$0.65 CSCL 10B

The investigation was conducted in argon and over a range of inlet total pressures from 9.5 to 1.3 psia (6.6 to 0.9 N/cm² abs). The corresponding Reynolds numbers ranged from 317,000 down to 41,000. Test results showed that efficiencies and equivalent mass flow decreased with decreasing Reynolds number. These decreases in performance were greater than those of a 6.02-in. (15.3-cm) radial-inflow turbine which was designed for the same application. Author

N68-37265*# National Aeronautics and Space Administration. Lewis Research Center, Cleveland, Ohio. EFFECTS OF FREEZING ON PRIMARY SILVER OXIDE ZINC

CELLS

Richard E. Johnson Washington Oct. 1968 11 p

(NASA-TM-X-1681) CFSTI: HC\$3.00/MF\$0.65 CSCL 10C

An investigation was conducted to determine the effects of freezing on primary silver oxide-zinc cells. Three freezing rates of 4.77° F/min. (2.66 K/min), 0.81° F/min (0.45 K/min) and 0.19° F/min (0.10 K/min) were used. In addition, some cells underwent a slow (28-day) freeze-thaw cycle to -50° F (227° K). No harmful effects were noted, either to the cell itself or its performance.

N68-37935*# National Aeronautics and Space Administration. Lewis Research Center, Cleveland, Ohio.

COMPARISON BETWEEN CEMENTED AND SOLDERED COVERGLASS FOR SILICON SOLAR CELLS

Jacob D. Broder Washington Nov. 1968 11 p refs

(NASA-TM-X-1687) CFSTI: HC\$3.00/MF\$0.65 CSCL 10A

A comparison was made of the spectral response of cemented and soldered cover glass on a current commercial silicon solar cell. Cover glass transmission factors were determined in the range of 0.4 to 0.95 micron with a filter-wheel solar simulator. Soldered and cemented cell short circuit current spectral response was calculated as a function of the effectiveness of the cover-glass radiation protection, for a bombardment dose of 10¹⁶ 1-MeV electrons per square centimeter. Author

N68-37943*# National Aeronautics and Space Administration. Lewis Research Center, Cleveland, Ohio.

EXPERIMENTAL PERFORMANCE OF A 5-INCH SINGLE-STAGE AXIAL-FLOW TURBINE DESIGNED FOR A BRAYTON CYCLE SPACE POWER SYSTEM

Donald E. Huleski and Samuel M. Futral, Jr. Washington Nov. 1968 22 p refs

(NASA-TM-X-1666) CFSTI: HC\$3.00/MF\$0.65 CSCL 10B

The turbine investigated was designed to drive a six stage, axial flow compressor for a 10-kilowatt, two shaft space power system. Tests were made using argon at an inlet pressure of 2.9 psia (2.0 N/cm² abs) and an inlet temperature of 582 [°]R (323 K). Test results showed that the turbine efficiency was below the design value. Data indicated the rotor tip sections performed poorly. The exit diffuser performed well.

04 BIOSCIENCES

Includes aerospace medicine, exobiology, radiation effects on biological systems; physiological and psychological factors. For related information see also: 05 Biotechnology.

N68-10122*# National Aeronautics and Space Administration. Langley Research Center, Langley Station, Va. APPLICATION OF CELL CULTURE AS A PRIMARY

TOXICITY SCREEN OF POSSIBLE SPACECRAFT. CONTAMINANTS Richard B. Hays Washington NASA Nov. 1967 13 p refs

(NASA-TN-D-4251) CFSTI: HC\$3.00/MF\$0.65 CSCL 06T

Cell culture has been investigated with regard to its applicability as a primary toxicity screen. Forty-nine compounds have been screened by this method. These compounds are all contaminants which may occur in manned spacecraft. The data presented indicate that cell culture can be a useful tool for selecting, from a long list, those compounds most likely to be toxic to a living system. The compounds tested might be ranked, in terms of decreasing toxicity to cells in culture, as follows: unsaturated aldehydes, amines, aldehydes, acids, ketones, and alcohols.

N68-11968*# Dudley Observatory, Albany, N. Y. THE MICROBIOLOGICAL FLORA OF THE GEMINI 9 SPACECRAFT BEFORE AND AFTER FLIGHT

John Hotchin (N. Y. State Dept. of Health), Peter Lorenz, Aletha Markusen (N. Y. State Univ., Albany), and Scott Covert (Albany Med. Coll., N. Y.) Washington NASA Dec. 1967 16 p refs (Grant NsG-155)

(NASA-CR-972) CFSTI: HC\$3.00/MF\$0.65 CSCL 06M

Three sites within the Gemini IX space capsule were investigated for microbiological contamination by swabbing before and after the flight. Bacterial or mold growth was observed in three sets of swabs taken before the flight and one set of swabs taken after the flight, and most of the swabs were then found heavily covered with dust. The results were obtained by the completely independent study of the eluted suspensions of the swabs by three research groups and, despite the considerable variation of the detailed results, they show that the inside of the Gemini IX space capsule was contaminated with microbiological materials both before and after the flight.

N68-12494*# General Technical Services, Inc., Upper Darby, Pa. TRANSIENT BEHAVIOR OF ARTERIAL SYSTEMS IN RESPONSE TO FLOW PULSES

E. D. Young Washington NASA Dec. 1967 35 p refs (Contract NASw-1066)

(NASA-CR-990) CFSTI: HC\$3.00/MF\$0.65 CSCL 06P

In this paper we hope to show the relation of transient analysis of fluid lines to harmonic analysis thereof, to indicate the practicality of formulating the transmission problem with respect to transients in the time domain and uniformly with respect to frequency or pulse width within the domain of linearity assumptions of Witzig, Iberall, Womersley, etc., to apply this transient analysis to a whole class of systems embracing in principle the normal range of mammalian arterial systems which should help to clarify the meaning of equivalence among various idealized models mentioned, to trace causual relations between familiar wave distortions seen in arterial trees and the basic geometry of the trees, or that of the equivalent system. Author N68-13432*# Israel Program for Scientific Translations, Ltd., Jerusalem.

BIOCHEMISTRY OF THE NERVOUS SYSTEM

A. V. Palladin 1967 136 p refs Transl. into ENGLISH of the publ. "Voprosy Biokhimii Nervnoi Sistemy" Kiev, Izd. Naukova Dumka, 1965 Publ. for NASA and NSF

(NASA-TT-F-439; TT-67-51375) CFSTI: HC \$3.00/MF \$0.65 CSCL 06A

Metabolism of the brain in various functional states, problems related to biochemistry of the brain and nervous system, and the use of radioactive isotopes for biochemical studies of the nervous system are discussed in reprints of conference papers. Other papers deal with the nervous system of hibernating animals, activity and localization of various subcellular cerebral functions separable by electrophoresis in agar gels, and the use of neurotropic drugs. M.W.R.

N68-14671* National Aeronautics and Space Administration, Washington, D. C.

AEROSPACE MEDICINE AND BIOLOGY—A CONTINUING BIBLIOGRAPHY WITH INDEXES

Nov. 1967 172 p refs

(NASA-SP-7011(43)) CFSTI: \$3.00 CSCL 06S

The abstracts and annotated indexes were selected from those introduced into the NASA Information System during October 1967. The references were previously announced by the Library of Congress, the American Institute of Aeronautics and Astronautics, and NASA. The emphasis is placed on the biological, physiological, psychological, and environmental effects to which man is subjected during and following simulated or actual flight in the earth's atmosphere or in interplanetary space. N.E.N.

N68-14725* National Aeronautics and Space Administration, Washington, D. C.

AEROSPACE MEDICINE AND BIOLOGY—A CONTINUING BIBLIOGRAPHY WITH INDEXES

Oct. 1967 153 p refs

(NASA-SP-7011(42)) CFSTI: \$3.00 CSCL 06S

The abstracts and indexes were selected from those introduced into the NASA Information System during September 1967. They appeared previously in the separate journals of the Library of: Congress, the American Institute of Aeronautics and Astronautics, and NASA. The emphasis is placed on the biological, physiological, and environmental effect to which man is subjected during aerospace flight.

N68-154777 # National Aeronautics and Space Administration, Washington, D. C.

PROBLEMS OF SPACE BIOLOGY. VOLUME 5: DYNAMICS OF THE CEREBRAL BLOOD VOLUME UNDER NORMAL CONDITIONS AND GRAVITATIONAL STRESSES

Yu. Ye. Moskalenko Feb. 1968 193 p refs Transl. into ENGLISH of the book "Problemy Kosmicheskoy Biologii. Tom V. Dinamika Krovenapolneniya Golovnogo Mozga.v Norme i pri Gravitatsionnykh Nagruzkakh" Leningrad, Nauka Press, 1967 (NASA-TT-F-492) CFSTI: HC\$3.00/MF\$0.65 CSCL 06S

04 BIOSCIENCES

The basic mechanisms responsible for compensating changes in the blood volume of the closed cranial cavity are described, based on data obtained by electroplethysmography, which makes it possible to judge the dynamics of the cerebral blood volume directly; and on critical analyses of other experimental material. A detailed assessment is made of some aspects of active and passive compensation of changes during gravitational stresses of more than 1 g, such as are encountered in space flight. Analytical data are also presented on the nature and activity of the basic mechanisms during compensation of periodic fluctuations in the blood volume resulting from cardiac activity, respiratory movements, third-order waves, and vascular reaction of the brain under normal conditions, including longitudinal gravitational accelerations of up to +1 g. To define these mechanisms, the dynamics of the cerebral blood volume as a partly isolated system are examined. M.G.L

N68-15899*# National Aeronautics and Space Administration, Washington, D. C.

AEROSPACE MEDICINE AND BIOLOGY: A CONTINUING BIBLIOGRAPHY WITH INDEXES

Dec. 1967 133 p refs

(NASA-SP-7011(44)) CFSTI: HC\$3.00/MF\$0.65 CSCL06S

Subject coverage concentrates on the biological, physiological, psychological, and environmental effects to which man is subjected during and following simulated or actual flight in the earth's atmosphere or in interplanetary space. Also included are such related topics as sanitary problems, pharmacology, toxicology, safety and survival, life support systems, exobiology, and personnel factors. Each entry consists of a standard citation accompanied by its abstract. Author

N68-16517*# National Aeronautics and Space Administration, Washington, D. C.

AEROSPACE MEDICINE AND BIOLOGY Continuing Bibliography With Indexes, During December 1967 Jan. 1968 130 p refs

(NASA-SP-7011(45) CFSTI: HC\$3.00/MF\$0.65 CSCL06S

Subject coverage concentrates on the biological, physiological, psychological, and environmental effects to which man is subjected during and following simulated or actual flight in the earth's atmosphere or in interplanetary space. References describing similar effects on biological organisms of lower order are also included. Such related topics as sanitary problems, pharmacology, toxicology, safety and survival, life support systems, exobiology, and personnel factors receive appropriate attention. Each entry consists of a standard citation accompanied by its abstract.

N68-20026*# National Aeronautics and Space Administration, Washington, D. C.

AEROSPACE MEDICINE AND BIOLOGY—A CONTINUING BIBLIOGRAPHY WITH INDEXES

Feb. 1968 175 p refs

(NASA-SP-7011(47)) CFSTI: HC\$3.00/MF\$0.65 CSCL 06S

Subject coverage concentrates on the biological, physiological, psychological, and environmental effects to which man is subjected during and following simulated or actual flight in the earth's atmosphere or in interplanetary space. References describing similar effects on biological organisms of lower order are also included. Such related topics as sanitary problems, pharmacology, toxicology, safety and survival, life support systems, exobiology, and personnel factors receive appropriate attention. Each entry consists of a standard citation accompanied by its abstract. Author N68-20027*# National Aeronautics and Space Administration, Washington, D. C. Scientific and Technical Information Div. AEROSPACE MEDICINE AND BIOLOGY—A CONTINUIN® BIBLIOGRAPHY WITH INDEXES

Mar. 1968 131 p refs For abstract see N68-20026 10-04 (NASA-SP-7011(48)) CFSTI: HC\$3.00/MF\$0.65 CSCL 06S

N68-21383*# National Aeronautics and Space Administration. Manned Spacecraft Center, Houston, Tex.

REVIEW OF NASA-MSC ELECTROENCEPHALOGRAM AND ELECTROCARDIOGRAM ELECTRODE SYSTEMS INCLUDING APPLICATION TECHNIQUES

J. L. Day Washington Apr. 1968 16 p refs

(NASA-TN-D-4398) CFSTI: HC\$3.00/MF\$0.65 CSCL 06B

The development and evaluation of a silver/silver chloride/gelatinate matrix electrode with a specially prepared electolytic paste are described. The system was developed to enhance readings of space flight electrocencephalogram, electrocardiogram, and respiration monitoring systems. Details of the electrode, electrolytic paste, harness assembly, and integument subsystems are given followed by a step by step presentation of application procedures. These electrodes are more artifact free than conventional electrodes will remain in place and provide a high quality signal for long periods. Dermatological and microbiological tests show that the paste and electrodes are nonirritating and cause insignificant microbial proliferation during 14-day periods. R.N.A.

N68-22194*# National Aeronautics and Space Administration, Washington, D. C.

AEROSPACE MEDICINE AND BIOLOGY-A CUMULATIVE INDEX

Jan. 1968 887 p refs Supersedes NASA-SP-7011(45)

(NASA-SP-7011(46); NASA-SP-7011(45)) CFSTI: HC \$3.00/MF \$0.65 CSCL 06S

This publication is a cumulative index to the past twelve issues (SP-7011(34) through SP-7011(45)) of the National Aeronautics and Space Administration's Continuing Bibliography titled Aerospace Medicine and Biology. The bibliography has been compiled through the cooperative efforts of the Aerospace Medicine and Biology Bibliography Project of the Library of Congress (LC), the American Institute of Aeronautics and Astronautics (AIAA), and the National Aeronautics and Space Administration (NASA). Entries prepared by the three contributing organizations are identified as follows: (1) NASA entries by their STAR accession numbers (N67-10000 series); (2) AIAA entries by their IAA accession numbers (A67-10000 series); and (3) LC entries identified by a number in the A67-80000 series.

N68-22882*# National Aeronautics and Space Administration, Washington, D. C.

AEROSPACE MEDICINE AND BIOLOGY. A CONTINUING BIBLIOGRAPHY WITH INDEXES

Apr. 1968 144 p

(NASA-SP-7011(49)) CFSTI: HC\$3.00/MF\$0.65 CSCL 06S

Subject coverage concentrates on the biological, physiological, psychological, and environmental effects to which man is subjected during the following simulated or actual flight in the earth's atmosphere or in interplanetary space. References describing similar effects on biological organisms of lower order are also included. Such related topics sanitary problems, pharmacology, toxicology, safety and survival, life support systems, exobiology, and personnel factors receive appropriate attention. Each entry consists of a standard citation accompanied by its abstract. Author

N68-24272*# Scientific Translation Service, La Canada, Calif. THE ORIGIN AND INITIAL DEVELOPMENT OF LIFE

A. I. Oparin Washington NASA May 1968 60 p refs Transl. into ENGLISH of the book "Vozniknoveniye i Nachal'noye Razvitiye Zhizni" Moscow, Meditsina, 1966

(Contract NASw-1496)

(NASA-TT-F-488) CFSTI: HC\$3.00/MF\$0.65 CSCL 06B

A book is presented on the history of the development of life on earth. A brief review of the attempts to solve the origin of life is given along with an objective chronology of the events leading to the origin and initial development of life. The initial stages in the development of carbon compounds is described, and the formation of the primary broth is examined. Details are given on the rise of prebiological systems, and the evolution and rise of primitive organisms with the subsequent evolution of primary organisms is described. B.S.D.

N68-25844*# National Aeronautics and Space Administration, Washington, D. C.

AEROSPACE MEDICINE AND BIOLOGY: A CONTINUING BIBLIOGRAPHY WITH INDEXES

May 1968 132 p refs

(NASA-SP-7011(50)) CFSTI: \$3.00 /MF \$0.65 CSCL 06S

Subject coverage concentrates on the biological, physiological, psychological, and environmental effects to which man is subjected during and following simulated or actual flight in the earth's atmosphere or in interplanetary space. References describing similar effects on biological organisms of lower order are also included. Such related topics as sanitary problems, pharmacology, toxicology, safety and survival, life support systems, exobiology, and personnel factors receive appropriate attention. Each entry consists of a standard citation accompanied by its abstract. Author

N68-26207*# National Aeronautics and Space Administration, Washington, D. C.

BIOREGENERATIVE SYSTEMS

1968 152 p refs Proc. of a Conf. held in Washington, D. C., 15-16 Nov. 1966

(NASA-SP-165) GPO: HC\$1.50; CFSTI: MF\$0.65 CSCL06M

Topics presented at this conference cover the application of Hydrogenomonas-chemosynthesis and algae-photosynthesis processes in future bioregenerative life support systems for long duration space travel. Advantages and disadvantages of both systems are outined and the possibility of a combined chemosyntheticphotosynthetic system is considered. G.G.

N68-28246*# National Aeronautics and Space Administration, Washington, D. C.

AEROSPACE MEDICINE AND BIOLOGY-A CONTINUING BIBLIOGRAPHY WITH INDEXES, MAY 1968

Jun. 1968 174 p refs

(NASA-SP-7011(51)) CFSTI: HC\$3.00/MF\$0.65 CSCL 06S

Subject coverage concentrates on the biological, physiological, pyschological, and environmental effects to which man is subjected during and following simulated or actual flight in the earth's atmosphere or in interplanetary space. References describing similar effects on biological organisms of lower order are also included. Such related topics as sanitary problems, pharmacology, toxicology, safety and survival, life support systems, exobiology, and personnel factors receive appropriate attention. Each entry consists of a standard citation accompanied by its abstract. Author

N68-28247*# Litton Systems, Inc., Minneapolis, Minn. MICROBIOLOGICAL EXPLORATION OF THE STRATOS-

PHERE. DEVELOPMENT AND FLIGHTS OF THE MARK 2 AND 3 SAMPLING SYSTEMS

Paul D. Pederson, Jr. Washington NASA Jun. 1968 139 p refs

(Contract NAS5-3888)

(NASA-CR-1101; TR-3172) CFSTI: HC \$3.00/MF \$0.65 CSCL 06M

Research to determine the existence and identity of viable microorganisms in the stratosphere was performed. This report covers all effort expended and includes the description of two sampling systems (Mark II and Mark III) which employ low-pressure drop media for the collection of viable microorganisms at low air densities. A total of seven operationally successful flights were conducted with samples obtained from altitude profiles ranging from 10,000 to 90,000 feet. Emphasis was on contamination control techniques to minimize or eliminate microbial background during all procedures associated with sample acquisition and analysis. Organisms recovered existed in low numbers generally varying inversely with altitude in the range of 10–2 to 10–4 organisms per ambient ft 3 air. A variety of bacterial and fungal species were isolated.

N68-28278*# Esso Research and Engineering Co., Linden, N. J. STUDY OF METHODS FOR CHEMICAL SYNTHESIS OF EDIBLE FATTY ACIDS AND LIPIDS Final Technical Report John W. Frankenfeld, ed. Washington NASA Jul. 1968 160 p refs

(Contract NAS2-3708)

(NASA-CR-1105) CFSTI: HC\$3.00/MF\$0.65 CSCL 06A

A survey and critical evaluation of existing methods for the synthesis of fatty acids and lipids from metabolic wastes under conditions of space travel was completed. An extensive literature search was conducted and the candidate processes were evaluated from the standpoints of chemical feasibility and nutritional value of the products. The only promising route involved synthesis of ethylene from carbon monoxide, polymerization to α -olefins via the Ziegler growth reaction, conversion to fatty acids by oxidative ozonolysis and combination with glycerol to form edible glycerides. Four methods for the synthesis of glycerol were discovered. The most promising are base catalyzed trimerization of formaldehyde followed by hydrogenation and hydrogenolysis of higher sugars which may be prepared by controlled polymerization of formaldehyde. The synthesis of glycerol is much less complicated than fatty acid production and hence is a recommended alternate. A series of recommendations for further research and development were drawn up. These are mostly in the area of engineering and nutrition. Author

N68-28829*# Esso Research and Engineering Co., Linden, N. J. STUDY OF METHODS FOR CHEMICAL SYNTHESIS OF EDIBLE FATTY ACIDS AND LIPIDS: FINAL SUMMARY John W. Frankenfeld, ed. Washington NASA Jul. 1968 97 p

refs

(Contract NAS2-3708)

(NASA-CR-1104) CFSTI: HC \$3.00/MF \$0.65 CSCL 06A

A survey and critical evaluation of existing methods for the synthesis of fatty acids and lipids from the metabolic wastes under conditions of space travel has been completed. An extensive literature search was conducted and the candidate processes were evaluated from the standpoints of chemical feasibility and nutritional value of the products. The only promising route involved synthesis of ethylene from carbon monoxide, polymerization to α -olefins via the Ziegler growth reaction, conversion to fatty acids by oxidative ozonolysis and combination with glycerol to form edible glycerides. A first approximation engineering design was made and some rough estimates of power requirements were drawn up. The system was found to be extremely complex and unreliable. Hence it is not recommended as a method for food preparation on board a space craft. Four methods for the synthesis of glycerol were discovered. The most promising are base catalyzed trimerization of formaldehyde followed by hydrogenation and hydrogenolysis of higher sugars which may be prepared by controlled polymerization of formaldehyde. The synthesis of glycerol is much less complicated than fatty acid production and hence is a recommended alternate. Dissert, Abstr.

04 BIOSCIENCES

N68-29128*# National Aeronautics and Space Administration, Washington, D. C.

THE ROLE OF THE VESTIBULAR ORGANS IN SPACE EXPLORATION

1968 437 p refs 3d Symp., Held at Naval Aerospace Med. Inst., Pensacola, Fla., 24–26 Jan. 1967 Sponsored by NAS-NRC (NASA-SP-152) GPO: HC\$3.25; CFSTI: MF\$0.65 CSCL 06S

In the conference papers presented, the problems of studying disorientation under space conditions is discussed in relation to the basic research being conducted on vestibular mechanisms. Attention is focused on circulation of the endolymph, efferent vestibular function and anatomical considerations, blood supply to the labyrinth, tests of otolith and canal function. For individual titles see N68-29128 through N68-29158.

N68-32707*# National Aeronautics and Space Administration, Washington, D. C.

AEROSPACE MEDICINE AND BIOLOGY A Continuing Bibliography with Indexes

Jul. 1968 150 p refs

(NASA-SP-7011(52)) CFSTI: HC\$3.00/MF\$0.65 CSCL06S

Subject coverage concentrates on the biological, physiological, psychological, and environmental effects to which man is subjected during and following simulated or actual flight in the earth's atmosphere or in interplanetary space. References describing similar effects on biological organisms of lower order are also included. Such related topics as sanitary problems, pharmacology, toxicology, safety and survival, life support systems, exobiology, and personnel factors receive appropriate attention. Each entry consists of a standard citation accompanied by its abstract. Author

N68-33005*# Stanford Research Inst., Menio Park, Calif. A PRELIMINARY STUDY OF THE AWAKENING AND STARTLE EFFECTS OF SIMULATED SONIC BOOMS

Jerome S. Lukas and Karl D. Kryter Washington NASA Sep. 1968 74 p refs

(Contract NAS1-6193)

(NASA-CR-1193) CFSTI: HC \$3.00/MF \$0.65 CSCL 05E

Results of experiments on the startling and awakening effects of sonic booms are presented. The objectives were to: (1) build and test a device and associated room where one could simulate the effects of sonic booms on a room in a house, and (2) conduct studies of the effects of the simulated indoor booms on people sleeping and performing manual tasks. The tentative findings are based on a study of a small, homogeneous group of subjects Author

N68-35069*# National Aeronautics and Space Administration, Washington, D. C.

AEROSPACE MEDICINE AND BIOLOGY: A CONTINUING BIBLIOGRAPHY WITH INDEXES

Aug. 1968 154 p refs

(NASA-SP-7011(53)) CFSTI: HC\$3.00/MF\$0.65 CSCL 06S

Subject coverage concentrates on the biological, physiological, psychological, and environmental effects to which man is subjected during and following simulated or actual flight in the earth's atmosphere or in interplanetary space. References describing similar effects on biological organisms of lower order are also included. Such related topics as sanitary problems, pharmacology, toxicology, safety and survival, life support systems, exobiology, and personnel factors receive appropriate attention. Each entry consists of a standard citation accompanied by its abstract. Author

N68-35103*# Stanford Research Inst., Menio Park, Calif. RELATIVE ANNOYANCE AND LOUDNESS JUDGEMENTS OF VARIOUS SIMULATED SONIC BOOM WAVEFORMS L. J. Shepherd and W. W. Sutherland Washington NASA Sep. 1968 59 p refs

(Contract NAS1-6193)

(NASA-CR-1192; LR-20922) CFSTI: HC \$3.00/MF \$0.65 CSCL 05E

A series of investigations were initiated in an effort to assess the effect of sonic boom signature modification on human subjective response, using Lockheed's sonic boom simulation facility. Subjective response was found to be influenced by changes in several signature parameter, including rise time, interpeak duration, and the addition of short duration transients to the signature bow wave. Detailed descriptions and the results of this series of experiments are described. Author

05 BIOTECHNOLOGY

Includes life support systems, human engineering; protective clothing and equipment; crew training and evaluation, and piloting. For related information see also: 04 Biosciences.

N68-10381*# Serendipity Associates, Chatsworth, Calif. A DESCRIPTIVE MODEL FOR DETERMINING OPTIMAL HUMAN PERFORMANCE IN SYSTEMS, VOLUME 4 Final Summary Report

Washington NASA Nov. 1967 51 p (Contract NAS2-2955) CSCL 05H (NASA-CR-879) CFSTI: HC\$3.00/MF\$0.65

This study was conducted to provide tools to aid in management decisions germane to the development of complex aerospace systems to the end that man be used in an optimal way. The study consists of five parts packaged in three reports and each part is focused on a particular area of concern to enable the necessary decision making, planning, and execution effort to be conducted. The reports are concerned with a simple model of a man-machine development cycle, a simple calculus for discrete systems, system development activities concerned with putting man in an aerospace system, some concepts and guidelines for developing man-machine systems, and an approach for determining the optimal role of man and allocation of functions in an aerospace system. The method by which the study was conducted is described in terms of 12 major tasks. Implications for future work are considered in detail. R.N.A.

N68-10648* Aerospace Products Research Corp., Santa Monica, Calif.

COMPUTER DRIVEN ELECTROLUMINESCENT VERTICAL SCALE INDICATOR

James A. Pellegrino and Jules L. Rosenbaum Washington NASA Nov. 1967 40 p

(Contract NAS7-420)

(NASA-CR-919) CFSTI: \$3.00 CSCL 09B

The effort expended in the design, development, and fabrication of two types of solid-state digitally controlled electroluminescent vertical scale indicators is outlined. One type is a single parameter indicator which employs one bargraph, with scale and parameter indication; and the other is a flight director which uses two adjacent bargraphs, with scale and parameter indication. The delivered indicators met all of the following specification requirements: fast dynamic response compatible with the SDS 920 Computer update-time capability of one to twenty milliseconds; automatic lamp brightness regulation; absence of glow, flicker, and cross-coupling in the lighted display; use of high-contrast display techniques; interchangeability and versatility compatibile with an instrument used in laboratory simulations; multicolor display capability; internal information storage; low power consumption, capable of operating at 2.5 watts. The objectives for simulator environments were met with the exception of temperature. Some difficulty was encountered in isolating problems which appeared under dynamic operation of the instruments. Author

N68-11510*# Webb Associates, Yellow Springs, Ohio. THE PRINCIPLE OF THE SPACE ACTIVITY SUIT Paul Webb and James F. Annis Washington NASA Dec. 1967 34 p refs (Contract NAS1-6872)

(NASA-CR-973) CFSTI: HC\$3.00/MF\$0.65 CSCL 05B

This paper describes in principle a Space Activity Suit (SAS) designed for an active astronaut working in a vacuum for up to four hours. The suit will consist of a powerful elastic net leotard combined with positive pressure breathing via helmet and trunk bladders. Under the terms of the present contract, an elastic sleeve-and-glove was constructed to demonstrate the principle of the full SAS suit. Subjects wore the garment in an arm chamber which produced negative pressures up to 200 mm Hg (8 in Hg). Exposures to near-vacuum conditions were accomplished in an altitude chamber where the total pressure was 155 mm Hg and the arm chamber pressure was 5 to 8 mm Hg. The near-vacuum exposure for 20 minutes produced no evidence of gaseous swelling; arterial and venous circulation was adequate; mobility and finger a dexterity were excellent; increase in arm volume from accumulation of tissue fluid was approximately 5%. The successful demonstration of principle indicates that a full SAS can be developed. As an alternative to gas-filled pressure suits, its advantages would be: improved mobility, flexibility, and dexterity at small metabolic cost; simplicity in approach; low risk to the astronaut if the netting is torn; and physiological temperature regulation without power or cooling machinery. Author

N68-13609*# National Aeronautics and Space Administration. Langley Research Center, Langley Station, Va.

A PILOTED FIXED-BASE SIMULATOR STUDY OF LOW-SPEED FLIGHT CHARACTERISTICS OF AN ARROW-WING SUPERSONIC TRANSPORT DESIGN William D. Grantham and Perry L. Deal Jan. 1968 39 p refs (NASA-TN-D-4277) CFSTI: HC\$3.00/MF\$0.65 CSCL 01B

A piloted fixed-base simulator study has been made to determine the low-speed flight characteristics of an arrow-wing supersonic transport configuration. The transport-type cockpit was equipped with normal flight controls and a flight instrument display representative of those found in current transport aircraft. The results indicated that although the longitudinal short-period damping ratio was at a good level (0.84), the pitch damping appeared to be low to the pilot because of the low frequency of the short-period oscillation. This low pitch damping and the sluggish pitch response made the longitudinal handling qualities of the basic configuration unsatisfactory. When the static stability, the damping in pitch, the elevator effectiveness, and the elevator to column gearing were increased by a sufficient amount. The lateral-directional handling qualities of the basic configuration were said to be unacceptable because of the poor roll control characteristics and the uncontrollable Dutch roll. When the effective dihedral was decreased by a sufficient amount, and the damping in roll and yawing moment due to roll were increased by a sufficient amount, the Cooper rating was improved to 2.5. Author

N68-13999* National Aeronautics and Space Administration. Lewis Research Center, Cleveland, Ohio.

CARDIAC R-WAVE DETECTOR Vernon D. Gebben Washington Jan. 1968 13 p refs

(NASA-TM-X-1489) CFSTI: \$3.00 CSCL 06B

A method of detecting the R-wave of the electrocardiac signal was developed for controlling the timing cycle of heart-assist pumps. Dependable separation of the R-wave from high-level electrical interferences was obtained from a circuit that contains high common-mode rejection, a band-pass filter, an amplitude detector, and a pulse-width discriminator. An experimental circuit was tested using copper surface electrodes located on the right arm and left leg. All false signals except those generated by vigorous motion or extreme muscle tensions were rejected by the circuit. Author

N68-14262*# Serendipity Associates, Chatsworth, Calif. A DESCRIPTIVE MODEL FOR DETERMINING OPTIMAL HUMAN PERFORMANCE IN SYSTEMS, VOLUME 1 Washington NASA Jan. 1968 166 p refs (Contract NAS2-2955)

(NASA-CR-876) CFSTI: HC\$3.00/MF\$0.65 CSCL 05H

CONTENTS:

1. A SIMPLE MODEL OF A MAN-MACHINE DEVELOPMENT CYCLE, PART A J. J. Wulff and J. N. Leonard 129 p refs (See N68-14263 05-05)

2. A SIMPLE CALCULUS FOR DISCRETE SYSTEMS, PART B J. J. Wulff, A. F. Pixley (Harvey Mudd Coll.), and J. N. Leonard 31 p refs (See N68-14264 05-19)

N68-15120*# Serendipity Associates, Chatsworth, Calif. A DESCRIPTIVE MODEL FOR DETERMINING OPTIMAL HUMAN PERFORMANCE IN SYSTEMS. VOLUME 2: PART A: SYSTEM DEVELOPMENT ACTIVITIES CONCERNED WITH PUTTING MAN IN AN AEROSPACE SYSTEM. PART B: DEVELOPMENT OF MAN-MACHINE SYSTEMS: SOME CONCEPTS AND GUIDELINES

Washington, D. C. NASA Jan. 1968 380 p refs (Contract NAS2-2955)

(NASA-CR-877, V. 2) CFSTI: HC\$3.00/MF\$0.65 CSCL 05H

The design and control of each of the identified man-related activities in an aerospace system model are described. Consideration is given to planning and controlling each activity in the system development cycle which pertains to the production of man-related end products such as trained personnel, job aids, and human-engineered interfaces. Each man-related activity is discussed in the context of the overall development cycle objectives which are dependencies upon other activities, demands of other activities, activities interactions, and the process of conducting the activity. The identified man-related activities are described in terms of activity groups. Selected terms are given for the common vernacular of the biotechnology and system engineering community. Tools for synthesizing aerospace systems are included with emphasis on the design and development of the man-related features of man-machine systems. B.S.D.

N68-15306*# Applied Physics Lab., Johns Hopkins Univ., Silver Spring, Md.

EXTENDED DURATION, RECOVERABLE PRIMATE SATELLITE

Washington NASA Jan. 1968 147 p

(NASA Order R-21-009-014)

(NASA-CR-926) CFSTI: HC\$3.00/MF\$0.65 CSCL 06K

The results are presented of a brief engineering study of a proposed six-month orbital physiological experiment generally referred to as the Primate Orbital Experiment. In this proposed Apollo application experiment, two live squirrel monkeys would be placed into a low earth orbit, then recovered alive approximately six months later, for examination on the ground. This study includes all spacecraft systems, life support, and instrumentation for an experiment package which could be transported into orbit by an Apollo spacecraft and function autonomously until picked up six months later through rendezvous with a second Apollo spacecraft. Presented are approaches to possible ways of integrating the animal-carrying satellite with Apollo during launch, and feasible life support and instrumentation techniques to maintain the animals alive in orbit for six months. Techniques for retrieval are suggested. Author N68-15901*# National Aeronautics and Space Administration, Washington, D. C.

THIRD ANNUAL NASA UNIVERSITY CONFERENCE ON MANUAL CONTROL

1967 435 p refs Conf. held Univ. of Southern Calif., Los Angeles, 1–3 Mar. 1967

(NASA-SP-144) CFSTI: HC\$3.00/MF\$0.65 CSCL 05H

In the conference proceedings presented, emphasis is placed on display devices, function models, decision processes, computer processing of manual control records, controlled elements, physiological modeling, and advanced modeling techniques. For individual titles, see N68-15902 through N68-15935.

N68-16594*# National Aeronautics and Space Administration. Langley Research Center, Langley Station, Va.

EVALUATION OF A CLOSED-CIRCUIT TELEVISION DISPLAY IN LANDING OPERATIONS WITH A HELICOPTER William Gracey, Robert W. Sommer, and Don F. Tibbs Washington Feb. 1968 20 p refs

(NASA-TN-D-4313) CFSTI: HC\$3.00/MF\$0.65 CSCL 05H

An instrument display consisting of a television monitor; vertical-type torquemeter was evaluated in simulated IFR (Instrument Flight Rules) approaches with a helicopter. The evaluation was made with three lenses having focal lengths of 12.5, 25, and 50 mm. The restricted-view tests with binocular vision showed that a view as small as 22.6° horizontal and 18.5° vertical has a detrimental effect on the control of longitudinal position attouchdown. The tests with monocular vision showed that the control difficulties increase with the loss of depth perception. The tests of the television display showed that the difficulties in controlling attitude and position increased as the helicopter approached the ground. The determination of position and position-rate information was made difficult because of the restricted views of the lenses. the image magnification and the low resolution and lack of depth perception of the televised scene. The tests demonstrated that, with the television display augmented by height information, the pilots were able to execute low-speed, steep approaches with an angular view as small as 22.6° by 18.5° and an image magnification as small as about 0.35. Author

N68-18014*# National Aeronautics and Space Administration. Langley Research Center, Langley Station, Va.

ANALYSIS OF HUMAN RESPONSE IN COMBINED CONTROL TASKS

Hugh P. Bergeron, James J. Adams, and George J. Hurt, Jr. Washington Mar. 1968 55 p refs

(NASA-TN-D-4356) CFSTI: HC \$3.00/MF \$0.65 CSCL 05H

The simulation consisted of a primary control task to which were added secondary or side tasks. A trajectory control problem was used as the primary control task for the pilot. The trajectory task was a fixed-base simulation of a lunar letdown. The task-loading effects on the letdown were found to be predominant during the final hover and translation phase. All multitask tests were made by using either the lunar-letdown simulation or the multiloop representation as the primary control task. The secondary or side tasks consisted of: (1) a system-failures task integral to a typical space vehicle, and (2) a well-defined motor response task. The study generated a quantitative index of the information processing characteristics of a full (multitask) simulation. A method, for determining the information processing requirements of a trajectory control task was devised to provide the quantity related to this index. By combining this quantity with the information processing measurements of the side tasks, the total workload for various combinations of tasks was determined. A quantitative analytical model was also generated for the multiloop control in a multitask simulation. A duty-cycle shaping technique developed in this study was used to generate the model. Author

 $\textbf{N68-18870}^{*}\#$ National Aeronautics and Space Administration, Washington, D. C.

TELEOPERATORS AND HUMAN AUGMENTATION. AN AEC-NASA TECHNOLOGY SURVEY

Edwin G. Johnson and William R. Corliss Dec. 1967 273 p (NASA-SP-5047) GPO: HC\$1.00; CFSTI: MF\$0.65 CSCL 05H

This book surveys general purpose, dexterous, cybernetic machines developed in the last 25 years, emphasizing the principal subsystems of contemporary designs of such teleoperators. The purpose of the work is to present the concepts and techniques of teleoperators now used in nuclear and aerospace work for possible adaptation in exploring the seas, increasing industrial productivity, and aiding physically handicapped persons. Covered are: (1) present and potential teleoperator applications; (2) subsystems and man-machine integration; (3) design principles of structure, control, actuator, and sensor subsystems; and (4) teleoperator terminal devices. A glossary and an extensive bibliography are included. K.W.

N68-19165*# Serendipity Associates, Chatsworth, Calif.

A DESCRIPTIVE MODEL FOR DETERMINING OPTIMAL HUMAN PERFORMANCE IN SYSTEMS. VOLUME 3: AN APPROACH FOR DETERMINING THE OPTIMAL ROLE OF MAN AND ALLOCATION OF FUNCTIONS IN AN AEROSPACE SYSTEM

Harold E. Price and Barbara J. Tabachnick Washington NASA Mar. 1968 1204 p refs

(Contract NAS2-2955)

(NASA-CR-878) CFSTI: HC\$3.00/MF\$0.65 CSCL05H

Conventions, sequence of activities, and research needs are considered in an effort to determine the role of man in space and the allocation of functions to men and machines in aerospace systems. The 11 conventions discussed include the local and remote segment, optimal manned design, man-rated performance, core performance, and roles of men in systems. Types and components of human performance, personnel support systems, man-machine comparisons, personnel products package, and automation are the other conventions implicit in a descriptive model for determining optimal human performance in aerospace systems. Activities are considered in terms of determining both the optimal role of man and the optimal allocation of function; and detailed data are appended on man-machine performance and crew support requirements.

N68-20339*# Environmental Research Associates, Randallstown, Md.

A STUDY OF THE PERFORMANCE OF AN ASTRONAUT DURING INGRESS AND EGRESS MANEUVERS THROUGH AIRLOCKS AND PASSAGEWAYS

Harry L. Loats, Jr. and William J. Bruchey, Jr. Washington NASA Apr. 1968 163 p refs

(Contract NAS1-4059)

(NASA-CR-971) CFSTI: HC\$3.00/MF\$0.65 CSCL 05H

The performance characteristics of a pressure-suited astronaut during ingress-egress through various geometry airlocks were studied by water immersion techniques. The buoyancy force induced by water displacement of a totally immersed subject was used to counteract all or part of his adjusted total weight to provide the desired simulated gravity level. The subject performed real-time maneuvers as determined from functional analysis of representative extravehicular and intravehicular tasks: The purpose of this phase of the contract was to generate additional data on refined experiments initiated under previous contractual phases and to expand the experiment scope to include rescue, replenishment and general maneuvers exterior to the airlock. The effect of the variation of airlock dimension and shape on the capabilities to perform manual ingress-egress was evaluated by comparative time-task analysis. Author

N68-20354*# National Aeronautics and Space Administration. Langley Research Center, Langley Station, Va.

EFFECTS OF PRESSURE SUITS AND BACKPACK LOADS ON MAN'S SELF-LOCOMOTION IN EARTH AND SIMULATED LUNAR GRAVITY

Amos A. Spady, Jr. and Randall L. Harris Washington Apr. 1968 46 p refs

(NASA-TN-D-4464) CFSTI: HC\$3.00/MF\$0.65 CSCL 05E

Studies were conducted to evaluate the effect of a state-of-the-art full pressure suit on man's self-locomotion capabilities in earth and simulated lunar gravity. Separate tests, with subjects wearing lightweight coveralls, were also conducted in simulated lunar gravity to determine the effect on locomotion of carrying backpack loads of up to 500 earth pounds. The simulated lunar tests were conducted on a modified version of the reduced-gravity walking simulator. Tests in earth gravity were performed on a portion of asphaltic concrete road of length equal to that provided by the modified lunar-gravity simulator. The gait characteristics of the subjects were determined by having the subjects walk and run at various speeds. The results obtained with the pressure suit indicated that pressurizing the suit to 3.7 psig did not appreciably affect the subject's self-locomotive gait characteristics in lunar gravity. The results of the load-carrying tests indicated that a subject, dressed in lightweight coveralls, could carry a backpack loaded with 500 earth pounds while walking, loping, and sprinting in lunar gravity. Author

N68-20357*# National Aeronautics and Space Administration, Washington, D. C.

AN INTRODUCTION TO THE ASSURANCE OF HUMAN PERFORMANCE IN SPACE SYSTEMS

1968 42 p refs Prepared by Martin Co.

(NASA-SP-6506) CFSTI: HC \$3.00/MF \$0.65 CSCL 05H To assess the role that man plays as a potential source of error in space technology, studies were conducted to determine what human performance assurance effort is appropriate for various projects and to show how this effort relates to various phases in the development cycle. A method for classifying programs and systems according to mission complexity and significance is developed, and human engineering and serviceability functions appropriate for specific development phases of the programs are categorized and described. Man-machine capabilities are summarized as an aid in determining the relative superiority of each. An example is presented in which the techniques are applied to a hypothetical micrometeoroid deep space satellite, a concept based on studies of an unmanned satellite program of medium-to-small cost and complexity. The reliability program provision for space system contractors, concerning prevention of human error, is included. M.G.J.

N68-21537*# National Aeronautics and Space Administration. Flight Research Center, Edwards, Calif.

FM HANDLING AND ANALOG-TO-DIGITAL CONVERSION OF BIOMEDICAL DATA FROM A 1,000-FLIGHT STUDY

Richard Carpenter and James Roman Washington Apr. 1968 12 p refs

(NASA-TN-D-4488) CFSTI: HC\$3.00/MF\$0.65 CSCL 06B

To collect, process, and analyze FM-recorded biomedical data from 1,000 flights in high performance aircraft and test vehicles, it was necessary to devise a handling facility that would prepare these data in a standard format for high speed computer processing. The handling system designed maintains the very high signal to noise ratio inherent in the original data acquisition equipment, provides pushbutton control for converting the medical information into a standard format for digital processing at either four or eight times faster than the original record speed, and provides an effective number of quality control checkpoints. The system is described in detail, and system design considerations are hiscussed in relation to preventing data degradation in both FM handling and digital conversion. Approximately 1,400 hours of

05 BIOTECHNOLOGY

flight data have been processed by this system in less than 600 hours without loss of data integrity. This system is suitable for preparing biomedical data in standard format for digital processing, since the system design can easily be changed to accommodate nonstandard input formats. Author

N68-21538*# National Aeronautics and Space Administration. Flight Research Center, Edwards, Calif.

RECORDING AND SIGNAL-CONDITIONING TECHNIQUES AND EQUIPMENT USED IN A 1,000-FLIGHT BIOMEDICAL STUDY

Richard Carpenter and James Roman Washington Apr. 1968 17 p refs

(NASA-TN-D-4487) CFSTI: HC\$3.00/MF\$0.65 CSCL 06B

The NASA Flight Research Center recently concluded a biomedical monitoring program involving 1,000 flights in high performance aircraft by students of the USAF Aerospace Research Pilot School and by NASA aerospace research pilots. To permit accurate and reliable data acquisition of electrocardiogram (ECG). respiration rate, and normal acceleration, it was necessary to design and develop a means of reliably recording and transcribing flight medical data in a format compatible with computer reduction. Signal conditioners and interconnecting harnesses were designed and fabricated, and guidelines were established for the construction of a five channel analog tape recorder to record these data while the recorder is being carried on the pilot with minimum interference or discomfort. The equipment operated reliably and enabled satisfactory data acquisition of biomedical information both in extended biomedical instrumentation studies and in remote site medical monitoring. Author

N68-21859*# California Univ., San Francisco. Medical Center. RELATIVE ROLES OF GRAVITATIONAL AND INERTIAL WORK IN THE ENERGY COST OF HUMAN LOCOMOTION H. J. Raiston and L. Lukin Washington NASA Apr. 1968 18 p refs

(Grant NsG-722)

(NASA-CR-1042) CFSTI: HC \$3.00/MF \$0.65 CSCL 06S

The metabolic cost of walking was measured during walking on the treadmill at various slopes—positive, level and negative—and before and after loading of the principal body segments. An equation derived from these studies relates metabolic demand to speed of walking under 1/6 g conditions, and is shown to be in acceptable agreement with the data obtained by other investigators for moderate speeds of walking under simulated 1/6 g conditions. The effects of load upon the metabolic cost of walking are shown to be critically dependent upon the segment of the body loaded. Loading of the extremities causes a much greater increase in the metabolic cost of walking than loading of the trunk, due to the greater magnitude of inertial (kinetic energy) work compared with gravitational work. The probable metabolic effects of restraint of free body motion, combined with difficult terrain, are briefly discussed. Author

N68-22448*# Rensselaer Polytechnic Inst., Troy, N. Y. FREQUENCY CODED THRESHOLD LOGIC UNIT FOR

PATIERN RECOGNITION APPLICATION

Rob Roy and David Hinks Washington NASA May 1968 72 p refs

(Grant NGR-33-018-014)

(NASA-CR-1035) CFSTI: HC\$3.00/MF\$0.65 CSCL 06B

The principles on which the central nervous system functions are investigated, and their application to pattern recognition problems are discussed. The concepts are then developed in the form of a frequency coded threshold logic element which will employ the advantageous techniques of information transmission exhibited by the sensory nervous system, and improve the performance of the pattern recognition system. The design develops a discriminant function that is a linear combination of weighted frequencies and computed simply as a pulse count; the operating characteristics of the system are delineated. The concept of frequency coding is used to provide a method in which modern digital techniques may be applied to incorporate speed and reliability into the design. The hardware requirements of the proposed design are given in detail and require only moderate expenditure of equipment. B.S.D.

N68-24756*# National Aeronautics and Space Administration. Manned Spacecraft Center, Houston, Tex. FLAMMABLE AND TOXIC MATERIALS IN THE OXYGEN

ATMOSPHERE OF MANNED SPACECRAFT

John H. Kimzey Washington May 1968 30 p refs

(NASA-TN-D-3415) CFSTI: HC\$3.00/MF\$0.65 CSCL 05E

A preliminary study of the considerations necessary in selecting materials for use in an oxygen-rich atmosphere revealed that a major design effort must be directed toward reducing the toxic and flammable contaminants of the atmosphere. The effect of zero gravity in preventing convection is one aspect of research that deserves considerable effort since heat transfer and flammability are two major fields directly affected. Other research is needed in human tolerances, static electricity, removal of low-molecular-weight gas, fire extinguishment, overall characteristics of materials exposed for long periods in pure oxygen, and in the development of adequate test procedures. Author

N68-25060*# National Aeronautics and Space Administration. Ames Research Center, Moffett Field, Calif.

A PIEZOELECTRIC TRANSDUCER FOR MEASURING CARDIAC AND GROSS MOTOR ACTIVITY OF SMALL ORGANISMS

Vernon L. Rogallo, Robert S. Jenkins, and Gordon J. Deboo Washington May 1968 11 p refs

(NASA-TN-D-4590) CFSTI: HC\$3.00/MF\$0.65 CSCL 06B

The transducer system incorporates both mechanical and electrical noise rejection features. The mechanical feature is achieved by a dual arrangement, essentially two transducers, one of which senses the organism activity and noise while the second senses only the noise. Subtraction of the output of the individual transducers results in a cancellation of the environmental noise. The electrical noise rejection is achieved by low-noise preamplifiers with differential input to reject 60 Hz. A low-noise-RC-active filter is used to eliminate frequencies outside the bandwidth of interest. It was found that the rejection features provided sufficient discrimination against environmental noise to allow the transducer to be used in a normal laboratory environment. The instrument is sufficiently sensitive to measure heart rates in insects, reptiles, mammals, and developing chick embryos as young as 3 days.

N68-26690*# Systems Technology, Inc., Hawthorne, Calif.

PILOT DYNAMIC RESPONSE TO SUDDEN FLIGHT CONTROL SYSTEM FAILURES AND IMPLICATIONS FOR DESIGN

David H. Weir and Walter A. Johnson Washington NASA Jun. 1968 152 p refs

(Contract NAS2-3607)

(NASA-CR-1087; TR-165-1) CFSTI: HC \$3.00/MF \$0.65 CSCL 05H

The dynamic response of the human pilot is studied during sudden changes in the effective controlled element dynamics caused by flight control system failure. Experimental results from single-loop and multiple-loop fixed-base studies are presented. A hypothesis of graceful degradation is shown to be valid which states that the pilot's transition response and performance are improved if the difference in controlled element dynamics at failure is reduced. The design implications of this principle are detailed. A model for the pilot's dynamic response is presented which accounts for his behavior during the several phases of transition. Author

N88-26701*# Webb Associates, Yellow Springs, Ohio. AUTOMATIC CONTROL OF WATER COOLING IN SPACE SUITS

Paul Webb, James F. Annis, and Samuel J. Troutman Washington NASA Jun. 1968 91 p refs

(Contract NASw-1529)

(NASA-CR-1085) CFSTI: HC \$3.00 /MF \$0.65 CSCL 06K

Accurate and timely control of the powerful cooling available in a water cooled garment (WCG) is important during periods when work varies widely, as in extravehicular activity, and with it the need for cooling. The relationship between metabolic rate (MR) and the suit inlet water temperature (Twi) can be expressed as an ordinary differential equation: $\tau T_{wi} = -T_{wi} + B_4(MR_0-MR)$. An experimental Q controller was used to automatically control heat removal (Q) from men wearing a new WCG while working on a treadmill. The input to the controller was a continuous oxygen consumption signal. The cooling water was recirculated through a closed loop where the man was the heat source and a controllable thermoelectric cooler was the heat sink. After initial experiments where variation in the controller gain and time constant were explored, automatic control was evaluated in two subjects doing four different patterns of work, including brief periods of intermittent work. Physiological responses were good, and control was smooth Author and accurate.

N68-28319*# IIT Research Inst., Chicago, III.

PRELIMINARY STUDY OF ADVANCED LIFE-SUPPORT TECHNOLOGY FOR A MARS SURFACE MODULE

R. E. Mitchell and M. Burns Washington NASA Jun. 1968 189 p refs

(Contract NASr-65(15))

(NASA-CR-1083) CFSTI: HC \$3.00/MF \$0.65 CSCL 06K

This study represents an initial step in the direction of subsystem definition for extended manned missions on Mars and is centered primarily around a review of the current literature and state-of-the-art techniques. A mission profile of four men for six months is analyzed. From this baseline assumption, a Mars surface module configuration is projected, and subsystems in life support, power, and environmental control most candidate for the proposed mission are assessed.

N68-28833*# Garrett Corp., Los Angeles, Calif.

THE EFFECTS OF LUNAR GRAVITY ON METABOLIC RATES

W. G. Robertson and E. C. Wortz Washington NASA Jul. 1968 91 p refs

(Contract NAS9-6494)

(NASA-CR-1102; Rept.-67-2174) CFSTI: HC \$3.00/MF \$0.65 CSCL 06S

Experiments were conducted to determine the effects of simulated lunar gravity on the metabolic cost of work in both the A-5-L and the RX-2 full pressure suits. Lunar gravity simulation was accomplished using a modified Hewes and Spady inclined-plane simulator and a 6-degree-of-freedom (DOF) suspension simulator. Six subjects wearing the A-5-L and RX-2 pressure suits were instrumented for determining metabolic rates; data were collected for walking and upper-torso exercises during ventilated and pressurized modes of operation for each suit. Results show that the metabolic rates for walking are lower in the 1/6-g environment than in the 1-g environment. There were no significant differences in the energy costs of walking between the RX-2 and the A-5-L pressure suits at 1/6 g with the suits pressurized. Pressurization results in a slight but significant increase in metabolic rate in the RX-2. Pressurization of the A-5-L results in a significant increase in metabolic rate in all exercise modes in each simulator. There were no significant differences between suits while performing upper-torso tasks in the pressurized mode during 1/6-q simulation. Author

N68-28847*# Decision Science, Inc., San Diego, Calif. MODELING THE HUMAN OPERATOR WITH FINITE-STATE MACHINES

L. J. Fogel and Roger A. Moore Washington NASA Jul. 1968 236 p refs

(Contract NAS1-6739)

(NASA-CR-1112) CFSTI: HC \$3.00/MF \$0.65 CSCL 05H

The prospect of using finite-state machines to represent arbitrary analog transducers and the human operator in his performance of flight control is considered in this experimental investigation, together with the use of evolutionary programming as a means for finding such representations. A series of tasks of increasing difficulty which demonstrate this capability are presented, ranging from the characterization of relatively simple linear analog "pilots", through more complex nonlinear analog "pilots", and on to the human pilot acting both in a simulator and in flight. The findings of the investigation demonstrate that finite-state machines do offer a suitable means for representing the human operator in terms of his stimulus-response behavior with respect to non-convergent tracking tasks. In addition, alternative hypotheses concerning the logic of pilot behavior were examined in order to reveal their relative worth on the basis of the available empirical evidence. Additional tasks are outlined which may well be addressed through the use of the technique described in this report. Author

N68-30602*# Bolt, Beranek, and Newman, Inc., Van Nuys, Calif. THE NOISINESS OF TONES PLUS NOISE

Karl S. Pearsons, Richard D. Horonjeff, and Dwight E. Bishop Washington NASA Aug. 1968 89 p refs (Contract NAS1-6364)

(NASA-CR-1117; Rept.-1520) CFSTI: HC \$3.00/MF \$0.65 CSCL 06P

A series of judgment tests were conducted to investigate subjective judgments of single, modulated and multiple tones plus noise. The subjects were asked to judge which of two sounds, tones plus noise or noise alone, was noisier (or in some cases louder). Stimuli included both broadband and octave band noises together with single tones at 250, 500, 1000, 2000, and 4000 Hz. Amplitude and frequency modulated tones of 500 and 2000 Hz were also employed. Multiple tone stimuli included 2 and 5 tone complexes with overall frequency spacings of 1/10, 1/3, 1, 4/3 and 2 octaves. Analysis of the judgment results were made using calculated perceived noise level and pure tone correction procedures. Author

N68-31480*# Biotechnology, Inc., Arlington, Va.

EFFECT OF HEAT STRESS AND PROLONGED ACTIVITY ON PERCEPTUAL-MOTOR PERFORMANCE

Raymond E. Reilly and James F. Parker, Jr. Washington NASA Aug. 1968 58 p refs

(Contract NASw-1329)

(NASA-CR-1153) CSCL06S

This study was concerned with the assessment of the effects of two stress conditions on 16 basic dimensions of perceptual-motor performance. Subjects were tested under conditions of heat stress (86°F effective temperature for a period of six hours) and prolonged activity (24-hour continuous activity, with two 2-hour rest periods). In general, perceptual-motor performance levels were well maintained under these stress conditions and there was essentially no change in performance effectiveness during the 24-hour period of prolonged activity. Under heat stress, oral temperature and pulse rate increased significantly, lending support to the inference of increased arousal. Under prolonged activity, no change was noted in oral temperature, pulse rate, or blood pressure. This was consistent with the general lack of change in the performance measures indicating this level of stress was well tolerated. The findings of this investigation demonstrate the usefulness of the integrated measurement system as a device for the study of human performance. Author

N68-31911*# Massachusetts Inst. of Tech., Cambridge. A THEORY AND MODEL OF HUMAN LEARNING **BEHAVIOR IN A MANUAL CONTROL TASK**

Albert Ernest Prevss Washington NASA Aug. 1968 138 p refs

(Grant NsG-577)

(NASA-CR-1124) CFSTI: HC \$3.00/MF \$0.65 CSCL 05H

A theory is presented for the explanation of human learning behavior in a manual control task. In the performance of a psychomotor task, a human operator responds to sensory stimuli with limb movements. This psycho-physiological phenomenon is conceptualized herein as a single channel information processing system. A sensor, a decision center and an effector are the serially connected components of the system. In the decision center responses are selected from a set of possible alternatives. Stored in memory are apriori estimates of the probability that a specific response should be inforced at the moment of decision. Response selection is determined by a rule which takes the priors into account. Learning is effected by a revision of the priors based on the weighting of certain evidence. The model of human learning behavior is a computer program obtained from a translation of the theory into machine language. Model behavior is compared with subject behavior measured in a motor skill experiment performed at M. I. T.'s Man Vehicle Laboratory. Author

N68-32100*# National Aeronautics and Space Administration. Flight Research Center, Edwards, Calif.

A SIMPLE LABORATORY METHOD FOR REDUCTION OF RHYTHM AND RATE IN LARGE-SCALE MONITORING OF ELECTROCARDIOGRAM

James Roman, Fred M. Larmie (Northrop Corp., Edwards, Calif.), and Tulio R. Figarola (Lovelace Found., Edwards, Calif.) Washington Aug. 1968 15 p refs Prepared in cooperation with Northrop Corp. and Lovelace Found. Field Teams at Edwards, Calif. (NASA-TN-D-4751) CFSTI: HC \$3.00/MF \$0.65 CSCL 06B

A laboratory system for rapid reduction of large amounts of continuously recorded ECG information has been developed. The system consists of 60-times-real-time playback device which generates one pulse for each cardiac cycle, appropriate signal conditioning and logic circuitry, and a counting and printing system. Practical means for culling out noisy information, at 60 times real time, are provided. In addition, modifications to the commercially available parts of the system have been made that significantly increase the reliability of diagnosis of ectopic events by the average investigator. Author

N68-33009*# Boeing Co., Philadelphia, Pa. SUBJECTIVE RESPONSE TO SYNTHESIZED FLIGHT NOISE SIGNATURES OF SEVERAL TYPES OF V/STOL AIRCRAFT Ernest G. Hinterkeuser and Harry Sternfeld, Jr. Washington

NASA Aug. 1968 98 p refs (Contract NAS1-7083)

(NASA-CR-1118; D8-0907A) CFSTI: HC \$3.00 / MF \$0.65 CSCL 05E

The acoustical signatures of various types of V/STOL aircraft sized for 60 passengers and a 500 mile range were analytically predicted, and tape recordings synthesizing these sounds were prepared. Test subjects listened to these sounds and compared their annoyance with that of a jet airplane. Perceived noise levels were calculated, and the levels which produced equal annoyance to the jet were determined. Each aircraft was analyzed to determine the distance it must maintain from observers in order not to exceed the annoyance of the jet airplane during terminal and flight operations. A second analysis was made to identify the noise reduction required for each aircraft in order to operate at specified distances at a specified level of annoyance. The aircraft studied were helicopters, fan lift, jet lift, and tilt wing VTOL and a turbofan STOL. Author

N68-33304*# Bolt, Beranek, and Newman, Inc., Cambridge, Mass. THE HUMAN AS AN OPTIMAL CONTROLLER AND INFORMATION PROCESSOR

Sheldon Baron and David L. Kleinman Washington Sep. 1968 76 p refs

(Contract NAS12-104)

(NASA-CR-1151; Rept.-1571) CFSTI: HC \$3.00 / MF \$0.65 CSCL 05H

A mathematical model of the human operator in multivariable control tasks is developed by considering the human as a control and information-processing system. The model contains elements for describing the operator's inherent physiological limitations as well as his instrument-monitoring, data-reconstruction, and control behavior. Special emphasis is placed on the instrument-monitoring aspects of the model. The human's limitations are modelled by combining them into an equivalent perceptual time delay and an equivalent observation noise. The main assumption underlying the subsequent theoretical investigations is that the well-trained, well-motivated operator behaves in a near optimal manner, subject to the constraints imposed by the above limitations. Thus, the operator's control behavior is assumed to be that of an ideal feedback controller. The human's data-reconstruction process is chosen so as to obtain a "best" estimate of the state of the controlled element based on information obtained from "sampling" the various instruments Author

N68-35102*# Lafayette Clinic, Detroit, Mich. SYSTEM AND PROCESS DEVELOPMENT FOR SELECTION **OF HIGH STRESS TOLERANCE PERSONNEL** Albert F. Ax Washington NASA Sep. 1968 84 p refs (Contract NAS2-1031)

(NASA-CR-1122) CFSTI: HC\$3.00/MF\$0.65 CSCL06B

A system was developed for digital computer processing of psychophysiological data. It employs oscilloscope and oscillograph display, analog magnetic tape storage, A/D conversion, digital tape storage and a large digital computer (IBM 7094). The computing programs developed select all points of interest and compute their type, time of occurence, amplitude and curvature. Two substantive studies were completed. The classical conditioning of autonomic responses in schizophrenia and healthy subjects demonstrated a marked impairment in the performance of autonomic conditioning by schizophrenic patients. A pilot study of non-schizophrenic low motivation subjects revealed a disability for autonomic conditioning similar to that found in chronic schizophrenia. These findings suggest that autonomic conditioning may serve as an index for the diagnosis of both schizophrenia and low motivation and permit the speculation that a low aptitude for autonomic learning may be a contributing factor to both schizophrenia and low social motivation. Finally a study of physiological concomitants of psychological differentiation suggests that the degree of autonomic response differentiation may be correlated with the cognitive style of perceptual discrimination. Author

N68-35109*# Stanford Research Inst., Menlo Park, Calif. RESEARCH STUDY OF A FUNDUS TRACKER FOR **EXPERIMENTS IN STABILIZED VISION**

D. H. Kelly and H. D. Crane Washington NASA Sep. 1968 49 p refs

(Contract NAS2-3995)

(NASA-CR-1121) CFSTI: HC\$3.00/MF\$0.65 CSCL 06B

An image stabilization method is discussed that involves the tracking of retinal blood vessels and other structures of the back of the eye-i.e., a fundus tracker. The method involves projecting a scanning pattern onto the retina, and detecting the translational and rotational movements of the reflected pattern by means of a certain type of high-speed correlation processing of the video signal. A particularly simple, circular scan method for this purpose is implemented by inverting a standard fundus camera in order to project the scan pattern onto the retina. The correlation processing is presently simulated on a digital computer at slow speed. This

05 BIOTECHNOLOGY

simulation program will be used for overall evaluation of the tracking system as well as to help in design of the required high-speed correlation equipment. This fundus tracker technique may provide greater precision of tracking than is provided by con-tact-lens techniques, as well as the potential for greater convenience of use.

N68-36457*# National Aeronautics and Space Administration. Ames Research Center, Moffett Field, Calif.

USE OF AN ELECTROLUMINESCENT DISPLAY IN MANUAL TRACKING AND IN A READING TASK

Frank Neuman and John D. Foster Washington Oct. 1968 22 p refs

(NASA-TN-D-4841) CFSTI: HC\$3.00/MF\$0.65 CSCL 05H

The purpose of this research was to determine whether performance differences existed between electromechanical and electroluminescent (EL) displays in a closed loop manual tracking task and in reading accuracy tests. Both displays had vertical scales, which are considered acceptable for spacecraft use. Studies were made with two EL displays, a single-scale, and a double-scale bargraph display. Pursuit tracking of sine and random waves and readability tests were conducted. The double scale instrument was used in the tracking tasks and the single scale instrument in the readability tests. The discreteness of the EL instrument's 128 vertical scale segments (12.6/cm) did not appear to cause any problems in either task. In the tracking tasks, the electroluminescent instruments were comparable to the electromechanical instruments in the region of their flat frequency response. In the readability tests, in which the environmental illumination was changed, readability of the EL instruments reduced rapidly with increasing environmental illumination above 550 lumens/m². However, at the low ambient light conditions expected in a spacecraft environment, less than 1 lumen/m², the readability was adequate. Author

N68-36461 *# National Aeronautics and Space Administration. Langley Research Center, Langley Station, Va.

A SYNTHESIS OF HUMAN RESPONSE IN CLOSED-LOOP TRACKING TASKS

James J. Adams and Hugh P. Bergeron Washington Oct. 1968 35 p refs

(NASA-TN-D-4842) CFSTI: HC\$3.00/MF\$0.65 CSCL 05H

Experiments have been conducted to determine the variability in a human subject's control stick response to the stimulus of displayed displacement and of rate of change of displacement to aid in the implementation of the time variations to be included in a linear model of the human subject. Additional tracking tests were made to obtain a definition of the characteristics of the random signal to be added to the model. These two factors, the time variations and the random signal, were then added to the linear model, and the resulting composite model was placed in analog representations of single loop and multiloop systems. The results demonstrate that this composite model reproduces the dynamic characteristics of the time histories and mean square system error which more closely match the response obtained with the human subject than does the linear model.

N68-37819*# Lockheed Missiles and Space Co., Sunnyvale, Calif. DISCRIMINATION OF INCREASES IN THE BRIGHTNESS OF A FLASHING BEACON

R. S. Lincoln, S. Seidenstein and C. V. Juliano Washington NASA Oct. 1968 47 p 8 refs

(Contract NAS1-6801)

(NASA-CR-1220) CFSTI: HC \$3.00 /MF \$0.65 CSCL 05E

The effects, on pilot judgments, of four variables were studied: beacon flash rate, beacon on time, beacon intensity, and rate of vehicle closure. The 25 subjects viewed a point source beacon, represented by a xenon arc lamp, through a lens that provided a virtual image of the beacon at a point near infinity. Flash rate and on time were controlled by motor driven cams, while closure rate was controlled with a servomotor that rotated a circular neutral filter, the density of which increased linearly. Initial brightness was varied with a second circular filter. In a counter-balanced experimental design each subject was exposed to combinations of all four variables, each at five levels. On certain trials, a steady rather than a flashing beacon was employed. The principal measure of performance was the time required to discriminate a change in beacon brightness, measured from the initiation of a trial to its termination by the subject when he was absolutely sure that the brightness of the beacon had increased. The results indicated that the thresholds for brightness increase were positively related to the rate at which the brightness of the beacon increased. Author

06 CHEMISTRY

Includes chemical analysis and identification (e.g., spectroscopy). For applications see: 17 Materials, Metallic; 18 Materials, Nonmetallic; and 27 Propellants.

N68-10497*# National Aeronautics and Space Administration, Lewis Research Center, Cleveland, Ohio. APPLICATION OF LIQUID-LAYER SOLID-SAMPLE SPARK TECHNIQUE TO SPECTROCHEMICAL SPARK SOURCE Ramon M. Barnes Washington Nov. 1967 15 p refs

(NASA-TM-X-1429) CFSTI: HC \$3.00/MF \$0.65 CSCL 07D Improved analytical results were obtained when a thin layer of water or aqueous solution was aspirated onto the surface of a flat metal sample during spark analysis. Studies with liquid layers applied to aluminum alloy standards demonstrated that increaser sampling and line emission produced increased analytical curv slopes and count precision for the determination of impurities. Spr exposure times were reduced by one-half to one-fifth. The sol from a solution layer was used to replace the aluminum inte standard in both the spark analysis of aluminum alloys and the . arc analysis of the sample electrode material vapor deposited on the counter electrode. In spark analysis when a liquid layer was applied, interfering emission from atmospheric elements and from the counter electrode material was minimized, and the physical appearance of the spark crater showed no oxide formation. Inductance of the spark circuit and aspiration rate influences were investigated. Application of this method to the analysis of refractory and superalloys is indicated by the results of the analysis. Author

N68-11512*# National Aeronautics and Space Administration. Lewis Research Center, Cleveland, Ohio. STABILIZATION OF DC ARCS IN STATIC ARGON

ATMOSPHERES FOR USE IN SPECTROCHEMICAL ANALYSIS

William A. Gordon Washington Dec. 1967 26 p refs (NASA-TN-D-4236) CFSTI: HC\$3.00/MF\$0.65 CSCL 07D

The use of metal cathodes in an argon atmosphere was investigated and found to be highly effective in achieving a positionally stable arc column. Visual and spectral evaluations of refractory metal cathodes, including graphite, thoriated tungsten, rhenium, tantalum, molybdenum, niobium, and platinum, were made to ascertain the most suitable cathode material for this application. From these studies a combination tantalum-graphite cathode was developed. This special cathode produced arcs characterized by a diffuse cathode emission, which resulted in a stable arc column. A simple model of the arc column, based on the mechanisms of cathodic gas streaming and thermionic emission, was used to explain experimental observations relevant to stability of arcs in argon. The emission spectrum of stabilized arcs was evaluated for use in spectrochemical analysis. It was found that, under the specified conditions, the excitation characteristics of the stabilized arc were essentially the same as when conventional graphite cathodes were used. It was therefore possible to integrate the special cathode into analytical procedures by substituting for graphite cathodes. Moreover, each special cathode was used for 100 to 200 analyses with no intervening treatment. Author

N68-11621*# National Aeronautics and Space Administration. Marshall Space Flight Center, Huntsville, Ala.

THE COMPUTATION OF THE PARTIAL VOLUMES OF THE COMPONENTS IN SOLUTION

Joseph S. Rosen (Computer Sci. Corp., Huntsville, Ala.) Washington Dec. 1967 10 p refs

(NASA-TN-D-4199) CFSTI: HC\$3.00/MF\$0.65 CSCL 07D

Described is a method for calculating partial volumes of the components in solution. The method is applicable to both aqueous and nonaqueous solutions of both electrolytes and nonelectrolytes. S.C.W.

N68-14093*# National Aeronautics and Space Administration. Lewis Research Center, Cleveland, Ohio. SYNTHESIS OF ULTRAHIGH MOLECULAR-WEIGHT POLY(ETHYLENE TERREPHTHALATE) Li-Chen Hsu Washington Jan. 1968 13 p refs

(NASA-TN-D-4335) CFSTI: HC\$3.00/MF\$0.65 CSCL 111

This study was conducted to synthesize poly(ethylene terephthalate) or PET of number-average molecular weight of the order of 120,000. PET of number-average molecular weight of the order of 120,000 was prepared with a gas chromatograph apparatus through solid-state polymerization technology. PET particles were packed in the column, heated to a temperature somewhat below the melting temperature, and flushed with a carrier gas until the desired molecular weight was reached. Parameters studied were the catalyst, the particle size, the molecular weight of the starting material, the reaction temperature and time, and the flow rate and nature of the carrier gas. The results showed that ester interchange catalysts such as tetraisopropyl titanate, zinc acetate-antimony trioxide, and cobaltous acetate are capable of increasing the molecular weight of PET. Small particle size and high molecular weight of the starting material are essential for obtaining products of ultrahigh molecular weight. The polymerization of PET in the solid state starts around 175°C (448°K); the molecular weight of the final product increased with increasing temperature for the period of time studied. Molecular weights are also increased by increasing the carrier gas flow rate to a certain practicable value. which varies with other polymerization conditions. Author

N68-18219*# National Aeronautics and Space Administration. Marshall Space Flight Center, Huntsville, Ala.

LATTICE STRUCTURES IN SOLUTIONS

Joseph S. Rosen Washington Mar. 1968 17 p refs

(NASA-TN-D-4297) CFSTI: HC\$3.00/MF\$0.65 CSCL 07D

The concept of an irregular and random arrangement of ions in solution is rejected. The interionic distances of the crystal lattice structure, assumed to be retained in solution, are maintained by the equilibrium between cohesive and repulsive forces on the ions in solution. This concept of a lattice structure in solution may have an important relation to the theory of an ionic atmosphere in electrolytic solutions. Calculations are presented for various concentrations of the alkali halides; for concentrations when no water is present, the interionic distances for the alkali halides agree with results obtained by other methods.

N68-19434*# National Aeronautics and Space Administration. Lewis Research Center, Cleveland, Ohio. RADIATION-INDUCED REDUCTION OF DIVALENT COPPER

SALTS IN SOLUTIONS Warren H. Philipp and Stanley J. Marsik Washington Mar. 1968

17 p refs

(NASA-TN-D-4451) CFSTI: HC\$3.00/MF\$0.65 CSCL 07C

Aqueous solutions of divalent copper salts containing soluble organic compounds were irradiated with 2-million-volt electrons. In

06 CHEMISTRY

the presence of oxidizable organic compounds le.g., methanol, glycerine, and formaldehyde), the divalent copper ion is reduced on irradiation. From solutions of either copper(II) sulfate or copper(II) perchlorate, free copper forms, G(Cu) (atoms per 100 eV or 1.6×10^{-17} J) = 2.2. A study involving concentration parameters in the copper(II)-sulfate-methanol-water system showed that two reaction mechanisms are operative. In general, when the water is the major constituent, the initial and rate-controlling reaction is the decomposition of water by radiation to form hydrogen atoms and hydroxyl radicals. The methanol is rapidly oxidized by the hydroxyl radicals and thereby leaves an excess of reducing hydrogen radicals in the system. At high methanol concentrations, the initial process is the direct interaction of the radiation with the methanol molecules, which results in the removal of hydrogen atoms from the carbon atoms. In both mechanisms, these hydrogen atoms then reduce the divalent copper. Author

N68-21430*# National Aeronautics and Space Administration. Ames Research Center, Moffett Field, Calif.

METHOD AND RESULTS OF STUDYING VAPOR DEPOSITION NUCLEATION PROCESSES BY IN SITU ELECTRON MICROSCOPY

Helmut Poppa Washington Apr. 1968 30 p refs

(NASA-TN-D-4506) CFSTI: HC\$3.00/MF\$0.65 CSCL 07D

The kinetics of nucleation in some simple substrate-overgrowth systems have been measured quantitatively by improved in situ electron microscopy techniques. The nucleation of bismuth and silver on evaporated carbon and the nucleation of bismuth on evaporated SiO substrates were studied as a function of substrate temperature and impinging flux. The results were analyzed in terms of the phenomenological theory of nucleation and in terms of Walton's atomistic model of condensation from the vapor phase. Both theoretical concepts led to specific conclusions concerning such nucleation parameters as the number of atoms in the critical nucleus n* and the free energy of desorption ΔG_{des} The substrate temperature and impingement flux dependence of the maximum number of particles deposited on the substrate surface were determined and tentatively interpreted on the basis of nucleation limited surface migration. Some nucleation induction time observations were made and were related to the clustering kinetics of adatoms, the growth process of individual nuclei, and the instrument limitations of the detection method. Author

N68-29959*# National Aeronautics and Space Administration. Goddard Space Flight Center, Greenbelt, Md.

PROPERTIES OF SELECTED RADIOISOTOPES. A BIBLIOGRAPHY, PART 1: UNCLASSIFIED LITERATURE

Dale Harris, comp. and Joseph Epstein, comp. Washington 1968 189 p refs

(NASA-SP-7031) CFSTI: HC \$3.00/MF \$0.65 CSCL 18H

Increasing interest in the application of substantial quantities of radioisotopes for propulsion, energy conversion, and various other thermal concepts emphasizes a need for accurate information describing the nuclear, chemical, and physical properties of these isotopes. This document presents, in a single reference, an annotated bibliography and sets of properties for nine of the more attractive isotopes available for use in power production. These isotopes are: Strontium-90: Cesium-134; Cesium-137; Cesium-144; Promethium-147; Polonium-210; Plutonium-238; Curium-242; and Curium-244.

N68-30044*# National Aeronautics and Space Administration. Lewis Research Center, Cleveland, Ohio.

ON THE INFLUENCE OF NONUNIFORM MAGNETIC FIELDS ON FERROMAGNETIC COLLOIDAL SOLS

S. Stephen Papell and Otto C. Faber, Jr. Washington Aug. 1968 27 p refs

(NASA-TN-D-4676) CFSTI: HC\$3.00/MF\$0.65 CSCL 07D

Description of a laboratory method for preparing magnetic sols, composed of ferromagnetic submicrometer particles as a stable colloidal dispersion in n-heptane, is presented. A fluid of this nature was subjected to nonuniform magnetic fields in a vertically mounted solenoid type electromagnet. Fluid accelerations of up to 7.2 g's were experienced by the magnetic sol without affecting the stability of the colloid system. Body force measurements were made on fluids containing a range of particle concentrations by weight from 1.58 to 13.41 percent that were subjected to magnetic inductions of from 0 to 2.75 teslas in magnetic gradients up to 22.3 teslas per meter. The relations between magnetic induction, magnetic gradient, particle concentration, and body force were examined, and the data are presented herein. An analysis was made from basic considerations that resulted in a general equation that effectively describes the trends in the data. Author

N68-30582*# National Aeronautics and Space Administration. Lewis Research Center, Cleveland, Ohio.

LOW-ENERGY ELECTRON DIFFRACTION STUDY OF OXYGEN ADSORPTION ON, MOLYBDENUM (111) SURFACE John Ferrante and Gilbert C. Barton Washington Aug. 1968 19 p refs

(NASA-TN-D-4735) CFSTI: HC\$3.00/MF\$0.65 CSCL 07D

Low energy electron diffraction was used to study oxygen absorption on, and thermal stability of, the Mo (111) surface. The crystal was subjected to oxygen exposures ranging from 0 to 10-4 torr-sec. The oxygen exposures resulted in four new surface structures, a chemisorbed structure and three others identified as chemical faceting into (112) planes. The latter required heating the crystal to 700°C to form completely. Differences from oxygen adsorption on W (111) were observed. Oxidation of the surface at room temperature was demonstrated. The surface was found to be thermally stable when heated for several minutes at 2100°C. Author

N68-31948*# National Aeronautics and Space Administration. Lewis Research Center, Cleveland, Ohio.

A SERVOCONTROLLER FOR PROGRAMMING SAMPLE VAPORIZATION IN DIRECT CURRENT ARC SPECTROCHEMICAL ANALYSIS

William A. Gordon Washington Aug. 1968 32 p refs (NASA-TN-D-4769) CFSTI: HC\$3.00/MF\$0.65 CSCL 07D

A method was developed for controlling atomic emission and sample vaporization in dc arc spectrochemical analysis. Automatic adjustments in arc current were made to cause the rate of atomic emission to follow a prescribed program. With a stabilized arc in argon the vaporization of silver chloride was repeatable to about 1 percent. The control system consisted of a spectrometer with multiplier-phototube detector, a curve-following programmer, a controller, a dc current supply, and an argon arc chamber. The control system was used with a stabilized arc in argon and also with a wandering arc in air. Author

07 COMMUNICATIONS

Includes communications equipment and techniques; noise; radio and communications blackout; modulation telemetry; tracking radar and optical observation; and wave propagation. For basic research see: 23 Physics, General; and 21 Navigation.

N68-11475*# National Aeronautics and Space Administration. Langley Research Center, Langley Station, Va.

A GENERAL METHOD FOR DESIGNING CIRCULAR ARRAY ANTENNAS TO OBTAIN QUASI-OMNIDIRECTIONAL PATTERNS

C. R. Cockrell and W. F. Croswell Washington Dec. 1967 21 p refs

(NASA-TN-D-4254) CFSTI: HC\$3.00/MF\$0.65 CSCL 09F

A criterion is established for determining the number of sources needed around the periphery of a spacecraft to obtain small far-field pattern fluctuations; that is quasi-omnidirectional antenna patterns. The criterion assumes that the source pattern is expressible as a finite Fourier cosine series and that the circumference in wavelengths of the body is greater than or equal to 10. The number of sources obtained by using this criterion will always be adequate; however, if the representation of the source pattern is known, an optimum number of sources can be obtained. The criterion is not valid when the source pattern is isotropic. Two curves are given which relate the number of sources and the circumference of the body in wavelengths for 0.5 dB or less and 2.0 dB or less fluctuation. Author

N68-17542*# Israel Program for Scientific Translations, Ltd., Jerusalem.

MEASUREMENT OF PULSE DISTORTION IN DIGITAL INFORMATION TRANSMISSION

K. A. Brusilovskii 1968 96 p refs Transl. into ENGLISH of the publ. "Izmereniya Iskazhenii Impul'sov v Sistemakh Peredachi Diskretnoi Informatsii" Moscow, Izd. Nauka, 1965 p 1–92 Published for NASA and NSF

(NASA-TT-F-434; TT-67-51370) CFSTI: HC \$3.00/MF \$0.65 CSCL 09D

Theoretical analyses of various problems connected with digital data channel measurements are presented, along with the statistical features of noise distortion and error distribution in communication channels. Evaluation criteria are developed for the noiseproof features of communication channels and for elements in the statistical treatment of signals, noises, distortions, and errors in digital data transmission systems handling uniformly coded binary data. A mathematical model is formulated for error analysis in such systems. The fundamental properties and generation of test signals are described, and design criteria are given for noncontact, solid-state, switching element transistor and ferrite measuring instruments. Questions relating to the optimum design of a digital indicator register and a transistorized output relay are discussed. A bibliography of related works is included. E.J.S.

N68-18123*# National Aeronautics and Space Administration. Langley Research Center, Langley Station, Va.

THE APERTURE ADMITTANCE OF A GROUND-PLANE-MOUNTED WAVEGUIDE ILLUMINATING A PERFECTLY CONDUCTING SHEET

J. Earl Jones and C. T. Swift Washington Mar. 1968 52 p refs

(NASA-TN-D-4366) CFSTI: HC\$3.00/MF\$0.65 CSCL 09F

The Fourier transform technique is applied to derive an expression for the aperture admittance of a ground-plane-mounted. transverse electric and magnetic (TEM) mode-excited parallel-plate waveguide illuminating a perfectly conducting sheet. Based on the aperture admittance expression, an equivalent circuit is developed. It is shown that there is a 1:1 correspondence between elements of the equivalent circuit and higher order modes which exist in the parallel-plate waveguide formed by the ground plane and the reflecting sheet. For the special case where the configuration is treated as a microwave circuit tee junction, the waveguide widths which give the best impedance match are seen to be 0.04 wavelength for the feed guide and 0.03 wavelength for the second guide. Numerical computations of the reflection coefficient, derived from the aperture admittance, are compared with both the experimental and theoretical results of a similar problem which is solved by application of the geometrical theory of diffraction. Finally, for various aperture widths, a Smith chart is employed to show that as the distance between the aperture and the reflecting sheet is increased, the admittance locus tends to coalesce about the admittance value for an infinite half-space. Author

N68-18178*# National Aeronautics and Space Administration. Ames Research Center, Moffett Field, Calif.

PERFORMANCE OF SEVERAL CONVOLUTIONAL AND BLOCK CODES WITH THRESHOLD DECODING

Frank Neuman and Dale R. Lumb Washington Mar. 1968 74 p refs

(NASA-TN-D-4402) CFSTI: HC\$3.00/MF\$0.65 CSCL 09D

The performance of several codes applicable to space communications telemetry links was evaluated. The study was limited to high rate and relatively short constraint length codes. specifically the (15,7) and (73,45) block codes and the (24,12) and (44,22) convolutional codes. Two types of threshold decoding schemes were applied, namely, majority decoding and the more powerful put complex a posteriori probability (APP) decoding. The gaussian data channel and the decoders were simulated on a general purpose computer. The results show that APP decoding has approximately a 1.5 dB advantage over majority decoding. The most powerful code studied, (73,45) with APP decoding, gives a 2.1 dB improvement over a seventh bit parity check code. Also, new error deletion schemes were designed and tested for the codes studied. Because of their constant computation rate, these codes are candidates for high data rate channels. For the low data rates required for deep space missions such as Pioneer, however, the code performances reported here form a basis of comparison with the more powerful sequential decoding of convolutional codes, a variable computation rate decoding technique. Author

N68-18247*# National Aeronautics and Space Administration., Goddard Space Flight Center, Greenbelt, Md.

THEORETICAL AND PRACTICAL RESOLUTION LIMITS FOR PROCESSING PULSE FREQUENCY MODULATION TELEMETRY

07 COMMUNICATIONS

Thomas J. Karras and Paul Heffner Washington Mar. 1968 29 $p\ refs$

(NASA-TN-D-4180) CFSTI: HC\$3.00/MF\$0.65 CSCL 09F

The importance of knowing the meaning, methods of computation, and proper use of the equivalent noise bandwidth (ENBW) of a system is presented. From this, a normalized relation for expressing the signal energy per bit of information and the noise power density of the noise in the signal will be developed and compared to the most common $S_{rms}\!/N_{rms}$ measurement. A universal Pulse Frequency Modulation (PFM) telemetry data processing line incorporates two processing subsystems, a low resolution processor and a high resolution processor. The low resolution processor resolves the data measurement to 1 percent of the data spectrum. while the high resolution processor resolves the data measurement within 0.02 percent to 1 percent. The resolution given by the high resolution processor is a direct function of the input signal-to-noise ratio. The theoretical and actual performance of both modes of processing are described. Reference is made to three presently transmitting PFM satellites. Author

N68-18542*# National Aeronautics and Space Administration. Goddard Space Flight Center, Greenbelt, Md. WAVEFORM DISTORTION IN A MAXIMUM-LIKELIHOOD DARLINGTON DETECTOR FOR M-ARY PFM SIGNALS Paul J. Heffernan Washington Mar. 1968 36 p refs

(NASA-TN-D-4294) CFSTI: HC\$3.00/MF\$0.65 CSCL 09F

This paper describes a proposed pulse frequency modulation digital communication system for satellite applications. The heart of the proposed system is a maximum-likelihood detector of the spectrum-analysis type discussed by Darlington. It is shown that the proposed technique is in principle an ideal M-ary system. A general description is followed by an analysis of anticipated departures from the theoretic system-in particular, waveform distortion due to finite bandwidth, slope mismatch, and phase and amplitude ripple. General results are derived, from which permissible tolerances for departures from the theoretical system may be computed.

N68-18616*# National Aeronautics and Space Administration. Langley Research Center, Langley Station, Va.

A QUASI-OMNIDIRECTIONAL SLOT ARRAY ANTENNA FOR SPACECRAFT USE AT MICROWAVE FREQUENCIES W. F. Croswell, C. M. Knop, and D. M. Hatcher Washington Mar.

(NASA-TN-D-4362) CFSTI: HC\$3.00/MF\$0.65 CSCL 09F

1968 60 p refs

The theory, design, and development of a resonant array of circumferential shunt slots cut in the broad wall of a ring waveguide, which is recessed into a circular metallic cylinder and dielectric coated in the recessed region, are presented. This antenna is suitable for narrow bandwidth space-vehicle applications, since it is essentially flush mounted, provides nearly omnidirectional coverage in the plane perpendicular to the vehicle axis, and provides a broad pattern in the planes which are parallel to and pass through this axis. The theory used for the design of the array is based upon the approximate synthesis method of Knudsen and Chu, in conjunction with the work of Wait for slots on dielectric-coated cylinders. The tolerance problems encountered in the development of the array and their solutions are discussed. Author

N68-18703*# National Aeronautics and Space Administration. Electronics Research Center, Cambridge, Mass.

ATTENUATION AND DISPERSION OF LONGITUDINAL WAVES IN VISCOUS, PARTLY IONIZED GASES David Kahn Washington Mar. 1968 9 p refs

(NASA-TM-X-1458) CFSTI: HC\$3.00/MF\$0.65 CSCL 201

The propagation of longitudinal waves in three fluid, partly ionized gases is studied as a function of the collision and plasma-to-wave-frequency ratios. A collisional approach is taken with the full Boltzmann equations (together with Maxwell's equations) serving as the starting point, the intention being to describe wave dispersion and absorption in the collisional regime, and to include the viscous and heat conduction effects on the wave propagation from the beginning as an integral part of the theory. Author

N68-19624*# National Aeronautics and Space Administration, Washington, D. C.

CONSTRUCTING INEXPENSIVE AUTOMATIC PICTURE-TRANSMISSION GROUND STATIONS

Charles H. Vermillion 1968 68 p refs

(NASA-SP-5079) CFSTI: HC \$3.00/MF \$0.65 CSCL 17B

This report describes how one can procure or build the antenna, FM receiver, and other components for an Automatic Picture Transmission (APT) ground station. Detailed drawings and parts lists are included. Installation, alignment, and operation of the APT ground station are also described. APT ground stations are inexpensive and reliable. They can be built from surplus parts for under \$500 or procured for as low as \$5000. With them, scientists, local weather stations, amateurs, and others can receive satellite-taken photographs of the Earth as APT-equipped satellites pass overhead. It is currently planned that APT systems compatible with the ground station will be flown on Nimbus and ESSA satellites at least until 1972. It is probable that similar or advanced APT systems will be available after 1972, although these programs are still in a tentative planning stage.

N68-20333*# National Aeronautics and Space Administration. Langley Research Center, Langley Station, Va.

THE INPUT ADMITTANCE OF A RECTANGULAR APERTURE ANTENNA LOADED WITH A DIELECTRIC PLUG Calvin T. Swift and Douglas M. Hatcher Washington Apr. 1968

27 p refs

(NASA-TN-D-4430) CFSTI: HC\$3.00/MF\$0.65 CSCL 09F

A waveguide-fed rectangular aperture antenna, loaded with a dielectric plug, is considered as a variational problem. The formulation results in an aperture-admittance expression which contains the self and mutual admittances of the transverse electric waveguide modes TE_{01} and TE_{03} . The theoretical results show that a gross distortion of the aperture field and a significant decrease in the aperture admittance occurs when the plug becomes a resonant cavity for the TE_{03} mode. The input admittance is compared with microwave measurements for the condition in which the external half-space is air. The theory is generally in good agreement with experiment over the entire waveguide band, including the frequency interval around resonance. It is noted that the plug can be used to tune out the susceptance and improve the match of the antenna. Author

N68-22019*# National Aeronautics and Space Administration. Goddard Space Flight Center, Greenbelt, Md. OPTICAL AND MICROWAVE COMMUNICATIONS: A

COMPARISON

F. Kalil Washington May 1968 46 p refs

(NASA-TN-D-3984) CFSTI: HC\$3.00/MF\$0.65 CSCL 17B

Some preliminary comparisons are made of microwave, millimeter, and optical communication systems for space communication from a spacecraft at Mars distances. An attempt is made to be realistic with regard to technology. Some discussion of thermal, quantum, and sky noise is included, as well as some discussion and analyses of microwave, millimeter wave, and optical technology; acquisition and tracking; and some mission analysis. Based on the considerations herein, it appears likely that in the radio spectrum, the S-Band is the better place to operate. However, it also appears likely that optical communication systems have the greater potential for higher data rates—up to about 10⁸ bps at Mars distances.

N68-22746*# Ohio State Univ., Columbus.

THE TEM RADIATION PATTERN OF A THIN-WALLED PARALLEL-PLATE WAVEGUIDE ANALYZED BY A SURFACE INTEGRATION TECHNIQUE

D. C. F. Wu Washington NASA May 1968 52 p refs

(Grant NsG-488)

(NASA-CR-1052; Rept.-1691-23) CFSTI: HC \$3.00/MF \$0.65 CSCL 09F

The radiation pattern of a TEM mode thin-walled parallel-plate waveguide is analyzed by a surface integration technique in conjunction with wedge diffraction theory. The surface integral is obtained by the Green's second identity. The fields on the surface are calculated by plane wave diffraction and first order interactions between two edges of the guide. The surface integration technique provides an improvement in the accuracy of the pattern as compared to the wedge diffraction method. Author

N68-24845*# National Aeronautics and Space Administration. Manned Spacecraft Center, Houston, Tex.

AN INTEGRATED-CIRCUIT DIRECT-COUPLED AMPLIFIER FOR SPACECRAFT USE

Guss E. Wenzel Washington May 1968 72 p refs

(NASA-TN-D-4584) CFSTI: HC\$3.00/MF\$0.65 CSCL 09F

The integrated-circuit direct-coupled differential-amplifier design is based on a previous phase of development and has advanced the state-of-the-art of direct-coupled amplifiers to the extent that the stability and driff characteristics are equal to, or superior to, the conventional high performance chopper direct current amplifier. The circuit diagrams and the physical layout of, the various components are presented. The amplifier performance, when powered from a typical flight battery, is described by various tables and plots of test data. Author

N68-25852*# National Aeronautics and Space Administration. Electronics Research Center, Cambridge, Mass. CODING SCHEMES FOR RUN-LENGTH INFORMATION

BASED ON POISSON DISTRIBUTION

W. W. Happ Washington Jun. 1968 19 p refs

(NASA-TN-D-4572) CFSTI: HC\$3.00/MF\$0.65 CSCL 09D

The Shannon-Fano-Huffman Redundancy Reduction Procedure is extended to one-parameter and two-parameter Poisson distribution resulting from run-length information streams. Figures-of-merit are established to compare Huffman coding to fixed-word-length binary coding on the basis of (1) average number of coding digits per message, (2) signal-to-noise ratio in analog-to-digital conversion due to bit errors, and (3) design criteria primarily of interest to the system designer and not readily amenable to quantitative analysis. To ascertain whether or not Huffman coding leads to a unique and optimum code, other equally good optimum solutions were obtained. Optimization and uniqueness criteria are examined and applications to data compression are discussed.

N68-25918*# National Aeronautics and Space Administration. Langley Research Center, Langley Station, Va.

AN OMNIDIRECTIONAL FLUSH-MOUNTED MICROWAVE ANTENNA WITH A SIMPLE FEED FOR USE ON SPACECRAFT

C. R. Cockrell and W. F. Croswell Washington Jun. 1968 28 p refs

(NASA-TN-D-4555) CFSTI: HC\$3.00/MF\$0.65 CSCL 09F

The qualitative theory, design, and development of a parallel-plate waveguide-fed antenna, suitable for flush-mounted broad-band spacecraft applications are presented. The antenna makes use of wedge-like metal posts placed uniformly about the periphery of the feed plates to provide both structural strength and practical interconnection routes for cables without disrupting the antenna impedance and patterns. Measurements taken on the antenna which is mounted on spheroids up to 50 wavelengths in circumference are presented, equatorial patterns are omnidirectional within ± 0.25 dB, and polar patterns have beam widths similar to a half-wave dipole. Author

N68-26621 *# Andrew Corp., Chicago, III. THE DIELECTRIC CLAD AXIAL SLOT ANTENNA

C. M. Knop, J. J. Meier, and O. K. Kim Washington NASA Jun. 1968 201 p refs

(Contract NAS1-6242)

(NASA-CR-1057) CFSTI: HC \$3.00 /MF \$0.65 CSCL 09F

The input admittance of a rectangular waveguide whose opening forms an axial slot on a metal cylinder of outer radius, a, which is coated with a concentric layer of homogeneous dielectric of outer radius, b, and of relative dielectric constant, ϵ_r , is analyzed. The analysis is accomplished by relating this input admittance to the external admittance by equating the complex power flow on each side of the slot. The external admittance is found by expanding the fields in the exterior of the cylinder in the form of a Fourier mode expansion following Wait, and casting the expression for the integration of Poynting's vector over the physical space of the slot into one over mode space via Parseval's theorem. The slot width is made small enough so that the higher order modes produced at the slot in the waveguide due to the slot-cylinder transition are negligible. Additionally, the guide is dielectric loaded, so as to realize sufficiently high attenuation at the slot location of the higher order modes produced at the excitation point for a given length of auide. Author

N68-27063*# Martin Co., Orlando, Fla.

PROPAGATION OF MILLIMETER AND SUBMILLIMETER WAVES

V. E. Derr Washington NASA Aug. 1967 225 p refs

(Contract NAS12-10)

(NASA-CR-863; OR-8549) CFSTI: HC \$3.00/MF \$0.65 CSCL 17B

The instrumentation development for absorption measurements is discussed. Calculations and a search for O, submillimeter transitions are described. Spectroscopic investigations of the Stark effect in water have been used to confirm level assignment and to determine a new value of the dipole moment of water by a more accurate dc voltage method. A chemical analog of water, D20, has been observed near 300 GHz. A discussion of orientation relaxation theory is presented, as well as a consideration of quadrupole interaction in CO2. A computer program that is suitable for computation of low J value transitions in asymmetric top molecules has been developed for the Kivelson-Wilson theory of centrifugal effects. Based on all available data from 100 to 1000 to be met by antenna systems that are concerned with earth lunar missions which include lunar rendezvous, lunar landing, and earth rendezvous; and other promising antenna techniques whose development can be expected to provide enhanced performance and Author flexibility in over-all mission design.

N68-28135*# Hughes Aircraft Co., Culver City, Calif. STUDY OF ADVANCED ANTENNA TECHNIQUES FOR RENDEZVOUS RADAR

B. J. Forman, S. N. Vodopia, and W. H. Kummer Washington NASA May 1967 52 p refs

(Contract NAS1-2621)

(NASA-CR-764) CFSTI: HC\$3.00/MF\$0.65 CSCL 171

A study of advanced antenna techniques for rendezvous and lunar landing radar systems is reported. The study was made in order to better define the antenna requirements for future manned spacecraft missions and to demonstrate the extent to which these requirements can be met within the present state-of-the-art. Recommendations have been made for antenna techniques that show promise in extending antenna technology. One such technique, which employs diode-irises to accomplish electronic-beam scanning, has been investigated and shown to be feasible. Technical material

07 COMMUNICATIONS

presented discusses results of the investigation on electronic scanning using diode-irises. The design and complete electrical performance of an X-band 10-element slot array is given. Included is a summary of a previous report which details the requirements GHz, the absorption spectrum of water is computed by two methods with different form factors, in order to present a comparison. Author

N68-28272*# Systems Technology, Inc., Hawthorne, Calif. AN EXPERIMENTAL INVESTIGATION OF COMPENSATORY AND PURSUIT TRACKING DISPLAYS WITH RATE AND ACCELERATION CONTROL DYNAMICS AND A DISTURB-ANCE INPUT

R. W. Allen and H. R. Jex Washington NASA Jun. 1968 77 p refs

(Contract NAS2-3746)

(NASA-CR-1082; TR-170-1) CFSTI: HC \$3.00/MF \$0.65 CSCL 17G

Four instrument-rated pilots were trained and tested with a series of different tracking displays and controlled element dynamics to validate some anomalous previous experiments and to provide a sounder data base for a theory of manual control displays. Quasi-random (sum of 9 sinusoids) inputs were used. Compensatory (C) and pursuit (P) display modes were investigated along with a hybrid pursuit-plus-disturbance (P+D) display mode. For P+D the command input was displayed conventionally, while a separate, uncorrelated disturbance input was applied to the controlled element. Rate control and acceleration control dynamics were investigated. The training data show that all pilots learned quickly to perform about equally well with all displays when controlling rate dynamics. With acceleration dynamics they took much longer to learn and the results showed more variability. In the main experiment, the error performance was not sensitive to display mode, while the describing function data showed that differences in the pilot's behavior did occur, with opposing effects leading to the constant net error. Author

N68-29528*# National Aeronautics and Space Administration. Electronics Research Center, Cambridge, Mass. M-ARY POISSON DETECTION AND OPTICAL

COMMUNICATIONS

Sherman Karp and Robert M. Gagliardi (Univ. of Southern Calif., Los Angeles) Washington Jun. 1968 26 p refs

(NASA-TN-D-4623) CFSTI: HC\$3.00/MF\$0.65 CSCL 17H

This report presents an investigation of the problem of maximum likelihood detection of one of M Poisson processes in a background of additive Poisson noise. When the observables correspond to counts of emitted photoelectrons, the problem models a discrete version of a coherent M-ary optical communication system using photon counters in the presence of background radiation. Consideration is given to an average distance and a detection probability criterion. The advantages of an M-ary-pulsed intensity set (Poisson intensities wholly concentrated in a single counting interval) are demonstrated. The performance of such intensity sets is exhibited in terms of error probabilities, pulse widths, signal-to-noise ratio, and channel capacity. Behavior as a function of number of intensities M is also discussed. By appropriate conversion these latter results may be used for determining power requirements in an optical pulse position modulation system. Author

N68-31639*# National Aeronautics and Space Administration. Electronics Research Center, Cambridge, Mass.

RESEARCH ON FIELD-ALIGNED PROPAGATION OF HF RADIOWAVES USING ALOUETTE 2 TOPSIDE SOUNDER DATA AND DIGITAL RAY-TRACING TECHNIQUES Jayaram Ramasastry, Edward J. Walsh, and John R. Herman (Lowell Technol. Inst. Res. Found.) Washington Aug. 1968 34 p refs Presented at the AGARD meeting, Oslo, 19–23 Aug. 1968 (NASA-TN-D-4748) CFSTI: HC \$3.00/MF \$0.65 CSCL 17B

The first part of this technical note covers the study of guidance of HF radiowaves along field-aligned paths using the topside sounder data from the Alouette 2 satellite. More than 100,000 Alouette 2 ionograms have been used in this analysis and an unusually high percentage of occurrence of conjugate echoes has been observed in the data of some equatorial stations. Two interesting types of ionograms containing conjugate echo traces are presented. A self-consistent explanation based on the assumption of multiple reflections between conjugate points of the field line passing through the satellite is presented. The second part of the note covers the results of the digital ray tracing study of the guidance of HF radiowaves along field-aligned ionization irregularities in the magnetosphere of the earth. The results reported here on the HF ducting phenomenon is directed primarily towards determining whether such a mechanism may be utilized to study the magnetospheric phenomena and whether it can be useful as a reliable communication link. Author

N68-33042*# Stanford Research Inst., Menlo Park, Calif. THE EFFECTS OF A PLASMA IN THE NEAR-ZONE FIELD OF AN ANTENNA, 2

W. C. Taylor Washington NASA Sep. 1968 38 p refs (Contract NAS1-7024)

(NASA-CR-1149) CFSTI: HC\$3.00/MF\$0.65 CSCL 09F

Measurements are reported on the effects on an antenna of a plasma in the near field. In one phase of the program, admittance measurements were performed with a Teflon-plugged waveguide slot antenna radiating into the flowing ionized gas of an arc-driven shock tube. The electron density was varied above and below the critical density at two different values of shock-tube pressure. The results are compared with theoretical predictions. Measurements were also made in the same shock tube to determine the ionization rise times in normal-shock-heated air and other planetary gas mixtures. The principal results of these measurements were to supply the ionization rise history in air and in a 90-percent $N_2/10$ -percent $\rm CO_2$ mixture over a wide range of pressures and shock speed. Author

N68-35140*# National Aeronautics and Space Administration. Goddard Space Flight Center, Greenbelt, Md.

ON THE DECREASE OF THE RADAR CROSS SECTION OF THE APOLLO COMMAND MODULE DUE TO REENTRY PLASMA EFFECTS

John W. Marini Washington Sep. 1968 22 p refs

(NASA-TN-D-4784) CFSTI: HC\$3.00/MF\$0.65 CSCL 17I

A number of mechanisms have been proposed to explain the observed decreases. One of these is the plasma sheath which, at certain combinations of altitude and speed, may act as an absorbant coating. In another, the inhomogeneous plasma sheath may present to the incident radar wave a reflecting surface having, because of its shape, a lower cross section than the original body surface. With the reentry object, radar frequency, and radar look-angle fixed, the regions where these mechanisms are likely to have effect depends primarily on the altitude and speed of the object. The regions of decrease caused by the two mechanisms listed are determined. The case considered is that of a C-band radar observing a large directly approaching object. Neither the possibility of a decrease caused by photoionization nor the effect of the sheath on a radar observing the object at other than a head-on view has yet been treated. Because of the incomplete and tentative nature of the analyses and because of a lack of field data on reentries of the Apollo type, it is premature to say whether the effects constitute a practical tracking problem. Author

N68-35172*# Ohio State Univ., Columbus. THE REFLECTION COEFFICIENT OF A TEM MODE PARALLEL-PLATE WAVEGUIDE ILLUMINATING A CONDUCTING SHEET: THE LARGE WEDGE ANGLE CASE W. D. Burnside, L. L. Tsai, and R. C. Rudduck Washington NASA Sep. 1968 46 p refs

(Grant NGR-36-008-048)

(NASA-CR-1174) CFSTI: HC \$3.00 /MF \$0.65 CSCL 20N

The reflection coefficient of a large wedge angle parallel plate waveguide operating in the TEM mode and illuminating a perfectly conducting sheet is analyzed by wedge diffraction techniques. The interactions between the waveguide aperture and the reflector are represented by bouncing cylindrical waves. The scattering of these cylindrical waves by the guide aperture produces four subsequent component cylindrical waves, which in turn reflect back onto the guide. These component cylindrical waves are determined through analysis and are represented by equivalent line sources which then couple power into the guide. The continuation of this reiteration process then includes the contribution of the higher order interactions (or bounces). Good agreement is obtained between the calculated results and measurements. The calculated results also agree with those obtained by the plane wave approach in the region of mutual validity for both analyses. Author

N68-35174*# National Aeronautics and Space Administration. Electronics Research Center, Cambridge, Mass. THE DESIGN OF A PULSE POSITION MODULATED (PPM)

OPTICAL COMMUNICATION SYSTEM

Sherman Karp and Robert M. Gagliardi (Univ. of Southern Calif., Los Angeles) Washington Oct. 1968 25 p refs

(NASA-TN-D-4814) CFSTI: HC\$3.00/MF\$0.65 CSCL 17B

In recent literature the advantages of an idealized narrow width pulse position modulated (PPM) optical communication system, using coherent sources and direct photo-detection, have been shown. In this report, the practical design of such an operating PPM link is considered. System performance, in terms of error probabilities and information rates, are derived in terms of key parameters, such as power levels, number of PPM signals, pulse width, and bandwidths. Both background radiation and receiver thermal noise are included. Design procedures utilizing these data are outlined. Whenever possible, optimal design values and parameter trade-offs, in terms of maximizing information rate or minimizing transmitter power, are shown. The effect on performance of photomultipliers and their inherent statistics is also presented. Although the basic analysis is derived in terms of photon counts, the necessary system optics equations are introduced to allow for overall optical hardware design. The primary underlying assumption is that synchronization is maintained at all times between transmitter and receiver. Author

N68-35522*# National Aeronautics and Space Administration. Electronics Research Center, Cambridge, Mass. PROBLEMS AND PROGRAMS ON THE USE OF

SUBMILLIMETER WAVES IN SPACE

Max R. Nagel Washington 1968 49 p refs (NASA-SP-182) CFSTI: HC\$3.00/MF\$0.65 CSCL 09F

æŝ.

The development and the present status of the technology associated with the use of submillimeter waves in field and space applications are described. A compilation of tables, graphs, and other data on the performance of modern submillimeter components is given, along with a list of the most recent literature on the subject. Some of the more significant achievements and the potential of submillimeter waves in the atmospheric and astronomical disciplines and in spaceflight-related operations, are discussed. A review of related programs currently sponsored by the National Aeronautics and Space Administration is given and high priority research needs that may lead to a more effective utilization of submillimeter radiation in space are pointed out. Author N68-35524*# National Aeronautics and Space Administration. Langley Research Center, Langley Station, Va.

HIGHER-ORDER-MODE EFFECTS ON THE APERTURE ADMITTANCE OF A RECTANGULAR WAVEGUIDE COVERED WITH DIELECTRIC AND PLASMA SLABS

C. R. Cockrell Washington Oct. 1968 44 p refs (NASA-TN-D-4774) CFSTI: HC\$3.00/MF\$0.65 CSCL 09F

Variational expressions of the admittance of a rectangular aperture covered with homogeneous material are derived. The electric field inside the waveguide is assumed to be a dominant mode plus the first higher order symmetrical mode. Admittance expressions are also given for semi-infinite media. Admittance calculations for polystyrene slabs are given. These calculations are shown to agree closely with results in the literature. Also given are calculations for lossy plasma slabs with electron densities both above and below the critical density. For plasma slabs approximately equal to or greater than 1/3 λ_0 , the medium can be considered semi-infinite, particularly for overdense plasmas. For changing slab thickness, the field of the higher order mode has a greater effect on the admittance in the dielectric slab than in the plasma slab. However, this effect is small; hence, only the dominant mode field is needed for computing aperture admittance. Author

N68-35537*# National Aeronautics and Space Administration. Langley Research Center, Langley Station, Va.

ELECTROMAGNETIC PROPERTIES OF A CIRCULAR APERTURE IN A DIELECTRIC-COVERED OR UNCOVERED GROUND PLANE

M. C. Bailey, S. N. Samaddar (Raytheon Co., Alexandria, Va.), and Calvin T. Swift Washington Oct. 1968 30 p refs

(NASA-TN-D-4752) CFSTI: HC\$3.00/MF\$0.65 CSCL 09F

The problem of an aperture fed by a circular waveguide excited in the dominant transverse electric mode $(TE_{1,1})$ is considered. The input admittance in the aperture reference plane for the case of a homogeneous lossy dielectric cover of finite thickness and the radiation patterns for the case of no cover are computed from integral transforms, for which a TE_{11} mode variation of the electric field is assumed at the aperture. Computations for the uncoated antenna show that the patterns and aperture admittance are similar to those of a square aperture with a field distribution given by the TE_{01} rectangular mode. It is noted that the uncoated aperture is well matched above midband of the circular waveguide in contrast to the open-end rectangular waveguide. This inherent property would be advantageous for possible use of the open-end circular waveguide as an antenna. Author

N68-36105*# National Aeronautics and Space Administration. Electronics Research Center, Cambridge, Mass.

ERROR PROBABILITIES FOR MAXIMUM LIKELIHOOD DETECTION OF M-ARY POISSON PROCESSES IN POISSON NOISE

Sherman Karp, Martin G. Hurwitz, and Robert M. Gagliardi (Univ. of Southern Calif., Los Angeles) Washington Oct. 1968 48 p refs

(NASA-TN-D-4721) CFSTI: HC\$3.00/MF\$0.65 CSCL 09D

Some of the recent results in the detection of a Poisson distributed signal in Poisson noise are considered. Curves for error probabilities are presented for the case of detecting one of M equiprobable signals over a broad range of parameter values. Implicit in these results for system applications is the use of photon counting receivers. Attention is given to the optical communication and radar problems for this receiver structure and significant parameters are translated into those used in the report. A complete description of the computational procedures used for making the error probability calculations is given. Author

07 COMMUNICATIONS

N68-36333*# National Aeronautics and Space Administration. Goddard Space Flight Center, Greenbelt, Md.

SELF-SYNCHRONIZING BI-ORTHOGONAL CODED PCM TELEMETRY SYSTEM

Warner Miller, Ronald Muller, Thomas Taylor, and John Yagelowich Washington Oct. 1968 29 p refs

(NASA-TR-R-292) CFSTI: HC\$3.00/MF\$0.65 CSCL 09F

Details are given on the complete design, theory, and experimental statistics of a self-synchronizing, biorthogonal coded PCM telemetry system for space communications. By selecting a proper code set, word synchronization is acquired without using a parallel channel and is maintained at a signal-to-noise ratio below 4 db. With the code's property of comma freedom, work synchronization can be achieved with a circuit requiring only a few logic modules. With the use of this circuit, signal detection can be performed in real time without the use of a computer. The measured probability of word error corresponds to a signal-to-noise ratio that is within 1 db of theoretical predictions; this is 3 db better than is obtained with the standard PCM systems now used on spacecraft.

O8 COMPUTERS

Includes computer operation and programming; and data processing. For basic research see: 19 Mathematics.

N68-13897*# Philco Corp., Houston, Tex. COMPUTER ASSISTED INSTRUCTION. FEASIBILITY STUDY

Richard L. Balogh and Don L. Purdum Washington NASA Jan. 1968 445 p refs

(Contract NAS9-1261)

(NASA-CR-917; PHO-TR-307) CFSTI: HC \$3.00/MF \$0.65 CSCL 09B

Results of a study to assess the potential of using advanced concepts for training flight controllers are presented. Existing computer systems are reviewed and analyzed, and their applicability to flight controller training is deterimed. The functional requirements for an optimum computer assisted system are developed. Costs incurred by programmed instruction are evaluated, and a study is made to determine if this is a cost-effective method of training NASA flight controllers. C.T.C.

N68-15798*# National Aeronautics and Space Administration. Lewis Research Center, Cleveland, Ohio.

NUMERICAL PROCEDURES FOR CALCULATING REAL FLUID PROPERTIES OF NORMAL AND PARAHYDROGEN Fredric N. Goldberg and Angela M. Haferd Washington Feb. 1968 62 p refs

(NASA-TN-D-4341) CFSTI: HC\$3.00/MF\$0.65 CSCL 20M

The library of single function calls can be used efficiently without initial estimates. When physical conditions are known, engineering estimates of density may be included for additional speed in calculation. The procedures are designed to calculate a specified function of one or two input parameters. Independent variables consist of the combinations temperature-density, pressure-density, temperature-pressure, enthalpy-pressure, or entropy-pressure. Ideal and saturation properties may also be calculated as functions of either temperature or pressure. The program is written in separate modules that can be modified easily in the future to include new data. These modules can be used as a subset of functions when computer space is not available for the entire library in complex programs. The discussion includes techniques used, resolution of inherent physical and mathematical problems, and consistency of results based on National Bureau of Standards data. Computer time and storage estimates are given with a manual of instructions for the programmer. A listing of the program is included as used in the library of functions at the Lewis Author Research Center.

N68-17154*# Little (Arthur D.), Inc., Cambridge, Mass. APPLICATION OF STATISTICAL ASSOCIATION TECH-NIQUES FOR THE NASA DOCUMENT COLLECTION

Paul E. Jones, Robert M. Curtice, Vincent E. Giuliano, and Murray E. Sherry Washington NASA Feb. 1968 111 p refs (Contract NASw-1051)

(NASA-CR-1020) CFSTI: HC \$3.00/MF \$0.65 CSCL 05B

Computer programs for batched associative search of the NASA coordinate-indexed document collection have been prepared and tested. Cooccurrence counts for the approximately 18,000 terms used to index about 100,000 documents were obtained and association matrices based on various subsets of these counts

were developed. One section of the report describes the system as a whole; the remainder is focused on a discussion of the behavior of the system observed during tests of the programs. Author

N68-18144*# Avco Corp., Wilmington, Mass. INVESTIGATION OF THE DYNAMIC CHARACTERISTICS OF A V ANTENNA FOR THE RAE SATELLITE, PHASE A Final Report

Washington NASA Mar. 1968 211 p refs

(Contract NAS5-9179)

(NASA-CR-962; RAD-TR-65-28) CFSTI: HC \$3.00/MF \$0.65 CSCL 09F

This report presents the results of the first phase of an investigation of the dynamic characteristics of the Radio Astronomy Explorer satellite equipped with a double-V antenna. During this first phase, computer programs which will provide the analytical tools necessary for continued study of the satellite dynamic performance have been prepared. For this purpose, a flexible-body analog computer program, a rigid-body digital computer program, and a flexible-body digital computer program were developed. The first two programs have been checked out and are fully described and included in this report, together with results of checkout runs. The flexible-body computer program is being checked out; the detailed derivation and description of the simulation is contained in this report. It is recommended that the next phase of the study provide for improvement in the accuracy and capability of the computer simulations and evaluation of satellite and control system dynamics, damping requirements, and overall satellite design. Author

N68-18179*# National Aeronautics and Space Administration. Goddard Space Flight Center, Greenbelt, Md.

A LOGARITHMIC ENCODER FOR BINARY WORD COMPRESSION

Joseph A. Sciulli Washington Mar. 1968 12 p refs

(NASA-TN-D-4290) CFSTI: HC\$3.00/MF\$0.65 CSCL 09D

The present paper describes a logarithmic encoding device which has had particular application in energetic particle detection experiments. The paper provides a generalized encoding error analysis in order to evaluate the performance of the device. Both peak and average error are derived in terms of word size and desired accuracy. The implementation of a flexible logarithmic encoder is also described. Author

N68-18620*# National Aeronautics and Space Administration. Lewis Research Center, Cleveland, Ohio.

ANALYTICAL INVESTIGATION OF SUPERSONIC TURBOMACHINERY BLADING. 1: COMPUTER PROGRAM FOR BLADING DESIGN

Louis J. Goldman and Vincent J. Scullin Washington Mar. 1968 66 p refs

(NASA-TN-D-4421) CFSTI: HC\$3.00/MF\$0.65 CSCL 10A

A FORTRAN IV computer program for the design of supersonic blading based on establishing vortex flow within the blade passage is presented. The method of characteristics, as applied to the

08 COMPUTERS

two-dimensional isentropic flow of a perfect gas, was utilized for the blade design. The equations necessary for the design are developed. The information required for the program consists of an inlet flow angle, specification of the inlet, outlet, and lower- and upper-circular-surface Mach numbers, and the specific-heat ratio. The program output consists of the blade coordinates and, if desired, a printer plot of the blade profile and flow passage. In addition, supersonic starting and flow separation calculations are performed by the program and obtained as output. An example is included to indicate the use of the program and the results obtainable. Author

N68-19336*# National Aeronautics and Space Administration. Electronics Research Center, Cambridge, Mass. SOME ARGUMENTS FAVORING NON-CONVENTIONAL

TYPES OF COMPUTERS

Wayne A. Lea Washington Mar. 1968 35 p refs (NASA-TM-X-1544) CFSTI: HC\$3.00/MF\$0.65 CSCL 09B

This paper considers the basic question of the adequacy of conventional, general-purpose digital computers, and whether new, non-conventional machine structures would be useful for expanding the capabilities of machine performance, to permit automatic solution of problems previously handled only by humans. Included in the class of "non-conventional" machines discussed herein are hybrid machines, multiprocessors, highly parallel computers, Holland and SOLOMON machines, bionics models, diffused-function anastomotic networks, pattern recognition machines, "linguistically intelligent" machines, and other more exotic machines. Several arguments favoring non-conventional machine structures are presented. Considered separately are arguments based on: (a) the opinions of certain experts; (b) ultimate theoretical capabilities of various machine types; (c) structures of biological counterparts in brains and nervous systems; (d) the potential for natural-language programming; (e) relative computational economies and efficiencies; and (f) the potential for successful development of new types of computer structures. Such arguments demonstrate the problems one can get into by confining study to present-day digital computer organizations, and the potential advantages of new, user-oriented Author designs.

N68-21499*# National Aeronautics and Space Administration. Lewis Research Center, Cleveland, Ohio.

COMPUTER PROGRAMS FOR PLANE COLLISIONLESS SHEATHS BETWEEN FIELD-MODIFIED EMITTER AND THERMALLY IONIZED PLASMA EXEMPLIFIED BY CESIUM Susan L. Button and James F. Morris Washington Apr. 1968

70 p refs (NASA-TM-X-1562) CFSTI: \$3.00 CSCL 201

Two computer programs coded in FORTRAN IV are described for plane collisionless positive-ion and electron emission sheaths. Given the emitter temperature, emitter work function, atomic ionization potential, plasma electron and ion number density, and plasma electron, ion, and atom temperatures, the programs compute current densities, potential drop through the sheath, charge density, electron field, and sheath distance. Author

N68-22510*# National Aeronautics and Space Administration. Goddard Space Flight Center, Greenbelt, Md.

SPACE SCIENCES DATA PROCESSING

George H. Ludwig Washington May 1968 19 p refs (NASA-TN-D-4508) CFSTI: HC \$3.00/MF \$0.65 CSCL 09D

Spacecraft carrying large numbers of scientific instruments presently transmit data at the rate of approximately 150 million data points per day which must be converted from raw digital form into a conceptually meaningful form for analysis. The task of processing these data rapidly and accurately is a large one, done in several steps. The first step involves converting the raw receiver output signals into computer compatible digital form, including signal clean-up, establishment of synchronization, and time decoding. In the newest processing lines, this first step also includes a moderate amount of editing and quality checking. The remaining steps employ large-scale computers for further editing, establishing accurate timing, computing spacecraft attitude, and sorting to provide data tapes for individual experimenters. The experimenters are responsible, at present, for further reduction to a more meaningful form. These operations include additional sorting, storage, compilation, computation, and display. Author

N68-24310*# National Aeronautics and Space Administration. Goddard Space Flight Center, Greenbelt, Md.

DUAL DETECTION SYSTEM FOR AIMP PFM DATA PROCESSING

Thomas J. Karras Washington May 1968 18 p

(NASA-TN-D-4561) CFSTI: \$3.00 CSCL 09F

A dual detection system, used at present to process PFM telemetry data for satellites AIMP D and E at GSFC, has proved superior to a single threshold detection system. The dual system consists of: (1) threshold detection of 128 individual filters during buildup, when the filters are excited with a PFM burst, and (2) "auction detection," i.e., one filter (out of 128) which contains the largest amplitude near the end of the filter buildup. The threshold method is used only for system synchronization; the auction method is used only for data recovery. Auction and threshold detection use the same bank of filters. Up to 10 percent more data recovery on actual AIMP satellite tapes is being achieved; diminution up to one half in rms error in the experimenters analog data is expected. Test results on reprocessed telemetry data have shown a definite improvement in data recovery and resolution. The incoming signal-to-noise threshold of the system has not been lowered, because line synchronization has remained unchanged. Author

N68-24967*# National Aeronautics and Space Administration. Lewis Research Center, Cleveland, Ohio.

COMPUTER PROGRAM FOR SYMBOLIC REDUCTION OF BLOCK DIAGRAMS USING FORMAC

Carl F. Lorenzo and Paul Swigert Washington, D. C. Jun. 1968 78 p refs

(NASA-TN-D-4617) CFSTI: HC\$3.00/MF\$0.65 CSCL 09B

Techniques have been established and a computer program has been written (in the experimental language, FORMAC) to symbolically reduce arbitrary block diagrams for desired transfer functions. Symbolic solutions are determined in several forms including an expanded form in terms of the driving frequency and system constants. Programs are written to numerically evaluate the symbolic solutions for real and imaginary parts and magnitude ratio and phase angle. The programs have been applied to several research problems which include both lumped and distributed parameter systems. The latter forms are built into the program and are handled automatically. Author

N68-25002*# National Aeronautics and Space Administration. Manned Spacecraft Center, Houston, Tex.

HYDRA 1 DATA DISPLAY SYSTEM

Roger L. Hodgkins and Donald R. Osgood Washington May 1968 22 p

(NASA-TN-D-4554) CFSTI: HC\$3.00/MF\$0.65 CSCL 09B

Details are given on the Hydra 1 which is an extremely flexible and versatile data display system. A television monitor screen serves as a working surface upon which an operator can develop, or create, graphic displays such as written documents, charts, diagrams, graphs, background slides, and other graphic art through the use of special control keyboards and operating techniques. An operator can create, rearrange, delete, or add to the graphic display to develop any desired format. Upon completion of a graphic display, it can be recorded in a magnetic tape library, plotted on an X-Y plotter, recorded as a punched paper tape, or recorded as a frame of a sequential playback magnetic tape. Displays recorded in the magnetic tape library can be recalled for examination or revision. N68-25268*# National Aeronautics and Space Administration. Goddard Space Flight Center, Greenbelt, Md.

DIGITAL SPECTRAL ANALYSIS

Anthony J. Villasenor Washington Jun. 1968 49 p refs (NASA-TN-D-4510) CFSTI: HC\$3.00/MF\$0.65 CSCL 09B

This paper presents some mathematical considerations of spectral analysis and some FORTRAN computer programs that use the Fast Fourier Transform algorithm of Cooley and Tukey. These programs compute Fourier amplitude and phase spectra, cross-power spectra, auto- and cross-correlation, and filtered spectra, as well as some other frequency domain functions. Author

N68-26640 *# National Aeronautics and Space Administration. Lewis Research Center, Cleveland, Ohio.

PRACTICAL STABILITY CRITERION AND ITS APPLICATION TO DIGITAL SIMULATION

Leslie L Scalzott and Carl F. Lorenzo Washington Dec. 1967 36 p refs

(NASA-TN-D-4203) CFSTI: HC\$3.00/MF\$0.65 CSCL 09B

A stability criterion has been developed for use with digital simulations or graphical data. The criterion used is a simple one, which basically requires ultimate state boundedness of the time function representing the system output. Techniques are established so that a transient of finite duration may be used as a practical indication of stability. A stability test utilizing the criterion has been implemented into a general digital program which will allow the determination of system stability directly by computer. This program and criterion was demonstrated for three applications representing: (1) a linear system, (2) a continuously nonlinear system, and (3) a discontinuously nonlinear system. Author

N68-29404*# National Aeronautics and Space Administration. Flight Research Center, Edwards. Calif.

X-15 ANALOG AND DIGITAL INERTIAL SYSTEMS FLIGHT EXPERIENCE

Melvin E. Burke Washington Jul. 1968 22 p refs

(NASA-TN-D-4642) CFSTI: HC\$3.00/MF\$0.65 CSCL 17G

Two different types of inertial flight data systems, an analog system and a digital system, have been used during the X-15 program to provide primary flight information for the X-15 pilot. This use has afforded an opportunity to compare the two mechanization concepts in the same operating environment. The two systems, although having basically different computers, use similar inertial measurements units. Equation mechanization is different primarily because of the difference in computers. The development problems on the analog system were considerably more complex than those with the digital system, inasmuch as the analog unit was the first of the miniature units conceived and thus was put into operation before it could be refined. These development problems ultimately brought about the redesign of the analog system and the utilization of the digital system. The performance of the analog and digital systems has been adequate for X-15 requirements. The performance of the digital system has indicated that it is a highly accurate mechanization, with the only significant problem that of the computer susceptibility to power transients. The digital system also provides a more flexible mechanization than the analog system through the programming capabilities of the computer. Author

N68-30240*# National Aeronautics and Space Administration. Manned Spacecraft Center, Houston, Tex.

SOME LABORATORY TECHNIQUES OF WAVE ANALYSIS WITH APPLICATION TO THE APOLLO PROGRAM Roy A. Watlington Aug. 1968 49 p refs

(NASA-TM-X-1599; S-157) CFSTI: HC \$3.00/MF \$0.65 CSCL 09B

Time and frequency correlation, root-mean-square time histories, and power-spectral density analysis techniques are applied not only in perfecting communication systems but also in gaining vital information on the chemical and physical nature of things. The sophisticated instruments and techniques of the present age have

made it possible to record, synthesize, and analyze wave data rapidly and in depth. This paper examines and discusses some of the major techniques of wave analysis being applied to the Apollo Program, describes the instrumentation involved, and provides an illuminating mathematical foundation for the analyses. Author

N68-31499*# North American Rockwell Corp., Anaheim, Calif. STUDY OF SPACEBORNE MULTIPROCESSING, PHASE 2. **VOLUME 1: SUMMARY**

L. J. Koczela Washington NASA Aug. 1968 45 p ref (Contract NAS12-108)

(NASA-CR-1158; C6-1476.22/33, V. 1) CFSTI: HC \$3.00/MF \$0.65 CSCL 09B

This final report presents the results of a research study of an advanced multiprocessor computer organization for future space missions. The organization is entitled the "Distributed Array Memory and Processor" computer. A manned Mars lander mission was selected as a representative mission for application and the computer requirements were developed. The organization developed utilizes an array of cells capable of a high degree of computational parallelism. The feasibility of such cells is dependent upon future LSI technology. Research was carried out in the hardware design and software analysis of this organization. This volume contains a Author summary of the results of the study.

N68-32055*# National Aeronautics and Space Administration. Lewis Research Center, Cleveland, Ohio.

ANALOG COMPUTER SIMULATION OF A DC ARC EMISSION SPECTROMETER CONTROL SYSTEM TO DEFINE **REQUIREMENTS FOR OPTIMUM CONTROL** Daniel J. Lesco Washington Aug. 1968 27 p refs

(NASA-TN-D-4770) CFSTI: HC\$3.00/MF\$0.65 CSCL 09B The use of an analog computer in the simulation of a dc arc and its control system is described. The detailed model design is presented. Control parameters determined with the model are shown to be optimum with the real system. Repeatability of system control to a programmed input to ± 1 percent is achieved. for both the model and the real system. Data from the model and the arc system show close agreement except in some areas of arc Author instability.

N68-32159*# National Aeronautics and Space Administration, Washington, D. C.

VISUAL INFORMATION DISPLAY SYSTEMS, A SURVEY 1968 101 p refs Prepared by Auerbach Corp.

(NASA-SP-5049) GPO: HC\$0.60; CFSTI: MF\$0.65 CSCL 09B

Visual information display systems that are computer connected or updated with computer-generated information were surveyed, with emphasis on alphanumeric and graphic devices. Details are included for the three basic elements of display systems: (1) human beings and task dependent parameters; (2) hardware components such as cathode ray tubes, generators, screens, and man-machine reactive input devices; and (3) computer systems, programming and software development. Checkout and control are considered for large-scale checkout, ground monitor, and control systems. Interactive displays systems described include mathematical, design automation, and educational display systems. Reservation and information access systems are mentioned for on-line information storage and retrieval display systems; and Manned Spacecraft Center simulation displays, General Electric computed displays, and computer-produced movies are cited as simulation display systems. Cockpit displays and image enhancement are also discussed. Separate bibliographies are listed for each of the major topics considered in this survey. M.W.R.

N68-35193*# Radio Corp. of America, Princeton, N. J. **MOS FIELD-EFFECT-TRANSISTOR TECHNOLOGY** J. T. Wallmark, W. A. Boesenberg, E. C. Ross, D. Flatley, and H. Parker Washington NASA Sep. 1968 67 p refs (Contract NAS1-5794)

08 COMPUTERS

(NASA-CR-1113) CFSTI: HC \$3.00/MF \$0.65 CSCL 09B

Integrated metal oxide semiconductor (MOS) circuit technology was studied as part of a laminated-ferrite memory project. The target was the development of a 64-transistor word-driver circuit. but the technology was also applied to a 100-transistor load circuit for the decoder. The developments included: (1) a contact metallization technique suitable for low temperature, low pressure circuit connections; (2) a circuit encapsulation and passivation technique compatible with the packaging and connection technique; (3) a high-density, long-life packaging technique; and (4) fabrication of long-life MOS transistors. Word driver strips with the expected performance and with acceptable yield were fabricated. A detailed account is given of silver contact stability, a key point in the circuit packaging. Also investigated were insulators for the gate region and the crossovers, gate healing techniques, and mask limitations on vield. Author

N68-35560*# Autonetics, Anaheim, Calif.

STUDY OF SPACEBORNE MULTIPROCESSING-PHASE 2. VOLUME 2: TECHNICAL DESCRIPTION Final Report

L. J. Koczela Washington NASA Sep. 1968 391 p refs

(Contract NAS12-108)

(NASA-CR-1159; C6-1476.22/33, v. 2) CFSTI: HC \$3.00/MF \$0.65 CSCL 09B

Results are presented on a research study of an advanced multiprocessor computer organization for future space missions. The organization is entitled the "Distributed Array Memory and Processor" computer. A manned Mars lander mission was selected as a representative mission for application and the computer requirements were developed. The organization developed utilizes an array of cells capable of a high degree of computational parallelism. The feasibility of such cells is dependent upon future large scale integration technology. Research was carried out in the hardware design and software analysis of this organization. Author

N68-37254*# Wolf Research and Development Corp., West Concord, Mass.

DATA DISPLAY PROGRAMMING

Washington NASA Sep. 1968 304 p refs

(Contract NAS5-9756-47)

(NASA-CR-1107) CFSTI: HC \$3.00 /MF \$0.65 CSCL 09B

Consideration is given to the problem of developing more efficient means by which the physical scientist might intimately control the complex data processing operations involved in the analysis and meaningful interpretation of large volumes of sensor data from scientific satellites. Areas of computer graphics technology in which pioneering efforts might prove fruitful are defined and approaches conceived. The results of pilot tests to evaluate proposed techniques from a human factors viewpoint are given. Specific techniques include information transfer via uncommon display media (full color; flicker; animation) and approaches to facilitate the use of a single input device as the means of processing control. Specifications are developed for an advanced hardware-software system for manipulating and displaying large volumes of data. A man computer communication station design is recommended which permits finger pointing as a means of input and peripheral equipment to service the display and input devices. Computer software to support man-computer communication is specified using a hierarchical approach. Author

09 ELECTRONIC EQUIPMENT

Includes electronic test equipment and maintainability; component parts, e.g., electron tubes, tunnel diodes, transistors; integrated circuitry; microminiaturization. For basic research see: 10 Electronics. For related information see also: 07 Communications and 21 Navigation.

N68-10420*# Melpar, Inc., Fails Church, Va. THIN-FILM PERSONAL COMMUNICATIONS AND TELEMETRY SYSTEM (TFPCTS) Washington NASA Nov. 1967 33 p (Contract NAS9-3924)

(NASA-CR-914) CFSTI: HC\$3.00/MF\$0.65 CSCL 09F

The final electrical design of the Thin-Film Personal Communications and Telemetry System (TFPCTS) is proposed and discussed. A block diagram of the entire system is depicted, along with diagrams of the transmitter, receiver, and thin-film universal very high frequency modules. Project scheduling is described; and a PERT chart showing the module delivery data is given. Module processing information and mask drawings for the first IF module, are also given. L.S.

N68-13617*# Stanford Research Inst., Menlo Park, Calif. MICROWAVE TECHNIQUE DEVELOPMENT FOR ADVANCED RADIO ASTRONOMY AND RADIOMETRY MISSIONS

B. M. Schiffman and Leo Young Washington NASA Jan. 1968 78 p refs

(Contract NAS12-126)

(NASA-CR-979) CFSTI: HC\$3.00/MF\$0.65 CSCL 09A

A scale model ($f_o=20$ GHz) of a birefringent wave filter for millimeter wavelengths is described. The filter consists of five cascaded identical half-wave plates, or crystals, each composed of an artificial anisotropic dielectric medium with its reference axis tilted at some prescribed angle to the plane of the input polarization. The design and analysis of an individual plate and the analysis of multielement filters are discussed. The experimental filter was tested in the range of 18–33 GHz, and its measured performance was found to compare well with the theoretical performance over a major portion of the range of frequencies used in the tests. A synthesis procedure for optimum (equal-ripple stop band) response multielement filters is given, together with tables of plate angles for such filters. This procedure combines the Fourier approximation method with the general synthesis method.

N68-15649*# National Aeronautics and Space Administration. Lewis Research Center, Cleveland, Ohio.

SEMICONDUCTOR SWITCHES FOR AEROSPACE ALTERNATING-CURRENT POWER APPLICATIONS James Vrancik Washington Feb. 1968 35 p refs

(NASA-TM-X-1495) CFSTI: HC\$3.00/MF\$0.65 CSCL 09A

The purpose of this investigation was to obtain insight into the merits and drawbacks of ac static switches, with particular attention to their application as aerospace power switches. Several ac static switches utilizing various semiconductor devices were studied with attention given to power loss, harmonic content, leakage, and temperature effects. The main desirable characteristics are probable high reliability (based on the fact that there are no known wear out modes) and long life, no moving parts, high vibration and shock resistance, and immunity to atmospheric conditions. A specific design was made to provide an example application for the devices and circuits investigated. A breadboard-type three-phase static switch for space use was designed, built, and tested. The breadboard switch was used as a motor starter for a 4-ampere fuel pump motor. The switch performance was determined and the power loss found to be 12 watts while transferring 800 watts (1.4 kVA). Other characteristics determined were harmonic content (\leq 1.0 percent) and leakage (resistance in off state \geq 50 k Ω). The switch was tested over a heat-sink temperature range of -40° to 80°C. Author

N68-15892*# General Electric Co., Schenectady, N. Y. DEVELOPMENT OF HIGH-TEMPERATURE VAPOR-FILLED THYRATRONS AND RECTIFIERS

Arthur W. Coolidge, Jr. Washington NASA Feb. 1968 98 p refs

(Contract NAS3-6005)

(NASA-CR-994) CFSTI: HC\$3.00/MF\$0.65 CSCL 09A

High-temperature vapor-filled diodes and thyratrons were studied for potential use as power-conditioning elements in future space applications. A 600°C thallium-filled diode was developed using a barium-system cathode. Alkali-halide fills intended for use at 600°C did not produce successful results. Cesium-filled diodes for use at 300°C were also studied. After the accumulation of extensive data from the investigation of diodes, a cesium-filled thyratron was designed and three sample tubes-rated at 15 amperes average, 300 volts forward, and 500 volts inverse-were constructed. One thyratron tube was operated for 1500 hours. Author

N68-16530*# National Aeronautics and Space Administration. Lewis Research Center, Cleveland, Ohio.

EFFECTS OF CABLE AND CIRCUIT PARAMETERS ON THE PRECISION CALIBRATION OF A CHARGE AMPLIFIER

John J. Smithrick and Ira T. Myers Washington Feb. 1968 22 p refs

(NASA-TN-D-4300) CFSTI: HC\$3.00/MF\$0.65 CSCL 09A

The effects of cable and circuit parameters on the precision calibration of a charge amplifier for microsecond pulses, such as those obtained from semiconductor diode particle detectors, are evaluated. The precision calibration method is described. A mercury-wetted relay pulse generator driving a 1-picofarad capacitor was used as a charge generator. The accuracy of the calibration was ± 0.4 percent.

N68-19062*# National Aeronautics and Space Administration. Electronics Research Center, Cambridge, Mass. CHARACTERISTICS OF TUNNELING P-NJUNCTIONS

John B. Hopkins Washington Mar. 1968 22 p refs (NASA-TN-D-4403) CFSTI: HC\$3.00/MF\$0.65 CSCL 09A

Procedures have been developed for the calculation of current-voltage characteristics of tunneling p-n junctions in semiconductors, given material constants and impurity-doping parameters. Accuracy higher than that acquired in similar efforts has been attained. When a digital computer is used, numerical differentiation permits calculation of parameters relevant to microwave mixing and detecting applications for tunnel and backward diodes in any elemental or compound semiconductor. Typical results are indicated. Author

N68-19185*# National Aeronautics and Space Administration. Langley Research Center, Langley Station, Va.

AN AUTOMATIC BALANCING SYSTEM FOR USE ON FRICTIONLESSLY SUPPORTED ATTITUDE-CONTROLLED TEST PLATFORMS

Norman M. Hatcher and Richard N. Young Washington Mar. 1968 24 p ref

(NASA-TN-D-4426) CFSTI: HC\$3.00/MF\$0.65 CSCL 14B

An automatic balancing system for frictionlessly supported, attitude-controlled test platforms about axes that are commonly orthogonal to the gravity vector is discussed. The system determines imbalance during limit-cycle operation by measuring the difference in total impulse exerted by opposing torquers that are used for attitude control in each axis to be balanced during some time interval. The system then moves a small weight by an appropriate distance to compensate for the measured imbalance. A model of the automatic balancing system has been constructed and tested on an air-bearing-supported platform that was fitted with sun sensors and a reaction-iet attitude-control system. Results indicated that the automatic balancing system can consistently balance this platform more accurately than it can be balanced manually, and that it can maintain this balance throughout prolonged test periods. The average accuracy to which the system balanced the platform during the tests was approximately 3000 dyne-dm. The system is compatible with present-day attitude-control systems, requires little power, and can be made small in weight and volume. Author

N68-22302*# National Aeronautics and Space Administration, Washington, D. C.

RECENT ADVANCES IN DISPLAY MEDIA

1968 129 p refs Symp. held at Cambridge, Mass., 19-20 Sep. 1967

(NASA-SP-159) GPO: HC\$1.00; CFSTI: MF\$0.65 CSCL 17G

CONTENTS:

1. COMPUTER-MANAGED DISPLAY SYSTEM FOR ADVANCED COMMERCIAL TRANSPORTS W. C. Dersch and R. T. Johnson (Boeing Co.) p 1–9 refs (See N68-22303 12-09)

2. DISPLAY REQUIREMENTS FOR ADVANCED MANNED SPACECRAFT R. C. Duncan (NASA. Electron. Res. Center) p 11-21 (See N68-22304 12-09)

3. MEDIA REQUIREMENTS FOR GENERAL AVIATION C. H. Gould and R. L. Winblade p 23–24 (See N68-22305 12-14)

4. RECENT ADVANCES IN CATHODE-RAY-TUBE DISPLAY DEVICES J. A. Davis (Purdue Univ.) p 25–39 refs (See N68-22306 12-09)

5. CARRIER INJECTION ELECTROLUMINESCENCE J. Hanlet and R. W. Haas (Marquardt Corp.) p 41-49 refs (See N68-22307 12-09)

6. THERMOCHROMIC DISPLAYS D. Grafstein, R. P. Burkowski, M. Kornblau, and W. L. Flint (Gen. Precision Inc.) p 53-61 refs (See N68-22308 12-09)

7. PROPERTIES AND APPLICATIONS OF PHOTOCHROMIC GLASSES R. J. Araujo (Corning Glass Works) p 63–69 refs (See N68-22309 12-09)

8. FLUIDIC DISPLAYS J. Van Der Heyden (Martin Co.) p 71-80 refs (See N68-22310 12-12)

9. MAGNETIC DISPLAY DEVICES R. C. Sinnott (Sinnott Corp.) p 81-88 refs (See N68-22311 12-09)

10. ELECTROSTATIC DISPLAYS P. Rice (Stanford Res. Inst.) p 89–92 refs (See N68-22312 12-09)

11. A SURVEY OF LASER DISPLAY D. W. Kennedy, C. R. Grauling, A. J. Devaney, and R. D. Wright (NASA. Electron. Res. Center) p 93–109 refs (See N68-22313 12-16) 12. THE PLASMA DISPLAY—A DIGITALLY CONTROLLABLE, HIGH BRIGHTNESS DISPLAY WITH AN INHERENT MEMORY R. H. Willson (Westinghouse Elec. Corp.) p 113–121 (See N68-22314 12-25)

13. MULTICOLOR ELECTROLUMINESCENT DISPLAYS K. P. Lally (Huyck Sys. Co.) p 123-129 refs (See N68-22315 12-09)

14. CONSIDERATIONS FROM ENGINEERING PSYCHOLOGY R. C. Casperson (Dunlap and Assoc., Inc.) p 133–142 refs (See N68-22316 12-05)

15. DISPLAY MEDIA: SUMMARY, INTERPOLATIONS, AND EXTRAPOLATIONS G. Kovatch and E. H. Hilborn (NASA. Electron. Res. Center) p 143–146 (See N68-22317 12-09)

N68-24387*# National Aeronautics and Space Administration. Langley Research Center, Langley Station, Va.

SUPPRESSION OF TEMPERATURE RISE IN LOSSY DIODES INSIDE RESONANT CAVITIES BY APPLICATION OF PRESSURIZED LIQUID NITROGEN

Hans-Juergen C. Blume Washington May 1968 31 p refs (NASA-TN-D-4556) CFSTI: HC\$3.00/MF\$0.65 CSCL 09A

The suppression of temperature rise in lossy diodes due to electrical power dissipation inside resonant cavities of low noise devices such as parametric amplifiers is essential in maintaining optimum low noise performance. This suppression can be achieved by the application of pressurized liquid nitrogen inside the cavity. The expected temperature of the lossy diode under this condition is estimated by (1) a calculation based on the heat-flow equations, and (2) a salt-solution test. The results are correlated with direct measurements which reveal a temperature rise of 3.3°K above the temperature of liquid nitrogen at 1 atmosphere. The resonant frequency shift due to the liquid nitrogen dielectric is estimated and its correlation with measurements is included. The results indicate that this type of cooling can be successfully used and is particularly effective for parametric amplifiers with medium quality varactor diodes. Author

N68-24388*# National Aeronautics and Space Administration. Electronics Research Center, Cambridge, Mass. LOW DRIVE TEMPERATURE STABLE MEMORY CORES Howard Lessoff Washington May 1968 10 p refs

(NASA-TN-D-4573) CFSTI: HC \$3.00/MF \$0.65 CSCL 09A

Details are given on the use of calcium and molybdenum as substitutes in the preparation of temperature-stable memory cores. Substituted lithium compositions which effectively improve core uniformity and lower the power required in memory application have been developed for memory cores. These improvements have been achieved by control of the ceramic structure, lowering of the coercivity, and reduction of the sintering temperature. Author

N68-24389*# National Aeronautics and Space Administration. Goddard Space Flight Center, Greenbelt, Md.

A DIGITAL VOLTAGE-CONTROLLED OSCILLATOR FOR PHASE LOCK LOOPS

Dominick E. Santarpia and Thomas E. McGunigal Washington May 1968 16 p refs

(NASA-TN-D-4521) CFSTI: HC\$3.00/MF\$0.65 CSCL 09E

The development of a digital voltage-controlled oscillator phase lock loop is described. A large frequency-tracking range and high phase stability are conflicting requirements of a conventional voltage-controlled oscillator; however, a digitally controlled frequency synthesizer performing in place of the conventional tracking oscillator will provide the stability and spectral purity of a very good 1-MHz standard over very wide frequency excursions. Author N68-26662*# National Aeronautics and Space Administration. Lewis Research Center, Cleveland, Ohio.

EFFECTS OF NUCLEAR RADIATION ON A HIGH-RELIA-BILITY SILICON POWER DIODE I-CHANGE IN 1-5 DESIGN CHARACTERISTICS

Julian F. Been Washington Jun. 1968 37 p refs

(NASA-TN-D-4620) CFSTI: HC \$3.00/MF \$0.65 CSCL 09A

Tests were conducted on 100 diodes in the NASA Plum Brook Reactor facility, which was designed to simulate a SNAP-8 nuclear environment. The diodes were irradiated in different operational and temperature modes for approximately 480 hr, with a resultant diode exposure to a total fast-neutron fluence (energies of 0.1 MeV and above) of 5×10^{13} neutrons/cm² and to a total gamma dose of 3×10^7 rads (C). Results showed that this diode could be reliably used in a nuclear electric generating system such as SNAP-8 provided that the total radiation levels were within those of the tests. No catastrophic failures occurred. The electrical characteristic that would limit the useful lifetime of the device with increased radiation is the forward voltage drop at high current levels. Author

N68-28668*# National Aeronautics and Space Administration. Electronics Research Center, Cambridge, Mass.

RADIATION AND COUPLING BETWEEN TWO COLLINEAR OPEN ENDED WAVEGUIDES

Robert J. Mailloux Washington Jul. 1968 50 p refs

(NASA-TN-D-4656) CFSTI: HC\$3.00/MF\$0.65 CSCL 09A

An experimental and theoretical study of collinear coupled waveguides radiating through a common perfectly conducting ground plane was described. The problem is formulated as a set of simultaneous integral equations and solved approximately by expanding the aperture field in a Fourier series. The special case of a single isolated waveguide is treated first, and the results are compared with experiment as well as with the approximate results of Lewin. Attention is given to the edge singularities. The more general case of two collinear coupled waveguide slots is solved by the same numerical method using the symmetrical properties of the geometry. Phase and amplitude of the mutual coupling are evaluated and compared with experiment. Considerable attention is given to comparing more simple approximations with this result, and on several occasions it is pointed out how these can be used and what error the additional approximations introduce. Author

N68-28879*# National Aeronautics and Space Administration. Marshall Space Flight Center, Huntsville, Ala. FLAT CONDUCTOR CABLE TECHNOLOGY

Washington 1968 54 p

(NASA-SP-5043) GPO: HC \$0.40; CFSTI: MF \$0.65 CSCL 09A

Technical information necessary for engineering consideration of flat conductor cable (FCC) systems as integral parts of future electronic programs is reported. The FCC is made of rolled flat conductors laminated between thin flexible plastic insulating films. Flat plugs and receptacles are used to form FCC systems. Copper is the most often used conductor, and polyesters (Mylar), polyimides (Kapton), and fluorocarbons (Teflon) are frequently chosen for the insulating films. Fabrication procedures, advantages, and limitations of use are detailed. Conventional wiring and FCC system costs are compared, and electrical characteristics data are tabulated. The FCC is recommended for electrical systems design where weight, space, cost reduction, lead time, reliability, and uniform electrical characteristics are of prime importance. Suggested areas of use are aircraft wiring, communications and radar equipment, computers, radio and television equipment, instruments and controls, appliances, and automotive harnesses F.O.S.

N68-29525*# ARINC Research Corp., Annapolis, Md. MICROELECTRONIC DEVICE DATA HANDBOOK. VOLUME 1: TEXT

Washington NASA Jul. 1968 302 p refs

(Contract NAS12-528)

(NASA-CR-1110; Rept.-548-01-7-803, V. 1) CFSTI: HC \$3.00/MF \$0.65 CSCL 09A

Volume 1 of a two volume handbook which was designed as a quick reference document for use by design engineers, technicians, parts specialists, and contractors in the selection and application of microelectronic devices in space systems; is reported. Emphasis is placed upon considerations affecting reliability of systems employing such devices. This volume comprises six sections of user oriented technical discussion, ranging from design, manufacture, use of the devices in subsystems, and specifications to reliability and failure physics. S.C.W.

N68-29526*# ARINC Research Corp., Annapolis, Md. MICROELECTRONIC DEVICE DATA HANDBOOK. VOLUME 2: MANUFACTURER AND SPECIFIC DEVICE INFORMATION

Washington NASA Jul. 1968 163 p

(Contract NAS12-528) (NASA-CR-1111; Rept.-548-01-7-803, V. 2) CFSTI: HC \$3.00/MF

(NASA-CR-1111; Rept.-548-01-7-803, V. 2) CFS11: HC \$3.00/MF \$0.65 CSCL09A

Volume II of a two volume handbook which was designed as a quick reference document for use by design engineers, technicians, parts specialists, and contractors in the selection and application of microelectronic devices in space systems; is reported. This volume lists and gives the characteristics of approximately 2,000 devices, arranged to facilitate device selection. Included are separate sections for linear circuits, digital circuits, and digital arrays. The reported catalog of micorelectronic devices is restricted to those devices that are integral units and that cannot be broken down into smaller segments without destruction of the entire unit. The catalog is further restricted, in general, to those devices in which all active and passive elements necessary to a fully operable circuit are included and intraconnected in one package. Names of companies engaged in manufacturing standard microelectronic devices are listed along with basic information on the nature of their devices. Included are outline drawings, schematic drawings, and printouts for each of the three classes of devices considered. S.C.W.

N68-30501*# National Aeronautics and Space Administration. Electronics Research Center, Cambridge, Mass.

ON ELECTROMAGNETIC SWITCHING PROPERTIES OF A BI-STABLE FLUIDIC ELEMENT WITH NON-DESTRUCTIVE MEMORY

Joseph S. Koziol, Jr. and Robert De Furia Washington Aug. 1968 39 p refs

(NASA-TM-X-1613) CFSTI: HC\$.300/MF\$0.65 CSCL 09E

The feasibility is discussed of controlling a magnetically permeable liquid bead with an electromagnet between two stable states of a particular system. Several useful properties of the switching system, namely, magnetomotive force required for switching, switching time, and ambient acceleration field limits are determined in terms of the system parameters. This concept suggests a simple, bi-stable, low-power, electric-to-fluid transducer with non-destructive memory. (The fluid bead retains its last stable state with all power off.) Development of a magnetically permeable liquid with high surface tension did not reach the stage for implementation, at the completion of the analysis, to permit experimental verification of the analytical results contained herein. Author

09 ELECTRONIC EQUIPMENT

N68-33224*# Hartman-Huyck Systems Co., Huntington Station, N. Y.

A CATHODE RAY TUBE SUITABLE FOR VIEWING UNDER HIGH AMBIENT

Donald Amberger Washington NASA Sep. 1968 84 p refs (Contract NAS12-97)

(NASA-CR-1185) CFSTI: HC \$3.00/MF \$0.65 CSCL 09A

A high contrast cathode ray tube, employing nonreciprocal optical filtering techniques was developed. The non-reciprocal filter design consists of a UV bandpass filter, a fluorescent film and a visible bandpass filter. All elements are transparent. The filter is between the observer and an ultra-violet emitting cathodoluminescent phosphor. Incident light strikes the visible filter and is partially absorbed. The remaining ambient passes through the transparent fluorescent film and is absorbed by the UV filter. The two filter layers have no mutual bandpass. Return diffuse reflection or emission from the fluorescent film and any return reflection from the phosphor are therefore eliminated. Attention is focused on the problem of eliminating diffuse reflection.

 $\bf N68\text{-}37944\ensuremath{^{\ast}\#}\xspace$ Administration. Lewis Research Center, Cleveland, Ohio.

ELECTRICAL STRESS ANALYSIS OF A MICROTHRUSTOR POWER CONDITIONER

Vincent R. Lalli Washington Nov. 1968 23 p refs

(NASA-TM-X-1686) CFSTI: HC\$3.00/MF\$0.65 CSCL 10B

Obtaining suitable power conditioning equipment for propulsion experiments is a critical problem. Data obtained on several space projects indicated that failure was caused partly by overstressed electrical parts. A microthruster power conditioner was experimentally analyzed to reveal the problems associated with worst case overstressed parts. The power conditioner was then modified to eliminate these existing overstressed conditions and has since operated continuously for more than 7000 hours. Author

10 ELECTRONICS

Includes circuit theory; and feedback and control theory. For applications see: 09 Electronic Equipment. For related information see: Specific Physics Categories.

N68-11513*# National Aeronautics and Space Administration. Ames Research Center, Moffett Field, Calif. THEORETICAL ERROR ANALYSIS OF A DOPPLER RANGE-RATE AND PHASE-MODULATED RANGE TRACKING

SYSTEM Kenneth J. Bures and Gerald L. Smith Washington Dec. 1967 47 p refs

(NASA-TN-D-4267) CFSTI: HC\$3.00/MF\$0.65 CSCL 09F

A detailed error analysis is presented for a particular type of range and range-rate tracking system. Results are given in the form of analytical expressions for the variances of the various types of errors that affect tracking data. The expressions are written in terms of system parameters so that they can be applied to a wide range of specific systems and tracking situations. The majority of the errors considered are random, but some are bias like and others are deterministic. The equations given constitute an error model from which data weighing factors can be obtained for use in data processing for the construction of the best estimate of the trajectory of a space vehicle.

N68-11789*# National Aeronautics and Space Administration. Goddard Space Flight Center, Greenbelt, Md. STATISTICAL TESTS FOR SIGNAL DETECTION James C. Morakis Washington Dec. 1967 83 p refs (NASA-TR-R-273) CFSTI: HC\$3.00/MF\$0.65 CSCL 09D

Some of the problems arising from maximum likelihood decision systems in time varying channels are solved by first introducing simple statistics which are functions of the outputs of the correlators of an n-ary detection system. Then methods are developed to use the statistics to a) attach a confidence level to each decision in a maximum likelihood decision system, b) control the error rate at the expense of data rejection, and c) define the critical region for an optimum generalized decision system. These improvements and optimizations are accomplished by taking advantage of the information already available in the sample representing the outputs of n-ary detection systems. The six statistics that are investigated are simple functions of the largest correlator output, the mean, the standard deviation, the sample mean, the sample variance, the next to the largest correlator output, and the smallest correlator output. Author

N68-16749*# National Aeronautics and Space Administration. Goddard Space Flight Center, Greenbelt, Md.

EFFECTS OF CORRELATED NOISE WITH APPLICATIONS TO APOLLO TRACKING PROBLEMS

B. Kruger Washington Feb. 1968 59 p refs

(NASA-TN-D-4121) CFSTI: HC\$3.00/MF\$0.65 CSCL 09D

The standard deviation η_i and the rms standard deviation $\overline{\eta}$ of least-squares fitted polynomials are analyzed in this paper. The general equations derived are demonstrated on several Apollo tracking problems: It is shown that $\overline{\eta}$ does not improve for higher sampling rates of angular data than 2 or 5 per second, for narrow and wide bandwidth setting of the angular servoloops, respectively. (Apollo GO, NO-GO decision.) The effect of negative correlation of measurement errors is analyzed. The effect of phase noise in range rate data is reduced by a factor \sqrt{N} due to the negative correlation of -1/2 between adjacent measurement points. The effect of random-walk phase noise on the range rate data is shown to be proportional to the two-way propagation time of the signal.

The maximum error in a least-squares fitted polynomial is also analyzed. Author

N68-19229*# Douglas Aircraft Co., Inc., Newport Beach, Calif. RESEARCH ON THE UTILIZATION OF PATTERN RECOGNITION TECHNIQUES TO IDENTIFY AND CLASSIFY OBJECTS IN VIDEO DATA Final Report Washington NASA Mar. 1968 285 p refs (Contract NAS12-30)

(NASA-CR-999; SM-48464-F) CFSTI: HC \$3.00/MF \$0.65 CSCL 09F

The study consisted of a literature survey to select pattern recognition methods for testing, controlled recognition experiments to test the performance of the selected methods on five specimen classification tasks, and a hardware feasibility study, culminating in three potential designs for a spaceborne recognition system. Six methods for generating property filters and eight algorithms for designing decision functions were tested. Lunar photographs and Nimbus pictures of cloud patterns were used in the experiments. Decision networks were designed to perform three recognition tasks on the photographic data. Three recognition systems were designed: (1) parallel/analog, (2) sequential/hybrid, and (3) sequential/digital. Each has an image dissector tube which views the scene and scans the sensed image through a small aperture. The first implements all property filters separately in analog form. The second uses a single property filter repetitively with a diode matrix containing the weighting elements for each computed property. The third uses a compact core storage unit and an arithmetic unit with a combination hardware and software program to implement the required property filters. All three systems can classify TV pictures in real time. Author

N68-19882*# National Aeronautics and Space Administration, Langley Research Center, Langley Station, Va.

AN ANNOTATED BIBLIOGRAPHY OF COMPUTER-AIDED CIRCUIT ANALYSIS AND DESIGN

Charles W. Meissner, Jr. Washington 1968 44 p refs (NASA-SP-7023) CFSTI: HC\$3.00/MF\$0.65 CSCL 09C

An annotated bibliography is presented on computer aided circuit analysis and design with emphasis on the application of computers to the analysis of electronic circuits. The bibliography presents a listing of authors and their works, and a chronology of the development of computer aided analysis. The bibliography covers the period from 1956 to 1966. B.S.D.

N68-21122*# National Aeronautics and Space Administration. Lewis Research Center, Cleveland, Ohio.

COLLISIONLESS CYLINDRICAL DIODE

Charles M. Goldstein Washington Apr. 1968 41 p refs

(NASA-TN-D-4516) CFSTI: HC\$3.00/MF\$0.65 CSCL 09C

A complete formulation and numerical results for the collisionless space-charge problem of a cylindrical diode with thermionically emitted electrons are presented. This formulation allows calculation of the current-voltage characteristics from the Schottky retarding region to saturation. In addition, the onset of the Schottky retarding region is unambiguously defined. Author

10 ELECTRONICS

N68-24338*# National Aeronautics and Space Administration. Lewis Research Center, Cleveland, Ohio.

ATLAS-CENTAUR FLIGHT PERFORMANCE FOR SURVEYOR MISSION A

Washington May 1968 148 p refs

(NASA-TN-D-4580) CFSTI: HC\$3.00/MF\$0.65 CSCL 22D

The first operational Atlas-Centaur launch vehicle AC-10, with Surveyor spacecraft SC-1, was launched May 30, 1966. Surveyor was the first earth-launched spacecraft to soft land, under controlled conditions, on the lunar surface. Landing on the lunar surface occurred on June 2, 1966. This report includes a flight performance evaluation of the Atlas-Centaur launch vehicle systems from lift-off through spacecraft separation and Centaur retromaneuver.

N68-28307*# General Precision, Inc., Little Falls, N. J. ADDITIONAL STUDIES OF QUASI-OPTIMUM FEEDBACK CONTROL TECHNIQUES

Bernard Friedland, Frederick E. Thau, Sanford Welt, Chong K. Ling, and Michael Schilder Washington NASA Jul. 1968 144 p refs

(Contract NAS2-3636)

(NASA-CR-1099) CFSTI: HC \$3.00/MF \$0.65 CSCL 09A

A quasi-optimal control technique was investigated by approximating a complicated dynamic process by a simpler process, designing a control system for the latter, and amending the design to account for any difference between the original process and the approximation. The simplified process must be a reasonably faithful representation of the original process and the solution of the two-point boundary-value problem governing the optimal control law of the process must be reducible to manageable proportions. The correction to the optimal control law requires evaluation of a correction matrix with a matrix Riccati equation, whose solution matrix is then used to correct the solution to the simplified process. Theoretical studies on the performance of the quasi-optimal control law as well as stochastic optimum control are reported. Applications are included for the three-axis attitude control of a space vehicle; minimum-time, bounded acceleration rendezvous in a central force field; and an aircraft landing problem. Some aspects of the inverse optimal control problem are considered for a class of nonlinear autonomous systems. M.W.R.

N68-33767*# Hughes Aircraft Co., Fullerton, Calif. TRANSISTOR DESIGN EFFECTS ON RADIATION RESISTANCE

C. C. Berggren and V. R. Honnold Washington NASA Sep. 1968 97 p refs

(Contract NAS1-6954)

(NASA-CR-1167) CFSTI: HC \$3.00 /MF \$0.65 CSCL 09A

Analytical expressions relating transistor design parameters to radiation induced gain degradation were developed. Emitter efficiency and base transport injection level effects have received prime consideration. Several statistically designed experiments, which employed custom designed planar transistor variations, were conducted to evaluate the theoretical conclusions. The need for accurate profile information, to correlate with radiation induced gain degradation, is established. Shallow junctions and low base doping are shown to contribute significantly to radiation resistance. Author

N68-37293*# Israel Program for Scientific Translations. Ltd., Jerusalem.

MULTIVARIABLE CONTROL SYSTEMS [SISTEMY MNOGOSVYAZNOGO REGULIROVANIYA] M. V. Meerov 1968 294 p refs Transl. into ENGLISH of the book "Sistemy Mnogosvyaznogo Regulirovaniya" Moscow, Izd. Nauka, 1965 Support by NASA and NSF

(NASA-TT-F-435; TT-67-51371) CFSTI: HC \$3.00/MF \$0.65 CSCL 09C

The fundamental properties of multivariable automatic control systems (MCS) are elucidated and reviewed. The current methods and techniques are assessed and evaluated for the synthesis and analysis of MCS. Mathematical descriptions of some typical MCS, representative of metallurgy and oil industries, are presented. Equations of MCS consisting of single variable subsystems are derived for steady state and transient conditions. The matrix of error coefficients is determined for the case of plant and control coupling of the individual variable. The general structural properties of MCS are investigated with emphasis on infinite gain stability. Noninteraction and variance problems are discussed with respect to structural properties of a certain class of systems. Fixed structure systems with their properties equivalent to adaptive systems and variational aspects of MCS are reported.

N68-37906*# Chrysler Corp., New Orleans, La. APPLICATIONS STUDY OF ELECTROADHESIVE DEVICES Richard P. Krape Washington NASA Oct. 1968 90 p 3 refs (Contract NAS1-7303)

(NASA-CR-1211) CFSTI: HC \$3.00/MF \$0.65 CSCL 13H

A summary is presented on studies to determine the feasibility of using electroadhesion as a means for aiding astronauts in performance of on-board and EVA experiments. Mathematical and experimental analyses were conducted to define the factors that control or affect the electroadhesion phenomenon. The parameters analyzed were: resistivity, coating thickness, current density, surface conditions, polarity, temperature, time, environmental conditions, and chemical nature of coating materials. Five types of electroadhesor mountings were investigated; power supply requirements and techniques for controlling electroadhesor operation were studied. Three prototype electroadhesor models were designed, fabricated, and tested to establish preliminary operational data. Evaluation included tests for static pull force, skid force, and battery longevity. In practice, electroadhesion was found to occur when any suitable insulator material was placed between two electrodes charged in a manner to allow a small current to pass from one to the other. The intimacy of the contacting surfaces was found the most difficult condition to establish and maintain. B.P.

11

FACILITIES, RESEARCH AND SUPPORT

Includes airports; lunar and planetary bases including associated vehicles; ground support systems; related logistics; simulators; test facilities (e.g., rocket engine test stands, shock tubes, and wind tunnels); test ranges; and tracking stations.

N68-10384* Sandia Corp., Albuquerque, N. Mex. CONTAMINATION CONTROL PRINCIPLES Washington NASA 1967 51 p refs (Contract NASw-12324)

(NASA-SP-5045) CFSTI: \$3.00 CSCL 14B

A basic contamination control model is outlined to define the overall field in terms of contaminants and environments which they affect. Contamination control considerations and principles in product design are discussed followed by detailed descriptions of clean rooms, clean work stations, and other work enclosures used to control airborne contaminants. The discussion also covers processes and methods used in cleaning product surface; contamination in liquids, gases, and solids; the effects and means of controlling radiation and microbial contamination; methods of detecting the various types of contaminants; controlling contamination in packaging, transport, and storage; and personnel control and management at contamination control facilities. R.N.A.

N68-14115*# National Aeronautics and Space Administration. Lewis Research Center, Cleveland, Ohio.

A 4500°R (2500°K) FLOWING-GAS FACILITY

Jack G. Slaby, Byron L. Siegel, William F. Mattson, and William L. Maag Washington Jan. 1968 32 p refs

(NASA-TM-X-1506) CFSTI: HC\$3.00/MF\$0.65 CSCL 14B

The design and operation of a high-temperature flowing-gas heater is described. The heater consists of four identical heater stages, each individually controlled. The heating elements consist of flat tungsten plates which are electrically resistance heated by high direct-current power supplies and operate at surface temperatures above 5000° R (2780° K). The maximum power that can be transferred to the gas is about 1.5 megawatts. The gas flows through the four heater stages in series. Gas temperatures exceeding 4500° R (2500° K) were obtained with hydrogen, helium, and nitrogen. Operating life of the heater elements was 10 hours or more. Power supply selection; connection of high current busing to the heater; heater expansion at operating temperature; materials compatibility, and heater surface temperature profiles associated with the physical dimensions of the heater, are discussed.

N68-15777*# Physics International Co., San Leandro, Calif. EXPLOSIVE HYPERVELOCITY LAUNCHERS

E. T. Moore, Jr. Washington NASA Feb. 1968 74 p refs

(Contract NAS2-3577)

-9

(NASA-CR-982; PIFR-051) CFSTI: HC \$3.00/MF \$0.65 CSCL 14B

This report summarizes the analytical and experimental effort that demonstrates the feasibility of using a two-stage explosively driven light gas gun to obtain high projectile velocities. The second stage of this gun consists of an explosive lensing system that is used to produce an implosively formed piston whose velocity can be increased uniformly. The uniformly accelerated piston is shown to generate a nearly constant base pressure for projectile accelerations. Velocities as high as 12.2 km/sec have been obtained for a 0.17-gram magnesium-lithium projectile. Author N68-15858*# National Aeronautics and Space Administration. Marshall Space Flight Center, Huntsville, Ala.

VISUAL SIMULATION FACILITY FOR EVALUATION OF LUNAR SURFACE ROVING VEHICLES

F. L. Vinz, M. H. Knighton, H. F. Lahser, L. G. Thomas, J. T. Howell, et al Washington Feb. 1968 41 p refs

(NASA-TN-D-4276) CFSTI: HC\$3.00/MF\$0.65 CSCL 14B

A fixed base visual simulator was developed to serve primarily as an engineering tool which would include man-machine interaction in evaluations of preliminary Lunar Surface Vehicle design. Visual cues are obtained by means of a visual simulator consisting of a camera and model unit and a projector and screen providing a 30°×50° field-of-view of a three-dimensional terrain model. The crew station consists of a general-purpose two-man cockpit designed for maximum flexibility. The crew station and the general-purpose analog computers are interconnected through an interface console featuring a removable patch panel and containing power supplies, relay racks, servo panels, limiters, and other items common to most simulators. The terrain model is scaled 150:1 and has a maximum dimension of 12 x 27 feet. Maximum camera-model separation is eight inches. Lunar surface details required in the manufacture of the model were reduced from Ranger VIII photographs and supplied by the Branch of Astro-Geology. Terrain surface irregularities are detected by sensors mounted around the camera optics. Author

N68-16695*# National Aeronautics and Space Administration. Lewis Research Center, Cleveland, Ohio.

DESIGN AND PERFORMANCE OF TWO VACUUM Chambers and solar simulators for Sölar-Cell Research

Adolph C. Spagnuolo Washington Feb. 1968 18 p refs (NASA-TM-X-1503) CFSTI: HC\$3.00/MF\$0.65 CSCL 14B

A facility containing a 5-foot- (1.52-m-) and a 2-foot- (0.61-m-) diameter space-environmental chamber with two solar-radiation simulators and support equipment is described. The facility is designed for testing solar cells, thermoelectric and thermionic devices, and related components at vacuum levels in the 10^{-8} - to 10^{-9} -tor $(10^{-6}\text{-}$ to $10^{-7}\text{-N/m}^2)$ range. The pumping systems and liquid-nitrogen-cooled shrouds are described. Information concerning a test apparatus and a solar-cell installation method is also included.

N68-18460*# National Aeronautics and Space Administration. Lewis Research Center, Cleveland, Ohio.

SNAP-8 SIMULATOR LOOP MECHANICAL DESIGN

Alfred S. Valerino, James C. Wood, and Joseph F. Reznik Washington NASA Mar. 1968 65 p refs

(NASA-TM-X-1515) CFSTI: HC\$3.00/MF\$0.65 CSCL 14B

A SNAP-8 system simulation facility was designed, assembled, and tested. Design flow rates of the three-loop system were 32,000 lb/hr of eutectic NaK in both the primary and heat-rejection loops and 9100 lb/hr of Hg in the power loop. The turbine, radiator, and nuclear reactor were simulated. A prototype boiler and condenser were employed. Fluid circulation was obtained by electromagnetic pumps and a centrifugal pump for NaK and Hg, respectively. Test results indicated errors in Hg vapor flow rate due

11 FACILITIES, RESEARCH AND SUPPORT

to erosion and/or corrosion of the entrance and throat sections of choked venturis. The location of spark-plug-type liquid-level indicators in the expansion tanks of the NaK loops resulted in frequent shorting of the indicators. Gas and vacuum lines located atop the tanks were often plugged. Metal flexible hoses installed to alleviate thermal expansion of the piping by lateral movement of the hoses were safely employed in the liquid metal loops. The NaK electric heater employed as the heat source in the primary loop was replaced because of external leaks and electric shorting of the heater-element lead wires. Author

N68-19207*# National Aeronautics and Space Administration. Lewis Research Center, Cleveland, Ohio.

OUTGASSING OF WATER VAPOR FROM CONCRETE SURFACES IN VACUUM ENVIRONMENT

Adolph C. Spagnuolo and Edward A. Maslowski Washington Mar. 1968 11 p refs

(NASA-TM-X-1536) CFSTI: HC\$3.00/MF\$0.65 CSCL 14B

The amount of water loss by outgassing from two borated and two nonborated concrete blocks was measured at vacuum levels of 0.1 and 30 torr $(1.3 \times 10^1 \text{ and } 3.9 \times 10^3 \text{ N/m}^2)$. The nonborated blocks were also baked out in a furnace and subsequently placed in a 100-percent humidity chamber to investigate the reabsorption power of the concrete. The amount of water loss proved to be approximately 0.06 lb/ft² (0.03 kg/m²) for the nonborated and 0.320 lb/ft² (0.16 kg/m²) for the borated blocks. The concrete reabsorbed 70 percent of the water loss within the first 20 hours in the 100-percent humidity chamber. Aurthor

N68-19273*# North American Aviation, Inc., Los Angeles, Calif. PROPULSION SYSTEM DYNAMIC SIMULATION THEORY AND EQUATIONS

Arnold W. Martin Washington NASA Mar. 1968 222 p refs (Contract NAS2-3268)

(NASA-CR-928; NA-67-384) CFSTI: HC \$3.00/MF \$0.65 CSCL 14B

This report presents the theory, equations and assumptions for a propulsion system dynamic simulation program with emphasis on the air induction system. Although the simulation program was developed and used primarily for the XB-70, the theory and equations are sufficiently general to be applicable to a wide range of inlet configurations and flight conditions. Similarly, while the majority of simulation runs have utilized a digital computer in conjunction with the General Electric Company's "Dynasyar" program, the simulation is adaptable to other computing systems, and to analog computers.

N68-22737*# National Aeronautics and Space Administration. Lewis Research Center, Cleveland, Ohio.

VIEWING DEVICES FOR OBSERVING FLOW CONDITIONS IN HOT MERCURY SYSTEMS

Lawrence A. Mueller and David W. Medwid Washington May 1968 22 \ensuremath{p} refs

(NASA-TM-X-1578) CFSTI: HC\$3.00/MF\$0.65 CSCL 14B

Windows for both a mercury condensing tube and a mercury-boiler-outlet tube were investigated. A key factor in window design was proper matching of the thermal expansion coefficients of the window, the window sealants, and the window-support structure. The window for the mercury-condensing tube was tested with flowing condensing mercury at 670°F (628°K) and 15 psia $(10\ {}^5\text{ N/m}^2)$. At room temperature, the window was also subjected to 20-g random vibration. The boiler window was heated in a furnace to 1350°F (1005°K) with gas pressurization of 350 psig $(2.4 \times 10^6\ \text{N/m}^2)$.

N68-23357*# Stevens Inst. of Tech., Hoboken, N. J. A LABORATORY SCALE MODEL TECHNIQUE FOR INVESTIGATING PNEUMATIC TIRE HYDROPLANING H. Dugoff and I. R. Ehrlich Washington NASA May 1968 39 p

refs

(Contract NSR-31-003-016)

(NASA-CR-1074; Rept.-1223) CFSTI: HC \$3.00/MF \$0.65 CSCL 01B

A new technique is developed for laboratory investigation of pneumatic-tire hydroplaning through experiment with small-scale tires on a treadmill runway-simulator. The tires are mounted on a modified aircraft-landing-gear assembly which permits freedom in heave under variable vertical load and allows measurement of the longitudinal force exerted on the tire. The treadmill is capable of speeds up to 90 feet per second, and is outfitted with a water-supply system and a nozzle which delivers a water layer 1-foot wide, of variable thickness, at matching speed. The model tires are fabricated of polyurethane foam the density of which is varied to simulate variations in pneumatic-tire inflation pressure. Correlation of detailed load-deformation data for model and prototype tires demonstrates that geometric similarity is achieved under static conditions. Dimensional analysis has been employed to derive additional requirements for dynamic similarity and to develop a design for the initial series of experiments. Author

N68-24560*# National Aeronautics and Space Administration. Ames Research Center, Moffett Field, Calif.

A HIGH ENTHALPY PLASMA GENERATOR FOR ENTRY HEATING SIMULATION

Charles E. Shepard, Donald M. Ketner, and John W. Vorreiter Washington May 1968 19 $p\ refs$

(NASA-TN-D-4583) CFSTI: HC\$3.00/MF\$0.65 CSCL 14B

The constricted arc supersonic jet has a variety of applications, the most important probably being the simulation of entry heating from interplanetary missions. Within a constricted arc supersonic iet apparatus, a supersonic nozzle with an elongated throat, or arc constrictor, a direct-current arc and a longitudinal flow of gas are maintained. The working fluid, which may be air or any other gas, is heated as it passes near the arc, becomes electrically conductive and eventually becomes a part of the arc core. The arc core temperature is maintained by current flow while the gas passes through the supersonic nozzle into the test section. At present, total enthalpies and impact pressures corresponding to flight at 10 km/s at 60 km altitude and 30 km/s at 100 km altitude can be achieved. The three major limitations on performance are the maximum wall heat flux that can be removed by the cooling water, the maximum current that can be maintained without electrode erosion and subsequent stream contamination, and the maximum voltage gradient that can be maintained without destructive arc-over. Author

N68-24966*# Ling-Temco-Vought, 'nc., Anaheim, Calif. LTV Research Center, Western Div.

THE SHOCK EXPANSION TUBE AND ITS APPLICATION AS A SONIC BOOM SIMULATOR

Hugo E. Dahlke, George T. Kantarges, Thomas E. Siddon, and John J. van Houten Washington, D. C. NASA Jun. 1968 46 p refs

(Contract NAS1-5652)

(NASA-CR-1055; TR-0-71200/TTR-125) CFSTI: HC \$3.00/MF \$0.65 CSCL 14B

The generation of simulated sonic booms by mechanically bursting a pressurized diaphragm in a shock tube and expanding through an acoustic horn is described. An analysis of the expansion tube phenomena is presented, the characteristics of the various wave and wave interactions in the tube-horn combination are established and projected in an x-t diagram. Mathematical expressions for these characteristic wave motions are computed for the expansion tube. The simulator can generate double blast waves with a maximum peak pressure of 27 psf at 10 feet from the horn (on axis) using static pressure of 30 psig. The boom duration is variable from 10 to 600 msec. Subjective data were obtained for quantitative evaluation. Data showing the shape of the blast wave pressure signatures, the radiation pattern on the gound, and blast wave pressure as a function of distance from the simulator are presented. Author

N68-25853*# National Aeronautics and Space Administration. Langley Research Center, Langley Station, Va.

EVALUATION OF A FULL-SCALE LUNAR-GRAVITY SIMULATOR BY COMPARISON OF LANDING-IMPACT TESTS OF A FULL-SCALE AND A 1/6-SCALE MODEL

Ulysse J. Blanchard Washington Jun. 1968 47 p refs Film Supplement Number L-993 to this report is available on Ioan from NASA Langley Res. Center, Langley Station, Va.

(NASA-TN-D-4474) CFSTI: HC\$3.00/MF\$0.65 CSCL 14B

In order to subject the structural components of the prototype lunar module (LM) to the dynamic loads and conditions imposed during lunar-landing impact, full-scale tests were needed. To conduct such full-scale tests on earth, lunar gravity must be simulated. A lunar-gravity simulator for conducting landing-impact tests of a full-scale vehicle was constructed and evaluated. Results of landing tests of a full-scale test model of the LM conducted on the lunar-gravity simulator compare favorably with results of free-body tests of a similar 1/6-scale dynamic model conducted under earth gravity. Landing-gear strokes, center-of-gravity accelerations, and pitching motions were in good agreement. The full-scale simulator adequately reproduces two-dimensional landing-impact dynamics and is suitable for conducting detailed studies of prototype LM structure during landing impact. The effect of structural elasticity on landing motions and stability could also be investigated with the simulator. Author

N68-28311*# National Aeronautics and Space Administration. Goddard Space Flight Center, Greenbelt, Md. CLEAN-ROOM FACILITIES FOR EXPLORER 35 SPACECRAFT

Francis N. Le Doux Washington Jun. 1968 16 p (NASA-TN-D-4577) CFSTI: HC\$3.00/MF\$0.65 CSCL 14B

Costly delays and failures in past spacecraft projects have been attributed to the inadequacy or lack of contamination control. Currently, NASA requires that automated spacecraft with mission in the near vicinity of the moon be biologically decontaminated to a level of no more than 2.59 imes 106 viable spore forms at time of launch. To reduce particulate and biological contamination of Explorer XXXV, various classes of clean rooms were used. Debris generating operations were performed in uncontrolled areas with protection for flight hardware in the near vicinity. Decontamination, conformal coating, and encapsulation of electronics were performed in a class 10,000 conventional clean room; spacecraft buildup and some engineering tests were conducted in a class 100,000 conventional clean room. Electronic systems field checkout, cleaning and decontamination of small hand tools, instrument assembly, and/or functional operation tests, final spacecraft decontamination and assembly, and bioassaying were conducted in a class 100 bio-clean room environment. All clean room areas were restricted in number of personnel, clean-room dress, deportment, and procedures. On the basis of the biorecords, it was determined that the Explorer XXXV surfaces contained not more than 9 \times 105 microorganisms before decontamination. This low level has been attributed to the various clean-room environments and contamination controls utilized during assembly and/or testing. Author

N68-28947*# National Aeronautics and Space Administration. Langley Research Center, Langley Station, Va.

DESCRIPTION AND INITIAL CALIBRATION OF THE LANGLEY 20-INCH HYPERSONIC ARC-HEATED TUNNEL Raymond E. Midden and Bennie W. Cocke, Jr. Washington Jul. 1968 26 p refs

(NASA-TN-D-4653) CFSTI: HC\$3.00/MF\$0.65 CSCL 14B

Four different throat sizes (0.483, 0.680, 0.965, and 1.366 cm) were investigated to determine the effect of throat size on arc-heater performance in a 20-inch hypersonic arc-heated tunnel. The 1.366 cm-dia throat was found to be the most efficient. Three different center electrodes were evaluated, and electrode size and shape were found to have a large effect on arc-heater performance. This tunnel has an enthalpy range from 2790 to 27 900 kJ/kg. Four interchangeable nozzles (5.08, 8.39, 16.75, and 50.80 cm exits) are used to vary heating rate and model stagnation pressure at fixed arc-heater conditions. With these four nozzles the heating rate can be varied from 17 to 1700 W/cm2 (on a 3.81-cm-dia hemisphere-cylinder model), and the model stagnation pressure can be varied from 0.01 to 2.7 atm. Hemisphere-cylinder models up to 10.15 cm in diameter have been tested in the 50.80-cm nozzle exit, and models up to 6.35 cm in diameter have been tested in the 16.75 cm nozzle exit. Author

N68-29478*# National Aeronautics and Space Administration. Goddard Space Flight Center, Greenbelt, Md.

COLD WALL THERMAL VACUUM, THERMAL DESIGN CHECK FOR FULLY INSULATED EXPERIMENT PACKAGES Charles Dan Washington Jul. 1968 13 p refs

(NASA-TN-D-4644) CFSTI: HC\$3.00/MF\$0.65 CSCL 20M

Past procedure for testing the thermal balance of fully insulated experiment packages involved a solar-simulation test on the flight model as well as on the prototype. Experience gained during the OGO III spacecraft tests indicated that the solar simulation portion of the subsystem test could be eliminated for the flight model experimients without loss of confidence in the design. In the new procedure, validation of the flight model thermal balance is achieved, instead, by calculating the solar stabilization temperatures using data from a "cold-wall design check" and comparing the results v with the solar-simulation test previously performed on the prototype model. Analytical development and procedures for employing this simplified approach are discussed. Author

N68-29957*# National Aeronautics and Space Administration. Langley Research Center, Langley Station, Va. ANALYSIS AND MECHANIZATION OF THREE AND FOUR

ANALYSIS AND MECHANIZATION OF THREE AND FOUR GIMBAL SYSTEMS

John W. Wilson Washington Aug. 1968 33 p refs

(NASA-TN-D-4689) CFSTI: HC\$3.00/MF\$0.65 CSCL 14B

An approximate algebraic technique which extends the usefulness of three-gimbal systems is presented. In analyzing the three gimbal problem, the Euler angles are explored about the singular points and are found to be, in general, non-unique. This non-uniqueness is eliminated by minimizing the magnitude of the discontinuities at the singular points. An approximate mathematical model of the inverse Euler angle problem is developed which chooses the solution with minimum discontinuity and, in addition, replaces high rates over large angles by small discontinuities. A computer circuit is devised for this model. A proposed four gimbal system is investigated and a mathematical model is derived by finding a necessary differential constraint on the fourth angle to maintain a nonsingular formulation. This constraint is then used to derive a particular mathematical formulation in an essentially algebraic form, from which a computer circuit is developed. The rate equations of the four angles are also derived. Existing four gimbal stable platforms are analyzed and discussed. Author

N68-30317*# National Aeronautics and Space Administration, Washington, D. C.

VENTURE INTO SPACE: EARLY YEARS OF GODDARD SPACE FLIGHT CENTER

Alfred Rosenthal 1968 369 p refs

(NASA-SP-4301) GPO: HC\$2.50; CFSTI: MF\$0.65 CSCL 14B

The historical origins and traditions of this NASA Center, named in honor of Dr. Robert H. Goddard, one of the pioneers in the theory of space exploration, are described in terms of early rocket research and the growing interest in rocket technology after World War 2. The contributions of Project Vanguard to the United States space effort are reviewed, and it is pointed out that the personnel from Vanquard and other NACA laboratories formed the nucleus of the scientific team at the Center, which was dedicated on March 16, 1961. Organizational growth is traced, and project assignments are defined. The development of the tracking, data acquisition, and data reduction facilities is discussed, and details are given on the Goddard-managed satellites and space probes, the boosters that placed these satellites into orbit, and the sounding rocket flights. Organization charts and reports of procurement actions are included. The history covers the period through 1963, which is considered to be the end of Act One of the Space Age. M.G.J.

N68-30598*# National Aeronautics and Space Administration. Lewis Research Center, Cleveland, Ohio.

WATER CONDENSATION EFFECTS OF HEATED VITIATED AIR ON FLOW IN A LARGE SUPERSONIC WIND TUNNEL Robert W. Cubbison and Edward T. Meleason Aug. 1968 12 p (NASA-TM-X-1636) CFSTI: HC\$3.00/MF\$0.65 CSCL 14B

Natural gas was burned directly in the air stream of the Lewis 10- by 10-foot supersonic wind tunnel to control stagnation temperature. The test section Mach number was varied from 2.0 to 3.5, and stagnation temperature was varied to a maximum of 1140° R (634 K). Condensation of water vapor in the nozzle caused a decrease in test section Mach number and total pressure which was repeatable and accurately calibrated. The uniformity of the flow in the test section was similar to that of the unheated air. Author

N68-31592*# National Aeronautics and Space Administration. Langley Research Center, Langley Station, Va.

TEST SECTIONS FOR SMALL THEORETICAL WIND-TUNNEL-BOUNDARY INTERFERENCE ON V/STOL MODELS

Ray H. Wright Washington Aug. 1968 85 p refs

(NASA-TR-286) CFSTI: HC\$3.00/MF\$0.65 CSCL 14B

A wind-tunnel test section with closed upper wall, slotted side walls, and open lower boundary was found theoretically to produce zero tunnel-boundary lift interference on a small wing with horizontal wake mounted at the center of the test section. For this test section the variation of the interference with angle of the vortex wake behind a high-lift-coefficient model was not large. Because of the small slot widths required for zero interference and of the effects of boundary layer, the theory is regarded as unreliable for predicting the slot widths required; however, the variation of the interference with the slot width for widths somewhat greater than those needed for zero interference was found to be small. The interference in the region likely to be occupied by the tail of a model was investigated in some detail and was found to change with slot width and with wake angle more strongly than did the interference at the lifting element. A limited investigation of the lift interference in a test section with closed upper wall and slotted side and lower boundaries was made to obtain the theoretically indicated slot width required for zero lift interference at a center-mounted wing with the wake horizontal. Author

N68-33190*# National Aeronautics and Space Administration. Langley Research Center, Langley Station, Va.

DESCRIPTION AND OPERATING PARAMETERS OF A MACH 2 NOZZLE SYSTEM FOR THE LANGLEY 11-INCH CERAMIC-HEATED TUNNEL

Kenneth Sutton Washington Sep. 1968 69 p refs

(NASA-TN-D-4750) CFSTI: HC\$3.00/MF\$0.65 CSCL 14B

A Mach 2 nozzle system has been developed to operate interchangeably with existing Mach 4 and Mach 6 systems previously available for high-temperature materials research tests with air were made to determine the operating parameters and to define the test environment. Of particular concern were the definition of stream total temperature decay with time and the damage to test specimens due to stream contamination. The diameters of the calibration models and probes were approximately three-fourths of the diameter of the nozzle exit. Results show that the Mach 2 system has a linear decrease of total temperature of approximately 200°R (110°K) in a test time of 600 seconds for the standard operating range of chamber pressure of 115 to 165 psia (0.79 to 1.14 MN/m²). The total «temperature range as measured was 2100°R to 4000°R (1170°K to 2220°K). The damage to a test model due to stream contamination from the ceramic bed can be neglected for a significant number of experimental materials. Also, the comparison in pressure, heating-rate, and shear distributions indicates the suitability of material response tests at the stagnation region of a model. The results demonstrate the applicability of the Mach 2 system for an experimental program. Author

N68-35466*# National Aeronautics and Space Administration. Langley Research Center, Langley Station, Va.

A DIGITAL COMPUTER PROGRAM FOR CALCULATING THE PERFORMANCE OF SINGLE OR MULTIPLE DIAPHRAGM SHOCK TUBES FOR ARBITRARY EQUILIBRIUM REAL GAS MIXTURES

William L. Grose, John E. Nealy, and Jane T. Kemper Washington Oct. 1968 59 p refs

(NASA-TN-D-4802) CFSTI: HC\$3.00/MF\$0.65 CSCL 14B

A computer program written in FORTRAN IV language is presented which determines the performance of a shock tube. For specified initial gas composition and charging conditions, the program output includes velocity, pressure, density, enthalpy, temperature, sound speed, and species mole fractions at any point in the shock tube cycle. Several representative calculations illustrate the utility of the program. The program is applicable to both simple and buffered shock tubes as well as to the expansion tube. Author

N68-36522*# Washington Univ., Seattle.

THE EFFECT OF THE CONVERGING FLOW FIELD OF A TANDEM TEST SECTION ON LONGITUDINAL STABILITY MEASUREMENTS

Shojiro Shindo and Robert G. Joppa Washington NASA Oct. 1968 27 p refs

(Grant NGR-48-002-010)

(NASA-CR-1198) CFSTI: HC \$3.00/MF \$0.65 CSCL 14B

Calculations of the internal flow in tandem-test-section wind tunnels have shown the presence of converging flow in the large test section portion between the two contracting sections. Results of analytical and experimental work in a test section having length to height ratio of 3 show that the magnitude of the converging flow and its effect on longitudinal stability of a rigid rotor can be closely predicted. Maximum model sizes and satisfactory testing regions can be identified analytically. A prediction is made for two model sizes tested in a tunnel having length to height ratio of 1. Author

11 FACILITIES, RESEARCH AND SUPPORT

N68-37259*# National Aeronautics and Space Administration. Lewis Research Center, Cleveland, Ohio.

DESIGN AND PRELIMINARY OPERATION OF THE LEWIS MAGNETOHYDRODYNAMIC GENERATOR FACILITY

Lester D. Nichols, James L. Morgan, Lawrence A. Nagy, Joseph M. Lamberti, and Robert A. Ellson Washington Oct. 1968 26 p refs

(NASA-TN-D-4867) CFSTI: HC\$3.00/MF\$0.65 CSCL 14B

The closed loop facility has been designed to study the feasibility of an argon-cesium MHD generator. The construction details, performance, and some preliminary research data are discussed. The facility has operated for several hours at the following conditions: argon flow rate. 1.8 kg/sec; Mach number, 0.3 to 0.5; stagnation temperature, 2100°K. Thus far, open circuit voltages equal to 60 percent of theoretical value (at 50 V) were measured. In addition short circuit currents up to 0.8 A (per electrode pair) were measured. This is in agreement with the calculated value using equilibrium conductivity. Leakage currents prevented better performance.

12 FLUID MECHANICS

Includes boundary-layer flow; compressible flow; gas dynamics; hydrodynamics; and turbulence. For related information see also: 01 Aerodynamics; and 33 Thermodynamics and Combustion.

N68-10499*# Massachusetts Inst. of Tech., Cambridge. A THREE-DIMENSIONAL HARD SPHERES THEORY OF SCATTERING OF GAS ATOMS FROM A SOLID SURFACE Frank O. Goodman Washington NASA Nov. 1967 95 p refs (Grant NGR-22-009-121)

(NASA-CR-933) CFSTI: HC\$3.00/MF\$0.65 CSCL 20D

A three-dimensional model of the interaction of monatomic gases with solid surfaces is described. The solid surface is represented by similar, non-interacting, hard spheres, the centers of which form initially a regular two-dimensional array; an incident gas atom is represented by a hard sphere incident on this array. Collisions between the gas atom and the surface atoms obey the ordinary laws of classical hard spheres. The closely-related problems of the detailed velocity distribution of the gas atoms reflected from the surface, the energy and momentum accommodation coefficients and the forces exerted on a target by a directed gas beam, are discussed and illustrated by means of a fairly comprehensive set of results.

N68-10646* Stanford Research Inst., Menlo Park, Calif. IMPLOSIVELY ACCELERATED SHOCK TUBE DRIVER Stephen P. Gill and Robert C. Goettelman Washington NASA

Nov. 1967 66 p refs (Contract NAS2-3129)

(NASA-CR-950) CFSTI: \$3.00 CSCL 14B

The feasibility of using an implosive driver in a shock tube facility for research in high energy gasdynamics was investigated. Two implosive shock tube systems, one using a jetting driver and the other a jetless driver, were used to drive shock waves at velocities from 11 to 15 km/sec into dry air at initial pressures in the range 0.5 to 5 torr. The characteristics of the driver were investigated in a combined experimental and theoretical program, and the high energy gas flow behind the shock front was studied to determine experimentally its uniformity, purity, duration, and quality. It is concluded that the jetting driver, which consists of a cylinder of high explosive that progressively collapses a glass tube and projects a diffuse glass jet into the shock tube, can be of significant value as a shock tube driver for initial test gas pressures less than 1 torr. The diffuse glass jet is as effective as a perfect piston at these pressures, and a plane shock of nearly uniform velocity is driven into the test gas, followed by high energy flow of exceptional uniformity, quality, and purity. In addition, the test time grows at a rate nearly equal to that calculated for a perfect piston, and is insensitive to boundary layer phenomena. Author

N68-12892*# IIT Research Inst., Chicago, III.

EVALUATION OF TURBULENCE CORRELATIONS IN A COAXIAL FLOW OF DISSIMILAR FLUIDS

Antonio Montealegre, Gerard J. D'Souza, and Herbert Weinstein Washington NASA Jan. 1968 85 p refs

(Grant NsG-694)

(NASA-CR-961) CFSTI: HC\$3.00/MF\$0.65 CSCL 20D

A method of measuring fluctuations in velocity by means of a hot wire anemometer system has been developed and applied in a flow field where large concentration gradients exist. The flow field chosen is a coaxial flow of the two dissimilar fluids with a density ratio of 4:1. The fluid medium is air and the other fluid is Freon-12. The new method based on the use of an aspirating density probe in conjunction with the parallel wires, when applied to coaxial flow data, give values that are reasonably damped with respect to density fluctuations. Also, these correlations are found to be inapplicable in certain mean velocity ranges, i.e., at low and very high velocities. Results of calculations of velocity, density and fluctuations in velocity and density in coaxial flow of the air-freon system are presented and discussed. Author

N68-13612*# IIT Research Inst., Chicago, III. MEASUREMENT OF TURBULENT CORRELATIONS IN A COAXIAL FLOW OF DISSIMILAR FLUIDS

Gerard J. D'Souza, Anthony Montealegre, and Herbert Weinstein Washington NASA Jan. 1968 60 p refs (Grant NSG-694)

(NASA-CR-960) CFSTI: HC\$3.00/MF\$0.65 CSCL 20D

In this work axial turbulence intensities in a coaxial flow of dissimilar gases are presented. The system consisted of a circular freon 12 stream issuing into a faster and much larger air stream. The air-freon 12 density ratio is 1/4. The velocity ratios ranged from 40:1 to 5:1 with an absolute air velocity not exceeding 56.0 ft/sec. The magnitude of the axial turbulence intensities depends much on the velocity ratio of the streams. It is usually found to have a maximum value at some point between the centerline and the radius of the inner jet and then diminish to the free stream turbulence intensity. In the two cases of high air-freon velocity ratio a maximum turbulence intensity of 70% was obtained in the initial mixing region. Density fluctuations were also measured but these are shown to be damped by the measuring device. Values of the correlation between velocity and density fluctuations obtained are not valid and hence are not presented, as the damped density fluctuations affect this quantity considerably. A comparison is made between axial turbulence intensities for the heterogeneous case and those for the homogeneous case available in the literature. Author

N68-13619*# IIT Research Inst., Chicago, III. ANALYTICAL INVESTIGATION OF THE MIXING OF TWO PARALLEL STREAMS OF DISSIMILAR FLUIDS

Richard L. Baker and Herbert Weinstein Washington NASA Jan. 1968 128 p refs

(Grant NsG-694)

(NASA-CR-956) CFSTI: HC\$3.00/MF\$0.65 CSCL 20D

The free jet mixing of parallel streams of different fluids is of fundamental importance and interest. The degree of mixing depends on the regime of flow in the mixing region, i.e., laminar or turbulent, and the velocity and density ratios. In this work, similarity solutions were obtained for laminar and turbulent mixing of two parallel incompressible streams. The solutions apply to both similar and dissimilar fluids in the two streams with any velocity or density ratio and arbitrary laminar or turbulent Schmidt numbers. A solution is numerical in nature and a set of solutions are presented in tabular form for a spectrum of density, velocity and Schmidt numbers.

12 FLUID MECHANICS

N68-14641*# National Aeronautics and Space Administration. Lewis Research Center, Cleveland, Ohio.

EFFECTS OF WALL PRESSURE DISTRIBUTION AND LIQUID TEMPERATURE ON INCIPIENT CAVITATION OF FREON-114 AND WATER IN VENTURI FLOW

Royce D. Moore, Robert S. Ruggeri, and Thomas F. Gelder Washington Jan. 1968 25 p refs

(NASA-TN-D-4340) CFSTI: HC\$3.00/MF\$0.65 CSCL 20D

Incipient cavitation of Freon-114 (dichlorotetrafluoroethane) and of water was studied over a range of liquid temperatures in three different transparent venturis mounted in a small hydrodynamic tunnel. Flow velocity in the approach section of the venturis was varied from 18 to 65 feet per second (5.5 to 19.8 m/sec). The venturis were designed to provide systematic changes in wall pressure distribution. Circular arcs of differing radii provided transition from a 1.745-inch- (4.432-cm-) diameter approach section to a 1.375-inch- (3.492-cm-) diameter throat section. For Freon-114, the magnitude of thermodynamic effects of cavitation was significantly reduced for the milder pressure distributions and increased with liquid temperature. No thermodynamic effects of cavitation were observed for water over the temperature range studied. For both water and Freon-114, the incipient cavitation parameter was always less than the noncavitating minimum pressure coefficient, which indicated that the liquids locally experienced effective liquid tensions at the incipient condition. The magnitude of these tensions was strongly dependent on the wall pressure distribution and decreased with the milder pressure distribution. Author

N68-15329*# National Aeronautics and Space Administration.. Lewis Research Center, Cleveland, Ohio.

VENTURI SCALING STUDIES ON THERMODYNAMIC EFFECTS OF DEVELOPED CAVITATION OF FREON-114

Royce D. Moore and Robert S. Ruggeri Washington Feb. 1968 30 p refs

(NASA-TN-D-4387) CFSTI: HC\$3.00/MF\$0.65 CSCL 20D

Well-developed cavitation of Freon-114 (dichlorotetrafluorethane) was induced on the walls of a venturi in a recirculating hydrodynamic tunnel. The venturi, which had a throat diameter of 0.976 inch (2.48 cm), was a 0.7 scale of one previously tested. The approach velocity was varied from 20 to 50 feet per second (6.1 to 15.2 m/sec) at controlled liquid temperatures from 0° to 86°F (255.4° to 303.2°K). Pressures and temperatures were measured in the cavitated region and compared with the results of the 1.0-scale venturi. For geometrically similar cavities and fixed flow velocity, the measured cavity pressure and temperature depressions below free-stream values of vapor pressure and temperature were nearly the same for both the 0.7- and 1.0-scale venturis. Cavity pressure and temperature depression trends with liquid temperature and velocity were also similar in the 0.7-scale venturi as in the 1.0-scale venturi. A previously derived method for predicting the thermodynamic effects of cavitation is extended to include the effect of scale. Similarity parameters for developed cavitation were evaluated by using the minimum cavity pressure as a reference rather than the free-stream vapor pressure. The cavitation parameter was shown to be nearly the same value for both the 0.7- and 1.0-scaled venturis. Author

N68-15530*# IIT Research Inst., Chicago, III. STABILITY OF SHEAR FLOW WITH DENSITY GRADIENT AND VISCOSITY

Richard L. Baker, Tzvi Rozenman, and Herbert Weinstein Washington NASA Feb. 1968 58 p refs

(Grant NsG-694)

(NASA-CR-958) CFSTI: HC\$3.00/MF\$0.65 CSCL 20D

The stability of the mixing region between co-flowing streams of different velocity and density has never been adequately investigated, because a general similarity solution for velocity and density profiles has not been available until recently. A solution method for the homogeneous case was extended to the heterogeneous case in an attempt to find a neutral stability curve for the more complex case. The extension was based on a similarity solution obtained by the authors. A branch line of the neutral stability curve was found but curves with non-zero amplification and damping factors fell on the same side of the neutral stability curves. Author

N68-15571*# IIT Research Inst., Chicago, III.

EXPERIMENTAL INVESTIGATION OF THE MIXING OF TWO PARALLEL STREAMS OF DISSIMILAR FLUIDS

Richard L. Baker and Herbert Weinstein Washington NASA Jan. 1968 102 p refs

(Grant NsG-694)

(NASA-CR-957) CFSTI: HC\$3.00/MF \$0.65 CSCL 20D

In this work, velocity and density profiles for both homogeneous and heterogeneous systems were obtained. The range of density ratios was 1:1 to 7:1. The velocity ratio range was 1:1 to 5:1. Turbulence intensities were also measured for the homogeneous case. The experimental method was based on hot wire anemometry. The data obtained agreed well with the analytical investigations in the literature. Author

N68-15639*# National Aeronautics and Space Administration. Lewis Research Center, Cleveland, Ohio.

SCALE MODEL STUDY OF FLOW PATTERNS IN THE INLET MANIFOLD OF THE FUEL PUMP DRIVE TURBINE FOR THE M-1 HYDROGEN-OXYGEN ROCKET ENGINE

John F. Kline and Roy G. Stabe Washington Feb. 1968 11 p refs

(NASA-TM-X-1513) CFSTI: HC\$3.00/MF\$0.65 CSCL 21H

Flow conditions in the inlet manifold of the M-1 fuel pump-drive turbine were investigated using circumferential static pressure measurements in conjunction with smoke trace photographs. This manifold is toroidal with a single radial feedpipe. The study was prompted by reference tests which indicated a large variation in total pressure around the turbine nozzle which was attributed to manifold flow conditions. In addition, the possibility of flow asymmetry in the manifold was indicated by circumferential measurements of manifold static pressure. The results obtained from both the static pressure measurements and smoke flow traces indicated that the flow pattern within this manifold was essentially symmetrical about the feedpipe. The large observed circumferential variation in static pressure and associated flow patterns afforded a better understanding of reference nozzle exit total pressure Author patterns.

N68-16227*# National Aeronautics and Space Administration. Lewis Research Center, Cleveland, Ohio.

DYNAMIC PRESSURE LIMITS FOR FLAT PLATES AS RELATED TO NUCLEAR FUEL ELEMENTS

Roger L. Smith Washington Feb. 1968 29 p refs

(NASA-TN-D-4417) CFSTI: HC\$3.00/MF\$0.65 CSCL 18J

Tests with air or helium flowing over single flat plates were performed at room temperature to determine the values of dynamic pressure required to cause plate failure. Failure was defined as a deflection greater than 0.010 inch (0.0254 mm). The ranges of the plate dimensions used are given. The plate materials selected were lead, aluminum, copper, and steel, which provide ranges of Young's modulus of elasticity from 2×10^6 to 30×10^6 psi (1.38×10^6 to 20.7×10^6 N/cm³), and of Poisson's ratio from 0.288 to 0.42. Gas density varied from 0.025 to 1.0 pound per cubic foot (0.4 to 16 kg/m³). The experimental results were compared with an existing theoretical analysis which predicts dynamic pressure for sudden, complete plate collapse. The experimental results agree with the theoretical prediction for the

effect of the material properties, but disagree with the prediction for the effect of the plate and flow-channel dimensions. The large amount of experimental data scatter and the disagreement of these data with the theoretical prediction may be caused by leading-edge effect, flutter, turbulence, or other unknown factors. Author

N68-16839*# National Aeronautics and Space Administration. Washington, D. C.

STUDIES IN PHYSICAL GAS DYNAMICS

A. S. Predvoditelev, ed. Feb. 1968 267 p refs Transl. into ENGLISH of the book "Issledovaniya po Fizicheskoy Gazodinamike" Moscow, Nauka Press, 1966

(NASA-TT-F-505) CFSTI: HC\$3.00/MF\$0.65 CSCL 20D

A collection of articles is presented on basic research in physical gas dynamics, with emphasis placed on molecular band spectra, shock tube studies, and interactions between diatomic molecules. For individual titles, see N68-16840 through N68-16867.

N68-16897*# IIT Research Inst., Chicago, III.

EXPERIMENTAL INVESTIGATION OF TURBULENCE IN THE MIXING REGION BETWEEN COAXIAL STREAMS

Thomas S. Zawacki and Herbert Weinstein Washington NASA Feb. 1968 145 p refs

(Grant NsG-694)

(NASA-CR-959) CFSTI: HC\$3.00/MF\$0.65 CSCL 20D

An experimental study is made of axially symmetric, turbulent, incompressible, coflowing streams. Hot wire anemometry techniques are used to make measurements in three systems, the homogeneous system with a resultant density ratio of 1, and two heterogeneous systems, one with an inner to outer stream density ratio of 4 to 1, and another with an inner to outer stream density ratio of 7 to 1. The outer stream velocity was varied from 12 to 50 ft/sec. and the inner stream was changed to provide outer stream to inner stream velocity ratios of from 1 to 40. Data is presented for the relative axial turbulence intensity, the relative radial turbulence intensity, and the turbulent shear stress for various velocity ratios in the homogeneous system, in both the initial mixing region and the downstream or similar region. The maximum relative turbulence intensity found was 0.40. For the 4 to 1 density case, data is presented for average velocity, the average density, and the relative velocity turbulence intensity for various velocity ratios in both the initial mixing region and the downstream or similar region. The maximum relative turbulence intensity found was 0.70. Average density and velocity profiles are presented for the 7 to 1 density ratio in the near and downstream regions. Author

N68-16998*# National Aeronautics and Space Administration. Lewis Research Center, Cleveland, Ohio.

PERFORMANCE STUDY OF ROTATING GAS JET GENERATOR FOR STRONG TRAVELING TRANSVERSE ACOUSTIC MODES"

Marcus F. Heidmann Washington Feb. 1968 37 p refs (NASA-TN-D-4380) CFSTI: HC\$3.00/MF\$0.65 CSCL 21E

An experimental investigation is made of a traveling transverse acoustic mode generator which utilizes a rotating gas jet as an energy source. The gas jet is radially alined and located at the center of a short cylindrical cavity with an exhaust port at the center of one end plate. Jet rotation is varied over a range of speeds encompassing the rotational speeds of several spinning transverse acoustic modes and pressure amplitudes are measured at the circumference of the cavity. The effect of jet total pressure, jet configuration, and cavity diameter on amplitude is investigated. Pressure amplitude as a function of rotational speed for a single radial jet exhibits several conditions of resonance. One occurs when jet speed corresponds to the resonant frequency of the first transverse mode. Higher modes occur at lower rotational speeds when more than one pressure oscillation is obtained for each rotation of the jet. For all modes and jet configurations, pressure amplitudes increase with an increase in jet total pressure and flow rate. Maximum peak-to-peak pressure amplitudes for all conditions was 38 psi $(2.62 \times 10^5 \text{ N/m}^2)$ which corresponds to a sound pressure level of 192 decibels. The wave shape at all resonant conditions was symmetrical with time about the peak pressure and appeared free of shocks. The conversion efficiency of potential jet power to acoustic power was evaluated for all resonant conditions. In general, efficiency increased with an increase in jet total pressure. A maximum efficiency of 44% was observed with a divergent nozzle. Small diameter jets in a large diameter cavity generally gave highest efficiencies; however, the result depends on jet total pressure. Two radial jets gave improved efficiencies over a single jet in generating the second transverse mode. Efficiencies for the higher modes, however, were nearly an order of magnitude lower than for the first mode for each increase in mode number. Author

N68-17376*# National Aeronautics and Space Administration. Langley Research Center, Langley Station, Va.

PRESSURE AND FLOW FIELD STUDY AT MACH NUMBER 8 OF FLOW SEPARATION ON A FLAT PLATE WITH DEFLECTED TRAILING EDGE FLAP

Charles B. Johnson Washington Mar. 1968 99 p refs

(NASA-TN-D-4308) CFSTI: HC \$3.00/MF \$0.65 CSCL 20D

An experimental investigation was made of the flow separation on a flat plate model with a short trailing-edge flap deflected at angles of 10°, 20°, and 30° relative to the plate surface. These tests were conducted at a nominal free-stream Mach number of 8 and the nominal free-stream unit Reynolds number per foot was varied from 0.22×10^6 to 10.9×10^6 . Pressure measurements and schlieren studies were made for wall-to-total temperature ratios. Surface oil-flow studies were made at a wall-to-total temperature ratio of 0.43. Local similarity boundary-layer calculations were made upstream of the interaction region. Properties of the interaction and separated flow region were calculated with the boundary-layershock-wave interaction theory. Author

N68-17563*# National Aeronautics and Space Administration, Washington, D. C.

CALCULATION OF THE TURBULENT BOUNDARY LAYER AND OF TRANSITION ON A PLANE PLATE [ESSAI DE CALCUL DE LA COUCHE LIMITE TURBULENTE ET DE LA TRANSITION SUR UNE PLAQUE PLANE]

R. Hirsch Feb. 1968 191 p refs Transl. into ENGLISH from Publ. Sci. Tech. Min. Air (France), no. 393, 1963

(NASA-TT-F-520) CFSTI: HC\$3.00/MF\$0.65 CSCL 20D

Calculations of the turbulent boundary layer and transition on a plane plate are derived in detail, including the following: study of a solution of two Navier-Stokes equations inducing a stationary field analogous to the average turbulent field; existence of an asymptotic solution and determination of the development of friction; study of the effect of an exterior harmonic perturbation of wavelength λ . For a critical Reynolds number of 0.0037, the Blasius state is unable to exist and must be replaced by the newly developed state. The perturbations permitting such substitution and formed over the segment of 1/2 Rc are derived, and the calculations are extrapolated to the compressible state with heat exchange. Comparisons of the results with practical experiments show agreement with the Blasius theory of the laminar regime. A possibility exists to maintain the laminar state by replacing the rigid wall with an elastic membrane whose tension would be made dependent on the pulsation of the exterior perturbation which ordinarily causes passage to the turbulent state. Author

12 FLUID MECHANICS

N68-18146*# National Aeronautics and Space Administration. Lewis Research Center, Cleveland, Ohio.

COMPUTER PROGRAM FOR CALCULATING ISOTHERMAL, TURBULENTJET MIXING OF TWO GASES

Leo F. Donovan and Carroll A. Todd Washington Mar. 1968 42 p refs

(NASA-TN-D-4378) CFSTI: HC\$3.00/MF\$0.65 CSCL 20D

This report describes a computer program for solving a simplified model of the turbulent mixing that occurs between a central fuel jet and a surrounding, faster-moving coaxial stream of propellant. As such, this report constitutes a step toward a better understanding of this aspect of the gas-core nuclear rocket. Local values of time-averaged velocity and the mass fraction of fuel can be calculated for a reactor in less isothermal a minute on the IBM 7094. The von Mises transformation was used to convert the axisymmetric forms of the josthermal boundary layer momentum and diffusion equations to forms amenable to numerical solution. The effects of confining walls were not considered. The program can solve problems in which the initial velocities and densities of the two streams differ greatly, by using expressions for eddy viscosity that vary radially as well as axially. The effects of initial coaxial-stream- to jet-velocity and density ratios on velocity and mass fraction profiles are shown. An unspecified reference density occurs in the eddy viscosity formulation; the influences on velocity and mass fraction profiles of several choices for the reference density are illustrated. Radial and axial variations of eddy viscosity and the product of density and eddy viscosity are also given. Estimates are made of the effects of initial velocity ratio and initial density ratio on the mass of the major jet component contained within a given volume. The maximum and minimum amounts that could be present are included for comparison. Author

N68-18253*# National Aeronautics and Space Administration. Langley Research Center, Langley Station, Va.

PRESSURE AND HEAT TRANSFER ON BLUNT CURVED PLATES WITH CONCAVE AND CONVEX SURFACES IN HYPERSONIC FLOW

Davis H. Crawford Washington Mar. 1968 59 p refs

(NASA-TN-D-4367) CFSTI: HC\$3.00/MF\$0.65 CSCL 20M

Pressure and heat transfer have been measured in the presence of both favorable and adverse pressure gradients at Mach numbers of 6.8 and 9.6 and Reynolds numbers based on length from 0.5×10^{6} to 3.0×10^{6} . The pressure data were represented by a power law relationship, and the empirical constants from this relationship were used to calculate the heat transfer by a simplified method. This method allows similar compressible solutions of the laminar boundary layer with pressure gradient to be directly applied without the use of integral or iterative methods. The results of these calculations are compared with the experimental values and with the calculated results from a more complex laminar similarity method requiring a machine program and iterative procedures. Differences between the two theoretical methods are shown to be slight for many applications. Applications where the simple method is less accurate are defined. Author

N68-18997*# National Aeronautics and Space Administration. Ames Research Center, Moffett Field, Calif.

RESULTS OF INCLUDING A BOUNDARY SHOCK WAVE IN THE CALCULATION OF THE FLIGHT PARAMETERS OF A LARGE HIGH-SPEED METEOR

E. Dale Martin Washington Mar. 1968 58 p refs

(NASA-TN-D-4325) CFSTI: HC \$3.00/MF \$0.65 CSCL 20D

The results of including a boundary shock wave in the calculation of the flight parameters of a large high speed meteor with rapid vapor ablation are investigated. Calculations for the meteor use a data curve fitted graphically to the meteor tracking data. These calculations indicate that the proper range of conditions was present on the meteor for a significant portion of its trajectory, for

a very thin strong boundary shock to occur at the meteor surface in the vapor, according to the boundary shock wave theory. Accounting for the effects of the boundary shock wave decreases the pressure drag, but the viscous-compressive drag is high, so the effective drag coefficient is unchanged by the boundary shock. Detailed calculations of the flow about a large high speed meteor would be greatly affected by the boundary shock effects, but overall gross values of the heating and motion parameters calculated by methods used recently by H. J. Allen and N. A. James are valid because of their use of appropriate assumed values of certain parameters.

N68-19000*# National Aeronautics and Space Administration. Langley Research Center, Langley Station, Va.

FORCES AND MOMENTS PRODUCED BY AIR AND HELIUM JETS EXHAUSTING PARALLEL TO A FLAT PLATE IN A NEAR VACUUM

Joseph J. Janos and Sherwood Hoffman Washington Mar. 1968 40 p refs

(NASA-TN-D-4408) CFSTI: HC\$3.00/MF\$0.65 CSCL 20D

An investigation was conducted in the 41 foot vacuum sphere to determine the impingement forces, moments, and centers of pressure on a flat plate produced by small control type nozzles or jets discharging generally parallel to the plate in a near vacuum. The nozzles tested were conical, had approximately the same throat areas, utilized unheated gas, and had nominal exit Mach numbers of 1, 3, 5, and 7 for air, and 1, 3, and 7 for helium. The ratios of nozzle total pressure to ambient pressure varied from 15×10^{6} to about 22×10^{6} ; the ratios of nozzle exit pressure to ambient pressure varied from about 1.4×10^4 to 12×10^6 for the tests at a constant pressure altitude of 95 kilometers. Nozzle positions were varied longitudinally and vertically relative to the plate. Angle of incidence of the flat plate relative to the nozzle center line was varied between -2° and 10° for the air nozzles. The flat plate was detached from the nozzle and mounted on a balance to measure the impingement effects directly. Significant normal forces and moments were obtained and were found to be dependent on nozzle vertical position, longitudinal position, jet exit Mach number, jet flow turning angle, and angle of incidence of the plate. The largest normal force was equal to about 50% of the gross thrust of the Mach number 1 nozzle when located relatively close to the plate. The impingement forces decreased with increasing height or jet Mach number, and decreasing jet turning angle or angle of plate incidence. Helium jets produced lower impingement forces and moments than the corresponding air jets at comparable locations. Author

N68-19225*# National Aeronautics and Space Administration. Lewis Research Center, Cleveland, Ohio.

EXPERIMENTAL INVESTIGATION OF VAPOR INGESTION IN THE CENTAUR LIQUID HYDROGEN TANK

Raymond F. Lacovic and Andrew J. Stofan Washington Mar. 1968 16 p refs

(NASA-TM-X-1482) CFSTI: HC\$3.00/MF\$0.65 CSCL 20D

An investigation of vapor ingestion during liquid outflow was conducted in a 1/3.67 and 1/38 scale-model Centaur liquid hydrogen tank at the Lewis Research Center. The purpose of the investigation was to establish the height above the concave oblate ellipsoidal tank bottom at which vapor ingestion would occur for two tank outflow rates at various acceleration levels in order to define Centaur propellant residuals. Experimental values of the liquid height at which vapor ingestion occurs were obtained at normal gavity. A Froude number simulation was then used to relate the normal gravity experimental data to other acceleration levels. The experimental values were correlated with an analytical expression based on Bernoulli's equations. The analytical expression correlated well with the experimental values over the entire range of tank outflow rates. N68-19246*# National Aeronautics and Space Administration. Lewis Research Center, Cleveland, Ohio.

SIMILARITY SOLUTION FOR TURBULENT MIXING BETWEEN A JET AND A FASTER MOVING COAXIAL STREAM

Leo F. Donovan Washington Mar. 1968 27 p refs

(NASA-TN-D-4441) CFSTI: HC\$3.00/MF\$0.65 CSCL 20D

An analysis of turbulent mixing of a jet with a faster moving coaxial stream is presented, and a similarity solution is obtained for large initial ratios of coaxial-stream velocity to jet velocity. The analysis is compared with experimental data, and the velocity profiles at different axial positions are shown to be similar. Centerline velocities follow the predicted behavior reasonably well except for the smallest experimental velocity ratio: half-radii, an indication of the amount of jet spreading, vary as expected after a certain axial distance. The shear-stress distributions are not similar, even at the largest axial positions for which data are available. In addition, the similarity solution is extended to include constant-density mass transfer or heat transfer.

N68-19340*# National Aeronautics and Space Administration. Lewis Research Center, Cleveland, Ohio.

MODEL FOR FREQUENCY RESPONSE OF A FORCED FLOW, HOLLOW, SINGLE, TUBE BOILER

Eugene A. Krejsa Washington Mar. 1968 29 p refs

(NASA-TM-X-1528) CFSTI: HC\$3.00/MF\$0.65 CSCL 20D

A simple model is given for the frequency response of boiler inlet pressure to inlet flow. The boiler analyzed is a forced flow, single tube, shell and tube boiler with no inserts. The model yields a simple description of the boiler dynamic characteristics. The characteristics included in the model are boiler pressure drop, time required for the liquid temperature to reach saturation temperature, inertia of the liquid in the subcooled region, and mass storage due to the movement of the boundary between the subcooled and two-phase regions. The model is compared with experimental boiler frequency response data. The boiling fluid was Freon-113, which was heated by counterflowing hot water. The boiler exit quality ranged from 12 to 63 percent. Good agreement between the model and the data was obtained for qualities ranging from 23 to 63 percent.

N68-19709*# National Aeronautics and Space Administration. Langley Research Center, Langley Station, Va.

EVALUATION OF BOUNDARY LAYER AND WAKE SURVEY DATA REDUCTION TECHNIQUES IN COMPRESSIBLE FLOWS

K. R. Czarnecki and Russell B. Sorrells, III Washington Apr. 1968 32 p refs

(NASA-TN-D-4401) CFSTI: HC\$3.00/MF\$0.65 CSCL 20D

The analytical study was limited to turbulent boundary layers with no heat transfer and to a Mach number range from 0 to 10. The experimental portion of the investigation was confined to zero-heat-transfer turbulent-wake surveys made behind a swept wing at free-stream Mach numbers of 1.61 and 2.01. Results of the analytical boundary-layer calculations indicate that if simplified data-reduction techniques that neglect the deviation of the local Mach number from the average free-stream or normalizing value are utilized, sizable differences in momentum, displacement, and velocity thicknesses are incurred over much of the Mach number range for relatively small deviations in the local-flow characteristics or parameters. In general, use of the free-stream Mach number as a base both for determining velocity defects due to skin friction and for normalizing the thickness parameters, will introduce larger differences than use of local Mach number as the base for both items and interpretation of results as being obtained under stream conditions. Experimental wake data indicate that because of increased wake widths and reduced viscous heating or compressibility effects in comparison with boundary layers of equal momentum deficiency, the use of the free-stream-flow technique generally results in proportionately larger differences in wake-data reduction. Author

N68-20352*# National Aeronautics and Space Administration. Lewis Research Center, Cleveland, Ohio.

AN EXPERIMENTAL INVESTIGATION OF THE EFFECT OF GRAVITY ON A FORCED CIRCULATION PATTERN IN SPHERICAL TANKS

Steven G. Berenyi, Ralph C. Nussle, and Kaleel L. Abdalla Washington Apr. 1968 25 p refs

(NASA-TN-D-4409) CFSTI: HC\$3.00/MF\$0.65 CSCL 20D

An experimental investigation of the effect of gravity on a forced circulation pattern in spherical tanks was conducted. The tank systems tested were exposed to acceleration levels of approximately 0.005, 0.01, 0.02, 1.0, and less than 10^{-5} g. The flow pattern of an axisymmetric wall jet was experimentally established in three different size tanks. The results indicate that the minimum jet inlet velocity required to establish and maintain the flow pattern is a function of jet inlet thickness, tank radius, and gravity level. Author

N68-21365*# National Aeronautics and Space Administration. Lewis Research Center, Cleveland, Ohio.

AN EXPERIMENTAL STUDY OF LIQUID FLOW INTO A BAFFLED SPHERICAL TANK DURING WEIGHTLESSNESS

Charles R. Andracchio and Kaleel L. Abdalla Washington Apr. 1968 23 p refs

(NASA-TM-X-1526) CFSTI: HC\$3.00/MF\$0.65 CSCL 20D

Liquid flow into a baffled spherical tank during weightlessness was investigated. A sphere within a sphere configuration was tested using a partially wetting liquid and a totally wetting liquid while varying the percent initial filling in the tank. Both liquids can be pumped into the tank over a range of velocities which maintains the liquid-vapor interface in a stable orientation; the maximum value of these velocities is a function of initial liquid filling in the tank. A baffled tank allowed higher stable filling rates than an unbaffled tank; similarly, the partially wetting liquid allowed higher stable filling rates than the totally wetting liquid. The use of a deflector mounted on the baffle improved the stable filling rate of the totally wetting liquid at low initial fillings. Author

N68-21724*# National Aeronautics and Space Administration. Lewis Research Center, Cleveland, Ohio. VISCOSITY OF GAS MIXTURES

Richard S. Brokaw Washington Apr. 1968 27 p refs

(NASA-TN-D-4496) CFSTI: HC\$3.00/MF\$0.65 CSCL 20D

An approximate method is developed for predicting the viscosities of mixtures involving both nonpolar and polar gases. For nonpolar mixtures, only the viscosities and molecular weights of the constituents are required, in addition to the mixture composition. With polar gases, dipole moments, boiling points, and boiling-point densities are also needed. The method is tested by comparison with experimental data on 25 gas pairs comprising 280 mixtures. The average error is 0.7 percent; the maximum error is 3.7 percent. (Errors may be much larger if this method is used for gas mixtures involving ions, free radicals, or valence-unsaturated atoms.) Author

NG8-22087*# Tracor, Inc., Rockville, Md. AN ANALYTICAL STUDY OF THE MEASURED WALL PRESSURE FIELD UNDER SUPERSONIC TURBULENT BOUNDARY LAYERS

Thomas J. Black Washington NASA Apr. 1968 167 p refs (Contract NAS1-6952)

(NASA-CR-888; TRACOR-RL/67-070-U) CFSTI: HC \$3.00/MF \$0.65 CSCL 20D

This report presents the results of a short analytical study of the turbulent wall pressure field under supersonic shear layers.

12 FLUID MECHANICS

The study is based on a theory of wall turbulence which asserts that the turbulent transfer of mass, heat, momentum and energy within the boundary layer are essentially effected within discrete, horseshoe-vortex structures which are generated and maintained by powerful, localized non-linear instabilities within the sublayer and which move downstream over the wall in a characteristic, quasi-frozen, spatial array. In particular, the theory explains the generation of turbulent shear stress in terms of the dynamic interaction between these vortex systems and the basic shear flow through which they move. On the basis of this theory, new scaling laws are proposed for the turbulent wall pressure field under subsonic and supersonic layers. These laws feature quite different scaling parameters for the high and low frequency portions of the spectra and indicate the effect of pressure gradient on the spectra. Author

N68-22200*# United Aircraft Corp., East Hartford, Conn. EXPERIMENTAL INVESTIGATION OF CONTAINMENT IN CONSTANT-TEMPERATURE RADIAL-INFLOW VORTEXES John S. Kendall Washington NASA May 1968 49 p refs

(Contract NASw-847)

(NASA-CR-1029; F-910091-15) CFSTI: HC \$3.00/MF \$0.65 CSCL 20D

An experimental investigation was conducted to determine the containment characteristics of radial-inflow vortexes for potential application to a vortex-stabilized nuclear light bulb engine. Tests were conducted using 10-in.-dia by 30-in.-long vortex tubes. Air used to simulate the buffer gas was injected through ports in the peripheral walls of the vortex tubes. lodine mixed with one of four other gases (helium, nitrogen, sulfur hexafluoride or a heavy fluorocarbon, FC-77) was used to simulate the gaseous nuclear fuel. The amount and radial distribution of simulated fuel contrined in the vortex were determined using an axial light beam absorption technique. The effects on containment of changes in the following were investigated: (1) the geometry of the simulated-fuel injection configurations, (2) the number of thru-flow ports used, (3) the radial Reynolds number (a measure of the amount of flow withdrawn through the thru-flow ports) and the corresponding amount of bypass flow, and (4) the molecular weight of the simulated fuel. Author

N68-23353*# National Aeronautics and Space Administration. Lewis Research Center, Cleveland, Ohio.

CAPILLARY RISE IN THE ANNULAR REGION OF CONCENTRIC CYLINDERS DURING COAST PERIODS OF ATLAS CENTAUR FLIGHTS

Raymond F. Lacovic and James A. Berns Washington May 1968 14 p refs

(NASA-TM-X-1558) CFSTI: HC\$3.00/MF\$0.65 CSCL 20D

The Centaur space vehicle liquid oxygen and liquid hydrogen tanks each contain a mass sensing system which utilizes flow through a helical inlet tube into a probe consisting of two concentric cylinders. During the coast periods of the Atlas-Centaur flights, each mass sensing system acted as a capillary system under low gravity conditions. Data for the capillary rise height in the annular region of concentric cylinders as a function of time were obtained from the flights of three Atlas-Centaurs at acceleration levels of approximately 7.0×10^{-3} and 4.2×10^{-4} g with durations of up to 100 and 1341 seconds, respectively. The capillary rise data were correlated with an analytical expression which accurately described the fluid flow through the sensing system under low gravity conditions.

N68-23423*# National Aeronautics and Space Administration. Lewis Research Center, Cleveland, Ohio.

EFFECTS OF HIGH-WAVE AMPLITUDE AND MEAN FLOW ON A HELMHOLTZ RESONATOR

Bert Phillips Washington May 1968 21 p refs

(NASA-TM-X-1582) CFSTI: HC\$3.00/MF\$0.65 CSCL 21H

An experimental investigation was conducted to determine the effects of mean flow and high-wave amplitude on the impedance of a Helmholtz resonator. The oscillatory phase and pressure relations across the aperture of a resonator were measured and converted into values of acoustic resistance and reactance. The results indicate that (1) the aperture effective length in a rocket-engine environment should be considered approximately equal to the aperture thickness and (2) the acoustic resistance at high-wave amplitude can be considered to be a turbulent jet loss. Author

N68-23482*# Douglas Aircraft Co., Santa Monica, Calif. NARROW BAND CROSS-CORRELATION ANALYSIS OF FLUCTUATING PRESSURES BENEATH A TURBULENT BOUNDARY LAYER

C. M. Ailman and A. S. Hopkins Washington NASA May 1968 83 p refs

(Contract NAS1-6901)

(NASA-CR-1066; DAC-60874) CFSTI: HC \$3.00/MF \$0.65 CSCL 20D

Selected narrow-band cross-correlations were calculated for pressure fluctuations at a rigid wall under both a uniform and a disturbed turbulent boundary layer at supersonic speeds. Flow disturbances resulted from: (1) a forward-facing step-spoiler, (2) an aft-facing step (with a well-behaved, slowly growing turbulent boundary layer prior to the step); and (3) an impinging (and reflected) shock generated by an obstruction to the airstream some distance from the wall. The data are presented in terms of contours of equal correlation coefficient, spatial decays of the correlation, and convection velocities. Author

N68-24129*# National Aeronautics and Space Administration. Lewis Research Center, Cleveland, Ohio.

RAREFIED-GAS COUETTE FLOW AND HEAT TRANSFER BETWEEN PARALLEL PLATES BY MODEL SAMPLING Morris Perlmutter Washington May 1968 44 p refs

(NASA-TN-D-4579) CFSTI: HC \$3.00/MF \$0.65 CSCL 20D

A rarefied gas with hard sphere molecules enclosed between parallel walls is analyzed for the case of couette flow and heat transfer by a model sampling procedure. In one case, both walls are stationary and at different temperatures. In the other case, the upper wall is moving in a direction parallel to the lower wall and both walls are at the same temperature. The wall accommodation factor is taken as unity. The target molecule velocity distribution is presumed to be the sum of two different half-Maxwellians. The parameters describing the half-Maxwellians are assumed constant over a given zone. By scoring the properties of sample molecules as they pass scoring positions, the macroscopic quantities, of interest are obtained. The problem is iterated until these values agree with the assumed distribution values.

N68-24758*# National Aeronautics and Space Administration. Lewis Research Center, Cleveland, Ohio.

EFFECTS OF LIQUID DEPTH ON LATERAL SLOSHING UNDER WEIGHTLESS CONDITIONS

Jack A. Salzman, Thom A. Coney, and William J. Masica Washington May 1968 18 p refs

(NASA-TN-D-4458) CFSTI: HC\$3.00/MF\$0.65 CSCL 20D

As a part of the general study of liquid behavior in weightlessness, an experimental drop-tower investigation was conducted to determine the effects of shallow liquid depths on lateral sloshing in a zero Bond number environment. Contact angles were restricted to very near 0°, so that the sloshing equilibrium interface was hemispherical. Cylindrical tanks were tested with both hemispherical and flat bottoms. Natural frequency data were correlated as a function of normalized liquid depth for both tank bottom shapes, and damping data were compared with predictions from high Bond number theory.

N68-25866*# National Aeronautics and Space Administration. Lewis Research Center, Cleveland, Ohio.

LIQUID INFLOW TO INITIALLY EMPTY, HEMISPHERICAL ENDED CYLINDERS DURING WEIGHTLESSNESS

Eugene P. Symons, Ralph C. Nussle, and Kaleel L. Abdalla Washington Jun. 1968 16 p refs

(NASA-TN-D-4628) CFSTI: HC \$3.00/MF \$0.65 CSCL 20D

An experimental investigation was conducted in a weightless environment during which liquid was pumped into hemispherical ended cylinders which were initially void of liquid. During inflow, two distinct types of liquid-vapor interfaces were observed; a stable interface and an unstable interface. The stability of the liquid-vapor interface was correlated by a Weber number based on inlet line radius and inlet velocity. Results indicate that above a Weber number of 1.3, the interface became unstable. Furthermore, this filling process was independent of the radii of the experiment tanks (2 to 4 cm). No gross effects due to the viscosity of the test liquid were observed. Author

N68-26651*# National Aeronautics and Space Administration. Lewis Research Center, Cleveland, Ohio.

DETAILED PERFORMANCE OF A RADIAL-BLADED CENTRIFUGAL PUMP IMPELLER IN WATER

Max J. Miller and Richard F. Soltis Washington Jun. 1968 52 p refs

(NASA-TN-D-4613) CFSTI: HC \$3.00/MF \$0.65 CSCL 20D

Shrouded and unshrouded versions of a 7.44-in.-{18.89-cm-} diameter, radial-bladed centrifugal pump impeller were tested in room-temperature water. Detailed measurements permitted the calculations of both circumferential and spanwise distributions of flow and performance parameters over a wide range of flows. Primary emphasis is on essentially noncavitating flow conditions, although a limited amount of performance data obtained under cavitating flow conditions is presented.

N68-28282*# National Aeronautics and Space Administration. Langley Research Center, Langley Station, Va.

LOCAL AFTERBODY HEAT TRANSFER TO A BLUNT TWO-DIMENSIONAL CONFIGURATION AT MACH 8

Dennis M. Bushnell (M.S. Thesis-Va. Univ.) Washington Jul. 1968 50 p refs

(NASA-TN-D-4443) CFSTI: HC\$3.00/MF\$0.65 CSCL01A

Local heat-transfer rates and pressures were measured on a blunt two-dimensional configuration the afterbody of which was subjected to an extensive region of separated flow. The investigation was conducted at a free-stream Mach number of 8 and at free-stream Reynolds numbers based on the model face width of 2 inches (5.08 cm) from 1.27 \times 105 to 7.55 \times 105. The predictions from two theories were compared with the heat-transfer data obtained in the afterbody region. One of these theories was a constant-pressure integral method utilizing profiles from similar solutions for enthalpy and velocity distributions. The other theory was a local flat-plate method in which the velocity and enthalpy conditions obtained from the integral method in the reverse-flow region were used as effective free-stream quantities. Both theories were in reasonable agreement with the general level of the data. The integral method predicted the correct trend in the vicinity of the separation point, whereas the flat-plate method gave the correct trend over the aft portion of the afterbody. Author

N68-28364*# National Aeronautics and Space Administration. Lewis Research Center, Cleveland, Ohio.

MAXIMUM DROP DIAMETERS FOR THE ATOMIZATION OF LIQUID JETS INJECTED CONCURRENTLY INTO ACCELERATING OR DECELERATING GAS STREAMS Robert D. Ingebo Washington Jul. 1968 26 p refs

(NASA-TN-D-4640) CFSTI: HC\$3.00/MF\$0.65 CSCL 20D

The determining effect of six dimensionless groups on the maximum drop-diameter was studied for the atomization of jets of ethanol or water injected into nitrogen or helium gas streams cocurrently or into still air. Values of the ratio of orifice diameter to maximum drop-diameter D_o/D_m were obtained from photomicrographs of the sprays and related to dimensionless groups. Liquid-injection velocities covered a range of nearly 0 to 6250 cm/sec. Gas-stream velocities were varied from the still-air condition to helium-gas velocities of 14,000 cm/sec. Gas-stream accelerations ranged from 833,000 to 19,200,000 cm/sec², and decelerations of 672,000 to 4,880,000 cm/sec².

N68-28370*# National Aeronautics and Space Administration. Lewis Research Center, Cleveland, Ohio.

PHOTOGRAPHIC STUDY OF A BROMINE JET IN A COAXIAL AIRSTREAM

Maynard F. Taylor and Charles C. Masser Washington Jul. 1968 19 $\ensuremath{\text{p}}$ refs

(NASA-TN-D-4660) CFSTI: HC\$3.00/MF\$0.65 CSCL 20D

Photographs were taken of a bromine jet issuing into a coaxially flowing airstream. The bromine jet appeared laminar for jet velocities below 1.5 m/sec and airstream velocities below 2.1 m/sec. If either the jet or stream velocity exceeded the aforementioned velocity the bromine jet appeared nonlaminar. These velocities can be expressed as nondimensional parameters, jet Reynolds number and stream- to jet-velocity ratio. In terms of these parameters, the jet will have a laminar appearance if both the jet Reynolds number is less than about 2400 and the product of the stream- to jet-velocity ratio and the Reynolds number is less than about 3400. The investigation covered only the region from the injection point to five jet radii downstream.

N68-28801*# National Aeronautics and Space Administration. Flight Research Center, Edwards, Calif.

WIND-TUNNEL CALIBRATION OF A 40° CONICAL PRESSURE PROBE AT MACH NUMBERS FROM 3.5 TO 7.4 Frank W. Burcham, Jr. Washington Jul. 1968 26 p refs (NASA-TN-D-4678) CFSTI: HC\$3.00/MF\$0.65 CSCL 01A

A wind-tunnel calibration of a 40° included-angle flow-field cone probe was made over a Mach number range of 3.5 to 7.4. The cone probe was designed and fabricated to obtain flow-field, data on the X-15 airplane. Estimated accuracy of the calibration, was ± 2 percent in Mach number and $\pm 0.2^{\circ}$ in flow angularity at a Mach number of 7.4. Reynolds number effects were negligible over the test range of 0.65 million to 3.25 million per foot (0.20 million to 1.0 million per meter). A rake designed for flight on the X-15 was used to mount two cone probes. Slightly different calibrations resulted for the two cones because of differences in the cone afterbody configurations. Author

N68-28842*# National Aeronautics and Space Administration. Lewis Research Center, Cleveland, Ohio.

VISUAL OBSERVATIONS OF "FLOW THROUGH A RADIAL-BLADED CENTRIFUGAL IMPELLER

Richard F. Soltis and Max J. Miller Washington Jul. 1968 26 p refs

(NASA-TN-D-4282) CFSTI: HC\$3.00/MF\$0.65 CSCL 20D

A 7.44-inch-(18.89-cm-) diameter radial-bladed centrifugal impeller designed by the stream-filament technique was operated in water over a range of flow conditions. Flow through the blade passages was visualized by observing the movement of nylon tufts glued to the impeller and by injecting dye into fluid at the pump inlet. Photographs and film sequences of the tufts and dye in the rotating passages are presented. A comparison of visual observations is also made with the measured performance results and with the flow conditions within the blade passages as calculated from an analytical procedure.

N68-31593*# Stevens Inst. of Tech., Hoboken, N. J. HYDRODYNAMICS OF AIRCRAFT TIRE HYDROPLANING S. Tsakonas, C. J. Henry, and W. R. Jacobs Washington NASA Aug. 1968 46 p refs

12 FLUID MECHANICS

(Contract NSR-31-003-016)

(NASA-CR-1125; REPT.-1238) CFSTI: HC \$3.00/MF \$0.65 CSCL 01B

An approximate theory has been developed for a study of the hydroplaning tire by considering it as a planing surface of small aspect ratio in extremely shallow water. The results of this approximation exhibit hydrodynamic behavior similar to that of hydroplaning pneumatic tires and thus indicate that the tire hydroplaning pneumatic tires and thus indicate that the tire hydroplaning pneumatic. The analysis furnishes families of curves which can be considered to represent, qualitatively, the start of hydroplaning and thus give qualitative guidance for avoiding the undesirable hydroplaning condition. Author

N68-31960*# National Aeronautics and Space Administration. Lewis Research Center, Cleveland, Ohio.

NONCAVITATING AND CAVITATING PERFORMANCE OF TWO LOW-AREA-RATIO WATER JET PUMPS WITH THROAT LENGTHS OF 5.66 DIAMETERS

Nelson L. Sanger Washington Aug. 1968 34 p refs

(NASA-TN-D-4759) CFSTI: HC\$3.00/MF\$0.65 CSCL 13K

Performance of two jet pumps was determined over a range of spacings of the nozzle exit from the throat entrance of 0 to 2.9 throat diameters. Maximum measured efficiencies of 31.3 and 37.6 percent were achieved for nozzle- to throat-area ratios of 0.066 and 0.197, respectively. These efficiencies were improvements over those obtained for previously investigated jet pumps with throat lengths of 7.25 diameters. A simple one-dimensional analysis predicted noncavitating performance within 2 percent at the best-efficiency conditions. The point of total headrise deterioration due to cavitation was predicted with reasonable accuracy by each of two related parameters. Author

N68-32982*# National Aeronautics and Space Administration. Ames Research Center, Moffett Field, Calif.

STUDY OF OPTICAL RADIATION IN THE WAVELENGTH REGIONS OF 0.4216 μ , 0.4278 μ , 0.4825 μ , and 0.5165 μ behind normal shock waves in a simulated martian atmosphere

Anthony P. Modica (Avco Corp.), Harry B. Dyner (Avco Corp.), and James O. Arnold Washington Aug. 1968 10 p refs

(NASA-TM-X-1634) CFSTI: HC\$3.00/MF\$0.65 CSCL 20D

Shock-tube measurements of equilibrium and nonequilibrium radiation in a 50-percent CO_2 -50-percent N_2 gas mixture are analyzed and compared to theoretical estimates and other measurements. The ratio of the integrated radiation from the nonequilibrium zone behind the normal shock wave to the equilibrium radiation from an equal volume of gas is of particular interest. The measurements show no appreciable differences in nonequilibrium enhancement from four different spectral regions. Author

N68-33054*# National Aeronautics and Space Administration. Langley Research Center, Langley Station, Va.

DRAG DUE TO TWO-DIMENSIONAL SURFACE ROUGHNESS IN A TURBULENT BOUNDARY LAYER AT MACH 3 WITH AND WITHOUT HEAT TRANSFER

William J. Monta, K. R. Czarnecki, and William D. Deveikis Washington Sep. 1968 41 p refs

(NASA-TN-D-4746) CFSTI: HC\$3.00/MF\$0.65 CSCL 20D

An investigation was conducted on an ogive-cylinder model to determine the effect of heat transfer on the drag due to two fabrication roughness shapes (steps with grooves and circular arc waves) at Reynolds numbers from 36×10^6 to 195×10^6 . The results indicate only a slight effect of heat transfer and Reynolds number upon the roughness drag for the two configurations of the investigation. The zero heat transfer data are in good agreement with previously published results. The step roughness drag is correlated on the basis of a step-height Reynolds number and is in good agreement with both existing data and an existing prediction method based on effective dynamic pressure. For the wave-shaped wall, a nondimensional drag parameter was found to be a function

of the ratio of roughness height to boundary layer thickness for a constant value of the roughness thickness ratio h/l. At the lower values of h/l, the parameter is a unique function of the ratio of roughness cycle length to boundary layer thickness. Author

N68-33056*# National Aeronautics and Space Administration. Ames Research Center, Moffett Field, Calif.

FINITE AMPLITUDE WAVES IN FLUID-FILLED ELASTIC TUBES: WAVE DISTORTION, SHOCK WAVES, AND KOROTKOFF SOUNDS

Richard M. Beam Washington Sep. 1968 52 p refs (NASA-TN-D-4803) CFSTI: HC\$3.00/MF\$0.65 CSCL 20D

The Lagrangian form of the one-dimensional equations of motion for a fluid-filled elastic tube is developed. The resulting nonlinear equations are combined with a general nonlinear internal pressure cross sectional area relation for the tube to obtain the finite amplitude wave equation. After determination of the tube pressure-area relation which leads to a linear wave equation, a solution for the general wave equation is presented. The solution is applicable for simple waves in tubes with general pressure-area relations. The solution is then used to develop criteria for the steepening and nonsteepening of finite amplitude waves. The theory is further developed to include the calculation of wave distortion. The criterion for a sharp wave is derived and the critical length of tube required for a sharp wave to develop is determined. The propagation of the resulting sharp wave or shock wave is considered. The velocity and the energy loss formulas for the shock wave are developed. Finally, the analysis and experimental results are used to support new hypotheses for the mechanism and source of the Korotkoff sounds which have a major role in the indirect Author determination of blood pressure.

N68-33165*# National Aeronautics and Space Administration. Lewis Research Center, Cleveland, Ohio.

LIQUID DROPS: NUMERICAL AND ASYMPTOTIC SOLUTIONS OF THEIR SHAPES

Kenneth J. Baumeister and Thomas D. Hamill Washington Sep. 1968 34 p refs

(NASA-TN-D-4779) CFSTI: HC\$3.00/MF\$0.65 CSCL 20D

The shapes of liquid drops resting on flat surfaces were determined by a Runge-Kutta solution of the Laplace capillary equation. A characteristic length equal to the square root of surface tension divided by the product of density and gravity was used to nondimensionalize the numerical results. In addition, asymptotic solutions for small and large drops were combined to give explicit expressions for the maximum drop height and radius. These correlations apply for the complete range of liquid volumes and contact angles.

N68-33642*# National Aeronautics and Space Administration. Lewis Research Center, Cleveland, Ohio.

LAMINARIZATION OF A TURBULENT BOUNDARY LAYER AS OBSERVED FROM HEAT-TRANSFER AND BOUNDARY LAYER MEASUREMENTS IN CONICAL NOZZLES

Donald R. Boldman, James F. Schmidt, and Anne K. Gallagher Washington Sep. 1968 34 p refs

(NASA-TN-D-4788) CFSTI: HC\$3.00/MF\$0.65 CSCL 20D

Heat transfer measurements were obtained in 30° and 60° half-angle of convergence nozzles at a nominal stagnation temperature of 970°R (539 K) and over a range of stagnation pressures of 2.0 to 20.4 atmospheres (2.03×10^5 to 20.67×10^5 N/m²). These conditions provided nozzle throat Reynolds numbers based on diameter of about 6.0 $\times 10^5$ to 5.0 $\times 10^6$. Boundary layer time-mean velocity and temperature measurements were obtained at one station in a water cooled pipe inlet and at a subsonic (Mach number ≤ 0.08) station in each nozzle at stagnation pressures of 3.1 and 20.4 atmospheres (3.14 $\times 10^5$ and 20.67 $\times 10^5$ N/m²). The heat transfer and boundary layer surveys suggested the occurrence of laminarization of an initially turbulent boundary layer.

N68-34089*# National Aeronautics and Space Administration. Lewis Research Center, Cleveland, Ohio.

EFFECTS OF BOUNDARY LAYER BUILDUP IN SHOCK TUBES UPON CHEMICAL RATE MEASUREMENTS Marvin Warshay Washington Sep. 1968 18 p refs

(NASA-TN-D-4795) CFSTI: HC\$3.00/MF\$0.65 CSCL 20D

A theory by Mirels was employed to investigate the effects of boundary layer buildup in shock tubes upon dissociation rate measurements. A comparison was made of bromine dissociation rate constant which were obtained assuming no boundary layer buildup to those obtained when boundary layer was taken into account. Mirels' wholly turbulent boundary layer case was used in the latter calculations. At low temperatures (1264°K), where reaction rates are low, the measured rate constant increased significantly; at high temperatures (1827°K), where rates are high, the effect was negligible. In quantitative terms, the activation energy decreased from 31.5 to 30.0 kilocalories (1.32 \times 10⁵ to 1.26 \times 10⁵ j). Author

N68-35086*# Southwest Research Inst., San Antonio, Tex. FLOW-INDUCED VIBRATIONS OF A FLAT PLATE SUSPENDED IN A NARROW CHANNEL Final Report

Franklin T. Dodge and Arthur F. Muller Washington NASA Sep. 1968 62 p refs

(Contract NAS1-6714)

(NASA-CR-1186) CFSTI: HC \$3.00 /MF \$0.65 CSCL 181

Elastically restrained plates in narrow flow channels can vibrate excessively when the flow rate past them reaches some critical value. Because of the importance of this phenomenon in nuclear reactor design, an analytical study of such vibrations has been conducted. The theory is based upon the one-dimensional, hydraulic flow assumption and includes viscous pressure drops and energy losses at channel contractions and expansions. Since the vibrating plate influences the hydrodynamic loading and vice versa, the unknown flow velocity and plate vibration freugency are coupled and must be determined simultaneously. The results of the calculations for several typical flow situations show that the flow velocity necessary to induce vibrations decreases as the channel height-to-plate length ratio decreases; this is in substantial agreement with previous potential flow calculations although not with experimental data. Author

N68-35096*# Princeton Univ., N. J.

A METHOD OF CALCULATING COMPRESSIBLE TURBULENT BOUNDARY LAYERS

H. James Herring and George L. Mellor Washington NASA Sep. 1968 112 p refs

(Grant NGR-31-001-074)

(NASA-CR-1144) CFSTI: HC \$3.00 /MF \$0.65 CSCL 20D

The essential unknown quantity in a compressible turbulent boundary layer is shown to be the kinematic Reynolds stress, as in incompressible flow, and does not explicitly involve density fluctuations. Based on this, the incompressible turbulent viscosity proposed by Mellor is extended to include compressible flows. The same values of the three empirical constants, which were obtained solely from constant-property, constant-pressure experiments, are also used. Without making any further assumptions beyond those related to the usual time averaged boundary layer equations, this system of equations has been programmed for numerical solution. Solutions have been compared to a considerable amount of constant-pressure data in the range from subsonic flows to flows with Mach numbers around 5.0 and the comparisons are quite favorable. Much less pressure gradient data are available but comparison was made to some axisymmetric flow data taken in a positive pressure gradient which indicated fairly good prediction of the boundary layer growth, while at the same time pointing up a systematic error in the detailed profile shape prediction in regions of finite longitudinal curvature. Author

N68-35104*# National Aeronautics and Space Administration. Lewis Research Center, Cleveland, Ohio.

ANALYTICAL AND EXPERIMENTAL INVESTIGATION OF OUTFLOW RESIDUALS IN INTERCONNECTED SPHERICAL TANKS

Harold J. Kasper and Robert J. Boyle Washington Sep. 1968 36 p refs

(NASA-TN-D-4828) CFSTI: HC\$3.00/MF\$0.65 CSCL 21H

An analysis is presented for predicting the propellant distribution during outflow of multiple-interconnected spherical tanks for possible space vehicle application. Analytical and experimental data are presented for four spherical tanks using water as the working fluid. The effects on final liquid residuals were determined for tanks that: (1) did or did not utilize crossflow lines between tanks for liquid level equilibration, (2) were initially equally oun unequally loaded, and (3) had equal or unequal length outflow lines. The analysis adequately predicted the experimental residuals as well as the point at which crossflow lines ceased to be effective equilibration flow paths. Author

N68-35114*# National Aeronautics and Space Administration. Lewis Research Center, Cleveland, Ohio.

LIQUID REORIENTATION IN SPHERES BY MEANS OF LOW-G ACCELERATIONS

Thomas L. Labus and William J. Masica Washington Oct. 1968 32 p refs

(NASA-TM-X-1659) CFSTI: HC\$3.00/MF\$0.65 CSCL 20D

An experimental drop-tower investigation of liquid reorientation in spherical containers was conducted from two initial interface conditions. One initial condition was a centrally located vapor bubble (the interface configuration in a zero-Bond-number environment). A second initial condition was an essentially flat interface (the configuration in a relatively high-Bond-number environment). Liquid reorientation was observed to be axisymmetric under both initial conditions. Qualitative observations of the gross effects of percent liquid volume and acceleration on the reorientation process are presented. Also included are graphic profiles of the liquid-vapor interface at selected times during the reorientation process. Author

N68-35117*# National Aeronautics and Space Administration. Langley Research Center, Langley Station, Va.

EQUILIBRIUM NORMAL-SHOCK AND STAGNATION-POINT PROPERTIES OF HELIUM FOR INCIDENT-SHOCK MACH NUMBERS FROM 1 TO 30

Walter B. Olstad, Jane T. Kemper, and Roger D. Bengtson Washington Sep. 1968 51 $p\ refs$

(NASA-TN-D-4754) CFSTI: HC\$3.00/MF\$0.65 CSCL 20M

Charts are presented of the thermodynamic properties of helium, including the effects of ionization and particle interactions, for temperatures to 100,000 °K and pressures from 10-7 to 104 atmospheres. The properties behind the incident, standing, and reflected shocks and at the in-flight and shock-tube stagnation conditions are also presented for incident-shock Mach numbers from 1 to 30 and quiescent gas pressure from 10-7 to 1 atmosphere. Author

N68-35252*# Illinois Univ., Urbana.

DRAG ASSOCIATED WITH SEPARATED FLOW OVER TWO-DIMENSIONAL V-SHAPED NOTCHES UNDER TRANSONIC AND SUPERSONIC CONDITIONS

Ronald H. Howell and Helmut H. Korst Washington NASA Sep. 1968 87 p refs

(Grant NsG-13)

(NASA-CR-1132) CFSTI: HC \$3.00/MF \$0.65 CSCL 01A

The wall geometry was limited to two-dimensional symmetric notches defined by specifying the length and angle of the notch. For any given notch geometry the free stream Mach number was the primary variable while the viscous effects, specified by the boundary layer momentum thickness and the length Reynolds number, were secondary variables. The Mach number ranged from 0.5 to 1.2 and at 2, while the approaching boundary layer was

12 FLUID MECHANICS

always turbulent and reasonably well representative of fully developed shear layers along adiabatic flat plates with the momentum thickness Reynolds number from 7500 to 15000. To cover a wide range of boundary layer momentum thickness-to-notch-depth ratios, experiments were carried out with notches of various lengths and notch angles. Schlieren observations, pressure distributions, and direct drag force measurements were used in studying the viscid-inviscid flow phenomena controlling the drag of notches and the redevelopment of the boundary layer downstream of the disturbance. Author

N68-35823*# National Aeronautics and Space Administration. Lewis Research Center, Cleveland, Ohio.

LIQUID VAPOR INTERFACE CONFIGURATIONS IN TOROIDAL TANKS DURING WEIGHTLESSNESS

Eugene P. Symons and Kaleel L. Abdalla Washington Oct. 1968 13 p refs

(NASA-TN-D-4819) CFSTI: HC\$3.00/MF\$0.65 CSCL 20D

An experimental investigation was conducted in the Lewis Research Center drop tower facility to study the isothermal liquid-vapor interface configuration in a toroidal tank during weightlessness for a 0°-static-contact-angle liquid. Results are presented for a range of liquid volumes in tanks normally positioned horizontally and also for tanks mounted at angles to the gravity field prior to the weightless test. The angle tests simulated the effect of nonaxial maneuvers on the initial position of the liquid-vapor interface before entering weightlessness. Three basic interface configurations were observed and were shown to be dependent on tank mounting angle and liquid volume and to be independent of tank size. Author

N68-36071*# National Aeronautics and Space Administration. Langley Research Center, Langley Station, Va.

DETAILED DESCRIPTION AND RESULTS OF A METHOD FOR COMPUTING MEAN AND FLUCTUATING QUANTITIES IN TURBULENT BOUNDARY LAYERS

Ivan E. Beckwith and Dennis M. Bushnell Washington Oct. 1968 118 p refs

(NASA-TN-D-4815) CFSTI: HC\$3.00/MF\$0.65 CSCL20D

The conservation equations for mass, mean momentum, and turbulent kinetic energy for the incompressible turbulent boundary layer have been solved by an implicit finite-difference procedure. Mathematical models developed by Glushko for the production, dissipation, and diffusion of the turbulent kinetic energy in the flat plate turbulent boundary layer have been modified and used to calculate a nonequilibrium turbulent boundary layer subjected initially to a large adverse pressure gradient followed by a run of constant pressure. Comparisons of both mean and fluctuating flow properties have indicated generally good agreement between the calculated results and experimental measurements of Goldberg. The best overall agreement with data was obtained by reducing the scale of turbulence in the outer part of the boundary layer to about 70 percent of the flat plate values as used by Glushko. The calculations have indicated that further simple modifications to the turbulence scale function and to some of the mathematical models for the turbulence correlation terms should improve the accuracy of predictions for the Goldberg data. The authors have shown that the predictions in good agreement with data were obtained for other arbitrary pressure distributions. Author

N68-36343*# IIT Research Inst., Chicago, III.

ANALYTICAL INVESTIGATION OF INCOMPRESSIBLE TURBULENT SWIRLING FLOW IN PIPES

Avelino P. Rochino and Zalman Lavan Washington NASA Sep. 1968 137 p refs

(Grant NsG-694)

(NASA-CR-1169) CFSTI: HC\$3.00/MF\$0.65 CSCL 20D

Turbulent swirling flows in ducts were investigated analytically using mixing length theories. The governing equations for the mean flow were derived using Taylor's modified vorticity transport theory and the concept of isotropy of the transport coefficients. The similarity theory of von Karman was extended to swirling flows in a cylindrical geometry considering a three-dimensional fluctuating velocity field. The resulting similarity conditions were used to formulate the expression for eddy diffusivity in the entire flow field except for a small region near the pipe wall where a mixing length expression analogous to that assumed by Prandtl for parallel flow in channels was used. The tangential equation of motion was then solved numerically to study the decay of angular momentum in a swirling flow field inside a stationary pipe. It is pointed out that for pure rotational as well as irrotational flow, some of the similarity conditions become indeterminate suggesting that the said formulation may not be valid for these situations. Author

N68-36458*# National Aeronautics and Space Administration. Langley Research Center, Langley Station, Va.

LOW-DENSITY, LEADING-EDGE BLUNTNESS, AND ABLATION EFFECTS ON WEDGE-INDUCED LAMINAR BOUNDARY LAYER SEPARATION AT MODERATE ENTHALPIES IN HYPERSONIC FLOW

C. L. W. Edwards and John B. Anders Washington Oct. 1968 31 p refs

(NASA-TN-D-4829) CFSTI: HC\$3.00/MF\$0.65 CSCL 20D

A study of real gas wedge induced laminar boundary layer separation has been made. The investigation was conducted in low-density air on a highly cooled flat-plate model with interchangeable leading edges and various trailing edge flap angles. All tests were conducted in the Langley 1-foot hypersonic arc tunnel at a nominal free stream Mach number of 12, free stream unit Reynolds numbers from 1.1 \times 10⁴ to 2.7 \times 10⁴ per foot $(3.6 \times 10^4 \text{ to } 8.9 \times 10^4 \text{ per meter})$, and dimensionless stagnation enthalpies from 39.0 to 72.4. The extent of separation was found to increase with increasing leading edge bluntness at these test conditions. Significant low density effects are shown to delay the onset of separation in comparison with what would be expected from predictions by a strong interaction theory. The direct effect of mass addition on the extent of separation through ablative leading edges was found to be negligible; however, an indirect effect on the extent of separation due to leading edge regression was found to be significant. Author

N68-37067*# National Aeronautics and Space Administration. Langley Research Center, Langley Station, Va.

STUDIES OF FLOW DISTORTION IN THE TAILPIPES OF HYDROGEN PEROXIDE GAS GENERATORS USED FOR JET ENGINE SIMULATION

Leland B. Salters, Jr. and Nicholas C. Chamales Washington Oct. 1968 51 p refs

(NASA-TM-X-1671) CFSTI: HC\$3.00/MF\$0.65 CSCL 21E

An investigation was made of the effect of variation in configuration of hydrogen peroxide decomposition engines on the jet exhaust flow characteristics. Sixteen configurations of hydrogen peroxide decomposition engines were tested under static conditions over a jet exit total pressure to static pressure ratio range from 1.2 to 4.6 using hydrogen peroxide of approximately 90.5 percent concentration. Jet exit total pressure flow distortion was found to vary inversely with the contraction ratio of the tailpipe. The propellant distribution plate and catalyst bed retainer plate designs also influenced exhaust flow patterns. Flow straightener plates were effective in reducing flow distortion in the jet exhaust. Author

13 GEOPHYSICS

Includes aeronomy; upper and lower atmosphere studies; oceanography; cartography; and geodesy. For related information see also: 20 Meteorology; 29 Space Radiation; and 30 Space Sciences.

N68-10079*# Israel Program for Scientific Translations, Ltd., Jerusalem.

ELECTRICITY OF THE FREE ATMOSPHERE

I. M. Imyanitov and E. V. Chubarina 1967 216 p refs Transl. into ENGLISH of the publ. "Elektrichestvo Svobodnoi Atmosfery" Leningrad, Gidrometeorol. Izd., 1965 Published for NASA and NSF

(NASA-TT-F-425; TT-67-51374) CFSTI: HC \$3.00/MF \$0.65 CSCL 04A

A general picture of the electric structure of the atmosphere on cloudy and cloudless days, based on data obtained in systematic aircraft soundings of the atmosphere's electric field, is presented. Detailed tables of the initial data are included as well as data on the structure of the fair weather electric field, on the distribution of electric space charges and potentials in these conditions, and on the electric structure of stratus clouds. The data were gathered during the International Geophysical Year and the Year of International Geophysical Collaboration. R.N.A.

N68-10283*# Little (Arthur D.), Inc., Cambridge, Mass. THE APPLICATION OF HIGH TEMPERATURE RADIATIVE THERMAL CONDUCTIVITY OF MINERALS AND ROCKS TO A MODEL OF LUNAR VOLCANISM Washington, NASA Nov. 1967 73 p refs

(Contract NAS9-5840)

(NASA-CR-916) CFSTI: HC\$3.00/MF\$0.65 CSCL 08G

At the relatively high temperatures that probably exist deep in the lunar interior, heat flow takes place by both lattice conduction and radiative transfer. The radiative transfer which should be dominant at the higher temperatures is caused by a process of repeated emission and re-absorption of radiation modified by the effect of scattering by discontinuities such as inclusions or grain boundaries. The rate of emission depends on the blackbody spectral distribution at the temperature of the medium and on the optical constants n and k of the medium which are, in general, strong functions of the wavelength. The rate of re-absorption also depends on n and k. The scattering depends on the size and spatial distribution of the discontinuities in n and k. Author

N68-10369*# National Aeronautics and Space Administration. Goddard Space Flight Center, Greenbelt, Md.

TEMPORAL VARIATIONS OF MESOSPHERIC OXYGEN AND OZONE DURING AURORAL EVENTS

Kaichi Maeda and A. C. Aikin Washington, NASA, Nov. 1967 36 p refs

(NASA-TN-D-3993) CFSTI: HC\$3.00/MF\$0.65 CSCL 04A

Temporal solutions are given for the photochemical equations describing the distribution of ozone and atomic oxygen in an oxygen atmosphere for the equatorial and polar regions. Similar calculations are applied to auroral events. These calculations indicate a strong dependence of the distribution of mesospheric atomic oxygen on the intensity and energy spectrum of auroral electrons that dissociate molecular oxygen. It is shown that there can be no significant atmospheric ozone and atomic oxygen modifications due to soft spectrum electron events which appear to characterize most bright auroras. The hard spectrum auroral electrons which appear in most weak, quiet auroras should cause significant increases in the atomic oxygen and ozone concentrations below 80 km, provided that their flux is more than $10^{6} \, \mathrm{per} \, \mathrm{cm}^{2} \, \mathrm{sec.}$ Author

N68-11714* National Aeronautics and Space Administration. Goddard Space Flight Center, Greenbelt, Md. **GEOLOGIC APPLICATIONS OF ORBITAL PHOTOGRAPHY**

Paul D. Lowman, Jr. Washington Dec. 1967 42 p refs (NASA-TN-D-4155) CFSTI: HC\$3.00 CSCL 08G

The potential geologic applications of orbital photography (photography of the surface of the earth or similar bodies from orbiting spacecraft) with illustrations from various Gemini flights are summarized. Advantages of orbital over conventional aerial photography include: large area per photograph, rapid coverage, rapid repetition of coverage, world-wide coverage (subject to orbital parameters), absence of restrictions on dissemination of American photographs, availability of color at small added cost, and a wide range of scales. The major limitations of orbital photography include: restriction by orbital characteristics (inclination to equator, apogee, and perigee), the generally high global cloud cover, daylight restrictions, atmospheric scattering, resolution limit inherent in extremely small scales, loss of resolution and color fidelity in oblique photos, site acquisition, and degradation of film by radiation and other space environmental conditions. Three major geologic uses of orbital photography can be predicted: regional geologic mapping, monitoring of variable properties and geological education. Author

N68-18902*# National Aeronautics and Space Administration, Washington, D. C.

POTENTIAL APPLICATIONS OF SATELLITE GEODETIC TECHNIQUES TO GEOSCIENCES

1968 26 p

(NASA-SP-158) GPO: HC\$0.15; CFSTI: MF\$0.65 CSCL 08E

The possible applications of the techniques and capabilities of satellite geodesy to support other areas of science are assessed. Attention is centered on the nonmapping applications and the need for precise geometric and gravitational information to which the techniques of satellite geodesy can be applied. Some possible applications to the sciences of solid earth geophysics and geology. oceanography, glaciology, atmospheric sciences, technology, and space operations are summarized according to the physical quantities to be measured. The accuracies required to obtain useful information as well as the extent and frequency of coverage required are indicated. The applications are categorized according to those which can be accomplished with presently achievable accuracies; those which require an increase in accuracy with which ground stations can be located by using present satellite geodetic techniques, or an increase in the accuracy with which a satellite can be located in space at any given instant; and those requiring as yet untried M.G.J. instrumentation.

N68-20278*# National Aeronautics and Space Administration. Marshall Space Flight Center, Huntsville, Ala.

SCALAR AND COMPONENT WIND CORRELATIONS BETWEEN ALTITUDE LEVELS FOR CAPE KENNEDY, FLORIDA, AND SANTA MONICA, CALIFORNIA

Glenn E. Daniels and Orvel E. Smith Washington Apr. 1968 118 p refs

(NASA-TN-D-3815) CFSTI: HC\$3.00/MF\$0.65 CSCL 04A

The analysis of large quantities of atmospheric data for use in space vehicle design studies requires the application of statistical methods. An envelope of means or any given percentile derived from a sample of winds taken at discrete altitudes is not necessarily a mean profile and may not define a physically attainable wind profile. Coefficients of correlations with means and standard deviations may be used in a statistical model to derive realistic wind profiles. The statistics presented in this report are based on rawinsonde wind data samples for Cape Kennedy, Florida, and Santa Monica, California, which are greatly improved samples over those previously available. These samples represent an improvement in that they are from a more recent observational period with fewer missing measurements than earlier records and because the data have been carefully edited, checked, and serially completed for missing data. Author

N68-21543*# National Aeronautics and Space Administration. Goddard Space Flight Center, Greenbelt, Md.

THE GEOMAGNETIC SECULAR VARIATION 1900-1965

Joseph C. Cain and Shirley J. Hendricks Washington Apr. 1968 224 p refs Presented at the Intern. Union of Geodesy and Geophys. 14th Gen. Assembly, St. Gall, Switzerland, 30 Sep. 1967 (NASA-TN-D-4527) CFSTI: HC\$3.00/MF\$0.65 CSCL 04A

The GSFC (12/66) model of the main geomagnetic field uses linear and parabolic terms in time, to represent secular change over the interval 1900-1965. The predicted field is compared with observatory annual means to investigate systematic residuals. Deviations of the order of 100y occur for short spans of years and only in limited regions. Otherwise, the trends of the computed field parallel the observations. Secular-change charts agree well with those drawn by earlier analyses. The westward drift is generally apparent in the vector representation of the harmonic coefficients, except that a few terms predominantly undergo an amplitude change. The components below (g_6^6, h_6^6) that show a recognizable estward drift are the (3,2), (5,1), and (5,2) terms. Both dipole poles move smoothly northwestward over the interval, whereas the dipole position initially drifts eastward, reverses direction near 1920, and then moves westward at a rate up to about 0.07 degrees per year. Its 1965 position is found to be 78.8°N, 7.0°W. Author

N68-21904*# National Aeronautics and Space Administration. Ames Research Center, Moffett Field, Calif.

PHASE AND GROUP REFRACTIVE INDICES FROM THE COLLISIONLESS MAGNETOIONIC THEORY

Lawrence Colin, Kwok-Long Chan, and Jack G. K. Lee (Informatics, Inc.) Washington Apr. 1968 130 p refs

(NASA-TM-X-1553) CFSTI: \$3.00 CSCL 04A

Graphs of phase and group refractive indices computed from the collisionless magnetoionic theory are presented. The indices are computed for both the entire range of electron concentration and the intensity of the earth's magnetic field to be encountered by operational topside ionospheric sounders in the International Satellites for Ionospheric Studies (ISIS) series (Alouette I, Explorer XX, Alouette II, ISIS-A, ISIS-É).

N68-22462*# Scientific Translation Service, La Canada, Calif. SCATTERING OF LIGHT IN A TURBID MEDIUM

K. S. Shifrin Washington NASA Apr. 1968 217 p refs Transl. into ENGLISH of the book "Rasseyaniye Sveta v Mutnoy Srede" Moscow, Gosgeoltekhizdat., 1951 p 1–212 (Contract NASw-1496)

(NASA-TT-F-477) CFSTI: \$3.00 CSCL 04A

Presented is a systematic discussion of the theory of scattering and absorption of plane electromagnetic waves by particles of a turbid medium. Considered in the discussion are the following: linear dimensions of the particles, their electrical characteristics, and a general formulation of the problem of perturbation introduced by a particle into a field; fundamental formulas: partial waves: small particles; large particles; absorbing and fully reflecting particles having any dimensions; and particles with electrical properties deviating slightly from the surrounding medium properties. S.C.W.

N68-22861*# National Aeronautics and Space Administration. Goddard Inst. for Space Studies, N. Y.

RADIATIVE EQUILIBRIUM IN AN ATMOSPHERE WITH CONSTANT EINSTEIN ABSORPTION COEFFICIENT

Rupert Wildt and Sandra Schwartz Washington May 1968 51 p refs

(NASA-TN-D-4479) CFSTI: HC\$3.00/MF\$0.65 CSCL 04A

In the classical gray atmosphere, the phenomenological coefficient of absorption that enters into Kirchhoff's law is assumed to be independent of the frequency ($\kappa_p = \text{const} = \kappa^{-1}$). Strictly considered, this coefficient is the product obtained by multiplying the Einstein coefficient of true absorption by a frequency-dependent correction for induced emission (Rosseland factor). The alternative here examined is to set the Einstein coefficient constant, incorporate the effects of induced emission into the transfer formalism, and determine the march of the local thermodynamic equilibrium source function by numerical iteration. This second kind of gray atmosphere differs markedly from the classical one in respect to many physical characteristics and represents, in conventional terminology, the simplest nongray problem that is physically realistic.

N68-23436*# Massachusetts Inst. of Tech., Cambridge. CORRECTION OF BALLOON X-RAY ASTRONOMY DATA FOR THE EFFECTS OF ATMOSPHERIC ATTENUATION, K X-RAY ESCAPE, AND ENERGY RESOLUTION

James W. Overbeck Washington NASA May 1968 30 p refs (Grant NsG-386)

(NASA-CR-1045) CFSTI: HC\$3.00/MF\$0.65 CSCL04A

An X-ray flux from outside the atmosphere determines the counting rate of an X-ray detector beneath several g/cm^2 of atmosphere, but a unique inverse relationship does not exist. Therefore X-ray astronomy data analysis requires the computer simulation of the processes which transform assumed X-ray energy spectra into detectors' counting rates. The programs used by the author, E. Allen Womack, Jr., and Harvey D. Tananbaum are presented and are applied to a specific example. A set of conventions for presenting one's results as an X-ray spectrum above the atmosphere is also explained. Author

N68-23706*# North American Aviation, Inc., Downey, Calif. EARTHQUAKE PREDICTION FROM LASER SURVEYING R. A. Fowler Washington NASA 1968 37 p refs Prepared

for NASA

(NASA-SP-5042) GPO: HC \$0.35 CFSTI: MF \$0.65 CSCL 08K

A geodetic laser survey system is described that overcomes the uncertainty introduced by atmospheric fluctuations affecting the refractive index value; and the resultant variations in the velocity of the electromagnetic waves that ordinarily cause distortions in distance measurements are considered. Applications of such systems to earthquake prediction and engineering research, geodetic problems, dam construction, and space research are described. Probability maps and laser survey technology development are discussed in relation to earthquake prediction; and passive versus active systems as well as the limitations of existing systems are considered for precise measuring of long distances. The theory for atmospheric refractive index corrections using dispersion techniques is considered, along with the mathematical models required for making the necessary calculations. M.W.R. N68-25579*# Bendix Corp., Ann Arbor, Mich. Aerospace Systems Div.

STUDY OF MINERAL STABILITY IN THE LUNAR ENVIRONMENT Final Report

Washington, D. C. NASA Jun. 1968 285 p refs

(Contract NAS9-3734)

(NASA-CR-1034; BSR-2022) CFSTI: HC \$3.00 /MF \$0.65 CSCL 08G

Stability of selected earth minerals in simulated lunar environments were investigated through laboratory experiments. Analyses of the reactions of the minerals to exposure of vacuum and thermal environments and their chemical and structural stability when exposed to spacecraft and earth environments were studied. Short term experiments included validation of mineral identification of 14 minerals, and provision of insight into reactions expected and standards for comparison with results obtained from the long term experiments. Long term testing involved a single temperature cycle at simulated lunar vacuum environment, X-ray photographs of each sample at various stages of the temperature cycle, a four day simulation of spacecraft environment, and a two day exposure to earth environment. It was noted that the change in environment, even over a short time interval, was sufficient to cause major changes in some phases, and that predicted equilibrium stability relations should be the overriding factor in determining the phase occurring on the lunar surface. A.L.

N68-28222*# National Aeronautics and Space Administration. Goddard Space Flight Center, Greenbelt, Md.

THE RADIATION BALANCE OF THE EARTH-ATMOSPHERE SYSTEM FROM RADIATION MEASUREMENTS OF THE NIMBUS 2 METEOROLOGICAL SATELLITE Ehrhard Raschke Washington Jul. 1968 81 p refs

(NASA-TN-D-4589) CFSTI: HC\$3.00/MF\$0.65 CSCL 04A

Measurements of the reflected solar radiation and emitted infrared radiation were obtained over the entire globe from the Nimbus II meteorological satellite during the period from 16 May 1966 to 28 July 1966. From these measurements, the outgoing long-wave radiation flux, the albedo, and the radiation balance of the earth-atmosphere system were computed for five subperiods, each of a half month's length. The global albedo was found to be between 29 and 31 percent, which is less than earlier accepted values of 33 percent and more. The globally emitted long-wave radiation flux results in an equivalent black-body temperature of the planet earth of about 255°K, which is 3–4 degrees higher than was found in earlier studies. The global averages of the radiation balance obtained were between 0.002 cal cm-2 min-1 of surplus and 0.007 cal cm⁻² min⁻¹ deficit.

N68-28872*# National Aeronautics and Space Administration. Goddard Space Flight Center, Greenbelt, Md.

REMOTE DETECTION OF TERRAIN FEATURES FROM NIMBUS 1 HIGH RESOLUTION INFRARED RADIOMETER NIGHTIME MEASUREMENTS

Jean Pouquet Washington Jul. 1968 12 p refs Sponsored in part by NAS-NRC

(NASA-TN-D-4603) CFSTI: HC\$3.00/MF\$0.65 CSCL 08B

Brightness temperature analyses were made from nighttime Nimbus high resolution infrared data in the $3.5-4.2\mu$ region. Data for the northeast Sahara Desert and the Nile delta regions, obtained during September 1964, were selected. The brightness temperatures were found very useful because they detect: (1) the widespread humidity in the upper soil horizons, and (2) the heat storage capacity in various rock formations such as sands and alluvial deposits. N68-33416*# National Aeronautics and Space Administration. Flight Research Center, Edwards, Calif.

ATMOSPHERIC CONDITIONS ASSOCIATED WITH TURBULENCE ENCOUNTERED BY THE XB-70 AIRPLANE ABOVE 40,000 FEET ALTITUDE

L. J. Ehernberger Washington Sep. 1968 49 p refs

(NASA-TN-D-4768) CFSTI: HC\$3.00/MF\$0.65 CSCL 04B

High-altitude atmospheric turbulence has been encountered by the XB-70 airplane during flight test over the Western United States. The encounters from 36 flights were analyzed for the meteorological features associated with high-altitude turbulence. This study used data from an NACA VGH recorder carried on the airplane and from rawinsonde observations made near turbulence encounters at altitudes above 40,000 feet (12.200 meters). These data showed that turbulence of significant intensity at high altitudes is related to wind velocity, vertical wind shear, and the vertical temperature gradient. It is also indicated that the disturbances causing high-altitude turbulence can originate in both the lower atmosphere and the stratosphere. Author

N68-35151*# Teledyne Industries, Inc., Garland, Tex. SEISMIC EFFECTS OF SONIC BOOMS

Tom T. Goforth and John A. McDonald Washington NASA Sep. 1968 130 p refs

(Contract NAS1-6342)

(NASA-CR-1137) CFSTI: HC\$3.00/MF\$0.65 CSCL08K

Earth particle velocities produced by sonic booms were recorded at Edwards Air Force Base, California, the Tonto Forest Seismological Observatory near Payson, Arizona, and the Uinta Basin Seismological Observatory near Vernal, Utah. Analysis of the field data indicates that the seismic effects of sonic booms are largely confined, laterally, to the boom pressure envelope and vertically to the upper few meters of the earth's surface. The maximum particle velocity associated with a sonic boom is in response to the rapid pressure changes of the leading and trailing edges of the acoustic N-wave. Comparison of peak particle velocities recorded at Edwards Air Force Base show good agreement with theoretically-predicted values. Empirical relations developed from the recorded data indicate that peak particle velocity is linearly related to the maximum positive overpressure of the N-wave. On hard, well-consolidated rock, each pound per square foot of overpressure produces about 75 microns per second peak particle velocity. On more loosely-consolidated rock, each pound per square foot of overpressure produces about 100 microns per second peak particle velocity. Author

N68-35179*# National Aeronautics and Space Administration, Washington, D. C.

ON THE COMPUTATION OF SOLAR ELEVATION ANGLES AND THE DETERMINATION OF SUNRISE AND SUNSET TIMES

Harold M. Woolf (Natl. Meteorol. Center) Sep. 1968 23 p refs Prepared for NASA by the Natl. Meteorol. Center

(NASA-TM-X-1646) CFSTI: HC\$3.00/MF\$0.65 CSCL 04A

The complete procedure for precise computation of solar elevation angle as a function of latitude, longitude, data, and time is given. Construction of a graphical aid for determining times of sunrise and sunset, with a precision of one minute, as functions of latitude, longitude, date, and altitude is described. Author

14

INSTRUMENTATION AND PHOTOGRAPHY

Includes design, installation, and testing of instrumentation systems; gyroscopes; measuring instruments and gages; recorders; transducers; aerial photography; and telescopes and cameras.

N68-10057*# National Aeronautics and Space Administration. Flight Research Center, Edwards, Calif.

A USEFUL MODIFICATION OF THE WRIGHT SPIROMETER James Roman and Robert N. Sato Washington NASA Nov. 1967 13 p ref

(NASA-TN-D-4234) CFSTI: HC\$3.00/MF\$0.65 CSCL 14B

The Wright spirometer is a gas flowmeter for physiological use which is small and reliable. However, data collected with this device must be reduced manually, and the calibration curve is nonlinear at low flow values. The instrument was modified by fitting the output shaft with a spoked wheel that interrupts the light beam between a low-power light source and a photonsensor. This modification provides a digital electrical output that can be computer-reduced, permitting correction of the data for the nonlinearity of the calibration curve. The power drain is 96 milliwatts, which is small enough to be drawn from the battery supplies of most self-contained miniature tape recorders. Author

N68-10647* National Aeronautics and Space Administration. Goddard Space Flight Center, Greenbelt, Md.

THE APPLICATIONS TECHNOLOGY SATELLITE IMAGE DISSECTOR CAMERA EXPERIMENT

G. A. Branchflower, R. H. Foote, and D. Figgins Washington NASA Nov. 1967 15 $\,p$

(NASA-TN-D-4186) CFSTI: \$3.00 CSCL 14E

The image dissector camera experiment, which is scheduled to fly aboard the Applications Technology Satellite-C, is described. Camera system parameters are presented and a description of system operation, including the clock synchronizer and timing and control logic, is given. Ground support equipment is also discussed. Author

N68-11867*# National Aeronautics and Space Administration, Lewis Research Center, Cleveland, Ohio.

SENSITIVITY OF QUARTZ, PIEZOELECTRIC PRESSURE TRANSDUCERS AS A FUNCTION OF TEMPERATURE FROM 20° TO 477°K

Lloyd W. Canfil and William C. Nieberding Washington Dec. 1967 9 p refs

(NASA-TM-X-1479) CFSTI: HC\$3.00/MF\$0.65 CSCL 14B

Quasi-static calibrations were performed to determine the sensitivity of quartz. piezoelectric type, pressure transducers in the temperature range of 20° to 477° K. Results were obtained which show that the sensitivity at 20° K differs from the sensitivity at room temperature by 4 percent maximum. The corresponding difference at 477° K is 9 percent. The change in room temperature sensitivity due to each temperature excursion was negligible. The conclusion is reached that this type of transducer is particularly applicable to dynamic pressure measurement at cryogenic temperatures.

N68-12669*# National Research Corp., Cambridge, Mass. STUDY OF DENSITY CALIBRATION IN SPACE Final Report, Jun. 29, 1966–Jan. 16, 1967

P. Fowler and F. J. Brock Washington NASA Dec. 1967 46 p refs

(Contract NAS5-3959)

(NASA-CR-987) CFSTI: HC\$3.00/MF\$0.65 CSCL 14B

Methods of calibrating ion gauges and mass spectrometers were studied to determine a method for in-flight calibration of detectors installed on spacecraft. The method developed consists of diffusing a known hydrogen flux through the wall of a small diffuser tube into the detector enclosure which produces a pressure increment equal to the ratio of hydrogen flux to exhaust conductance, by raising the temperature of the tube with an internal heater which dissipates a prescribed power for a prescribed time interval. Three successive generations of prototype in-flight calibrators were designed and constructed and evaluated. The results indicate that the diffuser generates a hydrogen flux which is linear over a dynamic range of 3×10^5 , that calibration pulse heights are repeatable within ±2.0% and that pulse height variation can be maintained less than 1.0% for 30 seconds. The data indicate that the pressure decay rate, associated with the diffuser, following a calibration pulse is such that after 15 minutes the pressure is no more than several percent of the external pressure if the calibration pulse is no more than an order of magnitude above the external pressure, except for pressures less than 10-9 Torr, which Author require a longer recovery time.

N68-13973*# National Aeronautics and Space Administration, Lewis Research Center, Cleveland, Ohio.

DUCTILITY MECHANISMS AND SUPERPLASTICITY IN CHROMIUM ALLOYS

Joseph R. Stephens and William D. Klopp Washington Jan. 1968 32 p refs

(NASA-TN-D-4346) CFSTI: HC\$3.00/MF\$0.65 CSCL 11F

Alloys with lower ductile-to-brittle transition temperatures than that of unalloyed chromium ($\approx 300^{\circ}F$ or $422^{\circ}K$) included chromium -35 to 40 atom percent rhenium, chromium -15 to 24 atom percent ruthenium, chromium-30 atom percent cobalt, and chromium-30 to 50 atom percent iron. Equilibrium diagrams have two features in common, an intermediate σ phase, and a high maximum solubility of solute in chromium. The following observations were made on alloys with compositions approaching the solubility limit in the chromium-rhenium, chromium-ruthenium, and chromium-cobalt systems and the σ composition in the chromium-iron system: ductile-to-brittle transition temperature decreased significantly: grain size increased sharply with increasing solute content after annealing at a constant temperature; hardness decreased substantially; and initial deformation was primarily by twinning. The ductile-to-brittle transition temperatures of near saturated alloys can be related to the fractional difference in specific volume between the σ phase and the respective chromium-base solid solution. Chromium-30 atom percent cobalt and chromium-24 atom percent ruthenium alloys were tensile tested at elevated temperatures and exhibited superplasticity. Observation suggests the rhenium ductilizing effect and superplasticity may have common basic features. Author

N68-13974*# National Aeronautics and Space Administration, Lewis Research Center, Cleveland, Ohio.

FLIGHT EVALUATION OF AN ELECTROSTATIC ACCEL-EROMETER FOR MEASUREMENT OF LOW-LEVEL ORBITAL ACCELERATIONS

Daniel J. Lesco Washington Jan. 1968 13 p refs (NASA-TM-X-1488) CFSTI: HC\$3.00/MF\$0.65 CSCL 14B

The results of the first flight test of an experimental electrostatic accelerometer are presented. Measurements of liquid-hydrogen venting accelerations as low as 6×10^{-5} g were obtained aboard an orbiting Saturn S-IVB stage. Comparison of the accelerometer readings is made with other flight measurements. The time correlation between output data and attitude control system firings is also described. Author

N68-14018*# National Aeronautics and Space Administration. Lewis Research Center, Cleveland, Ohio.

DIGITAL READOUT AND CONTROL SYSTEM FOR A 64-INCH (1.63-m) SCATTERING CHAMBER

Lawrence P. Madson Washington Jan. 1968 13 p refs (NASA-TN-D-4324) CFSTI: HC\$3.00/MF\$0.65 CSCL 18D

This report describes an automatic digital position control system for scattering chamber now in use with the 60-inch (1.52-m) cyclotron at the Lewis Research Center. It features programmed remote control of detector positions with accuracies of ±0.03 degree for these positions. The system has been in continuous operation for a period of 6 months and has resulted in a 20 percent saving in experiment running time. Author

N68-15893*# National Aeronautics and Space Administration. Lewis Research Center, Langley Station, Va.

TEMPERATURE AND LIQUID-LEVEL SENSOR FOR LIQUID-HYDROGEN PRESSURIZATION AND EXPULSION STUDIES

Robert J. Stochl and Richard L. De Witt Washington Feb. 1968 23 p refs

(NASA-TN-D-4339) CFSTI: HC \$3.00/MF \$0.65 CSCL 14B

A temperature-measurement technique that uses thermopiles (i.e., thermocouples in series) as sensors was developed. The results of this development indicate (1) that an instrument rake using measurement stations constructed of thermopiles can measure temperatures to within ±1.65°K (for gas temperatures between 20° and 300°K) and (2) that, in addition to their use as temperature sensors, thermopile units can be used as point liquid-level sensors for subcooled liquid during liquid outflow. Tests indicate that thermopiles can detect liquid level to within ± 0.453 centimeter. Author

N68-15936*# National Aeronautics and Space Administration. Lewis Research Center, Cleveland, Ohio.

BIMETAL SENSOR FOR AVERAGING TEMPERATURE MEASUREMENT OF NONUNIFORM TEMPERATURE PROFILES

Ralph T. Dittrich and Michael P. Lynch Washington Nov. 1967 19 p refs

(NASA-TN-D-4242) CFSTI: HC\$3.00/MF\$0.65 CSCL 14B

A single-probe instrument was developed for measuring an average temperature over a nonuniform temperature profile. This probe uses the principle of differential thermal expansion of two different materials. The performance of such a probe was demonstrated experimentally by using a prototype probe for a single temperature indication over temperature profiles which varied as much as 750°C. Probe temperature measurements obtained during several runs averaged as much as 13°C lower than temperatures obtained from averaging the measurements of eight thermocouples equally spaced along the probe length; analysis shows that for steep temperature gradients the probe-measured temperature is a better average than the average temperature obtained from the eight thermocouples. The instrument can be adapted to wide temperature ranges by the proper selection of probe geometry and materials. Author

N68-16529*# National Aeronautics and Space Administration. Ames Research Center, Moffett Field, Calif.

FOR SATELLITE UNCERTAINTY ANALYSIS AN CALORIMETRIC MEASUREMENTS

John P. Millard Washington Feb. 1968 64 p refs

(NASA-TN-D-4354) CFSTI: HC\$3.00/MF\$0.65 CSCL 20M

The use of an uncertainty analysis for analyzing current data and for designing future satellite calorimetric experiments is described. Calorimetric experiments considered are those for measuring the radiative properties of solar absorptance and infrared emittance of test surfaces, and those for measuring the emissive and reflective properties of the sun and planets. The paper describes the uncertainty-analysis technique, lists all pertinent equations for each measurement, presents several illustrative examples, and includes a section on design guides for future experiments. Author

N68-16838*# Lockheed Electronics Co., Houston, Tex. ANALYSIS OF LUNA 9 PHOTOGRAPHY Washington NASA Feb. 1968 88 p (Contract NAS9-5191) (NASA-CR-980; LEC/HASD-671-40-019) CFSTI: HC \$3.00/MF \$0.65 CSCL 14E

The techniques and procedures used for a detailed scientific evaluation and analysis of Luna 9 spacecraft imagery is presented along with results and conclusions. A discussion is given on the nature and specifications of the spacecraft and its instruments. Included here also are the image transmissions and images received. Detailed descriptions of the image frames are given. These include: scale and panoramic coverage of the frames, azimuth and distances of the image features, size and classification of the surface materials, and size and classification of the visible craters. The procedures and techniques used for the above calculations are discussed. These are discussed as applied to monoscopic panoramas, dihedral mirror images, and stereoscopic panoramas. Author

N68-17329*# GCA Technology Div., GCA Corp., Bedford, Mass. IMPROVEMENT AND OPTIMIZATION OF A MASS SPECTROMETER EMPLOYING A PHOTOIONIZATION SOURCE

Walter P. Poschenrieder and Peter Warneck Washington Mar. 1968 55 p refs

(Contract NAS1-6335)

(NASA-CR-1018; GCA-TR-67-12-N) CFSTI: HC \$3.00/MF \$0.65 CSCI 20F

Further improvements of the photoionization mass spectrometer are described. The experiments performed showed the basic feasibility of analytical photoionization mass spectrometry. At the same time, certain limitations were indicated, particularly with regard to the discrimination of ions with different ionization potentials and coinciding mass numbers, e.g., CO and N2. This limitation could be traced back to two main sources: namely, the second and higher order uv spectrum produced by the grating, and uv light scattering the monochromator. A considerable improvement has been achieved by the use of uv filters which reduce the intensity of the higher order spectrum and scattering by about two orders of magnitude. Accordingly, the detection limit for CO in N2 was improved from 5000 to 100 ppm. The performance of a thin-metal indium filter was compared with an argon gas filter. Author

N68-18834*# National Aeronautics and Space Administration. Lewis Research Center, Cleveland, Ohio.

PRELIMINARY TESTS WITH MASS FLUX PROBE IN SUPERSONIC STREAM

Lloyd N. Krause and George E. Glawe Washington Mar. 1968 15 p refs

(NASA-TM-X-1524) CFSTI: HC\$3.00/MF\$0.65 CSCL 14B

This investigation was undertaken to determine experimentally the accuracy of a mass flux probe system using two inlet designs. One inlet design was sharp-lipped and had both the internal lip surfaces bevelled at 15° (symmetrical). A second inlet, which had

only an external 15° bevel (unsymmetrical), was initially sharp and then was progressively blunted to various degrees during the test program. The purpose of using the two shapes was to compare the ideal, sharp inlet lip with the blunt lip inlets that are considered necessary to achieve adequate cooling in streams developing high stagnation-point heat-transfer rates. The Mach number of the tests ranged from 2.0 to 2.6, and the total temperature ranged from 530° to 700°R (290° to 390°K) with a tunnel inlet Reynolds number of the order of 2.5×10^6 per foot (8.2×10^6 m⁻¹). The symmetrical sharp-lipped inlet yielded excellent results, while the unsymmetrical wedge inlet with both sharp and blunt lips had an effective capture area up to 4 percent greater than the geometric capture area.

N68-19001*# National Aeronautics and Space Administration. Lewis Research Center, Cleveland, Ohio.

INSTRUMENTATION OF A SNAP-8 SIMULATOR FACILITY

James N. Deyo and William T. Wintucky Washington Mar. 1968 61 p refs

(NASA-TM-X-1525) CFSTI: HC\$3.00/MF\$0.65 CSCL 18D

The philosophy and experience with high temperature instrumentation, pressure sensors, thermocouples, and flowmeters are discussed. Secondary and support instrumentation in the test facility and control room are also included. The approach described is based on the parameters to be measured as well as the time schedule, physical characteristics, and available instrumentation for the facility. Results include data handling, accuracy, and reliability of the system. Over 2000 hours of operation were accumulated, during which time the mercury loop was at operating temperature for about 1000 hours. More than 2000 data runs were taken. Author

N68-19642*# National Aeronautics and Space Administration. Electronics Research Center, Cambridge, Mass.

DESIGN OF A PRECISION TILT AND VIBRATION ISOLATION SYSTEM

Herbert Weinstock Washington Mar. 1968 169 p refs

(NASA-TR-R-281) CFSTI: HC\$3.00/MF\$0.65 CSCL 17G

The design of a two axis servomechanism leveling system controlled by gyroscopes and level sensors which is mounted on a massive conventional pneumatic isolation system is presented. At frequencies below 0.012 cps the system is controlled by the level sensors. From 0.012 cps to 25 cps the gyroscopes maintain control. Above 25 cps the servomechanism system is locked out and the test device and massive frame act as a rigid body mounted on springs, resulting in the isolation that would be provided by a damped 1 cps conventional vibration isolation system. The design alternatives for the system, the general design parameters required to meet the performance specification, and the specific components required to achieve these parameters are discussed. The isolation efficiency and other performance functions of a realizable design are presented. The design, assembly, and test results of an experimental single axis full scale model of the servomechanism portion of the system are reviewed. RNA

N68-20324*# National Aeronautics and Space Administration. Lewis Research Center, Cleveland, Ohio.

CRYOGENIC TEMPERATURE MEASUREMENT USING PLATINUM RESISTANCE THERMOMETERS

Donald H. Sinclair, Howard G, Terbeek, and Jerry H. Malone Washington Apr. 1968 37 p refs

(NASA-TN-D-4499) CFSTI: HC\$3.00/MF\$0.65 CSCL 20M

Results of evaluation tests on commercial platinum resistance thermometers (PRT) are reported. Three selective types of compact high-resistance PRT (1000 to 5000 ohms at 273.15°K) have proved to be stable, rugged, and sensitive. Resistance difference ratios as a function of temperature, called Z functions, conform closely to those of the high-quality standard PRT even in the nonlinear cryogenic range. Fixed point calibrations at 273.15°, 77.40°, and 20.20°K plus interpolation between points by Z ratios yield probable uncertainties less than $\pm 0.05°K$ from 20° to 300°K.

14 INSTRUMENTATION AND PHOTOGRAPHY

Also described are a calibration facility, cryostat, procedures for calibrating in liquid-hydrogen and liquid-nitrogen baths to $\pm 0.02^{\circ}$ K, and instrumentation for field installations. Author

N68-21169*# National Aeronautics and Space Administration. Goddard Space Flight Center, Greenbelt, Md.

THE OPERATION OF AN ELECTRON PARAMAGNETIC RESONANCE SPECTROMETER

F. E. Geiger, Jr. Washington Apr. 1968 13 p refs

(NASA-TN-D-4469) CFSTI: HC\$3.00/MF\$0.65 CSCL 20F

Discussed is the operation of an electron paramagnetic resonance microwave spectrometer and expressions are given for the signal obtained from a paramagnetic sample with RF susceptibility $\chi = \chi' - i\chi''$. Calculations are made to the second order of χ'' and χ' . Also studied are the effect of relative microwave power in the signal arm and in the bias or reference arm of the microwave bridge, and the effects of crystal detector characteristics on the optimum cavity reflection coefficient. Expressions for signals are developed for balanced-bridge operation with small phase or amplitude unbalance and for bridge operation with biasing arrangements for the detecting crystal.

N68-21384*# National Aeronautics and Space Administration. Lewis Research Center, Cleveland, Ohio.

PERFORMANCE OF A VENTURI METER WITH SEPARABLE DIFFUSER

Thomas J. Dudzinski, Robert C. Johnson, and Lloyd N. Krause Washington Apr. 1968 18 p refs

(NASA-TM-X-1570) CFSTI: HC\$3.00/MF\$0.65 CSCL 14B

The effects on venturi meter efficiency and discharge coefficient of a radial, outward step at the transition from throat to diffuser are reported over a Reynolds number range of 1×10^4 to 5×10^5 and over a Mach number range of 0.2 to 1.0. Step size was varied from 0 to 12.5 percent of the throat radius. Diffuser efficiency was dependent on Reynolds number, Mach number, and step size greater than 2 percent. The discharge coefficient was independent of Mach number, step size, and back-pressure variation for critical flow. Author

N68-21942*# National Aeronautics and Space Administration. Langley Research Center, Langley Station, Va. A LIGHTING STRATEGY FOR LUNAR ORBITER MISSION DESIGN

Friedrich O. Huck Washington May 1968 38 p refs

(NASA-TN-D-4501) CFSTI: HC\$3.00/MF\$0.65 CSCL 14E

An analysis is presented which relates quality of lunar photographs to Lunar Orbiter trajectory. Furthermore, since several parameters which affect picture quality are uncertain, a strategy is developed which optimizes confidence levels in detecting specific lunar surface detail. This strategy is illustrated by examining Lunar Orbiter's capability to reveal small obstables in the form of right-circular cones which have lunar reflective properties. Results show that the smallest lunar detail can be detected at high phase angles (angle between incident light and camera) and long exposure times; however, the effects of variances in lunar reflectance, vehicle trajectory, and image smear result in higher levels of confidence in the detection of larger detail at lower phase angles and shorter film exposures. Author

N68-22290*# National Aeronautics and Space Administration... Langley Research Center, Langley Station, Va.

FLIGHT INVESTIGATION OF CAPACITANCE-TYPE METEOROID DETECTOR USING AN INFLATABLE PARAGLIDER

James H. Siviter, Jr. Washington May 1968 42 p refs

(NASA-TN-D-4530) CFSTI: HC\$3.00/MF\$0.65 CSCL 14B One of the meteoroid-detection systems under development consists of thin-film multiple capacitors made of layers of aluminized polyethylene terephthalate (PET). The capacitor momentarily

discharges when penetrated by a hypervelocity projectile. The multilayer capacitor-type detector used in this experiment was designed to detect particle penetrations in 6.5, 20, and 45 microns of PET. Eighteen square meters of the micrometeoroid-detector material was attached to the wing of an inflatable paraglider. The paraglider provided a convenient mounting structure for the sensors and a means of recovering the sensors after the flight test. The packaged paraglider and sensors were boosted to an altitude of 93 kilometers where the paraglider was ejected and inflated. The inflated paraglider then continued along a ballistic trajectory to a maximum altitude of 154.7 kilometers. Sensor data were recorded for approximately 169 seconds at altitudes above 121 kilometers. The excessive noise on the telemetry-data channels made exact analysis of the penetration data inconclusive. The deploy nent and inflation of the paraglider were normal and it attained the proper flight attitude during reentry; however, the telemeter section failed to release, and, as a result, the reentry loads were excessive. Author

N68-22883*# National Aeronautics and Space Administration. Langley Research Center, Langley Station, Va.

CAPACITOR-TYPE METEOROID-PENETRATION SENSORS: DESCRIPTION AND TEST RESULTS

John J. Broderick Washington May 1968 109 p refs

(NASA-TN-D-4529) CFSTI: HC\$3.00/MF\$0.65 CSCL 14B

Capacitor sensors were tested and evaluated, in various configurations, under hypervelocity-impact conditions which simulate, as nearly as possible with present laboratory facilities, the impacts of meteoroids in space. Light-gas guns, explosive devices, electrostatic accelerators, and exploding-wire guns were used. Three types of signals were observed during hypervelocity perforations. The first is characterized by a complete discharge of the sensor within a few microseconds. The second is characterized by the rapid discharge of a substantial portion of the applied voltage. The third is characterized by the loss of less than about 10 percent of the applied voltage with the discharge time in excess of 10 µsec. During the test program most of the perforations resulted in small signals or no signals. The applied voltage was the only parameter observed which had a pronounced effect on the sensor operation. Completely charged capacitor sensors were not permanently shorted when perforated by small single hypervelocity projectiles; however, some uncharged and partially charged sensors were permanently shorted when perforated. Author

N68-24244*# National Aeronautics and Space Administration. Langley Research Center, Langley Station, Va.

INVESTIGATION OF TEMPERATURE MEASUREMENTS IN 300° TO 1100°K LOW-DENSITY AIR USING AN ELECTRON BEAM PROBE

William W. Hunter, Jr. Washington May 1968 37 p refs (NASA-TN-D-4500) CFSTI: HC\$3.00/MF\$0.65 CSCL 20M

Laboratory measurements of rotational and vibrational temperatures have been performed over a range from 300° to 1100°K in static low-density air with an electron beam probe. Rotational-temperature measurements were made from the (0,0) band of the first negative system of the nitrogen constituent of air. Some tests were also performed by using the (0,1) band of the first negative system of nitrogen. No substantial differences were noted between the results of the (0,1) band tests and those of the (0,0) band tests. The accuracy of the measured rotational temperatures was found to vary with gas temperature and gas number density. A difference existed between the measured rotational temperature and the gas temperature. This difference increased with increasing gas temperature. With the inclusion of an experimentally determined correction for the gas-number-density effect, the rotational-temperature measurements were made with an accuracy that varied from approximately 0 to -6 percent with increasing gas temperature. Vibrational-temperature measurements were made by using the intensity ratios of the (0,1) and (1,2) bands of the first negative system of nitrogen. The measurements were found to be within ± 20 percent of the gas temperature. Author

N68-25316*# Ling--Temco--Vought, Inc., Dallas, Tex. LTV Research Center.

INVESTIGATION OF THE CALIBRATION OF MICROPHONES FOR SONIC BOOM MEASUREMENT

John J. Van Houten and Ron Brown Washington, D. C. NASA Jun. 1968 60 p refs (Contract NAS1-5652)

(NASA-CR-1075; TR-0-71200/7TR-112) CFSTI: HC \$3.00/MF \$0.65 CSCL 14B

Examination of the various procedures available for microphone calibration indicated that application of the electrostatic actuator technique and the use of an infrasonic pistonphone would satisfy NASA's microphone calibration requirements. These instruments provide the equipment necessary for a comprehensive evaluation of microphones currently being used by NASA as well as those which may be used in the future. The system is capable of sinusoidal evaluation of the frequency response and sensitivity of a microphone over the range of 0.01 Hz to above 20 kHz. Sinusoidal sound pressure levels of 94 dB and 114 dB are achieved with the infrasonic pistonphone and sound pressures in excess of 128 dB are obtained by use of the electrostatic actuator system. The calibration procedure demonstrates the compatibility of steady state and transient response characteristics of the microphone and provides illustrations of idealized N-waveform measurement capability of currently available microphones and complementing instrumentation. Author

N68-25317*# National Aeronautics and Space Administration. Flight Research Center, Edwards, Calif.

CHARACTERISTICS AND USE OF X-15 AIR-DATA SENSORS Lannie D. Webb Washington, D. C. Jun. 1968 59 p refs (NASA-TN-D-4597) CFSTI: HC\$3.00 /MF\$0.65 CSCL 14B

The uses, techniques of correlation, and analysis of flight-guidance and air data sensors that have been flown on the X-15 airplane are examined. Methods by which meteorological balloons and high altitude rocketsondes were used to define the atmospheric envelope around the X-15 airplane are discussed. The application of onboard sensor data, meteorological data, and radar data in obtaining altitude, velocity, Mach number, and dynamic pressure is explained. Onboard systems considered are the nose-boom pitot-static tube, hypersonic flow-direction sensor (ball nose), fuselage static system, fuselage pitot probe, stagnation-temperature probe, and inertial flight-data system. Author

N68-25375*# National Aeronautics and Space Administration. Goddard Space Flight Center, Greenbelt, Md.

MONOMOLECULAR CONTAMINATION OF OPTICAL SURFACES

H. Shapiro and J. Hanyok Washington Jun. 1968 25 p refs (NASA-TN-D-4612) CFSTI: HC\$3.00 /MF\$0.65 CSCL 20F

This paper describes the measurement of ultraviolet reflectance change in mirrors, caused by oil contamination. Spacecraft equipped with such mirrors are tested in a vacuum generated by oil diffusion pumps. Within instrumental limits, our experimental mirrors show no change in reflectivity when the vacuum chamber is operated in the usual mode. Contamination is plotted against amount of oil deposited, the amount being measured by a quartz-crystal microbalance. The observed phenomena give a more complete picture of the contamination process than existed previously. Deposited oil, it is found, forms minute droplets on the surface of mirrors coated with MgF₂. The droplets can be evaporated from the surface at a much higher chamber pressure than the rated vapor pressure of the bulk liquid; this provides a way of cleaning the mirrors. It is possible to operate diffusion-pumped systems so as to minimize Author

N68-25518*# National Aeronautics and Space Administration. Goddard Space Flight Center, Greenbelt, Md.

AN AUTOCORRELATION APPROACH TO THE BROWN-TWISS INTERFEROMETER

Frank C. Jones Washington May 1968 29 p refs (NASA-TN-D-4480) CFSTI: HC\$3.00/MF\$0.65 CSCL 20F

Consideration is given to interference phenomena which occur with light produced by incoherent sources. Starting from the familiar interference pattern produced by two coherent sources, one can proceed in simple steps to a picture of two incoherent sources producing an interference pattern that moves about at random. This randomly moving pattern leaves behind a footprint in the form of the intensity autocorrelation function. This report describes how the autocorrelation function for an extended, incoherent source may be constructed. It is this function that is measured by the Brown-Twiss stellar interferometer.

N68-25830*# National Aeronautics and Space Administration. Goddard Space Flight Center, Greenbelt, Md.

THE INFLUENCE OF FIXTURE STRESS CONCENTRATIONS ON RING ACCELEROMETERS

James A. Nagy and Charles E. Henley, Jr. Washington May 1968 11 p refs

(NASA-TN-D-4540) CFSTI: HC \$3.00 /MF \$0.65 CSCL 14B

Tests have revealed that the most commonly used accelerometer can be subject to a subtle source of error from strains developed in vibration fixtures. Accelerometers mounted on supposedly rigid surfaces may show errors on the order of 100 percent at the very low frequencies below any resonances. A study was initiated to determine the nature of the fixture stress concentration and means of avoiding it. This paper describes the test methods used during the study and the results obtained. The test methods discussed include standard accelerometer calibration techniques; calibrations varying torque, position, and mounting hole angle; photoelastic techniques; base sensitivity checks; and tests with a transducer devised to detect the presence of base-strain in mounted accelerometers. Author

N68-25862*# National Aeronautics and Space Administration. Goddard Space Flight Center, Greenbelt, Md.

THE INTERPRETATION OF DAYTIME MEASUREMENTS BY THE NIMBUS 1 AND 2 HIGH RESOLUTION INFRARED RADIOMETERS

G. Kuers Washington Jun. 1968 23 p refs

(NASA-TN-D-4452) CFSTI: HC\$3.00/MF\$0.65 CSCL 20F

Dense cumulus clouds and fog banks have been selected to determine mean values of their reflectances by means of the High Resolution Infrared Radiometers (HRIR) of Nimbus I and Nimbus II in the wavelength region between 3.6μ and 4.2μ . While both instruments yielded satisfactory results at night, it became apparent that Nimbus I delivered too high reflectance values by day. It was concluded that spurious shortwave radiation entered the radiometer. The amount of the energy difference was used to determine the most probable cause of the malfunctioning, which was considered to be an uncoated rim or a crack of the interference filter.

N68-25903*# Northrop Corp., Hawthorne, Calif.

A STUDY OF AN ELECTRIC FIELD MEASURING INSTRUMENT

S. H. Levine and S. R. Harrison Washington NASA Jun. 1968 44 \ensuremath{p} refs

(Contract NAS2-4143)

(NASA-CR-970; NCL-67-39) CFSTI: HC \$3.00 /MF \$0.65 CSCL 14B

The feasibility of employing a cesium ion beam electric field meter has been experimentally investigated in the laboratory using two types of cesium ion sources. The first source used radiant heating, the other electron bombardment heating. Excellent results were obtained with these sources attaining a sensitivity for measuring electric fields of 0.03 volts/meter. Methods for attaining sensitivities of the order of 0.01 V/m are presented together with a preliminary theoretical investigation of the processes pertaining

to the production of cesium ions in the ionizer. Also, an electronic-readout system design is presented so that all aspects of constructing a cesium ion beam electric field instrument have been studied. Author

N68-26703*# Stanford Research Inst., Menio Park, Calif. CRYOGENIC MAGNETOMETER DEVELOPMENT Final Report, 1 Jul. 1964–7 Mar. 1967

William S. Goree, Bascom S. Deaver, Jr., V. W. Hesterman, and T. W. Barbee, Jr. Washington NASA Jun. 1968 72 p refs (Contract NAS2-2088, SRI Proj. PHU-5093)

(NASA-CR-1073) CFSTI: HC\$3.00 /MF\$0.65 CSCL 14B

A low field superconducting shield has been developed and used to provide stable magnetic fields of less than 10^{-6} G, maintained stable for as long as 6 days. The shield is a superconducting cylinder 91.5 cm long by 16.5 cm ID. The measured attenuation of externally applied axial field changes is a factor of 31 per shield radius. The Meissner effect and zero resistance property of superconductors has been used in the development of a magnetometer for measuring the absolute value of magnetic fields. This device has been used to measure fields as small as 2 imes 10 $^{-6}$ G. A magnetometer utilizing the unique zero resistance and quantized flux properties of superconductors has been developed and used to measure magnetic field changes as small as 5 imes10-7 G. The dc Josephson tunneling effect has been used to construct (1) magnetometers with field sensitivity as good as 10 G, (2) magnetic gradiometers with which field gradients of 10^{-8} G cm have been measured, (3) linear displacement detectors with which displacements of less than 1500 Å have been measured, and (4) a system for measuring static magnetic susceptibility, which was used to study the time dependence of the Meissner effect in hollow tin cylinders. Author

N68-28327*# National Aeronautics and Space Administration. Goddard Space Flight Center, Greenbelt, Md.

A PRECISION SPACECRAFT RADIOMETER FOR HECTOMETER WAVELENGTHS

C. R. Somerlock and J. Krustins Washington Jul. 1968 24 p refs

(NASA-TN-D-4634) CFSTI: HC\$3.00/MF\$0.65 CSCL 20F

The Radio Astronomy Explorer program at Goddard Space Flight Center has pointed out the need for sophisticated radio astronomy receivers for spacecraft use. Development of such a receiver is described with design details. The resulting instrument is a feedback radiometer of the Ryle-Vonberg type. It measures at nine different frequencies between 0.4 Mc and 10 Mc with a 60-db dynamic range centered at an antenna temperature of 106° K. The incorporation of a novel thermistor-bridge power meter yields a long-term measurement accuracy of $\pm 1/2$ db.

N68-28965*# Santa Barbara Research Center, Goleta, Calif. DUAL RADIOMETER ASSEMBLY FOR PROJECT SCANNER Stillman C. Chase Washington NASA Jul. 1968 95 p (Contract NAS1-3827)

(NASA-CR-1086) CFSTI: HC \$3.00/MF \$0.65 CSCL 20F

Design and performance data are presented on the radiometer assembly which is part of a spin-stabilized suborbital space probe payload used to make measurements in two far-infrared wavelength bands of the earth's horizon radiance profile. The equipment consists essentially of two vertical reflecting-type telescopes using true aspheric surfaces on both the primary and secondary mirrors, with flat object space scan mirrors to scan across the horizon as the vehicle spins. Performance specifications are summarized, and comparisons are given between the proposed design and the values actually obtained for the final systems. The difficulties encountered, which made these changes necessary, are explained. The problem areas which developed during the procurement, fabrication, assembly, and test phases are described in detail, and the data are presented as an aid in developing guidelines for future projects. M.G.J.

N68-29418*# National Aeronautics and Space Administration. Langley Research Center, Langley Station, Va.

PHOTOGRAPHIC PHOTOMETRY OF ARTIFICIAL METEORS Wendell G. Ayers Washington Jul. 1968 27 p refs (NASA-TN-D-4667) CFSTI: HC\$3.00/MF\$0.65 CSCL 03A

Two methods of photographic photometry of artificial meteors are presented. These methods relate the amount of radiation that is produced by an artificial meteor in the photographic region of the spectrum to the amount of radiation produced by stars appearing close to the meteor. The relationship is expressed in terms of absolute meteor magnitude. The first method is general and is used when an appreciable difference exists between the structure of the streak image formed by the meteor and of those formed by the stars. The second method is restricted and is used when little difference exists between the structure of the meteor and star images. Author

N68-29951*# National Aeronautics and Space Administration. Langley Research Center, Langley Station, Va.

STRIKING CHARACTERISTICS OF THE MAGNETRON IONIZATION GAGE IN HELIUM FROM 1.9×10^{-7} Torr to 7×10^{-10} Torr

William S. Lassiter Washington Aug. 1968 37 p refs (NASA-TN-D-4681) CFSTI: HC\$3.00/MF\$0.65 CSCL 14B

The striking characteristics of the magnetron gage were measured in helium over a pressure range of 1.9×10^{-7} torr (N₂) (25.3 μ N/m²) to 7×10^{-10} torr (N₂) (93.1 nN/m²). The measured striking characteristics on the upper branches of the striking characteristics diagram agree with the Townsend discharge theory except that, for a given pressure, the characteristics deviate slightly from the theoretical parabolic prediction. On the lower branches, a significant disagreement with theory was found to exist in the dependence of the minimum striking voltage with pressure. Otherwise, on the lower branches, the measured striking behavior agrees with the theoretical prediction and with measurements at higher pressures. Measured striking-time lags occurred in the magnetron gage at pressures bwlow 5×10^{-8} torr (N₂) (6.65 μ N/m²). The lags were determined to cause no significant error in the measurements of the striking characteristics.

N68-30127*# National Aeronautics and Space Administration. Langley Research Center, Langley Station, Va.

CALIBRATION OF 30° INCLUDED-ANGLE CONE FOR DETERMINING LOCAL FLOW CONDITIONS IN MACH NUMBER RANGE OF 1.51 TO 3.51

Walter A. Vahl and Robert L. Weirich Washington Aug. 1968 41 p refs

(NASA-TN-D-4679) CFSTI: HC\$3.00/MF\$0.65 CSCL 14B

A 30° included angle cone was calibrated to permit determination of the local Mach number, total pressure, and flow angles from measurements of total pressure at the cone apex and static pressure at four equally spaced orifices on the cone surface. The calibration data were obtained at Mach numbers of 1.51, 2.37, 2.96, and 3.51 over an angle of pitch range of 0° to 20°. The test Reynolds number ranged from 6.56 \times 10⁶ to 9.85 \times 10⁶ per meter. The test results indicate that the accuracy of Mach number determination varies from approximately ± 0.010 to ± 0.050 at Mach numbers of 1.51 to 3.51, respectively. The accuracy of the total-pressure measurement varies from approximately ±0.5 percent to ± 4.5 percent at Mach numbers of 1.51 to 3.51, respectively. The flow angles nay be determined within approximately $\pm 0.25^{\circ}$ for angles less than 10° and within approximately $\pm 0.50^{\circ}$ for angles greater than 10°. Generally, an iterative procedure is required only for accurate determination of the Mach numbers near or greater than 2.37, with angles of pitch above approximately 10°. Author

N68-31958*# National Aeronautics and Space Administration. Lewis Research Center, Cleveland, Ohio.

MODIFIED VIBRATION TRANSDUCER CALIBRATION SYSTEM WHICH DIRECTLY YIELDS A PLOT OF SENSITIVITY VERSUS FREQUENCY

William C. Nieberding, Edward F. Miller, and David L. Wright Washington Aug. 1968 16 p ref

(NASA-TN-D-4760) CFSTI: HC\$3.00/MF\$0.65 CSCL 14B

A commercially available vibration transducer calibration system was modified to directly produce an output plot of transducer sensitivity versus frequency over the range of frequencies from 10 to 10,000 Hz. This was accomplished by the insertion of a readily programmed automatic attenuation in the exciter control-system feedback loop to maintain constant vibration amplitude versus frequency. National Bureau of Standards primary calibration data are repeated to within ± 0.5 percent over the frequency range of 10 to 9000 Hz and within ± 1 percent from 9000 to 10,000 Hz. Calibrations are obtained in 15 minutes.

N68-33022*# National Research Corp., Cambridge, Mass. Norton Exploratory Research Div.

STUDY OF NEW METHODS TO MEASURE LOW PRESSURE Richard Hecht Washington NASA Aug. 1968 79 p refs (Contract NAS1-5347)

(NASA-CR-1120) CFSTI: HC \$3.00 /MF \$0.65 CSCL 14B

A theoretical and experimental evaluation of the concept of electrostatic control of capacitance-manometer sensitivity has been carried out. The results have been encouraging, although problems have been created by high-voltage breakdown at the electrode and diaphragm surfaces of the gauge. This breakdown can undoubtedly be eliminated by choosing more appropriate surface materials. It is hoped that absolute pressures well below 10-6 Torr can ultimately be measured with this gauge if uncertainties in work-function can be avoided; a voltage-modulation technique is suggested which should accomplish this. It is suggested that the use of superconducting-bolometers to detect the kinetic energy of incident gas molecules will permit absolute measurements of pressures as low as 5 \times 10-9 Torr, and also measurements of molecular beam densities as low as 106 molecules/cc. It is suggested that the juxtaposition of a low-frequency heater and a sensitive microphone will permit absolute pressure measurements as low as 10⁻⁶ Torr. Author

N68-33277*# National Aeronautics and Space Administration. Langley Research Center, Langley Station, Va.

INVESTIGATION OF ELECTRON-RADIATION-INDUCED DIELECTRIC BREAKDOWNS IN A TYPICAL CAPACITOR METEOROID DETECTOR SYSTEM

George M. Storti, George E. Rambo, Herbert D. Hendricks, and Thomas B. Ballard Washington Sep. 1968 29 p refs (NASA-TN-D-4738) CFSTI: HC\$3.00/MF\$0.65 CSCL 14B

The effects of electron radiation on capacitor-type detector systems similar to those used on the Pegasus satellite were investigated. Each system that was tested consisted of a polyurethane foam panel containing two capacitor-type-meteoroid detectors, several meters of polyethylene terephthalate insulated electrical leads. and other items such as rubber shock mounts and polyethylene terephthalate adhesive tape. Three different target thicknesses for the meteoroid detectors were tested, these thicknesses being 40. 200, and 400 microns (1.5, 8, and 16 mils). The incident kinetic energy of electrons used in the tests ranged from 30 keV to 1000 keV, and the temperature of the detector systems was maintained at either 197° K or 297° K. It was found that radiation-induced dielectric breakdowns were produced in the systems and that some of these signals were indicated as meteoroid penetrations. It was determined that the primary source of the breakdowns and, hence. the penetration indications was the polyethylene terephthalate insulated wire. The number of breakdowns and penetration indications

obtained for a fluence of 5×10^{13} e/cm² was found to be dependent on the incident kinetic energy of the electrons and the system temperature; that is, more breakdowns and penetration indications occurred at the lower temperature (197° K) and the lower energies (30 keV to 100 keV). Tests were performed with different modifications made to the signal processing circuits. Several of these modifications resulted in a significant reduction or the total elimination of the radiation-induced penetration indications. Finally, it was found that those systems containing 200 and 400 micron detectors with 200- and 400-micron-thick targets suffered severe decreases in resistance in the capacitor-type detectors. Author

N68-35105*# National Aeronautics and Space Administration. Lewis Research Center, Cleveland, Ohio.

USE OF AN ELECTRONIC VISUALIZATION TECHNIQUE IN THE STUDY OF GAS JOURNAL BEARING BEHAVIOR

Robert Y. Wong, Hugh A. Klassen, Robert C. Evans, and Donald J. Spackman Washington Oct. 1968 18 p Film Supplement Number C-259 to this report is available on Ioan from NASA. Lewis Res. Center, Cleveland

(NASA-TM-X-1609) CFSTI: HC\$3.00/MF\$0.65 CSCL 13H

A visualization technique was developed and applied to data obtained during a test of a pivoted-pad gas journal bearing. Clearance probe measurements, recorded on a data tape, were used to show motions of the bearing components relative to each other, on an oscilloscope screen, with bearing motions amplified relative to the journal diameter. Author

N68-35149*# Research Triangle Inst., Durham, N. C. AN INVESTIGATION OF THIN FILM OXYGEN PARTIAL PRESSURE SENSORS

T. M. Royal, J. J. Wortman, and L. K. Monteith Washington NASA Sep. 1968 61 p refs

(Contract NAS1-7087)

(NASA-CR-1182) CFSTI: HC\$3.00/MF\$0.65 CSCL 14B

Design, development, and testing of a laboratory model involving semiconducting zinc oxide and tin oxide films were investigated. Zinc oxide films at elevated temperatures were found to experience resistance changes greater than an order of magnitude when cycled from N_2 to O_2 environments. The zinc oxide films are relatively insensitive to other gases such as N_2 . Ar, He, CO_2 . A theoretical discussion of the physical mechanisms responsible for the observed phenomena is presented based on oxygen induced changes in the semiconductor donor and acceptor influences. A suitable film substrate, heater, electrical contacting technique, and housing was designed and fabricated into a sensing head. The sensor head was coupled with a control unit for maintaining a constant operating temperature to form the complete sensor.

N68-35152*# Virginia Univ., Charlottesville. Dept. of Physics. AN ANNULAR LITHIUM-DRIFTED GERMANIUM DETECTOR FOR STUDYING NUCLEAR REACTION GAMMA-RAYS

A. J. Levy, R. C. Ritter, and K. Ziock Washington NASA Sep. 1968 85 p refs

(Grant NsG-455)

(NASA-CR-1138) CFSTI: HC\$3.00/MF\$0.65 CSCL 18D

A fabrication technique was developed for truly annular Ge(Li) gamma detectors. Featuring spark-cutting to precisely control the undamaged germanium volume, the detector is capable of standard-geometry techniques such as are used with Nal detectors. Background material relevant to the annular geometry is presented. An extremely explicit, detailed description of the complete fabrication procedure is given, including special cutting, radiant diffusion, and drifting techniques developed here. Measured properties of several detectors are presented, with the emphasis being on the usefulness of the detector high energy gamma ray spectra. Author

14 INSTRUMENTATION AND PHOTOGRAPHY

N68-35534*# National Aeronautics and Space Administration. Lewis Research Center, Cleveland, Ohio.

AN INTEGRATING SPHERE SPECTRORADIOMETER FOR SOLAR SIMULATOR MEASUREMENTS

Orlando W. Uguccini Washington Oct. 1968 27 p refs (NASATN-D-4822) CFSTI: HC\$3.00/MF\$0.65 CSCL 20F

A spectroradiometer, utilizing an integrating sphere and a grating monochromator, and a technique for performing low error spectral measurements of solar simulators are described, together with their evaluation tests. A point by point technique is used in which the spectroradiometer is calibrated with an NBS spectral irradiance standard at each wavelength. Evaluation consisted of checking the calibration of several NBS spectral irradiance standards. Accuracy was also checked by correlating these measurements with measurements obtained with a filter radiometer. Results of the measurements of a carbon arc solar simulator and a xenon arc solar simulator are presented.

N68-35620*# National Aeronautics and Space Administration, Washington, D. C.

NASA CONTRIBUTIONS TO DEVELOPMENT OF SPECIAL-PURPOSE THERMOCOUPLES. A SURVEY C. Eugene Moeller 1968 97 p refs

(NASA-SP-5050) GPO: HC\$1.25; CFSTI: MF\$0.65 CSCL 14B

Special-purpose thermocouples, their characteristics, and their application to difficult problems are discussed in relation to innovations and contributions by NASA research programs. Historical development and thermocouple operational principles are reviewed, and mention is made of important symposia and seminars in the thermocouple field. Recent developments in thermoelectric materials for measuring cryogenic temperatures are described, as are thermoelectric materials and electrical insulators used in thermocouples for measurements above 3000°F. Special thermocouple applications for the measurement of gas, surface, and solids temperatures are discussed; as are new thermocouple developments in rocket nozzles, thermal protection systems, and high speed fluid dynamics. Energy-measuring devices that use special thermocouples are described, along with heat flux gauges, a radiant energy calorimeter, and an intrinsic thermocouple device. Developments associated with techniques of attaching thermocouples to test items are discussed, and test circuits to check out many thermocouples at remote locations are included. M.W.R.

N68-36021*# National Aeronautics and Space Administration. Lewis Research Center, Cleveland, Ohio.

A SMALL COMBINATION SENSING PROBE FOR MEASUREMENT OF TEMPERATUE, PRESSURE, AND FLOW DIRECTION

George E. Glawe, Lloyd N. Krause, and Thomas J. Dudzinski Washington Oct. 1968 20 p refs

(NASA-TN-D-4816) CFSTI: HC\$3.00/MF\$0.65 CSCL 14B

The design features and characteristics of a small combination sensing probe for the measurement of total temperature, total pressure, and flow direction of a gas stream are presented. Also, with proper consideration, a flow direction sensing hold hole indication can be used to determine static pressure. Experimental data are presented for the aerodynamic recovery and time response of the temperature sensor, the flow angle characteristics of the total pressure sensor, and the sensitivity of the flow direction wedge. These data were obtained over a subsonic Mach number range of $0.2 \le M < 1$, as well as at M = 1.4.

N68-36530*# Utah Univ., Salt Lake City. ENTRY LENGTH FOR THE ROCKET METEOROLOGICAL RADIATION SHIELD

Forrest L. Staffanson, Sadiq Alsaji, and Ronald Fazzio Washington NASA Oct. 1968 27 $\,p\,$ refs

(Grant NGR-45-003-025) (NASA-CR-1200) CFSTI: HC \$3.00 / MF \$0.65 CSCL 14B

A derivation is presented for the thermal entry length which determines the depth within a tubular radiation shield that a temperature sensor may be placed without incurring convective heat transfer between the shield and sensor. Data are presented as a function of shield diameter, altitude, and sensor viewing angle. It is concluded that radiation shields of the diameter of the 4-inch meteorological rocket will provide significant shielding to 80 km altitude and shields of the diameter of the 1-inch dart to 60 km. Author

15

MACHINE ELEMENTS AND PROCESSES

Includes bearings, seals, pumps, and other mechanical equipment; lubrication, friction, and wear; manufacturing processes and quality control; reliability; drafting; and materials fabrication, handling, and inspection.

N68-10120*# Martin Co., Baltimore, Md. PARTS AND MATERIALS APPLICATION REVIEW FOR SPACE SYSTEMS

J. P. Craig et al Washington NASA 1967 58 p refs Prepared for NASA

(NASA-SP-6505) CFSTI: HC \$3.00/MF \$0.65 CSCL 14A

Parts and materials application-review activity for project management of space systems is defined, and a guide for performance of effective reviews by parts and materials specialists and design engineers is provided. Parts application review is necessary with regard to: flammability and outgassing properties of parts; compatibility of leads with metal joining processes; compatibility of parts surfaces with coating and encapsulants; and environmental resistance and physical and electrical properties of coatings, encapsulants, and insulating materials. A method for selecting the scope of review activities appropriate to various levels of project requirements is illustrated by examples of projects and their hardware. S.P.

N68-10402*# Midwest Research Inst., Kansas City, Mo. ADVANCED VALVE TECHNOLOGY, A SURVEY

Louis C. Burmeister, John B. Loser, and Eldon C. Sneegas Washington NASA 1967 190 p refs Revised (NASA-SP-5019) GPO: \$1.00 CSCL 13K

The purpose of this book is to disseminate advanced valve technology throughout all branches of industry. To achieve this objective, it was necessary to (1) determine the present industrial state-of-the-art-this was accomplished by conducting interviews, a literature search, and discussions with application and systems engineers at NASA installations; (2) recognize new advances-valves which have qualified for newer missiles, advanced aircraft, and spacecraft usually represent improvements beyond the industrial state-of-the-art; and (3) report the new technology-when a considerable number of custom-made valves fall within a given category, the combined technology information in that category will often fall into a pattern and indicate new trends and approaches. New trends and techniques mentioned are concerned with leakage, materials, compatibility, contamination, wear, reliability, response time, repeatability, valve actuators, proportional flow control, heat transfer, high pressure and temperature, pressure surge protection, flutter and chatter, and unique designs and applications. R.W.H.

N68-10503* General Electric Co., Cincinnati, Ohio. Missile and Space Div.

DESIGN OF TWO ELECTROMAGNETIC PUMPS

G. E. Diedrich and J. W. Gahan Washington NASA Nov. 1967 103 p refs

(Contract NAS3-8500)

(NASA-CR-911) CSCL 13K

A design study program to determine three specific EM pump designs for possible use as boiler feed pumps in Rankine-cycle, space electric power systems is described. The three designs were: (1) 9 (b/sec, 240 psi pump for 1000°F potassium using a T-111 duct; (2) 9 (b/sec, 240 psi pump for 1000°F potassium using a 316 SS duct; and (3) 3.25 (b/sec, 240 psi pump for 1000°F potassium using a T-111 duct. A specific design for each of these ratings is described in detail. Complete calculated performance and evaluation for each design are also presented. Final design selection for each rating was based on efficiency, reliability, weight, and fabricability. In general, efficiency was optimized.

EQUIPMENT AND PROCEDURES FOR GLASS-BEAD PEENING TITANIUM-ALLOY TANKS

Thomas T. Bales, Charles R. Manning, Jr., and W. Barry Lisagor Washington Jan 1968 32 $\,p\,$ refs

(NASA-TN-D-4288) CFSTI: HC\$3.00/MF\$0.65 CSCL 13H

Glass-bead peening equipment which utilizes programmed motions has been developed and used to peen uniformly the inner surface of 26 titanium alloy spacecraft tanks for the alleviation of stress corrosion resulting from exposure to nitrogen tetroxide. The tanks which were peened varied from 20 inches to 14 feet (0.5 to 4.2 m) in length and from 12.5 to 51 inches (0.3 to 1.3 m) in diameter. The function of each component of the developed equipment and the procedures used for peening are described herein. Glass-bead peening parameters have been investigated and parameters were established which produced a compressive stress of approximately 100 ksi on the peened surface of titanium test strips. Ine effect of glass-bead peening on the mechanical properties of the titanium Ti-6AI-4V alloy was determined from tests conducted by using peened and unpeened standard tensile and V-notch specimens as well as from results of a burst test of a peened tank. A slight reduction in the yield and notch properties of the material was noted after peening; the ultimate tensile strength, elongation, and modulus of the material, however, were found to be unaffected. Author

N68-15010*# National Aeronautics and Space Administration. Lewis Research Center, Cleveland, Ohio.

REDUCED PRESSURE ENVIRONMENT EFFECTS ON ROLLING ELEMENT FATIGUE LIFE WITH SUPER REFINED MINERAL OIL LUBRICANT

David W. Reichard, Richard J. Parker, and Erwin V. Zaretsky Washington Jan. 1968 17 p refs

(NASA-TN-D-4348) CFSTI: HC\$3.00/MF\$0.65 CSCL 131

A modified NASA five-ball fatigue tester was used to investigate the effect of a reduced-pressure environment on rolling-element fatigue life, deformation, and wear of SAE 52100 steel balls with a super-refined naphthenic mineral oil used as the lubricant. Tests were conducted at atmospheric pressure, at a 20° contact angle, with a thrust load of 60 pounds (267 N) to produce an initial maximum Hertz stress of 800,000 psi (5.5×10⁹ N/m²) at a shaft speed of 4900 rpm with no heat added. The atmospheric-pressure tests served as reference data for tests conducted at a reduced pressure, approximately the vapor pressure of the lubricant. For these reduced-pressure tests, the ball specimens were lubricated by a quasi-mist method and by immersion in the lubricant. In both cases, all other test conditions were the same as those in the atmospheric-pressure tests. No significant difference in the fatigue lives was observed for tests conducted at atmospheric pressure and those conducted at reduced ambient pressure. The amounts of deformation and wear for the two pressure conditions differed little, regardless of the lubrication mode employed, which was an indication of a sufficient elastohydrodynamic lubricating film at the reduced-pressure levels. Author

15 MACHINE ELEMENTS AND PROCESSES

N68-16468*# National Aeronautics and Space Administration. Lewis Research Center, Cleveland, Ohio.

FRICTION TORQUE OF BALL BEARINGS IN VACUUM WITH SEVEN POLYTETRAFLUOROETHYLENE COMPOSITION RETAINER MATERIALS

Herbert W. Scibbe, Dean C. Glenn, and William J. Anderson Washington Feb. 1968 20 p refs

(NASA-TN-D-4355) CFSTI: HC\$3.00/MF\$0.65 CSCL 131

Self-lubricating retainer materials containing various weight percentages of polytetrafluoroethylene (PTFE), glass fibers, molybdenum disulfide (MoS₂), and bronze were evaluated in 20-millimeter-bore ball bearings operating in a vacuum of 10^{-6} torr (1.33×10⁻⁴ N/m²). The lubricating capability of the retainer materials was evaluated by measurement of the bearing friction torque. The test bearings were run at 3600 rpm with axial loads from 35 to 100 pounds for periods of approximately 1 hour. Although all retainer materials lubricated the bearings reasonably well, the best lubrication, as measured by the lowest average friction torque, was obtained with a bearing equipped with a retainer of 70 percent PTFE, 15 percent glass fibers, and 15 percent MoS2. In an initial run at a load of 50 pounds with this material, the bearing torque was high and erratic: in the next three consecutive runs, however, the torque remained at a low, constant level. In the following three consecutive runs, the bearing registered low. steady torque upon restart and thereby demonstrated good restart capability. During the time intervals of 24 hours or more between the runs, the bearing "soaked" in the vacuum chamber. The good performance with this retainer was partly attributed to a fabricating process that produced a homogeneous mixture of PTFE, glass fibers, and MoS₂ in the material. Author

N68-17564*# National Aeronautics and Space Administration. Lewis Research Center, Cleveland, Ohio.

NONCAVITATING PERFORMANCE OF TWO-AREA-RATIO WATER JET PUMPS HAVING THROAT LENGTHS OF 7.25 DIAMETERS

Nelson L. Sanger Washington Mar. 1968 62 p refs

(NASA-TN-D-4445) CFSTI: HC\$3.00/MF\$0.65 CSCL 13K

The performance of two jet pumps having low nozzle- to throat-area ratios was evaluated in a water facility and compared to theoretically predicted performance. The purposes of the investigation were to gain a better insight into the flow mechanisms involved in low-area-ratio jet pumps, and to compare the abilities of two existing one-dimensional analyses to predict jet pump performance over a wide range of operating conditions. Two nozzles were evaluated experimentally and the test pump consisted of one of the two nozzles and one test section, the latter having a throat diameter of 1.35 inches (3.43 cm), a throat length of 7.25 diameters, and a diffuser included angle of 8°6' (0.141 rad). The nozzles had exit diameters corresponding to nozzle- to throat-area ratios of 0.066 and 0.197. Each nozzle was operated at several spacings of the nozzle exit upstream from the throat entrance over a range of from 0 to 3 throat diameters. At small nozzle spacings (up to 1 throat diameter) a simple one-dimensional analysis predicted performance quite closely. The theory also demonstrated that low efficiencies exhibited at low ratios of secondary to primary (high pressure) flows are due to inefficient mixing, whereas low efficiencies at high flow ratios are due largely to friction losses. A modified theory, which attempted to account for the effect of the mixing profile in the throat, required more computational effort and did not improve correlation with experimental performance. Author

N68-19307*# National Aeronautics and Space Administration. Marshall Space Flight Center, Huntsville, Ala.

SHAPING OF PRECIPITATION-HARDENING STAINLESS STEELS BY CASTING AND POWDER-METALLURGY

J. G. Kura, V. D. Barth, and H. O. McIntire [1968] 51 p refs Prepared by Army Missile Command and Battelle Mem. Inst. (NASA Order H-76715; Contract DA-01-021-AMC-11651(Z)) (NASA-SP-5086; RSIC-491) CFSTI: HC \$3.00/MF \$0.65 CSCL 13H The state of the art of making shapes of precipitationhardenable stainless steels by methods other than machining from wrought materials is reviewed. The methods reviewed are casting and powder metallurgy. Of these methods, only casting is extensively practiced. Powder metallurgy is a promising procedure for 17-4 PH stainless, but techniques are not well advanced for handling the grades that contain titanium or aluminum such as PH 15-7 Mo and A-286. Author

N68-19343*# National Aeronautics and Space Administration. Marshall Space Flight Center, Huntsville, Ala. SUBFACE TREATMENTS FOR PRECIPITATION-HARDENING

STAINLESS STEELS

[1967] 64 p refs Prepared by Battelle Memorial Inst.

(Contract DA-01-021-AMC-11651(Z))

(NASA-SP-5090; RSIC-595) CFSTI: HC \$3.00/MF \$0.65 CSCL 13H

In this report, selected surface treatments that are applied to precipitation-hardenable stainless steels are discussed. The treatments covered are hard surfacing, electroplating, electroless plating, carburizing and decarburizing, nitriding, burnishing and other, finishing operations, explosive hardening, planishing, and peening. Each treatment is described and its application to the precipitation-hardenable stainless steels is discussed. Reasons for using the treatments are discussed, problem areas are identified, and recommendations for research are made. Author

N68-20056*# National Aeronautics and Space Administration. Marshall Space Flight Center, Huntsville, Ala.

ADHESIVE BONDING OF STAINLESS STEELS INCLUDING PRECIPITATION-HARDENING STAINLESS STEELS

R. E. Keith, M. D. Randall, and R. C. Martin [1966] 125 p Prepared by Battelle Memorial Inst.

(Contract DA-01-021-AMC-11651(Z))

(NASA-SP-5085; RSIC-599) CFSTI: HC \$3.00/MF \$0.65 CSCL 13H

The state of the art of adhesive bonding of stainless steels and precipitation-hardened stainless steels is given. The advantages and disadvantages of adhesive bonding are discussed along with typical joint designs, surface preparation procedures, and environmental factors that influence choice among the available adhesives and processing techniques. The bonding of stainless steels with organic and inorganic adhesives is discussed in relation to the preparation of the adherend surfaces and joints, the tests and standards for selecting the adhesive, and the testing and inspection of the adhesive bond. B.S.D.

N68-20'199*# National Aeronautics and Space Administration. Lewis Research Center, Cleveland, Ohio.

RESIDUAL STRESS AND SUBSURFACE HARDNESS CHANGES INDUCED DURING ROLLING CONTACT

David W. Reichard, Richard J. Parker, and Erwin V. Zaretsky Washington Apr. 1968 31 p refs

(NASA-TN-D-4456) CFSTI: HC\$3.00/MF\$0.65 CSCL 131

Subsurface residual stress measurements were made on SAE 52100 steel inner races from 207-size deep-groove ball bearings in which Δ H (ball hardness minus race hardness) ranged from -1.1 to 3.5 points Rockwell C. Nominal Rockwell C hardness of the inner and outer races was 63. These bearings had been run at an inner-race speed of 2750 rpm and a radial load of 1320 pounds (5874 N) producing maximum Hertz stresses of 352.000 and 336,000 psi (2425 $\times 10^{6}$ and 2315 $\times 10^{6}$ N/m²) at the inner and outer races, respectively. The lubricant was a super-refined naphthenic mineral oil. The residual stress measurements were made of various depths below the inner-race running track surface for a total of 19 of these bearings that had been run for nominally 200, 600, and 1600 hours. The measurements indicated that the maximum compressive residual stresses occur in approximately the same Δ H range for which the maximum fatigue lives were observed.

Additionally, no relation between running time and residual stress could be determined from these measurements. Although a subsurface hardness decrease was evident in all cases, no relation between these changes and ΔH or running time could be determined.

N68-20325*# National Aeronautics and Space Administration. Lewis Research Center, Cleveland, Ohio.

WEAR RATE AND FRICTION COEFFICIENT IN LIQUID NITROGEN AND HYDROGEN OF STEEL SLIDING ON POLYMER LAMINATES (VARIOUS FABRICS AND POLYMERS)

Donald W. Wisander and Robert L. Johnson Washington Apr. 1968 15 p refs

(NASA-TN-D-4463) CFSTI: HC\$3.00/MF\$0.65 CSCL 111

The polymers included PTFE (polytetrafluoroethylene), phenolic, epoxy, and melamine; the fabrics included glass, graphite, nylon, and cotton. The reference material used was not a laminate (80% PTFE, 15% glass fiber, and 5% graphite). Wear and friction experiments were conducted with a 3/16-inch- (4.8-mm-) radius hemispherical rider sliding on a flat disk, which was rotated to produce sliding velocities of 2300 feet per minute (701 m/min). The 304 stainless steel riders were under a 1-kilogram load against the polymer laminate disks. The results indicate that the graphite-fabric phenolic laminate is a potentially useful material for sliding contact in liquid nitrogen and that glass-fabric PTFE and graphite-fabric PTFE laminates are potentially useful in both liquid nitrogen and liquid hydrogen. The wear rates and coefficients of friction of 304 stainless-steel riders against the laminates were appreciably lower in liquid nitrogen than in liquid hydrogen Author

N68-20389*# General Electric Co., Schenectady, N. Y.

LEAKAGE TESTING HANDBOOK J. William Marr Washington NASA Apr. 1968 461 p refs

Prepared for JPL

(Contract NAS7-396).

(NASA-CR-952; S-67-1014) CFSTI: HC \$3.00/MF \$0.65 CSCL 14D

Theory of leakage testing is described; and individual methods of leakage testing, their limitations, sensitivities, and methods of use are delineated. The distinction between leakage measurement and leak location is considered in this handbook that also discusses reasons for leak testing, techniques of using leak testing equipment, flow characteristics encountered in leaks, necessary equipment and safety measures, and standards and calibration. Procedure for writing a leakage specification is given, and a guide is presented for selecting appropriate testing methods. Mass spectrometry, heated anode halogen detection, pressure change procedure, flow measurement, bubble testing, and radioisotope procedures are described. Other techniques considered are the halide torch, sonic detection, light absorption, chemical methods, high voltage discharges, and vacuum gauge responses. Several miscellaneous procedures are noted; and properties of tracer gases and precautions for their use are discussed. MWR

N68-20433*# National Aeronautics and Space Administration. Marshall Space Flight Center, Huntsville, Ala.

THERMAL AND MECHANICAL TREATMENT FOR PRECIPITATION-HARDENING STAINLESS STEELS

C. J. Slunder, A. F. Hoenie, and A. M. Hall [1967] 207 p refs Sponsored jointly with AEC Prepared by Battelle Mem. Inst. for Redstone Sci. Inform. Center

(NASA Order H-76715; Contract DA-01-021-AMC-11651(Z))

(NASA-SP-5089; RSIC-600) CFSTI: HC \$3.00/MF \$0.65 CSCL 13H

The thermal and mechanical treatments employed in the production and fabrication of precipitation-hardenable stainless steels are discussed. Particular emphasis is directed to the interaction of the processing variables and their effects on fabricability and mechanical properties. Equipment arc's procedures are described as well as problems likely to be encrimered and precautions to be observed in processing. Detailed processing information is presented for the precipitation-hardenable stainless steels considered to be applicable for missile and aerospace applications. Author

N68-21226*# National Aeronautics and Space Administration Lewis Research Center, Cleveland, Ohio.

INFLUENCE OF CRYSTAL STRUCTURE, ORIENTATION, AND SOLUBILITY ON ADHESION AND SLIDING FRICTION OF METAL SINGLE CRYSTALS IN VACUUM

Donald H. Buckley Washington Apr. 1968 22 p refs

(NASA-TN-D-4347; ASTM-STP-431) CFSTI: HC \$3.00/MF \$0.65 CSCL 11F

An investigation was conducted on the relation of friction to the adhesion or cohesion of metals in vacuum. Metal single crystals were used to determine planes, surface energy, work hardening, and crystal structure on friction and adhesion. The following characteristics were examined: (1) atomic plane matching across an interface, (2) the effect of plane atomic density, (3) orientation of coupled metals, (4) mutual solubility, and (5) the effect of crystal structure. The metal couples examined included the copper plane pairs: (100) on (100), (110) on (110), and (111) on (111), all three pairs matched planes and directions; and (110) on (100) and (111) on (100). The (111) plane of copper was also examined in contact with planes (0001) of cobalt, (111) of nickel, and (110) of tungsten. The (0001) plane of cobalt was also studied in contact with itself. The results of this investigation indicate that adhesion is markedly increased by small amounts of unidirectional sliding of the surfaces in contact. The adhesion measurements correlated with the friction coefficients: high friction coefficients were always accompanied by high adhesive forces. Author

N68-21241*# National Aeronautics and Space Administration. Marshall Space Flight Center, Huntsville, Ala.

MACHINING AND GRINDING OF ULTRAHIGH-STRENGTH STEELS AND STAINLESS STEEL ALLOYS

C. T. Olofson, J. A. Gurklis, and F. W. Boulger Redstone Arsenal, Ala. Redstone Sci. Inform. Center [1968] 217 p refs Prepared by Battelle Mem. Inst.

(NASA Order H-76715; Contract DA-01-021-AMC-11651(Z)) (NASA-SP-5084; RSIC-501) CFSTI: HC \$3.00/MF \$0.65 CSCL 13H

The state of the art of metal-removal operations for stainless and ultrahigh-strength steels is presented. It describes the methods currently employed for conventional machining, grinding, electrolytic, electric-discharge, and chemical-machining processes. The precautions that should be taken to avoid troubles resulting from the characteristics typical of these alloys are pointed out. Nine machining, two grinding, two cutting, and three unconventional metal-removal operations are discussed separately. Other sections discuss the classification of these alloys and their general response to machining variables. Author

N68-21429*# National Aeronautics and Space Administration. Marshall Space Flight Center, Huntsville, Ala.

WELDING OF PRECIPITATION-HARDENING STAINLESS STEELS

J. J. Vagi, R. M. Evans, and D. C. Martin [1968] 194 p refs Prepared by Battelle Memorial Inst.

(Contract DA-01-021-AMC-11651(Z))

(NASA-SP-5087; RSIC-598) CFSTI: HC \$3.00/MF \$0.65 CSCL 13H

The state of the art of the welding of precipitation-hardening stainless steels is reviewed. Welding preparations, specific welding processes, welding dissimilar metals, and joint quality are discussed. Author

15 MACHINE ELEMENTS AND PROCESSES

N68-21898*# National Aeronautics and Space Administration. Lewis Research Center, Cleveland, Ohio.

EVALUATION OF TANTALUM-TO-STAINLESS-STEEL TRANSITION JOINTS

Adolph C. Spagnuolo Washington Apr. 1968 29 p refs (NASA-TM-X-1540) CFSTI: HC\$3.00/MF\$0.65 CSCL 13E

Tantalum-to-stainless-steel bimetallic transition joints were tested to determine the overall strength of the brazed joint. Tensile tests were conducted on flat sheet and tubular specimens at elevated temperatures 1350°F and vacuum levels of 10-7 to 10-6 torr. Studies were also conducted to determine if any unfavorable interdiffusion embrittlement was taking place between the braze material and the parent metals, A 2.5-inch diameter by 0.125-inch wall bimetallic joint was subjected to the temperature 1350°F and pressure 350 psia levels expected in a liquid metal loop including 20 temperature cycles between 600°F and 1350°F. The tests indicated: (1) The parent material in all tensile specimens ruptured first, leaving the brazed area intact. (2) No significant interdiffusion occurred between the braze and the parent metals. (3) The 2.5-inch diameter tube remained leak tight after 150 hours of testing at 1350°F and 350 psia. Ultimate and yield strength data are also included for unalloyed tantalum rods, plate and sheet test specimens at 1350° F at vacuum levels of 10^{-8} to 10^{-7} torr. Author

N68-21965*# National Aeronautics and Space Administration. Lewis Research Center, Cleveland, Ohio.

EXPERIMENTS ON STABILITY OF HERRINGBONE GROOVED GAS-LUBRICATED JOURNAL BEARINGS TO HIGH COMPRESSIBILITY NUMBERS

Robert E. Cunningham, David P. Fleming, and William J. Anderson Washington Apr. 1968 21 p refs

(NASA-TN-D-4440) CFSTI: HC\$3.00/MF\$0.65 CSCL 13K

Experiments were conducted with six rotors, 1-1/2 inches (3.8 cm) in diameter by 12-1/4 inches (31.1 cm) long and equipped with two herringbone-grooved journals. These rotors were operated in plain cylindrical sleeves to high compressibility numbers with ambient air as a lubricant. Vertical orientation of the rotors without any applied radial load presented a test condition most conducive to existing half-frequency whirl (HFW). These experiments showed that HFW threshold speeds are very much dependent on radial clearance. Five rotors running at clearances from 370 to 500 microinches (9.4 to 12.7 µm) did not whirl up to the limiting speed of the air turbine drive. When the same rotors were operated at clearances ranging from 550 to 710 microinches (14 to 18 µm), HFW was experienced at fairly low speed ranges of from 14,750 to 27,900 rpm. Limited test results comparing a fully grooved with a partially grooved rotor showed the fully grooved rotor to be stable up to 60,830 rpm. The partially grooved rotor having the same operating parameters except for groove length exhibited HFW at 27,900 rpm. Agreement between experimental and theoretical results is generally quite good. Based on these results the theory tends to be somewhat conservative in defining zones of unstable, operation Author

N68-21979*# National Aeronautics and Space Administration. Lewis Research Center, Cleveland, Ohio.

A REVIEW OF LUBRICATION OF SLIDING AND ROLLING-ELEMENT ELECTRICAL CONTACTS IN VACUUM John S. Przybyszewski Washington Apr. 1968 33 p refs (NASA-TN-D-4476) CFSTI: HC\$3.00/MF\$0.65 CSCL 11H

The operation of sliding- or rolling-element electrical contacts in vacuum presents a problem because of the occurrence of high noise levels, high coefficients of friction and excessive wear rates due to the absence of beneficial surface films. Thin metallic films are seen as a promising method of lubrication. Three methods of thin film deposition and the endurance lives of these films (obtained from friction experiments) are discussed. On the basis of the reviewed experimental data, some conclusions are made regarding the performance of the various electric contact materials and lubricants in vacuum. N68-22778*# National Aeronautics and Space Administration, Washington, D. C.

METHOD OF BRAZING ALUMINUM TO STAINLESS STEEL FOR HIGH-STRESS-FATIGUE APPLICATIONS

D. C. Martin 1968 16 p refs Prepared by Battelle Memorial Inst.

(NASA-SP-5040) CFSTI: HC \$3.00/MF \$0.65 CSCL 13H

A procedure for minimizing the formation of intermetallic compounds in aluminum-stainless steel joints is discussed that uses a titanium coating on the stainless steel to act as a diffusion barrier. This Ti alloy layer is coated with an aluminum-silicon alloy, and the joint is made by brazing the Al part to the coated stainless steel part. In the case of an age-hardenable Al part, aging takes place after brazing. Applications of the procedure are mentioned: problems of joining Al to iron-base alloys are noted; and diffusion barrier for Ti and Al coatings, brazing, and joint properties are discussed. M.W.R.

N68-22810*# Case Inst. of Tech., Cleveland, Ohio.

A CRITICAL EVALUATION OF THE STATUS AND TRENDS IN HIGH SPEED FLUID FILM LUBRICATION

E. S. Kulinski and S. Ostrach Washington NASA May 1968 25 p refs

(Grant NGR-36-003-004)

(NASA-CR-1058) CFSTI: HC \$3.00/MF \$0.65 CSCL 11H

High speed lubrication (also denoted as turbulent and superlaminar lubrication) and relevant parts of the fluid mechanics literature are reviewed. It is contended on the basis of this review that existing turbulent journal bearing calculations are predicted on an unrealistic characterization of the lubricant film. Furthermore, an order-of-magnitude argument is presented which indicates that the neglect of inertial terms in the governing equations of turbulent lubrication is incorrect. It is concluded that fundamental investigations on the structure of high speed lubricant films must precede the formulation of an adequate theory, and the nature of these investigations is discussed. Author

N68-23356*# Chrysler Corp., Huntsville, Ala. DESIGN HANDBOOK UMBILICAL LOCKING MECHANISM DEVELOPMENT PROGRAM

David L. Cusick Washington NASA May 1968 72 p (Contract NAS8-20649)

(NASA-CR-1021) CFSTI: HC \$3.00/MF \$0.65 CSCL 13E

This handbook presents the techniques, developed in an intensive testing program, for use in designing ball-lock mechanisms for use on space vehicle umbilicals. In addition to the general design of this locking device and its component parts, this handbook covers the effects of component surface conditioning, temperatures from ambient to minus 196 degrees Centigrade (°C), materials and material hardness, and forces on the locking device up to 5000 pounds.

N68-23900*# National Aeronautics and Space Administration. Lewis Research Center, Cleveland, Ohio.

THE RELEASE OF HYDROGEN ON BALL MILLING CHROMIUM IN WATER

Alan Arias Washington May 1968 23 p refs

(NASA-TN-D-4569) CFSTI: HC \$3.00/MF \$0.65 CSCL 13H

During the ball milling process, chromium powder reacted with the water used as the grinding medium, and hydrogen was evolved. A film composed of Cr_2O_3 and CrO_2 formed on the powder surface during this reaction. This film was calculated to be about 6.7 Å (0.00067 μ m) thick. Although the specific surface area of the powder continuously increases, a large proportion of the particles also became welded to each other during the milling process. The welding sandwiched the oxide films between the powder particles. For this reason, the ratio of oxide formed to measured surface (and apparent thickness of the film) increase with ball-milling time. N68-24142*# National Aeronautics and Space Administration. Lewis Research Center, Cleveland, Ohio,

FRICTION AND WEAR IN CRYOGENIC LIQUIDS FOR COMPOSITES OF PHENOLIC AND OF POLYTETRAFLUO-ROETHYLENE OF VARIOUS PARTICLE SIZES AND CONCEN-TRATIONS

Donald W. Wisander, Lawrence P. Ludwig, and Robert L. Johnson Washington May 1968 17 p refs

(NASA-TN-D-4565) CFSTI: HC \$3.00/MF \$0.65 CSCL 11D Experiments conducted with phenolic-PTFE

(polytetrafluoroethylene) composites sliding against 440-C steel in

how the analysis of the state o

N68-24456*# National Aeronautics and Space Administration. Lewis Research Center, Cleveland, Ohio.

COOLING STUDIES WITH 40-MILLIMETER-BORE BALL BEARINGS USING LOW FLOW RATES OF 60°R (33°K) HYDROGEN GAS

David E. Brewe, Harold H. Coe, and Herbert W. Scibbe Washington Jun. 1968 27 p refs

(NASA-TN-D-4616) CFSTI: HC\$3.00/MF\$0.65 CSCL 131

Experiments and analyses were performed to determine ball bearing cooling requirments at shaft speeds to 35,000 rpm and thrust loads to 400 pounds (1780 N). A bronze-filled polytetrafluoroethylene retainer was used to lubricate the bearings. Bearing outer-race temperature varied as the inverse of hy-drogen gas flow rate through the bearing. From this inverse relation, a minimum flow equation was developed for the range of bearing operating conditions. The minimum flow rate required for bearing cooling was more sensitive to speed than to load increases. Film transfer to the inner-race grooves and retainer wear are indicated and discussed. Author

N68-25042*# Mechanical Technology, Inc., Latham, N. Y. Pratt and Whitney Aircraft, East Hartford, Conn.

RESEARCH AND DEVELOPMENT OF HIGH PERFORMANCE AXIAL-FLOW TURBOMACHINERY. VOLUME 2: DESIGN OF GAS BEARINGS

P. W. Curwen Washington NASA May 1968 332 p refs Prepared for Pratt and Whitney Aircraft

(Contract NAS3-4179)

(NASA-CR-801) CFSTI: HC\$3.00/MF\$0.65 CSCL 13I

Three variations of a basic gas-bearing rotor-support system have been designed, built, and tested for the NASA Brayton cycle axial-flow turbocompressor. The designs were experimentally evaluated in a full-scale rotor-bearing system test rig. All three bearing system designs performed satisfactorily and successfully passed the required acceptance tests. The final design represents a minimum bearing-friction-loss design consistent with whirl-free operation of the rotor. Following acceptance testing of the initial gas-bearing rotor-support system, an attempt was made to attain a 61% reduction in total journal bearing friction loss by modifying the bearings to operate at larger clearances. Upon test of the modified design, a low-frequency, stable rotor-whirl phenomenon was observed in the turbine bearing as the clearance was being increased to the larger value. Until the whirl phenomenon is better understood, it is recommended that the diametral clearances of the journal bearings be maintained at ≤0.00135 inches. This will assure whirl-free operation of the rotor. At these clearances, the final design represents a 34.3% reduction in total journal bearing friction loss relative to the initial design. Author

N68-28241*# National Aeronautics and Space Administration. Lewis Research Center, Cleveland, Ohio,

OPERATION OF A LIQUID FLUORINE PUMP IN CAVITATING FLOW AT AN INDUCER TIP SPEED OF 188 FEET PER SECOND (57.3 M/SEC)

Walter M. Osborn Washington Jun. 1968 15 p refs

(NASA-TM-X-1573) CFSTI: HC\$3.00/MF\$0.65 CSCL 13K

A combination cavitating inducer and main-stage impeller was operated in liquid fluorine for 36 minutes. The inducer tip relative flow velocity was approximately 188 feet per second. Both noncavitating and cavitating pump performance are presented. For approximately 18 minutes the inducer was operating with moderate to heavy cavitation. No cavitation damage was experienced. Titanium carbide cermet with nickel binder and aluminum oxide performed adequately as seal materials. Author

N68-28249*# National Aeronautics and Space Administration. Goddard Space Flight Center, Greenbelt, Md.

THE USE OF THE ELECTRON PROBE MICROANALYZER IN MATERIALS RESEARCH AND DEVELOPMENT Lawrence Kobren Washington Jun. 1968 25 p refs

(NASA-TN-D-4526) CFSTI: HC\$3.00/MF\$0.65 CSCL 14B

The electron probe microanalyzer, a versatile tool for the analysis of areas as small as one micron in diameter, has been used at Goddard Space Flight Center in applications ranging from materials research to analysis of failures in mechanical parts. Methods of using the probe and representative results obtained are illustrated by several examples that include bonding of thermoelectric materials, alloy development, and analysis of materials failures. Author

N68-28258*# National Aeronautics and Space Administration. Lewis Research Center, Cleveland, Ohio.

EFFECT OF BALL-RACE CONFORMITY ON SPINNING FRICTION

Marshall W. Dietrich, Richard J. Parker, and Erwin V. Zaretsky Washington Jul. 1968 19 p refs

(NASA-TN-D-4669) CFSTI: HC\$3.00/MF\$0.65 CSCL 131

Tests were conducted in the NASA spinning friction apparatus with SAE 52100 steel specimens with ball-groove conformities of infinity (ball on a flat), 60, 55, and 51 percent. The coefficient of spinning friction decreased with increasing maximum Hertz stress to a minimum value of approximately 0.05. For a constant stress, the coefficient of spinning friction increased with decreasing conformity (increasing percent conformity). Spinning torque increased with increasing stress for each conformity tested. For a given stress, spinning torque decreased with decreasing conformity. Author

N68-28260*# National Aeronautics and Space Administration. Lewis Research Center, Cleveland, Ohio.

EFFECT OF CRYSTAL TRANSFORMATION AND ATOMIC ORDERING ON FRICTION AND WEAR OF TWO COBALT-BASE ALLOYS IN VACUUM

William A. Brainard and Donald H. Buckley Washington Jul. 1968 19 p refs

(NASA-TN-D-4668) CFSTI: HC\$3.00/MF\$0.65 CSCL 20K

The effect of crystal and order-disorder tranformations on friction and wear for Be–Co and FeCo alloys were studied in sliding friction experiments in vacuum at elevated temperatures. The results show that friction increases fourfold for the beryllium-cobalt alloy during tranformation and that friction remains high until the reverse or cooling transformation occurs. The friction and wear of Be–Co are markedly superior to 440-C stainless steel. The order-disorder transformation in FeCo increases friction by a factor of 30 and also significantly increases wear. Increased sliding speed and loading affect the transformation. The friction behavior during heating is in good agreement with the type of order-temperature relation in FeCo.

15 MACHINE ELEMENTS AND PROCESSES

N68-28766*# National Aeronautics and Space Administration. Lewis Research Center, Cleveland, Ohio.

PRELIMINARY EVALUATION OF GREASES TO 316°C AND SOLID LUBRICANTS TO 816°C IN BALL BEARINGS

Harold E. Sliney and Robert L. Johnson Washington NASA Jul. 1968 21 p refs

(NASA-TN-D-4652) CFSTI: HC\$3.00/MF\$0.65 CSCL 11H

A special apparatus designed for the evaluation of high-temperature lubricants in 20-mm-bore ball bearings is described. The results of bearing runs at temperatures up to 1500° F in air are reported. At 450° and 600° F, a fluorocarbon grease lubricated the 440-C steel bearings for longer times than did polyphenyl ether and silicone greases thickened with dyes and/or MoS₂. Cobalt alloy ball bearings, lubricated either with barium fluoride-calcium fluoride coatings bonded to the cages or with porous metal cages impregnated with these fluorides, ran successfully at 1200° and 1500°F under a thrust load of 30 lb and at a shaft speed of 5000 rpm.

N68-28871*# National Aeronautics and Space Administration. Lewis Research Center, Cleveland, Ohio.

FRICTION AND WEAR UNDER FRETTING CONDITIONS OF MATERIALS FOR USE AS WIRE FRICTION DAMPERS OF COMPRESSOR BLADE VIBRATION

Max A. Swikert and Robert L. Johnson Washington Jul. 1968 17 p refs

(NASA-TN-D-4630) CFSTI: HC\$3.00/MF\$0.65 CSCL 131

Friction dampers are required to reduce the magnitude of vibrational stresses in high aspect ratio blading of compressors for advanced aircraft turbine engines. Fretting is a common problem with all types of friction dampers. Fretting experiments with simulated wire lace blade damping were conducted with Inconel 600. Experiments were run with or without oxide coatings in contact with maraging steel. Although two methods were used to form the oxide, high friction and low wear occurred with both. Further wear experimentation with oxidized material rubbing against itself showed that friction and wear were decreased by operation at a higher temperature (500°F).

N68-29918*# National Aeronautics and Space Administration. Lewis Research Center, Cleveland, Ohio. INFLUENCE OF SURFACE ACTIVE AGENTS ON FRICTION, DEFORMATION, AND FRACTURE OF LITHIUM FLUORIDE Donald H. Buckley Washington Aug. 1964 29 p refs

(NASA-TN-D-4716) CFSTI: HC\$3.00/MF\$0.65 CSCL 11H

Sliding friction experiments were conducted with lithium fluoride crystals in various environments. These included air, water, hexadecane without and with various organic acids, and a paraffinic oil containing oleic acid. Sliding was on the (001) plane in the [100] direction at a speed of 0.005 millimeter per second and under loads of 5 to 200 grams on a millimeter-diameter sapphire rider which contacted the lithium fluoride flat. The results indicate that the presence of surfactants influences deformation and fracture in lithium fluoride. Crystals deform plastically more readily with an adsorbed organic acid than without it; this is the Rehbinder effect. Friction coefficient was influenced by the presence of the acid, its chain length, and its concentration.

N68-31478*# Research Triangle Inst., Durham, N. C. PRACTICAL RELIABILITY. VOLUME 1: PARAMETER VARIATIONS ANALYSIS

Washington NASA Jul. 1968 92 p refs (Contract NASw-1448) (NASA-CR-1126) CSCL 14D

Concepts such as model, randomness, statistical ignorance, and statistical independence are explored and explained. The effects of variations of parameters can be evaluated by changing components in a physical model or by creating a conceptual/mathematical model of the system and then analyzing it. There are only a very few basic techniques for analysis of mathematical models and these are rather extensively treated. The uses to which these models and their analyses may be put are many and only a few of these are treated such as sensitivity and worst-case analyses, and calculation where extreme extrapolation is necessary. There is a brief discussion of the sources and uses of variations data both in purchased and in manufactured items. A series of appendices gives some mathematical details, thus saving constant reference to other books. Author

N68-31522*# National Aeronautics and Space Administration, Washington, D. C.

LUBRICATION, CORROSION AND WEAR. A CONTINUING BIBLIOGRAPHY WITH INDEXES Jul. 1968 240 p refs

(NASA-SP-7020(02)) CFSTI: HC\$3.00/MF\$0.65 CSCL11F

This publication is the second supplement to the continuing bibliography *Lubrication, Corrosion and Wear.* It contains references to reports and journal articles on lubricating systems, design and performance of bearings; special applications of lubricants, e.g., as heat transfer and anticorrosion agents; stress corrosion and faigue cracking in metals and alloys; friction and wear characteristics of materials; and corrosion types and techniques for corrosion prevention. In addition, references describing the instrumentation and methods for the testing of lubricants are included. Author

N68-31979*# Research Triangle Inst., Durham, N. C. PRACTICAL RELIABILITY. VOLUME 4: PREDICTION C. A. Krohn et al Washington NASA Aug. 1968 168 p refs (Contract NASw-1448)

(NASA-CR-1129) CFSTI: HC\$3.00/MF\$0.65 CSCL 14D

The features and techniques of reliability prediction are identified and brought together in this report. Part I is largely qualitative discussion concerned with introduction and perspective. Contents include discussion and opinions on the role of reliability prediction, on perspective features, e.g. program phase and hardware level, on the relation to other analyses, and on the problems. Part It is concerned with reliability measures or definitions concerning single items, including data sources. Part III is devoted to the reliability prediction techniques which are suitable for general use and to classical reliability models. This material is scattered throughout the references: the treatment here mainly identifies approaches and relates them, with reliance on the references. Included for multi-item models are logic, lifetime, environment and bound-crossing topics. The remaining Part IV is concerned with concepts related to the detailed treatment of failure modes without independence assumptions. This is food-for-thought material from the results of research on reliability prediction techniques. This material in Part IV, in general, is not suited for widespread application. The Appendix presents a ready reference on some basic probability laws and on various probability distributions. Author

N68-31980*# Research Triangle Inst., Durham, N. C. PRACTICAL RELIABILITY VOLUME 5: PARTS B. M. Berry Washington NASA Jul. 1968 78 p refs (Contract NASw-1448) (NASA-CR-1130) CFSTI: HC\$3.00/MF\$0.65 CSCL 14D

Parts reliability and associated problems are discussed. This includes those functions—selections, specification, verification, review processes, and data sources—which are involved in a successful parts program. Some of the costs associated with these functions are discussed and an attempt is made to define an ideal data bank.

N68-32760*# Research Triangle Inst., Durham, N. C. PRACTICAL RELIABILITY. VOLUME 2: COMPUTATION Washington NASA Aug. 1968 138 p refs (Contract NASw-1448)

(NASA-CR-1127) CFSTI: HC \$3.00 / MF \$0.65 CSCL 14D

This report places in perspective the role of automatic digital computations in design for reliability. It is intended for the design engineer, the systems engineer, and the test engineer as well as the reliability specialist. The degree of detail with which the various topics are treated is sufficient to enable the engineer not previously familiar with the subject to properly select and use the methods presented. The report first briefly describes the computer, how it is used, and some of the mathematical problem types that are amenable to computer solution. The orientation to reliability is then provided in a brief perspective of reliability tasks and the relation of the computer to them. Later sections treat specific reliability tasks and explore the mathematical methods related to them and how the computer is used to implement them. Some specific computer programs are identified and their uses illustrated by examples. Parameter variation analysis and reliability prediction are treated. The last section treats some recent developments in communicating with the computer which make it more suitable to engineering and reliability applications. Author

N68-32779*# Research Triangle Inst., Durham, N. C. PRACTICAL RELIABILITY. VOLUME 3: TESTING Washington NASA Aug. 1968 298 p refs (Contract NASw-1448)

(NASA-CR-1128) CFSTI: HC \$3.00 / MF \$0.65 CSCL 14D

Testing is discussed from an engineering viewpoint. The subject is structured in terms of basic test types, basic problem types amenable to treatment by the basic test types, and applications of testing in hardware programs. The emphasis is on basic principles and practical problems in implementing them. Generally, the discussion emphasizes testing for reliability rather than reliability testing in the formal sense. Part I is devoted to concepts, definitions and general procedures. In particular, a section on test classifications considers the many ways of viewing tests and some of the prevalent confusion in terminology is resolved. Parts II and III collectively treat the basic test and problem types. The manner of separating these discussions into the two parts serves to highlight an important consideration in testing which is often overlooked, viz., whether or not aging is important. Part IV contains discussions on several subjects including nondestructive testing, environmental testing, and accelerated testing which are common to several or all of the basic test types. Part V surveys the major applications of testing in hardware programs and draws special attention to applications associated with reliability. An Appendix contains discussions of the mathematical topics pertinent to testing. Author

N68-32977*# National Aeronautics and Space Administration. Lewis Research Center, Cleveland, Ohio,

EXTRUSION OF 1/2 AND 3/8-INCH-DIAMETER THIN-WALL **TUNGSTEN TUBING IN LENGTHS NEAR 10 FEET**

Charles Blankenship and Charles A. Gyorgak Washington Aug. 1968 15 p refs

(NASA-TM-X-1638) CFSTI: HC\$3.00/MF\$0.65 CSCL 13H

Thin-wall tungsten tubing was extruded in lengths of 7.5 to 10.6 feet (2.3 to 3.2 m) using the floating mandrel technique. Tubing diameters were either 1/2 or 3/8 inch (1.27 or 0.95 cm), and nominal wall thicknesses were 0.020 inch (0.05 cm). In most of the tubes, variations in diameter and wall thickness over a length of 8 to 10 feet (2.5 to 3 m) were less than 0.020 and 0.008 inch (0.05 and 0.02 cm), respectively. Feasibility of warm drawing (1300° F or 700° C) the extruded tubing was demonstrated. Drawing greatly improved tubing surface finish and dimensional tolerances. Author

N68-33227*# National Aeronautics and Space Administration. Lewis Research Center, Cleveland, Ohio.

INFLUENCE OF CHEMISORBED FILMS OF VARIOUS GASES ON ADHESION AND FRICTION OF TUNGSTEN IN VACUUM

Donald H. Buckley Washington Sep. 1968 25 p refs

(NASA-TN-D-4694) CFSTI: HC\$3.00/MF\$0.65 CSCL 11H

An investigation was conducted to determine the effect of various adsorbed gaseous species on the adhesion and friction

15 MACHINE ELEMENTS AND PROCESSES

of tungsten. Experiments were conducted in a vacuum of 10-10 $(1.33 \times 10^{-8} \text{ N/m}^2)$ with a hemispherical rider specimen ((100) tungsten) contacting a flat. The atomic planes of tungsten examined on the flat included the (100), (110), and the (210). The gases adsorbed to these tungsten surfaces included hydrogen, oxygen, carbon dioxide, hydrogen sulfide, and a homologous series of hydrocarbons (methane through decane), as well as ethylene and acetylene. The results of the study indicate that the presence of any gas, even hydrogen, on the tungsten surface will reduce adhesion and friction. Less than a monolayer of oxygen adsorbed on tungsten is sufficient to reduce appreciably the friction of tungsten crystals. For hydrocarbons, an increase in chain length (methane through decane) resulted in a progressive decrease in friction. Furthermore, with ethane, ethylene, and acetylene, friction decreased with increasing bond saturation. Author

N68-36075*# National Aeronautics and Space Administration. Lewis Research Center, Cleveland, Ohio.

FATIGUE LIFE OF 120 mm BORE BALL BEARINGS AT 600°F WITH FLUOROCARBON, POLYPHENYL ETHER, AND SYNTHETIC PARAFFINIC BASE LUBRICANTS

Eric N. Bamberger (G.E., Cincinnati), Edwin V. Zaretsky, and William J. Anderson Washington Oct. 1968 27 p refs

(NASA-TN-D-4850) CFSTI: HC\$3.00/MF\$0.65 CSCL 131

Groups of 120-mm bore angular-contact ball bearings made from AISI M-50 steel were fatigue tested at a temperature of 600°F and a speed of 12,000 rpm with a synthetic paraffinic oil, a fluorocarbon, and a 5P4E polyphenyl ether. Under a low oxygen environment, the synthetic paraffinic oil and the fluorocarbon gave bearing lives approximately 14 and 3 times AFBMA-predicted (catalog) life, respectively. With the polyphenyl ether, bearing life was less than AFBMA-predicted (catalog) life in an air environment. For the synthetic paraffinic oil and the fluorocarbon, bearing fatigue was subsurface initiated. For the polyphenyl ether, bearing failure was mainly from surface distress, wear, and superficial pitting. Author

N68-36098*# National Aeronautics and Space Administration. Lewis Research Center, Cleveland, Ohio.

INCOMPRESSIBLY LUBRICATED RAYLEIGH STEP JOURNAL BEARING. 1: ZERO-ORDER PERTURBATION SOLUTION

Bernard J. Hamrock and William J. Anderson Washington Oct. 1968 33 p refs

(NASA-TN-D-4839) CFSTI: HC\$3.00/MF\$0.65 CSCL 131

A theoretical analysis of the pressure distribution, load capacity, load angle, and friction force for a single-step concentric journal bearing is performed. The resulting expressions were evaluated on a digital computer. The maximum load capacity is obtained when the ratio of the step clearance to ridge clearance is 1.7 and the ratio of the angle subtended by the ridge to the angle subtended by the pad is 0.35. Finally, for relatively small radius-to-length ratios, the load capacity of the stepped journal, while concentric, is higher than the load capacity of a finite-length Sommerfeld bearing Author operating with an eccentricity ratio of 0.1.

N68-37214*# National Aeronautics and Space Administration. Lewis Research Center, Cleveland, Ohio.

CRITICAL SPEED ANALYSIS OF RIGID ROTORS ON **FLEXIBLE FOUNDATIONS**

Richard H. Cavicchi Washington Oct. 1968 47 p refs (NASA-TN-D-4858) CFSTI: HC\$3.00/MF\$0.65 CSCL 131

A critical speed analysis of undamped rigid rotors on flexible foundations reveals four conical mode solutions comprising forward and backward precession. There is also a two solution bouncing mode set dependent only on foundation to rotor mass and spring constant ratios. Although analysis of a firm foundation model omits two of the four conical mode solutions, close agreement exists

15 MACHINE ELEMENTS AND PROCESSES

between the two corresponding solutions. The flexible foundation analysis reduces to a simple firm foundation result when the foundation to rotor spring constant ratio is zero or infinite. Only three calculations are needed in this range to cover all intermediate values. Author

N68-37239*# National Aeronautics and Space Administration. Lewis Research Center, Cleveland, Ohio.

THE ROLE OF CHEMICAL REACTIONS IN THE MECHANISM OF COMMINUTION OF DUCTILE METALS INTO ULTRAFINE POWDERS BY GRINDING Alan Arias Washington Oct. 1968 32 p refs

(NASA-TN-D-4862) CFSTI: HC\$3.00/MF\$0.65 CSCL 13H

On grinding in pure water, zirconium, tantalum, iron, and stainless-steel powders were extensively comminuted and simultaneously oxidized with hydrogen release, whereas nickel, copper, and silver powders did not react with water and their particle sizes increase. On grinding nickel, copper, and silver in water pressurized with oxygen, nickel and copper became extensively comminuted and were oxidized, whereas silver did not react with oxygen and its particle size increased. From these results and other considerations, it is hypothesized that for extensive comminution of ductile metals and alloys to occur on grinding they must react with the grinding media. Author

16 MASERS

Includes applications of masers and lasers. For basic research see: 26 Physics, Solid-State.

N68-10467*# TRW Systems, Redondo Beach, Calif. PARTICLE ACCELERATION BY EVAPORATION PRESSURE R. F. Wuerker Washington NASA Nov. 1967 104 p refs (Contract NAS9-5113)

(NASA-CR-927; TRW-04848-6001-R0-000) CFSTI: HC \$3.00/MF \$0.65 CSCL 20E

Accelerating 100 micron sized particles to meteoric velocities of 20 km/sec was studied via focused radiation from a high intensity pulsed solid state laser system. The Q-switched mode gave the highest peak power and permitted operation at the threshold of material yield strength. A computation method developed for computing effective exhaust velocity directly from experimental values of initial mass, final mass, and terminal velocity of the particles was used to predict, via the rocket equation, the ratio of the amount of mass which would have to be ablated to take a given particle from rest to the 20 km/sec velocity. Titanium had an effective exhaust velocity of 4 to 6 km/sec, and from this an initial to final mass ratio of 0.0358 was computed. In other words, 96.4% of the original particles would have to be burned away to bring the remaining mass to the 20 km/sec velocity. Iron had an effective exhaust velocity of 5 km/sec. Although the effective exhaust velocities obtained were not large enough to accelerate matter to terminal velocities of 20 km/sec, the laser ablation approach appeared to be feasible for generating particles with velocities of about 10 km/sec. MWR

N68-14070*# Sylvania Electric Products, Inc., Mountain View, Calif.

STUDY OF VIBRATION MEASUREMENT BY LASER METHODS

Gail A. Massey Washington NASA Jan. 1968 74 p refs (Contract NAS2-3643)

(NASA-CR-985) CFSTI: HC\$3.00/MF\$0.65 CSCL 20E

Described are techniques for using laser radiation to detect and measure vibration of mechanical structures. Two methods were developed analytically and experimentally. One of these methods, the intermediate frequency optical heterodyne system, provides quantitative data about the motion of a particular very small area on the mechanical structure. The other method is a qualitative interference technique for observing the vibrational mode patterns, so that the number of points to be measured by other methods can be reduced. A breadboard optical heterodyne system was built, and detection of audio frequency vibrations at levels from one centimeter to less than 0.1 micron peak-to-peak has been achieved with a variety of surface materials. The performance of this system using two different types of demodulation circuits was investigated. A model structure was fabricated for tests involving comparisons of the qualitative and quantitative methods. It has been shown that a very good knowledge of the vibrational modes can be obtained using the two methods in combination. The qualitative interference method also has been extended to include the measurement of axes of rotation. Author

N68-29438*# National Aeronautics and Space Administration, Washington, D. C.

LASERS AND MASERS A Continuing Bibliography with Indexes, Apr.-Dec. 1967

Jun. 1968 366 p refs 3d Suppl. to NASA-SP-7009; See N65-25599

(NASA-SP-7009(03)) CFSTI: HC\$3.00/MF\$0.65 CSCL 20E

Bibliographic citations and informative abstracts are presented on all major studies associated with the research and development of lasers and masers. Emphasis is placed on laser and maser applications as they relate to ranging and communications systems, astronomy and optics, and metalworking. Fundamental studies of the physical and electronic properties, and the functioning and performance of lasers and masers are also cited. Subject and personal author indexes are included. Author

N68-33635*# National Aeronautics and Space Administration. Goddard Space Flight Center, Greenbelt, Md.

MICROWAVE PUMP REQUIREMENTS FOR FIELD OPERATIONAL BROADBAND RUTILE TRAVELING-WAVE MASERS

L. E. Rouzer Washington Sep. 1968 12 p refs

(NASA-TN-D-4764) CFSTI: HC\$3.00/MF\$0.65 CSCL 20E

This paper discusses microwave pump sources available for use in a field operational, rutile, broadband, traveling wave maser for the Applications Technology Satellite (ATS) program. Included is a brief resume of the current solid state microwave pump sources, klystrons, and the Hughes and OKI backward wave oscillators. The spin Hamiltonian for iron-doped rutile is given; its solution yields a pump frequency of 54.7 GHz and pump bandwidth of 500 MHz for a 4.065- to 4.195-GHz signal frequency. The suitability of the OKI backward wave oscillator for the application here considered has been determined; it is simple and comparatively inexpensive to operate in the field. The solid state modulator circuit capable of sweeping the OKI backward wave oscillator over 500 MHz is described; and the pump package, which maintains the tube temperature at 130°F (well within the operating range required by the tube) is discussed. Author

N68-35099*# Tennessee Univ., Tullahoma. Space Inst. APPLICATION OF NEGATIVE FEEDBACK TO REDUCTION OF GLOW DISCHARGE NOISE

C. W. Bray, F. M. Shofner, and T. B. Carlson Washington NASA Sep. 1968 23 p refs

(Grants NGR-43-001-021; NSF GK-1638)

(NASA-CR-1173) CFSTI: HC\$3.00/MF\$0.65 CSCL20F

Several researchers have studied the problem of discharge current modulation noise in the output radiation intensity of a d-c excited He-Ne laser. Work presented herein uses an analog circuit to demonstrate the feasibility of using negative feedback to reduce the discharge current noise and thereby reduce noise in the output radiation intensity. Author

N68-35175*# National Aeronautics and Space Administration. Electronics Research Center, Cambridge, Mass.

SURVEY OF CO2 LASER DEVELOPMENT FOR SPACE APPLICATIONS

Thomas R. Lawrence Washington Sep. 1968 51 p refs (NASA-TN-D-4794) CFSTI: HC\$3.00/MF\$0.65 CSCL20E

This report presents the status of CO_2 laser development. The first application of a CO_2 laser is expected to be in the development and testing of an optical communication link from a synchronous orbit to Earth using heterodyne detection. The

16 MASERS

transmitter for this link will be a small, low-powered, space-qualified CO_2 laser with stable, single frequency, single mode operation, and dependable, long operating life. In this report, the brief history of CO_2 laser development is surveyed and a simplified qualitative discussion of the CO_2 laser and the various additives is presented. Then the current level of development is compared to what is desired. It is found that the CO_2 laser is especially suited for single frequency operation; stable, single frequency CO_2 lasers have been built and tested in heterodyne communication systems in the laboratory. Many of the requirements for space qualification can be met by proper design. Author

N68-35593*# National Aeronautics and Space Administration. Lewis Research Center, Cleveland, Ohio.

STUDY OF PLASMA DIAGNOSTICS USING LASER INTERFEROMETRY WITH EMPHASIS ON ITS APPLICATION TO CESIUM PLASMAS

Richard B. Lancashire Washington Sep. 1968 21 p refs (NASA-TM-X-1652) CFSTI: HC\$3.00/MF\$0.65 CSCL 20I

A review of the background and current development of gas-laser diagnostics is presented. Included is a résumé of the plasma refractive index and the experimental techniques of the three-mirror laser interferometer and the laser heterodyne system. Sensitivity of the two techniques to electron and neutral-particle densities is covered with emphasis placed on the application of the techniques to a cesium plasma contained in a thermionic diode. The spatial resolution of the techniques as applied to a cesium diode is also presented.

17 MATERIALS, METALLIC

Includes cermets; corrosion; physical and mechanical properties of materials; metallurgy; and applications as structural materials. For basic research see: 06 Chemistry. For related information see also: 18 Materials, Nonmetallic; and 32 Structural Mechanics.

N68-10051*# National Aeronautics and Space Administration. Lewis Research Center, Cleveland, Ohio.

ELECTRON MICROSCOPY TECHNIQUE FOR DETERMINA-TION OF DISPERSOID DISTRIBUTION IN POWDER BLENDS Bruno C. Buzek Washington NASA Nov. 1967 11 p refs (NASA-TM-X-1468) CFSTI: HC\$3.00/MF\$0.65 CSCL 11F

The ability to clearly observe and distinguish between oxide and metal particles in a starting powder blend and to determine the initial distribution of the oxide prior to consolidation enables predictions to be made about the final distribution of the oxide particles in a fully consolidated product. A new electron-microscope specimen-preparation technique was developed to aid in making these predictions. This procedure makes it possible to ascertain the size and the degree of agglomeration of the oxide particles, unobstructed by the presence of the metal-matrix particles, before the compaction and sintering of the powder blend. The initial powder blend is envoloped with a thin layer of carbon, and the metal phase is leached out. The retained particles reveal the state of the dispersoid phase after the blending operation. Nickel, tungsten, chromium, and nichrome, each blended with thoria or alumina, were investigated using this technique. A good correlation exists between the dispersoid distribution in the initial blend and the state of agglomeration in the final sintered product. If small oxide particles were well distributed in the initial powder blend, they remained in the final product. If the small oxide particles were clustered in the original powder blend, they appeard as large particles similar in size to the initial clusters after consolidation. Author

N68-10104*# National Aeronautics and Space Administration. Lewis Research Center, Cleveland, Ohio.

EFFECT OF COVER GAS PRESSURES ON ACCELERATED CAVITATION DAMAGE IN SODIUM

Stanley G. Young and James R. Johnston Washington NASA Nov. 1967 24 p refs

(NASA-TN-D-4235) CSCL 11F

An investigation was made to study the effect of pressure on the resistance to cavitation damage of materials under consideration for components of liquid-metal power conversion systems. A vibratory apparatus was used to subject three materials, AISI 316 stainless steel, L-605, and Stellite 6B to accelerated cavitation damage in sodium at 800°F (700°K). Argon cover gas was used to maintain pressures up to 4 atmospheres (4×10^5 N/m²) during test. Volume loss and volume-loss rate measurements were used to compare the effects of pressure on the degree of damage. Metallographic studies were conducted to determine the nature of damage. Increasing cover-gas pressure significantly increased cavitation damage to all materials for all exposure times. The materials ranked in the same order with respect to resistance to cavitation damage at all pressures; Stellite 6B was most resistant, L-605 intermediate, and AISI 316 stainless steel least resistant. The steady-state volume-loss rate based on total specimen area increased linearly with cover-gas pressure. When the volume-loss rate data were normalized to include only the heavily damaged area of the specimens, the steady-state volume-loss rate

increased as a power function of pressure. Metallographic examination of axially sectioned specimens revealed undercutting and transgranular cracking as well as subsurface deformation for all materials. Author

N68-10498*# National Aeronautics and Space Administration, Lewis Research Center, Cleveland, Ohio.

DETERMINATION OF ELECTRIC POTENTIAL ACROSS THE OXIDE SCALE DURING OXIDATION OF TANTALUM, NIO-BIUM, AND MAGNESIUM

I Zaplatynsky Washington Nov. 1967 9 p refs

(NASA-TN-D-4240) CFSTI: HC\$3.00/MF\$0.65 CSCL 11F

According to Hauffe's theoretical treatment of the oxidation of metals, the oxide-gas interface is electrically negative with respect to the oxide-metal interface. The potential difference is considered to be one of the driving forces for oxidation. Experimental evidence, presented here, does not support this assumption. The polarity of measured potential is reversed and has a retarding effect on oxidation. The magnitude of the potential and its temperature dependence were determined for tantalum, niobium, and magnesium during oxidation in air. The magnitude of the potential does not depend upon oxide thickness. Features of the potential-temperature curves for tantalum and niobium correspond to significant changes in the oxidation rates of both metals.

N68-11511*# National Aeronautics and Space Administration. Lewis Research Center, Cleveland, Ohio.

CORROSION PRODUCT OF THE TANTALUM-INTERSTITIAL OXYGEN-POTASSIUM SYSTEM AT 1800°F(1255°K) C.WilliamHickam, Jr. Washington Dec. 196712prefs

(NASA-TN-D-4213) CFSTI: HC\$3.00/MF\$0.65 CSCL 11F

Described herein are the isolation and identification of the corrosion product formed by the exposure of oxygen-doped tantalum to potassium. The corrosion of tantalum by liquid potassium appears to be quantitatively dependent on the oxygen impurity content and to occur by the formation of a ternary oxide. When tantalum containing oxygen in the range of 1600 to 3800 ppm is exposed to potassium at 1800°F (1255°K), depletion of oxygen from tantalum occurs and the hygroscopic potassium tantalate K3TaO4 is isolated as the reaction product. These results imply that the total amount of "oxygen-effect" corrosion can be predicted when the total amount of interstitial oxygen in tantalum is known li.e., oxygen in solution in the metal initially plus oxygen that enters the metal from the environment during the life of the system). Since oxygen-effect corrosion is the most serious type of corrosion encountered by tantalum alloys in contact with potassium at elevated temperatures, the present results are significant for the design and operation of advanced space power systems. Author

N68-11522*# Lockheed-California Co., Burbank. STRESS CORROSION OF TITANIUM ALLOYS UNDER SIMULATED SUPERSONIC FLIGHT CONDITIONS

K. E. Weber and A. O. Davis Washington NASA Dec. 1967 77 p refs

(Contract NAS1-6361)

(NASA-CR-981) CFSTI: HC\$3.00/MF\$0.65 CSCL 11F

The effects of high altitude supersonic air flow on the titanium hot salt cracking process were studied. Two different types of self-stressed specimens were utilized in these tests; one type was developed by Lockheed and the other by NASA Langley. Specimens were prepared from both the Ti-8AI-1Mo-1V duplex annealed and the Ti-6AI-4V mill annealed alloys. Cracking data from specimens exposed in the wind tunnel were compared to similar data obtained from ordinary laboratory oven tests. The tests demonstrated that the air flow and reduced pressure conditions characteristic of high altitude supersonic flight environments do not eliminate hot salt cracking in these titanium alloys at the test temperatures used in this program. However, cracking in supersonic environments was generally less severe than in laboratory oven environments. As might be expected, some of the salt coating was removed from the specimens by the action of the high velocity air stream, and evidence of a correlation between salt removal and cracking damage was indicated. Author

N68-11637* National Aeronautics and Space Administration. Lewis Research Center, Cleveland, Ohio.

FATIGUE OF LIQUID ROCKET ENGINE METALS AT CRYOGENIC TEMPERATURES TO -452°F (4°K)

Alfred J. Nachtigall, Stanley J. Klima, and John C. Freche Washington Dec. 1967 54 p refs

(NASA-TN-D-4274) CFSTI: \$3.00 CSCL 11F

Axial tensile fatigue behavior of four candidate alloys for liquid rocket engines was investigated for smooth and notched (theoretical stress concentration factors $K_t > 17$) sheet specimens at a minimum-to-maximum cyclic stress ratio R of 0.14 in ambient air (70°F, 294°K), liquid nitrogen (-320°F, 77°K), and liquid helium (-452°F, 4°K). The materials tested were 2014-T6 aluminum alloy. Inconel 718, 5 percent aluminum-2.5 percent tin-titanium (5AI-2.5Sn-Ti) alloy, and AISI 301 stainless steel. The fatigue strength of smooth specimens was generally higher than that of notched specimens. Except for AISI 301 stainless steel the fatigue strength of unnotched specimens increased progressively with decreasing test temperature to $-452^{\circ}F$ (4°K). This trend was also observed for 2014-T6 aluminum alloy and Inconel 718 in the notched condition. In most instances, Inconel 718 and 301 stainless steel had the highest fatigue strength while the 5AI-2.5Sn-titanium and 2014-T6 aluminum alloys ranked third and fourth. The titanium alloy generally had the highest fatigue-strength-to-density ratio at all temperatures. The fatigue notch factor Kr increased with cyclic life for all materials at all test temperatures. Up to 100 cycles, the increase was small, and the fatigue notch factor was essentially equal to the tensile notch factor (ratio of smooth specimen tensile strength to notched specimen tensile strength). Inconel 718 generally had the lowest Kf over the life range considered at all temperatures. Author

N68-11644*# National Aeronautics and Space Administration. Lewis Research Center, Cleveland, Ohio.

DEPOSITION OF SPUTTERED MOLYBDENUM DISULFIDE FILMS AND FRICTION CHARACTERISTICS OF SUCH FILMS IN VACUUM

Talivaldis Spalvins and Hohn S. Przybyszewski Washington Dec. 1967 14 p refs

(NASA-TN-D-4269) CFSTI: HC \$3.00/MF \$0.65 CSCL 11H

Physical direct-current sputtering of molybdenum disulfide (MoS₂) is used to apply MoS₂ films as a solid lubricant for rotating and sliding components. This method does not use organic or inorganic binders or the process of burnishing. Friction experiments in vacuum $(10^{-11} \text{ torr or } 1.33 \times 10^{-9} \text{ N/m}^2)$ were conducted on these films. The coefficients of friction for the sputtered films were in agreement with the reported values in the literature. Stoichiometric films were obtained, and no dissociation was observed. There is a strong bonding (adherence) between the films and the substrate, as indicated by the long-endurance life of the lubricating films in friction experiments. The sputtered MoS₂ films had an accurate repeatability in terms of stoichiometry, adherence, thickness, and uniformity when the sputtering conditions were kept constant.

N68-11912*# National Aeronautics and Space Administration. Lewis Research Center, Cleveland, Ohio. CONTROL OF CONTAMINANTS IN LIQUID-METAL

SYSTEMS

Sol Gorland and Raymond Bilski Washington NASA Dec. 1967 21 p refs

(NASA-TM-X-1432) CFSTI: HC\$3.00/MF\$0.65 CSCL 18J

The contaminant controls and cleaning procedures used in the SNAP-8 simulation loop, consisting of two sodium-potassium (NaK) loops and one mercury (Hg) loop, minimized both startup and operational problems. Mercury wetting was induced in the boiler and condenser as determined by progressive improvement in the heat-transfer performance. The degree of wetting is an indication of the system cleanliness. The boiler was conditioned in approximately 250 hours of operation without wetting additives. After 384 hours of operation, analysis of a Hg sample by a distillation method indicated no contamination. Oxide plugging in the NaK loops was minimized using the loop-entry procedures developed in the investigation. No plugs occurred because of changes of repairs that required system entry, and only minor partial plugs occurred in over 1500 hours of operation of the NaK loops.

N68-12891*# National Aeronautics and Space Administration. Langley Research Center, Langley Station, Va.

STRESS-CORROSION CRACKING OF TI-6AI-4V TITANIUM ALLOY IN NITROGEN TETROXIDE

W. Barry Lisagor, Charles R. Manning, Jr., and Thomas T. Bales Washington Jan. 1968 33 p refs

(NASA-TN-D-4289) CFSTI: HC\$3.00/MF\$0.65 CSCL 11F

The stress-corrosion of Ti-6AI-4V titanium alloy in nitrogen tetroxide was investigated by using small laboratory-size self-stressed specimens and tanks. Tests were conducted from 65 °F to 165°F (290°K to 345°K) for purposes of determining the time for crack initiation. Stress levels from 25 to 100 ksi (170 to 690 MN/m²) were investigated and crack initiation was observed at all stress levels in approximately the same time. An excellent correlation was obtained between crack initiation time on laboratory specimens and failure time for tanks. Tests were also conducted on specimens which had been treated in some manner for the prevention of stress-corrosion attack. Organic and metallic coatings investigated proved to be unsatisfactory because of adherence problems or apparent permeation resulting in stress-corrosion attack. Surface treatments including peening techniques proved to be beneficial and glass-bead peening to introduce residual compressive stresses of high magnitude appeared to alleviate the problem entirely for the range of tests conducted. The residual stress level was determined by X-ray diffraction techniques and was found to be in excess of 100 ksi (690 MN/m²) on the surface. The prevention of stress-corrosion attack by chemical inhibition with 0.78 percent by mass nitric oxide (NO) added to the N2O4 was also substantiated by tests conducted at 165°F (345°K) for exposures of 170 hours. The mechanism of prevention remains unknown. Author

17 MATERIALS, METALLIC

N68-14888*# National Aeronautics and Space Administration. Lewis Research Center, Cleveland, Ohio.

TECHNIQUE FOR RECOVERY OF ALKALI-METAL **REACTION PRODUCTS**

Randall F. Gahn Washington Jan. 1968 11 p refs

(NASA-TN-D-4310) CFSTI: HC\$3.00/MF\$0.65 CSCL 07B

A procedure for the isolation and recovery of alkali-metal reaction products in an uncontaminated state is described. Separation of the reaction product from excess alkali metal is accomplished by vacuum distillation. All recovery operations are carried out in high-vacuum or inert gas atmospheres. Two typical examples of the application and reproducibility of the procedure are presented: (1) the recovery of potassium tantalate (KaTaOa) from the potassium-tantalum-oxygen reaction, and (2) the recovery of potassium monoxide (K2O) from the potassium-oxygen reaction. Reaction products are identified by both X-ray diffraction 1nd chemical analysis. Author

N68-15637*# National Aeronautics and Space Administration. Lewis Research Center, Cleveland, Ohio.

APPLICATION OF DIRECTIONAL SOLIDIFICATION TO A NASA NICKEL-BASE ALLOY (TAZ-8B)

John C. Freche, William J. Waters, and Richard L. Ashbrook Washington Feb. 1968 22 p refs

(NASA-TN-D-4390) CFSTI: HC\$3.00/MF\$0.65 CSCL 11F

A nickel-base alloy (TAZ-8B) has been developed which compares favorably in high-temperature strength with known high-strength nickel-base alloys. Although basically a cast material, the alloy also has workability potential. By applying directional solidification techniques, test specimens were produced with a preferred columnar grain orientation. Grain boundaries transverse to the major stress axis were largely eliminated. Substantial increases in ductility, ultimate tensile strength, and stress-rupture life were obtained with the alloy in the directional polycrystalline condition, as compared with the random polycrystalline condition. On the basis of calculated electron vacancy number, TAZ-8B would not be expected to form sigma phase. Only minor decreases in 1400°F (1033°K) ductility were observed after exposure for 1000 hours at 1600°F (1144°K). Tensile elongation decreased from 3.3 to 2.0 percent for the random polycrystalline material and from 6.5 to 6.0 percent for the directional polycrystalline material. The application of directional solidification to TAZ-8B resulted in alloy properties which are of interest for potential advanced gas turbine engine applications. Author

N68-17317*# National Aeronautics and Space Administration. Lewis Research Center, Cleveland, Ohio.

EFFECTS OF COMPOSITION AND HEAT TREATMENT ON HIGH-TEMPERATURE STRENGTH OF ARC-MELTED **TUNGSTEN-HAFNIUM-CARBON ALLOYS**

L. S. Rubenstein Washington Feb. 1968 31 p refs

(NASA-TN-D-4379) CFSTI: HC \$3.00/MF \$0.65 CSCL 11F The effects of composition, heat treatments, and substructure on

the strength and ductility of tungsten-hafnium-carbon (W-Hf-C) allovs were studied. The compositions ranged from 0.23 to 1.76 atomic percent for hafnium and from 0.179 to 0.942 atomic percent for carbon, with carbon to hafnium ratios from 0.17 to 2.80 and calculated amounts of hafnium carbide ranging up to 1.5 volume percent. The high-temperature tensile strengths of swaged, recrystallized, solution-annealed and aged alloys increased with increasing hafnium carbide contents up to approximately 0.5 volume percent, after which further additions caused a slight decrease in strength. The strongest alloys contained equiatomic amounts of carbon and hafnium. The 3500°F (2200°K) tensile strength for swaged material was linearly related to the inverse square root of the cell size. Limited tensile and microstructural studies indicated that the W-Hf-C alloys are heat treatable. The stress for a 3500°F (2200°K), 100-hour rupture life was approximately 14,000 psi $(96.5 \times 10^{6} \text{ N/m}^{2})$ in the swaged condition. A solution-annealed and aged specimen tested in 3500°F (2200°K) step-load creep tests required a stress of approximately 20,000 psi $(138 \times 10^6 \text{ N/m}^2)$ for a minimum creep rate of $6 \times 10^{-7} \text{ sec}^{-1}$, corresponding to an approximate 100-hour rupture life. These W-Hf-C alloys exhibit a sevenfold strength improvement over unalloyed tungsten at 3500°F (2200°K) that is related to the precipitate stabilized, fine dislocation structure formed within the cell boundaries. For high strength applications at 3500°F (2200°K), compositions composed of equiatomic amounts of carbon and hafnium, approximately 0.3 to 0.4 atomic percent, are recommended. Author

N68-17377* National Aeronautics and Space Administration. Langley Research Center, Langley Station, Va.

COATINGS AND SURFACE TREATMENTS FOR LONGTIME PROTECTION OF TI-8AI-1Mo-1V ALLOY SHEET FROM HOT SALT STRESS CORROSION

Bland A. Stein, H. Benson Dexter, and Dick M. Royster Washington Mar. 1968 51 p refs

(NASA-TN-D-4319) CFSTI: \$3.00 CSCL 11F

After longtime exposures at 600°F in air at sea-level atmospheric pressure, the coatings were electroplated nickel with black nickel overcoat for high emittance, electrophoretically deposited aluminum, and a dipped coating of polyimide resin. The surface treatments included a vibratory treatment and glass-bead peening. The study included both residual-stress and self-stressed specimens which were dipped in a 3.4-percent NaCl solution, dried and exposed at 600°F (590°K) in circulating air ovens. Relative deflection measured in room-temperature bend tests or relative shortening measured in compression tests were used as quantitative indicators of stress-corrosion cracking in the specimens. An electron probe microanalyzer was used to determine interdiffusion between coating and substrate. The results indicated that the nickel and aluminum coatings were effective in preventing hot-salt stress corrosion for at least 10,000 hours exposure, whereas the polyimide coating peeled off the surface after 500 hours exposure. The glass-bead-peening process appeared to be effective in preventing or alleviating hot-salt stress corrosion for at least 10,000 hours. The vibratory treatment process proved to be effective in preventing or alleviating hot-salt stress corrosion for exposures of 15,000 hours when specimens were treated for at least 26 hours after fabrication. Author

N68-17591*# Bendix Corp., Detroit, Mich. **OXIDATION RESISTANT MATERIALS FOR TRANSPIRATION** COOLED GAS TURBINE BLADES. 1: SHEET SPECIMEN SCREENING TESTS

Fred W. Cole, James B. Padden, and Andrew R. Spencer Washington NASA Feb. 1968 146 p (Contract NAS3-7269)

(NASA-CR-930) CFSTI: HC\$3.00/MF\$0.65 CSCL 11F

Twelve alloys were tested in sheet metal form to compare their suitability for use as transpiration cooled gas turbine blade materials. The alloys were N 155, TD nickel, TD nickel-chromium, Bendel 65-35, Chromel A, DH 242, GE 1541, Hoskins 875, RA 333. Hastelloy X, Udimet 500, and Haynes 25. Screening tests consisted of cyclic furnace oxidation at 1400°, 1600°, 1800°, 2000°, 2100°, and 2200°F for 4, 16, 64, 100, 200, 300, 400, 500, and 600 hours exposure time. Total oxidation and spalling were determined for each specimen along with variation in room temperature mechanical properties and microstructure. Electron beam welding feasibility was also investigated. Three best-compromise alloys were selected for later testing as wires to determine suitability for manufacturing space-wound or woven porous transpiration cooling materials. Author

N68-17624*# Westinghouse Electric Corp., Lima, Ohio. PROPERTIES OF MAGNETIC MATERIALS FOR USE IN HIGH-TEMPERATURE SPACE POWER SYSTEMS

P. E. Kueser, D. M. Pavlovic, D. H. Lane, J. J. Clark, and M. Spewock Washington NASA 1967 325 p refs (Contract NAS3-4162)

(NASA-SP-3043) GPO: HC\$2.25; CFSTI: MF\$0.65 CSCL 11F

Test data are given and evaluated for eight magnetic materials that were found suitable for use in high-temperature liquid alkali-metal system applications. In general, the magnetic materials tested can be grouped in three temperature ranges, together with their fields of application: (1) 600° to 800°F: Most materials qualify for this temperature range. However, Cubex alloy (3-1/4% Si-Fe, doubly oriented) is preferred for use in stators at inductions up to 18 kilogauss. H-11 steel (5%Cr, 1%Mo, Fe) and maraging steel (15-18% Ni, 8-9% Co, Fe) are recommended for rotors, and Supermendur (2% V, 49% Co, 49% Fe) in controls using high quality, saturable-core reactors. (2) 800° to 1100°F: Hiperco 27 alloy (27% Co, Fe) is suggested for high inductions and Cubex alloy for inductions up to 15 to 18 kilogauss in stators. In rotors, H-11 steel qualifies for lower temperatures and Nivco alloy (approximately 72% Co. 23% Ni) for the higher temperatures in this range. (3) 1100° to 1400°F: Hiperco 27 alloy is recommended for stators and Nivco alloy for rotors in this temperature range. Author

N68-17897*# National Aeronautics and Space Administration. Langley Research Center, Langley Station, Va.

EFFECTS OF LONGTIME ENVIRONMENTAL EXPOSURE ON MECHANICAL PROPERTIES OF SHEET MATERIALS FOR A SUPERSONIC TRANSPORT

Richard A. Pride, Dick M. Royster, Bland A. Stein, and James E. Gardner Washington Mar. 1968 26 p refs Presented at the Met. Soc. Session of the 96th Ann. Meeting of the Am. Inst. of Mining, Met. and Petrol. Engr., Inc., Los Angeles, 19–23 Feb. 1967 (NASA-TN-D-4318) CFSTI: HC\$3.00/MF\$0.65 CSCL 11F

Studies of the effects of longtime environmental exposure on mechanical properties of supersonic transport sheet materials have been conducted by the Langley Research Center. These materials include titanium alloys, stainless steels, aluminum alloys, and a composite. Titanium alloys and stainless steels have been investigated since 1961, and results have shown that exposures of 30,000 hours at 550°F (561°K) have had little effect on the strength characteristics. Hot-salt stress corrosion occurs in titanium alloys under certain combinations of stress, temperature, and time but does not appear to be a problem at the operating conditions of a Mach 2.7 supersonic transport. Aluminum alloys were investigated to provide materials information for the Mach 2 speed range and have been found to be temperature limited by longtime creep strength. Properties of the polyimide-resin-glass-fiber composite have been determined after 4000 hours exposure. This material appears to be suitable for extended use in a Mach 2.7 Author supersonic transport.

N68-18145*# National Aeronautics and Space Administration. Lewis Research Center, Cleveland, Ohio.

DEVELOPMENT OF A COBALT-TUNGSTEN FERROMAG-NETIC, HIGH-TEMPERATURE, STRUCTURAL ALLOY

Richard L. Ashbrook, Anthony C. Hoffman, Gary D. Sandrock, and Robert L. Dreshfield Washington Mar. 1968 44 p refs

(NASA-TN-D-4338) CFSTI: HC\$3.00/MF\$0.65 CSCL 11F Rotors for space power generators require a compromise between high-temperature strength and magnetic properties. Rotors must withstand high centrifugal stresses at high temperature and develop high induction for small exciting fields. Alloys considered for rotors include maraging steels. H-11 steel, and a cobalt-base alloy. Nivco. This report discusses work to develop alloys with

improved high-temperature strength and good high-temperature

magnetic properties. Because cobalt has the highest Curie

temperature of any metal and is a good base for high-temperature alloys, a NASA superalloy, cobalt-25 tungsten-1 titanium-1/2 zirconium-1/2 carbon was chosen for further study. Modifications of this alloy were screened for maximum magnetic induction Bmax at a maximum magnetizing force H_{max} of 100 oersteds (7958 A/m) over a range of temperatures. Below 1000°F (538°C), low tungsten alloys show inflections in a plot of B_{max} as a function of temperature due to the instability of the face-centered cubic (fcc) phase. Stability of the fcc increased with increasing tungsten and iron. A preferred alloy, Co-7-1/2W-2-1/2Fe- 1Ti-1/2Zr-1/2C, was evaluated for magnetic and mechanical properties in cast form and for mechanical properties as sheet. After aging at 1700°F (927°C) for 72 hours, this alloy had a coercive force of 10.5 oersteds (835 A/m) at 75°F(24°C), and a B_{max} of 11.5 and 10.3 kilogauss (1.15 and 1.03 T) at 1200° and 1400°F (649° and 760°C), respectively. The stress-rupture life at 1200° to 1400°F (649° to 760°C) was greater than that of the strongest high-temperature commercially available magnetic-structural alloy. Author

N68-18610*# National Aeronautics and Space Administration. Lewis Research Center, Cleveland, Ohio.

OXIDE DEFORMATION AND FIBER REINFORCEMENT IN A TUNGSTEN METAL OXIDE COMPOSITE

Charles P. Blankenship Washington Mar. 1968 41 p refs (NASA-TN-D-4475) CFSTI: HC\$3.00/MF\$0.65 CSCL 11D

Refractory oxide particles of urania (UO_2) and zirconia (ZrO_2) were added to a tungsten matrix and elongated into fibers by hot extrusion. Extrusion temperatures ranged from 3200° to 4000°F (1760° to 2200°C). The geometry of the oxide fibers appeared to be closest to that of an ellipsoid with the major axis alined in the extrusion direction. Oxide fibering was measured by an average length-to-width ratio of the fibers sectioned parallel to the major axis. The extent of oxide deformation was estimated in terms of strain components. Oxide-matrix deformation characteristics were related to the extrusion parameters by comparing the estimated oxide strain components to those of the composite. Author

N68-18999*# National Aeronautics and Space Administration. Lewis Research Center, Cleveland, Ohio.

USE OF SURFACE REPLICATION, EXTRACTION REPLICATION, AND THIN-FILM ELECTRON MICROSCOPY IN THE STUDY OF DISPERSION-STRENGTHENED MATERIALS

Charles A. Hoffman and Bruno C. Buzek Washington Mar. 1968 25 p refs

(NASA-TN-D-4461) CFSTI: HC\$3.00/MF\$0.65 CSCL 11F

An investigation was conducted on the relative merits of surface replication, extraction replication, and thin-film methods to evaluate the microstructures of dispersion-strengthened materials. Surface replication gave the best agreement of measured and nominal amounts of oxide whether the oxide was discrete and spheroidal (Ni+ThO₂) or plate-like and aggregated (Al+Al₂O₃); this method also gave the most satisfactory value of average particle size and average interparticle spacing. Extraction replication was also satisfactory for the former material but not for the latter; its validity was dependent on the shape of the oxide particles and its state of aggregation as well as the effectiveness of the extraction technique. The thin-film method was helpful in verifying the existence of the finer particles but gave considerably greater volume fractions of oxide particles compared to the respective nominal amounts. Particle-size-frequency distributions obtained from each of the three methods when applied to the $Ni+ThO_2$ essentially agreed. Stereoscopic, or three-dimensional, views of thin films gave better indication of the shape of the particles and the spatial Author relations between particles.

N68-19347*# National Aeronautics and Space Administration, Lewis Research Center, Cleveland, Ohio.

EFFECT OF SURFACE ROUGHNESS ON THE 0.66-MICRON NORMAL SPECTRAL EMITTANCE OF VAPOR-DEPOSITED RHENIUM FROM 1500°K TO 2100°K

Peter Cipollone Washington Mar. 1968 20 p refs

(NASA-TM-X-1514) CFSTI: HC\$3.00/MF\$0.65 CSCL 20L

The normal spectral emittance of vapor-deposited rhenium at a 0.66-micron effective wavelength is presented, and the results are compared to previously published data on bar and sheet rhenium. A dependence of the normal spectral emittance on surface roughness is demonstrated quantitatively. Author

N68-21431*# National Aeronautics and Space Administration. Lewis Research Center, Cleveland, Ohio.

ELECTRON MICROSCOPE TECHNIQUE SUGGESTED TO REVEAL MICROSTRUCTURES OF DISPERSION-STRENGTH-ENED MATERIALS

Bruno C. Buzek Washington Apr. 1968 9 p refs

(NASA-TM-X-1561) CFSTI: HC\$3.00/MF\$0.65 CSCL 13H

This report describes a preparation and replication method which has produced consistently good results for a number of materials. To show the effectiveness of the method evolved, measurements of volume percentages of dispersoids were compared with values obtained from chemical analysis. Typical microstructures of differently produced dispersion-strengthened materials are shown. The method that was found to be satisfactory uses conventional metallographic specimen preparation procedures up to the two final steps of polishing. For this final polishing, 3-micron and 1/2-micron diamond polishing compounds are necessary. This produces a flat and distortion-free surface. Etching of the samples should be extremely light. The etchants used depend on sample composition and history. The samples are then cleaned in an ultrasonic bath and further cleaned with plastic by dry stripping. Replication of samples with a conventional two-stage method of plastic-carbon and platinum shadowing follows. A good correlation was obtained between volume percent dispersoid measured on the resulting electron micrographs and the values obtained by chemical analysis. This replication procedure was found satisfactory for use with nickel, tungsten, chromium, cobalt, and their alloys. Author

N68-21654*# National Aeronautics and Space Administration. Lewis Research Center, Cleveland, Ohio.

MECHANISM AND KINETICS OF CORROSION OF Selected Iron and Cobalt Alloys in Refluxing Mercury

Louis Rosenblum, Coulson Scheuermann, Charles A. Barrett, and Warren H. Lowdermilk Washington Apr. 1968 54 p refs

(NASA-TN-D-4450) CFSTI: HC\$3.00/MF\$0.65 CSCL 11F

The cobalt-base HS-25 and H-8187 and the iron-base SICROMO-9M, AM-350, and AM-355 were corrosion tested in boiling mercury in the temperature range of 1000° to 1300°F for times as long as 5000 hours. Metallographic, chemical, and physical analyses were used to determine the extent and the nature of the corrosion. Corrosion mechanism and reaction kinetics were inferred through a comparison of experimental and theoretical kinetic constants. The experimental kinetic constants (i.e., the time-law constant b and the activation energy ΔH_i) were obtained from the test data by multiple regression analysis. The theoretical kinetic constants b; and AH; for each of i steps of proposed corrosion models were obtained from transport theory relations and the pertinent boundary conditions. Changes of mechanism during the progress of corrosion were indicated for all the alloys tested except the AM-350 and AM-355 alloys. The shifts from one corrosion regime to another were associated with changes in the nature and length of the corrosion-affected zone. Three corrosion regimes were characterized, linear I, parabolic, and linear II. The probable rate-determining step in the two linear rate regimes is boundary-layer diffusion. The probable rate-determining step in the parabolic rate regime is liquid diffusion. Author

N68-21768*# National Aeronautics and Space Administration. Lewis Research Center, Cleveland, Ohio.

CRACK GROWTH IN 2014-T6 ALUMINUM TENSILE AND TANK SPECIMENS CYCLICALLY LOADED AT CRYOGENIC TEMPERATURES

William S. Pierce Washington Apr. 1968 40 p refs

(NASA-TN-D-4541) CFSTI: HC\$3.00/MF\$0.65 CSCL 11F

The cryogenic low-cycle fatigue crack growth behavior of 2014-T6 aluminum through-notched uniaxial tensile and biaxial pressure vessel specimens was studied. Low-cycle crack growth data were obtained from the notched specimens at -320° and -423°F. Initial notch lengths from 0.125 to 1.0 inch and initial R ratios R_i (minimum to maximum initial stress intensity factor, Kmin.i/Kmax.i) from 0.07 to 0.36 were studied. The parameters Ri and Kmaxi appear to be useful for relating crack growth rates in pressure vessels to those in tensile specimens. At -320° and -423°F the crack growth rates were almost equal for the pressure vessel and corresponding tensile specimen provided the R_i and Kmax, values were held constant. The slopes of the curves for crack growth rate da/dN as a function of stress intensity factor range ΔK varied from 6 to 13 on a log-log plot. For a given ratio of maximum to critical stress intensity factor, the specimens tested at -423°F had longer lives than those tested at -320°F. Also, specimens run with higher Riratios had the longer cyclic lives for a given ratio of maximum to critical stress intensity. For similar values of R and K max the cyclic lives of tensile and tank specimens were almost equal, with the tensile specimens generally having longer lives. Author

N68-21917*# National Aeronautics and Space Administration. Marshall Space Flight Center, Huntsville, Ala. DEFORMATION PROCESSING OF PRECIPITATION-

HARDENING STAINLESS STEELS

D. E. Strohecker, A. F. Gerds, and F. W. Boulger Redstone Arsenal, Ala. Redstone Sci. Inform. Center [1968] 278 p refs Prepared by Battelle Mem. Inst. for Army Missile Command

(NASA Order H-76715; Contract DA-01-021-AMC-11651(Z))

(NASA-SP-5088; RSIC-495) CFSTI: HC \$3.00/MF \$0.65 CSCL 13H

Both primary and secondary fabrication methods for the precipitation-hardenable stainless steels are covered. Methods currently employed for primary fabrication of these alloys include rolling, extrusion, forging, and drawing of tube, rod, and wire. Secondary metalforming operations are those processes that produce finished or semifinished parts from sheet, bar, or tubing using additional metalforming operations. The following secondary forming no shear forming, drop hammer, trapped rubber, stretch, roll forming, dimpling, joggling, and sizing. Equipment and tooling used for the various operations are discussed and illustrated wherever possible.

N68-22338*# National Aeronautics and Space Administration. Lewis Research Center, Cleveland, Ohio.

THE EFFECT OF INTERFIBER DISTANCE AND TEMPERATURE ON THE CRITICAL ASPECT RATIO IN COMPOSITES

Robert W. Jech and Robert A. Signorelli Washington May 1968 26 p refs

(NASA-TN-D-4548) CFSTI: HC\$3.00/MF\$0.65 CSCL 11F

The effect of distance and temperature on the minimum fiber length to diameter ratio in a fiber composite was examined using a modified pullout test. Tungsten-wire-copper, iron-wire-lead, and iron-wire-cadmium specimens were used. Variation of the critical aspect ratio as a function of interfiber distance was determined for the iron-lead and iron-cadmium systems. Critical aspect ratio as a function of temperature was determined for the tungsten-copper system. Reduction of the interfiber distance increased the apparent shear strength of the matrix as indicated by

17 MATERIALS, METALLIC

a reduction of the critical aspect ratio. A rapid increase in the critical aspect ratio was noted at test temperatures in excess of 1000°F (540°C). Author

N68-22884*# National Aeronautics and Space Administration. Lewis Research Center, Cleveland, Ohio.

TEXTURE STRENGTHENING AND FRACTURE TOUGHNESS OF TITANIUM ALLOY SHEET AT ROOM AND CRYOGENIC TEMPERATURES

Timothy L. Sullivan Washington May 1968 32 p refs

(NASA-TN-D-4444) CFSTI: HC \$3.00/MF \$0.65 CSCL 11F

Preferred crystallographic orientation or texturing in metallic sheet can, under conditions of biaxial stress, result in strengthening considerably greater than that predicted for an isotropic material. Certain titanium alloys exhibit texturing. After it is rolled into sheet form, titanium alloyed with about 4 percent aluminum gives close to the ideal texture for maximum biaxial strengthening. The commercially available titanium alloy. Ti–5AI-2.5Sn, also exhibits texture strengthening. The effect of texturing on the yield, ultimate, notch, and weld strengths of both Ti-4AI-0.2O and Ti-5AI-2.5Sn extra-low-interstitial grade was determined by testing 0.020-inch-thick sheet in uniaxial and 1 to 2 biaxial stress fields at 20°, 77°, and 294°K. The biaxial test specimens were cylinders 6 inches in diameter and 18 inches long. In addition, plastic Poisson's ratios were determined at the three test temperatures. Author

N68-23560*# Boeing Co., Seattle Wash.

ULTRAVIOLET-PROTON RADIATION EFFECTS ON SOLAR CONCENTRATOR REFLECTIVE SURFACES Final Report, Jun. 1965–Aug. 1967

R. B. Gillette Washington NASA May 1968 146 p refs (Contract NAS1-5251)

(NASA-CR-1024) CFSTI: HC \$3.00/MF \$0.65 CSCL 11D

The effects of proton and ultraviolet radiation on the specular and diffuse reflectance of stretch-formed aluminum, electroformed nickel and magnesium substrate solar mirrors were studied in high vacuum at temperatures from -195° to 200° and energies from 2 to 30 keV. Ultraviolet exposures were vacuum deposited AI, which in some cases were overcoated with Si₂O₃ or SiO₂. The most severe mechanism of radiation-induced degradation was found to be proton blistering. Author

N68-24111*# National Aeronautics and Space Administration. Lewis Research Center, Cleveland, Ohio.

CREEP OF TANTALUM T-222 ALLOY IN ULTRAHIGH VACUUM FOR TIMES UP TO 10,000 HOURS

Robert H. Titran Washington May 1968 18 p refs

(NASA-TN-D-4605) CFSTI: HC\$3.00/MF\$0.65 CSCL 11F The long time creep behavior of fine-grained (0.016-mm)

Ta-9.11W-1.91Hf-0.01C was determined over the temperature range of 2000° to 2600°F (1093° to 1426°C) and in a vacuum of 10^{-8} torr (1.33×10^{-6} N/cm²). Creep stresses ranged from 2500 to 20.000 psi (17.5×10^{6} to 138×10^{6} N/m²) for test times up to 10,000 hours. At temperatures ranging from 2000° to 2600°F (1093° to 1426°C), stress levels to limit creep to 1 percent in 10,000 hours are 28,000 and 800 psi (193×10^{6} and 6×10^{6} N/m²), respectively. The stress dependence of the steady creep vas equivalent to an apparent activation energy of 150 kcal/g-mole (627 450 J/g-mole).

N68-24477*# National Aeronautics and Space Administration. Lewis Research Center, Cleveland, Ohio. YIELDING AND FRACTURE. IN TUNGSTEN AND

TUNGSTEN-RHENIUM ALLOYS

Peter L. Raffo Washington May 1968 36 p refs

(NASA-TN-D-4567) CFSTI: HC\$3.00/MF\$0.65 CSCL 11F

A study was made of the mechanical properties of vacuum arc-melted tungsten and tungsten-rhenium alloys in the temperature range 77° to 810°K in order to elucidate the mechanism by which rhenium additions lower the ductile-brittle transition temperature of tungsten. The temperature and strain-rate dependence of the yield stress of tungsten is reduced by alloying with rhenium. This is shown to be because of a reduction in the Peierls stress. The reduction in the transition temperature is attributed to the reduced Peierls stress through its effect on the mobility and rate of multiplication of dislocations. Author

N68-24558*# National Aeronautics and Space Administration. Lewis Research Center, Cleveland, Ohio.

ELECTRICAL AND MECHANICAL PROPERTIES OF A SUPERIOR HIGH-TEMPERATURE COBALT-IRON MAGNETIC MATERIAL

John P. Barranger Washington May 1968 22 p refs (NASA-TN-D-4551) CFSTI: HC\$3.00/MF\$0.65 CSCL 11F

The alternating current electrical and mechanical properties of high purity alloys of 9 weight percent iron, the balance being mostly cobalt, were determined at temperatures from 25° to 1000°C. Data are presented for four thicknesses from 0.002 inch (0.005 cm) to 0.012 inch (0.030 cm) and at six frequencies from 60 to 3200 hertz. The results of the measurements and comparisons with a commercial alloy indicate that the material is one of the best magnetic materials for high temperature transformer core applications. Author

N68-25318*# Louisiana State Univ., Baton Rouge. A STUDY OF SENSITIZATION IN TYPES 301 AND 304L STAINLESS STEELS USING MOESSBAUER SPECTROSCOPY O. W. Albritton Washington, D. C. NASA Jun. 1968 23 p

O. W. Albritton Washington, D. C. NASA Jun. 1968 23 p refs

(Grant NGR-19-001-024)

(NASA-CR-1077) CFSTI: HC \$3.00 /MF \$0.65 CSCL 11F

Mossbauer effect spectroscopy in conjunction with X-ray diffraction techniques were used to study the phenomenon of stainless steel sensitization. A ferromagnetic phase, thought to be pseudomartensite, has been found to exist in sensitized Type 301. Stresses generated in the matrix by morphology changes of the precipitated carbides is deemed responsible for the creation of this phase. No such phase was detected in the Type 304L. It was confirmed that the precipitated carbides were of the complex type. Furthermore, it was established that these carbides are paramagnetic. In the presence of austenite, the Mossbauer peak for the carbides is overshadowed. In single phase materials grain size has no effect on the Mossbauer spectrum. In multiphase materials the peak locations are unaffected by grain size, but quantitative evaluations are influenced.

N68-28365*# National Aeronautics and Space Administration. Lewis Research Center, Cleveland, Ohio.

COMPILATION OF THERMOPHYSICAL PROPERTIES OF

Harry W. Davison Washington Jul. 1968 23 p refs

(NASA-TN-D-4650) CFSTI: HC\$3.00/MF\$0.65 CSCL 20M

A compilation of properties including density, electrical resistivity, enthalpy, heat capacity, surface tension, thermal conductivity, vapor pressure, viscosity, Prandtl number, and thermal diffusivity is presented for temperatures between the melting point and normal boiling point of lithium. Empirical correlations were obtained by statistically fitting a polynomial to experimental data obtained from the literature.

N68-28818^{*}# National Aeronautics and Space Administration. Lewis Research Center, Cleveland, Ohio.

EFFECT OF 10²⁰ NEUTRON PER SQUARE CENTIMETER IRRADIATION ON EMBRITTLEMENT OF POLYCRYSTALLINE TUNGSTEN Charles L. Younger and Gilbert N. Wrights Washington Jul. 1968 59 p refs

(NASA-TM-D-4661) CFSTI: HC\$3.00/MF\$0.65 CSCL 11F

The effect of reactor irradiation on embrittlement of polycrystalline tungsten was investigated by comparing ductile-to-brittle transition of unirradiated and irradiated material. Tensile tests were conducted in the range 300° to 700°F (422 to 644 K). Bend tests, conducted at room temperature, provided additional data. Test results show that recrystallized tungsten irradiated with 1×10^{20} fast neutrons per cm ² is severely embrittled. The ductile-to-brittle transition temperature for the irradiated material increased by at least 300°F (167K), accompanied by an increase in the temperature-dependent yield point stress and decreases in the tensile fracture and extreme fiber bending stresses. The embrittlement appears to be a result of factors which decrease grain boundary strength and inhibit transgranular fracture. Also determined were irradiation effects on specimen dimensions, density, and electrical resistivity. Dimensional and density changes were small, but the electrical resistivity increased linearly with increasing irradiation and reached 87% at the highest irradiation exposure. It may be concluded that irradiation of unalloyed, polycrystalline tungsten with 1020 fast neutrons per cm2 and 1021 thermal neutrons per cm 2produces a very brittle tungsten-1-percent-rhenium alloy with strength greater than that of the starting material, but because of irradiation-induced point defects, dislocation loops, and defect clusters, the grain boundary strength is lower than originally. Author

N68-29379*# National Aeronautics and Space Administration. Goddard Space Flight Center, Greenbelt, Md.

HEAT TREATMENT FOR IMPROVED STRESS-CORROSION RESISTANCE OF 17-7 ph STAINLESS

Carl R. Johnson and John D. Grimsley Washington Jul. 1968 11 p refs

(NASA-TN-D-4673) CFSTI: HC\$3.00/MF\$0.65 CSCL 11F

This paper discusses stress-corrosion tests given to 17-7 ph stainless steel—previously subjected to different heat treatments—to fit it for the requirements of rocket-driven spacecraft. Two commercial treatments and one experimental treatment are described, and illustrated by micrographs. Author

N68-29954*# National Aeronautics and Space Administration. Lewis Research Center, Cleveland, Ohio.

SOME OBSERVATIONS CONCERNING THE OXIDATION OF THE COBALT-BASE SUPERALLOY L-605 (HS-25)

James S. Wolf and Gary D. Sandrock Washington Aug. 1968 40 p refs

(NASA-TN-D-4715) CFSTI: HC\$3.00/MF\$0.65 CSCL 11F

The concentration of the minor alloying elements silicon and manganese were found to strongly affect the oxidation behavior of L-605 in the temperature range 1000° to 1200° C. Silicon is also dominant in determining the post-aging ductility of this alloy. Plots were developed which indicate that it is possible to optimize both oxidation resistance and ductility of L-605 by restricting the silicon and manganese concentrations to the range 0.1 to 0.4 and 1.4 to 1.65 weight percent, respectively. A mechanism compatible with observed weight gains, scale structures, and scale compositions was proposed for the oxidation of L-605 and similar alloys.

N68-29987*# National Aeronautics and Space Administration. Lewis Research Center, Cleveland, Ohio.

HIGH TEMPERATURE CREEP-RUPTURE PROPERTIES OF A TUNGSTEN-URANIUM DIOXIDE CERMET PRODUCED FROM COATED PARTICLES

Robert J. Buzzard Washington Aug. 1968 26 p refs

(NASA-TM-X-1625) CFSTI: HC\$3.00/MF\$0.65 CSCL 11F Tungsten-50 volume percent uranium dioxide cermets, produced by roll compaction of tungsten-coated uranium dioxide particles and clad with tungsten, were creep-rupture tested at temperatures of 1080° to 1800°C (1975° to 3272°F) and stresses of 1740 to 14,500 psi (12 to 100 MN/m^2). Rupture life values ranged from 1 to 696 hrs. Additional rupture life values were predicted by use of the Manson-Haferd time-temperature parameter, lsotherms for 0.5 and 1.0 percent creep, and the end of second stage creep, also were constructed by use of this parameter. An attempt was made to describe the role of the UO₂ in the cermet's creep-rupture process. Author

N68-29992*# TRW Equipment Labs., Cleveland, Ohio. GENERATION OF LONG TIME CREEP DATA OF REFRACTORY ALLOYS AT ELEVATED TEMPERATURES

J. C. Sawyer and E. A. Steigerwald Washington NASA Aug. 1968 197 p refs

(Contract NAS3-2545)

(NASA-CR-1115; TRW-ER-7203) CFSTI: HC \$3.00/MF \$0.65 CSCL 11F

Creep tests were conducted on selected refractory alloys in a vacuum environment for times between 100 and 15,000 hours. Since the ultimate program goal was to provide design data for space electric power systems, particular emphasis was placed on measuring creep extension below 1%. The resulting data were evaluated in terms of the relative properties of columbium, molybdenum, tantalum, and tungsten-base alloys. In the 1800°F to 2200°F temperature range, the molybdenum-base alloys TZC and TZM possess the best creep properties for potential turbine applications. The variability of the creep properties as a function of heat of material was determined for the T-111 alloy. In addition to comparison of alloy creep properties, chemical analysis, metallography, and tensile test data are presented to characterize each of the materials before and after creep testing.

N68-30000*# National Aeronautics and Space Administration. Langley Research Center, Langley Station, Va.

HOT-SALT-STRESS-CORROSION CRACKING AND ITS EFFECT ON TENSILE PROPERTIES OF TI-8AI-1Mo-1V TITANIUM-ALLOY SHEET

Dick M. Royster Washington Aug. 1968 36 p refs (NASA-TN-D-4674) CFSTI: HC\$3.00/MF\$0.65 CSCL 11F

The concluding phase of an extensive experimental investigation of hot-salt-stress corrosion of the Ti-8AI-1Mo-1V titanium alloy was conducted on self-stressed and tensile specimens of a 0.050-inch- (1.3-mm) thick Ti-8AI-1Mo-1V titanium-alloy sheet (duplex annealed). The self-stressed specimens, with stresses of 50, 25, and 15 ksi (340, 170, and 100 MN/m²), were dipped in a 3.4 percent sodium cloride (NaCl) solution and exposed at temperatures from 400° to 600°F (480° to 590°K) for exposures up to 20,000 hours. Stress-corrosion cracking was obtained after approximately 17 hours at 600°F (590°K) for the 50 ksi (340 MN/m²) stress, but no stress-corrosion cracking was noted at 400°F (480°K) at any stress level investigated. The threshold stresses decrease with an increase in exposure temperature and time. The tensile corrosion specimens were coated with a thin layer of sait (NaCl) and exposed at temperatures from 500° to 600°F (530° to 590°K) at 50 ksi (340 MN/m²) stress for exposures up to 800 hours to develop and grow stress-corrosion cracks. The presence of stress-corrosion cracks resulted in a large drop in elongation and a moderate decrease in tensile strength: The properties deteriorated more for the transverse specimens than for the longitudinal tensile specimens. The residual tensile properties appeared to be dependent only on the depth of the cracks, regardless of the temperature or time at which the cracks were developed. The stress-corrosion cracks were intergranular, and maximum crack depth could be correlated with exposure time at 550° and 600°F (560° and 590°K). Author

17 MATERIALS, METALLIC

N68-30065*# National Aeronautics and Space Administration. Lewis Research Center, Cleveland, Ohio.

COMPATIBILITY OF SEVERAL IRON-BASE, COBALT-BASE, AND NICKEL-BASE ALLOYS WITH REFLUXING POTASSIUM AT 1800°F

John H. Sinclair Aug. 1968 20 p refs

(NASA-TM-X-1617; E-4337) CFSTI: HC \$3.00/MF \$0.65 CSCL 11F

Capsules of HS-25, Rene 41, Hastelloys N, C, and X, and AISI 318 were corrosion tested with refluxing potassium at 1800°F (982°C) for times up to 2000 hours. The objective was to determine the corrosion resistance of these alloys for possible use in facilities for ground testing of design concepts for space-power systems. Only AISI 318 appeared to be unsuitable from the standpoint of resistance to corrosion by potassium. The materials could arbitrarily be ranked into three groups in descending order of resistance to corrosion: Rene 41 and HS-25; then, Hastelloys N, C, and X (in that order); and finally, AISI 318.

N68-30066*# National Aeronautics and Space Administration. Lewis Research Center, Cleveland, Ohio.

CHROMIUM AND NICKEL POWDERS MADE BY REDUCTION OF THEIR OXIDES WITH MAGNESIUM, LITHIUM, OR SODIUM VAPORS

Alan Arias Aug. 1968 23 p refs

(NASA-TN-D-4714; E-4386) CFSTI: HC \$3.00/MF \$0.65 CSCL 11F

Chromium powder separable into $0.0068 \cdot \mu m$ colloidal and $0.16 \cdot \mu m$ coarse powder fractions was obtained by reduction of Cr_2O_3 with Mg vapor in a vacuum furnace. The coarse powder fraction was calculated to have 8 volume percent residual MgO plus MgO·Cr_2O_3 dispersoids, probably suitable for dispersion strengthening. Other chromium powders, 0.08- to 0.60 \cdot \mu m particle size and oxygen to surface area ratios of about 0.002 g/m², were made by reduction of Cr_2O_3 with Li and Na vapors. Nickel powder, 1.25 - μm particle size and with 0.114 percent oxygen, was made by reduction of NiO with Li vapor. Author

N68-30504*# National Aeronautics and Space Administration. Lewis Research Center, Cleveland, Ohio.

TENSILE PROPERTIES OF TANTALUM AND TUNGSTEN 10-FIBER BUNDLES AT 1000° F (812 K)

Ruluff D. McIntyre Washington Aug. 1968 21 p refs

(NASA-TN-D-4725) CFSTI: HC \$3.00/MF \$0.65 CSCL 20K This investigation studied the tensile properties of 10-fiber bundles and related these properties to single-fiber strength. Bundles comprised of both tantalum and tungsten fibers with 20, 50, and 80 percent tungsten fibers were also tested. A statistical study related bundle strengths to single-fiber strengths. Bundles of tungsten fibers were less strong than single fibers tested separately. Bundles of tantalum fibers were as strong as tantalum single fibers. Strength followed the rule of mixtures for bundles containing mixtures of tantalum and tungsten fibers. Author

N68-30605*# National Aeronautics and Space Administration. Lewis Research Center, Cleveland, Ohio.

SUPERPLASTICITY IN TUNGSTEN-RHENIUM ALLOYS

M. Garfinkle, W. R. Witzke, and W. D. Klopp Washington Aug. 1968 22 p refs

(NASA-TN-D-4728) CFSTI: HC\$3.00/MF\$0.65 CSCL 11F

Electron beam melted tungsten-rhenium alloys containing 20 to 28 atomic percent Re exhibited elongations of over 200 percent in tensile tests at 3630°F. Rapid grain growth rates in these alloys, relative to tungsten-rhenium alloys with lesser Re contents, and continuous recrystallization during tensile testing indicate the occurrence of enhanced diffusion processes. Strain rate sensitivities generally ranged between 0.2 and 0.3 for these alloys, but strain rate sensitivities as high as 0.8 were observed under the special conditions encountered immediately following initial recrystallization. These were well within the range associated with superplastic materials. Author

N68-31517*# National Aeronautics and Space Administration. Lewis Research Center, Cleveland, Ohio.

STRESS-STRAIN BEHAVIOR OF COLD-WELDED COPPER-COPPER MICROJUNCTIONS IN VACUUM AS DETERMINED FROM ELECTRICAL RESISTANCE MEASUREMENTS

John S. Przybyszewski Washington Aug. 1968 22 p refs (NASA-TN-D-4743) CFSTI: HC\$3.00/MF\$0.65 CSCL 11F

True stress-strain curves, developed from contact-resistance measurements between two OFHC copper specimens loaded and unloaded in vacuum, showed that the cold-welded junctions exhibited an amount of ductility generally characteristic of the specimen material. Junction ductility was greater when the experiment was kept vibration free. Deliberate vibration introduced during the loading cycle lowered the junction ductility. The contact-resistance-against-load data also seemed to indicate that impulsive forces could increase the area of contact under fixed load to a point where the contact area might revert to an elastic condition. Author

N68-31605*# National Aeronautics and Space Administration, Washington, D. C.

EFFECTS OF LOW TEMPERATURES ON THE MECHANICAL PROPERTIES OF STRUCTURAL METALS

H. L. Martin, P. C. Miller, A. G. Imgram, (Battelle Mem. Inst., Columbus) and J. E. Campbell (Battelle Mem. Inst., Columbus) 1968 65 p refs Revised

(NASA-SP-5012(01)) GPO: HC \$0.50; CFSTI: MF \$0.65 CSCL 11F

Industrial applications in aerospace and other fields are noted for cryogenic technology; and mechanical properties of metals at low temperatures are discussed in terms of alloying and welding effects and the fracture of preexisting flaws and notches. Testing procedures are outlined; and data are presented for aluminum, magnesium, nickel, steel, and titanium alloys. Tensile properties are tabulated for a wide variety of these alloys in base ; and welded forms. Studies indicate that the austenitic stainless steels retain high ductility and toughness at temperatures as low as $-423\,^\circ\text{F}.$ Higher strength with good toughness as low as $-320\,^\circ\text{F}$ can be provided with 9Ni-4Co steels. Use of various aluminum alloys is cited, and toughness values of certain age-hardened AI alloys are found to be marginal at low temperatures. High strength, low density, and corrosion resistance of titanium alloys are noted; as are the high ductilities of nickel alloys. Developments in gas liquefaction and separation, storage and handling of cryogenic fluids, low temperature heat exchange, quick freezing, superconductivity, and low temperature storage and surgical techniques are covered. M.W.R.

N68-33019*# Du Pont de Nemours (E.I.) and Co., Aiken, S. C. **ROLE OF HYDROGEN CHLORIDE IN HOT SALT STRESS CORROSION CRACKING OF TITANIUM ALUMINUM ALLOYS**

R. S. Ondrejcin and M. R. Louthan, Jr. Washington NASA Aug. 1968 29 p refs

(NASA Order R-124)

(NASA-CR-1133; DP(NASA)-1130) CFSTI: HC\$3.00/MF\$0.65 CSCL 11F

The reactions of titanium-aluminum alloys with andydrous HCI gas were studied, and the reaction products were found to be TiCl₂. TiCl₃. TiCl₄. Al₂Cl₈, and H₂. These products are considered to be intermediates in the hot salt stress corrosion cracking of titanium-aluminum alloys. These products are not normally identified because they oxidize and hydrolyze in the presence of oxygen, moisture, and heat. Fractographic examination of Ti-8Al-1 Mo-1V specimens cracked by hot salt and HCI showed the same fracture mechanism in both cases-mechanical rupture

accompanied by dislocation movement. It is proposed that stress-sorption is the mechanism of cracking, and that atomic hydrogen is the species sorbed. Author

N68-33278*# National Aeronautics and Space Administration. Lewis Research Center, Cleveland, Ohio.

INFLUENCE OF CHEMISORBED FILMS ON ADHESION AND FRICTION OF CLEAN IRON

Donald H. Buckely Washington Sep. 1968 14 p refs

(NASA-TN-D-4775) CFSTI: HC\$3.00/MF\$0.65 CSCL 11F

Studies were conducted in a vacuum of 10^{-10} torr with clean polycrystalline iron and with iron containing various films. Results indicate strong adhesive forces for the clean iron; because of the magnitude of these forces friction could not be measured. These forces were appreciably reduced in the presence of adsorbates. Carbon dioxide dissociated on the surface, resulting in metal oxide and carbon monoxide. Water vapor was more effective in reducing friction than was oxygen of the same exposure. With hydrocarbons, the number of carbon-to -carbon bonds influenced friction and adhesion. Friction decreases with chain length and with the number of carbon-to -carbon bonds for a particular chain length.

N68-33335*# Materials Research Corp., Orangeburg, N. Y. AN ALUMINUM NITRIDE MELTING TECHNIQUE Walter Class Washington NASA Sep. 1968 49 p refs (Contract NAS3-10659)

(NASA-CR-1171) CFSTI: HC\$3.00/MF0.65 CSCL 13H

Experimental studies were undertaken to evaluate the melting behavior of aluminum nitride and, particularly, to determine if pressures of \leq 200 atm were sufficient to suppress the decomposition of AlN at its melting point. To determine this as well as the actual melting point of AlN, crucible melting was accomplished in resistively heated crucibles and arc melting was carried out on a cooled copper hearth to achieve uncontaminated AlN melts. The former method permitted the achievement of pressure stabilized melts; although the graphite, rhenium, and tungsten crucible materials reacted with the AlN to prevent an accurate determination of its melting point. The AlN does, however, appear to melt between 2750 and 2850°C. A nitrogen atmosphere at a pressure of 1500 psi was sufficient to suppress decomposition, although this conclusion can be questioned because of the presence of chemical reaction. M.W.R.

N68-33684*# National Aeronautics and Space Administration. Lewis Research Center, Cleveland, Ohio.

REFRACTORY METAL FIBER NICKEL BASE ALLOY COMPOSITES FOR USE AT HIGH TEMPERATURES

Donald W. Petrasek, Robert A. Signorelli, and John W. Weeton Washington Sep. 1968 48 p refs Presented at the Soc. of Aerospace Mater. and Process Engr. 12th Natl. Symp. on Advan. in Structural Composites, Anaheim, Calif., 10–12 Oct. 1967 (NASA-TN-D-4787) CFSTI: HC\$3.00/MF\$0.65 CSCL 11F

The stress rupture properties of several refractory metal fiber-nickel base alloy composites were determined at 2000° and 2200°F. The effect of wire diameter, fiber content, fabrication history and compositions of the matrix and fiber on the stress rupture properties of the composite was determined. The 100-hour stress rupture strength obtained for the strongest composites tested at 2000° and 2200°F was 35,000 and 14,000 psi, respectively. Composite strength was related to the compatibility of the fibers with the matrix materials. Composite rupture strength can be optimized by proper fiber diameter selection.

N68-35098*# Bendix Corp., Madison Heights, Mich. OXIDATION RESISTANT MATERIALS FOR TRANSPIRATION COOLED GAS TURBINE BLADES. 2: WIRE SPECIMEN TESTS Fred W. Cole, James B. Padden, and Andrew R. Spencer Washington NASA Sep. 1968 125 p ref

(Contract NAS3-7269)

(NASA-CR-1184) CFSTI: HC\$3.00/MF\$0.65 CSCL 11F

Four alloys were selected on the basis of sheet specimen tests, reported in Summary Report CR-930, and tested in 0.005 inch diameter wire form to determine their suitability for use as transpiration cooled gas turbine blade materials. The alloys were N 155, TD nickel-chromium, DH 242, and Hastelloy X. Tests consisted of cyclic oxidation, continuous oxidation, stress rupture life, and stress-oxidation at 1400, 1600, 1800, and 2000°F, and up to 2100 and 2200°F for some tests. Exposure times ranged up to 100 hours except for cyclic oxidation tests where times were 4, 16, 64, 100, 100, 300, 400, 500 and 600 hours. Total specific oxidation weight gain, oxide spall and penetration, and mechanical properties were determined for each alloy. Metallographic examination showed microstructure and oxidation effects. TD nickel-chromium was superior, except for stress sensitivity resulting in internal oxidation. All alloys were limited to a useful service temperature near 1600-1700°F. Author

N68-35200*# Norton Research Corp., Cambridge, Mass. MECHANISM OF THE ATMOSPHERIC INTERACTION WITH THE FATIGUE OF METALS

M. J. Hordon and M. A. Wright Washington NASA Sep. 1968 54 p refs

(Contract NASw-1533)

(NASA-CR-1165) CFSTI: HC\$3.00/MF\$0.65 CSCL11F

In an investigation of the fatigue properties of aluminum in vacuum, experimental work was directed at cyclic frequency and tensile fatigue effects, and at the defect substructure generated in vacuum by fatigue stressing. The mean fatigue life was observed to depend on the cyclic rate of straining at all pressure levels. However, in the region of the critical pressure zone for fatigue life enhancement, changes in the cyclic frequency were noted to have a major effect on crack propagation. Measurements of the fatigue life under conditions limited to alternating tensile stresses alone showed that fatigue life enhancement or crack growth retardation in vacuum was not dependent on compressive stress distributions or fatigue crack closure. Finally, a well defined correlation was observed between the fatigue properties of aluminum and dislocation substructural distributions revealed by thin film electron microscopy. Author

N68-36076*# National Aeronautics and Space Administration. Lewis Research Center, Cleveland, Ohio.

CAVITATION DAMAGE OF STAINLESS STEEL, NICKEL, AND AN ALUMINUM ALLOY IN WATER FOR ASTM ROUND ROBIN TESTS

Stanley G. Young Washington Oct. 1968 20 p refs (NASA-TM-X-1670) CFSTI: HC\$3.00/MF\$0.65 CSCL 11F

Cavitation damage was determined for AISI type 316-stailess steel, nickel 270, and 6061-T6 aluminum as part of an ASTM round robin test program. A vibratory apparatus was used and tests

were conducted in water at 75°F under 1 atmosphere pressure. Volume loss, volume loss rate, and mean depth of penetration were determined, and metallographic studies were made of the damage specimens. Author

N68-36970*# National Aeronautics and Space Administration. Ames Research Center, Moffett Field, Calif.

THE INFLUENCE OF GASEOUS ENVIRONMENT ON THE SELF-ADHESION OF METALS

William P. Gilbreath Washington Oct. 1968 21 p refs (NASA-TN-D-4868) CFSTI: HC\$3.00/MF\$0.65 CSCL 11F

The self-adhesion of metal surfaces was measured in various gases with pressure, exposure duration, and temperature as variables. Aluminum, copper, gold, lead, magnesium, and titanium

17 MATERIALS, METALLIC

were studied in air, argon, carbon monoxide, ethylene, hydrogen, nitrogen, and oxygen. The results showed that loss of adhesion for a particular metal resulted from gas adsorption on its contacting surface and that the effect of environment upon adhesion could be related to the heat of adsorption for the particular metal-gas interaction. Author

N68-37053*# National Aeronautics and Space Administration. Langley Research Center, Langley Station, Va.

MECHANICAL PROPERTIES AND COLUMN BEHAVIOR OF THIN WALL BERYLLIUM TUBING

Donald R. Rummler, H. Benson Dexter, George H. Harth, III, and Raymond A. Buchanan Washington Oct. 1968 77 p refs (NASA-TN-D-4833) CFSTI: HC\$3.00/MF\$0.65 CSCL 11F

The results of an experimental investigation to determine the mechanical properties and column behavior of commercially produced beryllium tubing at room temperature are presented. The investigation included three types of extruded tubing and one type of plasma-sprayed and sintered tubing. The diameters of the tubes ranged from 0.25 to 0.75 inch (6.35 to 19.05 mm). Wall thickness was either 0.020 or 0.040 inch (0.508 or 1.016 mm). Microhardness measurements and metallurgical studies were performed to characterize the tubing microstructure. On the basis of the results of mechanical-property determinations and column tests, the extruded tubing appeared to be suitable for use in truss-type structures. Column buckling loads could be predicted satisfactorily by using the tangent modulus, derived from compressive stress-strain curves, in the inelastic column-buckling equation. The results also indicated that the reproducibility of the dimensions and the mechanical properties of the extruded beryllium tubing were comparable to that of other aircraft structural materials. Author

18 MATERIALS, NONMETALLIC

Includes corrosion; physical and mechanical properties of materials (e.g., plastics); and elastomers, hydraulic fluids, etc. For basic research see: 06 Chemistry. For related information see also: 17 Materials, Metallic; 27 Propellants; and 32 Structural Mechanics.

N68-11978*# Southern Research Inst., Birmingham, Ala. AN INVESTIGATION OF THE MECHANISMS OF HEAT TRANSFER IN LOW-DENSITY PHENOLIC-NYLON CHARS E. D. Smyly, C. M. Pyron, Jr. and C. D. Pears Washington NASA

E. D. Smyly, C. M. Pyron, Jr. and C. D. Pears Washington NASA Dec. 1967 100 p refs

(Contract NAS1-5448)

(NASA-CR-966) CFSTI: HC\$3.00/MF\$0.65 CSCL 111

The thermal conductivities of three phenolic-nylon chars having porosities of 0.79, 0.82, and 0.88 were measured in vacuum, nitrogen, and helium environments. The temperature range covered was from 400°F to 1000°F. The pressure range was from 0.002 to 760 torr. The specimens were obtained from virgin materials with densities of 19 $\rm lb/ft^3,$ 30 $\rm lb/ft^3,$ and 42 $\rm lb/ft^3$ by charring in a 30 percent nitrogen-70 percent argon plasma for 125 to 180 seconds. The input cold-wall heat flux density was 170 Btu/sec-ft². The thermal conductivity increased on changing the environment from vacuum to either nitrogen or helium. The increase was greater than could be accounted for by the simple addition of the thermal conductance of the environmental gas to the thermal conductivity measured in vacuum. This discrepancy was explained as an effect due to the thermal shorting of internal delaminations within the char. A thermal model which takes the delaminations into account was developed and correlated with the data. The correlation allowed the isolation of one important intrinsic property of the char, the thermal conductivity of the matrix, assuming that the model describes the physical situation. Author

N68-16623*# National Aeronautics and Space Administration. Lewis Research Center, Cleveland, Ohio.

GLASS-, BORON-, AND GRAPHITE-FILAMENT-WOUND RESIN COMPOSITES AND LINERS FOR CRYOGENIC PRESSURE VESSELS

Morgan P. Hanson Washington Feb. 1968 18 p refs

(NASA-TN-D-4412) CFSTI: HC \$3.00/MF \$0.65 CSCL 11D An experimental investigation was conducted to determine the tensile-strength properties of glass, boron, and graphite composites at 75°, -320°, and -423° F. Composite tensile-strength and interlaminar-shear-strength tests were made of rings. Tensile strengths of boron filaments were determined at 75° and -320°F. Strengths of glass composites were about 29 percent higher at cryogenic temperatures than at ambient temperature. Boron and graphite composite strengths were essentially the same in the temperature range investigated. Interlaminar shear strength in glass composites also increased from 75° to -320°F; boron and graphite showed no significant change within the temperature range. Filament translation efficiencies ranged from 58 to 69 percent for the materials investigated. Aluminum-foil liners that were adhesively bonded to the internal surface of glass-filament-wound cylinders withstood pressure cycling to 2.5 percent strain for a cyclic life ranging from 14 to 165 cycles at cryogenic temperatures. Liner failures were associated with buckling of the seam areas. Author

N68-18849*# International Business Machines Corp., Cambridge, Mass.

INVESTIGATION OF REFRACTORY DIELECTRICS FOR INTEGRATED CIRCUITS V. Y. Doo and D. R. Kerr Washington NASA Mar. 1968 81 p refs

(Contract NAS12-105)

(NASA-CR-995) CFSTI: HC\$3.00/MF\$0.65 CSCL 20L

Growth parameters for pyrolytic silicon nitride such as nucleation, reactant composition, substrate temperature, substrate preparation, and carrier gas were studied. Measurements were made in MNS (metal-nitride-silicon) and MNOS (metal-nitride-oxide-silicon) samples for surface charge density, electronic leakage and dielectric constant determination. The index of refraction and 48% HF etch rate were also measured. The masking property of silicon nitride for dopants which silicon dioxide fails to mask was investigated. Photolithographic techniques were developed so that conventional photoresist could be used. Silicon nitride torgether with silicon and diodes. The integrated circuits were thermally and electrically stressed, and the results on H_{FE} and junction breakdowns charges were recorded.

N68-19710*# National Aeronautics and Space Administration. Langley Research Center, Langley Station, Va.

EXPERIMENTAL AND THEORETICAL INVESTIGATION OF THE ABLATIVE PERFORMANCE OF FIVE PHENOLIC-NYLON-BASED MATERIALS

Allen G. McLain, Kenneth Sutton, and Gerald D. Walberg Washington Apr. 1968 32 p refs

(NASA-TN-D-4374) CFSTI: HC \$3.00/MF \$0.65 CSCL 111

Five composite ablation materials which contain various percentages of phenolic resin, powdered nylon, and silica (either as spheres or fibers) were tested in a 20-inch hypersonic arc-heated tunnel. The tests were carried out in air at a stream stagnation enthalpy of 4800 Btu/lbm, a cold-wall aerodynamic heating rate of 119 Btu/ft² sec, a stagnation pressure on the model surface of 0.066 atmosphere, and a free-stream Mach number of approximately 5. The data obtained from these tests were used to evaluate the ablative performance of each of the materials and have been compared with theoretical predictions of char-recession rate and (for two of the materials) thermal response. During the tests, char removal was due primarily to oxidation and the char-recession rates were not significantly affected by either mechanical failure of SiO 2-C reactions. The addition of 12.5 percent SiO₂ to the high-density materials produced a significant increase in both char integrity and char-virgin material interface strength but resulted in a decrease in thermal effectiveness. Reasonable agreement between measured and calculated char-recession rates was obtained by assuming chemical equilibrium at the char surface between the pyrolysis gases, the char, and the test stream, with CO as the primary reaction product. Reasonable agreement between measured and calculated thermal response could be obtained only when the char thermal conductivity was assumed to be approximately 1/3 of its measured value. Author

N68-20329*# National Aeronautics and Space Administration. Lewis Research Center, Cleveland, Ohio. CRYOGENIC POSITIVE EXPULSION BLADDERS

18 MATERIALS, NONMETALLIC

Raymond F. Lark Washington Apr. 1968 18 p refs Presented at the 1st Ann. Cryog. Polymers Conf., Cleveland, 25–27 Apr. 1967 Sponsored by Case Inst. of Technology

(NASA-TM-X-1555) CFSTI: HC\$3.00/MF\$0.65 CSCL 21H

The cryogenic flexibility of single and multiple plies of thin polymeric films was experimentally determined at -320° and -423°F. Of the films tested, thin Mylar films of 0.5 mil and less are the most flexible. The relations between cryogenic cycle life and film thickness and also for the number of plies of Mylar film are reported for the same two temperatures. Twist-and-flex cycle life of 0.25-mil Mylar C samples at -423°F ranges from 20 cycles for 1 ply to 400 cycles for 10 plies. Test results for spherical 12-inch diameter multi-ply Mylar, Kapton, and polyethylene film bladders are summarized. Bladder material combinations showing the lowest helium gas porosity after 25 liquid hydrogen positive expulsion cycles are: (1) twelve plies of 0.15-mil Mylar C in combination with 20 plies of 0.1-mil polyethylene film; and (2) ten plies of 0.5-mil Kapton in combination with three plies of 2-mil Nomex-Nylon paper. K.W.

N68-22391*# General Electric Co., Philadelphia, Pa. **COATING SELECTION PROGRAM: THEORY**

Frederick A. Costello, Thomas P. Harper, and Barbara Aston Washington NASA Apr. 1968 48 p refs

(Contract NASw-960)

(NASA-CR-1041; Doc.-65SD526) CFSTI: HC \$3.00/MF \$0.65 CSCL 20M

A rational and direct method has been developed for selecting the optical coating pattern for the external surface of a spacecraft, such that the spacecraft temperatures are as close as possible to the midpoint of their preselected ranges. The temperature control is maintained passively by radiation and conduction, using no active control devices. The complete range in mission environments is considered in the optimization procedure. The selection technique has been programmed for use on the GE 600 Series, IBM 7094, or any other computer that uses the standard IBM Fortran IV system. Author

N68-28264*# National Aeronautics and Space Administration. Goddard Space Flight Center, Greenbelt, Md.

CRITERIA FOR SELECTION OF WIRE INSULATIONS FOR USE IN SPACE APPLICATIONS

Vernon Krueger Washington Jul. 1968 17 p refs

(NASA-TN-D-4553) CFSTI: HC\$3.00/MF\$0.65 CSCL 111

The properties of five electrical insulation materials (Teflon TFE, Teflon FEP, Specification 44 outer space insulation, Novathene, and modified Rayolin-N) were compared, to provide a guide for selecting wire insulations in spacecraft. Of all the properties considered, the outgassing characteristics, radiation resistance, and weight of the materials were considered most important for space applications. Also considered were the workability of these insulations and the amount of fabrication deterioration that wires and cables using them can withstand. Author

N68-30597*# National Aeronautics and Space Administration. Lewis Research Center, Cleveland, Ohio.

POLYMER-FILM	COATING	OF	MAGNESIUM	FOR
PARABOLOIDAL MIRRORS				

Thaddeus S. Mroz and Robert B. King Washington Aug. 1968 13 p refs

(NASA-TN-D-4734) CFSTI: HC\$3.00/MF\$0.65 CSCL 11C

A material and a method were determined for coating large mechanically polished magnesium surfaces to provide a high quality surface, acceptable for further coating with vapor-deposited optical films. The coating material was a modified epoxy resin mixture. The application procedure consisted of surface preparation using commercially available chemical cleaning agents, spray application with commercially available equipment, and a carefully programmed curing schedule. Author N68-33034*# National Aeronautics and Space Administration. Lewis Research Center, Cleveland, Ohio.

EFFECT OF FILM PROCESSING ON CRYOGENIC PROPERTIES OF POLY(ETHYLENE TEREPHTHALATE) Roger E. Eckert and Tito T. Serafini Washington Aug. 1968 35 p refs

(NASA-TN-D-4762) CFSTI: HC\$3.00/MF\$0.65 CSCL 111

The effects of stretch temperature, heat-set temperature, and time on the cryogenic mechanical properties of PET film were studied by using a two-level factorial experiment. Amorphous PET sheet was oriented at either 85° or 95° C. The levels of heat-set temperature and time investigated were 190° and 210° C and 15 and 120 seconds, respectively. Film crystallinity was determined by the density gradient technique. Tensile properties were measured in liquid nitrogen and in liquid hydrogen. Biaxial burst properties were obtained in liquid nitrogen. The number of flexural cycles to failure in liquid hydrogen and room-temperature gas porosities after 25 such cycles were also determined. Author

N68-35100*# Astro Research Corp., Santa Barbara, Calif. AN EVALUATION OF BORON-POLYMER FILM LAYER COMPOSITES FOR HIGH-PERFORMANCE STRUCTURES R. F. Crawford Washington NASA Sep. 1968 40 p refs (Contract NAS7-427)

(NASA-CR-1114; ARC-R-276) CFSTI: HC \$3.00/MF \$0.65 CSCL 11I

A composite film of polyimide with boron vacuum-deposited on one side has become available for development as a structural material. The objective of the present investigation has been to evaluate the fabricability, mechanical properties, and structural efficiency potentials of this material for structural composites. Hollow tubular test specimens were readily fabricated by wrapping the composite film over mandrels and bonding layers together with epoxy adhesive. These specimens were then tested under axial and bending loads to determine their stiffness and strength. The most important attribute of this form of composite material is that it is bidirectional, in contrast to filaments, which are unidirectional. Structural efficiency analyses performed in this investigation showed that the potential weight savings offered by this bidirectional attribute can be significant for applications such as facings for sandwich cylinders and plates subjected to inplane compression, where biaxial stiffness benefits structural stability. Author

19

MATHEMATICS

Includes calculation methods and theory; and numerical analysis. For applications see: 08 Computers.

N68-10121*# National Aeronautics and Space Administration. Marshall Space Flight Center, Huntsville, Ala. THE RUNGE-KUTTA EQUATIONS BY QUADRATURE

METHODS

Joseph S. Rosen Washington NASA Nov. 1967 16 p refs (NASA-TR-R-275) CFSTI: HC\$3.00/MF\$0.65 CSCL 12A

This report gives a basically new approach to the formulation of the classic Runge-Kutta process. Dependence on the tedious Taylor expansions is obviated by a matrix equation which defines the Runge-Kutta equations for any order; furthermore, the elements of these matrices are obtained quite simply. The method of quadratures is used to determine the conditions on the parameters which characterize the process since these parameters determine the order of accuracy of these functions. Author

N68-10355*# National Aeronautics and Space Administration. Ames Research Center, Moffett Field, Calif.

DETERMINATION OF STRESSES IN ELASTIC SOLIDS USING THREE STRESS FUNCTIONS AND THREE EQUATIONS

Robert E. Reed, Jr. Washington NASA Nov. 1967 43 p refs (NASA-TN-D-4253) CFSTI: HC\$3.00/MF\$0.65 CSCL 20K

The classical equations of elasticity in terms of the stress components are reduced to a set of three equations in terms of the three Maxwell stress functions and arbitrary functions of integration. The sufficiency of these equations is due to the interrelationships between the six compatibility equations. The difficulty in choosing the arbitrary functions to fit a particular problem accents the advantages of using the inverse method to find solutions. A family of exact solutions is presented for stresses in a rectangular solid with certain applied stresses on two opposite faces, workless boundary conditions on two opposite faces, and the remaining two faces free of applied stress. Author

N68-11109*# Brown Univ., Providence, R. I. USE OF A TRANSCENDENTAL APPROXIMATION IN TRANSIENT CONDUCTION ANALYSIS

P. D. Richardson and W. W. Smith (Taco, Inc.) Washington NASA Dec. 1967 24 p refs

(Grant NGR-40-002-012)

(NASA-CR-955) CFSTI: HC\$3.00/MF\$0.65

A particular example of a transient conduction problem with a non-linear boundary condition is considered, for which other solutions have been obtained. This example consists of unsteady one-dimensional conduction in a semi-infinite slab with the boundary condition that the heat flux at the surface is proportional to the n-th power of the surface temperature and with the initial condition that the slab temperature is uniform, forming the reference zero (i.e. the zero of an appropriate empirical temperature scale). Solutions for this form of boundary condition are useful for a variety of problems. One practical problem for which they have been used is transient conduction due to unsteady radiation in an enclosure. N68-11494*# National Aeronautics and Space Administration. Langley Research Center, Langley Station, Va. PRODUCTS OF SOME GENERALIZED FUNCTIONS Robert C. Costen Washington Nov. 1967 36 p refs (NASA-TN-D-4244) CFSTI: HC\$3.00/MF\$0.65 CSCL 12A

The purpose of this report is to define a new class of generalized functions which includes products of all members of the class. Application is made to the families of generalized functions derived from tanh nx (hyperbolic tangent family) and from ne^{-n²x²} (Gaussian family), where n is a sequence index and x the independent variable. Elementary uses of the product analysis in physics are also presented. The hyperbolic tangent family of generalized functions has the following features: The Dirac delta functions $\delta_n(x)$ and its derivatives are polynomials in the Heaviside unit step function $H_n(x)$ multiplied by powers of the sequence index n. Conversely, powers of H_n(x) may be expressed as linear sums of $H_n(x)$, $\delta_n(x)$, $\delta'_n(x)$, . . . with coefficients containing powers of n. Products of these generalized functions are similarly expressed either as polynomials in $H_n(x)$ or as linear sums of $H_n(x)$, $\delta_n(x)$, $\delta_n(x), \ldots$ The Gaussian family of generalized functions has analogous features, but products are not the same in the two families. Author

N68-11639*# National Aeronautics and Space Administration. Lewis Research Center, Cleveland, Ohio.

MULTIPLE DECISION PROCEDURES FOR ANOVA OF TWO-LEVEL FACTORIAL FIXED-EFFECTS REPLICATION-FREE EXPERIMENTS

Arthur G. Holms and J. N. Berrettoni (Ph.D. Thesis—Western Reserve Univ.) Washington Dec. 1967 46 $p\ refs$

(NASA-TN-D-4272) CFSTI: HC\$3.00/MF\$0.65 CSCL 12A

For expensive areas of experimentation, such as alloy development, pressure vessel burst testing, and high-temperature protective coatings, the appropriate experiments consist of two-level fixed-effects factorial designs without replication. No adequate procedures have been available for the statistical analysis of such experiments. A procedure called "chain pooling" is introduced for testing the significance of terms of a model equation as fitted to the observations from a fractional factorial experiment. The procedure starts with a small group containing only the smallest of the ordered squared coefficients of the model equation in the denominator of a test statistic. Stepwise testing, in the increasing order of succeeding squared coefficients, pools insignificant squares into the denominator of the statistic, which is used for continued testing. Monte Carlo computations were performed to determine the decision error probabilities for many different variations of chain pooling and to compare the relative advantages of the variations for fractional factorial experiments with 2^4 , 2^5 , and 2^6 treatment combinations. These computations were performed with values of the significant coefficients distributed in such a manner as to contribute to high probabilities of decision errors, so that the recommended procedures Author are good against the worst possible conditions.

19 MATHEMATICS

N68-14077*# National Aeronautics and Space Administration. Marshall Space Flight Center, Huntsville, Ala.

DEVELOPMENT OF A GENERAL FORMULA EXPANDING THE HIGHER-ORDER DERIVATIVES OF THE FUNCTION TANH Z IN POWERS OF TANH Z AND A-NUMBERS Hans H. Hosenthien Washington Jan. 1968 13 p refs

(NASA-TN-D-4396) CFSTI: \$3.00/MF\$0.65 CSCL 12A

A general formula for the rth derivative of the function tanh z with respect to z is developed. This formula is a finite polynominal in powers of tanh z where the coefficients are of simple structure containing A-numbers. The A-numbers, $A_r^{(m)}$, of order m and degree r are introduced as an abbreviation for an expression containing C-numbers which are related to Euler's numbers. A recursion formula the A-numbers and their special properties are derived. The paper contains a tabulation of derivatives of tanh z from the first to the sixth order as well as a table of A-numbers covering all combinations of order and degree from 0 to 10. Author

N68-17334*# National Aeronautics and Space Administration. Langley Research Center, Langley Station, Va. BOUNDS FOR THE EIGENVALUES OF A MATRIX Kenneth R. Garren Washington Mar. 1968 45 p refs

(NASA-TN-D-4373) CFSTI: HC\$3.00/MF\$0.65 CSCL 12A

This paper provides a listing of techniques used to determine the eigenvalue bounds of a matrix defined over either the real or complex fields. Theorems concerning the condition of eigenvalues as a function of the related matrix are stated. Known theorems which determine the bounds are derived. Closed-form solutions are expressed in terms of (1) the matrix elements, (2) matrix norms, and (3) vectors and the eigenvalues of related matrices. Extensions of several results are made to infinite matrices. A comparison is made in terms of the relative size of the areas of eigenvalue inclusion for the various solutions. Examples in terms of eigenvalue bounds for particular matrices are given. Author

N68-17532*# National Aeronautics and Space Administration. Goddard Space Flight Center, Greenbelt, Md.

ON THE POINCARE-VON ZEIPEL AND BROWN-SHOOK METHODS OF THE ELIMINATION OF THE SHORT PERIOD TERMS FROM A HAMILTONIAN

P. Musen Washington Mar. 1968 36 p refs

(NASA-TN-D-4399) CFSTI: HC\$3.00/MF\$0.65 CSCL 12A

A comparison is drawn between the methods of Poincare-von Zeipel and Brown-Shook for the elimination of the short period terms from a Hamiltonian by means of canonical transformations. The general theory is developed, and a table of operators is supplied which serve both to eliminate short period effects of any order and to invert the canonical transformation, i.e., to express the original elements in terms of the elements affected only by the long period perturbations. The generating functions which produce these operators are the Taylor and the Lagrange operators. The Lagrange operator is a generalization of the classical operator to the case of several independent variables. In every attempt to solve the problem of the general perturbations using the electronic machines, the table of differential operators and the recurrence relations between them constitute an essential part of the programming. The elimination of the short period terms seems to be somewhat simpler in the Brown-Shook method than in Poincare-von Zeipel method. Author

N68-18455*# National Aeronautics and Space Administration. Goddard Space Flight Center, Greenbelt, Md.

PLANCK FUNCTIONS AND INTEGRALS-METHODS OF COMPUTATION

Thomas E. Michels Mar. 1968 39 p refs

(NASA-TN-D-4446) CFSTI: HC\$3.00/MF\$0.65 CSCL 20M

Black-body radiation is investigated with emphasis placed on a solution of the Planck integral, which is suitable for computer and hand calculation. A computer program using this method has been included as well as graphs and tables of Planck functions and Planck integrals, which can be used for a wide range of wave numbers, ν , $(=\lambda^{-1})$, and temperatures, T, in degrees Kelvin. A suitable range is: ν from 0.001 to 300,000 cm⁻¹ (λ from 10 meters to 333.3 angstroms) for temperatures between 1°K and 25,000°K.

N68-19144*# National Aeronautics and Space Administration. Langley Research Center, Langley Station, Va.

A NEW METHOD OF TESTING SMALL SAMPLES FOR GOODNESS OF FIT TO NORMAL POPULATIONS

Peter D. Argentiero and Robert H. Tolson Washington Mar. 1968 319 p refs

(NASA-TN-D-4405) CFSTI: HC\$3.00/MF\$0.65 CSCL 12A

The frequency function is derived for a normal population with unknown mean and variance and from which has been chosen a sample of specified size with zero mean and a standard deviation of one. Tables of areas and ordinates of this frequency function for sample sizes between 20 and 170 are provided. The existence of such tables provides a method of testing small samples for goodness of fit to normal populations without the necessity of replacing unknown population parameters with maximum likelihood estimates. Therefore, this method is an improvement of the usual method of testing the hypothesis that a sample has been chosen from a normal population with unspecified mean and variance. An example is given to illustrate the use of the tables.

N88-21100*# National Aeronautics and Space Administration. Marshall Space Flight Center, Huntsville, Ala. MULTI-STEP RUNGE-KUTTA METHODS

Joseph S. Rosen Washington Apr. 1968 23 p refs

(NASA-TN-D-4400) CFSTI: HC\$3.00/MF\$0.65 CSCL 12A

The multi-step methods presented in this report differ from the classic, single-step Runge-Kutta process by utilizing the numerical results of the previous integrations. As developed here, the multi-step process avoids the complex Taylor expansions of the functions involved and instead employs the writer's previously developed method of guadratures.

N68-21978*# National Aeronautics and Space Administration. Ames Research Center, Moffett Field, Calif.

ON THE CONSTRUCTION OF HIGHLY STABLE, EXPLICIT, NUMERICAL METHODS FOR INTEGRATING COUPLED ORDINARY DIFFERENTIAL EQUATIONS WITH PARASITIC EIGENVALUES

Harvard Lomax Washington Apr. 1968 46 p refs

(NASA-TN-D- 4547) CFSTI: HC\$3.00/MF\$0.65 CSCL 12A

A theory is developed for constructing explicit numerical methods for integrating coupled nonlinear ordinary differential equations with local eigenvalues that are greatly separated in magnitude. Applications are made to cases in which large negative eigenvalues are combined with small complex ones. The specific methods derived are compared with Runge-Kutta methods. The derived methods are not considered to be optimum and further improvements are anticipated. Author

N68-22809*# National Aeronautics and Space Administration. Goddard Space Flight Center, Greenbelt, Md. GENERAL LAGRANGIAN INTERPOLATION FORMULAS

19 MATHEMATICS

C. E. Velez Washington May 1968 17 p refs

(NASA-TN-D-4424) CFSTI: HC\$3.00/MF\$0.65 CSCL 12A

The development of high-degree interpolation polynomials which use the values of the function and its subsequent derivatives is discussed. It is shown that if data of this type are available, high-accuracy interpolation is possible under the restrictive conditions of large step-sizes and few data values. Author

N68-24141*# National Aeronautics and Space Administration." Lewis Research Center, Cleveland, Ohio.

A COMPUTER PROGRAM FOR REVERSION OF THE CUMULATIVE BINOMIAL PROBABILITY DISTRIBUTION Darl D. Bien Washington May 1968 13 p refs

(NASA-TM-X-1592) CFSTI: \$3.00 CSCL 12A

A technique for reversion of the cumulative binomial probability distribution and an efficient and rapid computer program using the technique are presented. Reversion of the binomial series is useful in calculating the element success probability in a specified parallel system with redundancy which will yield the specified system success probability (reliability). The program is not limited to reliability problems but can also be used in a variety of scientific and engineering problems involving the reversion of the binomial series. Author

N68-24565*# National Aeronautics and Space Administration. Manned Spacecraft Center, Houston, Tex.

THE DISTRIBUTION AND PROPERTIES OF A WEIGHTED SUM OF CHI SQUARES

A. H. Feiveson and F. C. Delaney Washington May 1968 42 p refs

(NASA-TN-D-4575) CFSTI: \$3.00 CSCL 12A

A study of some of the properties of a weighted sum of chi-square random variables is presented, including the derivation of approximations to the distribution of this sum and an evaluation of the Welch approximation for the distribution of the test statistic in the Behrens-Fisher problem. The study indicates that if equal sample sizes are selected, the Welch approximation to the Behrens-Fisher problem may be safely used. Author

N68-25841*# Innsbruck Univ. (Austria).

LIE SERIES FOR CELESTIAL MECHANICS, ACCELERA-TORS, SATELLITE STABILIZATION AND OPTIMIZATION F. Cap. F. Ehlotzky, D. Floriani, W. Groebner, H. Knapp et al Washington, D. C. NASA May 1968 202 p refs (Grant NGR-52-046-001)

(NASA-CR-1046) CFSTI: HC\$3.00/MF\$0.65 CSCL 12A

An overview is presented on some of the research work done in the field of Lie series and their physical, technical, and practical applications. The following problem areas are considered: (1) solution of a system of n-th order differential equations; (2) solution of differential equations resulting from the separation of Laplace equation in various coordinate systems; (3) numerical computation of satellite orbits; (4) calculation of particle orbits in accelerators; (5) optimization problem of soft landing on the moon with fuel minimization; and (6) equations of motion of satellites. An extensive bibliography of work done using Lie series is also included.

N68-25869*# National Aeronautics and Space Administration. Ames Research Center, Moffett Field, Calif.

A LEAST SQUARES METHOD FOR THE REDUCTION OF . FREE-OSCILLATION DATA

Phillip R. Wilcox and William L. Crawford Washington Jun. 1968 29 p refs

(NASA-TN-D-4503) CFSTI: HC\$3.00/MF\$0.65 CSCL 01A

The classical least squares curve fitting method is used to determine the frequency, amplitude, damping ratio, phase angle, and zero offset of both a one- and two-degree-of-freedom system from free oscillation data. The method is applied to a number of experimental transients with good results. Where possible, comparisons are made with the results of other methods. The least-squares method is found to be particularly useful in the analysis of two-degree-of-freedom systems where other techniques are difficult or impossible to apply. Author

N68-27457*# Pittsburgh Univ., Pa.

LYAPUNOV STABILITY FOR PARTIAL DIFFERENTIAL EQUATIONS. PART 1: LYAPUNOV STABILITY THEORY AND THE STABILITY OF SOLUTIONS TO PARTIAL DIFFERENTIAL EQUATIONS. PART 2: CONTRACTION GROUPS AND EQUIVALENT NORMS

Gabe R. Buis, William G. Vogt, and Martin M. Eisen Washington NASA Jun. 1968 127 p refs

(Grant NGR-39-011-039) (NASA-CR-1100) CFSTI: HC\$3.00/MF\$0.65 CSCL 12A

CONTENTS:

1. LYAPUNOV STABILITY THEORY AND THE STABILITY OF SOLUTIONS TO PARTIAL DIFFERENTIAL EQUATIONS G. R. Buis p 1-113 refs (See N68-27458 16-19)

2. CONTRACTION GROUPS AND EQUIVALENT NORMS W. G. Vogt, M. M. Eisen, and G. R. Buis p 114-122 refs (See N68-27459 16-19)

N68-28240*# National Aeronautics and Space Administration. Lewis Research Center, Cleveland, Ohio.

PLOT3D-A PACKAGE OF FORTRAN SUBPROGRAMS TO DRAW THREE-DIMENSIONAL SURFACES

R. Bruce Canright, Jr. and Paul Swigert Washington Jun. 1968 32 p refs

(NASA-TM-X-1598) CFSTI: HC\$3.00/MF\$0.65 CSCL 12A

PLOT3D is a package of FORTRAN subprograms to draw three-dimensional surfaces of the form z = f(x,y). The function f and the bounding values for x and y are the input to PLOT3D. The surface thus defined by PLOT3D may be drawn after arbitrary rotations. Output is by off-line incremental plotter or on-line microfilm recorder. PLOT3D is completely described along with its limitations, possible future modifications, and poetential uses. Sample output and listings of the subprograms are included. Written entirely in FORTRAN IV, PLOT3D is readily adaptable to other hardware. Author

N68-28281*# National Aeronautics and Space Administration. Ames Research Center, Moffett Field, Calif.

ON THE USE OF ALGEBRAIC METHODS IN THE ANALYSIS AND DESIGN OF MODEL-FOLLOWING CONTROL SYSTEMS

Heinz Erzberger Washington Jul. 1968 31 p refs

(NASA-TN-D-4663) CFSTI: HC\$3.00/MF\$0.65 CSCL 12A

This study gives an analysis of and offers design criteria for three configurations of model following. The three configurations studied are real model following, implicit model following or matching dynamics, and real model following with command inputs. It is assumed that model and plant are described by linear vector differential equations where the equations of the model may be of lower order than those of the plant. Algebraic tests are developed to determine under what conditions a feedback law exists that permits perfect following of the model by the closed-loop plant. The same set of tests is shown to be applicable to both real and implicit model following. This leads to the conclusion that real and implicit model following, although physically different, are

19 MATHEMATICS

mathematically equivalent if no unknown state disturbances or parameter variations occur during the control interval. However, the condition for perfect following with command inputs to the model contains an additional test not present in the first two configurations. If perfect following was shown to be possible, the control law that achieves it is calculated for the implicit model-following configuration. In the general case, this control law must generate both finite and impulse controls if the model is of lower order than the plant. A simple method of approximating the impulse control law to arbitrary accuracy is also given. The theory is illustrated with three examples, two of which are based on the lateral equation of motion of an aircraft.

N68-29275*# National Aeronautics and Space Administration. Ames Research Center, Moffett Field, Calif.

STABLE IMPLICIT AND EXPLICIT NUMERICAL METHODS FOR INTEGRATING QUASI-LINEAR DIFFERENTIAL EQUATIONS WITH PARASITIC-STIFF AND PARASITIC-SADDLE EIGENVALUES

Harvard Lomax Washington Jul. 1968 29 p refs

(NASA-TN-D-4703) CFSTI: HC\$3.00/MF\$0.65 CSCL 12A

Certain classes of coupled, quasi-linear, ordinary, differential equations contain eigenvalues in their associated matrix which make them difficult to integrate by means of conventional numerical differencing schemes, even when the solutions are continuous and nonsingular. Two classes of such parasitic eigenvalues are defined and general ways in which their effects can be suppressed are discussed. Author

N68-29407*# National Aeronautics and Space Administration. Goddard Space Flight Center, Greenbelt, Md.

OPTIMAL COMPUTING FORMS FOR THE TWO-BODY C AND S SERIES

C. R. Herron, E. R. Lancaster, and W. R. Trebilcock Washington Jul. 1968 20 p refs

(NASA-TN-D-4643) CFSTI: HC\$3.00/MF\$0.65 CSCL 12A

The recently developed universal form of the two-body problem involves several transcendental functions. Since these functions are evaluated so frequently, it is worthwhile to develop approximations that minimize the number of arithmetical operations required. This paper presents several such approximations, based on theories of Chebyshev and Knuth, with bounds for the errors incurred when using them. Author

N68-30594*# National Aeronautics and Space Administration. Goddard Space Flight Center, Greenbelt, Md.

A VECTOR APPROACH TO THE ALGEBRA OF ROTATIONS WITH APPLICATIONS

Paul B. Davenport Washington Aug. 1968 25 p refs

(NASA-TN-D-4696) CFSTI: HC\$3.00/MF\$0.65 CSCL 12A

A new type of vector multiplication defines a group (whose elements are vectors) isomorphic to the group of rotations. This allows a vector representation of rotations which has many advantages over the usual matrix or Eulerian angles approach, e.g., this vector representation avoids the need for trigonometric relationships and requires only three independent parameters. Several applications show the simplicity of this vector representation—in particular, an analytic solution to a least squares rotation problem. The differential equations defining the motion of a rigid body are obtained in terms of a vector differential equation. Author

N68-30804*# National Aeronautics and Space Administration. Ames Research Center, Moffett Field, Calif.

CALCULATIONS OF CHANDRASEKHAR'S X- AND Y-FUNCTIONS AND THEIR ANALOGS FOR NONCOHERENT ISOTROPIC SCATTERING Franklyn B. Fuller and B. Jeanne Hyett Washington Aug. 1968 147 p refs

(NASA-TN-D-4712) CFSTI: HC\$3.00/MF\$0.65 CSCL 12A

Results of calculations of the X- and Y-functions of Chandrasekhar, and of their analogs for noncoherent isotropic scattering are given. In the noncoherent work, a Doppler profile is assumed. The results are presented both as tables and in a convenient graphical form, conducive to understanding the behavior of these complicated functions. Moments of the X- and Y-functions are also presented. The method of calculation is based on reduction to the solution of an initial value problem. A simple analytic approximation derived from this method is briefly discussed. Author

N68-31961*# National Aeronautics and Space Administration. Lewis Research Center, Cleveland, Ohio.

AN EFFICIENT METHOD FOR COMPUTATION OF CHARACTER TABLES OF FINITE GROUPS

Gabriel Allen Washington Aug. 1968 29 p refs

(NASA-TN-D-4763) CFSTI: HC\$3.00/MF\$0.65 CSCL 12A

A systematic procedure is presented for constructing the character table of a given finite group. The use of this procedure makes the task of computing group character tables more straightforward than previously published procedures. Each step in the construction of the character tables is illustrated by worked out examples. Group tables, character tables, and class algebra tables for many of the common finite groups are included. Author

N68-33245*# National Aeronautics and Space Administration, Washington, D. C.

NUMERICAL ANALYSIS—ABSTRACTS OF PRESENTATIONS Raymond H. Wilson, Jr., ed. 1968 46 p refs Abstracts of papers presented at a workshop meeting on numerical analysis, held in Washington, D. C., 29–30 Jan. 1968

(NASA-SP-170) CFSTI: HC\$3.00/MF\$0.65 CSCL 12A

Abstracts are presented for the 34 papers given at a NASA workshop on numerical analysis applications to aerospace and related problems. Included are topics such as the integration of lunar motion, calculation of atmospheric properties, techniques for determining thermal radiation, nonlinear methods in aeroelasticity, and evaluation of the geopotential forces for an orbital ephemeris with given high-order harmonics. Other topics deal with heat transfer of a finned spacecraft cylinder, orbital lifetime predictions, optimization problems, and stress analysis. Papers also consider application of the convolution integral, series representations, Bairstow's method, potential theory, and error bounds for real roots. A Heuristic integration program is discussed as are Frechet and other derivatives in a Banach space, multidimensional integrals, truncation errors, biharmonic analysis, and use of the Householder algorithm for solving linear least squares problems. Nonlinear transformations, a boundary value problem solution, and certification of library subroutines are also treated. M.W.R.

N68-33426*# Pennsylvania State Univ., University Park. DIFFERENTIAL SYSTEMS

Robert Bradley McNeill Washington NASA Aug. 1968 61 p refs

(Grant NGR-39-009-041)

(NASA-CR-1164) CFSTI: HC\$3.00/MF\$0.65 CSCL 12A

An attempt is made to secure a comprehensive theory for linear and nonlinear differential systems under most general conditions. A generalized form of Bellman's fundamental lemma and the correct proof of Lagrange's variation of parameters formula is presented. Linear systems were studied with respect to the sets beta and zeta. Here an important necessary and sufficient theorem of Conti was generalized. Moreover, a stronger sufficiency theorem was shown, even though one of the original conditions was dropped. This allowed an obvious extension to the set zeta, which was unattainable via the original theorem. Nonlinear systems are studied by means of their accompanying integral equations. A converse theorem to a standard result is given. The concept of one vector being bounded with respect to another vector is introduced, and a series of theorems concerning this definition follows. Sharper upper bounds were derived. Finally, Lagrange's variation of parameters formula was extended to a certain class of nonlinear systems. Oscillation theorems are presented in order to strengthen previous derivations. Author

N68-35472*# TRW Systems Group, Redondo Beach, Calif. MATHEMATICAL PROBLEMS OF MODELING STOCHASTIC NONLINEAR DYNAMIC SYSTEMS

Richard E. Mortensen Washington NASA Sep. 1968 53 p refs

(Contract NAS2-4553)

(NASA-CR-1168) CFSTI: HC\$3.00/MF\$0.65 CSCL 12A

The purpose of this report is to introduce the engineer to the area of stochastic differential equations and to point out some of the mathematical techniques and pitfalls in this area. Topics discussed include continuous-time Markov processes, the Fokker-Planck-Kolmogorov equations, the Ito and Stratonovich stochastic calculi, and the problem of modeling physical systems. Author

N68-36525*# National Aeronautics and Space Administration. Lewis Research Center, Cleveland, Ohio.

ITERATED COMMUTATORS AND FUNCTIONS OF OPERATORS

Howard C. Volkin Washington Oct. 1968 18 p refs

(NASA-TN-D-4857) CFSTI: HC\$3.00/MF\$0.65 CSCL 12A

A new method is developed by which certain functions of the noncommuting operators A and B can be expressed in a systematic and efficient way in terms of successively higher commutators of the operators. The procedure is designed primarily for polynomials, exponential functions, and analytic functions of the operator (A + B). The method is related to the ordered-operator calculus of Feynman. Certain commutation properties of the operators A and B are represented by polynomials in A and B called iterated commutators. The functions are converted into equivalent forms involving the iterated commutators. All iterated commutators of degree (j + 1) in A and B are combined in a suitable sum to form a new operator $G_{(j)}$. By working only with the $G_{(j)}$ and their commutators, the calculations are simplified and the results are given in an extremely compact notation. Author

N68-36753*# National Aeronautics and Space Administration. Marshall Space Flight Center, Huntsville, Ata.

CLASSICAL FIFTH-, SIXTH-, SEVENTH-, AND EIGHTH-ORDER RUNGE-KUTTA FORMULAS WITH STEPSIZE CONTROL

Erwin Fehlberg Washington Oct. 1968 87 p refs

(NASA-TR-R-287) CFSTI: HC \$3.00 /MF \$0.65 CSCL 12A

In this paper we shall derive classical Runge-Kutta formulas of the fifth, sixth, seventh, and eighth order including a stepsize centrol procedure which is again based on a complete coverage of the leading local truncation error term. Naturally, these new formulas require more evaluations per step of the differential equations than the known classical Runge-Kutta formulas without stepsize control procedure. Author N68-37073*# National Aeronautics and Space Administration. Langley Research Center, Langley Station, Va.

A COMBINED NEWTON-RAPHSON AND GRADIENT PARAMETER CORRECTION TECHNIQUE FOR SOLUTION OF OPTIMAL-CONTROL PROBLEMS

Ernest S. Armstrong Washington Oct. 1968 64 p refs

(NASA-TR-R-293) CFSTI: HC\$3.00/MF\$0.65 CSCL 12A

A parameter correction technique is developed to solve a boundary value problem which frequently occurs in optimal control theory. It is assumed that an indirect optimal control method was applied to a controllable dynamic system with a two point boundary value problem resulting such that the boundary conditions take the form of a set of unknown parameters to be determined to meet an equal number of terminal conditions. The optimal control law is a piecewise continuous function with discontinuities occurring only at the zeros of certain continuous functions. A procedure is developed to improve upon an assumed set of parameters so that, by repetitive use of a correction formula, a monotonic decreasing sequence of values of a positive definite function that measures the terminal errors is produced. The direction of the correction vector is found to lie between the directions given by the gradient and the Newton-Raphson procedures. The procedure is applied to the determination of both planar and non-planar fuel optimal trajectories for a space vehicle which is launched from the surface of the moon and required to rendezvous with a space vehicle in a circular orbit. Author

20 METEOROLOGY

Includes climatology; weather forecasting; and visibility studies. For related information see also: 13 Geophysics; and 30 Space Sciences.

N68-10222* National Aeronautics and Space Administration. Goddard Space Flight Center, Greenbelt, Md.

AN EVALUATION OF SEA SURFACE TEMPERATURE AS MEASURED BY THE NIMBUS I HIGH RESOLUTION INFRARED RADIOMETER

Lewis J. Allison and James S. Kennedy (USAF) Washington NASA Nov. 1967 27 $p\ refs$

(NASA-TN-D-4078) CFSTI: \$3.00 CSCL 04B

An analysis of Nimbus I HRIR data over various parts of the world indicated limited success in deriving sea surface temperatures to within 3° to 6°K of aircraft radiation measurements (8-13 μ) and synoptic-climatological ship sea surface temperature data. At night, thin clouds which may fill the radiometer's field of view make it difficult to interpret the absolute values of derived sea surface temperature. During the daytime, the HRIR data is unusable for oceanographic temperature analysis because the contamination by reflected solar radiation mixes with the emitted radiation. Future satellite instrumentation, consisting of a HRIR radiometer (10–11 μ) when used in conjunction with television data, will delineate cloud free ocean areas and permit the daily derivation of sea surface temperatures from approximately 10 to 30% of the world's oceanic regions. Author

N68-17024*# National Aeronautics and Space Administration. Langley Research Center, Langley Station, Va.

WIND VELOCITY PROFILES MEASURED BY THE SMOKE-TRAIL METHOD AT WALLOPS ISLAND, VIRGINIA, 1963 AND 1964

Robert M. Henry and Robert W. Miller Washington Mar. 1968 111 p refs

(NASA-TN-D-4365) CFSTI: HC\$3.00/MF\$0.65 CSCL 04B

Forty-five detailed profiles were obtained for heights from 0.5 to 30 km. Two second-stage profiles for heights from 39 to 58 km are also included. The profiles cover all seasons, and the characteristics are generally similar to those of previously published smoke-trail profiles. Wind velocities in excess of the 99-percent extreme value are included. Closely spaced soundings show only small variations over horizontal distances of 2 km and time intervals of 1-1/2 hours.

N68-18246*# National Aeronautics and Space Administration. Langley Research Center, Langley Station, Va.

WIND DATA FROM THE 250-FOOT (76.2-METER) TOWER AT WALLOPS ISLAND, VIRGINIA

James A. Cochrane and Robert M. Henry Washington Mar. 1968 46 p refs

(NASA-TN-D-4395) CFSTI: HC \$3.00/MF \$0.65 CSCL 04B

A nearly continuous 3-1/2 year sample of low-level wind data has been collected from anemometers mounted at five levels on the 250-foot meteorological tower at Wallops Island, Virginia. Fifteen-minute averages of speed and direction were read out at hourly intervals. The statistical treatment and the homogeneity of the sample are discussed. Two types of statistical information--frequency-distribution data and statistical parameters---were computed from the sample. The frequency-distribution information is of three types: (1) percentage probabilities of being less than or equal to a given value of wind speed; (2) wind-speed limits for selected percentiles; and (3) frequency of speed-direction groups. The tabulation of fundamental statistical parameters provides further information on specific properties of the wind distribution. The parameters are presented for various combinations of hourly, monthly, and annual periods. The statistical data included in this report provide the best available information on the low-level wind environment and should be useful for establishing design criteria and supporting launch operations. Author

N68-19084*# National Aeronautics and Space Administration. Langley Research Center, Langley Station, Va.

MEASUREMENTS OF WINDS AND TEMPERATURES AT ALTITUDES UP TO 65 KILOMETERS IN THE SOUTHERN HEMISPHERE

James C. Manning and Lloyd W. Chamberlain (Weather Bur., Wallops Sta., Va.) Washington Mar. 1968 61 p refs (NASA-TN-D-4429) CFSTI: HC\$3.00/MF\$0.65 CSCL 04B

Meteorological data from 27 rocketsonde and corresponding radiosonde soundings off the west coast of South America are presented as plots of temperature and wind as functions of altitude. The wind data are shown in plots of west-to-east and south-to-north velocity components. Summary time and space cross sections of the data are also shown. Author

N68-20375*# National Aeronautics and Space Administration. Ames Research Center, Moffett Field, Calif. INVESTIGATION OF AIR-FLOW VELOCITY BY LASER

BACKSCATTER

Kent R. Bourquin and Fred H. Shigemoto Washington Apr. 1968 23 p refs

(NASA-TN-D-4453) CFSTI: HC\$3.00/MF\$0.65 CSCL 04B

An investigation of laser light backscatter properties from an atmosphere emphasized the effect of frequency shift. The detection scheme described is based on this effect and proved successful in the laboratory determination of flow velocity of a contaminated atmosphere. The results agree well with measurements taken with a hot wire anemometer. This investigation used a continuous wave laser radiating in the visible region. The velocity of an air stream containing a small concentration of contaminants was measured. Using this technique to detect clear air turbulence would require that Mie scattering predominate in the turbulent region. This technique does not presently appear practical for airborne detection of clear air turbulence considering the available laser transmitters and detectors, and the uncertain knowledge of the contaminating particle content in a turbulent region.

20 METEOROLOGY

N68-24020 Federal Aviation Administration, Atlantic City, N. J. National Aviation Facilities Experimental Center. CLEAR AIR TURBULENCE: A BIBLIOGRAPHY, 1950–1967

Final Report

Dorothy E. Bulford Mar. 1968 82 p refs (NA-68-17; AD-667731)

Clear air turbulence encounters can occur unexpectedly without any visual evidence or warning. As operations of higher altitude aircraft increase, the phenomenon is encountered more often. Clear air turbulence is defined as all turbulence in the free atmosphere of interest in aerospace operations that is not in or adjacent to visible convective activity (this includes turbulence found in cirrus clouds not in or adjacent to visible convective activity). This bibliography consists of 578 references to technical reports, articles in periodicals, and books published during the past 17 years. References about other forms of turbulence such as that occurring with storms and airplane wake vortices are not included. Author (TAB)

N68-25617*# National Aeronautics and Space Administration. Goddard Space Flight Center, Greenbelt, Md.

SOME METEOROLOGICAL OBSERVATIONS OF THE SOUTHERN HEMISPHERE STRATOSPHERE AND MESOSPHERE

J. S. Theon and J. J. Horvath (Mich. Univ., Ann Arbor) Washington Jun. 1968 12 p refs

(NASA-TN-D-4264) CFSTI: HC\$3.00/MF\$0.65 CSCL 04B

A sea-going experiment was carried out in 1965 to obtain rocket sounding measurements from the atmosphere of the Southern Hemisphere along the west coast of South America from the equator to 60°S. Results are presented for eight Nike Apache pitot-type tube experiments, which were among the 77 rocket soundings taken. Temperature structures in the Southern Hemisphere stratosphere and mesosphere were somewhat different from their Northern Hemisphere counterparts during the corresponding season; and, especially at temperate latitudes, the Southern Hemisphere upper atmosphere was characterized by a warmer stratopause and a colder mesopause. The geostrophic approximation provided a reasonably accurate means for obtaining winds up to 70 km altitude, and zonal wind patterns in this region were characterized by an easterly core centered at 30 to 35 km above the tropics as well as westerly flow that increased with latitude and altitude to a maximum of 60 km above 60°S. This circulation was associated with the developing winter polar vortex. MWR.

N68-25816*# Cornell Aeronautical Lab., Inc., Buffalo, N. Y. INVESTIGATION OF WARM FOG PROPERTIES AND FOG MODIFICATION CONCEPTS

Warren C. Kocmond and James E. Jiusto Washington, D. C. NASA Jun. 1968 70 p refs

(Contract NASr-156)

(NASA-CR-1071; CAL-RM-1788-P-17) CFSTI: HC \$3.00/MF \$0.65 CSCL 04B

Analytical and experimental investigations were conducted to examine the concept of modifying fog with hygroscopic material. The results indicate that it is possible to improve visibility in warm fog by seeding with micron-size salt particles (NaCl). The visibility in laboratory fog (produced in a 600 m³ chamber) was increased by factors of three to ten, with as little as 1.7 mg of NaCl m $^{-3}$ being effective. Only modest reductions (<1%) in ambient relative humidity were involved. Extrapolation of these results suggests that clearing a suitable landing zone for aircraft would not involve prohibitive amounts of seeding material. Recommendations are made for field testing the concept. Laboratory experiments also suggest that the formation of fog can be modified by seeding the atmosphere with salt nuclei prior to fog formation. While visibility improvements of a factor of two were achieved in the laboratory, the concept appears less practical for field use. An improved cloud nucleus chamber of the thermal gradient diffusion type was

designed and is described together with results of a third year of observations. A "haze chamber" for measuring the concentrations of large and giant nuclei is discussed. Author

N68-33036*# National Aeronautics and Space Administration. Goddard Space Flight Center, Greenbelt, Md.

TEMPERATURE, PRESSURE, DENSITY, AND WIND MEASUREMENTS IN THE STRATOSPHERE AND MESOSPHERE, 1966

W. S. Smith, J. S. Theon, P. C. Swartz, L. B. Katchen, and J. J. Horvath (Mich. Univ., Ann Arbor) Washington Aug. 1968 94 p refs

(NASA-TR-R-288) CFSTI: HC\$3.00/MF\$0.65 CSCL 048

Complete data are presented from a total of 43 rocket-borne experiments conducted at Wallops Island, Virginia: Churchill, Canada; Barrow, Alaska; Natal, Brazil; and Ascension Island in the South Atlantic Ocean during 1966. Temperature, pressure, density, and wind profiles from 39 grenade experiments, and temperature, pressure, and density profiles from four pitot static tube experiments covering the altitude range of approximately 30 to 90 kilometers have been compiled. No attempt has been made to analyze the meteorological significance of these data in this report. Error analyses are included for the results of each of the 39 grenade experiments. Author

N68-37869*# National Aeronautics and Space Administration. Goddard Space Flight Center, Greenbelt, Md.

A SATELLITE VIEW OF TYPHOON MARIE 1966 DEVELOPMENT

G. Warnecke, L. J. Allison, E. R. Kreins (Environ. Tech. Appl. Center) and L. M. McMillin (Allied Res. Assoc., Inc., Concord, Mass.) Nov. 1967 98 p 13 refs

(NASA-TN-D-4757) CFSTI: HC\$3.00/MF\$0.65 CSCL 04B

A complete documentation of Nimbus II High Resolution Infrared Radiometer data and ESSA-3 photographs is presented for the life-time of Typhoon Marie 1966. Particular emphasis was given to the earliest stages of noticeable storm development. The interpretation of the satellite data in combination with the sparse conventional observations from the central Pacific Ocean revealed meteorological conditions in the development area which are commonly found necessary for tropical storm development. Author

21 NAVIGATION

Includes guidance; autopilots; star and planet tracking; inertial platforms; and air traffic control. For related information see also: 07 Communications.

N68-11146* National Aeronautics and Space Administration. Electronics Research Center, Cambridge, Mass.

NUMERICAL STUDIES OF TRANSITIONS BETWEEN THE RESTRICTED PROBLEM OF THREE BODIES AND THE PROBLEM OF TWO FIXED CENTERS AND THE KEPLER PROBLEM

R. F. Hoelker Washington NASA Nov. 1967 33 p refs (NASA-TM-X-1465) CFSTI: \$3.00 CSCL 22C

For the comparison of the trajectories of the two fixed-center problem with those of the restricted problem of three bodies. fields of trajectories are numerically computed for six initial position conditions, all starting on the line of masses and perpendicularly to this line. The transition is studied by varying stepwise, for these fields, the rate of revolution of the primaries from zero to the equilibrium rate of circular motion. For the investigation of the behavior of trajectories in the transition from the Kepler problem to the restricted problem, the Kepler orbits are considered in a coordinate system rotating at the rate determined by the continuation of this system into that of the restricted problem. Transition characteristics are shown on samples of periodic orbits and of trajectory fields. In particular, the continuous transition of a family of Kepler orbits into periodic orbits about the smaller primary as well as about the L3-libration point is demonstrated. Author

N68-11521*# National Aeronautics and Space Administration. Langley Research Center, Langley Station, Va.

MIDCOURSE-GUIDANCE PROCEDURE WITH SINGLE POSITION FIX OBTAINED FROM ONBOARD OPTICAL MEASUREMENTS

Harold A. Hamer, Katherine G. Johnson, and W. Thomas Blackshear Washington NASA Dec. 1967 83 p refs

(NASA-TN-D-4246) CFSTI: HC\$3.00/MF\$0.65 CSCL 17G

A manual procedure is developed for midcourse-guidance application. The procedure required only limited onboard calculations and leads to guidance predictions sufficiently accurate for emergency or backup operations. Although high accuracy cannot be obtained by manual methods as compared with automatic methods, the accuracy of the present method is shown to be adequate to the point where a terminal guidance system could take over with relatively simple equipment. The method is applied to Earth-Moon trajectories and is studied in detail for an example lunar mission. Basically, the determination of only one position fix is required rather than the determination of a large number of position fixes as is usually required in any manual or automatic procedure. This condition is made possible by use of precalculated data which linearly relate deviations from the nominal trajectory at the time of the position fix to those farther along the trajectory. This procedure is especially important for lunar missions where time is limited for making measurements and calculations prior to the first midcourse maneuver. The effects on aim-point accuracy of measurement errors, maneuver errors, star selection, and linear approximation are discussed. Author

N68-11902*# National Aeronautics and Space Administration. Ames Research Center, Moffett Field, Calif.

FACTORS AFFECTING THE DESIGN AND USE OF A PHOTOGRAPHIC SEXTANT FOR SPACE NAVIGATION

Thomas M. Walsh Washington Dec. 1967 37 p refs (NASA-TN-D-4285) CFSTI: HC\$3.00/MF\$0.65 CSCL 17G

A study was made of design and use factors that are pertinent to the fabrication of a photographic instrument for obtaining sextant-type data and for providing target star identification information. The objective was to adapt the highly accurate techniques of astronomical photography and film readout to the space cabin environment. Of all the factors studied, the film was the most critical. Currently available emulsions lack either resolution, speed, or ease of development. Improvements in this area are expected and in the near future there should be no serious obstacles to sextant feasibility. However, current emulsions, if made available on flat glass plates, will suffice for sextant measurements that do not require landmark targets. Five basic sextant configurations are examined and one hardware concept is presented. A photographic sextant should be considered a serious alternative as a navigation instrument with a probable precision of better than 10 seconds of arc, with the added capability of providing data for target star identification. Author

N68-11949*# National Aeronautics and Space Administration. Langley Research Center, Langley Station, Va.

PRELIMINARY INFRARED HORIZON PROFILES FROM PROJECT SCANNER

Thomas B. McKee, Ruth I. Whitman, and Richard E. Davis Washington Dec. 1967 25 p refs

(NASA-TM-X-1483) CFSTI: HC\$3.00/MF\$0.65 CSCL 17G

Measured horizon radiance profiles in spectral bands of 615 cm⁻¹ to 715 cm⁻¹ (CO₂) and 315 cm⁻¹ to 475 cm⁻¹ (H₂O) from Project Scanner flight of August 16, 1966, are shown. Excellent agreement between measured and analytically predicted rádiance profiles in the CO₂ region verifies the analytical technique to within the experimental accuracy. The agreement of measured with predicted profiles and the lack of dependence on presence of clouds indicate the 615 cm⁻¹ to 715 cm⁻¹ region is a good candidate for use in attitude determination applications. Horizon profiles in the 315 cm⁻¹ to 475 cm⁻¹ region show a strong dependence on the presence of clouds which indicates that the spectral region would be a poor one for attitude determination applications.

N68-13558* National Aeronautics and Space Administration. Ames Research Center, Moffett Field, Calif.

NAVIGATOR PERFORMANCE USING A HAND-HELD SEXTANT TO MEASURE THE ANGLE BETWEEN A MOVING FLASHING LIGHT AND A SIMULATED STAR Bedford A. Lampkin Washington Jan. 1968 41 p refs

(NASA-TN-D-4174) CFSTI: \$3.00 17G

The performance of a navigator using a hand-held sextant was investigated. The primary variables were the rate of angular motion of the flashing light and the frequency and on time characteristics of the flashing light. Performance criteria were the standard deviation of the measurement data and the bias of the measured angle compared to the true angle. Measurements were made from a stationary sighting station and from a sighting station simulating spacecraft oscillatory motion. An effective technique was developed for training navigators to measure accurately with a sextant. This technique uses measurement error feedback to the operator subsequent to each measurement to inform him of his error and to aid him in improving his subsequent measurements. The performance during this experiment indicates that an experienced navigator using a hand-held sextant during rendezvous navigation may obtain data with an accuracy of better than 60 arc seconds. Author

N68-14732*# National Aeronautics and Space Administration. Langley Research Center, Langley Station, Va.

A STUDY OF THE EFFECT OF MEASUREMENT ERRORS UPON A RANGE CONTROLLER FOR AN ENTRY VEHICLE Jack A. White Washington Jan. 1968 32 p refs

(NASA-TN-D-4317) CFSTI: HC \$3.00/MF \$0.65 CSCL 17G

A study of a range controller for an entry vehicle has been made. Three basic path trajectories to simulate short-range entries, medium-range entries, and long-range entries requiring a skip maneuver were selected for the study. The range controller used a bang-bang control during the initial dive into the atmosphere and during the pull-up phase for medium- or long-range entry. Control during the other phases of the trajectory was achieved by a linear-type controller that is dependent upon the solution of desired altitude as a function of desired range. A random number procedure was used to determine the effect of random errors in measuring the vehicle velocity, altitude, and rate of change of altitude upon the effectiveness of the range controller to control the vehicle to the desired range. Results of this study show that the range controller was able to control the vehicle from the entry point for angular ranges varying from 18° to 250° The controller had about the same sensitivity to measurement errors for Author

medium-range and long-range entries.

N68-16836*# National Aeronautics and Space Administration. Manned Spacecraft Center, Houston, Tex.

LUNAR MODULE PILOT CONTROL CONSIDERATIONS

Clarke T. Hackler, James R. Brickel, Herbert E. Smith, and Donald C. Cheatham Washington Feb. 1968 46 p refs

(NASA-TN-D-4131) CFSTI: HC\$3.00/MF\$0.65 CSCL 05H

The role of the pilot in control of the lunar module during the lunar landing mission is discussed. A brief description is given of the lunar module mission phases and the lunar module and its primary and backup guidance, navigation, and control systems. The pilot interfaces with the control system are also discussed. The various simulation studies and flight tests that have been conducted are reviewed. The reasons for the departure from a near-fuel-optimum trajectory and the several aspects of shaping the trajectory for visibility and other piloting considerations following this departure are analyzed. Finally, the primary areas of pilot control in the various phases are examined in detail and are related to such areas of concern as guidance monitoring, landing site inspection and change, landing, engine shutdown, terminal rendezvous, and docking.

N68-18484*# Stanford Research Inst., Menlo Park, Calif. STUDY AND APPLICATIONS OF RETRODIRECTIVE AND SELF ADAPTIVE ELECTROMAGNETIC-WAVE PHASE CONTROLS TO A MARS PROBE

C. A. Hacking, R. B. Battelle, C. H. Dawson, R. C. Kunzelman, J. A. Martin et al Washington NASA Mar. 1968 231 p refs

(Contract NAS2-2933)

(NASA-CR-977) CFSTI: HC\$3.00/MF\$0.65 CSCL 17B

A theoretical study has been made of several aspects of communication by means of adaptive antenna techniques, from the earth to an interplanetary vehicle (bus), and between the bus and a smaller vehicle (capsule) launched from the bus to land on a planet. The study has been restricted to some of the antenna problems associated with such a communication system, particularly where the vehicle is spin-stabilized. The environment to be expected near a planet, particularly Mars, and its effects on the operation of an adaptive system is discussed in some detail. Consideration is given to the various phenomena associated with atmospheric entry, including plasma, atmospheric inhomogeneities, voltage breakdown, and so forth. Four separate antenna configurations that might be suitable for use on a spinning vehicle were investigated theoretically. Particular attention was paid to the retrodirective mode of operation. Several computer programs were written to analyze various aspects of these antennas. It is shown that the effect of spectral splitting can probably be made negligible by careful design of the antenna and adaptive circuitry. Author

N62-19061*# National Aeronautics and Space Administration. Ames Research Center, Moffett Field, Calif.

SATURN 5 MANUAL BACKUP GUIDANCE AND CONTROL PILOTED SIMULATION STUDY

Richard L. Kurkowski and Gordon H. Hardy Washington Mar. 1968 29 p refs

(NASA-TN-D-4481) CFSTI: HC\$3.00/MF\$0.65 CSCL 17G

Fixed base simulation studies of manual backup guidance and control for the Saturn V have been conducted. A manual attitude trim control system was devised using the spacecraft inertial platform and command module computer to provide a backup attitude control loop. The guidance loop was provided by the pilot who observed digital displays of trajectory parameters, compared them with nominal values, and input controller commands to bias vehicle attitude. Another backup system called the rate command system fed the pilot controller commands directly to the launch vehicle where they were summed with the launch vehicle rate gyro output. The two backup systems were evaluated first for upper stage guidance and control, from second stage ignition to earth orbit injection. The results indicate that either system could be used effectively to guide the vehicle into earth orbit. Evaluation of these two systems for the first stage flight showed that the rate command system was not suitable because the direct on-off signal from the controller adversely affected the sloshing and bending dynamics of the vehicle. The attitude trim system, however, was suitable for first stage control. Author

N68-19236*# National Aeronautics and Space Administration. Ames Research Center, Moffett Field, Calif.

SIMPLE PROCESSORS OF STAR TRACKER COMMANDS FOR STABILIZING AN INERTIALLY ORIENTED SATELLITE Robert D. Showman, Brian F. Doolin, and G. Michael Sullivan

Washington Mar. 1968 66 p refs

(NASA-TN-D-4490) CFSTI: HC\$3.00/MF\$0.65 CSCL 17G

The study develops processors which convert star tracker gimbal angle measurements to satellite attitude control signals. An exact processor is nonlinear and complex because the gimbal angles vary as the inertial orientation of the vehicle changes. In this paper, approximations to the exact processor are developed which greatly simplify the mechanization and yet allow satisfactory attitude control. Three approximate processors are derived from a perturbation analysis in which only the first-order terms are considered significant. The use of the three processors to derive attitude control signals for an example satellite such as the Orbiting Astronomical Observatory is investigated.

N68-21123*# National Aeronautics and Space Administration. Ames Research Center, Moffett Field, Calif.

NAVIGATOR PERFORMANCE STUDIES FOR SPACE NAVIGATION USING THE NASA CV-990 RESEARCH AIRCRAFT

Richard A. Acken and Donald W. Smith Washington Apr. 1968 20 p refs

(NASA-TN-D-4449) CFSTI: HC\$3.00/MF\$0.65 CSCL 17G

Manually operated hand-held sextants are being studied to determine whether they are sufficiently accurate for midcourse navigation phases of manned space flight. Studies carried out on the ground have been extended by using the NASA CV-990 aircraft to provide sighting conditions closely simulating those in spacecraft and to investigate further the measurement error due to lunar irradiance. The results of approximately 1200 measurements made during nine flights confirm results of simulator and ground-based studies which indicate that, with a hand-held sextant, an astronaut can be expected to make navigational measurements with errors having a standard deviation of approximately ± 10 arc seconds. A value for moon irradiance effect of approximately 25 arc seconds was established for the conditions of the experiment using a hand-held sextant. Author

N68-21366*# National Aeronautics and Space Administration. Langley Research Center, Langley Station, Va.

SIMULATOR STUDY OF PILOT CONTROL OVER THE LUNAR MODULE DURING ASCENT FROM THE LUNAR SURFACE BY USING VISUAL GUIDANCE CUES

Herman S. Fletcher, L. Keith Barker, and Gary P. Beasley Washington Apr. 1968 33 p refs

(NASA-TM-X-1549) CFSTI: HC\$3.00/MF\$0.65 CSCL 05H

A fixed-base simulator study was conducted to determine the ability of pilots to use a simple, visually guided piloting procedure to inject the ascent stage of the lunar module into a safe transfer orbit which had an apocynthion altitude of 80 nautical miles (148.16 kilometers). The pilot had control of the thrust along the longitudinal axis by means of an on-off switch and of the vehicle attitude by means of a rate-command or a rate-command-attitude-hold control system. The guidance procedure required the pilot to maintain three consecutive constant angles between the thrust axis and the line of sight to the down-range horizon, and to use an integrating accelerometer to indicate when to change the vehicle pitch attitude and when to terminate the thrust. While the tasks required for a simulated launch and transfer-orbit injection were performed by using visual references for guidance, resulting transfer orbits depended on the thrust alignment with the center of gravity and the type of control system. Appreciable pilot-control problems were created when the rate-command control system was used in combination with thrust misalignment, nonvertical-launch effects were of no consequence and easily controlled, and thrust errors as large as 2 percent did not affect the safety of the ascent. Author

N68-21652*# United Aircraft Corp., Farmington, Conn.

A STUDY OF THE CRITICAL COMPUTATIONAL PROBLEMS ASSOCIATED WITH STRAPDOWN INERTIAL NAVIGATION SYSTEMS

Washington NASA Apr. 1968 217 p refs

(Contract NAS12-91)

(NASA-CR-968: SCR-328-1) CFSTI: HC \$3.00/MF \$0.65 CSCL 17G

A detailed and comprehensive evaluation of the computational processes of strapdown inertial navigators are reported; the computational requirements and error sources are defined, and analytic models of the computational errors are developed. The analytic computational error models were developed with the aid of detailed digital simulations of the flight environment, the strapdown inertial sensors, the computer hardware and the numerical processes. The strapdown computational processes investigated were the determination of attitude, the resolution of accelerometer data into the inertial frame and the computation of position. Author

N68-21754*# National Aeronautics and Space Administration. Manned Spacecraft Center, Houston, Tex.

NAVIGATION AND GUIDANCE ANALYSIS OF A MARS PROBE LAUNCHED FROM A MANNED FLYBY SPACECRAFT Thomas B. Murtagh, Flora B. Lowes, and Victor R. Bond Washington Apr. 1968 70 p refs

(NASA-TN-D-4512) CFSTI: HC\$3.00/MF\$0.65 CSCL 17G

This study was initiated with the probe and spacecraft separation at the Mars sphere of influence and was terminated with the probe arrival at a specified entry altitude and the spacecraft arrival at Mars periapsis. The disclosures of the study indicate that the results are decidedly dependent on the initial spacecraft errors at the time of separation and on the system model errors assumed when processing navigation data. Author N68-23377*# National Aeronautics and Space Administration. Langley Research Center, Langley Station, Va. APPLICATION OF MAXIMUM LIKELIHOOD TECHNIQUES TO THE DESIGN OF OPTIMUM STAR TRACKERS Edwin C. Foudriat Washington May 1968 28 p refs (NASA-TN-D-4549) CFSTI: HC\$3.00/MF\$0.65 CSCL 17G

An analytical method was developed for the design of optimum star trackers. In the method both the measurement procedure and the measurement processing-the estimation of the star parameters from the measurement samples-are optimized. The method for measurement processing is based upon the use of maximum likelihood techniques. The equations to be satisfied for estimation of the position and intensity of a star are given with the assumption that the photoelectrons leaving the cathode obey Poisson statistics. With the properties of the maximum likelihood method and the Cramér-Rao inequality, a technique is developed for optimization of the measurement procedure. General equations are derived for the optimum measurement position on the cathode. The procedure is applied to the design of a slit-type star tracker where it is desired to determine the x position of a star image with a Gaussian intensity distribution. The results indicate the star-tracker slit width should be based upon star image size and be independent of star-to-background intensity ratio. The measurement procedure indicates sample should be made along the limb of the star image. Author

N68-24409*# National Aeronautics and Space Administration. Lewis Research Center, Cleveland, Ohio.

STABILITY ANALYSIS AND MINIMUM THRUST VECTOR CONTROL REQUIREMENTS OF BOOSTER VEHICLES DURING ATMOSPHERIC FLIGHT

Janos Borsody and Fred Teren Washington May 1968 44 \ensuremath{p} ref

(NASA-TN-D-4593) CFSTI: HC\$3.00/MF\$0.65 CSCL 17G

Generalized analytic results are derived to give a complete description of an open-loop minimal control requirement to maintain stability for a rigid-body vehicle configuration. The results are easily applicable to both pitch and yaw control planes at any flight time of interest by computing some vehicle dependent parameters and evaluating the given equations. The results show that, with good control system design, the deflection requirements can be reduced to about 56 percent of trim deflection. At the same time, because of the method of control, the maximum angle of attack and bending moments can also be substantially reduced. Author

N68-24512*# National Aeronautics and Space Administration. Ames Research Center, Moffett Field.

A HAND-HELD SEXTANT QUALIFIED FOR SPACE FLIGHT Bedford A. Lampkin and Donald W. Smith Washington May

1968 31 p refs

(NASA-TN-D-4585) CFSTI: HC\$3.00/MF\$0.65 CSCL 17G

A hand-held sextant has been developed and fabricated for use in space navigation. The instrument is space-flight rated. Experienced operators may obtain measurement data having an accuracy of better than 10 seconds of arc. The mechanical, optical, and electrical characteristics of the instrument are described in detail. A synopsis of the results of the environmental tests to which the instrument was subjected and a mechanical error model of the instrument are presented. Measurement data and analysis are presented which indicate the operational accuracy of the sextant. Author

N68-24555*# National Aeronautics and Space Administration. Goddard Space Flight Center, Greenbelt, Md.

STAR TRACKER CALIBRATION

Lawrence T. Draper Washington Jun. 1968 13 p refs (NASA-TN-D-4594) CFSTI: HC\$3.00/MF\$0.65 CSCL 17G

Optical star tracker calibrations varied among companies in the industry by as much as 250 percent. A calibration procedure has been developed which relates a standard of spectral irradiance to real stars by laboratory measurements and computations. Initial

21 NAVIGATION

results from trackers calibrated for the Aerobee Sounding Rocket Program indicate a calibration accuracy on the order of 15 percent. Author

N68-25103*# National Aeronautics and Space Administration. Ames Research Center, Moffett Field, Calif.

ON BOARD CALCULATIONS OF A TWO IMPULSE ABORT TO A PRESELECTED LANDING SITE

Robert B. Merrick Washington May 1968 27 p refs

(NASA-TN-D-4599) CFSTI: HC\$3.00/MF\$0.65 CSCL 22C

A two impulse maneuver allows great flexibility in the choice of a landing site. This paper assumes that a nominal two impulse abort trajectory has been selected before flight but that the velocity required to attain that abort trajectory from off nominal conditions will be computed manually on board the spacecraft. The method presented here accomplishes the entire plane change with the first impulse and restricts the application of this impulse to cetain preselected ranges. The basic theory is valid for any transfer, in either planocentric or heliocentric space, between two positions whose inertial coordinates are known at prescribed times. Consequently, the theory would allow the method to be used for computing aborts from inbound trajectories, but reasonable fuel limitations restrict its primary applicability to outbound trajectories. The computational procedure developed obtains three orthogonal components, in inertial axes, of the velocity to be gained for the first impulsive rocket firing and obtains the magnitude of second impulse. It is shown that the method is feasible for manual calculations, using four figure accuracy, with a family of graphs to match the time constraint. Author

N88-28236*# National Aeronautics and Space Administration. Manned Spacecraft Center, Houston, Tex.

NAVIGATION AND GUIDANCE SYSTEMS PERFORMANCE FOR THREE TYPICAL MANNED INTERPLANETARY MISSIONS

Flora B. Lowes and Thomas B. Murtagh Washington Jul. 1968 39 p refs

(NASA-TN-D-4629) CFSTI: HC\$3.00/MF\$0.65 CSCL 17G

The navigation and guidance systems performance for manned interplanetary flight is evaluated for three representative missions: a 1972 Venus flyby mission, a 1975 Mars flyby mission, and a 1977 Mars orbital mission. The navigation system has both Earth-based radar and onboard tracking capabilities for updating position and velocity estimates for a spacecraft and an unmanned probe. Fixed-time-of-arrival and variable-time-of-arrival guidance logic is used in the guidance system to compute velocity corrections and target dispersions. From the performance evaluation for the three missions considered, arrival accuracies and propellant requirements can be predicted for the spacecraft and probe in the three types of missions presented or in similar interplanetary missions.

N68-28262*# National Aeronautics and Space Administration. Langley Research Center, Langley Station, Va.

RADIOMETRIC MEASUREMENTS OF THE EARTH'S INFRARED HORIZON FROM THE X-15 IN THREE SPECTRAL INTERVALS

Antony Jalink, Jr., Richard E. Davis, and Dwayne E. Hinton Washington Jul. 1968 59 p refs

(NASA-TN-D-4654) CFSTI: HC\$3.00/MF\$0.65 CSCL 17G

Experimental data of the earth's horizon in three spectral intervals. 0.8 to 2.8 μ m, 10 to 14 μ m, and 14 to 20 μ m, have been obtained by using the X-15 research airplane. The resolution (field of view) of the data at the tangent point is approximately 2 kilometers, and the spatial position of the horizon profile is known to within 4 kilometers. The 14 to 20 μ m interval was shown to be the best spectral interval for horizon sensing because it exhibits the least variance at adequate radiant intensity. The 0.8 to 2.8 μ m and 10 to 14 μ m spectral intervals do not appear suitable for accurate horizon sensing because they are sensitive to low-altitude meteorological changes. The experimental data obtained verified, within experimental accuracy, the theory used to predict

the far infrared radiant energy due to carbon dioxide. The use of theory for spectral regions where high-altitude water-vapor data are required is questionable because no mixing-ratio information is available. The single-scattering theory cannot predict accurately the radiant energy in the near infrared region (<3.0 μ m). Author

N68-28361*# National Aeronautics and Space Administration. Ames Research Center, Moffett Field, Calif.

A TECHNIQUE FOR PASSIVE ATTITUDE CONTROL OF SOLAR ORIENTED INTERPLANETARY SPACECRAFT

Vernon K. Merrick, Francis J. Moran, and Bruce E. Tinling Washington Jul. 1968 26 p refs

(NASA-TN-D-4641) CFSTI: HC\$3.00/MF\$0.65 CSCL 17G

Solar pressure forces can provide restoring torques that aline a specified axis of a suitably shaped spacecraft toward the sun. Implementing a control system that employs these torques requires a means of damping oscillatory motion of the solar pointing axis. This paper examines a passive technique of damping by dissipating the energy of relative motion between a pair of connected bodies. Two systems are studied in which the relative motion occurs about a single hinge. Coupling between the attitude motions is caused by unequal rates of change of solar pressure torque with each independent attitude angle. The performance is compared with that of a third system that uses a two-degrees-of-freedom hinge and has no coupling between the attitude motions. Author

N68-28418*# National Aeronautics and Space Administration. Langley Research Center, Langley Station, Va.

ANALYSIS OF A STAR-FIELD MAPPING TECHNIQUE FOR USE IN DETERMINING THE ATTITUDE OF A SPIN-STABILIZED SPACECRAFT

T. M. Walsh and Robert L. Kenimer Washington Jul. 1968 22 p refs Presented at the Aerospace Electrotechnol. Symp. of the Intern. Conf. and Exhibit on Aerospace Electrotechnol., Phoenix, Ariz., 19–25 Apr. 1964

(NASA-TN-D-4637) CFSTI: HC\$3.00/MF\$0.65 CSCL 17G

In certain space experiments precise knowledge of the orientation of a spin-stabilized spacecraft is required. This requirement has resulted in the development of a unique technique of star mapping herein discussed. The star mapping is accomplished by optically scanning a band of the star field about the vehicle's equator. Determination of the orientation of the vehicle's spin axis and roll angle with respect to the celestial sphere is accomplished by cross correlation of the scanned star map with a known reference map of the celestial sphere. The spinning motion of the vehicle causes star images to pass over a reticle which is configured to generate two groups of coded pulses at the output of the sensor. The amplitudes of the signals out of the optical system will be proportional to the spectral radiance of the scanned stars, and thus classification of stars according to their visual magnitude is possible. The time of the occurrence of the two pulse groups is related to the azimuth angle of the star, and the time separation of the pulse groups is related to the star's evaluation angle. Author

N68-30126*# National Aeronautics and Space Administration. Langley Research Center, Langley Station, Va.

THE ORBITAL RECOVERY PROBLEM. PART 1: AN ANALYSIS TECHNIQUE FOR RAPID DETERMINATION OF RETURN OPPORTUNITIES AND LATERAL-RANGE REQUIREMENTS FOR RECALL TO RECOVERY NETWORKS Paul F. Holloway and E. Brain Pritchard Washington Jun. 1967 43 p refs

(NASA-TR-R-259) CFSTI: HC\$3.00/MF\$0.65 CSCL 17G

An analysis technique has been developed which makes possible a rapid, accurate solution of the orbital return problem in terms of the determination of recall opportunities and the lateral range requirements associated with these opportunities for the recovery of spacecraft. The methods of application of the analysis (NASA-CR-95808; RD-2005) CFSTI: HC \$3.00/MF \$0.65 CSCL 22C

The feasibility of using an electro-optical celestial scanning sensor on board the IMP spacecraft for determination of the spacecraft attitude by utilizing star measurements is discussed. The sensor basically consists of a wide-angle lens with a slit positioned on the focal surface, a photomultiplier detector positioned behind the slit aperture and star signal processing electronics. The sensor, which consists of no moving parts, rotates with the spin stabilized vehicle. After automatic identification of the stars detected, the vehicle attitude is determined by computer solution of the system constraint equations. The study effort was largely devoted to the areas of optical design, electrical design, mechanical design, signal detection analysis, system error analysis, and star identification. A recommended system design is determined. Author

N68-31938*# National Aeronautics and Space Administration. Langley Research Center, Langley Station, Va.

A CELESTIAL ATTITUDE MEASUREMENT INSTRUMENT FOR PROJECT SCANNER

T. M. Walsh, William C. Dixon, Jr., Dwayne E. Hinton, and James A. Holland Washington Aug. 1968 43 $\,p\,$ refs

(NASA-TN-D-4742) CFSTI: HC\$3.00/MF\$0.65 CSCL 03A

The Project Scanner horizon-definition experiment required independent spacecraft attitude measurements with an accuracy (1σ) of 0.016°. This requirement led to the development of a celestial attitude measurement procedure using a unique star-mapping technique. Successful application of this technique required the detection and identification of stars in a +3 visual magnitude A0 spectral class. Star mapping was accomplished by use of a passive optical instrument consisting of a telescope, a coded reticle, and a photomultiplier. The telescope was mounted with its optical axis normal to the Scanner spacecraft principal spin axis. Spin motion about this axis caused star images to transit the reticle. Each star transit was sensed by the photomultiplier as two sequences of coded pulses that were telemetered to a ground receiving station. The amplitudes of the received pulses were proportional to the photometric magnitude of the stars, and the time separation of two pulse groups generated by a single star transit were related to the elevation angle of the star within the field of view of the telescope. Time separations of pulse groups generated by different stars were related to their azimuth angle separations. Total-angular-separation computations were used to identify the stars. Author

N68-31957*# National Aeronautics and Space Administration. Langley Research Center, Langley Station, Va.

ATTITUDE DETERMINATION OF THE SPIN-STABILIZED PROJECT SCANNER SPACECRAFT

T. M. Walsh, Jean C. Keating, and Dwayne E. Hinton Washington Aug. 1968 62 p refs

(NASA-TN-D-4740) CFSTI: HC\$3.00/MF\$0.65 CSCL 17G

The Scanner experiment required continuous knowledge of the spacecraft celestial attitude with a one-sigma accuracy of 0.016°. The basic measurements used to obtain attitude information were sighting times of stars viewed by the star mapper on the Project Scanner vehicle. Each star sighting produced coded-pulse sequences the amplitudes of which were related to the visual magnitude of the star. The times of occurrences of these pulse

sequences were related to the angular separation between a pair of stars. These angular-separation data were used to identify the sighted stars. The right ascension and declination of the identified stars and their transit times were used to identify the values of a set of parameters in an assumed model of the vehicle dynamical equations of motion. These vehicle motion parameters were then used to determine the vehicle celestial attitude as a function of time. A brief discussion of the star mapper is presented and the technique used to detect transit times of stars from the coded signals of the star mapper is described. A complete description of the star identification and parameter identification procedures is presented. Author N68-33006*# National Aeronautics and Space Administration. Ames Research Center, Moffett Field, Calif.

THE EFFECT OF SOME TELESCOPE FACTORS ON VARIABILITY OF PERFORMANCE IN SEXTANT SIGHTING Robert J. Randle and Emmett C. Lampkin Washington Sep. 1968 24 p refs

(NASA-TN-D-4781) CFSTI: HC\$3.00/MF\$0.65 CSCL 17G

The use of a hand-held sextant for the acquisition of navigational information in space flight may be a practical and economical method for providing an emergency or supplemental

navigation mode. Telescope objective lens diameter, aperture stop diameter, and magnification effects on the variability of a set of angular measurements made with a conventional marine sextant were investigated. Sighting variability performance improved monotonically with increasing telescope powers. Reductions in objective lens size and aperture size were also associated with improved performance. Subjects varied significantly in their sighting ability; subjects who had the poorest performance were helped most by higher magnifications. Performance changes due to magnification changes were dependent upon the objective lens size used. Performance changes due to changes in objective lens size depended upon the aperture size. Author

N68-33271*# National Aeronautics and Space Administration. Langley Research Center, Langley Station, Va.

A MANUAL NAVIGATION METHOD FOR EVALUATING TRANSFER ORBITS FOR LUNAR LANDINGS

G. Kimball Miller, Jr. Washington Sep. 1968 41 p refs (NASA-TN-D-4756) CFSTI: HC\$3.00/MF\$0.65 CSCL 22C

An analytical investigation has been made of a manual navigation method which permits an astronaut in the lunar-landing module to evaluate his orbit as he transfers from an 80-nauticalmile (148.16-kilimeter) altitude circular orbit to a point approximately 50,000 feet (15,240 meters) above the lunar surface. The method can also be used to predict the altitude and velocity components at the point of nominal powered-descent initiation. When the local horizontal is known, the method requires only the astronaut's use of a sextant to measure the elevation angle to the command module and the depression angle to the lunar horizon relative to the local horizontal at a single specified measurement point and four simple guidance charts. The navigation method was evaluated for various off-nominal transfer orbits and measurement errors. It was found that the accuracy of the method was enhanced by choosing the measurement point located as late as possible in the transfer orbit. With the measurement point located 40° prior to the point of nominal powered-descent initiation, the basic navigation method generally predicts the altitude of the landing module at pericenter and at the point of powered-decent initiation to within 2500 feet (762.0 meters). The corresponding predicted velocity components at nominal powered-descent initiation are generally within ±4 feet per second (1.22 meters per second) of the actual values. The prediction error experienced under the influence of selected measurement errors (including an optical determination of the local horizontal) are approximately double those Author of the basic mehtod.

N68-33450*# National Aeronautics and Space Administration. Langley Research Center, Langley Station, Va.

INFRARED HORIZON PROFILES FOR SUMMER CONDITIONS FROM PROJECT SCANNER

Thomas B. McKee, Ruth I. Whitman, and Richard E. Davis Washington Aug. 1968 125 p refs

(NASA-TN-D-4741) CFSTI: HC\$3.00/MF\$0.65 CSCL 17G

Measured horizon radiance profiles in spectral bands of 615 cm⁻¹ to 715 cm⁻¹ (CO₂) and 315 cm⁻¹ to 475 cm⁻¹ (H₂O) from Project Scanner flight of August 16, 1966, are shown. Data cover a latitude range from 10°N to 57°N. Excellent agreement between measured and independently analytically predicted radiance profiles in the CO₂ region confirms that the analytical technique is within the experimental accuracy. The

21 NAVIGATION

agreement of measured with predicted profiles and the lack of dependence on the presence of clouds indicate that the 615 cm⁻¹ to 715 cm⁻¹ spectral region is a leading choice for attitude determination applications. Horizon profiles in the 315 cm⁻¹ to 475 cm⁻¹ spectral region show a strong dependence on the presence of clouds. Mixing ratios of water vapor deduced from the radiance measurements indicate little latitudinal variation and are less than 0.017 g/kg at altitudes between 16 km and 33 km. Author

N68-33456*# National Aeronautics and Space Administration. Ames Research Center, Moffett Field, Calif.

THE EFFECTS OF IRRADIATION AND STAR MAGNITUDE ON SEXTANT SIGHTING PERFORMANCE

Robert J. Randle and Emmett C. Lampkin Washington Sep. 1968 11 p refs

(NASA-TN-D-4780) CFSTI: HC\$3.00/MF\$0.65 CSCL 17G

A hand-held sextant may provide a practical and economical method of acquiring navigational information in space flight during an emergency or to supplement other navigation measurements. If this mode is chosen for space flight, it is mandatory that the limits of human performance with the sextant be established. The present study was designed to investigate variables which may affect sighting accuracy. Male college students with good visual acuity (Snellen 20/20 or better) and normal color vision were trained to make angle measurements with a marine sextant. The sextant was gimbal mounted and angle readings were recorded with a digital shaft encoder mounted on the shaft of the sextant vernier knob. In measuring the angular subtense of a simulated planetary disk, increases in disk brightness were associated with increases in the measured subtense. Changing the magnitude of the reference star did not significantly affect performance. Author

N68-33756*# National Aeronautics and Space Administration. Lewis Research Center, Cleveland, Ohio.

LOAD RELIEF AUTOPILOT ANALYSIS TO MINIMIZE LAUNCH VEHICLE PEAK THRUST VECTOR DEFLECTION REQUIREMENTS

Leslie L. Scalzott and Fred Teren Washington Sep. 1968 42 p refs

(NASA-TN-D-4786) CFSTI: HC\$3.00/MF\$0.65 CSCL 17G

A load relief autopilot design to minimize the maximum thrust vector deflection angle required to maintain vehicle stability during flight through design winds is analyzed. The feedback variables are angle of attack and flight path angle as well as attitude error and rate. A rigid body configuration is assumed, and sensor dynamics are not considered. Deflection angle and attitude error responses are presented for design winds. It is shown that the load relief autopilot analyzed results in a 50 percent decrease in deflection requirements for these winds as compared to a conventional autopilot designed to trim the vehicle.

N68-33904*# Systems Technology, Inc., Princeton, N. J. NEW METHODS IN ADAPTIVE FLIGHT CONTROL

Lee Gregor Hofmann and John J. Best Washington NASA Sep. 1968 43 p refs

(Contract NAS1-6813)

(NASA-CR-1152) CFSTI: HC \$3.00/MF \$0.65 CSCL 17G

A new approach to the design of adaptive control systems was developed. It is called the adaptive control function approach, and the systems so designed are called adaptive control function systems. This terminology is descriptive of the basic operating principle for these systems. The basic operating principle is that sums of properly modulated, conventional linear feedback and feedforward signals provide the control imputs needed to obtain specified responses in a number or output variables of a linear controlled element. The theoretical development in this report deals with linear, constant coefficient controlled elements only. With this restriction, the number of linearly independent controlled element responses which can be arbitrarily specified is equal to the number of independent control points. These specified responses then determine what the (ideal) control inputs should be.

22 NUCLEAR ENGINEERING

Includes nuclear reactors and nuclear heat sources used for propulsion and auxiliary power. For basic research see: 24 Physics, Atomic, Molecular, and Nuclear. For related information see also: 03 Auxiliary Systems; and 28 Propulsion Systems.

N68-10133*# National Aeronautics and Space Administration. Lewis Research Center, Cleveland, Ohio. SHIELDING REQUIREMENTS FOR THE NASA PLUM

BROOK HB-6 BEAMHOLE RADIATION EFFECTS FACILITY Harvey S. Bloomfield Washington NASA Nov. 1967 23 p refs

(NASA-TM-X-1461) CFSTI: HC\$3.00/MF\$0.65 CSCL 18F

The calculational methods and results used to design a shield assembly for the Plum Brook Reactor HB-6 beamhole facility are described. The function of this shield assembly is to provide adequate biological protection during reactor operation and to permit personnel access to a test chamber after shutdown. Radiation sources examined during reactor operation were neutrons and gamma rays scattered by an experimental package in the test chamber, direct core radiations, and radiation through rectangular slits which may be formed by misalinement of shield sections. Fission product decay gammas and neutron-induced gamma activity in the test chamber were the important radiation sources investigated after shutdown. The bulk of the calculations was performed by specialized digital computer shielding programs which accounted for considerable detail of the core-beamhole geometry. Calculational results compare favorably with experimental measurements on the final shield assembly. Author

N68-10134*# National Aeronautics and Space Administration. Lewis Research Center, Cleveland, Ohio.

DESIGN AND OPERATION OF A HIGH-TEMPERATURE TUNGSTEN-MESH GAS HEATER

Byron L. Siegel Washington, NASA Nov. 1967 26 p refs (NASA-TM-X-1466) CFSTI: HC\$3.00/MF\$0.65 CSCL 181

A high-temperature electrically heated gas heater was designed

and is operational. This heater uses interwound helical tungsten coils as mesh heating elements. The heater has heated 0.450 and 0.69 pound per second of nitrogen to 4530° and 4200° R with average mesh bank surface temperatures as high as 4430° and 4270° R respectively. The design of the heater is described and its advantages are discussed. *Problem areas associated with the design of a high-temperature heater, such as flow bypass, are described, and resulting solutions or recommendations are given. Author

N68-10291*# National Aeronautics and Space Administration. Lewis Research Center, Cleveland, Ohio.

COMPARISON OF ABSOLUTE CALCULATED AND MEASURED GAMMA AND NEUTRON DOSES IN TUNGSTEN-WATER-MODERATED CRITICAL ASSEMBLY Paul G. Klann and Walter A. Paulson Washington NASA Nov.

1967 55 p refs

(NASA-TN-D-4223) CFSTI: HC\$3.00/MF\$0.65 CSCL 18E

The mixed gamma and neutron dose was measured at 60 locations within the Tungsten-Water-Moderated Reactor critical assembly. Graphite wall thimble ionization chambers filled with carbon dioxide and polyethylene wall chambers filled with ethylene were used. The chambers were absolutely calibrated in a bremsstrahlung beam against a secondary calibration standard and in a reactor against a water filled calorimeter. These calibrations were used to obtain gamma and neutron response coefficients for the chambers which permitted partitioning of the measured mixed

radiation dose into a gamma dose and a neutron dose. The measured gamma doses were compared with an Athena Monte Carlo calculation. Good agreement was found for the 16 locations compared. The average deviation was 10 percent. In addition, the measured neutron doses were compared with a "first collision" calculation of the dose. The calculated neutron doses were uniformly low with an average deviation from the measurement of 18 percent. Author

N68-10561* Georgia Inst. of Tech., Atlanta.

INVESTIGATION OF RADIANT HEAT TRANSFER TO PARTICLE-SEEDED GASES FOR APPLICATION TO NUCLEAR ROCKET ENGINE DESIGN

Edward Y. H. Keng and Clyde Orr, Jr. Washington NASA Nov. 1967 50 p refs

(Grant NsG-273)

(NASA-CR-953) CFSTI: HC\$3.00/MF\$0.65 CSCL 21F

The objective of this research is to provide fundamental information on radiant heat transfer to aerosols to aid in the evaluation of various gaseous core nuclear rocket concepts. Both theoretical and experimental investigations have been pursued. View factors have been evaluated for a number of conditions considering a cylindrical geometry for the system, such results being generally applicable to high temperature technology. The experimental results agree well with theoretical predictions. A new aerosol generator has been designed to produce dense yet uniform aerosols, and preparation for the study of particle evaporation or sublimation in an intense radiant field are underway. An electrically heated tungsten furnace for this investigation is being assembled.

N68-14585*# National Aeronautics and Space Administration. Lewis Research Center, Cleveland, Ohio.

PARAMETRIC ANALYSIS OF RADIOISOTOPE CASCADED THERMOELECTRIC GENERATORS

James T. Ward and Robert Ruch Washington Jan. 1968 27 p refs

(NASA-TM-X-1501) CFSTI: HC \$3.00/MF \$0.65 CSCL 18B The generator consisted of a high-temperature silicongermanium first stage and a lower-temperature lead telluride second stage was placed concentrically around a cylindrical fuel block. Heat was rejected from the outer surface of the generator shell; in most cases, fins were required to augment the heat rejection. The Si-Ge hot-junction temperature range was 1089° to 1255°K. The PbTe hot-junction temperature was fixed at 811°K and the PbTe cold-junction temperature varied from 422° to 700°K. The fuel-block length-diameter ratio varied from 0.5 to 10.0. The fuel-block-volume power-density range was 0.5 to 10.0 watts per cm³ The generator power output was fixed at 250 watts electric. The performance of cascaded generators is also compared with the performance of single-stage Si-Ge generators. The results indicate that the cascaded generator operating at a Si-Ge hot-junction temperature of 1089°K had a minimum specific weight of 220 lbs per kilowatt electric (kWe) at an efficiency of nearly 7%. For a Si-Ge hot-junction temperature of 1255°K, the minimum specific weight was 170 lbs per kWe with an efficiency of over 8%. The single-stage Si-Ge generator with a hot-junction temperature of 1255°K had a minimum specific weight of 100 lbs per kWe at an efficiency slightly below 6%. Author

22 NUCLEAR ENGINEERING

N68-14986*# National Aeronautics and Space Administration. Lewis Research Center, Cleveland, Ohio.

ESTABLISHING ALLOWABLE TEMPERATURE GRADIENTS FOR TUNGSTEN-URANIUM DIOXIDE FUEL ELEMENTS USING EXPERIMENTAL CYCLIC STRAIN DATA Ivan B. Fiero Washington Jan. 1968 36 p ref

(NASA-TN-D-4279) CFSTI: HC\$3.00/MF\$0.65 CSCL 18J

To establish allowable limits for temperature difference in tungsten-uranium dioxide fuel elements, experimental thermal strain data were examined. The data were obtained by uniformly heating tungsten and tungsten-uranium dioxide composites for 50 thermal cycles. Since the materials were not cycled to failure, the allowable temperature differences established from the experimental data are not absolute maximum values, but represent design values with which fuel element configurations can be evaluated. These allowable temperature differences are those which would produce thermal strains equivalent to the experimental data. If the strains calculated for a given design are less than the experimental values, the fuel element should operate satisfactorily under the conditions considered. Author

N68-15197*# National Aeronautics and Space Administration, Lewis Research Center, Cleveland, Ohio.

ANALYSIS OF URANYL FLUORIDE SOLUTION REACTORS CONTAINING VOIDED TUBES

Wendell Mayo Washington Feb. 1968 26 p refs

(NASA-TN-D-4270) CFSTI: HC\$3.00/MF\$0.65 CSCL 18L

Critical experiments with fully enriched (93.2 percent uranium 235) uranyl fluoride-water solution reactors that contain arrays of large-diameter void tubes have been analyzed satisfactorily. This study evaluates a calculational method that involves the direct application of widely used multigroup computer programs and techniques to cases of extreme heterogeneous voids. Experimental critical solution heights for cores that contain no void tubes and for 19, 31, and 37 void tubes with a 7.658-centimeter diameter were obtained by using the NASA Zero Power Reactor-II facility. Both unreflected cores and cores radially reflected with 15.24 centimeters of water were considered. The void arrays with triangular lattice pitches of either 9.652 or 10.922 centimeters were centrally located in the 76.2-centimeter-diameter core tank. The critical heights of the voided reactors ranged from 21 to about 84 centimeters. Author

N68-15643*# National Aeronautics and Space Administration. Lewis Research Center, Cleveland, Ohio.

EXPERIMENTAL DETERMINATION OF NEUTRON FLUXES IN PLUM BROOK REACTOR HB-6 FACILITY WITH USE OF SULFUR PELLETS AND GOLD FOIL

John M. Bozek and Michael P. Godlewski Washington Feb. 1968 23 p refs

(NASA-TM-X-1497) CFSTI: HC\$3.00/MF\$0.65 CSCL 18M

Fast and thermal neutron fluxes were measured in the test cavity outside the HB-6 beam port in the Plum Brook reactor, with the use of sulfur pellets and gold foils. The dependence of flux on reactor power level, shim-control-rod position, water attenuator tank configuration, position in the test cavity, and perturbations by other experiments was investigated. Based on the measurements taken, the thermal and fast neutron fluxes for any combination of these parameters can be determined. Standard fluxes (which correspond approximately to an average flux in the test cavity at full reactor power) were 1.4×10^6 neutrons per second per square centimeter (nv) for thermal neutrons (E \leq 0.4 eV or 0.64 $\times 10^{-7}$ pJ) and 8.2 $\times 10^6$ neutrons per second per square centimeter (nv) for fast neutrons (E \geq 2.48 MeV or 0.396 pJ). The flux errors are estimated at ± 38 and ± 35 percent for thermal and fast neutrons.

N68-15792*# National Aeronautics and Space Administration, Lewis Research Center, Cleveland, Ohio.

SMALL HIGH-TEMPERATURE NUCLEAR REACTORS FOR SPACE POWER Edward Lantz, Wendell Mayo, Robert M. Westfall, and John L. Anderson, Jr. Washington Feb. 1968 19 p refs

(NASA-TN-D-4371) CFSTI: HC \$3.00/MF \$0.65 CSCL 18L

As a first step in a comparison of the relative performance of nuclear reactors and of other thermal sources for space power systems, criticality calculations were made for small, cylindrical, lithium-cooled reactors which use tungsten as the structural material. The nuclear fuels considered were plutonium-239, uranium-233, and uranium-235. These fuels were assumed to be in the form of pure metals, nitrides, and oxides. The radial neutron reflectors considered were beryllium oxide, molybdenum, and carbon. The calculations revealed that the smallest cores are those fueled with metallic U^{233} and $\mathsf{Pu}^{239}.$ These cores can be as small as 11 centimeters in diameter and 30.5 centimeters long; however, at desired operating temperatures these cores would contain molten fuel. The smallest solid fuel core contains uranium-233 nitride $(U^{233}N)$ in a core 13.5 centimeters in diameter and 30.5 centimeters long. The reactor diameters increase about 2.5 centimeters when the oxide fuel is used in place of the nitride. Cores fueled with U^{235} are considerably larger than those fueled with U^{233} Author

N68-15855*# National Aeronautics and Space Administration. Lewis Research Center, Cleveland, Ohio.

NUCLEAR DESIGN DATA FOR EXPERIMENTS TO BE CONDUCTED IN HORIZONTAL THROUGH HOLE 1 OF THE PLUM BROOK REACTOR

Robert G. Rohal, Patrick M. Finnegan, and E. J. Ciesla Washington Feb. 1968 31 p refs

(NASA-TM-X-1509) CFSTI: HC\$3.00/MF\$0.65 CSCL 18M

Three irradiation facilities have been designed for use in the Horizontal Through Hole 1 (HT-1) of the Plum Brook Reactor (PBR). These facilities are the Inpile Helium-Cooled Loop, the Single-Pass Argon-Cooled Facility, and the Inpile Capsule Facility. Experiments were conducted in HT-1 of the Plum Brook Mockup Reactor (MUR) to provide data for experiments employing these facilities. In these experiments, mockups of the three facilities were used to obtain the following information: (1) the thermal-neutron flux, which ranged from approximately 1×10^9 to 4×10^9 neutrons per square centimeter per second per kilowatt of reactor power along the axis of the inpile tubes; (2) the fission power in mockups of flat-plate fuel elements composed of tungsten and approximately 10 to 25 grams of fully enriched uranium, which ranged from approximately 0.04 to 0.10 watt per gram of enriched uranium per kilowatt of reactor power: (3) the gamma heating in the inpile tube structure, which ranged from approximately 0.5×10^{-4} to 1.0×10^{-4} watt per gram per kilowatt of reactor power; (4) the reactivity worth of the mock fuel elements and inpile tubes in both normal and accident conditions, which ranged from -4 to -40 cents, respectively. Author

N68-16056*# National Aeronautics and Space Administration. Lewis Research Center, Cleveland, Ohio.

CALCULATIONS TO SUPPORT OPERATION OF THE PLUM BROOK REACTOR

Harry J. Reilly, John H. Lynch, and Steven R. Borbash Washington Feb. 1968 25 ρ refs

(NASA-TM-X-1496) CFSTI: HC\$3.00/MF\$0.65 CSCL 181

Several calculations that have aided operation of the Plum Brook Reactor were described. First, a simple mathematical model and the resulting calculations which were done to study fuel utilization are described. A decision to buy 240-gram uranium 235 fuel elements and to use them three times each was made on the basis of the study. The power distribution in the mixed loading is discussed and is observed to be more uniform than that in a uniform fuel loading. Charge life weight factors are then derived; the derivation differs in approach and in results from previous derivations by others. Finally, a "xenon clock" on-line computer program in use at the Reactor is discussed, and an approximation useful for hand calculations of complex histories is derived. Author

N68-16478*# United Aircraft Corp., East Hartford, Conn. EXPERIMENTAL INVESTIGATION OF FLOW PATTERNS IN RADIAL-OUTFLOW VORTEXES USING A ROTATING-PERIPHERAL-WALL WATER VORTEX TUBE Arthur Travers Washington NASA Feb. 1968 68 p refs (Contract NASw-847)

(NASA-CR-991; F-910091-10) CFSTI: HC \$3.00/MF \$0.65 CSCL 21F

Experiments were conducted to determine whether the turbulence observed in radial outflow vortices is caused by fluid injection at the peripheral wall or by an instability inherent with the flow of fluid radially outward from the centerline of the vortex, to determine criteria for the flow conditions that lead to turbulence, and to determine whether a rotating peripheral wall, a rotating inner porous tube, and rotating endwalls have significant effects on flow patterns. Results indicate that radial outflow vortices are characterized by turbulence with large eddies that convect fluid from the central region of the vortex to near the peripheral wall. These flow patterns exist for both basic and axial flow vortex configurations and for wide ranges of the flow conditions. Laminar flow was encountered only with low rates of radial outflow and low superimposed axial velocities. Rotation of the end walls affected flow patterns in the basic vortex configuration for a limited range of the flow conditions. Rotation of the inner porous tube had no effect. Rotation of the inner porous tube and end walls did not affect the flow patterns in the axial flow vortex configuration. R.N.A.

N68-17022*# National Aeronautics and Space Administration. Lewis Research Center, Cleveland, Ohio.

EXPERIMENTAL DETERMINATION OF GAMMA EXPOSURE RATE IN PLUM BROOK HB-6 FACILITY

John M. Bozek Washington Feb. 1968 14 p refs

(NASA-TM-X-1490) CFSTI: HC\$3.00/MF\$0.65 CSCL 18H The gamma ray exposure rates in the HB-6 beam hole

The gamma ray exposure rates in the three beam with facility of the NASA Plum Brook Reactor were measured with lithium fluoride thermoluminescent dosimeters and argon-filled ion chambers. The exposure rates varied as a function of position in the test cavity and the time of measurement. To define and predict variations of the gamma exposure rate, an empirical relation between a standardized exposure rate and various reactor parameters was formulated. The standardized exposure rate, defined at 60 megawatts of reactor power, median values of reactor parameters, and the center of the radiation beam, were measured to be 7.6×10^4 roentgens per hour (19.6 (C/kg)/hr).

N68-17095*# National Aeronautics and Space Administration. Lewis Research Center, Cleveland, Ohio.

SUMMARY OF RADIATION EFFECTS ON THERMIONIC INSULATOR MATERIALS

John T. Mayer Washington Feb. 1968 37 p refs

(NASA-TN-D-4414) CFSTI: HC\$3.00/MF\$0.65 CSCL 18J

Nuclear thermionic power systems are presently being studied for possible space applications. One of the critical materials in such designs is the metal oxide ceramic used as an electrical insulator and seal between various components. Such materials must withstand high temperatures (1000°C and above) as well as fast neutron doses to 10^{22} neutrons per square centimeter. To gain insight into their behavior in such an environment, a literature survey has been conducted for radiation effects data on the following candidates: beryllia, alumina, thoria, zirconia, and yttria. The properties of interest include dimensional changes, thermal and electrical conductivity, strength, thermal expansion coefficient, elastic modulus, and breakdown voltage. A large amount of data were found on beryllia, but much less work has been done on the other oxides, especially zirconia, thoria, and yttria. Beryllia seemed to be the most promising material, and its radiation stability may be improved by the use of additives and/or fine grained low density material. However, the large gas production rate in beryllia may restrict its use in thermionic systems; the release of a significant amount of helium gas into the interelectrode space may affect converter performance. The

most successful tests on beryllia to date showed relatively minor changes after fast neutron doses to 9×10^{21} neutrons per square centimeter at 1000°C. In contrast, high temperature tests of alumina and yttria have resulted in gross fracturing at lower doses. No high temperature, high dose data on thoria or zirconia were found. Author

N68-17131*# United Aircraft Corp., East Hartford, Conn.

EXPLORATORY FLOW AND CONTAINMENT EXPERIMENTS IN A DIRECTED-WALL-JET VORTEX TUBE WITH RADIAL OUTFLOW AND MODERATE SUPERIMPOSED AXIAL FLOWS Fifth Interim Summary Technical Report, Sep. 15, 1965–May 30, 1967

Bruce V. Johnson Washington NASA Feb. 1968 85 p refs Sponsored in part by AEC

(Contract NASw-847)

(NASA-CR-992; F-910091-11) CFSTI: HC \$3.00/MF \$0.65 CSCL 21F

The containment characteristics of confined radial-outflow vortexes with superimposed axial flow were studied to determine whether high average simulated-fuel densities and high ratios of simulated propellant-to-fuel flow rates could be obtained. The experiments concentrated on two factors that influence simulated-fuel containment: (1) simulated-propellant injection methods in which the flow is injected from the peripheral wall of an axial-flow vortex tube with both axial and tangential (circumferential) components of velocity, and (2) simulated-fuel injection methods. Compared with the containment times measured with no axial component of injection velocity, improvements in containment time of as much as a factor of three-and-one-half were obtained in this investigation using injection with both axial and tangential components of velocity. However, the maximum containment times that were measured were approximately one to two orders of magnitude less than the value now estimated to be required for an economically practical, open-cycle gaseous-core nuclear rocket. Author

N68-18197*# National Aeronautics and Space Administration. Lewis Research Center, Cleveland, Ohio.

PRELIMINARY CONSIDERATIONS FOR FAST-SPECTRUM, LIQUID-METAL COOLED NUCLEAR REACTOR PROGRAM FOR SPACE-POWER APPLICATIONS

Gerald P. Lahti, Edward Lantz, and John V. Miller Washington, Mar. 1968 49 $p\ refs$

(NASA-TN-D-4315) CFSTI: HC\$3.00/MF\$0.65 CSCL 18L

A preliminary study was made in which reactor size and shield weight requirements were calculated for several compositions of uranium nitride and uranium dioxide fuel materials under various operating conditions. A fast-spectrum, lithium-cooled reactor was selected for the study since it potentially will result in the smallest reactor that is capable of operating at the required temperature levels. In order to determine man-rated shielding requirements, a 2-millirem-per-hour radiation dose at 66 feet was selected as a reasonable value, being of the same order of magnitude as that which would be received from galactic cosmic rays in interplanetary space. Nuclear criticality and the allowable fuel burnup limits essentially determine the required reactor size and resulting weight of the shielding. The importance of the other variables, such as allowable steady-state heat-transfer limits, coolant temperatures, flow rates, and coolant hole sizes, is only secondary in determining the weight of the reactor plus shield. Choice of the proper value for each of these parameters can be based on overall system performance, availability of design data, material limitations, and manufacturing feasibility. It appears that nuclear stability and control, fuel material development, and shielding optimization are areas Author requiring further study.

N68-18243*# United Aircraft Corp., East Hartford, Conn. CONTAINMENT EXPERIMENTS IN VORTEX TUBES WITH RADIAL OUTFLOW AND LARGE SUPERIMPOSED AXIAL FLOWS

John S. Kendall, Arthur E. Mensing, and Bruce V. Johnson Washington Mar. 1968 92 p refs

(Contract NASw-847)

(NASA-CR-993; F-910091-12) CFSTI: HC \$3.00/MF \$0.65 CSCL 21F

An experimental investigation was conducted to determine the heavy-gas containment characteristics of radial-outflow vortexes for potential application to a vortex-stabilized, open-cycle gaseous nuclear rocket engine. Tests were conducted in a constant-temperature vortex with Reynolds numbers based on the superimposed axial flow up to those expected in a full-scale engine. Air was employed to simulate the seeded hydrogen propellant and a heavy fluorocarbon was used in most tests to simulate the gaseous nuclear fuel. The effects on heavy-gas containment of changes in the vortex tube length-to-diameter ratio, the light-gas injection geometry and area, the ratio of average heavy-gas density to light-gas density, and the density of the heavy gas at injection were studied. The containment parameters varied significantly only with vortex tube length-to-diameter ratio and the ratio of average heavy-gas density to light-gas density. The results of some tests using helium injected near the centerline of the vortex indicated that the presence of a light gas in the central region of the vortex has a significant favorable effect on containment characteristics. Author

N68-18252*# National Aeronautics and Space Administration. Lewis Research Center, Cleveland, Ohio.

FEASIBILITY STUDY OF A TUNGSTEN WATER MODERATED NUCLEAR ROCKET. 7: SYSTEM DYNAMICS AND CONTROL ANALYSIS

James R. Mihaloew Washington Mar. 1968 98 p refs (NASA-TM-X-1426) CFSTI: HC\$3.00/MF\$0.65 CSCL 21F

A system dynamics and control analysis was performed on several versions of a tungsten water-moderated (TWMR) nuclear rocket system, to determine its overall feasibility and control requirements from chilldown to startup and power range operation. Results of steady-state mapping of the TWMR showed that heat exchanger hydrogen bypass was required to prevent icing in the water-moderator cooling heat exchanger. A comparative system analysis of the several TWMR versions showed that the all-topping cycle version with heat exchanger bypass was substantially superior with respect to system simplicity and flexibility at the design chamber pressure of 600 psia. However, a split-feed cycle version with heat exchanger bypass represented the most promising system because of its superior chamber pressure uprating potential. The control analysis of this version showed that chamber temperature control with a poison insertion-extraction scheme was extremely fast in response, but necessarily discontinuous. Chamber temperature control with heat exchanger bypass was comparatively slow but inherently continuous. A control system based on heat exchanger bypass for primary chamber temperature control and poison reactivity for augmentation was demonstrated satisfactorily over a typical operating cycle. Author

N68-18541*# National Aeronautics and Space Administration. Lewis Research Center, Cleveland, Ohio.

DETERMINATION OF INTERSECTION OF PARTICLE FLIGHT PATH WITH SURFACE OF HELICAL TUBULAR VOID REGION

Millard L. Wohl and Carl D. Bogart Washington Mar. 1968 25 p refs

(NASA-TN-D-4435) CFSTI: HC\$3.00/MF\$0.65 CSCL 18F

A method for determining the intersections of a nuclear particle flight path and the wall of a helical tubular duct is presented. FORTRAN listings of computer subroutines which perform the numerical analysis involved are included. The subroutines are useful in any Monte Carlo transport analysis where complex void configurations of helical or pseudohelical geometry are involved. Their immediate purpose in this work is to serve as geometry subroutines to be used in conjunction with 05-R, a Monte Carlo transport code. Author **N68-19146***# National Aeronautics and Space Administration. Lewis Research Center, Cleveland, Ohio.

NUCLEAR THERMIONIC SPACE POWER SYSTEM CONCEPT EMPLOYING HEAT PIPES

Colin A. Heath and Edward Lantz Washington Mar. 1968 24 p refs

(NASA-TN-D-4299) CFSTI: HC\$3.00/MF\$0.65 CSCL 18N

A space power system employing out-of-pile thermionic diodes and using concentric heat pipes for both heating and cooling of these diodes has been examined. For an early application, the out-of-pile thermionic diode has some advantages over an in-pile system because it is removed from the reactor environment. Moreover, the heat pipe permits emitter temperatures that are not much less than the temperature of the fuel clad. Laboratory data on the performance of heat pipes has been examined and the results used to estimate reasonable performance levels for thermionic diodes which were consequently incorporated into a small, fast-spectrum nuclear reactor concept. Performance levels and system weights including shield weights, have been estimated from first order calculations. The overall system can have the advantage of the safety inherent in heat pipe redundancy and the improved performance available from components that are removed from the reactor environment. Author

N68-19925*# National Aeronautics and Space Administration. Lewis Research Center, Cleveland, Ohio.

REACTIVITY EFFECTS CAUSED BY RADIAL POWER FLATTENING IN A SMALL, FAST-SPECTRUM REACTOR C. L. Whitmarsh, Jr. Washington Apr. 1968 13 p refs

(NASA-TN-D-4459) CFSTI: HC\$3.00/MF\$0.65 CSCL 181

The effect on criticality of flattening the radial power distribution in a small, reflector-controlled, fully enriched, fast-spectrum nuclear reactor was calculated. Compared to a uniformly fueled, fully enriched core, a decrease in reactivity occurred from reduced fuel inventory and an increase in reactivity occurred from enhanced reflector worth. Fuel distributions were also calculated to indicate the effects of (1) changing the power ratio of 1.1, and (2) changing the reflector thickness to 7.62 cm. Change (1) resulted in a zoned core with an enrichment variation from 71.3 percent in the central zone to 93.2 percent in the peripheral zone; whereas, for change (2) these values were 67 and 93.2 percent, respectively. The net reactivity loss (fuel loss-reflector worth increase) based on a 93.2 percent enriched uniformly-fueled core was 3 percent for either of these zoned cores. Power distortion in a reactor core is caused by reflector movement required to compensate for reactivity changes over the core lifetime. This effect in zoned cores was observed by calculating power shapes for the initial and the end-of-life reflector configurations for two zoned cores. Author

N68-20355*# National Aeronautics and Space Administration. Lewis Research Center, Cleveland, Ohio.

ACTIVATION OF SODIUM, LITHIUM, AND POTASSIUM IN COMPACT FAST REACTORS AND ITS EFFECT ON SHIELDING

Leonard Soffer Washington Apr. 1968 23 p refs

(NASA-TM-X-1512) CFSTI: HC\$3.00/MF\$0.65 CSCL 18J

Neutron activation of sodium (Na), lithium (Li), and potassium (K) used as possible coolants in a "typical" compact fast reactor were analytically investigated. The natural elements, all individual isotopes, and one common eutectic (NaK 78) were examined. Suitable energy dependent neutron fluxes were used in conjunction with activation cross sections to calculate saturated specific activities. Activation cross-section data for the elements studied were compiled and tabulated, and these data are judged to be adequate for engineering calculations. Results show that when zero holdup time is assumed, the best coolants, on the basis of unshielded activation dose rate, are K⁴⁰, K³⁹, Li⁷, and natural Li. The worst are K⁴¹ and Na. Because of low natural abundance, K⁴⁰ is impractical as a reactor coolant. Lithium dose rates are

very sensitive to holdup time beause of the short (0.8 sec) half-lives of the Li products. Holdup of even a few seconds greatly reduces the Li dose rates but not those for any other element. Lithium 7 held up for 8 seconds and gave the lowest activation dose rate of any coolant considered. The unshielded dose rate from the assumed fission product release was the highest of all. It was about two orders of magnitude greater than the zero-holdup Li⁷ rate, and about five orders of magnitude greater than the dose rate for Li⁷ held up for 8 seconds. Gas evolution resulting from coolant irradiation was also investigated and found to be negligible except for Li⁶.

N68-21111*# National Aeronautics and Space Administration. Lewis Research Center, Cleveland, Ohio.

POSTSHUTDOWN COOLING REQUIREMENTS OF TUNGSTEN WÄTER-MODERATED NUCLEAR ROCKET

Walter A. Paulson and Ray M. Crawford Washington Apr. 1968 23 p refs

(NASA-TM-X-1568) CFSTI: HC\$3.00/MF\$0.65 CSCL 21F

The postshutdown cooling requirements were calculated for the tungsten water-moderated reactor concept. The reactor was assumed to have operated at full power for 1 hour. An amount equivalent to 5.25 percent of the hydrogen used during the operation at full power is required to remove the energy generated after shutdown. The postshutdown cooling schedule requires continuous hydrogen flow for the first 1000 seconds followed by 23 pulsed cooling periods. The last hydrogen pulse occurs at 6.1 days after shutdown. The pulse flow rate is 0.3 pound per second (0.136 kg/sec) and the duration of the pulses range from 4250 seconds early in the schedule to 1300 seconds ta later times. Author

N68-21124*# United Aircraft Corp., East Hartford, Conn. OPTICAL ABSORPTION IN FUSED SILICA DURING TRIGA REACTOR PULSE IRRADIATION

R. Gagosz, J. Waters, F. C. Douglas, and M. A. De Crescente Washington NASA Apr. 1968 67 p refs

(Contract NASw-847)

(NASA-CR-1031; F-910485-1) CFSTI: HC \$3.00/MF \$0.65 CSCL 18J

An experimental investigation was conducted to determine the spectral transmission characteristics of fused silica before, during and after exposure to reactor irradiation pulses. The transmission measurements were carried out at three wavelengths (0.215, 0.625 and 1.0 microns) and at a range of temperatures from ambient to 900°C. Corning 7940 fused silica specimens in a corner cube configuration were mounted next to the reactor core face Peak neutron and gamma fluxes obtained from this reactor were approximately 5.4×10^{15} n/cm² sec and 6.1×10^7 R/sec, respectively. Neutron and gamma doses associated with these pulses were 2.3×10^{14} n/cm² and 2.6 $\times 10^{6}$ R, respectively. The effective time of the pulse obtained by dividing the total dose by the peak flux was approximately 0.043 sec. The transmission measurements were made immediately before, during and after the reactor pulses to monitor both the creation of irradiation induced absorption and the decay of the induced absorption after the pulse.

N68-21705*# National Aeronautics and Space Administration. Lewis Research Center, Cleveland, Ohio.

HOT ISOSTATIC COMPACTION OF TUNGSTEN-URANIUM DIOXIDE FUELS WITH HIGH-VOLUME FRACTION OF URANIUM DIOXIDE

Paul F. Sikora and Andrew C. Millunzi Washington Apr. 1968 19 p refs

(NASA-TM-X-1563) CFSTI: HC\$3.00/MF\$0.65 CSCL 18J

Dense (>98 percent of theoretical) tungsten-uranium dioxide cermets containing 30 to 70 volume percent uranium dioxide were fabricated by hot isostatic compaction of tungsten-coated uranium dioxide particles. Both thin plates (0.020-in. or 0.051-cm thick) and small-diameter rods (0.20-in. or 0.51-cm diam) were successfully

22 NUCLEAR ENGINEERING

produced at compaction conditions of $3100^{\circ}F$ ($1700^{\circ}C$) and 30,000 psi (207 MN/m^2). In addition to volume-fraction loading of uranium dioxide, other variables studied in this program were the effect of (a) fuel particle size in the range of 50° to 110° micron diameter, (b) molybdenum or a molybdenum alloy (TZM) in container assemblies, and (c) compaction schedule and pressure (up to 42,000 psi or 295 MN/m²). Fully dense cermets were produced with all combinations of the range of variables studied. The surface smoothness of the cermets was affected only by the choice of container materials. Containers produced from TZM resulted in smooth cermet surfaces; however, unalloyed molybdenum containers often resulted in irregular surfaces. The feasibility of applying a thin tungsten cladding to the cermet surfaces as an integral part of the compaction process was also demonstrated.

N68-21924*# National Aeronautics and Space Administration. Lewis Research Center, Cleveland, Ohio.

APPLICATIONS OF MONTE CARLO ANALYSIS TO TUNGSTEN RESONANCE ABSORPTION

Robert M. Westfall Washington May 1968 47 p refs (NASA-TN-D-4545) CFSTI: \$3.00 CSCL 18F

Calculational procedures for Monte Carlo analyses and tungsten resonance absorption are presented. The widely used flat spatial neutron source assumption is shown to overestimate the effective resonance integral of the large scattering resonance in W186 by 21 percent at a surface to mass ratio (S/M) of 0.5 cm²/g. Resonance overlap in natural W decreases the effective resonance integral by 18 to 7 percent over a S/M range of 0.16 to 4.0 cm²/g relative to calculations which ignore resonance overlap. Spatial self-shielding in a complex geometric cell is evaluated through comparison of Monte Carlo calculations with exact geometric and homogenized absorber region representations. The code EPIGRAM, which selects energy points for resonance cross sections, is reported. Author

N68-22022*# National Aeronautics and Space Administration. Lewis Research Center, Cleveland, Ohio.

GAMMA FLUX AND HEAT DEPOSITION IN PLUM BROOK REACTOR—COMPARISON OF CALCULATION AND EXPERIMENT

Robert J. Bacigalupi and Byron E. Thinger Washington Apr. 1968 24 p refs

(NASA-TM-X-1539) CFSTI: HC \$3.00/MF \$0.65 CSCL 18M

A computerized point-kernel technique (QAD-P5) was used to calculate a gamma-heating map of a thermionic diode experiment proposed to be irradiated in the Plume Brook reactor core. A replica of the diode was used in the low-power mockup reactor at Plum Brook to generate corresponding gamma-heating maps experimentally using lithium fluoride dosimetry. A detailed comparison of experimental and calculated values generally showed agreement to within ± 25 percent. Proper interpretation of the measured values is discussed herein. Author

N68-22038*# United Aircraft Corp., East Hartford, Conn.

STUDIES OF SPECIFIC NUCLEAR LIGHT BULB AND OPEN-CYCLE VORTEX STABILIZED GASEOUS NUCLEAR ROCKET ENGINES

G. H. Mc Lafferty and H. E. Bauer Washington NASA Apr. 1968 102 p refs

(Contract NASw-847)

(NASA-CR-1030; F-910093-37) CFSTI: HC \$3.00/MF \$0.65 CSCL 21F

Analytical studies were conducted to determine the characteristics of two specific vortex-stabilized gaseous nuclear rocket engines: a nuclear light bulb engine and an open-cycle engine. Both engines are based on the transfer of energy by thermal radiation from gaseous nuclear fuel suspended in a vortex to seeded hydrogen propellant. The two engines differ in that the nuclear light bulb engine employs an internally-cooled transparent wall to separate the fuel-containing vortex region from the propellant region, while the open-cycle engine relies entirely on fluid mechanics

containment for preferential retention of the nuclear fuel. The majority of the work has been directed toward the nuclear light bulb engine, since recent fluid mechanics results indicate that the fuel retention characteristics of an open-cycle vortex-stabilized engine are insufficient to provide economic fuel containment. The nuclear light bulb engine offers the possibility of providing essentially perfect containment of the nuclear fuel. The studies indicate approximate values of the thrust, weight, and specific impulse of both configurations. Author

N68-22088*# United Aircraft Corp., East Hartford, Conn. EXPERIMENTAL INVESTIGATION OF RADIAL-INFLOW VORTEXES IN JET-INJECTION AND ROTATING PERI-PHERAL-WALL WATER VORTEX TUBES

Arthur Travers Washington NASA Apr. 1968 38 p refs

(Contract NASw-847)

(NASA-CR-1028; F-910091-14) CFSTI: HC \$3.00/MF \$0.65 CSCL 21F

Experiments were conducted in water vortex tubes to determine the effects of peripheral-wall injection area and axial bypass on the flow pattern and location of the radial stagnation surface in radial-inflow vortexes. The particular type of flow pattern investigated contains a central cell region which is bounded on the outside by a radial stagnation surface which appears to be laminar. At the radius of the radial stagnation surface, all radial flow passes through the end wall boundary layers. The flow in the vortex is laminar for radii less than that of the radial stagnation surface and is turbulent at larger radii. Tests were conducted with different combinations of tangential injection and radial Reynolds numbers, different amounts of bypass flow, and different peripheral-wall injection areas. The characteristics of the flow and the radius of the radial stagnation surface were determined from observations and photographs of dye patterns. The results of the experiments were compared with the results of a previous theoretical investigation of confined vortex Author flows.

N68-23481*# United Aircraft Corp., East Hartford, Conn.

OPTICAL ABSORPTION IN TRANSPARENT MATERIALS FOLLOWING HIGH-TEMPERATURE REACTOR IRRADIA-TION

F. C. Douglas, R. Gagosz, and M. A. DeCrescente $% \left({\left[{R_{c}} \right]} \right)$ Washington NASA May 1968 90 p refs

(Contract NASw-847)

(NASA-CR-1032; F-910485-2) CFSTI: HC \$3.00/MF \$0.65 CSCL 18M

An experimental investigation was conducted to determine the optical absorption levels induced in fused silica as a result of exposure to nuclear reactor irradiation over a range of fast neutron fluxes, fast neutron doses, and reactor temperatures. Also included in the investigation were a limited number of specimens made from alumina, hot-pressed beryllia, and single crystal beryllia. Measurements of the ultraviolet transmittance spectrum were made prior to the reactor irradiation, after the reactor irradiation, and after a series of cobalt-60 gamma irradiations. Measurements were also made during and after heat treatments at elevated temperatures. The induced absorption coefficients were determined from these measurements at the centers of absorption bands located at 0.215 and 0.163 microns.

N68-23894*# National Aeronautics and Space Administration. Lewis Research Center, Cleveland, Ohio.

REACTIVITY INSERTIONS IN COMPACT REACTOR CORES DUE TO FUEL MOVEMENT

Robert E. Sullivan Washington May 1968 14 p refs

(NASA-TM-X-1587) CFSTI: HC\$3.00/MF\$0.65 CSCL 18J

The reactivity effect of fuel movement in several compact reactor cores, highly fueled with uranium-233 dioxide was calculated using a computer program to solve the Boltzmann transport equation. Author **N68-24559***# National Aeronautics and Space Administration. Lewis Research Center, Cleveland, Ohio.

REACTIVITY CONTROL OF FAST-SPECTRUM REACTORS BY REVERSIBLE HYDRIDING OF YTTRIUM ZONES

John L. Anderson, Wendell Mayo, and Edward Lantz Washington Jun. 1968 35 p refs

(NASA-TN-D-4615) CFSTI: HC\$3.00 /MF\$0.65 CSCL 18D

The temperature dependent equilibrium hydrogen content of yttrium hydride above 1173°K is investigated as a means of reactivity control for a cylindrical reactor using zones of hydride in various in core and reflector configurations. The temperature dependence is such that the control system is inherently self-regulating. Severe power peaking, dependent on the hydrogen density, occurs at the hydride core interfaces. Use of auxiliary control for startup reduces the control demand on the variable hydriding system and thus reduces the power peaking. A configuration for which the reactivity control satisfies required core life and power peaking limits is presented. Author

N68-25058*# National Aeronautics and Space Administration. Lewis Research Center, Cleveland Ohio.

AGES OF D(D,N)HE SUP 3 AND T(D,N)HE SUP 4 NEUTRONS IN WATER AND TUNGSTEN-WATER MIXTURES Roger L. Alexander, Donald F. Shook, and Donald Bogart Washington May 1968 22 p refs

(NASA-TN-D-4581) CFSTI: HC\$3.00/MF\$0.65 CSCL 18J

Ages for D-D and D-T neutrons were measured. Experimental and calculated ages were in agreement for water, but measured ages exceeded calculated ages for tungsten-water mixtures. The discrepancy increases with an increase in the volume fraction of metallic tungsten in the tungsten-water mixture. The most probable reasons for the discrepancy are incomplete data for the partial inelastic cross sections of the tungsten isotopes and the inadequacy of the evaporation model used to represent inelastic scattering above 1.5 MeV in the GAM II cross section compilation. Author

N68-26764*# National Aeronautics and Space Administration. Lewis Research Center, Cleveland, Ohio.

METHOD FOR CALCULATING ALLOWABLE CREEP STRESS IN LINEARLY INCREASING STRESS ENVIRON-MENT

Charles L. Whitmarsh, Jr. Washington Jan. 1968 12 p refs (NASA-TN-D-4352) CFSTI: HC \$3.00/MF \$0.65 CSCL 18J

An analytical technique was developed to calculate the allowable design stress for a specified creep limit of a material under conditions of linear stress buildup and constant temperature. The analysis utilizes constant-stress creep data in the integration of a stress-dependent creep rate over the material history. Allowable design stress limits for 1-percent creep of refractory metals in the temperature range 800° to 1600°K are increased by 25 to 57 percent when compared with calculations based on the constant end-of-life stress conditions.

N68-28304*# National Aeronautics and Space Administration. Lewis Research Center, Cleveland, Ohio.

AXIAL POWER TAILORING TO OBTAIN CONSTANT FUEL-CENTERLINE TEMPERATURE IN A NUCLEAR REACTOR

Harry W. Davison Washington Jul. 1968 43 p refs

(NASA-TN-D-4658) CFSTI: HC\$3.00/MF\$0.65 CSCL 18L

The total-power output from a nuclear reactor can be increased by tailoring the axial-power shape if reactor power is limited by fuel-centerline temperature. The potential power gains and the axial-power shape required to obtain a constant fuel-centerline temperature are calculated using steady-state heat-transfer calculations on a long fuel rod cooled externally by forced convection. Steady-state two-group neutron diffusion theory is used to predict the axial-fuel loading required to obtain the desired axial-power shape. Fuel loadings and neutron-flux distributions are presented for various axial-power shapes required in a reflected, water moderated, and cooled reactor. Author

N68-29390*# Florida Univ., Gainesville.

GRAPHITE TRIPLE POINT AND SOLIDUS-LIQUIDUS INTERFACE EXPERIMENTALLY DETERMINED UP TO 1000 ATMOSPHERES

Glen J. Schoessow Washington NASA July 1968 38 p refs (Contract NAS3-10412)

(NASA-CR-1148) CFSTI: HC \$3.00/MF \$0.65 CSCL 18J

A pressure cell with a resistance heated graphite test specimen in a helium atmosphere was used to experimentally determine the triple point of graphite and the solidus liquidus interface to 1000 atmospheres absolute. Four grades of graphite were tested for triple point pressure and temperature. The triple point pressure was determined to be 103 atmospheres absolute for the four grades. The temperature varied for each grade. The solidus liquidus interface from the triple point to 1000 atmospheres was experimentally determined for one grade of graphite. The melting temperature increased with increasing pressure from 7645°R at 103 atmospheres to 7750°R at 1000 atmospheres absolute based on a linear least squares fit.

N68-29950*# National Aeronautics and Space Administration. Lewis Research Center, Cleveland, Ohio.

NEUTRONIC EFFECTS ON MODERATOR INSERTION IN FAST-SPECTRUM REACTORS

Wendell Mayo Washington Aug. 1968 18 p refs

(NASA-TM-X-1614) CFSTI: HC\$3.00/MF\$0.65 CSCL 181

A study of the effects of insertion of yttrium hydride into fast-spectrum reactors was conducted. Large, negative moderator temperature coefficients of reactivity that became more negative with increasing moderation were found. Partial or primary reactor control could be based on this temperature coefficient. An increase in the mean prompt-neutron lifetime and a decrease in the positive reactivity coefficients of volumetric compression were observed whem moderator was added. Moderator addition, however, increases the core size and results in larger fast-neutron fluxes in the reflector, causing increased shield weight for compact nuclear spacepower systems. Author

N68-30516*# National Aeronautics and Space Administration. Lewis Research Center, Cleveland, Ohio.

CHARACTERISTICS OF A SPACE-POWER NUCLEAR REACTOR WITH CONSIDERATIONS FOR VENTING OR CONTAINING GASEOUS FISSION PRODUCTS John V. Miller Washington Aug. 1968 57 p refs

(NASA-TM-X-1631) CFSTI: HC\$3.00/MF\$0.65 CSCL 18L

A study of a fast spectrum, liquid metal cooled reactor in which the gaseous fission products were either completely vented, completely contained, or partially vented from the fuel element, was performed. Although several areas were found in which insufficient data are currently available to accurately analyze the problem, the characteristic behavior of the various concepts was determined using fuel temperature, cladding strain, and nuclear criticality as limiting conditions. The analysis shows that the concepts. This size advantage decreases as the strength of the cladding increases and as the allowable fuel temperature decreases. Author

N68-30750*# National Aeronautics and Space Administration. Lewis Research Center, Cleveland, Ohio.

NEUTRONIC CALCULATIONS OF FUEL AND POISON DRUM CONTROL OF REFRACTORY-METAL, FAST-SPECTRUM, SPACE POWER REACTORS

Robert M. Westfall and Wendell Mayo Washington Aug. 1967 24 p refs

(NASA-TN-D-4709) CFSTI: HC\$3.00/MF\$0.65 CSCL 18L

An analytical procedure was developed to evaluate drum control worths with one-dimensional, radial, discrete ordinate transport calculations. Two types of drum control were evaluated, one with fuel drums containing a heavy-metal reflector material, the other with poison drums containing beryllium oxide and boron carbide. The one-dimensional procedure gave small-core drum control worths which agree with two-dimensional calculations to within 7 percent. The control response curves from two-dimensional calculations agree with $\sin^2(\theta/2)$ curve to within 15 percent. Poison control drum worths are sufficient for 40-centimeter-diameter cores. Fuel control drums are applicable to cores as large as 80 centimeters in diameter.

N68-32968*# National Aeronautics and Space Administration. Lewis Research Center, Cleveland, Ohio.

ELECTRON-BOMBARDMENT FILAMENT DESIGNS FOR HEATING CYLINDRICAL THERMIONIC CONVERTERS Peter Cipollone Washington Aug. 1968 20 p refs

(NASA-TM-X-1630) CFSTI: HC\$3.00/MF\$0.65 CSCL 18N

The effect of axially varying the pitch of helical electron-bombardment heaters on the axial distribution of radial heat flux to an internally heated hollow cylinder was investigaged; the cylinder simulating the electron-emitting electrode of a thermionic converter. Measured axial distributions of temperature and corresponding calculated heat fluxes are presented for a series of five variable-pitch filaments and for mean emitter-surface temperatures of 1778 to 2038°K. These results are compared to similar data obtained with a uniform-pitch filament. Author

N68-32983*# General Electric Co., Pleasanton, Calif. THERMAL CONDUCTIVITY OF COATED PARTICLE URANIUM DIOXIDE TUNGSTEN CERMETS

L. N. Grossman Washington NASA Aug. 1968 27 p refs (Contract NAS3-8511)

(NASA-CR-1154) CFSTI: HC \$3.00 / MF \$0.65 CSCL 18J

The thermal conductivity of cermets fabricated by hot-pressing of tungsten (W) coated uranium dioxide (UO_2) was measured. Data obtained from specimens containing nominally 80 and 60 volume percent UO_2 were compared with theoretical predictions based on Bruggman's model. Excellent agreement was found between theory and experiment in the 80 volume percent case in the temperature range of 900 to 1500°C. Less satisfactory agreement was obtained in the 60 volume percent case between 600 and 1700°c; the discrepancies could not be explained. The experimental technique, specimen preparation, experimental results and post-experiment metallography are presented.

N68-34087*# National Aeronautics and Space Administration. Lewis Research Center, Cleveland, Ohio.

PRELIMINARY STUDY OF A THERMIONIC REACTOR CORE COMPOSED OF SHORT-LENGTH EXTERNALLY FUELED DIODES

Howard G. Yacobucci Washington Sep. 1968 69 p refs (NASA-TN-D-4805) CFSTI: HC\$3.00/MF\$0.65 CSCL 181

The characteristics of a thermionic reactor-core concept, aimed at incorporation of the best features of several previously proposed concepts, are studied. Optimization of diode dimensions resulted in a reference design for a 211-kW electric core. The design, which employs electrical zoning to reduce the detrimental effect of radial thermal power variation, was analyzed for various electrical failures. Equations were derived for calculating internal resistance losses in diodes that have an electrical conductor in parallel with an electrode. Author

N68-35073*# National Aeronautics and Space Administration. Lewis Research Center, Cleveland, Ohio.

COMPARISON OF SMALL WATER-GRAPHITE NUCLEAR ROCKET STAGES WITH CHEMICAL UPPER STAGES FOR UNMANNED MISSIONS

M. Ray Clark, Gary D. Sagerman, and Gerald P. Lahti Washington Sep. 1968 58 $\,p\,$ refs

(NASA-TN-D-4827) CFSTI: HC\$3.00/MF\$0.65 CSCL 21F

Payload performance and the radiation environment characteristics of this small reactor type (200 to 600 MW power)

in a nuclear upper stage are considered. Payload dose criteria indicate that any shielding requirement would be based on propellant heating considerations. Several approaches to propellant heating, including subcooled or slush hydrogen propellant and shielding, are compared. Potential performance gains are outlined for the Saturn 1B and 260-inch solid launch vehicles when employing orbital nuclear start engine firing, optimum nuclear thrust, and subcooled hydrogen propellant. Payload sensitivity to the nuclear-stage jettison weight and to the shielding approach to propellant heating is illustrated. Author

N68-35153*# General Electric Co., Cincinnati, Ohio. CB-12R SODIUM THERMAL CONVECTION LOOP

E. E. Hoffman and J. Holowach Washington NASA Sep. 1968 135 p refs

(Contract NAS3-2547)

(NASA-CR-1097; R67SD3014) CFSTI: HC \$3.00/MF \$0.65 CSCL 20M

A sodium thermal convection loop constructed of Cb-1Zr was tested for 1000 hours at temperatures up to 2380°F. The purpose of the experiment was to evaluate several of the components selected for subsequent use in a two-loop Cb-1Zr facility in which liquid sodium was to circulate in a primary loop and potassium was to circulate in a two-phase secondary loop. In general, the components tested performed satisfactorily. No significant corrosion of the Cb-1Zr by the high temperature sodium was observed and the level of the vacuum environment maintained during the experiment prevented deleterious contamination of the Cb-1Zr tubing. The results of chemical analysis indicated a migration of the loop to the cooler regions. Author

N68-35826*# United Aircraft Corp., East Hartford, Conn. OPTICAL ABSORPTION AND FLUORESCENCE IN FUSED SILICA DURING TRIGA PULSE IRRADIATION

R. Gagosz and J. Waters Washington NASA Sep. 1968 43 p refs

(Contract NASw-847)

(NASA-CR-1191; G-910485-3) CFSTI: HC \$3.00/MF \$0.65 CSCL 18J

An experimental investigation was conducted at the Mark Il pulse reactor to determine the spectral transmission characteristics during and after an irradiation pulse and to determine the cause of the apparent increase in transmission during the pulse and the apparent decrease of trnasmission after the pulse which had been observed in the previous test program. A total of 91 experiments were performed on six specimens at a range of temperatures from 500 to 900C. Transmission measurements were made at two wavelengths, 2150 and 3021 Angstroms. Corning 7940 fused silica specimens in a corner cube configuration were mounted next to the reactor core face at the internal end of a reactor beam port. Peak neutron and gamma fluxes obtained from this reactor were approximately $5=4 \times 10^{15} \text{ n/cm}^2\text{-sec}$ and $6.1 \times 10^7 \text{ R/sec}$. respectively. Neutron and gamma doses associated with these pulses were 2.3 \times 10⁻¹⁴ n/cm² and 2.0 \times 10⁶R, respectively. In addition to the transmittance tests, bypass and optical instrumentation tests were conducted to examine the influence of the optical instrumentation tests were conducted to examine the influence of the optical alignment parameters upon system operation. Fluorescent test were also conducted to obtain an applicable correction to the transmittance runs. Author

N68-36055*# National Aeronautics and Space Administration. Lewis Research Center, Cleveland, Ohio. HIGH POWER KINETICS OF A TWO DIMENSIONAL CIRCULATING LIQUID METAL FUEL REACTOR

Michael J. Kolar Washington Oct. 1968 54 p refs (NASA-TN-D-4840) CFSTI: HC\$3.00/MF\$0.65 CSCL 18K

A two dimensional model of a single channel unreflected circulating fuel reactor is used to investigate the effect of a radial temperature distribution on the neutron kinetics. A slug flow model with no delayed neutrons is used. The effects of a nonuniform radial heat source distribution and radial heat transfer are taken into account. Results show that radial heat transfer has little effect on the kinetics. Furthermore, if changes in multiplication are not too large, the flux and radial temperature distribution maintain their steady state shapes throughout the transient. For certain combinations of the physical parameters, resonances can occur in the time dependent flux and temperature. These resonances can be predicted by either a line reactor model or a two dimensional reactor model; however, a two dimensional model is necessary to predict the value of the steady state flux and temperature following Author a transient.

N68-36615*# United Aircraft Corp., East Hartford, Conn. EXPERIMENTAL STUDY OF MULTI-COMPONENT COAXIAL-FLOWJETS IN SHORT CHAMBERS

Bruce V. Johnson Washington NASA Oct. 1968 84 p refs (Contract NASw-847)

(NASA-CR-1190; G-910091-16) CFSTI: HC \$3.00/MF \$0.65 CSCL 21F

Fluid mechanics experiments were performed to obtain information applicable to an open cycle, coaxial flow, gaseous nuclear rocket engine. In this engine concept, gaseous nuclear fuel and a surrounding stream of seeded hydrogen propellant pass coaxially through a reactor chamber. The flow was simulated in the present experiments by multicomponent, constant temperature, coaxial flow jets in short chambers. The flow was studied using flow visualization techniques and concentration measurements. Author

N68-37209*# National Aeronautics and Space Administration. Lewis Research Center, Cleveland, Ohio.

VERY HIGH BURNUP VAPOR TRANSPORT FUEL PIN CONCEPTFOR LONG LIFE NUCLEAR REACTORS

Frank E. Rom, Patrick M. Finnegan, and Glen E. McDonald Washington Oct. 1968 33 p refs

(NASA-TN-D-4860) CFSTI: HC\$3.00/MF\$0.65 CSCL 18I

A very-high-burnup, vapor-transport fuel-pin concept is presented. Sample calculations using the design charts given in the report show that fission densities in the range of 10²⁰ to 10²¹ fissions per cubic centimeter are conservatively predicted. The fuel within the pin can be operated at sufficiently high inside surface temperatures so that fuel redistribution will occur by design. This feature accommodates and relieves the adverse effects of nonuniform power distribution, hot spots, and nonuniform burnup. Changes in reactor reactivity due to high burnup are minimized with the vapor-transport fuel-pin concept.

N68-37260*# National Aeronautics and Space Administration. Lewis Research Center, Cleveland, Ohio.

GAMMA HEATING IN THIN HEAVY-ELEMENT ABSORBERS

John H. Lynch, Richard J. Crum, and Harry J. Reilly Washington Oct. 1968 20 p refs

(NASA-TM-X-1680) CFSTI: HC\$3.00/MF\$0.65 CSCL 18K

The ratio of gamma heating per gram of tungsten to gamma heating per gram of water was calculated for the case of a thin tungsten detector in a water shield. One dimensional transport theory calculations were used to obtain response polynomials which predict this ratio as a function of source energy, shield thickness, and detector thickness. Electron transport effects were also examined Useful results are presented in the form of graphs. Author

N68-37927*# National Aeronautics and Space Administration. Lewis Research Center, Cleveland, Ohio.

EFFECT OF TURBULENT MIXING ON AVERAGE FUEL TEMPERATURES IN A GAS-CORE NUCLEAR ROCKET ENGINE Albert F. Kascak and Annie J. Easley Washington Nov. 1968 28 p refs

(NASA-TN-D-4882) CFSTI: HC\$3.00/MF\$0.65 CSCL 21F

A heat transfer analysis was made for a coaxial flow nuclear rocket. The analysis considers one-dimensional radial transfer of heat, by both radiation and turbulent mixing from a centrally located fissioning gas to a coaxially flowing propellant. The results compare the effective thermal conductivities for radiation and turbulent mixing. Also included are typical radial-temperature profiles at various axial locations and average fuel temperatures showing the effect of neglecting turbulent mixing. Turbulent mixing had a large effect on local temperature in regions where the fuel density was smallest. Therefore, the effect of turbulent mixing on the average fuel temperature was small.

23

PHYSICS, GENERAL

Includes acoustics, cryogenics, mechanics, and optics. For astrophysics see: 30 Space Sciences. For geophysics and related information see also: 13 Geophysics, 20 Meteorology, and 29 Space Radiation.

N68-10354*# National Aeronautics and Space Administration. Goddard Space Flight Center, Greenbelt, Md. OPTICAL ALIGNMENT OF SILICON CRYSTALS

Felix E. Geiger and Sidney Brashears (Electro-Mech. Res., Inc.) Washington NASA Nov. 1967 11 p refs

(NASA-TN-D-4187) CFSTI: HC\$3.00/MF\$0.65 CSCL 20L

The principles of optical alignment of crystals, specifically silicon, are discussed. A relatively simple apparatus is described which allows crystal orientation to within $\pm 2^{\circ}$ or better, depending on the crystal plane. Data are presented and optical reflection patterns are given which identify not only the usually given [100], [110], and [111] planes but also the [311] and [122] planes. The usefulness of the latter two is pointed out when crystal orientations in more than one direction are required. The relationship between reflectograms and stereographic projection of crystal planes, and the latter's use for identifying optical reflections, are pointed out. An Appendix gives some useful hints on cutting such crystal wafers as required in solar cell and transistor technology, and in the measurement of Hall effect, resistance, and electron spin resonance.

N68-10674* Mississippi State Univ., State College. MICROWAVE SPECTROSCOPY OF MOLECULES: BIBLI-OGRAPHY, 1964–1966

Gordon E. Jones, B. Wayne Castleman, and Rudolph G. Oswald Washington NASA Nov. 1967 42 p refs

(Grant NGR-25-001-008)

(NASA-CR-951) CFSTI: \$3.00 CSCL 07D

A bibliography is presented on the various studies pertaining to the adaptation of microwave spectroscopy to the problem of detecting and identifying contaminants in the atmosphere of closed space capsules. Emphasis is placed on the microwave measurement of gases, and the listings are grouped according to inorganic molecules and organic molecules. M.G.J.

N68-13115*# Lockheed Missiles and Space Co., Palo Alto, Calif. DESIGN AND CONSTRUCTION OF AN ENGINEERING MODEL SOLID CRYOGEN REFRIGERATOR FOR INFRARED DETECTOR COOLING AT 50°K

R. P. Caren and R. M. Coston Washington NASA Jan. 1968 65 p. refs

(Contract NAS5-9549)

(NASA-CR-988) CFSTI: HC\$3.00/MF\$0.65 CSCL 13A

Structural and thermal design evaluations for a spaceborne sublimating solid cryogenic refrigerator resulted in the development of a prototype stacked unit that uses two cylindrical cryogen containers and a common vacuum space. The argon and carbon dioxide containers keep infrared detector operating temperature down to about 52°K. The refrigerator is able to remain unvented and in solid state during spacecraft boost phase, as well as for several days of a hold phase before the temperature rises markedly. G.G.

N68-15950*# National Aeronautics and Space Administration. Manned Spacecraft Center, Houston, Tex.

SUBCRITICAL CRYOGENIC STORAGE DEVELOPMENT AND FLIGHT TEST

R. K. Allgeier Washington Feb. 1968 92 p refs

(NASA-TN-D-4293) CFSTI: HC\$3.00/MF\$0.65 CSCL 20M

A subcritical cryogenic nitrogen system was aboard Apollo-Saturn flight 203 on July 5, 1966. This flight completed development of this particular sub-critical system. This paper contains the development history, ground-test results, and flight-test results of a sub-critical cryogenic storage system which is designed to supply warm vapor regardless of the liquid orientation. A two-phase development program resulted in delivery of ground-test units and flight units. The successful flight test culminated development efforts with this subcritical system and demonstrated its feasibility. Author

N68-21444*# Michigan Univ., Ann Arbor. Dept. of Electrical Engineering.

ELECTROMAGNETISM IN MOVING, CONDUCTING MEDIA

Rudolph M. Kalafus (Ph.D. Thesis) Washington NASA Apr. 1968 95 p refs

(Grant NGR-23-005-107)

(NASA-CR-1025; Rept.-7322-3-T) CFSTI: HC \$3.00/MF \$0.65 CSCL 20C

Based on Minkowski's theory of the electrodynamics of moving bodies, the present work is concerned with the systematic solution of problems involving sources placed in a uniformly moving, conducting medium. In order to accomplish this it is first necessary to examine the two differing forms of Ohm's law for moving media that are found in the literature. It is concluded here that the two forms are equivalent and interchangeable, and that their apparent difference arises out of different definitions of conduction and convection currents. Another difficulty which is encountered when dealing with conducting media is related to the relaxation phenomenon. The total charge and current densities cannot be independently specified, but must be consistent with the relaxation phenomenon; for non-conducting media only the equation of continuity must be met. A scheme is developed here which involves a separation of currents and charges into source and response terms. The source terms can be specified independently, but the total charge must be consistent with Maxwell's equations. Vector and scalar potentials are developed from the field quantities, and partial differential equations for the potentials are derived for two classes of problems: static charge sources, and harmonic current sources. For unbounded regions potential solutions are found by the method of Green's functions, which satisfy the same differential equations. The differential equations are solved by transform methods, and the Green's functions are found in closed form. The medium is assumed to have constant scalar parameters of permittivity, permeability, and conductivity. The results are valid for all values of conductivity and frequency, and for relativistic velocities. Author

N68-24146*# National Aeronautics and Space Administration. Goddard Space Flight Center, Greenbelt, Md.

A THEORETICAL APPROACH TO THE DETERMINATION OF MAGNETIC TORQUES BY NEAR FIELD MEASUREMENT

J. C. Boyle, J. Greyerbiehl, and E. J. Mosher Washington May 1968 22 p refs

(NASA-TN-D-4485) CFSTI: HC\$3.00/MF\$0.65 CSCL 20C

Using the concept of stress in the medium as postulated by Faraday and developed mathematically by Maxwell and Jeans, equations are derived for the torque on a magnetic object immersed in an arbitrary magnetic field. The calculation requires a knowledge of the magnetic intensity vector over any closed surface which encompasses the magnetic object of interest. Torque equations are derived for the case where the closed surface is a sphere of arbitrary radius and also where the closed surface is a right circular cylinder. The validity of the equations is tested by applying them to a simple intensity distribution (that of a theoretical dipole) where the resultant torque is known a priori. There is also a discussion of permanent versus induced moments and a technique which can be used to separately identify these components based on near field information. Author

N68-25868*# National Aeronautics and Space Administration. Goddard Space Flight Center, Greenbelt, Md.

OPTICALLY INDUCED FREE-CARRIER LIGHT MODULATOR

C. Gruber and W. E. Richards Washington Jun. 1968 18 p refs

(NASA-TN-D-4608) CFSTI: HC \$3.00 /MF \$0.65 CSCL 20F

Laser modulators for optical communications systems have recently been the subject of great effort especially in visible or near-infrared regions. The availability of optical sources in these regions, where excellent atmospheric transmission "windows" exist, has prompted attempts to extend the previously developed modulation techniques to longer wavelengths. Existing devices have other disadvantages such as excessive drive power requirements for high-frequency/wide-bandwidth operation, multicomponent optical configurations, inability to modulate at high optical power levels, and (with one or two exceptions) low modulation index. The present paper describes an optical modulation technique that should be able to overcome many of these difficulties and, in addition, provide complete electrical isolation of the modulation element. In addition the technique can be used over a broad range of infrared wavelengths determined solely by the optical transmission characteristics of the modulator material. In brief, this technique uses optically generated free electrons (and/or holes) in a bulk semiconductor in order to change its transmission characteristics. Apart from its construction in suitable semiconducting material, the modulator requires an easily modulated optical pump signal. Author

N68-28259*# National Aeronautics and Space Administration. Lewis Research Center, Cleveland, Ohio.

AN EXPLANATION OF FITZGERALD'S AUDIOFREQUENCY RESONANCES AND SOUND BEAMS

Donald R. Behrendt and James P. Cusick Washington Jun. 1968 12 p refs

(NASA-TN-D-4625) CFSTI: HC\$3.00/MF\$0.65 CSCL 20A

Fitzgerald's method is used to investigate the origin of his audiofrequency resonant phenomena. The source of the phenomena is shown from experiment to arise from the stiffness of the sample-shaker interface and not from a process associated with the interior of the sample, as proposed by Fitzgerald. The resonance effects are explained in terms of conventional elastic theory. Author N68-30596*# National Aeronautics and Space Administration. Lewis Research Center, Cleveland, Ohio.

MEASUREMENT OF THE TRANSMISSIVITY OF A CARBON-PARTICLE-SEEDED NITROGENJET Chester D. Lanzo Washington Aug. 1968 18 p refs

(NASA-TN-D-4722) CFSTI: HC\$3.00/MF\$0.65 CSCL 20F

An experiment was conducted to measure the transmissivity of a flowing steam of nitrogen gas that had been seeded with nominal 0.009-micron carbon particles. The seed density and light-beam wavelength were the variables of the experiment. Seed density was varied from 10-5 to 10-4 g/cm³. Wavelength was varied from 200 millimicrons to 3500 millimicrons. The results are presented as a ratio of transmitted to incident light intensity, and as an absorption cross section. Scattering is assumed to be unimportant. The experimental results show that the absorption cross section decreases as the seed density increases. This is attributed to particle agglomeration. The measurements also show that, for all practical purposes, the absorption cross section is independent of wavelength for wavelengths from 200 to 3500 millimicrons.

N68-36460*# National Aeronautics and Space Administration. Electronics Research Center, Cambridge, Mass.

MATHEMATICAL DETERMINATION OF GEOMETRICAL IMAGE ABERRATIONS IN SINGLE AND DOUBLE MIRROR SYSTEMS

Martin G. Hurwitz and Hubert F. A. Tschunko Washington Oct. 1968 25 p refs

(NASA-TN-D-4692) CFSTI: HC\$3.00/MF\$0.65 CSCL 20F

The mathematical analyses to determine the image aberrations of single and double mirror systems are presented. The single mirrors, spherical and paraboloidal, are considered. Then, double mirror systems with paraboloidal primary and hyperboloidal secondary are considered, along with higher aspherics of the secondary and tolerances in the relative positions of the mirrors. This investigation is a first step in the evaluation of the imaging performance of single and double mirror systems. The general analysis available in the literature is not applicable without development for the special requirements of the present cast. This special raytracing is the prerequisite needed later for the Fourier transformations which serve to derive the image performance data necessary to the determination of wave optical aberrations. Author

N68-36470*# National Aeronautics and Space Administration. Ames Research Center, Moffett Field, Calif.

EFFECTS OF EDGE CONSTRAINTS ON OPTICAL QUALITIES OF A SPACECRAFT WINDOW

David N. Warner, Jr. and Thomas M. Walsh Washington Oct. 1968 37 p refs

(NASA-TN-D-4845) CFSTI: HC\$3.00/MF\$0.65 CSCL 22C

Some effects of edge constraints on optical qualities of Gemini spacecraft windows were determined experimentally. Frames approaching theoretical fixed-edge and free-edge constraints were designed and constructed for the investigation. Gemini window frames were also used so that the idealized frames could be compared to an operational window frame. Direct measurements were made of the flatness and wedge angle of the windowpanes. the resolution loss through the window, the angular deviation of a line of sight, and the distortion of a flat wave front traveling through the window assembly. Space pressure differentials were applied to the window to bow the panes and simulate the effect of the space environment. Tests showed that edge constraints on spacecraft windows significantly affect their optical qualities. The qualities become irregular, particularly at high incidence angles, as the panes are distorted in the simulated space environment. Although the clamped edge frames did not provide a strictly theoretical fixededge condition, they did allow less surface deflection, less angular deviation to the line of sight, and less distortion to a plane wave Author front.

N68-37792*# Israel Program for Scientific Translations, Ltd., Jerusalem.

ANALYTICAL MECHANICS. STABILITY OF MOTION. CELESTIAL BALLISTICS [ANALITICHESKAYA MEKHANIKA, USTOICHIVOST' DVIZHENIYA, NEBESNAYA BALLISTIKA]

A. I. Lur'e, ed. et al 1968 262 p 454 refs Transl. into ENGLISH of the "Proc. of the 2nd All-Union Conf. on Theoret. and Appl. Mech., Pt. 1" Moscow, Izd. Nauka, 1965 Conf. held at Moscow, 29 Jan. – 5 Feb. 1964 Sponsored jointly by NASA and NSF

(NASA-TT-F-503; TT-68-50305) CFSTI: HC \$3.00/MF \$0.65 CSCL 20

CONTENTS:

1. DEVELOPMENT OF THE THEORY OF CANONICAL EQUATIONS OF ANALYTICAL MECHANICS I. S. Arzhanykh p 1–10 refs (See N68-37793 24-23)

2. STABILITY AND INSTABILITY OF DYNAMIC SYSTEMS WITH MANY DEGREES OF FREEDOM V. I. Arnold p 11–14 (See N68-37794 24-23)

3. APPLICATION OF STABILITY THEORY TO STATIC AND DYNAMIC STABILITY PROBLEMS OF POWER SYSTEMS G. V. Aronovich et al p 15–26 refs (See N68-37795 24-23)

4. ABSOLUTE STABILITY OF NONLINEAR CONTROL SYSTEMS F. R. Gantmakher et al p 27-66 refs (See N68-37796 24-23)

5. CONTINUUM PROBLEMS FOR ANALYTICAL MECHANICS N. A. Kil'chevskii p 67–81 refs (See N68-37797 24-23)

6. PROBLEMS OF CONTROLLABILITY, OBSERVABILITY, AND STABILIZABILITY OF DYNAMIC SYSTEMS N. N. Krasovskii p 83-100 refs (See N68-37798 24-23)

7. OPTIMAL CONTROL AND STABILITY A. M. Letov p 101-123 refs (See N68-37799 24-23)

8. DEVELOPMENT OF THE METHOD OF LYAPUNOV FUNCTIONS IN STABILITY THEORY V. M. Matrosov p 124–140 refs (See N68-37800 24-23)

9. SOME PROBLEMS IN DYNAMIC STABILITY ANALYSIS OF MECHANICAL SYSTEMS WITH DEFORMABLE ELEMENTS G. N. Mikishev et al p 141–145 (See N68-37801 24-23)

10. EQUATIONS OF MOTION AND THE ROLE OF SMALL PARAMETERSIN THE DYNAMICS OF NONHOLONOMIC SYSTEMS Yu. I. Neimark et al p 146–156 refs (See N68-37802 24-23)

11. ANALYTICAL DYNAMICS AND OPTIMUM TRANSFER V. S. Novoselov p 157-169 refs (See N68-37803 24-23)

12. INVESTIGATION OF THE STABILITY OF MOTION OF SOLID BODIES WITH LIQUID-FILLED CAVITIES V. V. Rumyantsev p 170–188 refs (See N68-37804 24-23)

13. STABILITY OF SYSTEMS WITH DELAY S. N. Shimanov p 189-200 refs (See N68-37805 24-23)

14. OPTIMIZATION PROBLEMS IN THE MECHANICS OF LOW-THRUST SPACE FLIGHT G. L. Grodzovskii et al p 201-221 refs (See N68-37806 24-23)

15. GRAVITY ATTITUDE STABILIZATION OF SATELLITES V. A. Sarychev p 222-232 refs (See N68-37807 24-23)

16. SOME PROBLEMS OF ASTRODYNAMICS G. N. Duboshin et al p 233-238 (See N68-37808 24-23)

24

PHYSICS, ATOMIC, MOLECULAR, AND NUCLEAR

Includes atomic, molecular and nuclear physics. For applications see: 22 Nuclear Engineering. For related information see also: 29 Space Radiation.

N68-11037*# New York Univ., N. Y. QUANTUM MECHANICAL STUDY OF MOLECULES TRANSITION PROBABILITIES, EINSTEIN A COEFFICIENTS AND OSCILLATOR STRENGTHS OF SOME BAND SYSTEMS OF DIATOMIC MOLECULES

D. C. Jain and R. C. Sahni Washington NASA Dec. 1967 45 p refs

(Grant NsG-76)

(NASA-CR-975) CFSTI: HC\$3.00/MF\$0.65 CSCL 20H

The Franck-Condon factors and r-centroids based on the Rydberg-Klein-Rees potential energy curves, have been presented for some band systems of the CO+, N2, N2 and RbH molecules. The variation of the electronic transition moment with the internuclear distance, Re(r), has been determined by the r-centroid procedure for the band systems for which the experimental data on the relative intensity distribution is available. The absolute band strengths, Einstein A coefficients and oscillator strengths have been obtained for some band systems by employing the expression for the electric dipole transition moment, Re(r), and the lifetimes of the excited states. The influence of the vibration-rotation interaction on the transition probabilities of the band system of the RbH molecule was studied and it was found that for this and certain other similar band systems, the vibration-rotation interaction must be included in the theoretical interpretation of the results. The importance and possible applications of these results is also described. Author

N68-11074*# National Aeronautics and Space Administration. Lewis Research Center, Cleveland, Ohio.

SCATTERING OF 42-MEV (6.7-PJ) ALPHA PARTICLES FROM EVEN ISOTOPES OF CADMIUM

Norton Baron, Regis F. Leonard, and William M. Stewart Washington Nov. 1967 19 p refs

(NASA-TN-D-4256) CFSTI: HC\$3.00/MF\$0.65 CSCL 20H

Angular distributions were measured for the elastic and inelastic scattering of 42 MeV (6.7-pJ) alpha particles from isotopically enriched targets of cadmium 110, 112, 114, and 116. In each isotope, five excited states were seen and their excitation energies were determined to ±30 keV (±4.8 fJ). Angular distributions for three of these states were measured over the angular range 30° to 65° Their relative phases and excitation energies indicate that these states are the first 2^+ , the 3^- , and the two phonon 2^+ . It is suggested that the two other excited states result from a quadrupole-octupole two-phonon transition. A tentative spin assignment of 5 - was made for one of them. Elastic angular distributions were analysed using the optical model with a four parameter Woods-Saxon potential. Excellent fits have been obtained for the elastic scattering. Inelastic scattering has been analyzed using a distorted wave Born approximation calculation. These calculated inelastic angular distributions agree very well with the experimentally measured cross sections for scattering to one phonon states, and allow determination of deformation parameters which are in satisfactory agreement with those obtained elsewhere. Author

N68-11634*# Research Systems, Inc., Lexington, Mass. A STUDY OF TRACE CONTAMINANT IDENTIFICATION BY MICROWAVE DOUBLE RESONANCE SPECTROSCOPY Richard J. Volpicelli, Otto L. Stiefvater, and George W. Flynn Washington NASA Dec. 1967 99 p refs (Contract NAS1-6308)

(NASA-CR-967) CFSTI: \$3.00 CSCL 07D

A microwave double resonance spectrometer has been assembled that operates with pump frequencies between 12 GHz and 18 GHz and signal frequencies between 26.5 GHz and 40 GHz. The absorption cell consists of a coiled 100 ft section of X-band guide. Modulation of the double resonance phenomenon is achieved through frequency modulation of the pump radiation, the modulation frequency being 100 KHz. For each of the five molecules CH3CH2CH2CI, CH3CH2COOH, (CH3)2S, (CH₃CH₂COH₁) and CH2Cl2, one or two double resonance connections were selected and suitable for the identification of these compounds. The 3 amplitude of the double resonance signals was studied as a function of the sample pressure for both pure samples and samples diluted in air. In typical cases double resonance signals could be observed in the pressure range from 1 μ Hg to \approx 100 μ Hg. The smallest detectable amount of a gas contaminant was of the order

of \approx .3%. In mixtures of several gases with rich microwave spectra the double resonance technique affords a rapid and extremely specific method for identifying individual components, and there is no ambiguity due to interference from neighboring and/or overlapping lines with only one double resonance connection required to identify the compound from which it arises. Author

N68-11903*# New York Univ., N. Y.

QUANTUM MECHANICAL STUDY OF MOLECULES: Eigenvalues and Eigenvectors of Real Symmetric Matrices

G. R. Verma, C. D. La Budde, and R. C. Sahni Washington NASA Dec. 1967 48 p refs

(Grant NsG-76)

(NASA-CR-983) CFSTI: HC\$3.00/MF\$0.65 CSCL 20J

In this report, three general classes of methods for calculating the eigenvalues and eigenvectors of real symmetric matrices arising in quantum mechanical calculations are described: the Sturm sequence methods, the orthogonal reduction methods, and the step by step methods. The advantages and limitations of each method are pointed out. The report also includes the discussion of various methods of reducing real symmetric matrices to more compact convenient forms. Methods of reduction to tridiagonal form, and deflation of matrices to smaller order are described.

N68-15328*# National Aeronautics and Space Administration. Lewis Research Center, Cleveland, Ohio.

EXCITED STATES OF XENON 128

Glenn M. Julian, S. Jha (Western Reserve Univ.), and A. S. Johnston (Carnegie Inst. of Tech.) Washington Feb. 1968 19 p refs Submitted for publication

(NASA-TN-D-4305) CFSTI: HC\$3.00/MF\$0.65 CSCL 20H

Gamma rays accompanying the decay of 25 minute iodine 128 (¹²⁸I) and 3 minute cesium 128 (¹²⁸Cs) have been studied with 8- and 30-cubic centimeter lithium-drifted germanium spectrometers. Coincidences between gamma rays were studied using two 7.6 by 7.6 centimeter thallium-activated sodium iodide scintillators. A level scheme of Xenon 128 (¹²⁸Xe) has been constructed with levels at 443.2 (2⁺), 969.6 (2⁺), 1583.1 (0⁺, 1⁺, 2⁺), 2275.2, 2484.3, 2600.5, 2841.1, and 2862.8 keV. According to the hydrodynamical model, the near-spherical even-even nucleus ¹²⁸Xe could be expected to have a close-lying 0⁺=2⁺-4⁺ "vibrational triplet" at about twice the energy of the first excited state. Population of the 0⁺ and 2⁺ members of such a triplet would be allowed in the decay of 1⁺ 1²⁸J

24 PHYSICS, ATOMIC, MOLECULAR, AND NUCLEAR

and $1 + \frac{128}{Cs}$. A $2 + level of \frac{128}{Xe}$ at about twice the energy of the first excited state had been found in previous investigations. In the present study a search was made for the predicted 0 + triplet member. No evidence has been found for the existence of such a level. Author

N68-15638*# National Aeronautics and Space Administration. Lewis Research Center, Cleveland, Ohio.

A SEARCH FOR UNBOUND HELIUM 3 LEVELS WITH ISOBARIC SPIN 1/2

Robert E. Warner (Oberlin Coll.), John S. Vincent, and Edmund T. Boschitz Washington Feb. 1968 14 p refs

(NASA-TN-D-4377) CFSTI: HC\$3.00/MF\$0.65 CSCL 20H

An attempt was made to excite the unbound T = 1/2 states in helium 3 by $(\alpha - He^3)$ inelastic scattering. No states in He³ between 3- and 13-MeV excitation were found. The shape of the inelastic alpha particle spectrum was calculated with the assumption that phase space alone determines the shape. Precise fits to the observed spectra were not obtained, but the similarity between calculated and observed spectra gave evidence that a broad maximum in the 17.5° spectrum was caused by phase space rather than a level in He³. Other calculations with Baldin's formalism showed that no enhancement of the inelastic cross section near 8-MeV excitation in He³ should be expected.

N68-17898*# National Aeronautics and Space Administration. Langley Research Center, Langley Station, Va.

EXPERIMENTAL STUDY OF TRANSMISSION AND BACKSCATTER OF 0.075 TO 1.0 MeV ELECTRONS BY ALUMINUM AND STAINLESS STEEL

William E. Miller and Herbert D. Hendricks Washington Mar. 1968 22 p refs

(NASA-TN-D-4363) CFSTI: HC\$3.00/MF\$0.65 CSCL 18F

An experimental study of the transmission and backscatter coefficients for aluminum and stainless steel irradiated with 75-keV to 1-MeV electrons at normal and 45° incidence is reported. The transmission coefficients were greater and the backscatter coefficients were smaller at normal beam incidence than they were at 45° beam incidence for both materials. In all cases the aluminum had higher transmission coefficients and lower backscatter coefficients than did stainless steel. It was determined that the transmission and backscatter coefficients for both aluminum and stainless steel were independent of the number of layers of foils used to attain a given thickness. The ratio of the thickness for maximum backscatter to the extrapolated range was found to be nearly a constant for each material. Transmission curves independent of energy were constructed for aluminum and stainless steel for normal and 45° beam incidence. Author

N68-18118*# Geophysics Corp. of America, Bedford, Mass. STUDIES OF PHOTOABSORPTION BY ATOMIC HYDROGEN, OXYGEN, AND NITROGEN

R. B. Cairns and James A. R. Samson Washington Mar. 1968 119 p refs

(Contract NASw-1283)

(NASA-CR-998; GCA-TR-67-2-N) CFSTI: HC \$3.00/MF \$0.65 CSCL 20H

This report contains an account of experiments made to study the photoabsorption properties of atomic hydrogen, oxygen, and nitrogen. The ultimate objective was the quantitative measurement of atomic photoionization cross sections. The results of the experiments have been combined with recent theoretical estimates of the cross sections and information from spectroscopic studies. Author

N68-18254*# National Aeronautics and Space Administration. Lewis Research Center, Cleveland, Ohio. OPERATIONAL AMPLIFIERS FOR USE IN NUCLEAR SPECTROSCOPY Theodore E. Fessler Washington Mar. 1968 28 p refs (NASA-TN-D-4349) CFSTI: HC \$3.00/MF \$0.65 CSCL 18D

The design of pulse amplifier systems for use in nuclear research can be greatly simplified by the use of fast operational amplifiers. This report treats the design and use of operational amplifiers in circuits with rise times as low as 10 nanoseconds. A specific amplifier circuit is used to illustrate real amplifier performance. Phase-compensation methods and their relation to open-loop amplifier properties are described. Some closed-loop amplifier circuits are used to demonstrate practical phase compensation. Author

N68-18949*# National Aeronautics and Space Administration. Ames Research Center, Moffett Field, Calif.

A CRITICAL EVALUATION OF THE USE OF ULTRASONIC ABSORPTION FOR DETERMINING HIGH-TEMPERATURE GAS PROPERTIES

Warren F. Ahtye Washington Mar. 1968 70 p refs

(NASA-TN-D-4433) CFSTI: HC\$3.00/MF\$0.65 CSCL 20M

The usefulness of ultrasonic absorption for determining the values of high-temperature gas properties has been examined critically. The sources of ultrasonic absorption considered are: viscosity and thermal conductivity (classical absorption), thermal radiation, and relaxation effects due to dissociation, ionization, and electronic excitation by atomic collisions. The absorption values for argon and nitrogen were calculated in an attempt to explain the large disparity between classical values and those measured by Carnevale in a series of electric arc experiments. Ultrasonic absorption in oxygen and in hydrogen was also examined. The calculations show that it is possible to measure the transport coefficients of argon and hydrogen for two states. The transport coefficients of nitrogen and oxygen cannot be measured with any degree of accuracy at any temperature. The calculations show that the ultrasonic absorption associated with thermal radiation is so minute that the absorption technique is incapable of measuring total radiative intensities of atmospheric gases even at temperatures sufficiently high that single ionization occurs. It is shown that most of the anomalous absorption in nitrogen can be attributed to collisional excitation of the bound electrons in nitrogen atoms, but only if a high collisional efficiency exists. Author

N68-21227*# Tennessee Univ., Tullahoma. Space Inst. MIE-SCATTERING FUNCTION

F. Shahrokhi and P. Wolf Washington NASA Apr. 1968 17 \ensuremath{p} refs

(Grant NGR-43-001-021)

(NASA-CR-1022) CFSTI: HC\$3.00/MF\$0.65 CSCL 20H

For a comparison between experimental results and Mie-scattering theory, a series of calculations was made to find the normalized scattering function $f(\theta)$ from the tables of Legendre-polynomials by G. C. Clark and S. W. Churchill and from tables of scattering coefficients made by C. M. Chu, G. C. Clark, and S. W. Churchill. Author

N68-21949*# General Electric Co., Philadelphia, Pa. THE ROLE OF ENERGY IN DEFORMATION I. J. Gruntfest Washington Apr. 1968 31 p refs

(Contract NASw-1190)

(NASA-CR-1039) CFSTI: HC \$3.00/MF \$0.65 CSCL 20L

This report is a review of exploratory analytical studies of the influence of energy conservation on the mechanical behavior of a variety of materials in diverse test situations. The results are presented and discussed so to display their physical implications rather than the details of their development. The work is generally complementary to the existing body of theory relating to mechanical behavior. However, consideration of the necessary coupling between the thermal and mechanical fields in deforming materials does suggest some new approaches to the problems of fracture in solids and flow stability in fluids. Some insights into the role of microstructure in determining the behavior of solids are also suggested. The methods, some of which involve the use of electric analogs of the mechanical system, show how necking, yield and plastic flow may arise. In addition, scale effects are introduced which are likely to be of interest in geophysical phenomena. Author

N68-23893*# National Aeronautics and Space Administration. Lewis Research Center, Cleveland, Ohio.

CALCULATION OF CAPTURE CROSS SECTIONS FOR ION POLAR MOLECULE COLLISIONS INVOLVING METHYL CYANIDE

John V. Dugan, Jr., James H. Rice, and John L. Magee (Notre Dame, Univ.) Washington May 1968 19 p refs

(NASA-TM-X-1586) CFSTI: HC\$3.00/MF\$0.65 CSCL 07E

The cross sections (CS) for capture collisions between the symmetric top molecule CH₃CN and molecular ions are calculated numerically. These ion-molecule collisions were studied experimentally and have large reaction CS, Ω_R . Calculations are done to study the role of the added degree of rotational freedom by comparing capture CS for tops with linear molecules. The monoenergetic CS $\sigma_c(\epsilon_1)$ (where ϵ_1 is the ion energy and T_R is the top rotational temperature) are less than the maximum classical CS σ_{max} , but much larger than Langevin CS σ_L . The integrated σ_c , Ω_c . agree well with Ω_R for the collisions studied. The σ_c values for CH₃CN are nearly independent of target geometry. Author

N68-24661 *# National Aeronautics and Space Administration, Lewis Research Center, Cleveland, Ohio.

INELASTIC SCATTERING FORM FACTORS USING PROJECTED HARTREE-FOCK WAVE FUNCTIONS

Richard C. Braley and William F. Ford Washington May 1968 28 p refs

(NASA-TN-D-4566) CFSTI: HC\$3.00/MF\$0.65 CSCL 20H

The theory of inelastic scattering is formulated, using detailed nuclear wave functions which are obtained from nuclear structure calculations. The inelastic scattering is assumed to proceed through a direct reaction, and nuclear states are obtained by projecting states of $good (J^2, J_2)$ from a variational Hartree–Fock wave function. General expressions for transition amplitudes and the nuclear form factors are derived, and the form factors are compared with those based on the shell model and macroscopic collective model. It is concluded that the restrictions imposed in the Hartree–Fock model must be relaxed if the model is to give the correct order of magnitude for reaction cross sections.

N68-28250*# Northrop Corp., Hawthorne, Calif. Corporate Labs. STUDY ON A TECHNIQUE FOR DETECTING PHOTONS IN THE 100–1000 Å WAVELENGTH REGION Final Report, 15 Apr. 1965–15 Oct. 1967

O. P. Rustgi Washington NASA Jun. 1968 136 p refs (Contract NAS12-3)

(NASA-CR-1096) CFSTI: HC\$3.00/MF\$0.65 CSCL 20H

A general survey of the various modes of interaction of electromagnetic radiation in the 100–1000 Å region with matter was conducted. These interactions were analyzed in terms of photon efficiency, wavelength cut-off, minimum photon flux required for detection of these effects, ease of wavelength resolution through selective detectors. The transmittance of thin films and photoionization in gases are selected as the possible interactions resulting in selective detectors. Thin films of aluminum, bismuth, indium, titanium, and tin are prepared and supported on mosaic glass. Techniques are developed to seal the mosaic glass with a film to the metallic plate. This plate is then used as a filter as well as a window for a rare gas ion chamber to form the resultant

24 PHYSICS, ATOMIC, MOLECULAR, AND NUCLEAR

selective detector. Spectral response characteristics of selective detectors using (1) bismuth film with neon, argon, and krypton; (2) indium film with argon, krypton, and xenon; and (3) titanium film with argon, neon, and helium are presented with emphasis on selectivity of response. Author

N68-28265*# National Aeronautics and Space Administration, Lewis Research Center, Cleveland, Ohio.

COUPLED-CHANNELS METHOD FOR REARRANGEMENT COLLISIONS

Howard C. Volkin Washington Jul. 1968 70 p refs (NASA-TN-D-4633) CFSTI: HC\$3.00/MF\$0.65 CSCL 20H

The classification and construction of open-channel projection operators for a given rearrangement collision are developed from the unifying viewpoint of their projective spaces in the total Hilbert space of the system. The representative case of the pickup or stripping process is treated. The open-channel projection operators are constructed from the channel-subspace projectors with the help of generalized channel transformation functions. Various projection operators that can be obtained in closed form are identified. The use of the projection operators to obtain coupled equations describing the reaction is discussed, including their application to generalized potential models.

N68-29375*# National Aeronautics and Space Administration. Lewis Research Center, Cleveland, Ohio.

GAMMA RAY ANGULAR CORRELATIONS FOLLOWING INELASTIC SCATTERING OF 42-MeV ALPHA PARTICLES FROM MAGNESIUM 24

Regis F. Leonard, William M. Stewart, Norton Baron, and Richard C. Braley Washington Jul. 1968 28 p refs

(NASA-TN-D-4683) CFSTI: HC\$3.00/MF\$0.65 CSCL 20H

The angular correlation between inelastically scattered 42-MeV alpha particles and gamma rays emitted in the subsequent nuclear decay has been studied for the 1.37-MeV state of magnesium 24. The symmetry angle of the gamma distribution and the magnitude of the anisotropy of the gamma distribution have been measured for alpha scattering angles between 30° and 76°. The results are compared with the distorted-wave predictions and with the adiabatic and Wills-Cramer models. Observed symmetry angles do not display the large excursions away from the adiabatic line which were seen in earlier work on magnesium 24 at lower energies and more forward angles.

N68-29520*# National Aeronautics and Space Administration. Goddard Space Flight Center, Greenbelt, Md.

A NUMERICAL LEAST-SQUARE METHOD FOR RESOLVING COMPLEX PULSE HEIGHT SPECTRA

J. I. Trombka and R. L. Schmadebeck Washington 1968 175 p. refs

(NASA-SP-3044) GPO: HC\$1.50; CFSTI: MF\$0.65 CSCL 20H

A least square analysis method is presented for determining the differential energy spectrum from a measurement of the pulse height spectrum. Consideration is given to an empirical matrix inversion method which allows for calculating the relative intensity of the statistical variance based on counting statistics of the correlation between library components and the fit chi-square. In order to obtain a unique solution and a non-oscillating solution, physical constraints are included either as an iterative search mode for nonegativity or a component subtraction mode in the computer program. An assessment is made of the nonlinearities in the pulse height scale that can be attributed to gain shift and zero drift. A method for background subtraction and the use of the background as a library component in the least square analysis were considered. The details of the structure of the computer programs, the FORTRAN statement of the program, data for use in the program, and typical computer outputs are presented. B.S.D.

24 PHYSICS, ATOMIC, MOLECULAR, AND NUCLEAR

N68-30001*# National Aeronautics and Space Administration. Lewis Research Center, Cleveland, Ohio.

FISSION NEUTRON ATTENUATION IN LITHIUM-6, NATURAL LITHIUM HYDRIDE, AND TUNGSTEN

Gerald P. Lahti Washington Aug. 1968 24 p refs

(NASA-TN-D-4684) CFSTI: HC\$3.00/MF\$0.65 CSCL 18G

A fission-spectrum neutron-dose-rate-attenuation curve was computed by the discrete-ordinates method for Li⁶H and natural LiH for penetration depths up to 139.5 cm. Results were compared with a recent Monte Carlo calculation for natural LiH. A single value for an energy-independent-neutron-removal cross section for Li⁶ and natural Li in LiH was deduced for use in an Albert-Welton dose-attenuation kernel but is accurate for only a given range of penetration. The validity of fast-neutron-removal theory was demonstrated for the cases of W followed by LiH. From this penetration data, a neutron-removal cross section for W was calculated. Author

N68-33763*# National Aeronautics and Space Administration. Lewis Research Center, Cleveland, Ohio.

MEASUREMENT OF THE B 10 (n, α) Li 7, Li 7* RELATIVE CROSS SECTIONS IN THE keV REGION

Donald Bogart and Lowell L. Nichols (Batelle-Northwest) Washington Sep. 1968 25 p refs

(NASA-TN-D-4783) CFSTI: HC\$3.00/MF\$0.65 CSCL 20H

Relative cross sections for $10B(n,\alpha)$ 7Li, 7Li* were obtained from measurements of the counting ratios of a $10BF_3$ proportional counter and a precision long counter used to monitor relative neutron fluxes. Monoenergetic neutrons were produced by a Van de Graaff accelerator in the energy region from 30 to 800 keV. When the relative cross sections are normalized to a 1/v variation below 80 keV, the data lie above a 1/v line from 80 to 550 keV indicating departures of 15 percent at 140 keV and 20 percent at 220 keV. Recommended cross sections for $10B(n,\alpha)$ 7Li, 7Li* up to 1 MeV are obtained from recently available measurements and the known levels in ¹¹B.

N68-34175*# National Aeronautics and Space Administration. Lewis Research Center, Cleveland, Ohio.

ADSORPTION-DESORPTION BEHAVIOR OF HOMOGENE-OUS AND HETEROGENEOUS METAL SURFACES Thaine W. Reynolds Washington Sep. 1968 46 p refs

(NASA-TN-D-4789) CFSTI: HC\$3.00/MF\$0.65 CSCL 20L

Energy distribution relations which describe the desorption behavior from heterogeneous surfaces are presented. A graphical method of obtaining these is described, and the results are compared with a more exact computer-determined solution. Adsorption isotherms representing equilibrium coverage for the systems H_2 -W, CO-W, N_2 -W, CO-Mo, and N_2 -Mo are presented covering a pressure range from 10^{-12} to 1 torr, a fractional surface coverage from 0.02 to 0.98, and for the appropriate temperature range in each case.

N68-35535*# National Aeronautics and Space Administration. Langley Research Center, Langley Station, Va.

TABLES OF ENERGY AND ANGULAR DISTRIBUTIONS OF THICK TARGET BREMSSTRAHLUNG IN METALS

Clemans A. Powell, Jr. Washington Oct. 1968 35 p refs (NASA-TN-D-4755) CFSTI: HC\$3.00/MF\$0.65 CSCL 20H

Calculations are made for the angular and energy distributions of bremsstrahlung produced in thick elemental metallic targets by normally incident monoenergetic fluxes of electrons with energies of 0.50, 0.75, 1.00, 2.00, and 3.00 MeV. Results are given for magnesium, aluminum, titanium, manganese, iron, nickel, copper, tungsten, gold, and lead. The target thickness was chosen to be the mean range of the electrons in the particular target material for the electron energy of interest. The theoretical analysis of these data is based on the approximation of a thick target by a series of thin slabs each of which is considered to be a thin target for bremsstrahlung production, and includes the following secondary processes: (1) the effect of multiple electron scatterings. (2) electron backscatter out of the target. (3) electron-electron bremsstrahlung, and (4) the absorption and buildup of photons in the target. Results are compared with experimental thick target bremsstrahlung data for aluminum and iron. Although the agreement is good, the predicted values tend to overestimate the experimental data for low photon energies and underestimate for higher photon energies. The discrepancy between the predicted and experimental values increases with increasing angular displacement from the incident electron direction and with increasing atomic number of the target material. Author

N68-36070*# National Aeronautics and Space Administration. Langley Research Center, Langley Station, Va. EXPERIMENTAL INVESTIGATION AND ANALYSIS OF DIELECTRIC BREAKDOWNS INDUCED BY ELECTRON IRRADIATION IN POLYMER FILMS

George M. Storti Washington Oct. 1968 35 p refs (NASA-TN-D-4810) CFSTI: HC\$3.00/MF\$0.65 CSCL 20L

The phenomenon of dielectric breakdowns caused by electron irradiation was investigated in several polymeric materials. The frequency of occurrence of the breakdowns (as measured by the number of breakdowns occurring for a given fluence of electrons) was dependent on factors such as the electron kinetic energy, electron flux, sample radiation history, and sample temperature. Also, some materials (for example, Teflon) were found to be more susceptible to the dielectric breakdowns than others (for example, polyethylene). These results were interpreted in terms of a modified band model for organic insulators. This modified band model successfully explained many of the experimental observations. Consequently, relative depths of electron traps in some of the materials were surmised from the experimental data.

N68-37240*# National Aeronautics and Space Administration. Lewis Research Center, Cleveland, Ohio. THE EXCITATION SPECTRUM FOR A BOSE GAS WITH

REPULSIVE AND ATTRACTIVE INTERACTIONS Gerald V. Brown Washington Oct. 1968 69 p refs

(NASA-TN-D-4838) CFSTI: HC\$3.00/MF\$0.65 CSCL 20H

The correct qualitative features of the helium II elementary excitation spectrum are derived microscopically for a realistic interatomic potential. The strong repulsive core is included by using a reaction matrix in the Hamiltonian. The attractive well is successfully included by assuming a generalized Bose–Einstein condensation. The pair Hamiltonian is diagonalized by the thermodynamically equivalent Hamiltonian method. Numerically solutions yield spectra with phonon and roton regions. The spectrum energies are too high for the Yntema–Schneider potential. Another potential, constructed to fit virial coefficient data classically, gives better results. Spectra are presented for a series of attractive well strengths.

N68-37708*# Ling-Temco-Vought, Inc., Dallas, Tex. Nuclear Science Group.

INVESTIGATION OF ELECTRON INTERACTION IN MATTER Final Report, 9 Feb. 1967–9 Feb. 1968 Washington NASA Oct. 1968 338 p 14 refs (Contract NAS8-21055) (NASA-CR-1194; Rept.-0-7100/8R-2) CFSTI: HC \$3.00/MF \$0.65 CSCL 20H

CONTENTS:

1. MEASUREMENT OF ELECTRON SCATTERING IN ALUMINUM AT 1.0 MeV FOR NON-NORMAL INCIDENCE D. H. Rester and W. J. Rainwater, Jr. p 3-241 refs (See N68-37709 24-24)

2. ELECTRON-BREMSSTRAHLUNG CROSS SECTION

MEASUREMENTS AT INCIDENT ELECTRON ENERGIES OF 0.2, 1.0, 1.7, AND 2.5 MeV D. H. Rester and W. E. Dance p 243 -282 refs (See N68-37710 24-24)

3. ELECTRON BREMSSTRAHLUNG PRODUCED IN THICK TARGETS AT INCIDENT ELECTRON ENERGIES OF 0.2, 1.0, 2.0, AND 2.8 MeV W. E. Dance and D. H. Rester p 284–330 refs (See N68-37711 24-24)

25

PHYSICS, PLASMA

Includes magnetohydrodynamics. For applications see: 28 Propulsion Systems.

N68-11404*# National Aeronautics and Space Administration. Lewis Research Center, Cleveland, Ohio.

POWER TRANSFER TO ION CYCLOTRON WAVES IN A TWO ION SPECIES PLASMA

Donald R. Sigman and John J. Reinmann Washington Dec. 1967 13 p refs

(NASA-TM-X-1481) CFSTI: HC\$3.00/MF\$0.65 CSCL 20K

Calculations were made on the efficiency of using a Stix coil to transfer power to waves near the ion cyclotron frequencies of a cold, collisionless plasma consisting of two ion species. The mass ratio mb/ma of the ion species was 2, and the frequency region near and between the cyclotron frequencies (Ω_{ia} and Ω_{ib}) of each ion species was investigated. For wave frequencies ω less than Ω_{ib} , only the usual ion cyclotron resonance absorption peak is obtained. For $\Omega_{ia} > \omega > \Omega_{ib}$, two absorption peaks are obtained. The additional peak corresponds to power absorbed by fast wave modes associated with the heavier species. The wave set up nearer the cyclotron frequency of the lighter ion Ω_{ia} is a left-polarized wave, and power is absorbed primarily by modes whose wavelengths. which are parallel to the static magnetic field, are near the wavelength of the Stix coil. The second absorption peak occurs at lower frequencies where the power is absorbed by the right-polarized fast wave modes associated with the heavier species. There is a sharp cutoff on the low frequency side of this second absorption peak. Author

N68-14078*# Catholic Univ. of America, Washington, D. C. MAGNETOHYDRODYNAMIC FLOWS OVER A ROTATING DISK

Hsien-ping Pao Washington NASA Jan. 1968 25 p refs (Grant NsG-586)

(NASA-CR-989) CFSTI: HC\$3.00/MF\$0.65 CSCL 201

The flow of an incompressible viscous electrically conducting fluid over a rotating disk is investigated. In addition, a circular magnetic field is also imposed at the disk. One physical interest in this flow lies in the possibility of using such a magnetic field to shield a rotating body from excessive heating. Similarity assumptions lead to a reduction of the governing equations to a set of ordinary differential equations. These are integrated numerically. Some approximate solutions are also obtained. The role of the magnetic field here is to thicken the flow boundary layer and to reduce the strength of the axial flow field. That means, the magnetic field has a diffusing and stiffening effect upon the flow field. As a consequence, the frictional moment at the disk is reduced. For sufficiently large values of the applied magnetic field, the boundary layer separates from the surface of the disk. Author

N68-15747*# National Aeronautics and Space Administration. Lewis Research Center, Cleveland, Ohio.

ELECTRICAL PROPERTIES OF XENON-FILLED THERMIONIC DIODES IN RADIATION FIELD OF A NUCLEAR REACTOR Ralph Forman Washington Feb. 1968 17 p refs

(NASA-TN-D-4368) CFSTI: HC\$3.00/MF\$0.65 CSCL 181

Experimental data on nuclear-irradiated xenon-gas-filled thermionic diodes are presented. The characteristic curves for the irradiated diodes were studied as a function of xenon pressure (4 to 300 torr $(5 \times 10^2 \text{ to } 4 \times 10^4 \text{ N/m}^2)$), nuclear radiation intensity (gamma dose rate 10^8 to 6×10^8 rads/hr (10^6 to 6×10^8 J/(kg)(hr))), emitter temperature (1000° to 1200° C), and electrode

spacing (0.025 to 0.75 cm). Some interesting breakdown pehnomena occurred at voltages much lower than the first excitation potential. Some of the breakdown effects showed characteristics similar to those obtained in low-temperature cesium thermionic converters. There are regions corresponding to the unignited mode, preignition, and the ignited mode. In some cases, depending on the choice of radiation intensity, xenon pressure, and interelectrode spacing, these breakdown modes occur at applied voltages as low as 1 volt.

N68-16286*# National Aeronautics and Space Administration, Washington, D. C.

MOTION OF CONDUCTING BODIES IN A MAGNETIC FIELD

Ya. Ya. Liyelpeter, ed. Feb. 1968 152 p refs Transl. into ENGLISH of the book "Dvizheniye Provodyashchikh Tel v Magnitnom Pole" Riga, Izd. Zinatne, 1966

(NASA-TT-F-460) CFSTI: HC\$3.00/MF\$0.65 CSCL 201

CONTENTS:

1. STATE OF THE THEORY OF MAGNETOHYDODYNAMIC INDUCTION MACHINES WITH WORKING MEDIA OF LIQUID METAL Ya. Ya. Liyelpeter p 1-12 refs (See N68-16287 07-25)

2. ELECTROMAGNETIC PROCESSES IN AN IDEAL, INDUCTION MHD MACHINE A. K. Veze and L. Ya. Ulmanis p 13–37 refs (See N68-16288 07-25)

3. HIGHER SPATIAL HARMONICS OF THE MAGNETIC FIELD OF AN INDUCTION MHD MACHINE Yu. Ya. Mikel'son p 38-57 refs (See N68-16289 07-25)

4. TRANSVERSE EDGE EFFECT IN PLANE INDUCTION MAGNETOHYDRODYNAMIC MACHINES A. Ya. Vilnitis p 58–85 refs (See N68-16290 07-25)

5. LONGITUDINAL EDGE EFFECT IN LINEAR INDUCTION MHD MACHINES Ya. Ya. Valdmanis p 85–98 refs (See N68-16291 07-25)

6. PONDEROMOTIVE FORCES ACTING UPON CONDUCTIVE BODIES IN THE TRAVELING MAGNETIC FIELD OF A CYLINDRICAL INDUCTOR Yu. K. Krumin' p 99–121 refs (See N68-16292 07-25)

7. THEORY FOR THE PROPAGATION OF PULSED ELECTROMAGNETIC FIELDS IN MOVING CONDUCTIVE MEDIA G. Ya. Sermons p 121–147 refs (See N68-16293 07-25)

N68-16700*# National Aeronautics and Space Administration, Washington, D. C.

MAGNETOBREMS (SYNCHROTRON) EMISSION AND REABSORPTION [O MAGNITOTORMOYNOM (SINKHROT-RONNOM)]

V. L. Ginzburg, V. N. Sazonov, and S. I. Syrovatskiy Feb. 1968 41 p refs Transl. into ENGLISH from Preprint No. 83 of Lebedev Phys. Inst. (Moscow), 1967

(NASA-TT-F-521) CFSTI: HC \$3.00/MF \$0.65 CSCL 201

The problem of magnetic-acceleration (synchrotron) emission at helical motion of relativistic electrons emitting from a source with relativistic velocity is discussed and mathematically formulated. Problems of reabsorption of magnetobrems emission, with respect to radio emission by quasars, are reviewed, followed by a study of the motion of particles in a magnetic field in the presence of

25 PHYSICS, PLASMA

losses. Special emphasis is placed on this motion for particle aggregates of high energy density and the resultant changes in the magnetic field, with formulas for the change in energy of the particle group. Errors in formulas and conclusions by other authors are analyzed. Author

N68-17070*# National Aeronautics and Space Administration. Lewis Research Center, Cleveland, Ohio.

CORRELATION OF TRANSIENT SPECTRA WITH PERFORMANCE IN COAXIAL PLASMA GUNS

Charles J. Michels and Henry J. Hettel Washington Feb. 1968 32 p refs

(NASA-TN-D-4385) CFSTI: HC\$3.00/MF\$0.65 CSCL 201

The time-varying spectra of an argon plasma in a coaxial aun were measured. Two aun geometries were investigated, both with argon propellant. The transient spectra were obtained by viewing the plasma spectra in the exit plane of a polychromator with an electronic image converter camera used as a streak camera. Frame and streak camera views and magnetic probes were also used to study the discharges occurring in the guns. The transient spectrum of each gun was completely different. The geometry which exhibits relatively clean aroon spectra showed good performance. It operated internally crowbarred. The performance correlates well with both earlier theory and experiments and extends previous data. In contrast, the geometry which exhibited contaminant spectra showed poorer performance which does not agree with theory or past experimental data. This geometry operated in the multiple-moving-discharges mode. The discharge spectra showed no argon lines, and the contaminant lines were those from a pyrex gas baffle just upstream of the gas ports. The influence of the gas baffle on performance accounts for discrepancies with earlier data (both experimental and theoretical). The two different geometries of the guns served to demonstrate the usefulness of transient spectra diagnostics as an added tool in ascertaining when theory can correctly be applied to a given gun. A description of a two-channel transient voltage digitizer is given. The digitizer is used to record dynamically gun voltage and current at the rate of 5 million samples per second. It digitizes these samples and punches them on paper tape for data reduction by a conventional high-speed computer Author

N68-18485*# National Aeronautics and Space Administration. Lewis Research Center, Cleveland, Ohio.

ENHANCEMENT OF ION CYCLOTRON WAVES IN HYDROGEN HELIUM MIXTURES

Henry J. Hettel, Roman Krawec, George M. Prok, and Clyde C. Swett Washington Mar. 1968 35 p refs

(NASA-TN-D-4271) CFSTI: HC\$3.00/MF\$0.65 CSCL 201

The admixture of helium to a hydrogen plasma atmosphere has increased the radiofrequency power absorption in the ion-cyclotron mode. Measurements of power absorption, plasma radius, electron density, and magnetic flux density at the peak power point were obtained as a function of plasma composition. A relation was derived involving these experimental parameters and the ion density. It is shown that the observed power enhancement can be explained if it is assumed that the metastable states of the helium atoms react with hydrogen atoms and molecules to increase the plasma ion density. Author

N68-18614*# National Aeronautics and Space Administration. Electronics Research Center, Cambridge, Mass.

A STUDY OF THE POSSIBLE USES OF PLASMA FOR MILLIMETER WAVE GENERATION

Robert E. McIntosh Washington Mar. 1968 28 p refs

(NASA-TN-D-4309) CFSTI: HC\$3.00/MF\$0.65 CSCL 201

The millimeter wave portion of the frequency spectrum has not been utilized in communication systems because of a lack of practical, high-power mm wave generators. As conventional tube design techniques have been only moderately successful in extending the microwave power frequency frontier, a number of novel approaches for obtaining mm wave sources have been suggested. Two of these methods rely on the use of a gaseous plasma and are described in this technical note. The electron beam-plasma interaction and the plasma multiplier have been investigated during the last decade in the hope that one or the other might have some application at mm wavelengths. So far the expectations for these devices have not been realized because of many unresolved engineering problems. This report describes the major difficulties that must be overcome before further development in this area can proceed, and it attempts to evaluate the potential of both devices. Author

N68-20296*# National Aeronautics and Space Administration. Lewis Research Center, Cleveland, Ohio.

A COAXIAL-FLOW-STABILIZED ARC

Chester D. Lanzo Washington Apr. 1968 20 p refs (NASA-TN-D-4517) CFSTI: HC\$3.00/MF\$0.65 CSCL 20I

This report describes and evaluates a new experimental coaxial-flow-stabilized ac arc facility and presents the results of a study of the general characteristics of an ac arc which has been stabilized or held in place by the action of the coaxial flow of two different gases. The arc is maintained in a central jet of axially flowing argon, between an unstream and a downstream electrode. An outer stream of gas flows coaxially around the center argon jet. Both nitrogen and helium were used in the outer stream. Tests were conducted to determine qualitatively the effect of varying the relative velocities of the inner and outer gas streams. These tests were conducted at a chamber pressure of 8 to 25 psia (55×10^3) to 172×10^3 N/m²abs) and arc lengths of 1 to 12 inches (2.54 to 30.5 cm). Frequency was varied from 12 to 22 cps (12 to 22 Hz). Current levels of 500 to 1000 amperes were run. Visual observations were made, and voltage and current measurements were recorded. In addition, individual frames from a high-speed motion-picture film were examined. These data indicate that the coaxial, two-gas flow pattern causes stable arc operation and that the arc behavior is relatively insensitive to changes in the velocity of either gas stream. Author

N68-21623*# National Aeronautics and Space Administration. Lewis Research Center, Cleveland, Ohio.

PAIRS OF EMITTER AND COLLECTOR SHEATHS FOR CESIUM THERMIONIC DIODES

James F. Morris Washington Apr. 1968 56 p refs (NASA-TN-D-4419) CFSTI: HC\$3.00/MF\$0.65 CSCL 201

Coupled theoretic sheaths given approximate thermionic diodes. The sheaths result from particle emissions of electrodes affected by sheath fields and of cesium plasmas ionized by thermal electrons. By matching their net current densities, the analysis pairs collisionless emitter and collector sheaths to simulate diodes. Midway between the electrodes in both space and temperatures lie the plasmas at 1700° to 2000°K with 1012 and 1013 electrons per cubic centimeter. The emitters and collectors differ by 400° to 800°K. For these conditions, the computed outputs for the converters range from 0.01 to 1 watt per square centimeter. Although such powers fall below desired performance levels. they provide low-current checks for thermionic-diode experiments. Sheath properties for the present systems and for electrodes inplasmas with raised electron temperatures agree with equilibrium results. But the theory applies only for equilibria, near-equilibria, and relatively low net transports. Overall sheath characteristics correlate with electrode and plasma conditions. One helpful parameter is a hybrid, the emission Debye length, λ_{DE} \approx 6.9 (Te/NeP) $^{1/2}$ This variable correlates data for these sheaths better than the plasma Debye lenth. Effective sheath widths for the present study lie between 1.7 and 2.6 emission Debye lengths. The independent variables for the present graphic correlations of sheath properties involve only electrode and plasma parameters. Because one states these conditions at the outset, the graphs allow immediate estimates of sheath characteristics-without the complex iterative calculations. Author

N68-21691*# National Aeronautics and Space Administration. Ames Research Center, Moffett Field, Calif.

BOUNDARY CORRECTIONS FOR A THREE-COIL CONDUCTIVITY/VELOCITY PLASMA PROBE

Edward W. Vendell Washington Apr. 1968 32 p refs (NASA-TN-D-4538) CFSTI: HC\$3.00/MF\$0.65 CSCL 201

A three-coil plasma probe that measures both the electrical conductivity and velocity of laboratory plasmas having low magnetic Reynolds numbers has been developed and tested. As a first approximation, it was assumed that the plasma boundary was far from and much larger than the probe. The present work was undertaken to extend the previous theory by deriving factors that correct for the presence of cylindrical boundaries. As a check on this numerical work, several computed values were compared with electrical conductivity measured in cylinders of acid. Since the agreement was satisfactory, the boundary correction factors were used to reduce data taken as the probe was swept through an argon plasma generated by a constricted-arc wind tunnel. These resultant profiles represent local conductivity and velocity values for a free plasma jet having a cylindrical boundary. It was found that the raw data underestimates conductivity and overestimates velocity. Author

N68-22887*# National Aeronautics and Space Administration. Lewis Research Center, Cleveland, Ohio.

PERIODIC, SMALL-AMPLITUDE SOLUTIONS TO THE SPATIALLY UNIFORM PLASMA CONTINUITY EQUATIONS J. Reece Roth Washington May 1968 43 p Fefs

(NASA-TN-D-4472) CFSTI: HC\$3.00/MF\$0.65 CSCL 201

The coupled set of first-order nonlinear differential equations $= C_0 + C_1 \chi + C_2 y + C_3 \chi y + C_4 \chi^2 + C_5 y^2 \text{ and}$ $= A_0 + A_1 \chi + A_2 y + A_3 \chi y + A_4 \chi^2 + A_5 y^2$ are solved by an approximate method which gives y(t) in closed form for the particular case in which the variables χ and y vary periodically in time, the coefficients Ci and Ai are real, and the peak-to-peak variation of χ is of small amplitude relative to the mean value of χ . The peak-to-peak amplitude of y, however, is not necessarily small compared with the mean value of y. These equations are a generalized form of Volterra's problem of two conflicting populations, in which χ is the population density of the prey, and y is the population density of the predator, or vice versa. Similar equations may also be derived from the spatially uniform neutral and charged-particle continuity equations in the field of plasma physics. These equations then describe relatively low-frequency oscillations in the number density of electrons and neutral atoms in a partially ionized plasma. Author

N68-24161*# National Aeronautics and Space Administration. Ames Research Center, Moffett Field, Calif.

TABLES OF Fe I LINE INTENSITIES. VOLUME 1: TEMPERATURES FROM 1000° TO 6500°K. VOLUME 2: TEMPERATURES BETWEEN 6500° AND 20,000°K

William J. Borucki Washington 1968 219 p refs

(NASA-SP-3041) CFSTI: HC \$3.00/MF \$0.65 CSCL 201

Tables of intensities for the 2200 atomic lines listed by Corliss and Warner and Corliss and Bozman for Fe I are presented for temperatures between 1000° and 20,000°K. These tables should be useful in computing the absolute intensity and the spectral distribution for Fe I line radiation from optically thin media. determining the temperature of an observed plasma, and indicating the existence of a non-Boltzmann distribution of excited electronic states when such a condition exists. Author

N68-25630*# National Aeronautics and Space Administration. Lewis Research Center, Cleveland, Ohio.

EFFECTS OF ARRIVAL RATES OF ABSORBATE IONS AND ATOMS ON SURFACE COVERAGE, HENCE WORK FUNCTIONS, OF EMITTING ELECTRODES James F. Morris Washington Jun. 1968 10 p refs

(NASA-TN-D-4369) CFSTI: HC\$3.00/MF\$0.65 CSCL 201

This report gives equations for determining substrate surface coverages from arrival rates and desorption characteristics of adsorbate ions and atoms. With a correlating theory by Gyftopoulos and Steiner, these coverages yield estimates of work functions for emitting electrodes with partial monolayers of other metals on their surface. Author

N68-25821 *# Space Sciences, Inc., Waltham, Mass. PLASMA BOUNDARY INTERACTIONS-2

S. Aisenberg, P. Hu, V. Rohatgi, and S. Ziering Washington, D. C. NASA Jun. 1968 68 p refs (Contract NASw-1014)

(NASA-CR-1072) CFSTI: HC\$3.00 /MF\$0.65 CSCL 201

A study has been made of additional factors describing plasma-boundary interactions. The theoretical analysis of the sheath has been extended to include a transverse plasma flow outside the sheath region. The sheath model has been made more general, and also reveals the importance of the accommodation coefficients at the boundary surface. The presence of ionization and collisions in the sheath has also been studied theoretically. The interpretation of the experimentally observed threshold in the tangential electrode drag as a function of transverse magnetic field and of arc current has suggested the possibility of a threshold in the tangential accommodation coefficient. The threshold tangential energy appears to be proportional to the sputtering threshold and can be related to the threshold for displacement of surface atoms. The relationship between plasma phase velocity and particle velocity was studied and it was shown that there is not necessarily a simple connection: The related problem of arc retrograde motion (where plasma phase and particle motion have opposite signs) was studied and a simple model was proposed. It appears that the plasma propagates in the retrograde direction because of an increased net ion generation rate due to the inhibited diffusion loss of icos and electrons in the region of higher magnetic field. The importance of direct measurement of ion and atom velocity by means such as the Doppler shift is discussed. Author

N68-25877*# National Aeronautics and Space Administration. Lewis Research Center, Cleveland, Ohio.

GENERAL OPERATING CHARACTERISTICS OF A BACK STREAMING DIRECT-CURRENT PLASMA GENERATOR Roman Krawec Washington Jun. 1968 26 p refs

(NASA-TN-D-4604) CFSTI: HC\$3.00/MF\$0.65 CSCL 201

Experimental studies were performed on a plasma generator consisting of a filament and a hollow, gas-fed anode which were immersed in an axial magnetic field. The hydrogen plasma formed between the filament and anode was allowed to diffuse past the filament, through a transition section, and into a low-pressure test section. The plasma within the test section was characterized by having two groups of electrons which differed in temperature and had a peak density greater than 2×10^{12} centimeter ~ 3 . The no-plasma background pressure within the test chamber was an order of magnitude less than the peak electron density. Evidence was found indicating that thermal dissociation of the hydrogen molecule occurred within the hollow anode. Author

N68-25920*# National Aeronautics and Space Administration. Lewis Research Center, Cleveland, Ohio.

THERMODYNAMIC STUDY OF PLASMAS USING THE PRINCIPLE OF MAXIMUM ENTROPY

Norbert Stankiewicz Washington Jun. 1968 26 p refs

 (NASA-TN-D-4621) CFSTI: HC\$3.00/MF\$0.65 CSCL 201
 A maximum entropy (disorder) principle is used to determine the velocity distribution functions in a quiescent plasma (case 1), a current-carrying plasma (case 2), and a viscous plasma (case 3).

 The Saha equation (at the electron temperature) holds for case 1, and modified Saha equations hold for cases 2 and 3. The modification in case 2 is important only in situations where the directed energy

of the electrons is a substantial fraction of the total energy. The

results of case 3 are presented in a general form and need simplification before they can be applied to a specific situation. Author

N68-28154*# National Aeronautics and Space Administration. Lewis Research Center, Cleveland, Ohio.

COAXIAL PLASMA GUN RESEARCH AT LEWIS RESEARCH CENTER

Charles J. Michels Washington Jul. 1968 15 p refs

(NASA-TM-X-1600) CFSTI: HC\$3.00/MF\$0.65 CSCL 201

Research on coaxial plasma guns in an effort to determine their potential for space propulsion applications was undertaken at the Lewis Research Center. The experimental parametric examination of various gun geometries, the theoretical analysis of capacitor-bankvariable-mass distribution gun systems, and the plasma diagnostics of various geometries are summarized. The results of this program indicated that the efficiency (\approx 40 percent) was too low to be competitive with alternative systems. Propellant, switching, and heat-rejection systems proved to be complicated. Author

N68-29888*# Humphreys Corp., Concord, N. H. INDUCTION PLASMA HEATING: SYSTEM PERFORMANCE, HYDROGEN OPERATION AND GAS CORE REACTOR SIMULATOR DEVELOPMENT

Merle L. Thorpe Washington NASA Aug. 1968 47 p refs (NASA-CR-1143) CFSTI: HC\$3.00/MF\$0.65 CSCL 20I

The induction plasma heating system has been studied and optimized. A reliable 80 kW 3 in. diameter sheath system has been developed which permits efficiently heating argon core gas to arc temperatures surrounded by a high velocity sheath of hydrogen. This unit will permit studies of mixing, fuel addition and other related phenomena associated with such a heat addition system. Other studies of hydrogen heating and particle injection into the arc are described. Author

N68-30031*# National Aeronautics and Space Administration. Langley Research Center, Langley Station, Va.

DYNAMICS OF A ONE-DIMENSIONAL PLASMA SHEATH

Frank Hohl and Leo D. Staton Washington Jul. 1968 56 p refs

(NASA-TN-D-4651) CFSTI: HC\$3.00/MF\$0.65 CSCL 201

Analytical and numerical methods are used to investigate a bounded one-dimensional plasma with a fixed neutralizing ion background. A variational method is used to show that a large class of stationary solutions of the nonlinear Vlasov equations represent minimum-energy states. The consequence of the minimum-energy property is that the stationary states, which represent minimum-energy configurations, can never be completely reached. However, numerical experiments which simulate the system reveal the interesting property that the plasma approaches its stationary state closely whenever the initial energy is not too different from the energy of this stationary state.

N68-30093*# National Aeronautics and Space Administration. Lewis Research Center, Cleveland, Ohio.

ANALYSIS OF INTEGRATED CHARGED PARTICLE ENERGY SPECTRA FROM GRIDDED ELECTROSTATIC ANALYZERS

F. Reece Roth and Marion Clark (Cornell Univ., Ithaca) Washington Aug 1968 73 p refs

(NASA-TN-D-4718) CFSTI: HC\$3.00/MF\$0.65 CSCL 201

This report relates the shape of the retarding potential curve produced by gridded electrostatic analyzers to the floating potential, the kinetic temperature, and the half-angle subtended in velocity space by the particles. Special emphasis is placed on the case in which the particles are Maxwellianized, but restricted within an escape cone in velocity space of half-angle. The cases of pulsed and steady state supply of particles are both considered. A computer program is included which produces an iterated best fit of experimental integrated energy spectra to these analytical expressions, and provides the effective values of the kinetic temperature, floating potential, and escape cone angle. A series of experimental runs is analyzed with the computer program as an illustrative example, and the possible sources of error are discussed. Author

N68-30593*# National Aeronautics and Space Administration. Lewis Research Center, Cleveland, Ohio.

SOME INTERACTIONS OF POLYCRYSTALLINE TUNGSTEN ELECTRODES WITH CESIUM PLASMAS James F. Morris Washington Aug. 1968 17 p refs

(NASA-TN-D-4745) CFSTI: HC\$3.00/MF\$0.65 CSCL 201

At thermionic diode temperatures, work functions of tungsten electrode surfaces depend strongly on positive ion sheaths between these electrodes and cesium plasmas. The present theoretic study demonstrates this effect for a plane field-modified emitter with a collisionless positive ion sheath in a thermally ionized plasma. The analysis covers temperatures from 1700° to 2600°K; plasma electron number densities of 1012, 1013, and 1014 cm -3; and a bare work function of 4.59 V. Values for sheath voltages, work functions, and cesium arrival rates and coverages on tungsten result from equilibrium calculations. In addition to these variables, computations for elevated plasma electron temperatures yield net current densities. Throughout this work, the sheath drops lie below 1 V. And atom arrival rates approach total cesium arrival rates only at low temperatures and sheath voltages.

N68-30784*# National Aeronautics and Space Administration. Lewis Research Center, Cleveland, Ohio.

SHAPE OF A MAGNETICALLY BALANCED ARC

Marvin E. Goldstein and Willis H. Braun Washington Aug. 1968 34 p refs

(NASA-TN-D-4736) CFSTI: HC\$3.00/MF\$0.65 CSCL 201

An improved model is developed for predicting the shape of an electric arc balanced in transverse convective and magnetic fields. The improvement over the previous model is in the more accurate description of the external flow field. The techniques used are based on conformal mapping and are an extension of those methods developed for problems of free surface flows. Author

N68-31640*# National Aeronautics and Space Administration. Lewis Research Center, Cleveland, Ohio.

EMITTER AND COLLECTOR SHEATHS FOR CESIUM THERMIONIC DIODES WITH POLYCRYSTALLINE TUNGSTEN ELECTRODES

James F. Morris Washington Aug. 1968 13 p refs

(NASA-TN-D-4744) CFSTI: HC\$3.00/MF\$0.65 CSCL 201

Using electrode temperatures above and below those of thermally ionized plasmas, this analysis estimates sheath properties for polycrystalline tungsten emitters and collectors in cesium thermionic diodes. The fields of these positive ion sheaths modify particle emissions from the plane electrodes; the sheath voltages affect cesium arrival, hence contact ionization rates. Cesium coverage dicates the work function, which is 4.59 volts for a bare electrode. In this study the assigned temperatures run from 1600 to 2400 K for plasmas with 1012 and 1013 electrons per cubic centimeter. Tabulations give results for diodes putting out from 0 to 1 ampere per square centimeter. Graphic trends of electrode and sheath characteristics also appear. The analysis applies to equilibria and near-equilibria.

N68-32072*# National Aeronautics and Space Administration. Lewis Research Center, Cleveland, Ohio.

ANOMALOUS DIFFUSION IN A PLASMA FORMED FROM THE EXHAUST BEAM OF AN ELECTRON-BOMBARDMENT ION THRUSTER

Allan J. Cohen Washington Aug. 1968 30 p refs (NASA-TN-D-4758) CFSTI: HC\$3.00/MF\$0.65 CSCL 201 A 10-cm-diam. cylindrical anode with a grounded coaxial center rod was immersed in the low density ($n_e \approx 2 \times 107$ cm -3) exhaust beam of an ion thruster. A longitudinal magnetic field was applied. A theoretical and experimental study was made of the electron diffusion process in the beam plasma passing through the electrically floating anode. Anomalous diffusion and low frequency noise wer found. The mechanism of anomalous diffusion was considered similar to that reported by Kadomtsev and Nedospasov. Bohm's diffusion equation was found applicable and a constant of 1/8 (twice Bohm's value) was deduced experimentally. Rotation in the plasma was found by means of a correlation technique. The measured frequency of rotation ranged from 100 to 150 kHz.

N68-33021*# National Aeronautics and Space Administration. Lewis Research Center, Cleveland, Ohio.

COLLISIONLESS SHEATHS BETWEEN FIELD-MODIFIED EMITTERS AND THERMALLY IONIZED PLASMAS EXEMPLIFIED BY CESIUM

James F. Morris Washington Aug. 1968 62 p refs

(NASA-TN-D-4376) CFSTI: HC\$3.00/MF\$0.65 CSCL 201 The model, an iterative calculation method, and results for plane collisionless sheaths are presented. These sheaths separate thermally ionized plasmas from emitters of electrons, ion, and atoms and change emission with their fields. Still the model gives identical absolute potential changes through the sheath for ions and electrons, contrary to usual practice. For cesium, the emitter and plasma ion and atom temperatures range from 1600° to 2400°K with plasma electron temperatures up to 300°K higher. Plasma electron number densities are 1012 to 1015 per cubic centimeter. At these conditions work functions from 1.5 to 5 volts produce absolute potential drops from 0 to 1.5 volts for electron and positive-ion sheaths. And some currents greater than 102 amperes per square centimeter result. Certain generalizations apply: Sheath fields affect emissions and sheath characteristics significantly. The overall sheath characteristics correlate better with an emission Debye length (6.9 time the square root of the emitter

temperature (°K) divided by the plasma electron number density (cm^{-3})) than with the conventional Debye length. Where conditions comply with the assumptions of the model, effective sheath widths decrease from 2.6 to 2 emission Debye lengths as overall sheath drops grow from less than 0.1 to 1.5 volts. Author

N68-33372*# National Aeronautics and Space Administration. Langley Research Center, Langley Station, Va.

THE PREHEATING OF PLASMA IN A MEGAJOULE THETA-PINCH EXPERIMENT

W. A. Cilliers, Joseph Norwood, Jr., and G. K. Oertel Washington Sep. 1968 22 p refs

(NASA-TN-D-4708) CFSTI: HC\$3.00/MF\$0.65 CSCL 201

The preheating of plasma in a megajoule theta-pinch experiment was investigated and distinct modes of operation have been delineated. The criteria for satisfactory preionization are discussed. For typical experiments where a number of discharges from different capacitor banks are applied sequentially to a common load, these criteria are determined not only by the requirement for a reproducible and stable plasma, but also by the limitations on the voltage that can be applied to the coil without precipitating prefire of banks that should fire later in the sequence. A range of preheater energies and a bank voltage that are satisfactory for this particular experiment were determined. Streak photographic evidence of plasma conditions in the various modes is presented. Author

N68-35171*# Ohio State Univ., Columbus. INPUT ADMITTANCE AND REFLECTION COEFFICIENT OF A CIRCULAR APERTURE IN A GROUND PLANE COVERED BY A HOMOGENEOUS DIELECTRIC OR PLASMA SLAB R. E. van Doeren Washington NASA Sep. 1968 33 p refs (Grant NGR-36-008-048)

(NASA-CR-1177) CFSTI: HC \$3.00/MF \$0.65 CSCL 201

The reflection coefficient and admittance of a circular aperture in a ground plane radiating into a dielectric slab medium lying directly on the ground plane is considered. The work relies heavily on previous efforts by Compton and Rudduck. Calculations are performed for lossless dielectric and lossy plasma slabs. The admittance for lossless slabs is compared with the experimental data of others. Author

N68-37237*# National Aeronautics and Space Administration. Lewis Research Center, Cleveland, Ohio.

ANALYSIS OF ELECTROMAGNETIC WAVES ON A DIELECTRIC ROD IMMERSED IN A PLASMA INCLUDING A DISCUSSION OF DIAGNOSTIC APPLICATIONS

David L. Wright and Norman C. Wenger Washington Oct. 1968 31 p refs

(NASA-TN-D-4866) CFSTI: HC\$3.00/MF\$0.65 CSCL 201

The guided electromagnetic waves that propagate along a lossless dielectric rod immersed in isotropic and uniaxial plasmas are determined. For the uniaxial plasma, only the case where the optic axis is alined parallel to the dielectric rod is considered. Both plasmas are described by the linearized momentum transport equation for a cold, collisionless, electron fluid of uniform density. Numerical results for the propagation constants of the waves are presented as a function of the rod and plasma parameters for both the circularly symmetric and dipole modes. Important aspects of the results are discussed with particular emphasis on plasma diagnostic applications.

26 PHYSICS, SOLID-STATE

Includes semiconductor theory; and superconductivity. For applications see: 16 Masers. For related information see also: 10 Electronics.

N68-17594*# National Aeronautics and Space Administration. Lewis Research Center, Cleveland, Ohio.

DAMPING OF A TORSIONAL OSCILLATOR IN LIQUID HELIUM 4 AND 3 FROM 0.4° TO 2.5°K

Rayjor W. H. Webeler and David C. Hammer Washington Mar. 1968 refs

(NASA-TN-D-4381) CFSTI: HC\$3.00/MF\$0.65 CSCL 20L

The logarithmic decrements of a piezoelectric cylindrical quartz crystal driven in a torsional mode of vibration were determined as a function of temperature with the crystal immersed in liquid He³ and He⁴ These measurements were used to calculate the applicable "viscosity-density" product of these two liquids as a function of temperature. The results in the interval 2.14° to 2.20°K represent the most extensive and precise viscosity-density values for He⁴ that are available to data. Inspection of this viscosity-normal density product $(\eta_n \rho_n)$ data near the lambda point (T_{λ}) indicates that a discontinuity in $(\eta_n \rho_n)$ data may exist. Results between 2.0° and 1.35°K in liquid He⁴ are in agreement with three other investigations. Between 1.1° and 0.95°K, the data substantiate only the rotating viscometer results of Woods and Hollis Hallett. At temperatures below $0.6^\circ K,$ the phonon density temperature dependence is $T^{4.0\pm0.1},$ confirming the temperature dependence of the Landau expression for the phonon density. With the torsional crystal technique there was evidence of suppression of the phonon viscous contribution. Viscosity values for liquid He³ were determined between 0.4° and 2.5°K and are compared with the results of other investigators. Author

N68-18772*# National Aeronautics and Space Administration. Langley Research Center, Langley Station, Va.

LIGHT-INDUCED MODULATION OF ABSORPTION (LIMA) IN CADMIUM SULFIDE

Karl W. Boer and Edmund J. Conway Washington Mar. 1968 11 p refs

(NASA-TN-D-4466) CFSTI: HC\$3.00/MF\$0.65 CSCL 20L

The bulk optical absorption from 0.5 micrometer to 2 micrometers of cadmium sulfide single crystals has been modulated by a chopped continuous wave laser. Data showing the intensity and chopping frequency dependences are discussed. A few of the implications of these data are also mentioned. Author

N68-19924*# National Aeronautics and Space Administration. Langley Research Center, Langley Station, Va.

EFFECTS OF 22 MEV PROTON AND 2.4 MEV ELECTRON RADIATION ON BORON AND ALUMINUM-DOPED SILICON SOLAR CELLS

Gilbert A. Haynes and Walter E. Ellis Washington Apr. 1968 67 p refs

(NASA-TN-D-4407) CFSTI: HC\$3.00/MF\$0.65 CSCL 10A

A comparative analysis is presented of the effects of proton and electron irradiation on the electrical properties of boron-doped and aluminum-doped, N on P, silicon solar cells having base resistivities of 1 ohm-cm and 10 ohm-cm. Electrical measurements were made before and after irradiation at various flux levels up to 2.1×10^{12} protons per square centimeter at 22 MeV, and 1.0×10^{16} electrons per square centimeter at 2.4 MeV. Measurements of short-circuit current and maximum power under illumination with a tungsten light source and a solar simulator indicate that 1 ohm-cm aluminum-doped cells are slightly more resistant to damage by 2.4 MeV electrons than 1 ohm-cm boron-doped cells; however, 10 ohm-cm boron-doped cells were found to be more resistant to electron damage than 10 ohm-cm aluminum-doped cells. Spectral response measurements made before and after irradiation indicated no significant difference due to the type of doping element employed. From these spectral response curves, conversion factors were computed for use in predicting the output of solar cells in space sunlight from direct measurements under tungsten light or the solar simulator.

N68-20295*# National Aeronautics and Space Administration. Lewis Research Center, Cleveland, Ohio.

ELECTRON-BEAM, CRYSTALLIZATION OF SILICON, GERMANIUM, AND CADMIUM SULFIDE

John C. Evans, Jr. Washington Apr. 1968 24 p refs

(NASA-TN-D-4522) CFSTI: HC\$3.00/MF\$0.65 CSCL 20L

Amorphous semiconductor films were electron-beam irradiated, and the effects were observed in the electron microscope. This study shows that oriented polycrystalline films of silicon, germanium, and cadmium sulfide may be made by electron bombardment of their amorphous films deposited on glass and plastic substrates. This transition was shown to occur without deleterious effects upon the substrates. The film bombardment was conducted both in the electron microscope and in a separate vacuum drystallizer capable of electron-beam raster scanning. Electron micrographs and electron diffraction patterns were used to record the results of the film treatments. Both silicon and germanium films underwent amorphous-to-crystalline changes at substrate temperatures well below the melting points of the semiconductors. Nucleation and crystal growth by coalescence were observed. The compound semiconductor, cadmium sulfide, crystallized by passing through a quasi-liquid state without subliming in the vacuum environment. The thickness of the untreated films was such as to allow transmission electron microscopic studies. Author

N68-21219*# National Aeronautics and Space Administration. Ames Research Center, Moffett Field, Calif.

RADIATION DAMAGE IN THICK COPPER AND GOLD SPECIMENS PRODUCED BY LOW-ENERGY PROTONS

Howard F. Savage and Robert D. Morris Washington Apr. 1968 12 p refs

(NASA-TN-D-4452) CFSTI: HC\$3.00/MF\$0.65 CSCL 20L

The production of defects at 90°K in thick gold and copper foils by 50 to 400 keV protons and subsequent annealing characteristics of these metals have been studied. The thickness of the specimens was several times the calculated range of the protons. The defects formed in gold were uniformly distributed along

26 PHYSICS, SOLID-STATE

the proton range, whereas the defects formed in copper were more than twice as dense toward the end of the range as at the beginning. At doses from 10¹⁵ protons/cm² to at least the maximum of the tests, the change in electrical resistivity of both the gold and copper at incident energies between 50 and 400 keV can be decribed by a relation of the form $\Delta \rho = A\phi$, where $\Delta \rho$ is the increase in resistivity and ϕ is the dose. The recovery of gold upon isochronal annealing was similar to that observed for high-energy irradiations of thin specimens. Author

N68-21708*# National Aeronautics and Space Administration. Lewis Research Center, Cleveland, Ohio.

SPECTRAL EMISSIVITY OF HIGHLY DOPED SILICON

Curt H. Liebert and Ralph D. Thomas Washington Apr. 1968 26 p refs

(NASA-TN-D-4303) CFSTI: HC\$3.00/MF\$0.65 CSCL 20L

Measurements were made at temperatures of 300°, 882°, and 1074°K of the normal spectral emissivity of opaque, highly doped silicon. The silicon was doped with arsenic and boron to electron carrier concentrations of 2.2×10^{19} , 3.7×10^{19} , and 8.5×10^{19} electrons per cubic centimeter and hole carrier concentrations of 6.2×10^{19} and 1.4×10^{20} holes per cubic centimeter. The 300°K emissivity data were obtained at wavelengths from 2.5 to 35 microns. The high temperature emissivities were measured from 3.5 to 14.8 microns. Carrier concentrations and direct current resistivity of the silicon were also measured. The carrier concentrations were determined from Hall measurements made at 300°K. The direct current resistivity was measured at temperatures from 300° to 1200°K. These quantities were used in analytical calculations of the emissivities. Agreement of the Hagan-Rubens theory with experiment was found at wavelengths greater than 12 microns and at 300°K. Good agreement of the free carrier absorption theory with experiment was achieved at all wavelengths and temperatures investigated. The free carrier absorption theory predicts the emissivity in terms of the index of refraction and the absorption index. The values of these quantities are presented. A comparison of the values of the absorption index obtained with those obtained from the literature showed good Author qualitative agreement.

N68-22271*# National Aeronautics and Space Administration. Lewis Research Center, Cleveland, Ohio.

AN EXPLANATION OF ANOMALOUS NON-HOOKEAN DEFORMATION OF IONIC SINGLE CRYSTALS

James P. Cusick and Donald R. Behrendt Washington May 1968 34 p refs

(NASA-TN-D-4513) CFSTI: HC\$3.00/MF\$0.65 CSCL 20L

Previously published non-Hookean load-deflection data are reviewed. The results of this review show that roughness of the sample loading surfaces contributes to the measured deflection. Simple calculations presented herein show the effect of surface roughness on load-deflection data. Experiments are described in which two simultaneous deflection measurements are made; one measures bulk sample deflections only, the other measures bulk and loading surface deflections. Non-Hookean effects are observed only when surface deflections are included in the measurement. Finally, microscopic surface examination reveals surface roughness of the size needed to produce the non-Hookean effect. The non-Hookean effects are a consequence of the experimental techniques and do not reflect the bulk properties of the sample. Author

N68-24273*# National Aeronautics and Space Administration. Electronics Research Center, Cambridge, Mass.

MANY-BODY THEORY OF A RAPIDLY VARYING INHOMOGENEOUS ELECTRON GAS

John William Gadzuk Washington May 1968 94 p refs

(NASA-TR-R-283) CFSTI: HC\$3.00/MF\$0.65 CSCL 20L

The case of an inhomogeneous electron gas within which the density variation is significant over a spatial range of the order

of a Fermi wavelength is considered. The first considerations are directed towards the problem of a weak periodic potential in an interacting electron gas. The momentum-dependent self-energy is calculated for an electron propagating in the many-body medium of an electron gas plus a periodic lattice pseudo-potential. This is the equivalent of a quasi-particle energy spectrum and thus an orthogonalized plane wave energy band. It does not appear that the lattice drastically changes qualitative aspects of plane wave many-body theory. A dielectric formulation for a general inhomogeneous electron gas is presented. By introducing a new image technique, the dielectric function within the random phase approximation, which is valid in the surface region of an electron gas, is obtained. A Green's function formalism is developed for treating the static dielectric screening of a point impurity in an electron gas. The surface dielectric function is used with the impurity screening formalism to treat the problem of impurity screening in the surface region. Author

N68-24510*# National Aeronautics and Space Administration. Lewis Research Center, Cleveland, Ohio. IONIC CONDUCTIVITY OF SOLID MIXTURES William L. Fielder Washington May 1968 refs

(NASA-TN-D-4606) CFSTI: HC\$3.00/MF\$0.65 CSCL 20L

The conductivities of four solid mixtures were determined as a function of temperature: (1) the lithium fluoride-lithium chloride eutectic, (2) the lithium chloride-potassium chloride eutectic, (3) the lithium fluoride-sodium chloride eutectic, and (4) a 50-mole-percent mixture of sodium chloride and potassium chloride. Two conductivity regions were obtained for each of the four mixtures. The activation energies for the conductivity for the lower-temperature regions ranged from 14 to 27 kilocalories per mole (59 to 114 kJ/mole). These energies were similar to the cation migration energies for the single crystals of the alkali halides. The conductivity of the mixtures in the lower-temperature regions is best explained by the following mechanism: (1) formation of cation vacancies primarily by multivalent impurities, and (2) migration of the cations through these vacancies. The activation energies for the conductivity of the solid mixtures in the upper-temperature regions ranged from 5 to 9 kilocalories per mole (20 to 39 kJ/mole). These values are significantly smaller than those energy values that might be expected for a normal intrinsic process. The low activation energies may reflect an ion transport process through a liquid-like state (premelting) or along low-energy paths such as line or plane imperfections. Additional evidence is needed before an upper-temperature region mechanism can be suggested with certainty. Author

N68-24660*# National Aeronautics and Space Administration. Langley Research Center, Langley Station, Va.

HIGH ENERGY PROTON DAMAGE IN SILICON SURFACE BARRIER DETECTORS

Jag J. Singh and Emanuel Rind Washington May 1968 33 p refs

(NASA-TN-D-4528) CFSTI: HC\$3.00/MF\$0.65 CSCL 20L

The performance of a number of silicon surface barrier detectors has been studied under bombardment with 5.0-MeV, 20.0-MeV, and 40.0-MeV protons. The detectors investigated fall under three categories: (1) normal 100 microns deep; (2) normal 500 microns deep; and (3) fully depleted (dE/dx) type, 500 microns deep. Measurements made include rate of deterioration of charge collection efficiency, variation of resolving power, variation of leakage current, variation of noise level, and changes in detector capacitance as a function of the incident proton dose. From these several data, formulas giving relationships between the proton dose and the degree of detector resolving power deterioration have been developed for the normal and fully depleted type of detectors. Measurements clearly establish that: (1) the fully depleted detectors are more radiation damage resistant than the normal detectors; (2) the increased collecting field across the sensitive region reduces the damage sensitivity; and (3) the damage threshold of detectors made from lower resistivity materials is higher than that of those

made from higher resistivity materials. In the case of dE/dx detectors, there was no convincing evidence of any difference in degradation rates when viewed from the positive or negative sides of the detectors. Author

N68-25972*# Kansas Univ., Lawrence.

INVESTIGATION OF ELECTROCALORIC EFFECTS IN FERROELECTRIC SUBSTANCES Final Report, 1 Mar. 1964–1 Jul. 1967

Gordon G. Wiseman Washington NASA Jun. 1968 78 p refs (Grant NsG-575)

(NASA-CR-1080) CFSTI: HC \$3.00 /MF \$0.65 CSCL 20L

The electrocaloric effect in ferroelectric and pyroelectric substances was investigated in order to obtain a better understanding of the spontaneous electrical polarization in these substances. Quantitative measurements of the electrocaloric effect are feasible over a wide range of temperature. The accuracy and validity of such measurements were established by observing the effect in a substance while it was in its paraelectric phase where the results were predictable from the Curie-Weiss law. Measurements of the electrocaloric effect in the ferroelectric region further confirm the idea that the Langevin-type model which is based on long range interactions between dipoles characterized by an inner field parameter v is not sound. A useful characteristic of a material which is to be used as a radiation detector delivering its signal into a low-impedance detector is considered to be the pyroelectric coefficient. Under certain conditions the sensitivity of a pyroelectric radiation detector can be changed by a change in the applied field whereas in others it can be made independent of an applied field. A.L.

N68-26603*# Research Triangle Inst., Durham, N. C.

A STUDY OF CHARGE STORAGE IN SILICON OXIDE Resulting from Non-Penetrating Electron Irradiation

M. Simons, L. K. Monteith, and J. R. Hauser Washington NASA Jun. 1968 78 p refs

(Contract NAS1-6900)

(NASA-CR-1088) CFSTI: HC\$3.00 /MF\$0.65 CSCL 20L

Charge storage in silicon dioxide resulting from low energy electron irradiation has been observed. The positive charge build-up has been studied in MOS type structures for various oxide thicknesses as a function of beam energy, electron fluence, sample bias, electrode thickness, and a number of oxide-related parameters. The effective radiation-induced oxide charge appears to be a function of beam energy dissipated within the oxide near the oxide-silicon interface; this charge increases with electron fluence up to a saturation level which was observed in some steam-grown oxides: the experimentally observed dependence of induced charge on applied bias is compared with that predicted by several models for charge accumulation. Optical and thermal annealing of the trapped charge has been studied in an effort to derive information on the nature of the oxide trapping levels. Reduction of trapped charge by irradiation at small negative biases has also been explored. Finally the development of a two-carrier model for space charge build-up in an MOS structure is discussed and the experimental results obtained for silicon dioxide are related to device performance in the radiation environment. Author

N68-26627*# Research Triangle Inst., Durham, N. C. SEMICONDUCTOR PIEZOJUNCTION TRANSDUCERS J. J. Wortman Washington NASA Jun. 1968 94 p refs (Contract NASr-222)

(NASA-CR-1089) CFSTI: HC \$3.00 /MF \$0.65 CSCL 20L

Techniques for utilizing the piezojunction effect as the sensory element in transducers are discussed. A new technique for applying the phenomenon (silicon needle) in a broad class of mechanical transducers has been developed and demonstrated in several transducers. Particular emphasis was placed on accelerometers where it was shown that devices could be fabricated with resonant frequencies greater than 3 KC, capable of measuring ac and dc accelerations in the range from ± 1 g to ± 100 g. Several techniques were developed for providing a digital output for the piezojunction sensors. Author

N68-28239*# National Aeronautics and Space Administration. Lewis Research Center, Cleveland, Ohio.

LOW-TEMPERATURE RESISTANCE IN MINIMUM AND MAGNETORESISTANCE FOR DILUTE ALLOYS OF IRON IN COPPER

John S. Loomis and Wayne R. Hudson Washington Jul. 1968 12 p refs

(NASA-TN-D-4626) CFSTI: HC\$3.00/MF\$0.65 CSCL 20L

A temperature dependence of the Fe-Cu resistivity was compared with the predictions of Kondo and Nagaoka. The Nagaoka theory fits the experimental results better than the Kondo theory. The transverse magnetoresistance was measured as a function of temperature and magnetic field. For concentrations less than 0.03 at. % Fe in Cu, the magnetoresistance was positive and was approximately linear for higher magnetic fields. For Fe concentrations greater than 0.03 at. %, the magnetoresistance became increasingly negative with increasing concentrations. The magnetoresistance of the 0.073-at. %-Fe sample fit a magnetic field dependency of H 1.33.

N68-33228*# National Aeronautics and Space Administration. Goddard Space Flight Center, Greenbelt, Md.

ELECTRON SPIN RESONANCE OF LITHIUM-DIFFUSED SILICON

F. E. Geiger Washington Aug. 1968 28 p refs

(NASA-TR-R-290) CFSTI: HC\$3.00/MF\$0.65 CSCL 20L

Electron paramagnetic resonance was studied in floating-zone, lithium-diffused silicon. The resonances observed were identified as the result of Li-O complexes. The g-factor for the Li-O complex with the magnetic field H_0 in the (100) direction was found to be in good agreement with the calculated value obtained from the principal g-factors determined by Feher for crucible-grown silicon. Instrument sensitivity allowed the recording of Li-O and phosphorus donor hyperfine structure, thus permitting the Li-O concentration to be determined and the oxygen concentration in floating-zone silicon to be estimated. Irradiation of floating-zone, lithium-diffused silicon emptied the phosphorus donor levels and about 54 percent of the Li-O levels into deep traps; however, no new centers were found, although an unidentified structure was observed at approximately g = 2.006. The lithium-diffused sample of 0.16 ohm-cm resistivity gave a narrow (0.9 oersted), stress-sensitive resonance line. The resonance split into a doublet in the (100) direction. The resonance was attributed to lithium donor electrons in a ground state and donor wave functions arising from single conduction electron vallevs. Author

N68-35178*# National Bureau of Standards, Boulder, Colo. Inst. for Basic Standards.

SUPERCONDUCTION THIN FILMS

R. A. Kamper, L. O. Mullen, and D. B. Sullivan Washington NASA Sep. 1968 38 p refs

(NASA Order C-7756-B)

(NASA-CR-1189; NBS-9708) CFSTI: HC \$3.00/MF \$0.65 CSCL

Attention is concentrated mainly on the properties and applications of the Josephson effect at radio frequencies. The characteristics of the emitted radiation under various conditions were explored; a simple theory was constructed of the linewidth (which was verified); new principles were conceived for an absolute milli-degree thermometer and a picovoltmeter; a prototype of the picovoltmeter was built and tested; and a reliable method for fabricating good tunnel junctions between thin films of niobium and lead was developed. Author

26 PHYSICS, SOLID-STATE

N68-35356*# National Aeronautics and Space Administration. Lewis Research Center, Cleveland, Ohio.

ULTRASONIC ATTENUATION IN SUPERCONDUCTING TANTALUM

Zoltan W. Sarafi Washington Sep. 1968 23 p refs

(NASA-TN-D-2806) CFSTI: HC\$3.00/MF\$0.65 CSCL 20L

Ultrasonic attenuation was measured in single crystals of tantalum at frequencies from 30 to 330 MHz. The crystals were oriented in the (100) and (110) directions. The attenuations of longitudinal and transverse waves were measured as a function of temperature and magnetic field. Curves are presented showing the transition between the normal and superconducting states. The zero-temperature energy gaps obtained were 3.3 kT_c for both directions. The samples had q/ values intermediate between those used by other investigators, and a comparison of results indicated that the energy gap in tantalum is lower for samples with larger electronic mean-free paths. A state of the samples intermediate between the samples with larger electronic mean-free paths.

N68-37051*# National Aeronautics and Space Administration. Langley Research Center, Langley Station, Va. PROTON-PRODUCED DEFECTS IN n-TYPE SILICON Roger A. Breckenridge Washington Oct. 1968 27 p refs (NASA-TN-D-4830) CFSTI: HC\$3.00/MF\$0.65 CSCL 20L

Defect energy levels and concentrations were determined for n-type silicon single crystals with initial resistivities between 10 and 200 ohm-cm after 22.4 -MeV proton irradiations. Two defect energy levels were located: one at 0.17 eV below the bottom of the conduction band and one at 0.41 eV below the bottom of the conduction band. The introduction rate of the oxygen-vacancy complex was independent of the oxygen content of the silicon for the samples investigated. Heat treatment of Czochralski-grown silicon at 1000°C for 65 hours had no effect on the introduction rate of the oxygen-vacancy complex. Author

N68-37055*# National Aeronautics and Space Administration. Langley Research Center, Langley Station, Va.

EFFECTS OF ZINC CONCENTRATION ON OUTPUT OF ZINC DOPED GERMANIUM DETECTORS

Wilfred D. Hesketh Washington Oct. 1968 36 p refs (NASA-TN-D-4834) CFSTI: HC\$3.00/MF\$0.65 CSCL 20L

The effects of dopant concentration on the operation of far infrared detectors were investigated theoretically and experimentally. The theoretical investigation shows that an optimum dopant concentration does exist in extrinsic quantum detectors. This optimum point will vary with changes in the host or dopant material. The optimum will also vary with changes in the integrating chamber used. In the experimental investigation, an integrating chamber was constructed and evaluated for its characteristics. These characteristics, radiation loss coefficient due to reflections from the input port, and radiation loss due to absorption by the integrating chamber walls were then used in predicting the optimum dopant concentration of zinc doped germanium. Ten pairs of detectors were produced of various dopant concentration with equal dopant concentration in the two detectors of each pair. The output of the detectors was measured, the measurement being normalized to the maximum value and plotted. These curves were then compared with similarly normalized theoretical curves. The optimum dopant concentration occurred as predicted but with a greater slope on each side of the optimum point than was predicted. Author

27 PROPELLANTS

Includes fuels; igniters; and oxidizers. For basic research see: 06 Chemistry; and 33 Thermodynamics and Combustion. For related information see also: 28 Propulsion Systems.

N68-11645*# National Aeronautics and Space Administration. Lewis Research Center, Cleveland, Ohio.

EFFECT OF GRAVITY ON SELF-PRESSURIZATION OF SPHERICAL LIQUID-HYDROGEN TANKAGE

John C. Aydelott Washington Dec. 1967 21 p refs

(NASA-TN-D-4286) CFSTI: HC\$3.00/MF\$0.65 CSCL 13D

The information obtained from several experimental programs was examined in order to understand better the thermodynamic history of spherical, 9-inch- (23-cm-) diameter liquid-hydrogen tankage at both normal and reduced gravities. The rate of pressure rise in the hydrogen container was lower under reduced-gravity conditions than under normal-gravity conditions because of the increase in the liquid-wetted wall area and the increased boiling. The location of the sources of heat relative to the hydrogen liquid and vapor was the most important factor in determining the rate of pressure rise.

N68-17093*# National Aeronautics and Space Administration. Lewis Research Center, Cleveland, Ohio.

FEASIBILITY OF SUPPORTING LIQUID FUEL ON A SOLID WALL IN A RADIATING LIQUID-CORE NUCLEAR ROCKET CONCEPT

Henry A. Putre and Albert F. Kascak Washington Feb. 1968 29 p refs

(NASA-TN-D-4413) CFSTI: HC\$3.00/MF\$0.65 CSCL 21F

A reference liquid fuel nuclear rocket concept, previously analyzed, consists of a liquid carbide fuel mixture supported on the inside wall of a rotating tube. This report extends the original liquid fuel heat-transfer analysis for the reference engine by developing an expression for combined molecular and propellant induced turbulent heat transfer in the liquid fuel, and results in a more rigorous determination of support-wall temperature. In addition, two means of reducing support wall temperature without severly affecting rocket performance are investigated. For the reference fuel element configuration, with uniform heat source distribution in the liquid fuel, the support wall temperature calculated from the more complete turbulent analysis was 9830°R (5460°K). When the fuel was zoned into a region in the liquid near the propellant interface. the support wall temperature was about 1200°R (670°K) lower than for the unzoned case. A simplified mass-transfer analysis indicated that wall temperature reduction by fuel zoning does not appear feasible. The insulating effect of a stable opaque vapor layer built up at the solid liquid interface was also evaluated. Wall temperature was found to be reduced to 8500°R (4720°K) at 1430 seconds specific impulse by the vapor layer. Current wall materials, such as graphite used at 7200°R (4000°K) in conjunction with an opaque vapor layer, may permit operation at a reduced specific impulse of about 1250 seconds. Author

N68-21267*# National Aeronautics and Space Administration. Lewis Research Center, Cleveland, Ohio.

COMPUTER CODE FOR CALCULATING TEMPERATURE PROFILES IN A PROPELLANT TANK

Ronald L. Danilowicz Washington Apr. 1968 35 p refs (NASA-TM-X-1556) CFSTI: HC\$3.00/MF\$0.65 CSCL 20M

A FORTRAN IV computer code for determining temperature histories in a propellant tank due to wall and internal heating was written. The analysis, on which the code is based, is presented. The assumptions and approximations made are also discussed. Also included are instructions for use of the code, a sample problem, a flow chart and a complete listing of the code. Author

N68-21893*# Atlantic Research Corp., Alexandria, Va. STUDY OF PROPELLANT VALVE LEAKAGE IN A VACUUM Final Summary Report

Ralph D. Gift, Jonn A. Simmons, Jack M. Spurlock, Joseph P. Copeland, and Jaydee M. Miller Washington NASA Apr. 1968 12 p ref

(Contract NAS9-4494)

(NASA-CR-1047) CFSTI: HC\$3.00/MF\$0.65 CSCL 21H

Condensed summary report is presented of an investigation of the adverse effects of propellant leakage through propellant valves and into rocket injector manifolds and combustion chambers exposed to a vacuum environment. In space, during a nonfiring condition, these various regions of the engine are exposed to a vacuum environment. Consequently, should any propellant leak past the control valve, it can freeze and accumulate in the injector flow passages and combustion chamber. Investigation was conducted to study the likelihood that such accumulation may cause blockage of the propellant flow system or result in a catastrophic hard start. The investigation consisted of concurrent theoretical and experimental studies, with emphasis of consideration being given to the factors that could affect the performance of the Apollo Service Propulsion System and the Gemini Orbit Attitude Maneuvering System engines. Author

N68-28155*# National Aeronautics and Space Administration. Lewis Research Center, Cleveland, Ohio.

THE BOILOFF PROBLEM WITH METHANE FUEL IN SUPERSONIC AIRCRAFT

Richard J. Weber Washington Jul. 1968 15 p refs

(NASA-TM-X-1604) CFSTI: HC\$3.00/MF\$0.65 CSCL 21D

The benefits of employing methane fuel in supersonic aircraft are lessened by the tendency of the cryogenic fuel to boil away in flight. Boiloff due to ambient pressure reduction during climb appears to be the most difficult to avoid. Subcooling the fuel and using a soluble pressurant such as air or nitrogen is evaluated. Another solution is zero-ullage storage. Alternatively, it is suggested that the boiloff penalties with nonsubcooled fuel may be acceptable. In the study airplane gross weight is allowed to vary as required to yield the desired range and payload.

27 PROPELLANTS

N68-30077*# National Aeronautics and Space Administration. Lewis Research Center, Cleveland, Ohio.

ON THE SOLUBILITIES AND RATES OF SOLUTION OF GASES IN LIQUID METHANE

Robert R. Hibbard and Albert Evans, Jr. Aug. 1968 25 p refs

(NASA-TN-D-4701; E-4324) CFSTI: HC \$3.00/MF \$0.65 CSCL 21D

Curves are given which permit the easy calculation of the solubilities of oxygen, argon, carbon monoxide, nitrogen, neon, hydrogen, and helium in liquid methane at temperatures between 90 and 112 K. The solubilities of these gases decrease in the order in which they are listed above. It was also found that the rates of solution of gases in liquefied natural gas are very high. It appears that only the least soluble gases, neon, hydrogen and helium can be used as fuel system pressurants if liquefied natural gas is to be used in aircraft.

 $\textbf{N68-30313}^{*\#}$ National Aeronautics and Space Administration, Washington, D. C.

HIGH ENERGY PROPELLANTS: A CONTINUING BIBLIOGRAPHY WITH INDEXES

Jun. 1968 57 p refs

(NASA-SP-7002(04)) CFSTI: HC\$3.00/MF\$0.65 CSCL 211

References on high energy propellants announced in the NASA abstract journals during 1967 are presented in this continuing bibliography that contains subjects and author indexes. The 103 references deal with research and development studies on solid, liquid, and hybrid propellants and oxidizers as well as propellant, handling and storage, combustion characteristics, toxicity, hazards, and safety measures.

N68-32793*# TRW Systems, Cleveland, Ohio. ANALYTICAL PREDICTIONS OF DELIVERED SPECIFIC IMPULSE

Victor Quan Washington NASA Aug. 1968 137 p refs (Contract NAS9-4358)

(NASA-CR-1123; TRW-02874-6008-R000) CFSTI: HC \$3.00/MF\$0.65 CSCL 211

Summary data are presented on the four computer programs developed to calculate inviscid, one-dimensional and axisymmetric nonequilibrium nozzle flow fields accounting for the nonequilibrium effects of finite rate chemical reactions between gaseous combustion products and velocity and thermal lags between gaseous and condensed combustion products. Written in Fortran 4, these are the (1) one-dimensional reacting gas program, (2) one-dimensional two-phase reacting gas program, (3) axisymmetric reacting gas program, and (4) axisymmetric two-phase perfect gas program. Program limitations are delineated. Tabulated data are included on the results of studies undertaken to determine the chemical species and chemical reactions and reaction rates for typical propellant systems. The implicit integration method used in the programs is described, along with the transonic analyses used to construct the initial lines for the characteristics calculations in the axisymmetric programs. Graphs depicting the results of the four programs are included. M.G.J.

N68-35072*# National Aeronautics and Space Administration. Lewis Research Center, Cleveland, Ohio.

PERFORMANCE AND STABILITY CHARACTERISTICS OF NITROGEN TETROXIDE-HYDRAZINE COMBUSTORS Martin Hersch Washington Sep. 1968 23 p refs

(NASA-TN-D-4776) CFSTI: HC\$3.00/MF\$0.65 CSCL 21B Studies were conducted to determine the effects of various design and operating parameters on storable propellant rocket combustion. An injector incorporating like-on-like doublets forming parallel sheets achieved 95 percent of theoretical performance and gave best stability. Triplet injectors with unlike impingement had poorest stability characteristics. Increasing combustor length improved performance for parallel sheet but not for triplet injection. Effects of contraction ratio, propellant flow rate, and chamber pressure on performance were small. It was concluded that unlike impingement of hypergolic propellants may be initiating cause of high-frequency instability. Author

28

PROPULSION SYSTEMS

Includes air breathing, electric, liquid, solid, and magnetohydrodynamic propulsion. For nuclear propulsion see: 22 Nuclear Engineering. For basic research see: 23 Physics, General; and 33 Thermodynamics and Combustion. For applications see: 31 Space Vehicles. For related information see also: 27 Propellants.

N68-10496*# National Aeronautics and Space Administration, Lewis Research Center, Cleveland, Ohio. THERMAL INVESTIGATION OF AN ION ENGINE MICRO-

THRUSTOR

N. J. Stevens and D. C. Briehl Washington Nov. 1967 15 p refs (NASA-TM-X-1473) CFSTI: HC \$3.00/MF \$0.65 CSCL 21C

A cesium contact-ion microthrustor that was designed at the Lewis Research Center was studied to determine the heat transfer conditions necessary to minimize the heater power. The microthrustor was simulated on a resistance analog network which was balanced to an experimentally obtained set of temperatures and power inputs from a full-size thermal model test. No cesium was used in the thermal model. The major thermal losses were identified as conduction through the tank mounts and radiation from the hot feed tube insulation, accelerator, and cesium tank. The thermal model with these losses minimized was predicted to operate at 13.1 watts, and actually it operated at 12.9 watts. Application of modifications to the actual thrustor reduced the power requirements by the expected 13 percent.

N68-10502*# National Aeronautics and Space Administration. Langley Research Center, Langley Station, Va.

EFFECTS OF AXIAL GRADIENTS OF VELOCITY AND MAGNETIC FIELD, ELECTRODE STAGGER, AND ION SLIP ON PARAMETERS IN MHD ACCELERATORS

Frank Hohl Washington NASA Nov. 1967 40 p refs

(NASA-TN-D-4239) CFSTI: HC\$3.00/MF\$0.65 CSCL 201

The distributions of current and potential have been determined for two linear Faraday plasma accelerators. The equations describing the electrical parameters of accelerators were reduced to two dimensions and numerical analysis was used to solve the equations. The internal resistance of the accelerator, the Hall potential gradient, and various other parameters have been calculated as functions of: velocity and magnetic field gradients along the channel axis, ion slip, various amounts of stagger of electrodes, the ratio of electrode width to insulator width, and the Hall parameter. The results are compared with previous theoretical work and with experimentally obtained data.

N68-10562*# National Aeronautics and Space Administration, Lewis Research Center, Cleveland, Ohio.

PERFORMANCE TESTS OF A 1/2-MILLIPOUND (2.2 mN) AMMONIA RESISTOJET THRUSTOR SYSTEM

Harold Ferguson and James S. Sovey Washington Nov. 1967 19 p refs

(NASA-TN-D-4249) CFSTI: HC \$3.00/MF \$0.65 CSCL 21H Performance data were obtained and evaluated for a nominal 1/2-millipound-(2.2 mN) thrust resistojet system, with ammonia as the propellant. The system is defined to include the thrustors, the propellant storage and feed components, and the power and signal conditioning module. For a nominal system input power of 8 watts, the valves and power conditioning required 3 watts. The power delivered to the thrustor was 5 watts, of which approximately 1 watt represented augmented thrust power. For these conditions, a specific impulse of 140 seconds was obtained. The system was capable of maintaining specified thrust tolerances for either liquid or vapor propellant extraction and thus should be able to operate in a zero-gravity environment. Author N68-1.1829*# Israel Program for Scientific Translations, Ltd., Jerusalem.

RUSSIAN SOLID-FUEL ROCKETS [RAKETY NA TVERDOM TOPLIVE V ROSSII]

V. W. Sokol'skii 1967 242 p refs Transl. into ENGLISH from Izd. Akad. Nauk SSSR (Moscow), 1963 Prepared for NASA and NSF

(NASA-TT-F-415; TT-66-51152) CFSTI: \$3.00 CSCL 19G

A history of solid fuel rocketry in Russia is presented. Consideration is given to pyrotechnic rockets before the beginning of the 19th century, the earliest military application of rockets, rocket armament of the Russian army, other types of rockets in the second half of the 19th century, attempts to power aircraft by solid propellant rockets, and solid propellant rockets in Russia at the turn of the 20th century. C.T.C.

N68-15644*# National Aeronautics and Space Administration, Lewis Research Center, Cleveland, Ohio.

COMBUSTION IN STABILITY IN STEEL AND ABLATIVE ROCKET CHAMBERS

Ralph R. Goelz Washington Feb. 1968 11 p refs

(NASA-TM-X-1511) CFSTI: HC\$3.00/MF\$0.65 CSCL 21B

An investigation was conducted to compare the effects of ablative chambers and steel chambers on combustion instability in a hydrogen-oxygen rocket engine. Both uncharred and charred ablative materials were evaluated. Two concentric tube injectors were used for the testing at a chamber pressure of 300 psia (2070 kN/m²) and a nominal thrust of 20,000 pounds (89 kN). Hydrogen-injection temperature ramping was the basic stability rating technique. An instability amplitude comparison analysis was completed to detect amplitude variations for the two materials. Both the hydrogen-injection temperature ramping and the amplitude analysis lead to the same conclusion: There is no significant difference in stability limit or instability amplitude between the steel, charred ablative, and uncharred ablative chambers.

N68-16413*# National Aeronautics and Space Administration. Lewis Research Center, Cleveland, Ohio.

COLD-AIR PERFORMANCE EVALUATION OF SCALE MODEL OXIDIZER PUMP-DRIVE TURBINE FOR THE M-1 HYDROGEN-OXYGEN ROCKET ENGINE. 3: PERFORMANCE OF FIRST STATE WITH INLET-FEEDPIPE-MANIFOLD ASSEMBLY

Roy G. Stabe and John F. Kline Washington Feb. 1968 21 p refs

(NASA-TN-D-4392) CFSTI: HC\$3.00/MF\$0.65 CSCL 21H

The aerodynamic performance of the first stage of a 0.45-scale model of the oxygen pump-drive turbine for the M-1 rocket engine was determined experimentally. The first stage, including the inlet-feedpipe-manifold assembly, was tested over a range of speeds and pressure ratios. The results indicated that, at design equivalent speed and blade-jet speed ratio, the first-stage static and total efficiencies were very close to design values. The static and total efficiencies were 0.37 and 0.57 compared with the design values of 0.375 and 0.563, respectively. The equivalent weight flow at the design point was the same as that reported for the reference two-stage turbine investigation. The weight flow was reduced by a higher-than-design inlet-manifold total-pressure loss, a large

circumferential variation in manifold flow conditions, and a 3.7-percent deficit in nozzle throat area. The less-than-design throat areas changed the static-pressure distribution from design and reduced the nozzle-exit velocity. Results of a velocity diagram and a loss analysis of the first-state performance indicated that the rotor efficiency was 0.81 compared with the design value of 0.80. The nozzle performed better than design: the nozzle efficiency was 0.94 compared with the design value of 0.91. Author

N68-16632*# National Aeronautics and Space Administration. Lewis Research Center, Cleveland, Ohio.

COLD-AIR INVESTIGATION OF A TURBINE FOR HIGH-TEMPERATURE ENGINE APPLICATION. 2: DETAILED ANALYTICAL AND EXPERIMENTAL INVESTIGATION OF STATOR PERFORMANCE

Herman W. Prust, Jr., Harold J. Schum, and Frank P. Behning Washington Feb. 1968 45 p refs

(NASA-TN-D-4418) CFSTI: HC \$3.00/MF \$0.65 CSCL 21E

The effects on turbine stator performance of the blade features of low solidity and large profile and trailing-edge thicknesses were studied. At design mean-section critical velocity ratio of 0.790, the experimental results for the subject stator based on annular-sector data show an annular-sector, after-mix, kinetic-energy loss coefficient of approximately 0.05. The experimental performance of this stator was compared with the estimated performance of two stators with thinner profiles and higher solidities than the subject blading. This comparison indicated that the performance of the subject blading was not significantly affected by increased profile thickness, and that the mean-radius solidity of the subject blading of 1.39 was not too low for good performance. Good agreement was obtained between experimental and analytical mean-section performance for the subject stator and one of the reference stator bladings. These analytical results indicate that the large trailing-edge blockage of the subject stator (about 10 percent) caused a 1% loss of the kinetic energy available to the stator. Rather poor agreement was obtained for the subject stator between experimental annular-sector loss and annular-sector loss predicted from mean-section data. The after-mix kinetic energy loss coefficient obtained from radial integration was 0.010 larger than the predicted value at design critical velocity ratio. Author

N68-17028*# National Aeronautics and Space Administration. Ames Research Center, Moffett Field, Calif.

INVESTIGATION OF A LARGE-SCALE MIXED COMPRES-SION AXISYMMETRIC INLET SYSTEM CAPABLE OF HIGH PERFORMANCE AT MACH NUMBERS 0.6 TO 3.0

Norman E. Sorensen and Donald B. Smeltzer Washington Feb. 1968 180 p refs

(NASA-TM-X-1507) CFSTI: HC\$3.00/MF\$0.65 CSCL 21H

A model of a mixed-compression inlet with a 20 inch diameter capture area was designed and tested in combination with three subsonic diffuser designs. The majo objective was to investigate relatively short axisymmetric inlet systems capable of high performance over the complete Mach number range. The model was tested in a wind tunnel at Mach numbers from 0.6 to 3.2 and angles of attack from 0° to 8°. The Reynolds number was about 2×10^{6} per foot at Mach number 3.0. The supersonic diffuser of the inlet was designed with the aid of a computer program employing the method of characteristics. Preliminary tests showed that the supersonic portion of the inlet performed as predicted, but the flow separated in the subsonic diffuser limiting the performance at the engine face. The subsonic diffuser was then modified and the total pressure recovery was raised to 90% with about 11% boundary layer bleed mass flow from 86% recovery with 13-percent bleed. Off-design total-pressure recoveries were also improved about 4% over the Mach number range 1.55 to 3.0. The 1.50 capture diameter inlet, with vortex generators, showed an additional 1-percent improvement in recovery, but of more significance was the reduction in total pressure distortion at the engine face. The distortion was reduced to 6 to 7% from about 10% and the maximum recovery was improved to about 91% with about 11% boundary layer bleed mass flow. Without the generators the distortion of the 1.50-diameter inlet was about doubled (14%). The test results in the Mach number range 0.6 to 1.2 included details of experimentally measured additive drag. It was found that there was an optimum trade of additive drag for pressure recovery. Au*hor

N68-18216*# National Aeronautics and Space Administration. Lewis Research Center, Cleveland, Ohio.

COOLED BAFFLE DEVELOPMENT FOR M-1 ENGINE USING A SUBSCALE ROCKET ENGINE

E. William Conrad, John P. Wanhainen, and Jerome K. Curley Washington Oct. 1966 49 ρ refs (Declassified)

(NASA-TM-X-1267) CFSTI: HC\$3.00/MF\$0.65 CSCL 21H

A subscale rocket of 15,000 pounds thrust was used to provide a realistic environment for development of a suitable cooled baffle configuration for use in the M-1 engine development program. Chamber pressure, contraction ratio, mixture ratio, and injector elements were identical with the full-scale M-1 engine. Inasmuch as the size of an individual baffle compartment of the full-scale engine was approximated by the subscale engine, the heat transfer environment of the full-scale engine was also closely simulated. As a result of tests using a series of 25 baffles (segments of full scale) employing several cooling techniques, a configuration was developed that satisfied the design requirements and exhibited adequate durability. All baffle configurations employing transpiration cooling exhibited an unexpected multivalued flow characteristic curve, rendering these configurations unsuitable for use in the M-1 engine program. Author

N68-18221*# National Aeronautics and Space Administration. Lewis Research Center, Cleveland, Ohio.

CHANGE IN INDUCER NET POSITIVE SUCTION HEAD REQUIREMENT WITH FLOW COEFFICIENT IN LOW TEMPERATURE HYDROGEN (27.9" TO 36.6"R) Phillin R Meng Washington Mar. 1968 28 p refs

(NASA-TN-D-4423) CFSTI: HC\$3.00/MF\$0.65 CSCL 21H

An 84° flat plate helical inducer was used to evaluate

the thermodynamic effect of cavitation in low temperature liquid hydrogen over a range of flow coefficients. The range of liquid hydrogen temperatures studied was from 27.9° to 36.6° R. The tests were conducted at a rotative speed of 20 000 rpm over a range of flow coefficients from 0.060 to 0.076 (1200 to 1500 gal/min). For a given head coefficient ratio, the required net positive suction head increased as the fluid inlet temperature was lowered. This decrease in inducer performance was attributed to a decrease in the thermodynamic effect of cavitation at the lower fluid temperatures. For a given temperature the thermodynamic effect of cavitation increased with decreasing flow coefficient. This effect is attributed to changes in blade pressure distribution with flow coefficient. The measured values of required net positive suction head are in reasonable agreement with those obtained using a semiempirical prediction method. Author

N68-18249*# National Aeronautics and Space Administration. Lewis Research Center, Cleveland, Ohio.

EXPERIMENTAL INVESTIGATION OF ACOUSTIC LINERS TO SUPPRESS SCREECH IN STORABLE PROPELLANT ROCKET MOTORS

David W. Vincent, Bert Phillips, and John P. Wanhainen Washington Mar. 1968 47 p refs

(NASA-TN-D-4442) CFSTI: HC\$3.00/MF\$0.65 CSCL 21H

Several acoustic liners (Helmholtz type) were experimentally and theoretically evaluated to determine their effectiveness to suppress screech in a rocket motor. The liners were experimentally rated in a storable propellant (N₂O₄-50 percent hydrazine, 50 percent UDMH) rocket at a nominal chamber pressure of 100 psia (689 kN/m²) and 6700 pounds of thrust (29.8 kN). Liner design

variables investigated included aperture size. liner percent open area, liner length, and aperture shape. Tests were conducted in both a marginally stable and a spontaneously unstable combustor. Bomb pulses were used to rate stability in terms of the grains (grams) of explosive necessary to induce instability. Bomb pulses as high as 170 psi (1172 kN/m²) peak-to-peak were damped by liners when the liner resonant frequency was near the screech frequency. Calculated theoretical absorption coefficients assuming both flow and no flow past the apertures agreed with the experimental results. Full-length liners were not required for stabilization. Aperture size and shape had secondary effects. Longitudinal slots, which would be adaptable to regeneratively cooled configurations, were found to be as effective as circular apertures in suppressing screech.

N68-19581*# National Aeronautics and Space Administration. Lewis Research Center, Cleveland, Ohio.

OUT-OF-THE-ECLIPTIC-PLANE PROBE MISSION EMPLOY-ING ELECTRIC PROPULSION

Frank J. Hrach Washington Apr. 1968 35 p refs

(NASA-TN-D-4455) CFSTI: HC\$3.00/MF\$0.65 CSCL 21C

Measurements out of the ecliptic plane are necessary in the study of the Sun and heliocentric space. The present analysis investigates the use of a combined propulsion system to accomplish the out-of-the-ecliptic-plane probe mission. In the combined propulsion system studied herein, energy beyond Earth-escape energy is given to the vehicle by a booster, after which a low-thrust electric propulsion system begins operation. The chemical boosters considered are the Atlas-Agena and the Atlas-Centaur. Three values of electric propulsion system specific powerplant mass are examined, 50, 100, and 150 pounds per kilowatt jet. Results are presented for missions to final heliographic inclinations from 25° to 45°. The basic mission profile considered is one in which the distance from the Sun to the vehicle is held constant at a value of 1 astronomical unit, and in which the propulsion is terminated before the argument of latitude of the trajectory reaches 90°. The effects of variations from the basic profile are investigated. Author

N68-19708*# National Aeronautics and Space Administration. Lewis Research Center, Cleveland, Ohio.

EXPERIMENTAL EVALUATION OF SEVERAL ADVANCED ABLATIVE MATERIALS AS NOZZLE SECTIONS OF A STORABLE-PROPELLANT ROCKET ENGINE A. J. Pavli Washington Apr. 1968 23 p refs

(NASA-TM-X-1559) CFSTI: HC\$3.00/MF\$0.65 CSCL 21H

Eighteen ablative materials were evaluated for their relative erosion resistance in test firings of 22 nozzles in a storable-propellant engine of a 1.2-inch (3.05-cm) diameter throat at a chamber pressure of 100 psia (689.5 kN/m^2). The materials investigated were the phenolic, polyimide, phenolic plus polyamide, epoxy novalac, and phenyl-silane resins, reinforced with silica, quartz, and carbon-silica fibers. Quartz reinforcement was superior to silica with the three resins tested. The lower erosion rate is attributed to the higher melting temperature of quartz. Carbon-silica reinforcement exhibited the highest erosion rate. Its relatively poor performance is attributed to the rapid oxidation of the carbon. Ablatives made of phenolic resin had lower erosion rates than all other resins tested. Erosion at mixture ratios of 1.6 was greater than at mixture ratios of 2.0. Nozzle convergent entrance angle, throat radius of curvature, and source or resin supplier had no apparent effect on erosion resistance. A slight effect of fabrication technique on erosion was detected. Author

N68-20064*# National Aeronautics and Space Administration. Lewis Research Center, Cleveland, Ohio. EXPERIMENTAL INVESTIGATION OF REACTION

CONTROL, STORABLE BIPROPELLANT THRUSTORS R. James Rollbuhler Washington Apr. 1968 35 p refs (NASA-TN-D-4416) CFSTI: HC\$3.00/MF\$0.65 CSCL 21H

In order to evaluate the performance of low-thrust, chemical bipropellant rocket thrustors for possible applications in spacecraft reaction control systems, an experimental investigation was conducted with readily available thrustors. The thrustors were designed for a thrust of less than 5 pounds force (22.2 N), combustion-chamber pressures of 100 pounds per square inch absolute (68.9 M/cm²) or less, and for use with nitrogen tetroxide-hydrazine-type propellants. A high instrumented altitude test facility was used to test each of the thrustors over a range of test durations and oxidizer to fuel ratios. The maximum specific impulse obtained was 262 pounds force per pound mass per second (2570(N)(sec)/kg), and the maximum characteristic velocity was 5200 feet per second (1588 m/sec). Total impulses were measured for run times as short as 10 milliseconds. The average value of the specific impulse, at minimum run times, was about 25 percent of the maximum specific impulse for the same thrustor. Also reported are response times and combustor-wall temperatures. Author

N68-20186*# National Aeronautics and Space Administration, Lewis Research Center, Cleveland, Ohio.

SCALE 1/14.2 INVESTIGATION OF SUBMERGED NOZZLE FOR SL-3 260-INCH SOLID ROCKET

Reino J. Salmi and James J. Pelouch, Jr. Washington Apr. 1968 12 p refs Presented at the 2d AIAA-ICRPG Solid Propellant Conf., Anaheim, Calif., Jun. 1967

(NASA-TM-X-1546) CFSTI: HC\$3.00/MF\$0.65 CSCL 21H

The original submerged nozzle configuration for the SL-3 260-inch solid propellant rocket was modified to provide additional insulation and protection against the erosive effects of hot exhaust gases in the annular channel between the submerged nozzle lip and the rocket aft-end casing. Tests of the modified nozzle design indicated that the circumferential flow velocities in the annular channel were lower for the modified nozzle than for the original configuration for the case of an unburned or 100-percent grain. For the case of the 34-percent regressed grain, which reduced the flow velocities in the annular channel, flow Mach numbers approximately equal to those of the original nozzle were obtained with the modified nozzle.

N68-20187*# National Aeronautics and Space Administration. Lewis Research Center, Cleveland, Ohio.

DIVERGENT-FLOW CONTACT-IONIZATION ELECTRO-STATIC THRUSTOR FOR SATELLITE ATTITUDE CONTROL AND STATION KEEPING

Walter C. Lathern and John F. Staggs Washington Apr. 1968 25 p refs

(NASA-TN-D-4420) CFSTI: HC\$3.00/MF\$0.65 CSCL 21C

A divergent-flow contact-ionization electrostatic thrustor is described herein. This thrustor performed well at thrust levels between 0.89 and 1.56 millinewtons, a range that is applicable to satellite attitude-control and station-keeping missions. Power efficiencies up to 45 percent (excluding vaporizer and neutralizer powers) were obtained for operation at specific impulses from 5000 to 8000 seconds. No damage due to primary ion impingement was detected in about 200 hours of running. Accelerator drain currents were typically less than 2 percent of the beam current. Computer studies indicated an accelerator electrode lifetime in excess of 20,000 hours. Experimental data verified the computer predictions for electrostatic beam deflection up to about 15°. This deflection produced a component of thrust normal to the center plane of up to Author 30 percent of the total thrust of an undeflected beam. N68-21679*# National Aeronautics and Space Administration.

Lewis Research Center, Cleveland, Ohio. STABILIZING EFFECTS OF SEVERAL INJECTOR FACE BAFFLE CONFIGURATIONS ON SCREECH IN A 20,000 POUND-THRUST HYDROGEN-OXYGEN ROCKET

Ned P. Hannum, Harry E. Bloomer, and Ralph R. Goelz Washington Apr. 1968 41 p refs

(NASA-TN-D-4515) CFSTI: HC\$3.00/MF\$0.65 CSCL 21H

Experimental tests were conducted to assess the worth of injector face baffles as screech suppression devices. Seventeen injector face baffle configurations were evaluated with 94 hot firings. The number of injector face baffle compartments was varied from 3 to 100 with lengths from 1/2 to 2 inches (1.3 to 5.1 cm). Stability data were obtained at a chamber pressure of 300 pounds per square inch absolute and over a range of oxidant-fuel ratios of from 4 to 6. Hydrogen injection temperature was used to rate the stability of the various baffles. The baffle with the lowest self-triggering temperature was considered to be the most stable. The results indicate that injector face baffles 2 inches long produced acoustic stability to the minimum hydrogen injection temperature limit of the test facility with maximum compartment dimensions as large as 9.1 inches. Acoustic stability down to a hydrogen injection temperature of 55°R (31°K) could also be achieved with injector face baffles 1 inch in length when the maximum compartment dimension was less than 4 inches (10.2 cm). One of the configurations was, however, only marginally stable at the reduced temperature. Author

N68-22096*# National Aeronautics and Space Administration. Lewis Research Center, Cleveland, Ohio.

OPTIMAL FINITE-THRUST TRANSFER BETWEEN PLANET APPROACH AND DEPARTURE ASYMPTOTES WITH SPECIFIED INTERMEDIATE ORBIT

Edward A. Willis, Jr. Washington Apr. 1968 59 p refs (NASA-TN-D-4534) CFSTI: HC\$3.00/MF\$0.65 CSCL 22C

Optimal control and finite thrust aspects of the approach maneuver-planetocentric orbit-departure maneuver sequence at the destination planet of a round trip are studied. Solutions are developed for single maneuvers, and conditions for joining these into an optimal total trajectory are derived. Numerical results are presented for an elliptic parking orbit and typical asymptotic velocities and directions. It is shown that gravity losses and steering losses are not directly additive, low vehicle thrust to weight ratios are desirable, and trajectories with single-burn escape and capture maneuvers are usually advantageous. Author

N68-22272*# National Aeronautics and Space Administration. Lewis Research Center, Cleveland, Ohio.

EXPERIMENTAL EVALUATION OF 7.82-INCH (19.8-CM) DIAMETER THROAT INSERTS IN A STORABLE-PROPEL-LANT ROCKET ENGINE

Jerry M. Winter and Donald A. Peterson Washington Apr. 1968 47 p refs

(NASA-TM-X-1463) CFSTI: HC\$3.00/MF\$0.65 CSCL 21H

A total of 14 nozzle throat inserts of 7.82-inch diameter were evaluated for use with reinforced plastic thrust chambers. The propellants used were nitrogen tetroxide and a blend of 50 percent hydrazine with 50 percent unsymmetrical dimethyl-hydrazine. Primary failure mechanisms were determined for specific materials and design concepts. Detailed failure mechanisms were explored as a means of recommending material and design modifications to improve reliability and performance. Silicon carbide provided erosion protection for 100 seconds of continuous firing. However, both one-piece and segmented silicon carbide inserts failed structurally. Tungsten infiltrated with copper or silver had relatively high resistance to oxidation for approximately 250 seconds of run time. The copper-infiltrated insert was structurally sound after a firing duration of 340 seconds. Careful attention to substrate design and coating techniques appreciably increased the erosion resistance of coated inserts. A preferentially oriented pyrolytic graphite design was partly successful, but, to realize the full potential of this design, additional development work would be required. Only limited correlation between small- and large-size testing was obtained. However, the time to failure for large-scale monolithic inserts was extended over small-scale inserts. Author N68-22725*# National Aeronautics and Space Administration. Lewis Research Center, Cleveland, Ohio.

ANALYSIS OF FAN-TURBINE EFFICIENCY CHARACTERIS-TICS IN TERMS OF SIZE AND STAGE NUMBER

Warner L. Stewart and Arthur J. Glassman Washington May 1968 19 p refs

(NASA-TM-X-1581) CFSTI: HC\$3.00/MF\$0.65 CSCL 21E

This report presents a study of fan-drive turbine geometry and efficiency interrelations both in generalized form in terms of specific speed and specific diameter and for a selected set of representative turbofan engine conditions. Results are presented in terms of turbine efficiency and diameter variations as a function of number of stages for a range of fan speeds. Also shown are the variations in engine specific thrust and specific fuel consumption as functions of fan-turbine efficiency for the selected engine conditions. Author

N68-23354*# National Aeronautics and Space Administration. Ames Research Center, Moffett Field, Calif.

INVESTIGATION OF A NEARLY ISENTROPIC MIXED COMPRESSION AXISYMMETRIC INLET SYSTEM AT MACH NUMBERS 0.6 TO 3.2

Donald B. Smeltzer and Norman E. Sorensen Washington May 1968 152 p refs

(NASA-TN-D-4557) CFSTI: HC\$3.00/MF\$0.65 CSCL 21H

A 20-inch capture diameter model of a mixed-compression axisymmetric inlet system was designed and tested. The inlet system was 1.4 capture diameters long measured from the cowl lip to the engine face. The design Mach number was 3.0, and off-design performance was obtained by translation of the cowl. Vortex generators were employed just downstream of the throat to reduce the total-pressure recovery, and total-pressure distortion at the engine face. Tests were conducted over the Mach number range 0.6 to 3.2 at angles of attack from 0° to 8° and at a tunnel total pressure of 15 psia. The supersonic diffuser of the inlet was designed with the aid of a computer program which employs the method of characteristics. The subsonic diffuser was designed to have a linear variation of Mach number from the end of the throat to the engine face. Results indicated a level of performance at Mach number 3.0 of 90 to 93 percent total-pressure recovery at the engine face with a bleed mass-flow ratio of 7.5 to 12 percent and a total-pressure distortion level of about 10 percent. Author

N68-23477*# National Aeronautics and Space Administration. Lewis Research Center, Cleveland, Ohio.

EXPERIMENTAL INVESTIGATION OF MERCURY PROPELLANT FEED ISOLATORS FOR KAUFMAN THRUSTERS

Shigeo Nakanishi Washington May 1968 29 p refs

(NASA-TM-X-1579) CFSTI: HC\$3.00/MF\$0.65 CSCL 21C

Electrical breakdown voltages and leakage currents were experimentally determined for seven high-voltage isolator configurations designed for the mercury propellant feed system of a SERT II type Kaufman ion thruster. An isolator containing 40 insulated segments experienced no breakdown up to 5000 volts, but leakage current at 3000 volts was about 0.10 milliampere. A configuration utilizing a long propellent flow passage and large recombination surface areas operated at 3000 volts potential difference with a leakage current of less than 0.003 milliampere. Minimum breakdown voltage was 4400 volts.

N68-24614*# National Aeronautics and Space Administration. Langley Research Center, Langley Station, Va.

STUDY OF UNDEREXPANDED EXHAUST JETS OF AN X-15 AIRPLANE MODEL AND ATTACHED RAMJET ENGINE SIMULATOR AT MACH 6.86

Earl H. Andrews, Jr. and R. Clayton Rogers Washington May 1968 refs

(NASA-TM-X-1571) CFSTI: HC\$3.00/MF\$0.65 CSCL 21H

An investigation was conducted using a 0.02-scale model of the X-15 airplane with a ramiet engine simulator attached to the underside of its afterbody. The investigation was initiated to approximate the effects of the ramjet exhaust plume upon the external pressures of a nozzle extension of an X-15 engine. The nozzle extension was tested with and without a simulated manifold designed to collect and to eject overboard auxiliary gases from the X-15 airplane. The presence of the ramiet and its pylon tended to cause the afterbody surface pressures on the X-15 airplane to remain constant and not be affected by underexpanded exhaust plumes of the X-15 and ramiet nozzles. The pressure-measuring station nearest the base of the X-15 afterbody did, however, experience an increase as the exit-to-ambient static-pressure ratio of the X-15 nozzle increased. Static-pressure measurements and schlieren photographs indicated that the ramiet nozzle exhaust plume initially impinged upon the nonblowing X-15 nozzle extension at very small ratios of ramjet nozzle-exit pressure to ambient static pressure of 8 and 12 for angles of attack of 0° and 3°, respectively. Upward forces on the X-15 nozzle extension caused by operation of the ramjet nozzle were approximated; the forces without the manifold ring were greater than those with the ring. Author

N68-25099*# National Aeronautics and Space Administration. Lewis Research Center, Cleveland, Ohio.

MANAGEMENT OF CRYOGENIC PROPELLANTS IN A FULL SCALE ORBITING SPACE VEHICLE

Raymond F. Lacovic, Frederick C. Yeh, Steven V. Szabo, Jr., R. J. Brun, Andrew J. Stofan et al Washington May 1968 69 p refs

(NASA-TN-D-4571) CFSTI: HC\$3.00/MF\$0.65 CSCL21H

The fourth and eighth Atlas-Centaur vehicles were launched to study cryogenic propellant management during coast. Kinetic energies imparted to the liquid hydrogen at first engine cutoff caused liquid motion within the hydrogen tank resulting in subsequent venting of liquid hydrogen rather than gaseous hydrogen. The vented liquid impinged on the vehicle causing it eventually to tumble out of control. Energy dissipators were installed on the hydrogen tank pressurization line and boost pump return flow lines. A balanced thrust hydrogen vent system was installed to reduce vehicle disturbances. A slosh baffle was installed in the hydrogen tank and a thrust schedule for propellant settling and retention was established. These modifications reduced the total kinetic energy at first engine cutoff from 200 foot-pounds (270 J) to less than 50 foot-pounds. Information obtained on heat inputs to the tank was used to establish the capability of the hydrogen vent system. Also, a thermal survey was made of the hydrogen tank ullage; this survey provided information on temperature stratification of the ullage gas. The flight demonstrated a practical method for control of a cryogenic propellant in a full-scale orbiting space vehicle. The method of propellant control established for the Centaur vehicle is applicable to any space vehicle having short-term storage of cryogenic propellants in space. Author

N68-28644*# National Aeronautics and Space Administration. Lewis Research Center, Cleveland, Ohio.

SCREECH SUPPRESSION TECHNIQUES FOR ROCKET COM-BUSTORS USING EARTH-STORABLE PROPELLANTS

David W. Vincent, Daniel E. Sokolowski, and Harry E. Bloomer Washington Jun. 1968 38 p refs

(NASA-TM-X-1595) CFSTI: HC\$3.00/MF\$0.65 CSCL 21H

A rocket investigation was conducted using $N_2O_4/50$ percent hydrazine 50 percent unsymmetrical dimethyl hydrazine propellants to determine the effects of injector faceplate baffles, concentrated injection distribution with divergent chamber geometry, nozzle entrance length, and injector-element radial coverage. Injector faceplate baffles and concentrated propellant injections were stabilizing. No stability effect was noted by increasing the nozzle entrance length. Creation of an element void at the circumference of an injector was destabilizing. N68-26771 *# McDonnell-Douglas Co., Long Beach, Calif. Aircraft Div.

A STUDY OF TURBOFAN-ENGINE COMPRESSOR-NOISE-SUPPRESSION TECHNIQUES

Alan H. Marsh, I. Elias, J. C. Hoehne, and R. L. Frasca Washington NASA Jun. 1968 182 $\,p$ refs

(Contract NAS1-5256)

(NASA-CR-1056) CFSTI: HC\$3.00 /MF\$0.65 CSCL 21E

Preliminary engineering designs of nacelle acoustical treatments applicable to operational jet transports have been studied. The treatments are intended to be used to suppress compressor noise, especially during the landing approach. Studies were limited to the P&WA JT3D turbofan engine series as installed on the Douglas DC-8 airplane; however, the principles developed are applicable to other installations as well. Concepts were investigated involving application of narrow-band resonators and wide-band acoustical absorbers to the walls of the fan-discharge and inlet ducts. The concept of choked engine inlets was also considered. Analytical aerodynamic studies and wind tunnel model tests evaluated inlets with lightbulb-shaped centerbodies to provide narrower duct dimensions, and increased surface area for the addition of acoustical treatment. Tests were run to determine the flow resistance and the normal-incidence acoustical impedance and absorption coefficient of various duct-lining treatment configurations. Author

N68-28112*# Bendix Corp., Southfield, Mich. Research Labs, RESEARCH AND DEVELOPMENT OF A VORTEX VALVE FOR FLOW MODULATION OF A 16-PERCENT ALUMINIZED 5500°F PROPELLANT GAS

T. W. Keranen and A. Blatter Washington NASA Jun. 1968 137 p refs

(Contract NAS1-5199)

(NASA-CR-1091; Rept.-4227) CFSTI: HC \$3.00/MF \$0.65 USCL 13K

The flow of hot (5500°F) gas from a solid propellant gas generator has been successfully throttled by a fluidic, no-moving-part, vortex valve. The vortex valve has been demonstrated in a system simulating a hot gas secondary injection thrust vector control (SITVC) system. The hot gas vortex valves were controlled by a pilot stage utilizing a flapper-nozzle and vortex amplifier valve arrangement which modulated the flow of a 2000°F pilot stage solid propellant gas generator. Materials found suitable for the 5500°F hot gas application consist of silver-infiltrated tungsten, carbon or silica phenolic and solid carbon. The development effort consisted of six hot gas firings which demonstrated satisfactory material selection, hot gas flow modulation, and steady-state and dynamic performance of a simulated SITVC system.

N68-29378*# National Aeronautics and Space Administration. Lewis Research Center, Cleveland, Ohio.

ANALYSIS OF SEVERAL METHANE-FUELED ENGINE CYCLES FOR MACH 3.0 FLIGHT

Brent A. Miller Washington Jul. 1968 36 p refs (126-15-02-02-22)

(NASA-TN-D-4699) CFSTI: HC\$3.00/MF\$0.65 CSCL 21E

Several means of using methane's heat sink capacity for turbine cooling and for other purposes to improve engine specific impulse, specific thrust, and thrust per unit compressor frontal area were analyzed. Preheating of the methane with heat sources both internal and external to the engine was considered. In general, small gains in performance were obtained for the various cycles with respect to a reference turbojet cycle. No attempt was made to determine the weights of the various cycles considered. Author

N68-29953*# National Aeronautics and Space Administration. Lewis Research Center, Cleveland, Ohio.

COLD FLOW INVESTIGATION OF A LOW ANGLE TURBOJET PLUG NOZZLE WITH FIXED THROAT AND TRANSLATING SHROUD AT MACH NUMBERS FROM 0 TO 2.0

Donald L. Bresnahan and Albert L. Johns Washington Aug. 1968 39 p refs

(NASA-TM-X-1619) CFSTI: HC\$3.00/MF\$0.65 CSCL 21E

The performance of a full length plug nozzle can be maintained at a high level by extending the outer shroud with increases in nozzle pressure ratio from 2.5 to the design pressure ratio of 26.3. During acceleration, maximum external flow effects occurred at Mach 1.5 with performance losses of approximately 2.8 percent. At subsonic cruise, this loss was about 4.8 percent. Plug truncations to one-half and one-third of its full length resulted in losses of 1 and 1.7 percent, respectively, at Mach 2.0. Base bleed of about 1.5 percent of the primary flow optimized the performance of the truncated plugs. Author

N68-30040*# National Aeronautics and Space Administration. Langley Research Center, Langley Station, Va.

TURBOJET-ENGINE NOISE STUDIES TO EVALUATE EFFECTS OF INLET-GUIDE-VANE-ROTOR SPACING

John L. Crigler, W. Latham Copeland, and Garland J. Morris Washington Aug. 1968 32 p refs

(NASA-TN-D-4690) CFSTI: HC\$3.00/MF\$0.65 CSCL 21A

Experimental results are presented of a noise study which made use of a turbojet engine having an axial flow multiple stage compressor. The objective of this study was to investigate the effect of increased inlet guide vane-rotor spacing on the compressor interaction noise and engine performance, particularly at partial power conditions. The engine selected for this investigation was in the 2000-pound (8896-newton) thrust category and was readily modified by relocating the linlet guide vane assembly approximately six mean rotor blade chords ahead of the first stage rotor. The data are presented in the form of engine performance curves, poise radiation patterns, and frequency spectra. The data show that there is a substantial noise reduction due to the increased inlet guide vane-first stage rotor axial spacing. The reductions were as much as 14 dB for the condition of 80 percent rated rpm, the highest engine speed at which noise measurements were made. The noise reductions have been accomplished without any measurable loss in engine performance. Stationary components of the compressor which are exposed to pulsating flows are identified as sources of noise and are noted to have characteristic frequencies. Author

N68-30599*# National Aeronautics and Space Administration. Lewis Research Center, Cleveland, Ohio.

PERFORMANCE OF A WIND TUNNEL MODEL OF AN AERODYNAMICALLY POSITIONED VARIABLE FLAP EJECTOR AT MACH NUMBERS FROM 0 TO 2.0

Fred W. Steffen and John R. Jones Aug. 1968 35 p refs (NASA-TM-X-1639) CFSTI: HC\$3.00/MF\$0.65 CSCL 21E

A wind tunnel model of a variable flap ejector nozzle with an aerodynamically positioned shroud was evaluated over a range of Mach numbers from 0 to 2.0 at appropriate nozzle pressure ratios and statically at pressure ratios up to 26.0. Various power settings were simulated. Nozzle efficiency, pumping characteristics, boattail floating position, and boattail pressure drag were determined. The nozzle had typically high efficiencies at supersonic cruise and reheat acceleration conditions but rather low efficiency at subsonic cruise and dry acceleration conditions. The aerodynamically positioned shroud was stable at all simulated power settings and free stream Mach numbers.

N68-30604*# National Aeronautics and Space Administration. Lewis Research Center, Cleveland, Ohio.

M-1 INJECTOR DEVELOPMENT—PHILOSOPHY AND IMPLEMENTATION

Walter F. Dankhoff, Irving A. Johnsen, E. William Conrad, and William A. Tomazic Washington Aug. 1968 68 p refs

(NASA-TN-D-4730) CFSTI: HC\$3.00/MF\$0.65 CSCL 21H The M-1 injector design was a cooperative effort to achieve

high performance with completely stable operation. The approach

was based on the technology already established in the RL-10 and J-2 engine development programs, supplemented with the latest data obtained at NASA-Lewis. Small scale tests were conducted to verify design concepts prior to incorporation into the full scale hardware. Full scale injector testing demonstrated that the design goals were achieved. Author

N68-31476*# National Aeronautics and Space Administration. Lewis Research Center, Cleveland, Ohio.

TURBOJET AND TURBOFAN CYCLE CONSIDERATIONS AND ENGINE CONFIGURATIONS FOR APPLICATION IN LIGHTWEIGHT AIRCRAFT

Richard J. Roelke and Warner L. Stewart Washington Aug. 1968 17 p ref

(NASA-TM-X-1624) CFSTI: HC\$3.00/MF\$0.65 CSCL21E

Engine studies were made to define cycle characteristics of small turbojet and turbofan engines for a selected set of lightweight aircraft flight requirements. From these cycle studies, representative engine conditions were selected and used as a basis for the examination of associated engine configurations. Emphasis was placed on the types of turbomachinery involved and their associated diameters. Author

N68-32987*# General Motors Corp., Indianapolis, Inc. Allison Div.

EXPERIMENTAL INVESTIGATION OF ADVANCED CONCEPTS TO INCREASE TURBINE BLADE LOADING, 2: PERFORMANCE EVALUATION OF PLAIN ROTOR BLADE H. G. Lueders Washington NASA Aug. 1968 46 p refs (Contract NAS3-7902)

(NASA-CR-1172; EDR-4909, V. 2) CFSTI: HC \$3.00 / MF \$0.65 CSCL 21E

The overall performance of a single stage turbine designed with a rotor blade suction surface diffusion factor of 0.3 and negative rotor hub reaction was investigated over a range of equivalent speeds and expansion ratios. Total pressure surveys were made at the stator and rotor exits and a hot-wire survey was taken at the rotor trailing edge. The performance of turbine with this rotor-blade forms a base line that will be compared with advanced turbine blade loading concepts.

N68-35101*# Northern Research and Engineering Corp., Cambridge, Mass.

ANALYSIS OF GEOMETRY AND DESIGN POINT PERFORMANCE OF AXIAL FLOW TURBINES. 1: DEVELOPMENT OF THE ANALYSIS METHOD AND THE LOSS COEFFICIENT CORRELATION

A. F. Carter, M. Platt, and F. K. Lenherr Washington NASA Sep. 1968 113 p refs

(Contract NAS3-9418)

(NASA-CR-1181) CFSTI: HC \$3.00 / MF \$0.65 CSCL 21E

The development of a stream-filament analysis procedure is presented and a correlation of total-pressure-loss coefficients which forms the basis for a computer program with which the geometry and design-point performance of axial turbines is investigated. Since one of the principal features of the analysis procedure is the solution of the radial equilibrium equation taking into account radial gradients of enthalpy and entropy, the computer program based on this analysis will provide the turbine designer with the freedom to consider arbitrarily selected distributions of tangential velocities and radial distributions of work output as analysis variables. In addition, with the incorporation of a total-pressure-loss coefficient correlation, the computer program which results from the analysis can be used for a systematic investigation of the performance of alternative turbine designs for specified design Author requirements.

N68-35115*# National Aeronautics and Space Administration. Langley Research Center, Langley Station, Va.

A SIMPLIFIED EQUILIBRIUM HYDROCARBON-AIR COMBUSTION GAS MODEL FOR USE IN AIR-BREATHING ENGINE CYCLE COMPUTER PROGRAMS

Vincent R. Mascitti Washington Sep. 1968 48 p refs (NASA-TN-D-4747) CFSTI: HC\$3.00/MF\$0.65 CSCL 21A

Details are given on a simplified hydrocarbon-air combustion gas model, including the effects of dissociation for convenient use in engine cycle computer programs. The generalized model reduces to the hydrogen-air system as well as to the dissociating-air system. The exclusion of chemical species containing atomic nitrogen allows a considerable simplification of the composition equations. The thermodynamic properties of stoichiometric combustion of the kerosene-air and hydrogen-air systems are computed with the simplified model and compared with those of more comprehensive gas models. In addition, the effect of the neglected chemical species on the performance of an idealized subsonic combustion ramiet is presented. The simplified gas model has been used to define the limiting conditions for solid carbon and ammonia formation for fuel-rich gas mixtures. A computer program listing of the calculation procedure for the simplified gas model is presented. Author

N68-35594*# North American Rockwell Corp., Los Angeles, Calif. ANALYSIS OF PERFORMANCE CHARACTERISTICS IN GROUND EFFECT OF A LARGE SCALE V/STOL MULTI-FAN-IN-WING TRANSPORT MODEL

R. J. Oberto, D. J. Renselaer, and D. L. Alfano Washington NASA Oct. 1968 130 p ref

(Contract NAS2-4352)

(NASA-CR-1180) CFSTI: HC \$3.00 / MF \$0.65 CSCL 01C

Performance data obtained from static tests in ground effect of a large multi-fan-in-wing V/STOL transport model are described. The data include plots of propulsion systems performance, force and moment characteristics, and induced thermal conditions. Major test variables were height above ground plane, lift/cruise (L/C) nozzle angle, fan louver angle, fan speed, L/C engine power, and operations with L/C nozzles and fans in combination, L/C nozzles alone, and fans alone.

N68-35764*# National Aeronautics and Space Administration. Lewis Research Center, Cleveland, Ohio.

STATIC PERFORMANCE OF AN AUXILIARY INLET EJECTOR NOZZLE FOR SUPERSONIC-CRUISE AIRCRAFT George D. Shrewsbury and John R. Jones Washington Oct. 1968 41 p refs

(NASA-TM-X-1653) CFSTI: HC\$3.00/MF\$0.65 CSCL 21H

A model of an auxiliary inlet ejector nozzle was tested in the Lewis Research Center's static test facility over a range of nozzle pressure ratios of approximately 1.5 to 17. The model diameter was 33 cm. Secondary flows of from 0 to 10 percent of the primary nozzle flow were investigated. Configurations simulating takeoff, transonic acceleration, supersonic acceleration, and supersonic cruise were tested. The takeoff configurations were evaluated with and without noise suppressor chutes.

N68-36507*# National Aeronautics and Space Administration. Lewis Research Center, Cleveland, Ohio.

CENTAUR LAUNCH VEHICLE PROPELLANT UTILIZATION SYSTEM

Steven V. Szabo, Jr., James A. Berns, and Andrew J. Stofan Washington Oct. 1968 35 p refs

(NASA-TN-D-4848) CFSTI: HC\$3.00/MF\$0.65 CSCL 21H

The development history, configuration, and operation of the Centaur propellant utilization system is described. The system used capacitance mass sensors to sense boiling liquid oxygen and liquid hydrogen in the propellant tanks. The system electronics utilized signal levels in the nanoampere range for control. The system operation was verified on nine Atlas-Centaur flights; end propellant residuals were controlled to less than 20 kilograms of liquid hydrogen out of a total tanked propellant weight of 13 600 kilograms. Author N68-36512*# National Aeronautics and Space Administration. Lewis Research Center, Cleveland, Ohio.

PRELIMINARY TESTS OF A SINGLE-AXIS AMMONIA-RESISTOJET ATTITUDE CONTROL SYSTEM

Harold Ferguson, James S. Sovey, and Henry R. Hunczak Washington Oct. 1968 16 p refs

(NASA-TM-X-1677) CFSTI: HC\$3.00/MF\$0.65 CSCL 21H

Performance data are presented for an ammonia-resistojet attitude control system designed for use with stable platform type satellites in the 225- to 450-kg class. The system includes the fast-heatup thrusters (2 mN thrust), propellant storage and feed components, control logic, and power and signal conditioning. The ability of the system to acquire and maintain a soft limit cycle control mode within an attitude accuracy of $\pm 0.2^{\circ}$ was demonstrated. In particular, thruster performance was obtained which indicated that increased preheat time and pulse width cause significant decreases in propellant mass flow rate and thrust and an increase in specific impulse.

N68-36515*# National Aeronautics and Space Administration. Lewis Research Center, Cleveland, Ohio.

EFFECT OF THRUST PER ELEMENT ON COMBUSTION STABILITY CHARACTERISTICS OF HYDROGEN OXYGEN ROCKET ENGINES

Reino J. Salmi, John P. Wanhainen, and Ned P. Hannum Washington Oct. 1968 30 p refs

(NASA-TN-D-4851) CFSTI: HC\$3.00/MF\$0.65 CSCL 21H

The results obtained with a series of 10.78-inch (0.27-m) coaxial INJECTORS ON A -)!))-pound (88 964-N) thrust oxygen-hydrogen rocket engine operated at a chamber pressure of 300 psia (2.064 MN/m^2) were analyzed to determine the effects of injector thrust per element T/E on the combustion stability. The thrust per element ranged from about 20 to 2500 pounds (88.96 to 11 120 N). Based on the minimum hydrogen temperature for stable combustion, the combustion stability increased with increasing thrust per element. No combustion instability was observed at a thrust per element of 200 pounds (88.96 N) or above. Bombing of the 572 and 1000 pound (2542 and 4448 N) T/E injectors failed to induce combustion instability. The hydrogen transition temperatures of the unstable injectors showed agreement with two different correlating parameters.

N68-36617*# Northern Research and Engineering Corp., Cambridge, Mass.

ANALYSIS OF GEOMETRY AND DESIGN POINT PERFORMANCE OF AXIAL FLOW TURBINES. PART 2: COMPUTER PROGRAM

M. Platt and A. F. Carter Washington NASA Oct. 1968 319 \ensuremath{p} refs

(Contract NAS3-9418)

(NASA-CR-1187) CFSTI: HC\$3.00/MF\$0.65 CSCL 21E

The computer program which has been developed to solve the equations governing flow in an axial turbine is examined. A complete description of the program, an indication of its usage, and sample results obtained from the program are included. The computer program follows directly from the analysis and the loss coefficient correlation which were developed previously. The program can be used to analytically investigate the effects of changes in the design variables. The variables include: number of stages, annulus geometry, work distribution, stage work split, radial distribution of stator exit whirl velocity or flow angle, radial variations of the meridional components of streamline slope and curvature. and blade element loss characteristics when values other than the internally computed total pressure loss coefficients are considered necessary for the analysis. The coefficients of the total pressure loss coefficient correlations are also input items and, therefore, can be used as analysis variables. Author

28 PROPULSION SYSTEMS

N68-37264*# National Aeronautics and Space Administration. Lewis Research Center, Cleveland, Ohio.

EFFECT OF VARIABLE STATOR AREA ON PERFORMANCE OF A SINGLE STAGE TURBINE SUITABLE FOR AIR COOLING. 4: STATOR OVERALL PERFORMANCE WITH 70 PERCENT DESIGN AREA

Frank P. Behning, Bernard Bider, and Edward M. Szanca Washington Oct. 1968 18 p refs

(NASA-TM-X-1675) CFSTI: HC\$3.00/MF\$0.65 CSCL 21E

A program is being conducted to study a single stage turbine at stator area settings of 70, 100, and 130 percent of design. This report presents the overall stator performance at the closed setting and compares the results with those obtained from design tests. Results are presented in terms of mass flow, outlet flow angle, and blade surface static pressure and velocity distributions, as well as inner- and outer-wall static pressures as obtained over a range of stator pressure ratios. Author

29

SPACE RADIATION

Includes cosmic radiation; solar flares; solar radiation; and Van Allen radiation belts. For related information see also: 13 Geophysics; and 24 Physics. Atomic, Molecular, and Nuclear.

N68-16008*# National Aeronautics and Space Administration. Lewis Research Center, Cleveland, Ohio.

ર તે સ્ટાર્ગ ઇન્ટેસ્ટ

MCFLARE, A MONTE CARLO CODE TO SIMULATE SOLAR FLARE EVENTS AND ESTIMATE PROBABLE DOSES ENCOUNTERED ON INTERPLANETARY MISSIONS Gerald P. Lahti, Irving M. Karp, and Burt M. Rosenbaum

Washington Feb. 1968 55 p refs

(NASA-TN-D-4311) CFSTI: HC \$3.00/MF \$0.65 CSCL 03B

A computer program MCFLARE that uses Monte Carlo methods to simulate solar flare occurrences during an interplanetary space voyage is described. The total biological dose inside a shielded crew compartment due to the flares encountered during the voyage is determined. The computer program evaluates the doses obtained on a large number of trips having identical trajectories. From these results, a dose Dp having a probability p of not being exceeded during the voyage can be determined as a function of p for any shield material configuration. The user of the code selects any number of solar flares considered to be representative of the ones that will occur during future solar active periods. The flares are assumed to occur randomly during these periods. The dose at a distance of 1 astronomical unit (1.496 $\times10^8$ km) from the Sun from each of these flares behind any shield configuration investigated is input to the MCFLARE code. The code accounts for the dependence of the dose received from a flare on the distance from the Sun according to a $(1/r)^{\alpha}$ variation, where r is the distance from the Sun and the exponent α can be assigned any integral value including zero. To illustrate the use of the code, a trip to Mars and return is calculated, and estimated doses behind several thicknesses of aluminum shield and water shield are presented. A FORTRAN IV listing, data input instructions, and sample output are aiven. Author

N68-16837*# National Aeronautics and Space Administration. Marshall Space Flight Center, Huntsville, Ala.

AN ANALYSIS OF ENERGETIC SPACE RADIATION AND DOSE RATES

M. O. Burrell, J. J. Wright, and J. W. Watts Washington Feb. 1968 63 p refs

(NASA-TN-D-4404) CFSTI: HC\$3.00/MF\$0.65 CSCL 03B

Presented is a compendium of the environmental data on trapped and untrapped radiation. It considers the calculated tissue dose rates received from these radiations and the induced secondary radiation behind various shield thicknesses. Energetic radiation, as used here, refers to particles with energies greater than about 0.5 MeV. The results should be of practical value for preliminary analysis of the radiation hazard to man during space flight. Author

N68-19188*# National Aeronautics and Space Administration. Lewis Research Center, Cleveland, Ohio.

CALCULATIONS OF SOLAR PLASMA INTERACTION WITH MAGNETIC FIELD OF CURRENT LOOP AND TWO PARALLEL INFINITE LINES OF CURRENT

Daniel J. McKinzie, Jr. and Anthony L. Julius, Jr. Washington Mar. 1968 28 p refs

(NASA-TN-D-4304) CFSTI: HC\$3.00/MF\$0.65 CSCL 03B

An investigation was made of the forces resulting from the interaction of the unconfined magnetic field emanating from a space vehicle with the undisturbed solar wind. The integrated theoretical drag per unit area and the acceleration of a circular current loop exposed to the solar wind at zero degree angle of incidence were determined. Also, the integrated theoretical drag and lift per unit area, the restoring moment per unit area per unit length of span were determined for the case of two parallel infinite lines of current at a 45° angle of incidence. For the case of the current loop, the drag per unit area varied over a range of proton number densities from 10^{-6} to 10^{-8} particles per cubic meter and a magnetic field parameter from 10^{-4} to 10^{-2} tesla. An examination of the particle fluxes from a major solar flare showed it to have a negligible effect on the drag when compared with that from the solar wind. Accelerations were calculated for a hypothetical superconducting coil (hollow torus) that had a permanent unconfined magnetic field. For the case of the two parallel infinite lines of current at a 45° angle of incidence, the lift to drag ratio was approximately 1 to 6.8.

N68-21731*# National Aeronautics and Space Administration. Marshall Space Flight Center, Huntsville, Ala.

CALCULATIONS OF NON-DIFFUSE INFRARED RADIATION FROM THE LUNAR SURFACE INCIDENT ONTO A UNIT ELEMENT ABOVE THE SURFACE

James K. Harrison Washington Apr. 1968 38 p refs (NASA-TM-X-1567) CFSTI: HC\$3.00/MF\$0.65 CSCL 03B

This report presents the results of calculations of the thermal radiation from the lunar surface incident onto a flat surface of unit area located a small distance above the moon. The orientation and height of the flat surface vary. The thermal radiation from the moon's surface is assumed to be non-diffuse. The calculations show that the thermal energy flux incident onto the flat surface can differ significantly for a lunar surface that emits radiation in a non-diffuse manner when compared to a lunar surface that emits in a diffuse manner. Author

N68-22849*# Boeing Co., Seattle, Wash. STUDY OF RADIATION HAZARDS TO MAN ON EXTENDED MISSIONS

S. B. Curtis and M. C. Wilkinson Washington NASA May 1968 89 p refs

(Contract NASw-1362)

(NASA-CR-1037) CFSTI: HC \$3.00/MF \$0.65 CSCL 06R

This study attempts to identify the particle types and energies which are important in the evaluation of the radiation hazard on long manned missions outside the magnetosphere. Important areas where information is presently lacking are identified. Spectra of the various components of the galactic cosmic radiation have been compiled from experimental data gathered during the period of minimum solar activity. These spectra, as well as typical solar particle spectra, have been used to determine depth-dose curves and differential particle and dose spectra behind typical shielding thicknesses. From this analysis, the important energies for various thicknesses and various spectra have been determined. In general, low energy particles (below 100 MeV) appear to be the most important at the dose point in solar particle events. From the biological standpoint, very low energy particles are important only for very steep spectra. The high energy heavy component of the galactic cosmic rays is of considerable importance for thin shielding and it appears that low energy heavy particles may continue to be important at thicker shielding, although secondary production data are not available for a thorough analysis. Author

29 SPACE RADIATION

N68-25181*# National Aeronautics and Space Administration. Ames Research Center, Moffett Field, Calif.

EXTERNAL AERODYNAMICS OF THE MAGNETOSPHERE John R. Spreiter, Alberta Y. Alksne, and Audrey L. Summers Washington June 1968 73 p refs Presented at the Summer Inst. for Phys. of the Magnetosphere, Chestnut Hill, Mass., 19–28 Jun. 1967

(NASA-TN-D-4482) CFSTI: HC\$3.00/MF\$0.65 CSCL 04A

A unified basis for the entire discussion is provided by the equations of magnetohydrodynamics, augmented by relations from kinetic theory for certain small scale details of the flow. While the full complexity of magnetohydrodynamics is required for the formulation of the model and the establishment of the proper conditions to apply at the magnetosphere boundary, it is shown that the magnetic field actually experienced in space is usually sufficiently small that an adequate approximation to the solution can be obtained by first solving the simpler equations of gasdynamics for the flow and then using the results to calculate equations of gasdynamics for the flow and then using the results to calculate the deformation of the magnetic field. Numerous specific results are presented, including those for conditions in the solar wind, the shape of the magnetosphere boundary, and the flow and magnetic fields around the magnetosphere. The calculated results are compared with data obtained by numerous spacecraft, including Explorer 12, IMP-1, Pioneers VI and VII, and the Vela satellites. Author

N68-25818*# National Aeronautics and Space Administration. Lewis Research Center, Cleveland, Ohio.

ELECTRICAL CHARACTERISTICS OF A DC COMPACT ARC IN ARGON FROM 1 TO 10 ATMOSPHERES AND FROM 600 TO 1200 AMPERES

Arthur J. Decker and Gary C. Goldman Washington, D. C. Jun. 1968 9 p refs

(NASA-TM-X-1596) CFSTI: HC \$3.00 / MF \$0.65 CSCL 201

Voltages across an arc have been measured in argon in the pressure range of 1 to 10 atmospheres (10^5 to 10^6 N/m²), the current range of 600 to 1200 amperes, and with electrode separation varied from 1 to 2 inches (0.0254 to 0.0508 m). These measurements are summarized in the form of the empirical formula V=12.4(LP)^{2/3} - 1.18 P^{2/3} + 0.0116 I + 11.7 expressing arc voltage V as a function of arc current I in amperes, electrode separation L in inches, and pressure P in atmospheres, or V= 6.67×10^{-2} (LP)^{2/3} - 5.48×10^{-4} P^{2/3} + 0.0116 I + 11.7 where V is in volts, L is in meters, P is in newtons per square meter, and I is in amperes.

N68-25880*# National Aeronautics and Space Administration. Goddard Space Flight Center, Greenbelt, Md.

POLAR CAP ABSORPTIONS AND ASSOCIATED SOLAR TERRESTRIAL EVENTS THROUGHOUT THE 19TH SOLAR CYCLE

Yukio Hakura (NAS) Washington Jun. 1968 28 p refs

(NASA-TN-D-4473) CFSTI: HC\$3.00/MF\$0.65 CSCL 04A

Solar cycle variations in the emission of high-energy particles from the sun are examined, by using daily Polar Cap Absorption (PCA) indices, selected solar-terrestrial events, and satellite observations of low-energy solar protons. A close relationship between PCA's and type IV solar radio outbursts existed throughout the last solar cycle. The solar corpuscular activity showed three peaks in 1957, 1960, and 1963. The first peak is characterized by a random occurrence of type IV outbursts, PCA's and geomagnetic SSC's (geomagnetic storms with sudden commencement). Active centers were restricted in two parts of narrow heliographic longitudes during the second, the most prominent peak, giving a slight 27-day recurrence to the corpuscular activity. Finally, a pronounced peak of 27-day recurrence appeared during the third period. A recurrent series of solar Mev protons lasted 15 solar rotations, while those of geomagnetic Kp index and galactic cosmic ray intensity lasted 25 rotations. Author

N68-26128*# National Aeronautics and Space Administration, Washington, D. C.

PROTECTION AGAINST SPACE RADIATION

Arthur Reetz, Jr., ed. and Keran O'Brien, ed. 1968 627 p refs Proc. of the Spec. Sessions on Protect. against Space Radiation at the 13th Ann. Meeting of the Am. Nucl. Soc., San Diego, Calif., 11–15 Jun. 1967

(NASA-SP-169) CFSTI: HC\$3.00/MF\$0.65 CSCL 18F

Conference papers are presented on the basic interaction and transport of space radiation in materials, methods for space radiation shield penetration calculations, spacecraft shield design, and advanced shielding concepts for spacecraft. For individual titles see N68-26129-N68-26153.

N68-33370*# National Aeronautics and Space Administration. Goddard Space Flight Center, Greenbelt, Md.

EXPERIMENTAL TESTS OF THE SUPERNOVAE ORIGIN OF COSMIC RAYS

C. E. Fichtel and H. B. Ogelman Washington Sep. 1968 21 p refs

(NASA-TN-D-4732) CFSTI: HC\$3.00/MF\$0.65 CSCL 03B

The general problem of supernovae explosions as a possible origin of cosmic rays is reviewed. The shock wave theory of Colgate et al., the only detailed model of supernovae explosions to date, predicts a short, intense high energy gamma-ray pulse associated with the explosion and cosmic ray acceleration. Two experimental tests capable of detecting the predicted initial explosion are suggested. One is a spark-chamber gamma-ray telescope which, when flown above the earth's atmosphere, could detect pulses of protons above 30 mev. The other experiment, which is ground-based, could detect the fluorescence produced in the atmosphere by the electromagnetic pulse radiated by the supernova during its explosion. Author

Includes astronomy and astrophysics; cosmology; lunar and planetary flight and exploration; and theoretical analysis of orbits and trajectories. For related information see also: 11 Facilities, Research and Support; and 31 Space Vehicles.

N68-10164* National Aeronautics and Space Administration. Ames Research Center, Moffett Field, Calif. TABULATED COMMUNICATION CHARACTERISTICS OF A STEADY-STATE MODEL OF INTERPLANETARY SPACE Ronald J. Hruby, Austin H. Somes, John Dimeff, and Howard

(NASA-SP-3042) CFSTI: \$3,00 CSCL 03B

The changes in an electromagnetic wave as it passes through interplanetary and coronal space depend on the intervening plasma and magnetic fields. These changes are presented as a function of the transmission range and the view angle relative to the earth-sun line in the ecliptic plane. This information can be used to determine the total change in an electromagnetic wave between any two points in the earth-sun volume excluding the magnetosphere. Models for the electron density, the magnetic fields, and the solar wind were derived from the best available estimates and experimental data. Tabulated data are derived from a steady-state model of the coronal space corresponding to a simplified quiet sun. The spiral pattern of the magnetic field model is considered to have no disordering effects, and the model of the electron density is a function of solar radial distance only. The interplanetary space is considered to be a neutral plasma with equal densities of electrons and protons. Communication between any two points within the earth's orbit and in the ecliptic plane can be analyzed from the tabulated data. Author

N68-11145*# National Aeronautics and Space Administration. Langley Research Center, Langley Station, Va. THREE BALLISTIC CAMERA DATA REDUCTION METHODS APPLICABLE TO REENTRY EXPERIMENTS

John E. Hogge Washington Nov. 1967 42 p refs

(NASA-TN-D-4260) CFSTI: HC \$3.00/MF \$0.65 CSCL 22C Ballistic cameras were used to photograph a reentry test object against a star background in order to determine accurately the position, velocity, and deceleration of the object as it penetrates the earth's atmosphere. Three data reduction methods which are applicable to the determination of the reentry trajectories from the photographic records are discussed. One reduction method applies when the reentry image on each photographic plate can be approximated with a straight line. Another method applies when the reentry image is curved on each photographic plate. A third technique applies when the shutter of each of several cameras at different stations is synchronized in time.

N68-11369*# National Aeronautics and Space Administration. Goddard Space Flight Center, Greenbelt, Md. INVESTIGATIONS IN HANSEN'S PLANETARY THEORY

Peter Musen Washington Nov. 1967 24 p refs (NASA-TN-D-4169) CFSTI: HC\$3.00/MF\$0.65 CSCL 03C

The geometrical characteristics of Hansen's planetary theory favor the expansion of perturbations in terms of the disturbed mean anomalies of the auxiliary planets. This eliminates the need to expand the disturbing force and speeds up the convergence of series representing Hansen's coordinates. An economy is achieved on the expansions of odd negative power of the mutual distances. There is no need to form the derivatives of the first and higher orders of the disturbing function relative to the pseudo-time. Hansen's theory is more intimately connected with perturbations in the rectangular coordinates than with perturbations of the elements. For this reason, direct use is made of the differential equations of motion in rectangular coordinates relative to an inertial frame of reference. Hansen had to introduce the perturbations of the third coordinate by combining the direct kinematical considerations with the method of variation of constants. Hansen's W-function is not used because of the way the operations with periodic series are performed on electronic machines. However, the W-function is retained because it is intimately connected with determining perturbations in the mean anomaly and with forming the integrating operators. R.N.A.

N68-11456*# National Aeronautics and Space Administration, Washington, D. C.

INTERSTELLAR GRAINS

J. Mayo Greenberg, ed. and T. P. Roark, ed. 1967 275 p refs Presented at Rensselaer Polytech. Inst., Troy, N. Y., 24-26 Aug. 1965

(NASA-SP-140) GPO: \$1.25 CSCL 03B

Conference papers on observational and theoretical interpretations of interstellar grains are presented. The principal issues are identified as being the following: uniformity of the ratio of total to selective extinction; dielectric grains versus graphite or graphite core plus dielectric mantle grains; variations of the reddening law and of the wavelength dependence of polarization and their respective relations with localized phenomena and the problems of galactic structure; formation of interstellar molecules, mainly OH and H₂; diffuse interstellar lines; and the physics and chemistry of grain nucleation and growth. Discussions following the papers are also included. N.E.N.

N68-11630*# National Aeronautics and Space Administration. Manned Spacecraft Center, Houston, Tex..

AN EVALUATION OF THE THERMALLY RADIANT ENVIRONS OF A MAN ON THE LUNAR SURFACE

David H. Pereland Alan J. Chapman Washington Nov. 1967 72 p refs (NASA-TN-D-4243) CFSTI: HC\$3.00/MF\$0.65 CSCL 03B

Analytical methods were developed for determining the quantities of radiative thermal energy to provide a quantitative evaluation of the effects of the lunar thermal environment on a pressure-suited man. Evaluations were limited to lunar plains. A multicylinder man and a hemisphere-cylinder man were considered in the analysis. While emphasis was placed on the evaluation of

quantities of thermal radiation from the lighted side of the moon, the radiation on the dark portion was also considered and illustrated. The results of the investigation are presented in parametric form to allow the solution of specific problems over a wide range of variables. Author

N68-11754*# National Aeronautics and Space Administration, Manned Spacecraft Center, Houston, Tex.

A GENERAL ANALYTICAL METHOD FOR ARTIFICIAL-SATELLITE LIFETIME DETERMINATION

Frank Garcia, Jr. Dec. 1967 27 p refs

(NASA-TN-D-4281) CFSTI: HC\$3.00/MF\$0.65 CSCL 22A

An expression for obtaining the lifetimes of artificial satellites in circular orbits is developed. A complete derivation of the method is presented to allow the user to evaluate its assumptions according to specific needs. The accuracy of the developed method is verified using Earth and Mars as examples and comparing the results to the results obtained from numerically integrated and approximate analytical trajectories. Characteristic altitude histories are presented for the trajectory methods and the described analytical solution. Expressions for computing lifetimes of elliptical orbits are also included, with the necessary graphical presentations to provide rapid solution of these expressions. Author

N68-14089*# North American Aviation, Inc., Downey, Calif. GUIDANCE, FLIGHT MECHANICS AND TRAJECTORY OPTIMIZATION. VOLUME 3: THE TWO-BODY PROBLEM

G. E. Townsend and M. B. Tamburro Washington NASA Jan. 1968 87 p refs

(Contract NAS8-11495)

(NASA-CR-1002; SID-65-1200-3) CFSTI: HC \$3.00/MF \$0.65 CSCL 22C

The approximate analysis of the motion of near-earth satellites, and/or the generation of precise trajectories via derivatives of an Encke formulation or via an osculating conic formulation, is the fundamental objective of this monograph. This objective will be achieved by developing the classical solution and modifying its form to assure that a completely deterministic solution is available. The two-body problem was one of the earliest problems in dynamics to be solved. Thus, the material to be presented does not represent the current status of a rapidly changing field on analysis as do some of the presentations in other monographs. Rather, the material is intended to express the results of these previous analyses, to express the observations regarding indeterminacies in the most commonly used form of the solution, and to provide alternate formulations of the motion to avoid the computational problems. In addition, this presentation is intended to function as a reference volume providing detailed tabulations of equations relating the most basic parameters of the motion and the dynamics. Author

N68-14941*# National Aeronautics and Space Administration. Manned Spacecraft Center, Houston, Tex.

GEMINI SUMMARY CONFERENCE

Washington 1967 335 p refs Conf. held at NASA. Manned Spacecraft Center, 1–2 Feb. 1967

(NASA-SP-138) CFSTI: HC\$3.00/MF\$0.65 CSCL 22B

Gemini program highlights are presented, and flight results are discussed in terms of space orbital maneuvering, extravehicular activities, operational experiences, and onboard experiments. For individual titles, see N68-14942 through N68-14962.

N68-15193*# North American Aviation, Inc., Downey, Calif. GUIDANCE, FLIGHT MECHANICS AND TRAJECTORY OPTIMIZATION. VOLUME 4: THE CALCULUS OF VARIATIONS AND MODERN APPLICATIONS M. Mangad and M. D. Schwartz Washington NASA Jan. 1968 117 p refs

(Contract NAS8-11495)

(NASA-CR-1003; SID-65-1200-4) CFSTI: HC \$3.00/MF \$0.65 CSCL 22C

The discussions presented progress from the fundamental lemma to the Euler-Lagrange equations, to the transversality condition, to the incorporation of constraint equations, to other necessary conditions for extrema, to the problems of Bolza, Mayer and Lagrange, and finally to the bounded and unbounded control problems. In addition to providing the basis for formulating this class of problems, the monograph is intended to serve as a necessary introduction to subsequent discussions of the optimization problem. Author

N68-15484*# National Aeronautics and Space Administration. Lewis Research Center, Cleveland, Ohio.

SIMULTANEOUS CORRECTION OF VELOCITY AND MASS BIAS IN PHOTOGRAPHY OF METEORS

C. D. Miller Washington Feb. 1968 74 p refs

(NASA-TR-R-280) CFSTI: HC\$3.00/MF\$0.65 CSCL 03A

An analysis was made to investigate the magnitude of the weighting factor, specifically for application to photographic meteor data. As a result, a revised factor was obtained to operate upon actual counts of photographic meteors within various classes of velocity to provide a correct ratio of counts for all velocities reduced to any given lower mass limit. An expression was derived theoretically for maximum effective exposure on the photographic plate produced by a meteor in terms of the original mass of the particle, its velocity relative to earth's atmosphere, and the angle of its path to the zenith. The expression for maximum effective exposure was tested and revised by application to 100 test meteors that were believed to have provided approximately uniform effective exposure density. The revised expression for maximum effective exposure was combined with a widely accepted equation for the influx rate of meteors of mass greater than a stated value to obtain approximately the desired weighting factor. The analysis indicated a large change in value of the exponent of velocity relative to earth's atmosphere in the weighting factor, namely, from -2 downward at least to -3.85 and possibly as low as -4.22. Author

N68-15683*# Planning Research Corp., Washington, D. C. INTRODUCTION TO THE DERIVATION OF MISSION REQUIREMENTS PROFILES FOR SYSTEM ELEMENTS NASA 1967 91 p refs

(Contract NASw-1032)

(NASA-SP-6503) CFSTI: HC\$3.00/MF\$0.65 CSCL22A

The present report describes a methodology for deriving the mission requirements profiles of the subsystem and lower level hardware elements from the system profile. This methodology consists of: (1) identification of the parameters that relate the functions and operations of the lower elements to each specific function and operation of the overall system; (2) arrangement of the parameters in the order of their importance to that function and operation of the system (so that they can each be treated in accordance with the appropriate priority and allocation of resources); (3) resolution, through the selection and application of the most appropriate analytical or empirical techniques, of the influences of each parameter from the system level to the level of the element under consideration; (4) compilation of the parameters and their influences derived in this manner into the mission requirements profile for the element in question. The appendices to this document are devoted to the presentation of supplementary data regarding parameters and analytical techniques necessary for the implementation of the methology. Author

N68-15725*# Boeing Co., Seattle, Wash. LUNAR ORBITER 3: PHOTOGRAPHY Washington NASA Feb. 1968 128 p (Contract NAS1-3800) (NASA-CR-984; D2-100753-2, V. 2) CFSTI: HC \$3.00/MF \$0.65

INASA-CH-984; D2-100753-2, V. 2) CFS11: HC \$3.00/MF \$0.65 CSCL 22A

A description of Mission III planning, its conduct with respect to photography, and an analysis of the photographic results are presented. Data pertinent to analysis and interpretation of the photographs are included. The telephoto coverage provided resolution equivalent to 1 meter from a nominal altitude of 46 kilometers. In addition to normal near-vertical photography, photographs were obtained with convergent telephoto stereo coverage. Oblique-angle photography was employed to enhance interpretation of topographic features, to provide photographs of areas beyond the field of view of a vertical camera orientation, and to investigate photometric characteristics of the lunar surface. Operation of the cameras was satisfactory and high-quality photographs were obtained. By combining priority and final readouts, 82.8% of the planned primary-site, wide-angle coverage and 70.3% of the telephoto coverage was obtained. Author

N68-15741*# North American Aviation, Inc., Downey, Calif. GUIDANCE, FLIGHT MECHANICS AND TRAJECTORY OPTIMIZATION. VOLUME 6: THE N-BODY PROBLEM AND SPECIAL PERTURBATION TECHNIQUES

M. S. Allione, A. L. Blackford, J. C. Mendez, and M. M. Whittouck Washington NASA Feb. 1968 122 $\,p\,$ refs

(Contract NAS8-11495)

(NASA-CR-1005; SID-65-1200-6) CFSTI: HC \$3.00/MF \$0.65 CSCL 22C

The analytical formulations and the numerical integration methods available for the solution of the n-body problem are discussed. For large pertubative accelerations which are changing rapidly, the Cowell method of mathematical formulation is preferred. For phases of the flight where the force field is nearly conservative and/or nearly central with respect to the body, either Encke's method or the variation of parameters is recommended. Multistep predictor-corrector methods are considered to be significantly more efficient than other numerical integration techniques. The Gauss-Jackson method is suggested for general application, with the Adams-Moulton predictor-corrector method as a close alternate. The Lanczos and Nordsieck methods are classified as new and promising. The single-step Runge-Kutta method is considered desirable in some cases due to its stability. The Runge-Kutta method is also recommended as a starter for the multi-step methods. N.E.N.

N68-15748*# National Aeronautics and Space Administration. Washington, D. C.

SIGNIFICANT ACHIEVEMENTS IN SPACE SCIENCE 1966 1967 224 p refs

(NASA-SP-155) GPO: \$1.50 CSCL 03A

Scientific and technological advances are reported for the areas of space astronomy and bioscience, ionospheres and radio physics, particles and fields, planetary atmospheres and planetology, and solar physics. Considered to be among the year's highlights are the soft landing of Surveyor I and the photographs obtained by Lunar Orbiters I and II. Special mention is made of Explorer XXXIII's extended flight, the upper atmospheric data obtained by Explorer XXXII, and the interplanetary measurements taken by Pioneer VII in heliocentric orbit.

N68-15793*# National Aeronautics and Space Administration, Manned Spacecraft Center, Houston, Tex.

A COMPUTER PROGRAM FOR CALCULATING MODEL PLANETARY ATMOSPHERES David E. Pitts Washington Feb. 1968 63 p refs (NASA-TN-D-4292) CFSTI: HC \$3.00/MF \$0.65 CSCL 03B

The computer program presented here enables calculations to be made of a model atmosphere of a planet to one planetary radius above the surface. The variables calculated are altitude, temperature, pressure, density, specific weight, molecular weight, pressure scale height, density scale height, number density, mean particle velocity, mean free path, collision frequency, speed of sound, coefficient of viscosity, kinematic viscosity, and columnar mass. The calculations are usually made for atmospheres consisting of nitrogen, carbon dioxide, oxygen, argon, neon, hydrogen, helium, water vapor, carbon monoxide, and sufur dioxide. However, if the printouts of mean free path, collision frequency, coefficient of viscosity, and kinematic viscosity are ignored, calculations may be made for gases of any desired molecular weight.

N68-15891*# National Aeronautics and Space Administration. Manned Spacecraft Center, Houston, Tex.

SUMMARY OF GEMINI EXTRAVEHICULAR ACTIVITY Reginald M. Machell, ed. Washington 1967 336 p refs

(NASA-SP-149) CFSTI: HC\$3.00/MF\$0.65 CSCL 22A

The actual systems employed, the testing and qualifications of these systems, the preparation of the flight crews, and the operational and medical aspects were described from a developmental viewpoint. During the Gemini program, the basic feasibility of extravehicular activity was established. Other significant results were: (a) demonstration of retrieval of equipment from within the spacecraft adapter and from another satellite, (b) establishment of requirements for handholds, foot restraints, and body restraints, (c) evaluation of the dynamics of motion on a short tether, (d) preliminary evaluation of a hand held maneuvering device, (e) demonstration that the extravehicular workload could be maintained within the limits of the life support system and the capabilities of the pilot, and (f) demonstration that underwater zero-g simulation was valid in solving body restraint problems and in assessing workloads. The most significant limitations were the inability to perform extravehicular tasks without the proper body restraints, the mobility restrictions imposed by the design of the space suit, and the limited cooling capacity of life support systems using gaseous cooling. Recommendations are made for development of future extravehicular operations. Author

N68-16103*# North American Aviation, Inc., Downey, Calif. GUIDANCE, FLIGHT MECHANICS AND TRAJECTORY OPTIMIZATION. VOLUME 1: COORDINATE SYSTEMS AND TIME MEASURE

M. B. Tamburro, A. S. Abbott, and G. E. Townsend Washington NASA Feb. 1968 115 p refs

(Contract NAS8-11495)

(NASA-CR-1000; SID-65-1200-1) CFSTI: HC \$3.00/MF \$0.65 CSCL 22C

A complete description of a coordinate measuring system to determine particle position and velocity is given. Emphasis is placed on the coordinate frameworks utilized for trajectory problems and body oriented axis systems. Developed is a mathematical model that derives the equations of motion from the fundamental reference system of the moon orbit around the earth and finds solutions to yield the nutation and precession corrections to the basic reference frame. Finally, discussed are time standards employed in astronomical studies for the purpose of relating the rotating coordinate systems to measurements of celestial spheres. G.G.

N68-16750*# National Aeronautics and Space Administration. Langley Research Center, Langley Station, Va.

PHOTOMETRY OF AN IRON ARTIFICIAL METEOR REENTERING AT 11 KILOMETERS PER SECOND

J. B. Robertson and Wendell G. Ayers Washington Feb. 1968 27 p refs

(NASA-TN-D-4312) CFSTI: HC\$3.00/MF\$0.65 CSCL 22A

A man-made meteor was successfully produced in March of 1966 by reentering into the atmosphere a 5.7-gram steel pellet at 10.85 km/sec with a six-stage, solid-fuel Trailblazer II vehicle, the last stage of which was an explosive accelerator. The meteor was photographed with a system of cameras and spectrographs. The luminous power of the meteor as a function of time was determined from the photographs with stars for calibration. The velocity and deceleration of the meteor were determined from photographs taken by cameras with chopping shutters. The luminous efficiency of the meteor was calculated from the luminous power and velocity data. The panchromatic luminous efficiency was $(4.0\pm0.8)\times10^{-3}$ and the blue sensitive luminous efficiency was $(4.0\pm0.8) \times 10^{-3}$ and the blue sensitive luminous efficiency was $(2.1\pm0.4) \times 10^{-3}$. A spectrogram of the meteor on blue sensitive film showed that the radiation produced by the meteor in the spectral region from 3800 Å to 5000 Å was predominately line radiation from neutral iron. A filter photograph indicated considerable radiation in the spectral region from 4900 Å to 6500 Å. A large portion of this radiation may have been produced by iron oxide. Author

N68-17215*# North American Aviation, Inc., Downey, Calif. Space and Information Systems Div.

GUIDANCE, FLIGHT MECHANICS AND TRAJECTORY OPTIMIZATION. VOLUME 2: GUIDANCE EQUATIONS FOR ORBITAL OPERATIONS

G. E. Townsend, D. R. Grier, and A. L. Blackford Washington NASA Feb. 1968 121 $\,p$ refs

(Contract NAS8-11495)

(NASA-CR-1010; SID-66-1678-3; V. 11) CFSTI: HC \$3.00/MF \$0.65 CSCL 22C

This monograph develops the mathematical formulations of the maneuver in orbit problem and presents solutions for analyzing space missions and the associated guidance process. This is accomplished by isolating those factors which affect the motion of a vehicle and by defining the optimum sequence of events required to produce the desired motion. The maneuvers are considered in two general classes. The first class, referred to as gross maneuvers, contains all of those corrective strategies in which the individual corrections are of such mangitude as to require that the nonlinear equations describing the maneuver be solved explicitly to obtain the required accuracy. The second class of maneuvers contains all of the corrective strategies which are sufficiently small to allow the nonlinear equations describing them to be expanded in a first order series in the neighborhood of a pre-selected nominal trajectory without adversely affecting the accuracy of the analysis. This class of maneuvers, referred to as differential corrections or midcourse corrections, is treated by progressing from a simplified guidance process to optimal control as measured by several loss functions. Examples of application are also given. кw

N68-19064*# National Aeronautics and Space Administration. Ames Research Center, Moffett Field, Calif.

LUNAR BEACONS: A PRELIMINARY LOOK AT THEIR POSITION ESTIMATION AND THEIR USE IN LUNAR ORBIT ESTIMATION

Thomas M. Carson Washington Mar. 1968 20 p refs (NASA-TM-X-1529) CSCL 22A

In the estimation of a lunar orbit, various data sources could be used. This report considers the use of on-board range and range-rate measurements of lunar beacons as an addition to the normal use of range-rate measurements from earth-based stations. The analysis considers both the improvement of the orbit estimation and the estimation of the location of the location of the orbit estimation and the estimation of the location of the Schmidt-Kalman filtering process was used for the estimation. Random errors in the measurements and bias errors in the station and beacon locations were considered. Results show that the addition of on-board measurements of lunar beacons to earth-based range-rate measurements contributes significantly in the estimation of the orbit and in the knowledge of the beacon locations. Author

N68-19186*# North American Aviation, Inc., Downey, Calif. GUIDANCE, FLIGHT MECHANICS AND TRAJECTORY OPTIMIZATION. VOLUME 12: RELATIVE MOTION, GUIDANCE EQUATIONS FOR TERMINAL RENDEZVOUS

D. F. Bender and A. L. Blackford Washington NASA Apr. 1968 97 p refs

(Contract NAS8-11495)

(NASA-CR-1011; SID-66-1678-4) CFSTI: HC \$3.00/MF \$0.65 CSCL 22C

This monograph is intended to present a discussion of the principles and techniques of accomplishing a rendezvous between two spacecraft. In the context here, rendezvous is considered as the interface between the midcourse corrections of an orbital transfer maneuver which establishes the two spacecraft on nearly identical orbits and the docking maneuver which results in the physical contact of the two spacecraft. First consideration in the discussion is given to the development of the equations of relative motion of the two vehicles. To facilitate the use in guidance scheme, these equations are developed in various coordinate systems, with several choices for the independent variables, and with several simplifying assumptions. Next, guidance schemes are developed based on these equations of motion. As each guidance scheme is presented, its existance is in some way justified and the relative advantages and disadvantages as compared to the other schemes discussed. With this discussion enough information is available so that the elements of a rendezvous guidance scheme can be constructed for a particular set of conditions in which a rendezvous Author maneuver is required.

N68-19192*# St. Louis Univ., Mo. SUBSOLAR-MERIDIAN MEAN ANNUAL DISTRIBUTIONS FOR MARTIAN TROPOSPHERE BELOW 50 KILOMETERS F. C. Bates Washington NASA Mar. 1968 51 p refs (Grant NGR-26-006-016)

(NASA-CR-1043) CFSTI: HC\$3.00/MF\$0.65 CSCL038

Available observations of the Martian atmosphere were employed to estimate the composition of the homogeneous atmosphere and equivalent-mean-sea-level pressure. A mean-annual subsolar-meridian distribution of temperature, pressure and zonal-wind speed was then constructed for a depth of 50 km based on the foregoing estimates and: (1) a wave regime; (2) hydrostatic balance; (3) midlatitude scale height consistent with Mariner IV observation; (4) tropopause height varying from 30 km at the equator to 10 km at the pole; (5) mean jet-stream position at 45° latitude and 20 km; and (6) estimates from similarity to Earth and other rotating-fluid systems. These results were then extended to an estimate of wind and wind regimes, including secondary circulations such as extra-tropical cyclones and yellow-dust devils. Computations of heating rates in a ten-layer model were used to test soundings at several latitudes to determine required dynamic and/or advective compensation. Author

N68-19315*# North American Aviation, Inc., Downey, Calif. GUIDANCE, FLIGHT MECHANICS AND TRAJECTORY OPTIMIZATION. VOLUME 13: NUMERICAL OPTIMIZATION METHODS

J. E. McIntyre Washington NASA Mar. 1968 109 p refs

(Contract NAS8-11495)

(NASA-CR-1012; SID-66-1678-5) CFSTI: HC \$3.00/MF \$0.65 CSCL 22C

A monograph is presented on the second step in the optimization process, which generates numerical solutions. The three

fundamental numerical procedures—neighboring external, steepestdescent and quasilinearization—are presented, and their application to both classical and nonclassical problems are shown. Two numerical methods for locating the minimum value of a function space leads to the three fundamental techniques for locating the minimum value of a functional. The step by step calculation procedure used in each of these techniques is given for the classical Mayer problem and nonclassical versions of the Mayer problem arising in modern trajectory and control applications. The relative merits of each technique are discussed, and it is shown that the iterative numerical procedures used for solving nonlinear optimization problems consist in approximating the problem by a succession of linear problems. B.S.D.

N68-19330*# National Aeronautics and Space Administration. Ames Research Center, Moffett Field, Calif.

A FORTRAN PROGRAM FOR COMPUTATION OF MASS IN EARTH ORBIT REQUIRED FOR INTERPLANETARY MISSIONS

Samuel W. Pitts and Alfred C. Mascy Washington Apr. 1968 29 p ref

(NASA-TM-X-1541) CFSTI: HC\$3.00/MF\$0.65 CSCL 22A

A necessary parameter to be investigated in the analysis of space missions is the total assembled mass in Earth orbit, as it is a strong indicator in comparisons of the performance of various propulsion systems. The computer code described in this paper was designed to compute the mass in Earth orbit for round-trip stopover missions. flyby missions, and orbiter missions with a single-stage high-thrust system for each propulsive phase. The actual gravity losses suffered during each propulsive phase are computed by complete integration of the equations of motion, thereby permitting the propulsion system to be optimized. The program allows the input of planet ephemeris data so that it may be used for any planet.

N68-19590*# Wisconsin Univ., Madison. ULTRAVIOLET DAYGLOW AND STELLAR BRIGHTNESS MEASUREMENT FROM THE X-15 AIRCRAFT

Lowell R. Doherty Washington NASA Mar. 1968 22 p refs (Grant NsG-618)

(NASA-CR-1017) CFSTI: HC \$3.00/MF \$0.65 CSCL 03A

The design and operation of a two channel photometer used to obtain sky brightness data are described. These data were used in preparation for an airborne astronomical photography program using the X-15 aircraft. Four Nikon 35 mm camera bodies with motor driven film transport mechanisms were used for ultraviolet stellar photography. The optics consisted of a lens system in a barrel mount and a field flattener located immediately above the focal-plane shutter. A focal length of 108 mm was used. An interference filter was mounted in front of the lens as a limiting aperture, producing an f/5 system. A gyroscopic platform designed to provide a constant pointing direction within an rms fluctuation of one minute of arc supported the four cameras in a hatch behind the pilot's compartment. Four stars were identified on ultraviolet films taken on two flights, and daytime stellar brightness was calculated for these. F.J.S.

N68-19622*# National Aeronautics and Space Administration. Langley Research Center, Langley Station, Va.

LINE-OF-SIGHT VELOCITY AS AN INDICATOR OF PERICYNTHION ALTITUDE OF SELENOCENTRIC ORBITS James Lloyd Williams Washington Mar. 1968 18 p refs (NASA-TM-X-1508) CFSTI: HC\$3.00/MF\$0.65 CSCL 22C

An investigation was made to determine the feasibility of using simplified equations to predict the pericynthion of a selenocentric orbit. It was assumed that the angular rate of the line of sight with respect to a prominent lunar surface feature was available for positions along a ballistic trajectory. The equations used were derived in terms of this variable by utilizing the linearized rendezvous equations and certain parameters of a circular selenocentric orbit. The procedure used in the evaluation of these equations was to calculate the pericynthion of selected reference Hohmann trajectories and to compare the values calculated by these equations with the known reference orbit values. The results of the computations indicate that the pericynthion altitude predicted by the approximate equations generally is not accurate, and that the predicted pericynthion altitude is very sensitive to the reference orbit altitude, to the times at which measurements of the rotation of the line of sight are made, and to the length of time between the measurements of the angular rate of line of sight. Author

N68-19676*# North American Aviation, Inc., Downey, Calif. GUIDANCE, FLIGHT MECHANICS AND TRAJECTORY OPTIMIZATION. VOLUME 2: OBSERVATION THEORY AND SENSORS

B. J. Miller and A. S.*Abbott Washington NASA Mar. 1968 181 p refs

(Contract NAS8-11495)

(NASA-CR-1001; SID-65-1200-2. V. 2) CFSTI: HC \$3.00/MF \$0.65 CSCL 22C

Reported is a monograph which is designed to illustrate analytical methods used in the fields of guidance, flight mechanics, and trajectory optimization. Primary objectives are to present a comprehensive technical discussion of observation theory and sensors applicable to the navigation of boost and space vehicles. Discussed are the following: radiation theory and sensors; radiation sensing techniques; inertial theory and sensors; observation (state vector relationships); observation errors: state determination from evenly determined data; sensor requirements imposed upon a vehicle; and criteria for selecting observables to be measured. S.C.W.

N68-19985*# North American Aviation, Inc., Downey, Calif. GUIDANCE, FLIGHT MECHANICS AND TRAJECTORY OPTIMIZATION. VOLUME 14: ENTRY GUIDANCE EQUATIONS

M. B. Tamburro and E. F. Knotts Washington NASA Apr. 1968 149 p refs

(Contract NAS8-11495)

(NASA-CR-1013; SID-66-1678-6, V. 14) CFSTI: HC \$3.00/MF \$0.65 CSCL 22C

Theories proposed for entry guidance are summarized, and the ways in which they may be applied for a given vehicle mission combination are described. The basic entry performance interactions that must be considered when formulating a guidance system are examined, and a method of discerning between unacceptable and acceptable trajectories is introduced. Mathematical theories of entry guidance are derived in terms of paths for which closed-form solutions can be obtained, in terms of paths which are defined by a fast-time integration method, or in terms of controlling the vehicle in the neighborhood of a nominal trajectory known to exhibit desirable trajectory characteristics. The techniques used in the Gemini and Apollo entry guidance are reviewed. The point mass equations of motions are written in terms of vectors resolved in two noninertial coordinate systems, and approximate integrals of motion for various flight modes are formulated. Atmospheric models for entry performance and guidance studies are discussed. Supericircular and subcircular entry velocities are considered, and the factors involved in finalizing a guidance system are assessed. M.G.J.

N68-20084*# North American Aviation, Inc., Downey, Calif. GUIDANCE, FLIGHT MECHANICS AND TRAJECTORY OPTIMIZATION. VOLUME 7: THE PONTRYAGIN MAXIMUM PRINCIPLE J. E. McIntyre Washington NASA Apr. 1968 129 p refs (Contract NAS8-11495) (NASA-CR-1006; SID-65-1200-7, V. 7) CFSTI: HC \$3.00/MF

\$0.65 CSCL 22C

Pertinent concepts from the maxima-minima theory are reviewed, and some of the concepts used in the calculus of variations are examined. The similarity between the Pontryagin maximum principle and the calculus of variations is discussed, and it is pointed out that both lead to the same set of governing equations which the extremizing solution must satisfy. However, the maximum principle is considered to be a clearer and more concise statement of how the optimization is to be conducted, particularly when certain types of inequality constraints are present. The maximum principle is used to formulate and solve a variety of problems encountered in optimal trajectory and control analysis. The treatment includes both linear and nonlinear systems, and problems with control inequalities and state inequalities. Several comparisons and parallels are drawn with both the calculus of variations and the maxima-minima theory of the differential calculus. Special problems and applications warrenting additional investigation are cited, such as the singular arc problem and the optimization of stochastic systems. M.G.J.

N68-20192*# National Aeronautics and Space Administration. Langley Research Center, Langley Station, Va.

RELATIVISTIC MODELS OF THE UNIVERSE WITH PRESSURE EQUAL TO ZERO AND TIME-DEPENDENT UNIFORMITY

Windsor L. Sherman and Sylvia A. Wallace Washington Apr. 1968 42 p refs

(NASA-TR-R-282) CFSTI: HC\$3.00/MF\$0.65 CSCL03B

Previous work on the zero-density and approximate models of the universe is summarized. The zero-density model is improved so that it is a useful approximation of the exact model to greater values of the red shift, and regions of applicability of the approximate model are determined. Regions where closed-form solutions of the exact model exist, other than zero-density and zero-cosmical-constant models, are defined and the solutions are given. The results of calculations are presented that indicate, for the data considered, all the models, simplified and exact, appear to fit the data equally well even though there is wide variation in the density and acceleration parameters. In addition, the results of the calculations indicate that density and acceleration parameters should be determined as a pair from observational data. It is concluded that data consistent with that for galaxies at red shifts greater than one-half are required before a model universe can be selected and a simplified model defined. Author

N68-20353*# Johns Hopkins Univ., Baltimore, Md. INFRARED OBSERVATIONS OF THE OUTER SOLAR CORONA

Robert M. MacQueen Washington NASA Apr. 1968 54 p refs

(Grant NGR-21-001-044)

(NASA-CR-969) CFSTI: HC\$3.00/MF\$0.65 CSCL 03B

The 2.2 μ wavelength infrared outer solar corona was observed in two experiments: first, employing a ground-based telescope from a high altitude site near Pulacayo, Bolivia, during the 93 second totality of the eclipse of 12 November 1966; and second, employing a stratospheric balloon package with an infrared coronagraph, flown to an altitude of 28 km, during a 5.25 hour period, on 9 January 1967. The design and evaluation of the infrared balloon-borne coronagraph is discussed in detail, and the various origins of stray light investigated. The completed flight coronagraph was found to introduce a stray radiance of less than $3 \times 10^{-12} B_{\odot}$ where B_{\odot} is the radiance of the mean solar disk at wavelength 2.2 μ . During eclipse the corona was observed from $2R_{\odot}$ to $6R_{\odot}$ in the ecliptic plane, and at a single point perpendicular to the ecliptic at $5R_{\odot}$. Balloon observations covered the range 3.7 R_{\odot} to 10 R_{\odot} at position angles from 20° north to 40° south of the ecliptic, on the east limb of the sun. Author

N68-20356*# National Aeronautics and Space Administration. Goddard Space Flight Center, Greenbelt, Md.

A FAST METHOD OF ORBIT COMPUTATION

Karl Stumpff and E. H. Weiss (IBM, Greenbelt, Md.) Washington Apr. 1968 41 p refs

(NASA-TN-D-4470) CFSTI: HC\$3.00/MF\$0.65 CSCL 22C

The problem of rapidly computing trajectories of spacecrafts from their initial conditions has become very important. Classical methods rely almost exclusively on precise integration techniques, but results thus obtained are too slow over extended arcs, even on high-speed computers. Moreover, great accuracy is often unnecessary. Here we present a new method of computing approximate ephemerides of a small body (minor planet or artificial satellite). This method is 10 to 15 times faster than the well-known methods of Encke or Cowell. The errors are small (e.g., of the order of one part in a thousand) and the results converge to the N-body point-mass solution for small time steps. It is also possible to account for non-point-mass effects; this, however, has not yet been implemented.

N68-20368*# National Aeronautics and Space Administration. Lewis Research Center, Cleveland, Ohio.

ANALYTICAL CALCULATION OF PARTIAL DERIVATIVES RELATING LUNAR AND PLANETARY MIDCOURSE CORRECTION REQUIREMENTS TO GUIDANCE SYSTEM INJECTION ERRORS

Fred Teren and Gary L. Cole Washington Apr. 1968 39 p refs (NASA-TN-D-4518) CFSTI: HC\$3.00/MF\$0.65 CSCL 22C

This report describes a simplified analytical method for calculating partial derivatives relating midcourse correction velocity requirements to injection errors resulting from guidance system errors for lunar and planetary missions. The analytical method uses two-body equations of motion to describe the reference transfer orbit. These equations are linearized to obtain partial derivatives relating changes in terminal state conditions to changes at injection and midcourse. The partial derivatives are then used to calculate the required correction velocity. The analytical equations are easily programmed on a digital computer and require very little computer time. The only input variables required are the position and velocity components at injection from a reference trajectory. The analytical partial derivatives are compared to exact partial derivatives obtained from a detailed N Body computer simulation. A comparison of results is presented for two lunar and five planetary missions. The error in the approximate results is found to be less than 14 percent for all cases simulated. Author

N68-20449*# North American Aviation, Inc., Downey, Calif. GUIDANCE, FLIGHT MECHANICS AND TRAJECTORY OPTIMIZATION. VOLUME 8: BOOST GUIDANCE EQUATIONS

G. E. Townsend, A. S. Abbott, and R. R. Palmer Washington NASA Apr. 1968 134 p refs

(Contract NAS8-11495)

(NASA-CR-1007; SID-65-1200-8) CFSTI: HC \$3.00/MF \$0.65 CSCL 22C

Near optimum steering equations were developed for boost vehicles, with the constraint that solutions must be possible in less than real time on the small digital computer used in the guidance system of boost vehicles. Approaches discussed are path adaptive or iterative guidance, explicit guidance employing guidance polynomials, and perturbation guidance. The iterative and perturbation guidance approaches have been or are currently being applied to boost vehicles, and detailed equations are presented in both cases. Because of numerical problems implicit in the preflight simulation and construction of the coefficients of the polynomial, the third approach is not being considered for application. M.W.R.

N68-20450*# North American Aviation, Inc., Downey, Calif. GUIDANCE, FLIGHT MECHANICS AND TRAJECTORY OPTIMIZATION. VOLUME 9: GENERAL PERTURBATIONS THEORY

B. Kampos Washington NASA Apr. 1968 205 p refs (Contract NAS8-11495)

(NASA-CR-1008; SID-66-1678-1) CFSTI: HC \$3.00/MF \$0.65 CSCL 22C

Solutions obtained by general perturbations techniques were studied for applications to mission analysis and inflight phases of space programs. Data on oblateness, atmospheric drag, extraterrestrial gravitation, and solar radiation pressure perturbations are reviewed; and detailed analyses are presented for some of these. Dominant perturbations for most earth satellites are discussed in terms of the earth's oblateness; and development of the atmospheric perturbation and satellite motion is considered. A scheme for approximating the net result of all these perturbating influences is presented, along with a mechanization to effect the solution that is based on the optimum formulations of each phase of the analysis. M.W.R.

N68-20468*# North American Aviation, Inc., Downey, Calif. GUIDANCE, FLIGHT MECHANICS AND TRAJECTORY OPTIMIZATION. VOLUME 16: MISSION CONSTRAINTS AND TRAJECTORY INTERFACES

R. L. Robertson Washington NASA Apr. 1968 128 p refs (Contract NAS8-11495)

(NASA-CR-1015; SID-66-1678-8, V. 16) CFSTI: HC \$3.00/MF \$0.65 CSCL 22C

Launch, rendezvous, spatial, deorbit, and entry trajectory phases are considered for earth orbital missions in order to formulate the more important constraints required for a realistic mission. Details are considered for the launch window, range safety, and ascent trajectories during boost and for direct ascent, rendezvous compatible orbits, intermediate orbit rendezvous techniques, and terminal maneuver during rendezvous. Perturbation and lifetime, earth trace and coverage, lighting and eclipse geometry, and radiation aspects of the rendezvous trajectory are noted. The general deorbit maneuver is discussed, as is minimum energy/time deorbit, deorbit timing, and deorbit via intermediate orbit. Entry dynamics and entry heating are noted; and direct entry, lifting entry and equilibrium glide path, and maneuverability are considered. Recommended procedures are mentioned in light of the discussion on mission constraints and their relationship to trajectories. M.W.R.

N68-21077*# North American Aviation, Inc., Downey, Calif. GUIDANCE, FLIGHT MECHANICS AND TRAJECTORY OPTIMIZATION. VOLUME 10: DYNAMIC PROGRAMMING A. S. Abbott and J. E. Mc Intyre Washington NASA Apr. 1968 155 p refs

(Contract NAS8-11495)

(NASA-CR-1009; SID-66-1678-2, V. 10) CFSTI: HC \$3.00/MF \$0.65 CSCL 22C

Basic concepts of dynamic programming are presented along with their applications to simple multistage decision processes related to guidance, flight mechanics, and trajectory optimization. The principle of optimality and optimal value functions are discussed, as are the optimization of stochastic systems and the treatment of terminal constraints. Details are included for the limiting process in dynamic programming; with attention to the recursive and Bellman equations, Lagrange and Bolza problems, linear problem with quadratic cost, and the Pontryagin maximum principle. M.W.R. N68-21182*# National Aeronautics and Space Administration. Goddard Space Flight Center, Greenbelt, Md.

DETERMINING THE SPIN AXIS OF A SPINNING SATELLITE

F. O. Vonbun Washington Apr. 1968 11 p refs

(NASA-TN-D-4483) CFSTI: HC\$3.00/MF\$0.65 CSCL 22A Spin axis, a unit vector, is determined for a spinning satellite

using ground tracking information. Range rate information is found to be adequate for this purpose. The determination of the unit vector is necessary to check onboard sensors once the spacecraft is in orbit. In the case of a slight onboard malfunction, the spin axis could not be determined without this vector. Author

N68-21228*# National Aeronautics and Space Administration. Lewis Research Center, Cleveland, Ohio.

LOW VARIABLE THRUST INTERPLANETARY TRAJECTORY DATA

Edward J. Nime and John S. Mac Kay Washington Apr. 1968 88 p refs

(NASA-TN-D-4431) CFSTI: \$3.00 CSCL 22C

The Newton-Raphson algorithm method is used to generate a large number of low-thrust trajectories between Earth and the other planets in the solar system. These paths assume the use of an ideal, variable-thrust rocket that operates at constant jet power. Trajectories include planet flyby, or capture from Earth, and Earth flyby from the other planets. In all cases, the heliocentric travel angle is varied between 30° and 330° for seven different trip times. The data presented include the performance parameter and all the initial values needed to recompute the path. Several terminal conditions, such as velocity components for the flyby cases, are also included. Analytical techniques with numerical examples are presented which consider the application of the data to a variety of manned and unmanned missions and mission profiles. Author

N68-21231*# North American Aviation, Inc., Downey, Calif. GUIDANCE, FLIGHT MECHANICS AND TRAJECTORY OPTIMIZATION. VOLUME 15: APPLICATION OF OPTIMIZATION TECHNIQUES

A. S. Abbott and A. L. Blackford Washington NASA Apr. 1968 163 p refs

(Contract NAS8-11495)

(NASA-CR-1014; SID-66-1678-7) CFSTI: HC \$3.00/MF \$0.65 CSCL 22C

Trajectory and guidance problems encountered in space flight are discussed in the context of three optimization techniques applied to their solution-the Pontryagin maximum principle, the calculus of variations, and dynamic programming. In the problems considered, the formulation is simple enough to allow an analytic solution along with a more general formulation which requires a numerical technique. Although both the calculus of variations and the Pontryagin maximum principle are applied, it is pointed out that the two formulations yield the same results in terms of the equations to be solved and can be considered as different means of looking at one formulation of an optimization technique. While these two techniques lead to a set of first-order ordinary differential equations (for the Mayer-type problem), the application of dynamic programming leads to a set of partial differential equations. It is generally felt that on a theoretical level dynamic programming is not as strong or as applicable as the other two methods. However, the difference in approach could provide a different perspective to the structure of the problem. M.G.J.

N68-21442*# North American Aviation, Inc., Downey, Calif. GUIDANCE, FLIGHT MECHANICS AND TRAJECTORY OPTIMIZATION. VOLUME 17: GUIDANCE SYSTEM PERFORMANCE ANALYSIS

D. R. Grier Washington NASA Apr. 1968 221 p refs (Contract NAS8-11495) (NASA-CR-1016; SID-66-1678-9) CFSTI: HC \$3.00/MF \$0.65 CSCL 22C

A study of the methodology of system performance analysis which forms the principles and techniques of direct applicability in assessing guidance system performance and requirements: is reported. Methodology considered is directly applicable to a guidance system which is dependent upon particular mission considerations. Discussed are basic concepts of randomness and probability among which are considered: (1) Gaussian random variables, the multivariate Gaussian probability density function, and probabilities for Gaussian random vectors; (2) functions of random variables with particular emphasis on transformations of probability density functions and statistical moments of functions of random variables: (3) several particular functions of Gaussian random variables with emphasis upon the probability density functions and statistical moments; (4) several basic probability bounds which can generally be used to bound random variables when only lower order statistical moments are known; (5) several basic limiting theorems which generally concern the limiting behavior of sums of statistically independent random variables; (6) statistical property determinations with particular emphasis on estimating moments and examining the validity of assumptions concerning probability density functions; (7) the particular case of estimating statistical moments for Gaussian random variables; (8) basic methods of correlation and regression analyses; and (9) the use of confidence intervals and the method of hypothesis testing. S.C.W.

N68-21685*# North American Aviation, Inc., Downey, Calif.

GUIDANCE, FLIGHT MECHANICS AND TRAJECTORY OPTIMIZATION. VOLUME 5: STATE DETERMINATION AND/OR ESTIMATION

G. E. Townsend, D. R. Grier, R. R. Palmer, R. J. Ruggiero, and A. S. Abbott Washington NASA Apr. 1968 255 p refs

(Contract NAS8-11495)

(NASA-CR-1004; SID-65-1200-5) CFSTI: HC \$3.00/MF \$0.65 CSCL 22C

Attention is focused on the basic problem of generalizing precise information regarding the trajectory of an observed vehicle and the coefficients of the mathematical model used in the prediction from a set of observations made of the vehicle. The task of generating a reliable first approximation to the true trajectory is discussed, and optimum estimates of the deviation vector are developed. The development of simple measures of the degree of optimality in the estimator, and the generation of the estimation equations and estimation error for these measures are discussed. The classical least squares, weighted least squares, and minimum variance estimators are derived, and consideration is given to modern estimation in a recursive mode. Filter concepts are assessed and tailored to problems where the statistics involved are Gaussian, where the dynamics can be approximated by the linear model, and where the optimum estimator is a linear function of the deviations in the observables. Matrices relating the dynamics at various times relative to the nominal trajectory, and the matrix presenting the error data for the observables are derived. Recommendations for applying these data are made. MG.L

N68-21733*# National Aeronautics and Space Administration. Goddard Space Flight Center, Greenbelt, Md.

A HUMMINGBIRD FOR THE L₂ LUNAR LIBRATION POINT F. O. Vonbun Washington Apr. 1968 15 p refs

(NASA-TN-D-4468) CFSTI: HC\$3.00/MF\$0.65 CSCL 22C

This paper concerns a spacecraft not in a circumlunar orbit, but in a quasi-permanent position in the vicinity of the far-side lunar libration point L₂. Such a spacecraft would be a useful communications relay between the back of the moon and the earth. It could be so placed above the libration point as never to be occulted, thus making the communication link a continuous one, independent of time. The spacecraft would be in the lunar gravitational field and thus need permanent thrust to stay in place or to move slowly around a point in space like a hovering hummingbird. This report shows analytically the accelerations in the vicinity of L₂ and the specific impulses needed to keep a spacecraft there economically with a reasonable fuel-to-mass ratio ($m_f/m_o = 0.05$ to 0.15). This dictates the kinds of engines needed for such missions, where constant, small accelerations are needed over the lifetime of a spacecraft (in the order of 1 to 3 years). Author

N68-21802*# National Aeronautics and Space Administration, Washington, D. C.

PHYSICS OF PLANETS

V. I. Moroz Apr. 1968 416 p refs Transl. into English of the publ. "Fizika Planet" Moscow, Nauka Press, 1967

(NASA-TT-F-515) CFSTI: HC \$3.00/MF \$0.65 CSCL 03B

Planetary physics deals with the physical characteristics of the planets and their satellites: the temperature of the planet surface and atmosphere; the composition, density and vertical structure (i.e., the altitude dependence of temperature, composition and density) of the atmosphere, the nature of the cloud layer, circulation of the atmosphere, the nature of the observable surface features and surface layer, and lastly, the internal structure. Author

N68-21864*# Heliodyne Corp., Van Nuys, Calif. NON-LINÉAR ORBIT DETERMINATION METHODS Ali Hasan Nayfeh Washington NASA May 1968 43 p refs (Contract NAS1-6690)

(NASA-CR-1040) CFSTI: HC \$3.00/MF \$0.65 CSCL 22C

A non-linear correction method for orbit determination using range, azimuth, and elevation data is presented and justified mathematically and numerically. In contrast with conventional methods, such as the least-squares, the maximum likelihood, and the Kalman, this method holds in the non-linear, as well as in the linear regions. Moreover, this method does not require transition and normal matrices and, hence, avoids the problems associated with calculating and inverting them. The convergence and accuracy of the method have been demonstrated by calculations made on simulated orbits with varying levels of noise. The calculations demonstrate that the proposed method is non-linear and can be used as an editing procedure because it converges despite the combined effect of very bad reference orbits, extremely high levels of noise, wild data points, and critical orbits. The calculations show also that the errors of the resultant epoch state vectors are indeed very small. Author

N68-22202*# Virginia Polytechnic Inst., Blacksburg. TIME-OPTIMAL RENDEZVOUS FOR ELLIPTIC ORBITS Y. Kashiwagi and K. T. Alfriend Washington NASA May 1968

125 p refs (Grant NGR-47-004-006)

(NASA-CR-1036) CFSTI: HC\$3.00/MF\$0.65 CSCL 22C

Time-optimal rendezvous maneuvers are studied. The system considered in this report consists of two space vehicles namely, a target vehicle (non-maneuvering vehicle) and an interceptor vehicle (maneuvering vehicle) under the influence of the earth gravity. An interceptor vehicle has propulsive jet systems which can produce a variable thrust (positive or negative) independently in three perpendicular directions. The case where the target vehicle is in the elliptic orbit is mainly considered and some analytical difficulties involved in the circular orbit case are discussed. Several time-optimal trajectories for different configurations are shown. Author N68-22289*# National Aeronautics and Space Administration. Lewis Research Center, Cleveland, Ohio.

SOME NUMERICAL COMPARISONS OF THREE-BODY TRAJECTORIES WITH PATCHED TWO-BODY TRAJEC-TORIES FOR LOW THRUST ROCKETS

William C. Strack Washington May 1968 30 p refs

(NASA-TN-D-4559) CFSTI: HC\$3.00/MF\$0.65 CSCL 22C

The n-body problem for low-thrust vehicles with optimal thrust control is formulated for the case of constant thrust with coast. A successive two-body approximation to the n-body problem is also developed under the assumption of tangential thrust during the planetocentric leg. This approximation involves one arbitrary parameter—the planetocentric radius at the patch point—whose best value can be determined by comparison with n-body solutions. Numerical solutions of several three-body problems indicate that the patch radius should be about 300 earth radii for either a circular or a parabolic initial earth orbit.

N68-22860*# St. Louis Univ., Mo.

RADIATIVE HEATING AND COOLING FUNCTIONS FOR THE LOWER MARTIAN ATMOSPHERE UNDER THE CONDITION OF LOCAL THERMODYNAMIC EQUILIBRIUM (LTE)

Albert J. Pallmann Washington NASA May 1968 47 p refs (Grant NGR-26-006-016)

(NASA-CR-1044; Rept.-101) CFSTI: HC \$3.00/MF \$0.65 CSCL 03B

The physics of planetary radiation fields has been reexamined to derive formulas describing analytically the heating and cooling processes of the Martian atmosphere in local thermodynamic equilibrium (LTE). The computational algorithm required for the numerical solution of the radiative heating and cooling in the Martian atmosphere has been outlined. Spectral data for near and far IR CO , bands have been provided. A model was assumed for the Martian atmosphere in LTE, characterized by 100% CO2, plane-parallel stratification, with no particulates embedded, scattering by molecules excluded, and neglecting the reflection of solar radiation at the ground. However, radiative equilibrium has not been assumed, because this assumption would have made the heating and cooling rates identically zero. The radiative transfer theory, its computational algorithm, and the spectral data of CO2 and solar radiation for the Martian atmosphere, as presented in this paper, provide the means for computing the radiative heating and cooling rates for the atmosphere of Mars at any latitude, once the temperature sounding is given for the location. Author

N68-22885*# National Aeronautics and Space Administration. Goddard Space Flight Center, Greenbelt, Md.

ON THE APPLICATION OF SPINORS TO THE PROBLEMS OF CELESTIAL MECHANICS

Karl Stumpff Washington May 1968 44 p refs

(NASA-TN-D-4447) CFSTI: HC\$3.00/MF\$0.65 CSCL 03C

Since Newton, the stumbling-block in celestial mechanics was the three-body problem. Only restricted cases have yielded solutions. This paper describes a new tool for solving the perturbation problem—"spinors," a vectorial concept (in the complex plane) originally used in atomic physics but now applied to celestial mechanics. The two-body problem is discussed and two devices are introduced: "pseudo-time" and the Levi-Cività transformations. Then spinors are shown to make possible the extension of these transformations to three dimensions. Perturbation problems are discussed; notably a body moving around the sun and being acted on by the orbital motion of a major planet.

N68-24371*# National Aeronautics and Space Administration. Electronics Research Center, Cambridge, Mass.

THE EQUATIONS OF MOTION FOR OPTIMIZED PROPELLED FLIGHT EXPRESSED IN DELAUNAY AND POINCARE VARIABLES AND MODIFICATIONS OF THESE VARIABLES

William E. Miner Washington May 1968 79 p refs

(NASA-TN-D-4478) CFSTI: HC\$3.00/MF\$0.65 CSCL 22C

This document presents methods for developing the ordinary differential equations of motion in canonical form equivalent to the forms of Delaunay and Poincare. It also presents modifications to these forms so that three variables, which are constants of motion. result while the forms remain canonical. The equations of motion are for a vehicle propelled by constant thrust magnitude with a constant mass flow rate. The vehicle is moving in a central force field. The trajectories are optimum in the sense of classical calculus of variations in a neighborhood definable by the boundary conditions of the specific problem. Specific problems are not discussed in this document. The value of the document lies in two major areas: (1) The possible economics in numerical calculations which may result from using these ordinary differential equations, and (2) The application of the general perturbation theory of classical celestial mechanics to approximate solutions of these ordinary differential equations. Author

N68-24486*# National Aeronautics and Space Administration. Goddard Space Flight Center, Greenbelt, Md.

ASPECT DETERMINATION IN LUNAR SHADOW ON EXPLORER 35

Harold E. Jaylor Washington May 1968 12 p refs

(NASA-TN-D-4544) CFSTI: HC\$3.00/MF\$0.65 CSCL 22A

The Explorer 35 spacecraft experiences a small, temporary secular decrease in spin period (approximately 2 parts in 1000) during every pass through the lunar shadow. Because of this, the pseudo-sun pulse, generated when the spacecraft is in the shadow, no longer accurately indicates the sunward direction. Details are given on an empirical method of fitting a spin period of the form $a + b \exp(-t/t_0)$ to the aspect information available before and after the optical shadow (t is time since the spacecraft entered the shadow, and a, b, and t₀ are constants to be determined). The resulting aspect information is estimated to be within ± 10 degrees of the true direction.

N68-24557*# National Aeronautics and Space Administration. Ames Research Center, Moffett Field, Calif.

LANDING SITE DISPERSIONS OF AN UNCONTROLLED LANDER ON MARS

John S. White Washington May 1968 24 p refs

(NASA-TN-D-4587) CFSTI: HC\$3.00/MF\$0.65 CSCL 22A

A study was made to determine the accuracy with which a lander, descending from a bus orbit, can reach a specified landing site on Mars without using a range control system. This report considers both a lifting and a nonlifting lander-each with two different values of mass. Several different entry angles were considered. along with two different procedures for the deorbit maneuver: the use of the minimum deorbit velocity increment and the use of a constant deorbit velocity increment. The error sources considered are variations in the Martian atmosphere, variations in the actual lift of the vehicle, and errors in performing the deorbit maneuver. It is concluded that if minimum deorbit velocity increment is used with entry angles of -20° to -24° , the landing site accuracy will be on the order of 1°, which is of the same order as the present knowledge of the location of the landing site. Thus a range control system need not be included in the lander. Author

N68-25271*# National Aeronautics and Space Administration. Goddard Space Flight Center, Greenbelt, Md.

SPACE TRAJECTORIES AND ERRORS IN TIME, FREQUENCY, AND TRACKING STATION LOCATION

F. O. Vonbun Washington Jun. 1968 22 p refs

(NASA-TN-D-4507; NASA-TM-X-55798) CFSTI: HC \$3.00/MF \$0.65 CSCL 09F

This paper demonstrates analytically how errors in tracking station time and frequency synchronization, as well as errors in station location, influence the accuracy of trajectory determination. Two systems, whose data are presently used for most of the more accurate orbit determination schemes, are described: a range and range rate system, and a radar system. All other systems are actually combinations of these two basic systems. Rather simple analytical expressions are derived relating measuring errors with those of time and frequency synchronization, as well as ground tracking station location. For the range and range rate system, the error in range rate or is used as a yardstick, and all other quantities are derived from it. For the radar system (not measuring range rate directly), the total local position vector, as measured by such a system is used as the yardstick to determine the necessary time synchronization and station location accuracy. Numerical examples are presented. Author

N68-25385*# National Aeronautics and Space Administration. Goddard Space Flight Center, Greenbelt, Md.

THEORY OF THE INVESTIGATION OF THE ATMOSPHERE OF BINARY STARS BY ANALOGY BETWEEN GAS DYNAMICS AND SHALLOW-WATER FLOWS

Ernst W. Adams and Burkhard Schulz-Jander (Deut. Versuchsanstalt fur Luft- und Raumfahrt, Freiburg, West Ger.) Washington Jun. 1968 22 p refs

(NASA-TN-D-4520) CFSTI: HC\$3.00/MF\$0.65 CSCL 03B

Approximate solutions of the differential equations of continuum isentropic gas dynamics may be obtained for flows in the equatorial plane of a binary star atmosphere, by analogy between gas dynamics and shallow-water flows in a rotating water tank. The local inclination of the tank's bottom is proportional to the resulting local gravitational force at the corresponding point in the binary-star atmosphere. The analogy requires a constant polytropic coefficient of two. This application of the analogy rests on its extension to rotating systems with external force fields. A theoretical evaluation of the analogy (for the earth's atmosphere under hydrostatic conditions with polytropic coefficient equal to two) yields the correct "maximum" height of the atmosphere-where density reaches zero. This study is motivated by the possibility that it may be applied to the early stages of the evolution of the earth-moon system after its hypothetical fission. Author

N68-25867*# National Aeronautics and Space Administration. Goddard Space Flight Center, Greenbelt, Md. LOCAL-ERROR CONTROL AND ITS EFFECTS ON THE

OPTIMIZATION OF ORBITAL INTEGRATION C. E. Velez Washington Jun. 1968 24 p refs

(NASA-TN-D-4542) CFSTI: HC\$3.00 /MF\$0.65 CSCL 22C

In the numerical integration of orbits by a multistep process, it has been suggested that the application of a local error control may increase the efficiency of the integration without any significant loss of accuracy. This study develops methods of controlling the local error and examines the effects of these controls on the integration. It is shown that for various orbit types, controlling the local error can optimize the integration while maintaining the desired accuracy. Author

N68-25895*# Arizona Univ., Tucson. MULTISEGMENTED OPTIMAL TRAJECTORIES Thomas L. Vincent Washington NASA Jun. 1968 31 p refs (Grant NsG-580)

(NASA-CR-1103) CFSTI: HC\$3.00 /MF\$0.65 CSCL 22C

The problem of Bolza from the calculus of variations in terms of modern control notation has been extended in scope to include situations in which a number of subarcs in the state variable trajectory may occur in a variety of ways. The subarcs are allowed to be overlapping and /or separated. This allows for several subarcs to occur in the same interval of the independent variable and for subarcs which are separated by jumps in the independent and state variables. In addition, the differential equations of constraint and the integral quantity to be extremized are allowed to be of different form from subarc to subarc. The necessary minimizing conditions for the extended Bolza problem are obtained by extremizing a new functional which is related to it. This allows the optimizing conditions for the state and control variables to be obtained by applying the usual calculus of variations procedures and the optimizing conditions for the endpoints of the subarcs to be obtained using the ordinary theory of maxima and minima. Author

N68-25902 *# Michigan Univ., Ann Arbor.

TRAJECTORY OPTIMIZATION BY A DIRECT DESCENT PROCESS

L. E. Fogarty and R. M. Howe Washington NASA Jun. 1968 38 p refs

(Grant NASr-54(06))

(NASA-CR-1070) CFSTI: HC\$3.00/MF\$0.65 CSCL 22C

The problem considered is that of trajectory optimization using step-by-step descent to minimum cost along the direction of the cost gradient with respect to the control. Using a hybrid computer, the gradient is computed directly as the response to nearly impulsive control perturbations. A method is presented for computing the gradient when several terminal constraints are enforced. Examples of application of the method are presented. It is concluded that the direct gradient computation method has some significant advantages over other methods. Author

N68-26642*# National Aeronautics and Space Administration. Goddard Space Flight Center, Greenbelt, Md.

ON SOME POSSIBLE SIMPLIFICATIONS AND CHANGES IN HANSEN'S LUNAR THEORY

Peter Musen Washington Jun 1968 28 p refs

1

(NASA-TN-D-4562) CFSTI: HC\$3.00/MF\$0.65 CSCL 03B

Several devices which permit us to reduce the number of quantities which must be re-computed with each iteration cycle are introduced. We refer the motion of the satellite to an almost ideal system of coordinates with two axes lying in the mean orbital plane. The position of the satellite relative to the almost ideal system is determined by Hansen's coordinates 1 + ν and N₀ δz of the projection of the satellite on its mean orbital plane and by the "elevation" (of the satellite relative to this plane. The position of the almost ideal system itself with respect to an inertial system is determined by two uniform rotations, one around the normal to the orbital plane of the sun, and one around the normal to the mean orbital plane of the satellite. The problem of integration is reduced to solving a linear partial differential equation by means of successive approximation, or to expanding the integrating operator into a series of products of two linear operators. One of these operators is a linear partial differential operator and the other is the inverse of a linear partial differential operator with the constant coefficients. We propose here, as in the previous work, to compute Hansen elements $\xi,\,\Upsilon$ and Ψ separately and to fuse them into W bypassing Hansen's function W. Author

N62-26643*# National Aeronautics and Space Administration. Goddard Space Flight Center, Greenbelt, Md.

ON THE APPLICATION OF LIE-SERIES TO THE PROBLEMS OF CELESTIAL MECHANICS

Karl Stumpff Washington Jun. 1968 29 p refs

(NASA-TN-D-4460) CFSTI: HC\$3.00/MF\$0.65 CSCL 03C

Since Newton, the stumbling block in celestial mechanics has been the three-body problem. Only restricted cases have yielded solutions. This paper describes a device, the "Lie-Series," that first appeared in Lie's work on analytical transformations; Gröbner has shown that they can be used to solve systems of differential equations by applying differential operators to known functions or to invert systems of analytical functions. The series are applied to Kepler's problem of an undisturbed planet round the sun (two-body problem), to the study of perturbations, and to the process of obtaining the characteristics for any general dynamical problem. Author

N68-26689*# Northrop Corp., Hawthorne, Calif. GENETIC STATES OF SIMULATED LUNAR ROCKS Emanuel Azmon Washington NASA Jun. 1968 152 p refs (Contract NAS7-358)

(NASA-CR-1081; NCL-67-44R) CFSTI: HC \$3.00/MF \$0.65 CSCL03B

Concepts leading to beneficial uses of rocks on the moon were developed. Most of the raw materials used are commonly and abundantly available silicate rocks. It is hoped that similar silicates will be found to be common and abundant on the lunar surface. The concept developed in this study is that of a genetic state which is the state from which a rock of distinct characteristics is born. This state is a function of the pressure and temperature conditions that a rock material is exposed to, as well as of the history (time and rate of changes) of pressures and temperature. Specific genetic states of several rocks are shown as genetic diagrams in this report. Most of the phases that are shown in the diagrams to coexist are not in equilibrium with their system, but were "frozen" into existence by quenching prior to attainment of equilibrium.

N68-26702*# Lovelace Foundation for Medical Education and Research, Albuquerque, N. Mex.

THE INTANGIBLES OF HABITABILITY DURING LONG DURATION SPACE MISSIONS

T. M. Fraser Washington NASA Jun. 1968 83 p refs (Contract NASt-115)

(NASA-CR-1084) CFSTI: HC \$3.00 / MF \$0.65 CSCL 05E

The nature and meaning of habitability are discussed in relation to the requirements for long duration manned space missions. Several models of habitability are examined, and it is suggested that habitability can be considered as that equilibrium state, resulting from man-machine-environment-mission interactions which permits man to maintain physiological homeostasis, adequate performance, and psycho-social integrity. The attributes of habitability are examined, and indices of habitability are discussed. No attempt is made to examine all the requirements for optimum habitability, an exercise which would involve consideration of every aspect of the interactions occurring in the entire manmachine-environment-mission complex. Attention if focussed instead on some of the less common aspects, and a discussion ensues on requirements for free internal volume, configuration, privacy (territoriality), personal hygiene, illumination, decor, color, recreation, and the use of leisure time, during a long duration Author manned space mission.

N68-27475*# National Aeronautics and Space Administration, Washington, D. C. THE ZODIACAL LIGHT AND THE INTERPLANETARY

THE ZODIACAL LIGHT AND THE INTERPLANETARY MEDIUM J. L. Weinberg ed. (Hawaii Univ.) 1967 395 p refs Papers presented at the Symp. held in Honolulu, Hawaii, 30 Jan.–2 Feb. 1967

(NASA-SP-150) GPO: HC\$3.00; CFSTI: MF\$0.65 CSCL 03B

Conference papers on zodiacal light in the interplanetary medium deal with photometric and meteor observations, particle collection and impact, scattering properties, dynamics and the earth's dust cloud, solar wind, and the origin and evolution of zodiacal dust. For individual titles see N67-27475 to N67-27525.

N68-28113*# National Aeronautics and Space Administration. Marshall Space Flight Center, Huntsville, Ala.

MOTION OF AN ARTIFICIAL SATELLITE UNDER COMBINED INFLUENCE OF PLANAR AND KEPLERIAN FORCE FIELDS

Rowland E. Burns Washington Jul. 1968 57 p refs

(NASA-TN-D-4622) CFSTI: HC\$3.00/MF\$0.65 CSCL 22C

The development of the technology of artificial earth satellites has posed mathematical problems which heretofore were academic. One such problem is the radiation pressure perturbations of satellites with large area-to-mass ratios (i.e., Echo). The standard method of treatment of such a problem is a perturbational analysis of a purely Keplerian orbit which is disturbed by a radiation pressure field. It will be shown in this report that a generalized form of the two-body problem which more closely approximates the radiation pressure problem can be solved in closed form. Specifically, the problem of the motion of a satellite under the combined influence of Keplerian and planar force fields will be solved in terms of the elliptic functions. The assumption of a planar force field is still an approximation to the true radiation pressure problem because the divergence of the field is neglected. It is obvious that neglecting the divergence of the radiation pressure field is far less restrictive than disregarding the entire field. Perturbational treatment with the present solution as a model should converge far more readily than treatments which assume an initially Keplerian model. Author

N68-28192*# Arizona Univ., Tucson. CHRONOLOGICAL CATALOG OF REPORTED LUNAR

EVENTS Barbara M. Middlehurst, Jaylee M. Burley, Patrick Moore (Armagh Planetarium), and Barbara L. Welther (Smithsonian Astrophys.

Obs.) Washington NASA Jul. 1968 55 p refs (NASA-TR-R-277) CFSTI: HC\$3.00/MF\$0.65 CSCL03A

A catalog of reports of lunar events, or temporary changes on the moon, was compiled based on literature covering more than four centuries. In most cases, the original reference was consulted; Houzeau and Lancaster's *Bibliographie Général d'Astronomie* and the *Astronomischer Jahresbericht* were useful secondary sources. Each entry includes a brief description and date of the observation; the name of the observer(s), where these are known; and the reference. Author

N68-28251*# National Aeronautics and Space Administration. Goddard Space Flight Center, Greenbelt, Md.

ON THE PERTURBATIONS OF SMALL-ECCENTRICITY SATELLITES

T. L. Felsentreger Washington Jul. 1968 49 p refs

(NASA-TN-D-4531) CFSTI: HC\$3.00/MF\$0.65 CSCL 22C

Difficulties have been encountered in the orbit determination of nearly circular earth satellites when "first-order" analytic perturbation theories have been used. "First-order" usually means that periodic terms are developed to order J_2 (the second zonal harmonic coefficient in the earth's gravitational potential), the secular terms to order J_2^2 . If these theories are extended to include periodic terms of order J_2^2 and higher, the appearance of eccentricity as a divisor in the perturbations of eccentricity, mean anomaly, and argument of perigee causes many of these "higher-order" terms to be comparable in magnitude with the J_2 .

terms (for small-eccentricity satellites). Thus, the aforementioned difficulties can be attributed, at least in part, to the omission of these terms from the orbit-determination models. Von Zeipel's method is used to derive all such "small divisor" terms inclusive of J_2^3 and $(J_1/J_2)^3$, when J_1 is any odd zonal harmonic coefficient. Author

N68-28275*# Boeing Co., Seattle, Wash. LUNAR ORBITER 4. PHOTOGRAPHY Washington NASA Jul. 1968 78 p (Contract NAS1-3800)

(NASA-CR-1093; D2-100754-2, V. 2) CFSTI: HC \$3.00/MF \$0.65 CSCL 22A

Photographic mission design, actual photography, photographic supporting data, and operational performance for Lunar Orbiter 4 are detailed. Nearly complete coverage of the nearside and appreciable coverage of the farside of the moon were made at a resolution significantly better than earth-based observations. Nominal orbit parameters are included and general characteristics of mission photography along with meteoroid, energetic radiation, wind fogging, and light streaking effects are included. Perilune and apolune lunar landing sites are discussed and illustrated. Cameras, processor-dryer, and readout performances are summarized. M.W.R.

N68-28373*# Douglas Aircraft Co., Inc., Santa Monica, Calif. ULTRAHIGH VACUUM ADHESION RELATED TO THE LUNAR SURFACE

Washington NASA Jul. 1968 95 p refs

(Contract NAS7-307)

(NASA-CR-1090) CFSTI: HC\$3.00/MF\$0.65 CSCL 22A

To represent possible bounds to the types of silicate surfaces which may be found on the moon, two types of silicate surface preparation were used. The first consisted of forming the surface in air, representing the contaminated surface case. The other consisted of forming the surface at ultrahigh vacuum by cleavage, representing the clean surface. Adhesion force was measured as a function of load force, temperature, surface roughness, type of material, crystalline orientation, and degree of surface cleanliness. The adhesion between ultrahigh vacuum-formed silicate surfaces was found to be orders of magnitude greater than that between the air-formed surfaces. A strong long-range attractive force, indicative of surface charing, was also noted. It was concluded: (1) Adhesion phenomena are critically dependent upon the surface state. (2) The highest magnitude adhesion may be caused through the action of the normal atomic bonding forces, but the surface charging makes a significant contribution. (3) Though random charge separation associated with bond breakage could contribute to surface charging, a major contributors are the defect structures in the crystal lattice. M.G.J.

N68-28408*# National Aeronautics and Space Administration, Manned Spacecraft Center, Houston, Tex.

USE OF PLANETARY OBLATENESS FOR PARKING-ORBIT ALINEMENT

Joseph R. Thibodeau, III Washington Jul. 1968 27 p refs

(NASA-TN-D-4657) CFSTI: HC\$3.00/MF\$0.65 CSCL 22C A rapid analytical technique is used to determine

simultaneously the possible configurations of an elliptical parking orbit at Mars. Both the geometry of planetary approach and departure and the effects of planetary oblateness are used to determine the characteristics of those orbits which shift into proper alinement for departure and require no discrete propulsive maneuvers. The technique makes use of the separable nature of the equations that express secular rotation of the orbit plane and major axis. Preliminary results indicate that the orbital inclinations fall into narrow bands which are widely distributed over the interval of possible inclinations. N68-28409*# National Aeronautics and Space Administration. Langley Research Center, Langley Station, Va.

CORRELATION STUDY OF LUNAR RADII OBTAINED FROM PHOTOGRAPHIC AND LUNAR GRAVITATIONAL FIELD DATA

James R. Williams and William R. Wells Washington Jul. 1968 19 p refs

(NASA-TN-D-4636) CFSTI: HC\$3.00/MF\$0.65 CSCL 03A

A study has been made to determine the correlation of local lunar radii as determined from recent earth-based photographic studies and from lunar gravitational field coefficients obtained from lunar satellite tracking data. The photographic study is a recent local radii determination performed by the Army Map Service at 734 points over the visible lunar surface. The lunar gravitational field coefficients used in the analysis are the most recent determinations from independent studies of tracking data from Lunar Orbiters I to IV and the Russian satellite LUNA-10. The general result of the study is that all the currently determined gravity models are little correlated with the visible surface features of the moon excpet in a few isolated regions. Author

N68-28841*# National Aeronautics and Space Administration. Langley Research Center, Langley Station, Va.

DERIVATION OF APPROXIMATE EQUATIONS FOR SOLVING THE PLANAR RENDEZVOUS PROBLEM

Gene W. Sparrow and Douglas B. Price Washington Jul. 1968 31 p refs

(NASA-TN-D-4670) CFSTI: HC\$3.00/MF\$0.65 CSCL 22C

The desirability of obtaining simplified and accurate relative equations of motion for two-impulse rendezvous application resulted in the examination of the Clohessy and Wiltshire type of simplified equation. An analysis of these equations revealed that large errors were possible if the radial separation of the two vehicles was large. In an effort to develop more accurate equations for rendezvous, the apparent erroneous terms were replaced by exact terms. The resulting modified equations contained terms not present in the Clohessy and Wiltshire equations. When the modified equations were applied to the problem of rendezvous, they were found to be generally superior to the Clohessy and Wiltshire equations, particularly for long transfer angles. The scope of the investigation is limited to the case in which the target vehicle is in a circular orbit coplanar with the ferry vehicle's orbit.

N68-28884*# National Aeronautics and Space Administration. Langley Research Center, Langley Station, Va.

GRAVITATIONAL EXPERIMENTS WITH A COLLISIONLESS TWO-DIMENSIONAL COMPUTER MODEL

Frank Hohl and Stephen K. Park Washington Jul. 1968 26 \mathbf{p} refs

(NASA-TN-D-4646) CFSTI: HC\$3.00/MF\$0.65 CSCL 03B

A two-dimensional model is used to perform computer experiments for a collisionless self-gravitating system. The grativational field is obtained by solving the Poisson equation and the system is advanced stepwise in time. Computer simulations have been performed for systems with an initially uniform distribution over a region in x,y space, zero thermal velocity, and various values of initial solid-body rotation. Up to 4000 stars were used in the calculations. Author

N68-29988*# National Aeronautics and Space Administration. Manned Spacecraft Center, Houston, Tex.

MARS LANDING MISSION MODE COMPARISON

James J. Taylor and John T. McNeely Washington Aug. 1968 49 p refs

(NASA-TM-X-1629) CFSTI:HC\$3.00/MF\$0.65 CSCL 22A

Four modes of landing a vehicle on Mars are compared in this document. In addition, several variations to these four basic mission modes are suggested. The most efficient mission mode for a Mars landing depends on the type of trajectories used. Author

N68-30098*# Douglas Aircraft Co., Inc., Santa Monica, Calif. PLANETARY FLIGHT HANDBOOK. PART 6: MARS STOPOVER MISSION USING VENUS SWINGBYS Washington NASA 1968 98 p refs

(Contract NAS2-4175)

(NASA-SP-35, Pt. 6) GPO: HC \$0.75; CFSTI: MF \$0.65 CSCL 22C

Trajectory data are presented to aid in planning stopover missions to Mars that employ the Venus swincby mode, which yield substantial reductions in propulsive velocity and Earth entry speed requirements when used as part of a round trip stopover mission. Charts, graphs and tabular data are included for total round trip mission duration and stopover time at Mars. The tabular trajectory data are for inbound and/or outbound swingbys that are projected for the 1975 through 1999 period; and stopover times are of zero, 30, and 60 day duration. Data are restricted to those missions which combine a direct leg and a ballistic Venus swingby leg, and mission employing Venus swingbys on both outbound and inbound legs. Minimum mission velocity requirements and associated earth entry speeds for each opportunity are presented as a function of mission duration for both propulsive braking and aerodynamic braking at Mars. M.W.R.

N68-30244*# National Aeronautics and Space Administration. Langley Research Center, Langley Station, Va.

LUMINOUS EFFICIENCIES OF THREE NICKEL ARTIFICIAL METEORS BETWEEN 9.8 AND 11.4 KILOMETERS PER SECOND

T. Dale Bess Aug. 1968 24 p refs

(NASA-TN-D-4666; L-5774) CFSTI: HC \$3.00/MF \$0.65 CSCL 038

Results of the experimental measurements of luminous intensity and corresponding luminous efficiency parameters of three nickel artificial meteors are presented. These results are compared with experimental values of iron luminous efficiencies over the same velocity range. All data were reduced from photographs taken with ground-based meteor cameras located at three camera sites. All flights were from Wallops Island, Virginia, and Nike-Cajun rocket vehicles were used to reenter the artificial meteoroids. Light curves on blue-sensitive film were obtained for all three nickel meteors. whereas the light curve on panchromatic film was obtained only for the fastest meteor. Data from the third experiment indicated that the radiation for this nickel meteor was strongest in the ultraviolet region of the spectrum; the measured blue-light intensity was about twice that of the panchromatic intensity. The experiments showed that the luminous efficiencies of nickel and iron are about the same at velocities around 11 and 12 kilometers per second; however, for lower velocities the luminous efficiency of nickel is as much as a factor of 10 less than the corresponding iron efficiencies. Author

N68-30601*# National Aeronautics and Space Administration, Washington, D. C.

PLANETARY ATMOSPHERES Continuing Bibliography with Indexes, Jun. 1966–Dec. 1967

Jul. 1968 126 p refs

(NASA-SP-7017(02)) CFSTI: HC\$3.00/MF\$0.65 CSCL 03B

Bibliographic citations and informative abstracts are presented on the properties of the atmospheres of Mars. Venus, Jupiter, Mercury, and Saturn, along with references to such related subjects as extraterrestrial environments, planetary observation techniques, and theories of planetary origin. Also included are subjects and personal author indexes. The bibliography covers the reports and journal articles announced in NASA abstract journals during the period June 1966 through December 1967. M.G.J. **N68-31989*#** National Aeronautics and Space Administration. Lewis Research Center, Cleveland, Ohio.

A TRAJECTORY CODE FOR MAXIMIZING THE PAYLOAD OF MULTISTAGE LAUNCH VEHICLES

Omer F. Spurlock and Fred Teren Washington Aug. 1968 168 p refs

(NASA-TN-D-4729) CFSTI: HC\$3.00/MF\$0.65 CSCL 22C

A computer code is described that quickly maximizes the payload of a multistage launch vehicle. Calculus of variations

chniques are used to optimize the trajectory and propellant loadings (optional) of one to six stages. The flow rate and vacuum thrust of each stage are constant. The jettison weight is a linear function of the propellant loading. The computer time is greatly reduced by minimizing the integration of atmospheric (booster) portions of the trajectory. A table of booster burnout conditions is formed from a limited number of boost trajectories. The table is used in conjunction with an interpolation scheme to obtain initial conditions for the vacuum portion of the trajectory. Author

N68-32094*# National Aeronautics and Space Administration. Goddard Space Flight Center, Greenbelt, Md.

EXPLICIT UPPER BOUNDS FOR ERROR PROPAGATION IN THE N-BODY FIELD

Albert Rosen Washington Aug. 1968 18 p refs (NASA-TN-D-4511) CFSTI: HC\$3.00/MF\$0.65 CSCL 22C

A simple means for bounding the propagated trajectory error induced by an impulsive initial error in the n-body field is developed. Formulas are derived for the maximum acceptable initial error, given the mission tolerances, and for the maximum time of negligible propagated error, given the initial impulses and mission tolerances. An example illustrates the use of the results within the solar system.

 ${\bf N68\text{-}32631}\ensuremath{^{\#}}$ National Aeronautics and Space Administration, Washington, D. C.

LUNAR SURFACE STUDIES Continuing Bibliography With Indexes

Jun. 1968 115 p refs

(NASA-SP-7003(04)) CFSTI: HC\$3.00/MF\$0.65 CSCL 22A

Subject coverage concentrates on theory of lunar origin, the lunar atmosphere, and the physical characteristics of the lunar surface, such as topography, geology, and stratigraphy. References are also included to techniques of lunar observation, measurement, and analysis, e.g., photography, photometry, and spectrophotometry, as well as references to the instrumentation and equipment used in lunar investigations. Author

N68-32744*# Westinghouse Electric Corp., Baltimore, Md. DIGITAL PROGRAM FOR DYNAMICS OF NON-RIGID GRAVITY GRADIENT SATELLITES

James L. Farrel, James K. Newton, and James J. Connelly Washington Aug. 1968 99 p

(Contract NAS5-9753-10) (NASA-CR-1119) CFSTI: HC\$3.00 /MF\$0.65 CSCL 22A

A digital program has been written to determine the dynamic behavior of discretized models for gravity gradient satellite structures. Both passive (elastic reaction, damping) and active (controller) internal torques can be included in the computational model. The program can be utilized simply by observing straight-forward directions given in the introductory section of this report, and a concrete example (hinged assembly model of the Radio Astronomy Explorer satellite) of program adaptation is described in detail. To facilitate application to other configurations a clear separation is made between 1) computations applicable to a general gravity gradient satellite, and 2) specific RAE computations. Author

N68-32978*# National Aeronautics and Space Administration. Langley Research Center, Langley Station, Va.

THEORY AND RESULTS ON COLLECTIVE AND COLLISIONAL EFFECTS FOR A ONE-DIMENSIONAL SELF-GRAVITATING SYSTEM

Frank Hohl Washington Aug. 1968 80 p refs (NASA-TR-R-289) CFSTI: HC\$3.00/MF\$0.65 CSCL03B

The equilibrium properties of one-dimensional self-gravitating systems are investigated analytically. One-dimensional models are used to perform computer experiments tracing the evolution of stellar systems. The stationary solution of the Vlasov equation for a one-dimensional system of stars as computed for an interesting class of initial conditions is found to correspond to a minimum-energy configuration. The results of the numerical experiments are compared with theory. For initial energies far from the minimum equilibrium energy the system becomes unstable and breaks up into smaller clusters. A variational principle was applied to the one-dimensional stellar system to show that stationary distribution functions which decrease monotonically in going outward from the center of the system are stable. The one-dimensional model is of interest as an approximation to the distribution of velocity and mass normal to the galactic plane of a greatly flattened galactic system. Observational results for the gravitational force normal to the galactic plane of the Galaxy agree with the results obtained from the one-dimensional model. Thermalization effects for systems containing small numbers of stars were investigated. The fluctuation of the kinetic energy was found to be inversely proportional to the square root of the number of particles in the system. Author

N68-33055*# National Aeronautics and Space Administration. Ames Research Center, Moffett Field, Calif.

A METHOD FOR COMPUTING LUMINOUS EFFICIENCIES FROM METEOR DATA

Barrett S. Baldwin, Jr. and H. Julian Allen Washington Sep. 1968 70 p refs

(NASA-TN-D-4808) CFSTI: HC\$3.00/MF\$0.65 CSCL 22A

The details of a model for the ablation of a stone meteoroid passing through the atmosphere are presented. The model allows for a decrease in mean density due to frothing, which results from the intense heating at low atmospheric pressures. The present results are a refinement of a previously published analysis since new information on the properties of meteoritic materials has been utilized. A method was also found for taking into account a delay in light production resulting from the time required to vaporize chunks of froth in the meteor wake. The introduction of a frothing ablation model in an analysis of super-Schmidt meteor data allows an interpretation in terms of originally solid meteoroids for meteors previously thought to have been produced by fragile low-density meteoroids. At the same time, the computed luminous efficiency factor, $\tau_{\rm op}$, is found to vary substantially with velocity. Above 35 km/sec the value of $\tau_{\rm op}$ is close to that recommended by Verniani. As the velocity is reduced below 25 km/sec $\tau_{\rm op}$ increases to a level about six times greater. Author

N68-33169*# National Aeronautics and Space Administration, Washington, D. C.

AEROSPACE ELECTRONIC SYSTEMS TECHNOLOGY

1967 319 p refs Briefing for Ind. Held at MIT, 3–4 May 1967 Sponsored by the Electron. Ind. Assoc.

(NASA-SP-154) GPO: HC\$1.25; CFSTI: MF\$0.65 CSCL 22A

Conference papers are presented on NASA planning and requirements for electronic systems technology, with particular reference to mission goals; earth orbital, lunar, and planetary technologies; and avionics. For individual titles see N68-33169 through N68-33189. N68-33371*# National Aeronautics and Space Administration. Ames Research Center, Moffett Field, Calif.

ANALYSIS OF LAUNCH WINDOWS FROM CIRCULAR ORBITS FOR REPRESENTATIVE MARS MISSIONS

Larry A. Manning, Byron L. Swenson, and Jerry M. Deerwester Washington Sep. 1968 61 $\,p\,$ refs

(NASA-TM-X-1651) CFSTI: HC\$3.00/MF\$0.65 CSCL 22C

Round-trip missions to Mars were investigated to define representative launch windows and associated ΔV requirements. The 1982 inbound and the 1986 outbound Venus swingby missions were selected for analysis and serve to demonstrate the influence of the characteristics of the heliocentric trajectories on the launch-window velocity requirement. The analysis investigated the use of optimum one- and two-impulse transfers, plus, a restricted three-impulse transfer employing an intermediate elliptic orbit to transfer from a circular parking orbit to the departure hyperbolic asymptote. Insertion at planet arrival was into an orbit coplanar with the arrival asymptote and any required plane change was performed during the planet departure phase. The study indicates that, with a three-impulse transfer, the ΔV penalty to provide a launch window of 20 days at Earth or 60 days at Mars is no more than 5 to 10 percent above the minimum coplanar requirement. Therefore, use in mission analyses of the coplanar ΔV requirements would not result in large errors if three-impulse transfers are acceptable. However, the results also show that the use of coplanar departure velocity requirements is not a good approximation for these launch windows with one- or two-impulse transfers. Author

N68-34086*# North American Rockwell Corp., Downey, Calif. STUDY OF TECHNOLOGY REQUIREMENTS FOR ATMOSPHERE BRAKING TO ORBIT ABOUT MARS AND VENUS. VOLUME 1: SUMMARY, JANUARY-OCTOBER 1967

E. M. Repic Washington NASA Sep. 1968 28 p refs (Contract NAS-2-4135)

(NASA-CR-1131; SD-67-994-1) CFSTI: HC \$3.00/MF \$0.65 CSCL 22C

A detailed investigation was conducted to evaluate the advantages and disadvantages of an integrated aerobraking spacecraft. Included were parameter and conceptual design studies to define the spacecraft weights and sensitivity to variations in the environmental models assumed, crew size, mission profile, propellants, etc., as well as internal packaging arrangements. A second objective was to analyze the requirements for system simulation, testing, and qualification. A typical mission profile was developed so that the various operations and systems involved in a Mars landing mission could be viewed in perspective. Figures are drawn to show schematically the mission and an inboard profile of the aerobraker vehicle. Study results showed that (1) the selected aerobraker configurations exhibit satisfactory performance and packaging characteristics and (2) there is considerable commonality between the spacecraft systems required to accomplish the Mars and Venus missions if the parking orbit eccentricity and probe payload parameters are adjusted appropriately. Significant results are discussed in relation to aerobraking vehicle requirements, configuration analysis, sensitivity analysis, and modular approach to vehicle synthesis. B.S.D.

N68-34870* National Aeronautics and Space Administration, Washington, D. C.

EXPLORING SPACE WITH A CAMERA

Edgar M. Cortright, ed. and comp. 1968 227 p

(NASA-SP-168) GPO: \$4.25 CSCL 22A

Representative space photographs from among the thousands of pictures returned to earth during the past decade comprise this volume, which is presented in sections devoted to photography above the atmosphere, to the moon and beyond, and man's venture

into space. Some of the pictures were made by man-directed cameras, while others were relayed back to earth by unmanned spacearaft. Primarily a collection representing space accomplishments of the United States, the volume also includes some photographs taken during Soviet space probes. Cloud cover, storms, and other meteorological phenomena are shown in the photographs, for which written texts are included along with comments by NASA and other scientific personnel. Surveyor and Orbiter shots of the moon include photographs of craters, mares, and other formations. Shots from various Gemini flights depict the docking of the Agena target, man's space walk, the earth's features, and space phenomena. An appendix includes details of the major spacecraft launched by the United States. M.W.R.

N68-36077*# National Aeronautics and Space Administration. Langley Research Center, Langley Station, Va.

A SEMIGRAPHICAL METHOD FOR A DEORBIT TRAJECTORY DESIGN STUDY

Richard N. Green, William F. Hampshire II, and Sue W. Souders Washington Oct. 1968 25 $\,p$

(NASA-TN-D-4801) CFSTI: HC\$3.00/MF\$0.65 CSCL 20C

A semigraphical method to aid in the selection of a deorbit trajectory which is compatible with arbitrarily selected mission constraints is presented. The method is applicable to the case where the initial orbit about the planet and the deorbit trajectory are coplanar. Basically, the method consists of examining a family of candidate trajectories and eliminating, by a graphical cross plotting technique, those which violate the mission constraints. In addition, the trade offs which exist between the various demands on the trajectory become graphically obvious. The method is flexible in that the user is free to dictate the mission mode and the mission constraints. An example illustrating the use of the method for a Mars mission is presented.

N68-36459*# National Aeronautics and Space Administration. Langley Research Center, Langley Station, Va.

SIMPLIFIED TECHNIQUE FOR DETERMINING PERICYNTHION ALTITUDE OF LUNAR ORBITS L. Keith Barker Washington Oct. 1968 15 p refs

(NASA-TN-D-4811) CFSTI: HC\$3.00/MF\$0.65 CSCL 22C

A study has been made of a simplified technique for determining the pericynthion altitude of transfer orbits from a selenocentric circular orbit at 80 nautical miles (148 160 m) to a lower altitude. The transfer orbits had pericynthion altitudes ranging from 0 to 100,000 feet (30 480 m) and radial injection velocities between ± 10 ft/sec (± 3 m/sec). The technique consisted of measuring the angle between a reference vehicle in circular orbit and the lunar horizon at two specified times. Pericynthion altitude was then determined graphically from these measurements. The effects of errors in measuring the angles, in determining the sighting times, in the circular reference orbit, and in horizon uncertainties were considered. It appears that the technique would be useful for predicting the pericynthion altitude of the transfer orbits and, if necessary, for providing information for orbit corrections.

N68-37220*# National Aeronautics and Space Administration, Washington, D. C.

NASA SPACE VEHICLE DESIGN CRITERIA (ENVIRONMENT). MODELS OF MARS ATMOSPHERE (1967) May 1968 24 p refs

(NASA-SP-8010) CFSTI: HC \$3.00 /MF \$0.65 CSCL 03B

Three models of Martian atmosphere having minimum, mean, and maximum density profiles, respectively, were generated by NASA computer programs using temperature and molecular mass distributions, surface pressure, composition, radius of the planet, and acceleration of gravity at the planetary surface as computer inputs. Equations are included for the calculation of density, pressure, speed of sound, density scale height, number density, mean free path, and viscosity. Tables give these parameters for the minimum model for geometric altitudes from 0 to 190 km; for the mean model, 0 to 390 km; and the maximum model 0 to 2500 km. K.W.R.

31 SPACE VEHICLES

Includes launch vehicles; manned space capsules; clustered and multistage rockets; satellites; sounding rockets and probes; and operating problems. For basic research see: 30 Space Sciences. For related information see also: 28 Propulsion Systems; and 32 Structural Mechanics.

N68-10192*# National Aeronautics and Space Administration. Goddard Space Flight Center, Greenbelt, Md. ENVIRONMENTAL TEST CONTRIBUTION TO SPACE-

CRAFT RELIABILITY

Kenneth R. Mercy Washington, NASA, Nov. 1967 17 p Presented at Inst. of Environ. Sci. Ann. Tech. Meeting, Washington, D. C., 11 Apr. 1967

(NASA-TN-D-4181) CFSTI: HC\$3.00/MF\$0.65 CSCL 22B

Typical problems that have a major impact on some space programs are discussed. These problems include those that involve the interdependence of equipment in a system complex. The experiences obtained in producing reliable spacecraft for several programs (Relay, Syncom, Tiros, etc.) are analyzed. The techniques used to control and appraise space programs differ and are influenced by the spacecraft design, target dates, and budget restrictions. The validity of these techniques is indicated by the results of the test programs. Problem occurrences are analyzed relative to program phase. The results of this study are discussed with regard to optimizing techniques of quality and reliability planning for space hardware. Author

N68-11476*# National Aeronautics and Space Administration. Langley Research Center, Langley Station, Va.

A SIMULATOR STUDY OF PILOT CONTROL OF REMOTE ORBITAL DOCKING OF LARGE ATTITUDE-STABILIZED COMPONENTS

Donald R. Riley and William T. Suit Washington Dec. 1967 22 p refs

(NASA-TN-D-4263) CFSTI: HC\$3.00/MF\$0.65 CSCL 22A

A brief fixed-base-simulator study has been made to determine the ability of human pilots to perform orbital docking between two spherical tanks from a manned spacecraft positioned some distance away. All three vehicles were assumed attitude stabilized. The pilot was given translational control of the manned spacecraft and of one of the remotely located tanks by means of simple on-off reaction jets. Guidance cues were obtained from two light spots, displayed on a cylindrical screen, that symbolized the two fully illuminated spherical tanks. In the simulator, docking was considered complete when the two light spots were the same size and were positioned tangent to each other directly ahead of the pilot. The results of the investigation indicated that pilots could complete remote docking with acceptable terminal conditions except for longitudinal positioning. An upper limit to the energy exchange between tanks at contact was shown by the data for the three velocity components between tanks which were found to be of small magnitude and invariant with spacecraft range. Data on the longitudinal misalinement between tanks, however, indicated that, as range of the manned spacecraft was increased above a given value, docking success decreased. Author

N68-11520*# North American Aviation, Inc., Downey, Calif. INFLUENCE OF STRUCTURE AND MATERIAL RESEARCH ON ADVANCED LAUNCH SYSTEMS' WEIGHT, PERFORMANCE, AND COST Summary Report, May 25, 1965-Jun. 30, 1967 J. A. Boddy and J. C. Mitchell Washington NASA Dec. 1967 61 p refs

(Contract NAS7-368)

(NASA-CR-974; SID-67-542-1) CFSTI: HC \$3.00/MF \$0.65 CSCL 22D

This report summarizes results of a two-phase study effort completed under a program focusing on the development of programmed assistance in directing structures research. Phase I of this program involved modifying and utilizing existing automated analytical techniques to determine significant structures and materials research areas in current and predicted future expendable launch vehicle systems. The Phase I study covers the parametric synthesis of expendable launch vehicles and a more detailed design synthesis of some of the structural components of these vehicle systems. A definition of the vehicle systems and structural synthesis of Phase I is also summarized. The Phase II effort was an extension of the design synthesis to advanced structural concepts, application to the base-line vehicle systems of Phase I and the evaluation of the relative merits to provide direction for worthwhile areas for structures and material research. Parametric vehicle synthesis was further adapted to encompass vehicle systems with recoverable first stages. The recoverable stages considered were expendable stages with recoverable features, i.e., winged body shapes with flyback propulsion and landing provisions. Author

N68-11641* National Aeronautics and Space Administration. Langely Research Center, Langley Station, Va.

INVESTIGATION OF TETHERED STATION KEEPING

James R. Williams and James J. Adams Washington Dec. 1967 31 p refs

(NASA-TN-D-4258) CFSTI: \$3.00 CSCL 22A

A method of Gemini-Agena station keeping using a connecting tether has been investigated both by analysis and by static and moving-base piloted simulations. The method involves spinning the tethered combination about its common center of mass so that tension is maintained in the cable and the vehicles remain close to each other without contact. The analytical study shows that the tethered system is inherently stable while spinning about its axis of maximum moment of inertia. The simulations indicate that pilots can perform the maneuver and can minimize fuel usage with either of the two piloting techniques studied. Author

N68-11919*# National Aeronautics and Space Administration. Langley Research Center, Langley Station, Va.

FLIGHT TEST OF A 40-FOOT-NOMINAL-DIAMETER MODIFIED RINGSAIL PARACHUTE DEPLOYED AT A MACH NUMBER OF 1.64 AND A DYNAMIC PRESSURE OF 9.1 POUNDS PER SQUARE FOOT

Clinton V. Eckstrom, Harold N. Murrow, and John S. Preisser Washington Dec. 1967 28 p refs

(NASA-TM-X-1484) CFSTI: HC\$3.00/MF\$0.65 CSCL 22B

A ringsail parachute, modified to provide a total geometric porosity of 15 percent of the reference area, was flight tested. The payload for the flight test was an instrumented capsule from which the test parachute was ejected by a deployment mortar when the system was at a Mach number of 1.64 and a dynamic pressure

31 SPACE VEHICLES

of 9.1 pounds per square foot. The parachute deployed to suspension line stretch in 0.45 second with a resulting snatch force of 1620 pounds. Canopy inflation began 0.07 second later and the parachute projected area increased slowly to a maximum of 20 percent of that expected for full inflation. Because the parachute never reached the full-open condition, the large drag force normally associated with parachute inflation did not develop. The difference in rotation between the spinning payload and the deployed canopy has normally resulted in some twisting of the payload attachment bridle and riser system. The suspension lines also twisted, primarily because the partially inflated canopy could not restrict the twisting to the attachment bridle and risers. This twisting of the suspension lines hampered canopy inflation at a time when velocity and dynamic-pressure conditions were more favorable. It is concluded that the most probable cause of the failure of the parachute to inflate properly was excessive total porosity (geometric open area and cloth permeability) in the crown area of the canopy. Author

N68-11961*# National Aeronautics and Space Administration. Langley Research Center, Langley Station, Va.

FLIGHT TEST OF A 15-FOOT-DIAMETER (4.6-METER) 120° CONICAL SPACECRAFT SIMULATING PARACHUTE DEPLOYMENT IN A MARS ATMOSPHERE

Wayne L. Darnell, Allen B. Henning, and Reginald R. Lundstrom Washington Dec. 1967 76 $p\ refs$

(NASA-TN-D-4266) CFSTI: HC\$3.00/MF\$0.65 CSCL 22B

An experiment was conducted in Earth atmosphere which simulated the deployment of an 85.3-foot-diameter (26.0-meter) ringsail parachute behind a spacecraft entering a Mars Atmosphere when at an altitude of about 18,000 feet (5.5 kilometers). The spacecraft was a 120° cone having a base diameter of 15 feet (4.6 meters) and weighing 1687 pounds (765 kilograms). It was carried to an altitude of 130,300 feet (39.7 kilometers) above the Earth by a 26,000,000-ft³ (736240-m³) balloon. After release from the balloon over the White Sands Missile Range, rockets propelled the spacecraft to a Mach number of 1.19 and a dynamic pressure of 6.4 lbf/ft² (306 N/m²). The parachute was deployed by a parachute mortar. Onboard instrumentation consisted of motion picture cameras and a tape recorder which recorded the output from accelerometers and temperature sensors. Good data were obtained from all instrumentation. The parachute, which was deployed in a reefed condition, did not have sufficient drag to withdraw the instrumented payload from the spacecraft until it was disreefed. Temperatures measured at critical points in the spacecraft were within the desired operating range. Author

N68-13797*# National Aeronautics and Space Administration. Langley Research Center, Langley Station, Va.

PERFORMANCE OF A 19.7-METER-DIAMETER DISK-GAP-BAND PARACHUTE IN A SIMULATED MARTIAN ENVIRON-MENT

Richard J. Bendura, Earle K. Huckins, III, and Lucille C. Coltrane Washington Jan. 1968 38 p refs

(NASA-TM-X-1499) CFSTI: HC\$3.00/MF\$0.65 CSCL 22B

Inflation and drag characteristics of a 64.7-foot nominal-diameter disk-gap-band parachute deployed at a Mach number of 1.59 and a dynamic pressure of 11.6 psf (555 N/m²) were obtained from the second balloon-launched flight test of the Planetary Entry Parachute Program. In addition, parachute stability characteristics during the subsonic descent portion of the test are presented. After deployment, the parachute rapidly inflated to a full condition, partially collapsed, and then reinflated to a stable configuration. After reinflation, an average drag coefficient of about 0.55 based on nominal surface area was obtained. The parachute exhibited good stability characteristics during descent. The only major damage to the parachute during the test was the tearing of two canopy panels; a loss of less than 0.5 percent of nominal surface area resulted. N68-14092*# National Aeronautics and Space Administration. Langley Research Center, Langley Station, Va.

PERFORMANCE OF A 16.6-METER-DIAMETER MODIFIED RINGSAIL PARACHUTE IN A SIMULATED MARTIAN ENVIRONMENT

Charles H. Whitlock, Allen B. Henning, and Lucille C. Coltrane Washington Jan. 1968 39 p refs Film Supplement Number L-984 is Available on Loan from NASA Langley Research Center (NASA-TM-X-1500) CFSTI: HC \$3.00/MF \$0.65 CSCL 22B

Inflation, drag, and stability characteristics of a 54.5-foot nominal-diameter (16.6-meter) modified ringsail parachute deployed in the wake of a 15-foot-diameter (4.6-meter) spacecraft traveling at a Mach number of 1.6 and a dynamic pressure equal to 11.6 psf (555 N/m²) were obtained from the third balloon-launched flight test of the Planetary Entry Parachute Program. After deployment, the parachute inflated rapidly to a full condition, partially collapsed, and reinflated to a stable configuration. After reinflation, an average drag coefficient near 0.6 based on nominal surface area was obtained. During descent, an aerodynamic trim angle was observed in a plane near several torn sails. Amplitude of the trim was approximately 15° and oscillation about trim was less than 11°. Author

N68-14638* General Motors Corp., Santa Barbara, Calif. EXPERIMENTAL INVESTIGATIONS OF SIMULATED METEOROID DAMAGE TO VARIOUS SPACECRAFT STRUCTURES

A. R. McMillan Washington NASA Jan. 1968 145 p refs (Contract NAS9-3081)

(NASA-CR-915; TR-66-67) CFSTI: \$3.00 CSCL 22B

A theoretical and experimental program has been performed to evaluate high-velocity impact damage to structures composed of two thin metallic sheets spaced some distance apart. The results of this study are applicable to the impact of meteoroids against space vehicles. A hydrodynamic treatment, combined with experiments, shows that the damage mechanisms to be considered for the second sheet are gross deformation, tensile failure, and spallation. Gross deformation and tensile failure were treated with a blast-loaded thin-shell analysis, and spallation with a two-dimensional elastic-plastic treatment. Multisheet (more than two simple sheets) structures were also analyzed and found to provide less protection within the same total structural thickness and weight than two-sheet structures. Honeycombs between the two sheets were found to be detrimental to the impact resistance of two-sheet structures. An analysis was also performed to assess the area-time of exposure for a 0.99 probability of no failure. This analysis is presented. Author

N68-14965*# National Aeronautics and Space Administration, Washington, D. C.

SCIENTIFIC SATELLITES

William R. Corliss 1967 828 p refs (NASA-SP-133) GPO: \$3.00 CSCL 22B

A detailed compilation of the equipment and instrumentation of scientific satellites is presented, along with the history, status, and objectives of satellite science. Satellite systems described include navigation, guidance and control, communication and data handling equipment, and subsystem integration. Earth-based facilities and operations are also considered. The role of satellite dynamics is assessed, and launch vehicle and satellite design data are given. Various aspects of satellite science are discussed in terms of the geophysical and solar physics instruments, biological experiments, and the experiments associated with satellite astronomy. A bibliography of engineering reports is included. B.S.D.

N68-15570*# National Aeronautics and Space Administration. Marshall Space Flight Center, Huntsville, Ala. AUTOMATION IN SATURN 1 FIRST STAGE CHECKOUT B. J. Funderburk Washington Jan. 1968 84 p refs (NASA-TN-D-4328) CFSTI: HC\$3.00/MF\$0.65 CSCL 22D The first section of the document describes the hardware and software systems that have been used for or in support of automatic vehicle checkout in the laboratory and at the Michoud assembly facility. The remaining sections summarize the test procedures and computer programs used in vehicle checkout and present some observations that have been made after a review of the automation effort. The document includes information on the checkout of the Saturn I Block I stages SA-1 through SA-4, Saturn I Block II stages SA-5 through SA-10, and the upgraded Saturn I stages SA-201 through SA-206. Author

N68-16240*# National Aeronautics and Space Administration. Langley Research Center, Langley Station, Va.

EXPERIMENTAL STABILITY AND CONTROL RESULTS AT MACH 19 OF AN ENTRY VEHICLE DESIGNED FOR AN INTERMEDIATE LIFT-DRAG RATIO

Patrick J. Johnston and Robert D. Witcofski Washington Feb. 1968 52 p refs

(NASA-TN-D-4337) CFSTI: HC\$3.00/MF\$0.65 CSCL 22A

An exploratory investigation of the longitudinal, lateral, and directional stability and control characteristics of a lifting entry vehicle was conducted at a Mach number of 19 and a Reynolds number, based on length, of 3.05×10^6 . At these conditions the boundary layer is believed to be laminar over the model. The configuration, which was characterized by a large-volume fuselage, was designed to achieve a trimmed maximum lift-drag ratio of 2.0. Realistic centers of gravity dictated by packaging studies were employed to evaluate the stability results. The effects on stability and performance of wing planform shape and size, ventral body fins, wing-tip fins, and body camber were examined. The final configuration, which included a shoulder-height wing with tip fins, achieved a trimmed maximum lift-drag ratio slightly in excess of 2.0 and was stable in pitch and sideslip over the angle-of-attack range for which it could be trimmed in pitch. Author

N68-17094*# National Aeronautics and Space Administration. Lewis Research Center, Cleveland, Ohio.

DESCRIPTION AND FLIGHT PERFORMANCE RESULTS OF THE WASP SOUNDING ROCKET

Joseph A. Yuska, James F. de Pauw, and Lowell E. Steffens Washington Feb. 1968 35 p refs

(NASA-TM-X-1518) CFSTI: HC\$3.00/MF\$0.65 CSCL 22D

A general description of the design and construction of the WASP sounding rocket and of the performance of its first flight are presented. The purpose of the flight test was to place the 862 pound (391-kg) spacecraft above 250,000 feet (76.25 km) on free fall trajectory for at least 6 minutes in order to study the effect of "weightlessness" on a slosh dynamics experiment. The WASP sounding rocket fulfilled its intended mission requirements. The sounding rocket approximately followed a nominal trajectory. The payload was in free fall above 250,000 feet (76.25 km) for 6.5 minutes and reached an apogee altitude of 134 nautical miles (248 km). Flight data including velocity, altitude, acceleration, roll rate, and angle of attack are discussed and compared to nominal performance calculations. The effect of residual burning of the second stage motor is analyzed. The flight vibration environment is presented and analyzed, including root mean square (RMS) and power spectral density analysis. Author

N68-17498*# National Aeronautics and Space Administration. Langley Research Center, Langley Station, Va. AN INVESTIGATION OF LEAKAGE OF LARGE-DIAMETER O-RING SEALS ON SPACECRAFT AIR-LOCK HATCHES Otto F. Trout, Jr. Washington Mar. 1968 38 p refs

(NASA-TN-D-4394) CFSTI: HC\$3.00/MF\$0.65 CSCL 22A

An investigation has been conducted to determine the leakage of large-diameter O-ring seals for operable hatch doors and static joints with a vacuum of 1.0×10^{-6} torr on one side and atmospheric pressure on the other. The measuring techniques employed made it possible to determine the leakage of any hatch component of an air-lock system. Tests of O-ring seals 28 to 30

inches in diameter have indicated that helium leakages of less than 1.0×10^{-5} cc/sec (STP) are attainable with butyl, viton, and neoprene elastomers for operable hatch doors and static seals. Silicone elastomeric O-rings allowed considerably greater leakages. The results indicate that the leakage of O-ring seals is sufficiently low for atmospheric containment on manned spacecraft under the conditions of this investigation.

N68-17844*# National Aeronautics and Space Administration, Washington, D. C.

SURVEYOR 5 Preliminary Report

Dec. 1967 162 p refs (NASA-SP-163) CFSTI: HC\$3.00/MF\$0.65 CSCL 22A

CONTENTS:

1. PRINCIPAL SCIENTIFIC RESULTS L. D. Jaffe, S. A. Batterson, W. E. Brown, Jr., E. M. Christensen, S. E. Dwornik et al p 1-2 (See N68-17845 08-30)

2. INTRODUCTION B. Milwitzky and S. E. Dwornik p 3-8 (See N68-17846 08-31)

3. TELEVISION OBSERVATIONS FROM SURVEYOR V E. M. Shoemaker, R. M. Batson, H. E. Holt, E. C. Morris, J. J. Rennilson et al p 9-42 refs (See N68-17847 08-31)

4. LUNAR SURFACE MECHANICAL PROPERTIES E. M. Christensen, S. A. Batterson, H. E. Benson, R. Choate, R. E. Hutton et al p 43–87 refs (See N68-17848 08-30)

5. LUNAR SURFACE TEMPERATURES AND THERMAL CHARACTERISTICS J. W. Lucas, R. R. Garipay, W. A. Hagemeyer, J. M. Saari, J. Smith et al p 89–101 refs (See N68-17849 08-30)

6. ASTRONOMY R. H. Norton, J. E. Gunn, W. C. Livingston, G. A. Newkirk, and H. Zirin p 103-105 (See N68-17850 08-30)

7. CHEMICAL ANALYSIS OF THE MOON AT SURVEYOR 5 LANDING SITE: PRELIMINARY RESULTS A. L. Turkevich, E. J. Franzgrote, and J. H. Patterson p 107–132 refs (See N68-17851 08-30)

8. LUNAR SURFACE ELECTROMAGNETIC PROPERTIES J. Negus de Wys p 133-154 (See N68-17852 08-30)

9. LUNAR THEORY AND PROCESSES D. E. Gault, J. B. Adams, R. J. Collins, J. Green, G. P. Kuiper et al p 155–156 refs (See N68-17853 08-30)

10. APPENDIX A. A STUDY OF CONTAMINATION OF SURVEYOR 5 LANDING SITE BY MAIN RETRO EXHAUST A. L. Turkevich, E. J. Franzgrote, and J. H. Patterson p 157–158 (See N68-17854 08-30)

N68-18615*# National Aeronautics and Space Administration. Langley Research Center, Langley Station, Va.

COMPUTING PROGRAM FOR AXIAL DISTRIBUTION OF AERODYNAMIC NORMAL-FORCE CHARACTERISTICS FOR AXISYMMETRIC MULTISTAGE LAUNCH VEHICLES Ragan B. Madden Washington Mar. 1968 126 p refs

(NASA TN-D-4342) CFSTI: HC \$3.00/MF \$0.65 CSCL 22D

This report describes a digital computer program which calculates the axial distribution of aerodynamic normal-force characteristics for axisymmetric, multistage launch vehicles in the linear angle-of-attack range. In calculating these characteristics for a particular configuration the program utilizes available experimental data. These data cover a wide range of Mach numbers and geometric parameters and can be readily utilized to obtain similar characteristics for most launch-vehicle configurations. Author

N68-18743*# Jet Propulsion Lab., Calif. Inst. of Tech., Pasadena. MARINER-MARS 1964 Final Project Report Washington NASA 1967 356 p. refs

(NASA-SP-139) GPO: HCS2.50; CFSTI: MFS0.65 CSCL 228

This report presents the story of the Mariner-Mars 1964 project from the time of its inception until October 1, 1965, when

31 SPACE VEHICLES

two-way communications with the spacecraft were interrupted. By this date, the objectives of the project had been completed. However, since that time, spacecraft continued to function properly and a follow on project, called Marinei 4, was established to continue operations with the spacecraft through 1966 and 1967. Plans for tracking Mariner 4 in its path around the sun and for obtaining additional telemetry data, as discussed in this report, were successfully culminated during this follow on project. Author

N68-18822*# National Aeronautics and Space Administration. Langley Research Center; Langley Station, Va.

WATER PRESSURE AND ACCELERATIONS DURING LANDING OF A DYNAMIC MODEL OF THE APOLLO SPACECRAFT WITH A DEPLOYED-HEAT-SHIELD IMPACT-ATTENUATION SYSTEM

Sandy M. Stubbs Washington Mar. 1968 48 p refs Film Supplement Number L-980 to this report is available on loan from NASA. Langley Res. Center

(NASA-TN-D-4275) CFSTI: HC\$3.00/MF\$0.65 CSCL 22B

An experimental investigation was made to determine impact water pressures, accelerations, and landing dynamics of a 1/4-scale model of the command module of the Apollo spacecraft with a deployed heat shield for impact attenuation. The landing system consisted of four vertically oriented hydraulic struts and six horizontally mounted strain straps. A scaled stiffness aft heat shield was used on the model to simulate the structural deflections of the full-scale heat shield. Landings were made at simulated vertical parachute-letdown velocities of approximately 30 ft/sec (9.1 m/sec), full scale. Horizontal velocities from 0 to 50 ft/sec (15 m/sec), full scale, were tested, and the pitch attitudes ranged from -33° to 11°. Roll attitudes were 0° and 180°, and yaw attitude was 0°.

N68-19085*# National Aeronautics and Space Administration. Langley Research Center, Langley Station, Va.

AN ANALYTICAL PROCEDURE FOR PREDICTING THE TWO-DIMENSIONAL IMPACT DYNAMICS OF SPACECRAFT LANDING GEAR

James T. Howlett Washington Mar. 1968 42 p refs

(NASA-TN-D-4434) CFSTI: HC\$3.00/MF\$0.65 CSCL 22B

This paper presents a method for analyzing the dynamic behavior of two-dimensional impacting struts and trusses of the type presently used in the construction of landing gear for lunar landing vehicles. The struts and trusses may contain shock absorbers. The method uses lumped masses to represent the system, and two-dimensional motion is assumed. The equations of motion are numerically integrated to obtain response time histories of each of the mass points, and to allow detàiled analysis of the dynamic behavior of the system. Application of the method to a particular strut and truss indicates that axial elasticity is much more important than lateral elasticity in the dynamic behavoir. The present limitation of the method is the large amount of computer time required for problems in which the time period of interest is large compared with the period of the highest natural frequency of the system. Author

N68-19226*# National Aeronautics and Space Administration. Flight Research Center, Edwards, Calif.

EVALUATION OF LATERAL-DIRECTIONAL HANDLING QUALITIES OF PILOTED REENTRY VEHICLES UTILIZING A FIXED BASE SIMULATION

Frank J. van Leynseele Washington Mar. 1968 34 p refs (NASA-TN-D-4410) CFSTI: HC\$3.00/MF\$0.65 CSCL 22B

A simulator investigation was conducted to evaluate the lateral-directional handling qualities of piloted reentry vehicles. The lateral-directional parameters were chosen to represent a sample of dynamic characteristics typical of reentry-vehicle configurations. The evaluations were made by using a three-degree-of-freedom fixed-base simulator with a pseudo-outside world visual display (contact analog). The investigation showed that the pilots preferred the ratio of the roll transfer function numerator frequency to the

Dutch roll frequency to be unity, independent of the magnitude of bank angle to sideslip angle ratio. They objected to an excessive amount of sideslip-angle excitation with ailerons when the ratio of the roll transfer function numerator frequency to the Dutch roll frequency differed from unity, the bank angle to sideslip angle ratio was low, and the yawing moment due to aileron was large. The evaluation also established that large rolling-motion excursions led to pilot miscoordination when the roll transfer function numerator frequency to Dutch roll frequency was larger than unity and the bank angle to sideslip angle ratio was large. A comparison of the results obtained with the three-degree-of-freedom contact-analog simulator and results obtained during a related study with a five-degree-of-freedom variable-stability T-33 airplane showed good correlation. Author

N68-19275*# National Aeronautics and Space Administration. Langley Research Center, Langley Station, Va.

VEHICLE ATTITUDE DETERMINATION WITH A SINGLE ONBOARD CAMERA

Richard J. Bendura, Allen B. Henning, and Robert E. Smith, Jr. Mar. 1968 27 p. refs.

(NASA-TN-D-4359) CFSTI: HC \$3.00/MF \$0.65 CSCL 17G Application of a postflight photographic method for determining the attitude history of a vehicle equipped with a single onboard camera is presented. Also included is an appendix showing the equation and geometric relationships of the method. For application, a minimum of two earth-related points need be identified on each photograph and the location of the vehicle with respect to the earth must be determined. In addition, the orientation of the camera axes system with respect to the vehicle is required. The method requires no other onboard instrumentation. The method was applied in determining the spacecraft attitude for a portion of the first flight test of the Planetary Entry Parachute Program (PEPP). The spacecraft was equipped with two relatively lightweight and inexpensive 16-mm motion picture cameras which photographed the surface of the earth. Data were obtained for altitudes ranging from 130,000 to 143,000 feet (40 to 44 kilometers). A comparison is made of the results independently obtained from each camera with ground based tracking data and with an azimuth datum point from an onboard magnetometer direction finding system. Author

N68-20198*# National Aeronautics and Space Administration. Langley Research Center, Langley Station, Va.

STRESSES CAUSED BY AN IN PLANE LINE LOAD USED TO ROTATE A THIN-WALLED SPHERICAL SATELLITE

W. Jefferson Stroud and Nancy P. Sykes Washington Apr. 1968 36 p refs

(NASA-TN-D-4425) CFSTI: HC\$3.00/MF\$0.65 CSCL 22B

The stress resultants and deformations which are brought about by a sinusoidal in-plane line load acting along a great circle of a spherical satellite of the Echo type are calculated and are presented in contour plots and in tabular form. The line load is applied in order to rotate the thin-walled spherical satellite for station-keeping purposes. The line load is induced by the interaction of a current-carrying wire with the geomagnetic field. Linear membrane theory and numerical methods are used in the analysis. Author

N68-20467*# General Dynamics Corp., San Diego, Calif. EVALUATION OF THE EFFECTS OF SPACE ENVIRONMENT EXPOSURE ON INDEX OF REFRACTION AND EXTINCTION COEFFICIENTS OF APOLLO WINDOW MATERIALS

J. T. Neu, E. J. Philbin, P. Mahadevan, and J. Compton Washington NASA Apr. 1968 112 p refs (Contract NAS9-4948)

(NASA-CR-1019; GDC-DBE-67-001) CFSTI: HC \$3.00/MF \$0.65 CSCL 20F

Temperature and radiation effects were studied on fused silica, Vycor, and aluminosilicate glass used for Apollo windows. Transmittance and index of refraction were measured as a function of wavelength at room and elevated temperatures prior to irradiation with a dosage that simulated a 30-day Apollo mission. Transmittance measurements were repeated following this exposure, and additional measurements were made with a 3-day dose equivalent and also a 0.3-day dose. For the last, no change in transmittance was observed for any of the materials. For the prolonged exposure, there is a sizeable reduction in transmittance of all three materials in the ultraviolet region and very little change in the infrared at room temperature, and transmittance is lowered in both regions at elevated temperatures. While increased optical absorption in the ultraviolet lowers transmittance, the increased absorptance of the ultraviolet bands is not sufficiently high to affect refractive index. Extinction coefficients are also tabulated as a function of temperature for these Apollo window materials. M.W.R.

N68-21260*# National Aeronautics and Space Administration. Lewis Research Center, Cleveland, Ohio.

FEASIBILITY STUDY OF OPTIMUM ON-OFF ATTITUDE CONTROL SYSTEM FOR SPACECRAFT

John D. Regetz, Jr. and Thomas M. Nelson Washington Apr. 1968 24 p

(NASA-TN-D-4519) CFSTI: HC\$3.00/MF\$0.65 CSCL 22B

Attitude control of orbiting spacecraft is generally performed in an on-off mode; no corrective thrust is provided until a preset angular error is obtained. For a given disturbance torque, the phase-plane trajectory then depends on the size of the angular impulse imparted during thrusting. For comparatively large angular impulses, the trajectory contacts both deadband limits alternately; for small impulses, the disturbance reverses the spacecraft angular rate before it can contact one side of the deadband. If the thrustor firing time is controlled, a limit cycle can be obtained in which the maximum angular excursion within the deadband is such that the spacecraft just misses contacting the opposite deadband limit. The fuel consumption is then minimum because a single-sided trajectory is maintained, and the number of thrust pulses during a given control period is minimized because the time between firings is a maximum. A single-axis control system that provides this optimum trajectory was functionally designed and investigated by simulation on an analog computer. The system calculates spacecraft angular velocity and acceleration of the deadband limit, and determines the thrustor "on" time which produces the optimum trajectory.

N68-21443*# National Aeronautics and Space Administration, Washington, D. C.

SURVEYOR 6. A PRELIMINARY REPORT

Mar. 1968 173 p refs

(NASA-SP-166) CFSTI: HC\$3.00/MF\$0.65 CSCL 22B

Preliminary results of analyses of scientific data gathered during the Surveyor VI mission are reported. Assessed are the following: television observations from Surveyor VI; lunar surface mechanical properties; lunar surface temperatures and thermal characteristics; astronomical observations; chemical analyses of the moon at the Surveyor VI landing site; electromagnetic properties (magnet test); theory and processes relating to the lunar maria; and the selenographic location of Surveyor VI. S.C.W.

N68-21758*# National Aeronautics and Space Administration. Ames Research Center, Moffett Field, Calif.

AN ANALYTICAL INVESTIGATION OF THE AERODYNAMIC AND PERFORMANCE CHARACTERISTICS OF AN UNPOWERED ROTOR ENTRY VEHICLE

Alan D. Levin and Ronald C. Smith Washington Apr. 1968 43 p refs

(NASA-TN-D-4537) CFSTI: HC\$3.00/MF\$0.65 CSCL 22B

Analysis of the aerodynamic characteristics of a rotor in autorotative flight. These characteristics have been combined with those of a capsule to study the performance characteristics of a rotor entry vehicle. Performance parameters such as range, deceleration, and heating were determined for a vehicle entering the atmosphere from earth orbit. The effects of rotor to capsule diameter ratio on the entry parameters and the effect of delaying rotor deployment on the range capability were investigated. Substantial gains in lateral range can be obtained by the addition of a rotor to a lifting capsule while maximum deceleration changes very little. The aerodynamic heating on the rotor was found to be severe enough to require possibly delaying deployment of the rotor until after the peak heating region has been passed. Delaying rotor deployment reduced the lateral range capability. Author

N68-21778*# National Aeronautics and Space Administration. Langley Research Center, Langley Station, Va.

FLIGHT TEST OF A 30-FOOT-NOMINAL-DIAMETER CROSS PARACHUTE DEPLOYED AT A MACH NUMBER OF 1.57 AND A DYNAMIC PRESSURE OF 9.7 POUNDS PER SQUARE FOOT

John S. Preisser and Clinton V. Eckstrom Washington Apr. 1968 53 p refs

(NASA-TM-X-1542) CFSTI: HC\$3.00/MF\$0.65 CSCL 22B

A 30-foot (9.1-meter) nominal-diameter cross-type parachute with a cloth area (reference area) of 709 square feet (65.9 square meters) was flight tested. The test parachute was ejected from an instrumented payload by means of a mortar when the system was at a Mach number of 1.57 and a dynamic pressure of 9.7 psf. The parachute deployed to suspension-line stretch in 0.44 second with a resulting snatch-force loading of 1100 pounds. Canopy inflation began at 0.58 second and a first full inflation was achieved at approximately 0.77 second. The maximum opening load occurred at 0.81 second and was 4255 pounds. Calculated values of axial-force coefficient during the deceleration portion of the test varied between 0.35 and 1.05, with an average value of 0.69. During descent, canopy-shape variations had reduced to small amplitudes and resultant pitch-yaw angles of the payload with respect to the local vertical averaged less than 10°. The effective drag coefficient, based on the vertical components of velocity and acceleration during system descent, was 0.78. An earlier test of a 25.2-foot nominal-diameter cross parachute is described in appendix A, along with a brief analysis of the riser-line failure suffered during the test. Author

N68-21833*# National Aeronautics and Space Administration. Langley Research Center, Langley Station, Va.

PERFORMANCE OF A 16.6-METER-DIAMETER CROSS PARACHUTE IN A SIMULATED MARTIAN ENVIRONMENT Reginald R. Lundstrom, Wayne L. Darnell, and Lucille C. Coltrane Washington Apr. 1968 38 p refs

(NASA-TM-X-1543) CFSTI: HC\$3.00/MF\$0.65 CSCL 22B

Inflation and drag characteristics of a 54.4-foot nominal-diameter cross parachute, deployed at a Mach number of 1.65 and a dynamic pressure of 12.68 lb/sq ft, were obtained from the fourth balloon-launched flight test of the planetary entry parachute program. These data as well as the stability characteristics of the parachute during subsonic descent are presented. After deployment the parachute quickly inflated to a full condition, partially collapsed, and then gradually reinflated while undergoing rapid oscillations between overinflation and underinflation. The oscillations began while the parachute was still at supersonic speeds and continued to low subsonic speeds well below an altitude of 90.000 feet. These canopy instabilities produced large cyclic variations in the parachute's drag coefficient. The average value of drag coefficient was about 0.8 to 0.9 at subsonic speeds and slightly lower at supersonic speeds. These drag coefficient values were based on the actual fabric surface area of the parachute canopy. The parachute sustained minor damage consisting of two canopy tears and abrasions and tears on the riser line. It is believed that this damage did not produce a significant change in the performance of the parachute. Author

N68-22213*# National Aeronautics and Space Administration. Manned Spacecraft Center, Houston, Tex. CHEMICALLY INDUCED IGNITION IN AIRCRAFT AND SPACECRAFT ELECTRICAL CIRCUITRY BY GLYCOL/WATER SOLUTIONS

31 SPACE VEHICLES

W. R. Downs Washington Apr. 1968 17 p refs (NASA-TN-D-4327) CFSTI: \$3.00 CSCL 22B

Electrical circuitry of military aircraft and spacecraft consists, in part, of insulated silver-covered copper wires and components. This circuitry creates a potential flammability hazard when solutions of glycol/water come in contact with either a bare or a defectively insulated wire or component carrying direct current. The hazard arises from chemical reactivity of the silver-covered copper anode in contact with glycol/water solutions. Similar reactivity does not occur with pure copper, nickel-covered copper, or tin-plated copper elements in electric circuits. Some chemical and physical properties of glycol/water fluids are presented, and glycol-induced corrosion of metals and corrosion inhibitors are discussed. A tentative chemical mechanism for the reactions of glycol/water solutions with silver wire carrying direct current is proposed.

N68-22262*# National Aeronautics and Space Administration, Washington, D. C.

RUSSIAN ROCKETRY, A HISTORICAL SURVEY

I. A. Slukhai 1968 152 p refs Transl. into ENGLISH of the publ. "Rakety i Traditsii" Moscow, Voennoe Izd. Min. Oborony SSSR, 1965 Published by Israel Program for Sci. Transl. for NASA and NSF

(NASA-TT-F-426; TT-67-51363) CFSTI: HC \$3.00/MF \$0.65 CSCL 22A

The contribution of Soviet scientists and designers to rocket technology is recounted. Pre- and post-World War 2 activities are discussed, with emphasis placed on the role of the rocketeer in the Army, Air Force, and Navy. Space exploration achievements are noted, along with the use of meteorological rockets for studying the upper layers of the atmosphere. M.G.J.

N68-22301*# National Aeronautics and Space Administration. Langley Research Center, Langley Station, Va.

DYNAMIC STABILITY OF A 4.6-METER DIAMETER 120° CONICAL SPACECRAFT AT MACH NUMBERS FROM 0.78 TO 0.48 IN A SIMULATED MARTIAN ENVIRONMENT

Charles H. Whitlock and Richard J. Bendura Washington May 1968 28 p refs

(NASA-TN-D-4558) CFSTI: HC\$3.00/MF\$0.65 CSCL 22B

Subsonic dynamic stability characteristics of the spacecraft were determined from flight data in a simulated Martian environment. The results cover a Mach number range from 0.78 to 0.48, and a Reynolds number range from 200,000 to 100,000 (based on 15-foot (4.6 meter) spacecraft diameter). Assumptions of the analysis include linear static aerodynamics and invariant dynamic stability derivative $C_{mg} + C_{m\alpha}$, with angle of attack. Reduction of the data on a cycle-by-cycle basis gives $C_{mg} + C_{m\alpha}$, values near -0.135 with an uncertainty of ± 0.105 over the range of the test. Trajectory simulation studies indicate that a reasonable simulation can be obtained by using a damping coefficient of -0.135, and that ± 0.105 is a realistic value for the accuracy limit.

N68-22742*# National Aeronautics and Space Administration. Lewis Research Center, Cleveland, Ohio.

WIND TUNNEL INVESTIGATION OF FLUCTUATING PRESSURES ON A 1/10-SCALE CENTAUR MODEL AT TRANSONIC SPEEDS

Bernard J. Blaha Washington May 1968 19 p refs

(NASA-TM-X-1574) CFSTI: HC\$3.00/MF\$0.65 CSCL 22D

Wind tunnel tests of a 1/10-scale Centaur model with a Surveyor nose cone were conducted over a range from Mach 0.55 to 1.95 to determine amplitudes and frequencies of fluctuating pressures that exist on the model surface at these speeds. Tests were conducted for roll angles of 0°, 90°, and 180° at 0° angle of attack. Peak-to-peak fluctuating pressure levels up to 30 percent of tunnel dynamic pressure were measured immediately downstream of the cone shoulder, the umbilical island, and on the boost pump fairing. Background noise in the tunnel made a detailed frequency analysis impractical. Author N68-22953*# National Aeronautics and Space Administration. Manned Spacecraft Center, Houston, Tex.

STATIC LONGITUDINAL AERODYNAMIC CHARACTERIS-TICS OF SEVERAL CONFIGURATIONS USED IN THE DEVELOPMENT OF THE LITTLE JOE 2-APOLLO TEST VE-HICLE AT MACH NUMBERS FROM 0.056 TO 4.65 Robert H. Moore, Jr. Washington May 1968 225 p refs (NASA-TN-D-4439) CFSTI: HC \$3.00/MF \$0.65 CSCL 22D

Investigations were conducted to determine the static longitudinal aerodynamic characteristics of several configurations of the Little Joe-Apollo and Little Joe II-Apollo test vehicles at angles of attack from 0° to 90° at the low-subsonic Mach numbers and at angles of attack from -15° to $+15^{\circ}$ at transonic and supersonic Mach numbers. The tests covered Mach numbers from 0.056 to 4.65. The Little Joe-Apollo configuration was unstable at the subsonic and low-supersonic speeds. Test results indicate that the production-model Little Joe II-Apollo configuration (with trailing-edge control surfaces on the booster fins) is stable throughout the Mach number range tested and that the trailing-edge control surfaces are effective for all Mach numbers tested. This configuration was used in the developmental tests of the Apollo launch escape system.

N68-23438*# Stanford Research Inst., Menlo Park, Calif. DESIGN OF GUIDANCE AND CONTROL SYSTEMS FOR OPTIMUM UTILIZATION OF INFORMATION

L. Meier, J. Peschon, B. Ho, R. Larson, and R. Dressler Washington NASA May 1968 129 p refs

(Contract NAS2-3476; SRI Proj. 5967)

(NASA-CR-997) CFSTI: HC\$3.00/MF\$0.65 CSCL 09C

A comprehensive scheme is described for designing control systems in the presence of uncertainties about initial plant state and plant parameters, disturbance inputs, and measurement poises. The method is based upon treating these random effects as perturbations on a nominal trajectory corresponding to plant operation without the random effects and with a nominal control as input. As a first approximation, the deterministic optimum is used for the nominal control, with optimal linearized estimation and control of the plant about the nominal trajectory. Next, the sensitivity of system performance to the random effects is computed; if this sensitivity is too great, then improved performance may be obtained by use of adaptive control and modification of the nominal control. If adaptive control is not used, reduced sensitivity can also be obtained by modifying the linear estimation and control in addition to the nominal control. Performance computations are accurate to terms of second degree in the perturbations. Optimization of the measurement system from two points of view is considered. Author

N68-24738*# Boeing Co., Seattle, Wash. LUNAR ORBITER 3: PHOTOGRAPHIC MISSION SUMMARY Washington NASA May 1968 117 p (Contract NAS1-3800)

(NASA-CR-1069) CFSTI: HC\$3.00 /MF\$0.65 CSCL 22B

Summary information is given on the photographic mission of Lunar Orbiter III. The primary objective of the mission was to obtain. from lunar orbit, detailed photographic information of various lunar areas, to assess their suitability as landing sites for Apollo and Surveyor spacecraft, and to improve our knowledge of the moon. The performance of each of the subsystems is discussed along with the operational performance of the spacecraft. The general design of the spacecraft is given, and launch preparation and operations are delineated. The performance and function of each of the ground stations and facilities necessary to sustain mission operations are also considered. Details are given on the photographic, lunar environmental, tracking, and performance data obtained from the spacecraft. Tabulated data are presented on a comparison of predicted and actual performance. B.S.D. N68-24945*# General Dynamics Corp., San Diego, Calif. DYNAMIC STABILITY OF SPACE VEHICLES. VOLUME 12: RE-ENTRY VEHICLE LANDING ABILITY AND CONTROL B. J. Kuchta Washington NASA May 1968 80 p refs

(Contract NAS8-11486)

(NASA-CR-946) CFSTI: HC\$3.00/MF\$0.65 CSCL 22B

The control and stability aspects of spacecraft just prior to and during touchdown are considered. The ground rules and requirements set forth for landing criteria are based upon present day knowledge. Low lift-over-drag ratio operational spacecraft with a parachute recovery system are discussed with respect to maneuverable and nonmaneuverable landing systems. A description of the Apollo re-entry and landing system is used to describe the general problem areas and constraints of a re-entry and landing system. Horizontal landing spacecraft of fixed and variable geometry are answered, and a method for evaluating landing characteristics of horizontal landing spacecraft is presented. A powered rotor and sustained-propulsive-lift system are two powered modes examined to assist powered landing spacecraft. B.S.D.

N68-24964*# National Aeronautics and Space Administration. Langley Research Center, Langley Station, Va.

AERODYNAMIC CHARACTERISTICS OF A MODIFIED CONE-CONICAL-FRUSTUM ENTRY CONFIGURATION AT MACH 6.0

George C. Ashby, Jr. and W. Frank Staylor Washington, D. C. Jun. 1968 19 p refs

(NASA-TN-D-4598) CFSTI: HC\$3.00/MF\$0.65 CSCL 228

An investigation of the internal arrangement and the stability and control of a modified cone-conical frustum entry vehicle has been conducted. The internal arrangement was made to house eight men in orbit for 24 hours and included a propulsive lift system for hover and landing. The experimental tests were conducted at Mach 6.0 and a Reynolds number based on model length of 6.3×10^{6} Trailing-edge flaps symmetrically arranged were used to trim the vehicle. The results show that the configuration is stable about all axes and can be trimmed about a center of gravity at 60 percent of the length with a maximum lift-drag ratio of 1.57 and a static margin of 3.5 percent. Calculations made by using a basic Newtonian computer program predicted the forces very well but overestimated the moments.

N68-25358 *# National Aeronautics and Space Administration. Goddard Space Flight Center, Greenbelt, Md.

LUNAR FAR-SIDE COMMUNICATION SATELLITES

P. E. Schmid Washington, D. C. Jun. 1968 23 p refs (NASA-TN-D-4509) CFSTI: HC\$3.00/MF\$0.65 CSCL 22B

This report discusses a lunar communication satellite relaying signals to and from points up to 200 km above the lunar far side surface. Two lunar satellite geometries are considered, namely, a libration point satellite anchored 65,000 km behind the moon and a 1000 km lunar orbiting relay satellite.

N68-25577*# McDonnell-Douglas Co., St. Louis, Mo.

PROJECT GEMINI: A TECHNICAL SUMMARY

P. W. Malik and G. A. Souris Washington, D. C. NASA Jun. 1968 350 p

(Contract NAS9-170)

(NASA-CR-1106) CFSTI: HC\$3.00/MF\$0.65 CSCL 228

Spacecraft and major systems, overall mission planning, and experiments are detailed for the Gemini project. Following an introduction that notes the modular design concept, presents the major objectives, and stresses safety first; the spacecraft reentry module, adapter module, and heat protection are described. The structural qualification testing and the reliability and quality assurance programs are summarized. Attention is given to the electrical, communication and tracking, rendezvous radar, digital command, and time reference systems; as well as to the instrumentation and recording, guidance and control, propulsion, environmental control, escape, and landing and recovery systems. Pyrotechnics and the crew station are also considered, as are details for the target docking adapter and the augmented target docking adapter. M.W.R.

N68-25820*# National Aeronautics and Space Administration. Langley Research Center, Langley Station, Va.

THE FABRICATION AND TESTING OF PAGEOS 1

Louis A. Teichman Washington, D. C. Jun. 1968 55 p refs (NASA-TN-D-4596) CFSTI: HC\$3.00/MF\$0.65 CSCL 22B

As an aid in assuring the successful construction and deployment of PAGEOS I, detailed fabrication process specifications were prepared and an extensive testing program was conducted. This large body of information on fabrication processes, testing techniques, and material properties is summarized herein as an indication of the present state of the art of inflatable sphere technology. Author

N68-26645*# National Aeronautics and Space Administration. Langley Research Center, Langley Station, Va.

ANALYTICAL INVESTIGATION OF EFFECTS OF PHYSICAL AND AERODYNAMIC PARAMETERS ON DYNAMIC BEHAVIOR OF PROJECT FIRE REENTRY VEHICLE Jacob H. Lichtenstein Washington Jun. 1968 57 p refs

(NASA-TM-X-1589) CFSTI: HC\$3.00/MF\$0.65 CSCL 22B

The heat-transfer characteristics of a body entering the earth's atmosphere at superorbital velocities are important in the consideration of any planetary mission. In an attempt to measure these characteristics experimentally, Project Fire was undertaken. During the design phase of the reentry vehicle, information was necessary as to whether certain physical and aerodynamic parameters would become important design considerations. Consequently, an analytical study was undertaken to evaluate the effects of these parameters on the dynamic behavior of the reentry vehicle. The results of the investigation showed that changes in most of the parameters considered, for instance, ± 21 percent in the moments of inertia and ±50 percent in the spin rate, would not affect the dynamic behavior during the main heat-measuring period (the first 40 seconds) enough to cause serious design problems. However, mass-distribution asymmetry that would displace the center of gravity 1/8 inch (0.003 meter) or more from the vehicle axis of symmetry would create angle-of-attack disturbances large enough to be significant. Author

N68-26814*# Boeing Co., Seattle, Wash.

LUNAR ORBITER 4: PHOTOGRAPHIC MISSION SUMMARY, VOLUME 1

Washington NASA Jun. 1968 126 p

(NASA-CR-1054; D2-100754-1, V. 1) CFSTI: HC \$3.00/MF \$0.65 CSCL 22B

The objectives, launch preparation, and operations of the Lunar Orbiter 4 mission are described. The primary objective was to perform a broad systematic photographic survey of lunar surface features to serve as a basis for selecting sites for more detailed scientific study by subsequent orbital and landing missions. All mission objectives were accomplished. Some of the more significant accomplishments of the mission included: (1) the first photographic mapping mission of a celestial body, other than earth, from an orbiting spacecraft; (2) photographic coverage (over 99%) of nearside of the moon of resolutions at least 10 times better than Earth-based observations: (3) the first detailed near vertical photos of the geologic formations of the Orientale basin at the western limb; and (5) photo data by which photo sites for the Lunar Orbiter 5 mission were relocated to optimize and maximize the scientific data requirements. A.L.

N68-28198*# National Aeronautics and Space Administration. Langley Research Center, Langley Station, Va.

THE EXPLORER 23 MICROMETEOROID SATELLITE. DESCRIPTION AND RESULTS FOR THE PERIOD NOVEMBER 6, 1964, THROUGH NOVEMBER 5, 1965

31 SPACE VEHICLES

Robert L. O'Neal, comp. Washington Jun. 1968 111 p refs (NASA-TN-D-4284) CFSTI: HC\$3.00/MF\$0.65 CSCL 22A

The Explorer XXIII was placed in orbit on November 6, 1964, with a perigee of 464 km and an apogee of 980 km. It carried stainless-steel pressurized penetration detectors, impact detectors, and cadmium sulfide cells to provide data on the near-earth meteoroid environment. In addition, the spacecraft was designed to provide data on the effects of the space environment on the operation of capacitor type of penetration detectors and solar-cell power supplies. The spacecraft operated satisfactorily during the 1-year design life, and the objectives of the mission were accomplished. The puncture rates obtained for stainless steel on Explorer XXIII are close to the puncture rates obtained for beryllium copper on Explorer XVI. The confidence limits include the data points obtained from Explorer XVI. A total of two counts were recorded by the capacitor-detector experiment during the 1-year reporting period. No conclusions can be reached concerning the effects of the space environment on the detector operation. The capacitor-detector monitoring circuit indicated that both detectors maintained bias voltage during the 1-year period. The counting rates on the high- and medium-sensitivity meteoroid-impact-detection systems when converted to equivalent puncture rates gave much higher averages than did the pressurized-cell puncture rates. The data from these two systems appear questionable. A meteoroid penetration model was developed, and defined for stainless steel. Author

N68-28202*# Boeing Co., Seattle, Wash.

LUNAR ORBITER 5: PHOTOGRAPHY Final Report Washington NASA Jun. 1968 229 p

(Contract NAS1-3800)

(NASA-CR-1094; D2-100755-2. V. 2) CFSTI: HC \$3.00/MF \$0.65 CSCL 22A

This Lunar Orbiter final report contains a description of Mission V planning, its conduct with respect to photography, and an evaluation of the photographic results. Data pertinent to analysis and interpretation of the photographs by the user are included. Near-vertical, convergent telephoto stereo-scopic, and oblique photography was used to obtain the desired data. Either single- or multiple-frame sequences were taken for coverage appropriate for the particular site. All photography planned for the mission was accomplished and the photographs were reconstructed. Author

N68-28379*# National Aeronautics and Space Administration, Washington, D. C.

COMMUNICATIONS SATELLITES. A CONTINUING BIBLIOGRAPHY WITH INDEXES

Jul. 1968 38 p refs

(NASA-SP-7004(04)) CFSTI: HC\$3.00/MF\$0.65 CSCL 22B

Annotated references on communications satellites are taken from the reports and journals announced in the NASA abstract journals between April and December 1967. All aspects of communications satellite theory and technology are covered in the 100 abstracts presented; and topics covered include television broadcasting, telemetry, multistation systems, economic and legal problems, and specific satellites. A subject index and a personal author index are included for the references. M.W.R.

N68-28426*# Systems Technology, Inc., Hawthorne, Calif. A STUDY OF FULLY-MANUAL AND AUGMENTED-MANUAL CONTROL SYSTEMS FOR THE SATURN 5 BOOSTER USING ANALYTICAL PILOT MODELS

H. R. Jex, G. L. Teper, D. T. Mc Ruer, and W. A. Johnson Washington NASA Jul. 1968 105 p refs

(Contract NAS2-1868-5)

(NASA-CR-1079; TR-152-1)CFSTI: HC \$3.00/MF \$0.65 CSCL 22D

The preliminary design of manual control systems for large flexible boosters of the Saturn V class was investigated by manual control systems analysis techniques. The approach employed empirically based mathematical models for the pilot mission-derived design criteria and constraints; and a set of efficient control system analysis and synthesis tools. Two roles for the pilot were studied in detail: fully-manual control and a series pilot plus stability-augmented booster. The control system characteristics evolved included the different describing functions likely to be adopted by the pilot, and the best loop structure from the criteria of simplicity, good handling qualities, wind load relief, and attention of the pilot's remnant. It was shown that fully-manual control of one axis was feasible, but that tracking performance, load relief, and handling would be poor. The augmented-manual control system included lead-double-lag pitch equalization in the inner loop, an integrating filter downstream of the pilot in the outer loops, and pilot-selected switching between trajectory and load relief control modes by shifting his attention from the attitude to the accelerometer display. Author

N68-28690*# National Aeronautics and Space Administration. Lewis Research Center, Cleveland, Ohio.

THRUST-VECTOR CONTROL REQUIREMENTS FOR LARGE LAUNCH VEHICLES WITH SOLID-PROPELLANT FIRST STAGES

Fred Teren, Kenneth I. Davidson, Janos Borsody, and Carl J. Daniele Washington Jul. 1968 49 p refs

(NASA-TN-D-4662) CFSTI: HC\$3.00/MF\$0.65 CSCL 22D

Thrust vector deflection (TVD) requirements are calculated for control of two solid-based launch vehicles—the 260-inch solid-SIVB (with a family of payload shapes and densities) and a large two-stage clustered solid vehicle (SSOPM) designed to deliver 450,000 kg of payload to orbit. TVD requirements for 99 percent wind loads were found to be 2.4° and 1.17° for 260-inch solid-SIVB and SSOPM, respectively. Requirements for other effects added about 0.35° for both vehicles. About 1° of TVD is required for control during tailoff for SSOPM. The TVD requirements for winds are reduced by using stationary basefins or movable canards. Author

N68-28891*# Boeing Co., Seattle, Wash, LUNAR ORBITER 5. PHOTOGRAPHIC MISSION SUMMARY Washington NASA Jul. 1968 157 p (Contract NAS1-3800)

(NASA-CR-1095; D2-100755-1, V. 1) CFSTI: HC \$3.00/MF \$0.65 CSCL 22B

The mission of Lunar Orbiter 5 was to provide additional photography of specific candidate Apollo landing sites to complete the NASA photographic requirements for each site. In addition, specific areas and features were to be photographed to provide data for overall lunar scientific investigation. Presented in this report is a large number of selected lunar photographs obtained on this mission, including wide angle and telephoto frames. The report also contains program objectives and descriptions; launch vehicle and spacecraft preparations and operations; mission profile; spacecraft and subsystem performances; ground system performance; spacecraft and flight path control; photographic, environmental, and tracking data; performance telemetry; and mission K.W.

N68-28997*# Boeing Co., Seattle, Wash.

LUNAR ORBITER 4. EXTENDED-MISSION SPACECRAFT OPERATIONS AND SUBSYSTEM PERFORMANCE Washington NASA Jun. 1968 107 p

(Contract NAS1-3800)

(NASA-CR-1092; D2-100754-4, V. 4) CFSTI: HC \$3.00/MF \$0.65 CSCL 22B

This volume describes the spacecraft, its mission, flight and control operations, and spacecraft performance during the extended mission. Spacecraft command activities, telemetry, and flight path control are discussed, and data are presented on radiation and micrometeoroids. The purposes and functioning of special experiments on lunar surface conductivity, voice relay, ionosphere effects, and the Manned Space Flight Network/Apollo Goss Navigational Qualification Support are stated. Spacecraft subsystem performance data and results derived from periodic monitoring of spacecraft telemetry are provided. Also given are performance data of special flight tests on gyro drift, Canopus and star tracking, traveling wave tube amplifier operation and cycling, battery discharge, antenna rotation, camera functioning, and paint degradation. K.W.

N68-29962*# National Aeronautics and Space Administration. Langley Research Center, Langley Station, Va.

EXPERIMENTAL INVESTIGATION OF THE USE OF SOFT SIDE LEGS TO IMPROVE TOUCHDOWN STABILITY OF LEGGED LANDING VEHICLES

Robert W. Herr Washington Aug. 1968 23 p refs

(NASA-TN-D-4680) CFSTI: HC\$3.00/MF\$0.65 CSCL 22B

The effectiveness of a concept to improve the landing stability of lunar-module-type vehicles has been investigated experimentally by utilizing a 1/6-scale model of an early engineering version of the lunar module. Results of landing-stability tests made with equal-force shock absorbers in all four leg assemblies are compared with results obtained with very soft shock absorbers in the side legs. This comparison indicates that landing stability can be greatly improved with the use of soft side struts if the fore and aft feet are roughly alined with the flight path at touchdown. For touchdowns at large yaw angles, the landing stability with soft side shock absorbers was at least as good as that obtained with equal-force shock absorbers. Author

N68-29993*# National Aeronautics and Space Administration. Langley Research Center, Langley Station, Va.

FLIGHT TEST OF A 40-FOOT-NOMINAL-DIAMETER DISK-GAP-BAND PARACHUTE DEPLOYED AT A MACH NUMBER OF 2.72 AND A DYNAMIC PRESSURE OF 9.7 POUNDS PER SQUARE FOOT

Clinton V. Eckstrom and John S. Preisser Washington Aug. 1968 41 p refs

(NASA-TM-X-1623) CFSTI: HC\$3.00/MF\$0.65 CSCL 22B

A 40 foot nominal diameter (12.2 meter) disk-gap-band parachute was flight tested as part of the NASA Supersonic Planetary Entry Decelerator (SPED-1) Program. The test parachute was deployed from an instrumented payload by means of a deployment mortar when the payload was at an altitude to 158,500 feet (48.2 kilometers), a Mach number of 2.72, and a free stream dynamic pressure of 9.7 pounds per foot2 (465 newtons per meter²). Suspension line stretch occurred 0.46 second after mortar firing and the resulting snatch force loading was -8.1g. The maximum acceleration experienced by the payload due to parachute opening was -27.2g at 0.50 second after the snatch force peak for a total elapsed time from mortar firing of 0.96 second. A calculated average nominal axial force coefficient ranged from about 0.25 immediately after the first canopy opening to about 0.50 as the canopy attained a steady inflated shape. Although the canopy damage caused by the deployment bag penetration had no apparent effect on the functional capability of the test parachute. it may have affected parachute performance since the average effective drag coefficient of 0.48 was 9 percent less than that of a previously tested parachute of the same configuration. Author

N68-29995*# Boeing Co., Seattle, Wash.

LUNAR ORBITER 3: EXTENDED-MISSION SPACECRAFT OPERATIONS AND SUBSYSTEM PERFORMANCE Washington NASA Jul. 1968 128 p

(Contract NAS1-3800)

(NASA-CR-1109; D2-100753-4) CFSTI: HC \$3.00/MF \$0.65 CSCL 22B

This report covers spacecraft control and flight path analysis and control operations conducted during the Lunar Orbiter 3 extended mission and discussed spacecraft performance during these operations. Complete data packages have been prepared for each experiment. The highlights of each special exercise and experiment are summarized. The primary objective of the Lunar Orbiter 3 extended mission was to secure information that may be used to increase the scientific knowledge of the size and shape of the Moon, the properties of its gravitational field, and the lunar environment. Secondary objectives were to conduct special exercises to determine the limits of spacecraft capabilities, develop standard operating procedures, conduct experiments to provide additional scientific data, and explore the use of Lunar Orbiter subsystems for other applications. Author

N68-30032*# National Aeronautics and Space Administration. Manned Spacecraft Center, Houston, Tex.

A QUASI-STEADY STATE ANALYSIS OF THE DYNAMIC BEHAVIOR OF A CONIC BODY MOVING IN A NONUNIFORM WAKE

John De Fife and Theodore F. Hughes (ITT/Federal Elec. Corp.) Washington Aug. 1968 57 p refs

(NASA-TN-D-4691) CFSTI: HC\$3.00/MF\$0.65 CSCL 22C

During reentry, the Apollo command module creates a wake of turbulent and reverse-flow conditions. When the earth-landing-system protective cover (forward heat shield) of the command module is jettisoned and moves within this wake, the kinetic energy of the cover is substantially reduced because of the reverse flows. Equations were developed which allowed vectorial additions of wake velocities to those velocities of the forward heat shield. From these resultant vectors and from wind-tunnel aerodynamic data, forces and accelerations were calculated, and trajectories were generated which indicated that the reverse flows within the wake had a significant effect on the dynamic behavior of the protective cover and therefore caused recontact for low initial separation velocities.

N68-30631*# Boeing Co., Seattle, Wash. LUNAR ORBITER 5. EXTENDED-MISSION SPACECRAFT OPERATIONS AND SUBSYSTEM PERFORMANCE NASA Aug. 1968 121 p (Contract NAS1-3800)

(NASA-CR-1142; D2-100755-4, V. 4) CSCL 22 A

The Lunar Orbiter V spacecraft was tracked from the start of its extended mission on August 28, 1967 until it was intentionally crashed into the moon's nearside on January 31, 1968. During this period, the primary objectives of selenodetic data acquisition and lunar environment sampling were accomplished by ranging, tracking, and spacecraft telemetry monitoring. Included here are also descriptions of the spacecraft's flight and guidance control systems, and data on the performance of its subsystems. Author

N68-31477*# Boeing Co., Seattle, Wash. LUNAR ORBITER 2: EXTENDED MISSION SPACECRAFT OPERATIONS AND SUBSYSTEM PERFORMANCE NASA Aug. 1968 158 p CSCL: 22B

(NAS1-3800)

(NASA-CR-1141; D2-100752-4, V. 4) CFSTI: HC \$3.00/MF \$0.65

The Lunar Orbiter II spacecraft was tracked from the start of its extended mission until it was intentionally crashed on the Moon. Following this launch, Lunar Orbiter II was used primarily for Doppler and ranging calibrations. Selenodetic data that could be used in developing a lunar gravitational model that would be more meaningful were obtained by changing the Lunar Orbiter II orbit inclination from 11.9 to 17.5 degrees at the beginning of the extended mission. Lunar environmental events of significance were proton events indicated by telemetry. Looper radiation increased 39 rads during the first event and 32.5 rads during the second. Seven micrometeoroid hits were recorded during the extended mission.

31 SPACE VEHICLES

Special tests were conducted to obtain additional data on performance characteristics of the various subsystems with the spacecraft in unique attitudes and/or environmental configurations. Author

N68-31978*# National Aeronautics and Space Administration. Goddard Space Flight Center, Greenbelt, Md.

THE DYNAMIC CHARACTERISTICS OF SATELLITES HAVING LONG ELASTIC MEMBERS

Harold P. Frisch Washington Aug. 1968 42 p refs

(NASA-TN-D-4576) CFSTI: HC\$3.00/MF\$0.65 CSCL 22B

Many satellites, such as ATS-A, ATS-D, DODGE, RAE, etc., have clamped to the surface of their central body long elastic members which when set into vibratory motion can significantly influence the motion of the central body. If such a satellite is reasonably symmetrical, we can predict its dynamic characteristics by modeling the entire satellite as a symmetric double-beam system; that is, by a rigid symmetric central body having clamped to its surface two long, diametrically opposed uniform elastic beams with tip weights possessing identical physical and geometrical properties. In this paper, dimensionless equations which define the natural modes and frequencies of such a satellite system are derived and solved. The solutions are outlined in graphical form and then used to solve the equations that describe the elastic response of the satellite to an arbitrary periodic forcing function. The results in both graphical and analytical form make it possible to predict with slide-rule accuracy the natural frequencies of any satellite that can be modeled as a symmetric double-beam system. Author

N68-33008*# Boeing Co., Seattle, Wash.

MAINTAINABILITY OF MANNED SPACECRAFT FOR LONG-DURATION FLIGHTS. VOLUME 1: SUMMARY REPORT Washington NASA Aug. 1968 57 p refs (Contract NAS2-3705)

(NASA-CR-1108; D2-113204-1) CFSTI: HC \$3.00/MF \$0.65 CSCL 22B

A 99% probability of crew survival is a basic constraint in the analysis. Spacecraft of four representative but widely varying missions, one Earth-orbital and one interplanetary each in the mid-1970 and mid-1980 time periods, are examined to the replaceable component level. Detailed maintenance analyses of subsystems and components, vehicle configuration optimizations performed with a unique computer program, and statistical results of several hundred mission simulations are described and evaluated. The effects of hardware reliability and failure rates, skills, environmental factors, mission durations and resupply potential, and various resources are considered in many interrelationships. Optimum distributions of redundant and spare items to be included on board each spacecraft configuration for assuring mission success are identified, and their implications as to operational requirements and design philosophies are discussed. Tables, charts, and graphs summarizing analytical results and displaying parametric sensitivities are provided. Gross cost estimates are also included to indicate trends and place the respective missions in context relative to each Author other.

N68-33332*# National Aeronautics and Space Administration. Lewis Research Center, Cleveland, Ohio.

ATLAS-CENTAUR FLIGHT PERFORMANCE FOR SURVEYOR MISSION B

Washington Sep. 1968 152 p refs

(NASA-TM-X-1616) CFSTI: HC\$3.00/MF\$0.65 CSCL 22D

The second operational Atlas-Centaur launch vehicle AC-7, with Surveyor SC-2, was launched on September 20, 1966. The flight profile was a direct-ascent mission to inject the Surveyor into a lunar intercept trajectory. Subsequent to injection, a vernier engine on the Surveyor failed to fire. The spacecraft tumbled out of control and failed to complete the mission. This report includes a flight performance evaluation of the Atlas-Centaur launch vehicle systems from lift-off through spacecraft separation and Centaur retromaneuver. N68-33553*# National Aeronautics and Space Administration, Washington, D. C.

SURVEYOR 7 Preliminary Report

May 1968 304 p refs

(NASA-SP-173) CFSTI: HC\$3.00/MF\$0.65 CSCL 22B

Principal scientific results are presented on the Surveyor which successfully landed on the outer rim flank of the large crater Tycho in the southern part of the moon. The extensive data obtained from television observations and measurements of the lunar surface are analyzed to determine the mechanical properties, surface temperatures and thermal characteristics, electromagnetic properties, and radar reflectivity. Details are also given on the surface sampler and the alpha scattering experiment; preliminary results of the chemical analyses of these lunar soil samples are presented. Implications of the alpha scattering experiment are discussed in relation to lunar landing sites. Postlanding tracking acquisition and analysis to determine the selenocentric location of the probe are described. The ability of earth stations to direct very narrow laser beams to a specific location on the lunar surface was B.S.D. verified.

N68-33683*# National Aeronautics and Space Administration. Lewis Research Center, Cleveland, Ohio.

SUCCESSFUL RESTART OF A CRYOGENIC UPPER-STAGE VEHICLE AFTER COASTING IN EARTH ORBIT

Kenneth W. Baud, Steven V. Szabo, Jr., Ronald W. Ruedele, and James A. Berns Washington Sep. 1968 44 p refs

(NASA-TM-X-1649) CFSTI: HC\$3.00/MF\$0.65 CSCL 22D

Successful engine restart in space of an upper stage vehicle using cryogenic propellants was accomplished for the first time with the flight of the Atlas-Centaur vehicle, AC-9. The problems unique to the restart of a vehicle using cryogenic propellants and the design concepts for solving these problems on Centaur are discussed. AC-9 flight data pertinent to the problems are also presented. Author

N68-35022*# National Aeronautics and Space Administration. Manned Spacecraft Center, Houston, Tex.

FIRST U.S. MANNED SIX-PASS ORBITAL MISSION (MERCURY-ATLAS 8, SPACECRAFT 16)

John H. Boynton, ed. Washington Sep. 1968 225 p refs (NASA-TN-D-5807) CFSTI: HC \$3.00/MF \$0.65 CSCL 22A

The results and analyses of the third U.S. manned orbital mission are presented. The mission was accomplished October 3, 1962, as a phase of Project Mercury. Spacecraft and launch-vehicle descriptions, mission operations, and postflight analyses are included. Particular treatment is given to the investigations of spacecraft systems performance and aeromedical analyses of the pilot. Author

N68-35357*# National Aeronautics and Space Administration. Lewis Research Center, Cleveland, Ohio.

PERFORMANCE EVALUATION OF ATLAS-CENTAUR RESTART CAPABILITY IN EARTH ORBIT Washington Sep. 1968 213 p refs

(NASA-TM-X-1647) CFSTI: HC\$3.00/MF\$0.65 CSCL 22D

The flight of Atlas-Centaur launch vehicle AC-9 on October 26, 1966 was the final flight in the Centaur research and development program. The vehicle carried a mass model of the Surveyor spacecraft. The mass model was boosted into a simulated lunar intercept trajectory using a parking-orbit mode of ascent. This mode of ascent placed the Centaur in a circular orbit. After coasting under low-gravity conditions, the Centaur main engines were restarted to supply energy to attain the proper simulated lunar intercept trajectory. This report includes a flight performance evaluation of the Atlas-Centaur systems for the total launch vehicle mission. Author N68-36056*# National Aeronautics and Space Administration. Ames Research Center, Moffett Field, Calif.

ENTRIES FROM EARTH ORBIT THAT SIMULATE ACCELERATION STRESSES OF MANNED PLANETARY MISSIONS

Frederick G. Edwards Washington Oct. 1968 35 p refs

(NASA-TN-D-4847) CFSTI: HC\$3.00/MF\$0.65 CSCL 22C

The ability to duplicate the acceleration stress during a portion of the earth return of a planetary mission vehicle by appropriate control of an earth orbital vehicle is investigated. The results show that during the entry of an orbital spacecraft it is possible to approximately match the accleration profile corresponding to the initial dive, the capture maneuver, and part of a constant altitude deceleration phase of a planetary mission return entry. A two-step approach to the solution is examined: the analytical step results in a closed form approximate solution for the lift control. An analog computer simulation of the entries uses results from the analytical step and gives a more precise solution for the control. It also permits an evaluation of the cost to the earth entry vehicle in terms of the aerodynamic heating, range capability, and retro velocity requirements. Emphasis is placed on simulating the planetary mission entry at twice orbital velocity, but the results also apply to entry at other supercircular velocities. An Apollo type lifting entry vehicle was used for the examples presented. Author

N68-36106*# National Aeronautics and Space Administration. Langley Research Center, Langley Station, Va.

AN EXPLORATORY STUDY OF PARALLEL STAGE SEPARATION OF REUSABLE LAUNCH VEHICLES

John P. Decker and Joseph Gera Washington Oct. 1968 62 p refs

(NASA-TN-D-4765) CFSTI: HC\$3.00/MF\$0.65 CSCL 22D

An exploratory study was made of the separation of parallel staged reusable launch vehicles. Static longitudinal aerodynamic data were obtained for a representative two stage rocket powered reusable launch vehicle concept when the stages were in close proximity to each other. The effects of vertical spacing, longitudinal spacing, and incidence angle were determined at Mach numbers 3 and 6. To identify the problems associated with mutual stage interference during the separation maneuver, the equations of longitudinal motion were numerically integrated. The calculation was carried out for a limited number of initial conditions by using a portion of the wind tunnel data along with estimated values of the dynamic derivatives. The experimental results indicated large interference increments on the static stability and normal force characteristics of both vehicle stages. The static aerodynamic data were found to be dependent on the position and attitude of the second stage, the Mach number, and the relative sizes of the two stages. The relative sizes are dependent on the launch mode, the mission requirements, and the choice of propulsion system for the launch vehicle. The trajectory results indicated a strong dependence of the dynamic derivatives, initial attitude, and dynamic pressure on the separation maneuver. Author

N68-36971*# National Aeronautics and Space Administration. Lewis Research Center, Cleveland, Ohio.

ELECTROMAGNETIC COMPATIBILITY VERIFICATION FOR THE CENTAUR AND SURVEYOR SPACE VEHICLES

John P. Quitter and J. Robert Reiss Washington Oct. 1968 42 p refs

(NASA-TM-X-1673) CSCL 22B

A series of five instrumented electromagnetic compatibility tests were performed on interface circuits between the Surveyor spacecraft and Atlas-Centaur launch vehicle. These tests were performed to verify that the spacecraft would not be susceptible to conductively induced effects from the launch vehicle and complex electromagnetic environment. Initial tests employed spacecraft and launch vehicle simulators in conjunction with their complementary vehicle. The final test was performed on completely assembled flight configuration equipment. Test results indicated the spacecraft, launch vehicle, and launch complex were compatible and that conducted interference levels were below specified limits. Numerical data are presented. Author

N68-37074*# National Aeronautics and Space Administration. Langley Research Center, Langley Station, Va.

TRANSONIC AERODYNAMIC CHARACTERISTICS OF POWERED MODELS OF SEVERAL APOLLO LAUNCH-ESCAPE VEHICLE CONFIGURATIONS

Bobby Lee Berrier and Odis C. Pendergraft, Jr. Washington Oct. 1968 43 p refs

(NASA-TN-D-4843) CFSTI: HC\$3.00/MF\$0.65 CSCL 22B

An investigation of several models of Apollo launch escape vehicle configurations was made at Mach numbers from 0.70 to 1.30. The effects of command module strakes, a flow separation device, escape rocket tower modifications, nozzle cant angle, and offset thrust vector were investigated. The escape rocket exhaust was simulated with a hydrogen peroxide rocket mounted upstream of the command module. The angle of attack range was -5° to 31°, and the average Reynolds number based on the maximum command module diameter was 4.34×106 at a Mach number of 0.90. The results of the investigation indicate that axial force (drag) was decreased because of favorable jet interference by adding strakes to the command module, by using a ring attachment type of escape rocket tower, or by increasing nozzle cant angle. Author

N68-37900*# Astro Research Corp., Santa Barbara, Calif. LARGE LOW-FREQUENCY ORBITING RADIO TELESCOPE Hans U. Schuerch and John M. Hedgepeth Washington NASA Oct. 1968 56 p 10 refs

(Contract NAS7-426)

(NASA-CR-1201; ARC-R-282) CFSTI: HC \$3.00/MF \$0.65 CSCL 22B

Studies have been performed of the feasibility of a large (1500-meter) orbiting paraboloidal antenna for use in low-frequency (< 10 MHz) radio astronomy. Such a radio telescope would be extremely useful in a variety of scientific astronomical studies. A conceptual configuration has been evolved which consists of a tenuous conductive paraboloidal network which is deployed and stiffened by centrifugal forces due to spin about the axis of symmetry. Meridional tension forces are produced in the net by means of an extremely long deployable mast which runs along the axis of symmetry and forms the backbone of the structure. The entire configuration is deployed from a package suitable for launch on such vehicles as the Titan III. Results of the various theoretical and experimental analyses which have led to this baseline concept are summarized.

N68-37942*# National Aeronautics and Space Administration. Lewis Research Center, Cleveland, Ohio.

EXPERIMENTAL LONGITUDINAL DYNAMICS OF AN EMPTY STUB D ATLAS VEHICLE

William G. Costakis and Carl F. Lorenzo Washington Nov. 1968 56 p refs

(NASA-TM-X-1682) CFSTI: HC \$3.00/MF \$0.65 CSCL 22D

A test was conducted to determine the longitudinal dynamic characteristics of the Stub D Atlas without propellants or payload. The dynamic characteristics obtained are given in terms of modal damping ratios, vehicle mode shapes, and acceleration responses to a force input over the frequency range of 1 to 120 Hz. Natural frequencies were determined by comparing the acceleration response results with the mode shape and orthogonality test results. The results showed that a one-dimensional model may not be sufficient to predict the behavior of the vehicle. Author

STRUCTURAL MECHANICS

Includes structural element design and weight analysis; fatigue; thermal stress; impact phenomena; vibration; flutter; inflatable structures; and structural tests. For related information see also: 17 Materials, Metallic; and 18 Materials, Nonmetallic.

N68-10231*# General Dynamics Corp., San Diego, Calif. DYNAMIC STABILITY OF SPACE VEHICLES. VOLUME I: LATERAL VIBRATION MODES G. B. Paddock Washington NASA Nov. 1967 86 p refs

(Contract NAS8-11486)

(NASA-CR-935; GD/C-DDF-65-001) CFSTI: HC \$3.00/MF \$0.65 CSCL 20K

The lateral model development and modal calculations for a cylindrical space vehicle system and systems using clustered tanks are discussed along with the relative importance of physical characteristics and methods used to solve modal parameters. Emphasis is given to parameters important in control and stability analyses for which the system frequency of interest is generally below 20 cycles/second and guite often below 10 cycles/second. The general approach for dynamic solutions of these large systems is to develop a mathematical model describing the system's mass and structure, to calculate its normal modes of vibration, and, using normal mode theory, to apply the external forces and couple in the control system to obtain total response. The space vehicle in the lateral direction is represented by a series of lumped masses connected by elastic beams. By successive refinements, such as branch beams to include multiple load paths, concentrated masses attached to the beam by translational and rotational springs, or other possible independent structures or components, the model can simulate all significant motions. R.N.A.

N68-10233*# General Dynamics Corp., San Diego, Calif. DYNAMIC STABILITY OF SPACE VEHICLES. VOLUME IX: THE EFFECT OF LIFTOFF DYNAMICS ON LAUNCH VEHICLE STABILITY AND CONTROL

L. C. Engbrenghof Washington NASA Nov. 1967 30 p refs (Contract NAS8-11486)

(NASA-CR-943; GD/C-BTD-67-031) CFSTI: HC \$3.00/MF \$0.65 CSCL 20K

The analysis of liftoff dynamics concerns both rigid body and elastic motions of a rocket vehicle in the vicinity of the launch site. The analysis begins at engine ignition and ends when the vehicle clears all launch site facilities. Engine thrust, winds, launcher restraints, umbilical disconnects, and ducts are the forcing functions for the elastic and rigid body motions. Liftoff dynamics are analyzed to evaluate the possibility of a launching mishap. and to attain the highest value of launch availability (ratio of safe launch days over days in a given period) based on ground wind restrictions. The airborne system parameter variations used to solve liftoff dynamics problems include flight control system activation time, engine thrust vector angular alignment at liftoff, engine ignition sequence, and thrust buildup time histories. Launch site parameter variations used to solve liftoff dynamics problems include removal of nonessential hardware that might offer a flight path constraint, specification of acceptable retraction times for umbilical booms and other moving parts, and specification of force-time histories of launcher constraints. R.N.A.

N68-10280*# General Dynamics Corp., San Diego, Calif. DYNAMIC STABILITY OF SPACE VEHICLES. VOLUME II: DETERMINATION OF LONGITUDINAL VIBRATION MODES J. A. Staley Washington NASA Nov. 1967 65 p refs (Contract NAS8-11486) (NASA-CR-936; GD/C-BTD-67-053) CFSTI: HC \$3.00/MF \$0.65

(NASA-CR-936; GD/C-BTD-67-053) CFSTI: HC \$3.00/MF \$0.65 CSCL 22D

Elastic longitudinal models of multistage liquid and solid propellant vehicles, and vehicles with clustered tanks, are discussed, and methods are described for determining the dynamic characteristics needed for analyzing vehicle response and stability. The longitudinal model is considered to provide a mathematical representation of the real physical system, and the dynamic characteristics are determined from the mass, stiffness, and dynamic matrices. The equations for solution are formulated. The problems to be analyzed using longitudinal models include response to engine ignition and shutdown transients, release of a vehicle from its launcher, and the stability of engine-structure coupled oscillations. A second stability problem peculiar to liquid propellant vehicles with thin-skinned tanks involves coupling between structural motions and the tank pressure regulation system. It is pointed out that each of these problems may require different emphasis on details of the model used. M.G.J.

N68-10407*# Israel Program for Scientific Translations, Ltd., Jerusalem.

RIB-REINFORCED PLATES AND SHELLS

G. N. Savin and N. P. Fleishman 1967 342 p refs Transl. into ENGLISH of the Publ. "Plastinki i Obolochki s Rebrami Zhestkosti" Kiev, Nauk. Dumka, 1964 Prepared for NASA and NSF

(NASA-TT-F-427; TT-67-51364) CFSTI: HC \$3.00/MF \$0.65 CSCL 20K

Theoretical and analytical data are presented on the stress concentrations in plates and shells reinforced by stiffening ribs. The general theory of bending of thin plates is reviewed, and the fundamental differential equation and representation of the general solution are given. Detailed consideration is given to such problems as bending of thin plates reinforced by curved stiffening ribs; bending of thin plates with reinforced edges; plates reinforced by very thin ribs; inverse problems of plates with holes whose edges are reinforced by thin ribs; and shells with stiffening ribs. The most important results referring to the interaction between stiffening ribs and plates or shells are given as simple formulas, graphs, and tables. The data provided are discussed from the viewpoint of efficient design of the reinforcing elements, and the optimum structure of thin plates and shells with ribs. M.G.J.

N68-10568*# General Dynamics Corp., San Diego, Calif.

DYNAMIC STABILITY OF SPACE VEHICLES. VOLUME III: TORSIONAL VIBRATION MODES

R. Gieseke, R. Schuett, and D. Lukens Washington NASA Nov. 1967 63 p refs

(Contract NAS8-11486)

(NASA-CR-937; GD/C-DDF65-003, Vol. III) CFSTI: HC \$3.00/MF \$0.65 CSCL 22B

This monograph discusses the torsional model development and modal calculations for the cylindrical space vehicle system and also systems employing clustered tanks. Relative importance of physical characteristics is discussed as well as methods used by the industry for the solution of modal parameters. Primary attention

32 STRUCTURAL MECHANICS

is focused on parameters important in control and stability analyses for which the system frequency is generally below twenty cycles per second and quite often below ten cycles per second. Application for loads analysis follows the same principles outlined herein but may require more detailed representation in areas where loads or deflections can be critical. The models described are concerned with gross vehicle torsional motions and do not include the shell tangential deflection modes which do not contribute to gross vehicle control and stability. Related monographs describe lateral, longitudinal, and sloshing models. Stability and loads analytical methods using these models and modal parameters are also subjects of other monographs.

N68-10574*# General Dynamics Corp., San Diego, Calif. DYNAMIC STABILITY OF SPACE VEHICLES. VOLUME IV: FULL SCALE TESTING FOR FLIGHT CONTROL PARAMETERS

David R. Lukens Washington NASA Nov. 1967 50 p refs (Contract NAS8-11486)

(NASA-CR-938; GDC-BTD-67-049) CFSTI: HC \$3.00/MF \$0.65 CSCL 22B

This monograph on flight control testing is primarily concerned with the major thrust vector control system and its principal components. The types of data that can be determined from full-scale tests are: frequency response, deadbands, friction, nonlinearities, limits, and the effect of structural resonances. Control system test data are required because the response characteristics of the flight control system are influenced by the total system. Most flight control systems are sufficiently complicated and responsive as to require tests to verify performance. The underlying basis for all first-of-a-kind launch vehicle flight readiness assertions must be analytical in nature. The only reason that an analytical stability derivation can be used is based on the premise that the analytical model used in analysis and synthesis can be verified by tests. This requires that the flight control system be analyzed for several test configurations and that agreement between model and test be obtained for each configuration. Then and only then can the final design verification be performed with confidence. Author

N68-11054* General Dynamics Corp., San Diego, Calif. DYNAMIC STABILITY OF SPACE VEHICLES. VOLUME 6: FULL SCALE DYNAMIC TESTING FOR MODE DETERMINATION

D. R. Lukens, R. L. Turney, R. L. Fefferman, J. W. Kittle, and T. E. Reed Washington NASA Dec. 1967 62 p refs (Contract NAS8-11486)

(NASA-CR-940) CFSTI: \$3.00 CSCL 22B

This monograph discusses the concepts, techniques, and problems associated with full-scale dynamic test programs of large booster vehicles, both solid and liquid fueled. This discussion is aimed toward the measurement of the elastic modes that can affect control system analysis. It includes definitions of various excitation systems, suspension systems, mounting systems, instrumentation, data reduction methods, problem areas, and test planning. Author

N68-11089*# General Dynamics Corp., San Diego, Calif. DYNAMIC STABILITY OF SPACE VEHICLES. VOLUME 8: ATMOSPHERIC DISTURBANCES THAT AFFECT FLIGHT CONTROL ANALYSIS

B. A. Appleby and T. E. Reed Washington NASA Nov. 1967 40 p refs

(Contract NAS8-11486)

(NASA-CR-942; GD/C-BTD-67-057, V. 8) CFSTI: HC \$3.00/MF \$0.65 CSCL 22B

The exit phase of flight must, by definition, originate on or near the earth's surface and terminate at some point in space, which will be above the sensible atmosphere. Therefore, all or part of the exit phase of flight occurs in the sensible atmosphere. The

analysis of space vehicle systems for this phase of flight must necessarily include the effect of the atmosphere upon the launch vehicle. The atmosphere is non-stationary with respect to the earth's surface and its properties (e.g., density and temperature) vary with respect to time and altitude. These deviations of the non-stationary atmosphere from the stationary position are termed atmospheric disturbances. This monograph is concerned with data on atmospheric disturbances, the criteria derived from the data, and the analyses to be performed to determine the vehicle and control system response to atmospheric disturbances. Specifically excluded from the monograph are the methods of determining loads on the space vehicle structure and the details of analyses. The loads on space vehicle structures, while of great significance, are adequately covered in other literature. The details of analyses are covered in another monograph. The intent here is to discuss what analyses are to be performed and what atmospheric disturbances are to be used, not to present methods of analysis. Author

N68-11133*# General Dynamics Corp., San Diego, Calif. DYNAMIC STABILITY OF SPACE VEHICLES. VOLUME 11: ENTRY DISTURBANCE AND CONTROL

F. D. Steketee Washington NASA Nov. 1967 61 p refs

(Contract NAS8-11486) (NASA-CR-945; GD/C-BTD-67-023, V. 11) CFSTI: \$3.00/MF \$0.65 CSCL 22B

This monograph is divided into three basic sections. The first discusses handling qualities, disturbances, and re-entry corridor boundaries. These subjects define the required vehicle/control system characteristics and are considered as design criteria. The second section describes present state-of-the-art control systems for the fixed- and variable-lift vehicles and contains material on possible problem areas as well as a discussion of some new experimental control techniques. The purpose of this second section is to illustrate how re-entry control systems are currently being designed and to point out some of the problem areas that the designer should be aware of. The third section develops the small perturbation equations that are required for the analysis/synthesis problem. This section also expands the pitch mode equation to include density as an exponential function of altitude.

N68-11191*# Allied Research Associates, Inc., Concord, Mass. STRUCTURAL DESIGN SYNTHESIS APPROACH TO FILAMENTARY COMPOSITES

George Gerard and C. Lakshmikantham Washington NASA Nov. 1967 40 p refs

(Contract NASw-1378)

(NASA-CR-964; ARA-327-6) CFSTI: HC \$3.00/MF \$0.65 CSCL 20K

Developments of analysis methods for filamentary composites are discussed. Theoretical predictions of the stiffness and strength properties of a unidirectional composite based on a knowledge of the constituent properties are correlated with experiments for both tensile and compressive loadings. The analysis of multilayer or laminated composites based upon the unidirectional composite properties then requires the rather straightforward use of classical anisotropic shell theory. Some structural aspects of filamentary composites designed for biaxial loads are considered. In particular, certain design restrictions inherent in the use of such composites become evident when compared with the more familiar isotropic sheet. Some of these restrictions can be overcome by a close matching of filament orientations and stress field. These factors serve to emphasize the overwhelming importance of creative structural concepts in the design of successful filamentary composites. Author

N68-11282*# Allied Research Associates, Inc., Concord, Mass. MINIMUM WEIGHT DESIGN ASPECTS OF STIFFENED CYLINDERS UNDER COMPRESSION C. Lakshmikantham and H. Becker Washington NASA Nov. 1967 20 p refs

(Contract NASw-1378)

(NASA-CR-963; ARA-327-5) CFSTI: HC \$3.00/MF \$0.65 CSCL 20K

The effects of minimum weight design on structural stability are reviewed based on a literature survey. The influence of stiffener eccentricity and location on minimum weight design of stiffened cylinders is emphasized. Expressions are cited for determining the critical stress associated with local instabilities of a deep stiffened cylinder; and a governing equation for the general instability of deep-stiffened cylinders is considered. Tables summarize theoretical and experimental data on the effect of stiffener location on the critical stress. The importance of stiffener location is further examined in a comparison of the efficiencies of symmetrical and asymmetrical designs. E.C.

N68-11356*# National Aeronautics and Space Administration. Langley Research Center, Langley Station, Va.

BALLISTIC LIMIT OF ALUMINUM PLATES DETERMINED BY AN EXPLODING FOIL GUN TECHNIQUE

Emilio Alfaro-Bou and Robert G. Thomson Washington Dec. 1967 17 p refs

(NASA-TN-D-4259) CFSTI: HC\$3.00/MF\$0.65 CSCL 20K

An understanding of the perforation of finite-thickness plates is essential to the proper design of spacecraft to insure protection from meteoroid impact. An investigation was therefore initiated to determine the ballistic limits of finite-thickness plates and to compare these results with existing theoretical predictions. The impact of meteoroids on thin aluminum plates is simulated in an exploding foil gun facility. The exploding foil gun can fire a large number of shots in a relatively short time with a range of projectile velocities from 1 to 8 km/s. The exploding foil gun facility is used in an experimental program to determine the ballistic limits of aluminum plates of varying thickness. The information gathered from this experimental program indicates that the ballistic limit is linearly dependent on the plate thickness and the experimental data correlate well with the theory of ballistic limit developed from a visco-plastic model. Hence, the current practice of using semi-infinite penetration data in predicting the ballistic limits of thin plates is incorrect. Author

N68-11485*# General Dynamics Corp., San Diego, Calif. DYNAMIC STABILITY OF SPACE VEHICLES. VOLUME 5: IMPEDANCE TESTING FOR FLIGHT CONTROL PARAMETERS

David R. Lukens Washington NASA Dec. 1967 27 p refs (Contract NAS8-11486)

(NASA-CR-939; GD/C-BTD-67-045) CFSTI: HC \$3.00/MF \$0.65 CSCL 20K

Ways of determining equivalent rates that describe the local flexibility of launch vehicle control system structures and their mounting and associated brackets are presented. Recommended practices are enumerated and include impedance methods, typical forms of the impedance plot, determination of mechanical impedance by test, force and motion requirements, instrumentation requirements, use of impedance in stability and control analysis, and simulation of equivalent systems. It is noted that these spring rates and impedance techniques used to determine them may also be used to evaluate motions for clearance and environmental studies. C.T.C.

N68-11489*# Bolt, Beranek, and Newman, Inc., Cambridge, Mass. PANEL LOSS FACTORS DUE TO GAS-PUMPING AT STRUCTURAL JOINTS G. Maidanik and E. E. Ungar Washington NASA Nov. 1967 62 p refs

(Contract NAS5-9694)

(NASA-CR-954; Rept.-1475) CFSTI: HC \$3.00/MF \$0.65 CSCL 13M

The recently observed fact that the high-frequency structural damping due to riveted joints is associated with "gas-pumping" in the space between overlapping surfaces is subjected to theoretical and experimental study. A theory is developed, which attributes the damping of plates with riveted-on beams to viscous losses associated with the tangential gas motions in the beam-plate interspace that are generated by normal relative motions of the adjacent beam and plate surfaces. Reasonable agreement is found between theoretical predictions and experimental data obtained for three different gases over a wide range of pressures. Author

N68-11967*# North Carolina State Coll., Raleigh. MODAL DENSITY OF THIN CIRCULAR CYLINDERS David K. Miller and Franklin D. Hart Washington NASA Dec. 1967 66 p refs

(Grant NGR-34-002-035) •

(NASA-CR-897) CFSTI: HC\$3.00/MF\$0.65 CSCL 20M

A combined analytical and experimental study is made of the modal density of a thin cylindrical shell. Previous analytical work is discussed and an integral form solution is presented and evaluated numerically. Having cognizance of the experimental results, it is concluded that the integral form solution gives an accurate method for computing the cumulative number of resonant modes and the modal density of a thin cylindrical shell. Author

N68-12370*# National Aeronautics and Space Administration. Lewis Research Center, Cleveland, Ohio.

STRUCTURAL FEASIBILITY STUDY OF PRESSURIZED TANKS FOR LIQUID-METHANE FUELED SUPERSONIC AIRCRAFT

Rene E. Chambellan, Joseph F. Lubomski, and William A. Bevevino Washington Dec. 1967 48 p refs

(NASA-TN-D-4295) CFSTI: HC\$3.00/MF\$0.65 CSCL 20K

Light-weight pressurized tanks for the storage of liquid-methane fuel in the wings of supersonic transport aircraft were evaluated. Three types of tank structures were studied: (1) membrane tanks where the only loads in the tank skin are tensile, (2) modified semimonocoque tanks composed of a framework of rings and stringers covered by a pressure-tight skin, and (3) filamentary restrained membrane tanks where the outer skins of either metal or sealed fabric are restrained by wires or threads attached to the opposite skin. A typical wing void space having an approximately rectangular prismoidal shape was assumed as a tank envelope. The various tank designs were compared by the use of two numerical ratios, namely, the volumetric efficiency and tank-weight to contained-fuel-weight ratio. Volumetric efficiency is defined as the ratio of the volume of fuel stored in the tank to the storage void volume into which the tank is fitted. For the designs considered, exclusive of insulation, volumetric efficiencies ranged from 81.1 to 99.6 percent and tank-weight to contained-fuel-weight ratios ranged from 0.0241 to 0.0556. Author

N68-12864*# National Aeronautics and Space Administration. Langley Research Center, Langley Station, Va.

NONLINEAR FLUTTER OF A CIRCULAR CYLINDRICAL SHELL IN SUPERSONIC FLOW

David A. Evensen and Mervyn D. Olson (Natl. Aeron, Estab.) Washington Dec. 1967 30 p refs Prepared by National Research Council of Canada

(NASA-TN-D-4265; NRC-LR-486) CFSTI: HC \$3.00/MF \$0.65 CSCL 20K

32 STRUCTURAL MECHANICS

A nonlinear analysis is presented for calculating the limiting amplitudes of cylindrical shell flutter by using a four-mode approximation for the shell deflection. The aerodynamic pressure is approximated by linear piston theory, and the nonlinearity enters the problem through the nonlinear shallow-shell equations for the cylinder. The governing equations are reduced to four modal equations by applying Galerkin's method, and limit cycle solutions are obtained by the method of harmonic balance. Stability of the limit cycles is investigated numerically by integrating the modal equations on a digital computer. Two types of limit cycle flutter are obtained: two-mode standing-wave flutter, and four-mode circumferentially traveling-wave flutter. Under most conditions, the two-mode standing-wave flutter becomes unstable and transforms into four-mode traveling-wave flutter. The analysis indicates that flutter can occur at aerodynamic pressures below the linear flutter boundary. This fact may explain why recent results indicate a difference between experiments and linear theory for the flutter of cylindrical shells. Author

N68-14091*# National Aeronautics and Space Administration. Langley Research Center, Langley Station, Va.

INFLUENCE OF DISCRETE RING STIFFENERS AND PREBUCKLING DEFORMATIONS ON THE BUCKLING OF ECCENTRICALLY STIFFENED ORTHOTROPIC CYLINDERS David L. Block Washington Jan. 1958 70 p refs

(NASA-TN-D-4283) CFSTI: HC\$3.00/MF\$0.65 CSCL 20K

The buckling of eccentrically stiffened perfect orthotropic cylinders is the subject of an analytical investigation in which prebuckling deformations and the influence of discretely located ring stiffeners are taken into account. By using energy principles, nonlinear prebuckling equations and linear buckling equations are derived. Solutions for simply supported and clamped boundary conditions and for loadings of axial compression and internal or external pressure are obtained by the method of finite differences and a modified Gaussian elimination technique. Computed results for two types of simply supported large-diameter stiffened cylinders loaded in axial compression illustrate the influence on the buckling load of prebuckling deformations, discrete rings, and eccentricity of applied axial compressive loads; results for clamped longitudinally stiffened cylinders are compared with previous test results. The results show that the predicted buckling load may be substantially affected by consideration of prebuckling deformations, eccentric loading, and discreteness of rings and that agreement with experiment may be improved by including these factors. Author

N68-14584* Dynamic Science Corp., Monrovia, Calif. A GEOMETRICALLY NONLINEAR ANALYSIS OF ARBITRARILY LOADED SHELLS OF REVOLUTION R. E. Ball Washington NASA Jan. 1968 218 p refs (Contract NAS1-5804)

(NASA-CR-909) CFSTI: \$3.00 CSCL 20K

A digital computer program for the geometrically nonlinear analysis of thin elastic shells of revolution subjected to arbitrary load and temperature distributions was developed to predict snap buckling of spacecraft shell structures due to asymmetric loads such as those imposed by reentry flow or landing impact. The analysis was based upon Sanders' nonlinear shell theory for the condition of small strains and moderately small rotations. The nonlinear partial differential equations are reduced to a sequence of linearized uncoupled ordinary differential equations by expanding the variables into Fourier series in the circumferential direction, and treating the nonlinear terms as pseudo loads. The linearized equations are repeatedly solved, using a finite difference formulation in conjunction with a Gaussian elimination procedure, until the solution converges. N68-14640*# National Aeronautics and Space Administration. Langley Research Center, Langley Station, Va.

PLASTIC BEHAVIOR OF CIRCULAR PLATES UNDER TRANSVERSE IMPULSE LOADINGS OF GAUSSIAN DISTRIBUTION

Robert G. Thomson Washington Jan. 1968 33 p refs (NASA-TR-R-279) CFSTI: HC\$3.00/MF\$0.65 CSCL 20K

An analytical study of the plastic response of a circular plate of uniform thickness subjected to a normal axisymmetric impulse of Gaussian distribution is presented. The Gaussian impulse loading is assumed initially to impart a momentum to the plate. The plate is thereafter prescribed as free from external loads. The kinetic energy of motion is assumed to be dissipated in plastic deformation. The radial and circumferential strain and strain-rate distributions of the plastically deforming plate are determined as a function of time and space from derived deflection expressions. Only the bending action of the plate is taken into account and the plate material is assumed to behave as a perfectly plastic-rigid continuum. The possibility of a fracture or separation of the plate material occurring during deformation is discussed. Maximum values of strain and strain rate are shown to occur in the circumferential components, and a mode of failure by radial fractures is indicated. Author

N68-15476*# Boeing Co., Renton, Wash. FATIGUE-CRACK PROPAGATION AND FRACTURE-TOUGH-NESS CHARACTERISTICS OF 7079 ALUMINUM-ALLOY SHEETS AND PLATES IN THREE AGED CONDITIONS

S. H. Smith, T. R. Porter, and W. D. Sump Washington NASA Feb. 1968 96 p refs

(Contract NAS1-6474)

(NASA-CR-996) CFSTI: HC\$3.00/MF\$0.65 CSCL 11F

Tensile property, fatigue crack propagation, and fracture toughness tests were conducted to determine the effects of aging temperature and time, material thickness, specimen width, and configuration and physical environments of dry air, liquid nitrogen (-65°F), and distilled water on these properties. Residual strength characteristics were determined with surface-flawed specimens; precracked Charpy impact toughness tests also were conducted. The results showed that 7079 peak-age material has a faster rate of fatique crack growth and a lower fracture toughness and residual strength than underaged and overaged materials. Underaged material exhibited the greatest fracture toughness and essentially the same rate of fatigue crack growth as that of overaged material. A slower fatigue crack growth rate was found for a decrease in plate thickness, an increase in panel width, a dry-air environment compared to distilled water, and a -65°F temperature. High fracture toughness and residual strength values were found for a decrease in plate thickness, an increase in panel width, a longitudinal grain direction, and an increase from $-65^{\circ}F$ to room temperature. Author

N68-15769*# National Aeronautics and Space Administration. Lewis Research Center, Cleveland, Ohio.

ELASTOPLASTIC ANALYSIS OF CIRCULAR CYLINDRICAL INCLUSION IN UNIFORMLY STRESSED INFINITE HOMOGENEOUS MATRIX

Alexander Mendelson Washington Jan. 1968 24 p refs (NASA-TN-D-4350) CFSTI: HC\$3.00/MF\$0.65 CSCL 20K

Equations have been derived and a method has been presented for performing an elastoplastic analysis of a system consisting of a circular cylindrical inclusion in a homogeneous matrix uniformly stressed at infinity and in a condition of generalized plane strain. The material properties of the inclusion and the matrix, including their stress-strain curves are assumed to be arbitrary and independent of each other. Several examples, including the limiting cases of a hole and a rigid inclusion, are presented. It is shown that the constraints imposed by the rigid inclusion sharply reduce both the stress and strain concentration factors over those for the hole. The

32 STRUCTURAL MECHANICS

results for a system roughly approximating a graphite fiber in a resin matrix indicate that the fiber acts nearly as a rigid inclusion and that strain hardening properties of the matrix play only a minor role in determining the plastic strain concentration factor for the case of plane strain. Author

N68-15796*# Scientific Translation Service, La Canada, Calif. COMPUTATIONS OF ELASTIC TENSOMETRIC ELEMENTS G. F. Malikov, A. L. Shneyderman, and A. M. Shulemovich Washington NASA Feb. 1968 182 p refs Transl. into ENGLISH of the book "Raschety Uprugikh Tenzometricheskikh Elementov" Moscow. Mashinostr., 1964

(Contract NASw-1496)

(NASA-TT-F-513) CFSTI: HC \$3.00/MF \$0.65 CSCL 20K

The calculations for present-day elastic tensometric elements, and present methods for utilizing them are presented. Along with calculations for strength and rigidity, the problems of determining the nonlinearity of certain elastic elements are examined. Great attention is devoted to the use of statistical methods for experimentally determining several parameters characterizing the meterological properties of elastic elements. Author

N68-17045*# National Aeronautics and Space Administration. Lewis Research Center, Cleveland, Ohio.

ELASTIC-PLASTIC TORSION PROBLEM FOR STRAIN-HARDENING MATERIALS

Alexander Mendelson Washington Feb. 1968 23 p refs (NASA-TN-D-4391) CFSTI: HC\$3.00/MF\$0.65 CSCL 20K

A simple and straightforward procedure is presented for solving the elastic-plastic problem for the torsion of a solid prismatic bar made of a strain-hardening material. The procedure is based on the method of successive elastic solutions or successive approximations. For circular cross sections, the problem reduces to the solution of a nonlinear algebraic equation. For the case of a circular cross section with linear strain hardening, the solution is obtained in closed form. Results are presented for bars of rectangular and circular cross sections with linear strain hardening. Author

N68-17068*# National Aeronautics and Space Administration. Langley Research Center, Langley Station, Va.

ACCURACY STUDY OF FINITE DIFFERENCE METHODS

Nancy Jane Cyrus and Robert E. Fulton Washington Jan. 1968 29 p refs

(NASA-TN-D-4372) CFSTI: HC\$3.00/MF\$0.65 CSCL 20K

A method for studying the accuracy of finite difference approximations for linear differential equations is presented and utilized. Definitive expressions for the error in each approximation are obtained by using Taylor series to derive the differential equations which exactly represent the finite difference approximations. The resulting differential equations are accurately solved by a perturbation technique which yields the error directly. This method is used to assess the accuracy of two alternate forms of central finite difference approximations for solving boundary value problems in structural analysis which are governed by certain equations containing variable coefficients. A "half station approximation" in which finite difference approximations are made before expanding derivatives of function products is compared with a "whole station approximation" in which derivatives of function products are expanded first for string, beam, and axisymmetric circular plate problems. An example of a square membrane is given as an application of the method to partial differential equations. Author

N68-17588*# National Aeronautics and Space Administration. Langley Research Center, Langley Station, Va.

RESIDUAL-STATIC-STRENGTH AND SLOW-CRACK-GROWTH BEHAVIOR OF DUPLEX-ANNEALED TI-8AI-1M0-1V SHEET

I. E. Figgee Mar. 1968 29 p refs

(NASA-TN-D-4358) CFSTI: HC\$3.00/MF\$0.65 CSCL 20K

Tests were conducted at room temperature on centrally cracked Ti-8AI-1Mo-1V duplex-annealed sheet specimens 2, 4, 8, and 20 inches wide. Tests were also conducted on specimens 8 inches wide in which cracks had been propagated either at various cyclic-stress levels or at various temperatures prior to static testing. The residual strength (based on net section prior to loading) for a given ratio of crack length to specimen width was less for wide specimens than for narrow ones. No effect of prior stress or temperature history on the residual static strength was found. The slow-crack-growth data obtained were approximated reasonably well by an equation of the form $a_c/a = 1 + A(w/2a - 1)^B$ where ac is the half-length of the critical crack, a is the half-length of the initial crack, w is the specimen width, and A and B are constants which are determined empirically. Analysis of the residual-strength data by both the unified notch-strength analysis method and a modified version of this method is discussed. Author

N68-17651*# National Aeronautics and Space Administration. Langley Research Center, Langley Station, Va. FLUTTER OF BUCKLED, SIMPLY SUPPORTED, RECTANG-

ULAR PANELS AT SUPERSONIC SPEEDS

Robert W. Fralich and John A. McElman Washington Mar. 1968 17 p refs

(126-14-02-24-23)

(NASA-TN-D-4357) CFSTI: HC\$3.00/MF\$0.65 CSCL 20K

A theoretical flutter analysis is presented for buckled, simply supported panels subjected to supersonic flow over one surface. The analysis employs the Von Karman large-deflection plate theory and linearized static aerodynamic strip theory. A Galerkin procedure using four static mode shapes is employed to determine a set of differential equations which is programed on an analog computer. The character of the output of the analog is used to determine the flutter speed. Results are obtained for panels with ratios of length in the streamwise direction to length in the cross-flow direction equal to 1/2 and 1 for three specified in-plane edge-loading conditions. An assessment of effects of cross-flow coupling of the modes is made by comparison of the results with those obtained when cross-flow coupling between the modes is neglected. Author

N68-18721*# National Aeronautics and Space Administration. Ames Research Center, Moffett Field, Calif.

AN EXPERIMENTAL STUDY OF THE INFLUENCE OF THE TURBULENT BOUNDARY LAYER ON PANEL FLUTTER

Lado Muhlstein, Jr., Peter A. Gaspers, Jr., and Dennis W. Riddle Washington Mar. 1968 55 $p\ refs$

(NASA-TN-D-4486) CFSTI: HC\$3.00/MF\$0.65 CSCL 20K

Flutter dynamic pressure and flutter frequency were obtained for a rectangular unstressed isotropic panel with all edges clamped for the following sets of parameters: (a) Panel length-to-width ratio of 0.5. Mach number range of 1.05 to 1.40, and ratio of boundary-layer thickness to panel length of 0.032 to 0.111; (b) panel length-to-width ratio of 2.0, Mach number of 1.20, and ratio of boundary-layer thickness to panel length of 0.016 to 0.056. For the configurations tested, it is shown that the turbulent boundary layer has a large stabilizing influence on the flutter of flat panels. The effect on flutter dynamic pressure is maximum near M = 1.20and decreases rapidly with increasing Mach number. The effect on flutter frequency is minimum near M = 1.20 and increases with increasing Mach number.

N68-18769*# General Dynamics Corp., San Diego, Calif.

DYNAMIC STABILITY OF SPACE VEHICLES. VOLUME 7: THE DYNAMICS OF LIQUIDS IN FIXED AND MOVING CONTAINERS

32 STRUCTURAL MECHANICS

L. L. Fontenot Washington NASA Mar. 1968 149 p refs (Contract NAS8-11486)

(NASA-CR-941; GDC-BTD67-056) CFSTI: HC \$3.00/MF \$0.65 CSCL 22C

This analytic review on stability and control of liquid-rocket powered missiles and space vehicles discusses theoretical hydrodynamics necessary to describe the motion of a heavy liquid enclosed in a rigid vessel which is itself in motion. An energy formulation for the system is written for six degrees of freedom and the concept is then extended to the case of the planar motion of a liquid propellant vehicle having a single tank and engine. Planar equations of motion are used to obtain the perturbation equations and to identify the role of the liquid motions. By replacing the liquid in the propellant tank with a simple mechanical system, the planar perturbation equations for the whole vehicle are obtained. Comparison of liquid motions and mechanical system motions show that the mechanical systems can duplicate the action of the liquid. G.G.

N68-18825*# General Dynamics Corp., San Diego, Calif. DYNAMIC STABILITY OF SPACE VEHICLES. VOLUME 10: EXIT STABILITY

R. F. Ringland Washington NASA Mar. 1968 166 p refs (Contract NAS8-11486)

(NASA-CR-944; GD/C-BTD-67-029) CFSTI: HC \$3.00/MF \$0.65 CSCL 22A

Described are techniques in use for the stability analysis of launch vehicles during their flight through, and upon exit from, the earth's atmosphere. Indicated are analytical tools and techniques used in the analysis and synthesis of launch vehicle flight control systems during the actively propelled and controlled flight phases. The object of this presentation is to illustrate the applicability of standard computational techniques to the solution of complex flight control problems associated with large launch vehicles. Current space boosters are characterized, from the flight dominated by parasitic modes of response (elastic vehicle bending and, if liquid propelled, propellant sloshing). Reliance is placed on active flight control by means of thrust vector deflection for stability; fins are used, if at all, as passive elements to decrease the degree of instability in those instances where it proves impractical to adequately stabilize the vehicle with the control system gains allowable by consideration of system parasitics. Also fins may be indicated where abort systems require a reduced rate of attitude divergence in the event of a flight control system failure. Large in the above context refers to vehicles whose dynamic parameters vary slowly over a wide range. The rates of change of these parameters are far less than those of the dependent variables associated with the short-period modes of response. The analytical techniques presented are limited to systems that are, or can be approximated by, continuous systems; sampled data systems, digital autopilots, and the like are not considered. There is no coverage of the long-period modes due to guidance system action and guidance commands; rather, the guidance system is treated in a fashion similar to atmospheric disturbances: as a source of system excitation. Author

N68-19143*# National Aeronautics and Space Administration. Langley Research Center, Langley Station, Va.

FLUTTER OF CORRUGATION STIFFENED PANELS AT MACH 3 AND COMPARISON WITH THEORY

Herman L. Bohon Washington Mar. 1968 29 p refs

(NASA-TN-D-4321) CFSTI: HC\$3.00/MF\$0.65 CSCL 20K Details of an experimental study on flutter of

corrugation-stiffened panels are presented. The panels were tested at Mach 3 in the Langley 9- by 6-foot thermal structures tunnel under aerodynamic heating conditions. Flutter boundaries presented include a flat-panel portion and a thermally buckled panel portion. Comparison of the results from this investigation and other available data on corrugation-stiffened panels with conventional theory for panels simply supported on all edges indicates that theory is highly unconservative. However, accounting in the theory for the deflectional flexibility of the corrugations and supports at the ends of the corrugations brings theory and experiment into fair agreement. These results indicate that seemingly small details of edge conditions of corrugation-stiffened panels may cause drastic reductions in the dynamic pressure for flutter. Author

N68-19311*# Syracuse Univ. Research Inst., N. Y.

PLANE STRESS ANALYSIS OF AN EDGE-STIFFENED RECTANGULAR PLATE, TAKING INTO ACCOUNT BENDING AND SHEAR STIFFNESS OF THE STIFFENERS

Yu-wen Hsu and Charles Libove Washington NASA Mar. 1968 178 p refs

(Grant NsG-385)

(NASA-CR-978; ME-1065-678) CFSTI: HC \$3.00/MF \$0.65 CSCL 20K

A plane stress analysis, by means of Fourier series, is presented for an isotropic or orthotropic elastic rectangular plate bounded by four uniform edge stiffeners and subjected to any prescribed temperature distribution and boundary loads. Both the extensional and flexural (including transverse shear) stiffnesses of the stiffeners are considered, and the possibility is included that the plate is attached to the stiffeners along lines which are offset from their centroidal axes. At each corner the junction between the two meeting stiffeners is assumed to consist of a hinge and a coil spring. By varying the stiffness of the coil spring, any degree of joint rigidity, from that of a pure hinge to a perfectly rigid joint, can be simulated. Using this analysis, numerical results were obtained for a number of specific cases involving prescribed force loading or prescribed temperature distributions. As a check on the validity of the method, stresses were measured on a doubly symmetric edge stiffened square plate subjected to stiffener-end loads. Good agreement was obtained between the measured and computed values of the plate and stiffener stresses. Author

N68-20364*# National Aeronautics and Space Administration. Langley Research Center, Langley Station, Va.

RESPONSE CHARACTERISTICS OF IMPACTING PENE-TROMETERS APPROPRIATE TO LUNAR AND PLANETARY MISSIONS

John Locke McCarty and Huey D. Carden Washington Apr. 1968 81 p refs

(NASA-TN-D-4454) CFSTI: HC \$3.00/MF \$0.65 CSCL 20K

The objectives of this study were to evaluate the capability of the penetrometers to identify structural characteristics which potentially might exist for materials on the surface of the moon and planets and to study the effects of variations in both the penetrometer design and the conditions at impact. The effects on penetrometer impact characteristics-primarily acceleration time histories---of such variables as impact velocity and angle, penetrometer size and mass, environmental pressure, and target structure and penetration resistance were examined. The target materials included a rigid nonyielding plate, a cobble-pebble agglomerate, two grades of quartz and basalt sands, fine silica powder, and a low-density open-cell foam. The results demonstrate that suitably designed penetrometers perform satisfactorily over a wide range of impact conditions on a rigid surface and have ample sensitivity to permit the detection of low-density materials having a bearing strength considerably below that required to support manned landings. Author

N68-20954*# National Aeronautics and Space Administration. Langley Research Center, Langley Station, Va. EXPERIMENTAL MODES OF VIBRATION OF 14° CONICAL-FRUSTUM SHELLS WITH FREE ENDS John S. Mixson Washington Apr. 1968 18 p refs (NASA-TN-D-4428) CFSTI: HC\$3.00/MF\$0.65 CSCL 20K

In experimental studies of the vibrations of conical and cylindrical shells, some modes having different numbers of circumferential waves at different locations along the shell meridian have been obtained. (Such modes are termed "mixed modes" herein.) To investigate the occurrence of such modes, five conical-frustum shells were vibrated and their resonant frequencies and nodal patterns determined. The shells had a half-angle of 14° and three wall thicknesses. Three shells had butt-welded seams and two had lap-welded seams. The suspension-system stiffness was varied, and two types of excitation were used. Experimentally determined frequencies and the location of the circumferential node line are shown to be in good agreement at low frequencies with values calculated by means of inextensional shell theory. Mixed modes occurred when the shell or test setup departed substantially from ideal conditions. Examples of nonideal conditions include imperfections or lap-welded seams on the shell, stiff suspension systems, and forced response of two modes at nearly the same frequency. It is shown that the experimental nodal patterns of these modes can be obtained by superposition of theoretical modes of an ideal conical shell Author

 $\label{eq:N68-21099} \begin{array}{l} \text{Methad} \\ \text{N68-21099} \\ \ensuremath{\#} \\ \ensuremath{\text{National}} \\ \text{Aeronautics} \\ \text{and Space Administration.} \\ \ensuremath{\text{Langley Research Center, Langley Station, Va.} \\ \end{array}$

EXPERIMENTAL STUDY OF AEROELASTIC INSTABILITY OF OVEREXPANDED ROCKET NOZZLE EXTENSIONS W. J. Tuovila and Norman S. Land Washington Apr. 1968 18 p refs

(NASA-TN-D-4471) CFSTI: HC\$3.00/MF\$0.65 CSCL 21H

A brief exploratory investigation was conducted to study possible aeroelastic-instability phenomena which might occur for overexpanded flow through flexible nozzle extensions which are being considered for use in increasing the thrust of rocket engines at very high altitudes. Five conical extensions with a 22.5° half-angle and area ratios of 54 and 100 were fabricated from varying thicknesses of steel and glass-fiber laminates. Studies were conducted at constant stagnation pressure. Flow through the nozzle and extension started in an underexpanded condition but gradually changed to an overexpanded condition as the guiescent-flow ambient pressure increased. Two rigid aluminum-alloy models with geometry similar to that of the flexible models were used for pressure measurements and for visualization of flow across the exit and interior surface. For some flexible extensions, dynamic instability was observed which could be related by means of flow measurements to an overexpanded flow condition that caused buckling loads. The experimental data are summarized graphically to indicate nozzle extension parameters in the stable region for different loading conditions. The data may be useful as a guide for the preliminary design of nozzle extensions. Author

N68-21293*# National Aeronautics and Space Administration. Ames Research Center, Moffett Field, Calif.

THE PENETRATION OF POROUS PROJECTILES IN ALUMINUM AND PLASTIC TARGETS

Richard H. Fish Washington Apr. 1968 11 p refs

(NASA-TN-D-4505) CFSTI: HC\$3.00/MF\$0.65 CSCL 20K

Cylindrical projectiles of polyurethane plastic, with a fineness ratio of 2/3 and densities ranging from 1.17 gm/cc for the solid material to 0.065 gm/cc for the lightest porous material, impacted targets of 2024-T351 aluminum alloy and polycarbonate plastic at velocities from 3.45 to 7.08 km/sec. Solid projectiles with the fineness ratio appropriately reduced to give the same mass as some of the porous projectiles were also tested for comparison with the porous projectiles. The results of the investigation indicated that the solid projectiles penetrated as deeply as the porous projectiles of the same mass, but their crater shapes and volumes were different. The depths of penetration in the two different target materials could be correlated on the basis of the density ratio raised to the 2/3 power, without considering other physical properties such

as strength. Comparison of the data of the present investigation with other plastic-projectile data indicated that the present data fall in low-speed or transition regions of impact. Author

N68-21767*# National Aeronautics and Space Administration. Ames Research Center, Moffett Field, Calif. REMARKS ON IMPERFECTIONS OF AXIALLY LOADED

CYLINDERS

Robert E. Reed, Jr. Washington Apr. 1968 13 p refs

(NASA-TM-X-1552) CFSTI: HC\$3.00/MF\$0.65 CSCL 20K

A simple hypothesis is offered as an explanation for the large discrepancy between theory and experiment of axially compressed cylindrical shells. It is suggested that the very low experimental buckling loads (when buckling does not occur at the ends) are caused by local "flat spots." A critical size of imperfection is given and the buckled mode shape is discussed. These arguments are also applied to other common shell buckling problems. Author

N68-21869*# National Aeronautics and Space Administration. Langley Research Center, Langley Station, Va.

EXPERIMENTAL INVESTIGATION OF THE LONGITUDINAL VIBRATION OF A REPRESENTATIVE LAUNCH VEHICLE WITH SIMULATED PROPELLANTS

James A. Schoenster and Robert R. Clary Washington May 1968 67 p refs

(NASA-TN-D-4502) CFSTI: HC\$3.00/MF\$0.65 CSCL 22D

The results of an experimental investigation of the longitudinal vibration of a full-scale representative launch-vehicle structure are presented. The vibration characteristics of the vehicle supported upright were determined for frequencies between 5 and 100 hertz by means of force-controlled vibration techniques. Resonant frequencies, resonant response accelerations, and damping values were determined and the degree of nonresonant vibration was investigated. Static deflections of the propellant tanks due to various levels of simulated propellants were also measured. The vibration characteristics of the vehicle were influenced by the simulated propellants. The acceleration data were not always sufficient to identify and to separate the various modes of the vehicle. In these cases, a definition of the effect of the contained liquid on the vehicle structure was required for proper association of the modes. In general, there was good agreement between the resonant frequencies selected for detailed study when one source of excitation two sources of excitation, or the Kennedy-Pancu method of data interpretation were used. However, data obtained from the two sources of excitation and the Kennedy-Pancu plots indicate significant nonresonant amplitude contributions to the total response amplitude obtained with a single source of excitation. Author

N68-22275*# National Aeronautics and Space Administration. Lewis Research Center, Cleveland, Ohio.

METHOD FOR DETERMINING NORMAL MODES AND FREQUENCIES OF A LAUNCH VEHICLE UTILIZING ITS COMPONENT NORMAL MODES

James D. McAleese Washington May 1968 50 p refs

(NASA-TN-D-4550) CFSTI: HC\$3.00/MF\$0.65 CSCL 22D

The launch vehicle is idealized as a one-dimensional structure consisting of a main beam to which several flexible branches are attached. The normal modes of both the unrestrained main beam and the cantilevered branches are determined. An energy approach is expressed as the superposition of a finite number of free-free normal modes of the main beam and cantilever normal modes of the branches. Langrange's equations are then used to derive the equations of motion in matrix form, and an iterative method of solution is included for completeness.

32 STRUCTURAL MECHANICS

N68-23355*# Lockheed Aircraft Corp., Sunnyvale, Calif.

BUCKLING OF SHELLS OF REVOLUTION WITH VARIOUS WALL CONSTRUCTIONS. VOLUME 3: USER'S MANUAL FOR BOSOR

D. Bushnell, B. O. Almroth, and L. H. Sobel Washington NASA May 1968 120 \ensuremath{p} refs

(Contract NAS1-6073)

(NASA-CR-1051; Rept.-4-17-67-4) CFSTI: HC \$3.00/MF \$0.65 CSCL 20K

Presented is a comprehensive computer program for the analysis of shells of revolution with axisymmetric loading. The program includes nonlinear prebuckling effects and is very general with respect to geometry of meridian, shell wall design, edge conditions, and loading. Despite its generality the program is easy to use. Branches are provided such that for commonly occurring cases the input data involves only basic information such as geometrical and material properties. The computer program was verified by comparisons with other known solutions.

N68-23399*# IIT Research Inst., Chicago, III. HIGH PERFORMANCE STRUCTURES

Ralph L. Barnett and Paul C. Hermann Washington NASA May 1968 124 p refs

(Contract NASr-65(16))

(NASA-CR-1038) CFSTI: HC\$3.00/MF\$0.65 CSCL 20K

Materials selection, structural geometry development, prestressing, proof testing and statistical screening, and system energy were used as general design tools for studying optimum tension members, columns, and trusses. A design philosophy based on proof testing or statistical screening is introduced that turns the characteristic scatter in fracture and yield strengths into an asset by emphasizing the strong elements in a sample. Proof testing is considered to recast the performance aspects of brittle design into an economic framework. A statistical load redistribution for ductile tension members is proposed that takes size effect into account, and prestressing is used to eliminate local buckling in a tubular column. Two classical column designs were investigated which required the optimum longitudinal distribution of a specified total mass to prevent Euler buckling, energy-strength tradeoffs were considered, and the design of statically determinate trusses for minimum weight and deflection was studied. Optimum stiffness/weight beam, constant stress trusses, and end and triangular loaded cantilevers were investigated. M.W.R.

N68-23451*# Lockheed Aircraft Corp., Sunnyvale, Calif. BUCKLING OF SHELLS OF REVOLUTION WITH VARIOUS WALL CONSTRUCTIONS. VOLUME 2: BASIC EQUATIONS AND METHOD OF SOLUTION

D. Bushnell, B. O. Almroth, and L. H. Sobel Washington NASA May 1968 83 $p\ refs$

(Contract NAS1-6073)

(NASA-CR-1050; LAC-4-17-67-1, V. 2) CFSTI: HC \$3.00/MF \$0.65 CSCL 20K

Basic equations are formulated for the computer program used in prebuckling and stability analysis of the axisymmetric collapse and nonsymmetric bifurcation buckling behavior of cylinders, cones, and spherical and toroidal shell segments subjected to axial compressive loads. The method used in solving these equations is described. A set of more general stability equations is appended. E.J.S.

N68-23452*# General Dynamics Corp., San Diego, Calif.

DYNAMIC STABILITY OF SPACE VEHICLES. VOLUME 13: AERODYNAMIC MODEL TESTS FOR CONTROL PARAMETER DETERMINATION

David R. Lukens Washington NASA May 1968 26 p refs (Contract NAS8-11486)

(NASA-CR-947; GD/C-BTD-67-112, V. 13) CFSTI: HC \$3.00/MF \$0.65 CSCL 22B Introductory data are presented on, and procedures recommended for, aerodynamic model testing of control parameters required in the design and analysis of spacecraft flight control systems. Items to be considered in planning, designing, and conducting a model test for the determination of aerodynamic forces and moments are discussed in terms of wind tunnel apparatus and facilities. Force and pressure testing techniques are described as well as commonly used procedures for control effectiveness testing. Captive and free flight models used in dynamic stability tests are described.

N68-23453*# General Dynamics Corp., San Diego, Calif. DYNAMIC STABILITY OF SPACE VEHICLES. VOLUME 15: SHELL DYNAMICS WITH SPECIAL APPLICATIONS TO CONTROL PROBLEMS

L. E. Penzes Washington NASA May 1968 197 p refs (Contract NAS8-11486)

(NASA-CR-949; GD/C-BTD-67-120) CFSTI: HC \$3.00/MF \$0.65 CSCL 20K

The purpose of this monograph is to explain the foundations of thin-walled elastic shells and the basis of theoretical derivations. An attempt is made to fill the gap between the contents of dynamics textbooks and recently published literature and to explain the differences in their treatment of the subject. Examples and problems are given to demonstrate the use of the theories. Some static problems are discussed to compare them with equivalent dynamic problems. In addition, the applicability of shell vibration theory to missiles and launch vehicles is described. Attention is

focused on calculation of dynamic model parameters affecting stability and control. Emphasized are modes for which the system frequency falls within the bandwidth of the control system, i.e., below 20 Hz for a large space booster. K.W.

N68-23454*# General Dynamics Corp., San Diego, Calif. DYNAMIC STABILITY OF SPACE VEHICLES. VOLUME 14: TESTING FOR BOOSTER PROPELLANT SLOSHING PARAMETERS

D. M. Eggleston Washington NASA May 1968 37 p refs (Contract NAS8-11486)

(NASA-CR-948; GD/C-BTD-67-089, V. 14) CFSTI: HC \$3.00/MF \$0.65 CSCL 22B

Summary data are presented on the state-of-the-art in booster propellant slosh testing and a mathematical model, defined as that set of differential and functional equations used to represent the forces and moments exerted on the vehicle due to the liquid propellants, is formulated. Known digital computer programs for generating parameters for a pendulum or spring-mass model of the basic fluid motion are reviewed, and together with known data and techniques, are organized for convenient use in new situations and for new launch vehicles. Recommendations are included for the establishment of test objectives and planning criteria, facility design and instrumentation, test operations and disturbance effects, and data reduction and scaling techniques. E.J.S.

N68-24481*# Lockheed Aircraft Corp., Sunnyvale, Calif. BUCKLING OF SHELLS OF REVOLUTION WITH VARIOUS WALL CONSTRUCTIONS. VOLUME 1: NUMERICAL RESULTS

B. O. Almroth, D. Bushnell, and L. H. Sobel Washington NASA May 1968 58 p refs

(Contract NAS1-6073)

(NASA-CR-1049; Rept.-4-17-67-1) CFSTI: HC \$3.00 /MF \$0.65 CSCL 20K

Results are presented on a parameter study performed with the computer program BOSOR (Buckling of Shells of Revolution). The axisymmetric collapse and the nonsymmetric bifurcation buckling behavior is studied for cylinders, cones, and spherical and toroidal shell segments subjected to axial compressive loads. Particular emphasis is placed on the effects of eccentricity in load application and on the influence of elastic end rings. Author

N68-24508*# National Aeronautics and Space Administration. Ames Research Center, Moffett Field, Calif.

FLUCTUATING PRESSURES ON THE AFTERBODIES OF FIVE BLUNT ATMOSPHERE ENTRY VEHICLES

Robert C. Robinson, Bruno J. Gambucci, and Robert E. George Washington May 1968 56 p refs

(NASA-TN-D-4591) CFSTI: HC\$3.00/MF\$0.65 CSCL 22B

Pressure fluctuations were measured on the afterbodies of entry-vehicle configurations at angles of attack from -14° to $+14^{\circ}$ and Mach numbers from 0.60 to 3.50. The Reynolds number range was $2.0 \times 10^{\circ}$ to $6.5 \times 10^{\circ}$ based on model diameter. The models were typical of configurations which have been considered as entry vehicles for the Mars atmosphere. Forebody fineness ratios were 1/3 and 1/8 and the afterbodies were conical with half angles of 30° , 60° , and 80° . The pressure fluctuations measured at subsonic Mach numbers were of low reduced frequency (below 0.30) and were highly correlated. At supersonic Mach numbers the bandwidth of the fluctuations increased and the degree of correlation decreased with increasing Mach number. Author

N68-24802*# North American Aviation, Inc., Downey, Calif. SHELL ANALYSIS MANUAL

E. H. Baker, A. P. Cappelli, L. Kovalevsky, F. L. Rish, and R. M. Verette Washington NASA Apr. 1968 849 p refs (Contract NAS9-4387)

(NASA-CR-912) CFSTI: HC\$3.00/MF\$0.65 CSCL 20M

This shell analysis manual provides specific instructions, procedures, basic solutions, and recommendations to facilitate the expedient static structural analysis of shell-type spacecraft structures. It also provides an introduction to and reference for the practical static structural analysis of shells. Author

N68-24971*# North American Aviation, Inc., Columbus, Ohio. INFRARED RADIOMETRIC STRESS INSTRUMENTATION APPLICATION RANGE STUDY

Milo H. Belgen Washington NASA May 1968 144 p refs (Contract NAS1-6082)

(NASA-CR-1067) CFSTI: HC\$3.00 /MF\$0.65 CSCL 20K

Research was utilized to develop a simplified method for evaluating infrared stress measurement applications and to study typical attainable spatial resolutions and detectable stresses (for selected detectors and windows) as a function of test part temperature and stress oscillation frequency. It appears that room temperature infrared measurements might have accuracies of the same general magnitude as conventional instrumentation, and infrared is likely to be more favorable than conventional instrumentation relative to accuracy and other factors at elevated temperatures. Since infrared measurements yield data on the sum of principal stresses, various combinations of infrared and conventional strain instrumentation could yield many (undefined) types of data not previously within the state of the art. Infrared permits rapid spatial data acquisition by scanning with an analog electronic signal output. Author

N88-25104*# National Aeronautics and Space Administration. Ames Research Center, Moffett Field, Calif. PENETRATION RESISTANCE OF DOUBLE SHEET

STRUCTURES AT VELOCITIES TO 8.8 KM/SEC C. Robert Nysmith Washington May 1968 17 p refs

(NASA-TN-D-4568) CFSTI: HC\$3.00 /MF\$0.65 CSCL 20K

Small pyrex glass spheres were launched into aluminum double-sheet targets at velocities to 8.8 km/sec to determine the

32 STRUCTURAL MECHANICS

effects of total sheet thickness and sheet spacing upon penetration resistance. The ballistic limit of double-sheet structures consisting of two equally thick aluminum sheets was found to increase with increasing total sheet thickness and sheet spacing. In addition, for a particular ratio of total sheet thickness to projectile diameter, the effectiveness of sheet spacing increases with increasing impact velocity. The data indicate that for impacts at a given velocity the ratio of front-sheet thickness to projectile diameter that causes maximum vaporization or fragmentation or both will result in the most efficient meteor bumper. It is concluded that the double-sheet structure most efficient in resisting penetration will use that thickness for a front sheet and the remaining available mass in the rear sheet. Measurements were also made of the front-sheet hole diameter and the front-sheet mass loss. It was determined that the front-sheet hole diameter varies with the square root of the impact velocity and the 0.45 power of the front-sheet thickness and the front-sheet mass loss various with impact velocity and the square of the front-sheet thickness. Author

N68-25421*# National Aeronautics and Space Administration. Lewis Research Center, Cleveland, Ohio. CRITICAL-SPEED ANALYSIS OF FLEXIBLY MOUNTED

CRITICAL SPEED ANALYSIS OF FLEXIBLY MOUNTED RIGID ROTORS

Richard H. Cavicchi Washington Jun. 1968 54 p refs (NASA-TN-D-4607) CFSTI: HC\$3.00 /MF\$0.65 CSCL 131

A general solution of the frequency equation for rigid rotors in undamped bearings is derived for forward and backward precession. The solution is applied to a wide range of speeds and shapes, with variation in center-of-gravity location, to obtain maps of the frequency characteristics and locate major and nonsynchronous critical speeds. When the center of gravity is at the bearing centerline midpoint, a set of two solutions exists. An additional set of two solutions appears, however, when the center of gravity is away from this point. No forward-precession high-frequency critical speeds exist if the moment-of-inertia ratio equals or exceeds the critical-speed ratio. With the center of gravity midway between single-row ball bearings and the polar and diametral moments of inertia equal, a monsynchronous critical speed exists at all rotor speeds.

N68-25819*# National Aeronautics and Space Administration. Lewis Research Center, Cleveland, Ohio.

TARGET PRESSURE AND DAMAGE DATA FROM IMPACTS BY EXPLOSIVELY PROPELLED PROJECTILES

A. B. Wenzel and Nestor Clough Washington, D. C. Jun. 1968 21 p refs

(NASA-TM-X-1597) CFSTI: HC\$3.00/MF\$0.65 CSCL 20K

Data on maximum shock-generated pressures at several axial positions in 1100-0 aluminum and on crater dimensions in 316-stainless steel were obtained from impacts by explosively-fired aluminum projectiles. The aluminum projectiles with mass ranging from 0.408 to 0.626 grams, impacted the targets at velocities of 11 km/sec. Comparisons of pressure data with similar data from light-gas gun impacts are included, together with a discussion of the "throw-off pellet" technique used to obtain axial pressures. Author

N68-28238*# National Aeronautics and Space Administration. Lewis Research Center, Cleveland, Ohio.

USE OF WIRE LACING TO REDUCE BLADE VIBRATION IN AN AXIAL-FLOW COMPRESSOR ROTOR

Roy D. Hager, George W. Lewis, and Jack M. Wagner Washington Jul. 1968 22 $\,p\,$ refs

(NASA-TM-X-1603) CFSTI: HC\$3.00/MF\$0.65 CSCL 20K

The experimental axial-flow compressor rotor had a diameter of 20 inches (50.8 cm), a hub-tip ratio of 0.4, and a blade aspect ratio of 3.6. The rotor was tested with lacing wires installed near

32 STRUCTURAL MECHANICS

the blade leading and trailing edges close to the blade tip. The wires were installed to reduce a severe bending vibration encountered at approximately 45 percent of design speed. Blade vibratory stresses were reduced from approximately $\pm 110,000$ psi ($\pm 75.902 \times 107$ N/m²) for the undamped blade to approximately ± 1550 psi ($\pm 1.070 \times 107$ N/m²) for the blade with lacing wires. An estimated reduction in the overall rotor efficiency of 1.6 percentage points resulted from the use of the wires.

N68-28330*# National Aeronautics and Space Administration. Lewis Research Center, Cleveland, Ohio.

STUDY OF VIBRATION INDUCED STRESSES IN DESIGN OF FUEL-ELEMENT SUPPORT ASSEMBLY FOR TUNGSTEN WATER-MODERATED NUCLEAR REACTOR

Ivan B. Fiero and Donald W. Adams Washington Jul. 1968 49 p refs

(NASA-TM-X-1608) CFSTI: HC\$3.00/MF\$0.65 CSCL 181

The results of vibration tests on a concentric-tube fuel-element support structure for the Tungsten Water-Moderated Reactor are presented. The assembly is a composite material inner tube separated from a concentric aluminum outer tube by springs. The tests show that the assembly must be supported on both ends and at the center of the aluminum tube by the reactor structure. With a cold reactor, only one spring is necessary to ensure that the support tube will withstand lateral vibrational loads. When the reactor is hot, three springs are required. Stress distributions and parameters affecting bending vibration response are discussed. Author

N68-28335*# North American Rockwell Corp., Downey, Calif.

INFLUENCE OF STRUCTURE AND MATERIAL RESEARCH ON ADVANCED LAUNCH SYSTEMS WEIGHT, PERFORMANCE, AND COST. PHASE 3: DESIGN SYNTHESIS OF RECOVERABLE LAUNCH VEHICLE STRUCTURES

J. A. Boddy Washington NASA Jul. 1968 60 p refs

(Contract NAS7-368)

NASA-CR-1116; SD-67-1204-1) CFSTI: HC \$3.00/MF \$0.65 CSCL 22D

To obtain a realistic series of basepoint vehicle systems, a structural synthesis was conducted for the major structural shell components of the recoverable first stages. Conventional constructions such as skin stringer, waffle, and honeycomb sandwich, were considered for the pressurized and unpressurized shells. The synthesis accounted for the thermal environment evaluation and protection system synthesis for the reentry mode of the recoverable first stages of a series of multistage launch vehicles. Relative benefits to be derived from structures/materials improvements when applied to these recoverable stages were considered in terms of their weight reductions, performance improvements, and cost reductions. The computer programs for vehicle synthesis and structural design synthesis were consolidated with a master executive control program and the total program was demonstrated. B.S.D.

N68-28806*# National Aeronautics and Space Administration. Langley Research Center, Langley Station, Va

REDUCTION OF WIND-TUNNEL-MODEL VIBRATION BY MEANS OF A TUNED DAMPED VIBRATION ABSORBER INSTALLED IN THE MODEL

William B. Igoe and Francis J. Capone Washington Jul. 1968 28 p refs

(NASA-TM-X-1606) CFSTI: HC\$3.00/MF\$0.65 CSCL 20K

Some experimentally determined performance characteristics have been presented for a tuned damped vibration absorber which was designed to reduce the undesirable rigid body vibrations of a conventional wind tunnel force model. The model vibration was due to random excitation by wind tunnel airstream turbulence and buffeting. A tuned vibration absorber was used for this purpose because it was compact and did not require any force linkages across the force balance. The absorber was tuned to reduce vibrations in both the pitch and yaw planes simultaneously, but its effectiveness in yaw was restricted because the mass center of the absorber was near the node of the yaw vibration mode. In the pitch plane, the peak and root mean square amplitudes of the rear normal force

component fluctuations of the balance were reduced by approximately 50 percent at some wind-tunnel test conditions. Author

N68-28832*# National Aeronautics and Space Administration. Ames Research Center, Moffett Field, Calif.

MEMBRANE ANALYSIS OF SCALLOPED SHELLS Ravindra K. Vyas Washington Jul. 1968 53 p refs

(NASA-TN-D-4687) CFSTI: HC\$3.00/MF\$0.65 CSCL 20K

The main objective of this report is to contribute to the understanding of membrane forces in scalloped shells, particularly scalloped paraboloids. It is shown how the stress function approach can be applied to the scalloped paraboloids. In order to demonstrate the technique, two scalloped structures having practical significance as structural models for parachutes are discussed in detail. In the cases considered, it is shown that the stress function must satisfy a linear second-order partial-differential equation with variable coefficients. The basic method for solving this equation is given in the first appendix. These results show that the hoop and meridional stresses in the parachute type structure are lower than those in a corresponding shell of revolution. More significantly, the meridional stress in the parachute type shell decreases remarkably, and even becomes compressive, as the bulge of the scallop, defined by a positive parameter β , is increased. It is shown how a critical value, $\boldsymbol{\beta}_{\rm cr}$ of this bulge parameter can be obtained below which the shell would remain in a compressionless state. A singular solution used in prescribing rope tension near the opening of the parachute type shell may also be useful in other aspects of parachute analysis. Author

N68-30045*# National Aeronautics and Space Administration. Lewis Research Center, Cleveland, Ohio.

A NUMERICAL PROCEDURE FOR CALCULATING STRESS AND DEFORMATION NEAR A SLIT IN A THREE-DIMENSIONAL ELASTIC-PLASTIC SOLID David J. Ayres Washington NASA Aug. 1968 31 p refs

(NASA-TN-D-4717) CFSTI: HC\$3.00/MF\$0.65 CSCL 20K

A finite difference procedure for the computation of the stress in a three dimensional solid is presented. This iterative technique, based on Newton's method for determining the roots of a system of polynomials, is applicable to both linear and nonlinear problems. The sample problems that are treated are the analysis of a plate in plane strain with a slit at its center, the analysis of a thick plate with a rectangular slit through its thickness, and the analysis of a thick plate containing a semielliptical slit which extends only halfway through its thickness. The loading condition in all sample problems is uniaxial tension normal to the slit. Author

N68-30505*# National Aeronautics and Space Administration. Langley Research Center, Langley Station, Va.

EXPERIMENTAL STUDY OF VERTICAL IMPACTS OF AN LM-TYPE LANDING GEAR ASSEMBLY UNDER SIMULATED LUNAR GRAVITY

John Locke McCarty and Huey D. Carden Washington Aug. 1968 55 p refs

(NASA-TN-D-4711) CFSTI: HC\$3.00/MF \$0.65 CSCL 22B A study made to evaluate the response of a landing gear system on several penetrable target materials and to relate this response to that of penetrometers impacting the same materials. Testing included vertical impacts of a single landing gear unit at velocities up to approximately 3 m/sec. The test apparatus included a full-scale boilerplate pad and a vertical strut with stroking characteristics similar to those of LM. The mass of the system approximated 25, 50 and 100% of the anticipated vehicle landing mass. The target materials consisted to two grades of quartz sand (one in a densely packed state) and an open cell urethane foam. The results show that the maximum anticipated accelerations sensed by the vehicle occupants and equipment would not exceed 3.3g (earth) in a vertical landing. During strut compression, which is intensified with increasing target bearing strength, with system mass and with impact velocity, these accelerations are shown to be a function of only the crushing strength of the collapsible strut and the system mass. Pad accelerations increase with increasing impact velocity and increasing target penetration resistance and, during strut compression, are independent of the system mass. Data are presented which show that the penetration of the landing pad into particulate target materials can be reasonably estimated. Author

N68-31602*# National Aeronautics and Space Administration. Langley Research Center, Langley Station, Va.

INVESTIGATION OF A COMPARTMENTED-GAS-BAG LANDING SYSTEM HAVING MULTIPLE IMPACT CAPABILITIES

John R. McGehee Washington Aug. 1968 38 p refs

(NASA-TN-D-4710) CFSTI: HC\$3.00/MF\$0.65 CSCL 22B

The principles of the proposed landing system were investigated experimentally to determine the kinetic energy dissipating capability of the system. A simplified test vehicle, using unidirectional gas bags, was tested with both sharp-edged and fabric covered orifices between the compartments. A supplementary experimental investigation was conducted to determine the discharge parameters associated with various fabrics. In addition, equations were derived for computing time histories of acceleration, velocity, stroke, and compartment pressures to extend the usefulness of the investigation by permitting variation of the landing environment and test vehicle parameters. The results show a kinetic energy dissipation capability for the initial impact as great as 93 percent of the vehicle touchdown kinetic energy. Tests performed with aircraft fabric covered orifices yielded a slightly greater (approximately 5 percent) kinetic energy dissipation capability than was obtained with the sharp-edged orifices. The analytical investigation resulted in a computational procedure which provides fair agreement between computed and experimentally determined accelerations, pressures, and kinetic energy dissipation for the ranges of velocity and bag initial pressures investigated. Author

N68-31912*# General Electric Co., King of Prussia, Pa. PLATE-GAP MODEL OF A POROUS SOLID AND ITS APPLICATION TO IMPACT BY REDUCED DENSITY PROJECTILES

J. F. Heyda Washington NASA Aug. 1968 39 p refs (Contract NAS3-8512)

(NASA-CR-1140 CFSTI: HC\$3.00/MF\$0.65 CSCL20K

The sensitivity of the peak axial profiles, obtained using the impact model of an earlier report, to a change in the Hugoniot function assumed for the reduced density projectiles is examined briefly. The previous Hugoniot function, based on the Los Alamos equation of state for aluminum, is replaced by one based on the Plate-Gap model of a porous solid due to Thouvenin. A modification of this model is described in detail and its comparison with existing experimental data for six porous materials and the predictions of the theoretically based equation of state due to Wagner and Bjork for aluminum is noted. Comparison is also made of calculated peak axial pressures obtained using the impact model for the case of normal density aluminum projectiles impacting aluminum with experimental data obtained from corresponding jet projector impact shots. Author N68-31946*# National Aeronautics and Space Administration. Langley Research Center, Langley Station, Va.

PLASTIC BUCKLING OF PLATES AND SHELLS UNDER BIAXIAL LOADING

James P. Peterson Washington Aug. 1968 32 p refs

(NASA-TN-D-4706) CFSTI: HC\$3.00/MF\$0.65 CSCL 20K

Available elastic buckling equations are used in making the plastic buckling calculation by substituting wall stiffnesses derived from a plastic buckling theory for the elastic orthotropic wall stiffnesses associated with the elastic buckling equations. This method permits the calculation of the buckling load of many structures of current interest which cannot be handled by available methods. Buckling loads of cylinders and plates of conventional, sandwich, and laminated construction are easily calculated. The cylinders and plates may have stiffening members which may be eccentric (one-sided) and which may be made of a different material than the skin. For many structures, the effect of transverse shear can be taken into account in the buckling calculations. Author

N68-32051*# National Aeronautics and Space Administration. Langley Research Center, Langley Station, Va.

A THEORETICAL AND EXPERIMENTAL INVESTIGATION OF THE THRE-DIMENSIONAL VIBRATION CHARACTERIS-TICS OF A SCALED MODEL OF AN ASYMMETRICAL LAUNCH VEHICLE

Ellwood L. Peele, William M. Thompson, Jr., and Christine G. Pusey Washington Aug. 1968 56 $\,p\,$ refs

(NASA-TN-D-4707) CFSTI: HC\$3.00/MF\$0.65 CSCL 20K

The three-dimensional vibration characteristics of a dynamically scaled model of an asymmetrically clustered launch vehicle were investigated both analytically and experimentally. The matrix Holzer analysis formulated specifically for this model configuration is identified as being three-dimensional because it renders possible the analysis of motion which is coupled in three planes: lateral bending motion in two planes (pitch and yaw), torsional motion, and longitudinal motion. Previous two-dimensional analyses of similar configurations considered pitch-torsion uncoupled from yaw-longitudinal motion. The suitability of the analysis is evaluated by comparison of computed vibration characteristics with measured response of a near-replica scaled model to lateral excitation. On the basis of these comparisons, the procedure was found to be capable of predicting the major vibration characteristics. Additional comparison is made between computed data based on a coupled and uncoupled mathematical model. These comparisons indicate that for this configuration, the coupled and uncoupled analysis yielded essentially the same results. Author

N68-32074*# National Aeronautics and Space Administration. Langley Research Center, Langley Station, Va.

PREDICTION OF FATIGUE-CRACK-PROPAGATION BEHAVIOR IN PANELS WITH SIMULATED RIVET FORCES J. E. Figge and J. C. Newman, Jr. Washington Aug. 1968 33 p

refs

(NASA-TN-D-4702) CFSTI: HC\$3.00/MF\$0.65 CSCL 20K

Analytical and experimental studies were conducted to determine the rates of fatigue crack propagation in 7075-T6 aluminum alloy sheet specimens containing either symmetric or nonsymmetric cracks subjected to uniform end loads, concentrated loads, or combinations of both. The concentrated loads simulated rivet forces and were applied by a special hydraulic fixture which is described. These studies indicate that the curve of stress-intensity factor against crack growth rate obtained from tests on simple specimens of a given material tested at load ratios of 0.05 to -1 can be successfully used to predict the crack propagation behavior of complex specimens of the same material tested over the same range of load ratios. It was also observed that better predictions of life were obtained for panels subjected to concentrated forces when the stress intensity factors were obtained by using the measured strains on the uncracked panels rather than by using those obtained from the theoretical point load solutions. Author

32 STRUCTURAL MECHANICS

N68-32976*# Fundamental Methods Associates, Inc., New York. APPLICATION OF DUST FOR SPACE STRUCTURES

Carl N. Klahr, Sylven N. Cutler, and Kalman Kalikstein Washington NASA Aug. 1968 61 p ref

(Contract NASw-1374)

(NASA-CR-1136) CFSTI: HC \$3.00 /MF \$0.65 CSCL 22A

This report is concerned with the physical properties and applications of small particles-particles whose masses range from 100 micrograms to 1 micro-microgram. A dust structure will be defined to be a spatial distribution of discrete particles whose relative geometry is maintained by the particle trajectories or by individual particle motion, and not by conventional cohesive forces which hold solids or liquids together. Therefore, dust configurations can be considered a new type of physical structural material, having properties often unlike those of solids, liquids, or gases. Various means can be used to maintain the cross relative geometry of the spatial distribution which constitutes the dust structure. Dust structures have unique properties across the entire thermal and electromagnetic energy spectrum, from optical frequencies through microwave and radio frequencies. Their inertial and mechanical properties as well as their gross material behavior are also guite unusual. Author

N68-33057*# National Aeronautics and Space Administration. Langley Research Center, Langley Station, Va.

ON THE PREDICTION OF THE VIBRATORY BEHAVIOR OF FREE-FREE TRUNCATED CONICAL SHELLS

Eugene C. Naumann Washington Sep. 1968 34 p refs (NASA-TN-D-4772) CFSTI: HC\$3.00/MF\$0.65 CSCL 20K

An analytical procedure is described for the prediction of the frequencies and mode shapes for free-free truncated conical shells. The method utilizes simple power series modal assumptions in a Rayleigh–Ritz type solution procedure. Excellent agreement was obtained when analytical results were compared with experimentally obtained frequencies and meriodional mode shapes. Comparisons between analytical and experimental results are presented for truncated conical shells over the following range of parameters: (1) semivertex angles from 3.4° to 60.5° . (2) shell thicknesses from 0.0178 cm to 0.0813 cm, (3) shell truncation ratio (minimum radius/maximum radius) from 1/8 to 6/7. (4) shell maximum radius, cold rolled steel, and stainless steel.

N68-33092*# National Aeronautics and Space Administration. Langley Research Center, Langley Station, Va.

A MATRIX METHOD FOR STUDYING MOTIONS OF SPACECRAFT CONSISTING OF INTERCONNECTED RIGID BODIES

Richard E. Turner Washington Sep. 1968 47 p refs

(NASA-TN-D-4749) CFSTI: HC\$3.00/MF\$0.65 CSCL 20K

A system of matrix equations was developed which describes the interaction between two rigid bodies joined at a point. The relative motion of the bodies is treated by projection matrices. A projection matrix is found which determines the angular acceleration allowed by relative angular motion about a common attachment point. Another projection matrix is found which determines the components of relative angular acceleration of the two bodies caused by physical constraints on their relative angular motion. By using these matrices, an automatically applied. This equation, the translational momentum equation, the angular momentum equation, and the translational constraint equation form a set of equations which can be used to add rigid rotating bodies to a dynamical system to achieve a new dynamical system of any desired complexity. This method is useful when constraint forces and torques must be calculated. An example dynamical system which consists of a central hub with four rigid wings connected to the hub at four different attachment points is studied. The equations of motion for this system were integrated numerically, and some parameters which describe the motion of the system are presented graphically Author

N68-33168*# Southampton Univ. (England).

THE RESPONSE OF A SIMPLY SUPPORTED PLATE TO TRANSIENT FORCES. PART 2: THE EFFECT OF N-WAVES AT OBLIQUE INCIDENCE

Anthony Craggs Washington NASA Sep. 1968 25 p refs (Grant NGR-52-052-003)

(NASA-CR-1176) CFSTI: HC\$3.00/MF\$0.65 CSCL 20K

A numerical method is used to compute the response of a simply supported plate to an 'N' wave arriving at oblique incidence. The factors influencing the response under these conditions are: (1) the ratio of the pulse duration to the fundamental period of the plate and (2) the convection forcing terms which are different for each mode. Also, asymmetric modes are excited, which do not make any contribution when the wave is at normal incidence to the plate. The computed results show that both the convection terms and the asymmetrical modes make a significant contribution to the form of the response for the displacements, velocities, and accelerations, though their effects are more dominant in the accelerations than for any other parameter.

N68-33191*# National Aeronautics and Space Administration. Lewis Research Center, Cleveland, Ohio.

EFFECT OF RESIDUAL STRESS ON FRACTURE STRENGTH OF AISI 301 STAINLESS-STEEL AND TI-5AI-2.5Sn ELI TITANIUM CRACKED THIN WALL CYLINDERS

Frederick D. Calfo Washington Sep. 1968 27 p refs (NASA-TN-D-4777) CFSTI: HC\$3.00/MF\$0.65 CSCL 20K

Six-inch- (15.2-cm-) diameter cylinders containing through-cracks were fabricated from 0.020-inch- (0.051-cm-) thick Ti-5AI-2.5Sn ELI titanium and 0.022-inch(0.056-cm-) thick AISI 301 stainless steel. Stress-relieved and non-stress-relieved cylinders were pressurized to burst at -423° and -320° F (20° and 77° K). The residual bending stresses in the titanium alloy were reduced from 65.000 to 6000 psi (45,000 to 4000 N/cm²) by means of a stress-relieving heat treatment. The effect was an increase in fracture strength of about 10.000 to 15.000 psi (6900 to 10.400 N/cm²). A reduction of residual stresses from 60,000 to 30,000 psi (42,000 to 21,000 N/cm²) in the stainless-steel cylinders did not appreciably change their fracture strength.

N68-33225*# National Aeronautics and Space Administration. Marshall Space Flight Center, Huntsville, Ala. FREE VIBRATION OF A ROTATING BEAM-CONNECTED SPACE STATION

James La Mar Milner Washington Sep. 1968 99 p refs (NASA-TN-D-4753) CFSTI: HC\$3.00/MF\$0.65 CSCL 20K

The free vibration of a rotating beam-connected space station is analyzed with a mathematical model of the space station which represents the general three-dimensional motion of the various components of the system. The space station is composed of two space modules connected by flexible beam, and the system is caused to spin in the plane of its orbit in order to produce an artificial gravity environment within the space modules. The kinetic energy and potential energy of the space station are used to develop a Lagrangian function of the system. Hamilton's principle is used to determine a set of governing equations, and a set of boundary conditions representing a clamped-clamped attachment of the beam to each space module is applied to the ends of the beam. Within the limits of small deflection theory, the motion of the space station is shown to be uncoupled into two separate types of motion, one in the plane of rotation and the other perpendicular to the plane of rotation. An exact solution is obtained for the beam deflection in the plane of rotation. The application of the nonhomogeneous boundary conditions leads to a set of simultaneous equations in the frequency p2, from which a characteristic determinant is developed. A procedure to solve for the zeros of the characteristic determinant is programmed for digital solution on the IBM 7094 Author

N68-33226*# California Inst. of Tech., Pasadena. THE BUCKLING OF THIN-WALLED CIRCULAR CYLINDERS UNDER AXIAL COMPRESSION AND BENDING

F. R. Stuart, J. T. Goto, and E. E. Sechler Washington NASA Sep. 1968 48 p refs

(Grant NsG-18-59)

(NASA-CR-1160) CFSTI: HC \$3.00/MF \$0.65 CSCL 20K

A series of tests was conducted on both electroplated copper and Mylar cylinders under combined axial compression and bending. Great care was taken to assure that the cylinders were as perfect as was possible and loading and boundary conditions were carefully controlled. For the Mylar cylinders, corrections were made for both area and stiffness of the lap joint. Under these conditions, much higher values of the buckling stress were obtained than had been reported on by previous investigators. Author

N68-33266*# North Carolina State Coll., Raleigh. NOISE REDUCTION SHAPE FACTORS IN THE LOW FREQUENCY RANGE

J. Ronald Bailey and Franklin D. Hart Washington NASA Sep. 1968 52 p refs

(Grant NGR-34-002-035)

(NASA-CR-1155) CFSTI: HC\$3.00/MF\$0.65 CSCL 20A

An analysis is made of noise reduction of small enclosures in the low-frequency range where both panel and volume are stiffness controlled. The strong dependence on geometry of the compliance of flexible panels is illustrated. Shape factors for low-frequency noise reduction are established through expressions for the acoustic compliance of enclosures and the compliances of rectangular, circular, cylindrical, and spherical panels. A comparison is made of the noise reduction of enclosures involving these elements and having equal volume, panel thickness, and exposed surface area. It is observed that the stiffer, membrane-controlled spherical and cylindrical enclosures have greater noise reduction than enclosures having flexure-controlled flat panels. A companion experimental investigation is described and the results are discussed and compared with the theory.

N68-33419*# California Inst. of Tech., Pasadena. ALMOST SURE STABILITY OF LONG CYLINDRICAL SHELLS WITH RANDOM IMPERFECTIONS

Rena Scher Fersht Washington NASA Aug. 1968 24 p refs (Grant NsG-18-59)

(NASA-CR-1161) CFSTI: HC\$3.00/MF\$0.65 CSCL 20K

A Lyapunov method is used to obtain sufficient conditions for the buckling stability of cylindrical shells with axisymmetric random imperfections. A perturbed system of equations in the neighborhood of the prebuckling solution is investigated. By reducing the problem to a system of integral equations, the stability boundary value problem of a long shell is similar to that of a dynamical system with random parametric excitations. The method has been tested numerically for the case of axisymmetric random imperfections of a cylindrical shell under axial compression. Initial imperfections were assumed to have Gaussian distribution and an exponential cosine correlation function. The critical load was obtained as a function of the root mean square of the imperfections.

N68-33737*# Southampton Univ. (England). Inst. of Sound and Vibration Research.

THE RESPONSE OF A SIMPLY SUPPORTED PLATE TO TRANSIENT FORCES. PART 1: THE EFFECT OF N-WAVES AT NORMAL INCIDENCE

Anthony Craggs Washington NASA Sep. 1968 34 p refs (Grant NGR-52-025-003)

(NASA-CR-1175) CFSTI: HC\$3.00/MF\$0.65 CSCL 20K

A numerical method is presented for determining the response of a structure to transient forces of arbitrary form. It is used to evaluate the response of a simply supported plate to an 'n' wave at normal incidence. Three response parameters are considered: the displacement, the acceleration and the stress at a particular point on the plate. It is shown that the fundamental mode dominates the displacement and stress responses in all cases. However, there is a significant contribution from the higher modes in the accelerations. The maximum response occurs when the duration of the wave is equal to the fundamental period of the plate. Author

N68-33738*# National Aeronautics and Space Administration. Langley Research Center, Langley Station, Va.

AN EXPERIMENTAL AND ANALYTICAL VIBRATION STUDY OF THIN CYLINDRICAL SHELLS WITH AND WITHOUT LONGITUDINAL STIFFENERS

John L. Sewall and Eugene C. Naumann Washington Sep. 1968 56 p refs

(NASA-TN-D-4705) CFSTI: HC\$3.00/MF\$0.65 CSCL 20K

Aluminum alloy cylindrical shells with and without external or internal integral longitudinal stiffeners for four end-support conditions were investigated. The stiffeners were of rectangular cross section and were closely spaced over the shell surface. Analytical results were obtained by application of the energy method employing the Rayleigh-Ritz procedure, in which longitudinal modal components were approximated by an arbitrary number of elementary beam-vibration functions chosen to satisfy prescribed end conditions. Results show the minimum frequencies of the externally stiffened shell, in all cases, to be significantly higher than the minimum frequencies of the corresponding internally stiffened shells. Agreement between measured and calculated frequencies was significantly improved when the analysis included local transverse bending stiffness due to the stiffeners, and additional beam modes for support conditions other than simply supported. The effect of including stiffener rotatory inertia in the analysis was found to be negligible. Applications of the analysis to two ring-stiffened shells are included to show the extent to which the averaged-stiffener Author assumption is valid for these configurations.

N68-35071*# National Aeronautics and Space Administration. Lewis Research Center, Cleveland, Ohio.

ULTRASONIC DETECTION AND MEASUREMENT OF FATIGUE CRACKS IN NOTCHED SPECIMENS

Stanley J. Klima and John C. Freche Washington Sep. 1968 31 p refs To be Presented at the SESA Fall Meeting, San Francisco, 28 Oct.-1 Nov. 1968

(NASA-TN-D-4782) CFSTI: HC\$3.00/MF\$0.65 CSCL 13H

An ultrasonic technique was developed and used to observe the formation and growth of fatigue cracks in notched cylindrical specimens subjected to reversed axial fatigue loading. Fatigue curves showing cycles to initially detectable cracks as well as cycles to fracture were obtained for an aluminum-, a titanium-, and a cobalt-base alloy and for a maraging steel. Depth of initially detectable cracks ranged between approximately 0.0005 and 0.004 in. (0.013 and 0.10 mm). Also obtained were curves relating ultrasonic system output voltage to crack depths up to 0.030 in. (0.76 mm) for three materials. These curves were used to demonstrate the capability of the device for monitoring crack growth. Author

N68-35198*# California Inst. of Tech., Pasauena. BUCKLING OF CONICAL SHELLS UNDER AXIAL COMPRESSION

Johann Arbocz Washington NASA Sep. 1968 60 p refs (Grant NsG-18-59)

(NASA-CR-1162) CFSTI: HC \$3.00/MF \$0.65 CSCL 20K

An experimental investigation of the effect of the cone semivertex angle on the buckling load of a conical shell under axial compression was carried out. The effect of a specific type of initial imperfection was also investigated. The imperfection studied was axially symmetric in shape. The experiments were carried out with shells fabricated by a copper electroforming process. The shells had no longitudinal seams. Final results showed that the dependence of the buckling load on the semivertex angle is adequately represented by the linearized theory. Also the upper boundary to the experimental results of the cones with known axisymmetric initial imperfections agreed well with previously published analytical values. Author

32 STRUCTURAL MECHANICS

N68-35199*# California Inst. of Tech., Pasadena. EXPERIMENTAL INVESTIGATION OF THE EFFECT OF GENERAL IMPERFECTIONS ON THE BUCKLING OF CYLINDRICAL SHELLS

Johann Arbocz and C. D. Babcock, Jr. Washington NASA Sep. 1968 81 p refs

(Grant NsG-18-59)

(NASA-CR-1163) CFSTI: HC\$3.00/MF\$0.65 CSCL 20K

Results are presented on complete imperfection surveys carried out on cylindrical shells before and during the loading process up to the buckling load. A noncontact probe was used to make these surveys on electroformed copper shells. The data recording process was fully automatized and the data reduction was done on an IBM 7094. Three-dimensional plots were obtained of the measured initial imperfection surfaces and of the growth of these imperfections under increasing axial loading. The modal components of the measured imperfection surfaces were also obtained. Preliminary results indicated that the prebuckling deformation which apparently caused the reduction in buckling load from that of a perfect shell could not be represented by an isolated mode. Author

N68-35496*# National Aeronautics and Space Administration. Langley Research Center, Langley Station, Va.

DIVERGENCE OF SOME ALL-MOVABLE CONTROL SURFACES INCLUDING DRAG LOADING

Robert C. Goetz Washington Oct. 1968 33 p refs (NASA-TN-D-4793) CFSTI: HC\$3.00/MF\$0.65 CSCL01A

The aeroelastic divergence characteristics of some rigid all-movable control surfaces supported by a flexible shaft have been studied analytically, and the results have been compared with existing experimental data in the Mach number range from 1.64 to 15.4. The configuration studied was a blunt, double-wedge control surface supported by a long, thin cantilever that was weak in the lift direction and stiff in the drag direction. The results of the study indicate that a new type of divergence instability is inherent to this configuration. Its character is a mode of deflection consisting of lateral bending accompanied by torsional rotation. The analysis and experiments indicate that drag loadings, in addition to lift loadings, are important in this new divergence instability. Estimates obtained from a potential energy analysis using aerodynamic characteristics calculated from simple Newtonian theory were in fair agreement with the experimental results over the entire Mach number range; however, excellent agreement resulted when measured static aerodynamic derivatives were incorporated into the analysis for the Mach 6.8 and 15.4 experiments. Author

N68-35632*# General Dynamics Corp., San Diego, Calif. DYNAMIC STABILITY OF SPACE VEHICLES. STRUCTURAL DYNAMICS MODEL TESTING

J. W. Wissmann Washington NASA Sep. 1968 48 p refs (Contract NAS8-11486)

(NASA-CR-1195) CFSTI: HC \$3.00/MF \$0.65 CSCL 20K

The principles of realistic modeling are outlined in terms of dimensional analysis, and similitude and scaling laws which introduce a physical configuration for the prototype along with the one for the scale model. Mathematical representations for each are given. Scale factors sufficient for most routine model work are calculated, and the requirements for kinematic similitude and dynamic similitude are formulated. The practical advantages of distorted scale models are cited, and the mathematical representations are reformulated to account for the variables. An example is included to demonstrate how the analytical formulation of a problem can be used to advantage to design an experiment, to reduce the number of independent variables, and to account for model distortions. Consideration is also given to ways of treating scale effects which represent a special case of model distortions. Recommended test practices are identified as definition of the problem, justification of the use of models, assessment of the model design parameters, model engineering, test setup, test procedure, and data evaluation and interpretation. MGJ

N68-37840*# Lehigh Univ., Bethlehem, Pa.

FATIGUE CRACK PROPAGATION IN CYLINDRICAL SHELLS

W. M. Catanach, Jr and F. Erodogan Washington NASA Oct. 1968 112 p 24 refs

(Grant NGR-39-007-011)

(NASA-CR-1197) CFSTI: HC \$3.00 / MF \$0.65 CSCL 20K

This report presents some of the results of the experimental and theoretical studies on the fatigue crack propagation in cylindrical shells subjected to fluctuating internal pressure. Most of the fatigue tests are performed on 6063-T6 aluminum alloys. In the analysis of the experimental results, the stress intensity factor is used as the correlation parameter. A modified crack propagation model is developed to take into account the effect of bending stresses, which are superimposed on membrane loads around the crack in shells. To evaluate the stress intensity factor, the integral equations obtained by Folias are solved numerically after separating the singularities. Partly to verify the theoretical results, strain measurements were made around the crack tip on the outside of the aluminum and inside and outside of the plexiglas cylinders. The results indicate that over the range of crack propagation data covering 10-7 to 10-3 in/cycle, the model adopted in this study seems to be highly satisfactory. Author

Includes ablation, cooling, heating, heat transfer, thermal balance, and other thermal effects; and combustion theory. For related information see also: 12 Fluid Mechanics; and 27 Propellants.

N68-10368* National Aeronautics and Space Administration. Lewis Research Center, Cleveland, Ohio. TRANSIENT CHILLDOWN OF A SINGLE THICK-WALLED TUBE BY LIQUID AND GASEOUS HYDROGEN

Francis C. Chenoweth, James J. Watt, and Earl L. Sprague Washington NASA Nov. 1967 55 p refs (NASA-TN-D-4238) CSCL 20M

The flow and heat transfer characteristics during the startup of a nuclear rocket are of particular interest because of the bootstrap type of startup. An analytical procedure was assembled using state-of-the-art equations to provide a tool for predicting the transient flow and heat transfer characteristics of reactor components during the startup. The results of applying this analytical procedure to a single thick-walled tube, which was selected as typical of a passage in the reflector of a current nuclear reactor, are presented. Experiments were performed on a thick-walled tubular

test section to provide experimental data for comparison with predicted results. With the test section at room temperature, either liquid-hydrogen or cold-hydrogen-gas flow was directed through the 3/16-inch (0.476-cm) bore of the 55-inch (139.6-cm) long test section until it was thoroughly chilled. During most of the liquid-hydrogen chilldown, a saturated liquid was assumed to be at the inlet of the test section. During the gas chilldown, the inlet gas temperature varied from 470° to 360°R (261° to 200°K). Inlet pressures ranged from 20 to 50 psia $(1.38 \times 10^5 \text{ to } 3.45 \times 10^5 \text{ to } 3.55 \times 10^5 \text{ to } 3.$ N/m abs). The initial wall temperatures and the flow rate, the inlet enthalpy, and the inlet pressure as functions of time from the experimental test were used as input for the analytical procedure. Comparison of predicted and experimental material temperatures, pressures, and exit temperatures indicated that, when cold hydrogen gas was used as the chilling medium, excellent agreement was obtained. When liquid hydrogen was used, only the average chilldown rates of the test section agreed. Local predicted material temperature variations were traced to characteristics of the heat transfer correlations used. Pressure and exit temperature variations were related to an extreme sensitivity of predicted values to Author variations in inlet quality and flow rate.

N68-11038*# National Aeronautics and Space Administration. Ames Research Center, Moffett Field, Calif.

THE EFFECTS OF MOLECULAR STRUCTURE ON THE THERMOCHEMICAL PROPERTIES OF PHENOLICS AND RELATED POLYMERS

John A. Parker and Ernest L. Winkler Washington Nov. 1967 40 p refs Presented at the Symp. on Phenolic Chem., Natl. Meeting of Am. Chem. Soc., Miami, Fla., Apr. 1967

(NASA-TR-R-276) CFSTI: HC\$3.00/MF\$0.65 CSCL 111

Phenolic resins and related polymers were synthesized by established methods to provide different types of char-forming polymers for pyrolysis studies. Certain features of the molecular structure of these polymers which determine the char yield have been characterized. Pyrolysis studies were carried out under both thermogravimetric conditions and in environments simulating reentry ablation to relate the char yields of these polymers to their molecular structure. It has been possible to account for the char-forming reactions of these phenolic derived resins in terms of a general pyrolysis mechanism for these classes of polymers. An analysis based on this mechanism was developed which predicts from molecular structure the observed thermogravimetric char yields

accurately over a range from 11 to 65% yield. This analysis makes it possible to control the primary rates of vapor to char production as required for particular heat-shield applications. Composites from these polymers were developed and tested under one-dimensional pyrolysis simulating reentry ablation. Up to applied heating rates of about 25 cal cm⁻²sec⁻¹, the observed char yields agree quite closely with those obtained in thermogravimetric tests. It is tentatively concluded that the primary char-forming processes with these classes of materials are independent of polymer heating rate over a range of temperature rise rates varying from 2° to 5000°C per minute. With certain composites and at heating rates greater than 25 cal $cm^{-2}sec^{-1}$ an additional amount of char is formed due to secondary pyrolysis of vapor products within the char matrix induced by high char temperatures. These secondary processes seem to depend on surface temperature, impact pressure, and the chemical nature of the vapor products. Author

N68-11144* National Aeronautics and Space Administration. Langley Research Center, Langley Station, Va.

CHARTS FOR EQUILIBRIUM ISENTROPIC EXPANSION OF AIR BEHIND SHOCKS UP TO 50000 FEET PER SECOND (15.24 KILOMETERS PER SECOND)

Ernest V. Zoby and Wayne D. Erickson Washington Nov. 1967 51 p refs

(NASA-TN-D-4247) CFSTI: \$3.00 CSCL 20M

Isentropic state properties (enthalpy, temperature, and density) have been computed for equilibrium air as a function of pressure relative to the respective stagnation-point conditions behind normal shocks for a wide range of velocities and altitudes. The free-stream velocities ranged from 10,000 to 50,000 ft/sec and the altitudes ranged from 50,000 to 300,000 feet. These isentropic properties with the associated normal shock properties of pressure, temperature, and density were correlated with nonreacting perfect-gas isentropic and normal shock expressions. Charts of the correlation parameters are presented as well as a simple procedure for computing the properties.

N68-11491*# National Aeronautics and Space Administration. Lewis Research Center, Cleveland, Ohio.

WEAK LOCALLY HOMOGENEOUS TURBULENCE AND HEAT TRANSFER WITH COMBINED TWO-DIMENSIONAL SHEAR AND NORMAL STRAIN

Robert G. Deissler Washington Dec. 1967 26 p refs

(NASA-TN-D-4273) CFSTI: HC\$3.00/MF\$0.65 CSCL 20M

An analysis of the effects of shear and normal strain on weak turbulence and turbulent heat transfer is made using two-point correlation equations obtained from the Navier–Stokes and energy equations. The correlation equations are converted to spectral form by taking their Fourier transforms. The resulting first-order partial differential equations are then reduced to an equivalent set of ordinary differential equations. The normal strain is taken as two-dimensional, uniform, and incompressible, with a contraction occurring in the same transverse direction as the uniform shear and temperature gradients. The turbulence is assumed to be initially isotropic but becomes anisotropic in the presence of the shear and normal strain. Author

N68-11636* National Aeronautics and Space Administration. Lewis Research Center, Cleveland, Ohio.

MIST-FLOW HEAT TRANSFER USING SINGLE-PHASE VARIABLE-PROPERTY APPROACH

Yih-yun Hsu, Glenn R. Cowgill, and Robert C. Hendricks Washington Dec. 1967 81 p refs

(NASA-TN-D-4149) CFSTI: \$3.00 CSCL 20M

Film-boiling mist flow is treated as a single-phase flow with properties being synthesized from those of liquid and vapor phases weighted according to their respective volume fraction. Such a synthesizing approach renders it possible to apply the technique for single-phase turbulent flow to the two-pase flow. Computational results for film-boiling hydrogen at low pressure predicts the experimental data within 25 percent; the deviation between the analytical and experimental results increases gradually with increasing pressure. Further analysis showed that the deviation was due to the assumptions of a thermodynamic equilibrium and homogeneous distribution of void. A simplified design method is proposed so that the heat-transfer coefficient can be calculated from the Dittus-Boelter equation by specifying a reference temperature and a reference void fraction for computation of properties. The coefficient for determining such a reference temperature and void is primarily a function of the bulk void fraction. Author

N68-11642*# National Aeronautics and Space Administration. Lewis Research Center, Cleveland, Ohio.

HYDROGEN-OXYGEN CHEMICAL REACTION KINETICS IN ROCKET ENGINE COMBUSTION

Martin Hersch Washington Dec. 1967 20 p refs

(NASA-TN-D-4250) CFSTI: HC\$3.00/MF\$0.65 CSCL 07D Hydrogen-oxygen reaction times and concentration histories

of chemical species during reaction were calculated for rocket combustor conditions. Calculations were made for oxidant-fuel weight ratios of 1 and 10 and initial reactant temperatures of 1200° to 2500°K at a chamber pressure of 20 atmospheres $(2.0 \times 10^6 \text{ N/sq})$ m). The reaction time varied from about 0.01 second at 1200°K to a few microseconds at 2500°K. Calculations were made by using a numerical integration program and an analytical solution. The reaction mechanism used included five chain branching reactions and three recombination-type reactions. Author

N68-11721*# Israel Program for Scientific Translations, Ltd., Jerusalem.

HEAT AND MASS TRANSFER. VOLUME 1: CONVECTIVE HEAT EXCHANGE IN A HOMOGENEOUS MEDIUM [TEPLO-I MASSOPERENOS. KONVEKTIVNYI TEPLOOBMEN V ODNORODNOI SREDE]

A. V. Lykov, ed., and B. M. Smol'skii, ed. 1967 313 p refs Transl. into ENGLISH from Nauka i Tekhnika (Minsk), 1965 Published for NASA and NSF

(NASA-TT-F-431; TT-67-51367) CFSTI: \$3.00 CSCL 20M

Heat transfer and friction resistance in homogeneous media, convective processes, hydrodynamics, boundary layer flow, and unsteady state conditions are covered in a series of papers dealing with experiments in fluid and gas dynamics. For individual titles see N68-11722 to N68-11753. M.W.R.

N68-11811*# National Aeronautics and Space Administration. Ames Research Center, Moffett Field, Calif.

COMPARISON OF CONVECTIVE STAGNATION HEAT TRANSFER IN AIR, CO₂-N₂, AND CO₂-Ar₂ GAS MIXTURES Clifford M. Akin and Joseph G. Marvin Washington Nov. 1967 15 p refs

(NASA-TN-D-4255) CFSTI: HC\$3.00/MF\$0.65 CSCL 20M

Convective stagnation-point heat transfer was measured on hemispherical models in air, in 50% CO₂, 50% N₂, and in 65% CO₂, 35% Ar (by volume). The measurements were made in combustion-driven shock tubes over a total enthalpy range from 9.3×10^6 to 48×10^6 J/kg with corresponding stagnation-point pressures from 15 to 160 atmospheres. At the same stagnation enthalpy and pressure, no significant difference was found between the heat transfer measured in air and in the gas mixtures. This observation agrees with theory. The data were adequately predicted by theories which took into account the stagnation-point stagnation-point pressures of the present tests. Author

N68-14042*# National Aeronautics and Space Administration. Lewis Research Center, Cleveland, Ohio.

ANALYSIS OF TURBULENT LIQUID-METAL HEAT TRANSFER IN CHANNELS WITH HEAT SOURCES IN THE FLUID POWER-LAW VELOCITY PROFILE

Robert M. Inman Washington Jan. 1968 39 p refs

(NASA-TN-D-4336) CFSTI: HC\$3.00/MF\$0.65 CSCL 20M

An analysis is made to determine the heat-transfer characteristics for turbulent flow of a heat-generating liquid metal between parallel plates with wall heat transfer. The internal heat generation is uniform over the channel cross section and along its length. The wall heat transfer is also uniform along the channel length. The analysis applies in the thermal entrance region of the channel as well as far downstream. The fluid is assumed to have a fully developed, turbulent power-law velocity profile which is unchanging throughout the length of the channel. The idealized eddy diffusivity profile proposed by Poppendiek is used. Numerical results for the wall temperature distribution and Nusselt number variation are presented in graphical form for a 1/7-power-law velocity profile and for values of k ranging from 1 to 5. Results for the fully developed Nusselt numbers for liquid metal flow without internal heat generation are compared with existing calculations (based on the assumption that the eddy diffusivities of heat and momentum are equal) and exhibit good agreement. Author

N68-14052* National Aeronautics and Space Administration. Marshall Space Flight Center, Huntsville, Ala.

NONLINEAR HEAT TRANSFER AND TEMPERATURE DISTRIBUTION THROUGH FINS AND ELECTRIC FILAMENTS OF ARBITRARY GEOMETRY WITH TEMPERATURE-DEPENDENT PROPERTIES AND HEAT GENERATION

A. R. Shouman Washington Jan. 1968 44 p refs (NASA-TN-D-4257) CFSTI: \$3.00 CSCL 20M

A theoretical analysis was conducted of one-dimensional, steady-state, heat exchange by both convection and radiation between a rod or a fin and their surroundings. The analysis considers both the cases where the heat is being dissipated or received by the fin or rod. Both the infinite and finite length cases are considered. The surroundings equivalent temperature for radiation could be different from that for convection. The fin or rod could have an arbitrary geometry and its physical properties could be temperature dependent as well as displacement dependent. The analysis also considers the effect of heat generation or absorption. The exact solution of the problem for a constant area fin or rod with constant thermal properties is presented. The solution produces two functions of parametric nature. The different parameters are dependent on the boundary conditions. A computer program for evaluating the functions was written. It was shown that the heat generation or absorption cases are reducible to the simple case through a suitable transformation. After this transformation, the tabulated functions can be used for solving problems with internal heat generation or absorption. Author

N68-14240*# National Aeronautics and Space Administration. Lewis Research Center, Cleveland, Ohio.

CORRELATION OF LOCAL HEAT TRANSFER COEFFICIENTS FOR SINGLE PHASE TURBULENT FLOW OF HYDROGEN IN TUBES WITH TEMPERATURE RATIOS TO 23

Maynard F. Taylor Washington Jan. 1968 22 p refs (NASA-TN-D-4332) CFSTI: HC\$3.00/MF\$0.65 CSCL 20M

The existing methods of correlating and predicting single-phase turbulent heat-transfer coefficients with variable properties give coefficients which are sometimes in poor agreement with measured values. Each prediction method can be used only over a limited range of pressure, temperature, ratio of axial position to diameter, and ratio of surface to fluid bulk temperature ratio. Local heat-transfer coefficients for hydrogen from 10 investigations using symmetrically heated straight tubes were used to determine a single equation that will predict heat-transfer coefficients over a wide range of conditions including surface to fluid bulk temperature ratios to 23. Author

N68-14270*# National Aeronautics and Space Administration. Lewis Research Center, Cleveland, Ohio.

THEORETICAL TEMPERATURES OF THIN-FILM SOLAR CELLS IN EARTH ORBIT

Curt H. Liebert and Robert R. Hibbard Washington Jan. 1968

(NASA-TN-D-4331) CFSTI: HC \$3.00/MF \$0.65 CSCL 10A

An analysis was made and equations and charts were developed that make it easy to calculate the temperatures of opaque, thin, flat plates in a Sun-planet system. The analysis is general and includes the effects of sunlight, albedo, and Earth radiation at any altitude and for any orientation; it requires that the absorptance and emittance of the plate surfaces be known. This analysis was applied to three thin-film cadmium sulfide solar cells, and it uses experimentally determined optical properties to calculate equilibrium temperatures in various Earth orbits. The calculations consider the effect of painting the inactive side with a black paint or a white, zinc oxide (ZnO) paint and the effect of lowering the solar absorptance of the active side at wavelengths not used in photovoltaic energy conversion. The results show that the temperature of present day cells with the inactive side not painted may vary from 346° K in sunlight to 92°K in the Earth's shadow. It was observed that the temperatures in sunlight may be lowered by painting the inactive side with a ZnO paint. Further temperature reductions may be achieved by lowering the solar absorptance of the active side at wavelengths not used in photovoltaic energy Author conversion.

N68-15330*# National Aeronautics and Space Administration. Lewis Research Center, Cleveland, Ohio.

EXPERIMENTAL INVESTIGATION OF NUCLEATE BOILING BUBBLE DYNAMICS IN NORMAL AND ZERO GRAVITIES

Thomas H. Cochran, John C. Aydelott, and Charles M. Spuckler Washington Feb. 1968 23 p refs

(NASA-TN-D-4301) CFSTI: HC\$3.00/MF\$0.65 CSCL 20M

The effects of gravity on the dynamics of bubbles generated on a flat horizontal surface are investigated in the heat-flux range defined as the discrete bubble region over a range of subcoolings, fluid properties, and heat-transfer rates. The zero-gravity data were obtained by allowing the experiment package to free fall in a 2.2-second drop tower, which permitted the attainment of less than 10^{-5} times Earth gravity. Data taken from high-speed motion pictures indicated that boiling was independent of gravity at high subcooling and that the transition from the discrete bubble region occurred at a lower heat flux in zero gravity than in normal gravity. Application of an analysis to the data indicated that a newly defined pressure force was of importance in bringing about bubble separation.

N68-15742*# National Aeronautics and Space Administration. Lewis Research Center, Cleveland, Ohio.

TRANSIENT SOLIDIFICATION OF A FLOWING LIQUID ON A COLD PLATE INCLUDING HEAT CAPACITIES OF FROZEN LAYER AND PLATE Robert Siegel and Joseph M. Savino Washington Feb. 1968 27 p refs Presented at the ASME Winter Ann. Meeting, Pittsburgh, 17 Nov. 1967 /ts Paper No. 67-WA/HT-34

(NASA-TN-D-4353) CFSTI: HC\$3.00/MF\$0.65 CSCL 20M

An analysis is made of solidification within a flowing medium where a convective boundary condition is imposed on the moving interface of the solidifying layer. The configuration is one in which a frozen layer forms in a warm liquid as it is chilled while flowing over a plane wall that is convectively cooled on the opposite side. The analysis includes the heat capacities of both the wall and frozen layer. The solution for frozen layer thickness variation with time is given as a closed-form algebraic equation and in graphical form so that results can be readily evaluated for use in practical applications. Some illustrative examples are given for flowing water in contact with Inconel plates of various thicknesses to demonstrate the effect of the heat capacities and the liquid and cooland temperatures on the growth of the ice layer and the temperature distributions in the ice and wall.

N68-15833*# Dynamic Science Corp., Monrovia, Calif. COMBUSTION INSTABILITY PREDICTION USING A NONLINEAR BIPROPELLANT VAPORIZATION MODEL

R. J. Hoffman, R. O. Wright, and B. P. Breen Washington NASA Jan. 1968 100 p refs

(Contract NAS7-442)

(NASA-CR-920) CFSTI: HC\$3.00/MF\$0.65 CSCL 20B

An extension of the Priem-Guentert nonlinear annular combustion instability model for liquid rocket engines is presented. additions to the model include: droplet drag effects, propellant spray distributions, and independent heat and mass addition due to a bipropellant system. The addition of droplet drag to the transport equations produces a new dimensionless term, the drag parameter. Computer results show that droplet drag can produce large attenuations in sensitivity to combustion instability. Drop sprays are treated by defining a spray distribution function for both the fuel and oxidizer spray entering an annulus. Results of a parametric study of the influence of mean drop size and of standard deviation are presented. The instability equations were modified to independently calculate mass and heat addition, and these modifications were included in the computer solution. Generally, the independent addition of mass to the flow produced trends similar to the simultaneous addition of heat and mass. For comparison, a complete engine stability map was generated using both the bipropellant model and the monopropellant model. Significant differences are apparent in the predicted sensitivity to instability. Author

N68-15942*# National Aeronautics and Space Administration. Lewis Research Center, Cleveland, Ohio.

DISPLACEMENT OF DISINTEGRATING LIQUID JETS IN CROSS FLOW

Frederick P. Povinelli Washington Feb. 1968 21 p refs

(NASA-TN-D-4334) CFSTI: HC\$3.00/MF\$0.65 CSCL 21B

The displacement of three sizes of liquid jets breaking up in a crossflow was measured in a shock tube. Data were obtained for water, oxygen, n-heptane, and three glycerol-water mixtures in gas flows up to 1080 feet per second (329 m/sec). The displacement was approximately proportional to gas velocity squared and inversely proportional to jet diameter. Data were correlated with an empirical parameter. A simple model of jet displacement which includes the rate of mass removal also led to a correlation of the data. Author

N68-16300*# National Aeronautics and Space Administration. Lewis Research Center, Cleveland, Ohio.

POTENTIAL USE OF HIGH FREQUENCY INDUCTION HEATING FOR HIGH TEMPERATURE LIQUID METAL HEAT TRANSFER TESTING

John V. Miller Washington Feb. 1968 50 p refs

(NASA-TM-X-1510) CFSTI: HC\$3.00/MF\$0.65 CSCL 20M To investigate potential methods of obtaining high temperature liquid metal heat transfer data, several heating devices were examined and the problems of each are discussed. One promising

method is high frequency induction heating. The heating coil is physically separated from the test section, is maintained at a lower temperature than the test section, and therefore, can be constructed of low temperature materials. A thick walled cylinder, internally cooled with liquid metal, was analyzed to evaluate the characteristics of an inductively heated test section. Results indicate that, if the ratio of cylinder radius to current depth is greater than 6, internal heat generation in the cylinder's center is negligible. With a tungsten cylinder; high frequency equipment can obtain the necessary cylinder-radius to current-depth ratio without exceeding allowable thermal stress levels for tungsten. Based on an error analysis of an inductively heated test section, experimental determination of liquid metal heat transfer coefficients at high heat flux levels can be made to an accuracy of $\pm 10\%$ for reasonable tolerances on thermocouple placement and temperature measurements. Author

N68-16324*# National Aeronautics and Space Administration. Lewis Research Center, Cleveland, Ohio.

ANALYTICAL COMPARISON OF RANKINE CYCLE SPACE RADIATORS CONSTRUCTED OF CENTRAL, DOUBLE, AND BLOCK-VAPOR-CHAMBER FIN-TUBE GEOMETRIES

Henry C. Haller and Seymour Lieblein Washington Feb. 1968 62 p refs

(NASA-TN-D-4411) CFSTI: HC\$3.00/MF\$0.65 CSCL 13A

An analytical comparison of flat direct-condensing radiators constructed of three different finned tube geometries was made over a wide range of design variables for a 500-day mission, 500-kilowatt output high-temperature Rankine space electric power generating system which used potassium as the cycle working fluid. The fin-tube configurations considered were the central, the double, and the block vapor chamber geometries. The solid conducting fin geometries (central and double fin) were composed of stainless-steel-clad copper fins. The vapor-chamber fin radiator was evaluated for both stainless-steel-clad and all stainless-steel fins. The vapor-chamber fin-tube radiator consistently showed a significantly lower weight per kilowatt output (specific weight) than the two solid conducting fin radiators. A relatively small reduction in planform area per kilowatt output (specific planform area) at least weight condition was indicated for the vapor-chamber fin-tube radiator compared with the solid conducting fin-tube configurations. In general, the vapor-chamber fin-tube radiator can utilize larger tube diameters and fewer number of tubes than the solid conducting geometries with the least increase in specific weight and planform area. Author

N68-16683*# National Aeronautics and Space Administration. Lewis Research Center, Cleveland, Ohio.

MINIMUM FILM-BOILING HEAT FLUX IN VERTICAL FLOW OF LIQUID NITROGEN

Frederick F. Simon, S. Stephen Papell, and Robert J. Simoneau Washington Feb. 1968 36 p refs

(NASA-TN-D-4307) CFSTI: HC\$3.00/MF\$0.65 CSCL 20M

A study was made of the minimum film-boiling heat flux of liquid nitrogen flowing in a vertical, electrically heated tube. Inlet liquid velocities up to 3 meters per second were studied for reduced pressures P/P_c of 0.071, 0.20, and 0.40. An analysis of the wall conduction was used to predict the wall temperatures occurring at the minimum heat flux for an electrically heated system. The predicted wall temperatures were then used in conjunction with a heat-transfer analysis for predicting the minimum heat flux. The analytical results are in good agreement with the experimental data.

N68-17566*# National Aeronautics and Space Administration. Lewis Research Center, Cleveland, Ohio.

BOILING HEAT TRANSFER COEFFICIENTS, INTERFACE BEHAVIOR, AND VAPOR QUALITY IN ROTATING BOILER OPERATING TO 475 G's Vernon H. Gray, Paul J. Marto, and Allan W. Joslyn (NASA, Manned Spacecraft Center, Houston, Tex.) Washington Mar. 1968 41 p refs

(NASA-TN-D-4136) CFSTI: HC \$3.00/MF \$0.65 CSCL 20M

An experimental heated-wall rotating boiler was investigated with continuous through-flow water as the test fluid. Heat-transfer coefficients were obtained with the boiler stationary and at rotative accelerations to 200 g's. Heat fluxes up to 505,000 Btu per hour per square foot were employed in obtaining the coefficients. Photographic and boiler-performance data were obtained to 475 g's. Outlet vapor quality, measured by throttling calorimeters, varied from above 99 percent to several degrees of vapor superheat. High-speed motion pictures revealed that high accelerations nearly eliminated disturbances at the liquid-vapor interface, reduced the number and size of bubbles, and promoted direct evaporation across the interface by the mechanism of convective secondary-flow cells in the rotating fluid annulus. Boiling heat-transfer coefficients at low heat fluxes were increased by increases in acceleration. At high heat fluxes the opposite was true, although the variation in coefficient was small and comparable with that caused by surface conditioning and aging effects. The crossover points for the coefficients occurred at progressively higher heat-flux levels as acceleration was increased. A boiling heat-transfer coefficients as high as 9000 Btu per hour per square foot per °F was measured (at the highest heat-flux value). Boiler-test performance was quite satisfactory and warranted consideration of the rotating boiler concept in Rankine cycle systems for power generation.

Author

N68-18046*# National Aeronautics and Space Administration. Lewis Research Center, Cleveland, Ohio.

SELF EVACUATED MULTILAYER INSULATION OF LIGHTWEIGHT PREFABRICATED PANELS FOR CRYOGENIC STORAGE TANKS

Porter J. Perkins, Robert P. Dengler, L. R. Niendorf, and G. E. Nies Washington Mar. 1968 25 p refs

(NASA-TN-D-4375) CESTI HC\$3 00/ME\$0.65 CSCL 13D

A new concept for simplifying the application of radiation-shield insulation to cryogenic tanks was developed and tested for both ground and space performance. A vacuum-tight flexible casing of laminated aluminized Mylar encloses the multilayers, forming panels that are bonded to tank walls in an overlapping shingle arrangement. The panels, weighing only 0.34 pound per square foot (1.66 kg/m^2), are filled with carbon dioxide (CO₂) gas which cryopumps to provide required vacuum when the tank is filled with a cryogen. The thermal performance of this insulation was determined in flat-plate and cylindrical calorimeters. Of the many materials tested in the flat-plate calorimeter, polyurethane foam was chosen as the separator between radiation shields because of its small increase in heat flux when compressed to 14.7 psi (10.13 N/cm²) in panels evacuated in the atmosphere. During ground tests, insulation panels as large as 3 by 6 feet (0.91 by 1.83 m) were mounted on a cylindrical calorimeter of liquid hydrogen and cryopumped to at least 5×10^{-3} torr (6.66 × 10⁻⁵ N/cm²). This procedure resulted in a heat flux of 23 Btu per hour per square foot (261,000 J/(hr) (m²)) for an external temperature of 70°F (294°K). In simulated space tests, panels evacuated by outside vacuum resulted in a heat flux of 0.86 Btu per hour per square foot (9770 J/ (hr) (m²)) with outside surfaces at 70°F (294°K). Author

N68-18122*# National Aeronautics and Space Administration. Langley Research Center, Langley Station, Va.

A THREE-DIMENSIONAL ANALYSIS OF THE EFFECTS OF HEAT GENERATION IN PLATES

Robert R. McWithey Washington Jan. 1968 27 p refs (NASA-TN-D-4326) CFSTI: HC\$3.00/MF\$0.65 CSCL 20M

A method for determining three-dimensional steady-state temperature distributions is presented for plates in which heat is generated and conducted throughout the plate material. The solution for the temperature distribution is given in terms of a power series with respect to the plate thickness coordinate. The coefficients of the power series are dependent upon the temperature distribution over the plate surfaces. Specific attention is given to the determination of temperature distributions and plate deformations resulting from constant heat generation and from the absorption of electromagnetic radiation. Author

N68-18196*# National Aeronautics and Space Administration. Lewis Research Center, Cleveland, Ohio.

PRESSURE-RISE CHARACTERISTICS FOR A LIQUID HYDROGEN DEWAR FOR HOMOGENEOUS, NORMAL GRAVITY QUIESCENT, AND ZERO GRAVITY TESTS

Kaleel L. Abdalla, Thomas C. Frysinger, and Charles R. Andracchio Washington Sep. 1965 35 p refs (Declassified)

(NASA-TM-X-1134) CFSTI: HC\$3.00/MF\$0.65 CSCL 20M

The pressure-rise characteristics for a liquid-hydrogen Dewar were obtained by utilizing a scientific passenger pod on an Atlas intercontinental ballistic missile during a 21-minute gravity free flight. Results were compared with those from homogeneous and normal-gravity quiescent tests. Residual pod rotation created an undesirable acceleration field on the Dewar of approximately 10^{-3} g throughout the weightless flight time. Temperature instrumentation indicated wall drying during this period. The resultant pressure-rise characteristics were similar to those for the normal-gravity test. Author

N68-19187*# National Aeronautics and Space Administration. Lewis Research Center, Cleveland, Ohio. CONSIDERATIONS OF TURBINE COOLING SYSTEMS FOR

CONSIDERATIONS OF TURBINE COOLING SYSTEMS FOR MACH 3 FLIGHT

Francis S. Stepka Washington Apr. 1968 43 p refs (NASA-TN-D-4491) CFSTI: HC\$3.00/MF\$0.65 CSCL 20M

A method is presented for rapidly determining the approximate average midspan metal temperatures and coolant flow requirements of turbine airfoils cooled by compressor exit bleed air. Presented also are the potential reductions in airfoil metal temperatures, coolant flows, or increases in average turbine inlet gas temperatures that are possible by utilization of various airfoil cooling designs, cooling methods, and cooling systems other than the direct use of compressor exit bleed air. These additional cooling systems were direct cooling with engine fuels (Jet A or liquid methane) and the use of heat exchangers to reduce the compressor exit bleed air temperature. The cooling fluids that were used in the heat exchangers were: engine fuel, by-pass air in the fan exit duct of a turbofan engine, and ram air. The analysis was conducted to engines of aircraft cruising at Mach 3 at an altitude of 75,000 feet (22.8 km). Turbine inlet gas temperatures from 2270° to 3170°F (1515° to 2020°K) were investigated. Author

N68-20065*# National Aeronautics and Space Administration. Langley Research Center, Langley Station, Va.

APPROXIMATE RELATIONS FOR LAMINAR HEAT-TRANS-FER AND SHEAR-STRESS FUNCTIONS IN EQUILIBRIUM DISSOCIATED AIR

Ernest V. Zoby Washington Apr. 1968 21 p refs

(NASA-TN-D-4484) CFSTI: HC\$3.00/MF\$0.65 CSCL 20M

Simple, approximate equations have been developed for computing the normal derivatives of enthalpy and velocity evaluated. at the surface of a flat plate or cone and of a blunt axisymmetric body. These approximate equations were developed by correlating exact similar solutions to the laminar boundary-layer equations for equilibrium dissociated air. The results of these approximate equations represent the exact solutions within ± 10 percent. Author

N68-20066*# National Aeronautics and Space Administration. Lewis Research Center, Cleveland, Ohio.

ANALYSIS OF PRESSURE-DROP FUNCTION IN RANKINE SPACE POWER BOILERS WITH DISCUSSION OF FLOW MALDISTRIBUTION IMPLICATIONS Andrew A. Schoenberg and Donald R. Packe Washington Apr. 1968 64 p refs

(NASA-TN-D-4498) CFSTI: HC\$3.00/MF\$0.65 CSCL 13A

The analysis was performed for counterflow liquid-heated single-pass boilers of the type used in Rankine space power systems such as SNAP-8. The analysis takes into account the nonuniform axial distribution of heat flux, variable geometry factors, and the variation of the lengths of the preheat, boiling, and superheat regions. Comparison with data from a single-tube water boiler indicates that the analytical model predicts the pressure drop and its dependence on various boiler-input variables with an average error of less than 10 percent. With the use of results generated from the analytical model, effects on the pressure-drop function caused by variations in some of the geometric and thermodynamic parameters of the boiler were studied. From these studies, the following causes of the multivalued characteristic were established: (1) The magnitude of the multivalued effect is strongly influenced by a boiler-tube insert, but the characteristic could exist even with an open tube. (2) The multivalued characteristic can exist for either a choked nozzle or a constant pressure at boiler discharge. Methods for eliminating the multivalued characteristic and thus the potential for flow maldistribution are evaluated. Author

N68-20331*# National Aeronautics and Space Administration. Lewis Research Center, Cleveland, Ohio.

RADIANT-INTERCHANGE CONFIGURATION FACTORS FOR SPHERICAL AND CONICAL SURFACES TO SPHERES

James P. Campbell and Dudley G. McConnell Washington Apr. 1968 24 p refs

(NASA-TN-D-4457) CFSTI: HC\$3.00/MF\$0.65 CSCL 20M

Geometric configuration view factors have been calculated for a sphere and for cones radiating to a sphere. A computer program was set up to give configuration view factors not only for the entire radiating body but, also, for bands of the radiating body which permit the determination of the configuration view factor between any part of the radiating body and the sphere. The range of configurations consisted of equal radii spheres, and right-circular cones of semiapex angles of 15°, 30°, 45°, and 60° radiating to a sphere on the cone axis with radius equal to the cone base radius. Separations for all cases ranged from zero to 10 sphere radii. Curves are presented that give the configuration view factor for any configuration within the limits of the study. Author

N68-20338*# National Aeronautics and Space Administration, Lewis Research Center, Cleveland, Ohio.

LOCAL HEAT TRANSFER FOR WATER IN ENTRANCE REGIONS OF TUBES WITH TAPERED FLOW AREAS AND NONUNIFORM HEAT FLUXES

Nick J. Sekas and James R. Stone Washington Apr. 1968 18 p refs

(NASA-TM-X-1554) CFSTI: HC\$3.00/MF\$0.65 CSCL 20M

Local convective heat-transfer coefficients of water flowing through electrically heated circular tubes with axially varying heat fluxes and flow areas were investigated. Data were obtained in the turbulent flow regime with local Reynolds numbers from 8000 to 50 000 over a Prandtl number range of 1.6 to 4.5. Measurements of mass flow rate, heat flux, water bulk temperatures at tube inlet and outlet, and axial temperature distribution for each run were made and are presented in tabular form. Plots of local to fully developed Nusselt number ratio as a function of heated length-to-diameter ratio are presented. These data are compared with calculated values of the local to fully developed Nusselt number ratios based on a previously reported correlation of entrance effects with tubes of constant flow area and uniform heat flux. The calculated Nusselt number ratios generally approximated the present Author experimental results.

N68-20374*# National Aeronautics and Space Administration. Lewis Research Center, Cleveland, Ohio.

HEAT-TRANSFER CORRELATION FOR GAS FLOW ACROSS HEATED BANKS OF WIRE MESHES OR TUBES

Byron L. Siegal Washington Apr. 1968 25 p refs

(NASA-TN-D-4514) CFSTI: HC\$3.00/MF\$0.65 CSCL 20M

The heat-transfer data of this investigation for nitrogen flowing across a bank of electrically heated mesh were compared with the data of other investigators for the flow of hydrogen, nitrogen, helium, and air across single meshes, banks of meshes, and banks of tubes. The data covered the following ranges of variables: (1) Porosities from 0.37 to 0.88, (2) Wire or tube diameters from 0.0076 to 0.375 inch (0.0193 to 0.952 cm), (3) Surface temperatures to 5500° R (3050° K), (4) Outlet gas temperatures to 3160° R (1760° K), and (5) Reynolds numbers from 3 to 30,000. A heat-transfer correlation based on surface-temperature gas property evaluation, wire diameter, and average mesh flow area was found which correlated the data within ± 20 percent. Author

N68-21536*# National Aeronautics and Space Administration, Washington, D. C.

DIRECTIONAL DISTRIBUTION IN THE REFLECTION OF HEAT RADIATION AND ITS EFFECT ON HEAT TRANSFER

Benjamin Muench (Ph.D. Thesis-Swiss Tech. Coll., 1955) Apr. 1968 95 p refs Transl. into ENGLISH of the publ. "Die Richtungsverteilung bei der Reflexion von Waermestrahlung und ihr Einflus auf die Waermeuebertrangung" Zurich, 1955

(NASA-TT-F-497) CFSTI: HC\$3.00/MF\$0.65 CSCL 20M

The thermal radiation properties of a surface can be characterized by its emission and reflection coefficients. An experimental apparatus is described for measuring the reflection coefficient as a function of the incident and reflected directions. All directional distributions from the purely specular to the strongly scattering were found by superposition of purely specular and diffuse results. A good approximation was found for the tests on concentric spheres. Author

N68-21680*# National Aeronautics and Space Administration. Lewis Research Center, Cleveland, Ohio.

EXPERIMENTAL INVESTIGATION OF AN ACOUSTIC LINER WITH VARIABLE CAVITY DEPTH

Bert Phillips Washington Apr. 1968 53 p refs

(NASA-TN-D-4492) CFSTI: HC\$3.00/MF\$0.65 CSCL 21H

An acoustic liner with individually isolated resonators and variable cavity depths was tested with a nominal 20,000-pound thrust hydrogen-oxygen rocket engine. The liner damping was evaluated by comparing values of hydrogen-inlet temperature at transition into combustion instability. Three concentric tube injectors were studied. Test variables were liner cavity depth, number of liner rows, and axial position of the liner rows. Cavity gas temperature and composition were measured at the screech transition point. A flow-induced frequency shift using a theoretical axial gas velocity profile changed the calculated resonant frequency to a value matching the pretransition noise frequency. The amplitude of the pretransition noise oscillations associated with the three injectors affected liner damping. The most effective axial position of the resonators was determined to be closest to the injector. Effectiveness of row combinations of the resonators at some other positions was also determined. There was a much higher concentration of hydrogen and hence higher sonic velocity in the resonator cavities than had been predicted in previous reports. Author

N68-21704*# National Aeronautics and Space Administration. Lewis Research Center, Cleveland, Ohio.

EFFECT OF FINNED-TUBE ASSEMBLY TECHNIQUES ON THE HEAT-TRANSFER CHARACTERISTICS OF A SPACE RADIATOR

Lawrence A. Mueller Washington Apr. 1968 20 p refs

(NASA-TM-X-1557) CFSTI: HC\$3.00/MF\$0.65 CSCL 13A

Nine methods of fabricating a finned-tube space radiator were tested. Both mechanical and metallurgical joining of stainless-steel tubes to aluminum meteoroid armor and fins were investigated and compared with an all-aluminum radiator. The mechanically assembled sample had a heat-radiating capacity of 125 to 236 watts per foot of tube length (410 to 774 W/m), and the metallurgically assembled samples radiated 231 to 287 watts per foot (758 to 941 W/m). A brazed assembly had the best heat-transfer characteristics. Measured thermal resistance ranged from 0.07 to 1.5 (°F)(ft)/W (0.011 to 0.258 (°K)(m)/W). Also, the metallurgically joined specimens were not affected by thermal cycling; whereas, all the mechanically assembled specimens, except the bumper finned-tube sample, were affected.

N68-21732*# National Aeronautics and Space Administration. Lewis Research Center, Cleveland, Ohio.

PARTITION FUNCTIONS AND THERMODYNAMIC PROPERTIES TO HIGH TEMPERATURES FOR H $_3$ AND H $_2$ IONS

R. W. Patch and Bonnie J. McBride Washington Apr. 1968 77 p refs

(NASA-TN-D-4523) CFSTI: \$3.00 CSCL 20M

Tables of partition functions were compiled for H⁺₂ and at temperatures from 298.15° to 56,000°K. Tables of thermodynamic properties were compiled at temperatures from 298.15° to 10,000°K. The latter tables give the following thermodynamic functions for ideal gases: heat capacity at constant pressure, sensible enthalpy, entropy at 1 atmosphere, sensible free energy at 1 atmosphere, enthalpy, and free energy at 1 atmosphere. The heats of formation at 298.15°K are also given. Since no band spectra have been observed for either ion, all calculations were based on ab initio potential energy calculations found in or derived from the literature. All results for H₂⁺ are reliable up to 15,000°K, but results for H_3^+ are tentative at all temperatures. A digital computer program to calculate Wentzel-Kramers-Brillouin rotational energies from the potential energy of a diatomic molecule or molecular ion is also included. The program is in FORTRAN IV. Author

N68-22118*# National Aeronautics and Space Administration. Langley Research Center, Langley Station, Va.

EFFECTS OF SHOCK IMPINGEMENT AND OTHER FACTORS ON LEADING-EDGE HEAT TRANSFER

Dennis M. Bushnell Washington Apr. 1968 17 p refs Presented at the Conf. on Hypersonic Aircraft Technol., Moffett Field, Calif., 16–18 May 1967 Submitted for publication (NASA-TN-D-4543; NASA-SP-148) CFSTI: HC \$3.00/MF \$0.65 CSCL 20M

An investigation was conducted at a Mach number of 8 to determine the effects on stagnation-line heat transfer of shock impingement, chordwise grooves in the leading edge, and end contamination of the leading-edge boundary layer from an adjoining surface. Heat-transfer measurements were made along the leading edge of a 76° swept fin mounted on a flat plate. Tests were made with and without a series of small chordwise grooves cut into the leading edge to simulate construction details. Analysis of the observed heating distribution on the leading edge with the grooves indicates that some fraction of the stagnation-line boundary layer is bled off by the groove. The general level of heating was about the same as or less than the leading-edge heating data obtained on the same configurations without the grooves.

N68-22318^{*}# Tennessee Univ., Tullahoma. Space Inst. RADIATION HEAT TRANSFER IN ABSORBING, SCATTERING, AND EMITTING MEDIUM

F. Shakrokhi and P. Wolf Washington NASA Apr. 1968 22 p refs

(Grant NGR-43-001-021)

(NASA-CR-1023) CFSTI: HC\$3.00/MF\$0.65 CSCL 20M

Radiative heat flow is computed between plane parallel, plates with anisotropically scattering atmosphere. Results indicate that a usable solution to the problem can be obtained by simple iteration of the set of equations which result from approximation of the equation of radiation transfer. The iteration worked perfectly, the computer program is simple and short, and the method can accomodate the same, if not more, parameter variations than more analytical treatments.

N68-23513*# National Aeronautics and Space Administration. Manned Spacecraft Center, Houston, Tex.

ANALYSIS OF THREE-FLUID, CROSSFLOW HEAT EXCHANGERS

Noel C. Willis, Jr. Washington May 1968 114 p refs (NASA-TR-R-284) CFSTI: HC\$3.00/MF\$0.65 CSCL 13A

The detailed behavior of three-fluid, crossflow heat exchangers has been investigated. The equations governing the two-dimensional temperature distributions of the three fluids have been derived and nondimensionalized. Performance characteristics have been determined for a wide range of operating parameters for single-pass heat exchangers. The performance of two-pass heat exchangers for both cocurrent and countercurrent flow has been studied for selected operating conditions. Results have been presented graphically in terms of the temperature effectiveness of the two outer fluids as functions of heat-exchanger size for sets of fixed operating conditions. Nondimensional operating parameters have been defined which allow an efficient presentation of the large volume of performance data required to represent a practical range of operating conditions. Sample problems are included to illustrate the use of the performance graphs for design applications. Author

N68-24618*# National Aeronautics and Space Administration. Lewis Research Center, Cleveland, Ohio.

DETERMINATION OF CONVECTIVE HEAT-TRANSFER COEFFICIENTS ON ADIABATIC WALLS USING A SINUSOIDALLY FORCED FLUID TEMPERATURE Ronald G. Huff Washington Jun. 1968 34 p refs

(NASA-TM-X-1594) CFSTI: HC\$3.00/MF\$0.65 CSCL 20M

The response of an insulated wall, over which a heated fluid flows, to a sinusoidally forced fluid temperature was used to calculate the convective heat-transfer coefficients. An exact solution is given which accounts for thermal conductivity and the location of the sensed wall temperature in one-dimensional heat-transfer problems. Charts are included to aid in the calculation. A comparative analysis was made of solutions that do not account for thermal conductivity and the location of the sensed wall temperature and those that do. If the exact solution is not used, errors greater than 23 percent are possible. Author

N68-24965*# National Aeronautics and Space Administration. Lewis Research Center, Cleveland, Ohio.

MIXING AND REACTION STUDIES OF HYDRAZINE AND NITROGEN TETROXIDE USING PHOTOGRAPHIC AND SPECTRAL TECHNIQUES

Marshall C. Burrows Washington, D. C. Jun. 1968 26 p refs Film Supplement Number C-258 to this Report is Available on Loan from Lewis Research Center, Cleveland

(NASA-TN-D-4467) CFSTI: HC\$3.00/MF\$0.65 CSCL 21B

Distances required to atomize, mix, and react N_2H_4 and N_2O_4 were experimentally determined for a quadlet injector element. Atomization occurred in less than 1 inch (2.5 cm), and vaporizing NO₂ extended downstream for 4 inches (10.2 cm) or less. Hottest gases were in the oxidant-rich zones; fuel-rich gases appeared to be influenced by the decomposition reaction of hydrazine. Concentration profiles of H₂O determined from total radiation and gas temperature compared favorably with H₂O concentrations calculated for combustion profiles limited by either fuel or oxidant vaporization.

N68-25102 *# National Aeronautics and Space Administration. Lewis Research Center, Cleveland, Ohio.

EXPERIMENTAL VERIFICATION OF A DOUBLE DEAD TIME MODEL DESCRIBING CHUGGING IN LIQUID BIPROPELLANT ROCKET ENGINES John R. Szuch and Leon M. Wenzel Washington May 1968 38 p refs

(NASA-TN-D-4564) CFSTI: HC\$3.00/MF\$0.65 CSCL 21B

Stability limits were determined, experimentally, for a 2-inch (5.08 cm) diameter rocket engine. Liquid oxygen and gaseous hydrogen were the propellants. Chamber pressures of 650 and 300 psia (4.48×10.6 and 2.07×10.6 N/m²) were run with an oxidant-fuel ratio of 5.0 and a characteristic length of 95 inches (2.41). For comparison with experimental data, boundaries were generated on the analog computer using the chugging model proposed by the authors and calculated values of delay. Results agreed with regard to observed frequencies and boundary shape. Discrepancies in boundary location (required pressure drops) were attributed to a high combustion noise level.

N68-25122*# National Aeronautics and Space Administration. Lewis Research Center, Cleveland, Ohio.

VAPOR PRESSURE OF POTASSIUM TO 2170 °K

Kenneth J. Bowles Washington May 1968 12 p refs (NASA-TN-D-4535) CFSTI: HC\$3.00/MF\$0.65 CSCL 20M

A static capsule method was used to measure the vapor pressure of potassium from 945° to 2170°K. The resulting Kirchhoff-type vapor-pressure equation is given. The standard deviation in pressure is ± 1.23 percent. Data calculated from this equation were pooled with data calculated from potassium-vapor-pressure equations determined previously in four independent studies. The pooled equation is used as a standard curve against which all data are compared. Author

N68-25244*# Itek Corp., Palo Alto, Calif. Vidya Div.

AN ANALYSIS OF THE COUPLED CHEMICALLY REACTING BOUNDARY LAYER AND CHARRING ABLATOR, PART 1 Summary Report

Robert M. Kendall, Eugene P. Bartlett, Roald A. Rindal, and Carl B. Moyer Washington, D. C. NASA Jun. 1968 111 p refs (Contract NAS9-4599)

(NASA-CR-1060; Rept.-66-7, Pt. 1) CFSTI: HC \$3.00 /MF \$0.65 CSCL 20M

This report summarizes analyses and computational procedures for predicting the transient in-depth response of charring ablation materials, either coupled to a nonsimilar, laminar, multicomponent, chemically-reacting boundary-layer computational procedure or partially decoupled through the use of convective transfer coefficients. The computational procedure for charring ablators is an implicit finite difference procedure for an ablating surface material with several nonablating backup materials. It considers one-dimensional heat and mass transfer along thermal streamtubes of arbitrary cross-sectional area and permits a multiple-reaction model for gas decomposition and a general thermochemical surface boundary condition. The boundary-layer procedure utilizes a newly developed integral matrix solution procedure. It applies for general chemical systems, allowing rate-controlled surface reactions, and incorporates approximate formulations for mixture transport properties, including unequal diffusion and thermal diffusion coefficients for all species. Analyses are also presented for extending the boundary-layer computational procedure to include mixed equilibrium-nonequilibrium. homogeneous or heterogeneous general chemical systems and to include radiation absorption and emission, and for extending the charring ablation procedure to include char-density buildup due to coking reactions in depth. Author

N68-25312*# National Aeronautics and Space Administration. Lewis Research Center, Cleveland, Ohio.

ANALYTICAL INVESTIGATION OF ELECTRICALLY HEATED WIRE MESH FOR FLOWING GAS HEATERS

William F. Mattson and William L. Maag Washington June 1968 42 $\,p$ refs

(NASA-TN-D-4595) CSCL 13A

By specifying the gas, the flow rate, the system pressure, the desired inlet and outlet gas temperatures, and the power supply characteristics, a compatible wire mesh heater element design

can be determined. The calculations involve solving simultaneous equations for the heat generation rate, the convective heat transfer from the mesh to the gas, and the change in enthalpy of the gas at every axial position along the heater length. The method also enables the determination of the operating conditions of an existing mesh heater when used at some off design condition or with another das Author

N68-25917* # National Aeronautics and Space Administration. Langley Research Center, Langley Station, Va.

STATIC-TEMPERATURE DISTRIBUTION IN A FLAT PLATE COMPRESSIBLE TURBULENT BOUNDARY LAYER WITH **HEAT TRANSFER**

S. Z. Pinckney Washington Jun. 1968 45 p refs

(NASA-TN-D-4611) CFSTI: HC\$3.00/MF\$0.65 CSCL 20M An expression based on the differential equations for the local energy transfer and shear is derived for the relationship between the static temperature and the velocity in a zero-pressure-gradient turbulent boundary layer. The boundary conditions imposed by these governing equations showed the temperature-velocity relation to be at least a fourth degree polynomial which differs considerably from the second degree polynomial obtained by previous investigators. These governing equations are integrated by using as boundary conditions the value of a particular total-energy-deficiency parameter of the boundary layer at the station under consideration, the slope of the laminar-sublayer temperature-velocity profile at the wall (as determined from a modified Reynolds analogy), and the local free-stream and wall conditions. Results obtained by this method are compared with experimental temperature-velocity profile data and are found to correlate well with the experimental profiles. Author

N68-26641 *# Itek Corp., Palo Alto, Calif. Vidya Div.

AN ANALYSIS OF THE COUPLED CHEMICALLY REACTING BOUNDARY LAYER AND CHARRING ABLATOR. PART 3: NONSIMILAR SOLUTION OF THE MULTICOMPONENT LAMINAR BOUNDARY LAYER BY AN INTEGRAL MATRIX METHOD

Eugene P. Bartlett and Robert M. Kendall (Aerotherm Corp.) Washington NASA Jun. 1968 138 p refs Prepared jointly with Aerotherm Corp., Palo Alto, Calif.

(Contract NAS9-4599)

(NASA-CR-1062; Rept.-66-7, Pt. 3) CFSTI: HC \$3.00 /MF \$0.65 CSCL 20M

A laminar nonsimilar boundary-layer procedure is described which yields accurate solutions for a broad range of problems. In its current formulation, solutions can be obtained for any equilibrium chemical environment with specified rate-controlled reactions at the surface. It has been used to treat a variety of ablating and nonablating surface boundary conditions including coupled energy and mass balances. The formulation considers unequal diffusion and thermal diffusion coefficients for all species in a particularly convenient manner through a bifurcation approximation for binary diffusion coefficients. The multicomponent viscosity and thermal conductivity of the mixture are determined by use of Sutherland-Wassiljewa type approximations. The procedure is readily applicable to inclusion of one-dimensional radiation emission and absorption and a general nonequilibrium chemical model. The procedure combines features of the general integral relations approach with those of matrix solution techniques. Following the former, smooth functions (in particular, cubic spline functions) are chosen to relate the principal dependent variables to their derivatives. Author

N68-26650*# National Aeronautics and Space Administration. Lewis Research Center, Cleveland, Ohio. **BODY ROTATION EFFECTS ON MELTING ABLATION**

Thomas H. Cochran and Simon Ostrach (Case Inst. of Tech.) Washington Jun. 1968 40 p refs

(NASA-TN-D-4614) CFSTI: HC\$3.00/MF\$0.65 CSCL 20M

The effects of rotation on the ablation of an axisymmetric body composed of a highly viscous material and subject to deceleration in an airstream were studied analytically and experimentally. The tests were conducted so that a parameter representing the importance of rotation effects and which was obtained from a nondimensionalization of the governing equations was varied from 0 to 4.2. The results indicate that, although rotation had no effect on the ablation process in the vicinity of the stagnation point of the body, significant changes in the character of the generated waves and in the flange were caused by rotation. Liquid was thrown from the body in the vicinity of the flange when the spin parameter was 0.88 or greater. Author

N68-26692*# Itek Corp., Palo Alto, Calif. Vidya Div.

AN ANALYSIS OF THE COUPLED CHEMICALLY REACTING BOUNDARY LAYER AND CHARRING ABLATOR. PART FINITE DIFFERENCE SOLUTION FOR THE IN-DEPTH 2. **RESPONSE OF CHARRING MATERIALS CONSIDERING** SURFACE CHEMICAL AND ENERGY BALANCES

Carl B. Moyer and Roald A. Rindal Washington NASA Jun. 1968 142 p refs Prepared jointly with Aerotherm Corp., Palo Alto, Calif.

(Contract NAS9-4599)

(NASA-CR-1061; Rept.-66-7, Pt. 2) CFSTI: HC \$3.00 /MF \$0.65 CSCL 20M

An analysis of the in-depth response of materials exposed to a high temperature environment was presented, and a computer program based upon the analysis was described. The differential equations for the in-depth response are formulated and then cast into a finite difference form implicit in temperature. Three pyrolyzing constituents are allowed with an accurate model of observed pyrolysis kinetics. Heat flow in-depth is one-dimensional, but cross-section area may vary with depth. The program for in-depth response computation may be coupled to a variety of boundary conditions. One of the possible boundary conditions is a complete boundary layer solution described in other reports of this series. Another version of the program may be coupled to a general film coefficient model of the boundary layer; this boundary condition is described in some detail in the present report. Author

N68-26759*# National Aeronautics and Space Administration. Lewis Research Center, Cleveland, Ohio.

BOUNDARY CONDITIONS FOR THE DIFFUSION SOLUTION OF COUPLED CONDUCTION-RADIATION PROBLEMS

Marvin Goldstein and John R. Howell Washington Jun. 1968 42 p refs

(NASA-TN-D-4618) CFSTI: HC\$3.00/MF\$0.65 CSCL 20M

The boundary condition for use with the diffusion solution for coupled radiation and conduction energy transfer is derived. An effective slip coefficient is presented as a function of the conduction-radiation parameter. Comparison to exact numerical solutions is good for the geometry of infinite parallel black plates. In the course of the analysis, a uniformly valid asymptotic expansion for the combined conduction and radiation problem in a nongray medium in the optically thick regime, and an exact analytical solution to the radiation-conduction transport equation in the boundary regime are obtained. Author

N68-26815*# Itek Corp., Palo Alto, Calif. Vidya Div.

AN ANALYSIS OF THE COUPLED CHEMICALLY REACTING BOUNDARY LAYER AND CHARRING ABLATOR. PART 4: A UNIFIED APPROXIMATION FOR MIXTURE TRANSPORT PROPERTIES FOR MULTICOMPONENT BOUNDARY-LAYER APPLICATIONS

Eugene P. Bartlett, Robert M. Kendall, and Roald A. Rindal Washington NASA Jun. 1968 57 p refs (Contract NAS9-4599)

(NASA-CR-1063; Rept.-66-7, Pt. 4) CFSTI: HC \$3.00 /MF \$0.65 CSCL 20M

Self-consistent approximations for binary diffusion coefficients. multicomponent thermal diffusion coefficients and mixture viscosity and thermal conductivity are presented which greatly simplify the solution of multicomponent laminar boundary-layer problems. The basic premise of the approach is a bifurcation of binary diffusion coefficients, $D_{ij} = \overline{D} / F_i F_j$, where \overline{D} is a reference diffusion coefficient and F_i is a diffusion factor for species i. The primary utility of the bifurcation approximation in multicomponent boundary-layer applications is that it enables explicit solution of the Stefan-Maxwell relations for the diffusive mass fluxes, j. The approximation for multicomponent thermal diffusion coefficients is based upon generalization of a semi-empirical equation for correlating binary thermal diffusion data. Approximate relations for mixture viscosity and thermal conductivity of the Sutherland-Wassilijewa type are simplified by use of the bifurcation approximation for binary diffusion Author coefficients.

N68-26816*# Itek Corp., Palo Alto, Calif. Vidya Div.

AN ANALYSIS OF THE COUPLED CHEMICALLY REACTING BOUNDARY LAYER AND CHARRING ABLATOR. PART 5: A GENERAL APPROACH TO THE THERMOCHEMICAL SOLUTION OF MIXED EQUILIBRIUM-NONEQUILIBRIUM, HOMOGENEOUS OR HETEROGENEOUS SYSTEMS Robert M. Kendall Washington NASA Jun. 1968 45 p refs

(Contract NAS9-4599)

(NASA-CR-1064; Rept.-66-7, Pt. 5) CFSTI: HC \$3.00/MF \$0.65 CSCL 20M

A general equilibrium and nonequilibrium chemical state procedure is developed and applied mathematically to a number of open and closed thermodynamic systems. The conventional equilibrium relations are developed in terms of a set of base species. The base species concept is then extended in order to treat mixed equilibrium and nonequilibrium systems in a general fashion. The specification of controlling reactions is used to create non-redundant equation sets as equilibrium is approached. The treatment of open system mass balances within the basic framework of the state solution permits direct surface state calculations considering boundary-layer transfer relations and surface-condensed phase removal relations. The computer program which performs the equilibrium state solutions according to the methods presented, the Aerotherm Chemical Equilibrium (ACE) program is described briefly. The program which contains some of the nonequilibrium features of the analysis, the ACE/KINET program is also introduced. Author

N68-26817*# Itek Corp., Palo Alto, Calif. Vidya Div.

AN ANALYSIS OF THE COUPLED CHEMICALLY REACTING BOUNDARY LAYER AND CHARRING ABLATOR. PART 6: AN APPROACH FOR CHARACTERIZING CHARRING ABLATOR RESPONSE WITH IN-DEPTH COKING REACTIONS

Roald A. Rindal Washington NASA Jun. 1968 48 p refs (Contract NAS9-4599)

(NASA-CR-1065; Rept.-66-7, Pt. 6) CFSTI: HC \$3.00 /MF \$0.65 CSCL 20M

The analysis of a charring ablation material which may undergo subsurface coking of the pyrolysis gas is considered. Coking reactions considered include thermal cracking of gaseous hydrocarbons resulting in precipitation of carbon onto the char layer and, at higher temperatures, the subsequent internal chemical erosion of the char structure by the gaseous pyrolysis products. A generalized type of ablation material is defined which consists of inert, carbon, and reactive constituents. Three types of subsurface reactions are considered, 1) decomposition of up to three organic constituents to form initial char and pyrolysis gas resulting in kinetically controlled decomposition of the pyrolysis gas resulting of carbon precipitation and char desification. and 3) at high temperature, chemical erosion of the subsurface char matrix by the pyrolysis products according to the dictates of chemical equilibrium. A model is considered for evaluating the pressure distribution through the char layer of variable permeability. Differential equations are developed to represent the transfer of mass, energy, and momentum within the framework of the postulated phenomenological model. Author

N68-28100*# National Aeronautics and Space Administration. Langley Research Center, Langley Station, Va.

AN EXPERIMENTAL STUDY OF FLAME PROPAGATION IN SUPERSONIC PREMIXED FLOWS OF HYDROGEN AND AIR Griffin Y. Anderson and Allen R. Vick Washington Jun. 1968 34 p. refs.

(NASA-TN-D-4631) CFSTI: HC\$3.00/MF\$0.65 CSCL 20M

The results of an experimental study of a Mach 1.5 free jet of hydrogen-air mixture ignited by a coaxial, hot gas, pilot jet are presented. This configuration produces an approximately conical average flame surface propagating from the pilot jet into the unburned, supersonic mixture. Flash schlieren, direct, and time schlieren photographic observations of the flame and flow field are discussed for mixtures up to 1.3 times stoichiometric with stagnation temperatures of 300°K and 450°K. Flame cone half-angle measured from time schlieren photographs is found to increase rapidly with equivalence ratio to a maximum at 0.8 times stoichiometric and remain approximately constant thereafter. The maximum flame angle is approximately 9.2° for mixture stagnation temperature of 300°K and decreases to about 7.4° with an increase in temperature to 450°K. Unlike maximum flame angle, the computed velocity normal to the average flame surface or flame-propagation velocity increases with increasing stagnation temperature. Relative values of flame-propagation velocity computed from flame angles measured in supersonic mixtures for hydrogen, methane, ethane, and ethylene were found to be similar to relative laminar burning velocity data for these fuels. Author

 $\textbf{N68-28156}^{*\#}$ National Aeronautics and Space Administration. Lewis Research Center, Cleveland, Ohio.

CENTAUR/SURVEYOR NOSE FAIRING AERODYNAMIC HEATING INVESTIGATION

C. W. Eastwood, Jr. Washington Jul. 1968 20 p refs

(NASA-TM-X-1605) CFSTI: HC\$3.00/MF\$0.65 CSCL 20M

An experimental investigation was conducted to verify the structural integrity of the Centaur/Surveyor fiberglas nose fairing at the thermal and pressure environment predicted for the fourth Atlas/Centaur flight. Specimens of the fairing, including two coated with a protective subliming material, were exposed to the simulated aerodynamic heating and decreasing atmospheric pressure associated with the flight trajectory. Nose fairing specimen skin temperatures, bondline temperatures, and core pressure in the simulated environment are presented. Core pressure required to delaminate the skin-core assembly is given. Fairing skin temperatures from two subsequent Atlas/Centaur flights are compared with the experimental results.

N68-28371*# National Aeronautics and Space Administration. Lewis Research Center, Cleveland, Ohio.

FLOW AND WALL-TEMPERATURE SENSITIVITY IN PARALLEL PASSAGES FOR LARGE INLET TO EXIT DENSITY RATIOS IN SUBSONIC FLOW

Meyer Reshotko Washington Jul. 1968 31 p refs

(NASA-TN-D-4649) CFSTI: HC\$3.00/MF\$0.65 CSCL 20M

There is a large gas density decrease from reactor inlet to exit in a nuclear rocket. Under certain reactor operating conditions, the momentum pressure drop can be a large portion of the overall pressure drop. As a result, deviations in flow rate or passage diameter can cause the reactor walls to overheat. A simplified analytical investigation was made to find the sensitivity of the flow and wall temperature in heated passages as a function of Mach number for (1) a change in heat addition, and (2) nonuniform passage diameter. The Mach number range is from 0.2 to 0.9. Author

 $\textbf{N68-28530}^{*\#}$ National Aeronautics and Space Administration. Lewis Research Center, Cleveland, Ohio.

THERMAL RADIATION HEAT TRANSFER. VOLUME I: THE BLACKBODY, ELECTROMAGNETIC THEORY, AND MATERIAL PROPERTIES

Robert Siegel and John R. Howell Washington 1968 194 p refs

(NASA-SP-164) GPO: HC\$1.00; CFSTI: MF\$0.65 CSCL 20M

The importance of thermal radiation data to aerospace design is discussed, with attention focused on the inherent differences and complexities of radiation problems as compared with convection and conduction. The radiative behavior of the black body, or ideal radiating surface, is examined to serve as a standard for comparing the performance of real radiating bodies. Both unaveraged and averaged emissive, absorptive, and reflective properties are defined, and blackbody emission is given as a function of wavelength and temperature. Nomenclature is introduced for defining radiative properties, and these definitions are used for assessing the restrictions on the various forms of Kirchhoff's law relating emissivity to absorptivity. The reciprocal relations for reflectivities are derived. Equations for predicting the radiative properties of materials by classical electromagnetic theory are formulated. The radiative performance of real materials is discussed in terms of property variations with wavelength and temperature. Conversion factors are tabulated. Numerical examples are presented to delineate the use of the analytical relations and to bridge the gap between theory and practical application. F S

N68-30041# National Aeronautics and Space Administration. Langley Research Center, Langley Station, Va.

EFFECT OF CARBON DIOXIDE AND WATER VAPOR ON THE INDUCTION PERIOD OF THE HYDROGEN-OXYGEN REACTION

Casimir J. Jachimowski and William M. Houghton Washington Aug. 1968 15 p refs

(NASA-TN-D-4685) CFSTI: HC \$3.00/MF\$0.65 CSCL 21B The effect of carbon dioxide and water vapor on the induction period kinetics of the hydrogen-oxygen reaction was studied in a shock tube at temperatures between 1000° and 1500°K. The results show that carbon dioxide does not produce any noticeable effect, whereas water vapor appears to accelerate the hydrogen-oxygen reaction. The analysis of experimental data indicates that the accelerating influence of water vapor is due to two processes. One process is dominant at the higher temperatures, the chain branching reaction $0 + H_2 0 \rightarrow 20H$, and the other, an unidentified process, is dominant at the lower temperatures. Author

N68-30518*# National Aeronautics and Space Administration. Lewis Research Center, Cleveland, Ohio.

EFFECT OF CHAMBER PRESSURE, FLOW PER ELEMENT, AND CONTRACTION RATIO ON ACOUSTIC-MODE INSTABILITY IN HYDROGEN-OXYGEN ROCKETS

John P. Wanhainen, Charles E. Feiler, and C. Joe Morgan Washington Aug. 1968 35 p refs

(NASA-TN-D-4733) CFSTI: HC\$3.00/MF\$0.65 CSCL 21H

An experimental investigation of a 20,000-lb. (89-kN) thrust engine with a single coaxial-type injector was conducted to determine the effect of variations in chamber pressure, weight flow per element, and contraction ratio, by changing nozzle throat diameter, on tangential-acoustic-mode stability- characteristics of hydrogen-oxygen rocket engines. These characteristics were evaluated by determining the hydrogen-injection temperature below which combustion was unstable. A correlation of the stability limits was obtained as a function of the variables investigated. The roles of various parameters were also interpreted according to the mechanism assumed in the response-factor model of this propellant combination. Author N68-30747*# National Aeronautics and Space Administration. Langley Research Center, Langley Station, Va.

FLIGHT TEST ANALYSIS OF APOLLO HEAT SHIELD MATERIAL USING THE PACEMAKER VEHICLE SYSTEM Randolph A. Graves, Jr. and William G. Witte Washington Aug.

1968 34 p refs (NASA-TN-D-4713) CFSTI: HC \$3.00/MF \$0.65 CSCL 228

The Apollo heat-shield material was flight tested on the hemispherically blunted nose cap of a Pacemaker vehicle. Ablation and temperature data were obtained at the stagnation point and at the 22.5°, 45°, and 67.5° stations. Maximum pressures at these locations were 8.4, 6.7, 4.1, and 1.7, atmospheres, respectively. (1 atm = 101 325 N/m².) Recession rates at the 22.5°, 45°, and 67.5° stations were greater than predicted, and this result is attributed to the high levels of turbulent aerodynamic shear, which exceeded the threshold shear sensitivity of this material. Unequal absorption of the surface sealer into the porous heat-shield material modified its behavior and introduced uncentainties in the analysis during the early portions of the data period. Author

N68-31498*# National Aeronautics and Space Administration. Lewis Research Center, Cleveland, Ohio.

EXPERIMENTAL MEASUREMENTS OF THERMAL RADIATION PROPERTIES BY CYCLIC INCIDENT RADIATION

Ernie W. Spisz and John R. Jack Washington Aug. 1968 15 p refs

(NASA-TM-X-1618) CFSTI: HC\$3.00/MF\$0.65 CSCL 20M

A new experimental technique is developed to determine simultaneously the total hemispherical emittance, solar absorptance, and absorptance-emittance ratio for metals at cryogenic temperatures. The method compares the temperature response of thin metal samples to a sinusoidal perturbation of an imposed radiant intensity. Emittance data are presented for aluminum, copper, and 304 stainless steel over the temperature range of 150 to 500 K. From the data, the applicability of the cyclic radiant intensity method is evaluated, and the problems associated with extending the method to temperatures below 150K are discussed. Author

N68-31959*# National Aeronautics and Space Administration. Langley Research Center, Langley Station, Va.

A SIMPLIFIED METHOD FOR CALCULATING LAMINAR HEAT TRANSFER OVER BODIES AT AN ANGLE OF ATTACK Fred R. De Jarnette and Ruby M. Davis Washington Aug. 1968 21 p refs

(NASA-TN-D-4720) CFSTI: HC\$3.00/MF\$0.65 CSCL 20M

A simplified method is developed for calculating the ratio of the local to stagnation-point heat-transfer rate for bodies at an angle of attack with only the free-stream Mach number and the ratio of specific heats required as inputs. The viscous problem is simplified by using the axisymmetric analog for three-dimensional boundary layers (small cross flow in boundary layer) in conjunction with Lees' laminar heating rate for axisymmetric bodies. An approximate technique for determining the geometry of the inviscid surface streamline is presented. In this technique the direction of a streamline at a given point on the body is taken as the direction of the resultant of the free-stream velocity vector minus its normal component. For determining the inviscid surface properties, the modified Newtonian pressure distribution is used with isentropic flow along the surface. The heat transfer over spherically blunted cones with 15° and 30° semiapex angles at angles of attack of 0°, 10°, and 20° and a free-stream Mach number of 10.6 was computed. The values obtained agreed well with experimental data. Author

N68-32073*# National Aeronautics and Space Administration. Lewis Research Center, Cleveland, Ohio.

CONFORMAL MAPPING FOR STEADY TWO-DIMENSIONAL SOLIDIFICATION ON A COLD SURFACE IN FLOWING LIQUID

Robert Siegel Washington Aug. 1968 22 p refs (NASA-TN-D-4771) CFSTI: HC\$3.00/MF\$0.65 CSCL 20M

Conformal mapping has been applied to determine the shape of two-dimensional solidified layers formed on a cold surface immersed in a flowing warm liquid. The frozen region is represented by a rectangle in a potential plane, and the rectangle is mapped into the physical plane to determine the frozen boundary configuration. The method is demonstrated for solidification on a cold plate of finite width that is insulated along its edges. Author.

N68-32099*# National Aeronautics and Space Administration. Lewis Research Center, Cleveland, Ohio.

TESTS OF A SINGLE TUBE-IN-SHELL WATER-BOILING HEAT EXCHANGER WITH A HELICAL-WIRE INSERT AND SEVERAL INLET FLOW-STABILIZING DEVICES

James R. Stone and Nick J. Sekas Washington Aug. 1968 60 p refs

(NASA-TN-D-4767) CFSTI: HC\$3.00/MF\$0.65 CSCL 13A

Experimental data were obtained on a vertical-upflow, single tube-in-shell. 0.436-in.-(1.11-cm) inside diameter by 60.5-in.-(1.54-m) long, water-boiling heat exchanger with a helical-wire insert (wire-pitch-to-inside-diameter ratio 1.90). Entrance-region plugs, inlet orifices, and a venturi-type inlet were tested at boiling-fluid flow rates from 60 to 100 lb_m/hr (0.0075 to 0.0125 kg/sec) and exit pressure = 17 psia (= 15 kN/m²). Results are compared with those on a boiler with the same dimensions, but with no insert. Vapor superheat with heat-balance exit quality >1.0 was obtained. With no inlet device, with or without plugs the tendency for back-slugging instabilities was present. Orifices eliminated back-slugging, but exit quality of 1.0 was not obtained, although vapor superheat was indicated. The venturi eliminated back slugging and gave a heat-balance quality as high as 1.02; however, the flow range was limited. Author

N68-32988*# National Aeronautics and Space Administration. Lewis Research Center, Cleveland, Ohio.

COMPARISON OF EXPERIMENTAL AND PREDICTED HEAT TRANSFER CHARACTERISTICS FOR A CYLINDRICAL EJECTOR

Francis C. Chenoweth and Fred W. Steffen Washington Aug. 1968 25 p refs

(NASA-TM-X-1641) CFSTI: HC\$3.00/MF\$0.65 CSCL 20M

The heat transfer characteristics of a cylindrical ejector for a small afterburning turbojet engine operating at static sea level conditions were compared with film-cooling correlations based on an insulated wall. Since the ejector in this tests was not insulated, a correction for radiation and free-convection losses was derived and applied to the wall temperatures calculated using one of the correlations. Good agreement was obtained between the experimental and predicted wall temperatures. Author

N68-33167*# National Aeronautics and Space Administration. Lewis Research Center, Cleveland, Ohio.

ANALYTICAL INVESTIGATION OF THERMAL DEGRADA-TION OF HIGH-PERFORMANCE MULTILAYER INSULATION IN THE VICINITY OF A PENETRATION

William R. Johnson and Earl L. Sprague Washington Sep. 1968 60 p refs

(NASA-TN-D-4778) CFSTI: HC\$3.00/MF\$0.65 CSCL 20M

An analytical investigation was conducted to determine the thermal degradation of high-performance multilayer insulation on a liquid hydrogen tank in the vicinity of a penetration. Results were obtained with and without the use of a thermal buffer zone between the shields and the pentration, for various values of thermal contact resistance. Input variables to the program included radiation source temperature, penetration diameter, number of shields, shield emissivity, shield thermal conductivity, shield spacing, buffer zone dimensions, and buffer zone thermal conductivity. The results of the program are presented in graphical form, as well as in equations representing curve fits of the analytical data. Author

N68-33203*# Pratt and Whitney Aircraft, East Hartford, Conn. VAPOR CHAMBER FIN STUDIES. OPERATING CHARACTERISTICS OF FIN MODELS

H. R. Kunz, S. S. Wyde, G. H. Nashick, and J. F. Barnes Washington NASA Aug. 1968 95 p refs

(Contract NAS3-7622)

(NASA-CR-1139; PWA-3154) CFSTI: HC \$3.00/MF \$0.65 CSCL 13A

This report presents the test results from experiments on two vapor-chamber fin (heat pipe) geometries and compares these results with a theory developed and presented in a prior report. Typical temperature distributions were obtained for heat pipe operation plus limiting heat flux data which was compared to the theory. This comparison indicated that the theory showed the correct trends at low levels of heat flux. An effect of working fluid inventory was found which was not included in the present theory. Tests with a noncondensable gas present in the chamber were found to result in complete mixing of this gas with the working fluid vapor. Author

N68-33208*# National Aeronautics and Space Administration. Langley Research Center, Langley Station, Va.

SINGLE-THERMOCOUPLE METHOD FOR DETERMINING HEAT FLUX TO A THERMALLY THICK WALL

Floyd G. Howard Washington Sep. 1968 51 p refs

(NASA-TN-D-4737) CFSTI: HC\$3.00/MF\$0.65 CSCL 20M

A method that accounts for variable thermal properties has been developed for determining heat flux from a single temperature-time history within a thermally thick wall. The accuracy depends on the thermal depth of the measurement point, and ranges from good to excellent for a number of practical cases, with best results occurring nearest the heated surface in conjunction with a small computing interval. The method is believed to be as accurate, if not more so, than other methods utilizing multiple thermocouples. If measurement is near the heated surface and accurate, the method can detect sudden changes in slope of heat flux such as are experienced when boundary layer flow becomes transitional or when heating rate history fluctuates as a result of body motions in flight.

N68-34088*# National Aeronautics and Space Administration. Lewis Research Center, Cleveland, Ohio.

ANALYSIS OF BOILING ON A FIN

Y. Y. Hsu Washington Sep. 1968 23 p refs

(NASA-TN-D-4797) CFSTI: HC\$3.00/MF\$0.65 CSCL 20M

A simplified method of calculation is proposed to determine the performance of a fin exposed to various modes of boiling. The heat-transfer coefficients of boiling were approximated by segments of simple nth power functions of superheat. These functions provide the analytical solution of the temperature gradient in the fin as a function of temperature. Results compare favorably with those obtained from a small-increment numerical solution. Three examples are given to illustrate the application of fin concept to boiling heat-transfer processes.

N68-35116*# National Aeronautics and Space Administration. Langley Research Center, Langley Station, Va.

FLIGHT INVESTIGATION OF THE EFFECTS OF APOLLO HEAT-SHIELD SINGULARITIES ON ABLATOR PERFORMANCE

Thomas E. Walton, Jr., William G. Witte, and Brian J. O'Hare Washington Sep. 1968 62 $\,p$ refs

(NASA-TN-D-4791) CFSTI: HC\$3.00/MF\$0.65 CSCL 20M

A flight investigation was conducted to evaluate the performance of the Apollo ablative heat-shield material under perturbed heating conditions caused by several simulated Apollo heat-shield singularities. The recovered spacecraft, which contained simulations of the Apollo singularities, experienced an

order-of-magnitude less recession in the unperturbed areas than had been predicted. A recalculation of the surface recession utilizing revised rate-controlled oxidation constants obtained from arc-jet tests produced results compatible with the measured surface recession. With the exception of the upstream lip of both simulated umbilical fairings, no appreciable increase in surface recession attributable to the singularities was noted. The effects of simulated Apollo singularities on ablator performance were minor, as evidenced from the recovered spacecraft.

N68-35248*# Douglas Aircraft Co., Inc., Santa Monica, Calif. RADIATIVE AND CONVECTIVE HEATING DURING ATMOSPHERIC ENTRY

W. S. Rìgdon, R. B. Dirling, Jr., and M. Thomas Washington NASA Sep. 1968 52 $\,p$ refs

(Contract NAS1-7757)

(NASA-CR-1170) CFSTI: HC\$3.00/MF\$0.65 CSCL20M

The first solutions for radiation-convection coupled stagnation point heat transfer retaining complete spectral detail of the radiative transfer have been generated for a single entry condition both with and without mass injection. The problems associated with obtaining massive blowing solutions with radiation have been generated for a single entry condition both with and without mass injection with radiation have been identified and solution procedures developed. The effect of radiative boundary conditions at the wall has been investigated by obtaining solutions for transparent, black, and totally reflecting walls. The detailed spectral solutions reveal that the originally proposed approximate relation for the divergence of the radiative flux is not suitable for accurate real-gas radiative convective coupling analyses. Therefore, the radiative transfer processes have been investigated and the theoretical basis for a new approximate formulation for the divergence of the radiative flux has been established such as to account for the dominant real-gas radiative transfer effects. Author

N68-35468*# National Aeronautics and Space Administration. Langley Research Center, Langley Station, Va.

EMPIRICAL STAGNATION POINT HEAT-TRANSFER RELATION IN SEVERAL GAS MIXTURES AT HIGH ENTHALPY LEVELS

Ernest V. Zoby Washington Oct. 1968 21 p refs

(NASA-TN-D-4799) CFSTI: HC\$3.00/MF\$0.65 CSCL 20M

A simple empirical method was developed for computing stagnation point heating rates in arbitrary gas mixtures. The method was shown to be in good agreement with stagnation point heating results in air, argon, carbon dioxide, hydrogen, nitrogen, and mixtures of argon, carbon dioxide, and nitrogen for enthalpy potentials up to 50,000 Btu/lbm (1.17 \times 10⁵ joule/g). One useful application of the method is for parametric stagnation point-heat transfer studies. The method is in good agreement with the existing prediction methods and is in fair agreement with the existing experimental data. Author

N68-36072*# National Aeronautics and Space Administration. Langley Research Center, Langley Station, Va.

A STUDY OF THE REACTION-PLANE APPROXIMATION IN ABLATION ANALYSES

C. W. Stroud Washington Oct. 1968 21 p refs

(NASA-TN-D-4817) CFSTI: HC\$3.00/MF\$0.65 CSCL 20M

Equations which describe the reactive zone in charring ablators during steady state ablation are derived. Average reaction zone temperatures and reaction zone thicknesses are studied for half-order, and second-order reactions. This study was made for each of these reaction orders over a wide range of frequency factors and heats of pyrolysis. One technique used to simplify ablation analyses is to idealize the degradation process and assume that it occurs in a plane. The purpose of this paper is to investigate the validity of this technique as a good engineering approximation. Empirical relations are developed between the frequency factors and the average reaction zone temperature for the three reaction orders. These relations are used to locate the reaction zone in a reaction plane analysis. The resulting temperature profile is shown to be in substantial agreement with the profile obtained from a reaction in depth analysis. Author

34

GENERAL

Includes reports of a broad nature related to industrial applications and technology, and to basic research; defense aspects; law and related legal matters; and legislative hearings and documents.

N68-11307*# National Aeronautics and Space Administration, Washington, D. C.

NASA THESAURUS: SUBJECT TERMS FOR INDEXING SCIENTIFIC AND TECHNICAL INFORMATION. VOLUME 1: ALPHABETICAL LISTING A-L

Dec. 1967 441 p

(NASA-SP-7030) CFSTI: HC\$3.00/MF\$0.65 CSCL 05B

The NASA Thesaurus is an alphabetical listing of terms by which the documents in the NASA scientific and technical information system are indexed and retrieved. The first two volumes of the three-volume publication contain the subject terms and the complete cross-reference structure that comprise the Thesaurus proper; the final volume consists of four appendixes which arrange the Thesaurus elements in other ways for purposes of further explication and utility. The four appendixes are: Hierarchical Display (Appendix A); Category Term Listing (Appendix B); Permuted Index (Appendix C); and Postable Terms (Appendix D).

N68-11308*# National Aeronautics and Space Administration, Washington, D. C.

NASA THESAURUS: SUBJECT TERMS FOR INDEXING SCIENTIFIC AND TECHNICAL INFORMATION. VOLUME 2: ALPHABETICAL LISTING M-Z

Dec. 1967 428 p For abstract see N68-11307

(NASA-SP-7030) CFSTI: HC \$3.00/MF \$0.65 CSCL 05B

N68-11309*# National Aeronautics and Space Administration, Washington, D. C.

NASA THESAURUS: SUBJECT TERMS FOR INDEXING SCIENTIFIC AND TECHNICAL INFORMATION. VOLUME 3: APPENDIXES

Dec. 1967 651 p For abstract see N68-11307

(NASA-SP-7030) CFSTI: HC \$3.00/MF \$0.65 CSCL 05B

N68-21828*# National Aeronautics and Space Administration, Washington, D. C.

MANAGEMENT. A CONTINUING LITERATURE SURVEY WITH INDEXES, 1962–1967

Mar. 1968 29 p refs

(NASA-SP-7500) CFSTI: HC\$3.00/MF\$0.65 CSCL 05A

A compilation of references to unclassified reports and periodicals on the subject of management that may be found in the NASA scientific and technical information system is reported. The publication assembles groups of citations formerly announced in separate journals, Scientific and Technical Aerospace Reports (STAR) and International Aerospace Abstracts (IAA), to provide management with a convenient information tool. Contents include material generated or sponsored by NASA during the period 1962 through 1967. Abstracts in the survey are grouped under the followingcategories: program management, contract management, research and development, management tools and techniques; personnel management; urban management; management policy and philosophy; economics; and general which includes conference proceedings, reviews, patent information, speeches, and bibliographies. S.C.W.

N68-24567*# National Aeronautics and Space Administration, Washington, D. C.

MANAGEMENT: A CONTINUING LITERATURE SURVEY, WITH INDEXES, 1962–1967 May 1968 87 p refs

(NASA-SP-7500(02)) CFSTI: HC\$3.00 /MF\$0.65 CSCL 05A

A bibliography of annotated references to unclassified reports and journals articles on various aspects of management was taken from entries to the NASA information system between 1962 and 1967. Abstracts as well as subject matter, author, and corporate source indexes are presented. References are given under the general categories of program management, contract management, research and development, management tools and techniques, personnel management, urban management, management policy and philosophy, and economics. A category designated general includes conference proceedings, reviews, patent information, speeches, and other bibliographies. M.W.R.

 $\textbf{N68-25221}^{*\#}$ National Aeronautics and Space Administration, Washington, D. C.

CUMULATIVE INDEX TO NASA TECH BRIEFS, 1963–1967 Apr. 1968 376 p refs

(NASA-SP-5021(06)) CFSTI: HC\$3.00/MF\$0.65 CSCL 05B

This cumulative index to NASA Tech Brief lists single page descriptions of individual innovations, devices, methods, or concepts published from 1963 through 1967. A subject index, as well as indices relating Tech Brief number with originating source and number are provided. Subject categories covered are: electrical (electronic); physical sciences (energy sources); materials (chemistry); life sciences; mechanical; and computer programs. G.G.

N68-26813*# Boeing Co., Seattle, Wash.

STUDIES OF COST EFFECTIVE STRUCTURES DESIGN FOR FUTURE SPACE SYSTEMS—SUMMARY Final Report, 17 Oct. 1966–17 Oct. 1967

Bruce Allesina and E. F. Styer Washington NASA Jun. 1968 158 p refs

(Contract NAS7-525)

(NASA-CR-1068; D2-114116-1) CFSTI: HC \$3.00/MF \$0.65 CSCL 14A

The application of economics to aerospace design problems is discussed. The three major goals were: to define promising directions for structural research by applying the concept of minimum cost rather than maximum performance to structural design; to understand the relationship of the structure to the economics of the total system; and to identify and apply the interactions of the various aspects of program costs to point out the potential cost savings they imply. All goals were satisfied and some of the conclusions reached were: (1) Cost considerations should be employed early in a program. (2) A concerted program of cost data collection, economic methods development, and industry education in use of cost as a design criteria is required. (3) Proper balance should be established between costs and weights for design candidates at the part, subsystem, and systems level. (4) Sophistication in low earth orbit payloads should be de-emphasized, with more emphasis placed on use of larger launch vehicles. (5) Space program testing philosophy should be defined on a cost effective basis, measured against mission risk. A.L.

34 GENERAL

N68-29039*# National Aeronautics and Space Administration, Washington, D. C.

NASA SCIENTIFIC AND TECHNICAL REPORTS FOR 1967. A SELECTED LISTING

May 1968 424 p refs

(NASA-SP-7029) GPO: HC\$2.50; CFSTI: MF\$0.65 CSCL 05B

Bibliographic citations and abstracts arranged by subject categories are presented, selected from NASA reports that appeared in STAR. These documents listed were issued as part of the following NASA report series: Special Publications (NASA SP-),' Technical Reports (NASA TR-), Technical Notes (NASA TN D-), Technical Memorandums (NASA TM X-), Technical Translations (NASA TT F-), and Contractor Reports (NASA CR-). Indexes are included on subject, personal author, corporate source, report/accession number, and accession/report number. M.G.J.

N68-32769*# National Aeronautics and Space Administration, Washington, D. C.

BIBLIOGRAPHIES ON AEROSPACE SCIENCE A Continuing **Bibliography With Indexes**

Jul. 1968 134 p refs

(NASA-SP-7006(03)) CFSTI: HC\$3.00/MF\$0.65 CSCL 05B

An annotated bibliography is presented which provides references to bibliographies, literature searches, abstract compilations, literature reviews and surveys, and report listings pertaining to aerospace subjects. Technical reports containing comprehensive reference listings are included along with a subject index. B.S.D.

N68-33682*# National Aeronautics and Space Administration. Goddard Space Flight Center, Greenbelt, Md.

THE ROLE OF THE EXPERIMETER ASSOCIATED WITH **MULTI-EXPERIMENT SCIENTIFIC SATELLITES**

George H. Ludwig Washington Sep. 1968 14 p Presented at the AIAA Space Program Issues of the 70's Meeting, Seattle, 28 Aug. 1967

(NASA-TN-D-4731) CFSTI: HC\$3.00/MF\$0.65 CSCL 22B

The primary objective of the scientific investigators concerned with scientific spacecraft is to obtain interpretable measurements from their sensors. An additional primary objective of university investigators is to train students in the space sciences and research techniques. To achieve these objectives, the investigators must help define mission requirements: participate in mission planning, instrument development, integration and testing, prelaunch activities, and operations; and be prepared to analyze the data upon receipt. Prelaunch preparations must be kept as short as possible commensurate with reasonable success probabilities, provide a reasonable balance between system capability and simplicity, and provide flight data as rapidly as possible. Improvements to present flight programs can be made in several areas. The experiment life cycle needs shortening, and greater simplification of the experiment/spacecraft interfaces is desirable. Technical and management coordination should be simplified and made more direct. Experimenters need better financial management, improved ability to meet schedules, better quality control, and better preparation for data reduction after launch. Author

N68-35564*# National Aeronautics and Space Administration. Washington, D. C. A STUDY OF NASA UNIVERSITY PROGRAMS

1968 85 p refs (NASA-SP-185) CFSTI: HC\$3.00/MF\$0.65 CSCL 051

Selected samplings of NASA-university interactions were

made by interviews, university visits, and in-depth studies to assess the overall NASA university program, which has the dual goal of accomplishing the aeronautics and space mission and strengthening the universities involved. Scope of the NASA university program is considered in terms of relations to the total amount of federal university support, university community involvement, and individual programs; and a general summary is included of the research grants

and contracts in various areas, flight experiments, and university research centers and laboratories. Sustaining university programs are reviewed, including grants for traineeships, research programs, and facilities; and mention is made of personnel development programs in connection with the overall effort. M.W.R.

N68-37216*# Little (Arthur D.), Inc., Cambridge, Mass. SPACE TECHNOLOGY TRANSFER AND DEVELOPING NATIONS

Peter E. Glaser, Robert M. Jolkovski, Claudio Marqueron, and Walter M. Noel Washington NASA Oct. 1968 158 p refs (Contract NASw-1649)

(NASA-CR-1222) CFSTI: HC \$3.00 /MF \$0.65 CSCL 05A

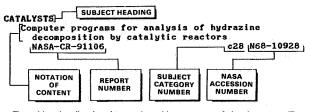
The potential for transferring space technology advances to aid developing nations was assessed using Brazil as a model. The NASA technical information file was searched to retrieve document abstracts relevant to Brazilian developmental needs in agriculture, public health, exploration and utilization of natural resources, industrialization, housing, education and training, communications, and transportation. More than 40 matches of need with technology were obtained. Included in the findings are: (1) Technology oriented searches (refrigeration and electric power, for example) provided a broader range of relevant abstracts than problem oriented searches for example, forest clearing and road construction. (2) Because all abstracts are in English, transfer to technology to developing nations would be impeded. (3) Abstracts containing information on principles, development status, application results, costs, and feasibility had the highest potential for matching. (4) Information search printouts in the form of document titles and key words only are inadequate for technology transfer matching. E.C.

SUBJECT INDEX

NASA SCIENTIFIC AND TECHNICAL REPORTS FOR 1968

A Selected Listing

Typical Subject Index Listing



The subject heading is a key to the subject content of the document. The Notation of Content (NOC), rather than the title of the document, is used to provide a more exact description of the subject matter. The report number helps to indicate the type of document cited (e.g., NASA report, translation, NASA contractor report). The subject category number indicates the subject category in the abstract section in which the citation is located. The NASA accession number denotes the number by which the citation is identified within the subject category. The NOC's are arranged under each subject heading in ascending accession number order.

Δ

- ABERRATION Mathematical determination of geometrical image aberrations in single and double mirror systems NASA-TN-D-4692 c23 N68-36460 ABLATION
 - Rotation effects on melting ablation on reentry of axisymmetric bodies NASA-TN-D-4614 c33 N68-26650
 - Ablation and temperature data for Apollo heat shield material using Pacemaker vehicle for flight test
 - NASA-TN-D-4713 c33 N68-30747 Frothing-sloughing ablation model for computing luminous efficiency factor from meteor data NASA-TN-D-4808 c30 N68-33055
 - Chemical reaction-plane approximation in ablation analyses
 - c33 N68-36072 NASA-TN-D-4817 Low density, leading edge bluntness, and ablation effects on wedge induced laminar boundary layer separation at moderate enthalpies in hypersonic flow
- NASA-TN-D-4829 c12 N68-36458 ABLATIVE MATERIALS
 - Effects of molecular structure on thermochemical properties of phenolic resins and related polymers NASA-TR-R-276
 - c33 N68-11038 Ablative and steel chambers effect on combustion instability in hydrogen oxygen rocket engine NASA-TM-X-1511 c28 N68-15644
 - Relative erosion resistance of ablative materials for nozzle sections of storable-propellant rocket engine
 - NASA-TM-X-1559 c28 N68-19708
 - Theoretical analysis of five composite ablation materials with various percentages of phenolic resin, powdered nylon, and silica NASA-TN-D-4374 c18 N68-197 c18 N68-19710
 - Analyses and finite difference procedure for predicting transient in-depth response of charring ablation materials NASA-CR-1060
 - c33 N68-25244 Coking reactions of pyrolysis gas in charring ablation material NASA-CR-1065
 - c33 N68-26817 Launch vehicle flight tests of effects of Apollo heat shield irregularities on ablative material performance NASA-TN-D-4791 c33 N68-35116
- ABLATIVE NOSE CONES Movement of forward heat shield in Apollo command module turbulent reverse flow wake c31 N68-30032 NASA-TN-D-4691 ABORT TRAJECTORIES Computational method for orbiting astronauts to determine required velocity for two impulse abort to landing site NASA-TN-D-4599 c21 N68-25103 ABSORBERS (EQUIPMENT) Wind tunnel model vibration reduced by use of tuned vibration damping absorber on aircraft model NASA-TM-X-1606 c32 N68-28806 ABSORPTION CROSS SECTIONS Source Control Boron 10/neutron, alpha particle/ lithium 7, lithium 7 resonance relative cross sections in keV region NASA-TN-D-4783 c24 N68-33763 ABSORPTION SPECTRA Laser modulated bulk optical absorption in cadmium sulfide single crystals NASA-TN-D-4466 c26 N68-18772 Applications of Monte Carlo analysis to tungsten resonance absorption NASA-TN-D-4545 c22 N68-21924 Coherent radiation methods of measuring absorption spectra in planetary atmosphere, and millimeter and submillimeter wave propagation c07 N68-27063 NASA-CR-863 Infrared horizon radiance profiles obtained during NASA-TN-D-4741 c21 N68-33450 ABSORPTIVITY Power transfer to ion cyclotron waves in two species plasma NASA-TM-X-1481 c25 N68 c25 N68-11404 ABSTRACTS Cumulative index to NASA survey on technology utilization of aerospace research output NASA-SP-5021/06/ c34 N68-25221 Bibliographic citations, abstracts, and indexes on selected NASA Scientific and Technical Reports for 1967 NASA-SP-7029 c34 N68-29039 NASA-SP-7029 c34 N68-291 Bibliographic citations, abstracts, and indexes on laser and maser research and development NASA-SP-7009/03/ c16 N68-294 Bibliographic citations, abstracts, and indexes on planetary atmospheres - June 1966 through December 1967 NASA-SP-7017/02/ c30 N68-300 CENEPATDES c16 N68-29438 c30 N68-30601 AC GENERATORS Reduction of apparent power requirement for phase controlled parasitically loaded turboalternator by multiple parasitic loads NASA-TN-D-4302 c03 N68-17110 Dynamic characteristics of parasitic loading speed controller for Brayton cycle turboalternator NASA-TM-X-1456 c03 N68-1 c03 N68-18702 Breadboard model of Brayton cycle alternator and voltage regulator-exciter NASA-TN-D-4697 c03 N68-29960 Performance test of homopolar inductor alternator for Brayton cycle space power system NASA-TN-D-4698 c c03 N68-30002
 - Numerical analysis of winding power loss of rotating ac generators in controlled atmospheres

ACCELERATION (PHYSICS)

NASA-TN-D-4849 c03 N68-37162 ACCLERATION (PHYSICS) Earth orbital vehicle control during entry phase to simulate manned planetary entry NASA-TN-D-4847 c31 N68-30 Landing loads and accelerations of the XB-70-1 c31 N68-36056 aircraft NASA-TN-D-4836 c02 N68-36073 ACCELEROMETERS Flight test of electrostatic accelerometer which eliminates null bias problem NASA-TM-X-1488 c14 N68-13974 Ring accelerometer errors from stresses developed by fixture vibrations NASA-TN-D-4540 c14 N68-25830 ACOUSTIC ATTENUATION Conference on sonic boom reduction in supersonic transport flight - shock wave propagation and refraction, prediction methods for acoustic attenuation, and aerodynamic engineering aspects NASA-SP-180 ACOUSTIC EXCITATION c02 N68-34907 Noise reduction in small enclosed structures in terms of physiological and psychological effects NASA-CR-1155 c32 N68-33266 ACOUSTIC IMPEDANCE Effects of high wave amplitude and mean flow on impedance of Helmholtz resonator NASA-TM-X-1582 ACOUSTIC INSTABILITY c12 N68-23423 Stability effects of several injector face baffle configurations on screech in hydrogen-oxygen rocket NASA-TN-D-4515 c28 N68-21679 Chamber pressure, contraction ratio, and flow per element effects on acoustic mode instability in hydrogen oxygen engines NASA-TN-D-4733 c33 N68-3051 c33 N68-30518 ACOUSTIC MEASUREMENTS Evaluation of ultrasonic absorption technique for measuring high temperature gas properties NASA-TN-D-4433 c24 N68-18949 c24 N68-18949 B-70 aircraft engine noise measurements and predictions NASA-TM-X-1565 c02 N68-21834 Acoustic measurements on jet engine intake system noise reduction suppressor cowlings NASA-TN-D-4639 c02 N68-29887 Ultrasonic attenuation measurements on single tantalum crystals at superconducting state NASA-TN-D-4806 c26 N68-35356 ACOUSTIC PROPERTIES Experimental, and theoretical evaluations of acoustic liners for screech suppression in rocket engines NASA-TN-D-4442 c28 N68-18249 Subjective response to far field noise characteristics of V/STOL aircraft sized to carry 60 passengers over 500 mile range NASA-CR-1118 c05 N68-33009 ACOUSTIC SIMULATION Effects of various simulated sonic boom waveforms on human subjective response NASA-CR-1192 c04 N68-ACTIVITY (BIOLOGY) Heat stress and prolonged activity effects on c04 N68-35103 human perceptual motor performance NASA-CR-1153 c05 N68-31480 ADAPTIVE CONTROL Human learning behavior theory in manual control task modeled as computer program NASA-CR-1124 c05 N68-31911 New methods for design of adaptive flight control systems NASA-CR-1152 c21 N68-33904 ADHESION Silicate surface preparation to represent lunar soil, and ultrahigh vacuum adhesion measurements NASA-CR-1090 c30 N68-28373 Influence of chemisorbed films of various gases on adhesion and friction of tungsten in vacuum NASA-TN-D-4694 c15 N68-33227 Influence of gaseous environment on self-adhesion of metal surfaces NASA-TN-D-4868 c17 N68-36970 Electroadhesive devices - theory, design,

fabrication, and testing NASA-CR-1211 c10 N68-37906

SUBJECT INDEX

ADHESION TESTS Reduction of adhesive forces and friction of iron polycrystals in vacuum by chemisorbed films NASA-TN-D-4775 c17 N68-33278 ADHESTVES Organic and inorganic adhesives for bonding of stainless steels and precipitation hardened stainless steels NASA-SP-5085 c15 N68-20056 ADSORPTION DRPTION Low energy electron diffraction study of oxygen adsorption on molybdenum /111/ surface NGGA-TM-D-4735 c06 N68-30582 Adsorption isotherm relations and transient desorption behavior of homogeneous and heterogeneous metal surfaces NASA-TN-D-4789 c24 N68-34175 AERODYNAMIC BALANCE Theoretical study of effect of pivot location on aerodynamic balance movement of variable sweep wings in incompressible flow NASA-TN-D-4635 c01 N68-28817 AERODYNAMIC BRAKES Wind tunnel evaluation of speed brake effects on supersonic characteristics of variable sweep fighter aircraft models NASA-TN-D-4773 c02 N68-33669 NASA-TN-D-4773 c02 No8-33 Technology requirements and spacecraft design studies for atmosphere braking to orbit about Mars and Venus NASA-CR-1131 c30 N68-34 c30 N68-34086 AERODYNAMIC CHARACTERISTICS Ground proximity effects on longitudinal, lateral, and control aerodynamic characteristics of tilt wing four propeller V/STOL wind tunnel model NASA-TN-D-4237 c02 N68-11519 c02 N68-11519 Performance characteristics during landing approach of large powered-lift jet transport NASA-TN-D-4261 c02 N68-11638 Pressure distributions and aerodynamic characteristics of Nimbus B fuel capsule in hypersonic flow NASA-TM-X-1487 c01 N68-11958 Inflation, and drag characteristics of disk gap band parachute in simulated low density Mars atmosphere NASA-TM-X-1499 c31 N68-13797 Aerodynamic ground effect measurements on low aspect ratio ogee wings NASA-TN-D-4329 c02 N68-14090 Inflation, drag, and stability characteristics of ringsail parachute deployed in simulated Mars atmosphere NASA-TM-X-1500 c31 N68-14092 Arodynamic factors, and effects on dynamic longitudinal stability characteristics of tilt wing V/STOL aircraft NASA-TN-D-4344 c02 N68-15941 Wind tunnel study of aerodynamic characteristics of three scale model multistage launch vehicles at supersonic and hypersonic speeds NASA-TM-X-1498 c01 N68-16299 Supersonic aerodynamic characteristics of model of air-to-surface missile NASA-TM-X-1491 c01 N68-16480 Wind tunnel study of lateral and directional aerodynamic characteristics of powered four-duct propeller VTOL scale model in transition NASA-TN-D-4343 co2 N68-17023 Aerodynamic characteristics of tension string, tension shell, and conical shapes in supersonic flow c01 N68-18720 NASA-TN-D-4360 Wind tunnel stability tests of twin engined NASA-TN-D-4489 c01 NGA c01 N68-1918 c01 N68-19189 Aerodynamic characteristics of large-scale model of tilt-wing V/STOL aircraft NASA-TN-D-4493 c01 N68-20370 Interference effects of canard controls on longitudinal aerodynamic characteristics of winged body in hypersonic flow NASA-TN-D-4436 c01 N68-2 Aerodynamic and performance characteristics of unpowered rotor reentry vehicle c01 N68-21579 c31 N68-21758 NASA-TN-D-4537

Simulated wing damage effects on aerodynamic characteristics of swept-wing airplane model NASA-TM-X-1550 col N68-22002 SUBJECT INDEX

AEROSOLS

Static longitudinal aerodynamic characteristics of configurations used in Little Joe/Apollo test vehicle development NASA-TN-D-4439 c31 N68-22953 Test apparatus and procedures for aerodynamic model tests of spacecraft control system parameters NASA-CR-947 c32 N68-23452 C32 NB8-234 Aerodynamic characteristics of modified conical lifting reentry vehicle at hypersonic speeds NASA-TN-D-4598 C31 N68-245 NASA-TN-D-4598 c31 N68-24964 Aerodynamic characteristics of scale model with augmented jet flap NASA-TN-D-4610 c01 N68-25919 Exhaust gas ingestion characteristics and induced aerodynamics for vertical takeoff lift engine fighter model in ground proximity NASA-CR-1098 c02 N68-28233 Aerodynamic characteristics of a stator modified gas turbine for single shaft Brayton cycle power system NASA-TM-X-1615 c03 N68-28870 Stabilizer and tail assembly effects on overall aerodynamic characteristics of lifting bodies at hypersonic speeds NASA-TM-X-1620 c01 N68-29952 Cold flow tests of aerodynamic characteristics of plug nozzle configuration for turbojet engines operating at supersonic speeds NASA-TM-X-1619 c28 N68-29953 Aerodynamic characteristics of two blunt half cone wedge entry configurations at supersonic speeds NASA-TM-X-1621 c01 N68-30030 NHOR-IN-X-1621 COI N68 Accurate methods for predicting longitudinal aerodynamic characteristics of two-lobed conical parawings with leading edge booms NASA-CR-1166 COI N68c01 N68-33765 Aerodynamic characteristics of several hypersonic boostglide configurations at Mach 2.30 to 4.63 c01 N68-33836 NASA-TM-X-1601 Deployment characteristics of dynamic and elastic parawing scale model for spacecraft recovery NASA-TN-D-4724 c02 N68-33879 Aerodynamic characteristics of subsonic cargo jet transport model in slotted transonic wind tunnel NASA-TN-D-4796 In slotted transport wind tun NASA-TN-Z-1660 col N68-35 Profile change effects on aerodynamic characteristics of twisted and cambered arrow wing at supersonic speed NASA-TN-D-4796 col N68-35 c01 N68-35617 c01 N68-35665 Wind turnel tests of a VTOL jet fighter to determine aerodynamic characteristics including stability NASA-TN-D-4812 c01 N68-36081 Aerodynamic characteristics of bodies of revolution at Mach numbers from 1.50 to 2.86 and angles of attack to 180 deg NASA-TM-X-1658 col N68-3 c01 N68-36193 Windshield and nose geometry effects on supersonic aerodynamic characteristics of tactical fighter model NASA-TM-X-1664 c02 N68-37066 Effects of simulated jet exhaust flow on transonic aerodynamic characteristics of Apollo launch escape vehicle models NASA-TN-D-4843 c31 N68-37074 Wind tunnel tests to determine low speed high lift aerodynamics of one-fifth scale variable sweep supersonic transport model NASA-TN-D-4844 c01 N68-37365 Longitudinal aerodynamic characteristics of parasol-wing model at supersonic speeds NASA-TN-D-4855 AERODYNAMIC COEFFICIENTS c01 N68-37854 Free flight aerodynamic characteristics of slender cone at hypersonic speeds NASA-TN-D-4245 c01 N68-10380 Effect of boattail juncture shape on pressure drag coefficients of isolated afterbodies of supersonic engine nacelles NASA-TM-X-1517 c01 N68-19237 MASA-IM-X-151/ Flight test of 30 foot nominal diameter cross parachute to measure shock loads, drag efficiency, and stability characteristics NASA-TM-X-1542 c31 N68-21778 Computer program for analyzing free flight motions of axisymmetric bodies to determine aerodynamic coefficients NASA-TN-D-4766 c01 N68-33081

of subsonic boattail at angle of attack NASA-TM-X-1662 c01 c01 N68-35672 AERODYNAMIC CONFIGURATIONS Volume addition effects on leeward surface of high lift drag ratio winged body at hypersonic speeds NASA-TN-D-4361 AERODYNAMIC DRAG c01 N68-17880 Inflation and drag characteristics of cross parachute in simulated Martian environment NASA-TM-X-1543 c31 N68 c31 N68-21833 Wind tunnel study to explore use of slot spoilers for direct control of flap induced lift and lateral aircraft control NASA-TN-D-4664 c01 N68-2883 Aerodynamic drag measurements and boundary layer flow over V notches at transonic and supersonic c01 N68-28830 speeds NASA-CR-1132 c12 N68-35252 AERODYNAMIC HEATING Aerodynamic heating, delamination and pressure in nose fairing honeycomb core of Atlas Centaur launch vehicle NASA-TM-X-1605 c33 N68-28156 Variable density hypervelocity wind tunnel tests on effects of several ramp-fairing, umbilical, and pad configurations on aerodynamic heating to Apollo command module NASA-TM-X-1640 c01 N68-35141 AERODYNAMIC STABILITY Aerodynamic stability characteristics of Apollo launch escape vehicle with canard surfaces deployed NASA-TN-D-4280 c01 N68-11640 Analytical methods for dynamic stability analyses of large launch vehicles during flight through and exit from earth atmosphere NASA-CR-944 c32 N68-18825 Planform design method, general characteristics, and aeroelastic stability of flexible lifting rotors NASA-TN-D-4465 c01 N68-1 Aeroelastic instability of overexpanded rocket c01 N68-19954 Aeroelastic instability of overexpanded rocker nozzle extensions NASA-TN-D-4471 c32 N68-: Flight test of 30 foot nominal diameter cross parachute to measure shock loads, drag c32 N68-21099 efficiency, and stability characteristics NASA-TM-X-1542 c31 N6 c31 N68-21778 Soviet engineering handbook on vibration and dynamic stability theory and calculations in helicopter design NASA-TT-F-519 c02 N68-23456 Flight test of 10-foot nominal-diameter disk-gap band parachute to determine deployment and inflation, opening shock loads, drag efficiency, and stability characteristics NASA-TM-X-1575 c02 N68-24245 MB3A-18-A-1975 Thrust vector deflection stability analysis for minimum control requirements of booster vehicles during atmospheric flight NASA-TN-D-4593 c21 N68-24409 Aerodynamic stability and control characteristics of supersonic aircraft NASA-TN-D-4578 c02 N68-24498 Wind tunnel tests of a VTOL jet fighter to determine aerodynamic characteristics including stability NASA-TN-D-4812 c01 N68-36081 AERODYNAMICS Aerodynamic parameters effect on dynamic behavior on reentry vehicle NASA-TM-X-1589 c31 N68-2664 c31 N68-26645 Supersonic aerodynamics of large angle cones NASA-TN-D-4719 c01 N68-31551 AEROELASTICITY Planform design method, general characteristics, and aeroelastic stability of flexible lifting rotors NASA-TN-D-4465 c01 N68-19954

 NASA-IN-D-4405
 CUL NGG-19554

 Aeroelastic instability of overexpanded rocket
 nozzle extensions

 NASA-TN-D-4471
 C32 N68-21099

 Aeroelastic divergence characteristics of moveable

 control surfaces, including drag loadings NASA-TN-D-4793 c32 N68-35496 AEROSOLS Radiant heat transfer to aerosols for application

Simulated wing effect on pressure drag coefficient

AEROSPACE ENGINEERING

SUBJECT INDEX

in gaseous core nuclear rocket engine designs NASA-CR-953 c22 N68-10561 AEROSPACE ENGINEERING Parts and materials application review for project management of space systems engineering c15 N68-10120 NASA-SP-6505 NABA-SF-5000 C15 N6 Advanced valve technology for aerospace use NASA-SP-5019 c15 N6 c15 N68-10402 Uses of submillimeter waves in aerospace technology, with bibliography NASA-SP-182 c07 N68-35522 AEROSPACE ENVIRONMENTS NASA-GE medicine and biology bibliography on physiological, psychological, and environmental effects on man during aerospace flights NASA-SP-7011/43/ C04 NAS-1467: Aerospace medicine and biology bibliography on c04 N68-14671 physiological, psychological, and environmental effects on man during aerospace flights NASA-SP-7011/42/ c04 N68-1472 c04 N68-14725 Liquid shroud cryogenic supercritical pressure storage system for space applications NASA-CR-1048 col c03 N68-22842 Circuit breakers and electric switch developments for future nuclear electric power generation systems operating in aerospace environments NASA-CR-1026 c03 N68-29 AEROSPACE MEDICINE c03 N68-29460 Aerospace medicine and biology bibliography on physiological, psychological, and environmental effects on man during aerospace flights NASA-SP-7011/43/ c04 N68-14671 Aerospace medicine and biology bibliography on physiological, psychological, and environmental effects on man during aerospace flights NASA-SP-7011/42/ c04 N68-14725 Aerospace medicine and biology bibliography NASA-SP-7011/44/ c04 N68-15899 Continuing bibliography on aerospace medicine and biological effects of space flight stress NASA-SP-7011/45/ c04 N68-16517 Annotated bibliography and indexes on aerospace medicine and biological effects - February 1968 Aerospace medicine and biology bibliography on medicine and biological effects - February 1968 NASA-SP-7011/47/ c04 N68-20026 Annotated bibliography and indexes on aerospace medicine and biological effects - March 1968 NASA-SP-7011/48/ c04 N68-20027 Cumulative index for NASA bibliography on aerospace medicine and biological effects -January 1968 NASA-SP-7011/46/ c04 N68-22194 Anotated bibliography and indexes on aerospace medicine and biological effects - April 1968 NASA-SP-7011/49/ c04 N68-224 Anotated bibliography and indexes on aerospace medicine and biological effects c04 N68-22882 May 1968 NASA-SP-7011/50/ c04 N68-25844 Annotated bibliography and indexes on aerospace medicine and biological effects - June 1968 NASA-SP-7011/51/ c04 N68c04 N68-28246 Annotated bibliography and indexes on aerospace medicine and biological effects - July 1968 NASA-SP-7011/52/ c04 N68-32707 Annotated bibliography on aerospace medicine and biology - August 1968 NASA-SP-7011/53/ c04 N68-350 c04 N68-35069 Annotated bibliography and indexes on aerospace medicine and biological effects - August 1968 NASA-SP-7011/54/ AEROSPACE SCIENCES cÕ4 N68-38051 Data collection and processing from space science satellites NASA-TN-D-4508 c08 N68-22510 Annotated bibliographies on aerospace science NASA-SP-7006/03/ c34 N68-3 AEROSPACE SYSTEMS c34 N68-32769 Descriptive model of system development activities and man machine systems for determining optimal human performance in aerospace systems NASA-CR-877, V. 2 co5 N68-15120 Optimal role of man in space, allocation of men and machines in aerospace systems, and descriptive model for determining optimal human performance human performance NASA-CR-878 c05 N68-19165 Human factors engineering techniques for reducing human errors in space systems development NASA-SP-6506 c05 N68-20357 c05 N68-20357

Cost effectiveness studies on structural design of future aerospace systems NASA-CR-1068 c34 N68-26813 Conference papers on NASA planning and projected requirements for advanced aerospace electronic systems technology NASA-SP-154 c30 N68-33169 Conference on numerical analysis applications to aerospace and related problems NASA-SP-170 c19 N68-332 AEROSPACE VEHICLES c19 N68-33245 Pyrotechnic shaped charge aerospace vehicle stage and shroud separation systems development NASA-TM-X-1607 c31 NG c31 N68-28869 AFTERBODIES Effect of boattail juncture shape on pressure drag coefficients of isolated afterbodies of supersonic engine nacelles NASA-TM-X-1517 c01 N68-1 Integral methods for predicting afterbody heat c01 N68-19237 transfer to blunt two dimensional configuration subjected to separated flow NASA-TN-D-4443 cl2 N68-2828 c12 N68-28282 Effect of geometry of conical afterbodies on base drag at subsonic and transonic speeds NASA-TN-D-4821 c01 N68-3705 c01 N68-37054 NASA-TN-D-4821 COI N68-AGENA ROCKET VEHICLES Gemini-Agena station keeping using connecting tether - Analysis and simulations NASA-TN-D-4258 c31 N68-Atlas-Agena and Atlas-Centaur combined c31 N68-11641 propulsion system for measurements out of three dimensional phenomena out of ecliptic plane NASA-TN-D-4455 c28 N68-19581 AIR BREATHING ENGINES Simplified equilibrium hydrocarbon-air combustion gas model for use in air breathing engine cycle computer programs NASA-TN-D-4747 c28 N68-35115 Simulated wing effect on pressure drag coefficient of subsonic boattail at angle of attack NASA-TM-X-1662 c01 c01 N68-35672 AIR CONDUCTIVITY Convective stagnation heat transfer of carbon dioxide, nitrogen-argon gas mixtures compared to air in shock tube tests NASA-TN-D-4255 c33 N68-11811 AIR COOLING Effect of variable stator geometry on performance of air cooling turbine NASA-TM-X-1632 c01 N68-29994 c01 N68-29994 ATR FLOW Air flow calibration over moving belt ground plane installed in wind tunnel and data for two blowing-flap models tested over moving belt NASA-TN-D-4228 col N68-10060 Reynolds number effect on single stage axial flow turbine in air NASA-TN-D-4383 c03 N68-16228 Approximate average midspan metal temperatures and coolant flow requirements for turbine airfoils cooled by compressor exit bleed air NASA-TN-D-4491 c33 N68-1 c33 N68-19187 Water vapor condensation effects of heated air on flow in large supersonic wind tunnels NASA-TM-X-1636 cl c11 N68-30598 AIR JETS Helium and air flow tests over single flat plates to determine dynamic pressure limits of nuclear fuel element plates NASA-TN-D-4417 c12 N68-1622 c12 N68-16227 Forces and moments produced by air and helium jets exhausting parallel to flat plate in near vacuum NASA-TN-D-4408 c12 N68-19000 AIR LOCKS Leakage of large diameter O ring seals on spacecraft air lock hatches NASA-TN-D-4394 c31 N68-17498 AIR SAMPLING

 AIR SAMPLING

 Air samplers, contamination, and sterilization in collection of microorganisms for microbiological exploration of stratosphere

 NASA-CR-1101
 c04 N68-28247

 AIR TRAFFIC CONTROL
 Simulated flight operations to evaluate problems encountered by supersonic transports in present air traffic control system

 NASA-TN-D-4638
 c02 N68-29372

AIRBORNE EQUIPMENT FM data handling facility for preparing analog physiological data obtained in flight for digital computations NASA-TN-D-4488 c05 N68-21537 Signal conditioning methods and equipment used for inflight recording of pilot biomedical data NASA-TN-D-4487 c05 N68-21538 AIRBGRNE/SPACEBORNE COMPUTERS Hardware design and computer programs for spaceborne multiprocessor computer system NASA-CR-1158 c08 N6 c08 N68-31499 Advanced multiprocessor computer organization for manned Mars lander mission NASA-CR-1159 c08 N68-35560 c08 N68-35560 AIRCRAFT BRAKES Runway surface texture conditions effect on wet runway braking friction coefficients created by aircraft tires NASA-TN-D-4323 c02 N68-14 c02 N68-14903 AIRCRAFT CONFIGURATIONS AIRCRAFT CUNFIGURATIONS Wind tunnel tests to determine low speed high lift aerodynamics of one-fifth scale variable sweep supersonic transport model NASA-TN-D-4844 AIRCRAFT CONTROL Simulated wind-tunnel investigation with jet-augmented flap NASA-TN-D-4278 c02 N68-11627 Pilot performance using compensatory and pursuit tracking displays with rate and acceleration control dynamics and disturbance input NASA-CR-1082 c07 N68-28272 Wind tunnel study to explore use of slot spoilers for direct control of flap induced lift and lateral aircraft control NASA-TN-D-4664 c01 N68-28830 AIRCRAFT DESIGN V/STOL short haul transport design considerations including noise characteristics NASA-CR-670/01/ c02 N68-11174 Estimation procedures for effect of design and flight characteristics of jets on ground noise c02 N68-26930 NASA-CR-1053 Feasibility of revised V/STOL design and flight plan concepts for short haul transport aircraft NASA-CR-743/1/ c02 N68-35177 AIRCRAFT ENGINES Cold air study of gas turbine for high temperature aircraft engine application NASA-TN-D-4389 col N68-15743 Wind tunnel tests of airframe installation effects on F-106B scale model with simulated underwing engine nacelles at Mach 0.56 to 1.46 NASA-TM-X-1683 AIRCRAFT FUEL SYSTEMS c02 N68-37941 Tankage systems for methane-fueled supersonic transport NASA-TM-X-1591 c02 N68-23895 AIRCRAFT HAZARDS Natural Incenso Natural electrical phenomena as aircraft fire hazards, with study of flame propagation in fuel vent systems NASA-CR-1076. co2 N68-26691 AIRCRAFT INSTRUMENTS Properties and imaging techniques of various display devices - computer directed visual Alight control boards, integrated optical man machine systems, and electro-optical methods NASA-SP-159 c09 N68-22 c09 N68-22302 AIRCRAFT LANDING NASA-TN-D-4261 (CRAFT LANDARG Performance characteristics during landing approach of large powered-lift jet transport NASA-TN-D-4261 c02 N68-11638 NASA-TN-D-4261 c02 N68-116 Simple model describing final airborne stages of landing transport aircraft manually NASA-TN-D-4438 c02 N68-21112 Statistical analysis of repeated acceleration and impact loads on airline transports NASA-TN-D-4586 c02 N68-24476 Cumulative errors associated with Category 2 and 3 operations, and terminal flight paths for low visibility landings NASA-CR-1188 c02 N68 AIRCRAFT MODELS Simulated wing damage effects on aerodynamic c02 N68-35595

characteristics of swept-wing airplane model NASA-TM-X-1550 c01 N68-22002 Wind tunnel model vibration reduced by use of

tuned vibration damping absorber on aircraft model NASA-TM-X-1606 c32 N68-28806 AIRCRAFT NOISE Subjective response to far field noise characteristics of V/STOL aircraft sized to carry 60 passengers over 500 mile range NASA-CR-1118 c05 N68-3 c05 N68-33009 NASA-CK-1118 Conference on sonic boom reduction in supersonic transport flight - shock wave propagation and refraction, prediction methods for acoustic attenuation, and aerodynamic engineering aspects NASA-SP-180 co2 N68-34907 Review of blade slap studies for determining noise in helicopters NASA-CR-1221 c02 N68-37932 AIRCRAFT PERFORMANCE Performance characteristics during landing approach of large powered-lift jet transport NASA-TN-D-4261 c02 N68-11638 Simulated flight test of double-Delta supersonic transport for performance characteristics, handling qualities, and climbing characteristics NASA-TN-D-4396 c02 N68-17391 Performance requirements and economic costs to reduce cruise sonic boom of supersonic transport NASA-TN-D-4677 c02 N68-28831 Beformance characteristics from static tests in ground effect of V/STOL transport model NASA-CR-1180 c28 N68-35594 NASA-CK-1180 C28 NG6-35594 AIRCRAFT PILOTS Optimum values of pitch rate damping, longitudinal control and speed stability for vertical takeoff aircraft /helicopters/ using pilot ratings NASA-TN-D-4824 c02 N68-28153 AIRCRAFT STABILITY Wind tunnel determination of longitudinal force characteristics for STOL aircraft scale models with varying wing aspect ratios NASA-TN-D-4448 c02 N68-18771 NASA-IN-D-4446 Variable-stability helicopter flight tests under instrument flight rules to determine effects of gross changes in longitudinal static stability for V/STOL handling qualities NASA-TN-D-4364 c02 N68-191 c02 N68-19184 AIRCRAFT TIRES Runway surface texture conditions effect on wet runway braking friction coefficients created by aircraft tires NASA-TN-D-4323 c02 N68-14903 Dynamic hydroplaning, viscous hydroplaning, and tire tread rubber reversion effects on tire traction on wet runways NASA-TN-D-4406 c02 N68-19620 Approximate theory for inviscid hydrodynamics of aircraft tire hydroplaning NASA-CR-1125 c12 N68-31593 AIRCRAFT WAKES UNART WARLS Jet wake effect of high bypass jet engine on wing-nacelle interference drag of subsonic transport model NASA-TN-D-4693 c01 N68-30595 NASA-IN-D-4693 CUI NGG-503 AIRFOIL PROFILES Tabulated performance data of full-scale rotary wings at high advance ratios and advancing tip Mach numbers based on wind tunnel tests NASA-TN-D-4632 col N68-2826 c01 N68-28268 AIRFOILS Pressure rise response of turbopumps to flucturating flow rates and unsteady flow about two dimensional linear cascade of airfoils c01 N68-21950 NASA-TN-D-4298 AIRFRAMES Wind tunnel tests of airframe installation effects on F-106B scale model with simulated underwing engine nacelles at Mach 0.56 to 1.46 NASA-TM-X-1683 c02 N68-37941 AIRLINE OPERATIONS CLINE UPERATIONS Summary of vertical gusts acceleration data collected for one type twin engine jet airplane during airline operations NASA-TN-D-4529 c02 N68-2229 Simulated flight operations to evaluate problems encountered by supersonic transports in present air traffic control super c02 N68-22291 air traffic control system NASA-TN-D-4638 c02 N68-29372 AIRSPEED Velocity, gust, and height data analysis from four-engine turbojet transport airplane

SUBJECT INDEX

NASA-TN-D-4330 c02 N68-16522 Helicopter height-velocity diagram analysis showing effects of density altitude and gross weight NASA-TN-D-4536 c02 N68-22033 ALGAE DE Bioregenerative life support systems for long duration space flights - Hydrogenomonas biosynthesis and algae photosynthesis processes NASA-SP-165 C04 N68-26207 ALGEBRA Vector representation of rotations and their algebra NASA-TN-D-4696 c19 N68-30594 ALKALI METALS Recovery of potassium tantalate and potassium monoxide to demonstrate procedure for isolation and recovery of alkali-metal reaction products in uncontaminated state NASA-TN-D-4310 ALOUETTE SATELLITES c17 N68-14888 Field-aligned propagation of high frequency radio waves using Alouette 2 satellite data NASA-TN-D-4748 c07 N68-31635 c07 N68-31639 ALPHA PARTICLES Search for unbound helium 3 levels with isobaric spin 1/2 NASA-TN-D-4377 c24 N68-15638 Angular correlation between inelastically scattered alpha particles and gamma rays emitted in subsequent nuclear decay of magnesium 24 NASA-TN-D-4683 c24 N68c24 N68-29375 NASA-TN-D-4683 c24 N68-293 Boron 10/neutron, alpha particle/ lithlum 7, lithlum 7 resonance relative cross sections in keV region NASA-TN-D-4783 c24 N68-3370 ALTERNATING CURRENT c24 N68-33763 Breadboard three-phase static switch for space alternating current power systems NASA-TM-X-1495 c09 N68-15649 Reliability of silicon rectifiers as inverters for alternating current power source for Atlas Centaur launch vehicles NASA-TM-X-1569 c03 N68-215 c03 N68-21562 CO3 N68-21562 Experimental evaluation of ferroresonant and feedback alternating current line voltage regulators in 15 kilowatt auxiliary power system NASA-TN-D-4627 CO3 N68-28101 c03 N68-28101 ALTITUBE Thrust and altitude effects on ground track noise during steep approaches of four engine, medium range, turbojet transports NASA-TN-D-4241 col N68-1125 Technique for determining pericynthion altitude of lunar transfer orbits NASA-TN-D-4811 c30 N68-3645 c01 N68-11253 c30 N68-36459 ALUMINUM Effects of 22 MeV proton and 2.4 MeV electron radiation on boron and aluminum doped silicon solar cells NASA-TN-D-4407 c26 N68-1: Brazing aluminum to titanium coated stainless steel to minimize formation of intermetallic c26 N68-19924 compounds in joint NASA-SP-5040 c15 N68-22778 Target pressure and damage data from impacts by explosively propelled aluminum projectile NASA-TM-X-1597 c32 NG c32 N68-25819 Fabrication and testing of Pageos 1 NASA-TN-D-4596 c31 N68-25820 Cyclic incident radiation method for measuring thermal emittance and absorption properties of metals at cryogenic temperatures NASA-TM-X-1618 c33 N68-314 c33 N68-31498 NASA-TN-X-1618 c33 N68-ALUMINUM ALLOYS Axial tensile fatigue of liquid rocket engine alloys at cryogenic temperatures NASA-TN-D-4274 c17 N68c17 N68-11637 NASA-IN-0-4274 Fatigue crack propagation and fracture toughness characteristics of 7079 aluminum alloys in underage, peak age, and overaged conditions NASA-CR-996 c32 N68-154 c32 N68-15476 Protective coatings and surface treatments for protection of Ti-8Al-1Mo-1V alloy sheet from hot-salt stress corrosion NASA-TN-D-4319 c17 N68-1 c17 N68-17377 Environmental exposure effects on mechanical properties of titanium alloy, stainless steel, aluminum alloy, and composite material sheets

c17 N68-17897 NASA-TN-D-4318 Transmission, and backscatter coefficients for electron irradiated aluminum, and stainless teel foils NASA-TN-D-4363 c24 N68-17898 Penetration of porous projectiles in aluminium and plastic targets NASA-TN-D-4505 c32 N68-21293 Crack propagation in aluminum notched tensile and pressure vessel specimens cyclically loaded at cryogenic temperatures NASA-TN-D-4541 Prediction of fatigue crack propagation behavior in aluminum alloy panels with simulated rivet c17 N68-21768 NASA-TN-D-4702 c32 N68-32074 Hot salt stress corrosion cracking of titanium aluminum alloys in presence of anhydrous hydrogen chloride NASA-CR-1133 c17 N68-33019 Cavitation damage of stainless steel, nickel, and aluminum alloy in water NASA-TM-X-1670 c17 N68-36076 ALUMINUM NITRIDES Crucible melting and arc melting of aluminum nitride and determination of its melting point NASA-CR-1171 c17 N68-33335 AMMONIA Performance test data for ammonia resistojet attitude control system of stable platform satellites NASA-TM-X-1677 AMPLIFIER DESIGN c28 N68-36512 Operational amplifiers for nuclear spectroscopy NASA-TN-D-4349 c24 N68-18 c24 N68-18254 AMPLIFIERS Cable and circuit parameters effects on calibration of charge amplifier for microsecond pulses NASA-TN-D-4300 c09 N68-16530 AMPLITUDES Effects of high wave amplitude and mean flow on impedance of Helmholtz resonator NASA-TM-X-1582 c12 N68-23423 NASA-IN-A-1502 ANALOG COMPUTERS Flexible body analog computer program and rigid body digital computer program for calculating dynamic characteristics of double-V antennas on Radio Astronomy Explorer satellite NASA-CR-962 c08 N68-Resolution limit analysis for pulse frequency modulation telemetry processing line c08 N68-18144 NASA-TN-D-4180 c07 N68-18247 ANALOG DATA Analog and digital inertial flight data systems for X-15 aircraft NASA-TN-D-4642 c08 N68-29 c08 N68-29404 ANALOG SIMULATION Analog simulation of dc arc emission spectrometer control system to define optimum control requirements NASA-TN-D-4770 c08 N68-32055 Synthesis of human response in closed loop tracking tasks NASA-TN-D-4842 c05 N68-36461 ANALOG TO DIGITAL CONVERTERS FM data handling facility for preparing analog physiological data obtained in flight for digital computations NASA-TN-D-4488 c05 N68-2. ANALYSIS (MATHEMATICS) c05 N68-21537 Transient solidification of flowing liquid on cold plate, including heat capacities of frozen layer and plate NASA-TN-D-4353 c33 N68-15742 Synchrotron emission at helical motion of relativistic electrons emitting from source with relativistic velocity NASA-TT-F-521 c25 N68-16700 Analysis and selection of design for plutonium 238 for Brayton cycle space powerplant NASA-TN-D-4600 c03 N68-25829 Laboratory methodology of signal analysis with application to Apollo program NASA-TM-X-1599 c08 N68-3 c08 N68-30240 Mathematical model of liquid metal fuel reactor to investigate temperature distribution on neutron kinetics

ALGAE

SUBJECT INDEX

APPLICATIONS TECHNOLOGY SATELLITES

NASA-TN-D-4840 c22 N68-36055 Critical speed analysis of rigid rotors on flexible foundations NASA-TN-D-4858 c15 N c15 N68-37214 ANALYZERS Analysis of integrated charged particle energy spectra from gridded electrostatic analyzers NASA-TN-D-4718 c25 N68-3 c25 N68-30093 ANEMOMETERS Statistical evaluation of sampled wind data from anemometers mounted on meteorological tower on Wallops Island NASA-TN-D-4395 c20 N68-18246 ANGLE DF ATTACK Simplified approximations for calculating laminar heat transfer over spherically blunted axisymmetric bodies at angle of attack NASA-TN-D-4720 c33 N68-31959 AFTORYNAU - Characteristics of bodies of revolution at Mach numbers from 1.50 to 2.86 and angles of attack to 180 deg NASA-TM-X-1658 c01 N68-34 ANGLES (GEDMETRY) Navigator performance using hand held sextant c01 N68-36193 to measure angle between moving flashing light and simulated star - space navigation NASA-TN-D-4174 c21 N68-13558 ANGULAR ACCELERATION JULAN ACCELENATION Summary of vertical gusts acceleration data collected for one type twin engine jet airplane during airline operations NASA-TN-D-4529 c02 N68-2229 c02 N68-22291 ANGULAR CORRELATION Angular correlation between inelastically scattered alpha particles and gamma rays emitted in subsequent nuclear decay of magnesium 24 NASA-TN-D-4683 c24 N68-29375 ANGULAR DISTRIBUTION Scattering of 42 MeV alpha particles from even cadhium isotopes NASA-TN-D-4256 c24 N68-1 c24 N68-11074 Tables of energy and angular distributions of thick target bremsstrahlung in metals NASA-TN-D-4755 c24 N68-3 c24 N68-35535 ANISOTROPIC MEDIA Simple iterative solution for radiative heat transfer in anisotropic media NASA-CR-1023 c33 N68 c33 N68-22318 ANNEALING Radiation damage in low energy proton irradiated thick copper and gold foils and subsequent annealing characteristics NASA-TN-D-4452 c26 N68-212. c26 N68-21219 ANNULAR NOZZLES Performance evaluation of annular plug and expansion-deflection nozzles including external flow effects at transonic Mach numbers NASA-TN-D-4462 c01 c01 N68-20330 ANTENNA ARRAYS General method for designing circular array antennas to obtain quasi-omnidirectional atterns NASA-TN-D-4254 c07 N68-11475 Computer analyses of retrodirective, and self adaptive antenna phase control techniques for Mars probe NASA-CR-977 c21 N68-18484 Quasi-ommidirectional resonant array of circumferential shunt slots in ring waveguides for narrow bandwidth space vehicle applications at microwave frequencies NASA-TN-D-4362 c07 N68-18616 Advanced antenna techniques for rendezvous and lunar landing radar systems NASA-CR-764 c07 N68-28135 ANTENNA FEEDS Aperture-admittance expression for waveguide-fed rectangular aperture antenna, loaded with dielectric plug NASA-TN-D-4430 c07 N68-20333 ANTENNA RADIATION PATTERNS General method for designing circular array antennas to obtain quasi-omnidirectional patterns NASA-TN-D-4254 c07 N68-11475 Flexible body analog computer program and rigid body digital computer program for calculating dynamic characteristics of double-V antennas on Radio Astronomy Explorer satellite

c08 N68-18144 NASA-CR-962 Thin walled parallel plate waveguide radiation pattern analyzed by surface integration technique NASA-CR-1052 c07 N68-22746 NASA-CR-1052 ANTIFRICTION BEARINGS Critical speed of flexibily mounted rigid rotors in undampened bearings NASA-TN-D-4607 c32 N68-25421 APERTURES HTURES Fourier transforms for aperture admittance of ground-plane-mounted waveguide illuminating conducting sheet NASA-TN-D-4366 c07 N68-transformer for waveguide for waveguide for a second seco c07 N68-18123 Aperture-admittance expression for waveguide-fed rectangular aperture antenna, loaded with dielectric plug NASA-TN-D-4430 c07 N68-20333 Reflection coefficient and admittance of circular aperture in ground plane covered by dielectric or plasma slab NASA-CR-1177 c25 N68-3517 APOLLO PROJECT c25 N68-35171 Aerodynamic stability characteristics of Apollo launch escape vehicle with canard surfaces deployed NASA-TN-D-4280 General equations for standard deviation, and rms standard deviation of least squares fitted polynomials applied to Apollo tracking problems NASA-TN-D-4121 c10 N68-16749 NASA-TN-D-4280 c01 N68-11640 NASA-TN-D-4121 cl0 N68-16749 Effects of simulated jet exhaust flow on transonic aerodynamic characteristics of Apollo launch aerodynamic characteristics of Apollo Faulen escape vehicle models NASA-TN-D-4843 APOLLO SPACECRAFT Simulator study of pilot control of remote orbital docking of large altitude stabilized components NASA-TN-D-4263 c31 N68-1 Instrumentation, systems engineering, and life support systems for Apollo primate orbital c31 N68-11476 experiment NASA-CR-926 c05 N68-15306 Development, ground tests, and flight performance of cryogenic nitrogen storage system for low gravity operation during Apollo-Saturn space flight NASA-TN-D-4293 c23 N68-15950 Impact water pressures, accelerations, and landing dynamics of scale model Apollo command module with deployed heat shield impact attenuation system NASA-TN-D-4275 c31 N68-18822 Static longitudinal aerodynamic characteristics of configurations used in Little Joe/Apollo test vehicle development NASA-TN-D-4439 c31 N68-22953 Movement of forward heat shield in Apollo command module turbulent reverse flow wake module turbulent reverse flow wake NASA-TN-D-4691 c31 N68-Ablation and temperature data for Apollo heat shield material using Pacemaker vehicle for flight test c31 N68-30032 NASA-TN-D-4713 c33 N6 Wind tunnel test data on static and dynamic c33 N68-30747 stability of Apollo command module configuration NASA-TN-D-4688 c01 N68-31445 Launch vehicle flight tests of effects of Apollo heat shield irregularities on ablative material performance NASA-TN-D-4791 c33 N68-35116 Apollo command module radar cross section decrease due to reentry plasma effects NASA-TN-D-4784 c07 N68-35140 Variable density hypervelocity wind tunnel tests on effects of several ramp-fairing, umbilical, and pad configurations on aerodynamic heating to Apollo command module NASA-TM-X-1640 c01 N68-35141 APPLICATIONS OF MATHEMATICS Formalism for treating products of generalized functions and applications in mathematical physics NASA-TN-D-4244 c19 N68-11494 Mathematical properties and computer programs for digital spectrum analyses NASA-TN-D-4510 c08 N68-25260 c08 N68-25268 APPLICATIONS TECHNOLOGY SATELLITES Image dissector camera flown aboard Applications

Technology Satellite-C for obtaining daylight cloud cover data NASA-TN-D-4186 c14 N68-10647 Microwave pump requirements for field operational broadband rutile traveling wave maser for Applications Technology Satellite program NASA-TN-D-4764 c16 N68-33635 APPROACH CONTROL Analog computed time histories and altitude-ground track plots of swept wing transport aircraft longitudinal response to wind shear and sustained gusts during landing approaches NASA-TN-D-4477 col N68-19180 APPROXIMATION Mathematical models and approximation methods for solving lateral vibration modes of cylindrical space vehicles and vehicles with clustered tanks NASA-CR-935 c32 N68-10231 NASA-CK-935 C32 N68-102 Numerical analyses of transitions between restricted problem of three bodies and problem of two fixed centers and Kepler problem NASA-TM-X-1465 C21 N68-111 c21 N68-11146 NASA-IN-X-1455 Plum Brook reactor support calculations -mathematical model for fuel utilization, power distribution in fuel loading, and approximate predictions of xenon poison transient NASA-TM-X-1496 C22 N68-160 c22 N68-16056 NAA-TN-A-1450 Successive approximation procedure for solving elastic-plastic problem for torsion of solid prismatic bar made of strain hardening material NASA-TN-D-4391 c32 N68-17045 Approximate equations for computing enthalpy and velocity derivatives at surface of flat plate, cone, or blunt axisymmetric body NASA-TN-D-4484 c33 N68-2006 c33 N68-20065 Approximate methods for predicting viscosities of gas mixtures involving both polar and nonpolar dases NASA-TN-D-4496 c12 N68-21724 Approximation method for calculating spanwise distribution of wind tunnel boundary interference on wing lift in rectangular perforated wall NASA-TR-R-285 c01 N68-24617 Simplified and accurate relative equations of motion for two impulse orbital rendezvous NASA-TN-D-4670 c30 N68c30 N68-28841 ARC DISCHARGES Coaxial flow stabilized ac arc facility NASA-TN-D-4517 c2 c25 N68-20296 ARC HEATING Effect of throat size and electrode size and shape on arc heating performance in 20-inch hypersonic tunnel NASA-TN-D-4653 c11 N68-28947 MELITING Crucible melting and arc melting of aluminum nitride and determination of its melting point C17 N68-33335 ARC MELTING ARC WELDING c15 N68-21429

Welding of precipitation hardening stainless steels NASA-SP-5087 ARGON Metal cathodes in argon atmospheres used to stabilize dc arcs for spectrochemical analysi NHSA-TN-D-4236 Convective stagnation heat transfer of carbon dioxide, nitrogen-argon gas mixtures compared to air in shock tube tests NASA-TN-D-4256 NASA-TN-D-4255 c33 N68-11811 Effects of Reynolds number change on performance of axial flow turbine working in argon NASA-TN-D-4432 c03 N68-18501 Electrical properties of direct current compact arc in argon under varying pressures, amperages, and electrode spacing NASA-TM-X-1596 c29 N68-25818 ARGON PLASMA Two channel transient voltage digitizer for correlation of transient spectra with performance in coaxial, argon plasma guns NASA-TN-D-4385 c25 N68-17070 Induction plasma heating system for hydrogen-argon simulated gas cooled reactor studies NASA-CR-1143 c25 N68-29888

NASA-CR-1143 c25 N68-29888 ARMATURES Numerical analysis of winding power loss of rotating ac generators in controlled atmospheres

SUBJECT INDEX

NASA-TN-D-4849 c03 N68-37162 ARROW WINGS Piloted fixed-base simulation of low speed flight characteristics of arrow wing supersonic transport aircraft NASA-TN-D-4277 c05 N c05 N68-13609 NASA-TN-D-4276 effects on aerodynamic characteristics of twisted and cambered arrow wing at supersonic speed NASA-TN-D-4796 c01 N68-350 NASA-TN-D-4796 col N68-35665 Wind tunnel tests at Mach 1.60, 2.36, and 2.96 to determine flow field properties near arrow wing body model for locating potential engine air inlets inlets NASA-TN-D-4809 c01 N68-37238 ARTERTES Transient analysis of arterial fluid lines with respect to time domains and pulse width NASA-CR-990 c04 c04 N68-12494 ARTIFICIAL SATELLITES Analytical method artificial satellite lifetime determination NASA-TN-D-4281 c30 N68-11754 Computer programs for rapidly computing approximate ephemerides of minor planet or artificial satellites NASA-TN-D-4470 c30 N68-20356 Artificial satellite motion under influence of planar and Keplerian force fields NASA-TN-D-4622 c30 N68-28113 Perturbation theory for artificial satellites with nearly circular orbits using Von Zeipel method NASA-TN-D-4531 c30 N68-28251 ASCENT Simulator study of pilot control over lunar module during ascent from lunar surface NASA-TM-X-1549 c21 N68-21366 ASCENT TRAJECTORIES Three numerical procedures for Mayer classical and non-classical problems in trajectory optimization NASA-CR-1012 ASTRONAUT LOCOMOTION c30 N68-19315 Space activity suit designed for active astronaut working in vacuum environments for up to four hours NASA-CR-973 c05 N68-11510 Pressure suits and backloads effects on locomotion in simulated lunar gravity NASA-TN-D-4464 ASTRONAUT PERFORMANCE c05 N68-20354 Descriptive model for determining optimal human performance in aerospace systems NASA-CR-879 c05 N68-10381 Lunar module backup guidance, navigation and pilot interfaces with control systems during lunar landing missions NASA-TN-D-4131 c21 N68-16836 Astronaut performance using manually hand-held sextants for midcourse navigation phases of manned space flight c21 N68-21123 NASA-TN-D-4449 ASTRONAUTS Water immersion simulation study of astronaut performance during airlock ingress or egress at reduced gravity NASA-CR-971 c05 N68-20339 NBSA-CR-971 Computational method for orbiting astronauts to determine required velocity for two impulse abort to landing site NASA-TN-D-4599 c21 N68-25103 ASTRONAVIGATION Manual navigation method for evaluating transfer orbits for lunar landings NASA-TN-D-4756 c21 N68-332 ASTRONOMICAL COORDINATES c21 N68-33271 Coordinate measuring system for flight control, and trajectory optimization NASA-CR-1000 c30 N68-16 c30 N68-16103 ASTRONOMICAL PHOTOGRAPHY Airborne stellar photometry and spectrometric determination of day sky brightness NASA-CR-1017 ASTRONOMICAL SPECTROSCOPY c30 N68-19590 Infrared observations of outer solar corona at wavelength of 22 microns NASA-CR-969 c30 N68-20353 ASTRONOMY Advances during 1966 in astronomy, exobiology,

ionospheric sciences, radio and solar physics, and planetary atmospheres and planetology NASA-SP-155 c30 N68-15748 ASTROPHYSTCS Observational and theoretical interpretations of interstellar grains - conference papers c30 N68-11456 NASA-SP-140 NASA-SP-140 c30 N68-114: ATLAS CENTAUR LAUNCH VEHICLE Reliability of silicon rectifiers as inverters for alternating current power source for Atlas Centaur launch vehicles NASA-TM-X-1569 c03 N68-215 Capillary rise in annular region of concentric culedons during scant provide of c03 N68-21562 cylinders during coast periods of Atlas-Centaur flights NASA-TM-X-1558 c12 N68-23353 Atlas Centaur launch vehicle with Surveyor 1 lunar probe NASA-TN-D-4580 c31 N68-24338 Cryogenic propellant management during coasting of Atlas Centaur vehicles NASA-TN-D-4571 c28 N68-25099 Aerodynamic heating, delamination and pressure in nose fairing honeycomb core of Atlas Centaur launch vehicle NASA-TM-X-1605 c33 N68-28156 Flight performance evaluation of Atlas-Centaur for Surveyor spacecraft SC-2 NASA-TM-X-1616 c31 N68-33332 Successful engine restart in space of upper stage vehicle using cryogenic propellants NASA-TM-X-1649 c31 N68-33683 Flight performance evaluation of Atlas Centaur restart capability in earth orbit NASA-TM-X-1647 c31 N68-35 c31 N68-35357 Electromagnetic compatibility verification for Surveyor spacecraft and Atlas Centaur launch vehicle NASA-TM-X-1673 c31 N68-36971 ATLAS LAUNCH VEHICLES Atlas-Agena and Atlas-Centaur combined propulsion system for measurements out of three dimensional phenomena out of ecliptic plane NASA-TN-D-4455 c28 N68-19581 Longitudinal dynamic characteristics of Stub D Atlas launch vehicle without propellants or payload NASA-TM-X-1682 c31 N68-37942 NASA-TM-X-1682 c31 N68-37942 ATMOSPHERIC ELECTRICITY Electric field of free atmosphere NASA-TT-F-425 c13 N68-10079 ATMOSPHERIC ENTRY Flight tests of ringsail parachute with 15 percent porosity, for planetary entry NASA-TM-X-1484 c31 N68-11919 Photographic and spectrometric observation of iron. artificial meteor launched from iron, artificial meteor launched from Trailblazer 2, and reentering at 11 kilometers per second NASA-TN-D-4312 c30 N68-167 Results of including boundary shock wave in calculation of flight parameters of large high c30 N68-16750 speed meteor NASA-TN-D-4325 c12 N68-18997 Entry guidance equations, reference trajectories, and guidance system mechanization NASA-CR-1013 c30 N68-19985 Pressure fluctuation measurements on afterbodies of blunt atmospheric entry vehicles NASA-TN-D-4591 c32 N68-24508 Aerodynamic characteristics of two blunt half cone wedge entry configurations at supersonic speeds NASA-TM-X-1621 col N68-30030 Radiative and convective heating during atmospheric entry NASA-CR-1170 c33 N68 ATMOSPHERIC ENTRY SIMULATION Flight test of conical spacecraft simulating parachute deployment in Mars atmosphere c33 N68-35248 Inflation, and drag characteristics of disk gap band parachute in simulated low density Mars atmosphere NASA-TM-X-1499 c31 N68-13797 Inflation and drag characteristics of cross parachute in simulated Martian environment NASA-TM-X-1543 c31 N68-21833

High enthalpy plasma generator for atmospheric

entry heating simulation NASA-TN-D-4583 c11 N68-24560 Randa in Det000 cll N68-2456 Earth orbital vehicle control during entry phase to simulate manned planetary entry NASA-TN-D-4847 c31 N68-3605 c31 N68-36056 ATMOSPHERIC MODELS FURTRAN computer program for calculating model planetary atmospheres and density and temperatue dispersion data for Apollo reentry NASA-TN-D-4292 c30 N68-15793 Carbon dioxide model for radiation heating and cooling functions of lower stratified Martian atmosphere in thermodynamic equilibrium NASA-CR-1044 c30 N68-22860
 NASA-CR-1044
 c30 N68-22860

 Gaseous motion and hydrodynamic model for analysis
 of binary star atmosphere

 NASA-TN-D-4520
 c30 N68-25385

 Models of Martian atmosphere based on minimum,
 mean, and maximum density profiles

 NASA-SP-8010
 c30 N68-37220

 ATMOSPHERIC PHYSICS
 C30 N68-37220
 USPHENIC PHYSICS Potential applications of geodetic satellites to geology, oceanography, glaciology, and atmospheric physics NASA-SP-158 cl3 N68-189 c13 N68-18902 NASA-CR-100 C13 N68-18: Subsolar-meridian mean annual distributions for Martian troposphere below 50 km NASA-CR-1043 ATMOSPHERIC PRESSURE C30 N68-19 c30 N68-19192 Charts of thermodynamic properties of helium showing effects of ionization, particle interactions, temperature, and atmospheric pressure NASA-TN-D-4754 ATMOSPHERIC SCATTERING c12 N68-35117 Scattering and absorption of plane electromagnetic waves by particles of turbid medium NASA-TT-F-477 c13 N68-22462 ATMOSPHERIC TURBULENCE Space vehicle and control system dynamic response to atmospheric disturbances NASA-CR-942 c32 N68-11089 NASA-CK-942 Handling qualities, disturbances and reentry corridor boundaries for spacecraft control system design NASA-CR-945 c32 N68-11133 Velocity, gust, and height data analysis from four-engine turbojet transport airplane NASA-TN-D-4330 c02 N68c02 N68-16522 Atmospheric conditions during turbulences encountered by XB-70 aircraft above 40,000 ft NASA-TN-D-4768 c13 N68-33416 NASA-TN-D-4768 ATOMIC ENERGY LEVELS Atomic line intensity tables for ionized iron atom at high temperatures NASA-SP-3041 c25 N68c25 N68-24161 Experimental determination of graphite triple point and liquid-solid interface NASA-CR-1148 c22 N68-2 c22 N68-29390 ATOMIC EXCITATIONS Helium 2 elementary excitation spectrum derived microscopically for realistic interatomic potential NASA-TN-D-4838 c24 N68-37240 ATOMIC STRUCTURE Crystal transformation and atomic ordering on wear and sliding friction in two cobalt alloys NASA-TN-D-4668 c15 N68-28260 ATOMIZING Maximum drop diameters for atomization of liquid jets injected concurrently into accelerating or decelerating gas streams NASA-TN-D-4640 c12 N68-28364 ATOMS Equations for determining substrate surface coverages from arrival rates and desorption characteristics of adsorbate ions and atoms c25 N68-25630 NASA-TN-D-4369 ATTENUATION Discrete ordinate computation of fission spectrum neutron dose rate attenuation curve for lithium hydrides and tungsten NASA-TN-D-4684 ATTENUATION COEFFICIENTS c24 N68-30001 Gallium arsenide laser modulator, attenuation coefficients, and semiconductors for optical communication systems NASA-TN-D-4608 c23 N68-25868

ATTITUDE CONTROL

ATTITUDE CONTROL Piloted simulation studies of Saturn 5 launch vehicle manual backup guidance and control NASA-TN-D-4481 c21 N68-19061 Automatic balancing system for frictionlessly supported, attitude control test platforms about axes commonly orthogonal to gravity vector NASA-TN-D-4426 c09 N68-19185 Passive damping technique for attitude control of solar orientated interplanetary spacecraft NASA-TN-D-4641 c21 N68-28361 c21 N68-28361 ATTITUDE INDICATORS Spacecraft attitude determination using single onboard camera NASA-TN-D-4359 c31 N68-19275 Attitude determination of spin-stabilized spacecraft using star mapping technique NASA-TN-D-4740 c21 N68-31957 NASA-IN-D-4740 Infrared horizon radiance profiles obtained during summer conditions with Project Scanner probe NASA-IN-D-4741 c21 N68-33450 AUDIO FREQUENCIES Fitzgeralds piezoelectric disk and theory on audio frequency resonances and sound beams in crystals NASA-TN-D-4625 c23 N68-28259 AURORAS Temporal solutions for photochemical equations describing distribution of ozone and oxygen during auroral events NASA-TN-D-3993 c13 N68-1 c13 N68-10369 AUSTENITIC STAINLESS STEELS Thermal and mechanical treatment for precipitation hardening stainless steels NASA-SP-5089 c15 N68-20433 Deformation processing of precipitation hardening stainless steels NASA-SP-5088 c17 N68-21917 Mossbauer spectroscopy used to study sensitization in austenitic stainless steels NASA-CR-1077 c17 N68-25318 Stress corrosion tests of heat treated austenitic stainless steels NASA-TN-D-4673 AUTOCORRELATION c17 N68-29379 Autocorrelation of incoherent stellar light measured by interferometer NASA-TN-D-4480 AUTOMATIC CONTROL c14 N68-25518 64 inch scattering chamber digital readout and control system for automatic processing of angle and experimental data NASA-TN-D-4324 cl4 N68-14018 Automatically controlled heat removal in water cooled space suits NASA-CR-1085 c05 N68-26701 Algebraic methods for analysis and design of model following control systems NASA-TN-D-4663 c19 N68-28281 AUTOMATIC CONTROL VALVES Vortex valve for hot gas flow modulation in secondary injection thrust vector control system NASA-CR-1091 c28 N68-28112 AUTOMATIC FLIGHT CONTROL Three axis fluidic automatic flight control system developed and flight tested NASA-CR-913 C02 N68-10047 Properties and imaging techniques of various display devices - computer directed visual flight control boards, integrated optical man machine systems, and electro-optical methods NASA-SP-159 C09 N68-22200 AUTOMATIC PICTURE TRANSMISSION Equipment specifications and engineering drawings for automatic picture transmission ground stations NASA-SP-5079 Automatic Pilots c07 N68-19624 Load relief autopilot to minimize launch vehicle thrust vector deflection angle required for vehicle stability during flight through design winds NASA-TN-D-4786 c21 N68-33756 AUTOMOBILES Wind tunnel study of scale model automobile ground plane boundary layer using moving-belt ground plane technique NASA-TN-D-4229 c01 N68-10093

SUBJECT INDEX

AUTOROTATION Helicopter height-velocity diagram analysis showing effects of density altitude and gross weight NASA-TN-D-4536 c02 N68-22033 AUXILIARY POWER SOURCES Development of nuclear thermionic space power system using thermionic diodes, and heat pipe flow for temperature control NASA-TN-D-4299 c22 N68-19146 NASA-IN-D-4299 c22 N68-1914 Geometric properties of expandable whirling membrane solar energy concentrator used in conjunction with electrical conversion systems for spacecraft auxiliary power units NASA-IN-D-4532 c03 N68-222 c03 N68-22258 Experimental evaluation of ferroresonant and perimental evaluation of terroroscant _____ feedback alternating current line voltage regulators in 15 kilowatt auxiliary power system NASA-TN-D-4627 c03 N68-28101 AXES OF ROTATION Spin axis for spinning satellite determined from range rate data NASA-TN-D-4483 AXIAL COMPRESSION LOADS c30 N68-21182 Imperfections of axially loaded cylindrical shells NASA-TM-X-1552 Computer program for analysis of shells of revolution with any revolution with axisymmetric loading NASA-CR-1051 c32 N68-23355 Bucking of thin-walled electroplated copper and Mylar circular cylinders under axial compression and bending NASA-CR-1160 c32 N68-33226 Buckling of conical shells under axial compression and effects of axially symmetric defects NASA-CR-1162 c32 N68-35198 Imperfection survey data on cylindrical shells before and during axial compression loading up to buckling load NASA-CR-1163 c32 N68-34 c32 N68-35199 AXIAL FLOW Axial turbulence measurements in coaxial flow of dissimilar gases NASA-CR-960 c12 N68-136 c12 N68-13612 Flow visualization and containment tests in directed-wall-jet vortex tube with radial outflow and moderate superimposed axial flows NASA-CR-992 c22 N68-17131 NASA-CA-592 Performance of single stage, axial flow turbine designed for Brayton cycle space power system NASA-TM-X-1666 c03 N68-37943 AXIAL FLOW TURBINES Similarity parameters used for examining geometry characteristics of axial flow turbines with high expansion ratio NASA-TN-D-4248 c01 N68-10529 Performance of two-stage axial flow turbine operating at different rotor tip clearance NASA-TN-D-4388 c03 N68 c03 N68-14639 Reynolds number effect on single stage axial flow turbine in air NASA-TN-D-4383 c03 N68-16228 Experimental design and performance test of two-stage axial-flow turbine designed for Brayton-cycle space power system Drayton-cycle provide c03 N68-16469 NASA-TN-D-4432 c03 N68-18501 Axial flow turbine compressor for space power plant NASA-CR-800 c03 N68-24596 Design and dynamic simulator testing of gas bearing rotor support for high performance axial flow turbomachinery NASA-CR-801 c15 N68-25042 Partial admission operation effects on performance of single stage axial flow turbine NASA-TN-D-4700 c03 N68-30241 Stream-filament analysis procedure and correlation of total pressure loss coefficients to form basis of computer program to investigate design point performance of axial turbines NASA-CR-1181 c28 N68 c28 N68-35101 Computer program for solving equations governing flow in axial turbines NASA-CR-1187 c28 N68-36617

Efficiency, mass flow rate, torque, and exit diffuser effectiveness of 5-inch axial flow

turbine NASA-TM-X-1679 c03 N68-37263 AXIAL LOADS Elastic buckling equations for calculating plastic buckling of plates and shells under biaxial loading NASA-TN-D-4706 c32 N68-31946 AXIAL STRAIN Plastic response of circular uniform plate to axisymmetric impulse load of Gaussian distribution NASA-TR-R-279 c32 N AXISYMMETRIC BODIES FORTRAN digital computer program for axial c32 N68-14640 distribution of aerodynamic normal force characteristics for axisymmetric, multistage launch vehicles in linear angle of attack ranges NASA-TN-D-4342 c31 N68-18615 NASA-TN-D-4342 c31 N68-1863 Approximate equations for computing enthalpy and velocity derivatives at surface of flat plate, cone, or blunt axisymmetric body NASA-TN-D-4484 c33 N68-2006 c33 N68-20065 model to unsteady aerodynamic loading in wind tunnel tests NASA-TN-D-4504 c01 N68-25916 Rotation effects on melting ablation on reentry of axisymmetric bodies NASA-TN-D-4614 c33 N68-26650 Simplified approximations for calculating laminar heat transfer over spherically blunted axisymmetric bodies at angle of attack NASA-TN-D-4720 c33 N68-31959 Computer program for analyzing free flight motions of axisymmetric bodies to determine aerodynamic coefficients AXISYMMETRIC FLOW Unstarted inlet flow field during restart cycle of axisymmetric mixed compression configuration at Mach 3 c01 N68-33081 NASA-TM-X-1547 c01 N68-21703 AZ THUTH Method of correcting azimuthal orientation of Explorer 35 spacecraft while in lunar shadow NASA-TN-D-4544 c30 N68-24486 B P- 70 ATRODARS

0 -	TU AIRGRAFI	
	Theory and equations for propul	sion system dynamic
	simulation	
	NASA-CR-928	c11 N68-19273
	B-70 aircraft engine noise measurements and	
	predictions	
	NASA-TM-X-1565	c02 N68-21834
	Flight tests for preliminary ev	aluation of
	handling qualities of unaugme	
	aircraft	
	NASA-TM-X-1584	c02 N68-23901
	Atmospheric conditions during t	urbulences
	encountered by XB-70 aircraft above 40.000 ft	
	NASA-TN-D-4768	c13 N68-33416
Landing loads and accelerations of the		
	aircraft	
	NASA-TN-D-4836	c02 N68-36073
BAC	KGROUND NOISE	
	Optical communications - maximu	m likelihood
	detection of M-ary Poisson processes in background of additive Poisson noise	
	NASA-TN-D-4623	c07 N68-29528
RAC	CKSCATTERING	007 NOC 25020
2	Transmission, and backscatter c	oofficients for
	electron irradiated aluminum.	
	steel foils	une statistess
	NASA-TN-D-4363	c24 N68-17898
	Laser light backscatter investi	
	velocity in contaminated atmospheres for	
	application to clear air turb	
	NASA-TN-D-4453	c20 N68-20375
	CTERIA	C20 N00-20070
DAV	Air samplers, contamination, an	à statilization in
	collection of microorganisms	
		for microulological
	exploration of stratosphere NASA-CR-1101	c04 N68-28247
-	FFLES	CU4 N00-2024/
DNI		- 661
Film and transpiration cooled baffles for M-1		
	engine NASA-TM-X-1267	c28 N68-18216
	MADA-10-1-160/	C20 N08-18210

Liquid flow into baffled spherical tank during eight lessness NASA-TM-X-1526 c12 N68-21365 Stability effects of several injector face baffle configurations on screech in hydrogen-oxygen rocket Cryogenic propellant management during coasting of Atlas Centaur vehicles NASA-TN-D-4571 c28 N68-25099 NASA-TN-D-4515 c28 N68-21679 Injector baffles for flame stability in combustion chambers using nitrogen tetroxide and hydrazine mixture NASA-TM-X-1595 c28 N68-26644 BALANCING Automatic balancing system for frictionlessly supported, attitude control test platforms about axes commonly orthogonal to gravity vector NASA-TN-D-4426 c09 N68-19185 BALL BEARINGS Reduced pressure effects on fatigue life of roller steel ball bearings with mineral oil lubricants NASA-TN-D-4348 c15 N68-15010 Friction torque of ball bearings in vacuum to determine lubricating capability of polytetrafluoroethylene-composition retainer materials NASA-TN-D-4355 c15 N68-16468 Subsurface residual stress on steel inner races from ball bearings during rolling contact NASA-TN-D-4456 c15 N68-20199 Cooling requirements of ball bearings operating in low flow rate hydrogen gas NASA-TN-D-4616 c15 N68-24456 Spinning friction and torque dependence on ball bearing-groove conformity NASA-TN-D-4669 c15 N68-28258 Test evaluation of high temperature greases and solid lubricants in thrust loaded ball bearings c15 N68-28766 NASA-TN-D-4652 High temperature tests to determine fatigue life of 120mm bore ball bearings with fluorocarbon, polyphenyl ether, and synthetic base paraffin base lubricants NASA-TN-D-4850 c15 N68-36075 BALLISTIC CAMERAS Ballistic camera data reduction methods for determining reentry body position, velocity, and deceleration NASA-TN-D-4260 c30 N68-11145 BALLISTICS Exploding foil gun technique for simulated meteoroid protection NASA-TN-D-4259 c32 N68-11355 Unmanned Mars probe tested for drag, lift, static and dynamic stability at Mach number 2 NASA-TN-D-4291 c01 N68-11936 BANDPASS FILTERS Ultraviolet filter and monochromator for mass spectrometer employing photoionization source NASA-CR-1018 c14 N68-17329 BASE PRESSURE Base pressure measurements at angle of attack for spherically blunted cones at hypersonic speed NASA-TN-D-4800 c01 N68-35668 BEACONS Human performance measured as function of reaction time required to discriminate change in beacon brightness NASA-CR-1220 c05 N68-37819 BEAN PLASMA AMPLIFIERS Electron beam-plasma interaction and plasma multiplier as possible millimeter wave generators NASA-TN-D-4309 c25 N68-18614 BELLMAN THEORY Qualitative theory of differential equations and conversion to integral equations NASA-CR-1164 c19 N68-33426 BENDING MOMENTS Rotor-hub bending moment measurements on hingeless rotor helicopter during abrupt maneuvers near ground NASA-TN-D-4574 BENDING VIBRATION c02 N68-24499 Stress analysis and wear tests in use of lacing wire as vibration damper on turbocompressor

BERYLLIUM

blades NASA-TM-X-1603 c32 N68-28238 BERYLLIUM Microstructure and mechanical properties of beryllium tubing and performance tests on support columns of beryllium NASA-TN-D-4833 c17 N68-37053 BIAS Simultaneous correction of velocity and mass bias in photography of meteors NASA-TR-R-280 c30 N68-15484 BIBLIOGRAPHIES Microwave molecular spectroscopy for identifying contaminants in space cabin atmospheres bibliography NASA-CR-951 c23 N68-10674 Survey on minimum weight design aspects of stiffened cylinders under compression c32 N68-11282 NASA-CR-963 Aerospace medicine and biology bibliography on physiological, psychological, and environmental effects on man during aerospace flights NASA-SP-7011/43/ c04 N68-14671 NADA-SF-7011/45/ CO4 No6-1467. Aerospace medicine and biology bibliography on physiological, psychological, and environmental effects on man during aerospace flights NASA-SP-7011/42/ CO4 N68-1472 c04 N68-14725 Aerospace medicine and biology bibliography NASA-SP-7011/44/ c04 N6 c04 N68-15899 NASA-SF-7/011/44/C04 N68-15899Continuing bibliography on aerospace medicine and
biological effects of space flight stressNASA-SP-7011/45/c04 N68-16517Annotated bibliography of computer-aided circuit
analysis and design
NASA-SP-7023c10 N68-19882 NADA-SF-7020 Annotated bibliography and indexes on aerospace medicine and biological effects - February 1968 NASA-SF-7011/47/ c04 N68-2002 c04 N68-20026 MADA-DF-1011/17/ Annotated bibliography and indexes on aerospace medicine and biological effects - March 1968 NASA-SP-7011/48/ c04 N68-200 c04 N68-20027 Management information bibliography NASA-SP-7500 c34 N68-21828 Cumulative index for NASA bibliography on aerospace medicine and biological effects -January 1968 NASA-SP-7011/46/ c04 N68-22194 Annotated bibliography and indexes on aerospace medicine and biological effects - April 1968 NASA-SP-7011/49/ c04 N68-2 c04 N68-22882 Bibliography of annotated references on management taken from entries to NASA information system between 1962 and 1967 - abstracts and indexes NASA-SP-7500/02/ c34 N68-24567 Annotated bibliography and indexes on aerospace medicine and biological effects - June 1968 NASA-SP-7011/51/ c04 N68-283 c04 N68-28246 NASA-SP-7011/51/ Annotated bibliography on communication satellite theory and technology NASA-SP-7004/04/ Bibliographic citations, abstracts, and indexes on selected NASA Scientific and Technical Reports for 1967 NASA-SP-7029 c34 N68-29039 Bibliographic citations, abstracts, and indexes on laser and maser research and development c16 N68-29438 NASA-SP-7009/03/ Nuclear, chemical, and physical properties of nine radioactive isotopes - annotated bibliography NASA-SP-7031 c06 N68-29959 Bibliography on solid, liquid, and hybrid high energy propellants and oxidizers, propellant handling and storage, toxicity and hazards, and safety measures NASA-SP-7002/04/ c27 N68-30313 bliographic citations, abstracts, and indexes on planetary atmospheres - June 1966 through Bibliographic citations, abstracts, December 1967 NASA-SP-7017/02/ c30 N68-30 Supplement to NASA bibliography on lubrication, c30 N68-30601 corrosion, and wear NASA-SP-7020/02/ c15 N6 Annotated bibliography and indexes on lunar c15 N68-31522 surface studies - 1967 NASA-SP-7003/04/ c30 N68-32631 Annotated bibliography and indexes on aerospace medicine and biological effects - July 1968 NASA-SP-7011/52/ c04 N68-32707 Annotated bibliographies on aerospace science

NASA-SP-7006/03/ c34 N68-32769 Annotated bibliography on aerospace medicine and biology - August 1968 NASA-SP-7011/53/ c04 Uses of submillimeter waves in aerospace c04 N68-35069 technology, with bibliography NASA-SP-182 c07 N68-35522 Annotated bibliography and indexes on aerospace medicine and biological effects - August 1968 NASA-SP-7011/54/ c04 N68-38051 BINARY DATA MARY DAIA Mathematical model of statistical channel characteristics in, and test instrumentation for, digital data transmission systems handling uniformly coded binary data NASA-TT-F-434 c07 N68-1754; c07 N68-17542 Logarithmic encoding procedure and error analysis for binary word compression NASA-TN-D-4290 c08 N68-18179 BINARY STARS Gaseous motion and hydrodynamic model for analysis of binary star atmosphere NASA-TN-D-4520 c30 N68-25385 BINOMIALS Computer program for reversion of cumulative binomial probability distribution NASA-TH-X-1592 cl9 N68-BIGASTRONAUTICS c19 N68-24141 Cumulative index for NASA bibliography on aerospace medicine and biological effects -January 1968 NASA-SP-7011/46/ c04 N68c04 N68-22194 BIOCHEMISTRY Biochemistry of nervous system, subcellular cerebral functions, brain metabolism, isotopic labeling for biochemical studies, and use of neurotropic drugs NASA-TT-F-439 c04 N68-13432 BIODYNAMICS Electroplethysmographic data on intercranial circulation, and dynamics of cerebral blood volume under normal conditions and gravitational stresses NASA-TT-F-492 c04 N68-15477 BIOINSTRUMENTATION Sensitive piezoelectric transducer with electric and mechanical noise rejection features for measuring cardiac and gross motor activity of small organisms NASA-TN-D-4590 c05 N68-25060 **BIOLOGICAL EFFECTS** Aerospace medicine and biology bibliography NASA-SP-7011/44/ c04 N6 c04 N68-15899 Continuing bibliography on aerospace medicine and biological effects of space flight stress NASA-SP-7011/45/ c04 N68-1651 c04 N68-16517 Annotated bibliography and indexes on aerospace medicine and biological effects - February 1968 NASA-SP-7011/47/ c04 N68-20026 Annotated bibliography and indexes on aerospace medicine and biological effects - March 1968 NASA-SP-7011/48/ c04 N68-20027 Annotated bibliography and indexes on aerospace medicine and biological effects - April 1968 NASA-SP-7011/49/ c04 N68-22 c04 N68-22882 Annotated bibliography and indexes on aerospace medicine and biological effects -May 1968 NASA-SP-7011/50/ c04 N68-25844 Annotated bibliography and indexes on aerospace medicine and biological effects - June 1968 NASA-SP-7011/51/ c04 N68-3 c04 N68-28246 Annotated bibliography and indexes on aerospace medicine and biological effects - July 1968 NASA-SP-7011/52/ c04 N68-32707 Annotated bibliography on aerospace medicine and biology - August 1968 NASA-SP-7011/53/ c04 N68-35069 Effects of various simulated sonic boom waveforms on human subjective response NASA-CR-1192 c04 N68-35103 Annotated bibliography and indexes on aerospace medicine and biological effects - August 1968 NASA-SP-7011/54/ c04 N68-38 c04 N68-38051 BIOLOGICAL EVOLUTION History of origin and initial development of carbon compounds, primitive organisms, and life on earth NASA-TT-F-488 c04 N68-24272

BIOSYNTHESIS Bioregenerative life support systems for long duration space flights - Hydrogenomonas biosynthesis and algae photosynthesis processes NASA-SP-165 c04 N68-26207 Survey and critical evaluation of existing methods for synthesis of fatty acids and lipids from metabolic wastes under conditions of space flight NASA-CR-1105 c04 N68-28278 Chemical feasibility and nutrional value in synthesis of edible fatty acids and lipids from metabolic wastes for space flight feeding NASA-CR-1104 BIREFRINGENCE Design, and evaluation of birefringent wave filter scale model for millimeter wavelengths radio astronomy NASA-CR-979 c09 N68-13617 BLACK BODY RADIATION Black body radiation - numerical solution for computer and hand calculation of total intensity over specified spectral range NASA-TN-D-4446 c19 N68-18455 C19 N68-18456 Thermal radiation heat transfer data, radiative properties of black bodies, and electromagnetic theory NASA-SP-164 BLADE TIPS c33 N68-28530 Hovering tests of extremely flexible lifting rotor to determine effects of rotor tip configuration and operating conditions on performance NASA-TN-D-4820 col N68-36334 Review of blade slap studies for determining noise in helicopters NASA-CR-1221 c02 N68-37932 BLAST LOADS Plastic response of circular uniform plate to axisymmetric impulse load of Gaussian distribution NASA-TR-R-279 c32 N68-14640 BLEEDING Effect of boundary layer bleed on heat transfer and pressure distributions over wedge-flap surface at hypersonic speeds NASA-TN-D-4686 c01 N68-29955 BLOOD VESSELS Design and operating characteristics of electro-optical instrument for tracking of retinal blood vessels in back of eye NASA-CR-1121 c05 N68 c05 N68-35109 BLUNT BODIES Integer relations method of determining inviscid shock layer flow and pressure distributions over blunt bodies NASA-TN-D-4397 c01 N68-15778 Steady hypersonic flow over blunt bodies with high rates of continuous mass and heat transfer from body surface NASA-TN-D-4252 c01 N68-17555 NBSA-IN-D-4232 Cul NGG-1/355 Approximate equations for computing enthalpy and velocity derivatives at surface of flat plate, cone, or blunt axisymmetric body NASA-TN-D-4484 c33 N68-20065 Wind tunnel investigation of pressure distribution on blunted 15 deg half-cone wedge lifting-entry body NASA-TN-D-4494 c01 N68-21681 Relationship of shock standoff distance, at sonic and stagnation points, to body geometry of blunt bodies at zero angle of attack NASA-TN-D-4539 c01 N68-21941 FORTRAN program for approximate calculation of supersonic ideal gas flow past blunt bodies with sonic corners NASA-TN-D-4563 c01 N68-25093 Integral methods for predicting afterbody heat transfer to blunt two dimensional configuration subjected to separated flow NASA-TN-D-4443 c12 N68-28282 BOATTAILS Effect of boattail juncture shape on pressure drag coefficients of isolated afterbodies of supersonic engine nacelles c01 N68-19237 NASA-TM-X-1517

NASA-TM-X-151/ Simulated wing effect on pressure drag coefficient of subsonic boattail at angle of attack NASA-TM-X-1662 col N68-35672 BODIES OF REVOLUTION Computer program for analysis of shells of revolution with axisymmetric loading NASA-CR-1051 c32 N68-23355 NASA-CR-1051 NASA-CR-1051 Numerical results of buckling of shells of revolution for computer program NASA-CR-1049 c32 N68-244 Design of bodies to produce specified sonic boom c32 N68-24481 signatures NASA-TN-D-4704 c01 N68-31484 Aerodynamic characteristics of bodies of revolution at Mach numbers from 1.50 to 2.86 and angles of attack to 180 deg NASA-TM-X-1658 c01 N68-30 c01 N68-36193 BODY-WING AND TAIL CONFIGURATIONS Wind tunnel tests of a VTOL jet fighter to determine aerodynamic characteristics including determine aerodynamic characteristics inc stability NASA-TN-D-4812 c01 NG BOEING 707 AIRCRAFT Effects of reduced landing speeds on flying qualities of Boeing 707 for simulated instrument approaches NASA-TN-D-4804 c02 NG c01 N68-36081 c02 N68-37075 BOILERS Boiling heat transfer coefficients, interface behavior, and vapor quality in heated wall rotating boilers with continuous through-flow of water as test fluid NASA-TN-D-4136 c33 N68-17 c33 N68-17566 Mathematical model for frequency response of forced flow, hollow, single tube boiler inlet pressure to inlet flow . NASA-TM-X-1528 c12 N68-19340 BOILING Fuel tank pressurization and supercooling of liquid methane to minimize fuel boiloff problems in supersonic aircraft NASA-TM-X-1604 c27 N68-28155 Single tube-in-shell water-boiling heat exchanger performance with helical wire insert and flow stabilizing devices NASA-TN-D-4767 c33 N68-32 c33 N68-32099 Fin performance analyzed by using heat transfer coefficients for various boiling modes NASA-TN-D-4797 c33 N68-34088 BOLOMETERS Superconducting bolometers for measuring very low pressures NASA-CR-1120 c14 N68-33022 BOLZA PROBLEMS Bolza problem of calculus of variations in terms of control coding applied to trajectories NASA-CR-1103 c30 N68-25895 BOOMS (EQUIPMENT) Dynamic characteristics of satellites having long elastic members by modeling as symmetric double beam system NASA-TN-D-4576 c31 N68-31978 BOOSTER ROCKET ENGINES Fully-manual and augmented-manual control systems for Saturn 5 booster studied by emperically based mathematical models for pilot NASA-CR-1079 c31 N68-28426 BOOSTER ROCKETS Techniques for full-scale dynamic testing of large solid or liquid fueled booster vehicles NASA-CR-940 c32 N68-11054 Observation theory and sensors applicable to navigation of boost and space vehicles NASA-CR-1001 c30 N68-19676 MASA-CA-1001 Color deflection stability analysis for minimum control requirements of booster vehicles during atmospheric flight MASA-TN-D-4593 c21 N68-24409 BOOSTGLIDE VEHICLES Aerodynamic characteristics of several hypersonic boostglide configurations at Mach 2.30 to 4.63 NASA-TM-X-1601 c01 N68-33836 RORON Tensile strength properties of glass, boron, and graphite filament wound resin composites and liners for cryogenic pressure vessels NASA-TN-D-4412 c18 c18 N68-16623 Effects of 22 MeV proton and 2.4 MeV electron radiation on boron and aluminum doped silicon solar cells

NASA-TN-D-4407 c26 N68-19924 Fabricability, mechanical properties, and BORON 10

structural efficiency potentials of boron-polymer film layer composites NASA-CR-1114 c18 N68-35100 BORON 10 Boron 10/neutron, alpha particle/ lithium 7, lithium 7 resonance relative cross sections in keV region NASA-TN-D-4783 BOUNDARY LAYER CONTROL c24 N68-33763 ADARY LATER CONINCL Air flow calibration over moving belt ground plane installed in wind tunnel and data for two blowing-flap models tested over moving belt NASA-TN-D-4228 Wind tunnel study of scale model automobile ground plane boundary layer using moving-belt ground plane technique NASA-TN-D-4229 col N68-10 c01 N68-10093 NASA-IN-D-4229 C01 N68-10 Effect of boundary layer bleed on heat transfer and pressure distributions over wedge-flap surface at hypersonic speeds NASA-TN-D-4686 C01 N68-29 BOUNDARY LAYER FLOW c01 N68-29955 Results of including boundary shock wave in calculation of flight parameters of large high speed meteor NASA-TN-D-4325 c12 N68-18997 Aerodynamic drag measurements and boundary layer flow over V notches at transonic and supersonic speeds NASA-CR-1132 c12 N68-35252 BOUNDARY LAYER SEPARATION Static pressure and flow field for flat plate model with short trailing-edge flap NASA-TN-D-4308 c12 N68-17376 Real gas wedge-induced laminar separation on cooled blunt flat plate at hypersonic speed NASA-TN-D-4320 coll N68-17899 Laminar flow separation on flat plate induced by deflected trailing-edge flap at hypersonic speed NASA-TN-D-4671 c01 N68-29405 Low density, leading edge bluntness, and ablation effects on wedge induced laminar boundary layer separation at moderate enthalpies in hypersonic flow NASA-TN-D-4829 BOUNDARY LAYER TRANSITION c12 N68-36458 Turbulent boundary layer and transition on plane plates NASA-TT-F-520 c12 N68~17563 Transition from laminar to turbulent flow in near wake of supersonic reentry body NASA-TN-D-4645 c01 N68-28220 BOUNDARY LAYERS Boundary layer buildup effects in shock tubes on dissociation rate measurements NASA-TN-D-4795 BOUNDARY VALUE PROBLEMS c12 N68-34089 Numerical analyses of transitions between restricted problem of three bodies and problem of two fixed centers and Kepler problem NASA-TM-X-1465 c21 N68-11146 NB3A-IN-A-1465 c21 N68-1114 Boundary conditions for diffusion solution of coupled heat transfer NASA-TN-D-4618 c33 N68-2675 Newton-Raphson and gradient parameter correction technique for solution of optimal control probleme c33 N68-26759 problems NASA-TR-R-293 c19 N68-37073 BOW WAVES Relationship of shock standoff distance, at sonic and stagnation points, to body geometry of blunt bodies at zero angle of attack NASA-TN-D-4539 c01 N68-21941 BRAIN Biochemistry of nervous system, subcellular cerebral functions, brain metabolism, isotopic labeling for biochemical studies, and use of neurotropic drugs NASA-TT-F-439 c04 N68-13432 BRAYTON CYCLE Experimental design and performance test of two-stage axial-flow turbine designed for Brayton-cycle space power system NASA-TN-D-4382 c03 N68-16469 Dynamic characteristics of parasitic loading speed controller for Brayton cycle turboalternator NASA-TM-X-1456 c03 N68-1 c03 N68-18702

Experimental evaluation of gas injection start of Brayton cycle turbocompressor operating on gas

bearings NASA-TM-X-1590 c03 N68-24757 Analysis and selection of design for plutonium 238 for Brayton cycle space powerplant NASA-TN-D-4600 c03 N68-25829 Comparative analysis of single-loop 100-kilowatt Brayton space power system using pure gas and gas-solid suspension as working fluids NASA-TN-D-4659 c03 N68-283 c03 N68-28280 Aerodynamic characteristics of a stator modified gas turbine for single shaft Brayton cycle power system NASA-TM-X-1615 c03 N68-28870 Breadboard model of Brayton cycle alternator and voltage regulator-exciter NASA-TN-D-4697 c03 N68-29960 Performance test of homopolar inductor alternator for Brayton cycle space power system NASA-TN-D-4698 c03 N Recuperator for closed Brayton cycle solar c03 N68-30002 energy space power system NASA-CR-1150 c03 N68-33062 Performance of single stage, axial flow turbine designed for Brayton cycle space power system NASA-TM-X-1666 c03 N68-37943 BRAZTI. Space technology transfer to developing nations using Brazil as model NASA-CR-1222 c34 N68-37 c34 N68-37216 BRAZING Brazing aluminum to titanium coated stainless steel to minimize formation of intermetallic compounds in joint NASA-SP-5040 BREADBOARD MODELS c15 N68-22778 Breadboard flueric circuitry used to drive pneumatic stepping motors NASA-TN-D-4495 c03 N68-21651 NASA-TN-D-4697 c03 N68-299 c03 N68-29960 BREMSSTRAHLUNG Tables of energy and angular distributions of thick target bremsstrahlung in metals NASA-TN-D-4755 c24 N68-3 c24 N68-35535 Electron scattering, bremsstrahlung cross sections, and spectral energy distributions NASA-CR-1194 c24 N68-BRIGHTNESS DISCRIMINATION c24 N68-37708 Human performance measured as function of reaction time required to discriminate change in beacon brightness NASA-CR-1220 c05 N68-37819 BROADBAND Microwave pump requirements for field operational broadband rutile traveling wave maser for Applications Technology Satellite program NASA-TN-D-4764 c16 N68-3363 c16 N68-33635 BROMINE Photographic study of bromine jet issuing into coaxially flowing airstream NASA-TN-D-4660 c12 N68-2 c12 N68-28370 BUBBLES Gravity effects on bubble dynamics generated during nucleate boiling NASA-TN-D-4301 c33 N68-15330 BUCKLING Prebuckling deformations, and ring stiffener effects on buckling load of eccentrically stiffened orthotropic cylinders NASA-TN-D-4283 c32 N68-14091 Digital computer program for prediction of snap buckling of spacecraft shell structures by geometric nonlinear analysis of thin elastic shells of revolution NASA-CR-909 c32 N68-14584 Imperfections of axially loaded cylindrical shells NASA-TM-X-1552 c32 N68-21767 Basic equations and method of solution for computerized analysis of shells of revolution with axisymmetric collapse and nonsymmetric bifurcation buckling behavior NASA-CR-1050 c32 N68-23451 Numerical results of buckling of shells of revolution for computer program NASA-CR-1049 c32 N68-24 Bucking of thin-walled electroplated copper and Mylar circular cylinders under axial c32 N68-24481

- compression and bending NASA-CR-1160 c32 N68-33226 Liapunov method used to obtain sufficient conditions for buckling stability of long cylindrical shells with random imperfections c32 N68-33419 NASA-CR-1161 Buckling of conical shells under axial compression and effects of axially symmetric defects NASA-CR-1162 c32 N68-35198 Imperfection survey data on cylindrical shells before and during axial compression loading to buckling load NASA-CR-1163 c32 N68-35199 BULK MODULUS Anomalous non-Hookean deformation of ionic
- single crystals NASA-TN-D-4513 c26 N68-22271 BURNING TIME
- Altitude of orbiting spacecraft corrected by thrustor firing time control system NASA-TN-D-4519 c31 N68-21260

- CADMIUM ISOTOPES Scattering of 42 MeV alpha particles from even cadmium isotopes NASA-TN-D-4256 c24 N68-13 c24 N68-11074
- CADMIUM SULFIDES Spectral response of cuprous sulfide-cadmium sulfide film photovoltaic cell to green light NASA-TN-D-4333 c03 N68-14 c03 N68-14082
- NASA THE 1992 Construction and performance of active cadmium sulfide thin film solar cell arrays NASA-TM-X-1519 c03 N68-20432
- CALCIUM Calcium, molybdenum, and lithium compounds as low drive temperature stable memory cores NASA-TN-D-4573 c09 N68-2438 COQ N68-24388
- NASA-TN-D-4573 C09 N6 CALCULUS OF VARIATIONS Guidance, flight mechanics, and trajectory optimization calculus of variations and modern applications
 - NASA-CR-1003 c30 N68-15193 Maxima-minima theory, Pontryagin principle, and calculus of variations for optimal trajectory and control analysis NASA-CR-1006 c30 N68-20 c30 N68-20084
 - Pontryagin maximum principle, calculus of variations, and dynamic programming optimization ternniques applied to trajectory and guidance problems NASA-CR-1014 c30 N68-21231
 - Bolza problem of calculus of variations in terms of control coding applied to trajectories NASA-CR-1103 c30 N68-25895
 - Variational calculus used in obtaining lift drag ratio attainable by slender conical body at hypersonic speeds NASA-CR-1156 c01 N68-33451
- CALIBRATING
- Quasi-static calibrations for determining quartz, piezoelectric type, pressure transducer sensitivity from 20 to 477 deg K NASA-TM-X-1479 c14 N68-1186 c14 N68-11867
- Diffusers for in-flight calibration of detectors installed in spacecraft NASA-CR-987 c14 N68-12669
- Cable and circuit parameters effects on calibration of charge amplifier for microsecond pulses
- NASA-TN-D-4300 c09 N68-16530
- MASA-IN-D-4300 CU9 NOG-1032 Optical star tracker calibration procedures NASA-TN-D-4594 c21 N68-2455 Precision calibration techniques for microphones used in sonic boom measurements NASA-CR-1075 c14 N68-2531 c21 N68-24555
- c14 N68-25316 Modified vibration transducer calibration system for directly producing sensitivity versus frequency range plots NASA-TN-D-4760
- c14 N68-31958 Spectroradiometer and technique for measuring spectral irradiance of solar simulators
- NASA-TN-D-4822 c14 N68-35534 CALIFORNIA
- Scalar and component wind correlations between altitude levels for statistical analysis of wind profiles at Cape Kennedy, Florida, and Santa Monica, California

c13 N68-20278 NASA-TN-D-3815 CALORIMETERS Uncertainty analysis for designing calorimetric experiments, and equations for measuring properties of planetary radiation NASA-TN-D-4354 c14 N68-16529 CAMBERED WINGS HBERED WINGS Profile change effects on aerodynamic characteristics of twisted and cambered arrow wing at supersonic speed NASA-TN-D-4796 c01 N68-35 c01 N68-35665 CAMERAS Image dissector camera flown aboard Applications Technology Satellite-C for obtaining daylight cloud cover data NASA-TN-D-4186 c14 N68-10647 Airborne stellar photometry and spectrometric determination of day sky brightness NASA-CR-1017 c30 N68-19 CANARD CONFIGURATIONS Aerodynamic stability characteristics of Apollo c30 N68-19590 launch escape vehicle with canard surfaces deployed NASA-TN-D-4280 c01 N68-11640 Interference effects of canard controls on longitudinal aerodynamic characteristics of winged body in hypersonic flow NASA-TN-D-4436 CANONICAL FORMS c01 N68-21579 Methods of eliminating short period terms from Hamiltonian by means of canonical transformation MASA-TN-D-4399 c19 N68-17 Development of equations of motion in canonical form equivalent to forms of Delaunay and c19 N68-17532 Poincare NASA-TN-D-4478 c30 N68-24371 CANTILEVER BEAMS Iterative procedure for calculating normal modes and frequencies of cantilever beam NASA-TN-D-4560 c02 N68-22886 CAPACITORS. Testing and evaluation of capacitor type meteoroid penetration NASA-TN-D-4524 c14 N68-22883 CAPILLARY FLOW Capillary rise in annular region of concentric cylinders during coast periods of Atlas-Centaur flights NASA-TM-X-1558 c12 N68-23 c12 N68-23353 Radiator concept based on capillary retention of liquid and potential extraterrestrial applications NASA-TN-D-4370 c03 N68-28310 CAPTLLARY TURES JLLARY TUBES Capillary rise in annular region of concentric cylinders during coast periods of Atlas-Centaur flights NASA-TM-X-1558 c12 N68-2: c12 N68-23353 CARBON COMPOUNDS Composition and heat treatment effects on high temperature strength of arc melted tungsten-hafnium-carbon alloys NASA-TN-D-4379 c17 N68-17317 History of origin and initial development of

- carbon compounds, primitive organisms, and life on earth NASA-TT-F-488 CARBON DIOXIDE c04 N68-24272
- Convective stagnation heat transfer of carbon dioxide, nitrogen-argon gas mixtures compared to air in shock tube tests NASA-TN-D-4255 c33 N68-11811 Carbon dioxide and water wapor effects on induction period kinetics of hydrogen-oxygen
- eaction NASA-TN-D-4685 c33 N68-30041
- Carbon dioxide laser development for space application NASA-TN-D-4794
- c16 N68-35175 CARGO AIRCRAFT Subsonic and transonic flutter and flow studies of T tail of large multijet cargo airplane
- NASA-TN-D-4316 c02 N68-17055 CASTING
- Shaping of precipitation hardened stainless steels by casting and powder metallurgy NASA-SP-5086 c15 N68-19307

CATALOGS (PUBLICATIONS)

CATALOGS (PUBLICATIONS) Chronological catalog of reported lunar events or temperature changes on moon recorded between 1540 and 1967 NASA-TR-R-277 c30 N68-28192 CATHODE RAY TUBES Properties and imaging techniques of various display devices - computer directed visual flight control boards, integrated optical man machine systems, and electro-optical methods NASA-SP-159 c09 N68-22: c09_N68-22302 Cathode ray tube with nonreciprocal optical filtering techniques for viewing under high ambient NASA-CR-1185 c09 N68-33224 CATHODES Metal cathodes in argon atmospheres used to stabilize dc arcs for spectrochemical analysis NASA-TN-D-4236 c06 N68-11512 CAVITATION CORROSION Cover gas pressures affecting accelerated cavitation damage in sodium NASA-TN-D-4235 c17 N68-10104 CAVITATION FLOW Effects of Freon, water flow temperatures, and pressures on incipient venturi cavitation NASA-TN-D-4340 cl2 NG c12 N68-14641 Thermodynamic effects on Freon cavitation on venturi scale model NASA-TN-D-4387 c12 N68-15329 Thermodynamic effects of cavitation in low temperature liquid hydrogen over range of flow coefficients using flat plate helical inducer NASA-TN-D-4423 c28 N68-18221 Cavitation performance of jet pumps having low ratios of nozzle to throat area NASA-TN-D-4592 c03 N68-24461 Liquid fluorine pump, impeller, and inducer corrosion resistance to cavitation flow NHOR-IN-X-1073 Noncavitating and cavitating performance of two low area ratio water jet pumps with throat lengths of 5.66 diameters NASA-TN-D-4759 C12 N68-319 NASA-TM-X-1573 c15 N68-28241 c12 N68-31960 Cavitation damage of stainless steel, nickel, and aluminum alloy in water NASA-TM-X-1670 c17 N68-36076 CAVITY RESONATORS Hydrogen-oxygen rocket engine used to test acoustic liner with isolated resonators and variable cavity depths NASA-TN-D-4492 c33 N68-21680 Effects of high wave amplitude and mean flow on impedance of Helmholtz resonator NASA-TM-X-1582 cl2 N68-23 c12 N68-23423 Suppression of temperature rise in lossy diodes inside resonant cavities by pressurized liquid nitrogen NASA-TN-D-4556 C09 N68-24387 CELESTIAL MECHANICS Vectorial concept for solving three body problem in celestial mechanics NASA-TN-D-4447 c30 N68-22885 Lie series applications to celestial mechanics, accelerators, satellite orbits, and optimization NASA-CR-1046 c19 N68-25841 c19 N68-25841 Application of Lie series to celestial mechanics mechanics NASA-TN-D-4460 c30 N68-26643 CELESTIAL NAVIGATION Celestial attitude measuring instrument using star mapping technique NASA-TN-D-4742 c21 N68-31938 CELLS (BIOLOGY) Cell culture method of screening contaminants which may appear in manned spacecraft NASA-TN-D-4251 c0 c04 N68-10122 CEMENTATION Comparison between cemented and soldered cover glass for radiation protection of silicon solar cells NASA-TM-X-1687 c03 N68-37935 CENTAUR LAUNCH VEHICLE Vapor ingestion during liquid outflow in scale model Centaur liquid hydrogen tank NASA-TM-X-1482 c12 N68-19225 Atlas-Agena and Atlas-Centaur combined propulsion system for measurements out of three dimensional phenomena out of ecliptic plane

SUBJECT INDEX

NASA-TN-D-4455 c28 N68-19581 Wind tunnel investigation of fluctuating pressures NASA-TM-X-1574 c31 N68-22742 on Centaur model surface at transonic spee NASA-TM-X-1574 c31 N68 Development, configuration, and operation of Centaur propellant utilization system NASA-TN-D-4848 c28 N68 c28 N68-36507 CENTERBODIES Performance of vortex generators installed aft of inlet throat on centerbody evaluated at Mach numbers 2.0 to 3.0 NASA-TN-D-4675 col N68-28795 c01 N68-28795 CENTRAL NERVOUS SYSTEM Frequency coded threshold logic unit for pattern recognition systems based on central nervous system NASA-CR-1035 c05 N68-22448 CENTRIFUGAL COMPRESSORS Overall performance tests in argon of six inch radial bladed centrifugal compressor NASA-TM-X-1622 c01 N68-30033 CENTRIFUGAL PUMPS Performance of centrifugal pump impeller in room temperature water NASA-TN-D-4613 c12 N68-26651 Visual observations to find flow distribution and coefficients through radial bladed centrifugal pump impeller NASA-TN-D-4282 CERAMIC COATINGS c12 N68-28842 Smooth surface coating of molybdenum alloys for cermets by hot isostatic compaction of tungsten-uranium dioxide fuels NASA-TM-X-1563 c22 N68-; CERAMIC NUCLEAR FUELS Thermal conductivity measurements on tungsten c22 N68-21705 coated uranium dioxide cermets NASA-CR-1154 c22 N68-32983 CEREBRAL CORTEX Biochemistry of nervous system, subcellular cerebral functions, brain metabolism, isotopic labeling for biochemical studies, and use of neurotropic drugs NASA-TT-F-439 c04 N68-13432 CERMETS Smooth surface coating of molybdenum alloys for cermets by hot isostatic compaction of tungsten-uranium dioxide fuels NASA-TM-X-1563 c22 N68-21 c22 N68-21705 High temperature creep rupture strength of tungsten uranium dioxide cermets NASA-TM-X-1625 c17 N68-29987 CESIUM High temperature tests on cesium diodes and vapor filled thyratrons NASA-CR-994 c09 N68-15892 CESIUM DIODES Pairs of emitter and collector sheaths for cesium thermionic diodes NASA-TN-D-4419 c25 N68-21623 CESIUM ENGINES Thermal design and analysis of cesium contact-ion microthrustor NASA-TM-X-1473 c28 N68-10496 CESTUM ION Cesium ion beam electric field measuring instruments NASA-CR-970 c14 N68-25903 CESIUM ISOTOPES Computer analysis of gamma ray spectra recordings from iodine 128, and cesium 128 decay NASA-TN-D-4305 c24 N68-15328 CESIUM PLASMA Dependence of tungsten electrode work functions on positive ion sheaths between electrodes and cesium plasmas NASA-TN-D-4745 c25 N68-30593 Emitter and collector sheaths for cesium thermionic diodes with polycrystalline tungsten electrodes NASA-TN-D-4744 c25 N68-31640 Iterative calculation model and results for plane collisionless sheaths between field modified emitter and thermally ionized cesium plasma NASA-TN-D-4376 c25 N68-33021 Laser interferometer and heterodyne system for cesium plasma diagnostics NASA-TM-X-1652 c16 N68-3 c16 N68-35593

CLEAN ROOMS

CHANDRASEKHAR EQUATION Tabular and graphical data on calculations of Chandrasekhars X and Y functions and analogs for noncoherent isotropic scattering c19 N68-30804 NASA-TN-D-4712 CHANNEL FLOW Hydraulic flow approximation for flow induced vibration analysis on flat plate suspended in narrow channel NASA-CR-1186 CHARGE DISTRIBUTION c12 N68-35086 Negative feedback for discharge current noise reduction in excited helium-neon laser NASA-CR-1173 c16 c16 N68-35099 CHARGED PARTICLES Analysis of integrated charged particle energy spectra from gridded electrostatic analyzers NASA-TN-D-4718 c25 N68-3 c25 N68-30093 CHARRING Analyses and finite difference procedure for predicting transient in-depth response of charring ablation materials NASA-CR-1060 c33 N6 c33 N68-25244 Coking reactions of pyrolysis gas in charring ablation material NASA-CR-1065 c33 N68-26817 Chemical reaction-plane approximation in ablation analyses NASA-TN-D-4817 c33 N68-36072 CHARTS Enthalpy, thalpy, temperature, and density charts for equilibrium isentropic expansion of air behind shock waves for wide range of velocities and altitudes NASA-TN-D-4247 CHEBYSHEV APPROXIMATION c33 N68-11144 Approximations to several transcendental functions in universal form of two body problem c19 N68-29407 NASA-TN-D-4643 CHECKOUT Automatic testing and checkout of Saturn 1 launch vehicles NASA-TN-D-4328 c31 N68-15570 CHEMICAL ANALYSIS Recovery of potassium tantalate and potassium monoxide to demonstrate procedure for isolation and recovery of alkali-metal reaction products in uncontaminated state NASA-TN-D-4310 c17 N68-14888 Servocontroller for programming atomic emission and sample vaporization in direct current arc spectrochemical analysis NASA-TN-D-4769 CHEMICAL ELEMENTS c06 N68-31948 Surveyor 5 configuration, television picture transmission, and experiments on measuring chemical elements in lunar surface NASA-SP-163 c31 N68 CHEMICAL EQUILIBRIUM c31 N68-17844 Computer program for solutions to equilibrium and nonequilibrium chemical state relations for open and closed thermodynamic systems NASA-CR-1064 c33 N68-26816 CHEMICAL PROPERTIES Nuclear, chemical, and physical properties of nine radioactive isotopes - annotated bibliography NASA-SP-7031 c06 N68-29959 CHEMICAL PROPULSION Small water-graphite nuclear rocket stages compared with chemical upper stages for use in unmanned spacecraft NASA-TN-D-4827 CHEMICAL REACTIONS c22 N68-35073 Corrosion products of oxygen doped tantalum exposed to potassium at 1800 deg F NASA-TN-D-4213 c17 N60 c17 N68-11511 NASA-IN-D-4213 C17 N68-1151 Flammability hazards chemically induced in aircraft and spacecraft electrical circuitry by glycol/water solutions NASA-TN-D-4327 c31 N68-2221 c31 N68-22213 Photographs, thermocouples, and emission spectra used to study mixing and reaction of hydrazine and nitrogen tetroxide NASA-TN-D-4467 c33 N68-2490 c33 N68-24965 Chemical reaction-plane approximation in ablation analyses NASA-TN-D-4817 c33 N68-36072 Role of chemical reactions in comminution

mechanism of ductile metals into ultrafine

powders by grinding NASA-TN-D-4862 c15 N68-37239 CHEMISORPTION Influence of chemisorbed films of various gases on adhesion and friction of tungsten in vacuum c15 N68-33227 NASA-TN-D-4694 Reduction of adhesive forces and friction of iron polycrystals in vacuum by chemisorbed films NASA-TN-D-4775 c17 N68-3327 c17 N68-33278 CHLORELLA UKELLA Bioregenerative life support systems for long duration space flights - Hydrogenomonas biosynthesis and algae photosynthesis processes NASA-SP-165 c04 N68-26207 CHOKES Inlet guide vane choking noise reduction in axial flow compressors NASA-TN-D-4682 c02 N68-29400 CHROMIUM ALLOYS c02 N68-29406 Chromium alloys with good low temperature ductility and superplasticity NASA-TN-D-4346 c14 c14 N68-13973 CHROMIUM OXIDES Hydrogen release in ball milling of high purity, coarse chromium powder in water NASA-TN-D-4569 c15 N68-Chromium and nickel powders from reduction of chromium and nickel oxides with magnesium, c15 N68-23900 lithium, or sodium vapors NASA-TN-D-4714 ~17 N68-30066 CIRCUIT BREAKERS Circuit breakers and electric switch developments for future nuclear electric power generation systems operating in aerospace environments NASA-CR-1026 c03 N68c03 N68-29460 CIRCUIT RELIABILITY Breadboard three-phase static switch for space alternating current power systems NASA-TM-X-1495 c09 N68-1 c09 N68-15649 CIRCUITS Electrical design and scheduling of components for thin film personal communications and telemetry sustem NASA-CR-914 c09 N68-10420 Cable and circuit parameters effects on calibration of charge amplifier for microsecond pulses NASA-TN-D-4300 CIRCULAR CYLINDERS c09 N68-16530 Bucking of thin-walled electroplated copper and Mylar circular cylinders under axial compression and bending NASA-CR-1160 c32 N68-33226 CIRCULAR ORBITS Analytical method artificial satellite lifetime determination NASA-TN-D-4281 c30 N68-11754 Simplified and accurate relative equations of motion for two impulse orbital rendezvous NASA-TN-D-4670 c30 N68-28841 Computer program technique for determination of opportunities for recall of spacecraft to multiple landing sites from circular or elliptical orbits NASA-TR-R-259 c21 N68-30126 Analysis of launch windows from circular orbits for representative Mars missions NASA-TM-X-1651 c30 N68-33371 CIRCULAR PLATES Plastic response of circular uniform plate to axisymmetric impulse load of Gaussian distribution NASA-TR-R-279 c32 N68-14640 CIRCULAR TUBES Convective heat transfer data for water flow in heated circular tubes with varying heat fluxes and flow areas NASA-TM-X-1554 c33 N68-20338 CLADDING Constant creep data accumulation for design stress analysis on cladding material thickness around cylindrical reactor fuel element NASA-TN-D-4352 CLASSICAL MECHANICS c22 N68~26764 Conference proceedings on classical mechanics, continuum mechanics, and motion stability NASA-TT-F-503 c23 N68-37792 CLEAN ROOMS

Contamination control principles

CLEANING

RADATOF-3045 cll N68-10384 Clean room facilities for Explorer 35 spacecraft spacecraft NASA-TN-D-4577 c11 N68-28311 CLEANING Contamination control principles NASA-SP-5045 c11 N68-10384 Contaminant controls and cleaning procedures in SNAP-8 simulation loop of liquid metals NASA-TM-X-1432 c17 N68-119 c17 N68-11912 RASA-18-2-14-32 CLEAR AIR TURBULENCE Laser light backscatter investigation of air flow velocity in contaminated atmospheres for application to clear air turbulence detectors NASA-TN-D-4453 C20 N68-2037 c20 N68-20375 CLIMBING FLIGHT Simulated flight test of double-Delta supersonic transport for performance characteristics, handling qualities, and climbing characteristics NASA-TN-D-4396 c02 N68-17391 c02 N68-17391 CLOSED CIRCUIT TELEVISION Evaluating closed circuit television display in helicopter landing operations NASA-TN-D-4313 c05 N68-16594 CLOSED CYCLES Design, fabrication and testing of Cb-12r thermal convection loop for evaluation of refractory metals in boiling and condensing potassium environments NASA-CR-1097 CLOSED ECOLOGICAL SYSTEMS c22 N68-35153 ISED ECOLOGICAL SYSTEMS Bioregenerative life support systems for long duration space flights - Hydrogenomonas biosynthesis and algae photosynthesis processes MASA-SP-165 c04 N68-26207 CLOUD COVER Image dissector camera flown aboard Applications Technology Satellite-C for obtaining daylight cloud cover data NASA-TN-D-4186 c14 N68-10647 CLOUD PHOTOGRAPHS Spaceborne photography of cloud cover and other meteorological phenomena, Surveyor and Orbiter lunar shots, and Gemini space walk and target docking NASA-SP-168 CLOUD SEEDING c30 N68-34870 Warm fog and fog modification by seeding with salt particles NASA-CR-1071 c20 N68-25816 COASTING FLIGHT Body alterations for reducing drag of missiles during coasting flight NASA-TM-X-1537 c01 N68-19206 NRSH-1R-X-1557 c01 N68-19206 Cryogenic propellant management during coasting of Atlas Centaur vehicles NASA-TN-D-4571 c28 N68-25099 COAXIAL FLOW Mixing of turbulent, incompressible, coaxial treams NASA-CR-959 c12 N68-16897 Similarity solution for turbulent mixing between jet and faster moving coaxial stream NASA-TN-D-4441 c12 N68-1924 c12 N68-19246 NASA-IN-D-4441 Cl2 NOS-19246 Coaxial flow stabilized ac arc facility NASA-TN-D-4517 c25 N68-20296 Coaxial injector thrust effects on combustion stability of hydrogen-oxygen rocket engine NASA-TN-D-4851 c28 N68-36515 COAXIAL PLASMA ACCELERATORS Two channel transient voltage digitizer for correlation of transient spectra with performance in coaxial, argon plasma guns NASA-TN-D-4385 c25 NG c25 N68-17070 COBALT ALLOYS Mechanism and kinetics of iron and cobalt alloys corrosion in refluxing mercury NASA-TN-D-4450 c17 N68-21654 Electrical and mechanical properties of high temperature cobalt-iron magnetic material NASA-TN-D-4551 c17 N68-24558 NASA-TN-D-4551c17 N68-24558Crystal transformation and atomic ordering on wear
and sliding friction in two cobalt alloys
NASA-TN-D-4668c15 N68-28260Oxidation resistance and ductility of cobalt heat
resistant alloys optimized by restriction of
silicon and manganese content
NASA-TN-D-4715c17 N68-29954

COCKPIT SIMULATORS Piloted fixed-base simulation of low speed flight characteristics of arrow wing supersonic transport aircraft NASA-TN-D-4277 c05 N68-13609 CONTING Coding schemes for data based on Poisson functions c07 N68-25852 NASA-TN-D-4572 Bolza problem of calculus of variations in terms of control coding applied to trajectories NASA-CR-1103 c30 N68-25895 COEFFICIENT OF FRICTION Runway surface texture conditions effect on wet runway braking friction coefficients created by aircraft tires NASA-TN-D-4323 c02 N68-14903 Wear rate and friction coefficient of steel sliding on polymer laminates determined in liquid nitrogen and hydrogen NASA-TN-D-4463 c15 N68-20325 Friction and wear in cryogenic liquids for phenolic and polytetrafluoroethylene composites of various particle sizes and concentrations NASA-TN-D-4565 c15 N68-2414 c15 N68-24142 NBSA-IN-D-4505 C10 NGC-2414 Spinning friction and torque dependence on ball bearing-groove conformity NASA-IN-D-4669 C15 N68-2825 Adsorbed surfactants influence on deformation and c15 N68-28258 friction coefficient of lithium fluoride single crystals during sliding friction NASA-TN-D-4716 c15 N68-2991 c15 N68-29918 COHERENT RADIATION Coherent radiation methods of measuring absorption spectra in planetary atmosphere, and millimeter and submillimeter wave propagation NASA-CR-863 c07 N68-27063 COLD FLOW TESTS Cold flow tests of aerodynamic characteristics of c07 N68-27063 plug nozzle configuration for turbojet engines operating at supersonic speeds NASA-TM-X-1619 c28 N68-29953 COLD PLASMAS Guided electromagnetic waves propagating along lossless dielectric rod immersed in isotropic and uniaxial plasmas determined for applications to plasma diagnostics NASA-TN-D-4866 c25 N68-37237 COLD SURFACES U DURFACED Transient solidification of flowing liquid on cold plate, including heat capacities of frozen layer and plate NASA-TN-D-4353 C33 N68-1574; c33 N68-15742 COLD WORKING Stress-strain diagrams for cold welded copper microjunctions in vacuum NASA-TN-D-4743 c17 N68-31517 COLLISIONLESS PLASMAS FORTRAN computer programs for plane collisionless sheaths between field modified emitter and sheaths between field modified emitter and thermally ionized plasma exemplified by cesium NASA-TM-X-1562 co8 N68-21499 Graphs of phase and group refractive indices computed from collisionless magnetoionic theory electron concentration and magnetic field intensity NASA-TM-X-1553 c13 N68-21904 Iterative calculation model and results for plane collisionless sheaths between field modified emitter and thermally ionized cesium plasma NASA-TN-D-4376 c25 N68c25 N68-33021 Guided electromagnetic waves propagating along lossless dielectric rod immersed in isotropic and uniaxial plasmas determined for applications to plasma diagnostics NASA-TN-D-4866 c25 N68-37237 COLLISIONS Classification and construction of open-channel projection operators for rearrangement collisions using subspaces of total Hilbert space of system NASA-TN-D-4633 c24 N68-28265 COLLOIDS Nonuniform magnetic field effect on ferromagnetic colloidal solutions NASA-TN-D-4676 c06 N68-3004 c06 N68-30044 COLUMNS (SUPPORTS) Materials selection, structural geometry, proof

COMPRESSORS

testing and statistical screening, prestressing, and system energy as tools for designing optimum trusses and other high performance structures NASA-CR-1038 c32 N68-23399 NABA-CR-1038 Nicrostructure and mechanical properties of beryllium tubing and performance tests on support columns of beryllium NASA-TN-D-4833 C17 NE0-2705-RUSTION CUANTY COMBUSTION CHAMBERS Ablative and steel chambers effect on combustion instability in hydrogen oxygen rocket engine NASA-TM-X-1511 Injector baffles for flame stability in combustion chambers using nitrogen tetroxide and hydrazine mixture NASA-TM-X-1595 c28 N68-26644 Dilution-jet mixing flow studies for gas turbine combustion chambers NASA-TN-D-4695 c01 N68-30128 Small uncooled combustion chamber tests of performance and stability characteristics of nitrogen tetroxide-hydrazine propellant NASA-TN-D-4776 c27 N68-35072 COMBUSTION EFFICIENCY Development, configuration, and operation of Centaur propellant utilization system NASA-TN-D-4848 c28 N68 c28 N68-36507 COMBUSTION STABLITY Combustion instability prediction using nonlinear bipropellant vaporization model NASA-CR-920 c33 N68-15833 Double dead-time model for combustion stability NASA-TN-D-4564 c33 N68-25102 NASA-TN-D-4564 c33 N68-2510 Chamber pressure, contraction ratio, and flow per element effects on acoustic mode instability in hydrogen oxygen engines NASA-TN-D-4733 c33 N68-30518 Coaxial injector thrust effects on combustion stability of hydrogen-oxygen rocket engine NASA-TN-D-4851 c28 N68-36515 COMMAND MODULES MAND HUDDLES Movement of forward heat shield in Apollo command module turbulent reverse flow wake NASA-TN-D-4691 c31 N68-3003; Wind tunnel test data on static and dynamic stability of Apollo command module c31 N68-30032 configuration NASA-TN-D-4688 c01 N68-31445 Apollo command module radar cross section decrease due to reentry plasma effects NASA-TN-D-4784 c07 N68-35140 Variable density hypervelocity wind tunnel tests on effects of several ramp-fairing, umbilical, and pad configurations on aerodynamic heating to Apollo command module NASA-TM-X-1640 c01 N68-35141 COMMUNICATION EQUIPMENT Electrical design and scheduling of components for thin film personal communications and telemetry system NASA-CR-914 c09 N68-10420 COMMUNICATION SATELLITES Achievements of application technology satellites, communication satellites, navigation and traffic control satellite program, weather satellites, and satellite geodesy NASA-SP-156 C31 N68-16015 Hovering lunar libration communication satellite stationary with respect to earth-moon system NASA-TN-D-4468 c30 N68-2173 NASA-TN-D-4468 c30 N68-21733 Data relay and tracking capability of lunar communication satellites above lunar far side surface NASA-TN-D-4509 c31 N68-25358 Annotated bibliography on communication satellite theory and technology NASA-SP-7004/04/ c31 N68-28379 COMMUTATORS Feynman formalisms for expressing iterated commutators and functions of operators NASA-TN-D-4857 COMPACTING c19 N68-36525 Smooth surface coating of molybdenum alloys for cermets by hot isostatic compaction of tungsten-uranium dioxide fuels NASA-TH-X-1563 c22 N68-21705 COMPATIBILITY

Corrosion resistance tests for compatibility of

several iron, cobalt, and nickel based alloys with refluxing potassium NASA-TH-X-1617 c17 N68-30 c17 N68-30065 NASA-TH-X-1617 C17 N62-3000 COMPENSATORY TRACKING Pilot performance using compensatory and pursuit tracking displays with rate and acceleration control dynamics and disturbance input NASA-CR-1082 c07 N68-282 c07 N68-28272 COMPONENT RELIABILITY Reliability prediction techniques for single item and multiitem problems NASA-CR-1129 c15 N68-31979 Component reliability including selection, specification, verification, review process, parts data sources NASA-CR-1130 c15 N68-31980 COMPONENTS Method for calculating partial volumes of components in solution NASA-TN-D-4199 c06 COMPOSITE MATENIALS c06 N68-11621 Structural design methods for analysis of multilayer or laminated filamentary composites NASA-CR-964 c32 N68-11191 Elastoplastic analysis of circular cylindrical inclusion in uniformly stressed infinite homogeneous matrices of composite materials for aerospace applications NASA-TN-D-4350 c32 N68-15769 NASA-TN-D-4350 C32 NGO-1977 Tensile strength properties of glass, boron, and graphite filament wound resin composites and liners for cryogenic pressure vessels NASA-TN-D-4412 c18 N68-166; c18 N68-16623 Environmental exposure effects on mechanical properties of titanium alloy, stainless steel, aluminum alloy, and composite material sheets NASA-TN-D-4318 c17 N68-17897 Interfiber distance and temperature effects on critical aspect ratio in composites NASA-TN-D-4548 c17 N68-2; c17 N68-22338 High temperature research on creep rupture strength of refractory metal fiber and nickel alloy composites NASA-TN-D-4787 c17 N68-33 Fabricability, mechanical properties, and structural efficiency potentials of c17 N68-33684 boron-polymer film layer composites NASA-CR-1114 COMPOSITE PROPELLANTS c18 N68-35100 POSITE PROPELLANES Double dead-time model for combustion stability analysis in liquid bipropellant rocket engines NASA-TN-D-4564 c33 N68-25102 Analysis in figure of propertant focket engines NAS-TN-D-4564 c33 N68-25102 COMPOSITE STRUCTURES Evaluation of self-evacuating multilayer radiation shields for cryogenic storage tanks NASA-TN-D-4375 c33 N68-18046 COMPRESSIBLE BOUNDARY LAYER Equations of motion for calculating compressible turbulent boundary layers NASA-CR-1144 c12 N68-35096 COMPRESSIBLE FLOW Boundary layer and wake survey data reduction techniques in compressible flows NASA-TN-D-4401 cl2 N68c12 N68-19709 COMPRESSION LOADS Liapunov method used to obtain sufficient conditions for buckling stability of long cylindrical shells with random imperfections cylindrical suchts -.... NASA-CR-1161 COMPRESSOR BLADES FORTRAN computer program for supersonic turbomachinery blading design calculations c08 N68 c32 N68-33419 NASA-TN-D-4421 c08 N68-18620 Stress analysis and wear tests in use of lacing wire as vibration damper on turbocompressor blades blades NASA-TM-X-1603 c32 N68-28238 Friction and fretting wear tests on materials used as friction dampers to reduce vibrational stresses in compressor blades for turbine engines NASA-TN-D-4630 c15 N68-28871 Overall performance tests in argon of six inch radial bladed centrifugal compressor NASA-TM-X-1622 c01 N68-30033 COMPRESSORS Approximate average midspan metal temperatures and coolant flow requirements for turbine airfoils cooled by compressor exit bleed air

COMPUTATION

NASA-TN-D-4491 c33 N68-19187 Combination temperature, pressure, and flow direction sensing probe to study rotating machinery NASA-TN-D-4816 c14 N68-36021 COMPUTATION Monte Carlo computations of decision error probabilities for chain pooling and variations for fractional factorial experiments NASA-TN-D-4272 c19 N68-11639 Computational method for orbiting astronauts to determine required velocity for two impulse abort to landing site NASA-TN-D-4599 NAON-IN-U-4559 c21 N68-25103 Computer applications to practical reliability NASA-CR-1127 NBSA-CK-112/ Computation of solar elevation angles and determination of sunrise and sunset times as function of latitude, longitude, and date NASA-TM-X-1646 c13 N68-35179 COMPUTER DESIGN Nonconventional computers for solving problems previously handled only by humans NASA-TM-X-1544 c08 N68-1 c08 N68-19336 Coding schemes for data based on Poisson functions NASA-TN-D-4572 c07 N68-25852 Machania (1872) - 4372 (1972) Advanced multiprocessor computer organization for manned Mars lander mission NASA-CR-1159 c08 N68-35560 COMPUTER PROGRAMMING Finite-state machines and evolutionary programming for representing and analyzing performance of human operator in control of dynamic systems NASA-CR-1112 c05 N68-284 c05 N68-28847 Computer applications to practical reliability NASA-CR-1127 c15 N68-32760 Error probabilities for maximum signal detection in presence of Poisson noise NASA-TN-D-4721 c07 N68-36105 Computer programming for control of complex data processing operations involved in analysis and interpretation of large volumes of sensor data from scientific satellites NASA-CR-1107 c08 N68-3725 c08 N68-37254 COMPUTER PROGRAMS Computer methods for calculating eigenvalue and eigenvectors of real symmetric matrices arising in problems of molecular quantum mechanics NASA-CR-983 c24 N68 c24 N68-11903 Digital computer program for prediction of snap buckling of spacecraft shell structures by geometric nonlinear analysis of thin elastic shells of revolution NASA-CR-909 c32 N68-14584 FORTRAN computer program for calculating model planetary atmospheres and density and temperatue dispersion data for Apollo reentry NASA-TN-D-4292 c30 N68-15793 Numerical procedures and computer program for calculating real fluid and thermodynamic properties of normal and parahydrogen NASA-TN-D-4341 c0 C08 N68-15798 Rhon-IN-0-4341 Flexible body analog computer program and rigid body digital computer program for calculating dynamic characteristics of double-V antennas on Radio Astronomy Explorer satellite NASA-CR-962 c08 N68-18144 Computer program for calculating isothermal, turbulent jet mixing flow of two gases in coaxial flow, gas gore nuclear reactors NASA-TN-D-4378 c12 N64 NASA-TN-D-4378 cl2 N68-18146 Computer analyses of retrodirective, and self adaptive antenna phase control techniques for Mars probe NASA-CR-977 c21 N68-18484 FORTRAN subroutines for determining intersections of nuclear particle flight path and wall of helical tubular duct NASA-TN-D-4435 c22 N68c22 N68-18541 FORTRAN digital computer program for axial distribution of aerodynamic normal force characteristics for axisymmetric, multistage launch vehicles in linear angle of attack ranges NASA-TN-D-4342 c31 N68-18615 c31 N68-18615

NASA-TN-D-4342 FORTRAN computer program for supersonic turbomachinery blading design calculations NASA-TN-D-4421 FORTRAN computer program for computing mass in

SUBJECT INDEX

earth orbit for round trip-stopover missions, flyby missions, and orbital missions with single-stage high-thrust system for each phase NASA-TM-X-1541 c30 N68-19330 Computer program for determining geometric configuration view factors for spherical and conical surfaces of spherical radiating bodies NASA-TN-D-4457 c33 N68-20331 Computer programs for rapidly computing approximate ephemerides of minor planet or artificial satellites NASA-TN-D-4470 c30 N68-20356 Computer program for calculating normalized Mie scattering functions NASA-CR-1022 c24 N68-21227 FORTRAN 4 computer program for calculating temperature profiles in propellant tank NASA-TM-X-1556 c27 N c27 N68-21267 FORTRAN computer program for calculating two dimensional subsonic inviscid flow for rotating or stationary circular cascade of blades on blade to blade stream surface of turbomachine NASA-TN-D-4525 c01 N68-21 c01 N68-21374 NASA-IN-U-4525 COI N68-2137 FORTRAN computer programs for plane collisionless sheaths between field modified emitter and thermally ionized plasma exemplified by cesium NASA-TM-X-1562 CO8 N68-2149 NASA-TM-X-1562 c08 N68-21499 Computer program for analysis of shells of revolution with axisymmetric loading NASA-CR-1051 c32 N68-23355 Basic equations and method of solution for computerized analysis of shells of revolution with axisymmetric collapse and nonsymmetric bifurcation buckling behavior NASA-CR-1050 c32 N68-23451 Computer program for reversion of cumulative binomial probability distribution NASA-TM-X-1592 c19 N68 c19 N68-24141 Numerical results of buckling of shells of revolution for computer program NASA-CR-1049 c32 N68-24481 Computer program for symbolic reduction of block diagrams to obtain transfer functions NASA-TN-D-4617 c08 N68-24967 FORTRAN program for approximate calculation of supersonic ideal gas flow past blunt bodies with sonic corners NASA-TN-D-4563 c01 N68-25093 Mathematical properties and computer programs for digital spectrum analyses NASA-TN-D-4510 c08 N68-2526 c08 N68-25268 Trajectory optimization by direct descent to minimum cost using iterative computer solutions NASA-CR-1070 c30 N68-25902 Computer program for finite difference equation analysis of in-depth response of materials exposed to high temperature environment NASA-CR-1061 c33 | c33 N68-26692 Computer program for solutions to equilibrium and nonequilibrium chemical state relations for open and closed thermodynamic systems c33 N68-26816 NASA-CR-1064 Numerical least square method for resolving complex pulse height spectra NASA-SP-3044 c24 N6 c24 N68-29520 Mathematical model and computer program for analysis of three and four gimbal systems Analysis of three and four gimbal systems NASA-TN-D-4689 cll N68-293 Computer program technique for determination of opportunities for recall of spacecraft to multiple landing sites from circular or elliptical orbits c11 N68-29957 NASA-TR-R-259 c21 N68-30126 Hardware design and computer programs for spaceborne multiprocessor computer system spaceborne multiprocessor computer system NASA-CR-1158 Supplementary information for computer program predicting lifting pressure and camber shape of composite planform in subsonic flow NASA-TN-D-4227, SUP. Computer program for trajectory optimization and payload maximization in multistage launch c08 N68-31499 . c01 N68-31515 vehicles NASA-TN-D-4729 c30 N68-3194 Digital program for dynamics of nonrigid gravity gradient satellites c30 N68-31989 NASA-CR-1119 c30 N68-32744

NBAR-CK-1119 C30 NG8-32/44 Computer program for analyzing free flight motions of axisymmetric bodies to determine aerodynamic

c30 N68-27475

coefficients NASA-TN-D-4766 c01 N68-33081 Stream-filament analysis procedure and correlation of total pressure loss coefficients to form basis of computer program to investigate design point performance of axial turbines NASA-CR-1181 c28 N68 c28 N68-35101 Simplified equilibrium hydrocarbon-air combustion gas model for use in air breathing engine cycle computer programs NASA-TN-D-4747 NASA-TN-D-4747 c28 N68-35115 Computer program in FORTRAN 4 for calculating shock tube performance for arbitrary equilibrium real gas mixtures NASA-TN-D-4802 c11 N68-35466 Computer program for solving equations governing flow in axial turbines NASA-CR-1187 c28 N68-366 c28 N68-36617 COMPUTER STORAGE DEVICES Metal oxide semiconductor field effect transistor circuit development and laminated electronic packaging for computer storage devices NASA-CR-1113 c08 c08 N68-35193 COMPUTERIZED DESIGN Computer methods for calculating radiation shield design for Plum Brook reactor HB-6 beamhole facility NASA-TM-X-1461 c22 N68-10133 FORTRAN 4 program for computerized design of two dimensional supersonic nozzles with sharp edged throats NASA-TM-X-1502 c01 N68-14747 Annotated bibliography of computer-aided circuit analysis and design NASA-SP-7023 c10 N68-19882 Visual information display systems that are computer connected or updated with computer generated information NASA-SP-5049 c08 N68-32159 NASA-SF-5049 Coo NoC-32159 Stream-filament analysis procedure and correlation of total pressure loss coefficients to form basis of computer program to investigate design point performance of axial turbines NASA-CR-1181 C28 N68-35101 COMPUTERIZED SIMULATION Feasibility of computer assisted flight controller training NASA-CR-917 c08 N68-13897 Computer program using Monte Carlo methods for simulating solar flares during interplanetary space flight NASA-TN-D-4311 c29 N68-16008 Analog computed time histories and altitude-ground track plots of swept wing transport aircraft longitudinal response to wind shear and sustained gusts during landing approaches NASA-TN-D-4477 c01 N68-1 c01 N68-19180 Theory and equations for propulsion system dynamic simulation NASA-CR-928 c11 N68-19273 Analytic computational error models for strapdown inertial navigation systems NASA-CR-968 c21 N68-21652 Two dimensional computer model for collisionless self gravitating galactic system with gravitational field obtained from Poisson equation NASA-TN-D-4646 c30 N68-28884 Human learning behavior theory in manual control task modeled as computer program NASA-CR-1124 c05 N68-319 c05 N68-31911 COMPUTERS Spirometer modification to permit computer reduction of respiratory flow data NASA-TN-D-4234 cl4 N c14 N68-10057 CONCENTRATION Effects of zinc concentration on output of zinc doped germanium infrared detectors NASA-TN-D-4834 c26 N68-37 c26 N68-37055 CONCENTRATION (COMPOSITION) Composition and heat treatment effects on high temperature strength of arc melted tungsten-hafnium-carbon alloys NASA-TN-D-4379 c17 N68-1 Organic additives and concentration effects on c17 N68-17317 radiation induced reduction of copper salts in aqueous solution NASA-TN-D-4451 c06 N68-19434

CONCENTRIC CYLINDERS Capillary rise in annular region of concentric cylinders during coast periods of Atlas-Centaur flights NASA-TM-X-1558 c12 N68-23353 CONCRETES Outgassing of water vapor from concrete surfaces in vacuum environments NASA-TM-X-1536 c11 N68-19207 CONDENSERS (LIQUIFIERS) Performance characteristics and operating parameters of three-fluid crossflow heat . exchangers NASA-TR-R-284 c33 N68-23513 CONDENSING Water vapor condensation effects of heated air on flow in large supersonic wind tunnels NASA-TM-X-1636 cll N68-3059 c11 N68-30598 Low temperature effects on tensile properties of aluminum, magnesium, nickel, steel, and titanium alloys Alloys NASA-SP-5012/01/ c17 N68-316 CONDITIONING (LEARNING) Human learning behavior theory in manual control task modeled as computer program NASA-CR-1124 c05 N68-319 c17 N68-31605 c05 N68-31911 CONDUCTIVE HEAT TRANSFER Boundary condition solution and transcendental approximation for transient heat conduction problem NASA-CR-955 c19 N68-11109 Conductive heat transfer mechanisms in low density phenolic-nylon chars NASA-CR-966 c18 N68-11978 Steady hypersonic flow over blunt bodies with high rates of continuous mass and heat transfer from body surface NASA-TN-D-4252 col N68-1755 Boundary conditions for diffusion solution of coupled heat transfer NASA-TN-D-4618 NUCTOR: 633 NE9-1 c01 N68-17555 c33 N68-26759 CONDUCTORS Electromagnetism in moving, conducting media – solution to problems involving static and radiation fields of static charges, and radiation fields of harmonic current sources NASA-CR-1025 c23 N68-21444 CONES Approximate equations for computing enthalpy and velocity derivatives at surface of flat plate, cone, or blunt axisymmetric body cone, or blunt NASA-TN-D-4484 c33 N68-20065 Base pressure measurements at angle of attack for spherically blunted cones at hypersonic speed NASA-TN-D-4800 c01 N68-35660 c01 N68-35668 Cone-cylinder models tested in supersonic wind tunnel to evaluate effect of wall reflected disturbances on model pressure distributions NASA-TM-X-1655 c01 N68-36134 CONFERENCES Observational and theoretical interpretations of interstellar grains - conference paper NASA-SP-140 c30 c30 N68-11456 Gemini Summary Conference NASA-SP-138 c30 N68-14941 Third annual NASA University Conference on Manual Control c05 N68-15901 NASA-SP-144 Sonic boom research /conference/ NASA-SP-147 c02 N68-21413 Properties and imaging techniques of various display devices - computer directed visual flight control boards, integrated optical man machine systems, and electro-optical methods NASA-SP-159 c09 N68-22 c09 N68-22302 Mnon-or-up Space radiation transport, spacecraft shielding design and advanced concepts, and methods for calculating radiation penetration through protective shields - conference Nack-222 NASA-SP-169 c29 N68-26128 Bioregenerative life support systems for long duration space flights - Hydrogenomonas biosynthesis and algae photosynthesis processes c04 N68-26207 NASA-SP-165 Photometric and meteor observations, scattering properties, particle collection and impact, solar wind, and origin and evolution of zodiacal light in interplanetary medium - conference

I-21

NASA-SP-150

CONFORMAL MAPPING

SUBJECT INDEX

Conference proceedings on role of vestibular organs in space exploration NASA-SP-152 c04 N68-29128 Conference papers on NASA planning and projected requirements for advanced aerospace electronic systems technology NASA-SP-154 c30 N68-33169 Conference on numerical analysis applications to aerospace and related problems NASA-SP-170 c19 N68-33245 transport flight - shock wave propagation and refraction, prediction methods for acoustic attenuation, and aerodynamic engineering aspects NASA-SP-180 c02 N68-34907 Conference proceedings on classical mechanics, continuum mechanics, and motion stability NASA-TT-F-503 c23 N68-37792 CONFORMAL MAPPING Mathematical model based on conformal mapping of shape of electric arc balanced in transverse convective and magnetic fields NASA-TN-D-4736 c25 N68-30784 Conformal mapping for steady two-dimensional solidification on cold surface in liquid flow NASA-TN-D-4771 c33 N68-32073 CONICAL BODIES Wind tunnel tests on pressure distribution, and shock shapes of conical blunted bodies moving at supersonic speeds in nitrogen, or helium media NASA-TN-D-4314 c01 N68-178 c01 N68-17896 NAA-TN-D-4014 Aerodynamic characteristics of modified conical lifting reentry vehicle at hypersonic speeds NASA-TN-D-4598 c31 N68-24964 Supersonic aerodynamics of large angle comes NASA-TN-D-4719 c01 N68 c01 N68-31551 Hypersonic heat transfer and pressure distribution on spherically blunted cone NASA-TN-D-4792 c01 N68-35497 Effect of geometry of conical afterbodies on base drag at subsonic and transonic speeds NASA-TN-D-4821 c01 N68-37054 c01 N68-37054 Flexibility effects on lift and pitching moments of low aspect ratio delta wing-conical-cylindrical body combinations at transonic speeds NASA-TN-D-4655 c01 N68-37065 Nonlinear lift and pressure distribution of slender conical bodies with strakes at low speed NASA-CR-1202 col N68-37255 CONICAL NOZZLES Forces and moments produced by air and helium jets exhausting parallel to flat plate in near vacuum NASA-TN-D-4408 Laminarization of turbulent boundary layer observed from heat transfer and boundary layer measurements in conical nozzles NASA-TN-D-4788 c12 N68-33642 CONICAL SHELLS Aerodynamic characteristics of tension string, tension shell, and conical shapes in supersonic flow NASA-TN-D-4360 c01 N68-18720 Resonant frequencies and nodal pattern modes of vibrating cylindrical and conical frustum shells NASA-TN-D-4428 c32 N68-20954 Rayleigh-Ritz method NASA-TN-D-4772 c32 N68-33057 c32 N68-33057 Buckling of conical shells under axial compression and effects of axially symmetric defects NASA-CR-1162 c32 N c32 N68-35198 CONSTRAINTS Resolution limit analysis for pulse frequency modulation telemetry processing line c07 N68-18247 NASA-TN-D-4180 NAA-IN-J-4120 Not-102-Semigraphical method to aid selection of descent trajectory compatible with mission constraints NASA-TN-D-4801 c30 N68-3607 Effects of edge constraints on optical qualities of Gemini spacecraft windows c30 N68-36077 NASA-TN-D-4845 c23 N68-36470 CONTAINMENT Containment tests of vortexes with radial outflow in basic vortex tube, and in axial-flow vortex tube NASA-CR-993 c22 N68-18243

Containment characteristics of radial inflow gases in vortex tubes NASA-CR-1029 c12 N68-22200 CONTAMINANTS Contaminant controls and cleaning procedures in SNAP-8 simulation loop of liquid metals NASA-TM-X-1432 c17 N68-11912 CONTAMINATION Contamination control principles NASA-SP-5045 c11 N68-10384 Air samplers, contamination, and sterilization in collection of microorganisms for microbiological exploration of stratosphere NASA-CR-1101 CONTINUITY EQUATION c04 N68-28247 Small amplitude solutions to spatially uniform plasma continuity equations for low frequency oscillations in electron density and neutral atoms NASA-TN-D-4472 c25 N68-22887 CONTINUUM FLOW Continuum fluid theory of solar wind and its interaction with geomagnetic field NASA-TN-D-4482 c29 N68-25181 CONTINUUM MECHANICS Conference proceedings on classical mechanics, continuum mechanics, and motion stability NASA-TT-F-503 c23 NG c23 N68-37792 CONTROL Multivariable control systems for industrial applications NASA-TT-F-435 c10 N68-37293 CONTROL BOARDS Properties and imaging techniques of various display devices - computer directed visual flight control boards, integrated optical man machine systems, and electro-optical methods NASA-SP-159 CONTROL ROCKETS c09 N68-22302 Altitude of orbiting spacecraft corrected by thrustor firing time control system NASA-TN-D-4519 c31 N68 c31 N68-21260 CONTROL RODS Vibration tests of concentric tube fuel element support structure for Tungsten Water Moderated Reactor NASA-TM-X-1608 CONTROL STABILITY c32 N68-28330 Impedance testing for flight control system parameters in studies of launch vehicle dynamic stability NASA-CR-939 c32 N68-11485 Hydrodynamic equations for stability, and control analyses on liquid propellant space vehicles NASA-CR-941 c32 N68-1876 c32 N68-18769 Dynamic stability of thin walled elastic shells and applications to space vehicle control problems NASA-CR-949 c32 N68-23453 co2 N68-23455 Control and stability aspects prior to spacecraft landing, and propulsive assist to landing spacecraft NASA-CR-946 c31 N68-24945 CONTROL SURFACES Aeroelastic divergence characteristics of moveable control surfaces, including drag loadings NASA-TN-D-4793 c32 NG c32 N68-35496 CONTROL VALVES Adverse effects of liquid propellant leakage past control valves in vacuum environment NASA-CR-1047 c27 N68-21893 c27 N68-21893 CONTROLLABILITY Handling qualities, disturbances and reentry corridor boundaries for spacecraft control system design system design NASA-CR-945 Variable-stability helicopter flight tests under instrument flight rules to determine effects of gross changes in longitudinal static stability for V/STOL handling qualities NASA-TN-D-4364 C02 N68-1916 c32 N68-11133 c02 N68-19184 NASA-TN-D-4364 c02 N68-1918 Flight simulator to evaluate lateral-directional handling qualities of piloted reentry vehicles NASA-TN-D-4410 c31 N68-1922 CONTROLLED ATMOSPHERES Contamination control principles MASA-CD-50A5 c11 N68-1039 c31 N68-19226 NASA-SP-5045 c11 N68-10384

NASA-TN-D-4849 c03 N68-37162 CONVECTIVE HEAT TRANSFER Convective heat exchange in homogeneous gas media, including heat exchange in homogeneous gas media, including heat transfer and friction resistance in pipes, hydrodynamics and heat transfer in jets, and intensification of convection NASA-TT-F-431 c33 N68-1172 c33 N68-11721 MADA-11-F-401 Convective stagnation heat transfer of carbon dioxide, nitrogen-argon gas mixtures compared to air in shock tube tests NASA-TN-D-4255 C33 N68-11811 One dimensional, steady state heat exchange by both convection and radiation between rods or fins and their surroundings NASA-TN-D-4257 c33 N68-14 c33 N68-14052 Single correlating equation for single phase forced convection heat transfer coefficients for turbulent flow through tubes over wide ranges of temperature ratios NASA-TN-D-4332 NASA-TN-D-4332 c33 N68-14240 Convective heat transfer data for water flow in heated circular tubes with varying heat fluxes and flow areas NASA-TM-X-1554 c33 N68-20338 Heat transfer correlation for nitrogen flowing across electrically heated banks of wire meshes or tubes NASA-TN-D-4514 c33 N68-20374 Convective heat transfer coefficients on adiabatic walls determined by sinusoidally forced fluid temperature NASA-TM-X-1594 c33 N68-24618 Radiative and convective heating during atmospheric entry NASA-CR-1170 c33 N68-35248 CONVERGENCE Converging flow effects on longitudinal stability measurements in tandem test section of wind tunnel NASA-CR-1198 c11 N68-36522 CONVERGENT-DIVERGENT NOZZLES Performance evaluation of annular plug and expansion-deflection nozzles including external flow effects at transonic Mach numbers NASA-TN-D-4462 c01 N68-20330 COOLING Transient chilldown of thick-walled tube simulating-nuclear rocket using liquid and gaseous hydrogen мнан-IN-D-4238 c33 N68-10368 Postshutdown cooling requirements of tungsten water moderated nuclear rocket engines NASA-TM-X-1568 c22 N68-2333 LING FM= COOLING FINS Effect of finned-tube assembly techniques on heat transfer characteristics of space radiator NASA-TM-X-1557 c33 N68 c33 N68-21704 Derating characteristics and limits of vapor chamber fins or heat pipes NASA-CR-1139 c33 N68c33 N68-33203 COOLING SYSTEMS Weight, heat transfer, and efficiency comparison for Rankine cycle space radiators constructed of three different finned tube geometries NASA-TN-D-4411 c33 N68-16324 Parametric mass analysis and comparison of two reactant cooling and storage units for lunar based hydrogen oxygen regenerative fuel cell system NASA-TN-D-4386 c03 N68-16631 Liquid shroud cryogenic supercritical pressure storage system for space applications NASA-CR-1048 c0 c03 N68-22842 COPPER Cyclic incident radiation method for measuring thermal emittance and absorption properties of metals at cryogenic temperatures NASA-TM-X-1618 c33 N68-314 c33 N68-31498 COPPER COMPOUNDS Organic additives and concentration effects on radiation induced reduction of copper salts in aqueous solution NASA-TN-D-4451 COPPER SULFIDES c06 N68-19434 Spectral response of cuprous sulfide-cadmium sulfide film photovoltaic cell to green light NASA-TN-D-4333 c03 N68-14082 CORNERS FORTRAN program for approximate calculation of

sonic corners NASA-TN-D-4563 c01 N68-25093 CORRELATION COEFFICIENTS Single correlating equation for single phase forced convection heat transfer coefficients for turbulent flow through tubes over wide ranges of temperature ratios NASA-TN-D-4332 c33 N68-14240 Two channel transient voltage digitizer for correlation of transient spectra with performance in coaxial, argon plasma guns NASA-TN-D-4385 Scalar and component wind correlations between altitude levels for statistical analysis of wind profiles at Cape Kennedy, Florida, and Santa Monica, California NASA-TN-D-3815 Heat transfer correlation for nitrogen flowing across electrically heated banks of wire meshes or tubes NASA-TN-D-4514 c33 N68-20374 Correlation of lunar radii estimates obtained from earth based photographic study and lunar orbiter gravitational field coefficient measures NASA-TN-D-4636 c30 N68-28409 CORROSION Mechanism and kinetics of iron and cobalt alloys corrosion in refluxing mercury NASA-TN-D-4450 c17 N68-21654 NASA-IN-D-4450 C17 N68-21 CORROSION PREVENTION Protective coatings and surface treatments for protection of Ti-8Al-IMo-IV alloy sheet from hot-salt stress corrosion NASA-TN-D-4319 c17 N68-17 c17 N68-17377 Supplement to NASA bibliography on lubrication, corrosion resistance to cavitation flow c15 N68-31522 NR5A-TM-X-1573 Corrosion resistance tests for compatibility of several iron, cobalt, and nickel based alloys with refluxing potassium NASA-TM-X-1617 ROSION Frere CORROSION TESTS Corrosion products of oxygen doped tantalum exposed to potassium at 1800 deg F exposed to porassium a. c17 N68-11511 NASA-TN-D-4213 c17 N68-11511 Oxidation resistant alloys tested for suitability as transpiration cooled gas turbine blades c17 N68-17591 c17 N68-17591 NASA-CK-930 cl7 N68-17 Corrosion resistance tests for compatibility of several fron, cobalt, and nickel based alloys with refluxing potassium NASA-TM-X-1617 cl7 N68-30 c17 N68-30065 Design, fabrication and testing of Cb-1Zr thermal convection loop for evaluation of refractory metals in boiling and condensing potassium environments NASA-CR-1097 c22 N68-35153 COSMIC NOISE Radio Astronomy Explorer satellite radiometer for measuring cosmic noise in vicinity of 100 meter wavelengths NASA-TN-D-4634 c14 N68-28327 COST ESTIMATES Cost effectiveness studies on structural design of future aerospace systems NASA-CR-1068 c34 N68-26813 COSTS Trajectory optimization by direct descent to minimum cost using iterative computer solutions NASA-CR-1070 c30 N68-2590 c30 N68-25902 Performance requirements and economic costs to reduce cruise sonic boom of supersonic transport NASA-TN-D-4677 c02 N68-28831 c02 N68-28831 COUETTE FLOW Rarefied gas couette flow and heat transfer between parallel plates analyzed by model sampling procedures NASA-TN-D-4579 cl2 NG c12 N68-24129 COUNTERFLOW MIERFLUW Mathematical model for deriving pressure drop against flow function of counterflow boiler tube in Rankine space power system NASA-TN-D-4498 c33 N68-20066

supersonic ideal gas flow past blunt bodies with

COUPLING

SUBJECT INDEX

COUPLING. Fourier series expansion of simultaneous integral equations for collinear coupled waveguides radiating through common perfectly conducting ground plane NASA-TN-D-4656 COUPLING CIRCUITS c09 N68-28668 Integrated circuit, direct coupled, differential amplifier for spacecraft signal conditioning NASA-TN-D-4584 c07 N68-2 c07 N68-24845 COWLINGS Wind tunnel investigation of techniques for reducing cowl drag of external compression inlet at Mach 2.49 NASA-TM-X-1516 coll N68-18189 Acoustic measurements on jet engine intake system noise reduction suppressor cowlings NASA-TN-D-4639 c02 N68-29887 CRACK INITIATION Stress corresion cracking of titanium aluminum vanadium alloy in nitrogen tetroxide under pressure NASA-TN-D-4289 CRACK PROPAGATION c17 N68-12891 Characteristics of 7079 aluminum alloys in underage, peak age, and overaged conditions NASA-CR-996 c32 N68-15476 Residual static strength and slow crack growth behavior of duplex annealed Ti-8A1-1Mo-1V sheet NASA-TN-D-4358 c32 N68-17588 Crack propagation in aluminum notched tensile and pressure vessel specimens cyclically loaded at cryogenic temperatures NASA-TN-D-4541 c17 N68-21768 nnsh-in-1-4341 Prediction of fatigue crack propagation behavior in aluminum alloy panels with simulated rivet forces NASA-TN-D-4702 c32 N68-32074 Ultrasonic detection and measurement of fatigue crack propagation in notched specimens of aluminum, titanium, and cobalt alloys and maraging steels NASA-TN-D-4782 c32 NG c32 N68-35071 Ratigue crack propagation in cylindrical shells with fluctuating internal pressure NASA-CR-1197 c32 N68-37840 NASA-CR-1197 CRACKING (FRACTURING) Hot salt stress corrosion cracking effects on tensile properties of titanium alloy sheets CLAR - D-4674 C17 N68-30000 CREEP ANALYSIS Constant creep data accumulation for design stress analysis on cladding material thickness around cylindrical reactor fuel element NASA-TN-D-4352 CREEP RUPTURE STRENGTH c22 N68-26764 High temperature creep rupture strength of tungsten uranium dioxide cermets NASA-TM-X-1625 c17 N68-29987 High temperature research on creep rupture strength of refractory metal fiber and nickel alloy composites NASA-TN-D-4787 c17 N68-33 CREEP STRENGTH c17 N68-33684 Creep behavior of tantalum alloys in ultrahigh vacuum for extended time periods NASA-TN-D-4605 c17 N68-24111 CREEP TESTS Creep test data on refractory metal alloys for use in spacecraft power supply systems NASA-CR-1115 c17 N68-2 c17 N68-29992 CRITICAL MASS Critical experiments analysis of uranyl fluoride solution reactors containing large-diameter voided tubes NASA-TN-D-4270 c22 N68-15197 CRITICAL VELOCITY Critical speed of flexibily mounted rigid rotors in undampened bearings NASA-TN-D-4607 c32 N68-25421 Critical speed analysis of rigid rotors on flexible foundations NASA-TN-D-4858 c15 N68-37214 CRUCIBLES Crucible melting and arc melting of aluminum nitride and determination of its melting point NASA-CR-1171 c17 N68-33335 CRUISING FLIGHT Wind tunnel tests of deflected slipstream cruise fan V/STOL aircraft wing NASA-TN-D-4262 CRYOGENIC EQUIPMENT c01 N68-11036 Design and construction of prototype spacecraft cryogenic refrigerator for infrared detector cooling NASA-CR-988 c23 N68-13115 Tensile strength properties of glass, boron, and graphite filament wound resin composites and liners for cryogenic pressure vessels NASA-TN-D-4412 cli c18 N68-16623 NHOR-IN-J-4412 CLB NOB-16623 Pressure rise characteristics of liquid hydrogen dewar for homogeneous, normal-gravity quiescent, and zero-gravity tests NASA-TM-X-1134 c33 N68-18196 c33 N68-18196 Platinum resistance thermometers tested and evaluated in cryogenic temperature measurement NASA-TN-D-4499 c14 N68-203 c14 N68-20324 CRYDGENIC FLUID STORAGE AGENIC FLUID STORAGE Evaluation of self-evacuating multilayer radiation shields for cryogenic storage tanks NASA-TN-D-4375 c33 N68-18046 Cryogenic flexibility of single and multiple plies of thin polymeric films tested at minus 320 deg and minus 423 deg F NASA-TM-X-1555 c18 N68-20329 Liquid shroud cryogenic supercritical pressure storage system for space applications NASA-CR-1048 c0 c03 N68-22842 c03 N68-28420 NASA-TN-D-4619 CRYOGENIC FLUIDS Friction and wear in cryogenic liquids for phenolic and polytetrafluoroethylene composites of various particle sizes and concentrations NASA-TN-D-4565 c15 N68-24142 c15 N68-24142 Fuel tank pressurization and supercooling of liquid methane to minimize fuel boiloff problems in supersonic aircraft NASA-TM-X-1604 c27 N68-28155 CRYOGENIC ROCKET PROPELLANTS Cryogenic propellant management during coasting of Atlas Centaur vehicles NASA-TN-D-4571 c28 N68-25099 Successful engine restart in space of upper stage vehicle using cryogenic propellants NASA-TM-X-1649 NASA-TM-X-1649 c31 N68-33683 Development, configuration, and operation of Centaur propellant utilization system NASA-TN-D-4848 c2 c28 N68-36507 CRYDGENIC STORAGE Development, ground tests, and flight performance of cryogenic nitrogen storage system for low gravity operation during Apollo-Saturn space flight NASA-TN-D-4293 CRYSTAL DEFECTS c23 N68-15950 Defect energy levels and concentrations for proton irradiated, n-type silicon single crystals NASA-TN-D-4830 c26 N68-37051 CRYSTAL GROWTH In situ electron microscopy for studying vapor deposition nucleation processes NASA-TN-D-4506 c06 N68-2 c06 N68-21430 CRYSTAL LATTICES Lattice structures in solution NASA-TN-D-4297 c06 N68-18219 CRYSTAL OPTICS Laser modulated bulk optical absorption in cadmium sulfide single crystals c26 N68-18772 NASA-TN-D-4466 CRYSTAL STRUCTURE Lattice structures in solution NASA-TN-D-4297 c06 N68-18219 Influence of crystal structure, orientation, and solubility on adhesion and sliding friction of metal single crystals in vacuum NASA-TN-D-4347 c15 N68-21226 Crystal transformation and atomic ordering on wear and sliding friction in two cobalt alloys NASA-TN-D-4668 c15 N68-28260 CRYSTAL SURFACES Techniques for, and applications of preferential etching of crystal surfaces to produce optical

alignment in silicon crystals NASA-TN-D-4187 reflections for crystal orientation and optical c23 N68-10354 NASA-IN-D-4167 Low energy electron diffraction study of oxygen adsorption on molybdenum /111/ surface NASA-IN-D-4735 c06 N68-305 c06 N68-30582 CRYSTALLOGRAPHY Fitzgeralds piezoelectric disk and theory on audio frequency resonances and sound beams in crystals NASA-TN-D-4625 c23 N68-28259 CULTURE TECHNIQUES Cell culture method of screening contaminants which may appear in manned spacecraft NASA-TN-D-4251 c04 N68-3 c04 N68-10122 CUMULUS CLOUDS Cumulus cloud and fog bank spectral reflectance observations using Nimbus satellites and infrared radiometers NASA-TN-D-4552 c14 N68-25862 CURVED PANELS Pressure and heat transfer on blunt concave and convex plates in hypersonic flow NASA-TN-D-4367 c12 N68-18253 CYBERNETICS Design and application potentials of general purpose, dexterous, cybernetic machines for human augmentation NASA-SP-5047 to today constant of the second sec c05 N68-18870 CYCLIC LOADS Crack propagation in aluminum notched tensile and pressure vessel specimens cyclically loaded at cryogenic temperatures NASA-TN-D-4541 c17 N68-21768 NB3A-IN-D-4541 C17 N68-2. Cyclic frequency, tensile fatigue effects, and defect substructure generated in vacuum by fatigue stressing of aluminum NASA-CR-1165 c17 N68-3: c17 N68-35200 CYLINDRICAL BODIES Torsional model development and model calculations for cylindrical space vehicle systems and systems employing clustered tanks NASA-CR-937 c32 N68-10568 NASA-CR-957 CO2 N Survey on minimum weight design aspects of stiffened cylinders under compression NASA-CR-963 C32 N c32 N68-11282 Cone-cylinder models tested in supersonic wind tunnel to evaluate effect of wall reflected disturbances on model pressure distributions NASA-TM-X-1655 coll N68-36134 Flexibility effects on lift and pitching moments low aspect ratio delta wing-conical of cylindrical body combinations at transonic speeds NASA-TN-D-4655 c01 N68-37065 Vibration modal response of thin cylindrical shells NASA-CR-897 c32 N68-11967 Nonlinear flutter of circular cylindrical shell in supersonic flow NASA-TN-D-4265 c32 N68-12864 Resonant frequencies and nodal pattern modes of vibrating cylindrical and conical frustum shells NASA-TN-D-4428 c32 N68-20954 Imperfections of axially loaded cylindrical shells NASA-TM-X-1552 c32 N68-21767 Liapunov method used to obtain sufficient conditions for buckling stability of long cylindrical shells with random imperfections NASA-CR-1161 c32 N68-33419 Vibration tests and analysis of thin cylindrical shells with and without longitudinal stiffener: NASA-TN-D-4705 c32 N68-337 c32 N68-33738 Imperfection survey data on cylindrical shells before and during axial compression loading up to buckling load NASA-CR-1163 c32 N68-35199 Fatigue crack propagation in cylindrical shells with fluctuating internal pressure NASA-CR-1197 c32 N68-378 CYLINDRICAL TANKS Effects of shallow liquid depths on lateral sloshing in cylindrical tanks under weightless c32 N68-37840 conditions NASA-TN-D-4458 c12 N68-24758 Liquid-vapor interface stability during liquid inflow in cylindrical tank during weightlessness NASA-TN-D-4628 c12 N68-25866 D

DAMPING Friction and fretting wear tests on materials used as friction dampers to reduce vibrational stresses in compressor blades for turbine engines NASA-TN-D-4630 c15 N68-28871 DATA ACQUISITION Mariner-Mars 1964 mission accomplishments NASA-SP-139 c31 c31 N68-18743 Data collection and processing from space science satellites NASA-TN-D-4508 c08 N68-22510 Performance characteristics of data acquisition flight test sensors used on X-15 aircraft NASA-TN-D-4597 c14 N68-25317 DATA CORRELATION Data correlation of thermophysical properties of saturated liquid lithium as function of temperature NASA-TN-D-4650 c17 N68-28365 DATA PROCESSING Error model for Doppler range rate and phase modulated range tracking system for which data weighting factors can be obtained for use in space vehicle trajectory analysis NASA-TN-D-4267 c10 N68-11513 Surveyor 6 scientific data analysis NASA-SP-166 c31 N68-21443 Data collection and processing from space science satellites NASA-TN-D-4508 c08 N68-22510 Computer programming for control of complex data processing operations involved in analysis and interpretation of large volumes of sensor data from scientific satellites NASA-CR-1107 c08 N68-37254 DATA PROCESSING EQUIPMENT 64 inch scattering chamber digital readout and control system for automatic processing of angle and experimental data NASA-TN-D-4324 c14 N68-14018 Dual detection system for processing AIMP satellite pulse frequency modulated telemetry data NASA-TN-D-4561 c08 N68-24310 DATA RECORDING A RECORDING Signal conditioning methods and equipment used for inflight recording of pilot biomedical data NASA-TN-D-4487 c05 N68-21538 NASA-TN-D-4487 DATA REDUCTION Spirometer modification to permit computer reduction of respiratory flow data NASA-TN-D-4234 c14 N c14 N68-10057 Ballistic camera data reduction methods for determining reentry body position, velocity, and deceleration NASA-TN-D-4260 c30 N68-1114 Logarithmic encoding procedure and error analysis c30 N68-11145 for binary word compression NASA-TN-D-4290 c08 N68-18179 Boundary layer and wake survey data reduction techniques in compressible flows NASA-TN-D-4401 c12 N68-19709 Surveyor 6 scientific data analysis NASA-SP-166 c31 N68-21443 Least squares determination of frequency, damping ratio, amplitude, and phase angle from free oscillation data NASA-TN-D-4503 c19 N68c19 N68-25869 Computer programming for control of complex data processing operations involved in analysis and interpretation of large volumes of sensor data from scientific satellites NASA-CR-1107 c08 N68-37254 DATA SYSTEMS FM data handling facility for preparing analog physiological data obtained in flight for http://www.actionsupersonalistics/actions/ NASA-TN-D-4488 c05 N Hydra 1 data display system for developing c05 N68-21537 graphic displays NASA-TN-D-4554 c08 N68-25002 Advanced multiprocessor computer organization for manned Mars lander mission NASA-CR-1159 c08 N68-35560 c08 N68-35560

DATA TRANSMISSION

DATA TRANSMISSION Mathematical model of statistical channel characteristics in, and test instrumentation for, digital data transmission systems handling uniformly coded binary data NASA-TT-F-434 c07 N68-17542 Data relay and tracking capability of lunar communication satellites above lunar far side surface NASA-TN-D-4509 DECISION THEORY c31 N68-25358 Dynamic programming and multistage decision processes in guidance, flight mechanics, and trajectory optimization NASA-CR-1009 c30 N68-2: c30 N68-21077 DECODING and block codes with threshold decoding for space telemetry NASA-TN-D-4402 c07 N68-18178 DEFECTS Buckling of conical shells under axial compression and effects of axially symmetric defects c32 N68-35198 NASA-CR-1162 nnon-G-1102 C32 N68-35 Imperfection survey data on cylindrical shells before and during axial compression loading up to buckling load NASA-CR-1163 C32 N68-35 c32 N68-35199 DEFLECTION Load relief autopilot to minimize launch vehicle thrust vector deflection angle required for vehicle stability during flight through design winds NASA-TN-D-4786 c21 N68-33756 DEFORMATION CORMATION Prebuckling deformations, and ring stiffener effects on buckling load of eccentrically stiffened orthotropic cylinders NASA-TN-D-4283 c32 N68 c32 N68-14091 Iterative solution for calculating deformation and stress concentration near slits in elastic-plastic solids NASA-TN-D-4717 DEGREES OF FREEDOM c32 N68-30045 Least squares determination of frequency, damping ratio, amplitude, and phase angle from free oscillation data NASA-TN-D-4503 c19 N68-25869 DELAMINATING Aerodynamic heating, delamination and pressure in nose fairing honeycomb core of Atlas Centaur launch vehicle NASA-TM-X-1605 c33 N68-28156 DELTA WINGS Simulated flight test of double-Delta supersonic transport for performance characteristics, handling qualities, and climbing characteristics NASA-TN-D-4396 co2 N68-17391 Sharp edge delta wing drag prediction by application of leading edge suction analogy of vortex lift NASA-TN-D-4739 c01 N68-31990 Flexibility effects on lift and pitching moments of low aspect ratio delta wing-conical-cylindrical body combinations at transonic speeds NASA-TN-D-4655 DENSITY DISTRIBUTION c01 N68-37065 Velocity and density profiles in mixing region between adjacent half jets of dissimilar fluids NASA-CR-957 c12 N68-1557 c12 N68-15571 Models of Martian atmosphere based on minimum, mean, and maximum density profiles NASA-SP-8010 c30 N68-37220 DENSITY MEASUREMENT Axial turbulence measurements in coaxial flow of dissimilar gases NASA-CR-960 c12 N68-13612 DEPLOYMENT Deployment characteristics of dynamic and elastic parawing scale model for spacecraft recovery NASA-TN-D-4724 c02 N68-3 c02 N68-33879 DESCENT TRAJECTORIES Trajectory optimization by direct descent to minimum cost using iterative computer solutions NASA-CR-1070 c30 N68-2590 c30 N68-25902 Semigraphical method to aid selection of descent

trajectory compatible with mission constraints NASA-TN-D-4801 c30 N68-36077

SUBJECT INDEX

DESORPTION Equations for determining substrate surface coverages from arrival rates and desorption characteristics of adsorbate ions and atoms c25 N68-25630 NASA-TN-D-4369 Adsorption isotherm relations and transient desorption behavior of homogeneous and heterogeneous metal surfaces NASA-TN-D-4789 c24 c24 N68-34175 DEUTERIUM Ages for D-D and D-T neutrons in water and tungsten-water mixtures NASA-TN-D-4581 c22 N68-25058 DIAGRAMS Helicopter height-velocity diagram analysis showing effects of density altitude and gross weight c02 N68-22033 NASA-TN-D-4536 Computer program for symbolic reduction of block diagrams to obtain transfer functions NASA-TN-D-4617 DIATOMIC MOLECULES c08 N68-24967 Quantum mechanical study of transition probabilities, Einstein A coefficients, and oscillator strengths of band systems of diatomic molecules NASA-CR-975 c24 N68-11037 Physical gas dynamics research - molecular band spectra, shock tube studies, and interactions between diatomic molecules NASA-TT-F-505 c12 N68-168 c12 N68-16839 DIELECTRIC PROPERTIES Dielectric formulation for inhomogeneous electron gas, and Green function formalism for treating static dielectric screening of point impurity in electron gas c26 N68-24273 NASA-TR-R-283 nnan-ix-x-263 c26 N68-242 Electron radiation induced dielectric breakdowns in capacitor meteoroid detection system NASA-TN-D-4738 c14 N68-332 DIELECTRICS c14 N68-33277 Pyrolytic silicon nitride dielectric for integrated circuits NASA-CR-995 c18 N68-18849 Dielectric temperature change effects observed in ferroelectric and pyroelectric substances NASA-CR-1080 c26 N6 c26 N68-25972 Dieletric clad axial slot antennas NASA-CR-1057 c07 N68-26621 Reflection coefficient and admittance of circular aperture in ground plane covered by dielectric or plasma slab NASA-CR-1177 c25 N68-35171 Fourier integration of electrical impedance expressions for nonlossy dielectric and lossy plamas NASA-TN-D-4774 c07 N68-35524 Electrical impedance and radiation distributions of circular waveguide by integral transformation NASA-TN-D-4752 c07 N68-35537 Analysis of dielectric breakdowns induced by electron irradiation in polymeric films NASA-TN-D-4810 c24 l c24 N68-36070 DIFFERENTIAL AMPLIFIERS Integrated circuit, direct coupled, differential amplifier for spacecraft signal conditioning NASA-TN-D-4584 DIFFERENTIAL CALCULUS c07 N68-24845 General Lagrangian interpolation formulas NASA-TN-D-4424 c19 DIFFERENTIAL EQUATIONS c19 N68-22809 Perturbation techniques for error analysis of finite difference approximations for linear differential equations NASA-TN-D-4372 c32 N68-17068 coupled nonlinear ordinary differential equations with parasitic eignevalues NASA-TN-D-4547 c19 N c19 N68-21978 Differential equations based on heat transfer and shear for temperature and velocity in turbulent boundary layers NASA-TN-D-4611 c33 N68-25917 Numerical methods for integrating nonlinear differential equations with parasitic eigenvalues NASA-TN-D-4703 c19 N68-29275 Qualitative theory of differential equations and

conversion to integral equations NASA-CR-1164 c19 N68-33426

Systems analysis logic applied to mathematical modeling of dynamic nonlinear stochastic processes NASA-CR-1168 c19 N68~35472 DIFFERENTIAL THERMAL ANALYSIS Thermal design and analysis of cesium contact-ion microthrustor NASA-TM-X-1473 c28 N68-10496 DIFFUSERS Experimental performance evaluation of radial inflow turbine with exit diffuser NASA-TM-X-1480 c03 N68c03 N68-11920 Diffusers for in-flight calibration of detectors installed in spacecraft c14 N68-12669 NASA-CR-987 Efficiency, mass flow rate, torque, and exit diffuser effectiveness of 5-inch axial flow turbine NASA-TM-X-1679 c03 N68-37263 DIFFUSION Electron paramagnetic resonance of lithium silicon NASA-TR-R-290 DIFFUSION COEFFICIENT c26 N68-33228 Bifurcation approximation for binary and thermal diffusion coefficients, mixture viscosity, and thermal conductivity of laminar boundary layer NASA-CR-1063 c33 N68-26815 Performance of single stage turbine with rotor blade surface diffusion factor of 0.3 NASA-CR-1172 DIFFUSION WELDING c28 N68-32987 Welding of precipitation hardening stainless steels NASA-SP-5087 c15 N68-21429 Electron probe X ray microanalyzer applied to material failure study, bonding, and other metallurgical analysis NASA-TN-D-4526 c15 N68-28249 DIGITAL COMPUTERS Solid-state digitally controlled electroluminescent vertical scale indicators NASA-CR-919 Constructions Digital computer program for prediction of snap buckling of spacecraft shell structures by geometric nonlinear analysis of thin elastic shells of revolution shells of revolution NASA-CR-909 c32 N68-14584 Flexible body analog computer program and rigid body digital computer program for calculating dynamic characteristics of double-V antennas on Radio Astronomy Explorer satellite c08 N68-18144 NASA-CR-962 NASA-CK-962 CUO NUO-10. Properties and imaging techniques of various display devices - computer directed visual flight control boards, integrated optical man machine systems, and electro-optical methods NASA-CK-962 NASA-SP-159 c09 N68-22302 Mathematical properties and computer programs for digital spectrum analyses NASA-TN-D-4203 COB NO Stability criterion for digital simulation NASA-TN-D-4203 COB NO c08 N68-25268 c08 N68-26640 Process development of system for digital computer processing of psychophysiological data to obtain high stress tolerance personnel NASA-CR-1122 c05 N68-35102 DIGITAL DATA Mathematical model of statistical channel characteristics in, and test instrumentation for, digital data transmission systems handling uniformly coded binary data NASA-TT-F-434 c07 N68-1754 c07 N68-17542 DIGITAL NAVIGATION Analog and digital inertial flight data systems for X-15 aircraft NASA-TN-D-4642 c08 N68-29404 DIGITAL SIMULATION Stability criterion for digital simulation NASA-TN-D-4203 c08 N DIGITAL TECHNIQUES c08 N68-26640 64 inch scattering chamber digital readout and control system for automatic processing of angle and experimental data and experimental data NASA-TN-D-43824 Two channel transient voltage digitizer for correlation of transient spectra with performance in coaxial, argon plasma guns NASA-TN-D-4385 c25 N68-17070

gradient satellites NASA-CR-1119 c30 N68-32744 DILUTION Dilution-jet mixing flow studies for gas turbine combustion chambers NASA-TN-D-4695 c01 N68-30128 DIMENSIONAL ANALYSIS Similarity parameters used for examining geometry characteristics of axial flow turbines with high expansion ratio NASA-TN-D-4248 c01 N68-10529 Dimensional analysis, and similitude and scaling laws for structural dynamics model testing of spacecraft dynamic stability NASA-CR-1195 c32 N68-3563 c32 N68-35632 DIODES High temperature tests on cesium diodes and vapor filled thyratrons NASA-CR-994 c09 N68-15892 Current-voltage characteristics of collisionless cylindrical diode with thermionically emitted electrons NASA-TN-D-4516 c10 N68-21122 Suppression of temperature rise in lossy diodes inside resonant cavities by pressurized liquid nitrogen NASA-TN-D-4556 c09 N68-24387 Effects of nuclear radiation on performance of diodes for use in SNAP 8 NASA-TN-D-4620 c09 N68-26662 Thermionic reactor core with short-length externally fueled diodes, and electrical failure analysis NASA-TN-D-4805 c22 N68-34087 DIRECT CURRENT Electrical properties of direct current compact arc in argon under varying pressures, amperages, and electrode spacing NASA-TM-X-1596 c29 N68-25818 DIRECTIONAL CONTROL Effect of wheel braking on directional control of pneumatic tires on pavement NASA-TN-D-4602 c02 N68-2531: DIRECTIONAL STABILITY c02 N68-25313 DIRECTIONAL STABILITY Longitudinal, lateral, and directional stability and control characteristics of lifting entry vehicle at Mach number of 19 NASA-TN-D-4337 DISCRETE FUNCTIONS c31 N68-16240 Discrete ordinate computation of fission spectrum neutron dose rate attenuation of fission spectrum hydrides and tungsten NASA-TN-D-4684 c24 N68-3000 c24 N68-30001 DISPERSIONS Electron microscopy technique for determining dispersoid distribution in powder blends NASA-TM-X-1468 c17 N68-10051 DISPLAY DEVICES Evaluating closed circuit television display in helicopter landing operations NASA-TN-D-4313 c05 N68-16594 Properties and imaging techniques of various display devices - computer directed visual flight control boards, integrated optical man machine systems, and electro-optical methods NASA-SP-159 c09 N68-22302 Hydra 1 data display system for developing graphic displays NASA-TN-D-4554 c08 N68-25002 Pilot performance using compensatory and pursuit tracking displays with rate and acceleration control dynamics and disturbance input NASA-CR-1082 c07 N68-28272 Visual information display systems that are computer connected or updated with computer generated information NASA-SP-5049 c08 N68-32159 Performance comparison of electromechanical and electroluminescent displays in closed loop manual tracking task and reading accuracy tests NASA-TN-D-4841 c05 N68-36457 DISSOCIATION Boundary layer buildup effects in shock tubes on dissociation rate measurements c12 N68-34089 NASA-TN-D-4795 DOSIMETERS

Gamma ray exposure rates in Plum Brook HB-6 facility measured with dosimeters and ion chambers

Digital program for dynamics of nonrigid gravity

c22 N68-17022 NASA-TM-X-1490 DRAG Unmanned Mars probe tested for drag, lift, static and dynamic stability at Mach number 2 NASA-TN-D-4291 col N68-11936 Aeroelastic divergence characteristics of moveable control surfaces, including drag loadings NASA-TN-D-4793 c32 NG c32 N68-35496 DRAG DEVICES Aerodynamic characteristics of tension string, tension shell, and conical shapes in supersonic flow NASA-TN-D-4360 c01 N68-18720 DRAG MEASUREMENT Sharp edge delta wing drag prediction by application of leading edge suction analogy of vortex lift NASA-TN-D-4739 c01 N68-31990 Acrodynamic drag measurements and boundary layer flow over V notches at transonic and supersonic speeds NASA-CR-1132 DRAG REDUCTION c12 N68-35252 Wind tunnel investigation of techniques for reducing cowl drag of external compression inlet at Mach 2.49 NASA-TM-X-1516 c01 N68-18189 Body alterations for reducing drag of missiles during coasting flight NASA-TM-X-1537 c01 N68-19206 DRAWINGS FORTRAN subroutines for plotting and drawing of three dimensional solid surfaces NASA-TM-X-1598 c19 N68-28240 DROP STZE Maximum drop diameters for atomization of liquid jets injected concurrently into accelerating or decelerating gas streams NASA-TN-D-4640 c12 N68-28364 c12 N68-28364 DROP TESTS Scale factors verification for parawing opening characteristics using experimental drop tests NASA-TN-D-4665 c02 N68-31956 Drop tower investigation of liquid reorientation in spherical containers NASA-TM-X-1659 c12 N68-351 c12 N68-35114 Drop test study on isothermal liquid-vapor interface configuration during weightlessness in toroidal shell NASA-TN-D-4819 c12 N68-35823 DROPS (LIQUIDS) Shapes of liquid drops resting on flat surfaces determined by Runge-Kutta solution of Laplace capillary equation NASA-TN-D-4779 c12 N68-33165 DUCTILITY Chromium alloys with good low temperature ductility and superplasticity NASA-TN-D-4346 c14 N68-13973 Oxidation resistance and ductility of cobalt heat resistant alloys optimized by restriction of silicon and manganese content NASA-TN-D-4715 c17 N68-29954 DUCTS FORTRAN subroutines for determining intersections of nuclear particle flight path and wall of helical tubular duct NASA-TN-D-4435 c22 N68-18541 DURABIL ITY Two stage potassium vapor turbine - materials support of performance and endurance tests NASA-CR-925 co3 N68-3 c03 N68-16351 DUST Physical properties and applications of dust structures in space technology NASA-CR-1136 c32 N68-32976 DYNAMIC CHARACTERISTICS Pressure rise characteristics of liquid hydrogen dewar for homogeneous, normal-gravity quiescent, and zero-gravity tests NASA-TM-X-1134 c33 N68-18196 Dynamic characteristics of parasitic loading speed controller for Brayton cycle turboalternator NASA-TM-X-1456 c03 N68-18702 Containment characteristics of radial inflow gases in vortex tubes NASA-CR-1029 c12 N68-22200

beam system NASA-TN-D-4576 c31 N68-31978 Mathematical model for computing equilibrium properties of one dimensional self-gravitating stellar system NASA-TR-R-289 c30 N68-32978 Dynamic response of subsonic inlet to external and internal disturbances NASA-TM-X-1648 c01 N68-33. Electronic visualization technique for studying c01 N68-33374 dynamic behavior of gas journal bearing NASA-TM-X-1609 c14 N68-35105 Static and dynamic characteristics of wind tunnel model of parallel staged reusable launch vehicle during stage separation NASA-TN-D-4765 c31 N68-36106 NB3A-IN-14-4705 Longitudinal dynamic characteristics of Stub D Atlas launch vehicle without propellants or payload NASA-TM-X-1682 DYNAMIC CONTROL c31 N68-37942 Effect of liftoff dynamics on launch vehicle stability and control NASA-CR-943 c32 N68 c32 N68-10233 DYNAMIC LOADS Full scale lunar gravitation simulator and 1/6 scale model NASA-TN-D-4474 c11 N68-25853 DYNAMIC MODELS Combustion instability prediction using nonlinear bipropellant vaporization model NASA-CR-920 c33 N68-15833 Three dimensional motion analysis and vibration characteristics of dynamically scaled model of asymmetrically clustered launch vehicle NASA-TN-D-4707 c32 N68-320 c32 N68-32051 NACATINT 4/07 C32 N68-3205 Dimensional analysis, and similitude and scaling laws for structural dynamics model testing of spacecraft dynamic stability NASA-CR-1195 c32 N68-3563 c32 N68-35632 DYNAMIC PRESSURE Helium and air flow tests over single flat plates to determine dynamic pressure limits of nuclear fuel element plates NASA-TN-D-4417 c12 N68-16227 Turbulent boundary layer effect on panel flutter NAS-TN-D-4486 Signal State of 40 foot parachute deployed at low supersonic speed and dynamic pressure NAS-TM-X-1623 DYNAMIC PROGRAMMING c32 N68-18721 c31 N68-29993 Dynamic programming and multistage decision processes in guidance, flight mechanics, and trajectory optimization NASA-CR-1009 c30 N68-21077 Pontryagin maximum principle, calculus of variations, and dynamic programming optimization techniques applied to trajectory and guidance problems NASA-CR-1014 DYNAMIC RESPONSE c30 N68-21231 Space vehicle and control system dynamic response to atmospheric disturbances NASA-CR-942 c32 N68-11089 Pilot dynamic response to sudden flight control system failures NASA-CR-1087 c05 I Effect of N waves at oblique incidence on c05 N68-26690 response of simply supported plate to transient loads NASA-CR-1176 c32 N68-33168 Dynamic response of subsonic inlet to external and internal disturbances NASA-TM-X-1648 c01 N68-33374 Numerical method for determining transient response of simply supported plate to n waves at normal incidence NASA-CR-1175 c32 N68-33737 DYNAMIC STABILITY Torsional model development and model calculations for cylindrical space vehicle systems and systems employing clustered tanks NASA-CR-937 c32 N68-10568 Unmanned Mars probe tested for drag, lift, static and dynamic stability at Mach number 2 c01 N68-11936 NASA-TN-D-4291 Static and dynamic longitudinal stability tests of fan in wing V/STOL aircraft model NASA-TN-D-4322 c02 N68-15894

DRAG

Dynamic characteristics of satellites having long elastic members by modeling as symmetric double

- Aerodynamic factors, and effects on dynamic longitudinal stability characteristics of tilt wing V/STOL aircraft NASA-TN-D-4344 c02 N68-1594 c02 N68-15941 NA3A-IN-7-4344 Subsonic dynamic stability characteristics of large conical spacecraft in simulated Martian
- environment NASA-TN-D-4558 c31 N68-22301 Recommended procedures for stability, control, and structural loading analysis of large liquid fueled rocket booster sloshing parameters NASA-CR-948 c32 N68-23454
- Wind tunnel test data on static and dynamic
- stability of Apollo command module configuration NASA-TN-D-4688 DYNAMIC STRUCTURAL ANALYSIS c01 N68-31445 Techniques for full-scale dynamic testing of large
 - solid or liquid fueled booster vehicles NASA-CR-940 c32 N68-11054 Digital program for dynamics of nonrigid gravity gradient satellites NASA-CR-1119 c30 N68-32744
 - Dimensional analysis, and similitude and scaling laws for structural dynamics model testing of spacecraft dynamic stability NASA-CR-1195 c32 N68-35632

E

EARTH (PLANET) Stability of selected earth minerals in simulated lunar environment tests NASA-CR-1034 c13 N68-25579 EARTH ATMOSPHERE Analytical methods for dynamic stability analyses of large launch vehicles during flight through and exit from earth atmosphere NASA-CR-944 c32 Evaluation of Nimbus satellite radiation c32 N68-18825 measurements and heat balance charts of earth atmosphere ATMOSPHERE NASA-TN-D-4589 c13 N68-7 EARTH-MARS TRAJECTORIES Planetary gravitation and oblateness used for parking orbit alignment in Mars mission NASA-TN-D-4657 c30 N68-7 c13 N68-28222 c30 N68-28408 EARTH-MOON SYSTEM Manual procedure for midcourse guidance and applications to Earth-Moon trajectories NASA-TN-D-4246 c21 N64 c21 N68-11521 EARTH ORBITS TH UNBITS Assessing cryogenic fluid requirements and storage methods for manned earth orbital and Mars flyby missions, and parametric data on thermal protection schemes NASA-TN-D-4619 c03 N68-2842 Earth orbital vehicle control during entry phase to simulate manned planetary entry c03 N68-28420 NASA-TN-D-4847 c31 N68-36056 EARTH SURFACE Measurement and interpretation of ground vibrations, produced by seismic effect of sonic booa NASA-CR-1137 c13 N68-35151 EARTHQUAKES Geodetic laser system for earthquake prediction and engineering research NASA-SP-5042 c13 N68-23706 ECHO SATELLITES Contour plots tabulated for stress resultants and deformations brought about by sinusoidal in plane line loads acting along great circles of spherical satellites of Echo type NASA-TN-D-4425 c31 N68-2015 c31 N68-20198 ECLIPTIC Atlas-Agena and Atlas-Centaur combined propulsion system for measurements out of three dimensional phenomena out of ecliptic plane NASA-TN-D-4455 c28 N68-19581 ECONOMICS Economic and suitability comparison of short haul transport aircraft concepts NASA-CR-986 c02 N68-13517 Space technology transfer to developing nations using Brazil as model NASA-CR-1222 c34 N68-372 c34 N68-37216 EFFICIENCY Efficiency and steady state performance of

cylindrical thermionic converter with rhenium emitter and niobium collector NASA-TN-D-4582 co3 N68-250 203 N68-25059 EIGENVALUES CONVALUES Computer methods for calculating eigenvalue and eigenvectors of real symmetric matrices arising in problems of molecular quantum mechanics NASA-CR-983 c24 N68-11905 c24 N68-11903 Mathematical models for determining eigenvalue bounds of matrix NASA-TN-D-4373 c19 Nd Explicit numerical methods for integrating c19 N68-17334 coupled nonlinear ordinary differential equations with parasitic eignevalues NASA-TN-D-4547 c19 c19 N68-21978 Numerical methods for integrating nonlinear differential equations with parasitic eigenvalues NASA-TN-D-4703 c19 N68-29275 Systematic procedure for constructing character table of finite group NASA-TN-D-4763 c19 N68-31 c19 N68-31961 EIGENVECTORS Computer methods for calculating eigenvalue and eigenvectors of real symmetric matrices arising in problems of molecular quantum mechanics NASA-CR-983 c24 N68-11903 Systematic procedure for constructing character table of finite group NASA-TN-D-4763 c19 N68-31961 Radiation equilibrium in atmosphere with constant Einstein absorption coefficient NASA-TN-D-4479 c13 N68-22861 EJECTORS Wind tunnel model tests of variable flap ejector nozzle with aerodynamically positioned shroud NASA-TM-X-1639 c28 N68-30599 NASA-TM-X-1639 c28 N68-3059 Heat transfer characteristics of cylindrical ejector for turbojet engine and shroud material temperature prediction c33 N68-3298 Static performance of an auxiliary inlet ejector nozzle for supersonic-cruise aircraft NASA-TM-X-1653 c28 N68-3576 ACTLC PUTE c33 N68-32988 c28 N68-35764 ELASTIC BODIES Classical equations of elasticity in terms of stress components reduced to three stress functions and three equations NASA-TN-D-4253 ELASTIC BUCKLING c19 N68~10355 Elastic buckling equations for calculating plastic buckling of plates and shells under biaxial loading NASA-TN-D-4706 ELASTIC CYLINDERS c32 N68-31946 DILL GILINDERS Theory of finite amplitude waves in fluid-filled elastic tubes, including wave distortion, shock wave propagation, and Korotkoff sounds NASA-TN-D-4803 C12 N68-33050 C12 N68-33050 c12 N68-33056 ELASTIC DEFORMATION Successive approximation procedure for solving elastic-plastic problem for torsion of solid prismatic bar made of strain hardening material NASA-TN-D-4391 c32 N68-17045 ELASTIC PROPERTIES Calculations for elastic tensometric elements and operation of tensometric force measuring devices NASA-TT-F-513 c32 N68-15796 Iterative solution for calculating deformation and stress concentration near slits in elastic-plastic solids NASA-TN-D-4717 c32 N68-30045 ELASTIC SCATTERING Scattering of 42 MeV alpha particles from even cadmium isotopes NASA-TN-D-4256 c24 N68-1 c24 N68-11074 ELASTIC SHELLS Digital computer program for prediction of snap buckling of spacecraft shell structures by geometric nonlinear analysis of thin elastic shells of revolution NASA-CR-909 c32 N68-14584 Dynamic stability of thin walled elastic shells and applications to space vehicle control problems NASA-CR-949 c32 N6 c32 N68-23453 ELASTIC WAVES Theory of finite amplitude waves in fluid-filled elastic tubes, including wave distortion, shock

ELASTOPLASTICITY

wave propagation, and Korotkoff sounds NASA-TN-D-4803 cl2 N68-33056 ELASTOPLASTICITY Elastoplastic analysis of circular cylindrical inclusion in uniformly stressed infinite homogeneous matrices of composite materials for aerospace applications NASA-TN-D-4350 c32 N68-15769 ELECTRIC ARCS Metal cathodes in argon atmospheres used to stabilize dc arcs for spectrochemical analysis NASA-TN-D-4236 c06 N68-11512 Coaxial flow stabilized ac arc facility c25 N68-20296 NASA-TN-D-4517 Electrical properties of direct current compact arc in argon under varying pressures, amperages, and electrode spacing NASA-TM-X-1596 c29 N68-25818 Mathematical model based on conformal mapping of shape of electric arc balanced in transverse convective and magnetic fields NASA-TN-D-4736 c25 N68-30784 Servecontroller for programming atomic emission and sample vaporization in direct current arc spectrochemical analysis NASA-TN-D-4769 c06 N68-31948 Analog simulation of dc arc emission spectrometer control system to define optimum control requirements NASA-TN-D-4770 ELECTRIC CHARGE c08 N68-32055 Cable and circuit parameters effects on calibration of charge amplifier for microsecond pulses NASA-TN-D-4300 c09 N68-16530 ELECTRIC CONDUCTORS Equipment specifications and electrical properties of flat conductor cable systems NASA-SP-5043 c09 N68-28870 ELECTRIC CONTACTS Summary data on deposition and endurance lives of thin metallic films used for lubricating sliding and rolling element electrical contacts in vacuum environments NASA-TN-D-4476 c15 N68-21979 ELECTRIC CURRENT Numerical analysis of electric current and potential distributions in linear Faraday plasma accelerators NASA-TN-D-4239 c28 N68-10502 ELECTRIC DISCHARGES Improved service life through reduction of self discharges in copper oxide-magnesium thermal cells NASA-TN-D-4306 c03 N68-20344 ELECTRIC ENERGY STORAGE Lunar surface layer considered to store solar energy for generating power during lunar night NASA-TM-X-1560 c03 N68-20363 ELECTRIC FIELDS Electric field of free atmosphere NASA-TT-F-425 c13 N68-10079 Cesium ion beam electric field measuring instruments NASA-CR-970 c14 N68-25903 ELECTRIC GENERATORS Cobalt-tungsten ferromagnetic, high temperature structural alloy for rotor applications in space power generators NASA-TN-D-4338 c17 N68-18145 ELECTRIC NETWORKS Formula for expanding higher order derivatives of function tanh z in powers of tanh z and A-numbers NASA-TN-D-4296 c19 N68-14077 ELECTRIC POTENTIAL Magnitude of electrical potential-temperature curve determined for tantalum, niobium, and magnesium during oxidation in air NASA-TN-D-4240 c17 N68-10498 Numerical analysis of electric current and potential distributions in linear Faraday plasma accelerators NASA-TN-D-4239 c28 N68-10502 Current-voltage characteristics of variable spaced thermionic converter with tungsten

emitter and nicbium collector NASA-CR-1033 c03 N68-23476

SUBJECT INDEX

ELECTRIC POWER PLANTS Electromagnetic pump designs for use as boiler feed pumps in Rankine cycle, space electric power plants NASA-CR-911 c15 N68-10503 ELECTRIC PROPULSION Algorithm for generating low variable thrust interplanetary trajectory data for mission analysis of electrical propulsion systems NASA-TN-D-4431 c30 N68 c30 N68-21228 ELECTRIC ROCKET ENGINES Performance tests on high voltage isolator for mercury propellant feed system of ion engine NASA-TM-X-1579 c28 N68-23477 ELECTRIC SWITCHES Breadboard three-phase static switch for space alternating current power systems NASA-TM-X-1495 c09 N68-15649 Circuit breakers and electric switch developments for future nuclear electric power generation systems operating in aerospace environments NASA-CR-1026 c03 N68-25 c03 N68-29460 FIFCTRIC WIRE Flammability hazards chemically induced in aircraft and spacecraft electrical circuitry by glycol/water solutions NASA-TN-D-4327 c31 N68-2221 c31 N68-22213 ELECTRICAL FAULTS Electrical properties of xenon filled thermionic diodes in nuclear reactor radiation field NASA-TN-D-4368 c25 N68-1574 c25 N68-15747 Electrical stress analysis of microthruster power conditioner NASA-TM-X-1686 c09 N68-37944 ELECTRICAL IMPEDANCE Plasma effects in antenna near zone field -admittance and ionization rise time measurements on Teflon-plugged waveguide slot antenna NASA-CR-1149 c07 N68-33042 Reflection coefficient and admittance of circular aperture in ground plane covered by dielectric or plasma slab NASA-CR-1177 c25 N68-35171 Fourier integration of electrical impedance expressions for nonlossy dielectric and lossy plamas NASA-TN-D-4774 c07 N68-35524 Electrical impedance and radiation distributions of circular waveguide by integral transformation NASA-TN-D-4752 ELECTRICAL INSULATION c07 N68-35537 Radiation effects on thermionic insulator materials – evaluation of beryllia, alumina, thoria, zirconia, and yttria NASA-TN-D-4414 c22 N68-17095 Flammability hazards chemically induced in aircraft and spacecraft electrical circuitry by glycol/water solutions NASA-TN-D-4327 c31 N68-22213 Radiation resistance, outgassing characteristics, and weight of five electrical insulation materials for spacecraft NASA-TN-D-4553 c18 N68-28264 Ruon 18-0-4555 Equipment specifications and electrical properties of flat conductor cable systems NASA-SP-5043 C09 N68-28879 ELECTRICAL PROPERTIES Electrical performance of rhenium niobium cylindrical thermionic converter NASA-TN-D-4533 c03 N68-21766 Mechanical, optical, and electrical characteristics of hand-held sextant for space flight NASA-TN-D-4585 c21 N68-24512 Electrical and mechanical properties of high temperature cobalt-iron magnetic material NASA-TN-D-4551 c17 N68-24558 Electrical properties of direct current compact arc in argon under varying pressures, amperages, and electrode spacing C29 N68-25818 Equipment specifications and electrical properties of flat conductor cable systems NASA-SP-5043 Thermal radiative and electrical properties of cadmium sulfide solar cell at low simulated solar intensities and temperatures NASA-TN-D-4818 c03 N68-3 c03 N68-35467

ELECTRICAL RESISTANCE Analytical investigation of electrical heated wire mesh for flowing gas heaters NASA-TN-D-4595 c33 N68-25312 ELECTRICAL RESISTIVITY Automated Hall effect and resistivity apparatus for studying electrical transport properties of semiconductors NASA-TM-X-1464 c03 N68-10103 Magnetohydrodynamic flow of incompressible viscous electrically conducting fluid over NASA-CR-989 c25 N68-14078 Ionic conductivities of solid mixtures of lithium fluoride-lithium chloride, lithium chloride-potassium chloride, lithium fluoride-sodium chloride, and sodium chloride-potassium chloride NASA-TN-D-4606 c26 N68-24510 ELECTRO-OPTICAL PHOTOGRAPHY Design and operating character rotating disk CUTRU-UPTICAL PHOTOGRAPHY Design and operating characteristics of electro-optical instrument for tracking of retinal blood vessels in back of eye NASA-CR-1121 c05 N68-35109 ELECTROCARDIOGRAPHY Electronic circuit for detection of R-wave of electrocardiac signal for control of time cycle of heart-assist pumps NASA-TM-X-1489 c05 N68-13999 Electrode-electrolytic paste system for space flight electroencephalogram, electrocardiogram, and respiration monitoring systems NASA-TN-D-4398 c04 N68-21383 Rapid reduction method of rhythm and rate information in large scale electrocardiogram monitoring NASA-TN-D-4751 c05 N68-32100 ELECTRODES Electrode design, inorganic separators, and performance tests of multiplate five ampere-hour silver-zinc battery cell NASA-CR-965 c03 N68-16321 Electrode-electrolytic paste system for space flight electroencephalogram, electrocardiogram, and respiration monitoring systems NASA-TN-D-4398 c04 N68-21383 Electrical performance of rhenium niobium cylindrical thermionic converter NASA-TN-D-4533 c03 f c03 N68-21766 Electrical properties of direct current compact arc in argon under varying pressures, amperages, and electrode spacing NASA-TM-X-1596 c29 N68-25818 Effect of throat size and electrode size and shape on arc heating performance in 20-inch hypersonic tunnel NASA-TN-D-4653 c11 N68-28947 Emitter and collector sheaths for cesium thermionic diodes with polycrystalline tungsten electrodes NASA-TN-D-4744 c25 N68-31640 NASA-IN-D-4744 Effects of electrolyte amount, drain rate, and electrode geometry on copper oxide-magnesium thermal cell performance NASA-TN-D-4790 ELECTROENCEPHALOGRAPHY C23 N08-34 c03 N68-34234 ELECTROLOGENALOGENEN Electrode-electrolytic paste system for space flight electroencephalogram, electrocardiogram, and respiration monitoring systems NASA-TN--4398 ELECTROLUMINESCENCE C04 N68-2138 c04 N68-21383 Solid-state digitally controlled electroluminescent vertical scale indicators NASA-CR-919 c05 N68-10648 Performance comparison of electromechanical and electroluminescent displays in closed loop manual tracking task and reading accuracy tests NASA-TN-D-4841 c05 N68-36457 ELECTROLYTES ELECTROLYTES Effects of electrolyte amount, drain rate, and electrode geometry on copper oxide-magnesium thermal cell performance NASA-TN-D-4790 c03 N68-34 ELECTROMAGNETIC COMPATIBILITY Electromagnetic compatibility verification for Surveyor spacecraft and Atlas Centaur launch which c03 N68-34234 vehicle NASA-TM-X-1673 c31 N68-36971 ELECTROMAGNETIC INTERACTIONS

Thermal radiation heat transfer data, radiative

properties of black bodies, and electromagnetic theory NASA-SP-164 c33 N68-28530 ELECTROMAGNETIC NOISE Radio Astronomy Explorer satellite radiometer for measuring cosmic noise in vicinity of 100 meter wavelengths NASA-TN-D-4634 cl4 N68-28 ELECTROMAGNETIC PROPERTIES c14 N68-28327 Electromagnetic switching properties of bistable, magnetically permeable liquid bead with nondestructive memory for gas flow control NASA-TM-X-1613 ELECTROMAGNETIC PUMPS c09 N68-30501 ELECTROMAGNETIC PUMPS Electromagnetic pump designs for use as boiler feed pumps in Rankine cycle, space electric power plants NASA-CR-911 ELECTROMAGNETIC RADIATION Detection of supernovae pulse by gamma ray c15 N68-10503 telescope and atmospheric scintillation method NASA-TN-D-4732 c29 N68-33370 ELECTROMAGNETIC WAVE TRANSMISSION Guided electromagnetic waves propagating along lossless dielectric rod immersed in isotropic and uniaxial plasmas determined for applications to plasma diagnostics NASA-TN-D-4866 c25 N68-37237 ELECTROMAGNETISM Electromagnetic processes in magnetohydrodynamic induction machines with working media of liquid metal NASA-TT-F-460 c25 N68-16286 ELECTROMECHANICAL DEVICES Performance comparison of electromechanical and electroluminescent displays in closed loop manual tracking task and reading accuracy NASA-TN-D-4841 c05 N6 ELECTRON ACCELERATORS tests c05 N68-36457 Synchrotron emission at helical motion of relativistic electrons emitting from source with relativistic velocity NASA-TT-F-521 c25 N68c25 N68-16700 ELECTRON BEAM WELDING Welding of precipitation hardening stainless steels NASA-SP-5087 c15 N68-21429 ELECTRON BEAMS Electron beam-plasma interaction and plasma multiplier as possible millimeter wave generators NASA-TN-D-4309 c25 N68-18614 Electron beam probe measurements of rotational and vibrational temperatures in static low-density air NASA-TN-D-4500 c14 N68 ELECTRON DENSITY (CONCENTRATION) Power transfer to ion cyclotron waves in two c14 N68-24244 species plasma NASA-TM-X-1481 c25 N68-11404 Small amplitude solutions to spatially uniform plasma continuity equations for low frequency oscillations in electron density and neutral atoms NASA-TN-D-4472 c25 N68-22887 Hydrogen plasma hot cathode generator and electron energy and density study NASA-TN-D-4604 c25 N68-25877 Plasma effects in antenna near zone field admittance and ionization rise time measurements on Teflon-plugged waveguide slot antenna NASA-CR-1149 c07 N68-33042 Fourier integration of electrical impedance expressions for nonlossy dielectric and lossy plamas NASA-TN-D-4774 ELECTRON DENSITY PROFILES c07 N68-35524 Graphs of phase and group refractive indices computed from collisionless magnetoionic theory electron concentration and magnetic field intensity NASA-TM-X-1553 ELECTRON DIFFRACTION c13 N68-21904 Low energy electron diffraction study of oxygen adsorption on molybdenum /111/ surface NASA-TN-D-4735 c06 N68-30 c06 N68-30582 ELECTRON DIFFUSION Electron diffusion process in beam plasma passing

through electrically floating anode NASA-TN-D-4758 c25 N68-32072 ELECTRON EMISSION Current-voltage characteristics of collisionless cylindrical diode with thermionically emitted electrons NASA-TN-D-4516 c10 N68-21122 Design evaluation of helical electron bombardment filaments for heating cylindrical thermionic converters NASA-TM-X-1630 c22 N68-32968 ELECTRON ENERGY Hydrogen plasma hot cathode generator and electron energy and density study NASA-TN-D-4604 c25 N68-25877 ELECTRON GAS Dielectric formulation for inhomogeneous electron gas, and Green function formalism for treating static dielectric screening of point impurity in electron gas NASA-TR-R-283 c26 N68-24273 ELECTRON IRRADIATION Transmission, and backscatter coefficients for electron irradiated aluminum, and stainless steel foils NASA-TN-D-4363 c24 N68-17898 Effects of 22 MeV proton and 2.4 MeV electron radiation on boron and aluminum doped silicon solar cells NASA-TN-D-4407 c26 N68-19924 Charge storage in silicon dioxide resulting from electron irradiation NASA-CR-1088 c26 N68-26603 Design evaluation of helical electron bombardment filaments for heating cylindrical thermionic converters NASA-TM-X-1630 c22 N68-32968 Analysis of dielectric breakdowns induced by electron irradiation in polymeric films NASA-TN-D-4810 c24 | c24 N68-36070 ELECTRON MICROSCOPES Electron microscopy technique for determining dispersoid distribution in powder blends dispersoid distribution in powder blends NASA-TM-X-1468 c17 N68-100 Use of surface replication, extraction replication, and thin film electron microscopy in study of microstructures of dispersion strengthened materials c17 N68-10051 NASA-TN-D-4461 c17 N68-18999 Electron microscopy of electron beam irradiated amorphous silicon, germanium, and cadmium sulfide semiconductor films NASA-TN-D-4522 c26 N68-203 c26 N68-20295 In situ electron microscopy for studying vapor deposition nucleation processes NASA-TN-D-4506 c06 N68-21430 Electron microscope technique for revealing microstructures of dispersion strengthened materials NASA-TM-X-1561 ELECTRON PARAMAGNETIC RESONANCE c17 N68-21431 Electron paramagnetic resonance signals from paramagnetic sample in microwave bridge NASA-TN-D-4469 c14 NASA-TN-D-4469 Electron paramagnetic resonance of lithium silicon NASA-TR-R-290 c26 N68-33228 ELECTRON PROBES Electron beam probe measurements of rotational and vibrational temperatures in static low-density air NASA-TN-D-4500 c14 N68-24244 Electron probe X ray microanalyzer applied to material failure study, bonding, and other metallurgical analysis NASA-TN-D-4526 c15 N68-3 c15 N68-28249 ELECTRON RADIATION Electron radiation induced dielectric breakdowns in capacitor meteoroid detection system NASA-TN-D-4738 ELECTRON SCATTERING c14 N68-33277 Electron scattering, bremsstrahlung cross sections, and spectral energy distributions NASA-CR-1194 c24 N68c24 N68-37708 ELECTRON TUNNELING Current-voltage characteristics of tunneling p-n junctions in semiconductors NASA-TN-D-4403 c09 N68 ELECTRONIC EQUIPMENT c09 N68-19062 Electronic circuit for detection of R-wave of

SUBJECT INDEX

electrocardiac signal for control of time cycle of heart-assist pumps NASA-TM-X-1489 c05 N68-13999 NASA-18-A-1469 Properties and Imaging techniques of various display devices - computer directed visual flight control boards, integrated optical man machine systems, and electro-optical methods NASA-SP-159 COS NG-13959 COS NG-22302 NASA-SP-159 CU9 NO6-2201 Conference papers on NASA planning and projected requirements for advanced aerospace electronic systems technology NASA-SP-154 C30 N68-3310 c30 N68-33169 Electronic visualization technique for studying dynamic behavior of gas journal bearing NASA-TM-X-1609 c14 N68-35 ELECTRONIC EQUIPMENT TESTS c14 N68-35105 ELECTRONIC EQUIPMENT TESTS Electrical properties of xenon filled thermionic diodes in nuclear reactor radiation field NASA-TN-D-4368 Product development and testing of thin film oxygen partial pressure sensors NASA-CR-1182 ELECTRONIC PACKAGING Metal oxide semiconductor field effect transistor circuit development and laminated electronic c25 N68-15747 c14 N68-35149 circuit development and laminated electronic packaging for computer storage devices NASA-CR-1113 c08 c08 N68-35193 ELECTRONIC TRANSDUCERS Piezojunction as sensor in transducers NASA-CR-1089 c c26 N68-26627 ELECTROPLETHYSMOGRAPHY Electroplethysmographic data on intercranial circulation, and dynamics of cerebral blood volume under normal conditions and gravitational stresses NASA-TT-F-492 ELECTROSTATIC CHARGE c04 N68-15477 Electromagnetism in moving, conducting media solution to problems involving static and radiation fields of static charges, and radiation fields of harmonic current sources NASA-CR-1025 c23 N68-21444 Charge storage in silicon dioxide resulting from electron irradiation NASA-CR-1088 c26 N68-26603 Analysis of integrated charged particle energy spectra from gridded electrostatic analyzers NASA-TN-D-4718 c25 N68-3 c25 N68-30093 Electroadhesive devices - theory, design, fabrication, and testing NASA-CR-1211 c10 N68-37906 ELECTROSTATIC ENGINES Divergent-flow contact-ionization electrostatic thrustor for satellite attitude control and stationkeeping NASA-TN-D-4420 c28 N68-20187 ELECTROSTATIC PROPULSION Performance tests on high voltage isolator for mercury propellant feed system of ion engine NASA-TM-X-1579 c28 N68-2: c28 N68-23477 ELECTROSTATICS Flight test of electrostatic accelerometer which eliminates null bias problem NASA-TM-X-1488 ELEVATION ANGLE c14 N68-13974 Computation of solar elevation angles and determination of sunrise and sunset times as function of latitude, longitude, and date NASA-TM-X-1646 c13 N68-33 ELLIPTICAL ORBITS c13 N68-35179 Analytical method artificial satellite lifetime determination NASA-TN-D-4281 c30 N68-11754 Computer program technique for determination of opportunities for recall of spacecraft to multiple landing sites from circular or elliptical orbits NASA-TR-R-259 c21 N68-30126 EMBRITTLEMENT Neutron irradiation effects on embrittlement of polycrystalline tungsten NASA-TN-D-4661 c17 N68-28 EMISSION SPECTRA c17 N68-28818 Physical gas dynamics research - molecular band spectra, shock tube studies, and interactions between diatomic molecules NASA-TT-F-505 c12 N68-16 c12 N68-16839 Surface roughness effects on normal spectral emittance of vapor deposited rhenium

NASA-TM-X-1514 c17 N68-19347 Emission and reflection coefficients of surface thermal radiation properties NASA-TT-F-497 c33 N68-21536 NASA-11-r-49/ C33 N66-2153 Photographs, thermocouples, and emission spectra used to study mixing and reaction of hydrazine 'and nitrogen tetroxide NASA-TN-D-4467 C33 N68-2496 Discrete ordinate computation of fission spectrum c33 N68-24965 neutron dose rate attenuation curve for lithium hydrides and tungsten NASA-TN-D-4684 c24 N68-30001 ENTTTERS Iterative calculation model and results for plane collisionless sheaths between field modified emitter and thermally ionized cesium plasma NASA-TN-D-4376 c25 N68-33021 ENERGY BANDS Quantum mechanical study of transition probabilities, Einstein A coefficients, and oscillator strengths of band systems of diatomic molecules NASA-CR-975 ENERGY CONVERSION c24 N68-11037 CRCY CUNVERSION Necking, yield, and plastic flow in electrical analogs of mechanical systems with respect to energy conversion effects on mechanical behavior of various materials NASA-CR-1039 C24 N68-21: C24 c24 N68-21949 ENERGY DISSIPATION Correction of balloon X ray astronomy data for atmospheric attenuation, escape, and energy resolution NASA-CR-1045 c13 N68-23436 Kinetic energy loss coefficients of stator blade row in open configuration row in open configuration NASA-TM-X-1635 Compartmented gas bag landing system with ommidirectional, multiple impact, and kinetic energy dissipation capabilities NASA-TN-D-4710 C32 N68-316 c03 N68-30506 c32 N68-31602 Numerical analysis of winding power loss of rotating ac generators in controlled atmospheres NASA-TN-D-4849 c03 N68-37162 ENERGY LEVELS Defect energy levels and concentrations for proton irradiated, n-type silicon single crystals NASA-TN-D-4830 c26 N68-37051 ENERGY SPECTRA Search for unbound helium 3 levels with isobaric spin 1/2 NASA-TN-D-4377 c24 N68-15638 Numerical least square method for resolving complex pulse height spectra NASA-SP-3044 c24 N6 c24 N68-29520 Analysis of integrated charged particle energy spectra from gridded electrostatic analyzers NASA-TN-D-4718 ENGINE COOLANTS c25 N68-30093 Approximate average midspan metal temperatures and coolant flow requirements for turbine airfoils cooled by compressor exit bleed air NASA-TN-D-4491 c33 N68-1 c33 N68-19187 ENGINE DESIGN Radiant heat transfer to aerosols for application in gaseous core nuclear rocket engine designs NASA-CR-953 c22 N68-10561 NASA-CR-1147 ENGINE INLETS Jet VTOL aircraft inlet temperature rise and induced recirculating flow patterns NASA-CR-1147 col N68 c01 N68-33043 Wind tunnel tests at Mach 1.60, 2.36, and 2.96 to determine flow field properties near arrow wing body model for locating potential engine air inlets NASA-TN-D-4809 c01 N68-37238 ENGINE NOISE V/STOL short haul transport design considerations including noise characteristics NASA-CR-670/01/ c02 N68-1117 B-70 aircraft engine noise measurements and c02 N68-11174 predictions NASA-TM-X-1565 c02 N68-21834 Nacelle design for turbofan engine compressor noise suppression on Douglas DC-8 aircraft NASA-CR-1056 c28 N68 c28 N68-26771 Estimation procedures for effect of design and

Alight characteristics of jets on ground noise NASA-CR-1053 co2 N68-26930

Acoustic measurements on jet engine intake system noise reduction suppressor cowlings NASA-TN-D-4639 c02 N68-29887 Turbojet engine noise reduction by increasing intake system guide vane-rotor blade spacing NASA-TN-D-4690 c28 N68-3 c28 N68-30040 ENGINE TESTS Analysis of several methane fueled engine cycles for supersonic flight NASA-TN-D-4699 c28 N68-29378 ENGINEERING DRAWINGS Equipment specifications and engineering drawings for automatic picture transmission ground stations NASA-SP-5079 ENTHALPY c07 N68-19624 Approximate equations for computing enthalpy and velocity derivatives at surface of flat plate, cone, or blunt axisymmetric body NASA-TN-D-4484 c33 N68-20065 High enthalpy plasma generator for atmospheric entry heating simulation c11 N68-24560 NASA-TN-D-4583 Low density, leading edge bluntness, and ablation effects on wedge induced laminar boundary layer separation at moderate enthalpies in hypersonic flow NASA-TN-D-4829 c12 N68-36458 ENTROPY Thermodynamics of plasmas using principle of maximum entropy NASA-TN-D-4621 c25 N68-25920 ENVIRONMENT SIMULATORS ENVIRONMENTAL CONTROL c11 N68-18460 Subsystem definition of advanced life support technology for Mars surface module NASA-CR-1083 c05 N68-28319 ENVIRONMENTAL ENGINEERING Assessment of environmental engineering and testing methods used in development of various spacecraft systems NASA-TN-D-4181 c31 N68-10192 Radiative thermal energy incident effects on pressure-suited man on lunar surface NASA-TN-D-4243 c30 N68-11630 ENVIRONMENTAL TESTS Environmental exposure effects on mechanical properties of titanium alloy, stainless steel, aluminum alloy, and composite material sheets NASA-TN-D-4318 c17 N68-17897 EPHEMERIDES Computer programs for rapidly computing approximate ephemerides of minor planet or artificial satellites c30 N68-20356 NASA-TN-D-4470 EPOXY RESINS Techniques for coating magnesium with epoxy resin films for paraboloid mirrors NASA-TN-D-4734 cl8 N68-3059 c18 N68-30597 EQUATIONS OF MOTION Equations of relative motion and guidance for orbital transfer and docking maneuvers in spacecraft rendezvous NASA-CR-1011 c30 N68-19186 Entry guidance equations, reference trajectories, and guidance system mechanization NASA-CR-1013 c30 N68-1998 c30 N68-19985 Two body equations of motion for calculating partial derivatives relating lunar and planetary midcourse correction requirements to guidance system injection errors NASA-TN-D-4518 c30 N68-20368 Matrix form of equations of motion used in iterative processes for determining normal modes and frequencies of launch vehicles NASA-TN-D-4550 c32 N68-22275 Development of equations of motion in canonical form equivalent to forms of Delaunay and Poincare NASA-TN-D-4478 c30 N68-24371 Simplified and accurate relative equations of motion for two impulse orbital rendezvous NASA-TN-D-4670 c30 N68c30 N68-28841

Attitude determination of spin-stabilized spacecraft using star mapping technique

EQUATIONS OF STATE

NASA-TN-D-4740 c21 N68-31957 Theory of finite amplitude waves in fluid-filled elastic tubes, including wave distortion, shock wave propagation, and Korotkoff sounds c12 N68-33056 NASA-TN-D-4803 Equations of motion for calculating compressible turbulent boundary layers NASA-CR-1144 EQUATIONS OF STATE c12 N68-35006 Computer program for solutions to equilibrium and nonequilibrium chemical state relations for open and closed thermodynamic systems NASA-CR-1064 c33 N68-26816 EQUILIBRIUM FLOW Enthalpy, temperature, and density charts for equilibrium isentropic expansion of air behind shock waves for wide range of velocities and altitudes c33 N68-11144 NASA-TN-D-4247 Steady state performance tests on single pass counterflow sodium-potassium cooled mercury Rankine cycle condenser NASA-TM-X-1548 EQUIPMENT SPECIFICATIONS c33 N68-20340 Analysis and evaluation of Lunik 9 spacecraft imagery, and specification of Lunik 9 spacecraft imagery, and specification of spacecraft and photographic instruments NASA-CR-980 cl4 N68-10 c14 N68-16838 Equipment specifications and engineering drawings for automatic picture transmission ground stations NASA-SP-5079 c07 N68-19624 Equipment specifications and electrical properties flat conductor cable systems NASA-SP-5043 c09 N68-28879 EROSION Relative erosion resistance of ablative materials for nozzle sections of storable-propellant rocket engine NASA-TM-X-1559 c28 N68-19708 ERROR ANALYSIS Error model for Doppler range rate and phase modulated range tracking system for which data weighting factors can be obtained for use in space vehicle trajectory analysis NASA-TN-D-4267 c10 N68-11513
 NHDA-IN-J-4267
 c10 N68

 Perturbation techniques for error analysis of finite difference approximations for linear differential equations
 NASA-TN-D-4372

 C32 N68 c32 N68-17068 Logarithmic encoding procedure and error analysis for binary word compression NASA-TN-D-4290 c08 N68-18179 Two body equations of motion for calculating partial derivatives relating lunar and planetary midcourse correction requirements to guidance system injection errors NASA-TN-D-4518 c30 N68-20368 Effects of time, frequency, and tracking station location errors on accuracy of trajectory analysis NASA-TN-D-4507 c30 N68-25271 Local error control for optimization of numerical Integration orbit calculation techniques NASA-TN-D-4542 c30 c30 N68-25867 Mathematical means for bounding propagated in n-body field NASA-TN-D-4511 c30 N68-32094 Cumulative errors associated with Category 2 and 3 operations, and terminal flight paths for low visibility landings NASA-CR-1188 c02 N68-35595 Error probabilities for maximum signal detection in presence of Poisson noise NASA-TN-D-4721 c07 N68-36105 ERRORS Parametric analysis of effects of concentrator surface errors and rim angle, collection system orientation error, and receiver temperature on paraboloid solar collector thermal efficiency NASA-TN-D-4415 c03 N68-18998 Human factors engineering techniques for reducing human errors in space systems development NASA-SP-6506 c05 N6 c05 N68-20357 ESSA 3 SATELLITE Nimbus 2 and ESSA 3 satellite observation photographs of typhoon Marie NASA-TN-D-4757

SUBJECT INDEX

ETCHING Techniques for, and applications of preferential etching of crystal surfaces to produce optical reflections for crystal orientation and optical alignment in silicon crystals NASA-TN-D-4187 C23 N68-1035 c23 N68-10354 Electroadhesive devices - theory, design, fabrication, and testing NASA-CR-1211 c10 EVAPORATION EVALUATION c10 N68-37906 EVAPURATION Particle acceleration by evaporation pressure using Q-switched laser beam NASA-CR-927 c16 N68-EVAPORATIVE COOLING c16 N68-10467 Evaluation of self-evacuating multilayer radiation shields for cryogenic storage tanks NASA-TN-D-4375 c33 N68-18046 EXCITATION Breadboard model of Brayton cycle alternator and voltage regulator-exciter NASA-TN-D-4697 c03 N68-29960 EXHAUST DIFFUSERS Performance of venturi meter with separable diffuser NASA-TM-X-1570 c14 N68 EXHAUST FLOW SIMULATION Jet VTOL aircraft inlet temperature rise and c14 N68-21384 induced recirculating flow patterns NASA-CR-1147 c01 N68-33043 Simulated wing effect on pressure drag coefficient of subsonic boattail at angle of attack NASA-TM-X-1662 c01 c01 N68-35672 Effects of simulated jet exhaust flow on transonic aerodynamic characteristics of Apollo launch escape vehicle models NASA-TN-D-4843 c31 N68-3 c31 N68-37074 EXHAUST GASES Hot-gas ingestion investigation of large-scale jet VTDL fighter type models NASA-TN-D-4609 c02 N68-28277 EXHAUST NOZZLES Approximation of ramjet exhaust plume effects on external pressure of nozzle extension of X-15 aircraft NASA-TM-X-1571 c28 N68-24614 Wind tunnel model tests of variable flap ejector nozzle with aerodynamically positioned shroud NASA-TM-X-1639 c28 N68-30599 NASA-1M-X-1039 c28 N68-3059 Heat transfer characteristics of cylindrical ejector for turbojet engine and shroud material temperature prediction NASA-TM-X-1641 c33 N68-3298 c33 N68-32988 EXOBIOLOGY Advances during 1966 in astronomy, exobiology, ionospheric sciences, radio and solar physics, and planetary atmospheres and planetology NASA-SP-155 c30 N68-15748 EXPANDABLE STRUCTURES ANJABLE SINGLORES Geometric properties of expandable whirling membrane solar energy concentrator used in conjunction with electrical conversion systems for spacecraft auxiliary power units NASA-TN-D-4532 c03 N68-22258 EXPERIMENTAL DESIGN Design data for gas cooled test loop, and inpile capsule facility from mockup reactor experiments NASA-TM-X-1509 c22 N68-15855 Experimental design and performance test of two-stage axial-flow turbine designed for Brayton-cycle space power system NASA-TN-D-4382 c03 N68-16469 EXPERIMENTATION Objectives of investigators associated with multiple experiment scientific satellites NASA-TN-D-4731 EXPLORER SATELLITES Clean room facilities for Explorer 35 spacecraft NASA-TN-D-4577 C11 N68 EXPLORER 23 SATELLITE Stainless steel Denetration data c34 N68-33682 c11 N68-28311 Automatical Action of the second state of the NASA-TN-D-4284 EXPLORER 35 SATELLITE c31 N68-28198 Method of correcting azimuthal orientation of Explorer 35 spacecraft while in lunar shadow

c20 N68-37869

NASA-TN-D-4544 EXPLOSIVE DEVICES c30 N68-24486 Two stage explosively driven light gas gun to obtain high projectile velocities NASA-CR-982 c11 N68-15777 EXPLOSIVES Target pressure and damage data from impacts by explosively propelled aluminum projectile NASA-TM-X-1597 c32 N68-254 c32 N68-25819 EXPULSION Temperature and liquid-level sensor for liquid hydrogen pressurization and expulsion studie NASA-TN-D-4339 c14 MARA c14 N68-15893 EXTINCTION Temperature and radiation effects on index of refraction and extinction coefficients of Apollo window materials NASA-CR-1019 EXTRATERRESTRIAL ENVIRONMENTS c31 N68-20467 Radiator concept based on capillary retention of liquid and potential extraterrestrial applications NASA-TN-D-4370 EXTRAVEHICULAR ACTIVITY c03 N68-28310 Extravehicular activity accomplishments in Gemini program NASA-SP-149 c30 N68-15891

F

F- 106 AIRCRAFT Wind tunnel tests of airframe installation effects on F-106B scale model with simulated underwing engine nacelles at Mach 0.56 to 1.46 NASA-TM-X-1683 ct c02 N68-37941 FABRICATION Normal and mechanical treatment for precipitation hardening stainless steels NASA-SP-5089 c15 N68-20433 FACTORIAL DESIGN Monte Carlo computations of decision error probabilities for chain pooling and variations for fractional factorial experiments NASA-TN-D-4272 c19 N68-11639 FAILURE Reliability prediction techniques for single item and multiitem problems NASA-CR-1129 c15 N68-31979 Thermionic reactor core with short-length externally fueled diodes, and electrical failure analysis NASA-TN-D-4805 c22 N c22 N68-34087 FAIRINGS Installation and fairing of flush, static pressure orifices on wing surfaces of supersonic aircraft NASA-TM-X-1530 col N68-19341 Aerodynamic heating, delamination and pressure in nose fairing honeycomb core of Atlas Centaur launch vehicle NASA-TM-X-1605 c33 N68-28156 Variable density hypervelocity wind tunnel tests on effects of several ramp-fairing, umbilical, and pad configurations on aerodynamic heating to Apollo command module NASA-TM-X-1640 c01 N68-35141 FAN IN WING AIRCRAFT Wind tunnel tests of deflected slipstream cruise fan V/STOL aircraft wing NASA-TN-D-4262 c01 N68-11036 cul N68-11036 Static and dynamic longitudinal stability tests of fan in wing V/STOL aircraft model NASA-TN-D-4322 co2 N68-15894 FAR FIELDS General method for designing circular array antennas to obtain quasi-omnidirectional patterns NASA-TN-D-4254 c07 N68-11475 Aircraft sonic boom characteristics predicted from near field data obtained in wind tunnel NASA-TM-X-1477 c02 N68-1 c02 N68-11772 NANA-THE STORE TO FAR FIELD NOT THE NOT THE NOT THE NOT THE STORE TO THE NOT THE STORE TO THE STORE ST FAR INFRARED RADIATION Systems analysis and performance test data on dual radiometer assembly for measuring far infrared wavelength bands of earths horizon

radiance profile

NASA-CR-1086 Faraday Effect c14 N68-28965 Numerical analysis of electric current and potential distributions in linear Faraday plasma accelerators NASA-TN-D-4239 c28 N68-10502 FAST NEUTRONS Fast and thermal neutron flux measurements in test cavity outside HB-6 beam port in Plum Brook reactor using sulfur pellets and gold foils NASA-TM-X-1497 c22 N68c22 N68-15643 FAST NUCLEAR REACTORS Size and shield weight requirements calculated for fast-spectrum, liquid-metal cooled nuclear reactor for space power application NASA-TN-D-4315 c22 N68-14 Neutron activation analysis of sodium, lithium, c22 N68-18197 and potassium in compact fast reactors and its effect on shielding NASA-TM-X-1512 c22 N68-2035 c22 N68-20355 Reactivity control of fast nuclear reactors Reactivity control of fast nuclear reactors containing yttrium hydride moderating zones NASA-TN-D-4615 c22 N68-24559 Neutronic effects of yttrium hydride moderator insertion in fast spectrum reactors NASA-TM-X-1614 c22 N68-29950 Neutronic calculations of fuel and poison drum control of refractory metal, fast spectrum space power reactors NASA-TN-D-4709 c22 N68-30750 FATIGUE (MATERIALS) Fatigue crack propagation and fracture toughness characteristics of 7079 aluminum alloys in underage, peak age, and overaged conditions NASA-CR-996 c32 N68c32 N68-15476 Prediction of fatigue crack propagation behavior in aluminum alloy panels with simulated rivet forces c32 N68-32074 NASA-TN-D-4702 NHOATIN-9-9702 Ultrasonic detection and measurement of fatigue crack propagation in notched specimens of aluminum, titanium, and cobalt alloys and maraging steels NASA-TN-D-4782 C32 N68-350 C32 c32 N68-35071 FATIGUE LIFE High temperature tests to determine fatigue life of 120mm bore ball bearings with fluorocarbon, polyphenyl ether, and synthetic base paraffin base lubricants NASA-TN-D-4850 c15 N68-36075 FATIGUE TESTS Axial tensile fatigue of liquid rocket engine alloys at cryogenic temperatures NASA-TN-D-4274 c17 N68c17 N68-11637 Stress corrosion tests of heat treated austenitic stainless steels NASA-TN-D-4673 c17 N68-29379 FATTY ACIDS Survey and critical evaluation of existing methods for synthesis of fatty acids and lipids from metabolic wastes under conditions of space flight NASA-CR-1105 c04 N68-28278 Chemical feasibility and nutrional value in synthesis of edible fatty acids and lipids from metabolic wastes for space flight feeding c04 N68-28829 NASA-CR-1104 FEED SYSTEMS Liquid fluorine pump, impeller, and inducer corrosion resistance to cavitation flow NASA-TM-X-1573 c15 N6 c15 N68-28241 FEEDBACK AMPLIFIERS Operational amplifiers for nuclear spectroscopy NASA-TN-D-4349 c24 NAR-18 c24 N68-18254 FEEDBACK CONTROL Limit cycle and control surface resonance characteristics of X-15 stability augmentation system NASA-TN-D-4287 c02 N68-11545 Synthesis of human response in closed loop tracking tasks NASA-TN-D-4842 FERROELECTRICITY c05 N68-36461 Dielectric temperature change effects observed in ferroelectric and pyroelectric substances NASA-CR-1080 FERROMAGNETIC MATERIALS c26 N68-25972 Cobalt-tungsten ferromagnetic, high temperature structural alloy for rotor applications in space

FEYNMAN DIAGRAMS

power generators NASA-TN-D-4338 c17 N68-18145 Nonuniform magnetic field effect on ferromagnetic colloidal solutions NASA-TN-D-4676 c06 N68-3004 c06 N68-30044 FEYNMAN DIAGRAMS Regnman formalisms for expressing iterated commutators and functions of operators NASA-TN-D-4857 c19 No c19 N68-36525 FIBERS Structural design methods for analysis of multilayer or laminated filamentary composites NASA-CR-964 c32 N68-11191 NASA-CR-964 FIELD EFFECT TRANSISTORS Metal oxide semiconductor field effect transistor circuit development and laminated electronic packaging for computer storage devices NASA-CR-1113 c08 c08 N68-35193 FIELD THEORY (PHYSICS) Artificial satellite motion under influence of planar and Keplerian force fields NASA-TN-D-4622 FIGHTER AIRCRAFT c30 N68-28113 Exhaust gas ingestion characteristics and induced aerodynamics for vertical takeoff lift engine fighter model in ground proximity NASA-CR-1098 c02 N68-28233 Windshield and nose geometry effects on supersonic aerodynamic characteristics of tactical fighter model NASA-TM-X-1664 c02 N68-37066 FILAMENT WINDING Tensile strength properties of glass, boron, and graphite filament wound resin composites and liners for cryogenic pressure vessels NASA-TN-D-4412 c18 N68-16623 FILM BOILING Film boiling mist flow heat transfer using single phase variable property NASA-TN-D-4149 c33 N68-11636 Minimum film boiling heat flux in vertical flow of liquid nitrogen NASA-TN-D-4307 c33 N68-16 FILM COOLING c33 N68-16683 Film and transpiration cooled baffles for M-1 engine NASA-TM-X-1267 FINITE DIFFERENCE THEORY c28 N68-18216 Perturbation techniques for error analysis of finite difference approximations for linear differential equations NASA-CR-1060 c33 N68c32 N68-17068 c33 N68-25244 computer program for finite difference equation analysis of in-depth response of materials exposed to high temperature environment NASA-CR-1061 c33 N68-26692 FINS Dne dimensional, steady state heat exchange by both convection and radiation between rods or fins and their surroundings NASA-TN-D-4257 c33 N68-14 c33 N68-14052 Fin performance analyzed by using heat transfer coefficients for various boiling modes NASA-TN-D-4797 c33 N68-34088 Nose shape and fin geometry effects on static stability of sounding rocket models in supersonic wind tunnel NASA-TM-X-1661 c01 N68-36509 FIRES Natural electrical phenomena as aircraft fire hazards, with study of flame propagation in fuel vent systems NASA-CR-1076 c02 N68-26691 FIRING (IGNITING) Unstarted inlet flow field during restart cycle of axisymmetric mixed compression configuration at Mach 3 NASA-TM-X-1547 c01 N68-21703 FISSION Discrete ordinate computation of fission spectrum neutron dose rate attenuation curve for lithium hydrides and tungsten NASA-TN-D-4684 FISSION PRODUCTS c24 N68-30001

Characteristics of liquid metal cooled reactor

SUBJECT INDEX

gaseous fission products vented or contained, for space power systems NASA-TM-X-1631 c22 N68-30 FLAME PROPAGATION c22 N68-30516 Natural electrical phenomena as aircraft fire hazards, with study of flame propagation in fuel vent systems NASA-CR-1076 c02 N68-26691 Flame propagation in supersonic premixed flows of hydrogen and air ignited by coaxial, hot gas, pilot jet NASA-TN-D-4631 c33 N68-28100 FLAME STABILITY Injector baffles for flame stability in combustion chambers using nitrogen tetroxide and hydrazine mixture NASA-TM-X-1595 c28 N68-26644 FLAMMABILITY Flammability hazards chemically induced in aircraft and spacecraft electrical circuitry by glycol/water solutions NASA-TN-D-4327 c31 N68-22213 Reduction of flammable and toxic materials for use in oxygen rich manned spacecraft cabin atmospheres c05 N68-24756 NASA-TN-D-3415 FLAPS (CONTROL SURFACES) Wind tunnel stability tests of twin engined turboprop aircraft with rotating cylinder flaps NASA-TN-D-4489 c01 N68-1918 c01 N68-19189 Effect of boundary layer bleed on heat transfer and pressure distributions over wedge-flap surface at hypersonic speeds NASA-TN-D-4686 c01 N68-2995 Wind tunnel model tests of variable flap ejector nozzle with aerodynamically positioned shroud NASA-TM-X-1639 c28 N68-3055 c01 N68-29955 c28 N68-30599 FLASH WELDING Welding of precipitation hardening stainless steels NASA-SP-5087 c15 N68-21429 FLAT LAYERS II LAILERD Transient solidification of flowing liquid on cold plate, including heat capacities of frozen layer and plate NASA-TN-D-4353 c33 N68-15743 c33 N68-15742 FLAT PLATES Helium and air flow tests over single flat plates to determine dynamic pressure limits of nuclear fuel element plates NASA-TN-D-4417 c12 N68-16227 Static pressure and flow field for flat plate model with short trailing-edge flap NASA-TN-D-4308 cl2 N68-17376 Real gas wedge-induced laminar separation on cooled blunt flat plate at hypersonic speed NASA-TN-D-4320 c01 N68-17899 Forces and moments produced by air and helium jets exhausting parallel to flat plate in near vacuum NASA-TN-D-4408 cl2 N68-19000 NASA-TN-D-4408 cl2 N68-19000
 Effect of two dimensional multiple sine wave protrusions on pressure and heat transfer distributions for flat plate in hypersonic flow NASA-TN-D-4437 c01 N68-19063
 Approximate equations for computing enthalpy and velocity derivatives at surface of flat plate, cone, or blunt axisymmetric body NASA-TN-D-4484 c33 N68-20063
 Numerical method for determining transient c01 N68-19063 c33 N68-20065 Numerical method for determining transient response of simply supported plate to n waves at normal incidence c32 N68-33737 NASA-CR-1175 Hydraulic flow approximation for flow induced vibration analysis on flat plate suspended in narrow channel NASA-CR-1186 c12 N68-35086 FLEXIBILITY Planform design method, general characteristics, and aeroelastic stability of flexible lifting rotors NASA-TN-D-4465 c01 N68-19954 Flexibility effects on lift and pitching moments of low aspect ratio delta wing-conical-cylindrical body combinations at transonic speeds NASA-TN-D-4655 c01 N68-37065 FLEXIBLE BODIES Critical speed analysis of rigid rotors on flexible foundations NASA-TN-D-4858 c15 No c15 N68-37214

FLIGHT TESTS

c02 N68-28153

FLIGHT Simulated study of effects of high altitude supersonic air flow on titanium alloy hot salt cracking process NASA-CR-981 c17 N68-11522 FLIGHT CHARACTERISTICS Sum CHARACTERISTICS Simulated flight test of double-Delta supersonic transport for performance characteristics, handling qualities, and climbing characteristics NASA-TN-D-4396 CO2 N68-17391 Flight tests for preliminary evaluation of handling qualities of unaugmented XB-70 aircreaft aircraft NASA-TM-X-1584 c02 N68-23901 Systems analysis and flight performance of Atlas Centaur launch vehicle with Surveyor 1 lunar probe NASA-TN-D-4580 c31 N68-24338 Aerodynamic stability and control characteristics of supersonic aircraft NASA-TN-D-4578 c02 N68-24498 Rotor-hub bending moment measurements on hingeless rotor helicopter during abrupt maneuvers near around NASA-TN-D-4574 c02 N68-24499 Mission and orbit parameter summary for Lunar Orbiter spacecraft flight NASA-CR-1141 c31 N68-31477 Flight performance evaluation of Atlas-Centaur for Surveyor spacecraft SC-2 NASA-TM-X-1616 c31 N68-33332 c31 N68-33 Flight performance evaluation of Atlas Centaur restart capability in earth orbit NASA-TM-X-1647 C31 N68-35 c31 N68-35357 Effects of reduced landing speeds on flying qualities of Boeing 707 for simulated instrument approaches NASA-TN-D-4804 c02 N68-37075 FLIGHT CONTROL Feasibility of computer assisted flight controller training NASA-CR-917 c08 N68-13897 Coordinate measuring system for flight control, and trajectory optimization NASA-CR-1000 c30 N68-16103 Piloted simulation studies of Saturn 5 launch vehicle manual backup guidance and control NASA-TN-D-4481 c21 N68 c21 N68-19061 Finite-state machines and evolutionary programming for representing and analyzing performance of human operator in control of dynamic systems NASA-CR-1112 c05 N68-28847 New methods for design of adaptive flight control systems systems NASA-CR-1152 c21 NG FLIGHT MECHANICS Guidance, flight mechanics, and trajectory optimization - calculus of variations and c21 N68-33904 modern applications NASA-CR-1003 c30 N68-15193 Non-citized formulation of guidance equations and solutions for orbital space missions WASA-CR-1010 c30 N68-17215 General perturbations theory applications to spacecraft guidance, flight mechanics, and trajectory optimization NASA-CR-1008 Dynamic programming and multistage decision processes in guidance, flight mechanics, and trajectory optimization NASA-CR-1009 c30 N68-21077 Guidance, flight mechanics, and trajectory optimization NASA-CR-1004 c30 N68-21685 FLIGHT PATHS Estimation procedures for effect of design and Estimation procedures for effect of design and flight characteristics of jets on ground noise NASA-CR-1053 colored colored colored colored Spacecraft performance, control, and flight path analysis of Lunar Orbiter 3 extended mission NASA-CR-1109 colored Cumulative errors associated with Category 2 and 3 operations, and terminal flight paths for low visibility landings NASA-CR-1188 c02 N68-35 FLIGHT PLANS Feasibility of revised V/STOL design and flight c02 N68-35595

FLIGHT SIMULATION Simulator study of pilot control of remote orbital docking of large altitude stabilized components NASA-TN-D-4263 c31 N68-11476 Piloted fixed-base simulation of low speed flight characteristics of arrow wing supersonic transport aircraft NASA-TN-D-4277 c05 N68-13609 Simulated flight test of double-Delta supersonic transport for performance characteristics, handling qualities, and climbing characteristics, NASA-TN-D-4396 c02 N68-17391 Simulated flight operations to evaluate problems encountered by supersonic transports in present c02 N68-17391 air traffic control system NASA-TN-D-4638 c02 N68-29372 FLIGHT SIMULATORS Flight simulator to evaluate lateral-directional handling qualities of piloted reentry vehicles NASA-TN-D-4410 c31 N68-19226 Simulator study of pilot control over lunar module during ascent from lunar surface c21 N68~21366 NASA-TM-X-1549 FLIGHT STRESS (BIOLOGY) FM data handling facility for preparing analog physiological data obtained in flight for digital computations NASA-TN-D-4488 c05 N68-21537 Signal conditioning methods and equipment used for inflight recording of pilot biomedical data c05 N68-21538 NASA-TN-D-4487 FLIGHT TEST INSTRUMENTS Performance characteristics of data acquisition Alight test sensors used on X-15 aircraft NASA-TN-D-4597 cl4 N6 c14 N68-25317 FLIGHT TEST VEHICLES Limit cycle and control surface resonance characteristics of X-15 stability augmentation system NASA-TN-D-4287 c02 N68-11545 Effects of reduced landing speeds on flying qualities of Boeing 707 for simulated instrument approaches NASA-TN-D-4804 c02 N68-37075 FLIGHT TESTS Three axis fluidic automatic flight control system developed and flight tested c02 N68-10047 NASA-CR-913 Flight tests of ringsail parachute with 15 percent porosity, for planetary entry NASA-TM-X-1484 c31 N68-11919 Flight test of conical spacecraft simulating parachute deployment in Mars atmosphere NASA-TN-D-4266 c31 N68c31 N68-11961 Flight test of electrostatic accelerometer which eliminates null bias problem NASA-TM-X-1488 cl4 N c14 N68-13974 Design and flight performance studies of Wasp sounding rocket NASA-TM-X-1518 c31 N68c31 N68-17094 MROR-117-A-1310 Variable-stability helicopter flight tests under instrument flight rules to determine effects of gross changes in longitudinal static stability for V/STOL handling qualities NASA-TN-D-4364 C02 N68-1910 c02 N68-19184 NASA-IN-24364 CU2 NGG-Flight test of 30 foot nominal diameter cross parachute to measure shock loads, drag efficiency, and stability characteristics NASA-TM-X-1542 c31 NGGc31 N68-21778 Flight test of capacitance type meteoroid impact detector of aluminum polyethylene terephthalate using inflatable paraglider NASA-TN-D-4530 c14 N68-2229 c14 N68-22290 Flight tests for preliminary evaluation of handling qualities of unaugmented XB-70 aircraft NASA-TM-X-1584 c02 N68-239 Flight test of 10-foot nominal-diameter disk-gap c02 N68-23901 band parachute to determine deployment and inflation, opening shock loads, drag efficiency, and stability characteristics NASA-TM-X-1575 c02 N68-24245 Aerodynamic stability and control characteristics of supersonic aircraft NASA-TN-D-4578 c02 N68-24498 Optimum values of pitch rate damping, longitudinal control and speed stability for vertical takeoff aircraft /helicopters/ using pilot ratings NASA-TN-D-4624 c02 N68

plan concepts for short haul transport aircraft NASA-CR-743/1/ c02 N68-35177

FLORIDA

Flight test of 40 foot parachute deployed at low supersonic speed and dynamic pressure NASA-TM-X-1623 c31 N68-29993 Launch vehicle flight tests of effects of Apollo heat shield irregularities on ablative material performance NASA-TN-D-4791 c33 N68-35116 Flow distribution in flight test and wind tunnel hypersonic flow of X-15 aircraft NASA-TN-D-4813 c01 N68-35173 FLORIDA Scalar and component wind correlations between altitude levels for statistical analysis of wind profiles at Cape Kennedy, Florida, and Santa Monica, California NASA-TN-D-3815 c13 N68-2 c13 N68-20278 FLOW CHARACTERISTICS Mathematical model for deriving pressure drop against flow function of counterflow boiler tube in Rankine space power system NASA-TN-D-4498 c33 N68-20066 Performance characteristics and operating parameters of three-fluid crossflow heat exchangers NASA-TR-R-284 c33 N68-23513 Analytical and experimental investigation of propellant distribution during outflow of spherical tanks for possible space vehicle application NASA-TN-D-4828 c12 N68-35104 FLOW COEFFICIENTS Thermodynamic effects of cavitation in low temperature liquid hydrogen over range of flow coefficients using flat plate helical inducer NASA-TN-D-4423 c28 N68-182; c28 N68-18221 FLOW DIRECTION INDICATORS Combination temperature, pressure, and flow direction sensing probe to study rotating machinery NASA-TN-D-4816 c14 N68-36021 FLOW DISTORTION Effect of hydrogen peroxide generator configurations on jet exhaust flow characteristics NASA-TM-X-1671 c12 N68-37067 FLOW DISTRIBUTION Flow conditions in inlet manifold of M-1 fuel pump drive turbine investigated using circumferential static pressure measurements in conjunction with smoke trace photographs NASA-TM-X-1513 cl2 N68-1563: c12 N68-15639 Flow distributions in radial outflow vortices using rotating peripheral wall water vortex tube NASA-CR-991 c22 N68-16478 MADA CR 551 Static pressure and flow field for flat plate model with short trailing-edge flap NASA-TN-D-4308 c12 N68-17376 Noncavitating flow mechanisms in two low area ratio water jet pumps with throat lengths of 7.25 diameters c15 N68-17564 NASA-TN-D-4445 Gravity effects on forced circulation pattern in spherical tanks NASA-TN-D-4409 c12 N68-20352 Comparison of mixed and isolated flow methods for cooled turbine performance using two simplified example turbines NASA-TM-X-1572 c01 N68-21692 COI N68-2169 Leading-edge heat transfer effects of three types of interfering flow fields NASA-TN-D-4543 C33 N68-2211 c33 N68-22118 Wind tunnel calibration of conical pressure probe over range of Mach numbers to determine flow field data for X-15 airplane NASA-TN-D-4678 c12 N68-28801 Visual observations to find flow distribution and coefficients through radial bladed centrifugal pump impeller NASA-TN-D-4282 c12 N68-28842 Wind tunnel calibration of 30 deg included angle cone for determination of local values of Mach number, total pressure, and flow distribution NASA-TN-D-4679 c14 N68-3012 c14 N68-30127 Jet VTOL aircraft inlet temperature rise and induced recirculating flow patterns NASA-CR-1147 NASA-CR-1147 c01 N68-33043 Conference on sonic boom reduction in supersonic

Conference on sonic boom reduction in supersonic transport flight — shock wave propagation and refraction, prediction methods for acoustic

attenuation, and aerodynamic engineering aspects NASA-SP-180 c02 N68-34907 NASA-SP-180 COE NASA-3490 Computation of mean and fluctuating quantities in turbulent boundary layers NASA-TN-D-4815 c12 N68-36071 Wind tunnel tests at Mach 1.60, 2.36, and 2.96 to determine flow field properties near arrow wing body model for locating potential engine air inlets NASA-TN-D-4809 FLOW EQUATIONS c01 N68-37238 Pressure rise response of turbopumps to flucturating flow rates and unsteady flow about two dimensional linear cascade of airfoils c01 N68-21950 NASA-TN-D-4298 FLOW GEOMETRY Similarity parameters used for examining geometry characteristics of axial flow turbines with high expansion ratio NASA-TN-D-4248 c01 N68-10529 handring 10-12-220 Heat transfer characteristics for turbulent flow of heat generating liquid metals between parallel plates with wall heat transfer NASA-TN-D-4336 c33 N68-1404 c33 N68-14042 Effect of geometry of conical afterbodies on base drag at subsonic and transonic speeds NASA-TN-D-4821 c01 N68-37054 c01 N68-37054 FLOW REGULATORS Vortex valve for hot gas flow modulation in secondary injection thrust vector control system NASA-CR-1091 c28 N68-28112 FLOW STABILITY Stability of shear flow with density gradient and viscosity c12 N68-15530 NASA-CR-958 Containment tests of vortexes with radial outflow in basic vortex tube, and in axial-flow vortex tube NASA-CR-993 c22 N68-18243 Wall injection area and axial bypass effects on flow pattern of stagnation surface in radial inflow vortexes NASA-CR-1028 c22 N68-22088 Single tube-in-shell water-boiling heat exchanger performance with helical wire insert and flow stabilizing devices NASA-TN-D-4767 c33 N68-32 c33 N68-32099 FLOW THEORY Turbulent boundary layer and transition on plane plates NASA-TT-F-520 c12 N68-17563 Leakage testing theory and testing methods handbook NASA-CR-952 c15 N68-20389 FLOW VELOCITY Hot-wire anemometer system for measuring velocity fluctuations in turbulent coaxial flow field of dissimilar fluids NASA-CR-961 c12 N68-12892 Analytical investigation of electrical heated wire mesh for flowing gas heaters NASA-TN-D-4595 c33 N68-25312 FLOW VISUALIZATION Flow visualization and containment tests in outflow and moderate superimposed axial flows NASA-CR-992 c22 N68-17131 FLOWMETERS Performance of venturi meter with separable diffuser NASA-TM-X-1570 c14 N68-21384 FLUID AMPLIFIERS Breadboard flueric circuitry used to drive pneumatic stepping motors NASA-TN-D-4495 c03 N68-21651 FLUID DYNAMICS Free jet mixing analysis for parallel streams of different fluids NASA-CR-956 cl2 N68-136 c12 N68-13619 Specific nuclear light bulb and open-cycle vortex stabilized gaseous nuclear rocket engine designs NASA-CR-1030 c22 N68-22038 Wall injection area and axial bypass effects on flow pattern of stagnation surface in radial inflow vortexes NASA-CR-1028 c22 N68-22088 Equations of motion for calculating compressible turbulent boundary layers NASA-CR-1144 c12 N68-35096

Converging flow effects on longitudinal stability measurements in tandem test section of wind tunnel NASA-CR-1198 c11 N68-36522 FLUID FLOW Window designs for mercury condensing tube and mercury boiler outlet tube NASA-TM-X-1578 c11 N68-22737 High speed fluid film lubrication NASA-CR-1058 c15 N68-22810 Convective heat transfer coefficients on adiabatic walls determined by sinusoidally forced fluid temperature NASA-TM-X-1594 c33 N68-24618 Fluid mechanics information applied to gaseous nuclear rocket engines NASA-CR-1190 c22 N68-30 c22 N68-36615 FLUID JETS Breakup, and displacement of liquid jets in crossflow of shock tube NASA-TN-D-4334 c33 N68-15942 Maximum drop diameters for atomization of liquid jets injected concurrently into accelerating or decelerating gas streams NASA-TN-D-4640 c12 N68-28364 FLUIDICS Three axis fluidic automatic flight control system developed and flight tested NASA-CR-913 c02 N68-10047 Fluidic analog to pulse frequency converter for pneumatic reactor control drum actuator system NASA-TN-D-4497 c03 N68-218 c03 N68-21835 magnetically permeable liquid bead with nondestructive memory for gas flow control NASA-TM-X-1613 c09 N68-30501 FLUORINE Liquid fluorine pump, impeller, and inducer corrosion resistance to cavitation flow NASA-TM-X-1573 c15 NG c15 N68-28241 FLUORINE COMPOUNDS Friction torque of ball bearings in vacuum to determine lubricating capability of polytetrafluoroethylene-composition retainer materials NASA-TN-D-4355 c15 N68-16468 FLUOROCARBONS High temperature tests to determine fatigue life of 120mm bore ball bearings with fluorocarbon, polyphenyl ether, and synthetic base paraffin base lubricants NASA-TN-D-4850 c15 N68-36075 FLUTTER ANALYSIS Nonlinear flutter of circular cylindrical shell in supersonic flow NASA-TN-D-4265 c32 N68-12864 Subsonic and transonic flutter and flow studies of T tail of large multijet cargo airplane NASA-TN-D-4316 c02 N68-17055 Flutter analysis on buckled supported rectangular panels under supersonic surface flow NASA-TN-D-4357 c c32 N68-17651 Experimental study, and theoretical analysis on supersonic flutter of corrugation stiffened panels NASA-TN-D-4321 c32 N68-19143 NASA-IN-D-4321 c32 N68-19143 FLUX (RATE) Fast and thermal neutron flux measurements in test cavity outside HB-6 beam port in Plum Brook reactor using sulfur pellets and gold foils NASA-IN-2-1497 c22 N68-15643 FLYBY MISSIONS FORTRAN computer program for computing mass in earth orbit for round trip-stopover missions, flyby missions, and orbital missions with single-stage high-thrust system for each phase NASA-TM-X-1541 c30 N68-1 Navigation and guidance analysis of Mars probe launched from manned flyby spacecraft NASA-TN-D-4512 c21 N68-2 c30 N68-19330 c21 N68-21754 Venus flyby, Mars flyby, and Mars orbital mission to evaluate navigation and guidance systems for manned interplanetary spacecraft NASA-TN-D-4629 c21 N68-28236 Assessing cryogenic fluid requirements and storage methods for manned earth orbital and Mars flyby missions, and parametric data on thermal protection schemes NASA-TN-D-4619

Trajectory data for stopover missions to Mars that employ Venus swingby mode NASA-SP-35, PT. 6 c30 N68-30(Analysis of launch windows from circular orbits for representative Mars missions c30 N68-30098 NASA-TM-X-1651 c30 N68-33371 FOG Warm fog and fog modification by seeding with salt particles NASA-CR-1071 c20 N68-25816 Cumulus cloud and fog bank spectral reflectance observations using Nimbus satellites and infrared radiometers NASA-TN-D-4552 c14 N68-25862 CE DISTRIBUTION Nonlinear lift and pressure distribution of slender conical bodies with strakes at low speed c01 N68-37255 FORCE DISTRIBUTION FOREBODIES Effect of model forebody shape on perforated supersonic wind tunnel wall interference NASA-TM-X-1656 FORM FACTORS c01 N68-36133 Inelastic scattering form factors using projected Hartree-Fock wave functions NASA-TN-D-4566 c24 N68-24661 FORMING TECHNIQUES Floating mandrel technique for extrusion of thin walled tungsten tubing NASA-TM-X-1638 c15 N68-32977 FURTRAN FORTRAN 4 program for computerized design of two dimensional supersonic nozzles with sharp edged throats NASA-TM-X-1502 c01 N68-14747 FORTRAN computer program for calculating model planetary atmospheres and density and temperatue dispersion data for Apollo reentry c30 N68-15793 NASA-TN-D-4292 FORTRAN subroutines for determining intersections of nuclear particle flight path and wall of helical tubular duct NASA-TN-D-4435 c22 N68-18541 NBAR-IN-D-4435 FORTRAN digital computer program for axial distribution of aerodynamic normal force characteristics for axisymmetric, multistage launch vehicles in linear angle of attack ranges NASA-TN-D-4342 c31 N68-18615 FORTRAN program for approximate calculation of supersonic ideal gas flow past blunt bodies with sonic corners NASA-TN-D-4563 c01 N68-25093 FORTRAN subroutines for plotting and drawing of three dimensional solid surfaces NASA-TM-X-1598 c19 N68-28240 FORTRAN 4 programs for calculating inviscid, one-dimensional and axisymmetric nonequilibrium nozzle flow fields and improving analytical predictions of delivered specific impulse NASA-CR-1123 c27 N68-32793 FOURIER SERIES Plane stress analysis using Fourier series of edge stiffened isotropic or orthotropic elastic rectangular plate subjected to prescribed temperature distribution and boundary loads NASA-CR-978 c.32 N68-19311 Fourier series expansion of simultaneous integral equations for collinear coupled waveguides radiating through common perfectly conducting ground plane NASA-TN-D-4656 c09 N68-280 FOURIER TRANSFORMATION c09 N68-28668 Fourier transforms for aperture admittance of ground-plane-mounted waveguide illuminating conducting sheet NASA-TN-D-4366 c07 N68c07 N68-18123 Fourier integration of electrical impedance expressions for nonlossy dielectric and lossy plamas NASA-TN-D-4774 c07 N68-35524 Mathematical determination of geometrical image aberrations in single and double mirror systems NASA-TN-D-4692 c23 N68-3646 c23 N68-36460 FRACTURE MECHANICS Necking, yield, and plastic flow in electrical analogs of mechanical systems with respect to energy conversion effects on mechanical behavior of various materials NASA-CR-1039 c24 N68-21949

I-39

c03 N68-28420

FRACTURE STRENGTH

FRACTURE STRENGTH Fatigue crack propagation and fracture toughness characteristics of 7079 aluminum alloys in underage, peak age, and overaged conditions NASA-CR-996 c32 N68-154 c32 N68-15476 Texture strengthening and fracture toughness of titanium alloy sheet at room and cryogenic temperatures NASA-TN-D-4444 c17 N68-22884 Residual stress effects on fracture strength of AISI 301 stainless steel and Ti-5Al-2.55n titanium cracked thin walled cylinders NASA-TN-D-4777 FREE ATMOSPHERE c32 N68-33191 Electric field of free atmosphere NASA-TT-F-425 FREE CONVECTION c13 N68-10079 Design, fabrication and testing of Cb-1Zr thermal convection loop for evaluation of refractory metals in boiling and condensing potassium environments NASA-CR-1097 c22 N68c22 N68-35153 FREE FLIGHT Free flight aerodynamic characteristics of slender cone at hypersonic speeds NASA-TN-D-4245 c01 N68-10380 Computer program for analyzing free flight motions of axisymmetric bodies to determine aerodynamic coefficients NASA-TN-D-4766 FREE VIBRATION c01 N68-33081 Prediction of vibration frequencies and modes for free-free truncated conical shells, using Rayleigh-Ritz method NASA-TN-D-4772 c32 N68-33 Mathematical model for analyzing free vibration of rotating beam-connected space station NASA-TN-D-4753 c32 N68-33 c32 N68-33057 c32 N68-33225 FREEZING Effects of freezing-melting cycles on primary silver oxide zinc batteries NASA-TM-X-1681 c03 N68c03 N68-37265 FREON Effects of Freen, water flow temperatures, and pressures on incipient venturi cavitation NASA-TN-D-4340 c12 N68-14641 Thermodynamic effects on Freon cavitation on venturi scale model NASA-TN-D-4387 c12 N68-15329 FREQUENCIES Critical speed analysis of rigid rotors on flexible foundations NASA-TN-D-4858 c15 N68-37214 FREQUENCY DISTRIBUTION Frequency function for testing small samples for goodness of fit to normal populations NASA-TN-D-4405 cl9 N68-191 FREQUENCY MODULATION c19 N68-19144 FM EQUENCY HUDDLATION FM data handling facility for preparing analog physiological data obtained in flight for digital computations NASA-TN-D-4488 c05 N68-2 FREQUENCY RANGES c05 N68-21537 Resolution limit analysis for pulse frequency modulation telemetry processing line NASA-TN-D-4180 c c07 N68-18247 FREQUENCY SYNTHESIZERS Digital voltage controlled oscillator for phase lock loops using coherent frequency synthesizer NASA-TN-D-4521 c09 N68-24389 FRETTING Friction and fretting wear tests on materials used as friction dampers to reduce vibrational stresses in compressor blades for turbine engines NASA-TN-D-4630 c15 N68-28871 FRICTION Friction and fretting wear tests on materials used as friction dampers to reduce vibrational stresses in compressor blades for turbine engines NASA-TN-D-4630 c15 N68-28871 Influence of chemisorbed films of various gases on adhesion and friction of tungsten in vacuum NASA-TN-D-4694 c15 N68-33227 FRICTION FACTOR

Influence of crystal structure, orientation, and solubility on adhesion and sliding friction of metal single crystals in vacuum

SUBJECT INDEX

NASA-TN-D-4347	c15 N68-21226
FRICTION MEASUREMENT Convective heat exchange in homogene	oue cae modia.
including heat transfer and fricti	on resistance
in pipes, hydrodynamics and heat t jets, and intensification of conve	ransfer in
jets, and intensification of conve NASA-TT-F-431	ction
FRICTION REDUCTION	c33 N68-11721
Sputtered molybdenum disulfide film	deposition and
friction characteristics in vacuum	
NASA-TN-D-4269	c17 N68-11644
Reduction of adhesive forces and fri polycrystals in vacuum by chemisor	
NASA-TN-D-4775	c17 N68-33278
FUEL CELLS	
Improved service life through reduct	
discharges in copper oxide-magnesi cells	um thermal
NASA-TN-D-4306	c03 N68-20344
Transient thermodynamic analysis for	development
of mathematical model that predict temperature and voltage-response of	s transient baracteristics
of fuel cell system	
NASA-TN-D-4601	c03 N68-25304
FUEL COMBUSTION	notion in
Hydrogen-oxygen chemical reaction ki rocket engine combustion	netics in
NASA-TN-D-4250	c33 N68-11642
FUEL FLOW REGULATORS	
Development, configuration, and oper Centaur propellant utilization sys	
NASA-TN-D-4848	c28 N68-36507
FUEL INJECTION	
Coaxial injector thrust effects on o	
stability of hydrogen-oxygen rocke NASA-TN-D-4851	c28 N68-36515
FUEL SYSTEMS	
Development, configuration, and open	
Centaur propellant utilization sys NASA-TN-D-4848	c28 N68-36507
FUEL TANK PRESSURIZATION	C20 N00-J0J07
Gravity effects on self-pressurizati	on of
spherical liquid hydrogen tankage	
NASA-TN-D-4286 Design and volumetric analysis of pr	c27 N68-11645
tanks for use in liquid-methane for	
supersonic transport aircraft	
NASA-TN-D-4295	c32 N68-12370
Fuel tank pressurization and superco liquid methane to minimize fuel bo	
in supersonic aircraft	
NASA-TM-X-1604	c27 N68-28155
FUEL TANKS Evaluation of self-evacuating multil	aver radiation
shields for cryogenic storage tan	
NASA-TN-D-4375	c33 N68-18046
Tankage systems for methane-fueled s	supersonic
transport NASA–TM–X–1591	c02 N68-23895
Comparative analysis of fuselage tar	
methane fueled supersonic aircraft	t -
NASA-TN-D-4837 Full scale tests	c02 N68-36074
Full scale tests of major thrust ver	ctor control
system parameters and verification	
operation	
NASA-CR-938 Fabrication and testing of Pageos 1	c32 N68-10574
NASA-TN-D-4596	c31 N68-25820
Full scale lunar gravitation simula	
1/6 scale model	c11 N68-25853
NASA-TN-D-4474 Functional Analysis	CII NO0-20800
Liapunov stability theory applied to	class of
partial differential equations, a	nd generation
of contraction groups related to e NASA-CR-1100	c19 N68-27457
FUNCTIONS (MATHEMATICS)	NIJ NU0-2/40/
Numerical procedures and computer p	rogram for
calculating real fluid and thermo	
properties of normal and parahydro NASA-TN-D-4341	c08 N68-15798
Tabular and graphical data on calcu	
Chandrasekhars X and Y functions	and analogs
for noncoherent isotropic scatter NASA-TN-D-4712	ing c19 N68-30804
Feynman formalisms for expressing i	
commutators and functions of operations	ators
NASA-TN-D-4857	c19 N68-36525

Comparative analysis of fuselage tanks for liquid

FIISFLAGES

GAS LUBRICANTS

methane fueled supersonic aircraft NASA-TN-D-4837 c02 N68-36074 G GALACTIC EVOLUTION Two dimensional computer model for collisionless self gravitating galactic system with gravitational field obtained from Poisson equation equation NASA-TN-D-4646 c30 N68-2 GALACTIC RADIATION Energetic space radiation and galactic cosmic radiation measured for radiation hazards in c30 N68-28884 manned space flight NASA-TN-D-4404 c29 N68-16837 Radiation hazards on extended manned space flights NASA-CR-1037 c29 N68-22845 c29 N68-22849 GALLIUM ARSENIDE LASERS Gallium arsenide laser modulator, attenuation coefficients, and semiconductors for optical communication systems NASA-TN-D-4608 c23 N68-25868 GAMMA RAYS Comparison of absolute calculated and measured gamma and neutron doses in tungsten water-moderated critical assembly NASA-TN-D-4223 c22 N68-10291 Computer analysis of gamma ray spectra recordings from iodine 128, and cesium 128 decay c24 N68-15328 NASA-TN-D-4305 Gamma ray exposure rates in Plum Brook HB-6 facility measured with dosimeters and ion chambers NASA-TM-X-1490 c22 N68-17022 Point-kernel computation and experimental measurements of gamma heating effects during thermionic diode irradiation NASA-TM-X-1539 c22 N66 Effects of nuclear radiation on performance of diodes for use in SNAP 8 c22 N68-22022 NASA-TN-D-4683 NASA-TN-D-4683 Angular correlation between inelastically scattered alpha particles and gamma rays emitted in subsequent nuclear decay of magnesium 24 NASA-TN-D-4683 C24 N68-29375 Detection of supernovae pulse by gamma ray telescope and atmospheric scintillation method NASA-TN-D-4732 c29 N68-33370 Fabrication and development of annular lithium drifted germanium detector for studying nuclear reaction gamma rays NASA-CR-1138 c14 N68-3515 c14 N68~35152 NASA-CK-1138 C14 M68-33 Ratio of gamma heating per gram of tungsten to gamma heating per gram of water for thin tungsten detector in water shield NASA-TM-X-1680 c22 N68-33 c22 N68-37260 GAS BAGS Compartmented gas bag landing system with omnidirectional, multiple impact, and kinetic energy dissipation capabilities NASA-TN-D-4710 c32 N68-31(c32 N68-31602 GAS BEARINGS Gas lubricated bearing system for turbine compressor NASA-CR-802 c03 N68-24597 Experimental evaluation of gas injection start of Brayton cycle turbocompressor operating on gas bearings NASA-TM-X-1590 c03 N68-24757 Design and dynamic simulator testing of gas bearing rotor support for high performance axial flow turbomachinery NASA-CR-801 c15 N68-25042 C15 N68-251 Electronic visualization technique for studying dynamic behavior of gas journal bearing NASA-TM-X-1609 C14 N68-351 GAS COOLED REACTORS c14 N68-35105 Design data for gas cooled test loop, and inpile capsule facility from mockup reactor experiments NASA-TM-X-1509 c22 N68-15855 c22 N68-15855 Reactivity effects caused by radial power flattening in gas cooled, fast-spectrum reactor NASA-TN-D-4459 c22 N68-19925 Induction plasma heating system for hydrogen-argon simulated gas cooled reactor studies NASA-CR-1143 ca c25 N68-29888

GAS COOLING Cooling requirements of ball bearings operating in low flow rate hydrogen gas NASA-TN-D-4616 c15 N68-24456 GAS DYNAMICS Convective heat exchange in homogeneous gas media, including heat transfer and friction resistance in pipes, hydrodynamics and heat transfer in jets, and intensification of convection NASA-TT-F-431 c33 N68-11721 Physical gas dynamics research - molecular band spectra, shock tube studies, and interactions between diatomic molecules NASA-TT-F-505 c12 N68-16839 Gaseous motion and hydrodynamic model for analysis of binary star atmosphere NASA-TN-D-4520 c30 N68-25385 GAS FLOW Axial turbulence measurements in coaxial flow of dissimilar gases NASA-CR-960 c12 N68-13612 High temperature flowing gas heater consisting of four stages for heating gases NASA-TM-X-1506 c11 N68-1411 c11 N68-14115 Helium and air flow tests over single flat plates to determine dynamic pressure limits of nuclear fuel element plates NASA-TN-D-4417 c12 N68-16227 Heat transfer correlation for nitrogen flowing across electrically heated banks of wire meshes or tubes NASA-TN-D-4514 c33 N68-20374 Containment characteristics of radial inflow gases in vortex tubes NASA-CR-1029 c12 N68-22200 Effects of high wave amplitude and mean flow on impedance of Helmholtz resonator c12 N68-23423 NASA-TM-X-1582 Cooling requirements of ball bearings operating in low flow rate hydrogen gas NASA-TN-D-4616 c15 N68-24456 GAS GUNS Exploding foil gun technique for simulated meteoroid protection NASA-TN-D-4259 c32 N68-11355 GAS HEATING High temperature tungsten mesh gas heater design and operation NASA-TM-X-1466 c22 N68-10134 High temperature flowing gas heater consisting of four stages for heating gases Analytical investigation of electrical heated wire mesh for flowing gas heaters NASA-TN-D-4595 C33 N68-25312 NASA-TM-X-1506 c11 N68-14115 GAS INJECTION Experimental evaluation of gas injection start of Brayton cycle turbocompressor operating on gas bearings NASA-TM-X-1590 c03 N68-24757 GAS IONIZATION Plasma effects in antenna near zone field -admittance and ionization rise time measurements on Teflon-plugged waveguide slot antenna NASA-CR-1149 c07 N68-33042 GAS JETS Performance tests of rotating gas jet generator for strong traveling transverse acoustic modes NASA-TN-D-4380 cl2 N68-169 c12 N68-16998 Photographic study of bromine jet issuing into coaxially flowing airstream NASA-TN-D-4660 c12 N68-2 c12 N68-28370 Transmissivity of carbon particle-seeded nitrogen jet for heat transfer predictions NASA-TN-D-4722 c23 N68-30596 GAS LASERS Negative feedback for discharge current noise reduction in excited helium-neon laser NASA-CR-1173 c16 N68-35099 Carbon dioxide laser development for space application NASA-TN-D-4794 c16 N68-35175 Laser interferometer and heterodyne system for cesium plasma diagnostics NASA-TM-X-1652 c16 N68-35593 GAS LUBRICANTS High revolutions per minute rotor stability of herringbone-grooved gas-lubricated journal

I-41

GAS-METAL INTERACTIONS

bearings NASA-TN-D-4440 c15 N68-21965 Gas lubricated bearing system for turbine compressor NASA-CR-802 c03 N68-24597 GAS-METAL INTERACTIONS Adsorption isotherm relations and transient desorption behavior of homogeneous and heterogeneous metal surfaces NASA-TN-D-4789 c24 N64 c24 N68-34175 Influence of gaseous environment on self-adhesion of metal surfaces NASA-TN-D-4868 c17 N68-36970 GAS MIXTURES Trace contaminant identification using microwave double resonance spectroscopy NASA-CR-967 c24 N68-11634 Approximate methods for predicting viscosities of gas mixtures involving both polar and nonpolar gases NASA-TN-D-4496 c12 N68-21724 Optical radiation measurements behind shock wave in simulated Mars atmosphere NASA-TM-X-1634 c12 N68-32982 Simplified equilibrium hydrocarbon-air combustion gas model for use in air breathing engine cycle computer programs NASA-TN-D-4747 c28 N68-35115 Empirical stagnation point-heat transfer relation in gas mixtures at high enthalpy potentials NASA-TN-D-4799 c33 N68-35468 GAS PRESSURE Cover gas pressures affecting accelerated cavitation damage in sodium NASA-TN-D-4235 c17 c17 N68-10104 GAS STREAMS Maximum drop diameters for atomization of liquid jets injected concurrently into accelerating or decelerating gas streams NASA-TN-D-4640 c12 N68-28364 c12 N68-28364 GAS TRANSPORT Evaluation of ultrasonic absorption technique for measuring high temperature gas properties NASA-TN-D-4433 c24 NG c24 N68-18949 Very high burnup vapor transport fuel pin concept for long life nuclear reactors NASA-TN-D-4860 c22 N68-37209 GAS TURBINE ENGINES c22 N68-37209 Directional solidification of nickel base alloy TAZ-8B to enhance potential for advanced gas turbine engine applications NASA-TN-D-4390 c17 N68-15 c17 N68-15637 Reynolds number effect on single stage axial flow turbine in air NASA-TN-D-4383 c03 N68-16228 Oxidation resistance evaluation for metal alloy cooling materials in high temperature gas turbine engines NASA-CR-1184 c17 N68-350 c17 N68-35098 NASA-CK-1164 C17 N68-35098 Performance of single stage, axial flow turbine designed for Brayton cycle space power system NASA-TM-X-1666 c03 N68-37943 GAS TURBINES Cold air study of gas turbine for high temperature aircraft engine application NASA-TN-D-4389 c01 N68-15743 Cold air study of high temperature gas turbine -blade feature effects on stator performance NASA-TN-D-4418 c28 N68-16632 Nechanical design and development test program for two-stage potassium vapor Rankine cycle turbine NASA-CR-923 c03 N68-17075 Approximate average midspan metal temperatures and coolant flow requirements for turbine airfoils cooled by compressor exit bleed air NASA-TN-D-4491 c33 N68-19187 Aerodynamic characteristics of a stator modified gas turbine for single shaft Brayton cycle power system NASA-TM-X-1615 c03 N68-28870 Dilution-jet mixing flow studies for gas turbine combustion chambers NASA-TN-D-4695 GASEOUS FISSION REACTORS c01 N68-30128 Effect of turbulent mixing on average fuel temperatures in gas-core nuclear rocket engine NASA-TN-D-4882 c22 N68-37927 GASEOUS ROCKET PROPELLANTS

Specific nuclear light bulb and open-cycle vortex

SUBJECT INDEX

stabilized gaseous nuclear rocket engine designs NASA-CR-1030 c22 N68-22038 GASES Influence of chemisorbed films of various gases on adhesion and friction of tungsten in vacuum NASA-TN-D-4694 c15 N68-33227 GEMINI FLIGHTS Geologic applications of orbital photography with illustrations from Gemini flights NASA-TN-D-4155 c13 N68-1171 c13 N68-11714 Spaceborne photography of cloud cover and other meteorological phenomena, Surveyor and Orbiter lunar shots, and Gemini space walk and target docking NASA-SP-168 GEMINI PROJECT c30 N68-34870 Gemini Summary Conference NASA-SP-138 c30 N68-14941 Extravehicular activity accomplishments in Gemini program NASA-SP-149 c30 N68-15891 qualification testing for Gemini project c31 N68-25577 NASA-CR-1106 GEMINI SPACECRAFT Gemini-Agena station keeping using connecting tether - Analysis and simulations NASA-TN-D-4258 c31 N68c31 N68-11641 Microbiological contamination of Gemini 9 spacecraft before and after flight NASA-CR-972 c04 N68-11968 Effects of edge constraints on optical qualities of Gemini spacecraft windows NASA-TN-D-4845 c23 N68-3643 GEODETIC SATELLITES c23 N68-36470 Achievements of application technology satellites, communication satellites, navigation and traffic control satellite program, weather satellites, and satellite geodesy NASA-SP-156 c31 N68-16015 Potential applications of geodetic satellites to geology, oceanography, glaciology, and atmospheric physics NASA-SP-158 c13 c13 N68-18902 GEODETIC SURVEYS Geodetic laser system for earthquake prediction and engineering research NASA-SP-5042 c13 N68-23706 GEOLOGY Geologic applications of orbital photography with illustrations from Gemini flights NASA-TN-D-4155 c13 N68-11714 Potential applications of geodetic satellites to geology, oceanography, glaciology, and atmospheric physics NASA-SP-158 c13 N68-18902 GEUMAGNETISM Geomagnetic field secular variation /1900 to 1965/ NASA-TN-D-4527 c13 N68-21543 Continuum fluid theory of solar wind and its interaction with geomagnetic field NASA-TN-D-4482 c29 N68-25181 GERMANIUM Fabrication and development of annular lithium drifted germanium detector for studying nuclear reaction gamma rays NASA-CR-1138 c14 N68-3515; c14 N68-35152 Effects of zinc concentration on output of zinc doped germanium infrared detectors NASA-TN-D-4834 c26 N68-37 GERMANIUM COMPOUNDS c26 N68-37055 Parametric analysis of radioisotope cascaded thermoelectric generators with Si-Ge first stage and PbTe second stage NASĂ-TM-X-1501 c22 N68-14585 Effective volume power density analysis for radicisotope power generator with silicon germanium thermoelectric elements NASA-TM-X-1453 c03 N68-14630 GIMBALS Mathematical model and computer program for analysis of three and four gimbal systems NASA-TN-D-4689 c11 N68-29957 GLACIOLOGY Potential applications of geodetic satellites to geology, oceanography, glaciology, and atmospheric physics NASA-SP-158 c13 c13 N68-18902

GLASS Precision glass-bead peening equipment for propellant tank surface corrosion protection NASA-TN-D-4288 c15 N68-13 c15 N68-12890 GLASS FIBERS Tensile strength properties of glass, boron, and graphite filament wound resin composites and liners for cryogenic pressure vessels NASA-TN-D-4412 c18 N68-166 c18 N68-16623 GLIDE PATHS Thrust and altitude effects on ground track noise during steep approaches of four engine, medium range, turbojet transports NASA-TN-D-4241 c01 N68-1125 c01 N68-11253 Optimum maneuvering of glide vehicle at hypersonic speeds NASA-CR-1078 c02 N68-25817 GLYCOLS Flammability hazards chemically induced in aircraft and spacecraft electrical circuitry by glycol/water solutions NASA-TN-D-4327 c31 N68-2221 c31 N68-22213 GRADIENTS Newton-Raphson and gradient parameter correction technique for solution of optimal control problems NASA-TR-R-293 c19 N68-37073 GRAPHIC ARTS Hydra 1 data display system for developing graphic displays NASA-TN-D-4554 c08 N68-25002 GRAPHITE Tensile strength properties of glass, boron, and graphite filament wound resin composites and liners for cryogenic pressure vessels c18 N68-16623 NASA-TN-D-4412 Experimental determination of graphite triple point and liquid-solid interface NASA-CR-1148 c22 N68c22 N68-29390 GRAPHS (CHARTS) Geomagnetic field secular variation /1900 to 1965/ NASA-TN-D-4527 c13 N68-21543 c13 N68-21543 Graphs of phase and group refractive indices computed from collisionless magnetoionic theory electron concentration and magnetic field intensity NASA-TM-X-1553 c13 N68-21904 Computation of solar elevation angles and determination of sunrise and sunset times as function of latitude, longitude, and date NASA-TM-X-1646 c13 GRAVITATIONAL EFFECTS Gravity effects on self-pressurization of c13 N68-35179 spherical liquid hydrogen tankage NASA-TN-D-4286 c27 N68-11645 Gravity effects on bubble dynamics generated during nucleate boiling NASA-TN-D-4301 c33 N68-15330 Electroplethysmographic data on intercranial circulation, and dynamics of cerebral blood volume under normal conditions and gravitational stresses NASA-TT-F-492 c04 N68-15477 Gravity effects on forced circulation pattern in spherical tanks NASA-TN-D-4409 c12 N68-3 c12 N68-20352 GRAVITATIONAL FIELDS Pressure rise characteristics of liquid hydrogen dewar for homogeneous, normal-gravity quiescent, and zero-gravity tests NASA-TM-X-1134 c33 N68-181 Two dimensional computer model for collisionless c33 N68-18196 self gravitating galactic system with gravitational field obtained from Poisson equation NASA-TN-D-4646 c30 N68-288 GRAVITY GRADIENT SATELLITES Digital program for dynamics of nonrigid gravity gradient satellites c30 N68-28884 NASA-CR-1119 c30 N68-32744 GRAY GAS Radiation equilibrium in atmosphere with constant Einstein absorption coefficient NASA-TN-D-4479 c13 N68-22861 GREASES Test evaluation of high temperature greases and solid lubricants in thrust loaded ball bearings NASA-TN-D-4652 c15 N68-28766 GREEN FUNCTION Dielectric formulation for inhomogeneous electron gas, and Green function formalism for treating static dielectric screening of point impurity in electron gas NASA-TR-R-283 c26 N68-24273 GRINDING (COMMINUTION) Role of chemical reactions in comminution mechanism of ductile metals into ultrafine powders by grinding NASA-TN-D-4862 c15 N68-37239 GRINDING MACHINES Machining and grinding of ultrahigh-strength steels and stainless steel alloys NASA-SP-5084 c15 N68-21241 GROOVES High revolutions per minute rotor stability of herringbone-grooved gas-lubricated journal hearings NASA-TN-D-4440 c15 N68-21965 Spinning friction and torque dependence on ball bearing-groove conformity NASA-TN-D-4669 c15 N68-28258 GROUND EFFECT Air flow calibration over moving belt ground plane installed in wind tunnel and data for two blowing-flap models tested over moving belt NASA-TN-D-4228 c01 N68-10060 Wind tunnel study of scale model automobile ground plane boundary layer using moving-belt ground plane technique NASA-TN-D-4229 col N68-10 c01 N68-10093 Ground proximity effects on longitudinal, lateral, and control aerodynamic characteristics of tilt wing four propeller V/STOL wind tunnel model NASA-TN-D-4237 c02 N68-1 c02 N68-11519 Aerodynamic ground effect measurements on low aspect ratio ogee wings NASA-TN-D-4329 c02 N68c02 N68-14090 Integral equations for inviscid flow field induced by rotor in ground effect NASA-CR-1027 coll N68-22475 Performance characteristics from static tests in ground effect of V/STOL transport model NASA-CR-1180 c28 N68-355 c28 N68-35594 GROUND STATIONS Equipment specifications and engineering drawings for automatic picture transmission ground stations NASA-SP-5079 c07 N68-19624 GROUND TRACKS Thrust and altitude effects on ground track noise during steep approaches of four engine, medium range, turbojet transports NASA-TN-D-4241 col N68-11253 c01 N68-11253 GROUP THEORY Liapunov stability theory applied to class of partial differential equations, and generation of contraction groups related to equivalent norms NASA-CR-1100 c19 N68-27457 Systematic procedure for constructing character table of finite group NASA-TN-D-4763 c19 N68-31 c19 N68-31961 GUIDANCE (MOTION) Guidance, flight mechanics, and trajectory optimization - calculus of variations and modern applications NASA-CR-1003 c30 N68-15193 Piloted simulation studies of Saturn 5 launch vehicle manual backup guidance and control NASA-TN-D-4481 c21 N68-19061 Dynamic programming and multistage decision processes in guidance, flight mechanics, and trajectory optimization NASA-CR-1009 c30 N68-21077 Design of guidance and control systems for optimum utilization of information c10 N68-23438 NASA-CR-997 GUIDE VANES Inlet guide vane choking noise reduction in axial flow compressors NASA-TN-D-4682 c02 N68-29406 Turbojet engine noise reduction by increasing Intake system guide vane-rotor blade spacing NASA-TN-D-4690 c28 N68-30040 GUST LOADS Velocity, gust, and height data analysis from four-engine turbojet transport airplane NASA-TN-D-4330 c02 N68-16522

GUSTS

Analog computed time histories and		
Andiod computed time distories and	altitude-ground	
track plots of swept wing transpo		
longitudinal response to wind shear and		
sustained gusts during landing ap		
NASA-TN-D-4477	c01 N68-19180	
Statistical analysis of repeated ac		
impact loads on airline transport		
NASA-TN-D-4586	c02 N68-24476	
GUSTS		
Summary of vertical gusts acceleration data		
collected for one type twin engin	e jet airplane	
during airline operations		
NASA-TN-D-4529	c02 N68-22291	
GYROSCOPES		
Precision tilt and vibration isolation system		
design		
NASA-TR-R-281	c14 N68-19642	
	CI4 NOC 19042	
H		
HABITABILITY		
HABITABILITY Spacecraft habitability for long du	ration manned	
HABITABILITY Spacecraft habitability for long du ' space flight missions		
HABITABILITY Spacecraft habitability for long du ' space flight missions NASA-CR-1084	ration manned c30 N68-26702	
HABITABILITY Spacecraft habitability for long du 'space flight missions NASA-CR-1084 HAFNIUM ALLOYS	c30 N68-26702	
HABITABILITY Spacecraft habitability for long du ' space flight missions NASA-CR-1084	c30 N68-26702	
HABITABILITY Spacecraft habitability for long du 'space flight missions NASA-CR-1084 HAFNIUM ALLOYS	c30 N68-26702 cts on high	
HABITABILITY Spacecraft habitability for long du 'space flight missions NASA-CR-1084 HAFNIUM ALLOYS Composition and heat treatment effe	c30 N68-26702 cts on high	
HABITABILITY Spacecraft habitability for long du 'space flight missions NASA-CR-1084 HAFNIUM ALLOYS Composition and heat treatment effe temperature strength of arc melte	c30 N68-26702 cts on high	
HABITABILITY Spacecraft habitability for long du 'space flight missions NASA-CR-1084 HAFNIUM ALLOYS Composition and heat treatment effe temperature strength of arc melte tungsten-hafnium-carbon alloys NASA-TN-D-4379	c30 N68-26702 cts on high d	
HABITABILITY Spacecraft habitability for long du 'space flight missions NASA-CR-1084 HAFNIUM ALLOYS Composition and heat treatment effe temperature strength of arc melte tungsten-hafnium-carbon alloys NASA-TN-D-4379 HALITES	c30 N68-26702 cts on high d c17 N68-17317	
HABITABILITY Spacecraft habitability for long du 'space flight missions NASA-CR-1084 HAFNIUM ALLOYS Composition and heat treatment effe temperature strength of arc melte tungsten-hafnium-carbon alloys NASA-TN-D-4379 HALITES Ionic conductivities of solid mixtu	c30 N68-26702 cts on high d c17 N68-17317 res of lithium	
HABITABILITY Spacecraft habitability for long du 'space flight missions NASA-CR-1084 HAFNIUM ALLOYS Composition and heat treatment effe temperature strength of arc melte tungsten-hafnium-carbon alloys NASA-TN-D-4379 HALITES Ionic conductivities of solid mixtu fluoride-lithium chloride, lithiu	c30 N68-26702 cts on high d c17 N68-17317 res of lithium m chloride-	
HABITABILITY Spacecraft habitability for long du 'space flight missions NASA-CR-1084 HAFNIUM ALLOYS Composition and heat treatment effe temperature strength of arc melte tungsten-hafnium-carbon alloys NASA-TN-D-4379 HALITES Ionic conductivities of solid mixtu fluoride-lithium chloride, lithiu potassium chloride, lithium fluor	c30 N68-26702 cts on high d c17 N68-17317 res of lithium m chloride- ide-sodium	
HABITABILITY Spacecraft habitability for long du 'space flight missions NASA-CR-1084 HAFNIUM ALLOYS Composition and heat treatment effe temperature strength of arc melte tungsten-hafnium-carbon alloys NASA-TN-D-4379 HALITES Ionic conductivities of solid mixtu fluoride-lithium chloride, lithiu	c30 N68-26702 cts on high d c17 N68-17317 res of lithium m chloride- ide-sodium	

HALL EFFECT Automated Hall effect and resistivity apparatus for studying electrical transport properties of semiconductors NASA-TM-X-1464 c03 N68-10103 HAMILTONIAN FUNCTIONS Methods of eliminating short period terms from Hamiltonian by means of canonical transformation NASA-TN-D-4399 HAMMERHEAD CONFIGURATION c19 N68-17532 Dynamic response of axisymmetric hammerhead model to unsteady aerodynamic loading in wind tunnel tests NASA-TN-D-4504 c01 N68-25916 HANDBOOKS NASA Thesaurus – A through L alphabetical listing of terms for indexing and retrieving

aerospace related documents NASA-SP-7030, V. 1 c34 N68-1: NASA Thesaurus - M through Z alphabetical listing of terms for indexing and retrieving aerospace related documents c34 N68-11307 NASA-SP-7030, V. 2 c34 M Appendices to NASA Thesaurus for indexing c34 N68-11308 scientific and technical information - category term listing, hierarchical display, permuted index, and postable terms NASA-SP-7030, V. 3 c34 Ni Leakage testing theory and testing methods c34 N68-11309 handbook NASA-CR-952 c15 N68-20389 Handbook on planetary physics NASA-TT-F-515 c30 N68-21802 Microelectronic device data handbook /text/ NASA-CR-1110 c09 NG c09 N68-29525 Microelectronic device data handbook /manufacturer and specific device information/ NASA-CR-1111 c09 N68-295 c09 N68-29526 HANSEN LUNAR THEORY

Hansen planetary theory NASA-TN-D-4169 c30 N68-11369 Modifications and simplifications of Hansen lunar theory NASA-TN-D-4562 c30 N68-26642 HARDWARE Hardware design and computer programs for spaceborne multiprocessor computer system

NASA-CR-1158 c08 N68-31499 Application of testing to hardware programs NASA-CR-1128 c15 N68-32779 HARMONIC GENERATORS Electromagnetism in moving conduction and c

Electromagnetism in moving, conducting media solution to problems involving static and

radiation fields of static charges, and radiation fields of harmonic current sources c23 N68-21444 NASA-CR-1025 HARTREE APPROXIMATION Inelastic scattering form factors using projected Hartree-Fock wave functions NASA-TN-D-4566 c24 N68-24661 HATCHES Leakage of large diameter O ring seals on spacecraft air lock hatches NASA-TN-D-4394 c31 | c31 N68-17498 HEART RATE Sensitive piezoelectric transducer with electric and mechanical noise rejection features for measuring cardiac and gross motor activity of small organisms NASA-TN-D-4590 c05 N68-25060 HEAT BALANCE Heat balance equations for optimizing optical coating patterns for spacecraft temperature control system NASA-CR-1041 c18 N68-22391 Evaluation of Nimbus satellite radiation measurements and heat balance charts of earth atmosphere c13 N68-28222 NASA-TN-D-4589 Analytical method for finding heat balance of insulated OGO experiment packages from thermal stability data and without solar simulation NASA-TN-D-4644 cll N68-294 c11 N68-29478 HEAT EXCHANGERS Steady state performance tests on single pass counterflow sodium-potassium cooled mercury Rankine cycle condenser NASA-TM-X-1548 c33 N68-20340 HEAT FLUX Boundary condition solution and transcendental approximation for transient heat conduction problem NASA-CR-955 c19 N68-11109 Minimum film boiling heat flux in vertical flow of liquid nitrogen NASA-TN-D-4307 c33 N68-16683 Control of the contro c33 N68-33203 Single-thermocouple method for measuring heat flux in thermally thick walls NASA-TN-D-4737 c33 N68-33208 HEAT GENERATION Three dimensional analysis for determining effects of heat generation in plates NASA-TN-D-4326 c33 N68-18122 HEAT PIPES Operating characteristics and limits of vapor chamber fins or heat pipes NASA-CR-1139 c33 N68-3 c33 N68-33203 HEAT RESISTANT ALLOYS Dividation resistant alloys tested for suitability as transpiration cooled gas turbine blades NASA-CR-930 c17 N68-17591 Cobalt-tungsten ferromagnetic, high temperature structural alloy for rotor applications in space power generators NASA-TN-D-4338 c17 N68-18145 Oxidation resistance and ductility of cobalt heat resistant alloys optimized by restriction of silicon and manganese content NASA-TN-D-4715 c17 N68-29954 Oxidation resistance evaluation for metal alloy cooling materials in high temperature gas turbine engines NASA-CR-1184 C17 N68-35 c17 N68-35098 HEAT SHIELDING Ablation and temperature data for Apollo heat shield material using Pacemaker vehicle for flight test NASA-TN-D-4713 c33 N68-30747 Launch wehicle flight tests of effects of Apollo heat shield irregularities on ablative material performance NASA-TN-D-4791 c33 N68-35116 HEAT STORAGE Lunar surface layer considered to store solar energy for generating power during lunar night NASA-TM-X-1560 c03 N68-20363 Automatically controlled heat removal in water cooled space suits NASA-CR-1085 c05 N68-26701

HEAT TOLERANCE Heat stress and prolonged activity effects on human perceptual motor performance NASA-CR-1153 c05 N68-31480 HEAT TRANSFER Film boiling mist flow heat transfer using single phase variable property NASA-TN-D-4149 c33 N68-11636 Weight, heat transfer, and efficiency comparison for Rankine cycle space radiators constructed of three different finned tube geometries c33 N68-16324 NASA-TN-D-4411 Pressure and heat transfer on blunt concave and convex plates in hypersonic flow NASA-TN-D-4367 c12 N68-18253 RHOR-IN-U-4307 Effect of two dimensional multiple sine wave protrusions on pressure and heat transfer distributions for flat plate in hypersonic flow NASA-TN-D-4437 c01 N68-19063 MAGN-IN-U-4407 Approximate equations for computing enthalpy and velocity derivatives at surface of flat plate, cone, or blunt axisymmetric body NASA-TN-D-4484 C33 N68-2000 c33 N68-20065 Effect of finned-tube assembly techniques on heat transfer characteristics of space radiator NASA-TM-X-1557 c33 N68-21704 Point-kernel computation and experimental measurements of gamma heating effects during thermionic diode irradiation NASA-TM-X-1539 c22 N68-2; c22 N68-22022 Leading-edge heat transfer effects of three types of interfering flow fields NASA-TN-D-4543 c33 N68-22118 Performance characteristics and operating parameters of three-fluid crossflow heat exchangers NASA-TR-R-284 c33 N68-23513 Rarefied gas couette flow and heat transfer between parallel plates analyzed by model sampling procedures NASA-TN-D-4579 c12 N68-24129 Differential equations based on heat transfer and shear for temperature and velocity in turbulent boundary layers NASA-TN-D-4611 c33 N68-25917 NASA-IN-D-4011 C35 NoB-2591 Integral methods for predicting afterbody heat transfer to blunt two dimensional configuration subjected to separated flow NASA-TN-D-4443 c12 N68-2828 c12 N68-28282 Thermal radiation heat transfer data, radiative properties of black bodies, and electromagnetic theory NASA-SP-164 c33 N68-28530 Effect of boundary layer bleed on heat transfer and pressure distributions over wedge-flap surface at hypersonic speeds NASA-TN-D-4686 c01 N68-29955 Transmissivity of carbon particle-seeded nitrogen jet for heat transfer predictions NASA-TN-D-4722 c23 N68-30596 Heat transfer characteristics of cylindrical ejector for turbojet engine and shroud material temperature prediction NASA-TM-X-1641 c33 N68-3298 c33 N68-32988 Heat transfer effect on drag due to surface roughness in supersonic turbulent boundary layer NASA-TN-D-4746 c12 N68-33054 Laminarization of turbulent boundary layer observed from heat transfer and boundary layer measurements in conical nozzles NASA-TN-D-4788 c12 N68-33642 Empirical stagnation point-heat transfer relation in gas mixtures at high enthalpy potentials NASA-TN-D-4799 c33 N68-35468 c33 N68-35468 HEAT TRANSFER COEFFICIENTS Single correlating equation for single phase forced convection heat transfer coefficients for turbulent flow through tubes over wide ranges of temperature ratios NASA-TN-D-4332 c33 N68-14240 Potential use of high frequency induction heating for high temperature liquid metal heat transfer testing NASA-TM-X-1510 c33 N68-16300 Boiling heat transfer coefficients, interface behavior, and vapor quality in heated wall rotating boilers with continuous through-flow of water as test fluid

c33 N68-17566 NASA-TN-D-4136 Computer program for determining geometric configuration view factors for spherical and conical surfaces of spherical radiating bodies NASA-TN-D-4457 c33 N68-20331 Convective heat transfer data for water flow in heated circular tubes with varying heat fluxes and flow areas NASA-TM-X-1554 c33 N68-20338 Heat transfer correlation for nitrogen flowing across electrically heated banks of wire meshes or tubes c33 N68-20374 NASA-TN-D-4514 NASA-IN-D-4514 Emission and reflection coefficients of surface thermal radiation properties NASA-TT-F-497 Convective heat transfer coefficients on adiabatic walls determined by sinusoidally forced fluid temperature NASA-TM-X-1594 c33 N68-24618 Operating characteristics and limits of vapor chamber fins or heat pipes NASA-CR-1139 c33 N68-33203 Fin performance analyzed by using heat transfer coefficients for various boiling modes NASA-TN-D-4797 c33 N68-34 c33 N68-34088 HEAT TREATMENT Composition and heat treatment effects on high temperature strength of arc melted tungsten-hafnium-carbon alloys NASA-TN-D-4379 c17 N68-17317 Thermal and mechanical treatment for precipitation hardening stainless steels NASA-SP-5089 c15 N68-20433 Stress corrosion tests of heat treated austenitic stainless steels NASA-TN-D-4673 c17 N68-29379 HEATING Ratio of gamma heating per gram of tungsten to gamma heating per gram of water for thin tungsten detector in water shield NASA-TM-X-1680 HEATING EQUIPMENT c22 N68-37260 High temperature tungsten mesh gas heater design and operation NASA-TM-X-1466 c22 N68-10134 High temperature flowing gas heater consisting of four stages for heating gases NASA-TM-X-1506 c11 N68-14115 HEIGHT Helicopter height-velocity diagram analysis showing effects of density altitude and gross weight NASA-TN-D-4536 c02 N68-22033 HELICAL INDUCERS Thermodynamic effects of cavitation in low temperature liquid hydrogen over range of flow coefficients using flat plate helical inducer NASA-TN-D-4423 c28 N68-18221 HELICAL WINDINGS NELIVAL WINDINGS Single tube-in-shell water-boiling heat exchanger performance with helical wire insert and flow stabilizing devices NASA-TN-D-4767 HELICOPTER CONTROL c33 N68-32099 Cptimum values of pitch rate damping, longitudinal control and speed stability for vertical takeoff aircraft /helicopters/ using pilot ratings NASA-TN-D-4624 c02 N68-28153 HELICOPTER DESIGN Soviet engineering handbook on vibration and dynamic stability theory and calculations in helicopter design NASA-TT-F-519 HELICOPTER PERFORMANCE c02 N68-23456 Rotor-hub bending moment measurements on hingeless rotor helicopter during abrupt maneuvers near ground NASA-TN-D-4574 c02 N68-24499 HELICOPTERS Evaluating closed circuit television display in helicopter landing operations NASA-TN-D-4313 c05 N68-16594 Helicopter height-velocity diagram analysis showing effects of density altitude and gross weight NASA-TN-D-4536 c02 N68-22033

HELIUM Helium and air flow tests over single flat plates

HELTUM

HELIUM 2

to determine dynamic pressure limits of nuclear fuel element plates NASA-TN-D-4417 c12 N68-16227 Metastable helium atom addition to hydrogen plasma for ion cyclotron mode enhancement NASA-TN-D-4271 c25 N68-18485 HELIUM 2 Helium 2 elementary excitation spectrum derived microscopically for realistic interatomic potential NASA-TN-D-4838 C24 N68-37240 HELIUM 3 Search for unbound helium 3 levels with isobaric spin 1/2 NASA-TN-D-4377 c24 N68-15638 HIGH ALTITUDE Simulated study of effects of high altitude supersonic air flow on titanium alloy hot salt cracking process NASA-CR-981 c17 N68~11522 HIGH ASPECT RATIO Relationship between fan drive turbine geometry and output efficiency of turbofan engine NASA-TM-X-1581 c28 N68-22 c28 N68-22725 HIGH ENERGY PROPELLANTS Bibliography on solid, liquid, and hybrid high energy propellants and oxidizers, propellant handling and storage, toxicity and hazards, and safety measures NASA-SP-7002/04/ c27 N68-30313 HIGH FREQUENCIES Field-aligned propagation of high frequency radio waves using Alouette 2 satellite data NASA-TN-D-4748 c07 N68-31639 c07 N68-31639 HIGH PRESSURE Electrical properties of direct current compact arc in argon under varying pressures, amperages, and electrode spacing NASA-TM-X-1596 c29 N68-25818 HIGH PRESSURE OXYGEN Reduction of flammable and toxic materials for use in oxygen rich manned spacecraft cabin atmospheres NASA-TN-D-3415 c05 N68-24756 HIGH RESOLUTION Resolution limit analysis for pulse frequency modulation telemetry processing line c07 N68-18247 NASA-TN-D-4180 Detection of terrain features from Nimbus 1 satellite high resolution infrared radiometer nighttime measurements NASA-TN-D-4603 c13 N68-28872 HIGH SPEED CAMERAS Spacecraft attitude determination using single onboard camera NASA-TN-D-4359 HIGH STRENGTH ALLOYS c31 N68-19275 Low temperature effects on tensile properties of aluminum, magnesium, nickel, steel, and titanium alloys NASA-SP-5012/01/ HIGH STRENGTH STEELS c17 N68-31605 Machining and grinding of ultrahigh-strength steels and stainless steel alloys NASA-SP-5084 c15 N68 c15 N68-21241 HIGH TEMPERATURE Spectral emissivity of highly doped silicon NASA-TN-D-4303 c26 N6 c26 N68-21708 Electrical and mechanical properties of high temperature cobalt-iron magnetic material NASA-TN-D-4551 c17 N6 c17 N68-24558 High temperature tensile properties of tungstenrhenium alloys NASA-TN-D-4728 c17 N68-30605 HIGH TEMPERATURE ENVIRONMENTS Two stage turbine suitable for use in wet potassium vapor at temperatures of 1400 to 1600 deg F NASA-CR-922 c03 N68-16439 Computer program for finite difference equation analysis of in-depth response of materials exposed to high temperature environment NASA-CR-1061 HIGH TEMPERATURE GASES c33 N68-26692 Physical gas dynamics research - molecular band spectra, shock tube studies, and interactions between diatomic molecules NASA-TT-F-505 c12 N68-16839 Evaluation of ultrasonic absorption technique for measuring high temperature gas properties

NASA-TN-D-4433 c24 N68-18949 Flame propagation in supersonic premixed flows of hydrogen and air ignited by coaxial, hot gas, pilot jet NASA-TN-D-4631 c33 N68-28100 Hot-reas ingestion investigation of large-scale jet VTOL fighter type models NASA-TN-D-4609 c02 N68-28277 HIGH TEMPERATURE LUBRICANTS H TEMPERATURE LUBRICANIS Test evaluation of high temperature greases and solid lubricants in thrust loaded ball bearings NASA-TN-D-4652 c15 N68-28766 HIGH TEMPERATURE RESEARCH High temperature tungsten mesh gas heater design and operation NASA-TM-X-1466 c22 N68-10134 High temperature tests on cesium diodes and vapor filled thyratrons NASA-CR-994 c09 N68-15892 Potential use of high frequency induction heating for high temperature liquid metal heat transfer testing NASA-TM-X-1510 c33 N68-16300 Atomic line intensity tables for ionized iron atom at high temperatures NASA-SP-3041 c25 N68-24161 High temperature research on creep rupture night temperature research on creep rupture strength of refractory metal fiber and nickel alloy composites NASA-TN-D-4787 c17 N68-33 HIGH TEMPERATURE TESTS Property data of magnetic materials for use in c17 N68-33684 high temperature liquid alkali-metal space power systems NASA-SP-3043 c17 N68-17624 High temperature creep rupture strength of tungsten uranium dioxide cermets NASA-TM-X-1625 c17 N68-29987 High temperature tests to determine fatigue life of 120mm bore ball bearings with fluorocarbon, polyphenyl ether, and synthetic base paraffin base lubricants NASA-TN-D-4850 c15 N68-36075 HILBERT SPACE Classification and construction of open-channel projection operators for rearrangement collisions using subspaces of total Hilbert space of system NASA-TN-D-4633 c24 N68-28265 HILSCH TUBES Flow distributions in radial outflow vortices using rotating peripheral wall water vortex tube NASA-CR-991 . c22 N68-16478 Flow visualization and containment tests in directed-wall-jet vortex tube with radial outflow and moderate superimposed axial flows NASA-CR-992 c22 N68-17131 Containment tests of vortexes with radial outflow in basic vortex tube, and in axial-flow vortex tube NASA-CR-993 c22 N68-18243 Wall injection area and axial bypass effects on flow pattern of stagnation surface in radial inflow vortexes NASA-CR-1028 c22 N68-22088 Containment characteristics of radial inflow gases in vortex tubes NASA-CR-1029 c12 N68-22200 HISTORIES History of Russian solid fuel rocketry NASA-TT-F-415 c28 NG History of NASA Goddard Space Flight Center c28 N68-11829 through 1963 NASA-SP-4301 c11 N68-30317 HONEYCOMB CORES Aerodynamic heating, delamination and pressure in nose fairing honeycomb core of Atlas Centaur launch vehicle NASA-TM-X-1605 HONEYCOMB STRUCTURES c33 N68~28156 Titanium alloy honeycomb with blackened walls as absorber of solar energy NASA-TN-D-4727 c03 N68~30751 HORIZON SCANNERS Horizon infrared radiance profiles from Scanner project c21 N68-11949 NASA-TM-X-1483 X-15 aircraft radiometric measurement of earth infrared horizon in three spectral intervals

NASA-TN-D-4654 c21 N68-28262 Infrared horizon radiance profiles obtained during summer conditions with Project Scanner probe NASA-TN-D-4741 c21 N68-33450 -TN-D-4741 HOT PRESSING Smooth surface coating of molybdenum alloys for cermets by hot isostatic compaction of tungsten-uranium dioxide fuels NASA-TM-X-1563 c22 N68-21705 HOT-WIRE ANEMOMETERS Hot-wire anemometer system for measuring velocity fluctuations in turbulent coaxial flow field of dissimilar fluids NASA-CR-961 c12 N68-12892 NASA-CK-961 C12 N68-12892 MOTSHOT WINN TUNNELS Wind tunnel tests on pressure distribution, and shock shapes of conical blunted bodies moving at supersonic speeds in nitrogen, or helium media NASA-TN-D-4314 C01 N68-17896 HOVERING Hovering tests of extremely flexible lifting rotor to determine effects of rotor tip configuration and operating conditions on performance c01 N68-36334 NASA-TN-D-4820 HUMAN BEINGS Aerospace medicine and biology bibliography on physiological, psychological, and environmental effects on man during aerospace flights c04 N68-14725 NASA-SP-7011/42/ HUMAN BODY Metabolic cost of walking on treadmills of various slope before and after loading of principal body segments NASA-CR-1042 c05 N68-21859 HUMAN FACTORS ENGINEERING Descriptive model of system development activities and man machine systems for determining optimal human performance in aerospace systems NASA-CR-877, V. 2 c05 N68-15120 Human factors engineering techniques for reducing human errors in space systems development NASA-SP-6506 c05 N66 c05 N68-20357 NASA-SP-0000 Properties and imaging techniques of various display devices - computer directed visual flight control boards, integrated optical man machine systems, and electro-optical methods NASA-SP-159 Kathematical model of human operator as optimal controllog and information processor controller and information processor NASA-CR-1151 ct c05 N68-33304 HUMAN PERFORMANCE Man machine development cycle and mathematical models for optimal human performance NASA-CR-876 c05 N68-14262 Descriptive model of system development activities and man machine systems for determining optimal human performance in aerospace systems NASA-CR-877, V. 2 c05 N68-15 Optimal role of man in space, allocation of men c05 N68-15120 and machines in aerospace systems, and descriptive model for determining optimal human performance NASA-CR-878 c05 N68-19165 Water immersion simulation study of astronaut performance during airlock ingress or egress at reduced gravity NASA-CR-971 c05 N68-20339 Human factors engineering techniques for reducing human errors in space systems development NASA-SP-6506 c05 N68-20357 Heat stress and prolonged activity effects on human perceptual motor performance NASA-CR-1153 C05 N68-31 Mathematical model of human operator as optimal controller and information processor c05 N68-31480 NASA-CR-1151 c05 N68-33304 Human performance measured as function of reaction time required to discriminate change in beacon brightness NASA-CR-1220 c05 N68-37819 HUMAN REACTIONS Human response analysis in combined trajectory control task, system-failures task, and motor response task NASA-TN-D-4356 c05 N68-18 c05 N68-18014 Judgment tests conducted to determine noise levels or loudness of tones plus noise NASA-CR-1117 c05 N68-30602 Awakening and startle effects of simulated sonic

booms NASA-CR-1193 c04 N68~33005 Synthesis of human response in closed loop tracking tasks NASA-TN-D-4842 HUMAN TOLERANCES c05 N68~36461 Process development of system for digital computer processing of psychophysiological data to obtain high stress tolerance personnel NASA-CR-1122 c05 N68-35102 HYBRID PROPELLANTS Bibliography on solid, liquid, and hybrid high energy propellants and oxidizers, propellant handling and storage, toxicity and hazards, and safety measures NASA-SP-7002/04/ c27 N68-3031 HYDRAULIC FLUIDS -27 N68-30313 Hydraulic flow approximation for flow induced vibration analysis on flat plate suspended in narrow channel NASA-CR-1186 c12 N68-35086 HYDRAZINES Photographs, thermocouples, and emission spectra used to study mixing and reaction of hydrazine and nitrogen tetroxide NASA-TN-D-4467 c33 N68-249 c33 N68-24965 Injector baffles for flame stability in combustion chambers using nitrogen tetroxide and hydrazine mixture NASA-TM-X-1595 c28 N68-26644 Small uncooled combustion chamber tests of performance and stability characteristics of nitrogen tetroxide-hydrazine propellant NASA-TN-D-4776 c27 N68-35072 HYDRIDES Neutronic effects of yttrium hydride moderator insertion in fast spectrum reactors NASA-TM-X-1614 c22 N68-23 HYDROCARBON COMBUSTION c22 N68-29950 Simplified equilibrium hydrocarbon-air combustion gas model for use in air breathing engine cycle computer programs NASA-TN-D-4747 HYDROCHLORIC ACID c28 N68-35115 Hot salt stress corrosion cracking of titanium aluminum alloys in presence of anhydrous hydrogen chloride NASA-CR-1133 c17 N68-33019 HYDRODYNAMIC EQUATIONS Hydrodynamic equations for stability, and control analyses on liquid propellant space vehicles c32 N68-18769 NASA-CR-941 HYDRODYNAMICS Convective heat exchange in homogeneous gas media, including heat transfer and friction resistance in pipes, hydrodynamics and heat transfer in jets, and intensification of convection NASA-TT-F-431 c33 N68-1172 c33 N68-11721 Approximate theory for inviscid hydrodynamics of aircraft tire hydroplaning NASA-CR-1125 c12 N68-31593 HYDROGEN Numerical procedures and computer program for calculating real fluid and thermodynamic properties of normal and parahydrogen NASA-TN-D-4341 c08 N68c08 N68-15798 Quantitative measurement of atomic photoionization cross sections of atomic hydrogen, oxygen, and nitrogen NASA-CR-998 c24 N68-18118 Cooling requirements of ball bearings operating in low flow rate hydrogen gas NASA-TN-D-4616 c15 N68-24456 Induction plasma heating system for hydrogen-argon simulated gas cooled reactor studies NASA-CR-1143 c25 N68-29888 Carbon dioxide and water vapor effects on induction period kinetics of hydrogen-oxygen reaction NASA-TN-D-4685 c33 N68-30041 HYDROGEN FUELS Hydrogen-oxygen chemical reaction kinetics in rocket engine combustion NASA-TN-D-4250 HYDROGEN IONS c33 N68-11642 Partition functions and thermodynamic properties to high temperatures for hydrogen triatomic and diatomic molecular ions NASA-TN-D-4523 c33 N68-21732

HYDROGEN OXYGEN ENGINES

HYDROGEN OXYGEN ENGINES Ablative and steel chambers effect on combustion instability in hydrogen oxygen rocket engine NASA-TM-X-1511 c28 N68-15644 NASA-TM-X-1511 c28 N68-15644 Stability effects of several injector face baffle configurations on screech in hydrogen-oxygen rocket NASA-TN-D-4515 c28 N68-21679 Hydrogen-oxygen rocket engine used to test acoustic liner with isolated resonators and variable cavity depths NASA-TN-D-4492 c33 N68-21680 Chamber pressure, contraction ratio, and flow per element effects on acoustic mode instability in hydrogen oxygen engines NASA-TN-D-4733 c33 N68-30518 Systems engineering and development of M-1 injector hydrogen oxygen engine NASA-TN-D-4730 c28 N68-30604 Coaxial injector thrust effects on combustion stability of hydrogen-oxygen rocket engine NASA-TN-D-4851 c28 N68-3 c28 N68-36515 HYDROGEN OXYGEN FUEL CELLS Parametric mass analysis and comparison of two reactant cooling and storage units for lunar based hydrogen oxygen regenerative fuel cell system system NASA-TN-D-4386 HYDROGEN PEROXIDE Effect of hydrogen peroxide generator configurations on jet exhaust flow c03 N68-16631 characteristics NASA-TM-X-1671 c12 N68-37067 HYDROGEN PLASMA Metastable helium atom addition to hydrogen plasma for ion cyclotron mode enhancement NASA-TN-D-4271 c25 N68-18485 Hydrogen plasma hot cathode generator and electron energy and density study NASA-TN-D-4604 c25 N68-25877 HYDROGENOMONAS Bioregenerative life support systems for long duration space flights — Hydrogenomonas biosynthesis and algae photosynthesis processes NASA-SP-165 HYDROPLANING c04 N68-26207 Dynamic hydroplaning, viscous hydroplaning, and tire tread rubber reversion effects on tire traction on wet runways NASA-TN-D-4406 c02 N68-19620 Laboratory scale model technique for investigating pneumatic tire hydroplaning NASA-CR-1074 c11 N68-23357 Approximate theory for inviscid hydrodynamics of aircraft tire hydroplaning NASA-CR-1125 c12 N68-31593 HYGROSCOPICITY Warm fog and fog modification by seeding with salt particles NASA-CR-1071 c20 N68-25816 HYPERBOLIC FUNCTIONS Formalism for treating products of generalized functions and applications in mathematical physics NASA-TN-D-4244 c19 N68-11494 HYPERGOLIC ROCKET PROPELLANTS Small uncooled combustion chamber tests of performance and stability characteristics of nitrogen tetroxide-hydrazine propellant NASA-TN-D-4776 HYPERSONIC FLIGHT c27 N68-35072 Variational calculus used in obtaining lift drag ratio attainable by slender conical body at hypersonic speeds NASA-CR-1156 Hypersonic Flow c01 N68-33451 Pressure distributions and aerodynamic characteristics of Nimbus B fuel capsule in hypersonic flow NASA-TM-X-1487 c01 N68-11958 Pressure and heat transfer on blunt concave and convex plates in hypersonic flow NASA-TN-D-4367 cl2 N68-18 c12 N68-18253 Interference effects of canard controls on longitudinal aerodynamic characteristics of winged body in hypersonic flow NASA-TN-D-4436 c01 N68-21579 Flow distribution in flight test and wind tunnel hypersonic flow of X-15 aircraft

SUBJECT INDEX

c01 N68-35173 NASA-TN-D-4813 Effect of leading edge bluntness on hypersonic two dimensional inlet type flows NASA-CR-1145 c01 N68-35523 Low density, leading edge bluntness, and ablation effects on wedge induced laminar boundary layer separation at moderate enthalpies in hypersonic flow NASA-TN-D-4829 c12 N68-36458 HYPERSONIC GLIDERS Aerodynamic characteristics of several hypersonic boostglide configurations at Mach 2.30 to 4.63 NASA-TM-X-1601 col N68-33836 HYPERSONIC HEAT TRANSFER Hypersonic heat transfer and pressure distribution on spherically blunted cone NASA-TN-D-4792 col N68-35497 HYPERSONIC REENTRY Aerodynamic parameters effect on dynamic behavior on reentry vehicle NASA-TM-X-1589 c31 N68-2664 c31 N68-26645 Luminous intensity and efficiency parameters for hypersonic reentry of nickel artificial meteors NASA-TN-D-4666 c30 N68-3024 c30 N68-30244 HYPERSONIC SPEED Free flight aerodynamic characteristics of slender cone at hypersonic speeds NASA-TN-D-4245 c01 N68-10380 Volume addition effects on leeward surface of high lift drag ratio winged body at hypersonic speeds NASA-TN-D-4361 c01 N68-17880 Aerodynamic characteristics of modified conical lifting reentry vehicle at hypersonic speeds NASA-TN-D-4598 c31 N68-24964 Optimum maneuvering of glide vehicle at hypersonic speeds NASA-CR-1078 c02 N68-25817 Laminar flow separation on flat plate induced by deflected trailing-edge flap at hypersonic speed NASA-TN-D-4671 c01 N68-29405 Stabilizer and tail assembly effects on overall aerodynamic characteristics of lifting bodies at hypersonic speeds NASA-TM-X-1620 c01 N68-299 Effect of boundary layer bleed on heat transfer and pressure distributions over wedge-flap c01 N68-29952 surface at hypersonic speeds NASA-TN-D-4686 c01 N68-29955 Base pressure measurements at angle of attack for spherically blunted cones at hypersonic speed NASA-TN-D-4800 coll N68-35668 HYPERVELOCITY IMPACT Simulated meteoroid high velocity impact damage to spacecraft structures composed of two metallic sheets NASA-CR-915 c31 N68-14638 Flight test of capacitance type meteoroid impact detector of aluminum polyethylene terephthalate using inflatable paraglider NASA-TN-D-4530 c14 N68-2229 HYPERVELOCITY PROJECTILES c14 N68-22290 Implosively accelerated shock tube driver for use in high energy gas dynamics research NASA-CR-950 c12 N68-10640 c12 N68-10646 Testing and evaluation of capacitor type meteoroid penetration NASA-TN-D-4524 c14 N68-22883 Penetration resistance of aluminum double sheet targets to projectile impact NASA-TN-D-4568 c32 N68-25104 Luminous intensity and efficiency parameters for hypersonic reentry of nickel artificial meteors NASA-TN-D-4666 c30 N68-3024 c30 N68-30244 HYPERVELOCITY WIND TUNNELS Effect of throat size and electrode size and shape on arc heating performance in 20-inch hypersonic tunnel NASA-TN-D-4653 c11 N68-28947 1 IMAGE DISSECTOR TUBES

Image dissector camera flown aboard Applications Technology Satellite-C for obtaining daylight cloud cover data NASA-TN-D-4186 c14 N68-10647 IMAGES

Mathematical determination of geometrical image

aberrations in single and double mirror systems NASA-TN-D-4692 c23 N68-3646 IMAGING TECHNIQUES c23 N68-36460 Properties and imaging techniques of various display devices - computer directed visual flight control boards, integrated optical man machine systems, and electro-optical methods NASA-SP-159 c09 N68-223 c09 N68-22302 IMP Solar simulation testing of anchored interplanetary monitoring platform D thermal design and protective coating NASA-TN-D-4112 C33 N68-10 Dual detection system for processing AIMP satellite pulse frequency modulated telemetry c33 N68-10299 data NASA-TN-D-4561 c08 N68-24310 IMPACT ACCELERATION Impact water pressures, accelerations, and landing dynamics of scale model Apollo command module with deployed heat shield impact attenuation system NASA-TN-D-4275 c31 N68-18822 Exploding foil gun technique for simulated meteoroid protection NASA-TN-D-4259 c32 N6 IMPACT LOADS IMPACT DAMAGE c32 N68-11355 Response characteristics of impacting penetrometers evaluated for use on lunar and planetary missions NASA-TN-D-4454 c32 N68-2 c32 N68-20364 NRDH-IN-U-4454 Target pressure and damage data from impacts by explosively propelled aluminum projectile NASA-TM-X-1597 C32 N68-250 IMPACT RESISTANCE c32 N68-25819 Penetration resistance of aluminum double sheet targets to projectile impact NASA-TN-D-4568 c32 N68-25104 Plate-gap model of porous solid and application to reduced density projectile impact NASA-CR-1140 c32 N68-31912 IMPACT TESTING MACHINES Testing and evaluation of capacitor type meteoroid penetration NASA-TN-D-4524 C14 N68-22883 IMPACT TESTS Penetration of porous projectiles in aluminium and plastic targets NASA-TN-D-4505 c32 N68-21293 Testing and evaluation of capacitor type meteoroid penetration NASA-TN-D-4524 c14 N68-22883 NASA-IN-D-4524 Compartmented gas bag landing system with omnidirectional, multiple impact, and kinetic energy dissipation capabilities NASA-TN-D-4710 IMPEDANCE MEASUREMENTS c32 N68-31602 Impedance testing for flight control system parameters in studies of launch vehicle dynamic stability NASA-CR-939 c32 N68-11485 IMPELLERS Performance of centrifugal pump impeller in room temperature water NASA-TN-D-4613 c12 N68-26651 IN-FLIGHT MONITORING Diffusers for in-flight calibration of detectors installed in spacecraft NASA-CR-987 c14 N68-12669 INCOHERENCE Autocorrelation of incoherent stellar light measured by interferometer NASA-TN-D-4480 INCOHERENT SCATTERING c14 N68-25518 Tabular and graphical data on calculations of Chandrasekhars X and Y functions and analogs for noncoherent isotropic scattering NASA-TN-D-4712 INCOMPRESSIBLE FLOW c19 N68-30804 Mixing of turbulent, incompressible, coaxial eans c12 N68-16897 NASA-CR-959 Theoretical study of effect of pivot location on aerodynamic balance movement of variable sweep wings in incompressible flow NASA-TN-D-4635 c01 N68-28817 Mixing length flow theory for analyzing incompressible turbulent swirling flow

in pipes NASA-CR-1169 INCOMPRESSIBLE FLUIDS c12 N68-36343 Magnetohydrodynamic flow of incompressible viscous electrically conducting fluid over rotating disk NASA-CR-989 c25 N68-: -INCONEL (TRADEMARK) Axial tensile fatigue of liquid rocket engine alloys at cryogenic temperatures NASA-TN-D-4274 c17 N68-: c25 N68-14078 c17 N68-11637 INDEPENDENT VARIABLES Aerodynamic parameters effect on dynamic behavior on reentry vehicle NASA-TM-X-1589 c31 N68-26645 Parameter variation analyses on mathematical models NASA-CR-1126 c15 N68-31478 INDEXES (DOCUMENTATION) NASA Thesaurus - A through L alphabetical listing of terms for indexing and retrieving aerospace related documents NASA-SP-7030, V. 1 c34 N68-1 NASA Thesaurus M through Z alphabetical listing of terms for indexing and retrieving aerospace related documents c34 N68-11307 aerospace related documents NASA-SP-7030, V. 2 Appendices to NASA Thesaurus for indexing scientific and technical information - category term listing, hierarchical display, permuted index, and postable terms NASA-SP-7030, V. 3 Annotated bibliography and indexes on aerospace medicine and biological effects - February 1968 NASA-SP-7011/47/ Co4 N68-2002C Annotated bibliography and indexes on aerospace medicine and biological effects - March 1968 NASA-SP-7011/48/ Co4 N68-20027 Cumulative index for NASA bibliography on aerospace medicine and biological effects -January 1968 c34 N68-11308 c34 N68-11309 c04 N68-20026 c04 N68-20027 January 1968 NASA-SP-7011/46/ c04 N68-22194 NASA-SF-7011/45/ Annotated bibliography and indexes on aerospace medicine and biological effects - April 1968 NASA-SP-7011/49/ c04 N68-22882 Cumulative index to NASA survey on technology utilization of aerospace research output NASA-SP-5021/06/ Annotated bibliography and indexes on aerospace medicine and biological effects c34 N68-25221 May 1968 NASA-SP-7011/50/ c04 N68-25 Annotated bibliography and indexes on aerospace c04 N68-25844 medicine and biological effects - June 1968 NASA-SP-7011/51/ c04 N68-28246 Bibliographic citations, abstracts, and indexes on selected NASA Scientific and Technical Reports for 1967 NASA-SP-7029 c34 N68-29039 Bibliographic citations, abstracts, and indexes on laser and maser research and development NASA-SP-7009/03/ c16 N68-29 c16 N68-29438 Bibliographic citations, abstracts, and indexes Bibliographic citations, abstracts, and indexes on planetary atmospheres - June 1966 through December 1967 NASA-SP-7017/02/ c30 N68-30601 Annotated bibliography and indexes on aerospace medicine and biological effects - July 1968 NASA-SP-7011/52/ c04 N68-32707 Annotated bibliography and indexes on aerospace medicine and biological effects - August 1968 NASA-SP-7011/54/ c04 N68-38 c04 N68-38051 INDICATING INSTRUMENTS Solid-state digitally controlled electroluminescent vertical scale indicators NASA-CR-919 c05 N68-10648 TNDUCTTON Carbon dioxide and water vapor effects on induction period kinetics of hydrogen—oxygen reaction NASA-TN-D-4685 c33 N68-3004 INDUCTION HEATING Potential use of high frequency induction heating c33 N68-30041 for high temperature liquid metal heat transfer testing NASA-TM-X-1510 c33 N68-16300 Induction plasma heating system for hydrogen-argon simulated gas cooled reactor studies NASA-CR-1143 c25 N68-29888

INDUCTORS

INDUCTORS Performance test of homopolar inductor alternator for Brayton cycle space power system NASA-TN-D-4698 c C03 N68-30002 INDUSTRIES Multivariable control systems for industrial applications NASA-TT-F-435 c10 N68-37293 INELASTIC SCATTERING Scattering of 42 MeV alpha particles from even cadmium isotopes NASA-TN-D-4256 c24 N68-11 c24 N68-11074 Search for unbound helium 3 levels with isobaric spin 1/2 NASA-TN-D-4377 c24 N68-15638 Inelastic scattering form factors using projected Hartree-Fock wave functions NASA-TN-D-4566 c24 N68-24661 Angular correlation between inelastically scattered alpha particles and gamma rays emitted in subsequent nuclear decay of magnesium 24 NASA-TN-D-4683 INERTIAL NAVIGATION c24 N68-29375 Analytic computational error models for strapdown inertial navigation systems NASA-CR-968 c21 N68-21652 NASA-CK-968 c21 N68-21 Analog and digital inertial flight data systems for X-15 aircraft NASA-TN-D-4642 c08 N68-29 INERTIAL REFERENCE SYSTEMS c08 N68-29404 Simple processors of star tracker commands for stabilizing inertially oriented satellite NASA-TN-D-4490 c21 N68-1: INFLATABLE GLIDERS c21 N68-19236 Flight test of capacitance type meteoroid impact Action of a luminum polyethylene terephthalate using inflatable paraglider NASA-TN-D-4530 c14 N68-2229 INFLATABLE STRUCTURES c14 N68-22290 Inflation, drag, and stability characteristics of ringsail parachute deployed in simulated Mars atmosphere NASA-TM-X-1500 c31 N68-14092 Deployment characteristics of dynamic and elastic parawing scale model for spacecraft recovery NASA-TN-D-4724 c02 N68-3 c02 N68-33879 INFLATING Inflation and drag characteristics of cross parachute in simulated Martian environment NASA-TM-X-1543 c31 N68 c31 N68-21833 INFORMATION RETRIEVAL NASA Thesaurus - A through L alphabetical listing of terms for indexing and retrieving aerospace related documents NASA-SP-7030, V. 1 c34 N68-1 NASA Thesaurus - M through Z alphabetical listing of terms for indexing and retrieving c34 N68-11307 listing of terms for indexing and retrieving aerospace related documents NASA-SP-7030, V. 2 c34 N68-11308 Appendices to NASA Thesaurus for indexing scientific and technical information - category term listing, hierarchical display, permuted index, and postable terms NASA-SP-7030, V. 3 c34 N68-11309 Statistical association techniques c34 N68-11308 c34 N68-11309 NASA-CR-1020 c08 N68-17154 NASA-CR-1020 COB NOS-1/154 Properties and imaging techniques of various display devices - computer directed visual flight control boards, integrated optical man machine systems, and electro-optical methods NASA-SP-159 CO9 N68-22302 Space technology transfer to developing nations using Brazil as model NASA-CR-1222 c34 N68-37 c34 N68-37216 INFORMATION THEORY Mathematical model of statistical channel characteristics in, and test instrumentation for, digital data transmission systems handling uniformly coded binary data NASA-TT-F-434 c07 N68-1754; INFRARED DETECTORS c07 N68-17542 Evaluation of sea surface temperature as measured by Nimbus 1 satellite high resolution infrared radiometer NASA-TN-D-4078 c20 N68-10222 Design and construction of prototype spacecraft cryogenic refrigerator for infrared detector cooling NASA-CR-988

SUBJECT INDEX

Infrared radiometric stress instrumentation system for estimating detectable stress measurements NASA-CR-1067 c32 N68-24971 Effects of zinc concentration on output of zinc doped germanium infrared detectors NASA-TN-D-4834 INFRARED PHOTOGRAPHY c26 N68~37055 Nimbus 2 and ESSA 3 satellite observation photographs of typhoon Marie NASA-TN-D-4757 c20 N68-37869 INFRARED RADIATION Calculations of nondiffuse infrared radiation from lunar surface incident onto unit element above surface NASA-TM-X-1567 c29 N68-21731 Detection of terrain features from Nimbus 1 satellite high resolution infrared radiometer nighttime measurements NASA-TN-D-4603 INFRARED SCANNERS c13 N68-28872 Horizon infrared radiance profiles from Scanner project NASA-TM-X-1483 c21 N68-11949 X-15 aircraft radiometric measurement of earth infrared horizon in three spectral intervals c21 N68-28262 NASA-TN-D-4654 Infrared horizon radiance profiles obtained during summer conditions with Project Scanner probe NASA-TN-D-4741 c21 N68-33450 INFRARED SPECTROPHOTOMETERS Cumulus cloud and fog bank spectral reflectance observations using Nimbus satellites and infrared radiometers NASA-TN-D-4552 c14 N68-25862 INFRARED SPECTROSCOPY Infrared observations of outer solar corona at wavelength of 22 microns NASA-CR-969 c30 N68-20353 INGESTION (ENGINES) Hot-gas ingestion investigation of large-scale jet VTOL fighter type models NASA-TN-D-4609 c02 N68-28277 TNJECTORS Injector baffles for flame stability in combustion chambers using nitrogen tetroxide and hydrazine mixture NASA-TM-X-1595 c28 N68-26644 Systems engineering and development of M-1 injector hydrogen oxygen engine c28 N68-30604 NASA-TN-D-4730 INLET FLOW Flow conditions in inlet manifold of M-1 fuel pump drive turbine investigated using circumferential static pressure measurements in conjunction with smoke trace photographs NASA-TM-X-1513 c12 N68-15639 Mathematical model for frequency response of forced flow, hollow, single tube boiler inlet pressure to inlet flow NASA-TM-X-1528 c12 N68-19340 Containment characteristics of radial inflow gases in vortex tubes NASA-CR-1029 c12 N68-22200 Liquid-vapor interface stability during liquid inflow in cylindrical tank during weightlessness NASA-TN-D-4628 c12 N68-25866 Analytical investigation of flow and wall temperature sensitivity in heated passages for large inlet to exit density ratios in subsonic flow of nuclear rocket NASA-TN-D-4649 c33 N68-28371 Effect of leading edge bluntness on hypersonic two dimensional inlet type flows NASA-CR-1145 c01 N68-35523 INLET NOZZLES Static performance of an auxiliary inlet ejector nozzle for supersonic-cruise aircraft NASA-TM-X-1653 c28 N68-35764 INLET PRESSURE Wind tunnel tests of mixed-compression axisymmetric inlet system to determine bleed mass flow ratio, pressure recovery and pressure distortion NASA-TN-D-4557 c28 N68-23354 INSTRUMENT APPROACH Effects of reduced landing speeds on flying qualities of Boeing 707 for simulated instrument approaches NASA-TN-D-4804 c02 N68-37075

c23 N68-13115

ION BEAMS

INSTRUMENT COMPENSATION Boundary correction factors for three coil conductivity/velocity plasma probe NASA-TN-D-4538 c25 N68-21691 INSTRUMENT ERRORS Ring accelerometer errors from stresses developed by fixture vibrations NASA-TN-D-4540 c14 N68-25830 INSTRUMENTS SNAP 8 simulator facility instrumentation NASA-TM-X-1525 c14 c14 N68-19001 INTAKE SYSTEMS Supersonic performance evaluation of mass flux probes with sharp symmetrical inlet, and with blunted unsymmetrical inlet NASA-TM-X-1524 c14 N68-184 c14 N68-18834 Acoustic measurements on jet engine intake system noise reduction suppressor cowlings NASA-TN-D-4639 c02 N68-29887 Turbojet engine noise reduction by increasing intake system guide vane-rotor blade spacing NASA-TN-D-4690 c28 N68-30040 INTEGRAL EQUATIONS Integral equations for inviscid flow field induced by rotor in ground effect NASA-CR-1027 coll N68-22475 Local error control for optimization of numerical integration orbit calculation techniques NASA-TN-D-4542 c30 N68-25867 Fourier series expansion of simultaneous integral equations for collinear coupled waveguides radiating through common perfectly conducting ground plane NASA-TN-D-4656 c09 N68-2866 Qualitative theory of differential equations and conversion to integral equations NASA-CR-1164 c19 N68-3342 INTEGRAL TRANSFORMATIONS c09 N68-28668 c19 N68-33426 Electrical impedance and radiation distributions of circular waveguide by integral transformation NASA-TN-D-4752 c07 N68-35537 INTEGRATED CIRCUITS Pyrolytic silicon nitride dielectric for integrated circuits NASA-CR-995 c18 N68-18849 Integrated circuit, direct coupled, differential amplifier for spacecraft signal conditioning NASA-TN-D-4584 c07 N68-248 c07 N68-24845 NASATIN-D-4004 INTERATOMIC FORCES Helium 2 elementary excitation spectrum derived microscopically for realistic interatomic potential NASA-TN-D-4838 INTERCRANIAL CIRCULATION c24 N68-37240 Electroplethysmographic data on intercranial circulation, and dynamics of cerebral blood volume under normal conditions and gravitational stresses NASA-TT-F-492 c04 N68-15477 INTERFACE STABILITY Liquid-vapor interface stability during liquid inflow in cylindrical tank during weightlessness NASA-TN-D-4628 c12 N68-25866 INTERFERENCE DRAG Jet wake effect of high bypass jet engine on wing-nacelle interference drag of subsonic transport model NASA-TN-D-4693 c01 N68-30595 INTERFERENCE LIFT Approximation method for calculating spanwise distribution of wind tunnel boundary interference on wing lift in rectangular perforated wall NASA-TR-R-285 c01 N68-24617 INTERFEROMETERS Autocorrelation of incoherent stellar light measured by interferometer NASA-TN-D-4480 c14 N68-25518 Laser interferometer and heterodyne system for cesium plasma diagnostics NASA-TM-X-1652 c16 N68-35593 INTERNAL COMPRESSION INLETS Design and performance testing of large scale mixed compression axisymmetric inlet at transonic and supersonic speeds NASA-TM-X-1507 c28 N68c28 N68-17028 Dynamic response of subsonic inlet to external and internal disturbances NASA-TM-X-1648 c01 N68-33374

INTERPLANETARY FLIGHT Simulator study of pilot control of remote orbital docking of large altitude stabilized components NASA-TN-D-4263 c31 N68-11476 NASA-TN-D-4263 c31 N68-11476 Computer program using Monte Carlo methods for simulating solar flares during interplanetary space flight NASA-TN-D-4311 c29 N68-16008 Optimal finite-thrust transfer between planet approach and departure asymptotes with specified intermediate orbit NASA-TN-D-4534 c28 N68-22096 Passive damping technique for attitude control of solar orientated interplanetary spacecraft NASA-TN-D-4641 c21 N68-28 Analysis of launch windows from circular orbits c21 N68-28361 for representative Mars missions NASA-TM-X-1651 c30 N68-33371 INTERPLANETARY MEDIUM Photometric and meteor observations, scattering properties, particle collection and impact, solar wind, and origin and evolution of zodiacal light in interplanetary medium - conference NASA-SP-150 c30 N68-27475 INTERPLANETARY NAVIGATION Venus flyby, Mars flyby, and Mars orbital mission to evaluate navigation and guidance systems for manned interplanetary spacecraft NASA-TN-D-4629 INTERPLANETARY SPACE c21 N68-28236 Tabulated communication characteristics of steady state model of interplanetary space NASA-SP-3042 c30 N68-10164 INTERPLANETARY SPACECRAFT Computer analyses of retrodirective, and self adaptive antenna phase control techniques for Mars probe NASA-CR-977 c21 N68-18484 Venus flyby, Mars flyby, and Mars orbital mission to evaluate navigation and guidance systems for manned interplanetary spacecraft NASA-TN-D-4629 INTERPLANETARY TRAJECTORIES c21 N68-28236 Manual procedure for midcourse guidance and applications to Earth-Moon trajectories NASA-TN-D-4246 c21 N68-11521 NASA-IN-D-4246 FORTRAN computer program for computing mass in earth orbit for round trip-stopover missions, flyby missions, and orbital missions with single-stage high-thrust system for each phase NASA-IM-X-1541 c30 N68-19330 NABA-IN-A-1541 Algorithm for generating low variable thrust interplanetary trajectory data for mission analysis of electrical propulsion systems NASA-TN-D-4431 INTERPOLATION c30 N68-21228 General Lagrangian interpolation formulas NASA-TN-D-4424 INTERSTELLAR MATTER c19 N68-22809 Observational and theoretical interpretations of INVESTIGATION INVESTIGATION Objectives of investigators associated with multiple experiment scientific satellites NASA-TN-D-4731 C34 N68-3366 INVISCID FLOW Integer relations method of determining inviscid shock layer flow and pressure distributions over blunt bodies 2466-79-0-4902 C01 N68-157 c34 N68-33682 NASA-TN-D-4397 c01 N68-15778 Steady hypersonic flow over blunt bodies with high rates of continuous mass and heat transfer nigh rates of continuous mass and heat transfer from body surface NASA-TN-D-4252 col N68-17555 Integral equations for inviscid flow field induced by rotor in ground effect NASA-CR-1027 col N68-22475 IODINE ISOTOPES Computer analysis of gamma ray spectra recordings from iodine 128, and cesium 128 decay NASA-TN-D-4305 c24 N68-1532 c24 N68-15328 ION BEAMS Cesium ion beam electric field measuring instruments NASA-CR-970 c14 N68-25903 Electron diffusion process in beam plasma passing through electrically floating anode NASA-TN-D-4758 c25 N68-32072

ION CURRENTS

SUBJECT INDEX

ION CURRENTS Ionic conductivities of solid mixtures of lithium fluoride-lithium chloride, lithium chloride-potassium chloride, lithium fluoride-sodium chloride, and sodium chloride-potassium chloride NASA-TN-D-4606 c26 N68-24510 ION CYCLOTRON RADIATION Power transfer to ion cyclotron waves in two species plasma NASA-TM-X-1481 c25 N68 c25 N68-11404 Metastable helium atom addition to hydrogen plasma for ion cyclotron mode enhancement NASA-TN-D-4271 c25 N68-18485 ION ENGINES Thermionic reactor core with short-length externally fueled diodes, and electrical failure analysis NASA-TN-D-4805 c22 N68-34087 TON SHEATHS Dependence of tungsten electrode work functions on positive ion sheaths between electrodes and cesium plasmas NASA-TN-D-4745 c25 N68-30593 Emitter and collector sheaths for cesium thermionic diodes with polycrystalline tungsten electrodes NASA-TN-D-4744 IONIC COLLISIONS c25 N68-31640 Numerical calculation of capture cross sections between ions and polar molecules NASA-TM-X-1586 c24 N68-23 c24 N68-23893 IONIC CRYSTALS Anomalous non-Hookean deformation of ionic single crystals NASA-TN-D-4513 IONIZATION c26 N68-22271 Charts of thermodynamic properties of helium showing effects of ionization, particle interactions, temperature, and atmospheric pressure NASA-TN-D-4754 IONIZATION CHAMBERS c12 N68-35117 Gamma ray exposure rates in Plum Brook HB-6 facility measured with dosimeters and ion chambers NASA-TM-X-1490 IONIZATION CROSS SECTIONS c22 N68-17022 Quantitative measurement of atomic photoionization cross sections of atomic hydrogen, oxygen, and ni trogen NASA-CR-998 c24 N68-18118 Electron scattering, bremsstrahlung cross sections, and spectral energy distributions NASA-CR-1194 c24 N68c24 N68-37708 IONIZATION GAGES Striking characteristics of magnetron ionization gages in helium over low pressure range NASA-TN-D-4681 c14 N68-29951 IONIZED GASES Attenuation and dispersion of longitudinal waves in viscous partly ionized gases NASA-TM-X-1458 c07 N68-187 IONOSPHERE c07 N68-18703 Advances during 1966 in astronomy, exobiology, ionospheric sciences, radio and solar physics, and planetary atmospheres and planetology NASA-SP-155 c30 N68-15748 TONS Lattice structures in solution NASA-TN-D-4297 c06 N68-18219 Equations for determining substrate surface coverages from arrival rates and desorption characteristics of adsorbate ions and atoms c25 N68-25630 NASA-TN-D-4369 IRON Atomic line intensity tables for ionized iron atom at high temperatures NASA-SP-3041 c25 N68-24161 Reduction of adhesive forces and friction of iron polycrystals in vacuum by chemisorbed films NASA-TN-D-4775 c17 N68-33278 IRON ALLOYS Mechanism and kinetics of iron and cobalt alloys corrosion in refluxing mercury NASA-TN-D-4450 c17 N68-21654 Electrical and mechanical properties of high temperature cobalt-iron magnetic material NASA-TN-D-4551 c17 N68-24558 Predictions for magnetoresistivity temperature

dependence of dilute alloys of iron in copper NASA-TN-D-4626 c26 N68-28239 Photographic and spectrometric observation of iron, artificial meteor launched from Trailblazer 2, and reentering at 11 kilometers per second NASA-TN-D-4312 IRRADIANCE c30 N68-16750 Spectroradiometer and technique for measuring spectral irradiance of solar simulators NASA-TN-D-4822 c14 c14 N68-35534 IRRADIATION **Grganic additives and concentration effects on** radiation induced reduction of copper salts in aqueous solution NASA-TN-D-4451 c06 N68-19434 ISENTROPE Enthalpy, temperature, and density charts for equilibrium isentropic expansion of air behind shock waves for wide range of velocities and altitudes NASA-TN-D-4247 c33 N68-11144 ISIS SATELLITES Graphs of phase and group refractive indices computed from collisionless magnetoionic theory electron concentration and magnetic field intensity NASA-TM-X-1553 c13 N68-21904 ISOLATORS Performance tests on high voltage isolator for mercury propellant feed system of ion engine NASA-TM-X-1579 c28 N68-2 C28 N68-23477 ISOTHERMAL FLOW Computer program for calculating isothermal, turbulent jet mixing flow of two gases in coaxial flow, gas gore nuclear reactors NASA-TN-D-4378 c12 N68 c12 N68-18146 ISOTHERMS Adsorption isotherm relations and transient Adsorption isotherm relations and transient desorption behavior of homogeneous and heterogeneous metal surfaces NASA-TN-D-4789 c24 N68-341 ISOTOPIC LABELING Biochemistry of nervous system, subcellular cerebral functions, brain metabolism, isotopic labeling for biochemical studies, and use of neurocompic druge c24 N68-34175 neurotropic drugs NASA-TT-F-439 c04 N68-13432 ISOTOPIC SPIN Search for unbound helium 3 levels with isobaric spin 1/2 NASA-TN-D-4377 c24 N68-15638 ISOTROPIC MEDIA Guided electromagnetic waves propagating along lossless dielectric rod immersed in isotropic and uniaxial plasmas determined for applications to plasma diagnostics NASA-TN-D-4866 c25 N68-37237 TSOTROPY Plane stress analysis using Fourier series of edge stiffened isotropic or orthotropic elastic rectangular plate subjected to prescribed temperature distribution and boundary loads NASA-CR-978 c32 N68-19311 ITERATION Feynman formalisms for expressing iterated commutators and functions of operators NASA-TN-D-4857 c19 c19 N68-36525 ITERATIVE SOLUTION Iterative and perturbation approaches to near optimum steering equations for boost vehicle guidance NASA-CR-1007 c30 N68-20449 Simple iterative solution for radiative heat transfer in anisotropic media NASA-CR-1023 c33 N68-22318 Iterative procedure for calculating normal modes and frequencies of cantilever beam NASA-TN-D-4560 c02 N68-22886

Trajectory optimization by direct descent to minimum cost using iterative computer solutions NASA-CR-1070 c30 N68-25902

Iterative solution for calculating deformation and stress concentration near slits in elastic-plastic solids NASA-TN-D-4717 c32 N68-30045

NASA-TN-D-4717 c32 N68-30045 Iterative calculation model and results for plane collisionless sheaths between field modified

LAMINAR FLOW

emitter and thermally ionized cesium plasma NASA-TN-D-4376 c25 N68-33021 J JET AIRCRAFT Performance characteristics during landing approach of large powered-lift jet transport NASA-TN-D-4261 c02 N68-11638 Subsonic and transonic flutter and flow studies of tail of large multijet cargo airplane c02 N68-17055 NASA-TN-D-4316 Summary of vertical gusts acceleration data collected for one type twin engine jet airplane during airline operations NASA-TN-D-4529 c02 N68-2229 c02 N68-22291 NASA-IN-D-4223 C02 N66-2229 JET AIRCRAFT NOISE Thrust and altitude effects on ground track noise during steep approaches of four engine, medium range, turbojet transports NASA-IN-D-4241 c01 N68-1125 c01 N68-11253 Aircraft sonic boom characteristics predicted from near field data obtained in wind tunnel NASA-TM-X-1477 c02 N68-1 c02 N68-11772 Estimation procedures for effect of design and flight characteristics of jets on ground noise NASA-CR-1053 c02 N68-26930 JET AMPLIFIERS Fluidic analog to pulse frequency converter for pneumatic reactor control drum actuator system NASA-TN-D-4497 c03 N68-21835 JET_BLAST_EFFECTS Exhaust gas ingestion characteristics and induced aerodynamics for vertical takeoff lift engine fighter model in ground proximity NASA-CR-1098 c02 N68-28233 JET ENGINES Acoustic measurements on jet engine intake system noise reduction suppressor cowlings NASA-TN-D-4639 c02 N68-29887 NASA-IN-D-4003 Jet wake effect of high bypass jet engine on wing-nacelle interference drag of subsonic transport model NASA-IN-D-4693 c01 N68c01 N68-30595 JET EXHAUST NASA-TN-D-4609 co2 N68-28277 c02 N68-28277 Effect of hydrogen peroxide generator configurations on jet exhaust flow characteristics NASA-TM-X-1671 c12 N68-37067 JET FLAPS Aerodynamic characteristics of scale model with augmented jet flap NASA-TN-D-4610 c01 N68-25 c01 N68-25919 JET FLOW Photographic study of bromine jet issuing into coaxially flowing airstream NASA-TN-D-4660 c12 N68-2 c12 N68-28370 JET IMPINGEMENT Forces and moments produced by air and helium jets exhausting parallel to flat plate in near vacuum NASA-TN-D-4408 c12 N68-19000 JET MIXING FLOW Free jet mixing analysis for parallel streams of different fluids NASA-CR-956 c12 N68-13619 Velocity and density profiles in mixing region between adjacent half jets of dissimilar fluids NASA-CR-957 c12 N68-1557 c12 N68-15571 Breakup, and displacement of liquid jets in crossflow of shock tube NASA-TN-D-4334 c33 N66 c33 N68-15942 Computer program for calculating isothermal, turbulent jet mixing flow of two gases in coaxial flow, gas gore nuclear reactors NASA-TN-D-4378 c12 NASA-TN-D-4441 NASA-TN-D-4441 Similarity solution for turbulent mixing between jet and faster moving coaxial stream NASA-TN-D-4441 c12 N68-10246 Dilution-jet mixing flow studies for gas turbine combustion chambers NASA-TN-D-4695 c01 N68-30128 JET PUMPS Noncavitating flow mechanisms in two low area ratio water jet pumps with throat lengths of 7.25 diameters c15 N68-17564 NASA-TN-D-4445

Cavitation performance of jet pumps having low ratios of nozzle to throat area c03 N68-24461 NASA-TN-D-4592 RHON-IN-U-4092 C03 N68-24 Noncavitating and cavitating performance of two low area ratio water jet pumps with throat lengths of 5.66 diameters NASA-TN-D-4759 c12 N68-31 c12 N68-31960 JOINTS (JUNCTIONS) Thermal degradation of high performance multilayer insulation on liquid hydrogen tank in vicinity of penetration NASA-TN-D-4778 JOSEPHSON JUNCTIONS c33 N68-33167 Superconduction thin films, and properties and applications of Josephson effect at radio frequencies NASA-CR-1189 c26 N68-35178 JOURNAL BEARINGS High revolutions per minute rotor stability of herringbone-grooved gas-lubricated journal bearings NASA-TN-D-4440 High speed fluid film lubrication NASA-CR-1058 c15 N68-21965 c15 N68-22810 Electronic visualization technique for studying dynamic behavior of gas journal bearing NASA-TM-X-1609 c14 N68-35105 Theoretical analysis of pressure distribution, load capacity, load angle, and friction force for single-step concentric journal bearing c15 N68-36098 NASA-TN-D-4839 JUDGMENTS Judgment tests conducted to determine noise levels or loudness of tones plus noise NASA-CR-1117 c05 N68-30602

K

KEPLER LAWS Artificial satellite motion under influence of planar and Keplerian force fields NASA-TN-D-4622 c30 N68-28113 KINETIC ENERGY Kinetic energy loss coefficients of stator blade row in open configuration NASA-TM-X-1635 c03 N68-30506
 nnon-in-A-1030
 c03 N68-304

 Compartmented gas bag landing system with omnidirectional, multiple impact, and kinetic energy dissipation capabilities NASA-TN-D-4710
 c32 N68-316

 KINETIC THEORY
 C32 N68-316
 c32 N68-31602 Real gas wedge-induced laminar separation on cooled blunt flat plate at hypersonic speed NASA-TN-D-4320 coll N68-17899 KINETICS Carbon dioxide and water vapor effects on induction period kinetics of hydrogen-oxygen reaction NASA-TN-D-4685 c33 N68-30041 Mathematical model of liquid metal fuel reactor to investigate temperature distribution on neutron kinetics NASA-TN-D-4840 c22 N68-36055

L

LABORATORY EQUIPMENT Laboratory scale model technique for investigating pneumatic tire hydroplaning NASA-CR-1074 cll N68-23357

LAMINAR BOUNDARY LAYER

Laminar boundary layer problems solved by integral matrix methods NASA-CR-1062 c33 N68-26641

Bifurcation approximation for binary and thermal diffusion coefficients, mixture viscosity, and thermal conductivity of laminar boundary layer NASA-CR-1063 c33 N66-268.

c33 N68-26815 Low density, leading edge bluntness, and ablation effects on wedge induced laminar boundary layer separation at moderate enthalpies in hypersonic flow NASA-TN-D-4829

c12 N68-36458 LAMINAR FLOW

FORTRAN computer program for calculating two

dimensional subsonic inviscid flow for rotating or stationary circular cascade of blades on blade to blade stream surface of turbomachine NASA-TN-D-4525 c01 N68-2137 c01 N68-21374

LAMINAR HEAT TRANSFER

SUBJECT INDEX

Transition from laminar to turbulent flow in near wake of supersonic reentry body NASA-TN-D-4645 c01 N68-28220 Laminar flow separation on flat plate induced by deflected trailing-edge flap at hypersonic speed NASA-TN-D-4671 col N68-29405 Laminarization of turbulent boundary layer observed from heat transfer and boundary layer measurements in conical nozzles NASA-TN-D-4788 LAMINAR HEAT TRANSFER c12 N68-33642 Simplified approximations for calculating laminar heat transfer over spherically blunted axisymmetric bodies at angle of attack NASA-TN-D-4720 c33 N68-31959 LAMINATES Wear rate and friction coefficient of steel sliding on polymer laminates determined in liquid nitrogen and hydrogen NASA-TN-D-4463 c15 N68-20325 Thermal degradation of high performance multilayer insulation on liquid hydrogen tank in vicinity of penetration NASA-TN-D-4778 c33 N68-33167 Metal oxide semiconductor field effect transistor circuit development and laminated electronic packaging for computer storage devices NASA-CR-1113 c08 c08 N68-35193 LANDING AIDS Evaluating closed circuit television display in helicopter landing operations NASA-TN-D-4313 c05 N68-16 c05 N68-16594 Comparimented gas bag landing system with omnidirectional, multiple impact, and kinetic energy dissipation capabilities NASA-TN-D-4710 c32 N68-31(c32 N68-31602 LANDING GEAR Mathematical prediction model for landing dynamics of impacting struts, and trusses of lunar vehicle landing gear NASA-TN-D-4434 Vertical impacts of LM-type landing gear system c31 N68-19085 under simulated lunar landings NASA-TN-D-4711 c32 N68-30505 LANDING LOADS Impact water pressures, accelerations, and landing dynamics of scale model Apollo command module with deployed heat shield impact attenuation system NASA-TN-D-4275 c31 N68-18822 Landing loads and accelerations of the XB-70-1 aircraft 0.02 N68-30 NASA-TN-D-4836 0.02 N68-30 c02 N68-36073 LANDING SIMULATION Vertical impacts of LM-type landing gear system under simulated lunar landings NASA-TN-D-4711 c32 N68-30 LANDING SITES c32 N68-30505 Landing site dispersions of unmanned spacecraft on Mars NASA-TN-D-4587 c30 N68-24557 Computer program technique for determination of opportunities for recall of spacecraft to multiple landing sites from circular or elliptical orbits NASA-TR-R-259 c21 N68-30126 LANDING SPEED Effects of reduced landing speeds on flying qualities of Boeing 707 for simulated instrument approaches NASA-TN-D-4804 c02 N68-37075 LAPLACE EQUATION Shapes of liquid drops resting on flat surfaces determined by Runge-Kutta solution of Laplace capillary equation NASA-TN-D-4779 c12 N68-33165 LASER MODES Laser light backscatter investigation of air flow velocity in contaminated atmospheres for application to clear air turbulence detectors NASA-TN-D-4453 c20 N68-20375 LASERS Feasibility of using laser radiation for detection and measurement of vibration of mechanical structures NASA-CR-985 c16 N68-14070 Laser modulated bulk optical absorption in cadmium sulfide single crystals NASA-TN-D-4466 c26 N68-18772

Geodetic laser system for earthquake prediction and engineering research NASA-SP-5042 c13 N68-23706 Bibliographic citations, abstracts, and indexes on laser and maser research and development NASA-SP-7009/03/ c16 N68-29438 LATERAL CONTROL Flight tests for preliminary evaluation of handling qualities of unaugmented XB-70 aircraft NASA-TM-X-1584 LATERAL OSCILLATION c02 N68-23901 Mathematical models and approximation methods for solving lateral vibration modes of cylindrical space vehicles and vehicles with clustered tanks NASA-CR-935 c32 N68-10231 LATERAL STABILITY LEKAL STABILITY Longitudinal, lateral, and directional stability and control characteristics of lifting entry vehicle at Mach number of 19 NASA-TN-D-4337 c31 N68-162 c31 N68-16240 NHSH-IN-D-4507 C31 N68-16240 Flight simulator to evaluate lateral-directional handling qualities of piloted reentry vehicles NASA-TN-D-4410 c31 N68-19226 LAUNCH ESCAPE SYSTEMS Aerodynamic stability characteristics of Apollo launch escape vehicle with canard surfaces deployed NASA-TN-D-4280 c01 N68-11640 Effects of simulated jet exhaust flow on transonic aerodynamic characteristics of Apollo launch escape vehicle models NASA-TN-D-4843 c31 N68-37074 LAUNCH VEHICLE CONFIGURATIONS FORTRAN digital computer program for axial distribution of aerodynamic normal force characteristics for axisymmetric, multistage launch vehicles in linear angle of attack ranges NASA-TN-D-4342 c31 N68-18615 Longitudinal vibration of full scale representative launch vehicle by means of force controlled vibration techniques NASA-TN-D-4502 LAUNCH VEHICLES c32 N68-21869 Impedance testing for flight control system parameters in studies of launch vehicle dynamic stability NASA-CR-939 c32 N68-11485 Influence of structure and materials research on weight, performance, and cost of advanced launch vehicle systems NASA-CR-974 c31 N68-1152 Analytical methods for dynamic stability analyses of large launch vehicles during flight through c31 N68-11520 and exit from earth atmosphere NASA-CR-944 c32 N68-18825 Iterative and perturbation approaches to near optimum steering equations for boost vehicle guidance NASA-CR-1007 c30 N68-20449 Thrust vector control for large launch vehicles with solid propellant first stages NASA-TN-D-4662 c31 N68-280 c31 N68-28690 Three dimensional motion analysis and vibration characteristics of dynamically scaled model of asymmetrically clustered launch vehicle NASA-TN-D-4707 c32 c32 N68-32051 LAUNCH WINDOWS Analysis of launch windows from circular orbits for representative Mars missions c30 N68-33371 NASA-TM-X-1651 LAYOUTS Electrical design and scheduling of components for thin film personal communications and telemetry system NASA-CR-914 c09 N68-10420 LEAD TELLURIDES Parametric analysis of radioisotope cascaded thermoelectric generators with Si-Ge first stage and PbTe second stage NASA-TM-X-1501 c22 N68-14585 LEADING EDGES Leading-edge heat transfer effects of three types of interfering flow fields NASA-TN-D-4543 c33 N68-22118 Accurate methods for predicting longitudinal aerodynamic characteristics of two-lobed conical parawings with leading edge booms NASA-CR-1166 c01 N6 c01 N68-33765

Effect of leading edge bluntness on hypersonic two dimensional inlet type flows NASA-CR-1145 c01 N68-35523 Low density, leading edge bluntness, and ablation effects on wedge induced laminar boundary layer separation at moderate enthalpies in hypersonic flow NASA-TN-D-4829 c12 N68-36458 LEAKAGE Leakage testing theory and testing methods handbook NASA-CR-952 c15 N68-20389 Adverse effects of liquid propellant leakage past control valves in vacuum environment NASA-CR-1047 c27 N68-21893 LEAST SQUARES METHOD AST SQUARES METHOD Least squares determination of frequency, damping ratio, amplitude, and phase angle from free oscillation data NASA-TN-D-4503 c19 N68-25869 Numerical least square method for resolving complex pulse height spectra NASA-SP-3044 c24 N68-29520 c19 N68-25869 c24 N68-29520 LIAPUNOV FUNCTIONS Liapuncy stability theory applied to class of partial differential equations, and generation of contraction groups related to equivalent norms NHON-CR-1100 Liapuncy method used to obtain sufficient conditions for buckling stability of long cylindrical shells with random imperfections NASA-CR-1161 c32 N68-33 c19 N68-27457 c32 N68-33419 LIBRATION Hovering lunar libration communication satellite stationary with respect to earth-moon system NASA-TN-D-4468 c30 N68-2173 LIE GROUPS c30 N68-21733 Lie series applications to celestial mechanics, accelerators, satellite orbits, and optimization NASA-CR-1046 Application of Lie series to celestial mechanics NASA-TN-D-4460 LIFE SUPPORT SYSTEMS c30 N68-26643 Space activity suit designed for active astronaut working in vacuum environments for up to four hours NASA-CR-973 c05 N68-11510 Instrumentation, systems engineering, and life support systems for Apollo primate orbital experiment NASA-CR-926 c05 N68-15306 Pressure suits and backloads effects on locomotion in simulated lunar gravity in simulated lunar yields NASA-TN-D-4464 c05 N68-20354 Bioregenerative life support systems for long duration space flights - Hydrogenomonas biosynthesis and algae photosynthesis processes NACA-SD-165 c04 N68-26207 Survey and critical evaluation of existing methods for synthesis of fatty acids and lipids from metabolic wastes under conditions of space flight NASA-CR-1105 c04 N68-28278 Subsystem definition of advanced life support technology for Mars surface module NASA-CR-1083 c05 N68-28319 LIFT Unmanned Mars probe tested for drag, lift, static and dynamic stability at Mach number 2 c01 N68-11936 NASA-TN-D-4291 Flexibility effects on lift and pitching moments of low aspect ratio delta wing-conicalcylindrical body combinations at transonic speeds NASA-TN-D-4655 c01 N68-37065 Nonlinear lift and pressure distribution of slender conical bodies with strakes at low speed NASA-CR-1202 c01 N68-37255 LIFT DEVICES N DEVICES Wind tunnel study to explore use of slot spoilers for direct control of flap induced lift and lateral aircraft control NASA-TN-D-4664 c01 N68-2883 c01 N68-28830 LIFT DRAG RATIO Volume addition effects on leeward surface of high lift drag ratio winged body at hypersonic eneeds NASA-TN-D-4361 c01 N68-17880

Supplementary information for computer program predicting lifting pressure and camber shape of composite planform in subsonic flow NASA-TN-D-4427, SUP. Col N68-31515 Variational calculus used in obtaining lift drag ratio attainable by slender conical body at hypersonic speeds NASA-CR-1156 c01 N68-33451 Aerodynamic characteristics of several hypersonic boostglide configurations at Mach 2.30 to 4.63 NASA-TM-X-1601 col N68-33836 LIFTING BODIES TING BUDIES Longitudinal, lateral, and directional stability and control characteristics of lifting entry vehicle at Mach number of 19 NASA-TN-D-4337 C31 N68-162 c31 N68-16240 Wind tunnel investigation of pressure distribution on blunted 15 deg half-cone wedge lifting-entry body body c01 N68-21681 NASA-TN-D-4494 c01 N68-21681 Modified approach for predicting lift body pressures and camber shape for planforms in subsonic flow NASA-TN-D-4427 c01 N68-28868 Stabilizer and tail assembly effects on overall aerodynamic characteristics of lifting bodies at hypersonic speeds NASA-TM-X-1620 LIFTING REENTRY VEHICLES c01 N68-29952 Flight simulator to evaluate lateral-directional handling qualities of piloted reentry vehicles NASA-TN-D-4410 c31 N68-19226 C31 N68-19: Aerodynamic characteristics of modified conical lifting reentry vehicle at hypersonic speeds NASA-TN-D-4598 C31 N68-24 c31 N68-24964 LIFTING ROTORS Planform design method, general characteristics, and aeroelastic stability of flexible lifting rotors NASA-TN-D-4465 c01 N68-19954 Integral equations for inviscid flow field induced by rotor in ground effect NASA-CR-1027 col N68-22475 Hovering tests of extremely flexible lifting rotor to determine effects of rotor tip configuration and operating conditions on performance NASA-TN-D-4820 c01 N68-36334 LIGHT AIRCRAFT Cycle characteristics and structural configuration of turbojet and turbofan engines for lightweight aircraft NASA-TM-X-1624 LIGHT GAS GUNS c28 N68-31476 Two stage explosively driven light gas gun to obtain high projectile velocities NASA-CR-982 c11 N68-15777 LIGHT MODULATION Laser modulated bulk optical absorption in cadmium sulfide single crystals NASA-TN-D-4466 LIGHT SCATTERING c26 N68-18772 Laser light backscatter investigation of air flow velocity in contaminated atmospheres for application to clear air turbulence detectors NASA-TN-D-4453 c20 N68-20 c20 N68-20375 Scattering and absorption of plane electromagnetic waves by particles of turbid medium NASA-TT-F-477 c13 N68-22462 LINE CURRENT Experimental evaluation of ferroresonant and feedback alternating current line voltage regulators in 15 kilowatt auxiliary power system NASA-TN-D-4627 c03 N68-28101 LINE SPECTRA Atomic line intensity tables for ionized iron atom at high temperatures NASA-SP-3041 c25 N68-24161 LINEAR PREDICTION Manual procedure for midcourse guidance and applications to Earth-Moon trajectories NASA-TN-D-4246 c21 N6 c21 N68-11521 LIPIDS Survey and critical evaluation of existing methods for synthesis of fatty acids and lipids from metabolic wastes under conditions of space flight c04 N68-28278 NASA-CR-1105

Chemical feasibility and nutrional value in synthesis of edible fatty acids and lipids from

LIQUEFTED GASES

SUBJECT INDEX

metabolic wastes for space flight feeding NASA-CR-1104 LIQUEFIED GASES c04 N68-28829 Solubilities of several gases in liquid methane and liquefied natural gas NASA-TN-D-4701 c27 N68-30077 LIQUID AMMONIA Performance tests of ammonia resistojet thrustor system for various spacecraft control maneuvers NASA-TN-D-4249 c28 N68-1056 c28 N68-10562 LIQUID ATOMIZATION Breakup, and displacement of liquid jets in crossflow of shock tube NASA-TN-D-4334 c33 N6 c33 N68-15942 NASA-1N-D-4534 C33 NBS-. LIQUID COOLED REACTORS Steady state performance tests on single pass counterflow sodium-potassium cooled mercury Rankine cycle condenser NASA-TM-X-1548 c33 N68-3 c33 N68-20340 LIQUID FLOW Transient solidification of flowing liquid on cold plate, including heat capacities of frozen layer and plate NASA-TN-D-4353 c33 N68-1574 c33 N68-15742 Liquid flow into baffled spherical tank during eightlessness NASA-TM-X-1526 Conformal mapping for steady two-dimensional solidification on cold surface in liquid flow c33 N68-32073 LIQUID-GAS MIXTURES Solubilities of several gases in liquid methane and liquefied natural gas NASA-TN-D-4701 c27 N68-30077 LIQUID HELIUM Damping of piezoelectric quartz crystal driven in torsional mode of vibration in liquid helium 3 and helium 4 NASA-TN-D-4381 c26 N68-17594 LIQUID HYDROGEN Transient chilldown of thick-walled tube simulating-nuclear rocket using liquid and gaseous hydrogen NASA-TN-D-4238 c33 N68-10368 Gravity effects on self-pressurization of spherical liquid hydrogen tankage NASA-TN-D-4286 c27 l c27 N68-11645 Temperature and liquid-level sensor for liquid hydrogen pressurization and expulsion studies NASA-TN-D-4339 cl4 N68-15 c14 N68-15893 Pressure rise characteristics of liquid hydrogen Pressure rise characteristics of liquid hydrogen dewar for homogeneous, normal-gravity quiescent, and zero-gravity tests NASA-TM-X-1134 c33 N68-18196 Thermodynamic effects of cavitation in low temperature liquid hydrogen over range of flow coefficients using flat plate helical inducer NASA-TN-D-4423 c28 N68-18221 c28 N68-18221 NBOR-IN-D-4425 Vapor ingestion during liquid outflow in scale model Centaur liquid hydrogen tank NASA-TM-X-1482 LIQUID INJECTION c12 N68-19225 Maximum drop diameters for atomization of liquid jets injected concurrently into accelerating or decelerating gas streams NASA-TN-D-4640 NASA-TN-D-4640 LIQUID METAL COOLED REACTORS Criticality calculations for small, cylindrical, lithium cooled reactors for space power systems c22 N68-15792 Size and shield weight requirements calculated for fast-spectrum, liquid-metal cooled nuclear reactor for space power application NASA-TN-D-4315 c22 N68-18197 мнэн-IN-U-4010 c22 N68-18 Characteristics of liquid metal cooled reactor gaseous fission products vented or contained, for space power systems NASA-TM-X-1631 c22 N68-30 c22 N68-30516 LIQUID METALS Heat transfer characteristics for turbulent flow of heat generating liquid metals between parallel plates with wall heat transfer NASA-TN-D-4336 c33 N c33 N68-14042 Rhon-IN-D-1000 Electromagnetic processes in magnetohydrodynamic induction machines with working media of liquid metal NASA-TT-F-460 c25 N68-16286

Potential use of high frequency induction heating for high temperature liquid metal heat transfer

testing NASA-TM-X-1510 c33 N68-16300 Property data of magnetic materials for use in high temperature liquid alkali-metal space power systems NASA-SP-3043 c17 N68-17624 Mathematical model of liquid metal fuel reactor to investigate temperature distribution on neutron kinetics NASA-TN-D-4840 c22 N68-36055 Development, ground tests, and flight performance of cryogenic nitrogen storage system for low gravity operation during Apollo-Saturn space flight NASA-TN-D-4293 c23 N68-15 Minimum film boiling heat flux in vertical flow c23 N68-15950 of liquid nitrogen NASA-TN-D-4307 c33 N68-16683 Suppression of temperature rise in lossy diodes inside resonant cavities by pressurized liquid nitrogen NASA-TN-D-4556 c09 N68-24387 LIQUID POTASSIUM Contaminant controls and cleaning procedures in SNAP-8 simulation loop of liquid metals c17 N68-11 c17 N68-11912 NASA-TM-X-1432 Design, and performance of facility for kankine cycle testing of two stage potassium vapor turbine turoine NASA-CR-924, V. 3 LIQUID PROPELLANT ROCKET ENGINES c03 N68-18044 Mathematical models for determining longitudinal vibration modes of multistage liquid and solid propellant vehicles, and clustered tank vehicles NASA-CR-936 c32 N68-10280 c32 N68-10280 Techniques for full-scale dynamic testing of large solid or liquid fueled booster vehicles c32 N68-11054 NASA-CR-940 Axial tensile fatigue of liquid rocket engine alloys at cryogenic temperatures NASA-TN-D-4274 c17 N68c17 N68-11637 Hydrodynamic equations for stability, and control analyses on liquid propellant space vehicles NASA-CR-941 c32 N68-18769 NASA-CR-941 Double dead-time model for combustion stability analysis in liquid bipropellant rocket engines NASA-TN-D-4564 C33 N68-25102 NASA-TN-D-4564 c3 LIQUID ROCKET PROPELLANTS Combustion instability prediction using nonlinear bipropellant vaporization model NASA-CR-920 c33 N68-15833 Feasibility of supporting liquid fuel on solid wall in radiating liquid core nuclear rocket concept NASA-TN-D-4413 RNDR-IN-D-4413 C27 N68-17093 Adverse effects of liquid propellant leakage past control valves in vacuum environment NASA-CR-1047 Bibliography on solid, liquid, and hybrid high energy propellants and oxidizers, propellant handling and storage, toxicity and hazards, and safety measures NASA-SP-7002/04/ LIQUID SLOSHING c27 N68-30313 Hydrodynamic equations for stability, and control analyses on liquid propellant space vehicles c32 N68-18769 NASA-CR-941 Recommended procedures for stability, control, and structural loading analysis of large liquid fueled rocket booster sloshing parameters NASA-CR-948 c32 N68-23454 Effects of shallow liquid depths on lateral sloshing in cylindrical tanks under weightless conditions NASA-TN-D-4458 c12 N68-24758 Drop test study on isothermal liquid-vapor interface configuration during weightlessness in toroidal shell NASA-TN-D-4819 c12 N68-35823 LIQUID SODIUM Contaminant controls and cleaning procedures in SNAP-8 simulation loop of liquid metals NASA-TM-X-1432 cl7 N68-11: LIQUID-SOLID INTERFACES c17 N68-11912 Experimental determination of graphite triple point and liquid-solid interface NASA-CR-1148 c22 N68-3 c22 N68-29390

LOW SPEED STABILITY

LIQUID SURFACES Liquid Layer solid sample spark technique for spectrochemical analysis of flat metal samples using conventional spark source NASA-TM-X-1429 c06 N68-1049 c06 N68-10497 LIQUID-VAPOR INTERFACES Liquid-vapor interface stability during liquid inflow in cylindrical tank during weightlessness NASA-TN-D-4628 c12 N68-25866 Drop test study on isothermal liquid-vapor interface configuration during weightlessness in toroidal shell NASA-TN-D-4819 c12 N68-35823 LITHIUM Criticality calculations for small, cylindrical, lithium cooled reactors for space power systems NASA-TN-D-4371 c22 N68-15792 Neutron activation analysis of sodium, lithium, and potassium in compact fast reactors and its and potassium in compact last reactors and its effect on shielding NASA-TM-X-1512 c22 N68-2035 Data correlation of thermophysical properties of saturated liquid lithium as function of c22 N68-20355 temperature NASA-TN-D-4650 c17 N68-28365 Electron paramagnetic resonance of lithium silicon NASA-TR-R-290 c26 N68-33228 Fabrication and development of annular lithium radrication and development of annular fitnium drifted germanium detector for studying nuclear reaction gamma rays NASA-CR-1138 c14 N68-3515 LITHIUM COMPOUNDS c14 N68-35152 Calcium, molybdenum, and lithium compounds as low drive temperature stable memory cores NASA-TN-D-4573 c09 N68-2438 c09 N68-24388 LITHIUM FLUORIDES Adsorbed surfactants influence on deformation and friction coefficient of lithium fluoride single crystals during sliding friction NASA-TN-D-4716 LITHIUM ISOTOPES c15 N68-29918 Boron 10/neutron, alpha particle/ lithium 7, lithium 7 resonance relative cross sections in keV region NASA-TN-D-4783 LITTLE JOE 2 LAUNCH VEHICLE c24 N68-33763 LITTLE JUE 2 LAUNCH VEHICLE Static longitudinal aerodynamic characteristics of configurations used in Little Joe/Apollo test vehicle development NASA-TN-D-4439 c31 N68-22 LOAD DISTRIBUTION (FORCES) c31 N68-22953 Plastic response of circular uniform plate to axisymmetric impulse load of Gaussian distribution NASA-TR-R-279 c32 N68-14640 LOADS (FORCES) Calculations for elastic tensometric elements and operation of tensometric force measuring devices NASA-TT-F-513 c32 N68-15796 c32 N68-15796 Reduction of apparent power requirement for phase controlled parasitically loaded turboalternator by multiple parasitic loads NASA-TN-D-4302 c03 N68-1711(c03 N68-17110 NASA-IN-D-4302 Contour plots tabulated for stress resultants and deformations brought about by sinusoidal in plane line loads acting along great circles of spherical satellites of Echo type NASA-IN-D-4425 C31 N68-2019 c31 N68-20198 nan-18-19-1425 Prediction of fatigue crack propagation behavior in aluminum alloy panels with simulated rivet forces NASA-TN-D-4702 c32 N68-32074 Load relief autopilot to minimize launch vehicle thrust vector deflection angle required for vehicle stability during flight through design winds NASA-TN-D-4786 c21 N68-33756 Theoretical analysis of pressure distribution, load capacity, load angle, and friction force for single-step concentric journal bearing NASA-TN-D-4839 c15 N68-36 LOCKS (FASTENERS) Handbook for designing ball lock mechanisms for use on space vehicles NASA-CR-1021 c15 N68-23 c15 N68-36098 c15 N68-23356 LOGARITHMIC RECEIVERS Logarithmic encoding procedure and error analysis for binary word compression NASA-TN-D-4290 c08 N68-18179

Modified control logic with random-number procedure to determine error effects on range controller of reentry vehicle NASA-TN-D-4317 c21 N68-14732 LOGIC DESIGN Formula for expanding higher order derivatives of function tanh z in powers of tanh z and A-numbers NASA-TN-D-4296 c19 N68-14077 LOGICAL ELEMENTS Frequency coded threshold logic unit for pattern recognition systems based on central nervous system NASA-CR-1035 LONGITUDINAL CONTROL Flight tests for preliminary evaluation of handling qualities of unaugmented XB-70 aircraft NASA-TM-X-1584 LONGITUDINAL STABILITY Longitudinal, lateral, and directional stability and control characteristics of lifting entry vehicle at Mach number of 19 NASA-TN-D-4337 C31 N68-1624 Analog computed time histories and altitude-arour system c05 N68-22448 c02 N68-23901 c31 N68-16240 Analog computed time histories and altitude-ground track plots of swept wing transport aircraft longitudinal response to wind shear and longitudinal response to wind shear and sustained gusts during landing approaches NASA-TN-D-4477 coll N68-19180 Variable-stability helicopter flight tests under instrument flight rules to determine effects of gross changes in longitudinal static stability for V/STOL handling qualities NASA-TN-D-4364 coll N68-19184 Interference effects of canard controls on longitudinal aerodynamic characteristics of longitudinal aerodynamic characteristics of winged body in hypersonic flow NASA-TN-D-4436 c01 N68-21579 Optimum values of pitch rate damping, longitudinal control and speed stability for vertical takeoff aircraft /helicopters/ using pilot ratings c02 N68-28153 NASA-TN-D-4624 c02 N68-2815 Converging flow effects on longitudinal stability measurements in tandem test section of wind tunnel NASA-CR-1198 c11 N68-36522 LONGITUDINAL WAVES Attenuation and dispersion of longitudinal waves in viscous partly ionized gases NASA-TM-X-1458 c07 N6A-187 c07 N68-18703 LOOPS Digital voltage controlled oscillator for phase lock loops using coherent frequency synthesizer NASA-TN-D-4521 c09 N68-2438 c09 N68-24389 LOSSLESS MATERIALS Fourier integration of electrical impedance expressions for nonlossy dielectric and lossy plamas NASA-TN-D-4774 c07 N68-35524 Electrical impedance and radiation distributions of circular waveguide by integral transformation NASA-TN-D-4752 c07 N68-35537 Guided electromagnetic waves propagating along lossless dielectric rod immersed in isotropic and uniaxial plasmas determined for applications to plasma diagnostics NASA-TN-D-4866 c25 N68-37237 LOW ASPECT RATIO Flexibility effects on lift and pitching moments of low aspect ratio delta wing-conical-cylindrical body combinations at transonic speeds NASA-TN-D-4655 LOW ASPECT RATIO WINGS c01 N68-37065 Aerodynamic ground effect measurements on low aspect ratio ogee wings NASA-TN-D-4329 c02 N68-LOW PRESSURE c02 N68-14090 Striking characteristics of magnetron ionization gages in helium over low pressure range NASA-TN-D-4681 c14 c14 N68-29951 Superconducting bolometers for measuring very low pressures NASA-CR-1120 c14 N68-33022 LOW SPEED STABILITY Low speed static and dynamic stability tests on scale model of double-delta supersonic commercial air transport configuration

LOGIC CIRCUITS

LOW TEMPERATURE ENVIRONMENTS

c02 N68-18250 NASA-TN-D-4179 Rotor-hub bending moment measurements on hingeless rotor helicopter during abrupt maneuvers near around NASA-TN-D-4574 c02 N68-24499 LOW TEMPERATURE ENVIRONMENTS Low temperature effects on tensile properties of aluminum, magnesium, nickel, steel, and titanium alloys NASA-SP-5012/01/ c17 N68-31605 LOW TEMPERATURE TESTS Cryogenic flexibility of single and multiple plies of thin polymeric films tested at minus 320 deg and minus 423 deg F NASA-TM-X-1555 c18 N68-20329 Texture strengthening and fracture toughness of titanium alloy sheet at room and cryogenic temperatures NASA-TN-D-4444 c17 N68-22884 Predictions for magnetoresistivity temperature dependence of dilute alloys of iron in copper NASA-TN-D-4626 c26 N68-28239 Cyclic incident radiation method for measuring thermal emittance and absorption properties of metals at cryogenic temperatures NASA-TM-X-1618 c33 N68~31498 LOW THRUST LUW INNUSI Algorithm for generating low variable thrust interplanetary trajectory data for mission analysis of electrical propulsion systems NASA-TN-D-4431 c30 N68 LOW THRUST PROPULSION c30 N68-21228 Performance of low thrust storable bipropellant thrustors in spacecraft reaction control system NASA-TN-D-4416 c28 N68-20064 Comparisons of three body trajectories with patched two body trajectories for low thrust rockets NASA-TN-D-4559 LOW VISIBILITY c30 N68-22289 VISIBILITY Cumulative errors associated with Category 2 and 3 operations, and terminal flight paths for low visibility landings NASA-CR-1188 c02 N68-3559 c02 N68-35595 LUBRICANTS Friction torque of ball bearings in vacuum to determine lubricating capability of polytetrafluoroethylene-composition retainer materials NASA-TN-D-4355 c15 N68-16468 High temperature tests to determine fatigue life of 120mm bore ball bearings with fluorocarbon, polyphenyl ether, and synthetic base paraffin base lubricants NASA-TN-D-4850 c15 N68-36075 LUBRICATION Sputtered molybdenum disulfide film deposition and friction characteristics in vacuum NASA-TN-D-4269 c17 N68-11644 High speed fluid film lubrication NASA-CR-1058 LUBRICATION SYSTEMS c15 N68-22810 Supplement to NASA bibliography on lubrication, corrosion, and wear NASA-SP-7020/02/ c15 N68-31522 LUMINOSITY Frothing-sloughing ablation model for computing luminous efficiency factor from meteor data NASA-TN-D-4808 c30 N68-33055 LUMINOUS INTENSITY Maximum likelihood techniques for design of optimum star trackers that determine position and magnitude NASA-TN-D-4549 c21 N68-23 c21 N68-23377 Luminous intensity and efficiency parameters for hypersonic reentry of nickel artificial meteors NSB-TN-D-4666 c30 N68-Effects of irradiation and star magnitude on sextant sighting performance NASA-TN-D-4780 c21 N68-LUNAR ATMOSPHERES c30 N68-30244 c21 N68-33456 Annotated bibliography and indexes on lunar surface studies - 1967 NASA-SP-7003/04/ c30 N6 c30 N68-32631 LUNAR COMMUNICATION Data relay and tracking capability of lunar communication satellites above lunar far side surface NASA-TN-D-4509 c31 N68-25358

SUBJECT INDEX

LUNAR ENVIRONMENT Stability of selected earth minerals in simulated lunar environment tests NASA-CR-1034 c13 N68-25579 Control, performance, and tracking Lunar Orbiter 5 in obtaining selenodetic and lunar environment data NASA-CR-1142 c31 N68-30631 LUNAR FAR SIDE Hovering lunar libration communication satellite stationary with respect to earth-moon system NASA-TN-D-4468 c30 N68-3 c30 N68-21733 Data relay and tracking capability of lunar communication satellites above lunar far side surface NASA-TN-D-4509 c31 N68-25358 LUNAR FLIGHT NR FLIVTI Design, mission, flight operations, experiment data, and subsystem performances for Lunar Orbiter 4 extended mission NASA-CR-1092 C31 N68-24 c31 N68-28997 LUNAR GEOLOGY Silicate rocks as simulators for study of genetic states of lunar surface rocks NASA-CR-1081 c30 N68-26689 Annotated bibliography and indexes on lunar surface studies - 1967 NASA-SP-7003/04/ LUNAR GRAVITATION c30 N68-32631 Full scale lunar gravitation simulator and 1/6 scale model NASA-TN-D-4474 cll N c11 N68-25853 Correlation of lunar radii estimates obtained from gravitational field coefficient measures NASA-TN-D-4636 LUNAR GRAVITATIONAL EFFECTS c30 N68-28409 Pressure suits and backloads effects on locomotion in simulated lunar gravity NASA-TN-D-4464 c05 N68-20354 Effects of simulated lunar gravity on metabolic rates while wearing pressure suits NASA-CR-1102 c05 N68-284 c05 N68-28833 LUNAR LANDING Nathematical prediction model for landing dynamics Mathematical prediction model for fanding dynamic of impacting struts, and trusses of lunar vehicle landing gear
 NASA-TN-D-4434
 C31 N68-190
 Pericynthion altitude of selenocentric orbits determined from angular rate of line of sight with respect to prominant lunar surface footnote on a ballicite trainectories c31 N68-19085 features along ballistic trajectories NASA-TM-X-1508 c3 c30 N68-19622 Full scale lunar gravitation simulator and 1/6 scale model NASA-TN-D-4474 c11 N68-25853 Advanced antenna techniques for rendezvous and lunar landing radar systems NASA-CR-764 c07 N68-28135 Vertical impacts of LM-type landing gear system under simulated lunar landings NASA-TN-D-4711 c32 N68-30505 Mission and orbit parameter summary for Lunar Orbiter spacecraft flight NASA-CR-1141 c31 N68-31477 Manual navigation method for evaluating transfer orbits for lunar landings NASA-TN-D-4756 c21 N68-33271 LUNAR LANDING MODULES Lunar module backup guidance, navigation and pilot interfaces with control systems during lunar landing missions NASA-TN-D-4131 C21 N68-10 c21 N68-16836 LUNAR LANDING SITES Photographs of perilune and apolune landing sites made by Lunar Orbiter 4 NASA-CR-1093 c30 N68-28275 Selected photographs and mission summary of Lunar Orbiter 5 NASA-CR-1095 c31 N68-28891 Principal scientific results on Surveyor 7 mission NASA-SP-173 c31 N68-33553 LUNAR MODULE Simulator study of pilot control over lunar module during ascent from lunar surface NASA-TM-X-1549 c21 N68-21366 c21 N68~21366 Full scale lunar gravitation simulator and 1/6 scale model

NASA-TN-D-4474 c11 N68-25853 Lunar module scale model study of use of soft side legs for improved touchdown stability of legged landing vehicles c31 N68-29962 LUNAR OBSERVATORIES Chronological catalog of reported lunar events or temperature changes on moon recorded between 1540 and 1967 NASA-TR-R-277 LUNAR ORBITER c30 N68-28192 Photographic mission planning and photograph interpretation for Lunar Orbiter 3 NASA-CR-984 c30 N68 c30 N68+15725 Optimization of confidence levels in detecting Junar surface detail in terms of viewing geometry and camera shutter speeds for Lunar Orbiter missions NASA-TN-D-4501 c14 N68-21942 Systems performance, lunar photography, and launch operations of Lunar Orbiter 3 photographic mission NASA-CR-1069 c31 N68-24738 Photographic summary report of Lunar Orbiter 4 mission NASA-CR-1054 c31 N68-26814 Photographic program summary and evaluation for Lunar Orbiter mission NASA-CR-1094 c31 N68-28202 Photographs of perilune and apolune landing sites made by Lunar Orbiter 4 NASA-CR-1093 c30 N68-28275 c30 N68-28275 Orbiter 5 NASA-CR-1095 c31 N68-28891 C31 N68-24 Design, mission, flight operations, experiment data, and subsystem performances for Lunar Orbiter 4 extended mission NASA-CR-1092 C31 N68-24 c31 N68-28997 Spacecraft performance, control, and flight path analysis of Lunar Orbiter 3 extended mission NASA-CR-1109 c31 N68-29995 Control, performance, and tracking Lunar Orbiter 5 in obtaining selenodetic and lunar environment data c31 N68-30631 NASA-CR-1142 Mission and orbit parameter summary for Lunar Orbiter spacecraft flight NASA-CR-1141 c31 N68c31 N68-31477 LUNAR ORBITS Onboard range and range rate measurements of lunar beacons for position and lunar orbit estimation NASA-TM-X-1529 Pericynthion altitude of selenocentric orbits determined from angular rate of line of sight with respect to prominant lunar surface c30 N68-19064 features along ballistic trajectories NASA-TM-X-1508 c30 c30 N68-19622 Technique for determining pericynthion altitude of lunar transfer orbits NASA-TN-D-4811 LUNAR PHOTOGRAPHS c30 N68-36459 Photographic program summary and evaluation for Lunar Orbiter mission NASA-CR-1094 c31 N68-28 c31 N68-28202 Selected photographs and mission summary of Lunar Orbiter 5 NASA-CR-1095 c31 N68-28891 Spaceborne photography of cloud cover and other meteorological phenomena, Surveyor and Orbiter lunar shots, and Gemini space walk and target docking NASA-SP-168 LUNAR PHOTOGRAPHY c30 N68~34870 Photographic mission planning and photograph interpretation for Lunar Orbiter 3 NASA-CR-984 c30 N68 c30 N68-15725 Analysis and evaluation of Lunik 9 spacecraft imagery, and specification of spacecraft and photographic instruments NASA-CR-980 c14 N68-16838 Systems performance, lunar photography, and launch operations of Lunar Orbiter 3 photographic mission NASA-CR-1069 c31 N68-24738 Photographic summary report of Lunar Orbiter 4 mission

NASA-CR-1054 c31 N68-26814 Photographs of perilune and apolune landing sites

made by Lunar Orbiter 4 NASA-CR-1093 c30 N68-28275 Correlation of lunar radii estimates obtained from earth based photographic study and lunar orbiter gravitational field coefficient measures NASA-TN-D-4636 c30 N68-28409 NASA-TN-D-4636 c30 N68-28409 Annotated bibliography and indexes on lunar surface studies - 1967 NASA-SP-7003/04/ c30 N68-32631 LUNAR ROVING VEHICLES Visual simulation facility for evaluation of lunar surface roving vehicles NASA-TN-D-4276 c11 N68-15858 LUNAR SHADOW Method of correcting azimuthal orientation of Explorer 35 spacecraft while in lunar shadow NASA-TN-D-4544 c30 N68-24486 LUNAR SOIL Lunar surface layer considered to store solar energy for generating power during lunar night NASA-TM-X-1560 c03 N68-20363 Response characteristics of impacting penetrometers evaluated for use on lunar and planetary missions NASA-TN-D-4454 c32 N68-2 c32 N68-20364 Silicate surface preparation to represent lunar NASA-CR-1090 c30 N68-28373 c30 N68-28373 LUNAR SPACECRAFT Nathematical prediction model for landing dynamics of impacting struts, and trusses of lunar vehicle landing gear NASA-TN-D-4434 c31 N6 c31 N68-19085 LUNAR TEMPERATURE Chronological catalog of reported lunar events or temperature changes on moon recorded between 1540 and 1967 NASA-TR-R-277 c30 N68-28192 LUNAR TOPOGRAPHY Lunar volcanism model based on high temperature radiative thermal conductivity of minerals and rocks NASA-CR-916 c13 N68-10283 Analysis and evaluation of Lunik 9 spacecraft imagery, and specification of spacecraft and photographic instruments NASA-CR-980 c14 N68-1 c14 N68-16838 Surveyor 5 configuration, television picture transmission, and experiments on measuring chemical elements in lunar surface NASA-SP-163 c31 N68-17844 Photographic program summary and evaluation for Lunar Orbiter mission NASA-CR-1094 c31 N68-287 c31 N68-28202 Selected photographs and mission summary of Lunar Orbiter 5 NASA-CR-1095 c31 N68-28891 Annotated bibliography and indexes on lunar surface studies - 1967 NASA-SP-7003/04/ c30 N6 c30 N68-32631 Principal scientific results on Surveyor 7 mission NASA-SP-173 c31 N68-33553 LUNAR TRAJECTORIES Technique for determining pericynthion altitude of lunar transfer orbits NASA-TN-D-4811 c30 N68-364 LUNIK 9 LUNAR PROBE c30 N68-36459 Analysis and evaluation of Lunik 9 spacecraft imagery, and specification of spacecraft and photographic instruments NASA-CR-980 c14 N68-16838

Μ

M- 1 ENGINE Flow conditions in inlet manifold of M-1 fuel pump drive turbine investigated using circumferential static pressure measurements in conjunction with smoke trace photographs NASA-TM-X-1513 cl2 N68-15633 Cold air performance test of scale model oxidizer pump drive turbine for M-1 engine - performance of first stare with inlat fordpine manifold c12 N68-15639 of first stage with inlet feedpipe manifold assembly NASA-TN-D-4392 c28 N68~16413

Aerodynamic performance of scale model oxygen pump-drive turbine for M-1 rocket engine NASA-TN-D-4393 c28 N68c28 N68-18188

MACH NUMBER

SUBJECT INDEX

Film and transpiration cooled baffles for M-1 engine NASA-TM-X-1267 c28 N68-18216 MACH NUMBER Performance of vortex generators installed aft of inlet throat on centerbody evaluated at Mach numbers 2.0 to 3.0 NASA-TN-D-4675 c01 N68-28795 Wind tunnel calibration of conical pressure probe over range of Mach numbers to determine flow field data for X-15 airplane NASA-TN-D-4678 c12 N68-28801 Wind tunnel calibration of 30 deg included angle cone for determination of local values of Mach number, total pressure, and flow distribution NASA-TN-D-4679 c14 N68-30 c14 N68-30127 MACHINE ORIENTED LANGUAGES Nonconventional computers for solving problems previously handled only by humans NASA-TM-X-1544 c08 N68-1 c08 N68-19336 MACHINING Machining and grinding of ultrahigh-strength steels and stainless steel alloys NASA-SP-5084 c15 N68c15 N68-21241 MAGMA Lunar volcanism model based on high temperature radiative thermal conductivity of minerals and rocks NASA-CR-916 MAGNESIUM CELLS c13 N68-10283 MAGNESIUM CELLS Effects of electrolyte amount, drain rate, and electrode geometry on copper oxide-magnesium thermal cell performance NASA-TN-D-4790 c03 N68-34 MAGNESIUM OXIDES c03 N68-34234 Magnitude of electrical potential-temperature curve determined for tantalum, niobium, and magnesium during oxidation in air NASA-TN-D-4240 c17 N68c17 N68-10498 MAGNETIC CORES Calcium, molybdenum, and lithium compounds as low drive temperature stable memory cores NASA-TN-D-4573 c09 N68-24388 CO9 N68-24388 MAGNETIC FIELDS Synchrotron emission at helical motion of relativistic electrons emitting from source with relativistic velocity NASA-TT-F-521 c25 No Interactions of unconfined magnetic fields c25 N68-16700 emanating from space vehicles with undisturbed solar wind NASA-TN-D-4304 c29 N68-19188 Theoretical approach to determination of magnetic torques on orbiting spacecraft by near-field measurement NASA-TN-D-4485 c23 N68-24146 Magnetometers for measuring stable magnetic fields produced by low field superconducting shields NASA-CR-1073 c14 N68-26703 Mathematical model based on conformal mapping of shape of electric arc balanced in transverse convective and magnetic fields NASA-TN-D-4736 c25 N68-30784 NACH IN 2010 Field-aligned propagation of high frequency radio waves using Alouette 2 satellite data NASA-TN-D-4748 c07 N68-3163 c07 N68-31639 MAGNETIC MATERIALS Electrical and mechanical properties of high temperature cobalt-iron magnetic material NASA-TN-D-4551 c17 N68-MAGNETIC PROPERTIES c17 N68-24558 Property data of magnetic materials for use in high temperature liquid alkali-metal space power systems NASA-SP-3043 c17 N68-MAGNETIC SHIELDING c17 N68-17624 Magnetometers for measuring stable magnetic fields produced by low field superconducting shields NASA-CR-1073 c14 N68-26703 MAGNETIC STORMS Polar cap absorption study of solar cycle variation in solar proton emissions from sun NASA-TN-D-4473 c29 N68-2: MAGNETOHYDRODYNAMIC FLOW c29 N68-25880 Magnetohydrodynamic flow of incompressible viscous electrically conducting fluid over rotating disk NASA-CR-989 c25 N68-14078

MAGNETOHYDRODYNAMIC GENERATORS Electromagnetic processes in magnetohydrodynamic induction machines with working media of liquid metal NASA-TT-F-460 c25 N68-16286 Closed loop facility designed to study MHD generator using argon-cesium working fluid NASA-TN-D-4867 c11 N68-37259 MAGNETOMETERS Magnetometers for measuring stable magnetic fields produced by low field superconducting shields NASA-CR-1073 c14 N68-26703 NASA-CR-1073 MAGNETORESISTIVITY NETORESISTIVITY Predictions for magnetoresistivity temperature dependence of dilute alloys of iron in copper 2260 - TW-D-4626 c26 N68-28239 MAGNETOSPHERE Interactions of unconfined magnetic fields emanating from space vehicles with undisturbed solar wind NASA-TN-D-4304 c29 N68 Continuum fluid theory of solar wind and its interaction with geomagnetic field c29 N68-19188 NASA-TN-D-4482 c29 N68-25181 MAGNETRONS Striking characteristics of magnetron ionization gages in helium over low pressure range NASA-TN-D-4681 c14 N68-29951 MAINTAINABILITY Maintainability of manned spacecraft for long duration flights NASA-CR-1108 MAN MACHINE SYSTEMS c31 N68~33008 Descriptive model for determining optimal human performance in aerospace systems NASA-CR-879 c05 N68-10381 Man machine development cycle and mathematical models for optimal human performance NASA-CR-876 c05 N68-14262 Descriptive model of system development activities and man machine systems for determining optimal human performance in aerospace systems MASA-CR-877, V. 2 c05 N68-Design and application potentials of general purpose, dexterous, cybernetic machines for c05 N68-15120 human augmentation NASA-SP-5047 c05 N68-18870 Optimal role of man in space, allocation of men and machines in aerospace systems, and descriptive model for determining optimal human performance NASA-CR-878 c05 N68-19165 Properties and imaging techniques of various display devices - computer directed visual flight control boards, integrated optical man machine systems, and electro-optical methods NASA-SP-159 c09 N68-22. c09 N68-22302 MANAGEMENT Bibliography of annotated references on management taken from entries to NASA information system between 1962 and 1967 - abstracts and indexes NASA-SP-7500/02/ c34 N68-24567 MANAGEMENT PLANNING Influence of structure and materials research on weight, performance, and cost of advanced launch vehicle systems NASA-CR-974 c31 N68-11520 Man machine development cycle and mathematical nodels for optimal human performance NASA-CR-876 c c05 N68-14262 Management information bibliography NASA-SP-7500 c34 N68-21828 MANEUVERS Optimum maneuvering of glide vehicle at hypersonic speeds NASA-CR-1078 c02 N68-25817 MANGANESE Oxidation resistance and ductility of cobalt heat resistant alloys optimized by restriction of silicon and manganese content NASA-TN-D-4715 c17 N68-29954 MANIFOLDS Flow conditions in inlet manifold of M-1 fuel pump drive turbine investigated using circumferential static pressure measurements in conjunction with smoke trace photographs NASA-TM-X-1513 c12 N68-15639 MANNED SPACE FLIGHT Descriptive model for determining optimal human

MASS DISTRIBUTION

performance in aerospace systems NASA-CR-879 c05 N68-10381 Energetic space radiation and galactic cosmic radiation measured for radiation hazards in manned space flight NASA-TN-D-4404 c29 N68-16837 Astronaut performance using manually hand-held manned space flight NASA-TN-D-4449 c21 N68c21 N68-21123 Properties and imaging techniques of various display devices - computer directed visual flight control boards, integrated optical man machine systems, and electro-optical methods NASA-SP-159 c09 N68-22 c09 N68-22302 Radiation hazards on extended manned space flights NASA-CR-1037 c29 N68-22849 Spacecraft habitability for long duration manned space flight missions NASA-CR-1084 c30 N68-26702 Venus flyby, Mars flyby, and Mars orbital nus flyby, mars flyby, and halo statter mission to evaluate navigation and guidance systems for manned interplanetary spacecraft NASA-TN-D-4629 c21 N68-28236 NASA-TN-D-4629 c21 N68-Maintainability of manned spacecraft for long duration flights NASA-CR-1108 c31 N68-33008 to simulate manned planetary entry NASA-TN-D-4847 c31 N68-36056 MANNED SPACECRAFT Cell culture method of screening contaminants which may appear in manned spacecraft NASA-TN-D-4251 c0 c04 N68-10122 NASA-IN-U-4201 Navigation and guidance analysis of Mars probe launched from manned flyby spacecraft NASA-TN-D-4512 c21 N68-21754 Maintainability of manned spacecraft for long duration flights NASA-CR-1108 c31 N68c31 N68-33008 MANUAL CONTROL Simulator study of pilot control of remote orbital docking of large altitude stabilized components NASA-TN-D-4263 c31 N68-11476 Third annual NASA University Conference on Manual Control NASA-SP-144 c05 N68-15901 Piloted simulation studies of Saturn 5 launch vehicle manual backup guidance and control NASA-TN-D-4481 c21 N68 c21 N68-19061 Simple model describing final airborne stages of landing transport aircraft manually NASA-TN-D-4438 c02 N68-21112 Fully-manual and augmented-manual control systems for Saturn 5 booster studied by emperically based mathematical models for pilot c31 N68-28426 NASA-CR-1079 Manual navigation method for evaluating transfer orbits for lunar landings NASA-TN-D-4756 c21 N68-332 c21 N68-33271 MANUALS Handbook for designing ball lock mechanisms for use on space vehicles NASA-CR-1021 c15 N68-23356 Instruction manual for static structural analyses on shell-type spacecraft structures NASA-CR-912 c32 N68-24802 MANY BODY PROBLEM Analytical formulations and numerical integration methods for many body problem and special perturbative techniques NASA-CR-1005 c30 N68-15741 NASA-CK-1005 Mathematical means for bounding propagated trajectory error induced impulsive initial error in n-body field NASA-TN-D-4511 C30 N68-32094 MAPPING Star field mapping technique for determining attitude of spin stabilized spacecraft NASA-TN-D-4637 c21 N68 c21 N68-28418 MARINER SPACE PROBES Mariner-Mars 1964 mission accomplishments NASA-SP-139 c31 c31 N68-18743 MARKOV PROCESSES Systems analysis logic applied to mathematical modeling of dynamic nonlinear stochastic processes NASA-CR-1168 c19 N68-35472

c30 N68-24557 NASA-TN-D-4587 Mars excursion module landing mission mode comparison NASA-TM-X-1629 c30 N68-29988 MARS ATMOSPHERE (3) AIRUSPIENE Flight test of conical spacecraft simulating parachute deployment in Mars atmosphere NASA-TN-D-4266 c31 N68-11963 Inflation, drag, and stability characteristics of ringsail parachute deployed in simulated Mars c31 N68-11961 atmosphere NASA-TM-X-1500 c31 N68-14092 Subsolar-meridian mean annual distributions for Martian troposphere below 50 km NASA-CR-1043 c30 N68-19192 Inflation and drag characteristics of cross parachute in simulated Martian environment NASA-TM-X-1543 c31 N68 c31 N68-21833 Carbon dioxide model for radiation heating and cooling functions of lower stratified Martian atmosphere in thermodynamic equilibrium NASA-CR-1044 c30 N68-2280 Optical radiation measurements behind shock wave c30 N68-22860 in simulated Mars atmosphere NASA-TM-X-1634 cl2 N68-3 Models of Martian atmosphere based on minimum, c12 N68-32982 mean, and maximum density profiles NASA-SP-8010 c30 N68-37220 MARS ENVIRONMENT Mariner-Mars 1964 mission accomplishments NASA-SP-139 c31 NASA-TN-D-3984 Subscript duration of microwave, millimeter, and optical communication systems for space communications from Mars spacecraft NASA-TN-D-3984 C07 N68-22010 Subsonic dynamic stability characteristics of large conical spacecraft in simulated Martian environment NASA-TN-D-4558 MARS EXCURSION MODULE c31 N68-22301 Subsystem definition of advanced life support technology for Mars surface module NASA-CR-1083 c05 N68-28319 Mars excursion module landing mission mode comparison NASA-TM-X-1629 c30 N68-29988 Technology requirements and spacecraft design studies for atmosphere braking to orbit about Mars and Venus NASA-CR-1131 c30 N68-34086 MARS PROBES Unmanned Mars probe tested for drag, lift, static and dynamic stability at Mach number 2 NASA-TN-D-4291 c01 N68-11 Computer analyses of retrodirective, and self adaptive antenna phase control techniques for c01 N68-11936 Mars probe NASA-CR-977 c21 N68-18484 Navigation and guidance analysis of Mars probe launched from manned flyby spacecraft NASA-TN-D-4512 c21 N68-2: c21 N68-21754 Trajectory data for stopover missions to Mars that employ Venus swingby mode NASA-SP-35, PT. 6 c30 N68-MARTENSITIC STAINLESS STEELS c30 N68-30098 Thermal and mechanical treatment for precipitation hardening stainless steels NASA-SP-5089 c15 N68-20433 Deformation processing of precipitation hardening stainless steels c17 N68-21917 NASA-SP-5088 MASERS Bibliographic citations, abstracts, and indexes on laser and maser research and development NASA-SP-7009/03/ c16 N68-29438 MASS c30 N68-19330 Simultaneous correction of velocity and mass bias in photography of meteors NASA-TR-R-280 c30 N68-15484 Coaxial plasma gun research for space propulsion

MARS (PLANET) Landing site dispersions of unmanned spacecraft

on Mars

MASS FLOW

SUBJECT INDEX

applications NASA-TM-X-1600 c25 N68-28154 MASS FLOW Cold air study of gas turbine for high temperature aircraft engine application NASA-TN-D-4389 c0 Wind tunnel tests of mixed-compression c01 N68-15743 axisymmetric inlet system to determine bleed mass flow ratio, pressure recovery and pressure distortion NASA-TN-D-4557 MASS FLOW RATE c28 N68-23354 Supersonic performance evaluation of mass flux probes with sharp symmetrical inlet, and with blunted unsymmetrical inlet NASA-TM-X-1524 cl4 N68-18 c14 N68-18834 Efficiency, mass flow rate, torque, and exit diffuser effectiveness of 5-inch axial flow turbine NASA-TM-X-1679 c03 N68-37263 MASS SPECTROMETERS Ultraviolet filter and monochromator for mass spectrometer employing photoionization source NASA-CR-1018 MASS TRANSFER c14 N68-17329 Steady hypersonic flow over blunt bodies with high rates of continuous mass and heat transfer from body surface NASA-TN-D-4252 c01 N68-1755 c01 N68-17555 MATERIALS HANDLING Contamination control principles NASA-SP-5045 c11 N68-10384 MATERIALS RECOVERY Recovery of potassium tantalate and potassium monoxide to demonstrate procedure for isolation and recovery of alkali-metal reaction products. in uncontaminated state NASA-TN-D-4310 c17 N68-14888 MATERIALS SCIENCE Influence of structure and materials research on weight, performance, and cost of advanced launch vehicle systems NASA-CR-974 MATERIALS TESTS c31 N68-11520 Two stage potassium vapor turbine - materials support of performance and endurance tests NASA-CR-925 c03 N68c03 N68-16351 Radiation effects on thermionic insulator materials - evaluation of beryllia, alumina, thoria, zirconia, and yttria NASA-TN-D-4414 c22 N68-1 MATHEMATICAL LOGIC c22 N68-17095 Systems analysis logic applied to mathematical modeling of dynamic nonlinear stochastic processes NASA-CR-1168 c19 N68-35472 MATHEMATICAL MODELS Tabulated communication characteristics of steady state model of interplanetary space NASA-SP-3042 c30 N68-10164 Mathematical models and approximation methods for solving lateral vibration modes of cylindrical space vehicles and vehicles with clustered tanks NASA-CR-935 c32 N68-10231 Mathematical models for determining longitudinal vibration modes of multistage liquid and solid propellant vehicles, and clustered tank vehicles NASA-CR-936 c32 N68-10280 Descriptive model for determining optimal human performance in aerospace systems NASA-CR-879 c05 N68-10381 Three dimensional model of monatomic gases interacting with solid surfaces represented by similar, noninteracting hard spheres NASA-CR-933 c c12 N68-10499 Analysis of shear and normal strain effects on weak turbulence and turbulent heat transfer using two point correlation equations obtained from Navier-Stokes and energy equations NASA-TN-D-4273 c33 N68-11491 NASA-TN-D-4273 Man machine development cycle and mathematical models for optimal human performance NASA-CR-876 c05 N68-14262 MAA-CK-G70 C03 NOD-1421 Plum Brook reactor support calculations -mathematical model for fuel utilization, power distribution in fuel loading, and approximate predictions of xenon poison transient NASA-TM-X-1496 C22 N68-1604 c22 N68-16056

Coordinate measuring system for flight control, and trajectory optimization NASA-CR-1000 c30 N68-16 c30 N68-16103 Mathematical models for determining eigenvalue bounds of matrix NASA-TN-D-4373 c19 N68-1 c19 N68-17334 NASA-IN-D-4373 Cls NoC-17354 Mathematical model of statistical channel characteristics in, and test instrumentation for, digital data transmission systems handling uniformly coded binary data NASA-IT-F-434 c07 N68-1754; c07 N68-17542 Machematical prediction model for landing dynamics of impacting struts, and trusses of lunar vehicle landing gear NASA-TN-D-4434 c31 N68-19085 Frequency function for testing small samples for goodness of fit to normal populations NASA-TN-D-4405 cl c19 N68-19144 Mathematical model for frequency response of forced flow, hollow, single tube boiler inlet pressure to inlet flow NASA-TM-X-1528 cl2 N68-19 c12 N68-19340 Mathematical model for deriving pressure drop against flow function of counterflow boiler tube in Rankine space power system c33 N68-20066 NASA-TN-D-4498 Zero density and approximate, relativistic models of universe NASA-TR-R-282 c30 N68-20192 Multi-step Runge-Kutta methods using method of quadratures NASA-TN-D-4400 c19 N68-21100 Simple model describing final airborne stages of landing transport aircraft manually NASA-TN-D-4438 c02 N68-21112 Analytic computational error models for strapdown inertial navigation systems NASA-CR-968 c21 N68-21652 Recommended procedures for stability, control, and structural loading analysis of large liquid fueled rocket booster sloshing parameters NASA-CR-948 c32 N68-23454 Double dead-time model for combustion stability analysis in liquid bipropellant rocket engines NASA-TN-D-4564 c33 N68-25102 Transient thermodynamic analysis for development of mathematical model that predicts transient temperature and voltage-response characteristics of fuel cell system NASA-TN-D-4601 c03 N68-25304 Model of plasma boundary interactions NASA-CR-1072 c25 N68-25821 Fully-manual and augmented-manual control systems for Saturn 5 booster studied by emperically based mathematical models for pilot c31 N68-28426 NASA-CR-1079 Two dimensional computer model for collisionless self gravitating galactic system with gravitational field obtained from Poisson equation NASA-TN-D-4646 c30 N68-28884 Mathematical model and computer program for analysis of three and four gimbal systems NASA-TN-D-4689 c11 N68-299 Mathematical model based on conformal mapping of c11 N68-29957 shape of electric arc balanced in transverse convective and magnetic fields NASA-TN-D-4736 c25 N68-30784 Parameter variation analyses on mathematical models NASA-CR-1126 c15 N68-31478 Mathematical means for bounding propagated trajectory error induced impulsive initial error n-body field NASA-TN-D-4511 c30 N68-32094 Mathematical model for computing equilibrium properties of one dimensional self-gravitating stellar system NASA-TR-R-289 c30 N68-32978 Frothing-sloughing ablation model for computing luminous efficiency factor from meteor data

c30 N68-33055 NASA-TN-D-4808 Mathematical model for analyzing free vibration of rotating beam-connected space station c32 N68-33225 NASA-TN-D-4753

Mathematical model of human operator as optimal controller and information processor NASA-CR-1151 c05 N68-33304

Simplified equilibrium hydrocarbon-air combustion

gas model for use in air breathing engine cycle computer programs NASA-TN-D-4747 c28 N68-35115 Systems analysis logic applied to mathematical modeling of dynamic nonlinear stochastic processes NASA-CR-1168 c19 N68-35472 Mathematical model of liquid metal fuel reactor to investigate temperature distribution on neutron kinetics NASA-TN-D-4840 c22 N68-36055 Computation of mean and fluctuating quantities in turbulent boundary layers NASA-TN-D-4815 c12 N68-36 Theoretical analysis of pressure distribution, load capacity, load angle, and friction force for single-step concentric journal bearing NASA-TN-D-4839 c15 N68-36 NASA-TN-D-4815 c12 N68-36071 c15 N68-36098 NASA-TN-D-4439 c15 N68-36098 Length of winding on torus in two ideal models NASA-TN-X-1674 c03 N68-37217 MATRICES (MATHEMATICS) Heat balance equations for optimizing optical coating patterns for spacecraft temperature control system NASA-CR-1041 c18 N68-22391 Laminar boundary layer problems solved by integral matrix methods NASA-CR-1062 c33 N68-26641 Matrix equations to describe motions of spacecraft consisting of interconnected rigid bodies NASA-TN-D-4749 c32 N68-33092 MATRIX METHODS RIX METHODS Elastoplastic analysis of circular cylindrical inclusion in uniformly stressed infinite homogeneous matrices of composite materials for aerospace applications NASA-TN-D-4350 c32 N68-15769 MATRIX THEORY Mathematical models for determining eigenvalue bounds of matrix NASA-TN-D-4373 c19 N68-17334 MAXIMA Maxima-minima theory, Pontryagin principle, and calculus of variations for optimal trajectory and control analysis NASA-CR-1006 MAXIMUM PRINCIPLE c30 N68-20084 Thermodynamics of plasmas using principle of maximum entropy NASA-TN-D-4621 c25 N68-25920 MAYER PROBLEM Three numerical procedures for Mayer classical and non-classical problems in trajectory optimization NASA-CR-1012 MEASURING INSTRUMENTS c30 N68~19315 Supersonic performance evaluation of mass flux probes with sharp symmetrical inlet, and with blunted unsymmetrical inlet NASA-TM-X-1524 cl4 N68-18 c14 N68-18834 Cesium ion beam electric field measuring instruments NASA-CR-970 c14 N68-25903 Celestial attitude measuring instrument using star mapping technique NASA-TN-D-4742 c21 N68-31938 MECHANICAL IMPEDANCE Impedance testing for flight control system parameters in studies of launch vehicle dynamic stability NASA-CR-939 c32 N68-11485 MECHANICAL PROPERTIES HANICAL PRUPERTIES Environmental exposure effects on mechanical properties of titanium alloy, stainless steel, aluminum alloy, and composite material sheets NASA-TN-D-4318 c17 N68-17897 Mechanical properties of tungsten and tungsten rhenium alloys NASA-TN-D-4567 c17 N68-2 c17 N68-24477 Mechanical, optical, and electrical characteristics of hand-held sextant for space flight NASA-TN-D-4585 c21 N68-24512 Electrical and mechanical properties of high temperature cobalt-iron magnetic material NASA-TN-D-4551 c17 N68-24558

Effects of stretch and heat-set temperatures and time on cryogenic mechanical properties of poly/ethyl terephthalate/ film

c18 N68-33034 NASA-TN-D-4762 Fabricability, mechanical properties, and structural efficiency potentials of boron-polymer film layer composites NASA-CR-1114 c18 N68-35100 Microstructure and mechanical properties of beryllium tubing and performance tests on support columns of beryllium NASA-TN-D-4833 c17 N6 c17 N68-37053 MEDICAL ELECTRONICS Design and operating characteristics of electro-optical instrument for tracking of retinal blood vessels in back of eye NASA-CR-1121 c05 N68-35109 MELTING POINTS Crucible melting and arc melting of aluminum nitride and determination of its melting point NASA-CR-1171 c17 N68-33335 MEMBRANE STRUCTURES Stress analysis and functions in membrane analysis of scalloped thin walled shells like parachutes NASA-TN-D-4687 c32 N68-28832 NASA-IN-D-soor MERCURY (METAL) Steady state performance tests on single pass counterflow sodium-potassium cooled mercury Rankine cycle condenser NASA-TM-X-1548 c33 N68-20340 Mechanism and kinetics of iron and cobalt alloys corrosion in refluxing mercury NASA-TN-D-4450 c17 N68-21654 Performance tests on high voltage isolator for mercury propellant feed system of ion engine NASA-TM-X-1579 c28 N68-23 c28 N68-23477 MERCURY MA- 8 FLIGHT Description and performance analysis of manned six-pass orbital mission /Mercury-Atlas 8/ NASA-TN-D-4807 c31 N68-3 c31 N68-35022 MERCURY VAPOR Window designs for mercury condensing tube and mercury boiler outlet tube NASA-TM-X-1578 c11 N68-22737 MESOSPHERE Nike Apache pitot tube rocket sounding measuring of Southern Hemisphere stratosphere and mesosphere along west coast of South America NASA-TN-D-4264 c20 N68-25617 Meteorological rocket soundings in stratosphere and mesosphere, 1966 - tables NASA-TR-R-288 Metabolic Wastes c20 N68-33036 Chemical feasibility and nutrional value in synthesis of edible fatty acids and lipids from metabolic wastes for space flight feeding NASA-CR-1104 c04 N68-28829 METABOLISM Metabolic cost of walking on treadmills of various slope before and after loading of principal body segments NASA-CR-1042 c05 N68-21859 Effects of simulated lunar gravity on metabolic rates while wearing pressure suits NASA-CR-1102 c05 N68~28833 METAL CRYSTALS Influence of crystal structure, orientation, and solubility on adhesion and sliding friction of metal single crystals in vacuum NASA-TN-D-4347 c15 N68-21226 METAL FATIGUE Axial tensile fatigue of liquid rocket engine alloys at cryogenic temperatures NASA-TN-D-4274 c17 N68-11637 Stress corrosion cracking of titanium aluminum vanadium alloy in nitrogen tetroxide under pressure NASA-TN-D-4289 c17 N68-12891 Cyclic frequency, tensile fatigue effects, and defect substructure generated in vacuum by fatigue stressing of aluminum NASA-CR-1165 c17 N68-35200 Ratigue crack propagation in cylindrical shells with fluctuating internal pressure NASA-CR-1197 c32 N68-37840 METAL FILMS Summary data on deposition and endurance lives of thin metallic films used for lubricating sliding and rolling element electrical contacts in vacuum environments NASA-TN-D-4476 c15 N68-21979

METAL FOILS

SUBJECT INDEX

METAL FOILS Transmission, and backscatter coefficients for electron irradiated aluminum, and stainless steel foils NASA-TN-D-4363 c24 N68-17898 Radiation damage in low energy proton irradiated thick copper and gold foils and subsequent annealing characteristics NASA-TN-D-4452 c26 N68-212 c26 N68-21219 METAL GRINDING Role of chemical reactions in comminution note of chemical reactions in communition mechanism of ductile metals into ultrafine powders by grinding NASA-TN-D-4862 cl5 N68 METAL HYDRIDES c15 N68-37239 Reactivity control of fast nuclear reactors containing yttrium hydride moderating zones NASA-TN-D-4615 c22 N68c22 N68-24559 METAL JOINTS Brazing aluminum to titanium coated stainless steel to minimize formation of intermetallic compounds in joint NASA-SP-5040 c15 N68-22778 METAL-METAL BONDING Organic and inorganic adhesives for bonding of stainless steels and precipitation hardened stainless steels c15 N68-20056 NASA-SP-5085 METAL OXIDE SEMICONDUCTORS Metal oxide semiconductor field effect transistor circuit development and laminated electronic packaging for computer storage devices NASA-CR-1113 c08 N68-35 c08 N68-35193 METAL PLATES Tables of energy and angular distributions of thick target bremsstrahlung in metals NASA-TN-D-4755 c2 c24 N68-35535 METAL POWDER Electron microscopy technique for determining dispersoid distribution in powder blends NASA-TM-X-1468 c17 N68-10051 chromium and nickel powders from reduction of chromium and nickel oxides with magnesium, lithium, or sodium vapors NASA-TN-D-4714 c17 N68-30066 Role of chemical reactions in comminution mechanism of ductile metals into ultrafine powders by grinding NASA-IN-D-4862 c15 N68 c15 N68-37239 METAL SHEETS Simulated meteoroid high velocity impact damage to spacecraft structures composed of two metallic sheets NASA-CR-915 c31 N68-14638 NASA-CK-915 Col NOC-14050 Environmental exposure effects on mechanical properties of titanium alloy, stainless steel, aluminum alloy, and composite material sheets NASA-TN-D-4318 c17 N68-17897 NASA-TN-D-4318 c17 N68-174 Penetration resistance of aluminum double sheet targets to projectile impact NASA-TN-D-4568 c32 N68-25104 METAL SURFACES Influence of gaseous environment on self-adhesion of metal surfaces NASA-TN-D-4868 c17 N68-3697 c17 N68-36970 METAL VAPORS Two stage turbine suitable for use in wet potassium vapor at temperatures of 1400 to 1600 deg F NASA-CR-922 c03 N68-16439 METALLOGRAPHY Electron probe X ray microanalyzer applied to material failure study, bonding, and other metallurgical analysis NASA-TN-D-4526 c15 N68-: c15 N68-28249 METASTABLE ATOMS Metastable helium atom addition to hydrogen plasma for ion cyclotron mode enhancement NASA-TN-D-4271 METEORITE COLLISIONS c25 N68-18485 Testing and evaluation of capacitor type meteoroid penetration NASA-TN-D-4524 c14 N68-22883 METEORITIC DAMAGE Simulated meteoroid high velocity impact damage to spacecraft structures composed of two metallic sheets NASA-CR-915 c31 N68-14638 Stainless steel penetration detector, impact

detector, and solar cell degradiation, to study ucterior, and solar cell degradiation, to study micrometeoroid impact damage and puncture rate, and radiation effects on Explorer 23 satellite NASA-TN-D-4284 c31 N68-2819 METEOROID PROTECTION c31 N68-28198 Exploding foil gun technique for simulated meteoroid protection NASA-TN-D-4259 c32 N c32 N68-11355 METEOROIDS Simultaneous correction of velocity and mass bias in photography of meteors NASA-TR-R-280 c30 N68-15484 Photographic and spectrometric observation of iron, artificial meteor launched from Trailblazer 2, and reentering at 11 kilometers per second NASA-TN-D-4312 c30 N68-16750 Results of including boundary shock wave in calculation of flight parameters of large high speed meteor NASA-TN-D-4325 c12 N68-18997 Two methods of photographic photometry of artificial meteoroids NASA-TN-D-4667 c14 l c14 N68-29418 Luminous intensity and efficiency parameters for hypersonic reentry of nickel artificial meteors NASA-TN-D-4666 c30 N68-3024 c30 N68-30244 Frothing-sloughing ablation model for computing luminous efficiency factor from meteor data NASA-TN-D-4808 c30 N68-33055 Electron radiation induced dielectric breakdowns in capacitor meteoroid detection system NASA-TN-D-4738 c14 N68-332 METEDROLOGICAL CHARTS Statistical evaluation of sampled wind data from c14 N68-33277 anemometers mounted on meteorological tower on Wallops Island NASA-TN-D-4395 c20 N68-18246 Evaluation of Nimbus satellite radiation measurements and heat balance charts of earth atmosphere NASA-TN-D-4589 c13 N68-28222 METEOROLOGY Atmospheric effects on sonic boom characteristics NASA-TN-D-4588 c02 N68-24662 METHANE Design and volumetric analysis of pressurized tanks for use in liquid-methane fueled supersonic transport aircraft NASA-TN-D-4295 c32 N68-12370 Tankage systems for methane-fueled supersonic transport NASA-TM-X-1591 c02 N68-23895 Fuel tank pressurization and supercooling of liquid methane to minimize fuel boiloff problems in supersonic aircraft NASA-TM-X-1604 c27 N68-28155 Analysis of several methane fueled engine cycles for supersonic flight NASA-TN-D-4699 c28 N68-29378 Solubilities of several gases in liquid methane and liquefied natural gas NASA-TN-D-4701 c27 N68-30077 Comparative analysis of fuselage tanks for liquid methane fueled supersonic aircraft NASA-TN-D-4837 c02 N68~36074 METHODOLOGY Laboratory methodology of signal analysis with application to Apollo program NASA-TM-X-1599 c08 N68-30240 MICROANALYSIS Electron probe X ray microanalyzer applied to material failure study, bonding, and other metallurgical analysis NASA-TN-D-4526 c15 N68c15 N68-28249 MICROBIOLOGY Air samplers, contamination, and sterilization in collection of microorganisms for microbiological exploration of stratosphere NASA-CR-1101 MICROELECTRONICS c04 N68-28247 Microelectronic device data handbook /text/ c09 N68-29525 NASA-CR-1110 Microelectronic device data handbook /manufacturer and specific device information/ NASA-CR-1111 c09 N68-295 c09 N68-29526 MICROHARDNESS

Subsurface residual stress on steel inner races from ball bearings during rolling contact

MIXING LENGTH FLOW THEORY

NASA-TN-D-4456 c15 N68-20199 MICROMETEOROIDS Flight test of capacitance type meteoroid impact detector of aluminum polyethylene terephthalate using inflatable paraglider NASA-TN-D-4530 c14 N68-2229 c14 N68-22290 NASA-IN-0-4330 Stainless steel penetration detector, impact detector, and solar cell degradiation, to study micrometeoroid impact damage and puncture rate, and radiation effects on Explorer 23 satellite NASA-TN-D-4284 c31 N68-28198 MICROMINIATURIZED ELECTRONIC DEVICES Integrated circuit, direct coupled, differential amplifier for spacecraft signal conditioning NASA-TN-D-4584 MICROORGANISMS c07 N68-24845 Microbiological contamination of Gemini 9 spacecraft before and after flight NASA-CR-972 c04 c04 N68-11968 MI CROPHONES Precision calibration techniques for microphones used in sonic boom measurements NASA-CR-1075 c14 N68-25316 MICROSTRUCTURE Use of surface replication, extraction replication, and thin film electron microscopy in study of microstructures of dispersion strengthened materials NASA-TN-D-4461 c17 N68 Electron microscope technique for revealing microstructures of dispersion strengthened c17 N68-18999 materials NASA-TM-X-1561 c17 N68-21431 Microstructure and mechanical properties of beryllium tubing and performance tests on support columns of beryllium NASA-TN-D-4833 c17 N68-37053 MICROTHRUST Thermal design and analysis of cesium contact-ion microthrustor NASA-TM-X-1473 c28 N68-10496 NADA TH A 1410 Performance tests of ammonia resistojet thrustor system for various spacecraft control maneuvers NASA-TN-D-4249 c28 N68-1056 c28 N68-10562 Electrical stress analysis of microthruster power conditioner NASA-TM-X-1686 c09 N68-37944 MICROWAVE ANTENNAS Omridirectional microwave parallel plate broadband antenna for spacecraft communications NASA-TN-D-4555 c07 N68-25918 MICROWAVE EQUIPMENT Trace contaminant identification using microwave double resonance spectroscopy NASA-CR-967 c24 N68-11634 MICROWAVE SPECTRA Microwave molecular spectroscopy for identifying contaminants in space cabin atmospheres bibliography NASA-CR-951 C23 N68-106 MICROWAVE TRANSMISSION Evaluation of microwave, millimeter, and optical communication systems for space communications c23 N68-10674 from Mars spacecraft NASA-TN-D-3984 c07 N68-22019 MI CROWAVES Microwave pump requirements for field operational broadband rutile traveling wave maser for Applications Technology Satellite program NASA-TN-D-4764 MIDCOURSE GUIDANCE c16 N68-33635 Manual procedure for midcourse guidance and applications to Earth-Moon trajectories NASA-TN-D-4246 c21 N6 c21 N68-11521 Mathematical formulation of guidance equations and solutions for orbital space missions NASA-CR-1010 c30 N68-17215 Two body equations of motion for calculating partial derivatives relating lunar and planetary midcourse correction requirements to guidance system injection errors NASA-TN-D-4518 c30 N68-20368 Astronaut performance using manually hand-held sextants for midcourse navigation phases of manned space flight NASA-TN-D-4449 c21 N68-21123 MIE SCATTERING Computer program for calculating normalized Mie scattering functions

NASA-CR-1022 Military Aircraft c24 N68-21227 Aerodynamic ground effect measurements on low aspect ratio ogee wings NASA-TN-D-4329 co2 N68c02 N68-14090 MILITARY TECHNOLOGY HILLIARY IECHNOLOGY Historical survey of Russian rocketry and space exploration NASA-TT-F-426 KILLIMETER WAVES Electron beam-plasma interaction and plasma c31 N68-22262 multiplier as possible millimeter wave generators NASA-TN-D-4309 c25 N68-18614 NASA-TN-D-4309 c25 N68-180. Evaluation of microwave, millimeter, and optical communication systems for space communications from Mars spacecraft c07 N68-220 Coherent radiation methods of measuring absorption spectra in planetary atmosphere, and millimeter and submillimeter wave c07 N68-22019 propagation NASA-CR-863 c07 N68-27063 MASA-UK-865 CUT N66-270 MILLING (MACHINING) Hydrogen release in ball milling of high purity, coarse chromium powder in water NASA-TN-D-4569 c15 N68-239 c15 N68-23900 MINERAL OILS Reduced pressure effects on fatigue life of roller steel ball bearings with mineral oil lubricants NASA-TN-D-4348 c15 N68-15010 MINERALS Stability of selected earth minerals in simulated lunar environment tests NASA-CR-1034 c13 N68-25579 MINIMA Maxima-minima theory, Pontryagin principle, and calculus of variations for optimal trajectory and control analysis NASA-CR-1006 c30 N68-20084 MIRRORS Ultraviolet measurements of oil contamination in optical mirrors NASA-TN-D-4612 c14 N68-25375 Mathematical determination of geometrical image aberrations in single and double mirror systems NASA-TN-D-4692 MISSILE CONFIGURATIONS c23 N68-36460 Body alterations for reducing drag of missiles during coasting flight NASA-TM-X-1537 c01 N68-19206 MISSILES Supersonic aerodynamic characteristics of model of air-to-surface missile NASA-TM-X-1491 c01 N68-16480 MISSION PLANNING BION FLANNING Development of mission requirement profile for subsystem components from overall system profile NASA-SP-6503 c30 N68-15683 Photographic mission planning and photograph interpretation for Lunar Orbiter 3 NASA-CR-984 c30 N68-15725 Mission constraints and trajectory interfaces for launch, rendezvous, spatial, deorbit, and entry phases of earth orbital mission NASA-CR-1015 c30 N68-20468 C3U N68-20 Spacecraft system design, mission planning, and qualification testing for Gemini project NASA-CR-1106 c31 N68-25 c31 N68-25577 Trajectory data for stopover missions to Mars that employ Venus swingby mode NASA-SP-35, PT. 6 c30 N68c30 N68-30098 Technology requirements and spacecraft design studies for atmosphere braking to orbit about Mars and Venus NASA-CR-1131 c30 N68-34086 MIXING Photographs, thermocouples, and emission spectra used to study mixing and reaction of hydrazine and nitrogen tetroxide NASA-TN-D-4467 c33 N68-2490 c33 N68-24965 MIXING LENGTH FLOW THEORY Free jet mixing analysis for parallel streams of different fluids NASA-CR-956 c12 N68-13619 Mixing length flow theory for analyzing incompressible turbulent swirling flow

in pipes NASA-CR-1169 c12 N68-36343

MODAL RESPONSE

MODAL RESPONSE Vibration modal response of thin cylindrical shells NASA-CR-897 c32 N68-11967 Longitudinal dynamic characteristics of Stub D Atlas launch vehicle without propellants or payload NASA-TM-X-1682 c31 N68-37942 MODELS Algebraic methods for analysis and design of model following control systems NASA-TN-D-4663 c19 N68-28281 MODERATORS Neutronic effects of yttrium hydride moderator insertion in fast spectrum reactors NASA-TM-X-1614 c22 N68-29950 MODULATORS Gallium arsenide laser modulator, attenuation coefficients, and semiconductors for optical communication systems NASA-TN-D-4608 c23 N68-2 c23 N68-25868 MODULUS OF ELASTICITY Classical equations of elasticity in terms of stress components reduced to three stress functions and three equations NASA-TN-D-4253 c19 N68-10355 MOLECULAR COLLISIONS Numerical calculation of capture cross sections between ions and polar molecules NASA-TM-X-1586 MOLECULAR INTERACTIONS c24 N68-23893 Physical gas dynamics research - molecular band spectra, shock tube studies, and interactions between diatomic molecules NASA-TT-F-505 c12 N68-16839 MOLECULAR IONS Partition functions and thermodynamic properties to high temperatures for hydrogen triatomic and diatomic molecular ions NASA-TN-D-4523 c33 N68-21732 MOLECULAR SPECTROSCOPY Microwave molecular spectroscopy for identifying contaminants in space cabin atmospheres bibliography NASA-CR-951 MOLECULAR STRUCTURE c23 N68-10674 Effects of molecular structure on thermochemical properties of phenolic resins and related polymers NASA-TR-R-276 MOLECULAR WEIGHT c33 N68-11038 Solid state polymerization technology for synthesis of ultrahigh molecular weight polyethylene terephthalate NASA-TN-D-4335 c06 N68-14093 MOLYBDENUM Calcium, molybdenum, and lithium compounds as low drive temperature stable memory cores NASA-TN-D-4573 c09 N68-2438 c09 N68-24388 Low energy electron diffraction study of oxygen adsorption on molybdenum /111/ surface NASA-TN-D-4735 c06 c06 N68-30582 MOLYBDENUM ALLOYS Protective coatings and surface treatments for protection of Ti-8Al-1Mo-1V alloy sheet from hot-salt stress corrosion NASA-TN-D-4319 c17 N68-1 c17 N68-17377 MOLYBDENUM DISULFIDES Sputtered molybdenum disulfide film deposition and friction characteristics in vacuum NASA-TN-D-4269 c17 N68-11644 MONATOMIC GASES Three dimensional model of monatomic gases interacting with solid surfaces represented by similar, noninteracting hard spheres NASA-CR-933 c c12 N68-10499 MONOCHROMATORS Ultraviolet filter and monochromator for mass spectrometer employing photoionization source NASA-CR-1018 c14 N68-17329 MONTE CARLO METHOD Monte Carlo computations of decision error probabilities for chain pooling and variations for fractional factorial experiments c19 N68-11639 NASA-TN-D-4272

SUBJECT INDEX

Computer program using Monte Carlo methods for simulating solar flares during interplanetary space flight NASA-TN-D-4311 c29 N68-16008 Applications of Monte Carlo analysis to tungsten resonance absorption NASA-TN-D-4545 c22 N68-21924 Rarefied gas couette flow and heat transfer between parallel plates analyzed by model sampling procedures NASA-TN-D-4579 c12 N68-24129 MOON Calculations of nondiffuse infrared radiation from lunar surface incident onto unit element above surface NASA-TM-X-1567 MOSSBAUER EFFECT c29 N68-21731 Mossbauer spectroscopy used to study sensitization in austenitic stainless steels NASA-CR-1077 MOTION PICTURES c17 N68-25318 Spacecraft attitude determination using single onboard camera NASA-TN-D-4359 c31 N68-19275 MOTION STABILITY Effect of liftoff dynamics on launch vehicle stability and control NASA-CR-943 c32 N68-10233 NASH-UN-945 C32 N68-11 Conference proceedings on classical mechanics, continuum mechanics, and motion stability NASA-TT-F-503 C23 N68-33 MULTIPROGRAMMING c23 N68-37792 Advanced multiprocessor computer organization for manned Mars lander mission NASA-CR-1159 c08 N68-3556 c08 N68-35560 MULTISTAGE ROCKET VEHICLES Kathematical models for determining longitudinal vibration modes of multistage liquid and solid propellant vehicles, and clustered tank vehicles NASA-CR-936 c32 N68-10280 Wind tunnel study of aerodynamic characteristics of three scale model multistage launch vehicles at supersonic and hypersonic speeds NASA-TM-X-1498 c01 N68-16299 NASA-IN-X-1490 FORTRAN digital computer program for axial distribution of aerodynamic normal force characteristics for axisymmetric, multistage launch vehicles in linear angle of attack ranges NASA-TN-D-4342 c31 N68-18615 Computer program for trajectory optimization and payload maximization in multistage launch vehicles NASA-TN-D-4729 c30 N68-31989 N N-TYPE SEMICONDUCTORS Defect energy levels and concentrations for proton irradiated, n-type silicon single crystals NASA-TN-D-4830 c26 N68-37051 NACELLES Effect of boattail juncture shape on pressure drag coefficients of isolated afterbodies of supersonic engine nacelles NASA-TM-X-1517 c01 N68-19237 Simulated wing effect on pressure drag coefficient of subsonic boattail at angle of attack NASA-TM-X-1662 c01 c01 N68-35672 Wind turnel tests of airframe installation effects on F-106B scale model with simulated underwing engine nacelles at Mach 0.56 to 1.46 NASA-TM-X-1683 c02 N68-37941 NASA PROGRAMS NASA Thesaurus – A through L alphabetical listing of terms for indexing and retrieving aerospace related documents NASA-SP-7030, V. 1 c34 N68-1: NASA Thesaurus - M through Z alphabetical listing of terms for indexing and retrieving aerospace related documents c34 N68-11307 NASA-SP-7030, V. 2 c34 M Appendices to NASA Thesaurus for indexing c34 N68-11308 scientific and technical information - category term listing, hierarchical display, permuted index, and postable terms NASA-SP-7030, V. 3 c34 N68-1 Third annual NASA University Conference on c34 N68-11309 Manual Control NASA-SP-144

c05 N68-15901

Cumulative index to NASA survey on technology NASA-SP-5021/06/ c34 N c34 N68-25221 History of NASA Goddard Space Flight Center through 1963 NASA-SP-4301 c11 N68-30317 Supplement to NASA bibliography on lubrication, corrosion, and wear NASA-SP-7020/02/ c15 N68-31522 Conference papers on NASA planning and projected requirements for advanced aerospace electronic systems technology NASA-SP-154 c30 N68-33169 NASA university programs in personnel training, aeronautics and space research, and laboratories and research centers NASA-SP-185 c34 N68-35564 NASA contributions to special-purpose thermocouple design and applications NASA-SP-5050 c c14 N68-35620 NAVIER-STOKES EQUATION Analysis of shear and normal strain effects on weak turbulence and turbulent heat transfer using two point correlation equations obtained from Navier-Stokes and energy equations NASA-TN-D-4273 c33 c33 N68-11491 NAVIGATION AIDS Telescope objective lens size, aperture size, and magnification effects on operator performance using marine sextants NASA-TN-D-4781 c21 N68-33006 NAVIGATORS Navigator performance using hand held sextant to measure angle between moving flashing light and simulated star - space navigation NASA-TN-D-4174 c21 N68-13558 NEAR ULTRAVIOLET RADIATION Spectral response of cuprous sulfide-cadmium sulfide film photovoltaic cell to green light NASA-TN-D-4333 c03 N68-14082 NEGATIVE FEEDBACK Negative feedback for discharge current noise reduction in excited helium-neon laser NASA-CR-1173 c16 N68-35099 NETWORK ANALYSIS Annotated bibliography of computer-aided circuit analysis and design NASA-SP-7023 c10 N68-19882 NEUROTROPISM Biochemistry of nervous system, subcellular cerebral functions, brain metabolism, isotopic labeling for biochemical studies, and use of neurotropic drugs NASA-TT-F-439 NEUTRON ACTIVATION ANALYSIS c04 N68-13432 /TRUN ACTIVATION ANALYSIS Neutron activation analysis of sodium, lithium, and potassium in compact fast reactors and its effect on shielding NASA-TM-X-1512 C22 N68-203 c22 N68-20355 NEUTRON EMISSION Comparison of absolute calculated and measured gamma and neutron doses in tungsten watermoderated critical assembly NASA-TN-D-4223 c22 N68-10291 Discrete ordinate computation of fission spectrum neutron dose rate attenuation curve for lithium hydrides and tungsten NASA-TN-D-4684 NEUTRON FLUX DENSITY c24 N68-30001 Fast and thermal neutron flux measurements in test cavity outside HB-6 beam port in Plum Brook reactor using sulfur pellets and gold foils NASA-TM-X-1497 c22 N68-15643 NEUTRON IRRADIATION Spectral transmission characteristics of fused silica before, during, and after exposure to reactor irradiation pulses NASA-CR-1031 c22 N68-21124 Reactor irradiation effects on optical absorption levels in fused silica NASA-CR-1032 c22 N68-2348 c22 N68-23481 Effects of nuclear radiation on performance of diodes for use in SNAP 8 NASA-TN-D-4620 c09 N68-26662 Neutron irradiation effects on embrittlement of polycrystalline tungsten NASA-TN-D-4661 c17 N68-28 c17 N68-28818 Spectral transmission measurements on fused silica during and after exposure to pulsed neutron

irradiation NASA-CR-1191 c22 N68-35826 NEUTRON SOURCES Ages for D-D and D-T neutrons in water and tungsten-water mixtures NASA-TN-D-4581 c22 N68-25058 NEUTRONS Mathematical model of liquid metal fuel reactor to investigate temperature distribution on neutron kinetics NASA-TN-D-4840 c22 N68-36055 NEWTON-RAPHSON METHOD Newton-Raphson and gradient parameter correction technique for solution of optimal control problems NASA-TR-R-293 c19 N68-37073 NTCKEL. Luminous intensity and efficiency parameters for hypersonic reentry of nickel artificial meteors NASA-TN-D-4666 c30 N68-30244 NICKEL ALLOYS ALL ALLUIS Directional solidification of nickel base alloy TAZ-8B to enhance potential for advanced gas turbine engine applications NASA-TN-D-4390 cl7 N68-15637 Oxidation resistant alloys tested for suitability as transpiration cooled gas turbine blades NASA-CP-D-030 cl7 N68-17503 c17 N68-15637 NASA-CR-930 c17 N68-17591 High temperature research on creep rupture strength of refractory metal fiber and nickel alloy composites NASA-TN-D-4787 c17 N68-33 c17 N68-33684 Cavitation damage of stainless steel, nickel, and aluminum alloy in water NASA-TM-X-1670 c17 N68-36076 NTCKEL OXIDES Chromium and nickel powders from reduction of chromium and nickel oxides with magnesium, lithium, or sodium vapors NASA-TN-D-4714 c17 N68-3 c17 N68-30066 NIMBUS SATELLITES Evaluation of sea surface temperature as measured by Nimbus 1 satellite high resolution infrared radiometer NASA-TN-D-4078 c20 N68-10222 Pressure distributions and aerodynamic characteristics of Nimbus B fuel capsule in hypersonic flow NASA-TM-X-1487 c01 N68-11958 Cumulus cloud and fog bank spectral reflectance observations using Nimbus satellites and infrared radiometers NASA-TN-D-4552 c14 N68-25862 Evaluation of Nimbus satellite radiation measurements and heat balance charts of earth atmosphere NASA-TN-D-4589 c13 N68-28 Detection of terrain features from Nimbus 1 satellite high resolution infrared radiometer c13 N68-28222 nighttime measurements NASA-TN-D-4603 c13 N68-28872 Nimbus 2 and ESSA 3 satellite observation photographs of typhoon Marie NASA-TN-D-4757 c20 N68-37869 NIMBUS 1 SATELLITE Cumulus cloud and fog bank spectral reflectance observations using Nimbus satellites and infrared radiometers c14 N68-25862 NASA-TN-D-4552 NIMBUS 2 SATELLITE Cumulus cloud and fog bank spectral reflectance observations using Nimbus satellites and infrared radiometers NASA-TN-D-4552 c14 N68-25862 NIGBIUM Magnitude of electrical potential-temperature curve determined for tantalum, niobium, and magnesium during oxidation in air NASA-TN-D-4240 c17 N68-10498 Electrical performance of rhenium niobium cylindrical thermionic converter NASA-TN-D-4533 c03 N68-21766 NASA-TN-D-4533 C03 No Current-voltage characteristics of variable spaced thermionic converter with tungsten emitter and niobium collector NASA-CR-1033 c03 No

Convective stagnation heat transfer of carbon dioxide, nitrogen-argon gas mixtures compared to

NITROGEN

c03 N68-23476

NITROGEN

air in shock tube tests NASA-TN-D-4255 c33 N68-11811 Quantitative measurement of atomic photoionization cross sections of atomic hydrogen, oxygen, and nitrogen NASA-CR-998 c24 N68-18118 Heat transfer correlation for nitrogen flowing across electrically heated banks of wire meshes or tubes NASA-TN-D-4514 NITROGEN TETROXIDE c33 N68-20374 Photographs, thermocouples, and emission spectra used to study mixing and reaction of hydrazine and nitrogen tetroxide NASA-TN-D-4467 c33 N68-2490 c33 N68-24965 Injector baffles for flame stability in combustion chambers using nitrogen tetroxide and hydrazine mixture NASA-TM-X-1595 c28 N68-26644 Small uncooled combustion chamber tests of performance and stability characteristics of nitrogen tetroxide-hydrazine propellant NASA-TN-D-4776 c27 N68-3 c27 N68-35072 NOISE (SOUND) Judgment tests conducted to determine noise levels or loudness of tones plus noise NASA-CR-1117 co5 N68-30602 NOISE INTENSITY Estimation procedures for effect of design and flight characteristics of jets on ground noise NASA-CR-1053 c02 N68-269 c02 N68-26930 c04 N68-35103 NOISE REDUCTION Experimental, and theoretical evaluations of acoustic liners for screech suppression in rocket engines NASA-TN-D-4442 c28 N68-18249 Sensitive piezoelectric transducer with electric and mechanical noise rejection features for measuring cardiac and gross motor activity of small organisms NASA-TN-D-4590 c05 N68-25060 Nacelle design for turbofan engine compressor Noise suppression on Douglas DC-8 aircraft NASA-CR-1056 c28 N68 c28 N68-26771 Performance requirements and economic costs to reduce cruise sonic boom of supersonic transport NASA-TN-D-4677 c02 N68-28831 Inlet guide vane choking noise reduction in axial flow compressors NASA-TN-D-4682 c02 N68-29406 Acoustic measurements on jet engine intake system noise reduction suppressor cowlings NASA-TN-D-4639 c02 N68-29887 Turbojet engine noise reduction by increasing intake system guide vane-rotor blade spacing NASA-TN-D-4690 c28 N68-3 c28 N68-30040 Noise reduction in small enclosed structures in terms of physiological and psychological effects NASA-CR-1155 c32 N68-33266 conference on sonic boom reduction in supersonic transport flight - shock wave propagation and refraction, prediction methods for acoustic attenuation, and aerodynamic engineering aspects NASA-SP-180 c02 N68-34907 Negative feedback for discharge current noise reduction in excited helium-neon laser NASA-CR-1173 c16 N68c16 N68-35099 Review of blade slap studies for determining noise in helicopters NASA-CR-1221 NOISE TOLERANCE c02 N68-37932 Awakening and startle effects of simulated sonic booms NASA-CR-1193 c04 N68-33005 NONEQUILIBRIUM FLOW FORTRAN 4 programs for calculating inviscid, one-dimensional and axisymmetric nonequilibrium nozzle flow fields and improving analytical predictions of delivered specific impulse NASA-CR-1123 27 N68-3279: 27 N68-3279: c27 N68-32793 NONLINEAR EQUATIONS LINEAK EQUALIUND Numerical methods for integrating nonlinear differential equations with parasitic eigenvalues NASA-TN-D-4703 c19 N68-29275 NONLINEARITY

Nonlinear flutter of circular cylindrical shell in

SUBJECT INDEX

supersonic flow NASA-TN-D-4265 c32 N68-12864 Nonlinear correction method for orbit determination using range, azimuth, and elevation data NASA-CR-1040 NONUNIFORM MAGNETIC FIELDS c30 N68-21864 Nonuniform magnetic field effect on ferromagnetic colloidal solutions NASA-TN-D-4676 c06 N68-3004 c06 N68-30044 NORMAL DENSITY FUNCTIONS Methodology used in guidance system performance analysis /assessment/ NASA-CR-1016 c30 N68-21442 NOSE CONES Wind tunnel investigation of pressure distribution on blunted 15 deg half-cone wedge lifting-entry body NASA-TN-D-4494 c01 N68-21681 NOSES (FOREBODIES) Windshield and nose geometry effects on supersonic aerodynamic characteristics of tactical fighter model NASA-TM-X-1664 c02 N68-37066 NOTCH TESTS Ultrasonic detection and measurement of fatigue crack propagation in notched specimens of aluminum, titanium, and cobalt alloys and maraging steels NASA-TN-D-4782 NOZZLE DESIGN c32 N68-35071 FORTRAN 4 program for computerized design of two dimensional supersonic nozzles with sharp edged throats NASA-TM-X-1502 c01 N68-14747 Submerged nozzle design for SL-3 260-inch solid propellant rocket engines NASA-TM-X-1546 c28 N68-20186 Aeroelastic instability of overexpanded rocket nozzle extensions NASA-TN-D-4471 NOZZLE EFFICIENCY c32 N68-21099 Performance evaluation of annular plug and expansion-deflection nozzles including external flow effects at transonic Mach numbers NASA-TN-D-4462 c01 N68-20330 NOZZLE FLOW Cavitation performance of jet pumps having low ratios of nozzle to throat area NASA-TN-D-4592 c03 N68-24461 NBSA-IN-D-4592 COS NBS-2446. FORTRAN 4 programs for calculating inviscid, one-dimensional and axisymmetric nonequilibrium nozzle flow fields and improving analytical predictions of delivered specific impulse NASA-CR-1123 c27 N68-32793 NOZZLE GEOMETRY Noncavitating flow mechanisms in two low area ratio water jet pumps with throat lengths of 7.25 diameters NASA-TN-D-4445 c15 N68-1 Effects of shroud geometry on performance of collapsible plug nozzle at Mach numbers from c15 N68-17564 0 to 2.0 NASA-TM-X-1657 c01 N68-36132 NUCLEAR CHEMISTRY Nuclear, chemical, and physical properties of nine radioactive isotopes — annotated bibliography NASA-SP-7031 c06 N68-29959 NASH-SF-7031 NUCLEAR ELECTRIC POWER GENERATION Reactivity effects caused by radial power flattening in gas cooled, fast-spectrum reactor NASA-TN-D-4459 c22 N68-1992 c22 N68-19925 NASA-IN-U-4459 C22 N68-1992; Circuit breakers and electric switch developments for future nuclear electric power generation systems operating in aerospace environments NASA-CR-1026 c03 N68-2946 c03 N68-29460 NUCLEAR FUEL ELEMENTS Establishing allowable temperature gradients for tungsten-uranium dioxide fuel elements using experimental cyclic strain data NASA-TN-D-4279 c22 N68-14986 Criticality calculations for small, cylindrical, lithium cooled reactors for space power systems NASA-TN-D-4371 c22 N68-1579 c22 N68-15792 Plum Brook reactor support calculations -mathematical model for fuel utilization, power distribution in fuel loading, and approximate predictions of xenon poison transient NASA-TM-X-1496 c22 N68-16 c22 N68-16056

Helium and air flow tests over single flat plates to determine dynamic pressure limits of nuclear fuel element plates NASA-TN-D-4417 NASA-TN-D-4417 c12 N68-16227 Constant creep data accumulation for design stress analysis on cladding material thickness around cylindrical reactor fuel element NASA-TN-D-4352 c22 N68-26764 Vibration tests of concentric tube fuel element support structure for Tungsten Water Moderated Reactor NASA-TM-X-1608 c32 N68-28330 Very high burnup vapor transport fuel pin concept for long life nuclear reactors NASA-TN-D-4860 c22 N68-37209 NUCLEAR FUELS Neutronic calculations of fuel and poison drum control of refractory metal, fast spectrum space power reactors NASA-TN-D-4709 Effect of turbulent mixing on average fuel temperatures in gas-core nuclear rocket engine NASA-TN-D-4882 NUCLEAR POWER REACTORS c22 N68-30750 c22 N68-37927 Criticality calculations for small, cylindrical, lithium cooled reactors for space power systems NASA-TN-D-4371 c22 N68-15792 Axial power tailoring to obtain constant fuel-centerline temperature in nuclear reactor NASA-TN-D-4658 c22 N68-28304 Mathematical model of liquid metal fuel reactor to investigate temperature distribution on neutron kinetics NASA-TN-D-4840 NUCLEAR RADIATION SPECTROSCOPY c22 N68-36055 Operational amplifiers for nuclear spectroscopy NASA-TN-D-4349 c24 N68-18 NUCLEAR REACTOR CONTROL c24 N68-18254 System dynamics and control analysis of tungsten water moderated nuclear rocket NASA-TM-X-1426 c22 N68-18252 CZZ N68-182 Fluidic analog to pulse frequency converter for pneumatic reactor control drum actuator system NASA-TN-D-4497 CO3 N68-218 NASA-TN-D-4497 c03 N68-2 Reactivity control of fast nuclear reactors containing yttrium hydride moderating zones NASA-TN-D-4615 c22 N68-2 Axial power tailoring to obtain constant fuel-centerline temperature in nuclear reactor NASA-TN-D-4658 c22 N68-2 LEAR REACTINES c03 N68-21835 c22 N68-24559 c22 N68-28304 NUCLEAR REACTORS LEAN NEACTING Spectral transmission characteristics of fused silica before, during, and after exposure to reactor irradiation pulses NASA-CR-1031 c22 N68-21124 Reactivity insertions in compact reactor cores due to fuel movement NASA-TM-X-1587 c22 N68-23894 Very high burnup vapor transport fuel pin concept for long life nuclear reactors NASA-TN-D-4860 c22 N68-37209 NUCLEAR RESEARCH AND TEST REACTORS c22 N68-37209 Design data for gas cooled test loop, and inpile capsule facility from mockup reactor experiments NASA-TM-X-1509 c22 N68-15855 NUCLEAR ROCKET ENGINES Transient chilldown of thick-walled tube simulating-nuclear rocket using liquid and gaseous hydrogen NASA-TN-D-4238 c33 N68-10368 Feasibility of supporting liquid fuel on solid wall in radiating liquid core nuclear rocket concept NASA-TN-D-4413 c27 N68-17093 System dynamics and control analysis of tungsten water moderated nuclear rocket NASA-TM-X-1426 c22 N68-1825 C22 N68-1 Postshutdown cooling requirements of tungsten water moderated nuclear rocket engines NASA-TM-X-1568 C22 N68-2 c22 N68-18252 stabilized gaseous nuclear rocket engine designs NASA-CR-1030 c22 N68-21111 Analytical investigation of flow and wall temperature sensitivity in the formation of the sensitivity in the temperature sensitivity in heated passages for large inlet to exit density ratios in subsonic flow of nuclear rocket NASA-TN-D-4649 c33 N68-283 c33 N68-28371

Thermionic reactor core with short-length

externally fueled diodes, and electrical failure analysis NASA-TN-D-4805 c22 N68-34087 NH5A-IN-D-4800 C22 N68-Small water-graphite nuclear rocket stages compared with chemical upper stages for use in unmanned spacecraft NASA-TN-D-4827 C22 N68c22 N68-35073 Fluid mechanics information applied to gaseous nuclear rocket engines NASA-CR-1190 c22 N68-36615 Effect of turbulent mixing on average fuel temperatures in gas-core nuclear rocket engine NASA-TN-D-4882 c22 N68-379 NUCLEATE BOILING c22 N68-37927 Gravity effects on bubble dynamics generated during nucleate boiling NASA-TN-D-4301 c33 N68-15330 NUCLEATION In situ electron microscopy for studying vapor deposition nucleation processes NASA-TN-D-4506 c06 N68-21430 NUMERICAL ANALYSIS Numerical analysis of electric current and potential distributions in linear Faraday plasma accelerators c28 N68-10502 NASA-TN-D-4239 Numerical procedures and computer program for calculating real fluid and thermodynamic properties of normal and parahydrogen NASA-TN-D-4341 COB N68-15798 Feasibility of supporting liquid fuel on solid wall in radiating liquid core nuclear rocket concept NASA-TN-D-4413 c27 N68-17093 Black body radiation - numerical solution for computer and hand calculation of total intensity over specified spectral range NASA-TN-D-4446 c19 N68-18455 Three numerical procedures for Mayer classical and non-classical problems in trajectory optimization NASA-CR-1012 c30 N68-19315 radiation fields of harmonic current sources NASA-CR-1025 c23 N68-21444 Geomagnetic field secular variation /1900 to 1965/ NASA-TN-D-4527 c13 N68-21543 c13 N68-21543 Calculations of nondiffuse infrared radiation from lunar surface incident onto unit element above surface NASA-TM-X-1567 c29 N68-21731 Numerical calculation of capture cross sections between ions and polar molecules NASA-TM-X-1586 c24 N68-230 c24 N68~23893 Conference on numerical analysis applications to aerospace and related problems NASA-SP-170 c19 N68-33245 Runge-Kutta formulas of high order with stepsize control through leading truncation error term NASA-TR-R-287 c19 N68-36 c19 N68-36753 Numerical analysis of winding power loss of rotating ac generators in controlled atmospheres NASA-TN-D-4849 c03 N68-37162 c03 N68-37162 NUMERICAL INTEGRATION Analytical formulations and numerical integration methods for many body problem and special perturbative techniques NASA-CR-1005 c30 N68-15741 Explicit numerical methods for integrating coupled nonlinear ordinary differential equations with parasitic eignevalues c19 N68-21978 NASA-TN-D-4547 NASA-IN-D-4547 Local error control for optimization of numerical integration orbit calculation techniques NASA-IN-D-4542 Numerical methods for integrating nonlinear differential equations with parasitic eigenvalues NASA-TN-D-4703 cl9 N68-29275 Runge-Kutta formulas of high order with stepsize control through leading truncation error term NASA-TR-R-287 cl9 N68-36753 NUTRITIONAL REQUIREMENTS Chemical feasibility and nutrional value in synthesis of edible fatty acids and lipids from metabolic wastes for space flight feeding NASA-CR-1104 c04 N68-28829 O RING SEALS

SUBJECT INDEX

0 O RING SEALS Leakage of large diameter O ring seals on spacecraft air lock hatches NASA-TN-D-4394 c31 | OBLIQUE SHOCK WAVES c31 N68-17498 Effect of N waves at oblique incidence on response of simply supported plate to transient loads NASA-CR-1176 c32 N68-33168 OCEANOGRAPHY Potential applications of geodetic satellites to geology, oceanography, glaciology, and atmospheric physics NASA-SP-158 c13 N68-18902 **OCEANS** Evaluation of sea surface temperature as measured by Nimbus 1 satellite high resolution infrared radiometer NASA-TN-D-4078 c20 N68-10222 OGEE SHAPE Aerodynamic ground effect measurements on low aspect ratio ogee wings NASA-TN-D-4329 c02 N68c02 N68-14090 0G0 Analytical method for finding heat balance of insulated OGO experiment packages from thermal stability data and without solar simulation NASA-TN-D-4644 cll N68c11 N68-29478 OILS Ultraviolet measurements of oil contamination in optical mirrors NASA-TN-D-4612 OMNIDIRECTIONAL ANTENNAS c14 N68-25375 General method for designing circular array antennas to obtain quasi-omnidirectional patterns NASA-TN-D-4254 c07 N68-11475 Quasi-connidirectional resonant array of circumferential shunt slots in ring waveguides for narrow bandwidth space vehicle applications at microwave frequencies NASA-TN-D-4362 c07 N68-18616 Omnidirectional microwave parallel plate broadband antenna for spacecraft communications NASA-TN-D-4555 c07 N68-25918 ONBOARD EQUIPMENT Spacecraft attitude determination using single onboard camera NASA-TN-D-4359 c31 N68-19275 ONE DIMENSIONAL FLOW Dynamics of bounded one dimensional plasma sheath NASA-TN-D-4651 c25 N68-3003 c25 N68-30031 OPERATOR PERFORMANCE Finite-state machines and evolutionary programming for representing and analyzing performance of human operator in control of dynamic systems NASA-CR-1112 c05 N68-28847 NBAR-GR-1112 COUNCE Telescope objective lens size, aperture size, 'and magnification effects on operator performance using marine sextants NASA-TN-D-4781 c21 N68-33006 OPERATORS (MATHEMATICS) Classification and construction of open-channel projection operators for rearrangement collisions using subspaces of total Hilbert space of system NASA-TN-D-4633 c24 N68-28265 Feynman formalisms for expressing iterated commutators and functions of operators NASA-TN-D-4857 c19 N68-36525 OPERATORS (PERSONNEL) Feasibility of computer assisted flight controller c19 N68-36525 training NASA-CR-917 c08 N68-13897 Mathematical model of human operator as optimal controller and information processor NASA-CR-1151 c c05 N68-33304 OPTICAL COMMUNICATION Evaluation of microwave, millimeter, and optical communication systems for space communications from Mars spacecraft NASA-TN-D-3984 c07 N68-22019 Gallium arsenide laser modulator, attenuation coefficients, and semiconductors for optical communication systems

NASA-TN-D-4608

Optical communications - maximum likelihood detection of M-ary Poisson processes in background of additive Poisson noise NASA-TN-D-4623 c07 N68-29528 Design of pulse position modulation optical communication system NASA-TN-D-4814 c07 N68-35174 OPTICAL FILTERS Cathode ray tube with nonreciprocal optical filtering techniques for viewing under high ambient c09 N68-33224 NASA-CR-1185 OPTICAL MEASUREMENT Ultraviolet measurements of oil contamination in optical mirrors NASA-TN-D-4612 OPTICAL PROPERTIES c14 N68-25375 Mechanical, optical, and electrical characteristics of hand-held sextant for space flight NASA-TN-D-4585 c21 N68-24512 Effects of edge constraints on optical qualities of Gemini spacecraft windows NASA-TN-D-4845 c23 N68-3647 c23 N68-36470 OPTICAL REFLECTION Techniques for, and applications of preferential etching of crystal surfaces to produce optical reflections for crystal orientation and optical alignment in silicon crystals c23 N68-10354 NASĂ-TN-D-4187 Heat balance equations for optimizing optical coating patterns for spacecraft temperature control system NASA-CR-1041 c18 N68c18 N68-22391 OPTICAL TRACKING Optical star tracker calibration procedures NASA-TN-D-4594 c21 NG c21 N68-24555 OPTIMAL CONTROL Altitude of orbiting spacecraft corrected by thrustor firing time control system NASA-TN-D-4519 c31 N68-21260 Optimal finite-thrust transfer between planet approach and departure asymptotes with specified intermediate orbit NASA-TN-D-4534 c28 N68-22096 Design of guidance and control systems for optimum utilization of information NASA-CR-997 c10 N68-23438 Thrust vector deflection stability analysis for minimum control requirements of booster vehicles during atmospheric flight NASA-TN-D-4593 c21 N68-24409 NASA-TN-D-4593 C21 N68-24409 Optimum values of pitch rate damping, longitudinal control and speed stability for vertical takeoff aircraft /helicopters/ using pilot ratings NASA-TN-D-4624 C02 N68-28153 Algebraic methods for analysis and design of model following control systems NASA-TN-D-4663 c19 N68-28281 Quasi-optimal control technique for space vehicle attitude, bounded acceleration rendezvous in NASA-CR-1099 cl0 N NASA-CR-1099 Analog simulation of dc arc emission spectrometer control system to define optimum control requirements NASA-TN-D-4770 c08 N68-32055 Mathematical model of human operator as optimal controller and information processor NASA-CR-1151 c05 N68-33304 Newton-Raphson and gradient parameter correction technique for solution of optimal control problems NASA-TR-R-293 c19 N68-37073 OPTIMIZATION Dytimum design geometry for high radial inflow turbine performance efficiency NASA-TN-D-4384 c03 N68-1 c03 N68-15943 Optimum maneuvering of glide vehicle at hypersonic speeds NASA-CR-1078 c02 N68-25817 Lie series applications to celestial mechanics, accelerators, satellite orbits, and optimization NASA-CR-1046 c19 N68-25841

Local error control for optimization of numerical integration orbit calculation techniques NASA-TN-D-4542 c30 N68-25867 Trajectory optimization by direct descent to

Trajectory optimization by direct descent to minimum cost using iterative computer solutions

c23 N68-25868

c30 N68-25902 NASA-CR-1070 Oxidation resistance and ductility of cobalt heat resistant alloys optimized by restriction of silicon and manganese content NASA-TN-D-4715 c17 N68-2; c17 N68-29954 ORBIT CALCULATION Computer programs for rapidly computing approximate ephemerides of minor planet or artificial satellites NASA-TN-D-4470 c30 N68-20356 Nonlinear correction method for orbit determination using range, azimuth, and elevation data NASA-CR-1040 c30 N68-21864 Local error control for optimization of numerical integration orbit calculation techniques NASA-TN-D-4542 c30 N c30 N68-25867 Perturbation theory for artificial satellites with nearly circular orbits using Von Zeipel method NASA-TN-D-4531 c30 N68-28251 ORBIT DECAY Analytical method artificial satellite lifetime determination NASA-TN-D-4281 ORBIT PERTURBATION c30 N68-11754 Trajectory optimization by direct descent to minimum cost using iterative computer solutions NASA-CR-1070 c30 N68-25902 ORBITAL MECHANICS Hansen planetary theory NASA-TN-D-4169 c30 N68-11369 Mathematical formulation of guidance equations and solutions for orbital space missions NASA-CR-1010 c30 N68-17215 Modifications and simplifications of Hansen lunar theory NASA-TN-D-4562 c30 N68-26642 Planetary gravitation and oblateness used for parking orbit alignment in Mars mission NASA-TN-D-4657 c30 N68c30 N68-28408 Analysis of launch windows from circular orbits for representative Mars missions NASA-TM-X-1651 Orbital Rendezvous c30 N68-33371 Time optimal rendezvous trajectories for variable thrust intercepting and orbiting space vehicles NASA-CR-1036 c30 N68-22202 Simplified and accurate relative equations of motion for two impulse orbital rendezvous NASA-TN-D-4670 c30 N6 ORBITAL VELOCITY c30 N68-28841 Computational method for orbiting astronauts to determine required velocity for two impulse abort to landing site NASA-TN-D-4599 c21 N68-25103 ORBITAL WORKERS Space activity suit designed for active astronaut working in vacuum environments for up to four hours NASA-CR-973 c05 N68-11510 ORGANISMS History of origin and initial development of carbon compounds, primitive organisms, and life on earth NASA-TT-F-488 c04 N68-24272 ORIENTATION Drop tower investigation of liquid reorientation in spherical containers NASA-TH-X-1659 c12 N68-351 c12 N68-35114 CI2 NOC ORTHOTROPIC CYLINDERS Prebuckling deformations, and ring stiffener effects on buckling load of eccentrically stiffened orthotropic cylinders NASA-TN-D-4283 c32 N68 c32 N68-14091 ORTHOTROPIC PLATES Plane stress analysis using Fourier series of edge stiffened isotropic or orthotropic elastic rectangular plate subjected to prescribed temperature distribution and boundary loads NASA-CR-978 c32 N68-19311 OSCILLATING CYLINDERS Vibration tests and analysis of thin cylindrical shells with and without longitudinal stiffeners NASA-TN-D-4705 c32 N68-3373 c32 N68-33738 OSCILLATION DAMPERS Passive damping technique for attitude control of solar orientated interplanetary spacecraft NASA-TN-D-4641 c21 N68-28361 c21 N68-28361

OSCILLATORS Digital voltage controlled oscillator for phase lock loops using coherent frequency synthesizer NASA-TN-D-4521 c09 N68-2438 c09 N68-24389 OUTGASSING Outgassing of water vapor from concrete surfaces in vacuum environments NASA-TM-X-1536 c11 N68-19207 NBDR-IN-A-1000 Cll N68-1920' Radiation resistance, outgassing characteristics, and weight of five electrical insulation materials for spacecraft NASA-TN-D-4553 Cl8 N68-2826 c18 N68-28264 OXIDATION Magnitude of electrical potential-temperature curve determined for tantalum, niobium, and magnesium during oxidation in air NASA-TN-D-4240 c17 N68c17 N68-10498 OXIDATION RESISTANCE Oxidation resistant alloys tested for suitability as transpiration cooled gas turbine blades c17 N68-17591 NASA-CR-930 Didation resistance and ductility of cobalt heat resistant alloys optimized by restriction of silicon and manganese content NASA-TN-D-4715 c17 N68-29954 Oxidation resistance evaluation for metal alloy cooling materials in high temperature gas turbine engines NASA-CR-1184 c17 N6 c17 N68-35098 OXIDES Electron microscopy technique for determining dispersoid distribution in powder blends c17 N68-10051 NASA-TM-X-1468 OXYGEN Temporal solutions for photochemical equations describing distribution of ozone and oxygen during auroral events NASA-TN-D-3993 c13 N68-10369 Corrosion products of oxygen doped tantalum exposed to potassium at 1800 deg F NASA-TN-D-4213 c17 N64 c17 N68-11511 Hydrogen-oxygen chemical reaction kinetics in rocket engine combustion NASA-TN-D-4250 c33 N68-11642 Quantitative measurement of atomic photoionization cross sections of atomic hydrogen, oxygen, and nitrogen NASA-CR-998 c24 N68-18118 Carbon dioxide and water vapor effects on induction period kinetics of hydrogen-oxygen reaction NASA-TN-D-4685 c33 N68-30041 Product development and testing of thin film oxygen partial pressure sensors NASA-CR-1182 c14 N68-35149 OXYGEN METABOLISM Bioregenerative life support systems for long duration space flights - Hydrogenomonas biosynthesis and algae photosynthesis processes NASA-SP-165 c04 N68-26207 OZONE Temporal solutions for photochemical equations describing distribution of ozone and oxygen during auroral events NASA-TN-D-3993 c13 N68-1 c13 N68-10369

Ρ

P-N JUNCTIONS Current-voltage characteristics of tunneling p-n junctions in semiconductors NASA-TN-D-4403 c09 N68-19062 Piezojunction as sensor in transducers NASA-CR-1089 c c26 N68-26627 PAGEOS SATELLITE Fabrication and testing of Pageos 1 NASA-TN-D-4596 c31 N68-25820 PANEL FLUTTER Plutter analysis on buckled supported rectangular panels under supersonic surface flow NASA-TN-D-4357 c32 N68-1765 c32 N68-17651 Turbulent boundary layer effect on panel flutter NASA-TN-D-4486 c32 N68-187 c32 N68-18721 Experimental study, and theoretical analysis on supersonic flutter of corrugation stiffened panels NASA-TN-D-4321 PARABOLIC ANTENNAS c32 N68-19143 Feasibility of orbiting paraboloidal antenna for

low frequency radio astronomy NASA-CR-1201 PARABOLIC REFLECTORS c31 N68-37900 Parametric analysis of effects of concentrator surface errors and rim angle, collection system orientation error, and receiver temperature on paraboloid solar collector thermal efficiency NASA-TN-D-4415 c03 N68-18998 PARABOLOID MIRRORS Techniques for coating magnesium with epoxy resin films for paraboloid mirrors NASA-TN-D-4734 c18 N68-3059 c18 N68-30597 PARACHURE DESCENT Flight test of 10-foot nominal-diameter disk-gap band parachute to determine deployment and inflation, opening shock loads, drag efficiency, and stability characteristics NASA-TM-X-1575 co2 N68-24245 Scale factors verification for parawing opening characteristics using experimental drop tests NASA-TN-D-4665 c02 N68-31956 PARACHUTES Flight tests of ringsail parachute with 15 percent porosity, for planetary entry NASA-TM-X-1484 c31 N68-11919 Right test of conical spacecraft simulating parachute deployment in Mars atmosphere NASA-TN-D-4266 c31 N68 c31 N68-11961 Inflation, and drag characteristics of disk gap band parachute in simulated low density Mars atmosphere NASA-TM-X-1499 c31 N68-13797 Inflation, drag, and stability characteristics of ringsail parachute deployed in simulated Mars atmosphere NASA-TM-X-1500 c31 N68-14092 NASA-TM-X-1500 c31 N68-Flight test of 30 foot nominal diameter cross parachute to measure shock loads, drag efficiency, and stability characteristics NASA-TM-X-1542 c31 N68-2 NASA-TM-X-1542 Inflation and drag characteristics of cross parachute in simulated Martian environment NASA-TM-X-1543 NASA-TM-X-1543 c31 N68-21833 Flight test of 10-foot nominal-diameter disk-gap band parachute to determine deployment and inflation, opening shock loads, drag efficiency, and stability characteristics NASA-TM-X-1575 co2 N68-24245 Wind tunnel studies of static aerodynamic characteristics of multilobe gliding parachute NASA-TN-D-4672 c01 N68-28447 Stress analysis and functions in membrane analysis of scalloped thin walled shells like parachutes Flight test of 40 foot parachute deployed at low supersonic speed and dynamic pressure NASA-TM-X-1623 AFFTNO c32 N68-28832 c31 N68-29993 PARAFFINS High temperature tests to determine fatigue life of 120mm bore ball bearings with fluorocarbon, polyphenyl ether, and synthetic base paraffin base lubricants NASA-TN-D-4850 c15 N68-36075 PARALLEL PLATES Thin walled parallel plate waveguide radiation pattern analyzed by surface integration technique NASA-CR-1052 c07 N68-22746 Rarefied gas couette flow and heat transfer between parallel plates analyzed by model sampling procedures NASA-TN-D-4579 c12 N68-24129 Omnidirectional microwave parallel plate broadband antenna for spacecraft communications NASA-TN-D-4555 c0 c07 N68-25918 NASA-IN-D-4555 c07 N68-25 Reflectance of wedge angle parallel plate waveguides in transverse electromagnetic mode illuminating reflecting sheet NASA-CR-1174 c07 N68-35 c07 N68-35172 PARAWINGS Scale factors verification for parawing opening characteristics using experimental drop tests NASA-TN-D-4665 c02 N68-31956 MAGA-IN-U-5005 C02 N68 Accurate methods for predicting longitudinal aerodynamic characteristics of two-lobed conical parawings with leading edge booms NASA-CR-1166 c01 N68 c01 N68-33765 Deployment characteristics of dynamic and elastic parawing scale model for spacecraft recovery NASA-TN-D-4724 c02 N68-33 c02 N68-33879 SUBJECT INDEX

PARKING ORBITS Planetary gravitation and oblateness used for parking orbit alignment in Mars mission NASA-TN-D-4657 c30 N68-PARTIAL DIFFERENTIAL EQUATIONS c30 N68-28408 Uncertainty analysis for designing calorimetric experiments, and equations for measuring properties of planetary radiation NASA-TN-D-4354 c14 N68-16 Liapunov stability theory applied to class of c14 N68-16529 partial differential equations, and generation of contraction groups related to equivalent norms NASA-CR-1100 c19 N68-274 c19 N68-27457 PARTIAL PRESSURE Product development and testing of thin film oxygen partial pressure sensors NASA-CR-1182 c14 N68-35149 PARTICLE ACCELERATION NASA-CR-927 c16 N68c16 N68-10467 PARTICLE ACCELERATORS Lie series applications to celestial mechanics, accelerators, satellite orbits, and optimization NASA-CR-1046 c19 N68-25841 PARTICLE EMISSION Polar cap absorption study of solar cycle variation in solar proton emissions from sun NASA-TN-D-4473 c29 N68-2 c29 N68-25880 PARTICLE FLUX DENSITY FORTRAN subroutines for determining intersections of nuclear particle flight path and wall of helical tubular duct NASA-TN-D-4435 c22 N68-18541 PARTICLE INTERACTIONS Charts of thermodynamic properties of helium showing effects of ionization, particle interactions, temperature, and atmospheric pressure NASA-TN-D-4754 c12 N68-35117 PARTICLE MOTION Synchrotron emission at helical motion of relativistic electrons emitting from source with relativistic velocity NASA-TT-F-521 c25 N68-16700 PARTICLES Physical properties and applications of dust structures in space technology NASA-CR-1136 c32 N68-PARTITIONS (MATHEMATICS) c32 N68-32976 Partition functions and thermodynamic properties to high temperatures for hydrogen triatomic and diatomic molecular ions NASA-TN-D-4523 PATTERN RECOGNITION c33 N68-21732 Spaceborne pattern recognition system for identifying and classifying objects in video data NASA-CR-999 c10 N68-19229 Frequency coded threshold logic unit for pattern recognition systems based on central nervous system NASA-CR-1035 c05 N68-22448 PAVEMENTS Effect of wheel braking on directional control of pneumatic tires on pavement NASA-TN-D-4602 c02 N68-25313 PAYLOAD MASS RATIO Computer program for trajectory optimization and payload maximization in multistage launch vehicles NASA-TN-D-4729 c30 N68-31989 PAYLOADS Dynamic response of axisymmetric hammerhead model to unsteady aerodynamic loading in wind tunnel tests NASA-TN-D-4504 c01 N68-25916 PEENING Precision glass-bead peening equipment for propellant tank surface corrosion protection NASA-TN-D-4288 c15 N68-1 c15 N68-12890 PENETRATION Stainless steel penetration detector, impact detector, and solar cell degradiation, to study micrometeoroid impact damage and puncture rate, and radiation effects on Explorer 23 satellite NASA-TN-D-4284 c31 N68-28198 PENETROMETERS Response characteristics of impacting

penetrometers evaluated for use on lunar and lanetary missions NASA-TN-D-4454 c32 N68-20364 PERFORMANCE Efficiency and steady state performance of cylindrical thermionic converter with rhenium emitter and niobium collector NASA-TN-D-4582 c03 N68-25 c03 N68-25059 PERFORMANCE PREDICTION Optimum design geometry for high radial inflow turbine performance efficiency NASA-TN-D-4384 c03 N68-1 c03 N68-15943 Mathematical prediction model for landing dynamics of impacting struts, and trusses of lunar vehicle landing gear NASA-TN-D-4434 c31 N68-19085 Relationship between fan drive turbine geometry and output efficiency of turbofan engine and output efficiency of tarootan engine NASA-TM-X-1581 Transfent thermodynamic analysis for development of mathematical model that predicts transfent temperature and voltage-response characteristics of fuel cell system NASA-TN-D-4601 NASA-TN-D-4601 c03 N68-25304 Supplementary information for computer program predicting lifting pressure and camber shape of composite planform in subsonic flow NASA-TN-D-4427, SUP. c01 N68-31515 Noncavitating and cavitating performance of two low area ratio water jet pumps with throat lengths of 5.66 diameters NASA-TN-D-4759 c12 N68-31960 Reliability prediction techniques for sizele item c03 N68-25304 c01 N68-31515 c12 N68-31960 Reliability prediction techniques for single item and multiitem problems NASA-CR-1129 PERFORMANCE TESTS c15 N68-31979 Design, and evaluation of birefringent wave filter scale model for millimeter wavelengths radio astronomy NASA-CR-979 c09 N68-13617 Performance of two-stage axial flow turbine operating at different rotor tip clearance NASA-TN-D-4388 c03 N68-14639 NASA-TN-U-4300 Cold air study of gas turbine for high temperature aircraft engine application NASA-TN-D-4389 c01 N68-15743 High temperature tests on cesium diodes and vapor filled thyratrons NASA-CR-994 c09 N68-15892 Development, ground tests, and flight performance of cryogenic nitrogen storage system for low gravity operation during Apollo-Saturn space flight NASA-TN-D-4293 c23 N68-15950 Electrode design, inorganic separators, and performance tests of multiplate five ampere-hour silver-zinc battery cell NASA-CR-965 c03 N68-16321 Two stage potassium vapor turbine - materials support of performance and endurance tests NASA-CR-925 co3 N68-1 c03 N68-16351 Cold air performance test of scale model oxidizer pump drive turbine for M-1 engine - performance of first stage with inlet feedpipe manifold assembly NASA-TN-D-4392 c28 N68-16413 Experimental design and performance test of two-stage axial-flow turbine designed for Brayton-cycle space power system NASA-TN-D-4382 c03 N68-16469 Evaluation of self-evacuating multilayer radiation shields for cryogenic storage tanks NASA-TN-D-4375 c33 N68-18046 Aerodynamic performance of scale model oxygen pump-drive turbine for M-1 rocket engine NASA-TN-D-4393 c28 N68c28 N68-18188 effects of Reynolds number change on performance of axial flow turbine working in argon whoth IN-D-4432 C03 N68-18501 Supersonic performance evaluation of mass flux probes with sharp symmetrical inlet, and with blunted unsymmetrical inlet NASA-TM-X-1524 c14 N69 1007 Performance of low thrust storable bipropellant thrustors in spacecraft reaction control system NASA-TN-D-4416 c28 N68-20064 Steady state performance tests on single pass counterflow sodium-potassium cooled mercury Rankine cycle condenser

c33 N68-20340 NASA-TM-X-1548 Comparison of mixed and isolated flow methods for cooled turbine performance using two simplified example turbines NASA-TM-X-1572 c01 N68-21692 Performance tests on high voltage isolator for mercury propellant feed system of ion engine NASA-TM-X-1579 c28 N68-23477 Performance characteristics and operating parameters of three-fluid crossflow heat exchangers c33 N68-23513 NASA-TR-R-284 Performance of centrifugal pump impeller in room temperature water NASA-TN-D-4613 c12 N68-26651 Effects of nuclear radiation on performance of diodes for use in SNAP 8 NASA-TN-D-4620 c09 N68-26662 Systems analysis and performance test data on dual radiometer assembly for measuring far infrared wavelength bands of earths horizon radiance profile NASA-CR-1086 c14 N68-28965 Performance test of homopolar inductor alternator for Brayton cycle space power system NASA-TN-D-4698 c c03 N68-30002 Overall performance tests in argon of six inch radial bladed centrifugal compressor NASA-TM-X-1622 c(c01 N68-30033 Partial admission operation effects on performance of single stage axial flow turbine NASA-TN-D-4700 NASA-TN-D-4700 c03 N68-30241 Cycle characteristics and structural configuration of turbojet and turbofan engines for lightweight aircraft NASA-TM-X-1624 c28 N68-31476 Scale factors verification for parawing opening characteristics using experimental drop tests NASA-TN-D-4665 c02 N68-31956 Application of testing to hardware programs c15 N68-32779 NASA-CR-1128 Performance of single stage turbine with rotor blade surface diffusion factor of 0.3 NASA-TN-D-4790 Cost and cost of the second s c28 N68-32987 c03 N68-34234 Design, fabrication and testing of Cb-1Zr thermal convection loop for evaluation of refractory metals in boiling and condensing potassium environments NASA-CR-1097 c22 N68-35153 Flight performance evaluation of Atlas Centaur restart capability in earth orbit NASA-TM-X-1647 c31 N68-35357 Turbine performance with 130 percent design stator NASA-TM-X-1663 c03 N68-35536 NASA-IM-A-1003 Hovering tests of extremely flexible lifting rotor to determine effects of rotor tip configuration and operating conditions on performance NASA-TN-D-4820 col N68-36334 Microstructure and mechanical properties of beryllium tubing and performance tests on support columns of beryllium NASA-TN-D-4833 c17 N68-37053 Efficiency, mass flow rate, torque, and exit diffuser effectiveness of 5-inch axial flow turbine NASA-TM-X-1679 c03 N68-37263 Performance tests of stator component in closed position and effects on performance of single stage turbine suitable for air cooling NASA-TM-X-1675 c28 c28 N68-37264 Performance of single stage, axial flow turbine designed for Brayton cycle space power system NASA-TM-X-1666 c03 N68-37943 PERIODIC FUNCTIONS Methods of eliminating short period terms from Hamiltonian by means of canonical transformation NASA-TN-D-4399 c19 N68-17532 PERSONNEL SELECTION Process development of system for digital computer processing of psychophysiological data to obtain high stress tolerance personnel NASA-CR-1122 co5 N68-35102

I-73

PERTURBATION

PERTURBATION Analytical formulations and numerical integration methods for many body problem and special perturbative techniques NASA-CR-1005 c30 N68-15741 NASA-CK-1005 PERTURBATION THEORY Hansen planetary theory NASA-TN-D-4169 c30 N68-11369 Perturbation techniques for error analysis of finite difference approximations for linear differential equations NASA-TN-D-4372 c32 N68-: c32 N68-17068 Iterative and perturbation approaches to near optimum steering equations for boost vehicle guidance NASA-CR-1007 c30 N68-20449 General perturbations theory applications to spacecraft guidance, flight mechanics, and trajectory optimization NASA-CR-1008 c30 N68 c30 N68-20450 Predictions for magnetoresistivity temperature dependence of dilute alloys of iron in copper NASA-TN-D-4626 c26 N68-28239 Perturbation theory for artificial satellites with nearly circular orbits using Von Zeipel method NASA-TN-D-4531 c30 N68-28251 PHASE CONTROL Computer analyses of retrodirective, and self adaptive antenna phase control techniques for Mars probe NASA-CR-977 c21 N68-18484 PHASE LOCKED SYSTEMS Digital voltage controlled oscillator for phase lock loops using coherent frequency synthesizer NASA-TN-D-4521 c09 N68-2438 c09 N68-24389 PHENOLIC RESINS Effects of molecular structure on thermochemical properties of phenolic resins and related polymers NASA-TR-R-276 c33 N68-11038 Conductive heat transfer mechanisms in low density phenolic-nylon chars NASA-CR-966 c18 N68-11978 Theoretical analysis of five composite ablation materials with various percentages of phenolic resin, powdered nylon, and silica NASA-TN-D-4374 c18 N68-197 c18 N68-19710 PHENOLS Friction and wear in cryogenic liquids for phenolic and polytetrafluoroethylene composites of various particle sizes and concentrations NASA-TN-D-4565 c15 N68-2414 c15 N68-24142 PHOTOCHEMICAL REACTIONS Temporal solutions for photochemical equations describing distribution of ozone and oxygen during suroral events NASA-TN-D-3993 c13 N68-10369 PHOTOGRAPHIC EQUIPMENT Analysis and evaluation of Lunik 9 spacecraft imagery, and specification of spacecraft and photographic instruments NASA-CR-980 c14 N68-16838 Design and operating characteristics of electro-optical instrument for tracking of retinal blood vessels in back of eye NASA-CR-1121 PHOTOGRAPHIC MEASUREMENT c05 N68-35109 Two methods of photographic photometry of artificial meteoroids NASA-TN-D-4667 c14 c14 N68-29418 PHOTOGRAPHIC RECORDING Photographic program summary and evaluation for Lunar Orbiter mission NASA-CR-1094 c31 N68-28202 Photographic study of bromine jet issuing into coaxially flowing airstream NASA-TN-D-4660 cl2 N68-24 PHOTOGRAPHIC TRACKING Ballistic camera data reduction methods for c12 N68-28370 determining reentry body position, velocity, and deceleration NASA-TN-D-4260 c30 N68-11145 Factors affecting design and use of photographic sextant for space navigation NASA-TN-D-4285 c21 N68-11902 PHOTOGRAPHS Photographs, thermocouples, and emission spectra used to study mixing and reaction of hydrazine and

nitrogen tetroxide

SUBJECT INDEX c33 N68-24965 NASA-TN-D-4467 PHOTOGRAPHY Simultaneous correction of velocity and mass bias In photography of meteors NASA-TR-R-280 PHOTOINTERPRETATION c30 N68-15484 Photographic mission planning and photograph interpretation for Lunar Drbiter 3 NASA-CR-984 PHOTOIONIZATION c30 N68-15725 Ultraviolet filter and monochromator for mass spectrometer employing photoionization source NASA-CR-1018 c14 N68-17329 Quantitative measurement of atomic photoionization cross sections of atomic hydrogen, oxygen, and nitrogen NASA-CR-998 c24 N68-18118 Transmittance of thin films and photoionization of gases in selective detectors set for photons in ultraviolet spectrum NASA-CR-1096 c24 N68-28250 PHOTOMETRY Photometric and meteor observations, scattering properties, particle collection and impact, solar wind, and origin and evolution of zodiacal light in interplanetary medium - conference c30 N68-27475 NASA-SP-150 Two methods of photographic photometry of artificial meteoroids NASA-TN-D-4667 PHOTOMULTIPLIER TUBES c14 N68-29418 Celestial attitude measuring instrument using star mapping technique NASA-TN-D-4742 c21 N68-31938 PHOTONS Transmittance of thin films and photoionization of gases in selective detectors set for photons in ultraviolet spectrum NASA-CR-1096 c24 N68-2825 c24 N68-28250 PHOTOSYNTHESIS Bioregenerative life support systems for long duration space flights - Hydrogenomonas biosynthesis and algae photosynthesis processes NASA-SP-165 c04 N68-26207 PHOTOVOLTAIC CELLS Spectral response of cuprous sulfide-cadmium sulfide film photovoltaic cell to green light NASA-TN-D-4333 PHYSICAL PROPERTIES c03 N68-14082 Nuclear, chemical, and physical properties of nine radioactive isotopes - annotated bibliography NASA-SP-7031 c06 N68-29959 Physical properties and applications of dust structures in space technology NASA-CR-1136 c32 N68-32976 PHYSIOLOGICAL EFFECTS SIDLOGICAL EFFECTS
 Aerospace medicine and biology bibliography on physiological, psychological, and environmental effects on man during aerospace flights
 NASA-SP-7011/43/
 c04 N68-1467
 Aerospace medicine and biology bibliography on c04 N68-14671 physiological, psychological, and environmental effects on man during aerospace flights NASA-SP-7011/42/ c04 N68-1472 c04 N68-14725

- NASA-SP-7011/42/ c04 N68-14725 FM data handling facility for preparing analog physiological data obtained in flight for digital computations NASA-TN-D-4488 c05 N68-21537 Signal conditioning methods and equipment used for inflight recording of pilot biomedical data NASA-TN-D-4487 c05 N68-21538 Heat stress and prolonged activity effects on human percentual motor performance
- human perceptual motor performance NASA-CR-1153 PHYSIOLOGICAL RESPONSES c05 N68-31480
- Noise reduction in small enclosed structures in terms of physiological and psychological effects NASA-CR-1155 c32 N68-33266
- PIEZOELECTRIC CRYSTALS Damping of piezoelectric quartz crystal driven in torsional mode of vibration in liquid helium 3 and helium 4 NASA-TN-D-4381
- c26 N68-17594 PIEZOELECTRIC GAGES
- Fitzgeralds piezoelectric disk and theory on audio frequency resonances and sound beams in crystals NASA-TN-D-4625 c23 N68-28259

PLASMA GUNS

PIEZOELECTRIC TRANSDUCERS Quasi-static calibrations for determining quartz, piezoelectric type, pressure transducer sensitivity from 20 to 477 deg K NASA-TM-X-1479 cl4 N68-1186 c14 N68-11867 Sensitive piezoelectric transducer with electric and mechanical noise rejection features for measuring cardiac and gross motor activity of small organisms NASA-TN-D-4590 c05 N68-25060 Piezojunction as sensor in transducers NASA-CR-1089 c26 N68-26627 PILOT PERFORMANCE Simulator study of pilot control of remote orbital docking of large altitude stabilized components NASA-TN-D-4263 c31 N68-11476 Signal conditioning methods and equipment used for Inflight recording of pilot biomedical data NASA-TN-D-4487 c05 N68-21538 NASA-TN-D-4487 Pilot dynamic response to sudden flight control system failures NASA-CR-1087 c05 N68-26690 Pilot performance using compensatory and pursuit tracking displays with rate and acceleration control dynamics and disturbance input NASA-CR-1082 c07 C07 N68-28272 PIPE FLOW C FLUW Development of nuclear thermionic space power system using thermionic diodes, and heat pipe flow for temperature control NASA-TN-D-4299 c23 Mixing length flow theory for analyzing c22 N68-19146 incompressible turbulent swirling flow in pipes NASA-CR-1169 c12 N68-36343 PIPES (TUBES) Convective heat exchange in homogeneous gas media, nvective heat exchange in homogeneous gas media including heat transfer and friction resistance in pipes, hydrodynamics and heat transfer in jets, and intensification of convection NASA-TT-F-431 c33 N68-1172 c33 N68-11721 Window designs for mercury condensing tube and mercury boiler outlet tube NASA-TM-X-1578 cll N68-23 c11 N68-22737 Floating mandrel technique for extrusion of thin walled tungsten tubing NASA-TM-X-1638 c15 N68-32977 Microstructure and mechanical properties of beryllium tubing and performance tests on support columns of beryllium NASA-TN-D-4833 c17 N68-37053 PITCH Judgment tests conducted to determine noise levels or loudness of tones plus noise NASA-CR-1117 c05 N68-30602 NASA-CR-1117 PITCH (INCLINATION) Wind tunnel stability tests of pinch of modified half ring wing body and swept wing body combinations at supersonic speeds NASA-TM-X-1551 c01 N68-21940 PITCHING MOMENTS Forces and moments produced by air and helium jets exhausting parallel to flat plate in near vacuum NASA-TN-D-4408 c12 N68-19000 Flexibility effects on lift and pitching moments of low aspect ratio delta wing-conical-cylindrical body combinations at transonic speeds NASA-TN-D-4655 c01 N68-37065 PTVOTS Theoretical study of effect of pivot location on NASA-TN-D-4635 of effect of proof location on wings in incompressible flow NASA-TN-D-4635 c01 N68-288 PLANCKS CONSTANT c01 N68-28817 Black body radiation - numerical solution for computer and hand calculation of total intensity over specified spectral range NASA-TN-D-4446 c19 N68-18455 PLANETARY ATMOSPHERES Advances during 1956 in computer 1956 in Advances during 1966 in astronomy, exobiology, ionospheric sciences, radio and solar physics, and planetary atmospheres and planetology NASA-SP-155 c30 N68-15748 FORTRAN computer program for calculating model planetary atmospheres and density and temperatue dispersion data for Apollo reentry NASA-TN-D-4292 c30 N68-15793 Handbook on planetary physics

NASA-TT-F-515 c30 N68-21802 Coherent radiation methods of measuring absorption spectra in planetary atmosphere, and millimeter and submillimeter wave propagation NASA-CR-863 c07 N68-27063 NASA-GR 000 Bibliographic citations, abstracts, and indexes on planetary atmospheres - June 1966 through December 1967 NASA-SP-7017/02/ c30 N68-306 Optical radiation measurements behind shock wave c30 N68-30601 in simulated Mars atmosphere NASA-TM-X-1634 c12 N68-32982 PLANETARY GRAVITATION Planetary gravitation and oblateness used for parking orbit alignment in Mars mission NASA-TN-D-4657 c30 N68-7 c30 N68-28408 PLANETARY LANDING Mars excursion module landing mission mode comparison NASA-TM-X-1629 c30 N68-29988 Advanced multiprocessor computer organization for manned Mars lander mission NASA-CR-1159 c08 N68-3556 c08 N68-35560 PLANETARY RADIATION Equations, charts, and analysis to calculate theoretical temperatures of thin film solar cells in earth orbit NASA-TN-D-4331 c33 N68-: c33 N68-14270 Uncertainty analysis for designing calorimetric experiments, and equations for measuring properties of planetary radiation NASA-TN-D-4354 cl4 NO PLANETARY TEMPERATURE c14 N68-16529 Subsolar-meridian mean annual distributions for Martian troposphere below 50 km NASA-CR-1043 c30 N68-19192 PLANETS Advances during 1966 in astronomy, exobiology, ionospheric sciences, radio and solar physics, and planetary atmospheres and planetology NASA-SP-155 c30 N68-15748 PLANFORMS Modified approach for predicting lift body pressures and camber shape for planforms in subsonic flow NASA-TN-D-4427 c01 N68-28868 Supplementary information for computer program predicting lifting pressure and camber shape of composite planform in subsonic flow NASA-TN-D-4427, SUP. col N68-31515 PLASMA ACCELERATORS c01 N68-31515 Numerical analysis of electric current and potential distributions in linear Faraday plasma accelerators NASA-TN-D-4239 c28 N68-10502 PLASMA CONTROL Plasma preheating in megajoule theta pinch device for subsequent magnetic compression NASA-TN-D-4708 c25 N68-33372 PLASMA DIAGNOSTICS Laser interferometer and heterodyne system for cesium plasma diagnostics NASA-TM-X-1652 c16 N68-33 c16 N68-35593 Guided electromagnetic waves propagating along lossless dielectric rod immersed in isotropic and uniaxial plasmas determined for applications to plasma diagnostics NASA-TN-D-4866 c25 N68-37237 PLASMA DYNAMICS Dynamics of bounded one dimensional plasma sheath NASA-TN-D-4651 c25 N68-3003. PLASMA GENERATORS c25 N68-30031 High enthalpy plasma generator for atmospheric entry heating simulation NASA-TN-D-4583 c11 N68-24 c11 N68-24560 Hydrogen plasma hot cathode generator and electron energy and density study NASA-TN-D-4604 c25 N68-25877 PLASMA GUNS Two channel transient voltage digitizer for correlation of transient spectra with performance in coaxial, argon plasma guns NASA-TN-D-4385 c25 NG c25 N68-17070 Coaxial plasma gun research for space propulsion applications NASA-TM-X-1600 c25 N68-281 c25 N68-28154 Electron diffusion process in beam plasma passing through electrically floating anode

PLASMA HEATING

NASA-TN-D-4758 c25 N68-32072 PLASMA HEATING Induction plasma heating system for hydrogen-argon simulated gas cooled reactor studies NASA-CR-1143 c c25 N68-29888 Plasma preheating in megajoule theta pinch device for subsequent magnetic compression NASA-TN-D-4708 PLASMA INTERACTIONS c25 N68-33372 Plasma effects in antenna near zone field -admittance and ionization rise time measurements on Teflon-plugged waveguide slot antenna NASA-CR-1149 PLASMA OSCILLATIONS c07 N68-33042 Small amplitude solutions to spatially uniform plasma continuity equations for low frequency oscillations in electron density and neutral atoms NASA-TN-D-4472 c25 N6 PLASMA-PARTICLE INTERACTIONS Electron beam-plasma interaction and plasma c25 N68-22887 multiplier as possible millimeter wave generators NASA-TN-D-4309 c25 N68-18614 Scattering and absorption of plane electromagnetic waves by particles of turbid medium NASA-TT-F-477 c13 N68-22462 Dependence of tungsten electrode work functions on positive ion sheaths between electrodes and cesium plasmas NASA-TN-D-4745 c25 N68-30593 PLASMA PROBES PLASMA PRODES Boundary correction factors for three coil conductivity/velocity plasma probe NASA-TN-D-4538 c25 N PLASMA PROPULSION c25 N68-21691 Coaxial plasma gun research for space propulsion applications NASA-TM-X-1600 c25 N68-28154 PLASMA RESONANCE Power transfer to ion cyclotron waves in two species plasma NASA-TM-X-1481 c25 N68-11404 PLASMA SHEATHS FORTRAN computer programs for plane collisionless sheaths between field modified emitter and thermally ionized plasma exemplified by cesium NASA-TM-X-1562 c08 N68-21499 Pairs of emitter and collector sheaths for cesium thermionic diodes NASA-TN-D-4419 c25 N68-21623 Model of plasma boundary interactions NASA-CR-1072 c25 N68-25821 Dynamics of bounded one dimensional plasma sheath NASA-TN-D-4651 NASA-TN-D-4651 c25 N68-30031 Iterative calculation model and results for plane collisionless sheaths between field modified emitter and thermally ionized cesium plasma NASA-TN-D-4376 c25 N68-33021 Apollo command module radar cross section decrease due to reentry plasma effects NASA-TN-D-4784 c07 N68-35140 PLASMA SLABS aperture in ground plane covered by dielectric or plasma slab NASA-CR-1177 c25 N68-35171 PLASMAS (PHYSICS) Small amplitude solutions to spatially uniform plasma continuity equations for low frequency oscillations in electron density and neutral atoms NASA-TN-D-4472 c25 N68-22887 Model of plasma boundary interactions NASA-CR-1072 c25 N68-25821 Thermodynamics of plasmas using principle of maximum entropy NASA-TN-D-4621 c25 N68-25920 Fourier integration of electrical impedance expressions for nonlossy dielectric and lossy plamas NASA-TN-D-4774 PLASTIC COATINGS c07 N68-35524 Techniques for coating magnesium with epoxy resin films for paraboloid mirrors NASA-TN-D-4734 c18 N68-3059 c18 N68-30597 PLASTIC DEFORMATION

Plastic response of circular uniform plate to

SUBJECT INDEX

axisymmetric impulse load of Gaussian distribution NASA-TR-R-279 c32 N68-14640 Successive approximation procedure for solving elastic-plastic problem for torsion of solid prismatic bar made of strain hardening material NASA-TN-D-4391 c32 N68-17045 NASA-IN-0-4091 Correction Correction Non-17 Necking, yield, and plastic flow in electrical analogs of mechanical systems with respect to energy conversion effects on mechanical behavior of various materials NASA-CR-1039 c24 N68-21949 Adsorbed surfactants influence on deformation and friction coefficient of lithium fluoride single crystals during sliding friction NASA-TN-D-4716 c15 N68-29918 c15 N68-29918 Elastic buckling equations for calculating plastic buckling of plates and shells under biaxial loading NASA-TN-D-4706 PLASTIC PROPERTIES c32 N68-31946 Chromium alloys with good low temperature ductility and superplasticity NASA-TN-D-4346 c14 c14 N68-13973 Iterative solution for calculating deformation and stress concentration near slits in elastic-plastic solids NASA-TN-D-4717 c32 N68-30045 PLASTICS Wear rate and friction coefficient of steel sliding on polymer laminates determined in liquid nitrogen and hydrogen NASA-TN-D-4463 c15 N68-20325 PLATES (STRUCTURAL MEMBERS) Three dimensional analysis for determining effects of heat generation in plates NASA-TN-D-4326 c33 N68-18122 Elastic buckling equations for calculating plastic buckling of plates and shells under biaxial loading NASA-TN-D-4706 c32 N68-31946 Effect of N waves at oblique incidence on response of simply supported plate to transient loads NASA-CR-1176 c32 N68-33168 PLATINUM Platinum resistance thermometers tested and evaluated in cryogenic temperature measurement NASA-TN-D-4499 c14 N68-203 c14 N68-20324 PLAYBACKS Rapid reduction method of rhythm and rate information in large scale electrocardiogram monitoring c05 N68-32100 NASA-TN-D-4751 PLOTTING FORTRAN subroutines for plotting and drawing of three dimensional solid surfaces NASA--TM-X-1598 c19 N68-28240 PLUG NOZZLES Performance evaluation of annular plug and expansion-deflection nozzles including external flow effects at transonic Mach numbers NASA-TN-D-4462 c01 c01 N68-20330 Cold flow tests of aerodynamic characteristics of plug nozzle configuration for turbojet engines operating at supersonic speeds NASA-TM-X-1619 c28 N68-2 Effects of shroud geometry on performance of collapsible plug nozzle at Mach numbers from c28 N68-29953 0 to 2.0 NASA-TM-X-1657 c01 N68-36132 PLUM BROOK REACTOR Computer methods for calculating radiation shield design for Plum Brook reactor HB-6 beamhole facility NASA-TM-X-1461 c22 N68-10133 Fast and thermal neutron flux measurements in test cavity outside HB-6 beam port in Plum Brook reactor using sulfur pellets and gold foils NASA-TM-X-1497 c22 N68-15643 MADATINTATIAN Plum Brook reactor support calculations -mathematical model for fuel utilization, power distribution in fuel loading, and approximate predictions of xenon poison transient NASA-TM-X-1496 NFG C22 N68-160 c22 N68-16056 PLUMES Approximation of ramjet exhaust plume effects on external pressure of nozzle extension of X-15 aircraft

POTASSIUM

NASA-TM-X-1571 PLUTONIUM 238 c28 N68-24614 Analysis and selection of design for plutonium 238 for Brayton cycle space powerplant NASA-TN-D-4600 PNEUMATIC CONTROL c03 N68-25829 Fluidic analog to pulse frequency converter for NASA-TN-D-4497 co3 N68-21835 PNEUMATIC EQUIPMENT Breadboard flueric circuitry used to drive pneumatic stepping motors NASA-TN-D-4495 c03 N POINCARE PROBLEM c03 N68-21651 Development of equations of motion in canonical form equivalent to forms of Delaunay and Poincare NASA-TN-D-4478 c30 N68-24 POISONING (REACTION INHIBITION) Neutronic calculations of fuel and poison drum c30 N68-24371 control of refractory metal, fast spectrum space power reactors NASA-TN-D-4709 c22 N68-30750 POISSON DENSITY FUNCTIONS Coding schemes for data based on Poisson functions NASA-TN-D-4572 c07 N68-25852 NHOATIN-10-4572 CO7 NG Optical communications - maximum likelihood detection of M-ary Poisson processes in background of additive Poisson noise NASA-TN-D-4623 CO7 NG c07 N68-29528 Error probabilities for maximum signal detection in presence of Poisson noise NASA-TN-D-4721 c07 N68-36105 POLAR CAP ABSORPTION Polar cap absorption study of solar cycle variation in solar proton emissions from sun NASA-TN-D-4473 c29 N68-2 c29 N68-25880 POLAR GASES Approximate methods for predicting viscosities of gas mixtures involving both polar and nonpolar dases NASA-TN-D-4496 c12 N68-21724 POLYAMIDE RESINS Conductive heat transfer mechanisms in low density phenolic-nylon chars NASA-CR-966 c18 N68-11978 Theoretical analysis of five composite ablation materials with various percentages of phenolic resin, powdered nylon, and silica NASA-TN-D-4374 c18 N68-197 c18 N68-19710 POLYCARBONATES Penetration of porous projectiles in aluminium and plastic targets NASA-TN-D-4505 c32 N68-21293 POLYCRYSTALS Electron microscopy of electron beam irradiated amorphous silicon, germanium, and cadmium sulfide semiconductor films NASA-TN-D-4522 c26 Emitter and collector sheaths for cesium c26 N68-20295 thermionic diodes with polycrystalline tungsten electrodes NASA-TN-D-4744 c25 N68-31640 POLYETHYLENE TEREPHTHALATE Solid state polymerization technology for synthesis of ultrahigh molecular weight polyethylene terephthalate NASA-TN-D-4335 c06 c06 N68-14093 NASA-IN-D-4335 Flight test of capacitance type meteoroid impact detector of aluminum polyethylene terephthalate using inflatable paraglider NASA-TN-D-4530 cl4 N68-2229 c14 N68-22290 Fabrication and testing of Pageos 1 NASA-TN-D-4596 c31 N68-25820 NASA-TN-D-4596 c31 POLYMER CHEMISTRY Solid state polymerization technology for synthesis of ultrahigh molecular weight polyethylene terephthalate NASA-TN-D-4335 c06 c06 N68-14093 POLYMERIC FILMS Cryogenic flexibility of single and multiple plies of thin polymeric films tested at minus 320 deg and minus 423 deg F NASA-TM-X-1555 c18 N68-20329 Effects of stretch and heat-set temperatures and time on cryogenic mechanical properties of poly/ethyl terephthalate/ film

NASA-TN-D-4762 c18 Fabricability, mechanical properties, and structural efficiency potentials of c18 N68-33034 boron-polymer film layer composites NASA-CR-1114 c18 N68-35100 Analysis of dielectric breakdowns induced by electron irradiation in polymeric films NASA-TN-D-4810 c24 N68 c24 N68-36070 POLYMERIZATION Solid state polymerization technology for synthesis of ultrahigh molecular weight polyethylene terephthalate NASA-TN-D-4335 c06 c06 N68-14093 POLYNOMIALS General equations for standard deviation, and rms standard deviation of least squares fitted polynomials applied to Apollo tracking problems NASA-TN-D-4121 c10 N68-16749 General Lagrangian interpolation formulas NASA-TN-D-4424 cl9 POLYPHENYL ETHER c19 N68-22809 High temperature tests to determine fatigue life of 120mm bore ball bearings with fluorocarbon, polyphenyl ether, and synthetic base paraffin base lubricants NASA-TN-D-4850 c15 N68-36075 POLYTETRAFLUOROETHYLENE POLYURETHANE FOAM c15 N68-24142 Penetration of porous projectiles in aluminium and Penetration of porous projectiles in aluminium plastic targets NASA-TN-D-4505 c32 N68-21 PONTRYAGIN PRINCIPLE Maxima-minima theory, Pontryagin principle, and calculus of variations for optimal trajectory and control analysis NASA-CR-1006 c30 N68-20 c32 N68-21293 c30 N68-20084 Pontryagin maximum principle, calculus of variations, and dynamic programming optimization techniques applied to trajectory and guidance problems NASA-CR-1014 c30 N68-21231 POPULATIONS Frequency function for testing small samples for goodness of fit to normal populations NASA-TN-D-4405 c19 N68-191 c19 N68-19144 **POROUS MATERIALS** Plate-gap model of porous solid and application to reduced density projectile impact NASA-CR-1140 c32 N68-31912 NASA-TM-X-1529 c30 N68-19064 POSITION INDICATORS Maximum likelihood techniques for design of optimum star trackers that determine position and magnitude NASA-TN-D-4549 c21 N68-23 c21 N68-23377 POSTFLIGHT ANALYSIS Flight performance evaluation of Atlas-Centaur for Surveyor spacecraft SC-2 NASA-TM-X-1616 c31 N68-33332 Description and performance analysis of manned six-pass orbital mission /Nercury-Atlas 8/ NASA-TN-D-4807 c31 N68-35022 POTASSIUM Corrosion products of oxygen doped tantalum exposed to potassium at 1800 deg F NASA-TN-D-4213 c17 N6 c17 N68-11511 Two stage potassium vapor turbine - materials support of performance and endurance tests NASA-CR-925 c03 N68c03 N68-16351 CU3 N68 Two stage turbine suitable for use in wet potassium vapor at temperatures of 1400 to 1660 deg F NASA-CR-922 c03 N68-16439 Mechanical design and development test program for two-stage potassium vapor Rankine cycle turbine NASA-CR-923 c03 N68-17075 NASA-CA-925 Neutron activation analysis of sodium, lithium, and potassium in compact fast reactors and its effect on shielding NASA-TM-X-1512 c22 N68-203 c22 N68-20355 Vapor pressure measurements of potassium to 2170 deg K

NASA-TN-D-4535 c33 N68-25122 POTASSIUM OXIDES Recovery of potassium tantalate and potassium monoxide to demonstrate procedure for isolation and recovery of alkali-metal reaction products in uncontaminated state NASA-TN-D-4310 c17 N68-14888 POWDER METALLURGY Shaping of precipitation hardened stainless steels by casting and powder metallurgy NASA-SP-5086 c15 N68-19307 Hydrogen release in ball milling of high purity, coarse chromium powder in water NASA-TN-D-4569 c15 N68-23900 POWER CONDITIONING Electrical stress analysis of microthruster power conditioner NASA-TM-X-1686 POWER EFFICIENCY c09 N68-37944 Reduction of apparent power requirement for phase controlled parasitically loaded turboalternator by multiple parasitic loads NASA-TN-D-4302 c03 N68-17110 Axial power tailoring to obtain constant fuel-centerline temperature in nuclear reactor NASA-TN-D-4658 c22 N68-2 c22 N68-28304 Partial admission operation effects on performance of single stage axial flow turbine NASA-TN-D-4700 c03 N68-30241 POWER PLANTS Property data of magnetic materials for use in high temperature liquid alkali-metal space power systems NASA-SP-3043 c17 N68-1763 PRECIPITATION HARDENING Use of surface replication, extraction replication, and thin film electron microscopy c17 N68-17624 in study of microstructures of dispersion strengthened materials NASA-TN-D-4461 c17 N68-18999 Shaping of precipitation hardened stainless steels by casting and powder metallurgy NASA-SP-5086 c15 N68-19307 Hard surfacing, electroplating, electrodeless plating, carburizing, nitriding, burnishing, explosive hardening, planishing, and peening of precipitation-hardenable stainless steels NASA-SP-5090 c15 N68-19343 Thermal and mechanical treatment for precipitation hardening stainless steels NASA-SP-5089 c15 N68-20433 Electron microscope technique for revealing microstructures of dispersion strengthened materials NASA-TM-X-1561 c17 N68-21431 Deformation processing of precipitation hardening stainless steels NASA-SP-5088 c17 N68-21917 PREDICTIONS Sharp edge delta wing drag prediction by application of leading edge suction analogy of vortex lift NASA-TN-D-4739 c01 N68-31990 PREMIXED FLAMES Flame propagation in supersonic premixed flows of hydrogen and air ignited by coaxial, hot gas, pilot jet NASA-TN-D-4631 c33 N68-28100 PRESSURE DISTRIBUTION Pressure distributions and aerodynamic characteristics of Nimbus B fuel capsule in hypersonic flow NASA-TM-X-1487 c01 N68-11958 Cold air study of gas turbine for high temperature aircraft engine application NASA-TN-D-4389 c01 N68-15743 Integer relations method of determining inviscid shock layer flow and pressure distributions over blunt bodies NASA-TN-D-4397 c01 N68-15778 Wind tunnel tests on pressure distribution, and shock shapes of conical blunted bodies moving at supersonic speeds in nitrogen, or helium media NASA-TN-D-4437 NASA-TN-D-4437 Effect of two dimensional multiple sine wave protrusions on pressure and heat transfer distributions for flat plate in hypersonic flow NASA-TN-D-4437 COI N68-199063 c01 N68-17896

c01 N68-19063 Wing surface pressure data from large scale wind

SUBJECT INDEX

tunnel tests of propeller driven short takeoff aircraft NASA-TM-X-1527 c02 N68-19065 Wind tunnel investigation of pressure distribution on blunted 15 deg half-cone wedge lifting-entry bodv NASA-TN-D-4494 c01 N68-21681 Effect of boundary layer bleed on heat transfer and pressure distributions over wedge-flap surface at hypersonic speeds NASA-TN-D-4686 c01 N68-29955 Hypersonic heat transfer and pressure distribution on spherically blunted cone NASA-TN-D-4792 c01 N68-35497 Theoretical analysis of pressure distribution, load capacity, load angle, and friction force for single-step concentric journal bearing NASA-TN-D-4839 c15 N68-36098 Cone-cylinder models tested in supersonic wind tunnel to evaluate effect of wall reflected disturbances on model pressure distributions NASA-TM-X-1655 col N68-3 c01 N68-36134 Nonlinear lift and pressure distribution of slender conical bodies with strakes at low speed c01 N68-37255 NASA-CR-1202 PRESSURE DRAG Effect of boattail juncture shape on pressure drag coefficients of isolated afterbodies of supersonic engine nacelles NASA-TM-X-1517 c01 N68-19237 Simulated wing effect on pressure drag coefficient of subsonic boattail at angle of attack NASA-TM-X-1662 c01 | c01 N68-35672 Effect of geometry of conical afterbodies on base drag at subsonic and transonic speeds NASA-TN-D-4821 c01 N68-37054 c01 N68-37054 PRESSURE DROP Mathematical model for deriving pressure drop against flow function of counterflow boiler tube in Rankine space power system NASA-TN-D-4498 c33 N68-20066 PRESSURE EFFECTS Reduced pressure effects on fatigue life of roller steel ball bearings with mineral oil lubricants steel ball bearings and c15 N68-15010 NASA-TN-D-4348 Wind tunnel investigation of fluctuating pressures NASA-TM-X-1574 PRESSURE GAGES Installation and fairing of flush, static pressure orifices on wing surfaces of supersonic aircraft NASA-TM-X-1530 c01 N68-19341 c01 N68-19341 PRESSURE GRADIENTS Pressure fluctuation measurements on afterbodies of blunt atmospheric entry vehicles NASA-TN-D-4591 PRESSURE MEASUREMENTS c32 N68-24508 Pressure rise characteristics of liquid hydrogen dewar for homogeneous, normal-gravity quiescent, and zero-gravity tests NASA-TM-X-1134 c33 N68-18196 c33 N68-18196 Pressure and heat transfer on blunt concave and convex plates in hypersonic flow NASA-TN-D-4367 c12 N68-183 c12 N68-18253 Approximation of ramjet exhaust plume effects on external pressure of nozzle extension of X-15 aircraft NASA-TH-X-1571 c28 N68-24614 Wind tunnel calibration of 30 deg included angle cone for determination of local values of Mach number, total pressure, and flow distribution NASA-TN-D-4679 c14 N68-301; c14 N68-30127 Superconducting bolometers for measuring very low pressures NASA-CR-1120 c14 N68-33022 Base pressure measurements at angle of attack for spherically blunted cones at hypersonic speed NASA-TN-D-4800 PRESSURE OSCILLATIONS c01 N68-35668 Selected band cross correlation analysis of fluctuating pressures under turbulent boundary layer flow NASA-CR-1066 c12 N68-23482 PRESSURE RECOVERY Wind tunnel tests of mixed-compression axisymmetric inlet system to determine bleed mass flow ratio, pressure recovery and pressure distortion NASA-TN-D-4557 c28 N68-23354

PRESSURE SENSORS Quasi-Static calibrations for determining quartz, piezoelectric type, pressure transducer sensitivity from 20 to 477 deg K NASA-TM-X-1479 c14 N68-11867 c14 N68-11867 Temperature and liquid-level sensor for liquid hydrogen pressurization and expulsion studies NASA-TN-D-4339 c14 N68-15 c14 N68-15893 Wind tunnel calibration of conical pressure probe over range of Mach numbers to determine flow field data for X-15 airplane NASA-TN-D-4678 c12 N68 Product development and testing of thin film c12 N68-28801 oxygen partial pressure sensors MADA-CK-1182 c14 N68-35149 Combination temperature, pressure, and flow direction sensing probe to study rotating machinery machinery NASA-TN-D-4816 c14 N68-36021 PRESSURE SUITS Pressure suits and backloads effects on locomotion in simulated lunar gravity NASA-TN-D-4464 c05 N68-20354 Effects of simulated lunar gravity on metabolic rates while wearing pressure suits NASA-CR-1102 c05 N68-280 c05 N68-28833 PRESSURE VESSELS Tensile strength properties of glass, boron, and graphite filament wound resin composites and liners for cryogenic pressure vessels NASA-TN-D-4412 c18 N68-1 NASA-TN-D-4412 Crack propagation in aluminum notched tensile and pressure vessel specimens cyclically loaded at cryogenic temperatures NASA-TN-D-4541 c17 N68-21768 PRESTRESSING Materials selection, structural geometry, proof testing and statistical screening, prestressing, and system energy as tools for designing optimum trusses and other high performance structures NASA-CR-1038 C32 N68-23399 PRISMATIC BARS Successive approximation procedure for solving elastic-plastic problem for torsion of solid prismatic bar made of strain hardening material NASA-TN-D-4391 c32 N68-17045 PROBABILITY DISTRIBUTION FUNCTIONS Maximum likelihood techniques for design of optimum star trackers that determine position and magnitude NASA-TN-D-4549 c21 N68-23377 Computer program for reversion of cumulative binomial probability distribution NASA-TM-X-1592 c19 N68 c19 N68-24141 Listribution and properties of weighted sum of chi squares random variables NASA-TN-D-4575 c19 N68-24141 cliphotocological chi NASA-TN-D-4575 c19 N68-24565 PROBABILITY THEORY Uncertainty analysis for designing calorimetric experiments, and equations for measuring properties of planetary radiation NASA-TN-D-4354 c14 N68-165 Error probabilities for maximum signal detection c14 N68-16529 in presence of Poisson noise NASA-TN-D-4721 c07 N68-36105 PROBLEM SOLVING Nonconventional computers for solving problems previously handled only by humans NASA-TM-X-1544 c08 N68-19336 Nonlinear correction method for orbit determination using range, azimuth, and elevation data NASA-CR-1040 c30 N68-21864 Vectorial concept for solving three body problem in celestial mechanics NASA-TN-D-4447 c30 N68-22885 Laminar boundary layer problems solved by integral matrix methods NASA-CR-1062 c33 N68-26641 PRODUCT DEVELOPMENT Systems engineering and development of M-1 injector hydrogen oxygen engine NASA-TN-D-4730 c28 N68-30604 Product development and testing of thin film oxygen partial pressure sensors NASA-CR-1182 c14 N68-35149 PRODUCTS Formalism for treating products of generalized functions and applications in mathematical

physics NASA-TN-D-4244 PROJECT MANAGEMENT c19 N68-11494 Parts and materials application review for project management of space systems engineering NASA-SP-6505 c15 c15 N68-10120 PROJECTILE CRATERING Penetration of porous projectiles in aluminium and plastic targets NASA-TN-D-4505 c32 N68-21293 PROJECTILES Exploding foil gun technique for simulated meteoroid protection NASA-TN-D-4259 c32 N c32 N68-11355 Target pressure and damage data from impacts by explosively propelled aluminum projectile NASA-TM-X-1597 c32 N68-250 c32 N68-25819 Plate-gap model of porous solid and application to reduced density projectile impact NASA-CR-1140 c32 N68-31912 PROPELLANT COMBUSTION Hydrogen-oxygen chemical reaction kinetics in rocket engine combustion NASA-TN-D-4250 c33 N68c33 N68-11642 Combustion instability prediction using nonlinear bipropellant vaporization model NASA-CR-920 c33 N68-15833 PROPELLANT STORABILITY Performance of low thrust storable bipropellant thrustors in spacecraft reaction control system NASA-TN-D-4416 c28 N68-20064 NASA-TN-D-4416 PROPELLANT TANKS Precision glass-bead peening equipment for propellant tank surface corrosion protection NASA-TN-D-4288 c15 N68-13 c15 N68-12890 Vapor ingestion during liquid outflow in scale model Centaur liquid hydrogen tank NASA-TH-X-1482 cl2 N68-1: c12 N68-19225 FORTRAN 4 computer program for calculating temperature profiles in propellant tank NASA-TM-X-1556 c27 N68-21267 Thermal degradation of high performance multilayer insulation on liquid hydrogen tank in vicinity of penetration NASA-TN-D-4778 c33 N68-33167 Analytical and experimental investigation of propellant distribution during outflow of spherical tanks for possible space vehicle application c12 N68-35104 NASA-TN-D-4828 Drop tower investigation of liquid reorientation in spherical containers NASA-TM-X-1659 c12 N68-351 PROPELLER SLIPSTREAMS c12 N68-35114 PROPELLER SLIPSIRERS Wind tunnel determination of longitudinal force characteristics for STOL aircraft scale models with varying wing aspect ratios NASA-TN-D-4448 c02 N68-187 PROPULSION SYSTEM CONFIGURATIONS c02 N68-18771 Effect of hydrogen peroxide generator configurations on jet exhaust flow characteristics NASA-TM-X-1671 c12 N68-37067 Thermal design and analysis of cesium contact-ion microthrustor NASA-TM-X-1473 c28 N68-10496 Performance tests of ammonia resistojet thrustor system for various spacecraft control maneuvers NASA-TN-D-4249 c28 N68-1056 c28 N68-10562 PROPULSIVE EFFICIENCY Coaxial plasma gun research for space propulsion applications NASA-TM-X-1600 PROTECTIVE CLOTHING c25 N68-28154 Radiative thermal energy incident effects on pressure-suited man on lunar surface c30 N68-11630 NASA-TN-D-4243 PROTECTIVE COATINGS Solar simulation testing of anchored interplanetary monitoring platform D thermal design and protective coating NASA-TN-D-4112 c33 N68-1 c33 N68-10299 Protective coatings and surface treatments for protection of Ti-8A1-1Mo-1V alloy sheet from hot-salt stress corrosion NASA-TN-D-4319 c17 N68-17377 Heat balance equations for optimizing optical coating patterns for spacecraft temperature

control system NASA-CR-1041 c18 N68-22391 Electron probe X ray microanalyzer applied to material failure study, bonding, and other metallurgical analysis NASA-TN-D-4526 c15 N68-28249 PROTON DAMAGE High energy proton damage in silicon surface barrier detectors NASA-TN-D-4528 c26 N68-240 PROTON IRRADIATION Effects of 22 MeV proton and 2.4 MeV electron radiation on boron and aluminum doped silicon c26 N68-24660 solar cells NASA-TN-D-4407 c26 N68-19924 NASA-IN-D-4407 Radiation damage in low energy proton irradiated thick copper and gold foils and subsequent annealing characteristics NASA-TN-D-4452 Ultraviolet-proton radiation effects on solar concentrator reflective surfaces NASA-CP-1924 C20 N68-1992 C20 N68-2122 C20 N68-212 C20 N68c26 N68-21219 c17 N68-23560 Defect energy levels and concentrations for proton irradiated, n-type silicon single crystals NASA-TN-D-4830 c26 M68-3705 PROTOTYPES Electroadhesive devices - theory, design, fabrication, and testing NASA-CR-1211 c10 N68-37906 Noise reduction in small enclosed structures in terms of physiological and psychological effects NASA-CR-1155 PSYCHOACOUSTICS PSYCHOLOGICAL EFFECTS Aerospace medicine and biology bibliography on Aerospace medicine and biology bibliography on physiological, psychological, and environmental effects on man during aerospace flights NASA-SP-7011/43/ c04 N68-1467 Aerospace medicine and biology bibliography on physiological, psychological, and environmental effects on man during aerospace flights NASA-SP-7011/42/ c04 N68-1472 (PUNDBWSTRICOV) c04 N68-14671 c04 N68-14725 PSYCHOPHYSIOLOGY Process development of system for digital computer processing of psychophysiological data to obtain high stress tolerance personnel NASA-CR-1122 c05 N68-35102 PULSE AMPLITUDE Numerical least square method for resolving complex pulse height spectra NASA-SP-3044 c24 NG c24 N68-29520 PULSE CODE MODULATION Self-synchronizing, biorthogonal coded pulse code modulation telemetry system for communicating with unmanned spacecraft NASA-TR-R-292 c07 N68-36333 PULSE COMMUNICATION Waveform distortion in maximum likelihood Darlington detector for M-ary pulse frequency modulation signals NASA-TN-D-4294 c07 N68-18542 PULSE DURATION Transient analysis of arterial fluid lines with respect to time domains and pulse width NASA-CR-990 c04 N68-12494 PULSE FREQUENCY MODULATION TELEMETRY Resolution limit analysis for pulse frequency modulation telemetry processing line NASA-TN-D-4180 c c07 N68-18247 Waveform distortion in maximum likelihood Darlington detector for M-ary pulse frequency modulation signals NASA-TN-D-4294 c07 N68-18542 Dual detection system for processing AIMP satellite pulse frequency modulated telemetry data NASA-TN-D-4561 c08 N68-24310 PULSE POSITION MODULATION Design of pulse position modulation optical communication system NASA-TN-D-4814 PULSED RADIATION c07 N68-35174 Detection of supernovae pulse by gamma ray telescope and atmospheric scintillation method NASA-TN-D-4732 c29 N68-333 NASA-TN-D-4732 c29 N68-33370 Spectral transmission measurements on fused silica during and after exposure to pulsed neutron irradiation

NASA-CR-1191

SUBJECT INDEX

PHMP IMPELLERS Liquid fluorine pump, impeller, and inducer corrosion resistance to cavitation flow NASA-TM-X-1573 cl5 N6 c15 N68-28241 Visual observations to find flow distribution and coefficients through radial bladed centrifugal pump impeller NASA-TN-D-4282 c12 N68-28842 PUMPS Electronic circuit for detection of R-wave of electrocardiac signal for control of time cycle of heart-assist pumps NASA-TM-X-1489 c05 N68-13999 c05 N68-13999 PURSUIT TRACKING Pilot performance using compensatory and pursuit tracking displays with rate and acceleration control dynamics and disturbance input NASA-CR-1082 c07 C07 N68-28272 PYROELECTRICITY Dielectric temperature change effects observed in ferroelectric and pyroelectric substances NASA-CR-1080 c26 N68-25972 PYROLYSIS Coking reactions of pyrolysis gas in charring ablation material NASA-CR-1065 c33 N68-26817 Chemical reaction-plane approximation in ablation analyses NASA-TN-D-4817 c33 N68-36072 PYROLYTIC MATERIALS Pyrolytic silicon nitride dielectric for integrated circuits NASA-CR-995 c18 N68-18849 PYROTECHNICS Pyrotechnic shaped charge aerospace vehicle stage and shroud separation systems development NASA-TM-X-1607 c31 N6 c31 N68-28869 Ο Q SWITCHED LASERS Particle acceleration by evaporation pressure using Q-switched laser beam NASA-CR-927 c16 N68c16 N68-10467 QUADRATURES Quadrature methods of formulating Runge-Kutta equations NASA-TR-R-275 c19 N68-10121 Multi-step Runge-Kutta methods using method of quadratures NASA-TN-D-4400 c19 N68-21100 NASA-IN-D-4400 C19 N68-2. QUANTUM ELECTROBYNAMICS Electromagnetism in moving, conducting media -solution to problems involving static and radiation fields of static charges, and radiation fields of harmonic current sources NASA-CR-1025 QUANTUM MECHANICS c23 N68-21444 Quantum mechanical study of transition probabilities, Einstein A coefficients, and oscillator strengths of band systems of diatomic molecules NASA-CR-975 c24 N68-11037 Computer methods for calculating eigenvalue and eigenvectors of real symmetric matrices arising in problems of molecular quantum mechanics NASA-CR-983 c24 N68 c24 N68-11903 QUARTZ TRANSDUCERS NILE INMODUCERS Quasi-static calibrations for determining quarts, piezoelectric type, pressure transducer sensitivity from 20 to 477 deg K NASA-TM-X-1479 C14 N68-1186 c14 N68-11867 QUASI-STEADY STATES Mathematical model for computing equilibrium properties of one dimensional self-gravitating stellar system NASA-TR-R-289 c30 N68-32978

R

RADAR CROSS SECTIONS Apollo command module radar cross section decrease due to reentry plasma effects NASA-TN-D-4784 CO7 N68-35140 RADAR TRACKING Effects of time, frequency, and tracking station

Effects of time, frequency, and tracking station location errors on accuracy of trajectory analysis NASA-TN-D-4507 c30 N68-25271

c22 N68-35826

RADIAL FLOW Experimental performance evaluation of radial inflow turbine with exit diffuser NASA-TM-X-1480 c03 N68-11920 Optimum design geometry for high radial inflow turbine performance efficiency NASA-TN-D-4384 c03 N6 Flow visualization and containment tests in directed-wall-jet vortex tube with radial c03 N68-15943 outflow and moderate superimposed axial flows NASA-CR-992 c22 N68-12 c22 N68-17131 Visual observations to find flow distribution and coefficients through radial bladed centrifugal pump impeller NASA-TN-D-4282 RADIATION ABSORPTION c12 N68-28842 Radiation equilibrium in atmosphere with constant Einstein absorption coefficient NASA-TN-D-4479 c13 N68-22861 RADIATION DETECTORS Electronic circuit for detection of R-wave of electrocardiac signal for control of time cycle heart-assist pumps NASA-TM-X-1489 c05 N68-13999 Transmittance of thin films and photoionization of gases in selective detectors set for photons in ultraviolet spectrum NASA-CR-1096 c24 N68-28250 Fabrication and development of annular lithium drifted germanium detector for studying nuclear reaction gamma rays NASA-CR-1138 c14 N68-3515 c14 N68-35152 NASA-CK-1138 c14 N68-3: Ratio of gamma heating per gram of tungsten to gamma heating per gram of water for thin tungsten detector in water shield NASA-TM-X-1680 c22 N68-3: c22 N68-37260 RADIATION DISTRIBUTION Horizon infrared radiance profiles from Scanner project NASA-TM-X-1483 c21 N68-11949 Electromagnetism in moving, conducting media solution to problems involving static and radiation fields of static charges, and radiation fields of harmonic current sources NASA-CR-1025 c23 N68-21444 Electrical impedance and radiation distributions of circular waveguide by integral transformation NASA-TN-TN-752 NASA-TN-D-4752 RADIATION DOSAGE c07 N68-35537 Comparison of absolute calculated and measured gamma and neutron doses in tungsten water-moderated critical assembly NASA-TN-D-4223 c22 N68 c22 N68-10291 Energetic space radiation and galactic cosmic radiation measured for radiation hazards in manned space flight NASA-TN-D-4404 c29 N68-16837 Gamma ray exposure rates in Plum Brook HB-6 facility measured with dosimeters and ion chambers NASA-TM-X-1490 c22 N68-17022 High energy proton damage in silicon surface barrier detectors NASA-TN-D-4528 c26 N68-24660 Space radiation transport, spacecraft shielding design and advanced concepts, and methods for calculating radiation penetration through protective shields - conference NASA-SP-169 c29 N68-26 c29 N68-26128 RADIATION EFFECTS Electrical properties of xenon filled thermionic diodes in nuclear reactor radiation field NASA-TN-D-4368 c25 N68-1574 Radiation effects on thermionic insulator c25 N68-15747 materials - evaluation of beryllia, alumina, thoria, zirconia, and yttria NASA-TN-D-4414 c22 N68-17095 Temperature and radiation effects on index of refraction and extinction coefficients of Apollo window materials NASA-CR-1019 NASA-CR-1019 c31 N68-20467 Spectral transmission characteristics of fused silica before, during, and after exposure to reactor irradiation pulses NASA-CR-1031 c22 N68-2 c22 N68-21124 Radiation damage in low energy proton irradiated thick copper and gold foils and subsequent annealing characteristics NASA-TN-D-4452 c26 N68-212 c26 N68-21219

Point-kernel computation and experimental measurements of gamma heating effects during thermionic diode irradiation NASA-TM-X-1539 c22 N68-22022 Reactor irradiation effects on optical absorption levels in fused silica c22 N68-23481 NASA-CR-1032 Ultraviolet-proton radiation effects on solar concentrator reflective surfaces NASA-CR-1024 c17 N68-23560 Neutron irradiation effects on embrittlement of polycrystalline tungsten NASA-TN-D-4661 c17 N68 Effects of irradiation and star magnitude on sextant sighting performance NASA-TN-D-4780 c21 N68 c17 N68-28818 c21 N68-33456 Analytical expressions to determine transistor design effects on radiation resistance NASA-CR-1167 c10 N68-3 c10 N68-33767 RADIATION HAZARDS Energetic space radiation and galactic cosmic radiation measured for radiation hazards in manned space flight NASA-TN-D-4404 c29 N68-16837 NASA-TN-U-4404 Radiation hazards on extended manned space flights NASA-CR-1037 c29 N68-22849 NASA-CR-1037 RADIATION PROTECTION Comparison between cemented and soldered cover glass for radiation protection of silicon solar cells NASA-TM-X-1687 c03 N68-37935 RADIATION SHIELDING Computer methods for calculating radiation shield design for Plum Brook reactor HB-6 beamhole facility NASA-TM-X-1461 c22 N68-10133 MASA-IM-X-1461 Size and shield weight requirements calculated for fast-spectrum, liquid-metal cooled nuclear reactor for space power application NASA-TN-D-4315 Neutron activation analysis of sodium, lithium, and potassium in compact fast reactors and its effect on shielding NASA-TM-X-1512 c22 N68-20355 Space radiation transport, spacecraft shielding design and advanced concepts, and methods for calculating radiation penetration through protective shields - conference NASA-SP-169 c29 N68-26128 Thermal entry length of temperature sensor placement in tubular radiation shield NASA-CR-1200 c1 c14 N68-36530 RADIATION TOLERANCE Radiation resistance, outgassing characteristics, and weight of five electrical insulation materials for spacecraft NASA-TN-D-4553 c18 N68-2826 c18 N68-28264 Analytical expressions to determine transistor design effects on radiation resistance NASA-CR-1167 c10 N68-33 c10 N68-33767 RADIATIVE HEAT TRANSFER Lunar volcanism model based on high temperature radiative thermal conductivity of minerals and rocks NASA-CR-916 c13 N68-10283 Radiant heat transfer to aerosols for application in gaseous core nuclear rocket engine designs NASA-CR-916 NASA-CR-953 c22 N68-10561 One dimensional, steady state heat exchange by both convection and radiation between rods or fins and their surroundings NASA-TN-D-4257 NASA-TN-D-4257 c33 N68-14052 Feasibility of supporting liquid fuel on solid wall in radiating liquid core nuclear rocket concept NASA-TN-D-4413 c27 N68-17093 Computer program for determining geometric configuration view factors for spherical and conical surfaces of spherical radiating bodies NASA-TN-D-4457 c33 N68-20331 Simple iterative solution for radiative heat transfer in anisotropic media NASA-CR-1023 c33 N68-22318 Carbon dioxide model for radiation heating and cooling functions of lower stratified Martian atmosphere in thermodynamic equilibrium NASA-CR-1044 c30 N68-Boundary conditions for diffusion solution of c30 N68-22860

Boundary conditions for diffusion solution of coupled heat transfer

NASA-TN-D-4618 c33 N68-26759 Tabular and graphical data on calculations of Chandrasekhars X and Y functions and analogs for noncoherent isotropic scattering c19 N68-30804 NASA-TN-D-4712 Radiative and convective heating during atmospheric entry NASA-CR-1170 c33 c33 N68-35248 RADII Correlation of lunar radii estimates obtained from earth based photographic study and lunar orbiter gravitational field coefficient measures NASA-TN-D-4636 c30 N68-28409 RADIO ANTENNAS Flexible body analog computer program and rigid body digital computer program for calculating dynamic characteristics of double-V antennas on Radio Astronomy Explorer satellite NASA-CR-962 c08 N68-18144 RADIO ASTRONOMY Feasibility of orbiting paraboloidal antenna for low frequency radio astronomy NASA-CR-1201 c31 N68-37900 RADIO ASTRONOMY EXPLORER SATELLITE Flexible body analog computer program and rigid body digital computer program for calculating dynamic characteristics of double-V antennas on Radio Astronomy Explorer satellite NASA-CR-962 c08 N68-18144 Radio Astronomy Explorer satellite radiometer for measuring cosmic noise in vicinity of 100 meter wavelengths NASA-TN-D-4634 c14 N68-28327 RADIO BEACONS Onboard range and range rate measurements of lunar beacons for position and lunar orbit estimation NASA-TM-X-1529 c30 N68-19064 RADIO FILTERS Design, and evaluation of birefringent wave filter scale model for millimeter wavelengths radio astronomy NASA-CR-979 c09 N68-13617 **RADIO FREQUENCIES** Superconduction thin films, and properties and applications of Josephson effect at radio frequencies NASA-CR-1189 c26 N68-35178 RADIO PHYSICS Advances during 1966 in astronomy, exobiology, ionospheric sciences, radio and solar physics, and planetary atmospheres and planetology NASA-SP-155 c30 N68-15748 RADIO SPECTRA Radio Astronomy Explorer satellite radiometer for measuring cosmic noise in vicinity of 100 meter wavelengths NASA-TN-D-4634 c14 N68-28327 RADIO WAVES Field-aligned propagation of high frequency radio waves using Alouette 2 satellite data NASA-TN-D-4748 c07 N68-31639 RADIOACTIVE DECAY Computer analysis of gamma ray spectra recordings from iodine 128, and cesium 128 decay NASA-TN-D-4305 c24 N68-15328 C24 N68-15328 Angular correlation between inelastically scattered alpha particles and gamma rays emitted in subsequent nuclear decay of magnesium 24 NASA-TN-D-4683 C24 N68-20375 RADIOACTIVE ISOTOPES Nuclear, chemical, and physical properties of nine radioactive isotopes — annotated bibliography NASA-SP-7031 c06 N68-29959 NASA-SP-7031 RADIOISOTOPE BATTERIES Parametric analysis of radioisotope cascaded thermoelectric generators with Si-Ge first stage and PbTe second stage NASA-TM-X-1501 c22 N68 c22 N68-14585 Effective volume power density analysis for radioisotope power generator with silicon germanium thermoelectric elements NASA-TM-X-1453 c03 N68-14630 RADIOMETERS X-15 aircraft radiometric measurement of earth infrared horizon in three spectral intervals NASA-TN-D-4654 c21 N68-28262

NASA-TN-D-4654 c21 N68-2826 Radio Astronomy Explorer satellite radiometer for measuring cosmic noise in vicinity of 100 meter wavelengths

NASA-TN-D-4634 c14 N68-28327 Detection of terrain features from Nimbus 1 satellite high resolution infrared radiometer nighttime measurements c13 N68-28872 NASA-TN-D-4603 Systems analysis and performance test data on dual radiometer assembly for measuring far infrared wavelength bands of earths horizon radiance profile NASA-CR-1086 c14 N68-28965 RADTOSONDES Meteorological wind, and temperature data from atmospheric radiosonde soundings in Southern Hemisphere NASA-TN-D-4429 c20 N68~19084 RAMJET ENGINES Unstarted inlet flow field during restart cycle of axisymmetric mixed compression configuration at Mach 3 NASA-TM-X-1547 c01 N68-21703 Approximation of ramjet exhaust plume effects on external pressure of nozzle extension of X-15 aircraft NASA-TM-X-1571 c28 N68-24614 RANDOM SAMPLING Frequency function for testing small samples for goodness of fit to normal populations c19 N68-19144 NASA-TN-D-4405 RANDOM VARIABLES Methodology used in guidance system performance analysis /assessment/ NASA-CR-1016 c30 N68-21 c30 N68-21442 Distribution and properties of weighted sum of chi squares random variables NASA-TN-D-4575 RANGE AND RANGE RATE TRACKING c19 N68~24565 c10 N68-11513 Choord range and range rate measurements of lunar beacons for position and lunar orbit estimation NASA-TM-X-1529 c30 N68-19064 Spin axis for spinning satellite determined from range rate data NASA-TN-D-4483 c30 N68-21182 RANGE FINDERS Modified control logic with random-number nourred control logic with random-humber procedure to determine error effects on range controller of reentry vehicle NASA-TN-D-4317 c21 N68-14 RANKINE CYCLE c21 N68-14732 Electromagnetic pump designs for use as boiler feed pumps in Rankine cycle, space electric power plants NASA-CR-911 c15 N68-1 c15 N68-10503 NASA-CR-911 cl5 N68-10503 Weight, heat transfer, and efficiency comparison for Rankine cycle space radiators constructed of three different finned tube geometries NASA-TN-D-4411 c33 N68-16324 Mechanical design and development test program for two-stage potassium vapor Rankine cycle turbine NASA-CR-923 c03 N68-17075 Design, and performance of facility for Rankine cycle testing of two stage potassium vapor turbine NASA-CR-924, V. 3 c03 N68-18044 SNAP 8 simulator using primary sodium-potassium loop, mercury loop operating on Rankine cycle, and heat rejection sodium-potassium loop NASA-TM-X-1515 c11 N68-184 c11 N68-18460 Mathematical model for deriving pressure drop against flow function of counterflow boiler tube in Rankine space power system NASA-TN-D-4498 c33 N68-20066 Steady state performance tests on single pass counterflow sodium-potassium cooled mercury Rankine cycle condenser NASA-TM-X-1548 c33 N68-20340 Lunar surface layer considered to store solar energy for generating power during lunar night NASA-TM-X-1560 c03 N68-20363 Primary loop transients during startup of Rankine cycle space power system in SNAP 8 simulator NASA-TN-D-4546 c03 N68-22257 c03 N68-22257 RAREFIED GASES Rarefied gas couette flow and heat transfer between parallel plates analyzed by model sampling

REFRACTIVITY

procedures NASA-TN-D-4579 c12 N68-24129 Electron beam probe measurements of rotational and vibrational temperatures in static low-density air NASA-TN-D-4500 c14 N68-24244 RAY TRACING Mathematical determination of geometrical image aberrations in single and double mirror systems NASA-TN-D-4692 c23 N68-36460 RAYLEIGH-RITZ METHOD Prediction of vibration frequencies and modes for free-free truncated conical shells, using Rayleigh-Ritz method NASA-TN-D-4772 c32 N68-33057 REACTION KINETICS Hydrogen-oxygen chemical reaction kinetics in rocket engine combustion NASA-TN-D-4250 c33 N68c33 N68-11642 Boundary layer buildup effects in shock tubes on dissociation rate measurements NASA-TN-D-4795 c12 N68-34089 REACTIVITY Reactivity effects caused by radial power flattening in gas cooled, fast-spectrum reactor NASA-TN-D-4459 c22 N68-1992 c22 N68-19925 Reactivity insertions in compact reactor cores due to fuel movement NASA-TM-X-1587 c22 N68-23894 REACTOR CORES Criticality calculations for small, cylindrical, lithium cooled reactors for space power systems NASA-TN-D-4371 c22 N68-15792 Computer program for calculating isothermal, turbulent jet mixing flow of two gases in coaxial flow, gas gore nuclear reactors NASA-TN-D-4378 c12 c12 N68-18146 Reactivity insertions in compact reactor cores due to fuel movement NASA-TM-X-1587 NROR-IN-A-1507 C22 N68-2385 Analytical investigation of flow and wall temperature sensitivity in heated passages for large inlet to exit density ratios in subsonic flow of nuclear rocket NASA-TN-D-4649 C33 N68-2837 c22 N68-23894 c33 N68-28371 Thermionic reactor core with short-length externally fueled diodes, and electrical failure analysis NASA-TN-D-4805 c22 N68-34087 REACTOR DESIGN Radiant heat transfer to aerosols for application in gaseous core nuclear rocket engine designs NASA-CR-953 c22 N68-10 NNON-UK-953 C22 N68-10561 Design data for gas cooled test loop, and inpile capsule facility from mockup reactor experiments NASA-TM-X-1509 Anon-in-A-1509 Analysis and selection of design for plutonium 238 for Brayton cycle space powerplant powerplant NASA-TN-D-4600 REACTOR TECHNOLOGY c03 N68-25829 Critical experiments analysis of uranyl fluoride solution reactors containing large-diameter voided tubes NASA-TN-D-4270 c22 N68-15197 READING Performance comparison of electromechanical and electroluminescent displays in closed loop manual tracking task and reading accuracy tests NASA-TN-D-4841 c05 N68-36457 READOUT 64 inch scattering chamber digital readout and control system for automatic processing of angle and experimental data NASA-TN-D-4324 c14 N68-14018 REAL GASES Real gas wedge-induced laminar separation on cooled blunt flat plate at hypersonic speed NASA-TN-D-4320 c01 N68-17899 nnon-IN-D-4320 Computer program in FORTRAN 4 for calculating shock tube performance for arbitrary equilibrium real gas mixtures NASA-TN-D-4802 SUVEDANE I ANNO-2 RECOVERABLE LAUNCH VEHICLES Structural design synthesis of recoverable launch vehicle structures NASA-CR-1116 c32 N68-28335 Static and dynamic characteristics of wind tunnel model of parallel staged reusable launch vehicle during stage separation NASA-TN-D-4765 RECTANGULAR PANELS c31 N68-36106 Flutter analysis on buckled supported rectangular panels under supersonic surface flow NASA-TN-D-4357 c32 N68-1765: c32 N68-17651 RECTANGULAR PLATES Plane stress analysis using Fourier series of edge stiffened isotropic or orthotropic elastic rectangular plate subjected to prescribed temperature distribution and boundary loads NASA-CR-978 c32 N68-19311 NASA-CR-976 c32 N68-193 REDUCTION (CHEMISTRY) Organic additives and concentration effects on radiation induced reduction of copper salts in aqueous solution Aqueous solution NASA-TN-D-4451 c06 N68-Chromium and nickel powders from reduction of chromium and nickel oxides with magnesium, lithium, or sodium vapors NASA-TN-D-4714 c17 N68c06 N68-19434 c17 N68-30066 NASA-TN-D-4714 cl7 N68-3006 REDUNDANCY ENCODING Logarithmic encoding procedure and error analysis for binary word compression NASA-TN-D-4290 c08 N68-1817 c08 N68-18179 REENTRY Rotation effects on melting ablation on reentry of axisymmetric bodies NASA-TN-D-4614 c33 N68-26650 NADATINUTTOT REENTRY EFFECTS Apollo command module radar cross section decrease due to reentry plasma effects 007 N68-35140 NASA-TN-D-4784 REENTRY GUIDANCE Handling qualities, disturbances and reentry c07 N68-35140 corridor boundaries for spacecraft control system d_psign NASA-CR-945 c32 N68-11133 NASA-CKT-345 REENTRY PHYSICS FORTRAN computer program for calculating model planetary atmospheres and density and temperatue dispersion data for Apollo reentry C30 N68-15 temperatue dispersion data for Apollo reality NASA-TN-D-4292 c30 N68-157 Photographic and spectrometric observation of iron, artificial meteor launched from Trailblazer 2, and reentering at 11 kilometers c30 N68-15793 per second NASA-TN-D-4312 c30 N68-16750 REENTRY SHIELDING Effects of molecular structure on thermochemical properties of phenolic resins and related polymers NASA-TR-R-276 c33 N68-11038 REENTRY VEHICLES Ballistic camera data reduction methods for determining reentry body position, velocity, and deceleration NASA-TN-D-4260 c30 N68-11145 Modified control logic with random-number procedure to determine error effects on range controller of reentry vehicle NASA-TN-D-4317 c21 N68-14732 Aerodynamic and performance characteristics of unpowered rotor reentry vehicle NASA-TN-D-4537 c31 N68-21758 Pressure fluctuation measurements on afterbodies of blunt atmospheric entry vehicles NASA-TN-D-4591 c32 N68-24508 Aerodynamic characteristics of two blunt half cone wedge entry configurations at supersonic speeds NASA-TM-X-1621 c01 N68-30030 REFLECTANCE Reflection coefficient and admittance of circular aperture in ground plane covered by dielectric or plasma slab NASA-CR-1177 c25 N68-35171 Reflectance of wedge angle parallel plate waveguides in transverse electromagnetic mode illuminating reflecting sheet NASA-CR-1174 c07 N68-35172 REFLECTORS Reflectance of wedge angle parallel plate waveguides in transverse electromagnetic mode illuminating reflecting sheet NASA-CR-1174 REFRACTIVITY c07 N68-35172 Temperature and radiation effects on index of refraction and extinction coefficients of Apollo window materials

REFRACTORY MATERIALS

NASA-CR-1019 c31 N68-20467 REFRACTORY MATERIALS Property data of magnetic materials for use in high temperature liquid alkali-metal space power systems NASA-SP-3043 c17 N68-17624 REFRACTORY METAL ALLOYS Creep test data on refractory metal alloys for use in spacecraft power supply systems NASA-CR-1115 c17 N68-29992 Design, fabrication and testing of Cb-1Zr thermal convection loop for evaluation of refractory metals in boiling and condensing potassium environments NASA-CR-1097 c22 N68-35153 REFRACTORY METALS Neutronic calculations of fuel and poison drum control of refractory metal, fast spectrum space power reactors NASA-TN-D-4709 c22 N68-30750 High temperature research on creep rupture alloy composites alloy composites NASA-TN-D-4787 c17 N68-330 REFRIGERATING MACHINERY Design and construction of prototype spacecraft cryogenic refrigerator for infrared detector c17 N68-33684 cooling NASA-CR-988 c23 N68-13115 REGENERATION (PHYSIOLOGY) Bioregenerative life support systems for long duration space flights - Hydrogenomonas biosynthesis and algae photosynthesis processes NASA-SP-165 c04 N68-2620 c04 N68-26207 REGENERATIVE FUEL CELLS Parametric mass analysis and comparison of two reactant cooling and storage units for lunar based hydrogen oxygen regenerative fuel cell system NASA-TN-D-4386 c03 N68-16631 REGENERATORS Recuperator for closed Brayton cycle solar energy space power system NASA-CR-1150 REINFORCED PLATES c03 N68-33062 Stress concentrations in rib-reinforced plates and shells, and effects on structural design NASA-TT-F-427 c32 N c32 N68-10407 REINFORCED SHELLS Stress concentrations in rib-reinforced plates and shells, and effects on structural design NASA-TT-F-427 c32 N68-10407 NASA-TT-F-427 c32 N68-10407 Vibration tests and analysis of thin cylindrical shells with and without longitudinal stiffener: NASA-TN-D-4705 c32 N68-3373 c32 N68-33738 REINFORCING FIBERS Divide deformation and fiber reinforcement in tungsten-urania and tungsten-zirconia elongated into fibers by hot extrusion NASA-TN-D-4475 c17 N68-18610 c17 N68-18610 Interfiber distance and temperature effects on critical aspect ratio in composites NASA-TN-D-4548 c17 N68-22338 NADA-IN-D-4040 Tensile properties of tantalum and tungsten 10-fiber bundles NASA-TN-D-4725 cl7 N66 c17 N68-30504 High temperature research on creep rupture strength of refractory metal fiber and nickel alloy composites NASA-TN-D-4787 c17 N68-33 c17 N68-33684 RELATIVISTIC THEORY Zero density and approximate, relativistic models of universe NASA-TR-R-282 Relativistic velocity c30 N68-20192 Synchrotron emission at helical motion of relativistic electrons emitting from source with relativistic velocity NASA-TT-F-521 RELIABILITY ENGINEERING c25 N68-16700 Design and performance testing of large scale mixed compression axisymmetric inlet at transonic and supersonic speeds NASA-TM-X-1507 c28 N68-17028 Microelectronic device data handbook /text/ NASA-CR-1110 c09 N68-29525 Microelectronic device data handbook /manufacturer and specific device information/ NASA-CR-1111 c09 N68-29526

SUBJECT INDEX

Reliability prediction techniques for single item and multiitem problems NMON-CK-1129 C15 N68-3 Component reliability including selection, specification, verification, review process, parts data sources NASA-CR-1130 C15 N68-3 NASA-CR-1129 c15 N68-31979 c15 N68-31980 Computer applications to practical reliability NASA-CR-1127 Application of testing to hardware programs c15 N68-32760 NASA-CR-1128 c15 N68-32779 REMOTE CONTROL Design and application potentials of general purpose, dexterous, cybernetic machines for human augmentation NASA-SP-5047 c05 N68-18870 RENDEZVOUS GUIDANCE Advanced antenna techniques for rendezvous and lunar landing radar systems NASA-CR-764 c07 N68-28135 RENDEZVOUS TRAJECTORIES Mission constraints and trajectory interfaces for launch, rendezvous, spatial, deorbit, and entry phases of earth orbital mission NASA-CR-1015 c30 N68-20468 Time optimal rendezvous trajectories for variable thrust intercepting and orbiting space vehicles NASA-CR-1036 c30 N68-22202 Quasi-optimal control technique for space vehicle attitude, bounded acceleration rendezvous in free space, and aircraft landing problem NASA-CR-1099 c10 N68-23 c10 N68-28307 REPLICAS Use of surface replication, extraction replication, and thin film electron microscopy in study of microstructures of dispersion strengthened materials NASA-TN-D-4461 c17 N68-18999 REGUTREMENTS Development of mission requirement profile for subsystem components from overall system profile NASA-SP-6503 c30 N68-15683 RESEARCH FACILITIES History of NASA Goddard Space Flight Center through 1963 NASA-SP-4301 c11 N68-30317 Closed loop facility designed to study MHD generator using argon-cesium working fluid NASA-TN-D-4867 RESEARCH PROJECTS c11 N68-37259 NASA university programs in personnel training, aeronautics and space research, and laboratories and research centers NASA-SP-185 c34 N68-35564 RESIDUAL STRESS Residual static strength and slow crack growth behavior of duplex annealed Ti-8A1-1Mo-1V sheet NASA-TN-D-4358 c32 N68-17588 Subsurface residual stress on steel inner races from ball bearings during rolling contact c15 N68-20199 NASA-TN-D-4456 Residual stress effects on fracture strength of AISI 301 stainless steel and Ti-5Al-2.5Sn titanium cracked thin walled cylinders NASA-TN-D-4777 RESISTANCE THERMOMETERS c32 N68-33191 Platinum resistance thermometers tested and evaluated in cryogenic temperature measurement NASA-TN-D-4499 c14 N68-20324 RESISTOJET ENGINES Performance tests of ammonia resistojet thrustor system for various spacecraft control maneuvers NASA-TN-D-4249 c28 N68-10562 Performance test data for ammonia resistojet attitude control system of stable platform satellites NASA-TM-X-1677 c28 N68-36512 RESONANCE Applications of Monte Carlo analysis to tungsten resonance absorption NASA-TN-D-4545 c22 N68-219 Boron 10/neutron, alpha particle/ lithium 7, lithium 7 resonance relative cross sections in c22 N68-21924 keV region NASA-TN-D-4783 c24 N68-33763 RESONANT FREQUENCIES Turbulent boundary layer effect on panel flutter NASA-TN-D-4486 c32 N68-18721

Resonant frequencies and nodal pattern modes of vibrating cylindrical and conical frustum shells NASA-TN-D-4428 c32 N68-20954 Matrix form of equations of motion used in iterative processes for determining normal modes and frequencies of launch vehicles NASA-TN-D-4550 c32 N68-22275 Fitzgeralds piezoelectric disk and theory on audio frequency resonances and sound beams in crystals NASA-TN-D-4625 c23 N68-28259 Prediction of vibration frequencies and modes for free-free truncated conical shells, using Rayleigh-Ritz method NASA-TN-D-4772 c32 N68-33057 RESONANT VIBRATION Limit cycle and control surface resonance characteristics of X-15 stability augmentation system NASA-TN-D-4287 RESPIRATORY RATE c02 N68-11545 Spirometer modification to permit computer reduction of respiratory flow data NASA-TN-D-4234 RESTARTABLE ROCKET ENGINES c14 N68-10057 Successful engine restart in space of upper stage vehicle using cryogenic propellants NASA-TM-X-1649 c31 N68-33683 Flight performance evaluation of Atlas Centaur restart capability in earth orbit c31 N68-33683 NASA-TM-X-1647 c31 N68-35357 RETICLES Celestial attitude measuring instrument using star mapping technique NASA-TN-D-4742 c21 N68-31938 RETINA Design and operating characteristics of electro-optical instrument for tracking of retinal blood vessels in back of eye c05 N68-35109 NASA-CR-1121 RETROREFLECTION Computer analyses of retrodirective, and self adaptive antenna phase control techniques for Mars probe NASA-CR-977 c21 N68-18484 REVIEWING Parts and materials application review for project management of space systems engineering NASA-SP-6505 c15 N68-10120 **REYNOLDS NUMBER** Reynolds number effect on single stage axial flow turbine in air NASA-TN-D-4383 c03 N68-1622 c03 N68-16228 Effects of Reynolds number change on performance of axial flow turbine working in argon NASA-TN-D-4432 c03 N68-1850 c03 N68-18501 RHENTUM Surface roughness effects on normal spectral emittance of vapor deposited rhenium NASA-TM-X-1514 c17 N68-19347 Electrical performance of rhenium nioblum cylindrical thermionic converter NASA-TN-D-4533 c03 N68-21766 RHENIUM ALLOYS Mechanical properties of tungsten and tungsten rhenium alloys NASA-TN-D-4567 c17 N68-24 c17 N68-24477 High temperature tensile properties of tungstenrhenium alloys NASA-TN-D-4728 c17 N68-30605 RIGID ROTORS Critical speed of flexibily mounted rigid rotors in undampened bearings NASA-TN-D-4607 c32 N68-25421 Critical speed analysis of rigid rotors on flexible foundations NASA-TN-D-4858 c15 NG RIGID STRUCTURES c15 N68-37214 Prebuckling deformations, and ring stiffener effects on buckling load of eccentrically stiffened orthotropic cylinders NASA-TN-D-4283 c32 N68 c32 N68-14091 Plane stress analysis using Fourier series of edge stiffened isotropic or orthotropic elastic rectangular plate subjected to prescribed temperature distribution and boundary loads NASA-CR-978 c32 N68-19311

Matrix equations to describe motions of spacecraft consisting of interconnected rigid bodies

NASA-TN-D-4749 c32 N68-33092 RING WINGS Longitudinal aerodynamic characteristics of parasol-wing model at supersonic speeds NASA-TN-D-4855 c01 c01 N68-37854 RIVETED JOINTS High frequency structural damping due to riveted joints associated with gas pumping between overlapping surfaces NASA-CR-954 c32 N68-11489 ROCKET ENGINE DESIGN Specific nuclear light bulb and open-cycle vortex stabilized gaseous nuclear rocket engine designs NASA-CR-1030 c22 N68-22038 Failure mechanisms for specific materials and design concepts for storable propellant rocket engines NASA-TM-X-1463 ROCKET ENGINES c28 N68-22272 Experimental, and theoretical evaluations of acoustic liners for screech suppression in rocket engines NASA-TN-D-4442 c28 N68-1824 Relative erosion resistance of ablative materials for nozzle sections of storable-propellant c28 N68-18249 rocket engine NASA-TM-X-1559 c28 N68-19708 Divergent-flow contact-lonization electrostatic thrustor for satellite attitude control and stationkeeping NASA-TN-D-4420 ROCKET LAUNCHING c28 N68-20187 Effect of liftoff dynamics on launch vehicle stability and control NASA-CR-943 c32 N68 c32 N68-10233 ROCKET LININGS Experimental, and theoretical evaluations of acoustic liners for screech suppression in rocket engines NASA-TN-D-4442 c28 N68-18249 Hydrogen-oxygen rocket engine used to test acoustic liner with isolated resonators and variable cavity depths NASA-TN-D-4492 c33 N68-21680 BOCKET NOSE CONES Aerodynamic heating, delamination and pressure in nose fairing honeycomb core of Atlas Centaur launch vehicle NASA-TM-X-1605 c33 N68-28156 Nose shape and fin geometry effects on static stability of sounding rocket models in supersonic wind tunnel NASA-TM-X-1661 c01 N68-36509 ROCKET NOZZLES Aeroelastic instability of overexpanded rocket nozzle extensions NASA-TN-D-4471 c32 N68-21099 ROCKET SOUNDING Nike Apache pitot tube rocket sounding measuring of Southern Hemisphere stratosphere and mesosphere along west coast of South America NASA-TN-D-4264 c20 N68-2 c20 N68-25617 Meteorological rocket soundings in stratosphere and mesosphere, 1966 - tables NASA-TR-R-288 c20 N68-33036 ROCKET THRUST Coaxial injector thrust effects on combustion stability of hydrogen-oxygen rocket engine NASA-TN-D-4851 c28 N68-ROCKET VEHICLES c28 N68-36515 Historical survey of Russian rocketry and space exploration NASA-TT-F-426 c31 N68-22 c31 N68-22262 ROCKETS History of Russian solid fuel rocketry NASA-TT-F-415 c28 N68-11829 ROCKS Silicate rocks as simulators for study of genetic states of lunar surface rocks NASA-CR-1081 c30 N68-26689 RODS One dimensional, steady state heat exchange by both convection and radiation between rods or fins and their surroundings NASA-TN-D-4257 c33 N68-14052 ROLL Flight simulator to evaluate lateral-directional handling qualities of piloted reentry vehicles NASA-TN-D-4410 c31 N68-19226

ROLLER BEARINGS

ROLLER BEARINGS Reduced pressure effects on fatigue life of roller steel ball bearings with mineral oil lubricants NASA-TN-D-4348 c15 N68-15010 ROLLING CONTACT LOADS Reduced pressure effects on fatigue life of roller steel ball bearings with mineral oil lubricants NASA-TN-D-4348 ROOM TEMPERATURE c15 N68-15010 Performance of centrifugal pump impeller in room temperature water NASA-TN-D-4613 c12 N68-26651 ROTARY STABILITY High revolutions per minute rotor stability of herringbone-grooved gas-lubricated journal bearings NASA-TN-D-4440 c15 N68-21965 ROTARY WINGS Planform design method, general characteristics, and aeroelastic stability of flexible lifting rotors NASA-TN-D-4465 NAGA IN 59-4405 Soviet engineering handbook on vibration and dynamic stability theory and calculations in helicopter design NASA-TT-F-519 c02 N68-23 c02 N68-23456 Tabulated performance data of full-scale rotary wings at high advance ratios and advancing tip Mach numbers based on wind tunnel tests NASA-TN-D-4632 c01 N68-28268 Review of blade slap studies for determining noise in helicopters NASA-CR-1221 c02 N68-37932 ROTATING DISKS Magnetohydrodynamic flow of incompressible viscous electrically conducting fluid over rotating disk NASA-CR-989 c25 N68-14078 ROTATING ENVIRONMENTS Boiling heat transfer coefficients, interface behavior, and vapor quality in heated wall rotating boilers with continuous through-flow of water as test fluid NASA-TN-D-4136 c33 N68-175 c33 N68-17566 ROTATING GENERATORS Performance tests of rotating gas jet generator for strong traveling transverse acoustic modes NASA-TN-D-4380 c12 N68-165 c12 N68-16998 ROTATION Vector representation of rotations and their algebra NASA-TN-D-4696 ROTOR AERODYNAMICS c19 N68-30594 Aerodynamic and performance characteristics of unpowered rotor reentry vehicle NASA-TN-D-4537 c31 N68-21758 Tabulated performance data of full-scale rotary wings at high advance ratios and advancing tip Mach numbers based on wind tunnel tests NASA-TN-D-4632 col N68-282 c01 N68-28268 ROTOR BLADES (TURBOMACHINERY) Turbolet engine noise reduction by increasing intake system guide vane-rotor blade spacing NNON-IN-U-4690 Performance of single stage turbine with rotor blade surface diffusion factor of 0.3 NASA-CR-1172 ROTORS Rotor-hub bending moment measurements on hingeless rotor helicopter during abrupt maneuvers near ground NASA-TN-D-4574 ROUND TRIP TRAJECTORIES c02 N68-24499 Trajectory data for stopover missions to Mars that employ Venus swingby mode NASA-SP-35, PT. 6 c30 N68c30 N68-30098 RUBY LASERS Particle acceleration by evaporation pressure using Q-switched laser beam NASA-CR-927 c16 N68-RUNGE-KUTTA NETHOD c16 N68-10467 Quadrature methods of formulating Runge-Kutta equations NASA-TR-R-275 c19 N68-10121 Multi-step Runge-Kutta methods using method of quadratures NASA-TN-D-4400 c19 N68-21100 Shapes of liquid drops resting on flat surfaces determined by Runge-Kutta solution of Laplace

SUBJECT INDEX

capillary equation NASA-TN-D-4779 c12 N68-33165 Runge-Kutta formulas of high order with stepsize control through leading truncation error term NASA-TR-R-287 c19 N68-36753 RUNWAY CONDITIONS Runway surface texture conditions effect on wet runway braking friction coefficients created by aircraft tires NASA-TN-D-4323 c02 N68-14903 RUNWAYS Dynamic hydroplaning, viscous hydroplaning, and tire tread rubber reversion effects on tire traction on wet runways NASA-TN-D-4406 c02 N68-19620 RUTILE Microwave pump requirements for field operational broadband rutile traveling wave maser for Applications Technology Satellite program NASA-TN-D-4764 c16 N68-33635 S SAMPLERS Air samplers, contamination, and sterilization in collection of microorganisms for microbiological exploration of stratosphere NASA-CR-1101 SATELLITE ATTITUDE CONTROL c04 N68-28247 Simple processors of star tracker commands for stabilizing inertially oriented satellite NASA-TN-D-4490 c21 N68-1 c21 N68-19236 Divergent-flow contact-ionization electrostatic thrustor for satellite attitude control and stationkeeping NASA-TN-D-4420 c28 N68-2018 Quasi-optimal control technique for space vehicle c28 N68-20187 attitude, bounded acceleration rendezvous in free space, and aircraft landing problem NASA-CR-1099 c10 NG c10 N68-28307 NASA-TN-D-4637 C21 N68 c21 N68-28418 Performance test data for ammonia resistojet attitude control system of stable platform satellites NASA-TM-X-1677 SATELLITE CONTROL c28 N68-36512 Altitude of orbiting spacecraft corrected by thrustor firing time control system NASA-TN-D-4519 c31 N68 c31 N68-21260 SATELLITE DESIGN Equipment, instrumentation, communications, design, launch vehicles, and guidance of scientific satellites NASA-SP-133 C31 N6 c31 N68-14965 SATELLITE GUIDANCE Two body problem for satellite guidance, flight mechanics, and trajectory optimization analyses NASA-CR-1002 c30 N68-1408 c30 N68-14089 NASA-SP-133 Non-ck-1002 Calibration communications, design, launch vehicles, and guidance of scientific satellites NASA-SP-133 C31 NG c31 N68-14965 Guidance, flight mechanics, and trajectory optimization c30 N68-21685 NASA-CR-1004 Design, mission, flight operations, experiment data, and subsystem performances for Lunar Orbiter 4 extended mission NASA-CR-1092 c31 N68-28997 RADA-UK-1092 C31 NG SATELLITE INSTRUMENTS Equipment, instrumentation, communications, design, launch vehicles, and guidance of scientific satellites NASA-SP-133 C31 NG CATELITE LINEARD c31 N68-14965 SATELLITE LIFETIME Analytical method artificial satellite lifetime determination NASA-TN-D-4281 SATELLITE OBSERVATION c30 N68-11754 Cumulus cloud and fog bank spectral reflectance observations using Nimbus satellites and infrared radiometers NASA-TN-D-4552 SATELLITE ORBITS c14 N68-25862 Lie series applications to celestial mechanics, accelerators, satellite orbits, and optimization NASA-CR-1046 c19 N68-25841

SEMICONDUCTORS (MATERIALS)

c01 N68-37365

NASA-TN-D-4844

Artificial satellite motion under influence of planar and Keplerian force fields NASA-TN-D-4622 c30 N68-28113 Dynamic characteristics of satellites having long elastic members by modeling as symmetric double beam system NASA-TN-D-4576 c31 N68-31978 SATELLITE ROTATION Spin axis for spinning satellite determined from range rate data NASA-TN-D-4483 c30 N68-211 c30 N68-21182 Rotation effects on melting ablation on reentry of axisymmetric bodies NASA-TN-D-4614 c33 N68-26650 SATELLITE TELEVISION Nimbus 2 and ESSA 3 satellite observation photographs of typhoon Marie NASA-TN-D-4757 c20 N68-37869 SATELLITES Equipment, instrumentation, communications, design, launch vehicles, and guidance of scientific satellites NASA-SP-133 SATURN LAUNCH VEHICLES c31 N68-14965 UNN LAUNCH VEHICLES Development, ground tests, and flight performance of cryogenic nitrogen storage system for low gravity operation during Apollo-Saturn space flight NASA-TN-D-4293 SATURN 1 LAUNCH VEHICLES c23 N68-15950 Automatic testing and checkout of Saturn 1 launch vehicles NASA-TN-D-4328 c31 N68-SATURN 1B LAUNCH VEHICLES Small water-graphite nuclear rocket stages compared with chemical upper stages for use in unmanned spacecraft NASA-TN-D-4827 c22 N68c31 N68-15570 c22 N68-35073 NASA-IN-J-toc; SATURN 5 LAUNCH VEHICLES Piloted simulation studies of Saturn 5 launch vehicle manual backup guidance and control NASA-NASA-TN-D-4481 c21 N68-19061 Fully-manual and augmented-manual control systems for Saturn 5 booster studied by emperically based mathematical models for pilot NASA-CR-1079 c31 N68-28426 SCALE MODELS Wind tunnel study of scale model automobile ground plane boundary layer using moving-belt ground plane technique NASA-TN-D-4229 col N68-10 c01 N68-10093 Design, and evaluation of birefringent wave filter scale model for millimeter wavelengths radio astronomy NASA-CR-979 c09 N68-13617 Thermodynamic effects on Freon cavitation on venturi scale model NASA-TN-D-4387 c12 N68-15329 Wind tunnel study of lateral and directional aerodynamic characteristics of powered four-duct propeller VTOL scale model in transition NASA-TN-D-4343 co2 N c02 N68-17023 Low speed static and dynamic stability tests on scale model of double-delta supersonic commercial air transport configuration NASA-TN-D-4179 c02 c02 N68-18250 Aerodynamic characteristics of large-scale model of tilt-wing V/STOL aircraft NASA-TN-D-4493 col N68-203 c01 N68-20370 Laboratory scale model technique for investigating pneumatic tire hydroplaning NASA-CR-1074 c11 N68-23357 Full scale lunar gravitation simulator and 1/6 scale model NASA-TN-D-4474 c11 N68-25853 Aerodynamic characteristics of scale model with augmented jet flap NASA-TN-D-4610 c01 N68-25 c01 N68-25919 Exhaust gas ingestion characteristics and induced aerodynamics for vertical takeoff lift engine fighter model in ground proximity NASA-CR-1098 c02 N68-28 c02 N68-28233 Lunar module scale model study of use of soft side legs for improved touchdown stability of legged legs for improved touchdown stability of legged landing vehicles NASA-TN-D-4680 c31 N68-29962 Wind tunnel tests to determine low speed high lift aerodynamics of one-fifth scale variable sweep supersonic transport model

SCALING LAWS Scale factors verification for parawing opening characteristics using experimental drop tests NASA-TN-D-4665 c02 N68-31956 Dimensional analysis, and similitude and scaling laws for structural dynamics model testing of spacecraft dynamic stability NASA-CR-1195 c32 N68-35632 SCALLOPING Stress analysis and functions in membrane analysis of scalloped thin walled shells like parachutes NASA-TN-D-4687 c32 N68-28832 SCATTERING COEFFICIENTS Computer program for calculating normalized Mie scattering functions NASA-CR-1022 c24 N68-21227 SCIENTIFIC SATELLITES Data collection and processing from space science c24 N68-21227 satellites NASA-TN-D-4508 c08 N68-22510 Objectives of investigators associated with multiple experiment scientific satellites NASA-TN-D-4731 c34 N6 c34 N68-33682 Computer programming for control of complex data processing operations involved in analysis and interpretation of large volumes of sensor data from scientific satellites NASA-CR-1107 c08 N68-37254 SCINTILLATION COUNTERS Detection of supernovae pulse by gamma ray telescope and atmospheric scintillation method NASA-TN-D-4732 c29 N68-333 c29 N68-33370 SCREEN EFFECT Dielectric formulation for inhomogeneous electron gas, and Green function formalism for treating static dielectric screening of point impurity in electron gas NASA-TR-R-283 c26 N68-24273 SECONDARY INJECTION Vortex valve for hot gas flow modulation in secondary injection thrust vector control system NASA-CR-1091 c28 N68-28112 SEISHOGRAPHS Measurement and interpretation of ground vibrations, produced by seismic effect of sonic boom NASA-CR-1137 c13 N68-35151 SELECTION Component reliability including selection, specification, verification, review process, parts data sources NASA-CR-1130 SELF ADAPTIVE CONTROL SYSTEMS c15 N68-31980 Computer analyses of retrodirective, and self adaptive antenna phase control techniques for Mars probe NASA-CR-977 SELF LUBRICATING MATERIALS c21 N68-18484 Friction torque of ball bearings in vacuum to determine lubricating capability of polytetrafluoroethylene-composition retainer materials NASA-TN-D-4355 c15 N68-16468 Friction and wear in cryogenic liquids for phenolic and polytetrafluoroethylene composites of various particle sizes and concentrations NASA-TN-D-4565 c15 N68-2 c15 N68-24142 SEMICONDUCTING FILMS Electron microscopy of electron beam irradiated amorphous silicon, germanium, and cadmium sulfide semiconductor films NASA-TN-D-4522 c26 N68-20 c26 N68-20295 SEMICONDUCTOR DEVICES Automated Hall effect and resistivity apparatus for studying electrical transport properties of semiconductors c03 N68-10103 NASA-TM-X-1464 Breadboard three-phase static switch for space alternating current power systems NASA-TM-X-1495 c09 N68-15649 Fabrication and development of annular lithium drifted germanium detector for studying nuclear reaction gamma rays NASA-CR-1138 cl4 N68 SEMICONDUCTORS (MATERIALS) Current-voltage characteristics of tunneling p-n junctions in semiconductors NASA-TN-D-4403 c09 N68 c14 N68-35152 c09 N68-19062

SENSORIMOTOR PERFORMANCE

Gallium arsenide laser modulator, attenuation coefficients, and semiconductors for optical communication systems NASA-TN-D-4608 SENSORIMOTOR PERFORMANCE c23 N68-25868 Heat stress and prolonged activity effects on human perceptual motor performance NASA-CR-1153 c05 N68-SEPARATED FLOW c05 N68-31480 Static pressure and flow field for flat plate model with short trailing-edge flap NASA-TN-D-4308 c12 N68-17376 Integral methods for predicting afterbody heat transfer to blunt two dimensional configuration subjected to separated flow c12 N68-28282 NASA-TN-D-4443 Laminar flow separation on flat plate induced by deflected trailing-edge flap at hypersonic speed NASA-TN-D-4671 c01 N68-29405 SEPARATORS Electrode design, inorganic separators, and performance tests of multiplate five ampere-hour silver-zinc battery cell NASA-CR-965 c03 N68-16321 SERIES (MATHEMATICS) Formula for expanding higher order derivatives of function tanh z in powers of tanh z and A-numbers NASA-TN-D-4296 c19 N68-14077 SERVICE LIFE Improved service life through reduction of self discharges in copper oxide-magnesium thermal cells NASA-TN-D-4306 c03 N68-20344 Very high burnup vapor transport fuel pin concept for long life nuclear reactors NASA-TN-D-4860 c22 N68-3720 c22 N68-37209 SERVOCONTROL Servocontroller for programming atomic emission and sample vaporization in direct current arc spectrochemical analysis NASA-TN-D-4769 c06 N68-31 c06 N68-31948 SERVOMECHANISMS Design and application potentials of general purpose, dexterous, cybernetic machines for human augmentation NASA-SP-5047 c05 N68-18870 Precision tilt and vibration isolation system design NASA-TR-R-281 c14 N68-19642 SEXTANTS Factors affecting design and use of photographic sextant for space navigation NASA-TN-D-4285 c21 N68-11902 Navigator performance using hand held sextant to measure angle between moving flashing light and simulated star - space navigation NASA-TN-D-4174 c2 c21 N68-13558 Astronaut performance using manually hand-held sextants for midcourse navigation phases of manned space flight NASA-TN-D-4449 c21 N68-21123 Mechanical, optical, and electrical characteristics of hand-held sextant for space flight NASA-TN-D-4585 c21 N68-24512 Telescope objective lens size, aperture size, and magnification effects on operator performance using marine sextants c21 N68-33006 NASA-TN-D-4781 Effects of irradiation and star magnitude on sextant sighting performance NASA-TN-D-4780 SHAPED CHARGES c21 N68-33456 Pyrotechnic shaped charge aerospace vehicle stage and shroud separation systems development NASA-TM-X-1607 c31 N68-2886 c31 N68-28869 SHAPES Shapes of liquid drops resting on flat surfaces determined by Runge-Kutta solution of Laplace capillary equation NASA-TN-Q-4779 c12 N68-33 NHON-IN-U-4779 c12 N68-3 Nose shape and fin geometry effects on static stability of sounding rocket models in supersonic wind tunnel NASA-TM-X-1661 c01 N68-3 c12 N68-33165 c01 N68-36509 SHARP LEADING EDGES Sharp edge delta wing drag prediction by application of leading edge suction analogy of

SUBJECT INDEX

vortex lift NASA-TN-D-4739 c01 N68-31990 SHEAR FLOW Stability of shear flow with density gradient and viscosity c12 N68-15530 NASA-CR-958 SHEAR LAYERS Analysis of turbulent wall pressure field under supersonic shear layers NASA-CR-888 c12 N68-22087 SHEAR STRAIN Analysis of shear and normal strain effects on weak turbulence and turbulent heat transfer using two point correlation equations obtained from Navier-Stokes and energy equations NASA-TN-D-4273 SHELL STABILITY c33 N68-11491 Dynamic stability of thin walled elastic shells and applications to space vehicle control problems NASA-CR-949 c32 N68-23453 Liapunov method used to obtain sufficient conditions for buckling stability of long cylindrical shells with random imperfections NASA-CR-1161 c32 N68-3 c32 N68-33419 SHELLS (STRUCTURAL FORMS) Computer program for analysis of shells of revolution with axisymmetric loading NASA-CR-1051 c32 N68-23355 NASA-CR-1051 Numerical results of buckling of shells of revolution for computer program NASA-CR-1049 c32 N68-24481 Elastic buckling equations for calculating plastic buckling of plates and shells under biaxial loading NASA-TN-D-4706 c32 N68-31946 SHOCK LAYERS Integer relations method of determining inviscid shock layer flow and pressure distributions over blunt bodies NASA-TN-D-4397 c01 N68-157 c01 N68-15778 SHOCK LOADS Flight test of 30 foot nominal diameter cross parachute to measure shock loads, drag efficiency, and stability characteristics NASA-TM-X-1542 c31 N68-2177 Flight test of 10-foot nominal-diameter disk-gap c31 N68-21778 band parachute to determine deployment and inflation, opening shock loads, drag efficiency, and stability characteristics NASA-TM-X-1575 c02 N68-24245 SHOCK SIMULATORS Awakening and startle effects of simulated sonic booms NASA-CR-1193 c04 N68-33005 SHOCK TUBES Implosively accelerated shock tube driver for use in high energy gas dynamics research NASA-CR-950 c c12 N68-10646 NASA-TT-F-505 C12 N68-100 Physical gas dynamics research - molecular band spectra, shock tube studies, and interactions between diatomic molecules NASA-TT-F-505 c12 N68-160 c12 N68-16839 Shock expansion tube characteristics and use as sonic boom simulator NASA-CR-1055 c11 N68-24966 Boundary layer buildup effects in shock tubes on dissociation rate measurements NASA-TN-D-4795 c12 N68-34089 NNSA-IN-D-4/30
 C12 N68-34089
 Computer program in FORTRAN 4 for calculating shock tube performance for arbitrary equilibrium real gas mixtures
 NASA-TN-D-4802
 C11 N68-35466
 SHOCK WAVE INTERACTION Breakup, and displacement of liquid jets in crossflow of shock tube NASA-TN-D-4334 c33 N6 c33 N68-15942 SHOCK WAVE PROFILES Wind tunnel tests on pressure distribution, and shock shapes of conical blunted bodies moving at supersonic speeds in nitrogen, or helium media NASA-TN-D-4314 col N68-178 c01 N68-17896 SHOCK WAVE PROPAGATION Implosively accelerated shock tube driver for use in high energy gas dynamics research MADA-CK-950 cl2 N68-10646 Theory of finite amplitude waves in fluid-filled elastic tubes, including wave distortion, shock wave propagation, and Korotkoff sounds

NASA-TN-D-4803 c12 N68-33056 Conference on sonic boom reduction in supersonic transport flight - shock wave propagation and refraction, prediction methods for acoustic attenuation, and aerodynamic engineering aspects NASA-SP-180 c02 N68-34907 NASA-SP-180 SHOCK WAVES Enthalpy, temperature, and density charts for equilibrium isentropic expansion of air behind shock waves for wide range of velocities and altitudes NASA-TN-D-4247 c33 N68-11144 Results of including boundary shock wave in calculation of flight parameters of large high speed meteor NASA-TN-D-4325 c12 N68-18997 Relationship of shock standoff distance, at sonic and stagnation points, to body geometry of blunt bodies at zero angle of attack NASA-TN-D-4539 c01 N68-21941 Optical radiation measurements behind shock wave in simulated Mars atmosphere NASA-TM-X-1634 SHORT TAKEOFF AIRCRAFT Wind tunnel tests of deflected slipstream cruise c12 N68-32982 fan V/STOL aircraft wing NASA-TN-D-4262 c01 N68-11036 Economic and suitability comparison of short haul transport aircraft concepts NASA-CR-986 c02 N68-13517 Wind tunnel determination of longitudinal force with varying wing aspect ratios NASA-TN-D-4448 c02 N68-187 c02 N68-18771 Wing surface pressure data from large scale wind tunnel tests of propeller driven short takeoff aircraft NASA-TM-X-1527 c02 N68-19065 SHROUDED NOZZLES Wind tunnel model tests of variable flap ejector nozzle with aerodynamically positioned shroud c28 N68-30599 NASA-TM-X-1639 Effects of shroud geometry on performance of collapsible plug nozzle at Mach numbers from to 2.0 NASA-TM-X-1657 c01 N68-36132 SHROUDS Pyrotechnic shaped charge aerospace vehicle stage and shroud separation systems development NASA-TM-X-1607 c31 N6 c31 N68-28869 SHUTDOWNS Postshutdown cooling requirements of tungsten water moderated nuclear rocket engines NASA-TM-X-1568 c22 N68-2 c22 N68-21111 SIDESLIP Flight simulator to evaluate lateral-directional handling qualities of piloted reentry vehicles NASA-TN-D-4410 c31 N68-19226 NASA-TN-D-4410 c31 N Sideslip angle effects on static stability characteristics of T tail transport configuration NASA-TM-X-1665 c01 N68-36112 SIGMA 7 Description and performance analysis of manned six-pass orbital mission /Mercury-Atlas 8/ NASA-TN-D-4807 c31 N68-35022 SIGNAL ANALYSIS Laboratory methodology of signal analysis with application to Apollo program NASA-TM-X-1599 c08 Rapid reduction method of rhythm and rate c08 N68-30240 information in large scale electrocardiogram monitoring NASA-TN-D-4751 c05 N68-32100 SIGNAL ANALYZERS Signal conditioning methods and equipment used for inflight recording of pilot biomedical data NASA-TN-D-4487 co5 N68-21538 NASA-TN-D-4487 SIGNAL DETECTION NAE DELECTION Statistical tests for signal detection and correlation coefficients NASA-TR-R-273 c10 N c10 N68-11789 Electron paramagnetic resonance signals from paramagnetic sample in microwave bridge NASA-TN-D-4469 c14 N68-21169 Optical communications - maximum likelihood detection of M-ary Poisson processes in background of additive Poisson noise NASA-TN-D-4623 c07 N68-29528

Error probabilities for maximum signal detection in presence of Poisson noise NASA-TN-D-4721 c07 N68-36105 SIGNAL DISTORTION Waveform distortion in maximum likelihood Darlington detector for M-ary pulse frequency modulation signals NASA-TN-D-4294 SIGNAL ENCODING c07 N68-18542 Performance evaluation of several convolutional and block codes with threshold decoding for space telemetry NASA-TN-D-4402 c07 N68-181 Frequency coded threshold logic unit for pattern recognition systems based on central nervous c07 N68-18178 sustem NASA-CR-1035 c05 N68-22448 SIGNAL PROCESSING Resolution limit analysis for pulse frequency modulation telemetry processing line NASA-TN-D-4180 c07 N68-18247 SIGNATURES Design of bodies to produce specified sonic boom signatures NASA-TN-D-4704 c01 N68-31484 SILICATES Silicate rocks as simulators for study of genetic states of lunar surface rocks NASA-CR-1081 c30 N68-26689 Silicate surface preparation to represent lunar soil, and ultrahigh vacuum adhesion measurements NASA-CR-1090 c30 N68-28373 SILICON Techniques for, and applications of preferential etching of crystal surfaces to produce optical reflections for crystal orientation and optical alignment in silicon crystals NASA-TN-D-4187 c23 N68-10354 Spectral emissivity of highly doped silicon NASA-TN-D-4303 c26 N68-21708 Oxidation resistance and ductility of cobalt heat resistant alloys optimized by restriction of silicon and manganese content NASA-TN-D-4715 c17 N69-20051 Electron paramagnetic resonance of lithium silicon NASA-TR-R-290 c26 N68-33228 c26 N68-33228 SILICON COMPOUNDS Parametric analysis of radioisotope cascaded thermoelectric generators with Si-Ge first stage and PbTe second stage NASA-TM-X-1501 c22 N68-14585 Effective volume power density analysis for radioisotope power generator with silicon germanium thermoelectric elements NASA-TM-X-1453 co3 NG c03 N68-14630 SILICON CONTROLLED RECTIFIERS Reliability of silicon rectifiers as inverters for alternating current power source for Atlas Centaur launch vehicles NASA-TM-X-1569 c03 N68-215 c03 N68-21562 SILICON DIOXIDE Reactor irradiation effects on optical absorption levels in fused silica NASA-CR-1032 c22 N68-23481 Charge storage in silicon dioxide resulting from electron irradiation NASA-CR-1088 c26 N68-26603 Spectral transmission measurements on fused silica during and after exposure to pulsed neutron irradiation NASA-CR-1191 c22 N68-35826 SILICON JUNCTIONS

 SILICUN JUNCTIUNS

 Defect energy levels and concentrations for proton

 irradiated, n-type silicon single crystals

 NASA-TN-D-4830
 c26 N68-37051

 SILICON NITRIDES

 Pyrolytic silicon nitride dielectric for

 integrated circuits

 NASA-CR-995

 c18 N68-18849

 SILICON RADIATION DETECTORS High energy proton damage in silicon surface barrier detectors barrier detectors NASA-TN-D-4528 c26 N68-24660 SILVER ZINC BATTERIES Electrode design, inorganic separators, and performance tests of multiplate five ampere-hour silver-zinc battery cell NASA-CR-965 c03 N68-16321

Effects of freezing-melting cycles on primary

SIMILARITY THEOREM

silver oxide zinc batteries NASA-TM-X-1681 SIMILARITY THEOREM c03 N68-37265 Similarity solution for turbulent mixing between jet and faster moving coaxial stream NASA-TN-D-4441 c12 N68-1924 c12 N68-19246 SIMILITUDE LAW Dimensional analysis, and similitude and scaling laws for structural dynamics model testing of spacecraft dynamic stability NASA-CR-1195 c32 N68-35632 SIMULATORS Shock expansion tube characteristics and use as sonic boom simulator NASA-CR-1055 c11 N68-24966 SINE WAVES Effect of two dimensional multiple sine wave protrusions on pressure and heat transfer distributions for flat plate in hypersonic flow NASA-TN-D-4437 c01 N68-19063 SINGLE CRYSTALS Anomalous non-Hookean deformation of ionic single crystals NASA-TN-D-4513 c26 N68-22271 Adsorbed surfactants influence on deformation and friction coefficient of lithium fluoride single crystals during sliding friction NASA-TN-D-4716 c15 N68-29918 Ultrasonic attenuation measurements on single tantalum crystals at superconducting state NASA-TN-D-4806 c26 N68 c26 N68-35356 SINGLE-PHASE FLOW Film boiling mist flow heat transfer using single phase variable property NASA-TN-D-4149 c33 N68-11636 SKID LANDINGS Dynamic hydroplaning, viscous hydroplaning, and tire tread rubber reversion effects on tire traction on wet runways NASA-TN-D-4406 c02 N68-19620 SLEEP DEPRIVATION Awakening and startle effects of simulated sonic booms NASA-CR-1193 404 N68-33005 SLENDER BODIES Nonlinear lift and pressure distribution of slender conical bodies with strakes at low speed NASA-CR-1202 col N68-37255 SLENDER CONES Free flight aerodynamic characteristics of slender cone at hypersonic speeds NASA-TN-D-4245 c01 N68-103 Variational calculus used in obtaining lift drag c01 N68-10380 ratio attainable by slender conical body at hypersonic speeds NASA-CR-1156 c01 N68-33451 SLIDING FRICTION Crystal transformation and atomic ordering on wear and sliding friction in two cobalt alloys NASA-TN-D-4668 c15 N68-2826 Adsorbed surfactants influence on deformation and c15 N68-28260 friction coefficient of lithium fluoride single crystals during sliding friction NASA-TN-D-4716 c15 N68-29918 SLITS Iterative solution for calculating deformation and stress concentration near slits in elastic-plastic solids NASA-TN-D-4717 c32 N68-30045 SLOT ANTENNAS Quasi-ommidirectional resonant array of circumferential shunt slots in ring waveguides for narrow bandwidth space vehicle applications at microwave frequencies NASA-TN-D-4362 c07 N68-18616 Dieletric clad axial slot antennas NASA-CR-1057 c07 N68-26621 Plasma effects in antenna near zone field admittance and ionization rise time measurements on Teflon-plugged waveguide slot antenna NASA-CR-1149 SLOTTED WIND TUNNELS c07 N68-33042 Aerodynamic characteristics of subsonic cargo jet transport model in slotted transonic wind tunnel NASA-TM-X-1660 col N68-35617 SMOKE TRAILS Wind velocity profiles measured by smoke trail method at Wallops Island, Va., in 1963 and

I-90

SUBJECT INDEX

1964 NASA-TN-D-4365 c20 N68-17024 SNAP 8 Contaminant controls and cleaning procedures in SNAP-8 simulation loop of liquid metals NASA-TM-X-1432 c17 N68-11 c17 N68-11912 SNAP 8 simulator using primary sodium-potassium loop, mercury loop operating on Rankine cycle, and heat rejection sodium-potassium loop NASA-TM-X-1515 c11 N68-18460 SNAP 8 simulator facility instrumentation NASA-TM-X-1525 cl4 c14 N68-19001 Primary loop transients during startup of Rankine cycle space power system in SNAP 8 simulator NASA-TN-D-4546 c03 N68-2225 c03 N68-22257 Effects of nuclear radiation on performance of diodes for use in SNAP 8 NASA-TN-D-4620 c09 N68-26662 SODIUM Cover gas pressures affecting accelerated cavitation damage in sodium c17 N68-10104 NASA-TN-D-4235 Neutron activation analysis of sodium, lithium, and potassium in compact fast reactors and its effect on shielding NASA-TM-X-1512 c22 N68-203 c22 N68-20355 SODIUM CHLORIDES Warm fog and fog modification by seeding with salt particles NASA-CR-1071 c20 NASAc20 N68-25816 SOLAR CELLS Equations, charts, and analysis to calculate theoretical temperatures of thin film solar cells in earth orbit NASA-TN-D-4331 c33 N68-14270 Design and performance of two vacuum chambers and solar-radiation simulators for solar-cell research NASA-TM-X-1503 c11 N68-16695 Effects of 22 MeV proton and 2.4 MeV electron radiation on boron and aluminum doped silicon solar cells NASA-TN-D-4407 c26 N68-19924 Construction and performance of active cadmium sulfide thin film solar cell arrays NASA-TM-X-1519 c03 N68-20432 NASA-TM-X-1519 Cook Not 2000. Stainless steel penetration detector, impact detector, and solar cell degradiation, to study micrometeoroid impact damage and puncture rate, and radiation effects on Explorer 23 satellite The Cook State S NASA-TN-D-4284 c31 N68-28198 Thermal radiative and electrical properties of cadmium sulfide solar cell at low simulated solar intensities and temperatures NASA-TN-D-4818 a03 N68-35467 Comparison between cemented and soldered cover glass for radiation protection of silicon solar cells NASA-TM-X-1687 c03 N68-37935 SOLAR COLLECTORS Parametric analysis of effects of concentrator surface errors and rim angle, collection system orientation error, and receiver temperature on paraboloid solar collector thermal efficiency NASA-TN-D-4415 c03 N68-18998 Geometric properties of expandable whirling membrane solar energy concentrator used in conjunction with electrical conversion systems for spacecraft auxiliary power units NASA-TN-D-4532 c03 N68-2225 c03 N68-22258 SOLAR CORONA Infrared observations of outer solar corona at Wavelength of 22 microns NASA-CR-969 SOLAR COSMIC RAYS c30 N68-20353 Energetic space radiation and galactic cosmic radiation measured for radiation hazards in manned space flight NASA-TN-D-4404 c29 N68-16837 SOLAR CYCLES Polar cap absorption study of solar cycle variation in solar proton emissions from sun NASA-TN-D-4473 c29 N68-25880 SOLAR ENERGY ABSORBERS Titanium alloy honeycomb with blackened walls as absorber of solar energy NASA-TN-D-4727 c03 N68-30751 SOLAR FLARES Computer program using Monte Carlo methods for

simulating solar flares during interplanetary space flight NASA-TN-D-4311 SOLAR GENERATORS c29 N68-16008 Lunar surface layer considered to store solar energy for generating power during lunar night NASA-TN-X-1560 c03 N68-20363 SOLAR PHYSICS Advances during 1966 in astronomy, exobiology, ionospheric sciences, radio and solar physics, and planetary atmospheres and planetology NASA-SP-155 c30 N68-15748 SOLAR PROTONS Polar cap absorption study of solar cycle variation in solar proton emissions from sun NASA-TN-D-4473 c29 N68-25880 SOLAR RADIATION Radiative thermal energy incident effects on pressure-suited man on lunar surface NASA-TN-D-4243 c30 N68 c30 N68-11630 Radiation hazards on extended manned space flights NASA-CR-1037 Carbon dioxide model for radiation heating and cooling functions of lower stratified Martian c29 N68-22849 atmosphere in thermodynamic equilibrium NASA-CR-1044 c30 c30 N68-22860 SOLAR RADIO BURSTS Polar cap absorption study of solar cycle variation in solar proton emissions from sun NASA-TN-D-4473 c29 N68-2 SOLAR REFLECTORS c29 N68-25880 Ultraviolet-proton radiation effects on solar concentrator reflective surfaces NASA-CR-1024 c17 N68-23560 SOLAR SIMULATION Solar simulation testing of anchored interplanetary monitoring platform D thermal design and protective coating NASA-TN-D-4112 c33 N68-1 c33 N68-10299 Thermal radiative and electrical properties of cadmium sulfide solar cell at low simulated solar intensities and temperatures NASA-TN-D-4818 SOLAR SIMULATORS c03 N68-35467 Design and performance of two vacuum chambers and solar-radiation simulators for solar-cell research NASA-TM-X-1503 c11 N68-16695 Spectroradiometer and technique for measuring spectral irradiance of solar simulators NASA-TN-D-4822 c14 c14 N68-35534 SOLAR SYSTEM Handbook on planetary physics NASA-TT-F-515 c30 N68-21802 SOLAR WIND Interactions of unconfined magnetic fields emanating from space vehicles with undisturbed solar wind NASA-TN-D-4304 c29 N68-19188 Continuum fluid theory of solar wind and its interaction with geomagnetic field c29 N68-25181 NASA-TN-D-4482 NAGA-IN-D-4462 Photometric and meteor observations, scattering properties, particle collection and impact, solar wind, and origin and evolution of zodiacal light in interplanetary medium - conference NASA-SP-150 C30 N68-27475 DDDD C30 SOLDERED JOINTS Tantallum-stainless steel bimetallic joints tested to determine overall strength of brazed joint NASA-TM-X-1540 c15 N68-21898 SOLDERING Comparison between cemented and soldered cover glass for radiation protection of silicon solar cells NASA-TM-X-1687 c03 N68-37935 SOLID LUBRICANTS Test evaluation of high temperature greases and solid lubricants in thrust loaded ball bearings c15 N68-28766 NASA-TN-D-4652 SOLID PHASES ID FIRELS Ionic conductivities of solid mixtures of lithium fluoride-lithium chloride, lithium chloride-potassium chloride, lithium fluoride-sodium chloride, and sodium chloride-potassium chloride NASA-TN-D-4606 C26 N68-24510 NASA-IN-D-4000 620 NOO-243 SOLID PROPELLANT ROCKET ENGINES Mathematical models for determining longitudinal

propellant vehicles, and clustered tank vehicles NASA-CR-936 c32 N68-10280 C32 N68-10280 Techniques for full-scale dynamic testing of large solid or liquid fueled booster vehicles NASA-CR-940 C32 N68-11054 History of Russian solid fuel rocketry NASA-TT-F-415 c28 N68-114 Submerged nozzle design for SL-3 260-inch solid propellant rocket engines c28 N68-11829 NASA-TM-X-1546 c28 N68-20186 Thrust vector control for large launch vehicles with solid propellant first stages With solid properiant first stages NASA-TN-D-4662 Load relief autopilot to minimize launch vehicle thrust vector deflection angle required for vehicle stability during flight through design c31 N68-28690 winds NASA-TN-D-4786 c21 N68-33756 SOLID ROCKET PROPELLANTS Bibliography on solid, liquid, and hybrid high energy propellants and oxidizers, propellant handling and storage, toxicity and hazards, and safety measures NASA-SP-7002/04/ SOLID SURFACES c27 N68-30313 Three dimensional model of monatomic gases interacting with solid surfaces represented by similar, noninteracting hard spheres NASA-CR-933 cl2 N68-10499 Feasibility of supporting liquid fuel on solid wall in radiating liquid core nuclear rocket concept NASA-TN-D-4413 c27 N68-17093 FORTRAN subroutines for plotting and drawing of three dimensional solid surfaces NASA-TM-X-1598 c19 N68-28240 SOLIDIFICATION Directional solidification of nickel base alloy TAZ-8B to enhance potential for advanced gas turbine engine applications NASA-TN-D-4390 c17 N68-15 c17 N68-15637 Transient solidification of flowing liquid on cold plate, including heat capacities of frozen layer and plate NASA-TN-D-4353 c33 N68-15742 c33 N68-15742 Conformal mapping for steady two-dimensional solidification on cold surface in liquid flow NASA-TN-D-4771 c33 N68-32073 SOLUBILITY Solubilities of several gases in liquid methane and liquefied natural gas NASA-TN-D-4701 c27 N68-30 c27 N68-30077 SOLUTIONS Method for calculating partial volumes of components in solution NASA-TN-D-4199 c06 N68-11621 Lattice structures in solution NASA-TN-D-4297 c06 N68-18219 Nonuniform magnetic field effect on ferromagnetic colloidal solutions NASA-TN-D-4676 c06 N68-30044 c06 N68-30044 SONIC BOOMS Aircraft sonic boom characteristics predicted from near field data obtained in wind tunnel NASA-TM-X-1477 c02 N68-11772 Sonic boom research /conference/ c02 N68-21413 NASA-SP-147 Atmospheric effects on sonic boom characteristics NASA-TN-D-4588 c02 N68-2466 c02 N68-24662 Shock expansion tube characteristics and use as sonic boom simulator NASA-CR-1055 c11 N68-24966 Precision calibration techniques for microphones used in sonic boom measurements NASA-CR-1075 c14 N68-25316 Performance requirements and economic costs to reduce cruise sonic boom of supersonic transport NASA-TN-D-4677 c02 N68-28831 Design of bodies to produce specified sonic boom signatures NASA-TN-D-4704 c01 N68-31484 Awakening and startle effects of simulated sonic booms NASA-CR-1193 c04 N68-33005 Numerical method for determining transient

response of simply supported plate to n waves at normal incidence NASA-CR-1175 c32 N68-33737

Conference on sonic boom reduction in supersonic transport flight - shock wave propagation and refraction, prediction methods for acoustic attenuation, and aerodynamic engineering aspects NASA-SP-180 c02 N68-34907 NASA-SP-180 CO2 NGC-3490 Effects of various simulated sonic boom waveforms on human subjective response NASA-CR-1192 c04 N68-3510 c04 N68-35103 Measurement and interpretation of ground vibrations, produced by seismic effect of sonic boom NASA-CR-1137 c13 N68-35151 SOUND FIELDS Subjective response to far field noise characteristics of V/STOL aircraft sized to carry 60 passengers over 500 mile range NASA-CR-1118 c05 N68-33009 SOUND GENERATORS Performance tests of rotating gas jet generator for strong traveling transverse acoustic modes NASA-TN-D-4380 c12 N68-169 SOUND PRESSURE c12 N68-16998 Target pressure and damage data from impacts by explosively propelled aluminum projectile NASA-TM-X-1597 c32 N68-25819 SOUND WAVES Fitzgeralds piezoelectric disk and theory on audio frequency resonances and sound beams in crystals NASA-TN-D-4625 c23 N68-28259 SOUNDING ROCKETS Nose shape and fin geometry effects on static stability of sounding rocket models in supersonic wind tunnel NASA-TM-X-1661 c01 N68-36509 SOUTH AMERICA Nike Apache pitot tube rocket sounding measuring of Southern Hemisphere stratosphere and mesosphere along west coast of South America NASA-TN-D-4264 c20 N68-25617 SOUTHERN HEMISPHERE Meteorological wind, and temperature data from atmospheric radiosonde soundings in Southern Hemisphere NASA-TN-D-4429 c20 N68-19084 Nike Apache pitot tube rocket sounding measuring of Southern Hemisphere stratosphere and mesosphere along west coast of South America NASA-TN-D-4264 c20 N68-25617 SPACE COMMUNICATION Tabulated communication characteristics of steady state model of interplanetary space NASA-SP-3042 c30 N68-10164 Carbon dioxide laser development for space application NASA-TN-D-4794 c16 N68-35175 with unmanned spacecraft NASA-TR-R-292 SPACE ENVIRONMENT SIMULATION c07 N68-36333 Space activity suit designed for active astronaut working in vacuum environments for up to four hours NASA-CR-973 c05 N68-11510 Design and performance of two vacuum chambers and solar-radiation simulators for solar-cell research NASA-TM-X-1503 c11 N68-16695 Analytical method for finding heat balance of insulated GGO experiment packages from thermal stability data and without solar simulation NASA-TN-D-4644 cll N68-294 SPACE EXPLORATION c11 N68-29478 Historical survey of Russian rocketry and space exploration NASA-TT-F-426 c31 N68-22262 Conference proceedings on role of vestibular organs in space exploration NASA-SP-152 c04 N68-29128 SPACE FLIGHT Development of nuclear thermionic space power system using thermionic diodes, and heat pipe flow for temperature control NASA-TN-D-4299 c22 N60 History of NASA Goddard Space Flight Center c22 N68-19146 through 1963 NASA-SP-4301 c11 N68-30317 SPACE FLIGHT FEEDING Chemical feasibility and nutrional value in

synthesis of edible fatty acids and lipids from metabolic wastes for space flight feeding NASA-CR-1104 c04 N68-28825 c04 N68-28829 SPACE GLOSSARIES NASA Thesaurus - A through L alphabetical listing of terms for indexing and retrieving aerospace related documents NASA-SP-7030, V. 1 c34 N68-1 NASA Thesaurus - M through Z alphabetical listing of terms for indexing and retrieving c34 N68-11307 aerospace related documents NASA-SP-7030, V. 2 c34 N68-1130 Appendices to NASA Thesaurus for indexing scientific and technical information - category term listing, hierarchical display, permuted c34 N68-11308 index, and postable terms NASA-SP-7030, V. 3 c34 N68-11309 SPACE MISSIONS Mission constraints and trajectory interfaces for launch, rendezvous, spatial, deorbit, and entry phases of earth orbital mission NASA-CR-1015 c30 N68-20468 Mars excursion module landing mission mode comparison NASA-TM-X-1629 c30 N68-29988 Principal scientific results on Surveyor 7 mission NASA-SP-173 c31 N68-33553 Technology requirements and spacecraft design studies for atmosphere braking to orbit about Mars and Venus NASA-CR-1131 SPACE NAVIGATION c30 N68-34086 Factors affecting design and use of photographic sextant for space navigation NASA-TN-D-4285 c21 N68-11902 Navigator performance using hand held sextant to measure angle between moving flashing light and simulated star - space navigation NASA-TN-D-4174 c21 N66 Observation theory and sensors applicable to navigation of boost and space vehicles c21 N68-13558 NASA-CR-1001 c30 N68-19676 Navigation and guidance analysis of Mars probe launched from manned flyby spacecraft NASA-TN-D-4512 c21 N68-Telescope objective lens size, aperture size, and magnification effects on operator c21 N68-21754 performance using marine sextants NASA-TN-D-4781 c21 N68-33006 NASA-IN-D-4701 C21 NO-33000 Effects of irradiation and star magnitude on sextant sighting performance NASA-IN-D-4780 C21 N68-33456 SPACE POWER UNIT REACTORS Size and shield weight requirements calculated for fast-spectrum, liquid-metal cooled nuclear reactor for spectrom, and fastion reactor for space power application NASA-TN-D-4315 c22 N68-18197 Analysis and selection of design for plutonium 238 for Brayton cycle space powerplant NASA-TM-X-1631 c22 N68-30 c03 N68-25829 c22 N68-30516 mnow-in-A-1031 c22 N68-30516 Neutronic calculations of fuel and poison drum control of refractory metal, fast spectrum space power reactors NASA-TN-D-4709 c22 N68-30750 CP DPCPAME SPACE PROGRAMS Space technology transfer to developing nations using Brazil as model NASA-CR-1222 c34 N68-37216 SPACE STATIONS Mathematical model for analyzing free vibration of rotating beam-connected space station c32 N68-33225 NASA-TN-D-4753 SPACE SUITS Space activity suit designed for active astronaut working in vacuum environments for up to four hours NASA-CR-973 c05 N68-11510 Automatically controlled heat removal in water cooled space suits NASA-CR-1085 c05 N68-20 c05 N68-26701 SPACE VEHICLE CHECKOUT PROGRAM Automatic testing and checkout of Saturn 1 launch vehicles

NASA-TN-D-4328 SPACEBORNE PHOTOGRAPHY c31 N68-15570 Geologic applications of orbital photography with illustrations from Gemini flights NASA-TN-D-4155 c13 N68-11714 Optimization of confidence levels in detecting lunar surface detail in terms of viewing geometry and camera shutter speeds for Lunar Orbiter missions NASA-TN-D-4501 c14 N68-21942 Spaceborne photography of cloud cover and other meteorological phenomena, Surveyor and Orbiter lunar shots, and Gemini space walk and target docking NASA-SP-168 c30 N68-34870 SPACECRAFT Dimensional analysis, and similitude and scaling laws for structural dynamics model testing of spacecraft dynamic stability NASA-CR-1195 c32 N68-356 SPACECRAFT CABIN ATMOSPHERES c32 N68-35632 Microwave molecular spectroscopy for identifying contaminants in space cabin atmospheres · bibliography NASA-CR-951 c23 N68-10674 Reduction of flammable and toxic materials for use in oxygen rich manned spacecraft cabin atmospheres NASA-TN-D-3415 SPACECRAFT CABIN SIMULATORS c05 N68-24756 Water immersion simulation study of astronaut c05 N68-20339 SPACECRAFT COMMUNICATION Performance evaluation of several convolutional and block codes with threshold decoding for space telemetry NASA-TN-D-4402 c07 N68-18178 Waveform distortion in maximum likelihood Darlington detector for M-ary pulse frequency modulation signals NASA-TN-D-4294 c07 N68-18542 COT N68-18542 Omnidirectional microwave parallel plate broadband antenna for spacecraft communications NASA-TN-D-4555 COT N68-25918 SPACECRAFT CONFIGURATIONS Surveyor 5 configuration, television picture transmission, and experiments on measuring chemical elements in lunar surface
 MRAM-SF-103
 c31 N68-174

 Technology requirements and spacecraft design studies for atmosphere braking to orbit about Mars and Venus
 c30 N68-34

 NASA-CR-1131
 c30 N68-34
 NASA-SP-163 c31 N68-17844 c30 N68-34086 SPACECRAFT CONSTRUCTION MATERIALS Influence of structure and materials research on Weight, performance, and cost of advanced launch vehicle systems NASA-CR-974 c31 N68-11520 Reduction of flammable and toxic materials for use in oxygen rich manned spacecraft cabin atmospheres NASA-TN-D-3415 c05 N68-24756 NASA-IN-U-3415 c05 N68-24756 Radiation resistance, outgassing characteristics, and weight of five electrical insulation materials for spacecraft NASA-TN-D-4553 c18 N68-28264 SPACECRAFT CONTAMINATION Column c18 N68-28264 Cell culture method of screening contaminants which may appear in manned spacecraft NASA-TN-D-4251 c04 c04 N68-10122 Microbiological contamination of Gemini 9 spacecraft before and after flight NASA-CR-972 c04 N68-11968 SPACECRAFT CONTROL Full scale tests of major thrust vector control system parameters and verification of system operation NASA-CR-938 c32 N68-10574 Space vehicle and control system dynamic response to atmospheric disturbances NASA-CR-942 c32 N68-1108 c32 N68-11089 Handling qualities, disturbances and reentry corridor boundaries for spacecraft control system design NASA-CR-945 c32 N68-11133 NASA-CK-945 C32 N68-1 Lunar module backup guidance, navigation and pilot interfaces with control systems during lunar landing missions NASA-TN-D-4131 c21 N68-1 c21 N68-16836

Hydrodynamic equations for stability, and control analyses on liquid propellant space vehicles NASA-CR-941 c32 N68-1 c32 N68-18769 Simulator study of pilot control over lunar module during ascent from lunar surface NASA-TM-X-1549 c21 N68-21366 MBSA-IN-X-1949 Time optimal rendezvous trajectories for variable thrust intercepting and orbiting space vehicles NASA-CR-1036 c30 N68-22202 Test apparatus and procedures for aerodynamic model tests of spacecraft control system parameters NASA-CR-947 c32 N68-23452 Passive damping technique for attitude control of solar orientated interplanetary spacecraft NASA-TN-D-4641 c21 N68-28363 MRGH-IN-D-4641 Spacecraft performance, control, and flight path analysis of Lunar Drbiter 3 extended mission NASA-CR-1109 Control, performance, and tracking Lunar Orbiter 5 in obtaining selenodetic and lunar environment data NASA-CR-1142 SPACECRAFT DESIGN c31 N68-30631 Assessment of environmental engineering and testing methods used in development of various spacecraft systems NASA-TN-D-4181 c31 N68-10192 Solar simulation testing of anchored interplanetary monitoring platform D thermal design and protective coating NASA-TN-D-4112 c33 N68-10299 General method for designing circular array antennas to obtain quasi-omnidirectional patterns NASA-TN-D-4254 c07 N68-11475 Spacecraft system design, mission planning, and qualification testing for Gemini project NASA-CR-1106 SPACECRAFT DOCKING c31 N68-25577 Simulator study of pilot control of remote orbital docking of large altitude stabilized components NASA-TN-D-4263 c31 N68~11476 Equations of relative motion and guidance for orbital transfer and docking maneuvers in spacecraft rendezvous NASA-CR-1011 SPACECRAFT ELECTRONIC EQUIPMENT c30 N68-19186 Spaceborne pattern recognition system for identifying and classifying objects in video data NASA-CR-999 c10 N68-19229 NASA-CR-999 Microelectronic device data handbook /text/ NASA-CR-1110 c09 N68-29525 Microelectronic device data handbook /manufacturer and specific device information/ c09 N68-29526 NASA-CR-1111 Advanced multiprocessor computer organization for manned Mars lander mission NASA-CR-1159 c08 N68-355 SPACECRAFT ENVIRONMENTS Spacecraft habitability for long duration manned c08 N68-35560 space flight missions NASA-CR-1084 c30 N68-2 Subsystem definition of advanced life support c30 N68-26702 technology for Mars surface module NASA-CR-1083 c05 N68-28319 SPACECRAFT GUIDANCE Lunar module backup guidance, navigation and pilot interfaces with control systems during lunar landing missions NASA-TN-D-4131 c21 N68-16836 Mathematical formulation of guidance equations and solutions for orbital space missions NASA-CR-1010 c c30 N68-17215 Equations of relative motion and guidance for orbital transfer and docking maneuvers in spacecraft rendezvous NASA-CR-1011 c30 N68-19186 Observation theory and sensors applicable to navigation of boost and space vehicles NASA-CR-1001 c30 N68-1967 Entry guidance equations, reference trajectories, and guidance system mechanization c30 N68-1998 c30 N68-19676 NASA-CR-1013 c30 N68-19985 Iterative and perturbation approaches to near optimum steering equations for boost vehicle guidance NASA-CR-1007 c30 N68-20449

General perturbations theory applications to spacecraft guidance, flight mechanics, and trajectory optimization NASA-CR-1008 c30 N68-20450 Methodology used in guidance system performance analysis /assessment/ NASA-CR-1016 c30 N68-21442 Navigation and guidance analysis of Mars probe launched from manned flyby spacecraft NASA-TN-D-4512 c21 N68-21 NASA-IN-D-4512 c21 N68-2 Venus flyby, Mars flyby, and Mars orbital mission to evaluate navigation and guidance systems for manned interplanetary spacecraft NASA-IN-D-4629 c21 N68-20 c21 N68-21754 c21 N68-28236 Attitude determination of spin-stabilized spacecraft using star mapping technique spacecraft using star mapping technique NASA-TN-D-4740 c21 N68-319 SPACECRAFT INSTRUMENTS Diffusers for in-flight calibration of detectors installed in spacecraft NASA-CR-987 c14 N68-1260 c21 N68-31957 c14 N68-12669 Instrumentation, systems engineering, and life support systems for Apollo primate orbital experiment NASA-CR-926 c05 N68-15306 NASA-UN-920 Spacecraft attitude determination using single onboard camera NASA-TN-D-4359 SPACECRAFT LANDING Control and stability aspects prior to spacecraft c31 N68-19275 landing, and propulsive assist to landing spacecraft NASA-CR-946 c31 N68-24945 SPACECRAFT LAUNCHING Equipment, instrumentation, communications, design, launch vehicles, and guidance of scientific satellites NASA-SP-133 C31 NG c31 N68-14965 NASA-32-133 SPACECRAFT ORBITS Mission and orbit parameter summary for Lunar Orbiter spacecraft flight NASA-CR-1141 c31 N68c31 N68-31477 SPACECRAFT PERFORMANCE Systems performance, lunar photography, and launch operations of Lunar Orbiter 3 photographic mission NASA-CR-1069 c31 N68-24738 Design, mission, flight operations, experiment data, and subsystem performances for Lunar Drbiter 4 extended mission NASA-CR-1092 C31 N68-2 c31 N68-28997 Spacecraft performance, control, and flight path analysis of Lunar Orbiter 3 extended mission c31 N68-29995 NASA-CR-1109 Control, performance, and tracking Lunar Orbiter 5 in obtaining selenodetic and lunar environment data NASA-CR-1142 c31 N68-30 Description and performance analysis of manned c31 N68-30631 six-pass orbital mission /Mercury-Atlas 8/ c31 N68-35022 NASA-TN-D-4807 SPACECRAFT POWER SUPPLIES Electromagnetic pump designs for use as boiler feed pumps in Rankine cycle, space electric power plants power plants NASA-CR-911 c15 N68-1(Breadboard three-phase static switch for space alternating current power systems NASA-TM-X-1495 c09 N68-15 Experimental design and performance test of two-stage axial-flow turbine designed for Brauton-curbo concer source sustant c15 N68-10503 c09 N68-15649 Brayton-cycle space power system NASA-TN-D-4382 c03 N68-16469 MADA-IN-D-4362 Effects of surface Mach numbers, inlet flow angle and specific heat ratio on geometric features of supersonic impulse turbine blade sections over Mach number range of 1.5 to 5.0 NASA-IN-D-4422 C03 N68-20276 Geometric properties of expandable whirling membrane solar energy concentrator used in conjunction with electrical conversion systems NASA-TN-D-4532 c03 N68-22258 Axial flow turbine compressor for space power plant NASA-CR-800 c03 N68-24596

Comparative analysis of single-loop 100-kilowatt Brayton space power system using pure gas and gas-solid suspension as working fluids

c03 N68-28280 NASA-TN-D-4659 Creep test data on refractory metal alloys for use in spacecraft power supply systems NASA-CR-1115 c17 N68-29992 Recuperator for closed Brayton cycle solar energy space power system NASA-CR-1150 SPACECRAFT PROPULSION c03 N68-33062 Control and stability aspects prior to spacecraft landing, and propulsive assist to landing spacecraft NASA-CR-946 SPACECRAFT RADIATORS c31 N68-24945 Weight, heat transfer, and efficiency comparison for Rankine cycle space radiators constructed of three different finned tube geometries NASA-TN-D-4411 c33 N68-16324 Effect of finned-tube assembly techniques on heat transfer characteristics of space radiator NASA-TM-X-1557 c33 N68-21704 Comparative analysis of single-loop 100-kilowatt Brayton space power system using pure gas and gas-solid suspension as working fluids NASA-TN-D-4659 c03 N68-28280 Radiator concept based on capillary retention of liquid and potential extraterrestrial applications NASA-TN-D-4370 NASA-TN-D-4370 SPACECRAFT RECOVERY c03 N68-28310 SPACECRAFT RECOVERY Computer program technique for determination of opportunities for recall of spacecraft to multiple landing sites from circular or elliptical orbits NASA-TR-R-259 c21 N68-30 SPACECRAFT RELIABILITY c21 N68-30126 Assessment of environmental engineering and testing methods used in development of various spacecraft systems NASA-TN-D-4181 c31 N68-101 Maintainability of manned spacecraft for long c31 N68-10192 duration flights NASA-CR-1108 SPACECRAFT SHIELDING c31 N68-33008 CECKAFT SHIELDING Space radiation transport, spacecraft shielding design and advanced concepts, and methods for calculating radiation penetration through protective shields - conference NASA-SP-169 c29 N68-26 c29 N68-26128 SPACECRAFT STABILITY Mathematical models and approximation methods for solving lateral vibration modes of cylindrical space vehicles and vehicles with clustered tanks NASA-CR-935 c32 N68-10231 Simple processors of star tracker commands for stabilizing inertially oriented satellite NASA-TN-D-4490 c21 NG c21 N68-19236 Subsonic dynamic stability characteristics of large conical spacecraft in simulated Martian environment NASA-TN-D-4558 c31 N68-22301 Dynamic stability of thin walled elastic shells and applications to space vehicle control problems NASA-CR-949 c32 N68-23453 Control and stability aspects prior to spacecraft landing, and propulsive assist to landing spacecraft NASA-CR-946 c31 N6 c31 N68-24945 SPACECRAFT STERILIZATION Clean room facilities for Explorer 35 spacecraft spacecrait NASA-TN-D-4577 cll N68-28 SPACECRAFT STRUCTURES Digital computer program for prediction of snap buckling of spacecraft shell structures by geometric nonlinear analysis of thin elastic shells of revolution NASA-CR-909 c32 N68-14 cll N68-28311 c32 N68-14584 Simulated meteoroid high velocity impact damage to spacecraft structures composed of two metallic sheets NASA-CR-915 c31 N68-14638 Instruction manual for static structural analyses on shell-type spacecraft structures ON Shell-Type spaceorall structure NASA-CR-912 C32 N68-24802 SPACECRAFT TRACKING General equations for standard deviation, and rms standard deviation of least squares fitted polynomials applied to Apollo tracking problems c32 N68-24802

NASA-TN-D-4121 c10 N68-16749 Effects of time, frequency, and tracking station location errors on accuracy of trajectory analysis NASA-TN-D-4507 SPACECRAFT TRAJECTORIES c30 N68~25271 Two body problem for satellite guidance, flight mechanics, and trajectory optimization analyses NASA-CR-1002 c30 N68-14089 Entry guidance equations, reference trajectories, and guidance system mechanization NASA-CR-1013 c30 N68-19985 Nathematical means for bounding propagated trajectory error induced impulsive initial error in n-body field NASA-TN-D-4511 c30 N68-32094 Matrix equations to describe motions of spacecraft consisting of interconnected rigid bodies NASA-TN-D-4749 c32 N68-33092 SPARK GAPS Liquid layer solid sample spark technique for spectrochemical analysis of flat metal samples using conventional spark source NASA-TM-X-1429 c06 N68-10497 SPECIFIC HEAT Transient solidification of flowing liquid on cold plate, including heat capacities of frozen layer and plate NASA-TN-D-4353 c33 N68-1574 c33 N68-15742 SPECIFIC IMPULSE FORTRAN 4 programs for calculating inviscid, one-dimensional and axisymmetric nonequilibrium nozzle flow fields and improving analytical predictions of delivered specific impulse NASA-CR-1123 c27 N68-32793 SPECTRAL EMISSION Spectral transmission characteristics of fused silica before, during, and after exposure to reactor irradiation pulses NASA-CR-1031 c22 N68-2 c22 N68-21124 Spectral emissivity of highly doped silicon NASA-TN-D-4303 c26 N68-21708 Spectral transmission measurements on fused silica during and after exposure to pulsed neutron irradiation NASA-CR-1191 c22 N68-35826 SPECTRAL ENERGY DISTRIBUTION Atomic line intensity tables for ionized iron atom at high temperatures NASA-SP-3041 c25 N68-24161 Electron scattering, bremsstrahlung cross sections, and spectral energy distributions NASA-CR-1194 c24 N68-3 c24 N68-37708 SPECTRAL REFLECTANCE Cumulus cloud and fog bank spectral reflectance observations using Nimbus satellites and infrared radiometers NASA-TN-D-4552 c14 N68-25862 SPECTROMETERS Servicentroller for programming atomic emission and sample vaporization in direct current arc spectrochemical analysis NASA-TN-D-4769 c06 N68-3194 Analog simulation of dc arc emission spectrometer c06 N68-31948 control system to define optimum control requirements NASA-TN-D-4770 c08 N68-32055 SPECTRORADIOMETERS Spectroradiometer and technique for measuring spectral irradiance of solar simulators NASA-TN-D-4822 SPECTROSCOPIC ANALYSIS c14 N68-35534 Trace contaminant identification using microwave double resonance spectroscopy NASA-CR-967 c24 N68-11634 SPECTROSCOPY Mossbauer spectroscopy used to study sensitization in austenitic stainless steels NASA-CR-1077 c17 N68-25318 SPECTRUM ANALYSIS Liquid layer solid sample spark technique for spectrochemical analysis of flat metal samples using conventional spark source NASA-TM-X-1429 c06 N68-10497 Metal cathodes in argon atmospheres used to stabilize dc arcs for spectrochemical analysis NASA-TN-D-4236 c06 N68-11512 Trace contaminant identification using microwave

Trace contaminant identification using microwave double resonance spectroscopy

NASA-CR-967 c24 N68-11634 Spectral response of cuprous sulfide-cadmium sulfide film photovoltaic cell to green light NASA-TN-D-4333 c03 N68-14 c03 N68-14082 Mathematical properties and computer programs for digital spectrum analyses NASA-TN-D-4510 c08 N68-25268 Helium 2 elementary excitation spectrum derived microscopically for realistic interatomic potential c24 N68-37240 NASA-TN-D-4838 SPEED CONTROL Dynamic characteristics of parasitic loading speed controller for Brayton cycle turboalternator NASA-TM-X-1456 c03 N68-18702 SPHERES Computer program for determining geometric configuration view factors for spherical and conical surfaces of spherical radiating bodies NASA-TN-D-4457 c33 N68-20331 SPHERICAL TANKS Gravity effects on self-pressurization of spherical liquid hydrogen tankage c27 N68-11645 NASA-TN-D-4286 Gravity effects on forced circulation pattern in spherical tanks NASA-TN-D-4409 c12 N68-20352 Liquid flow into baffled spherical tank during weightlessness NASA-TM-X-1526 c12 N68-21365 Analytical and experimental investigation of propellant distribution during outflow of spherical tanks for possible space vehicle application NASA-TN-D-4828 c12 N68-35104 Drop tower investigation of liquid reorientation in spherical containers NASA-TM-X-1659 c12 N68-351 c12 N68-35114 SPHYGMOGRAPHY Theory of finite amplitude waves in fluid-filled elastic tubes, including wave distortion, shock wave propagation, and Korotkoff sounds NASA-TN-D-4803 c12 N68-33056 SPIKES (AERODYNAMIC CONFIGURATIONS) Unstarted inlet flow field during restart cycle of axisymmetric mixed compression configuration at Mach 3 NASA-TM-X-1547 c01 N68-21703 c12 N68-33056 c01 N68-21703 SPIN STABILIZATION Spin axis for spinning satellite determined from range rate data NASA-TN-D-4483 c30 N68-21182 Star field mapping technique for determining attitude of spin stabilized spacecraft NASA-TN-D-4637 c21 N68 c21 N68-28418 SPIN TESTS Spinning friction and torque dependence on ball bearing-groove conformity NASA-TN-D-4669 c15 N68-28258 SPIROMETERS Spirometer modification to permit computer reduction of respiratory flow data NASA-TN-D-4234 c14 N SPOILER SLOT AILERONS c14 N68-10057 Wind tunnel study to explore use of slot spoilers for direct control of flap induced lift and lateral aircraft control NASA-TN-D-4664 c01 N68-28830 SPUTTERING Sputtered molybdenum disulfide film deposition and friction characteristics in vacuum c17 N68-11644 NASA-TN-D-4269 STABILITY Load relief autopilot to minimize launch vehicle thrust vector deflection angle required for vehicle stability during flight through design winds NASA-TN-D-4786 c21 N68-33756 STABILITY TESTS Analytical methods for dynamic stability analyses of large launch vehicles during flight through and exit from earth atmosphere NASA-CR-944 c32 N68-18825 Double dead-time model for combustion stability analysis in liquid bipropellant rocket engines NASA-TN-D-4564 c33 N68-25102

Stability of selected earth minerals in simulated lunar environment tests NASA-CR-1034 c13 N68-25579

STABILIZATION

STABILIZATION Limit cycle and control surface resonance characteristics of X-15 stability augmentation system NASA-TN-D-4287 c02 N68-11545 Stability criterion for digital simulation NASA-TN-D-4203 c08 No c08 N68-26640 STABILIZED PLATFORMS Automatic balancing system for frictionlessly supported, attitude control test platforms about axes commonly orthogonal to gravity vector NASA-TN-D-4426 c09 N68-19185 Precision tilt and vibration isolation system design NASA-TR-R-281 c14 N68-19642 Performance test data for ammonia resistojet attitude control system of stable platform satellites NASA-TM-X-1677 c28 N68-36 STABILIZERS (FLUID DYNAMICS) Stabilizer and tail assembly effects on overall c28 N68-36512 aerodynamic characteristics of lifting bodies at hypersonic speeds NASA-TM-X-1620 c01 N68-29952 STAGE SEPARATION Pyrotechnic shaped charge aerospace vehicle stage and shroud separation systems development NASA-TM-X-1607 c31 N68-28869 c31 N68-28869 Small water-graphite nuclear rocket stages compared with chemical upper stages for use in unmanned spacecraft NASA-TN-D-4827 c22 N68c22 N68-35073 Static and dynamic characteristics of wind tunnel model of parallel staged reusable launch vehicle during stage separation NASA-TN-D-4765 c31 N68-36106 STAGNATION FLOW Wall injection area and axial bypass effects on flow pattern of stagnation surface in radial inflow vortexes NASA-CR-1028 STAGNATION POINT c22 N68-22088 Convective stagnation heat transfer of carbon dioxide, nitrogen-argon gas mixtures compared to air in shock tube tests NASA-TN-D-4255 c33 N68-11811 Empirical stagnation point-heat transfer relation in gas mixtures at high enthalpy potentials c33 N68-11811 NASA-TN-D-4799 c33 N68-35468 STAINLESS STEELS Axial tensile fatigue of liquid rocket engine alloys at cryogenic temperatures NASA-TN-D-4274 c17 N68c17 N68-11637 Tungsten-stainless steel sensor for averaging temperature measurement of nonuniform temperature profiles temperature profiles NASA-TN-D-4242 cl4 N68-10500 Environmental exposure effects on mechanical properties of titanium alloy, stainless steel, aluminum alloy, and composite material sheets cl7 N68-17897 Transmission, and backscatter coefficients for electron irradiated aluminum, and stainless steel foils NASA-TN-D-4363 c24 N68-17898 NAA-IN-24363 C24 NOO-17090 Shaping of precipitation hardened stainless steels by casting and powder metallurgy NASA-SP-5086 c15 N68-19307 MASA-SF-3080 C10 NOO-1550. Hard surfacing, electroplating, electrodeless plating, carburizing, nitriding, burnishing, explosive hardening, planishing, and peening of precipitation-hardenable stainless steels NASA-SP-5090 c15 N68-19343 Organic and inorganic adhesives for bonding of stainless steels and precipitation hardened stainless steels NASA-SP-5085 c15 N68-2 c15 N68-20056 Wear rate and friction coefficient of steel sliding on polymer laminates determined in liquid nitrogen and hydrogen NASA-TN-D-4463 c15 N68-20325 Machining and grinding of ultrahigh-strength steels and stainless steel alloys NASA-SP-5084 c15 N68c15 N68-21241 Welding of precipitation hardening stainless. steels NASA-SP-5087 c15 N68-21429

Tantallum-stainless steel bimetallic joints

SUBJECT INDEX

tested to determine overall strength of brazed joint NASA-TM-X-1540 c15 N68-21898 Brazing aluminum to titanium coated stainless steel to minimize formation of intermetallic compounds in joint NASA-SP-5040 c15 N68-22778 NAA-32-3040 C13 Nob-2277 Stainless steel penetration detector, impact detector, and solar cell degradiation, to study micrometeorold impact damage and puncture rate, and radiation effects on Explorer 23 satellite NASA-TN-D-4284 C31 N68-2819 c31 N68-28198 Cyclic incident radiation method for measuring thermal emittance and absorption properties of metals at cryogenic temperatures NASA-TM-X-1618 c33 N68-31498 Residual streas effects on fracture strength of AISI 301 stainless steel and Ti-5A1-2.5Sn titanium cracked thin walled cylinders NASA-TN-D-4777 c32 N68-33191 Cavitation damage of stainless steel, nickel, and aluminum alloy in water NASA-TM-X-1670 c17 N68-36076 STAR DISTRIBUTION c17 N68-36076 N DISINIBUTION Star field mapping technique for determining attitude of spin stabilized spacecraft NASA-TN-D-4637 c21 N68-284: Two dimensional computer model for collisionless self gravitating galactic system with gravitational field obtained from Poisson c21 N68-28418 equation NASA-TN-D-4646 c30 N68-28884 STAR TRACKERS Simple processors of star tracker commands for stabilizing inertially oriented satellite NASA-TN-D-4490 c21 N68-1 c21 N68-19236 Maximum likelihood techniques for design of optimum star trackers that determine position and magnitude NASA-TN-D-4549 c21 N68-23377 Optical star tracker calibration procedures NASA-TN-D-4594 c21 N68-24555 NASA-TN-D-4594 c21 N68-24555 Celestial attitude measuring instrument using star mapping technique NASA-TN-D-4742 c21 N68-31938 STATIC AERODYNAMIC CHARACTERISTICS Instruction manual for static structural analyses on shell-type spacecraft structures NASA-CR-912 c32 N68-24802 MBDR-GK-912 Static and dynamic characteristics of wind tunnel model of parallel staged reusable launch vehicle during stage separation NASA-TN-D-4765 C31 N68-36106 STATIC FIRING Full scale tests of major thrust vector control system parameters and verification of system operation NASA-CR-938 c32 N68-10574 STATIC LOADS Dynamic characteristics of parasitic loading speed controller for Brayton cycle turboalternator NASA-TM-X-1456 c03 N68-18702 STATIC PRESSURE Flow conditions in inlet manifold of M-1 fuel pump drive turbine investigated using circumferential static pressure measurements in conjunction with smoke trace photographs NASA-TM-X-1513 c12 N68-15639 static pressure and flow field for flat plate model with short trailing-edge flap NASA-TN-D-4308 Installation and fairing of flush, static pressure orifices on wing surfaces of supersonic aircraft NASA-TM-X-1530 c01 N68-19341 STATIC STABILITY Static and dynamic longitudinal stability tests of fan in wing V/STOL aircraft model NASA-TN-D-4322 co2 N68-15894 Wind tunnel studies of static aerodynamic characteristics of multilobe gliding parachute NASA-TN-D-4672 col N68-28447 Wind tunnel test data on static and dynamic stability of Apollo command module configuration NASA-TN-D-4688 COL NOB-1N-D-4688 COL N68-31445 Sideslip angle effects on static stability characteristics of T tail transport configuration configuration NASA-TM-X-1665 c01 N68-36112

STRESS ANALYSIS

STATIC TESTS Performance characteristics from static tests in ground effect of V/STOL transport model NASA-CR-1180 c28 N68-35594 Static performance of an auxiliary inlet ejector nozzle for supersonic-cruise aircraft NASA-TM-X-1653 c28 c28 N68-35764 Electroadhesive devices - theory, design, fabrication, and testing NASA-CR-1211 c10 N68-37906 STATIONKEEPING Control Con c31 N68-11641 stationkeeping NASA-TN-D-4420 c28 N68-20187 Hovering lunar libration communication satellite stationary with respect to earth-moon system NASA-TN-D-4468 c30 N68-21733 STATISTICAL ANALYSIS General method for designing circular array antennas to obtain quasi-omnidirectional patterns NASA-TN-D-4254 c07 N68-11475 Statistical association techniques NASA-CR-1020 c08 N68-17154 Mathematical model of statistical channel characteristics in, and test instrumentation for, digital data transmission systems handling uniformly coded binary data NASA-TT-F-434 c07 N68-1754; c07 N68-17542 Statistical evaluation of sampled wind data from anemometers mounted on meteorological tower on Wallops Island NASA-TN-D-4395 c20 N68-18246 Frequency function for testing small samples for goodness of fit to normal populations NASA-TN-D-4405 c19 N68-191 c19 N68-19144 Methodology used in guidance system performance analysis /assessment/ NASA-CR-1016 c30 N68-21442 impact loads on airline transports NASA-TN-D-4586 c02 N68-24476 Parameter variation analyses on mathematical models NASA-CR-1126 STATISTICAL DECISION THEORY c15 N68-31478 Monté Carlo computations of decision error probabilities for chain pooling and variations for fractional factorial experiments NASA-TN-D-4272 c19 N STATISTICAL TESTS Statistical tests for signal detection and c19 N68-11639 correlation coefficients NASA-TR-R-273 c10 N68-11789 STATOR BLADES Cold air study of high temperature gas turbine -blade feature effects on stator performance NASA-TN-D-4418 c28 N68-166 c28 N68-16632 Kinetic energy loss coefficients of stator blade row in open configuration NASA-TM-X-1635 c03 N68-3056 c03 N68-30506 Turbine performance with 130 percent design stator NASA-TM-X-1663 c03 N68-35536 STATORS Aerodynamic characteristics of a stator modified gas turbine for single shaft Brayton cycle power system NASA-TM-X-1615 c03 N68-28870 NASA-TM-X-1615 c03 N68-28870 Effect of variable stator geometry on performance of air cooling turbine NASA-TM-X-1632 c01 N68-29994 Performance tests of stator component in closed position and effects on performance of single stage turbine suitable for air cooling NASA-TM-X-1675 c28 N68-37264 performance tests STEEL STRUCTURES Ablative and steel chambers effect on combustion instability in hydrogen oxygen rocket engine NASA-TM-X-1511 c28 N68-15644 STEERING Iterative and perturbation approaches to near optimum steering equations for boost vehicle guidance NASA-CR-1007 c30 N68-20449

STELLAR EVOLUTION Mathematical model for computing equilibrium properties of one dimensional self-gravitating stellar system NASA-TR-R-289 c30 N68-32978 STELLAR LUMINOSITY Airborne stellar photometry and spectrometric determination of day sky brightness c30 N68-19590 NASA-CR-1017 Autocorrelation of incoherent stellar light measured by interferometer NASA-TN-D-4480 c14 N68-25518 STEP FUNCTIONS Runge-Kutta formulas of high order with stepsize control through leading truncation error term NASA-TR-R-287 STIFFENING c19 N68-36753 Survey on minimum weight design aspects of stiffened cylinders under compression NASA-CR-963 c3 c32 N68-11282 Prebuckling deformations, and ring stiffener effects on buckling load of eccentrically stiffened orthotropic cylinders NASA-TN-D-4283 c32 NG c32 N68-14091 NASATIN-D-4203 STOCHASTIC PROCESSES Optical communications - maximum likelihood detection of M-ary Poisson processes in background of additive Poisson noise NASA-TN-D-4623 c07 N6 c07 N68-29528 STORABLE PROPELLANTS Relative erosion resistance of ablative materials for nozzle sections of storable-propellant rocket engine NASA-TM-X-1559 c28 N68-19708 Failure mechanisms for specific materials and design concepts for storable propellant rocket engines NAŠA-TM-X-1463 c28 N68-22272 STORAGE TANKS Parametric mass analysis and comparison of two reactant cooling and storage units for lunar based hydrogen oxygen regenerative fuel cell system NASA-TN-D-4386 c03 N68-16631 STRAIN HARDENING Elastoplastic analysis of circular cylindrical inclusion in uniformly stressed infinite homogeneous matrices of composite materials for aerospace applications NASA-TN-D-4350 c32 N68-15769 Successive approximation procedure for solving elastic-plastic problem for torsion of solid prismatic bar made of strain hardening material c32 N68-17045 NASA-TN-D-4391 STRATOSPHERE Nike Apache pitot tube rocket sounding measuring of Southern Hemisphere stratosphere and mesosphere along west coast of South America c20 N68-25617 NASA-TN-D-4264 Air samplers, contamination, and sterilization in collection of microorganisms for microbiological exploration of stratosphere NASA-CR-1101 c04 N68-28247 Meteorological rocket soundings in stratosphere and mesosphere, 1966 - tables NASA-TR-R-288 c20 N68-33036 Atmospheric conditions during turbulences encountered by XB-70 aircraft above 40,000 ft NASA-TN-D-4768 c13 N68-33 c13 N68-33416 STRESS (PSYCHOLOGY) Process development of system for digital computer processing of psychophysiological data to obtain high stress tolerance personnel NASA-CR-1122 co5 N68-35102 STRESS ANALYSIS Elastoplastic analysis of circular cylindrical inclusion in uniformly stressed infinite homogeneous matrices of composite materials for aerospace applications NASA-TN-D-4350 Residual static strength and slow crack growth behavior of duplex annealed Ti-8A1-1Mo-1V c32 N68-15769 sheet NASA-TN-D-4358 c32 N68-17588 Plane stress analysis using Fourier series of edge stiffened isotropic or orthotropic elastic rectangular plate subjected to prescribed temperature distribution and boundary loads NASA-CR-978 c32 N68-19311

STRESS CONCENTRATION

SUBJECT INDEX

Subsurface residual stress on steel inner races from ball bearings during rolling contact NASA-TN-D-4456 . c15 N68-201 Texture strengthening and fracture toughness of titanium alloy sheet at room and cryogenic NASA-TN-D-4456 c15 N68-20199 temperatures NASA-TN-D-4444 c17 N68-22884 Stress analysis and wear tests in use of lacing wire as vibration damper on turbocompressor blades NASA-TM-X-1603 c32 N68-28238 Electrical stress analysis of microthruster power conditioner NASA-TM-X-1686 c09 N68-37944 STRESS CONCENTRATION Stress concentrations in rib-reinforced plates and shells, and effects on structural design NASA-TT-F-427 c32 N68-10407 Ring accelerometer errors from stresses developed by fixture vibrations NASA-TN-D-4540 c14 N68-25830 Iterative solution for calculating deformation and stress concentration near slits in elastic-plastic solids NASA-TN-D-4717 NASA-TN-D-4717 c32 N68-30 Cyclic frequency, tensile fatigue effects, and defect substructure generated in vacuum by fatigue stressing of aluminum NASA-CR-1165 c17 N68-35 STRESS CORROSION c32 N68-30045 c17 N68-35200 Simulated study of effects of high altitude supersonic air flow on titanium alloy hot salt cracking process NASA-CR-981 c17 N68-11522 Precision glass-bead peening equipment for propellant tank surface corrosion protection NASA-TN-D-4288 c15 N68-12890 Stress corrosion cracking of titanium aluminum vanadium alloy in nitrogen tetroxide under pressure NASA-TN-D-4289 c17 N68-12891 Protective coatings and surface treatments for protection of Ti-8A1-1Mo-1V alloy sheet from hot-salt stress corrosion NASA-TN-D-4319 c17 N68-17377 Stress corrosion tests of heat treated austenitic stainless steels c17 N68-29379 NASA-TN-D-4673 Hot salt stress corrosion cracking effects or tensile properties of titanium alloy snec(s NASA-TN-D-4674 c17 N68-3 c17 N68-30000 Hot salt stress corrosion cracking of titanium aluminum alloys in presence of anhydrous hydrogen chloride NASA-CR-1133 c17 N68-33019 STRESS FUNCTIONS Classical equations of elasticity in terms of stress components reduced to three stress functions and three equations NASA-TN-D-4253 c19 N6 c19 N68-10355 Stress analysis and functions in membrane analysis of scalloped thin walled shells like parachutes NASA-TN-D-4687 c32 N68-28832 STRESS MEASUREMENT Infrared radiometric stress instrumentation system for estimating detectable stress measurements NASA-CR-1067 c32 N68-24971 NASA-UK-1057 C32 NOS-STRESS-STRAIN DIAGRAMS Stress-strain diagrams for cold welded copper microjunctions in vacuum NASA-TN-D-4743 c17 N68-31517 STRESS-STRAIN-TIME RELATIONS Constant creep data accumulation for design stress analysis on cladding material thickness around cylindrical reactor fuel element c22 N68-26764 NASA-TN-D-4352 STRESS WAVES Numerical method for determining transient response of simply supported plate to n waves at normal incidence NASA-CR-1175 c32 N68-3 STRESSED-SKIN STRUCTURES Aerodynamic characteristics of tension string, c32 N68-33737 tension shell; and conical shapes in supersonic flow NASA-TN-D-4360 c01 N68-18720 STRUCTURAL ANALYSIS High frequency structural damping due to riveted joints associated with gas pumping between

overlapping surfaces NASA-CR-954 c32 N68-11489 Design data for gas cooled test loop, and inpile capsule facility from mockup reactor experiments NASA-TM-X-1509 c22 N68-15855 Optimum design geometry for high radial inflow turbine performance efficiency NASA-TN-D-4384 c03 N68-1 c03 N68-15943 Basic equations and method of solution for computerized analysis of shells of revolution with axisymmetric collapse and nonsymmetric bifurcation buckling behavior NASA-CR-1050 c32 N68-23451 Instruction manual for static structural analyses on shell-type spacecraft structures NASA-CR-912 c32 N68-24802 Cycle characteristics and structural configuration of turbojet and turbofan engines for lightweight aircraft NASA-TM-X-1624 c28 N68-31476 NASA-TM-X-1624 c28 Fabricability, mechanical properties, and structural efficiency potentials of boron-polymer film layer composites NASA-CR-1114 c18 c18 N68-35100 STRUCTURAL DESIGN Stress concentrations in rib-reinforced plates and shells, and effects on structural design NASA-TT-F-427 c32 N c32 N68-10407 Structural design methods for analysis of multilayer or laminated filamentary composites NASA-CR-964 c32 N68-11191 Design, and evaluation of birefringent wave filter scale model for millimeter wavelengths radio astronomy NASA-CR-979 c09 N68-13617 Design, and performance of facility for Rankine cycle testing of two stage potassium vapor turbine NASA-CR-924, V. 3 c03 N68 FORTRAN computer program for supersonic turbomachinery blading design calculations c03 N68-18044 c08 N68-18620 NASA-TN-D-4421 Planford design method, general characteristics, and aeroelastic stability of flexible lifting rotors NASA-TN-D-4465 c01 N68-19954 Relationship between fan drive turbine geometry and output efficiency of turbofan engine c28 N68-22725 NASA-TM-X-1581 Window designs for mercury condensing tube and mercury boiler outlet tube NASA-TM-X-1578 c11 N68-22737 Handbook for designing ball lock mechanisms for use on space vehicles NASA-CR-1021 c15 N68-23356 MASA-CR-1021 Materials selection, structural geometry, proof testing and statistical screening, prestressing, and system energy as tools for designing optimum trusses and other high performance structures NASA-CR-1038 c32 N68-23399 Constant creep data accumulation for design stress analysis on cladding material thickness around cylindrical reactor fuel element NASA-TN-D-4352 c22 N68-26764 Cost effectiveness studies on structural design of future aerospace systems NASA-CR-1068 c34 N68-26813 Structural design synthesis of recoverable launch vehicle structures NASA-CR-1116 c32 N68-28335 STRUCTURAL ENGINEERING Assessment of environmental engineering and testing methods used in development of various spacecraft systems NASA-TN-D-4181 c31 N68-101 c31 N68-10192 Influence of structure and materials research on weight, performance, and cost of advanced launch vehicle systems NASA-CR-974 c31 N68-11520 Non-CR 574 Structural design synthesis of recoverable launch vehicle structures NASA-CR-1116 c32 N68-2833

NASA-CR-1116 c32 N68-28335 STRUCTURAL RELIABILITY Design and volumetric analysis of pressurized tanks for use in liquid-methane fueled supersonic transport aircraft

NASA-TN-D-4295 c32 N68-12370 STRUCTURAL STABILITY

Impedance testing for flight control system

SUPERSONIC FLOW

parameters in studies of launch vehicle dynamic stability NASA-CR-939 c32 N68-11485 Lunar module scale model study of use of soft side legs for improved touchdown stability of legged landing vehicles NASA-TN-D-4680 c31 N68-2996 STRUCTURAL VIBRATION Flutter analysis on buckled supported rectangular c31 N68-29962 panels under supersonic surface flow NASA-TN-D-4357 c c32 N68-17651 Experimental study, and theoretical analysis on supersonic flutter of corrugation stiffened panels NASA-TN-D-4321 c32 N68-19143 Noise reduction in small enclosed structures in terms of physiological and psychological effects NASA-CR-1155 c32 N68-33266 Hydraulic flow approximation for flow induced vibration analysis on flat plate suspended in narrow channel NASA-CR-1186 STRUCTURAL WEIGHT c12 N68-35086 Survey on minimum weight design aspects of stiffened cylinders under compression NASA-CR-963 c3 c32 N68-11282 SUBMERGED BODIES Water immersion simulation study of astronaut performance during airlock ingress or egress at reduced gravity NASA-CR-971 c05 N68-20339 SUBMILLIMETER WAVES Coherent radiation methods of measuring absorption spectra in planetary atmosphere, and millimeter and submillimeter wave propagation NASA-CR-863 c07 N68-27063 Uses of submillimeter waves in aerospace technology, with bibliography NASA-SP-182 c07 c07 N68-35522 SUBROUTINES FORTRAN subroutines for plotting and drawing of three dimensional solid surfaces NASA-TM-X-1598 SUBSONIC AIRCRAFT c19 N68-28240 Aerodynamic characteristics of subsonic cargo jet transport model in slotted transonic wind tunnel NASA-TM-X-1660 c01 N68-35617 c01 N68-35617 SUBSONIC FLOW Analytical investigation of flow and wall temperature sensitivity in heated passages for large inlet to exit density ratios in subsonic flow of nuclear rocket NASA-TN-D-4649 c33 N68-28371 Modified approach for predicting lift body pressures and camber shape for planforms in subsonic flow NASA-TN-D-4427 c01 N68-28868 Effect of geometry of conical afterbodies on base drag at subsonic and transonic speeds NASA-TN-D-4821 c01 N68-37054 c01 N68-37054 SUBSONIC FLUTTER Subsonic and transonic flutter and flow studies of T tail of large multijet cargo airplane NASA-TN-D-4316 c02 N68-17055 SUBSONIC SPEED Subsonic dynamic stability characteristics of large conical spacecraft in simulated Martian environment NASA-TN-D-4558 c31 N68-22301 Pressure fluctuation measurements on afterbodies of blunt atmospheric entry vehicles NASA-TN-D-4591 c32 N68-24508 SUBSTRATES Equations for determining substrate surface coverages from arrival rates and desorption characteristics of adsorbate ions and atoms NASA-TN-D-4369 c25 N68-25630 SUITABILITY Economic and suitability comparison of short haul transport aircraft concepts NASA-CR-986 c02 N68-13517 SUMMARIES Gemini Summary Conference NASA-SP-138 c30 N68-14941 SUN Computation of solar elevation angles and determination of sunrise and sunset times as function of latitude, longitude, and date

c13 N68-35179 NASA-TM-X-1646 SUNRISE Computation of solar elevation angles and determination of sunrise and sunset times as function of latitude, longitude, and date NASA-TM-X-1646 c13 N68-35179 SUPERCONDUCTIVITY Superconduction thin films, and properties and applications of Josephson effect at radio frequencies NASA-CR-1189 c26 N68-35178 Ultrasonic attenuation measurements on single tantalum crystals at superconducting state NASA-TN-D-4806 SUPERCONDUCTORS c26 N68-35356 Magnetometers for measuring stable magnetic fields produced by low field superconducting shields NASA-CR-1073 c14 N68-26703 SUPERCOOLING Fuel tank pressurization and supercooling of liquid methane to minimize fuel boiloff problems in supersonic aircraft NASA-TM-X-1604 c27 N68-28155 SUPERNOVAE Detection of supernovae pulse by gamma ray telescope and atmospheric scintillation method NASA-TN-D-4732 c29 N68-3333 c29 N68-33370 SUPERSONIC AIRCRAFT Piloted fixed-base simulation of low speed flight characteristics of arrow wing supersonic transport aircraft NASA-TN-D-4277 c05 N68-13609 Installation and fairing of flush, static pressure orifices on wing surfaces of supersonic aircraft Ansa-TH-X-1530 coll values of supersonic arroration of the second c01 N68-19341 of supersonic aircraft NASA-TN-D-4578 c02 N68-24498 Atmospheric effects on sonic boom characteristics NASA-TN-D-4588 c02 N68-24662 Fuel tank pressurization and supercooling of liquid methane to minimize fuel boiloff problems in supersonic aircraft NASA-TM-X-1604 c27 N68-28155 Comparative analysis of fuselage tanks for liquid methane fueled supersonic aircraft NASA-TN-D-4837 c02 N68-36074 c02 N68-36074 SUPERSONIC COMMERCIAL AIR TRANSPORT CRSUNIC COMMERCIAL AIR TRANSPORT Low speed static and dynamic stability tests on scale model of double-delta supersonic commercial air transport configuration NASA-TN-D-4179 co2 N68-18; c02 N68-18250 Sonic boom research /conference/ NASA-SP-147 c02 N68-21413 SUPERSONIC DIFFUSERS Wind tunnel tests of mixed-compression axisymmetric inlet system to determine bleed mass flow ratio, pressure recovery and pressure distortion NASA-TN-D-4557 SUPERSONIC DRAG c28 N68-23354 Heat transfer effect on drag due to surface roughness in supersonic turbulent boundary layer NASA-TN-D-4746 c12 N68-33054 SUPERSONIC FLIGHT Analysis of several methane fueled engine cycles for supersonic flight NASA-TN-D-4699 c28 N68-29378 Static performance of an auxiliary inlet ejector nozzle for supersonic-cruise aircraft NASA-TM-X-1653 c2 c28 N68-35764 SUPERSONIC FLOW Nonlinear flutter of circular cylindrical shell in supersonic flow NASA-TN-D-4265 c32 N68-12864 FORTRAN 4 program for computerized design of two dimensional supersonic nozzles with sharp edged throats NASA-TM-X-1502 c01 N68-14747 Flutter analysis on buckled supported rectangular panels under supersonic surface flow NASA-TN-D-4357 c c32 N68-17651 Aerodynamic characteristics of tension string, tension shell, and conical shapes in supersonic flow NASA-TN-D-4360 c01 N68-18 Analysis of turbulent wall pressure field under supersonic shear layers c01 N68-18720

SUPERSONIC FLUTTER

SUBJECT INDEX

NASA-CR-888 c12 N68-22087 FORTRAN program for approximate calculation of supersonic ideal gas flow past blunt bodies with sonic corners NASA-TN-D-4563 coll N68-25093 Flame propagation in supersonic premixed flows of hydrogen and air ignited by coaxial, hot gas, pilot jet NASA-TN-D-4631 c33 N68-28100 NASA-IN-D-4031 Supersonic aerodynamics of large angle cones NASA-TN-D-4719 Wind tunnel tests at Mach 1.60, 2.36, and 2.96 to determine flow field properties near arrow wing body model for locating potential engine air inlets NASA-TN-D-4809 SUPERSONIC FLUTTER c01 N68-37238 Experimental study, and theoretical analysis on supersonic flutter of corrugation stiffened panels NASA-TN-D-4321 SUPERSONIC INLETS c32 N68-19143 Wind tunnel investigation of techniques for reducing cowl drag of external compression inlet at Mach 2.49 NASA-TM-X-1516 c01 N68-18189 Supersonic performance evaluation of mass flux probes with sharp symmetrical inlet, and with blunted unsymmetrical inlet NASA-TM-X-1524 Dynamic response of subsonic inlet to external and internal disturbances NASA-TM-X-1648 c01 N68-33374 SUPERSONIC JET FLOW Simulated study of effects of high altitude supersonic air flow on titanium alloy hot salt cracking process NASA-CR-981 c17 N68-11522 SUPERSONIC NOZZLES Description and operating parameters of Mach 2 nozzle system for 11-inch ceramic heated wind tunnel NASA-TN-D-4750 SUPERSONIC SPEEDS c11 N68-33190 Supersonic aerodynamic characteristics of model of air-to-surface missile NASA-TM-X-1491 c01 N68-16480 Design and performance testing of large scale mixed compression axisymmetric inlet at transonic and supersonic speeds NASA-TM-X-1507 c28 N68c28 N68-17028 Wind tunnel tests on pressure distribution, and shock shapes of conical blunted bodies moving at supersonic speeds in nitrogen, or helium media NASA-TN-D-4314 c01 N68-178 c01 N68-17896 Cold flow tests of aerodynamic characteristics of plug nozzle configuration for turbojet engines operating at supersonic speeds NASA-TM-X-1619 c28 N68-299 c28 N68-29953 Flight test of 40 foot parachute deployed at low supersonic speed and dynamic pressure c31 N68-29993 NASA-TM-X-1623 Aerodynamic characteristics of two blunt half cone Aerodynamic characteristics of two blunt half con-wedge entry configurations at supersonic speeds NASA-TM-X-1621 coll N68-3003 Wind tunnel evaluation of speed brake effects on supersonic characteristics of variable sweep c01 N68-30030 fighter aircraft models NASA-TN-D-4773 c02 N68-33669 Aerodynamic drag measurements and boundary layer flow over V notches at transonic and supersonic speeds NASA-CR-1132 c12 N68-35252 Aerodynamic characteristics of bodies of revolution at Mach numbers from 1.50 to 2.86 and angles of attack to 180 deg NASA-TM-X-1658 c01 N68-3 c01 N68-36193 Windshield and nose geometry effects on supersonic aerodynamic characteristics of tactical fighter model NASA-TM-X-1664 SUPERSONIC TRANSPORTS c02 N68-37066 Design and volumetric analysis of pressurized tanks for use in liquid-methane fueled supersonic transport aircraft supersonic transport aircrait NASA-TN-D-4295 Simulated flight test of double-Delta supersonic transport for performance characteristics, handling qualities, and climbing characteristics

NASA-TN-D-4396 c02 N68-17391 Tankage systems for methane-fueled supersonic transport NASA-TM-X-1591 c02 N68-23895 Verformance requirements and economic costs to reduce cruise sonic boom of supersonic transport NASA-TN-D-4677 c02 N68-28831 Simulated flight operations to evaluate problems encountered by supersonic transports in present air traffic control system NASA-TN-D-4638 c02 N68-29372 Conference on sonic boom reduction in supersonic transport flight - shock wave propagation and refraction, prediction methods for acoustic attenuation, and aerodynamic engineering aspects NASA-SP-180 c02 N68-34907 Wind tunnel tests to determine low speed high lift aerodynamics of one-fifth scale variable sweep supersonic transport model NASA-TN-D-4844 c01 N68-37365 SUPERSONIC TURBINES FORTRAN computer program for supersonic turbomachinery blading design calculations c08 N68-18620 NASA-TN-D-4421 Effects of surface Mach numbers. inlet flow angle and specific heat ratio on geometric features of supersonic impulse turbine blade sections over Mach number range of 1.5 to 5.0 NASA-TN-D-4422 SUPERSONIC WAKES Transition from laminar to turbulent flow in near c03 N68-20276 wake of supersonic reentry body NASA-TN-D-4645 SUPERSONIC WIND TUNNELS c01 N68-28220 Water vapor condensation effects of heated air on flow in large supersonic wind tunnels NASA-TM-X-1636 cll N68-3059 c11 N68-30598 Effect of model forebody shape on perforated supersonic wind tunnel wall interference NASA-TM-X-1656 c01 N68-36133 Cone-cylinder models tested in supersonic wind tunnel to evaluate effect of wall reflected disturbances on model pressure distributions NASA-TM-X-1655 col N68-3 c01 N68-36134 SUPPORT SYSTEMS Development of mission requirement profile for subsystem components from overall system profile NASA-SP-6503 c30 N68-15683 SUPPRESSORS Acoustic measurements on jet engine intake system noise reduction suppressor cowlings NASA-TN-D-4639 SURFACE DISTORTION c02 N68-29887 Effect of two dimensional multiple sine wave protrusions on pressure and heat transfer distributions for flat plate in hypersonic flow NASA-TN-D-4437 col N68-1996 NASA-TN-D-4437 coll N68-19063 Imperfections of axially loaded cylindrical shells NASA-TM-X-1552 c32 N68-21767 SURFACE FINISHING Hard surfacing, electroplating, electrodeless plating, carburizing, nitriding, burnishing, explosive hardening, planishing, and peening of precipitation-hardenable stainless steels NASA-SP-5090 SURFACE GEOMETRY c15 N68-19343 Supplementary information for computer program predicting lifting pressure and camber shape of composite planform in subsonic flow NASA-TN-D-4427, SUP. SURFACE PROPERTIES c01 N68-31515 Emission and reflection coefficients of surface thermal radiation properties NASA-TT-F-497 c33 N68-21536 SURFACE REACTIONS Silicate surface preparation to represent lunar soil, and ultrahigh vacuum adhesion measurements NASA-CR-1090 c30 N68-28373 SURFACE ROUGHNESS NASA-TN-D-4323 NUMBER AND ACT OF A CONSTRUCTION OF A CONSTRUCT OF c02 N68-14903 Heat transfer effect on drag due to surface roughness in supersonic turbulent boundary layer NASA-TN-D-4746 SURFACE ROUGHNESS EFFECTS c12 N68-33054 Surface roughness effects on normal spectral

emittance of vapor deposited rhenium NASA-TM-X-1514 c c17 N68-19347 SURFACE TEMPERATURE Evaluation of sea surface temperature as measured by Nimbus 1 satellite high resolution infrared radiometer NASA-TN-D-4078 c20 N68-10222 NASA-IN-D-4078 c20 N68-Equations, charts, and analysis to calculate theoretical temperatures of thin film solar cells in earth orbit NASA-TN-D-4331 c33 N68-SURVEYOR LUNAR PROBES c33 N68-14270 Surveyor 5 configuration, television picture transmission, and experiments on measuring chemical elements in lunar surface NASA-SP-163 Surveyor 6 scientific data analysis c31 N68-17844 NASA-SP-166 c31 N68-21443 Flight performance evaluation of Atlas-Centaur for Surveyor spacecraft SC-2 NASA-TM-X-1616 c31 N68-33332 Principal scientific results on Surveyor 7 míssion NASA-SP-173 c31 N68-33553 Spaceborne photography of cloud cover and other meteorological phenomena, Surveyor and Orbiter lunar shots, and Gemini space walk and target docking NASA-SP-168 c30 N68-34870 Electromagnetic compatibility verification for Surveyor spacecraft and Atlas Centaur launch vehicle NASA-TM-X-1673 c31 N68-36971 SURVEYOR 1 LUNAR PROBE Systems analysis and flight performance of Atlas Centaur launch vehicle with Surveyor 1 lunar probe NASA-TN-D-4580 c31 N68-24338 SWEAT COOLING Oxidation resistant alloys tested for suitability as transpiration cooled gas turbine blades c17 N68-17591 NASA-CR-930 Film and transpiration cooled baffles for M-1 engine NAŠA-TM-X-1267 c28 N68-18216 SWEPT WINGS Simulated wing damage effects on aerodynamic characteristics of swept-wing airplane model NASA-TM-X-1550 c01 N68-22002 NASA-TM-X-1550 SWITCHING CIRCUITS Electromagnetic switching properties of bistable, magnetically permeable liquid bead with nondestructive memory for gas flow control NASA-TM-X-1613 SYMBOLIC PROGRAMMING c09 N68-30501 Computer program for symbolic reduction of block diagrams to obtain transfer functions NASA-TN-D-4617 c08 N68-2490 c08 N68-24967 SYNCHRONISM Self-synchronizing, biorthogonal coded pulse code modulation telemetry system for communicating with unmanned spacecraft NASA-TR-R-292 c07 N68-3633; c07 N68-36333 SYNCHROTRON RADIATION Synchrotron emission at helical motion of relativistic electrons emitting from source with relativistic velocity NASA-TT-F-521 c25 N68-16700 SYSTEM FAILURES Human response analysis in combined trajectory control task, system-failures task, and motor response task NASA-TN-D-4356 c05 N68-18 Pilot dynamic response to sudden flight control c05 N68-18014 system failures NASA-CR-1087 c05 N68-26690 Electron radiation induced dielectric breakdowns in capacitor meteoroid detection system NASA-TN-D-4738 c14 c14 N68-33277 SYSTEMS ANALYSIS Development of mission requirement profile for subsystem components from overall system profile NASA-SP-6503 c30 N68-15683 System dynamics and control analysis of tungsten water moderated nuclear rocket NASA-TM-X-1426 c22 N68-18252 Systems analysis and flight performance of Atlas Centaur launch vehicle with Surveyor 1

lunar probe

c31 N68-24338 NASA-TN-D-4580 Systems performance, lunar photography, and launch operations of Lunar Orbiter 3 photographic mission NASA-CR-1069 c31 N68-24738 Fully-manual and augmented-manual control systems for Saturn 5 booster studied by emperically based mathematical models for pilot c31 N68-28426 NASA-CR-1079 Systems analysis and performance test data on dual radiometer assembly for measuring far infrared wavelength bands of earths horizon radiance profile NASA-CR-1086 c14 N68c14 N68-28965 NASA-CK-1086 cl4 N66-28 Technology requirements and spacecraft design studies for atmosphere braking to orbit about Mars and Venus NASA-CR-1131 c30 N68-34 c30 N68-34086 Systems analysis logic applied to mathematical modeling of dynamic nonlinear stochastic processes NASA-CR-1168 c19 N68-35472 SYSTEMS ENGINEERING Instrumentation, systems engineering, and life support systems for Apollo primate orbital experiment NASA-CR-926 c05 N68-15306 Design and performance testing of large scale mixed compression axisymmetric inlet at transonic and supersonic speeds NASA-TM-X-1507 c28 N68-17028 Design and flight performance studies of Wasp sounding rocket NASA-TM-X-1518 c31 N68-17094 Effects of surface Mach numbers, inlet flow angle and specific heat ratio on geometric features of supersonic impulse turbine blade sections over Mach number range of 1.5 to 5.0 NASA-TN-D-4422 c03 N68-20276 Design of guidance and control systems for optimum utilization of information NASA-CR-997 c10 N68-23438 Spacecraft system design, mission planning, and qualification testing for Gemini project NASA-CR-1106 c31 N68-25577 Laboratory methodology of signal analysis with application to Apollo program NASA-TM-X-1599 c08 N68-30240 Systems engineering and development of M-1 injector hydrogen oxygen engine NASA-TN-D-4730 c28 N68-30604 Design of bodies to produce specified sonic boom signatures NASA-TN-D-4704 c01 N68-31484 Hardware design and computer programs for spaceborne multiprocessor computer system NASA-CR-1158 c08 N6 c08 N68-31499 Design evaluation of helical electron bombardment filaments for heating cylindrical thermionic converters NASA-TM-X-1630 c22 N68-32968 Recuperator for closed Brayton cycle solar energy space power system NASA-CR-1150 c03 N68-33062 New methods for design of adaptive flight control systems NASA-CR-1152 c21 N68-33904 Process development of system for digital computer processing of psychophysiological data to obtain high stress tolerance personnel NASA-CR-1122 c05 N68-35102 Design of pulse position modulation optical communication system NASA-TN-D-4814 c07 N6 c07 N68-35174 Multivariable control systems for industrial applications NASA-TT-F-435 c10 N68-37293 Т T TAIL SURFACES Subsonic and transonic flutter and flow studies of T tail of large multijet cargo airplane c02 N68-17055 NASA-TN-D-4316 Sideslip angle effects on static stability characteristics of T tail transport

configuration NASA-TM-X-1665 col N68-36112

I-101

TABLES (DATA)

SUBJECT INDEX

TABLES (DATA) Wing surface pressure data from large scale wind tunnel tests of propeller driven short takeoff aircraft NASA-TM-X-1527 c02 N68-19065 Convective heat transfer data for water flow in heated circular tubes with varying heat fluxes and flow areas NASA-TM-X-1554 c33 N68-20338 Tabulated performance data of full-scale rotary wings at high advance ratios and advancing tip Mach numbers based on wind tunnel tests NASA-TN-D-4632 c01 N68-28268 Systematic procedure for constructing character table of finite group NASA-TN-D-4763 c19 N68-31961 and mesosphere, 1966 - tables NASA-TR-R-288 c20 N68-33036 Tables of energy and angular distributions of thick target bremsstrahlung in metals NASA-TN-D-4755 TAIL ASSEMBLIES c24 N68-35535 Stabilizer and tail assembly effects on overall aerodynamic characteristics of lifting bodies at hypersonic speeds NASA-TM-X-1620 c01 N68-29952 TANK GEOMETRY Analytical and experimental investigation of propellant distribution during outflow of spherical tanks for possible space vehicle application NASA-TN-D-4828 c12 N68-35104 TANTALUM Corrosion products of oxygen doped tantalum exposed to potassium at 1800 deg F NASA-TN-D-4213 c17 N68-11511 Tantallum-stainless steel bimetallic joints tested to determine overall strength of brazed ioint NASA-TM-X-1540 c15 N68-21898 Tensile properties of tantalum and tungsten 10-fiber bundles NASA-TN-D-4725 c17 N68-30504 Ultrasonic attenuation measurements on single tantalum crystals at superconducting state NASA-TN-D-4806 TANTALUM ALLOYS c26 N68-35356 Creep behavior of tantalum alloys in ultrahigh vacuum for extended time periods NASA-TN-D-4605 c17 N68-24111 TANTALUM OXIDES Magnitude of electrical potential-temperature curve determined for tantalum, niobium, and magnesium during oxidation in air NASA-TN-D-4240 c17 N68c17 N68-10498 TARGET THICKNESS Tables of energy and angular distributions of thick target bremsstrahlung in metals NASA-TN-D-4755 c24 N68-35535 TASKS Human response analysis in combined trajectory control task, system-failures task, and motor response task NASA-TN-0-4356 c05 N68-18014 TEACHING MACHINES Feasibility of computer assisted flight controller training NASA-CR-917 c08 N68-13897 TECHNOLOGY UTILIZATION utilization of aerospace research output c34 N68-25221 NASA-SP-5021/06/ Space technology transfer to developing nations using Brazil as model NASA-CR-1222 c34 N68-37216 TELEMETRY Performance evaluation of several convolutional and block codes with threshold decoding for space telemetry NASA-TN-D-4402 c07 N68-18178 Non-TR D 4702 Self-synchronizing, biorthogonal coded pulse code modulation telemetry system for communicating with unmanned spacecraft NASA-TR-R-292 c07 N68-3633 c07 N68-36333 TELESCOPES Celestial attitude measuring instrument using star mapping technique NASA-TN-D-4742 c21 N68-31938 Telescope objective lens size, aperture size, and magnification effects on operator performance using marine sextants NASA-TN-D-4781 c21 N68-TELEVISION TRANSMISSION c21 N68-33006 Surveyor 5 configuration, television picture transmission, and experiments on measuring chemical elements in lunar surface NASA-SP-163 c31 N68-17844 TEMPERATURE CONTROL High temperature flowing gas heater consisting of four stages for heating gases NASA-TM-X-1506 c11 N68-14115 System dynamics and control analysis of tungsten water moderated nuclear rocket NASA-TM-X-1426 c22 N68-18252 Development of nuclear thermionic space power system using thermionic diodes, and heat pipe flow for temperature control NASA-TN-D-4299 c22 N68-1 Approximate average midspan metal temperatures c22 N68-19146 and coolant flow requirements for turbine airfoils cooled by compressor exit bleed air NASA-TN-D-4491 c33 N68-1 c33 N68-19187 NRSA-IN-0-4491 CS3 NGG-Heat balance equations for optimizing optical coating patterns for spacecraft temperature control system NASA-CR-1041 c18 N68c18 N68-22391 TEMPERATURE DISTRIBUTION Three dimensional analysis for determining effects of heat generation in plates NASA-TN-D-4326 c33 N68-18122 Approximate average midspan metal temperatures and coolant flow requirements for turbine airfoils cooled by compressor exit bleed air NASA-TN-D-4491 c33 N68-19187 Mathematical model of liquid metal fuel reactor to investigate temperature distribution on neutron kinetics NASA-TN-D-4840 TEMPERATURE EFFECTS c22 N68-36055 Simulated study of effects of high altitude supersonic air flow on titanium alloy hot salt cracking process NASA-CR-981 c17 N68-11522 Effects of Freen, water flow temperatures, and pressures on incipient venturi cavitation NASA-TN-D-4340 cl2 N68-14 c12 N68-14641 RESETING AND A CONTRACT OF A C window materials NASA-CR-1019 c31 N68-20467 C31 N68-2/ Interfiber distance and temperature effects on critical aspect ratio in composites NASA-TN-D-4548 c17 N68-22 c17 N68-22338 Window designs for mercury condensing tube and mercury boiler outlet tube NASA-TM-X-1578 c11 N68-22737 Dielectric temperature change effects observed in ferroelectric and pyroelectric substances NASA-CR-1080 c26 N68-25972 Predictions for magnetoresistivity temperature dependence of dilute alloys of iron in copper NASA-TN-D-4626 c26 N68-28239 Effects of stretch and heat-set temperatures and time on cryogenic mechanical properties of poly/ethyl terephthalate/ film NASA-TN-D-4762 c18 N68 c18 N68-33034 Charts of thermodynamic properties of helium showing effects of ionization, particle interactions, temperature, and atmospheric nteractions, temperature, and atmospheric pressure NASA-TN-D-4754 cl2 N68-3511 TEMPERATURE GRADIENTS Establishing allowable temperature gradients for tungsten-uranium dioxide fuel elements using c12 N68-35117 experimental cyclic strain data NASA-TN-D-4279 c22 N68-14986 Suppression of temperature rise in lossy diodes inside resonant cavities by pressurized liquid nitrogen NASA-TN-D-4556 TEMPERATURE MEASUREMENT c09 N68-24387 Meteorological wind, and temperature data from atmospheric radiosonde soundings in Southern Hemisphere NASA-TN-D-4429 c20 N68-19084 Platinum resistance thermometers tested and evaluated in cryogenic temperature measurement

NASA-TN-D-4499 c14 N68-20324 Electron beam probe measurements of rotational and vibrational temperatures in static low-density NASA-TN-D-4500 c14 N68-24244 Vapor pressure measurements of potassium to 2170 deg K NASA-TN-D-4535 c33 N68-25122 Ablation and temperature data for Apollo heat shield material using Pacemaker vehicle for flight test NASA-TN-D-4713 c33 N68-30747 Jet VTOL aircraft inlet temperature rise and induced recirculating flow patterns NASA-CR-1147 col N68-33043 Single-thermocouple method for measuring heat flux in thermally thick walls NASA-TN-D-4737 c33 N68-33208 TEMPERATURE MEASURING INSTRUMENTS Temperature and liquid-level sensor for liquid hydrogen pressurization and expulsion studies NASA-TN-D-4339 cl4 N68-15893 Combination temperature, pressure, and flow direction sensing probe to study rotating machinery NASA-TN-D-4816 c14 N68-36021 Thermal entry length of temperature sensor placement in tubular radiation shield NASA-CR-1200 c14 N c14 N68-36530 TEMPERATURE PROFILES Boundary condition solution and transcendental approximation for transient heat conduction problem NASA-CR-955 c19 N68-11109 Tungsten-stainless steel sensor for averaging temperature measurement of nonuniform temperature measurement of nonunfform temperature profiles NASA-TN-D-4242 c14 NG FORTRAN 4 computer program for calculating temperature profiles in propellant tank c14 N68-15936 NASA-TM-X-1556 c27 N68-21267 Differential equations based on heat transfer and shear for temperature and velocity in turbulent boundary layers NASA-TN-D-4611 c33 N68-2591 c33 N68-25917 TENSILE PROPERTIES Axial tensile fatigue of liquid rocket engine alloys at cryogenic temperatures NASA-TN-D-4274 c17 N68-11 Directional solidification of nickel base alloy c17 N68-11637 TAZ-8B to enhance potential for advanced gas turbine engine applications NASA-TN-D-4390 c17 N68-1 c17 N68-15637 Hot salt stress corrosion cracking effects on tensile properties of titanium alloy sheets NASA-TN-D-4674 c17 N68-30000 Tensile properties of tantalum and tungsten 10-fiber bundles NASA-TN-D-4725 c17 N68-30504 High temperature tensile properties of tungstenrhenium alloys NASA-TN-D-4728 c17 N68-30605 Low temperature effects on tensile properties of aluminum, magnesium, nickel, steel, and titanium alloys NASA-SP-5012/01/ c17 N68-31605 TENSILE STRENGTH Tensile strength properties of glass, boron, and graphite filament wound resin composites and liners for cryogenic pressure vessels NASA-TN-D-4412 cl8 N68-166 c18 N68-16623 Composition and heat treatment effects on high temperature strength of arc melted tungsten-hafnium-carbon alloys NASA-TN-D-4379 c17 N68-17317 Tantallum-stainless steel bimetallic joints tested to determine overall strength of brazed joint NASA-TM-X-1540 c15 N68-21898 TENSILE TESTS Calculations for elastic tensometric elements and operation of tensometric force measuring devices NASA-TT-F-513 c32 N68-15796 Crack propagation in aluminum notched tensile and pressure vessel specimens cyclically loaded at cryogenic temperatures NASA-TN-D-4541 c17 N68-21768 TENSOMETERS Calculations for elastic tensometric elements and

operation of tensometric force measuring devices NASA-TT-F-513 c32 N68-15796 TEREPHTHALATE Effects of stretch and heat-set temperatures and time on cryogenic mechanical properties of poly/ethyl terephthalate/ film NASA-TN-D-4762 c18 N68-33034 TERMINAL BALLISTICS NAIMAL BALLISILG Penetration resistance of aluminum double sheet targets to projectile impact NASA-TN-D-4568 Plate-gap model of porous solid and application to reduced density projectile impact 632 N68-31912 NASA-CR-1140 TERMINAL GUIDANCE Cumulative errors associated with Category 2 and 3 operations, and terminal flight paths for low visibility landings NASA-CR-1188 c02 N68-35595 TERRAIN Detection of terrain features from Nimbus 1 satellite high resolution infrared radiometer nighttime measurements nightime measurements NASA-TN-D-4603 c13 N68-23 TERRAIN ANALYSIS Optimization of confidence levels in detecting lunar surface detail in terms of viewing geometry and camera shutter speeds for Lunar Orbiter missions NASA-TN-D-4501 c14 N68-23 TEST EQUIPMENT c13 N68-28872 c14 N68-21942 Automatic testing and checkout of Saturn 1 launch vehicles NASA-TN-D-4328 TEST FACILITIES c31 N68-15570 Visual simulation facility for evaluation of lunar surface roving vehicles NASA-TN-D-4276 Design, and performance of facility for Rankine cycle testing of two stage potassium vapor turbine turbine NASA-CR-924, V. 3 c03 N68-180 SNAP 8 simulator using primary sodium-potassium loop, mercury loop operating on Rankine cycle, and heat rejection sodium-potassium loop c03 N68-18044 NASA-TM-X-1515 c11 N68-18460 SNAP 8 simulator facility instrumentation NASA-TM-X-1525 c14 c14 N68-19001 Test apparatus and procedures for aerodynamic model tests of spacecraft control system parameters NASA-CR-947 c32 N68-23452 TEST FIRING Stability effects of several injector face baffle configurations on screech in hydrogen-oxygen rocket NASA-TN-D-4515 c28 N68-21679 TEST VEHICLES Static longitudinal aerodynamic characteristics of configurations used in Little Joe/Apollo test vehicle development NASA-TN-D-4439 c31 N68-22953 TESTS Leakage testing theory and testing methods handbook NASA-CR-952 c15 N68~20389 TETHERLINES Gemini-Agena station keeping using connecting tether - Analysis and simulations NASA-TN-D-4258 c31 N68c31 N68-11641 THEOREM PROVING Qualitative theory of differential equations and conversion to integral equations NASA-CR-1164 c19 N68-334 c19 N68-33426 Newton-Raphson and gradient parameter correction technique for solution of optimal control problems NASA-TR-R-293 c19 N68-3707 THEORETICAL PHYSICS Theoretical approach to determination of magnetic c19 N68-37073 torques on orbiting spacecraft by near-field measurement NASA-TN-D-4485 c23 N68-24146 THERMAL CONDUCTIVITY Lunar volcanism model based on high temperature radiative thermal conductivity of Sinerals and rocks NASA-CR-916 c13 N68-10283 Theoretical analysis of five composite ablation

materials with various percentages of phenolic resin, powdered nylon, and silica NASA-TN-D-4374 c18 N68-197 c18 N68-19710 NASA-TN-D-4374 Bifurcation approximation for binary and thermal diffusion coefficients, mixture viscosity, and thermal conductivity of laminar boundary layer NASA-CR-1063 C33 N68-26815 Thermal conductivity measurements on tungsten coated uranium dioxide cermets NASA-CR-1154 THERMAL CYCLING TESTS c22 N68-32983 Establishing allowable temperature gradients for tungsten-uranium dioxide fuel elements using experimental cyclic strain data NASA-TN-D-4279 c22 N68-14986 THERMAL DEGRADATION Thermal degradation of high performance multilayer insulation on liquid hydrogen tank in vicinity of penetration NASA-TN-D-4778 c33 N68-33167 THERMAL DIFFUSION Bifurcation approximation for binary and thermal diffusion coefficients, mixture viscosity, and thermal conductivity of laminar boundary layer NASA-CR-1063 c33 N68-2683 c33 N68-26815 THERMAL EMISSION Calculations of nondiffuse infrared radiation from lunar surface incident onto unit element above surface NASA-TM-X-1567 c29 N68-21731 THERMAL ENERGY Radiative thermal energy incident effects on pressure-suited man on lunar surface NASA-TN-D-4243 c30 N68-11630 THERMAL INSULATION shields for cryogenic storage tanks NASA-TN-D-4644 NASA-TN-D-4644 Analytical method for finding heat balance of insulated OGO experiment packages from thermal stability data and without solar simulation NASA-TN-D-4644 cll N68-294 c33 N68-18046 c11 N68-29478 Thermal degradation of high performance multilayer insulation on liquid hydrogen tank in vicinity of penetration NASA-TN-D-4778 c33 N68-33167 Thermal entry length of temperature sensor placement in tubular radiation shield NASA-CR-1200 c14 No c14 N68-36530 THERMAL NEUTRONS

 INERNAL NEUTRONS

 Fast and thermal neutron flux measurements in test

 cavity outside HB-6 beam port in Plum Brook

 reactor using sulfur pellets and gold foils

 NASA-TM-X-1497
 c22 N68-15643

 THERMAL PROTECTION

 Assessing cryogenic fluid requirements and storage methods for manned earth orbital and Mars flyby missions, and parametric data on thermal protection schemes NASA-TN-D-4619 THERMAL RADIATION c03 N68-28420 Uncertainty analysis for designing calorimetric experiments, and equations for measuring properties of planetary radiation NASA-TN-D-4354 cl4 N68-16 c14 N68-16529 Emission and reflection coefficients of surface thermal radiation properties NASA-TT-F-497 c33 N68-21 c33 N68-21536 Thermal radiation heat transfer data, radiative properties of black bodies, and electromagnetic theory NASA-SP-164 c33 N68-28530 Thermal radiative and electrical properties of cadmium sulfide solar cell at low simulated solar intensities and temperatures NASA-TN-D-4818 THERMAL STABILITY c03 N68-35467 Calcium, molybdenum, and lithium compounds as low drive temperature stable memory cores NASA-TN-D-4573 c09 N68-2438 c09 N68-24388 THERMIONIC CATHODES Pairs of emitter and collector sheaths for cesium thermionic diodes c25 N68-21623 NASA-TN-D-4419 Design evaluation of helical electron bombardment filaments for heating cylindrical thermionic converters NASA-TM-X-1630 c22 N68-32968

SUBJECT INDEX

THERMIONIC CONVERTERS. Electrical performance of rhenium niobium cylindrical thermionic converter NASA-TN-D-4533 c03 N68-21766 Current-voltage characteristics of variable spaced thermionic converter with tungsten emitter and niobium collector NASA-CR-1033 c03 N68-23476 MAA dr. 2005 Efficiency and steady state performance of cylindrical thermionic converter with rhenium emitter and niobium collector NASA-TN-D-4582 c03 N68-25 c03 N68-25059 bombardment filaments for heating cylindrical thermionic converters NASA-TM-X-1630 THERMIONIC DIODES c22 N68-32968 Electrical properties of xenon filled thermionic diodes in nuclear reactor radiation field NASA-TN-D-4368 c25 NG c25 N68-15747 Development of nuclear thermionic space power system using thermionic diodes, and heat pipe flow for temperature control NASA-TN-D-4299 c22 N68-19146 Non-IN-D-12-32 NOO-I Point-kernel computation and experimental measurements of gamma heating effects during thermionic diode irradiation NASA-TM-X-1539 c22 N68-2: c22 N68-22022 Emitter and collector sheaths for cesium thermionic diodes with polycrystalline tungsten electrodes electrodes NASA-TN-D-4744 c25 N68-316 THERMIONIC EMISSION Current-voltage characteristics of collisionless cylindrical diode with thermionically emitted c25 N68-31640 electrons NASA-TN-D-4516 c10 N68-21122 THERMIONIC POWER GENERATION Radiation effects on thermionic insulator materials - evaluation of beryllia, alumina, thoria, zirconia, and yttria NASA-TN-D-4414 THERMOCHEMICAL PROPERTIES c22 N68-17095 Effects of molecular structure on thermochemical properties of phenolic resins and related olymers NASA-TR-R-276 c33 N68-11038 THERMOCOUPLES Photographs, thermocouples, and emission spectra used to study mixing and reaction of hydrazine and nitrogen tetroxide NASA-TN-D-4467 c33 N68-24965 Single-thermocouple method for measuring heat flux in thermally thick walls NASA-TN-D-4737 c33 N68-33208 NASA contributions to special-purpose thermocouple design and applications NASA-SP-5050 c c14 N68-35620 THERMODYNAMIC EFFICIENCY Weight, heat transfer, and efficiency comparison for Rankine cycle space radiators constructed of three different finned tube geometries NASA-TN-D-4411 c33 N68-16324 Parametric analysis of effects of concentrator surface errors and rim angle, collection system orientation error, and receiver temperature on paraboloid solar collector thermal efficiency NASA-TN-D-4415 co3 N68-18998 c22 N68-28304 THERMODYNAMIC EQUILIBRIUM Radiation equilibrium in atmosphere with constant Einstein absorption coefficient NASA-TN-D-4479 c13 N68-22861 THERMODYNAMIC PROPERTIES Numerical procedures and computer program for calculating real fluid and thermodynamic properties of normal and parahydrogen NASA-TN-D-4341 c0 c08 N68-15798 NASA-IN-D-4341 Approximate equations for computing enthalpy and velocity derivatives at surface of flat plate, cone, or blunt axisymmetric body NASA-TN-D-4484 C33 N68-2000 c33 N68-20065 Partition functions and thermodynamic properties to high temperatures for hydrogen triatomic and diatomic molecular ions NASA-TN-D-4523 c33 N68-21732

Data correlation of thermophysical properties of

THRUST CHAMBERS

saturated liquid lithium as function of temperature temperature NASA-TN-D-4650 c17 N68 Charts of thermodynamic properties of helium showing effects of ionization, particle interactions, temperature, and atmospheric c17 N68-28365 pressure NASA-TN-D-4754 c12 N68-35117 THERMODYNAMICS Thermodynamic effects on Freon cavitation on venturi scale model NASA-TN-D-4387 c12 N68-15329 Gravity effects on bubble dynamics generated during nucleate boiling NASA-TN-D-4301 c33 N68-15330 Thermodynamic effects of cavitation in low temperature liquid hydrogen over range of flow coefficients using flat plate helical inducer NASA-TN-D-4423 Transient thermodynamic analysis for development of mathematical model that predicts transient temperature and voltage-response characteristics of fuel colt of fuel cell system NASA-TN-D-4601 c03 N68-25304 Thermodynamics of plasmas using principle of maximum entropy NASA-TN-D-4621 c25 N68-25920 Computer program for solutions to equilibrium and nonequilibrium chemical state relations for open and closed thermodynamic systems NASA-CR-1064 c33 N68-26816 NASA-CK-1054 Coordination Stream-filament analysis procedure and correlation of total pressure loss coefficients to form basis of computer program to investigate design point performance of axial turbines NASA-CK-1054 NASA-CR-1181 c28 N68-35101 THERMOELASTICITY Infrared radiometric stress instrumentation system for estimating detectable stress measurements NASA-CR-1067 c32 N68-24971 NASA-CR-1067 c32 N68-2 THERMOELECTRIC COOLING Automatically controlled heat removal in water cooled space suits NASA-CR-1085 c05 N68-2 THERMOELECTRIC GENERATORS c05 N68-26701 Parametric analysis of radioisotope cascaded thermoelectric generators with Si-Ge first stage and PbTe second stage NASA-TM-X-1501 c22 N68-14585 Effective volume power density analysis for radioisotope power generator with silicon germanium thermoelectric elements NASA-TM-X-1453 c03 NG c03 N68-14630 THERMOPHYSICAL PROPERTIES Cyclic incident radiation method for measuring thermal emittance and absorption properties of metals at cryogenic temperatures NASA-TM-X-1618 c33 N68-31498 THETA PINCH Plasma preheating in megajoule theta pinch device for subsequent magnetic compression NASA-TN-D-4708 c25 N68-33372 Single-thermocouple method for measuring heat flux in thermally thick walls NASA-TN-D-4737 c33 N68-33208 THIN FILMS THICK WALLS Electrical design and scheduling of components for thin film personal communications and telemetry system NASA-CR-914 c09 N68-10420 Sputtered molybdenum disulfide film deposition and friction characteristics in vacuum NASA-TN-D-4269 c17 N68-11644 NAA-IN-24205 C17 NOO-110 Use of surface replication, extraction replication, and thin film electron microscopy in study of microstructures of dispersion strengthened materials NASA-TN-D-4461 c17 N68-18999 Construction and performance of active cadmium sulfide thin film solar cell arrays NASA-TM-X-1519 c03 N68-2 c03 N68-20432 MASA-TH-A-IDIS COS N68-20433 Summary data on deposition and endurance lives of thin metallic films used for lubricating sliding and rolling element electrical contacts in vacuum environments NASA-TN-D-4476 c15 N68-21979 Product development and testing of thin film oxygen partial pressure sensors

NASA-CR-1182 c14 N68-35149 Superconduction thin films, and properties and applications of Josephson effect at radio frequencies NASA-CR-1189 THIN WALLED SHELLS c26 N68-35178 Vibration modal response of thin cylindrical shells NASA-CR-897 c32 N68-11967 Contour plots tabulated for stress resultants and deformations brought about by sinusoidal in plane line loads acting along great circles of spherical satellites of Echo type NASA-TN-D-4425 c31 N68-20198 Resonant frequencies and nodal pattern modes of vibrating cylindrical and conical frustum shells NASA-TN-D-4428 c32 N68-20954 Dynamic stability of thin walled elastic shells and applications to space vehicle control problems NASA-CR-949 c32 N68-23453 Stress analysis and functions in membrane analysis of scalloped thin walled shells like parachutes NASA-TN-D-4867 c32 N68-28 Residual stress effects on fracture strength of AISI 301 stainless steel and Ti-5A1-2.5SR titanium cracked thin walled cylinders NASA-TN-D-4777 c32 N68-33 c32 N68-28832 c32 N68-33191 THIN WALLS Floating mandrel technique for extrusion of thin walled tungsten tubing Walled tungsten tubing NASA-TM-X-1638 c15 N68-325 Bucking of thin-walled electroplated copper and Mylar circular cylinders under axial compression and bending NASA-CR-1160 c32 N68-332 c15 N68-32977 c32 N68-33226 THREE BODY PROBLEM Numerical analyses of transitions between restricted problem of three bodies and problem of two fixed centers and Kepler problem c21 N68-11146 NASA-TM-X-1465 Comparisons of three body trajectories with patched two body trajectories for low thrust rockets NASA-TN-D-4559 c30 N68-22289 Vectorial concept for solving three body problem in celestial mechanics NASA-TN-D-4447 c30 N68-22885 Application of Lie series to celestial mechanics NASA-TN-D-4460 THREE DIMENSIONAL FLOW c30 N68-26643 Performance characteristics and operating parameters of three-fluid crossflow heat exchangers NASA-TR-R-284 c33 N68-23513 THREE DIMENSIONAL MOTION Three dimensional motion analysis and vibration characteristics of dynamically scaled model of asymmetrically clustered launch vehicle NASA-TN-D-4707 c32 c32 N68-32051 THRESHOLD DETECTORS (DOSIMETERS) Dual detection system for processing AIMP satellite pulse frequency modulated telemetry data NASA-TN-D-4561 c08 N68-24310 THROATS Cavitation performance of jet pumps having low ratios of nozzle to throat area NASA-TN-D-4592 c03 N68-2 c03 N68-24461 Performance of vortex generators installed aft of inlet throat on centerbody evaluated at Mach numbers 2.0 to 3.0 NASA-TN-D-4675 c01 N68-28795 Effect of throat size and electrode size and shape on arc heating performance in 20-inch hypersonic tunnel NASA-TN-D-4653 c11 N68-28947 Noncavitating and cavitating performance of two low area ratio water jet pumps with throat lengths of 5-66 diameters NASA-TN-D-4759 cl2 N68-31 c12 N68-31960 THRUST AUGMENTATION Aerodynamic characteristics of scale model with augmented jet flap NASA-TN-D-4610 c01 N68-25 c01 N68-25919 THRUST CHAMBERS Failure mechanisms for specific materials and

THRUST CONTROL

SUBJECT INDEX

design concepts for storable propellant rocket engines NASA-TM-X-1463 c28 N68-22272 THRUST CONTROL Optimal finite-thrust transfer between planet approach and departure asymptotes with specified intermediate orbit NASA-TN-D-4534 THRUST LOADS c28 N68-22096 Test evaluation of high temperature greases and solid lubricants in thrust loaded ball bearings NASA-TN-D-4652 c15 N68-28766 THRUST MEASUREMENT Thrust and altitude effects on ground track noise during steep approaches of four engine, medium range, turbojet transports NASA-TN-D-4241 c01 N68-1125 c01 N68-11253 THRUST VECTOR CONTROL Full scale tests of major thrust vector control system parameters and verification of system operation NASA-CR-938 c32 N68-10574 Performance of low thrust storable bipropellant thrustors in spacecraft reaction control system NASA-TN-D-4416 c28 N68-20064 Altitude of orbiting spacecraft corrected by thrustor firing time control system c31 N68-21260 NASA-TN-D-4519 Thrust vector deflection stability analysis for minimum control requirements of booster vehicles during atmospheric flight NASA-TN-D-4593 c21 N68-24409 Vortex value for hot gas flow modulation in secondary injection thrust vector control system NASA-CR-1091 c28 N68-28112 NASA-CK-1091 c28 N68-2811 Thrust vector control for large launch vehicles with solid propellant first stages NASA-TN-D-4662 c31 N68-2865 Load relief autopilot to minimize launch vehicle thrust vector deflection angle required for vehicle stability during flight through design winde c31 N68-28690 winds NASA-TN-D-4786 c21 N68-33756 THYRATRONS High temperature tests on cesium diodes and vapor filled thyratrons NASA-CR-994 c09 N68-1589 TILT WING AIRCRAFT c09 N68-15892 Ground proximity effects on longitudinal, lateral, and control aerodynamic characteristics of tilt wing four propeller V/STOL wind tunnel model NASA-TN-D-4237 c02 N68-11519 Aerodynamic factors, and effects on dynamic longitudinal stability characteristics of tilt c02 N68-11519 wing V/STOL aircraft NASA-TN-D-4344 c02 N68-15941 Aerodynamic characteristics of large-scale model of tilt-wing V/STOL aircraft NASA-TN-D-4493 c01 N68-203 c01 N68-20370 TIME FUNCTIONS Transient analysis of arterial fluid lines with respect to time domains and pulse width NASA-CR-990 c04 N68-12 c04 N68-12494 TIME MEASUREMENT Coordinate measuring system for flight control, and trajectory optimization NASA-CR-1000 c30 N68-16 c30 N68-16103 Geomagnetic field secular variation /1900 to 1965/ NASA-TN-D-4527 c13 N68-21543 TIME OPTIMAL CONTROL Time optimal rendezvous trajectories for variable thrust intercepting and orbiting space vehicles NASA-CR-1036 c30 N68-22202 TIP DRIVEN ROTORS Performance of two-stage axial flow turbine operating at different rotor tip clearance NASA-TN-D-4388 c03 N68 c03 N68-14639 TIRES Laboratory scale model technique for investigating pneumatic tire hydroplaning NASA-CR-1074 cll N68-23357 Effect of wheel braking on directional control of pneumatic tires on pavement NASA-TN-D-4602 c02 N68-2531 c02 N68-25313 TITANTUM Protective coatings and surface treatments for protection of Ti-8A1-1Mo-IV alloy sheet from hot-salt stress corrosion NASA-TN-D-4319 c17 N68-17377

TITANTUM ALLOYS Simulated study of effects of high altitude supersonic air flow on titanium alloy hot salt cracking process NASA-CR-981 -c17 N68-11522 Precision glass-bead peening equipment for propellant tank surface corrosion protection NASA-TN-D-4288 c15 N68-12890 Stress corrosion cracking of titanium aluminum vanadium alloy in nitrogen tetroxide under pressure NASA-TN-D-4289 c17 N68-12891 Residual static strength and slow crack growth behavior of duplex annealed Ti-8A1-1Mo-1V sheet c32 N68-17588 NASA-TN-D-4358 NASA-TN-D-4358 cos not 17800 Environmental exposure effects on mechanical properties of titanium alloy, stainless steel, aluminum alloy, and composite material sheets NASA-TN-D-4318 cl7 N68-17897 NASA-TN-D-4318 c17 N68-1 Brazing aluminum to titanium coated stainless steel to minimize formation of intermetallic compounds in joint NASA-SP-5040 c15 N68-2 c15 N68-22778 Texture strengthening and fracture toughness of titanium alloy sheet at room and cryogenic temperatures NASA-TN-D-4444 c17 N68-22884 Hot salt stress corrosion cracking effects on tensile properties of titanium alloy sheets NASA-TN-D-4674 c17 N68-30000 NASA-TN-D-4674 Titanium alloy honeycomb with blackened walls as absorber of solar energy NASA-TN-D-4727 c03 N68-30751 Hot salt stress corrosion cracking of titanium aluminum alloys in presence of anhydrous hydrogen chloride NASA-CR-1133 c17 N68-33019 Residual stress effects on fracture strength of AISI 301 stainless steel and Ti-5Al-2.5Sn titanium cracked thin walled cylinders NASA-TN-D-4777 c32 N68-33191 TOROIDAL SHELLS Drop test study on isothermal liquid-vapor interface configuration during weightlessness in toroidal shell NASA-TN-D-4819 c12 N68-35823 TOROUE Theoretical approach to determination of magnetic torques on orbiting spacecraft by near-field measurement NASA-TN-D-4485 c23 N68-24146 NASA-TN-D-4485 c23 N88-24 Spinning friction and torque dependence on ball bearing-groove conformity NASA-TN-D-4669 c15 N68-28 TORSIONAL VIBRATION c15 N68-28258 Torsional model development and model calculations for cylindrical space vehicle systems and systems employing clustered tanks NASA-CR-937 c32 N68-10568 Damping of piezoelectric quartz crystal driven in torsional mode of vibration in liquid helium 3 and helium 4 c26 N68-17594 NASA-TN-D-4381 TORUSES Length of winding on torus in two ideal models NASA-TM-X-1674 c03 N68-3 c03 N68-37217 TOUCHDOWN Lunar module scale model study of use of soft side legs for improved touchdown stability of legged landing vehicles NASA-TN-D-4680 c31 N68-29962 TOXIC HAZARDS Reduction of flammable and toxic materials for use in oxygen rich manned spacecraft cabin atmospheres NASA-TN-D-3415 c05 N68-24756 TRACE CONTAMINANTS Trace contaminant identification using microwave double resonance spectroscopy NASA-CR-967 c24 N68-11634 Ultraviolet measurements of oil contamination in optical mirrors NASA-TN-D-4612 c14 N68-25375 TRACKING (POSITION) Performance comparison of electromechanical and electroluminescent displays in closed loop manual tracking task and reading accuracy test NASA-TN-D-4541 c05 N68-364 c05 N68-36457

TRANSIENT RESPONSE

TRACTION Dynamic hydroplaning, viscous hydroplaning, and tire tread rubber reversion effects on tire traction on wet runways NASA-TN-D-4406 c02 N68-19620 TRAILBLAZER 2 REENTRY VEHICLE Photographic and spectrometric observation of iron, artificial meteor launched from Trailblazer 2, and reentering at 11 kilometers per second NASA-TN-D-4312 c30 N68-16750 Attitude determination of spin-stabilized spacecraft using star mapping technique NASA-TN-D-4740 c21 c21 N68-31957 TRAILING-EDGE FLAPS Static pressure and flow field for flat plate model with short trailing-edge flap NASA-TN-D-4308 cl2 N68c12 N68-17376 Laminar flow separation on flat plate induced by deflected trailing-edge flap at hypersonic speed NASA-TN-D-4671 TRAINING SIMULATORS c01 N68-29405 Visual simulation facility for evaluation of lunar surface roving vehicles NASA-TN-D-4276 c11 N68-15858 TRAJECTORIES Comparisons of three body trajectories with patched two body trajectories for low thrust rockota NASA-TN-D-4559 c30 N68-22289 Bolza problem of calculus of variations in terms of control coding applied to trajectories NASA-CR-1103 c30 N6 c30 N68-25895 TRAJECTORY ANALYSIS Error model for Doppler range rate and phase modulated range tracking system for which data weighting factors can be obtained for use in space vehicle trajectory analysis NASA-TN-D-4267 c10 N68-115 c10 N68-11513 Results of including boundary shock wave in calculation of flight parameters of large high speed meteor NASA-TN-D-4325 c12 N68-18997 Maxima-minima theory, Pontryagin principle, and calculus of variations for optimal trajectory and control analysis NASA-CR-1006 c30 N68-20084 Algorithm for generating low variable thrust interplanetary trajectory data for mission analysis of electrical propulsion systems NASA-TN-D-4431 c30 N68-21228 Semigraphical method to aid selection of descent trajectory compatible with mission constraints NASA-TN-D-4801 c30 N68-360 c30 N68-36077 TRAJECTORY CONTROL Modified control logic with random-number procedure to determine error effects on range controller of reentry vehicle NASA-TN-D-4317 c21 N68-14732 Human response analysis in combined trajectory control task, system-failures task, and motor response task NASA-TN-D-4356 c05 N68-18 c05 N68-18014 Pericynthion altitude of selenocentric orbits determined from angular rate of line of sight with respect to prominant lunar surface features along ballistic trajectories NASA-TM-X-1508 c3 c30 N68-19622 TRAJECTORY OPTIMIZATION Two body problem for satellite guidance, flight mechanics, and trajectory optimization analyses NASA-CR-1002 c30 N68-14089 Guidance, flight mechanics, and trajectory optimization - calculus of variations and modern applications NASA-CR-1003 c30 N6 c30 N68-15193 Coordinate measuring system for flight control, and trajectory optimization NASA-CR-1000 c30 N68-16 c30 N68~16103 Mathematical formulation of guidance equations and solutions for orbital space missions NASA-CR-1010 c30 N68-17215 Three numerical procedures for Mayer classical and non-classical problems in trajectory optimization NASA-CR-1012 c30 N68-19315 General perturbations theory applications to spacecraft guidance, flight mechanics, and trajectory optimization

c30 N68-20450 NASA-CR-1008 Mission constraints and trajectory interfaces for launch, rendezvous, spatial, deorbit, and entry phases of earth orbital mission NASA-CR-1015 c30 N68-20468 NASA-CK-1015 C30 N68-2 Dynamic programming and multistage decision processes in guidance, flight mechanics, and trajectory optimization NASA-CR-1009 C30 N68-2 c30 N68-21077 Pontryagin maximum principle, calculus of variations, and dynamic programming optimization techniques applied to trajectory and guidance problems NASA-CR-1014 c30 N68-21231 Guidance, flight mechanics, and trajectory optimization NASA-CR-1004 c30 N68-21685 Effects of time, frequency, and tracking station location errors on accuracy of trajectory analysis NASA-TN-D-4507 c30 N68-25271 Planetary gravitation and oblateness used for parking orbit alignment in Mars mission NASA-TN-D-4657 c30 N68-NASA-TN-D-4657 c30 N68-28408 Computer program for trajectory optimization and payload maximization in multistage launch vehicles NASA-TN-D-4729 TRANSCENDENTAL FUNCTIONS c30 N68-31989 Boundary condition solution and transcendental approximation for transient heat conduction problem NASA-CR-955 c19 N68-11109 Approximations to several transcendental functions in universal form of two body problem NASA-TN-D-4643 c19 N68-29407 TRANSDUCERS Modified vibration transducer calibration system for directly producing sensitivity versus frequency range plots NASA-TN-D-4760 c14 N6 c14 N68-31958 TRANSFER FUNCTIONS Formula for expanding higher order derivatives of function tanh z in powers of tanh z and A-numbers NASA-TN-D-4296 c19 N68-14077 C19 N68-1407 Computer program for symbolic reduction of block diagrams to obtain transfer functions NASA-TN-D-4617 c08 N68-2496 c08 N68-24967 TRANSFER ORBITS Two body equations of motion for calculating partial derivatives relating lunar and planetary midcourse correction requirements to guidance mindourse correction requirements to guidance system injection errors NASA-TN-D-4518 c30 N68-20368 Optimal finite-thrust transfer between planet approach and departure asymptotes with specified intermediate orbit NASA-TN-D-4534 c28 N68-22096 Manual navigation method for evaluating transfer orbits for lunar landings NASA-TN-D-4756 c21 N68-33271 Analysis of launch windows from circular orbits for representative Mars missions NASA-TM-X-1651 c30 N68-33371 Technique for determining pericynthion altitude of lunar transfer orbits NASA-TN-D-4811 c30 N68-364 c30 N68-36459 TRANSFORMATIONS (MATHEMATICS) Methods of eliminating short period terms from Hamiltonian by means of canonical TRANSIENT LOADS Effect of N waves at oblique incidence on response of simply supported plate to transient c19 N68-17532 loads NASA-CR-1176 c32 N68-33168 TRANSIENT OSCILLATIONS Least squares determination of frequency, damping ratio, amplitude, and phase angle from free oscillation data NASA-TN-D-4503 TRANSIENT RESPONSE c19 N68-25869 Analyses and finite difference procedure for predicting transient in-depth response of charring ablation materials NASA-CR-1060 c33 N6 c33 N68-25244 Numerical method for determining transient

I-107

TRANSISTOR CIRCUITS

SUBJECT INDEX

response of simply supported plate to n waves at normal incidence NASA-CR-1175 c32 N68-33737 TRANSISTOR CIRCUITS Metal oxide semiconductor field effect transistor circuit development and laminated electronic packaging for computer storage devices NASA-CR-1113 c08 N68-35193 TRANSISTORS Analytical expressions to determine transistor design effects on radiation resistance NASA-CR-1167 c10 N68-33 c10 N68-33767 TRANSITION PROBABILITIES Quantum mechanical study of transition probabilities, Einstein A coefficients, and oscillator strengths of band systems of diatomic molecules NASA-CR-975 TRANSMISSIVITY c24 N68-11037 Transmissivity of carbon particle-seeded nitrogen jet for heat transfer predictions NASA-TN-D-4722 c23 N68-30596 c23 N68-30596 TRANSMITTANCE Transmittance of thin films and photoionization of gases in selective detectors set for photons in ultraviolet spectrum NASA-CR-1096 c24 N68-28250 TRANSONIC FLOW Subsonic rebw Subsonic and transonic flutter and flow studies of T tail of large multijet cargo airplane NASA-TN-D-4316 c02 N68-17055 Effect of geometry of conical afterbodies on base drag at subsonic and transonic speeds NASA-TN-D-4821 c01 N68-3705 c01 N68-37054 TRANSONIC NOZZLES Performance evaluation of annular plug and expansion-deflection nozzles including external flow effects at transonic Mach numbers NASA-TN-D-4462 c01 c01 N68-20330 TRANSONIC SPEED Design and performance testing of large scale mixed compression axisymmetric inlet at transonic and supersonic speeds NASA-TM-X-1507 c28 N68-17028 Wind tunnel investigation of fluctuating pressures on Centaur model surface at transonic speed NASA-TM-X-1574 c31 N68-22742 Aerodynamic drag measurements and boundary layer flow over V notches at transonic and supersonic speeds c12 N68-35252 NASA-CR-1132 Flexibility effects on lift and pitching moments of low aspect ratio delta wing-conicalcylindrical body combinations at transonic speeds NASA-TN-D-4655 c01 N68-37065 Effects of simulated jet exhaust flow on transonic aerodynamic characteristics of Apollo launch escape vehicle models NASA-TN-D-4843 c31 N68-37074 TRANSPORT AIRCRAFT V/STOL short haul transport design considerations including noise characteristics NASA-CR-670/01/ c02 N68-11174 Thrust and altitude effects on ground track noise during steep approaches of four engine, medium range, turbojet transports NASA-TN-D-4241 c01 N68-1125 c01 N68-11253 Economic and suitability comparison of short haul transport aircraft concepts NASA-CR-986 c02 N68-13517 Velocity, gust, and height data analysis from four-engine turbojet transport airplane NASA-TN-D-4330 c02 N68c02 N68-16522 Simple model describing final airborne stages of landing transport aircraft manually NASA-TN-D-4438 c02 N68-21112 Statistical analysis of repeated acceleration and impact loads on airline transports NASA-TN-D-4586 c02 N68-24476 Jet wake effect of high bypass jet engine on wing-nacelle interference drag of subsohic transport model NASA-TN-D-4693 col N68-30595 Feasibility of revised V/STOL design and flight plan concepts for short haul transport aircraft NASA-CR-743/1/ col2 N68-35177 Aerodynamic characteristics of subsonic cargo jet.

transport model in slotted transonic wind tunnel

NASA-TM-X-1660 c01 N68-35617 Sideslip angle effects on static stability characteristics of T tail transport configuration NASA-TM-X-1665 TRANSPORT PROPERTIES c01 N68-36112 Automated Hall effect and resistivity apparatus for studying electrical transport properties of semiconductors NASA-TM-X-1464 c03 N68-10103 FORTRAN subroutines for determining intersections of nuclear particle flight path and wall of c03 N68-10103 helical tubular duct NASA-TN-D-4435 c22 N68-18541 TRANSPORT THEORY Space radiation transport, spacecraft shielding design and advanced concepts, and methods for calculating radiation penetration through protective shields - conference NASA-SP-169 c29 N68-26128 TRANSVERSE WAVES Performance tests of rotating gas jet generator for strong traveling transverse acoustic modes NASA-TN-D-4380 c12 N68-169 TRAPPED MAGNETIC FIELDS c12 N68-16998 Plasma preheating in megajoule theta pinch device for subsequent magnetic compression NASA-TN-D-4708 c25 N68-3337 c25 N68-33372 TRAVELING WAVE MASERS Microwave pump requirements for field operational broadband rutile traveling wave maser for Applications Technology Satellite program NASA-TN-D-4764 c16 N6 c16 N68-33635 TRAVELING WAVES Performance tests of rotating gas jet generator for strong traveling transverse acoustic modes NASA-TN-D-4380 c12 N68-169 c12 N68-16998 Effect of N waves at oblique incidence on response of simply supported plate to transient loads NASA-CR-1176 c32 N68-33168 TRITIUM Ages for D-D and D-T neutrons in water and tungsten-water mixtures NASA-TN-D-4581 c22 N68-25058 NASA-IN-D-4001 C22 N68-25058 TRUNCATION ERRORS Runge-Kutta formulas of high order with stepsize control through leading truncation error term NASA-TR-R-287 c19 N68-36753 TRUSSES Materials selection, structural geometry, proof testing and statistical screening, prestressing, and system energy as tools for designing optimum trusses and other high performance structures NASA-CR-1038 c32 N68-23399 NASA-UK-1036 TUBE HEAT EXCHANGERS Single tube-in-shell water-boiling heat exchanger performance with helical wire insert and flow stabilizing devices NASA-TN-D-4767 C33 N68-3209 c33 N68-32099 TUNGSTEN Tungsten-stainless steel sensor for averaging temperature measurement of nonuniform temperature profiles NASA-TN-D-4242 cl4 N68 Oxide deformation and fiber reinforcement in c14 N68-15936 tungsten-urania and tungsten-zirconia elongated into fibers by hot extrusion NASA-TN-D-4475 c17 N68-1861 c17 N68-18610 Postshutdown cooling requirements of tungsten water moderated nuclear rocket engines c22 N68-21111 NASA-TM-X-1568 Applications of Monte Carlo analysis to tungsten resonance absorption NASA-TN-D-4545 c22 N68-21924 Current-voltage characteristics of variable spaced thermionic converter with tungsten emitter and niobium collector NASA-CR-1033 c03 N68-23476 Ages for D-D and D-T neutrons in water and tungsten-water mixtures NASA-TN-D-4581 c22 N68-25058 Neutron irradiation effects on embrittlement of polycrystalline tungsten NASA-TN-D-4661 c17 N68-28818 Tensile properties of tantalum and tungsten 10-fiber bundles NASA-TN-D-4725 c17 N68-30504 Emitter and collector sheaths for cesium

thermionic diodes with polycrystalline tungsten electrodes NASA-TN-D-4744 c25 N68-31640 Floating mandrel technique for extrusion of thin walled tungsten tubing NASA-TM-X-1638 c15 N68-32977 Thermal conductivity measurements on tungsten coated uranium dioxide cermets NASA-CR-1154 c22 N68-32983 Influence of chemisorbed films of various gases on adhesion and friction of tungsten in vacuum NASA-TN-D-4694 c15 N68-33227 TUNGSTEN ALLOYS Composition and heat treatment effects on high temperature strength of arc melted tungsten-hafnium-carbon alloys NASA-TN-D-4379 c17 N68-17317 Mechanical properties of tungsten and tungsten rhenium alloys NASA-TN-D-4567 c17 N68-24477 High temperature tensile properties of tungstenrhenium alloys NASA-TN-D-4728 c17 N68-30605 TUNGSTEN OXIDES Establishing allowable temperature gradients for tungsten-uranium dioxide fuel elements using experimental cyclic strain data NASA-TN-D-4279 TUNNEL DIODES c22 N68-14986 Current-voltage characteristics of tunneling p-n junctions in semiconductors NASA-TN-D-4403 c09 N68 c09 N68-19062 TURBIDITY Scattering and absorption of plane electromagnetic waves by particles of turbid medium NASA-TT-F-477 c13 N68-22462 TURBINE BLADES Reynolds number effect on single stage axial flow turbine in air NASA-TN-D-4383 c03 N68-16228 Cold air study of high temperature gas turbine – blade feature effects on stator performance NASA-TN-D-4418 c28 N68-16632 Oxidation resistant alloys tested for suitability as transpiration cooled gas turbine blades NASA-CR-930 c17 N68 c17 N68-17591 Effects of surface Mach numbers, inlet flow angle and specific heat ratio on geometric features of supersonic impulse turbine blade sections over Mach number range of 1.5 to 5.0 NASA-TN-D-4422 c03 N68-20276 TURBINE ENGINES Friction and fretting wear tests on materials used as friction dampers to reduce vibrational stresses in compressor blades for turbine engines NASA-TN-D-4630 c15 N68-28871 Performance of single stage turbine with rotor blade surface diffusion factor of 0.3 NASA-CR-1172 TURBINE PUMPS c28 N68-32987 Cold air performance test of scale model oxidizer pump drive turbine for M-1 engine - performance of first stage with inlet feedpipe manifold assembly NASA-TN-D-4392 c28 N68-16413 Pressure rise response of turbopumps to flucturating flow rates and unsteady flow about two dimensional linear cascade of airfoils NASA-TN-D-4298 c01 N68-21950 TURBINES Experimental performance evaluation of radial inflow turbine with exit diffuser NASA-TM-X-1480 c03 N68-11920 Optimum design geometry for high radial inflow turbine performance efficiency NASA-TN-D-4384 c03 N68-15 c03 N68-15943 Effect of variable stator geometry on performance of air cooling turbine NASA-TM-X-1632 c01 N68-29994 Turbine performance with 130 percent design stator NASA-TM-X-1663 c03 N68-35536 Combination temperature, pressure, and flow direction sensing probe to study rotating machinery NASA-TN-D-4816 c14 N68-36021 Performance tests of stator component in closed position and effects on performance of single

stage turbine suitable for air cooling NASA-TM-X-1675 c28 N68-37264 TURBOCOMPRESSORS Axial flow turbine compressor for space power plant NASA-CR-800 c03 N68-24596 Gas lubricated bearing system for turbine compressor NASA-CR-802 c03 N68-24597 Experimental evaluation of gas injection start of Brayton cycle turbocompressor operating on gas bearings NASA-TM-X-1590 c03 N68-24757 Design and dynamic simulator testing of gas bearing rotor support for high performance axial flow turbomachinery NASA-CR-801 c15 N68-25042 Nacelle design for turbofan engine compressor noise suppression on Douglas DC-8 aircraft NASA-CR-1056 c28 N68c28 N68-26771 Stress analysis and wear tests in use of lacing wire as vibration damper on turbocompressor blades NASA-TM-X-1603 c32 N68-28238 Inlet guide vane choking noise reduction in axial flow compressors NASA-TN-D-4682 c02 N68-29406 TURBOFAN ENGINES Relationship between fan drive turbine geometry and output efficiency of turbofan engine NASA-TM-X-1581 c28 N68-22 c28 N68-22725 Nacelle design for turbofan engine compressor noise suppression on Douglas DC-8 aircraft NASA-CR-1056 c28 N68-26771 Cycle characteristics and structural configuration of turbojet and turbofan engines for lightweight aircraft NASA-TM-X-1624 c28 N68-31476 TURBOGENERATORS Reduction of apparent power requirement for phase controlled parasitically loaded turboalternator by multiple parasitic loads NASA-TN-D-4302 c03 N68-17110 Dynamic characteristics of parasitic loading speed controller for Brayton cycle turboalternator NASA-TM-X-1456 c03 N68-1 c03 N68-18702 TURBOJET ENGINES Simulated wind-tunnel investigation with jet-augmented flap NASA-TN-D-4278 c02 N68-1162 Cold flow tests of aerodynamic characteristics of plug nozzle configuration for turbojet engines c02 N68-11627 operating at supersonic speeds NASA-TM-X-1619 c28 N68-29953 Turbojet engine noise reduction by increasing intake system guide vane-rotor blade spacing NASA-TN-D-4690 c28 N68-3 c28 N68-30040 Cycle characteristics and structural configuration of turbojet and turbofan engines for lightweight aircraft NASA-TM-X-1624 c28 N68-31476 Heat transfer characteristics of cylindrical ejector for turbojet engine and shroud material temperature prediction NASA-TM-X-1641 c33 N68-32988 Jet VTOL aircraft inlet temperature rise and induced recirculating flow patterns NASA-CR-1147 c01 N68 c01 N68-33043 TURBOMACHINE BLADES FORTRAN computer program for calculating two dimensional subsonic inviscid flow for rotating or stationary circular cascade of blades on blade to blade stream surface of turbomachine NASA-TN-D-4525 col N68-2137 TURBOMACHINERY c01 N68-21374 FORTRAN computer program for supersonic turbomachinery blading design calculations NASA-TN-D-4421 c08 N68 c08 N68-18620 TURBOPROP AIRCRAFT Velocity, gust, and height data analysis from four-engine turbojet transport airplane NASA-TN-D-4330 TURBOPROP ENGINES c02 N68-16522 Wind tunnel stability tests of twin engined turboprop aircraft with rotating cylinder flaps NASA-TN-D-4489 c01 N68-19189 TURBOSHAFTS Design and dynamic simulator testing of gas bearing rotor support for high performance axial

flow turbomachinery NASA-CR-801 c15 N68-25042 TURBULENCE EFFECTS Analysis of turbulent wall pressure field under supersonic shear layers NASA-CR-888 c12 N68-22087 TURBULENCE METERS Hot-wire anemometer system for measuring velocity fluctuations in turbulent coaxial flow field of dissimilar fluids NASA-CR-961 cl2 N68-1289 c12 N68-12892 TURBULENT BOUNDARY LAYER Turbulent boundary layer and transition on Turbulent boundary 1995. plane plates NASA-TT-F-520 Turbulent boundary layer effect on panel flutter C32 N68-18721 C32 N68-18721 C32 N68-18721 Boundary layer and wake survey data reduction techniques in compressible flows NASA-TN-D-4401 c12 N68c12 N68-19709 Selected band cross correlation analysis of fluctuating pressures under turbulent boundary layer flow NASA-CR-1066 c12 N68-23482 Heat transfer effect on drag due to surface roughness in supersonic turbulent boundary layer NASA-TN-D-4746 c12 N68-33054 Laminarization of turbulent boundary layer observed from heat transfer and boundary layer measurements in conical nozzles NASA-TN-D-4788 c12 N68-336 Equations of motion for calculating compressible c12 N68-33642 turbulent boundary layers NASA-CR-1144 c12 N68-35096 Computation of mean and fluctuating quantities in turbulent boundary layers NASA-TN-D-4815 c12 N68-3607 c12 N68-36071 TURBULENT FLOW Axial turbulence measurements in coaxial flow of dissimilar gases NASA-CR-960 c12 N68 Mixing of turbulent, incompressible, coaxial c12 N68-13612 streams NASA-CR-959 c12 N68-16897 High speed fluid film lubric_tion NASA-CR-1058 c15 N68-22810 Differential equations based on heat transfer and shear for temperature and velocity in turbulent boundary layers NASA-TN-D-4611 c33 N68-25917 Transition from laminar to turbulent flow in near wake of supersonic reentry body NASA-TN-D-4645 c01 N68-28220 Computation of mean and fluctuating quantities in turbulent boundary layers NASA-TN-D-4815 c12 N68-36071 Mixing length flow theory for analyzing incompressible turbulent swirling flow in pipes in pipes NASA-CR-1169 c12 N68-3634 TURBULENT HEAT TRANSFER Analysis of shear and normal strain effects on weak turbulence and turbulent heat transfer using two point correlation equations obtained c12 N68-36343 from Navier-Stokes and energy equations NASA-TN-D-4273 c33 N68-11491 Heat transfer characteristics for turbulent flow of heat generating liquid metals between parallel plates with wall heat transfer NASA-TN-D-4336 c33 N c33 N68-14042 Single correlating equation for single phase forced convection heat transfer coefficients for turbulent flow through tubes over wide ranges of temperature ratios NASA-TN-D-4332 c33 N68-14240 Velocity and density profiles in mixing region between adjacent half jets of dissimilar fluids NASA-CR-957 TURBULENT MIXING NASA-CR-957 cl2 N68-15571 Similarity solution for turbulent mixing between jet and faster moving coaxial stream NASA-TN-D-4441 cl2 Neg 10000 Effect of turbûlent mixing on average fuel temperatures in gas-core nuclear rocket engine NASA-TN-D-4882 c22 N68-37927 TURBULENT WAKES Boundary layer and wake survey data reduction techniques in compressible flows

NASA-TN-D-4401 c12 N68-19709 NNDA-IN-U-4401 cl2 N68-19709 Movement of forward heat shield in Apollo command module turbulent reverse flow wake NASA-TN-D-4691 c31 N68-30032 TURING MACHINES c31 N68-30032 Finite-state machines and evolutionary programming for representing and analyzing performance of human operator in control of dynamic systems NASA-CR-1112 co5 N68-280 TWISTED WINGS Profile change effects on aerodynamic c05 N68-28847 Profile change effects on aerodynamic characteristics of twisted and cambered arrow wing at supersonic speed NASA-TN-D-4796 col N68-356 TWO BODY PROBLEM Numerical analyses of transitions between restricted problem of three bodies and problem of two fixed centers and Kepler problem NASA-TM-Y-1665 col N68-111 c01 N68-35665 c21 N68-11146 NASA-TM-X-1465 Two body problem for satellite guidance, flight mechanics, and trajectory optimization analyses NASA-CR-1002 c30 N68-1408 c30 N68-14089 Comparisons of three body trajectories with patched two body trajectories for low thrust NASA-TN-D-4559 c30 N68-22289 NASA-IN-D-4509 c30 N68-22289 Approximations to several transcendental functions in universal form of two body problem NASA-TN-D-4643 c19 N68-29407 TWO DIMENSIONAL BODIES Integral methods for predicting afterbody heat transfer to blunt two dimensional configuration subjected to separated flow NASA-TN-D-4443 cl2 N68-28283 TWO DIMENSIONAL FLOW c12 N68-28282 FORTRAN computer program for calculating two dimensional subsonic inviscid flow for rotating or stationary circular cascade of blades on blade to blade stream surface of turbomachine NASA-TN-D-4525 col N68-21 c01 N68-21374 Effect of leading edge bluntness on hypersonic two dimensional inlet type flows NASA-CR-1145 c01 N68-33 c01 N68-35523 TWO FLUID MODELS Free jet mixing analysis for parallel streams of different fluids NASA-CR-956 TWO STAGE TURBINES c12 N68-13619 Performance of two-stage axial flow turbine operating at different rotor tip clearance NASA-TN-D-4388 c03 N68 c03 N68-14639 Two stage potassium vapor turbine - materials support of performance and endurance tests NASA-CR-925 c03 N68c03 N68-16351 Cold air performance test of scale model oxidizer pump drive turbine for M-1 engine - performance of first stage with inlet feedpipe manifold assembly NASA-TN-D-4392 c28 N68-16413 Two stage turbine suitable for use in wet potassium vapor at temperatures of 1400 to 1600 deg F NASA-CR-922 c03 N68-16439 Mechanical design and development test program for two-stage potassium vapor Rankine cycle turbine NASA-CR-923 c03 N68-17075 Design, and performance of facility for Rankine cycle testing of two stage potassium vapor turbine Turbine NASA-CR-924, V. 3 c03 N68-Aerodynamic performance of scale model oxygen pump-drive turbine for M-1 rocket engine NASA-TN-D-4393 c28 N68c03 N68-18044 c28 N68-18188
 wnow-im-u-4030
 c28 N68-18187

 Comparison of mixed and isolated flow methods for cooled turbine performance using two simplified example turbines
 with the simplified

 NASA-TM-X-1572
 c01 N68-21692
 c01 N68-21692 TYPHOONS Nimbus 2 and ESSA 3 satellite observation photographs of typhoon Marie NASA-TN-D-4757 c20 N68-37869 U U.S.S.R.

History of Russian solid fuel rocketry NASA-TT-F-415 c28 N68-11829 Historical survey of Russian rocketry and space exploration

VACIUM DEPOSITION

NASA-TT-F-426 Ultrahigh Vacuum c31 N68-22262 Creep behavior of tantalum alloys in ultrahigh vacuum for extended time periods NASA-TN-D-4605 c17 N68-24111 Silicate surface preparation to represent lunar soil, and ultrahigh vacuum adhesion measurements NASA-CR-1090 c30 N68-2837 ULTRASONIC TESTS Evaluation of ultrasonic absorption technique for c30 N68-28373 measuring high temperature gas propertie NASA-TN-D-4433 c24 N NASA-TN-D-4433 c24 N68-18949 Ultrasonic detection and measurement of fatigue Ultrasonic detection and measurement of fatigue crack propagation in notched specimens of aluminum, titanium, and cobalt alloys and maraging steels NASA-TN-D-4782 c32 N68-3 Ultrasonic attenuation measurements on single tantalum crystals at superconducting state NASA-TN-D-4806 c26 N68-3 c32 N68-35071 c26 N68-35356 ULTRAVIOLET RADIATION Mitraviolet filter and monochromator for mass spectrometer employing photoionization source NASA-CR-1018 c14 N68-17329 Ultraviolet-proton radiation effects on solar concentrator reflective surfaces c17 N68-23560 NASA-CR-1024 Transmittance of thin films and photoionization of gases in selective detectors set for photons in ultraviolet spectrum NASA-CR-1096 c24 N68-28250 c24 N68-28250 Cathode ray tube with nonreciprocal optical filtering techniques for viewing under high ambient NASA-CR-1185 c09 N68-33224 ULTRAVIOLET SPECTRA Reactor irradiation effects on optical absorption levels in fused silica NASA-CR-1032 UMBILICAL CONNECTORS c22 N68-23481 Handbook for designing ball lock mechanisms for use on space vehicles NASA-CR-1021 c15 N68-23356 Variable density hypervelocity wind tunnel tests on effects of several ramp-fairing, unbilical, and pad configurations on aerodynamic heating to Apollo command module NASA-TM-X-1640 col N68-351 UNDAMPED OSCILLATIONS c01 N68-35141 Critical speed of flexibily mounted rigid rotors in undampened bearings NASA-TN-D-4607 c32 N68-254 c32 N68-25421 UNTVERSE Zero density and approximate, relativistic models of universe NASA-TR-R-282 UNIVERSITY PROGRAM c30 N68-20192 Third annual NASA University Conference on Manual Control NASA-SP-144 c05 N68-15901 NASA university programs in personnel training, aeronautics and space research, and laboratories and research centers NASA-SP-185 c34 N68-35564 UNMANNED SPACECRAFT Unmanned Mars probe tested for drag, lift, static and dynamic stability at Mach number 2 NASA-TN-D-4291 c01 N68-11936 Evaluation of microwave, millimeter, and optical communication systems for space communications from Mars spacecraft NASA-TN-D-3984 c07 N68-22019 Landing site dispersions of unmanned spacecraft on Mars NASA-TN-D-4587 UPPER ATMOSPHERE c30 N68-24557 Tabulated data on velocity distribution of upper air winds at Wallops Island NASA-TN-D-4570 c20 N68-240 c20 N68-24028 UPWASH Approximation method for calculating spanwise distribution of wind tunnel boundary interference on wing lift in rectangular perforated wall NASA-TR-R-285 URANIUM FLUORIDES c01 N68-24617 Critical experiments analysis of uranyl fluoride solution reactors containing large-diameter

voided tubes NASA-TN-D-4270 c22 N68-15197 URANIUM OXIDES Establishing allowable temperature gradients for tungsten-uranium dioxide fuel elements using experimental cyclic strain data NASA-TN-D-4279 c22 N68-149 c22 N68-14986 Oxide deformation and fiber reinforcement in tungsten-urania and tungsten-zirconia elongated into fibers by hot extrusion NASA-TN-D-4475 c17 N68-18610 c17 N68-18610 Smooth surface coating of molybdenum alloys for cermets by hot isostatic compaction of tungsten-uranium dioxide fuels NASA-TM-X-1563 c22 N68-21705 Thermal conductivity measurements on tungsten coated uranium dioxide cermets NASA-CR-1154 c22 N68-32983 URANIUM 235 Plum Brook reactor support calculations -mathematical model for fuel utilization, power distribution in fuel loading, and approximate predictions of xenon poison transient NASA-TM-X-1496 C22 N66-529 c22 N68-16056 ν V GROOVES

Aerodynamic drag measurements and boundary layer flow over V notches at transonic and supersonic speeds c12 N68-35252

NASA-CR-1132 V/STOL AIRCRAFT V/STOL short haul transport design considerations

- V/SILL short haul transport design considerations including noise characteristics NASA-CR-670/01/ c02 N68-11174 Ground proximity effects on longitudinal, lateral, and control aerodynamic characteristics of tilt wing four propeller V/STOL wind tunnel model NASA-TN-D-4237 c02 N68-11519

 - NASA-TN-D-4237 CUZ NOS-11019 Static and dynamic longitudinal stability tests of fan in wing V/STOL aircraft model NASA-TN-D-4322 CO2 N68-15894 Aerodynamic factors, and effects on dynamic longitudinal stability characteristics of tilt
 - c02 N68-15941
 - longitudinal stability characteristics of tilt wing V/STOL aircraft NASA-TN-D-4344 co2 N68-1594 Variable-stability helicopter flight tests under instrument flight rules to determine effects of gross changes in longitudinal static stability for V/STOL handling qualities NASA-TN-D-4364 co2 N68-191 c02 N68-19184
 - Aerodynamic characteristics of large-scale model of tilt-wing V/STOL aircraft NASA-TN-D-4493
 - c01 N68-20370 Test sections for small theoretical wind tunnel boundary interference on V/STOL models NASA-TR-R-286 cl1
 - c11 N68-31592
 - NASA-1K-K-286 CII NOS-Subjective response to far field noise characteristics of V/STOL aircraft sized to carry 60 passengers over 500 mile range NASA-CR-1118 c05 N68-
 - NASA-CR-1118 COST Solution of the state of t
- ground effect of V/STOL transport model NASA-CR-1180 c28 c28 N68-35594 VACUUM
- Influence of chemisorbed films of various gases on adhesion and friction of tungsten in vacuum NASA-TN-D-4694 c15 N68-33227
- Cyclic frequency, tensile fatigue effects, and defect substructure generated in vacuum by fatigue stressing of aluminum NASA-CR-1165 c17 N68-35 VACUUM CHAMBERS c17 N68-35200
- Design and performance of two vacuum chambers and solar-radiation simulators for solar-cell research
- NASA-TM-X-1503 cll N68-16695 Hydrogen plasma hot cathode generator and electron energy and density study NASA-TN-D-4604 c25 N68-25877 VACUUM DEPOSITION
- Sputtered molybdenum disulfide film deposition and friction characteristics in vacuum NASA-TN-D-4269 c17 N68-11644

VACUUM EFFECTS

VACUUM EFFECTS Outgassing of water vapor from concrete surfaces in vacuum environments NASA-TM-X-1536 c11 N68-19207 Adverse effects of liquid propellant leakage past control valves in vacuum environment NASA-CR-1047 c2 c27 N68-21893 Summary data on deposition and endurance lives of thin metallic films used for lubricating sliding and rolling element electrical contacts in vacuum environments NASA-TN-D-4476 c15 N68-21979 VALVES Advanced valve technology for aerospace use NASA-SP-5019 c15 N68-10402 VANADIUM Protective coatings and surface treatments for protection of Ti-8A1-1Mo-1V alloy sheet from hot-salt stress corrosion NASA-TN-D-4319 c17 N68-1 c17 N68-17377 VAPOR DEPOSITION Surface roughness effects on normal spectral emittance of vapor deposited rhenium NASA-TM-X-1514 In situ electron microscopy for studying vapor deposition nucleation processes c17 N68-19347 NASA-TN-D-4506 c06 N68-21430 VAPOR PRESSURE Vapor pressure measurements of potassium to 2170 deg K NASA-TN-D-4535 c33 N68-25122 VAPORIZING Combustion instability prediction using nonlinear bipropellant vaporization model NASA-CR-920 c33 No c33 N68-15833 VAPORS Vapor ingestion during liquid outflow in scale model Centaur liquid hydrogen tank NASA-TM-X-1482 cl2 N68-1 NASA-CR-1139 NASA-CR-1139 NASA-CR-1139 NASA-CR-1139 NASA-CR-1139 NASA-CR-1139 VARIABLE GEOMETRY STRUCTURES Effect of variable stator geometry on performance of air cooling turbine NASA-TM-X-1632 VARIABLE SWEEP WINGS Theoretical study of effect of pivot location on c01 N68-29994 aerodynamic balance movement of variable sweep wings in incompressible flow NASA-TN-D-4635 c01 N68-28817 Wind tunnel evaluation of speed brake effects on supersonic characteristics of variable sweep fighter aircraft models NASA-TN-D-4773 c02 N68-33669 Wind tunnel tests to determine low speed high lift aerodynamics of one-fifth scale variable sweep supersonic transport model NASA-TN-D-4844 VARIABLE THRUST c01 N68-37365 Algorithm for generating low variable thrust interplanetary trajectory data for mission analysis of electrical propulsion systems NASA-TN-D-4431 c30 N68-21228 VECTORS (MATHEMATICS) Vectorial concept for solving three body problem in celestial mechanics NASA-TN-D-4447 c30 N68-228 c30 N68-22885 Vector representation of rotations and their algebra NASA-TN-D-4696 c19 N68-30594 VELOCITY DISTRIBUTION Simultaneous correction of velocity and mass bias in photography of meteors NASA-TR-R-280 c30 N68-15484 Stability of shear flow with density gradient and viscosity NASA-CR-958 c12 N68-15530 Velocity and density profiles in mixing region between adjacent half jets of dissimilar fluids NASA-CR-957 c12 N68-15571 Tabulated data on velocity distribution of upper air winds at Wallops Island NASA-TN-D-4570 c20 N68-2407 C20 N68-24028 VENTING Cryogenic propellant management during coasting of

Atlas Centaur vehicles NASA-TN-D-4571 c28 N68-25099

SUBJECT INDEX

VENTURT TURES Effects of Freon, water flow temperatures, and pressures on incipient venturi cavitation NASA-TN-D-4340 c12 NG c12 N68-14641 Thermodynamic effects on Freon cavitation on venturi scale model NASA-TN-D-4387 c12 N68-15329 Performance of venturi meter with separable diffuser NASA-TM-X-1570 c14 N68-21384 VERTICAL AIR CURRENTS Statistical analysis of repeated acceleration and impact loads on airline transports Impact loads on alfilme transports NASA-TN-0-4586 VERTICAL TAKEOFF AIRCRAFT Wind tunnel tests of deflected slipstream cruise fan V/STOL aircraft wing NASA-TN-0-4262 Economic and suitability comparison of short haul -02 N68-24476 c01 N68-11036 transport aircraft concepts NASA-CR-986 c02 N68-13517 Wind tunnel study of lateral and directional aerodynamic characteristics of powered four-duct propeller VTOL scale model in transition c02 N68-17023 NASA-TN-D-4343 NASA-TN-D-4343 c02 N68-17023 Optimum values of pitch rate damping, longitudinal control and speed stability for vertical takeoff aircraft /helicopters/ using pilot ratings NASA-TN-D-4624 c02 N68-28153 Exhaust gas ingestion characteristics and induced aerodynamics for vertical takeoff lift engine fighter model in ground proximity NASA-CR-1098 c02 N68-28233 Hot-gas ingestion investigation of large-scale jet VTOL fighter type models NASA-TN-D-4609 c02 N68-28277 Jet VTOL aircraft inlet temperature rise and induced recirculating flow patterns NASA-CR-1147 c01 N68-33043 Wind tunnel tests of a VTOL jet fighter to determine aerodynamic characteristics including stability NASA-TN-D-4812 VESTIBULES c01 N68-36081 Conference proceedings on role of vestibular organs in space exploration NASA-SP-152 c04 N68-29128 VIBRATION Modified vibration transducer calibration system for directly producing sensitivity versus frequency range plots NASA-TN-D-4760 c14 N68-319 c14 N68-31958 VIBRATION DAMPING High frequency structural damping due to riveted joints associated with gas pumping between overlapping surfaces NASA-CR-954 c32 N68-11489 Damping of piezoelectric quartz crystal driven in torsional mode of vibration in liquid helium 3 and helium 4 NASA-TN-D-4381 c26 N68-17594 Stress analysis and wear tests in use of lacing wire as vibration damper on turbocompressor blades c32 N68-28238 NASA-TM-X-1603 Wind tunnel model vibration reduced by use of tuned vibration damping absorber on aircraft model NASA-TM-X-1606 VIBRATION ISOLATORS Precision tilt and vibration isolation system design NASA-TR-R-281 VIBRATION MEASUREMENT c14 N68-19642 Preasibility of using laser radiation for detection and measurement of vibration of mechanical structures NASA-CR-985 c16 N68-14070 Measurement and interpretation of ground vibrations, produced by seismic effect of sonic boom NASA-CR-1137 c13 N68-35151 VIBRATION MODE Mathematical models and approximation methods for solving lateral vibration modes of cylindrical space vehicles and vehicles with clustered tanks NASA-CR-935 c32 N68-10231 Mathematical models for determining longitudinal vibration modes of multistage liquid and solid

WALL PRESSURE

propellant vehicles, and clustered tank vehicles NASA-CR-936 c32 N68-10280 NASA-CR-936 Torsional model development and model calculations for cylindrical space vehicle systems and systems employing clustered tanks NASA-CR-937 c32 N68-10568 Vibration modal response of thin cylindrical shells NASA-CR-897 c32 N68-11967 Resonant frequencies and nodal pattern modes of vibrating cylindrical and conical frustum shells NASA-TN-D-4428 c32 N68-20954 Iterative procedure for calculating normal modes and frequencies of cantilever beam NASA-TN-D-4560 c02 N68-22886 Three dimensional motion analysis and vibration characteristics of dynamically scaled model of asymmetrically clustered launch vehicle NASA-TN-D-4707 c32 c32 N68-32051 Prediction of vibration frequencies and modes for free-free truncated conical shells, using Rayleigh-Ritz method NASA-TN-D-4772 VIBRATION TESTS c32 N68-33057 Techniques for full-scale dynamic testing of large solid or liquid fueled booster vehicles NASA-CR-940 c32 N68-11054 Longitudinal vibration of full scale representative launch vehicle by means of force controlled vibration techniques NASA-TN-D-4502 Vibration tests of concentric tube fuel element support structure for Tungsten Water Moderated Reactor NASA-TM-X-1608 c32 N68-28330 Vibration tests and analysis of thin cylindrical shells with and without longitudinal stiffeners NASA-TN-D-4705 c32 N68-33738 VIBRATIONAL STRESS Soviet engineering handbook on vibration and dynamic stability theory and calculations in helicopter design NASA-TT-F-519 c02 N68-23456 Friction and fretting wear tests on materials used as friction dampers to reduce vibrational stresses in compressor blades for turbine engines NASA-TN-D-4630 c15 N68-28871 VIDEO DATA Spaceborne pattern recognition system for identifying and classifying objects in video data NASA-CR-999 c10 N68-19229 VISCOSITY Stability of shear flow with density gradient and viscosity NASA-CR-958 c12 N68c12 N68-15530 VISCOUS FLUIDS Magnetohydrodynamic flow of incompressible viscous electrically conducting fluid over rotating disk NASA-CR-989 c25 N68-14078 VISUAL AIDS Properties and imaging techniques of various display devices - computer directed visual flight control boards, integrated optical man machine systems, and electro-optical methods NASA-SP-159 c09 N68-223 c09 N68-22302 Visual information display systems that are computer connected or updated with computer generated information NASA-SP-5049 c08 N68-32159 VISUAL OBSERVATION Visual observations to find flow distribution and coefficients through radial bladed centrifugal pump impeller NASA-TN-D-4282 cl2 N68-286 Electronic visualization technique for studying c12 N68-28842 dynamic behavior of gas journal bearing NASA-TM-X-1609 c14 k c14 N68-35105 VISUAL PERCEPTION Human performance measured as function of reaction time required to discriminate change in beacon brightness NASA-CR-1220 c05 N68-37819 VOID RATIO Critical experiments analysis of uranyl fluoride solution reactors containing large-diameter

NASA-TN-D-4270 c22 N68-15197 Lunar volcanism model based on high temperature radiative thermal conductivity of minerals and rocks NASA-CR-916 VOLT-AMPERE CHARACTERISTICS c13 N68-10283 Current-voltage characteristics of tunneling p-n junctions in semiconductors NASA-TN-D-4403 c09 N68 c09 N68-19062 Current-voltage characteristics of collisionless cylindrical diode with thermionically emitted electrons c10 N68-21122 NASA-TN-D-4516 NRDATIN-U-4016 c10 N68-21122 Transient thermodynamic analysis for development of mathematical model that predicts transient temperature and voltage-response characteristics of fuel cell system NASA-TN-D-4601 c03 N68-25304 VOLTAGE REGULATORS Experimental evaluation of ferroresonant and feedback alternating current line voltage regulators in 15 kilowatt auxiliary power system NASA-TN-D-4627 c03 N68-28101 Breadboard model of Brayton cycle alternator and voltage regulator-exciter NASA-TN-D-4697 c03 N68-29960 VOLUMETRIC ANALYSIS Method for calculating partial volumes of components in solution NASA-TN-D-4199 c06 N68-11621 Design and volumetric analysis of pressurized tanks for use in liquid-methane fueled supersonic transport aircraft NASA-TN-D-4295 c32 N68-12370 NASA-IN-D-4235 C32 NG-12370 VON ZEIPEL METHOD Perturbation theory for artificial satellites with nearly circular orbits using Von Zeipel method NASA-IN-D-4531 C30 N62-28251 VORTEX BREAKDOWN Containment characterístics of radial inflow gases in vortex tubes NASA-CR-1029 c12 N68-22200 VORTEX GENERATORS Analysis of turbulent wall pressure field under supersonic shear layers NASA-CR-888 c12 N68-22087 NASA-CR-888 cl2 N68-22087 Performance of vortex generators installed aft of inlet throat on centerbody evaluated at Mach numbers 2.0 to 3.0 NASA-TN-D-4675 c01 N68-28799 VORTEX INJECTORS Wall injection area and axial bypass effects on flow pattern of stagnation surface in radial c01 N68-28795 inflow vortexes NASA-CR-1028 c22 N68-22088 VORTICES Flow distributions in radial outflow vortices using rotating peripheral wall water vortex tube NASA-CR-991 c22 N68-16478 NASA-CK-991 Flow visualization and containment tests in directed-wall-jet vortex tube with radial outflow and moderate superimposed axial flow NASA-CR-992 c22 N68-1 c22 N68-17131 Containment tests of vortexes with radial outflow in basic vortex tube, and in axial-flow vortex tube NASA-CR-993 c22 N68-18243 Vortex value for hot gas flow modulation in secondary injection thrust vector control system NASA-CR-1091 c28 N68-28112 W WALKING Metabolic cost of walking on treadmills of various slope before and after loading of principal body segments NASA-CR-1042 co5 N68-21859 WALL FLOW Selected band cross correlation analysis of fluctuating pressures under turbulent boundary layer flow NASA-CR-1066

voided tubes

- NASA-CR-1066 c12 N68-23482 WALL PRESSURE Analysis of turbulent wall pressure field under
- supersonic shear layers NASA-CR-888 c12 N68-22087

WALL TEMPERATURE Feasibility of supporting liquid fuel on solid wall in radiating liquid core nuclear rocket concept NASA-TN-D-4413 c27 N68-17093 Convective heat transfer coefficients on adiabatic walls determined by sinusoidally forced fluid temperature temperature NASA-TM-X-1594 Analytical investigation of flow and wall temperature sensitivity in heated passages for large inlet to exit density ratios in subsonic flow of nuclear rocket c33 N68-24618 NASA-TN-D-4649 c33 N68-28371 Heat transfer characteristics of cylindrical ejector for turbojet engine and shroud material temperature prediction NASA-TM-X-1641 c33 N68-3298 c33 N68-32988 Single-thermocouple method for measuring heat flux in thermally thick walls NASA-TN-D-4737 c33 N68-33208 WALLOPS ISLAND Wind velocity profiles measured by smoke trail method at Wallops Island, Va., in 1963 and 1964 NASA-TN-D-4365 c20 N68-17024 Tabulated data on velocity distribution of upper air winds at Wallops Island NASA-TN-D-4570 c20 N68-240 c20 N68-24028 WASP SOUNDING ROCKET Design and flight performance studies of Wasp sounding rocket NASA-TM-X -1518 c31 N68-17094 WASTE UTILIZATION Survey and critical evaluation of existing methods for synthesis of fatty acids and lipids from metabolic wastes under conditions of space flight NASA-CR-1105 c04 N68-28278 WATER Boiling heat transfer coefficients, interface behavior, and vapor quality in heated wall rotating boilers with continuous through-flow of water as test fluid NASA-TN-D-4136 c33 N68-17 c33 N68-17566 Performance of centrifugal pump impeller in room temperature water NHOH-IN-U-4613 cl2 N68-26651 Cavitation damage of stainless steel, nickel, and aluminum alloy in water NASA-TM-X-1670 cl7 N69-26030 WATER LANDING Impact water pressures, accelerations, and landing dynamics of scale model Apollo command module with deployed heat shield impact attenuation system NASA-TN-D-4275 c31 N68-18822 WATER MODERATED REACTORS Comparison of absolute calculated and measured gamma and neutron doses in tungsten watermoderated critical assembly NASA-TN-D-4223 c22 N68-10291 System dynamics and control analysis of tungsten water moderated nuclear rocket NASA-TM-X-1426 c22 N68-18252 Postshutdown cooling requirements of tungsten water moderated nuclear rocket engines NASA-TM-X-1568 c22 N68-21111 Vibration tests of concentric tube fuel element support structure for Tungsten Water Moderated Reactor NASA-TM-X-1608 c32 N68-28330 WATER PRESSURE Effects of Freon, water flow temperatures, and pressures on incipient venturi cavitation NASA-TN-D-4340 c12 N68-1 c12 N68-14641 WATER VAPOR Outgassing of water vapor from concrete surfaces in vacuum environments NASA-TM-X-1536 c11 N68-19207 Carbon dioxide and water vapor effects on induction period kinetics of hydrogen-oxygen reaction NASA-TN-D-4685 c33 N68-30041 Water vapor condensation effects of heated air on flow in large supersonic wind tunnels NASA-TM-X-1636 cll N68-3059 c11 N68-30598 WAVE ATTENUATION

Attenuation and dispersion of longitudinal waves

SUBJECT INDEX

in viscous partly ionized gases NASA-TM-X-1458 WAVE DISPERSION c07 N68-18703 Attenuation and dispersion of longitudinal waves in viscous partly ionized gases NASA-TM-X-1458 c07 N68-18703 WAVE FRONT DEFORMATION Test sections for small theoretical wind tunnel boundary interference on V/STOL models NASA-TR-R-286 c11 c11 N68-31592 WAVE FUNCTIONS Inelastic scattering form factors using projected Hartree-Fock wave functions NASA-TN-D-4566 c24 N68-24661 Field-aligned propagation of high frequency radio waves using Alouette 2 satellite data NASA-TN-D-4748 c0 c07 N68-31639 WAVEFORMS Rapid reduction method of rhythm and rate information in large scale electrocardiogram monitoring NASA-TN-D-4751 c05 N68~32100 WAVEGUIDES Fourier transforms for aperture admittance of ground-plane-mounted waveguide illuminating conducting sheet NASA-TN-D-4366 c07 N68-18123 Quasi-omnidirectional resonant array of circumferential shunt slots in ring waveguides for narrow bandwidth space vehicle applications at microwave frequencies NASA-TN-D-4362 c07 N68-18616 Aperture-admittance expression for waveguide-fed rectangular aperture antenna, loaded with dielectric plug c07 N68-20333 NASA-TN-D-4430 Thin walled parallel plate waveguide radiation pattern analyzed by surface integration technique c07 N68-22746 NASA-CR-1052 Fourier series expansion of simultaneous integral equations for collinear coupled waveguides radiating through common perfectly conducting radiating through common perfectly conducting ground plane NASA-TN-D-4656 c09 N68-28 Reflectance of wedge angle parallel plate waveguides in transverse electromagnetic mode illuminating reflecting sheet NASA-CR-1174 c07 N68-35 c09 N68-28668 c07 N68-35172 Electrical impedance and radiation distributions of circular waveguide by integral transformation NASA-TN-D-4752 c07 N68-35537 WEAR TESTS Wear rate and friction coefficient of steel sliding on polymer laminates determined in liquid nitrogen and hydrogen NASA-TN-D-4463 c15 N68-20325 Crystal transformation and atomic ordering on wear and sliding friction in two cobalt alloys NASA-TN-D-4668 c15 N68-28260 Friction and fretting wear tests on materials used as friction dampers to reduce vibrational stresses in compressor blades for turbine engines NASA-TN-D-4630 c15 N68-28871 WEATHER STATIONS Statistical evaluation of sampled wind data from anemometers mounted on meteorological tower on Wallops Island NASA-TN-D-4395 c20 N68-18246 WEDGE FLOW Real gas wedge-induced laminar separation on cooled blunt flat plate at hypersonic speed NASA-TN-D-4320 c01 N68-17899 WEDGES AGES Effect of boundary layer bleed on heat transfer and pressure distributions over wedge-flap surface at hypersonic speeds NASA-TN-D-4686 c01 N68-29 c01 N68-29955 NASA-IN-J-3000
 WEIGHT (MASS)
 Weight, heat transfer, and efficiency comparison for Rankine cycle space radiators constructed of three different finned tube geometries -33 N68-1633 NASA-TN-D-4411 c33 N68-16324 Radiation resistance, outgassing characteristics, and weight of five electrical insulation materials for spacecraft NASA-TN-D-4553 c18 N68-28264

WEIGHT ANALYSIS GHT ANALYSIS Survey on minimum weight design aspects of stiffened cylinders under compression NASA-CR-963 c32 N68-11282 Size and shield weight requirements calculated for fast-spectrum, liquid-metal cooled nuclear reactor for space power application NASA-TN-D-4315 c22 N68-18197 WEIGHTING FUNCTIONS Distribution and properties of weighted sum of chi squares random variables NASA-TN-D-4575 c19 N68-24565 WEIGHTLESSNESS Liquid flow into baffled spherical tank during weightlessness NASA-TM-X-1526 c12 N68-213 Effects of shallow liquid depths on lateral sloshing in cylindrical tanks under weightless c12 N68-21365 conditions NASA-TN-D-4458 c12 N68-24758 Liquid-vapor interface stability during liquid inflow in cylindrical tank during weightlessness NASA-TN-D-4628 c12 N68-25866 WEIGHTLESSNESS SIMULATION Water immersion simulation study of astronaut performance during airlock ingress or egress at reduced gravity NASA-CR-971 c05 N68-20339 NAN CR 5/1 Pressure suits and backloads effects on locomotion in simulated lunar gravity NASA-TN-D-4464 c05 N68-20354 WELDED JOINTS Stress-strain diagrams for cold welded copper microjunctions in vacuum NASA-TN-D-4743 WHEEL BRAKES c17 N68-31517 Effect of wheel braking on directional control of pneumatic tires on pavement NASA-TN-D-4602 c02 N68-25313 WIND DIRECTION Tabulated data on velocity distribution of upper air winds at Wallops Island NASA-TN-D-4570 c20 N68-240; WIND MEASUREMENT c20 N68-24028 Statistical evaluation of sampled wind data from Anemometers mounted on meteorological tower on Wallops Island NASA-TN-D-4395 c20 N68-182 c20 N68-18246 WIND PROFILES W FRUFILED Scalar and component wind correlations between altitude levels for statistical analysis of wind profiles at Cape Kennedy, Florida, and Santa Monica, California NASA-TN-D-3815 cl3 N68-20 c13 N68-20278 WIND SHEAR Analog computed time histories and altitude-ground track plots of swept wing transport aircraft longitudinal response to wind shear and sustained gusts during landing approaches NASA-TN-D-4477 col NG c01 N68-19180 WIND TUNNEL CALIBRATION Wind tunnel calibration of conical pressure probe over range of Mach numbers to determine flow field data for X-15 airplane NASA-TN-D-4678 c12 N68-2880 c12 N68-28801 Wind tunnel calibration of 30 deg included angle come for determination of local values of Mach number, total pressure, and flow distribution NASA-TN-D-4679 c14 N68-30 c14 N68-30127 Description and operating parameters of Mach 2 nozzle system for 11-inch ceramic heated wind tunnel NASA-TN-D-4750 WIND TUNNEL MODELS c11 N68-33190 Air flow calibration over moving belt ground plane installed in wind tunnel and data for two blowing-flap models tested over moving belt NASA-TN-D-4237 Ground proximity effects on longitudinal, lateral, and control aerodynamic characteristics of tilt wing four propeller V/STOL wind tunnel model NASA-TN-D-4237 CO2 N68-11519 Simulated wind-tunnel investigation with jet-augmented flap NASA-TN-D-4278 c02 N68-11627 Aircraft sonic boom characteristics predicted from near field data obtained in wind tunnel NASA-TM-X-1477 c02 N68-1 c02 N68-11772 Wind tunnel study of aerodynamic characteristics

of three scale model multistage launch vehicles at supersonic and hypersonic speeds NASA-TM-X-1498 c01 N68-Wind tunnel study of lateral and directional c01 N68-16299 aerodynamic characteristics of powered four-duct propeller VTOL scale model in transition NASA-TN-D-4343 co2 N68-17023 NASA-IN-D-4343 C02 N68-17023 Wind tunnel determination of longitudinal force characteristics for STOL aircraft scale models with varying wing aspect ratios NASA-TN-D-4448 C02 N68-18771 Wind tunnel investigation of fluctuating pressures on Centaur model surface at transonic speed NASA-TM-X-1574 c31 N68-22742 Test apparatus and procedures for aerodynamic ... apparatus and procedures for aerodynam model tests of spacecraft control system parameters NASA-CR-947 c32 N68-23452 Wind tunnel model vibration reduced by use of tuned vibration damping absorber on aircraft model NASA-TM-X-1606 c32 N68-28806 Wind tunnel model tests of variable flap ejector nozzle with aerodynamically positioned shroud NASA-TM-X-1639 c-28 N68-30 Test sections for small theoretical wind tunnel boundary interference on V/STOL models NASA-TR-R-286 c11 N68-31 c28 N68-30599 c11 N68-31592 NASA-TK-R-286 c11 N68-315 Wind tunnel evaluation of speed brake effects on supersonic characteristics of variable sweep fighter aircraft models NASA-TN-D-4773 c02 N68-3366 c02 N68-33669 NASA-IN-3-4775 Aerodynamic characteristics of subsonic cargo jet transport model in slotted transonic wind tunnel NASA-TM-X-1660 col N68-35617 Wind tunnel tests of a VTOL jet fighter to determine aerodynamic characteristics including stability NASA-TN-D-4812 c01 N68-36081 Effect of model forebody shape on perforated supersonic wind tunnel wall interference NASA-TM-X-1656 c01 N68 NASA-TM-X-1656 coll N68-36133 Windshield and nose geometry effects on supersonic aerodynamic characteristics of tactical fighter model NASA-TM-X-1664 Effect of hydrogen peroxide generator configurations on jet exhaust flow c02 N68-37066 characteristics NASA-TM-X-1671 c12 N68-37067 Effects of simulated jet exhaust flow on transonic aerodynamic characteristics of Apollo launch escape vehicle models escape venicle models NASA-TN-D-4843 Wind tunnel tests at Mach 1.60, 2.36, and 2.96 to determine flow field properties near arrow wing body model for locating potential engine air c31 N68-37074 inlets NASA-TN-D-4809 c01 N68-37238 Longitudinal aerodynamic characteristics of parasol-wing model at supersonic speeds NASA-TN-D-4855 WIND TUNNEL NOZZLES c01 N68-37854 Description and operating parameters of Mach 2 nozzle system for 11-inch ceramic heated wind tunnel NASA-TN-D-4750 cll N68-331 WIND TUNNEL STABILITY TESTS Wind tunnel tests of deflected slipstream cruise fan V/STOL aircraft wing NASA-TN-D-4262 c01 N68-110 c11 N68-33190 c01 N68-11036 Aerodynamic stability characteristics of Apollo launch escape vehicle with canard surfaces deployed NASA-TN-D-4280 c01 N68-11640 Design and performance testing of large scale mixed compression axisymmetric inlet at transonic and supersonic speeds NASA-TM-X-1507 c28 N68-17028 Low speed static and dynamic stability tests on scale model of double-delta supersonic commercial air transport configuration NASA-TN-D-4179 c02 c02 N68-18250 wind tunnel stability tests of twin engined turboprop aircraft with rotating cylinder flaps NASA-TN-D-4489 col N68-1918

WHDA-IN-D-4489 c01 N68-19189 Wind tunnel stability tests of pinch of modified half ring wing body and swept wing body combinations at supersonic speeds

WIND TUNNEL WALLS

SUBJECT INDEX

NASA-TM-X-1551 c01 N68-21940 Dynamic response of axisymmetric hammerhead model to unsteady aerodynamic loading in wind tunnel tests NASA-TN-D-4504 c01 N68-25916 Wind tunnel studies of static aerodynamic Nasa-TN-D-4672 col N68-28447 Wind tunnel test data on static and dynamic stability of Apollo command module configuration NASA-TN-D-4688 c01 N68-31445 Test sections for small theoretical wind tunnel boundary interference on V/STOL models NASA-TM-X-1661 c11 N68-31592 c01 N68-36509 Converging flow effects on longitudinal stability measurements in tandem test section of wind tunnel NASA-CR-1198 c11 N68-36522 Windshor-Gr-1136 Wind tunnel tests to determine low speed high lift aerodynamics of one-fifth scale variable sweep supersonic transport model NASA-TN-D-4844 CO1 N68-37365 WIND TUNNEL WALLS Approximation method for calculating spanwise distribution of wind tunnel boundary interference on wing lift in rectangular perforated wall NASA-TR-R-285 c01 N68-24617 Effect of model forebody shape on perforated supersonic wind tunnel wall interference NASA-TM-X-1656 c01 N68-36133 Cone-cylinder models tested in supersonic wind tunnel to evaluate effect of wall reflected disturbances on model pressure distributions NASA-TM-X-1655 c01 N68-36134 WIND TUNNELS Wind tunnel study of scale model automobile ground plane boundary layer using moving-belt ground plane technique NASA-TN-D-4229 c01 N68-100 Wind tunnel investigation of techniques for c01 N68-10093 reducing cowl drag of external compression inlet at Mach 2.49 NASA-TM-X-1516 coll N68-18189 WIND VARIATIONS Atmospheric conditions during turbulences encountered by XB-70 aircraft above 40,000 ft NASA-TN-D-4768 c13 N68-33 c13 N68-33416 WIND VELOCITY Meteorological wind, and temperature data from atmospheric radiosonde soundings in Southern Hemisphere NASA-TN-D-4429 c20 N68-1900 Tabulated data on velocity distribution of upper air winds at Wallops Island NASA-TN-D-4570 c20 N68-2400 WIND VELOCITY MEASUREMENT c20 N68-19084 c20 N68-24028 Wind velocity profiles measured by smoke trail method at Wallops Island, Va., in 1963 and 1964 c20 N68-17024 NASA-TN-D-4365 WINDING Length of winding on torus in two ideal models NASA-TM-X-1674 WINDOWS (APERTURES) c03 N68-37217 Temperature and radiation effects on index of refraction and extinction coefficients of Apollo window materials NASA-CR-1019 c31 N68-20467 •JHOOW Gesigns for mercury condensing tube and mercury boiler outlet tube NASA-TM-X-1578 cl1 N68-2273 Effects of edge constraints on optical qualities of Gemini spacecraft windows NASA-TN-D-4845 c23 N68-3647 Window designs for mercury condensing tube and c11 N68-22737 c23 N68-36470 WINDSHIELDS Windshield and nose geometry effects on supersonic aerodynamic characteristics of tactical fighter model NASA-TM-X-1664 c02 N68-37066 **WING CAMBER** Notified approach for predicting lift body pressures and camber shape for planforms in subsonic flow

NASA-TN-D-4427 c01 N68-28868 WING FLAPS Wind tunnel study to explore use of slot spoilers for direct control of flap induced lift and lateral aircraft control NASA-TN-D-4664 c01 N68-28830 WING PROFILES IG PROFILES Wind tunnel stability tests of pinch of modified half ring wing body and swept wing body combinations at supersonic speeds NASA-TM-X-1551 col N68-2194 c01 N68-21940 NRON-IN-X-1001 COI N68-21: Profile change effects on aerodynamic characteristics of twisted and cambered arrow wing at supersonic speed NASA-TN-D-4796 COI N68-35 c01 N68-35665 WING SPAN Wing surface pressure data from large scale wind tunnel tests of propeller driven short takeoff aircraft NASA-TM-X-1527 c02 N68-19065 WING TANKS Design and volumetric analysis of pressurized tanks for use in liquid-methane fueled supersonic transport aircraft NASA-TN-D-4295 WINGED VEHICLES c32 N68-12370 Volume addition effects on leeward surface of high lift drag ratio winged body at hypersonic speeds NASA-TN-D-4361 c01 N68-17880 WINGS Approximation method for calculating spanwise distribution of wind turnel boundary interference on wing lift in rectangular perforated wall NASA-TR-R-285 c01 N68-24617 NTRE Stress analysis and wear tests in use of lacing wire as vibration damper on turbocompressor blades NASA-TM-X-1603 c32 N68-28238 WIRE BRIDGE CIRCUITS Electron paramagnetic resonance signals from paramagnetic sample in microwave bridge c14 N68-21169 NASA-TN-D-4469 WIRE CLOTH Analytical investigation of electrical heated wire mesh for flowing gas heaters NASA-TN-D-4595 c33 N68-25312 WORK FUNCTIONS Equations for determining substrate surface coverages from arrival rates and desorption characteristics of adsorbate ions and atoms c25 N68-25630 NASA-TN-D-4369 Dependence of tungsten electrode work functions on positive ion sheaths between electrodes and cesium plasmas NASA-TN-D-4745 WORKING FLUIDS c25 N68-30593 Electromagnetic processes in magnetohydrodynamic induction machines with working media of liquid metal NASA-TT-F-460 c25 N68-16286 Comparative analysis of single-loop 100-kilowatt Brayton space power system using pure gas and gas-solid suspension as working fluids NASA-TN-D-4659 c03 N68-2820 c03 N68-28280 Х

- X- 15 AIRCRAFT Wind tunnel study of flow field beneath X-15 aircraft fuselage at supersonic to hypersonic speeds NASA-TM-X-1469 c02 N68-11147
 - Limit cycle and control surface resonance characteristics of X-15 stability augmentation system
 - NASA-TN-D-4287 c02 N68-11545 Airborne stellar photometry and spectrometric determination of day sky brightness
 - NASA-CR-1017 c30 N68-19590 Approximation of ramjet exhaust plume effects on external pressure of nozzle extension of X-15 aircraft
 - NASA-TM-X-1571 c28 N68-24614 Performance characteristics of data acquisition flight test sensors used on X-15 aircraft NASA-TN-D-4597 c14 NG
 - c14 N68-25317

ZODIACAL LIGHT

X-15 aircraft radiometric measurement of earth infrared horizon in three spectral intervals NASA-TN-D-4654 c21 N68-28262 Wind tunnel calibration of conical pressure probe over range of Mach numbers to determine flow field data for X-15 airplane NASA-TN-D-4678 c12 N68-28801 Analog and digital inertial flight data systems for X-15 aircraft NASA-TN-D-4642 c08 N68-294 c08 N68-29404 No. IN D-4042 Flow distribution in flight test and wind tunnel hypersonic flow of X-15 aircraft NASA-TN-D-4813 col N68-3513 c01 N68-35173 X RAY ABSORPTION Correction of balloon X ray astronomy data for atmospheric attenuation, escape, and energy resolution NASA-CR-1045 c13 N68-23436 X RAY ANALYSIS Electron probe X ray microanalyzer applied to material failure study, bonding, and other metallurgical analysis NASA-TN-D-4526 c15 N68-28249 X RAY ASTRONOMY Correction of balloon X ray astronomy data for atmospheric attenuation, escape, and energy resolution NASA-CR-1045 c13 N68-23436 X RAY DIFFRACTION Recovery of potassium tantalate and potassium monoxide to demonstrate procedure for isolation and recovery of alkali-metal reaction products in uncontaminated state NASA-TN-D-4310 X RAY SPECTROSCOPY c17 N68-14888 Correction of balloon X ray astronomy data for atmospheric attenuation, escape, and energy resolution NASA-CR-1045 c13 N68-23436 X-Y PLOTTERS Modified vibration transducer calibration system for directly producing sensitivity versus frequency range plots NASA-TN-D-4760 c14 N68-31958 XENON Electrical properties of xenon filled thermionic diodes in nuclear reactor radiation field NASA-TN-D-4368 c25 N68-15747 Plum Brook reactor support calculations nathematical model for fuel utilization, power distfibution in fuel loading, and approximate predictions of xenon poison transient NASA-TM-X-1496 c22 N68-160

Ý

c22 N68-16056

YIELD STRENGTH Necking, yield, and plastic flow in electrical analogs of mechanical systems with respect to energy conversion effects on mechanical behavior of various materials NASA-CR-1039 YTTRIUM COMPOUNDS c24 N68-21949 Reactivity control of fast nuclear reactors Reactivity control of last nuclear reactors
 containing yttrium hydride moderating zones
 NASA-TN-D-4615
 c22 N68-24559
 Neutronic effects of yttrium hydride moderator
 insertion in fast spectrum reactors
 NASA-TM-X-1614
 c22 N68-29950

Ζ

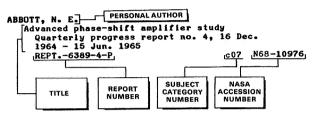
ZINC Effects of zinc concentration on output of zinc doped germanium infrared detectors NASA-TN-D-4834 c26 N68-370 ZIRCONIUM OXIDES c26 N68-37055 Oxide deformation and fiber reinforcement in tungsten-urania and tungsten-zirconia elongated into fibers by hot extrusion NASA-TN-D-4475 ZODIACAL LIGHT c17 N68-18610 DIACAL LIGHT Photometric and meteor observations, scattering properties, particle collection and impact, solar wind, and origin and evolution of zodiacal light in interplanetary medium - conference 20 NG2-22475 c30 N68-27475 NASA-SP-150

PERSONAL AUTHOR INDEX

NASA SCIENTIFIC AND TECHNICAL REPORTS FOR 1968

A Selected Listing

Typical Personal Author Index Listing



Listings in this index are arranged alphabetically by personal author. The title of the document provides the user with a brief description of the subject matter. The report number helps to indicate the type of document cited (e.g., NASA report, NASA contractor report). The subject category number indicates the subject category in the abstract section in which the citation is located. The NASA accession number denotes the number by which the citation is identified within the subject category. The titles are arranged under each personal author in ascending accession number order.

Α

```
ABBOTT, A. S.
Guidance, flight mechanics and trajectory
optimization. Volume 1 - Coordinate
systems and time measure
         NASA-CR-1000
                                                                  c30 N68-16103
     Guidance, flight mechanics and trajectory optimization. Volume 2 - Observation theory
         and sensors
     NASA-CR-1001 c30 N
Guidance, flight mechanics and trajectory
optimization. Volume 8 - Boost guidance
                                                                  c30 N68-19676
         equations
NASA-CR-1007
                                                                  c30 N68-20449
     Guidance, flight mechanics and trajectory optimization. Volume 10 - Dynamic
         programming
     NASA-CR-1009
Guidance, flight mechanics and trajectory
optimization. Volume 15 - Application
                                                                  c30 N68-21077
         of optimization techniques
         NASA-CR-1014
                                                                  c30 N68-21231
     Guidance, flight mechanics and trajectory optimization. Volume 5 - State
         determination and/or estimation
         NASA-CR-1004
                                                                  c30 N68-21685
 ABDALLA, K. L.
      Pressure-rise characteristics for a liquid
        hydrogen dewar for homogeneous, normal gravity
quiescent, and zero gravity tests
NASA-TM-X-1134 c33 N68-181
                                                                  c33 N68-18196
     NASA-TM-X-1134 c33 N68
An experimental investigation of the effect
of gravity on a forced circulation pattern
in spherical tanks
NASA-TN-D-4409 c12 N68
                                                                  c12 N68-20352
      An experimental study of liquid flow into
a baffled spherical tank during weightlessness
NASA-TM-X-1526 c12 N68-213
                                                                  c12 N68-21365
     Liquid inflow to initially empty,
hemispherical ended cylinders during
         weightlessness
         NASA-TN-D-4628
                                                                  c12 N68-25866
      Liquid vapor interface configurations in
         toroidal tanks during weightlessness
         NASA-TN-D-4819
                                                                  c12 N68-35823
 ACKEN. R. A.
      Navigator performance studies for space
navigation using the NASA CV-990
research aircraft
         NASA-TN-D-4449
                                                                  c21 N68-21123
ACKER, L. W.
Sound measurements on a full-scale
```

jet-engine inlet-noise-suppressor cowling NASA-TN-D-4639 C02 N68-29887 ADAMS, D. W. Study of vibration induced stresses in design of fuel-element support assembly for tungsten water-moderated nuclear reactor NASA-TM-X-1608 c32 N68-28330 ADAMS, E. W. Theory of the investigation of the atmosphere of binary stars by analogy between gas dynamics and shallow-water flows NASA-TN-D-4520 c30 c30 N68-25385 ADAMS, J. J. Investigation of tethered station keeping NASA-TN-D-4258 c31 N68-11641 Analysis of human response in combined control tasks NASA-TN-D-4356 c05 N68-18014 synthesis of human response in closed-loop tracking tasks NASA-TN-D-4842 c05 N68-36461 AHTYE, W. F. A critical evaluation of the use of ultrasonic absorption for determing high-temperature gas properties NASA-TN-D-4433 c24 N68-18949 AIKIN, A. C. Temporal variations of mesospheric oxygen and ozone during auroral events NASA-TN-D-3993 c13 N68-10369 AILMAN. C. M. Narrow band cross-correlation analysis of fluctuating pressures beneath a turbulent boundary layer NASA-CR-1066 c12 N64 c12 N68-23482 AISENBERG, S. Plasma boundary interactions - 2 NASA-CR-1072 c25 N68-25821 AKIN. C. M. Comparison of convective stagnation heat transfer in air, CO2-N2, and CO2-Ar gas mixtures NASA-TN-D-4255 c33 N68-11811 ALBRITTON, O. W. A study of sensitization in types 301 and 304L stainless steels using Moessbauer spectroscopy NASA-CR-1077 c17 N68-25318 ALEXANDER, R. L. Ages of D/d,n/He sup 3 and T/d,n/He sup 4 neutrons in water and tungsten-water mi NASA-TN-D-4581 c22 mixtures c22 N68-25058 ALFANO, D. L. Analysis of performance characteristics in ground effect of a large scale V/STOL multi-fan-in-wing transport model NASA-CR-1180 c28 N68-35594 ALFARO-BOU, E. Ballistic limit of aluminum plates determined by an exploding foil gun technique NASA-TN-D-4259 c32 N68-: c32 N68-11355 ALFRIEND, K. T. Time-optimal rendezvous for elliptic orbits NASA-CR-1036 c30 N68-22202 ALKSNE, A. Y. External aerodynamics of the magnetosphere NASA-TN-D-4482 c29 N68-25181 ALLEN, G. An efficient method for computation of character tables of finite groups NASA-TN-D-4763 c19 N68-31961 ALLEN, H. J. A method for computing luminous efficiencies from meteor data NASA-TN-D-4808 c30 N68-33055

ALLEN, R. W.

ALLEN. R. W. An experimental investigation of compensatory and pursuit tracking displays with rate and acceleration control dynamics and a disturbance input NASA-CR-1082 c07 N68-28272 ALLESINA, B. Studies of cost effective structures design for future space systems - Summary Final report, 17 Oct. 1966 - 17 Oct. 1967 NASA-CR-1068 c34 N68-26813 NASA-UK-1000 C34 NOO-ALLGEIER, R. K. Subcritical cryogenic storage development and flight test NASA-TN-D-4293 c23 N68-15950 Cryogenic storage systems for earth-orbital and Mars-flyby missions NASA-TN-D-4619 c03 N6 c03 N68-28420 ARSA-IN-D-4019 COS NOS-ALLIONE, M. S. Guidance, flight mechanics and trajectory optimization. Volume 6 - The N-body problem and special perturbation techniques NASA-CR-1005 c30 N68c30 N68-15741 ALLISON, L. J. An evaluation of sea surface temperature as measured by the Nimbus 1 high resolution infrared radiometer NASA-TN-D-4078 c20 N c20 N68-10222 A satellite view of Typhoon Marie 1966 development NASA-TN-D-4757 c20 N68-37869 ALMROTH, B. O. Buckling of shells of revolution with various wall constructions. Volume 3 - User*s manual for BOSOR NASA-CR-1051 c32 N68-23355 Buckling of shells of revolution with various wall constructions. Volume 2 - Basic equations and method of solution NASA-CR-1050 c32 N68-23451 Buckling of shells of revolution with various wall constructions. Volume 1 - Numerical results NASA-CR-1049 c32 N68-24481 ALSAJI, S. Entry length for the rocket meteorological radiation shield NASA-CR-1200 c14 N68-36530 AMBERGER, D. A cathode ray tube suitable for viewing under high ambient NASA-CR-1185 c09 N68-33224 ANDERS, J. B. An Ders, J. B. A real-gas study of low-density wedge-induced laminar separation on a highly cooled blunt flat plate at M infinity equals 12 NASA-TN-D-4320 c01 N68-17899 NASA-TN-D-4320 c01 N6 Low-density, leading-edge bluntness, and ablation effects on wedge-induced laminar boundary layer separation at moderate enthalpies in hypersonic flow NASA-TN-D-4829 c12 N68-36458 ANDERSON, A. F. Recuperator for solar Brayton cycle system NASA-CR-1150 c03 No c03 N68-33062 ANDERSON, G. Y. An experimental study of flame propagation in supersonic premixed flows of hydrogen and air NASA-TN-D-4631 c33 N68-28100 ANDERSON, J. L., JR. Small high-temperature nuclear reactors for space power NASA-TN-D-4371 c22 N68-15792 Reactivity control of fast-spectrum reactors by reversible hydriding of yttrium zones NASA-TN-D-4615 c22 N68 c22 N68-24559 ANDERSON, W. J. Friction torque of ball bearings in vacuum with seven polytetrafluoroethylene composition retainer materials NASA-TN-D-4355 c15 N68 Experiments on stability of herringbone grooved gas-lubricated journal bearings to c15 N68-16468 high compressibility numbers NASA-TN-D-4440 c15 N68-21965 NASA-IN-D-4440 c15 N68 Fatigue life of 120 mm bore ball bearings at 600 deg F with fluorocarbon, polyphenyl ether, and synthetic paraffinic base lubricants

NASA-TN-D-4850 c15 N68-36075 Incompressibly lubricated Rayleigh step journal bearing. 1 - Zero-order perturbation solution NASA-TN-D-4839 c15 N ANDRACCHIG, C. R. Pressure-rise characteristics for a liquid c15 N68-36098 hydrogen dewar for homogeneous, normal gravity quiescent, and zero gravity tests NASA-TM-X-1134 c33 N68-181 NASA-TM-X-1134 c33 N68-18196 An experimental study of liquid flow into a baffled spherical tank during weightlessness NASA-TM-X-1526 NASA-TM-X-1526 c12 N68-21365 ANDREWS, E. H., JR. Study of underexpanded exhaust jets of an X-15 airplane model and attached ramjet engine simulator at Mach 6.86 NASA-TM-X-1571 c28 N68-24614 ANNIS, J. F. The principle of the space activity suit NASA-CR-973 c05 N68-11510 Automatic control of water cooling in space suits NASA-CR-1085 c05 N68-26701 ADYAGI, K. Large-scale wind-tunnel investigation of a model with an external jet-augmented flap NASA-TN-D-4278 c02 NG c02 N68-11627 APPLEBY, B. A. Dynamic stability of space vehicles. Volume 8 - Atmospheric disturbances that affect flight control analysis c32 N68-11089 NASA-CR-942 ARBOCZ, J. Buckling of conical shells under axial compression NASA-CR-1162 c32 N68-35198 Experimental investigation of the effect of general imperfections on the buckling of cylindrical shells NASA-CR-1163 c32 N6 c32 N68-35199 ARGENTIERO, P. D. A new method of testing small samples for goodness of fit to normal populations NASA-TN-D-4405 c19 c19 N68-19144 ARIAS, A. The release of hydrogen on ball milling chromium in water NASA-TN-D-4569 c15 N68-23900 Chromium and nickel powders made by reduction of their oxides with magnesium, lithium, or sodium vapors NASA-TN-D-4714 c17 N68-30066 The role of chemical reactions in the mechanism of comminution of ductile metals mechanism of comminution of ductile metals into ultrafine powders by grinding NASA-TN-D-4862 cl5 N68-: ARMSTRONG, E. S., JR. A combined Newton-Raphson and gradient parameter correction technique for solution of optimal-control problems c15 N68-37239 ARNOLD, J. U. Study of optical radiation in the wavelength regions of 0.4216 mu, 0.4278 mu, 0.4835 mu, and 0.5165 mu behind normal shock waves in c19 N68-37073 a simulated Martian atmosphere c12 N68-32982 NASA-TM-X-1634 ARRANCE, F. C. Inorganic separator for a high temperature silver-zinc battery NASA-CR-965 c03 N68-16321 ASHBROOK, R. L. Application of directional solidification to a NASA nickel-base alloy /TAZ-8B/ NASA-TN-D-4390 c17 N68-15637 Development of a cobalt-tungsten ferromagnetic, high-temperature, structural alloy NASA-TN-D-4338 c17 N68-18145 ASHBY, G. C., JR. Effects of lee-surface volume addition on longitudinal aerodynamics of a high-lift-drag-ratio wing-body configuration at mach 6.0 NASA-TN-D-4361 Aerodynamic characteristics of a modified cone - Conical-frustum entry configuration at Mach 6.0 at Mach 6.0 c01 N68-17880

BARTLETT, E. P.

NASA-TN-D-4598 c31 N68-24964 ASTON, B. Coating selection program - Theory NASA-CR-1041 c18 N68-22391 System and process development for selection of high stress tolerance personnel NASA-CR-1122 c05 N68-35102 NASA-CHT1126 AYDELOTT, J. C. Effect of gravity on self-pressurization of spherical liquid-hydrogen tankage NASA-TN-D-4286 C27 NG c27 N68-11645 Experimental investigation of nucleate boiling bubble dynamics in normal and zero gravities NASA-TN-D-4301 c33 N68-15330 AYERS, W. G. Photometry of an iron artificial meteor reentering at 11 kilometers per second NASA-TN-D-4312 c30 c30 N68-16750 NASA-TN-D-4312 C30 N68-Photographic photometry of artificial meteors NASA-TN-D-4667 c14 N68c14 N68-29418 A numerical procedure for calculating stress numerical procedure for calculating off and deformation near a slit in a three-dimensional elastic-plastic solid NASA-TN-D-4717 c32 N68-30045 AZMON, E. Genetic states of simulated lunar rocks NASA-CR-1081 c30 N68-26689

В

BABCOCK, C. D., JR. Experimental investigation of the eff general imperfections on the buckli	lect of ing of
cylindrical shells NASA-CR-1163	c32 N68-35199
BACIGALUPI, R. J.	C32 N00-33133
Gamma flux and heat deposition in Plu	ım Brook
reactor - Comparison of calculation	
experiment	
NASA-TM-X-1539	c22 N68-22022
BADDOUR, M. F.	
Critical electrical aspects of	
alternating-current power source for Centaur space vehicle	
NASA-TM-X-1569	c03 N68-21562
BAILEY, J. R.	
Noise reduction shape factors in the	low
frequency range	
NASA-CR-1155	c32 N68-33266
BAILEY, M. C.	
Electromagnetic properties of a circu	
aperture in a dielectric-covered of ground plane	r uncovered
NASA-TN-D-4752	c07 N68-35537
BAKER. E. H.	CUI NOO 00007
Shell analysis manual	
NASA-CR-912	c32 N68-24802
BAKER, R. L.	
Analytical investigation of the mixing the m	
parallel streams of dissimilar flu	
NASA-CR-956	c12 N68-13619
Stability of shear flow with density	gradient
and viscosity NASA-CR-958	c12 N68-15530
Experimental investigation of the mi	
two parallel streams of dissimilar	
NASA-CR-957	c12 N68-15571
BALDWIN, B. S., JR.	
A method for computing luminous effi	ciencies
from meteor data	
NASA-TN-D-4808	c30 N68-33055
BALES, T. T. Equipment and procedures for glass-be	
peening titanium-alloy tanks	eau
NASA-TN-D-4288	c15 N68-12890
Stress-corrosion cracking of Ti-6Al- titanium alloy in nitrogen tetroxi	de
NASA-TN-D-4289	c17 N68-12891
BALL, C. L.	
Overall performance in argon of a 6-	
radial-bladed centrifugal compress NASA-TM-X-1622	
NASA-TM-X-1622 BALL, R. E.	c01 N68-30033
A geometrically nonlinear analysis o	•
arbitrarily loaded shells of revol	ution
NASA-CR-909	c32 N68-14584
	<u> </u>
	I

BALLARD, T. B. Investigation of electron-radiation-induced dielectric breakdowns in a typical capacitor meteoroid detector system NASA-TN-D-4738 c14 N68-33277 BALOGH, R. L. Computer assisted instruction. Feasibility study NASA-CR-917 c08 N68-13897 BAMBERGER, E. N. Fatigue life of 120 mm bore ball bearings at 600 deg F with fluorocarbon, polyphenyl ether, and synthetic paraffinic base lubricants NASA-TN-D-4850 c15 BARBEE, T. W., JR. Cryogenic magnetometer development Final report, 1 Jul. 1964 - 7 Mar. 1967 NASA-CR-1073 c14 c15 N68-36075 c14 N68-26703 BARGER, R. L. Design of bodies to produce specified sonic-boom signatures NASA-TN-D-4704 c01 N68-31484 BARKER. L. K. KLEK, L. K. Simulator study of pilot control over the lunar module during ascent from the lunar surface by using visual guidance cues NASA-TM-X-1549 c21 NG Simplified technique for determining pericynthion altitude of lunar orbits NASA-TM-D-431 c21 N68-21366 pericynthion altitude of lunar oroits NASA-TN-D-4811 c30 N68-BARNA, G. J. Investigation of the use of the lunar surface layer to store energy for generating power during the lunar night c30 N68-36459 NASA-TM-X-1560 c03 N68-20363 Analysis and selection of design conditions for a radioisotope Brayton-cycle space powerplant NASA-TN-D-4600 c03 N68-25829 BARNES, J. F. Vapor chamber fin studies. Operating characteristics of fin models NASA-CR-1139 c33 N68-33203 BARNES, R. M. Application of liquid-layer solid-sample spark technique to spectrochemical spark source NASA-TM-X-1429 c06 N68-10497 BARNETT, R. L. High performance structures NASA-CR-1038 c32 N68-23399 BARON, N. Scattering of 42-MeV /6.7-pJ/ alpha particles from even isotopes of cadmium NASA-TN-D-4256 c24 c24 N68-11074 Gamma ray angular correlations following inelastic scattering of 42-MeV alpha particles from magnesium 24 NASA-TN-D-4683 c24 N68-29375 BARON, S. The human as an optimal controller and information processor NASA-CR-1151 c05 N68-33304 BARRANGER, J. P. Electrical and mechanical properties of a superior high-temperature cobalt-iron magnetic material NASA-TN-D-4551 c17 N68-24558 NASA-IN-D-4551 c. BARRETT, C. A. Mechanism and kinetics of corrosion of selected iron and cobalt alloys in refluxing mercury NASA-TN-D-4450 c. c17 N68-21654 BARTH, V. D. Shaping of precipitation-hardening stainless steels by casting and powder-metallurgy NASA-SP-5086 c15 N68-19307 NASA-SP-5086 C. BARTLETT, E. P. An analysis of the coupled chemically reacting boundary layer and charring ablator, part 1 Summary report NASA-CR-1060 C: c33 N68-25244 An analysis of the coupled chemically reacting boundary layer and charring ablator. Part 3 - Nonsimilar solution of the multicomponent laminar boundary layer by an integral matrix method NASA-CR-1062 c33 N68-26641

An analysis of the coupled chemically reacting boundary layer and charring ablator. Part 4 -A unified approximation for mixture transport properties for multicomponent boundary-layer applications NASA-CR-1063 c33 N68-26815 BARTON, G. C. Low-energy electron diffraction study of oxygen adsorption on molybdenum /111/ surface NASA-TN-D-4735 c06 N68-30582 BARTON, R. L. Experimental verification of scale factors for parawing opening characteristics NASA-TN-D-4665 c02 N68-31956 BATES, F. C. Subsolar-meridian mean annual distributions for Martian troposphere below 50 kilometers NASA-CR-1043 c30 N68c30 N68-19192 BATTELLE, R. B. Study and applications of retrodirective and self adaptive electromagnetic-wave phase controls to a Mars probe NASA-CR-977 c21 c21 N68-18484 BAUD, K. W. Successful restart of a cryogenic upper-stage vehicle after coasting in earth orbit NASA-TM-X-1649 c31 N68-3 c31 N68-33683 BAUER, H. E. Studies of specific nuclear light bulb and open-cycle vortex stabilized gaseous nuclear rocket engines NASA-CR-1030 c22 N68-22038 BAUMEISTER, K. J. Liquid drops - Numerical and asymptotic solutions of their shapes NASA-TN-D-4779 cl: c12 N68-33165 BEAM, R. M. Finite amplitude waves in fluid-filled elastic tubes - Wave distortion, shock waves, and Korotkoff sounds NASA-TN-D-4803 cl2 N68-3 c12 N68-33056 NASA-IN-D-4803 cl2 N6 BEASLEY, G. P. Simulator study of pilot control over the lunar module during ascent from the lunar surface by using visual guidance cues NASA-TM-X-1549 c21 N6 c21 N68-21366 BECKER, H. Minimum weight design aspects of stiffened cylinders under compression NASA-CR-963 c32 N68-11282 MBDH-GR-900 BECKWITH, I. E. Detailed description and results of a method for computing mean and fluctuating quantities in turbulent boundary layers (12 N68-36 NASA-TN-D-4815 c12 N68-36071 BEEN, J. F. Effects of nuclear radiation on a high-reliability silicon power diode I-change in I-5 design characteristics NASA-TN-D-4620 c09 N68-2 c09 N68-26662 NASA-TN-D-4418 c28 N68-16632 Effect of variable stator area on performance of a single-stage turbine suitable for air cooling, 1 - Stator overall performance with 130-percent design area NASA-TM-X-1632 c01 N68-29994 NASA-IN-A-1032 Effect of variable stator area on performance of a single-stage turbine suitable for air cooling. 3 - Turbine performance with 130-percent design stator area NASA-TM-X-1663 CO3 N68c03 N68-35536 Effect of variable stator area on performance of a single stage turbine suitable for air cooling. 4 - Stator overall performance with 70 percent design area NASA-TM-X-1675 c28 N68 c28 N68-37264 BEHRENDT, D. R. An explanation of anomalous non-Hookean deformation of ionic single crystals c26 N68-22271 NASA-TN-D-4513 An explanation of Fitzgerald*s audiofrequency resonances and sound beams NASA-TN-D-4625 c23 N68-3 c23 N68-28259

BELGEN, M. H. Infrared radiometric stress instrumentation application range study NASA-CR-1067 c32 N68-24971 GIZ NGA-BENDER, D. F. Guidance, flight mechanics and trajectory optimization. Volume 12 - Relative motion, guidance equations for terminal rendezvous NASA-CR-1011 c30 N68c30 N68-19186 BENDURA, R. J. Performance of a 19.7 meter diameter disk gap band parachute in a simulated Martian environment NASA-TM-X-1499 c31 N68-13797 Vehicle attitude determination with a single onboard camera NASA-TN-D-4359 c31 N68-19275 Dynamic stability of a 4.6-meter-diameter 120 deg conical spacecraft at Mach numbers from 0.78 to 0.48 in a simulated Martian environment NASA-TN-D-4558 c31 N68-22301 NASA-TN-D-4558 c31 N68-2; BENGTSON, R. D. Equilibrium normal-shock and stagnation-point properties of helium for incident-shock Mach numbers from 1 to 30 NASA-TN-D-4754 c12 N68-3; PEDENUT c c12 N68-3; c12 N68-35117 BERENYI, S. G. An experimental investigation of the effect of gravity on a forced circulation pattern in spherical tanks NASA-TN-D-4409 c12 N68-2 BERGERON, H. P. Analysis of human response in combined control c12 N68-20352 tasks NASA-TN-D-4356 c05 N68-18014 A synthesis of human response in closed-loop tracking tasks NASA-TN-D-4842 c05 N68-36461 BERGGREN, C. C. Transistor design effects on radiation resistance NASA-CR-1167 c10 N68-33767 BERNS, J. A. Capillary rise in the annular region of concentric cylinders during coast periods of Atlas Centaur flights NASA-TM-X-1558 c12 N68-7 Management of cryogenic propellants in a full scale orbiting space vehicle NASA-TN-D-4571 c28 N68-7 c12 N68-23353 c28 N68-25099 NAGA-IN-J-4071 Successful restart of a cryogenic upper-stage vehicle after coasting in earth orbit NASA-IM-X-1649 c31 N68c31 N68-33683 Centaur launch vehicle propellant utilization system NASA-TN-D-4848 c28 N68-36507 BERRETTONI, J. N. Multiple decision procedures for ANOVA of two-level factorial fixed-effects replicationfree experiments NASA-TN-D-4272 c19 N68-11639 BERRIER, B. L. Transonic aerodynamic characteristics of powered models of several Apollo launch-escape vehicle configurations NASA-TN-D-4843 c31 N c31 N68-37074 BERRY, B. M. Practical reliability. Volume 5 - Parts c15 N68-31980 NASA-CR-1130 BERRY, W. B. Effect of green light on spectral response of cuprous sulfide-cadium sulfide photovoltaic cells NASA-TN-D-4333 c03 N68-14082 BESS, T. D. Luminous efficiencies of three nickel artificial meteors between 9.8 and 11.4 kilometers per second NASA-TN-D-4666 c30 N68-30244 BEST, J. J. New methods in adaptive flight control NASA-CR-1152 c21 N68-33904 BEVEVINO, W. A. Structural feasibility study of pressurized tanks for liquid-methane fueled supersonic aircraft NASA-TN-D-4295 c32 N68-12370 Comparative study of fuselage tanks for liquid

methane fueled supersonic aircraft NASA-TN-D-4837 c02 N68-36074 BIDER, B. Cold-air investigation of a turbine for hightemperature-engine application. 3 - Overall stage performance NASA-TN-D-4389 c01 N68-15743 NBAR-IN-U-4309 col N68-157 Effect of a variable stator area on performance of a single-stage turbine suitable for air cooling. 2 - Stator detailed losses with 130 percent design area NASA-TM-X-1635 co3 N68-305 c03 N68-30506 NASA-IM-X-1635 COJ N68-Effect of variable stator area on performance of a single stage turbine suitable for air cooling. 4 - Stator overall performance with 70 percent design area NASA-TM-X-1675 C28 N68-3 c28 N68-37264 BIEN, D. D. A computer program for reversion of the cumulative binomial probability distribution NASA-TM-X-1592 c19 N68-24141 Analysis and selection of design conditions for a radioisotope Brayton-cycle space powerplant NASA-TN-D-4600 BIFANO, W. J. Parametric analysis of radioisotope c03 N68-25829 thermoelectric generators NASA-TM-X-1453 c03 N68-14630 Electrical performance of a rhenium-niobium cylindrical thermionic converter NASA-TN-D-4533 c03 Thermal performance of a rhenium niobium cylindrical thermionic converter c03 N68-21766 NASA-TN-D-4582 c03 N68-25059 Preliminary analysis of a titanium alloy honeycomb solar absorber having blackened walla NASA-TN-D-4727 c03 N68-30751 BIGGERS, J. C. An investigation of full-scale helicopter rotors at high advance ratios and advancing tip Mach numbers NASA-TN-D-4632 c01 N68-28268 BILSKI, R. Control of contaminants in liquid-metal systems NASA-TM-X-1432 c17 N68-11912 BISHOP, D. E. The noisiness of tones plus noise NASA-CR-1117 c05 N68-30602 BLACK, T. J. An analytical study of the measured wall pressure field under supersonic turbulent boundary layers NASA-CR-888 cl2 N6 c12 N68-22087 BLACKFORD, A. L. Guidance, flight mechanics and trajectory optimization. Volume 6 - The N-body problem and special perturbation techniques NASA-CR-1005 c30 N68-15741 Guidance, flight mechanics and trajectory optimization. Volume 11 - Guidance equations for orbital operations NASA-CR-1010 c30 NASA-CK-1010 c30 N68-Guidance, flight mechanics and trajectory optimization. Volume 12 - Relative motion, guidance equations for terminal rendezvous NASA-CR-1011 c30 N68-Cuidance 1011 c30 N68-17215 c30 N68-19186 Guidance, flight mechanics and trajectory optimization. Volume 15 - Application of optimization techniques NASA-CR-1014 c30 | BLACKSHEAR, W. T. Midcourse-guidance procedure with single c30 N68-21231 position fix obtained from onboard optical measurements Measurements NAS-TN-D-4246 c21 N68-1157 BLACKSTOCK, T. A. Experimental pressure distributions and aerodynamic characteristics of a low-fineness-ratio cylinder at a Mach number of 10.5 and c21 N68-11521 ratio cylinder at a mach number of 10.5 angles of attack from 0 deg to 90 deg NASA-TM-X-1487 c01 I BLAHA, B. J. Wind tunnel investigation of fluctuating pressures on a 1/10-scale Centaur model at transonic speeds c01 N68-11958 NASA-TM-X-1574 c31 N68-22742

1-123

Wind tunnel investigation of airframe installation effects on underwing engine nacelles at Mach numbers from 0.56 to 1.46 NASA-TM-X-1683 c02 N68-37941 NASA-TM-X-1683 CU2 No BLAIR, A. B., JR. Wind tunnel investigation of three proposed launch vehicles at Mach numbers from 2.30 to 4.63 NASA-TM-X-1498 c01 N6 c01 N68-16299 BLAIR, L. S. Parametric analysis of radioisotope thermoelectric generators NASA-TM-X-1453 c03 N68-14630 BLANCHARD, U. J. Evaluation of a full-scale lunar-gravity simulator by comparison of landing-impact tests of a full-scale and a 1/6-scale model NASA-TN-D-4474 cll N68c11 N68-25853 BLANKENSHIP, C. P. Oxide deformation and fiber reinforcement in a tungsten metal oxide composite NASA-TN-D-4475 c Extrusion of 1/2 and 3/8-inch-diameter c17 N68-18610 thin-wall tungsten tubing in lengths near 10 feet NASA-TM-X-1638 c15 N68-32977 BLATTER, A. Research and development of a vortex valve for flow modulation of a 16-percent aluminized 5500 deg F propellant gas NASA-CR-1091 c28 N68-2 c28 N68-28112 BLOCK, D. L. Influence of discrete ring stiffeners and prebuckling deformations on the buckling of eccentrically stiffened orthotropic cylinders NASA-TN-D-4283 c32 N68-14 c32 N68-14091 BLOCK, H. B. Experimental investigation of reactor-loop transients during startup of a simulated SNAP-8 system NASA-TN-D-4546 c03 N68-22257 NASA-TN-D-4546 c03 N68-22 BLOOMER, H. E. Stabilizing effects of several injector face baffle configurations on screech in a 20,000 pound-thrust hydrogen-oxygen rocket NASA-TN-D-4515 c28 N68-21 Screech suppression techniques for rocket combustors using earth-storable propellants NASA-TM-X-1595 c28 N68-26 BLOOMETFIN. H. S. c28 N68-21679 c28 N68-26644 BLOOMFIELD, H. S. Shielding requirements for the NASA Plum Brook HB-6 beamhole radiation effects facility NASA-TM-X-1461 c22 BLUME, H. J. C. Suppression of temperature rise in lossy c22 N68-10133 diodes inside resonant cavities by application of pressurized liquid nitrogen NASA-TN-D-4556 c09 N68-243 c09 N68-24387 BOCCIO, J. L. Effect on bluntness on hypersonic two-dimensional inlet type flows NASA-CR-1145 c c01 N68-35523 NAA-CR-974
 Coll NGG
 Coll NGG c31 N68-11520 Influence of structure and material research on advanced launch systems weight, performance, and cost. Phase 3 - Design synthesis of recoverable launch vehicle structures NASA-CR-1116 c32 N68-28335 BOER, K. W. Light-Induced Modulation of Absorption /LIMA/ in cadmium sulfide NASA-TN-D-4466 c26 N68-18772 BOESENBERG, W. A. MOS field-effect-transistor technology NASA-CR-1113 c c08 N68-35193 BOGART, C. D. Determination of intersection of particle flight path with surface of helical tubular void region NASA-TN-D-4435 c22 N68-18541 BOGART, D. Ages of D/d,n/He sup 3 and T/d,n/He sup 4

neutrons in water and tungsten-water mixtures NASA-TN-D-4581 c22 N68-25058 Measurement of the B 10/n, alpha/Li 7, Li 7* relative cross sections in the keV region NASA-TN-D-4783 c24 N68-33763 BOHON, H. L. Flutter of corrugation stiffened panels at MACH 3 and comparison with theory NASA-TN-D-4321 c32 N68-19143 BOLAN, P. Research and development of high-performance axial-flow turbomachinery, Volume 1 -Design of turbine-compressor NASA-CR-800 c03 N68 c03 N68-24596 BOLDMAN, D. R. Laminarization of a turbulent boundary layer as observed from heat-transfer and boundary layer measurements in conical nozzles NASA-TN-D-4788 c12 N68 BOLLENBACHER, G. Experimental evaluation of a voltage regulator-exciter for a 15 kilovolt-ampere c12 N68-33642 Brayton cycle alternator NASA-TN-D-4697 c03 N68-29960 MASH IN-D-455, BOND, V. R. Navigation and guidance analysis of a Mars probe launched from a manned flyby spacecraft NASA-TN-D-4512 c21 N68-21 c21 N68-21754 BORBASH, S. R. Calculations to support operation of the Plum Brock reactor NASA-TM-X-1496 c22 N68-16056 BORSDDY, J. Stability analysis and minimum thrust vector control requirements of booster vehicles during atmospheric flight NASA-TN-D-4593 c21 N68-24409 Thrust-vector control requirements for large launch vehicles with solid-propellant first stages NASA-TN-D-4662 c31 N68-28690 BORUCKI, W. J. Tables of Fe I line intensities. Volume 1 - Temperatures from 1000 deg to 6500 deg K. Volume 2 - Temperatures between 6500 deg and 20,000 deg K NASA-SP-3041 c25 N68-24161 BOSCHITZ, E. T. A search for unbound helium 3 levels with isobaric spin 1/2 NASA-TN-D-4377 c24 N68-15638 BOSS, R. E. Parts and materials application review for space systems NASA-SP-6505 c15 N68-10120 BOULGER, F. W. Machining and grinding of ultrahigh-strength steels and stainless steel alloys NASA-SP-5084 c15 N68-21241 Deformation processing of precipitationhardening stainess steels NASA-SP-5088 BOURQUIN, K. R. Investigation of air-flow velocity by c17 N68-21917 laser backscatter NASA-TN-D-4453 c20 N68-20375 BOWLES, K. J. Vapor pressure of potassium to 2170 deg K NASA-TN-D-4535 c33 c33 N68-25122 BOYLE, J. C. A theoretical approach to the determination of magnetic torques by near field measurement NASA-TN-D-4485 c23 N68-24146 BOYLE, R. J. Analytical and experimental investigation of outflow residuals in interconnected spherical tanks NASA-TN-D-4828 c12 N68-35104 BOYNTON, J. H. BOYNTON, J. H. First U.S. manned six-pass orbital mission /Mercury-Atlas 8, spacecraft 16/ NASA-TN-D-4807 c31 No c31 N68-35022 BOZEK, J. M. Experimental determination of neutron fluxes in Plum Brook reactor HB-6 facility with use of sulfur pellets and gold foil NASA-TM-X-1497 c22 N68 c22 N68-15643 Experimental determination of gamma exposure

rate in Plum Brook HB-6 facility NASA-TM-X-1490 c22 N6 BRAINARD, W. A. Effect of crystal transformation and atomic c22 N68-17022 ordering on friction and wear of two cobalt-base alloys in vacuum NASA-TN-D-4668 c15 N68-28260 BRALEY, R. C. Inelastic scattering form factors using projected Hartree-Fock wave functions NASA-TN-D-4566 c24 N68-24661 NASA-TN-D-4566 c24 NG. Gamma ray angular correlations following inelastic scattering of 42-MeV alpha particles from magnesium 24 NASA-TN-D-4683 c24 NG BRANCHFLOWER, G. A. The applications technology satellite image c24 N68-29375 dissector camera experiment NASA-TN-D-4186 c14 N68-10647 BRANDHORST, H. W., JR. Effect of green light on spectral response of cuprous sulfide-cadium sulfide photovoltaic cells NASA-TN-D-4333 c03 N68-14082 23.4 square-foot /2.17-SQ-M/ cadmium sulfide thin-film solar cell array NASA-TM-X-1519 c c03 N68-20432 BRASHEARS, S. Optical alignment of silicon crystals NASA-TN-D-4187 c23 N68-10354 BRAUN, W. H. Shape of a magnetically balanced arc NASA-TN-D-4736 c25 N68-30784 BRAY, C. W. Application of negative feedback to reduction of glow discharge noise NASA-CR-1173 BRAZZIEL, M. E. c16 N68-35099 Summary of VGH data collected on one type of twin-engine jet airplane during airline operations NASA-TN-D-4529 c02 i BRECKENRIDGE, R. A. Proton-produced defects in n-type silicon NASA-TN-D-4830 c26 j c02 N68-22291 c26 N68-37051 BREEN, B. P. Combustion instability prediction using a nonlinear bipropellant vaporization model c33 NG NASA-CR-920 c33 N68-15833 NASA-CR-920 C53 BRESNAHAN, D. L. Cold flow investigation of a low angle turbojet plug nozzle with fixed throat and translating shroud at Mach numbers from 0 to 2.0 NASA-TM-X-1619 c28 N68-29953 BREWE, D. E. Cooling studies with 40-millimeter-bore ball bearings using low flow rates of 60 deg R /33 deg K/ hydrogen gas NASA-TN-D-4616 c15 N68 c15 N68-24456 BRICKEL, J. R. Lunar module pilot control considerations NASA-TN-D-4131 c21 c21 N68-16836 BRIEHL, D. C. Thermal investigation of an ion engine microthrustor NASA-TM-X-1473 c28 N68-10496 BROCK, F. J. Study of density calibration in space Final report, Jun. 29, 1966 - Jan. 16, 1967 NASA-CR-987 c14 N68 c14 N68-12669 RODER, J. D. Comparison between cemented and soldered cover glass for silicon solar cells NASA-TM-X-1687 c03 N68-37935 BRODERICK, J. J. Capacitor-type meteoroid-penetration sensors -Description and test results NASA-TN-D-4524 c14 N68-2 c14 N68-22883 BROKAW, R. S. Viscosity of gas mixtures NASA-TN-D-4496 c12 N68-21724 BROOKS, C. W., JR. Interference effects of canard controls on the longitudinal aerodynamic characteristics of a winged body at Mach 10 NASA-TN-D-4436 c01 N68-21 c01 N68-21579 BROWN, G. V. The excitation spectrum for a Bose gas with

CAMPBELL, J. E.

repulsive and attractive interactions NASA-TN-D-4838 c2 c24 N68-37240 BROWN, R. Investigation of the calibration of microphones for sonic boom measurement NASA-CR-1075 c14 NU BRUCHEY, W. J., JR. A study of the performance of an astronaut c14 N68-25316 during ingress and egress maneuvers through airlocks and passageways NASA-CR-971 c05 N68-20339 NASA-VA-S/I BRUN, R. J. Management of cryogenic propellants in a full scale orbiting space vehicle NASA-TN-D-4571 c28 N68c28 N68-25099 BRUSILOVSKII, K. A. Measurement of pulse distortion in digital information transmission NASA-TT-F-434 c07 N68-17542 BUCHANAN, R. A. Mechanical properties and column behavior of thin wall beryllium tubing NASA-TN-D-4833 c17 N68c17 N68-37053 BUCKLEY, D. H. Influence of crystal structure, orientation, and solubility on adhesion and sliding friction of metal single crystals in vacuum NASA-TN-D-4347 c15 N68-21226 Effect of crystal transformation and atomic ordering on friction and wear of two cobalt-base alloys in vacuum NASA-TN-D-4668 c15 N68-2 c15 N68-28260 Influence of surface active agents on friction, deformation, and fracture of lithium fluoride c15 N68-29918 NASA-TN-D-4716 Influence of chemisorbed films of various gases on adhesion and friction of tungsten in ບລວມມກ NASA-TN-D-4694 c15 N68-33227 Influence of chemisorbed films on adhesion and friction of clean iron NASA-TN-D-4775 c17 N68-33278 BUIS, G. R. Lyapunov stability for partial differential equations. Part 1 - Lyapunov stability theory and the stability of solutions to partial differential equations. Part 2 -Contraction groups and equivalent norms NASA-CR-1100 c19 c19 N68-27457 NASA-CR-1100 c19 N68 BURCHAM, F. W., JR. Wind-tunnel calibration of a 40 deg conical pressure probe at Mach numbers from 3.5 to 7.4 NASA-TN-D-4678 c12 N68-28801 BURES, K. J. Theoretical error analysis of a Doppler range-rate and phase-modulated range tracking system NASA-TN-D-4267 c10 BURKE, M. E. X-15 analog and digital inertial systems c10 N68-11513 flight experience NASA-TN-D-4642 c08 N68-29404 BURLEY, J. M. Chronological catalog of reported lunar events events NASA-TR-R-277 BURMEISTER, L. C. Advanced valve technology, a survey NASA-SP-5019 c30 N68-28192 c15 N68-10402 BURNS, M. Preliminary study of advanced life-support technology for a Mars surface module NASA-CR-1083 c c05 N68-28319 BURNS, R. E. Motion of an artificial satellite under combined influence of planar and Keplerian, force fields NASA-TN-D-4622 c30 N68-28113 NASA-IN-D-4522 C30 NoG-2013 BURNSIDE, W. D. The reflection coefficient of a TEM mode parallel-plate waveguide illuminating a conducting sheet - The large wedge angle case NASA-CR-1174 c07 N68-35172 BURRELL, M. O. An analysis of energetic space radiation and dose rates NASA-TN-D-4404 c29 N68-16837

BURROWS, M. C. Mixing and reaction studies of hydrazine and nitrogen tetroxide using photographic and spectral techniques C33 N68 NASA-TN-D-4467 c33 N68-24965 BUSEMANN, A. Optimum maneuvers of hypervelocity vehicles NASA-CR-1078 c02 NG c02 N68-25817 NASA-CN-1070 BUSHNELL, D. Buckling of shells of revolution with various wall constructions. Volume 3 - User*s manual for BOSOR NASA-CR-1051 c32 N68-7 Different capable of revolution with various c32 N68-23355 Buckling of shells of revolution with various wall constructions. Volume 2 - Basic equations and method of solution NASA-CR-1050 c32 N68-23451 Buckling of shells of revolution with various wall constructions. Volume 1 ~ Numerical results NASA-CR-1049 c32 N68-24481 BUSHNELL, D. M. Effects of shock impingement and other factors on leading-edge heat transfer NASA-TN-D-4543 c33 Local afterbody heat transfer to a blunt c33 N68-22118 two-dimensional configuration at Mach 8 c12 N68-28282 NASA-TN-D-4443 NASA-TN-D-4443 Heat transfer and pressure distributions on spherically blunted 25 deg half-angle cone at Mach 8 and angles of attack up to 90 deg NASA-TN-D-4792 C01 N68-35497 Detailed description and results of a method for computing mean and fluctuating quantities in turbulent boundary layers NASA-TN-D-4815 c12 N68-36071 BUTION, S. L. Computer programs for plane collisionless sheaths between field-modified emitter and thermally ionized plasma exemplified by cesium co8 N68-214 NASA-TM-X-1562 c08 N68-21499 BUZEK, B. C. Electron microscopy technique for determination of dispersoid distribution in powder blends NASA-TM-X-1468 c17 N68-10051 Use of surface replication, extraction replication, and thin-film electron microscopy in the study of dispersion-strengthened materials NASA-TN-D-4461 c17 N68-18999 Electron microscope technique suggested to reveal microstructures of dispersion-strengthened materials NASA-TM-X-1561 c17 N68-21431 NASA-TM-X-1561 c17 BUZZARD, R. J. High temperature creep-rupture properties of a tungsten-uranium dioxide cermet produced from coated particles NASA-TM-X-1625 c17 N68-29987 BYRDSONG. T. A. Investigation of the effect of wheel braking on side-force capability of a pneumatic tire NASA-TN-D-4602 c02 N68-2 c02 N68-25313

С

CAIN, J. C.		
The geomagnetic secular variation 19	00-19	65
NASA-TN-D-4527	c13	N68-21543
CAIRNS, R. B.		
Studies of photoabsorption by atomic	hydı	ogen,
oxygen, and nitrogen		
NASA-CR-998	c24	N68-18118
CALFO, F. D.		
Effect of residual stress on fracture	a sti	ength
of AISI 301 stainless-steel and		-
Ti-5Al-2.5Sn ELI titanium cracked	thin	
wall cylinders		
NASA-TN-D-4777	c32	N68-33191
CALOGERAS, J. E.		
Wind tunnel investigation of technique	ies i	or
reducing cowl drag of an axisymmet	ric	
external-compression inlet at Mach	2.49)
NASA-TM-X-1516	c01	N68-18189
CAMPBELL, J. E.		
Effects of low temperatures on the me	ochai	lical
	sunai	
properties of structural metals		
NASA-SP-5012/01/	c17	N68-31605

CAMPBELL, J. F.

CAMPBELL, J. F. Supersonic aerodynamics of large-angle cones NASA-TN-D-4719 col N68 c01 N68-31551 CAMPBELL, J. P. Radiant-interchange configuration factors for spherical and conical surfaces to spheres NASA-TN-D-4457 c33 N68-20331 NASA-TN-D-4457 c33 N68-203 CANFIL, L. W. Sensitivity of quartz, piezoelectric pressure transducers as a function of temperature from 20 deg to 477 deg K NASA-TM-X-1479 c14 N68-114 CANRIGHT, R. B., JR. PLOT3D - A package of FORTRAN subprograms to draw three-dimensional surfaces NASA-TM-X-1598 c19 N68-282 CAP. F. c14 N68-11867 c19 N68-28240 CAP, F. Lie series for celestial mechanics, accelerators, satellite stabilization and optimization NASA-CR-1046 c19 N68-25841 CAPONE, F. J. Reduction of wind-tunnel-model vibration by means of a tuned damped vibration absorber installed in the model NASA-TM-X-1606 c32 N68c32 N68-28806 CAPPELLI, A. P. Shell analysis manual NASA-CR-912 c32 N68-24802 CARDEN, H. D. Response characteristics of impacting penetrometers appropriate to lunar and planetary missions NASA-TN-D-4454 c32 N68 Experimental study of vertical impacts of an c32 N68-20364 LM-type landing gear assembly under simulated lunar gravity NASA-TN-D-4711 c32 N68-30505 CAREN, R. P. Design and construction of an engineering model solid cryogen refrigerator for infrared detector cooling at 50 deg K NASA-CR-988 c23 N68-13 c23 N68-13115 And the back of a construction of negative feedback to reduction of glow discharge noise NASA-CR-1173 c16 N68-35099 CARNEL, M. M. Wind tunnel investigation of three proposed launch vehicles at Mach numbers from 2,30 to 4,63 NASA-TM-X-1498 c01 N68-16299 Aerodynamic characteristics of several hypersonic boost-glide-type configurations at Mach numbers from 2.30 to 4.63 NASA-TM-X-1601 col N68-33 c01 N68-33836 CARPENTER, R. FM handling and analog-to-digital conversion of biomedical data from a 1,000-flight study NASA-TN-D-4488 c05 N68-21537 Recording and signal-conditioning techniques and equipment used in a 1,000-flight biomedical study NASA-TN-D-4487 c05 N68-21538 CARSON, T. M. Lunar beacons - A preliminary look at their position estimation and their use in lunar orbit estimation NASA-TM-X-1529 c30 N68-19064 NASA-TM-X-1029 CARTER, A. F. Analysis of geometry and design point performance of axial flow turbines. 1 -Development of the analysis method and the loss coefficient correlation NASA-CR-1181 C28 N68c28 N68-35101 Analysis of geometry and design point performance of axial flow turbines. Part 2 - Computer program NASA-CR-1187 c28 N68-36617 CARY, A. M., JR. Effect of two-dimensional multiple sine-wave protrusions of the pressure and heat-transfer distributions for a flat plate at Mach 6 NASA-TN-D-4437 c01 N68-19063 MASH-IN-D-4407 CASTLEMAN, B. W. Microwave spectroscopy of molecules -Bibliography, 1964-1966 NASA-CR-951 c23 N68-10674

PERSONAL AUTHOR INDEX

CATANACH, W. M., JR. Fatigue crack propagation in cylindrical shells NASA-CR-1197 c32 N68-37840 CAVICCHI, R. H. Critical-speed analysis of flexibly mounted rigid rotors NASA-TN-D-4607 c32_N68-25421 Critical speed analysis of rigid rotors on flexible foundations NASA-TN-D-4858 c15 No c15 N68-37214 CHAMALES, N. C. Studies of flow distortion in the tailpipes of hydrogen peroxide gas generators used for jet engine simulation NASA-TM-X-1671 c12 N68-37067 NASATINTATION CHAMBELLAN, R. E. Structural feasibility study of pressurized tanks for liquid-methane fueled supersonic aircraft NASA-TN-D-4295 c32 N68-12370 Tankage systems for a methane-fueled supersonic transport NASA-TM-X-1591 c02 N68-23895 Comparative study of fuselage tanks for liquid methane fueled supersonic aircraft NASA-TN-D-4837 c02 N68-36074 CHAMBERLAIN, L. W. Measurements of winds and temperatures at altitudes up to 65 kilometers in the Southern Hemisphere NASA-TN-D-4429 c20 N68-19084 NASA-TN-D-4429 c20 N68-190 CHAMBERS, J. R. Static and dynamic longitudinal stability derivatives of a powered 0.18-scale model of a fan-in-wing VTOL aircraft TAN-IN-WING VIDE arterer. NASA-TN-D-4322 c02 N68-1 Calculation of the dynamic longitudinal stability of a tilt-wing V/STOL aircraft and correlation with model flight tests 02 N68-1 c02 N68-15894 NASA-TN-D-4344 c02 N68-15941 CHAN, K.-L. CHAN, K.-L.
 Phase and group refractive indices from the collisionless magnetoionic theory NASA-TM-X-1553
 CHAPMAN, A. J.
 An evaluation of the thermally radiant c13 N68-21904 environs of a man on the lunar surface NASA-TN-D-4243 c30 c30 N68-11630 CHAPMAN, G. T. CHAPMAN, G. T. A computer program for systematically analyzing free-flight data to determine the aerodynamics of axisymmetric bodies NASA-TN-D-4766 c01 c01 N68-33081 CHASE, S. C. Dual radiometer assembly for Project Scanner NASA-CR-1086 c14 N68 c14 N68-28965 CHEATHAM, D. C. Lunar module pilot control considerations NASA-TN-D-4131 c21 N68-16836 CHENOWETH, F. C. Transient chilldown of a single thick-walled tube by liquid and gaseous hydrogen NASA-TN-D-4238 c33 N68 c33 N68-10368 NASA-TN-D-4238 c33 Comparison of experimental and predicted heat transfer characteristics for a cylindrical ejector NASA-TM-X-1641 c33 c33 N68-32988 CHESTNUTT, D. Noise reduction by means of inlet-guide-vane choking in an axial-flow compressor NASA-TN-D-4682 c02 N68 c02 N68-29406 CHU, T. Y. Research and development of high-performance ALIAL-IIOW turbomachinery. Volum Design of backup gas bearings NASA-CR-802 CHUBARINA, E. V. Electricity of the free atmosphere NASA-TT-F-425 CTESIA. F. axial-flow turbomachinery. Volume 3 c03 N68-24597 c13 N68-10079 NASA-TI-F-425 cl3 N6 CIESLA, E. J. Nuclear design data for experiments to be conducted in Horizontal Through Hole 1 of the Plum Brook Reactor NASA-TM-X-1509 c2: CILLIERS, W. A. The preheating of plasma in a megajoule c22 N68-15855 theta-pinch experiment NASA-TN-D-4708 c25 N68-33372

COSGROVE, W. J.

CIPOLLONE, P. Effect of surface roughness on the 0.66-micron normal spectral emittance of vapor-deposited rhenium from 1500 deg K to 2100 deg K NASA-TM-X-1514 C17 N68-15 C17 N68-15 g n c17 N68-19347 Electron-bombardment filament designs for heating cylindrical thermionic converters NASA-TM-X-1630 c22 N6 c22 N68-32968 CLARK, J. J. Properties of magnetic materials for use in high-temperature space power systems NASA-SP-3043 c17 N68-17624 CLARK, M. Analysis of integrated charged particle energy spectra from gridded electrostatic analyzers c25 N68-30093 NASA-TN-D-4718 CLARK, M. R. Comparison of small water-graphite nuclear rocket stages with chemical upper stages for unmanned missions NASA-TN-D-4827 c22 N68-35073 CLARY, R. R. Experimental investigation of the longitudinal vibration of a representative launch vehicle with simulated propellants NASA-TN-D-4502 c32 N68-2 c32 N68-21869 CLASS, W. An aluminum nitride melting technique NASA-CR-1171 c17 N68-33335 CLOUGH, N. Target pressure and damage data from impacts by explosively propelled projectiles NASA-TM-X-1597 c c32 N68-25819 NH3R-IM-X-1397 c32 N68 COCHRAN, T. H. Experimental investigation of nucleate boiling bubble dynamics in normal and zero gravities NASA-TN-D-4301 c33 H Body rotation effects on melting ablation c33 N68-15330 NASA-TN-D-4614 c33 N68-26650 COCHRANE, J. A. Wind data from the 250-foot /76.2-meter/ tower at Wallops Island, Virginia NASA-TN-D-4395 c20 N68-18246 Revised upper-air wind data for Wallops Island based on serially completed data for the years 1956 to 1964 NASA-TN-D-4570 c20 NG COCKE, B. W., JR. Description and initial calibration of the c20 N68-24028 Langley 20-inch hypersonic arc heated tunnel NASA-TN-D-4653 c11 N68-28947 COCKRELL, C. R. A general method for designing circular array antennas to obtain guasi-omnidirectional patterns NASA-TN-D-4254 c07 N68-11475 An omnidirectional flush-mounted microwave antenna with a simple feed for use on spacecraft NASA-TN-D-4555 c07 N68-25918 Higher-order-mode effects on the aperture admittance of a rectangular waveguide covered with dielectric and plasma slabs c07 N68-35524 NASA-TN-D-4774 COE, H. H. Cooling studies with 40-millimeter-bore ball bearings using low flow rates of 60 deg R /33 deg K/ hydrogen gas NASA-TN-D-4616 c15 N68 c15 N68-24456 COHEN, A. J. Anomalous diffusion in a plasma formed from the exhaust beam of an electron-bombardment ion thruster NASA-TN-D-4758 c25 N68-32072 COHEN, R. Research and development of high-performance axial-flow turbomachinery. Volume 1 -Design of turbine-compressor c03 N68 c03 N68-24596 COLE, F. W. Oxidation resistant materials for transpiration cooled gas turbine blades. 1 -Sheet specimen screening tests NASA-CR-930 c17 N68-17 c17 N68-17591 Oxidation resistant materials for transpiration cooled gas turbine blades. 2 - Wire specimen tests

c17 N68-35098 NASA-CR-1184 COLE, G. L. Analytical calculation of partial derivatives relating lunar and planetary midcourse correction requirements to guidance system injection errors NASA-TN-D-4518 c30 N68-20368 COLEMAN, To L. Trends in repeated loads on transport airplanes NASA-TN-D-4586 c02 N68-24476 COLIN, L. Phase and group refractive indices from the collisionless magnetoionic theory NASA-TM-X-1553 c13 NG c13 N68-21904 COLTRANE, L. C. Performance of a 19.7 meter diameter disk gap band parachute in a simulated Martian environment c31 N68-13797 NASA-TM-X-1499 Performance of a 16.6-meter-diameter modified ringsail parachute in a simulated Martian environment NASA-TM-X-1500 c31 N68 c31 N68-14092 Performance of a 16.6-meter-diameter cross parachute in a simulated Martian environment NASA-TM-X-1543 c31 N68-2 c31 N68-21833 COMPTON, J. Evaluation of the effects of space environment exposure on index of refraction and extinction coefficients of Apollo window materials NASA-CR-1019 c31 N68-20467 CONPTON, W. B., III Effect on base drag of recessing the bases of conical afterbodies at subsonic and transonic speeds NASA-TN-D-4821 c01 N68-37054 NASA-IN-J-9021 CONEY, T. A. Effects of liquid depth on lateral sloshing under weightless conditions NASA-IN-D-4458 c12 NG CONNELLY, J. J. Digital program for dynamics of non-rigid cravity gradient satellites c12 N68-24758 gravity gradient satellites NASA-CR-1119 c30 N68-32744 NASH-UNTILLE CONRAD, E. W. Cooled baffle development for M-1 engine using a subscale rocket engine NASA-TM-X-1267 c28 c28 N68-18216 M-1 injector development - Philosophy and implementation c28 N68-30604 NASA-TN-D-4730 NASA-TN-D-4730 c2 CONWAY, E. J. Light-Induced Modulation of Absorption /LIMA/ in cadmium sulfide NASA-TN-D-4466 c2 c26 N68-18772 NASA-IN-D-4446 C20 NOS-COOK, A. M. Wind tunnel investigation of the low speed high lift aerodynamics of a one-fifth scale variable sweep supersonic transport NASA-IN-D-4844 c01 N68-COOLDERST C01 N68c01 N68-37365 NASH-IN-D-4844 CUI NGG COOLIDGE, A. W., JR. Development of high-temperature vapor-filled thyratrons and rectifiers NASA-CR-994 CO9 N68 c09 N68-15892 COPELAND, J. P. Study of propellant valve leakage in a vacuum Final summary report NASA-CR-1047 c27 N68c27 N68-21893 COPELAND, W. L. Turbojet-engine noise studies to evaluate effects of inlet-guide-vane-rotor spacing NASA-TN-D-4690 c28 N68-30040 CORLISS, V. R. Scientific satellites c31 N68-14965 NASA-SP-133 Teleoperators and human augmentation. An AEC-NASA technology survey c05 N68-18870 NASA-SP-5047 NASA-59-5047 CUB NG8-18870 CORSIGLIA, V. R. Aerodynamic characteristics of a large-scale model with unswept wing and augmented jet flap NASA-TN-D-4610 col N68-25919 CORTRIGHT, E. M. Exploring space with a camera NASA-SP-168 c30 N68-34870 COSGROVE, W. J. A generalized experimental investigation of hot gas recirculation and ingestion

for jet VTOL aircraft NASA-CR-1147 c01 COSTAKIS, W. G. Experimental longitudinal dynamics of an c01 N68-33043 empty Stub D Atlas vehicle NASA-TM-X-1682 c31 N68-37942 COSTELLO, F. A. Coating selection program - Theory NASA-CR-1041 c18 N68-22391 COSTEN, R. C. Products of some generalized functions NASA-TN-D-4244 ci c19 N68-11494 COSTON, R. M. Design and construction of an engineering model solid cryogen refrigerator for infrared detector cooling at 50 deg K NASA-CR-988 c23 N68-13 c23 N68-13115 COUCH, L. M. Experimental pressure distributions on a blunt lifting-entry body at Mach 3.71 NASA-TN-D-4494 c01 N68-2 c01 N68-21681 COVERT, S. The microbiological flora of the Gemini 9 spacecraft before and after flight NASA-CR-972 c04 N68-11968 COWGILL, G. R. Mist-flow heat transfer using single-phase variable-property approach NASA-TN-D-4149 c33 N68-11636 CRAGGS, A. The response of a simply supported plate to transient forces. Part 2 - The effect of N-waves at oblique incidence NASA-CR-1176 c32 NG c32 N68-33168 MHON-CN-1170 C32 N6 The response of a simply supported plate to transient forces. Part 1 - The effect of N-waves at normal incidence NASA-CR-1175 C32 N6 c32 N68-33737 CRAIG, J. P. Parts and materials application review for space systems NASA-SP-6505 c15 N68-10120 CRANE, H. D. Research study of a fundus tracker for experiments in stabilized vision NASA-CR-1121 c05 N68-35109 CRANE, H. L. Effects of reduced airspeed for landing approach on flying qualities of a large jet transport equipped with powered lift NASA-TN-D-4804 c02 N68-3 c02 N68-37075 CRAWFORD, D. H. Pressure and heat transfer on blunt curved plates with concave and convex surfaces in hypersonic flow NASA-TN-D-4367 c12 i CRAWFORD, R. F. An evaluation of boron-polymer film layer c12 N68-18253 composites for high-performance structures NASA-CR-1114 c18 N68 c18 N68-35100 CRAWFORD, R. M. Postshutdown cooling requirements of tungsten water-moderated nuclear rocket NASA-TM-X-1568 c22 NG CRAWFORD, V. L. A least squares method for the reduction of free-oscillation data NASA-TN-D-4503 c19 NG c22 N68-21111 c19 N68-25869 CREEL, T. R., JR. Pressure distributions and aerodynamic characteristics of 90 deg and 15 deg blunted cones in nitrogen and helium at Mach 20 NASA-TN-D-4314 CO1 N68-17 c01 N68-17896 CRIGLER, J. L. Turbojet-engine noise studies to evaluate effects of inlet-guide-vane-rotor spacing NASA-TN-D-4690 c28 N68-30040 CROSVELL, W. F. A general method for designing circular array antennas to obtain quasi-omnidirectional patterns NASA-TN-D-4254 c07 N68-11475 A quasi-omnidirectional slot array antenna for spacecraft use at microwave frequencies NASA-TN-D-4362 c07 N68-18616 An omnidirectional flush-mounted microwave antenna with a simple feed for use on spacecraft NASA-TN-D-4555 c07 N68-25918

PERSONAL AUTHOR INDEX

CRUM. R. J. Gamma heating in thin heavy-element absorbers c22 N68-37260 NASA-TM-X-1680 CUBBISON, R. W. An experimental investigation of the restart area ratio of a Mach 3.0 axisymmetric mixed compression inlet NASA-TM-X-1547 CO1 N68-21703 Water condensation effects of heated vitiated air on flow in a large supersonic wind tunnel NASA-TM-X-1636 cl1 N68-30598 NASA-TM-X-1636 cl1 N68-CUNNINGHAM, R. E. Experiments on stability of herringbone grooved gas-lubricated journal bearings to high compressibility numbers NASA-TN-D-4440 cl5 N68-CURLEY, J. K. Cooled baffle development for M-1 engine c15 N68-21965 using a subscale rocket engine NASA-TM-X-1267 c28 N68-18216 CURRERI, J. S. Performance of a multiple single-pass counterflow NaK-cooled mercury Rankine cycle condenser NASA-TM-X-1548 c33 N68-20340 CURTICE, R. M. Application of statistical association techniques for the NASA document collection NASA-CR-1020 c08 N68-17154 CURTIS, S. B. Study of radiation hazards to man on extended missions NASA-CR-1037 c29 N68-22849 CURWEN, P. W. Research and development of high performance axial-flow turbomachinery. Volume 2 - Design of gas bearings NASA-CR-801 c15 c15 N68-25042 CUSICK, D. L. Design handbook umbilical locking mechanism development program NASA-CR-1021 c15 N6 c15 N68-23356 CUSICK, J. P. An explanation of anomalous non-Hookean An explanation of ionic single crystals NASA-TN-D-4513 c26 N68-An explanation of Fitzgerald*s audiofrequency c26 N68-22271 resonances and sound beams NASA-TN-D-4625 c23 N68-28259 CUTLER, S. N. Application of dust for space structures NASA-CR-1136 c32 N68-32976 CYRUS, N. J. Accuracy study of finite difference methods NASA-TN-D-4372 c32 N6 c32 N68-17068 CZARNECKI, K. R. Evaluation of boundary layer and wake survey data reduction techniques in compressible flows NASA-TN-D-4401 c12 N68-19709 Drag due to two-dimensional surface roughness in a turbulent boundary layer at Mach 3 with and without heat transfer NASA-TN-D-4746 c12 N68-33054 D DAHLKE, H. E. The shock expansion tube and its application as a sonic boom simulator NASA-CR-1055 c11 N68-24966 DAN, C. Cold wall thermal vacuum, thermal design check for fully insulated experiment packages NASA-TN-D-4644 c11 DANIELE, C. J. c11 N68-29478

Thrust-vector control requirements for large launch vehicles with solid-propellant first stages NASA-TN-D-4662 c31 N68-28690 DANIELS, G. E. Scalar and component wind correlations

- NASA-TN-D-4662 c31 N68-28590 DANIELS, G. E. Scalar and component wind correlations between altitude levels for Cape Kennedy, Florida, and Santa Monica, California NASA-TN-D-3815 c13 N68-20278 DANILOWICZ, R. L. Computer code for calculating temperature
- profiles in a propellant tank NASA-TM-X-1556 c27 N68-21267

DEXTER, H. B.

DANKHOFF. W. F. M-1 injector development - Philosophy and implementation NASA-TN-D-4730 c28 N68-30604 DARNELL, W. L. Flight test of a 15-foot-diameter /4.6-meter/ 120 deg conical spacecraft simulating parachute deployment in a Mars atmosphere NASA-TN-D-4266 c31 N6 NA5A-TN-D-4266 Performance of a 16.6-meter-diameter cross parachute in a simulated Martian environment NA5A-TM-X-1543 ENDROW DAVENPORT, P. B. A vector approach to the algebra of rotations with applications NASA-TN-D-4696 c19 N68c19 N68-30594 DAVIDSON, K. I. Thrust-vector control requirements for large launch vehicles with solid-propellant first stages NASA-TN-D-4662 c31 N68-28690 NASH-IN-D-4002 DAVIES, T. L. Cryogenic storage systems for earth-orbital and Mars-flyby missions NASA-TN-D-4619 c03 N6 c03 N68-28420 DAVIS, A. Q. Stress corrosion of titanium alloys under simulated supersonic flight conditions NASA-CR-981 c17 c17 N68-11522 DAVIS, R. E. Preliminary infrared horizon profiles from Project Scanner NASA-TM-X-1483 c2: Radiometric measurements of the earth*s c21 N68-11949 infrared horizon from the X-15 in three spectral intervals NASA-TN-D-4654 c21 N68-28262 Infrared horizon profiles for summer conditions from Project Scanner NASA-TN-D-4741 c21 N68-33450 DAVIS, R. M. A simplified method for calculating laminar heat transfer over bodies at an angle of attack NASA-TN-D-4720 c33 N68-31959 DAVIS, R. W. Performance of centerbody vortex generators in an axisymmetric mixed-compression inlet at Mach numbers from 2.0 to 3.0 NASA-TN-D-4675 c01 N68-28795 DAVISON, H. W. Axial power tailoring to obtain constant fuel-centerline temperature in a nuclear reactor NASA-TN-D-4658 c22 N68-28304 Compilation of thermophysical properties of liquid lithium NASA-TN-D-4650 c17 N68-28365 DAWSON, C. H. Study and applications of retrodirective and self adaptive electromagnetic-wave phase controls to a Mars probe NASA-CR-977 c21 c21 N68-18484 DAY, J. L. Review of NASA-MSC electroencephalogram and electrocardiogram electrode systems including application techniques NASA-TN-D-4398 c04 N68-21383 NADATIN-J-1000 DE CRESCENTE, M. A. Optical absorption in fused silica during TRIGA reactor pulse irradiation C22 1 NASA-CR-1031 c22 N68-21124 NASA-CK-1031 C22 NGC DE FIFE, J. A quasi-steady state analysis of the dynamic behavior of a conic body moving in a nonuniform wake NASA-TN-D-4691 c31 N68c31 N68-30032 DE FURIA. R. On electromagnetic switching properties of a bi-stable fluidic element with non-destructive memory NASA-TM-X-1613 c09 N68-30501 DE JARNETTE, F. R. A simplified method for calculating laminar heat transfer over bodies at an angle of attack NASA-TN-D-4720 c33 N68-31959 DE PAUW, J. F. D'escription and flight performance results

of the Wasp sounding rocket NASA-TM-X-1518 c31 N68-17094 DE ROSE, C. E. Ballistic-range tests of a drag-ring configuration at Mach numbers around 2 NASA-TN-D-4291 c01 c01 N68-11936 DE WITT, R. L. Temperature and liquid-level sensor for liquid-hydrogen pressurization and expulsion studies NASA-TN-D-4339 c14 N68-15893 NASA-TN-D-4339 C14 N68-156 DEAL, P. L. Flight investigation of performance characteristics during landing approach of a large powered-lift jet transport NASA-TN-D-4261 C02 N68-116 A piloted fixed-base simulator study of low-speed flight characteristics of an arrow-wing c02 N68-11638 supersonic transport design c05 N68-13609 NASA-TN-D-4277 NASA-IN-D-4277 CU5 NBS-. DEARING, J. D. Effect of hinge-line bleed on heat transfer and pressure distribution over a wedge-flap combination at Mach 10.4 NASA-TN-D-4686 c01 N68-29955 NASA-TN-D-4686 c01 DEAVER, B. S., JR. Cryogenic magnetometer development Final report, 1 Jul. 1964 - 7 Mar. 1967 NASA-CR-1073 c14 c14 N68-26703 DEB00, G. J. A piezoelectric transducer for measuring cardiac and gross motor activity of small organisms NASA-TN-D-4590 c05 N68-25060 NASA-IN-J-4050 DECKER, A. J. Electrical characteristics of a dc compact arc in argon from 1 to 10 atmospheres and from 600 to 1200 amperes NASA-TM-X-1596 c29 N6 c29 N68-25818 DECKER, J. P. An exploratory study of parallel stage separation of reusable launch vehicles NASA-TN-D-4765 c31 c31 N68-36106 DECKERT, W. H. Large-scale wind-tunnel tests of a deflected slipstream STOL model with wings of various aspect ratios NASA-TN-D-4448 c02 N68-18771 NAGA-IN-D-4490 Large-scale wind-tunnel investigation of an airplane model with a tilt wing of aspect ratio 8.4, and four propellers, in the presence of a ground plane NASA-IN-D-4493 c01 NG c01 N68-20370 DECRESCENTE, M. A. Optical absorption in transparent materials following high-temperature reactor irradiation NASA-CR-1032 c22 D DEERWESTER, J. M. Analysis of launch windows from circular orbits for representative Mars missions NASA-TM-X-1651 c30 M c22 N68-23481 c30 N68-33371 DEISSLER, R. G. Weak locally homogeneous turbulence and heat transfer with combined two-dimensional shear and normal strain NASA-TN-D-4273 c33 N68-11491 DELANEY, F. C. The distribution and properties of a weighted sum of chi squares NASA-TN-D-4575 c19 N68-24565 DENGLER, R. P. Self evacuated multilayer insulation of lightweight prefabricated panels for cryogenic storage tanks NASA-TN-D-4375 c c33 N68-18046 DERR, V. E. Propagation of millimeter and submillimeter waves NASA-CR-863 c07 N68-27063 NASA-CR-863 c07 N68-27 DEVEIKIS, W. D. Drag due to two-dimensional surface roughness in a turbulent boundary layer at Mach 3 with and without heat transfer NASA-IN-D-4746 DEXTER, H. B. Coatings and surface treatments for c12 N68-33054 longtime protection of Ti-8Al-1Mo-1V alloy sheet from hot salt stress corrosion NASA-TN-D-4319 c17 N68-17377

Mechanical properties and column behavior of thin wall beryllium tubing NASA-TN-D-4833 c17 N68 c17 N68-37053 DEYO, J. N. Instrumentation of a SNAP-8 simulator facility NASA-TM-X-1525 c14 N68-19001 DI CARLO, D. J. Flight investigation to determine the effect of longitudinal characteristics on low-speed instrument operation NASA-TN-D-4364 c02 N68-19184 DICKINSON, S. O. Large-scale wind-tunnel tests of a deflected slipstream STOL model with wings of various aspect ratios NASA-TN-D-4448 c02 N68-18771 NASA-IN-D-4440 CC2 No Large-scale wind-tunnel investigation of an airplane model with a tilt wing of aspect ratio 8.4, and four propellers, in the presence of a ground plane NASA-IN-D-4493 CO1 No c01 N68-20370 DIEDRICH, G. E. Design of two electromagnetic pumps NASA-CR-911 c15 N68-10503 DIETRICH, M. W. Effect of ball-race conformity on spinning friction NASA-TN-D-4669 c15 N68-28258 DIMEFF, J. Tabulated communication characteristics of a steady-state model of interplanetary space NASA-SP-3042 c30 N68-10164 DIRLING, R. B., JR. Radiative and convective heating during atmospheric entry NASA-CR-1170 c33 N68-35248 DIXON, W. C., JR. A celestial attitude measurement instrument for Project Scanner NASA-TN-D-4742 c21 N68-31938 DDDGE, F. T. Flow-induced vibrations of a flat plate suspended in a narrow channel Final report NASA-CR-1186 c12 N68-35086 DOGGETT, R. V., JR. Effects of flexibility on lift and pitchingmoment characteristics of a series of low aspect-ratio wing-body combinations at transonic speeds NASA-TN-D-4655 c01 N68-37065 NASA-TN-D-4655 col N DOHERTY, L. R. Ultraviolet dayglow and stellar brightness measurement from the X-15 aircraft NASA-CR-1017 c30 N c30 N68-19590 NASA-CATION DONOVAN, L. F. Computer program for calculating isothermal, turbulent jet mixing of two gases NASA-TN-D-4378 cl2 N68 c12 N68-18146 Similarity solution for turbulent mixing between a jet and a faster moving coaxial stream NASA-TN-D-4441 c12 N68-19246 DOO, V. Y. Investigation of refractory dielectrics for integrated circuits NASA-CR-995 c18 N64 c18 N68-18849 NASA-CK-995 c18 N68-1 DOQLIN, B. F. Simple processors of star tracker commands for stabilizing an inertially oriented satellite NASA-TN-D-4490 c21 N68-1 c21 N68-19236 DUUGLAS, F. C. Optical absorption in fused silica during TRIGA reactor pulse irradiation c22 N68-21124 NASA-CR-1031 Optical absorption in transparent materials following high-temperature reactor irradiation NASA-CR-1032 c22 N68-23481 DOWNS, W. R. Chemically induced ignition in aircraft and spacecraft electrical circuitry by glycol/water solutions NASA-TN-D-4327 c31 c31 N68-22213 DRAPER, L. T. Star tracker calibration

NASA-TN-D-4594 c21 N68-24555 DRESHFIELD, R. L. Development of a cobalt-tungsten ferromagnetic, high-temperature, structural allov NASA-TN-D-4338 c17 N68-18145 DRESSLER, R. F. Design of guidance and control systems for optimum utilization of information NASA-CR-997 -10 N68-23438 DROBA, D. J. Dynamic characteristics of parasitic loading speed controller for 10 kilowatt Brayton cycle turboalternator NASA-TM-X-1456 c03 N68-18702 DSOUZA, G. J. Evaluation of turbulence correlations in a coaxial flow of dissimilar fluids NASA-CR-961 c12 N68-12892 C12 N Measurement of turbulent correlations in a coaxial flow of dissimilar fluids NASA-CR-960 c12 N c12 N68-13612 DUDZINSKI, T. J. Performance of a venturi meter with separable diffuser NASA-TM-X-1570 c14 N68-21384 A small combination sensing probe for measurement of temperature, pressure, and flow direction NASA-TN-D-4816 c14 h DUGAN, J. V., JR. Calculation of capture cross sections for ion polar molecule collisions involving c14 N68-36021 methyl cyanide NASA-TM-X-1586 c24 N68-23893 DUGDF, H. A laboratory scale model technique for investigating pneumatic tire hydroplaning NASA-CR-1074 cll N6 DUSTIN, M. O. Design and performance of flueric analog to c11 N68-23357 pulse frequency converter NASA-TN-D-4497 c03 N68-21835 DYNER, H. B. Study of optical radiation in the wavelength regions of 0.4216 mu, 0.4278 mu, 0.4835 mu, and 0.5165 mu behind normal shock waves in a simulated Martian atmosphere NASA-TM-X-1634 c12 N68-32982

E

EASLEY, A. J. Effect of turbulent mixing on average fuel temperatures in a gas-core nuclear rocket engine NASA-TN-D-4882 c22 N68-37927 EASTWOOD, C. W., JR. Centaur/Surveyor nose fairing aerodynamic heating investigation NASA-TM-X-1605 c33 1 c33 N68-28156 Two-stage potassium test turbine. Volume 3 -Test facilities NASA-CR-924, V. 3 c03 N68c03 N68-18044 ECKERT, R. E. Effect of film processing on cryogenic properties of poly/ethylene terephthalate/ NASA-TN-D-4762 c18 N68 c18 N68-33034 NASA-IN-D-4762 ECKSTROM, C. V. Flight test of a 40-foot-nominal-diameter modified ringsail parachute deployed at a Mach number of 1.64 and a dynamic pressure of 9.1 pounds per square foot NASA-TM-X-1484 c31 N68-11919 Flight test of a 30 foot nominal diameter cross parachute deployed at a Mach number of 1.57 and a dynamic pressure of 9.7 pounds per square foot NASA-TM-X-1542 c31 N68-21778 Flight test of a 40-foot nominal diameter disk gap band parachute deployed at a Mach number of 1.91 and a dynamic pressure of 11.6 pounds per square foot NASA-TM-X-1575 c02 N68-24245 Flight test of a 40-foot-nominal-diameter disk-gap-band parachute deployed at a Mach number of 2.72 and a dynamic pressure of 9.7 pounds per square foot

NASA-TM-X-1623 c31 N68-29993 EDKIN, R. A. Experimental evaluation of a voltage regulator-exciter for a 15 kilovolt-ampere Brayton cycle alternator NASA-TN-D-4697 c03 N68-29960 Performance characteristics of 15 kVA homopolar inductor alternator for 400 Hz Brayton-cycle space-power system NASA-TN-D-4698 c03 N68-3 EDWARDS, C. L. W. A real-gas study of low-density wedge-induced laminar separation on a highly cooled blunt flat plate at M infinity equals 12 NASA-TN-D-4320 c01 N68-1 Low-density, leading-edge bluntness, and ablation effects on wedge-induced laminar boundary layer separation at moderate enthalpies in hypersonic flow NASA-TN-D-4829 c12 N68-3 EDWARDS, F. G. Entries from earth orbit that simulate acceleration stresses of manned planetary NASA-TN-D-4698 c03 N68-30002 c01 N68-17899 c12 N68-36458 acceleration stresses of manned planetary missions NASA-TN-D-4847 c31 N68-36056 EGGEESTON, D. N. Dynamic stability of space vehicles. Volume 14 - Testing for booster propellant sloshing parameters NASA-CR-948 c32 N68-23454 NASA-CK-948 c EHERNBERGER, L. J. Atmospheric conditions associated with turbulence encountered by the XB-70 airplane above 40,000 feet altitude NASA-TN-D-4768 c13 N68-33416 EHLOTZKY, F. Lie series for celestial mechanics, accelerators, satellite stabilization and optimization NASA-CR-1046 c19 N68-25841 EHRLICH, I. R. A laboratory scale model technique for investigating pneumatic tire hydroplaning NASA-CR-1074 cll N6 c11 N68-23357 EICHBLATT, D. L. Experimental verification of scale factors for parawing opening characteristics NASA-TN-D-4665 c02 N68-31956 EISEN, M. M. JERN, H. H. Lyapunov stability for partial differential equations. Part 1 - Lyapunov stability theory and the stability of solutions to partial differential equations. Part 2 -Contraction groups and equivalent norms NASA-CR-1100 C19 N6. c19 N68-27457 EISENBERG, J. D. Tankage systems for a methane-fueled supersonic transport NASA-TN-X-1591 c02 N68-23895 ELIAS, I. A study of turbofan-engine compressor noise suppression techniques NASA-CR-1056 c28 N68-26771 NASA-UN-1000 ELLIS, W. E. Effects of 22 MeV proton and 2.4 MeV electron radiation on boron and aluminum-doped silicon solar cells c26 N68-19924 ELLSON, R. A. Design and preliminary operation of the Lewis magnetohydrodynamic generator facility Lewis magnetonydrodynamic generator lating NASA-TN-D-4867 cll N68-37 ENGBRENGHOF, L. C. Dynamic stability of space vehicles. Volume 9 - The effect of liftoff dynamics on launch vehicle stability and control c11 N68-37259 NASA-CR-943 c32 N68-10233 RADH-ON-345 ENGLEBY, D. S. Two-stage potassium test turbine. Volume 4 - Materials support of performance and endurance tests NASA-CR-925 c03 N68-16351 EPSTEIN, J. Properties of selected radioisotopes. bibliography, part 1 - Unclassified A literature NASA-SP-7031 c06 N68-29959 ERDOGAN, F. Fatigue crack propagation in cylindrical

FELSENTREGER, T. L.

shells NASA-CR-1197 c32 N68-37840 Charts for equilibrium isentropic expansion of air behind shocks up to 50000 feet per second /15.24 kilometers per second/ NASA-TN-D-4247 c ERZBERGER, H. On the use of algebraic methods in the c33 N68-11144 analysis and design of model-following control systems NASA-TN-D-4663 c19 N68-28281 NASA-TN-D-4663 c19 N68-EVANS, A., JR. On the solubilities and rates of solution of gases in liquid methane NASA-TN-D-4701 c27 N68-EVANS, J. C., JR. Electron-beam, crystallization of silicon, germanium, and cadmium sulfide NASA-TN-D-4522 c26 N68-EVANS, R. C. c27 N68-30077 c26 N68-20295 EVANS, R. C. Injection start of a Brayton cycle turbocompressor operating on gas bearings in a closed loop NASA-TM-X-1590 c03 N68-24757 Use of an electronic visualization technique in the study of gas journal bearing behavior NASA-TM-X-1609 c14 N68-35105 EVANS, R. M. Welding of precipitation-hardening stainless steels NASA-SP-5087 c15 N68-21429 NASA-SP-5087 c15 N6 EVENSEN, D. A. Nonlinear flutter of a circular cylindrical shell in supersonic flow NASA-TN-D-4265 c32 N6 c32 N68-12864 EVERHART, P. E. Experimental pressure distributions and aerodynamic characteristics of a low-finenessangles of attack from 0 deg to 90 deg NASA-TM-X-1487 c01 N68-11958 F FABER, O. C., JR. On the influence of nonuniform magnetic fields on ferromagnetic colloidal sols NASA-TN-D-4676 c06 N68-30044 NASA-TN-D-4676 cub f FARREL, J. L. Digital program for dynamics of non-rigid gravity gradient satellites NASA-CR-1119 c30 f c30 N68-32744

FARRELL, J. Procedures for estimating the effects of design and operational characteristics of jet aircraft on ground noise NASA-CR-1053 c02 N68-26930 FAZZIO, R. Entry length for the rocket meteorological radiation shield NASA-CR-1200 c14 N68-36530

c14 N68-36530 NASA-CK-1200 c14 | FEFFERMAN, R. L. Dynamic stability of space vehicles. Volv 6 - Full scale dynamic testing for mode determination Volume NASA-CR-940 c32 N68-11054 FEHLBERG, E. Classical fifth-, sixth-, seventh-, and eighth-order Runge-Kutta formulas with stepsize control NASA-TR-R-287 c19 N68-36753 FEILER, C. E. Sound measurements on a full-scale jet-engine inlet-noise-suppressor cowling NASA-TN-D-4639 c02 N68-29887 Effect of chamber pressure, flow per element, and contraction ratio on acoustic-mode instability in hydrogen-oxygen rockets NASA-TN-D-4733 c33 N68-30518 FEIVESON, A. H. The distribution and properties of a weighted c19 N68-24565

sum of chi squares NASA-TN-D-4575 cl9 N68-24565 FELSENTREGER, T. L. On the perturbations of small-eccentricity satellites NASA-TN-D-4531 c30 N68-28251

I-131

FERGUSON, H.

PERSONAL AUTHOR INDEX

FERGUSON, H. Performance tests of a 1/2-millipound /2.2 mN/ ammonia resistojet thrustor system NASA-TN-D-4249 c28 N68-10562 Preliminary tests of a single-axis ammonia-resistojet attitude control system NASA-TM-X-1677 c28 N68-36512 FERRANTE. J. Low-energy electron diffraction study of oxygen adsorption on molybdenum /111/ surface NASA-TN-D-4735 c06 N68-30582 FERRIS, A. T. Free-flight and wind-tunnel studies of deployment of a dynamically and elastically scaled inflatable parawing model NASA-TN-D-4724 c02 N68-33879 FERSHT, R. S. Almost sure stability of long cylindrical shells with random imperfections NASA-CR-1161 c32 | FESSLER, T. E. Operational amplifiers for use in nuclear c32 N68-33419 spectroscopy NASA-TN-D-4349 c24 N68-18254 FICHTEL, C. E. Experimental tests of the supernovae origin of cosmic ravs NASA-TN-D-4732 FIELDER, W. L. Ionic conductivity of solid mixtures c29 N68-33370 NASA-TN-D-4606 c26 N68-24510 NASA-IN-U-4000 FIERO, I. B. Establishing allowable temperature gradients for tungsten-uranium dioxide fuel elements using experimental cyclic strain data NASA-TN-D-4279 c22 N68-1 Study of vibration induced stresses in design of fuel-element support assembly for turgeton-moderated nuclear reactor c22 N68-14986 tungsten water-moderated nuclear reactor NASA-TM-X-1608 c32 N c32 N68-28330 FIGARCLA, T. R. A simple laboratory method for reduction of rhythm and rate in large-scale monitoring of electrocardiogram NASA-TN-D-4751 c05 N68-32100 FIGGE, I. E. Residual static strength and slow crack growth behavior of duplex-annealed Ti-8A1-1Mo-1V sheet NASA-TN-D-4358 c32 N68-175 Prediction of fatigue-crack-propagation behavior in panels with simulated rivet forces c32 N68-17588 NASA-TN-D-4702 c32 N68-32074 FIGGINS, D. The applications technology satellite image dissector camera experiment NASA-TN-D-4186 c14 N68-10647 FINK, R. W. Two-stage potassium test turbine. Volume 2 -Mechanical design and development NASA-CR-923 c03 N68c03 N68-17075 FINNEGAN, P. M. Nuclear design data for experiments to be conducted in Horizontal Through Hole 1 of the Plum Brook Reactor NASA-TM-X-1509 c22 N68-15855 Very high burnup vapor transport fuel pin concept for long life nuclear reactors NASA-TN-D-4860 c22 N68-37209 FISCHER, R. L. E. Dynamic characteristics of parasitic loading speed controller for 10 kilowatt Brayton cycle turboalternator NASA-TM-X-1456 c03 N68-18702 FISH. R. H. The penetration of porous projectiles in aluminum and plastic targets NASA-TN-D-4505 c32 c32 N68-21293 FLATLEY, D. MOS field-effect-transistor technology NASA-CR-1113 c08 N68-35193 FLEISHAN, N. P. Rib-reinforced plates and shells NASA-TT-F-427 c32 N68-10407 FLEMING, D. P. Experiments on stability of herringbone grooved gas-lubricated journal bearings to high compressibility numbers

NASA-TN-D-4440 c15 N68-21965 NASA-IN-U-4440 FLETCHER, H. S. Simulator study of pilot control over the lunar module during ascent from the lunar surface by using visual guidance cues NASA-IM-X-1549 c21 N6 c21 N68-21366 NASA-IN-A-4045 FLORIANI, D. Lie series for celestial mechanics, accelerators, satellite stabilization and NASA-CR-1046 c19 N68-25841 FLYNN, G. W. A study of trace contaminant identification by microwave double resonance spectroscopy NASA-CR-967 c24 N68-11634 NASA-CR-967 FOGARTY, L. E. Trajectory optimization by a direct descent process NASA-CR-1070 c30 N68-25902 FOGEL, L. J. Modeling the human operator with finite-state NASA-CR-1112 c05 N68-28847 FONTENOT, L. L. Dynamic stability of space vehicles. Volume 7 — The dynamics of liquids in fixed and moving containers NASA-CR-941 c32 N68-18769 FOOTE, R. H. The applications technology satellite image dissector camera experiment NASA-TN-D-4186 c14 N68-10647 NASA-TN-D-4160 CT 10, W. F. Inelastic scattering form factors using projected Hartree-Fock wave functions NASA-TN-D-4566 c2. FORD, c24 N68-24661 NH3A-IN-U-4306 c24 FORMAN, B. J. Study of advanced antenna techniques for rendezvous radar NASA-CR-764 c07 c07 N68-28135 FORMAN, R. Electrical properties of xenon-filled thermionic diodes in radiation field of a nuclear reactor NASA-TN-D-4368 c25 N68-15747 FOSTER, G. V. Aerodynamic characteristics of two blunt, half-cone wedge entry configurations at Mach numbers from 2.30 to 4.63 NASA-TM-X-1621 co1 c01 N68-30030 NASA-IN-A-1021
 COI NOS-3
 FOSTER, J. D.
 Use of an electroluminescent display in manual tracking and in a reading task
 NASA-TN-D-4841
 FOUDRIAT, E. C.
 Application of maximum likelihood techniques c05 N68-36457 to the design of optimum star trackers NASA-TN-D-4549 c21 c21 N68-23377 FOWLER, P. Study of density calibration in space Final report, Jun. 29, 1966 - Jan. 16, 1967 NASA-CR-987 c14 N68 c14 N68-12669 FOWLER, R. A. Earthquake prediction from laser surveying NASA-SP-5042 c13 N c13 N68-23706 FOX, C. H., JR. Hypersonic aerodynamic characteristics of low-wave-drag elliptical-body-tail combinations as affected by changes in stabilizer configuration NASA-TM-X-1620 c01 N68-29952 NASA-TN-D-4357 C01 FRALICH, R. W. Flutter of buckled, simply supported, rectangular panels at supersonic speeds NASA-TN-D-4357 C32 c32 N68-17651 FRANKENFELD, J. W. Study of methods for chemical synthesis of edible fatty acids and lipids Final technical report NASA-CR-1105 c04 N68-28278 Study of methods for chemical synthesis of edible fatty acids and lipids - Final summary NASA-CR-1104 FRASCA, R. L. c04 N68-28829 A study of turbofan-engine compressor noise suppression techniques NASA-CR-1056 c28 N68-26771

GEORGE, R. E.

FRASER, T. M. The intangibles of habitability during long duration space missions NASA-CR-1084 c30 | FRECHE, J. C. Fatigue of liquid rocket engine metals at c30 N68-26702 cryogenic temperatures to minus 452 deg F /4 deg K/ NASA-TN-D-4274 c17 N68-11637 Application of directional solidification to a NASA nickel-base alloy /TAZ-8B/ NASA-TN-D-4390 cli Ultrasonic detection and measurement of c17 N68-15637 fatigue cracks in notched specimens FREEMAN, D. C., JR.
 Low-subsonic flight and force investigation of a supersonic transport model with a double-delta wing c32 N68-35071 c02 N68-18250 NASA-TN-D-4179 FRIEDLAND, B. Additional studies of quasi-optimum feedback control techniques NASA-CR-1099 c10 N68-28307 FRISCH, H. P. The dynamic characteristics of satellites having long elastic members NASA-TN-D-4576 c31 c31 N68-31978 FRY. B. L. Supplement to feasibility of V/STOL concepts for short-haul transport aircraft NASA-CR-743/1/ c02 N68-35177 FRYSINGER, T. C. Pressure-rise characteristics for a liquid hydrogen dewar for homogeneous, normal gravity quiescent, and zero gravity tests NASA-TM-X-1134 c33 N68-18196 FULLER, D. E. Preliminary study of drag reduction for coasting missiles at Mach numbers from 1.57 to 4.63 NASA-TM-X-1537 coll N66 Effects of nose shape and fin geometry on static stability of a high-fineness-ratio c01 N68-19206 sounding rocket NASA-TM-X-1661 c01 N68-36509 NASA-IN-X-IODI CUI NOG-FULLER, F. B. Calculations of Chandrasekhar*s X and Y functions and their analogs for noncoherent isotropic scattering NASA-TW-P-4212 NASA-TN-D-4712 c19 N68-30804 FULTON, R. E. Accuracy study of finite difference methods NASA-TN-D-4372 c32 N6 c32 N68-17068 FUNDERBURK, B.J. Automation in Saturn 1 first stage checkout NASA-TN-D-4328 c31 N68-15570 FUTRAL, S. M., JR. Experimental performance evaluation of a 6.02-inch /15.29-cm/ radial-inflow turbine with an exit diffuser NASA-TM-X-1480 c03 N68-11920 Experimental performance of a 5-inch /13 cm/ axial-flow turbine over a range of Reynolds number NASA-TM-X-1679 c03 N68-37263 Experimental performance of a 5-inch single-stage axial-flow turbine designed for a Brayton cycle space power system NASA-TM-X-1666 c03 N68-37943 G

GADZUK, J. V.	
Many-body theory of a rapidly v	arving
inhomogeneous electron gas	
NASA-TR-R-283	c26 N68-24273
GAGLIARDI, R. M.	
M-ary Poisson detection and opt	ical
communications	
NASA-TN-D-4623	c07 N68-29528
The design of a Pulse Position	Modulated
/PPM/ optical communication s	
NASA-TN-D-4814	c07 N68-35174
Error probabilities for maximum	likelihood
detection of M-ary Poisson pr	ocesses in
Poisson noise	
NASA-TN-D-4721	c07 N68-36105

GAGOSZ, R. Optical absorption in fused silica during TRIGA reactor pulse irradiation NASA-CR-1031 c22 N68-21124 following high-temperature reactor irradiation NASA-CR-1032 c22 N68-23481 Optical absorption and fluorescence in fused silica during TRIGA pulse irradiation GAHAN, J. W. Design of two electromagnetic pumps NASA-CR-191 GAHN, R. F. c22 N68-35826 c15 N68-10503 Technique for recovery of alkali-metal reaction products NASA-TN-D-4310 c c17 N68-14888 GALLAGHER, A. K. Laminarization of a turbulent boundary layer as observed from heat-transfer and boundary layer measurements in conical nozzles NASA-TN-D-4788 c12 N68-33642 GAMBUCCI, B. J. Fluctuating pressures on the afterbodies of five blunt atmosphere entry vehicles NASA-TN-D-4591 c32 N68-24508 hannerhead models to unsteady aerodynamic loading NASA-TN-D-4504 c01 N68-25916 GAMSE, B. Large-scale wind-tunnel tests of an airplane model with two propellers and rotating cylinder flaps NASA-TN-D-4489 c01 N68 c01 N68-19189 GARCIA, F., JR. A general analytical method for artificial-satellite lifetime determination NASA-TN-D-4281 c30 N68-11754 GARDNER, J. E. Effects of longtime environmental exposure on mechanical properties of sheet materials for a supersonic transport NASA-TN-D-4318 c17 N68-17897 GARFINKLE, M. Superplasticity in tungsten-rhenium alloys NASA-TN-D-4728 c GARREN, J. F., JR. Study of the optimum values of several c17 N68-30605 parameters affecting longitudinal handling qualities of VTOL aircraft NASA-TN-D-4624 c02 N68-28153 GARREN, K. R. Bounds for the eigenvalues of a matrix NASA-TN-D-4373 c c19 N68-17334 GARRICK, I. E. A summary of results on sonic-boom pressure signature variations associated with atmospheric conditions NASA-TN-D-4588 c02 N68-24662 GASPERS, P. A., JR. An experimental study of the influence of the turbulent boundary layer on panel flutter NASA-TN-D-4486 c32 N68c32 N68-18721 GEBBEN, V. D. Cardiac R-wave detector NASA-TM-X-1489 c05 N68-13999 GEIGER, F. E., JR. Optical alignment of silicon crystals NASA-TN-D-4187 c c23 N68-10354 The operation of an electron paramagnetic resonance spectrometer NASA-TN-D-4469 c14 N68-21169 Electron spin resonance of lithium-diffused silicon NASA-TR-R-290 c26 N68-33228 GELDER, T. F. Effects of wall pressure distribution and liquid temperature on incipient cavitation of Freon-114 and water in venturi flow NASA-TN-D-4340 cl2 N68-14 c12 N68-14641 GENTRY, G. L., JR. Aerodynamic characteristics of a five jet VTOL configuration in the transition speed range NASA-TN-D-4812 c01 N68-36081 GEORGE, R. E. Fluctuating pressures on the afterbodies of five blunt atmosphere entry vehicles

GERA, J.

PERSONAL AUTHOR INDEX

NASA-TN-D-4591 c32 N68-24508 Dynamic response of a family of axisymmetric hammerhead models to unsteady aerodynamic loading NASA-TN-D-4504 c01 N68-25916 GERA, J. An exploratory study of parallel stage separation of reusable launch vehicles NASA-TN-D-4765 c31 c31 N68-36106 GERARD, G. Structural design synthesis approach to filamentary composites NASA-CR-964 c3 c32 N68-11191 GERDS. A. F. Deformation processing of precipitation-hardening stainless steels NASA-SP-5088 c17 c17 N68-21917 GERSTEIN, M. A study of aircraft fire hazards related to natural electrical phenomena Final report, Jun. 1966 - Jul. 1967 NASA-CR-1076 c02 N68-26691 GIESEKE, R. Dynamic stability of space vehicles. Volume 3 - Torsional vibration modes NASA-CR-937 c32 N68-10568 GIFT, R. D. Study of propellant valve leakage in a vacuum Final summary report NASA-CR-1047 c27 N68-21893 GILBERT, L. J. Reduction of apparent-power requirement of phase-controlled parasitically loaded turboalternator by multiple parasitic loads NASA-TN-D-4302 GILBREATH, W. P. c03 N68-17110 The influence of gaseous environment on the self-adhesion of metals NASA-TN-D-4868 c17 N6 c17 N68-36970 GILL, S. P. Implosively accelerated shock tube driver NASA-CR-950 c12 N68-10646 NASA-CR-930 C12 NOS-GILLETTE, R. B. Ultraviolet-proton radiation effects on solar concentrator reflective surfaces Final report, Jun. 1965 - Aug. 1967 NASA-CR-1024 c17 N68-2 c17 N68-23560 GILROY, W. K. Research and development of high-performance axial-flow turbomachinery. Volume 1 -Design of turbine-compressor NASA-CR-800 c03 N68 c03 N68-24596 GILYARD, G. B. Preliminary flight evaluation of the stability and control derivatives and dynamic characteristics of the unaugmented XB-70-1 airplane including comparisons with predictions NASA-TN-D-4578 c02 N68-24498 GINZBURG, V. L. Magnetobrems /synchrotron/ emission and reabsorption NASA-TT-F-521 c25 N68-16700 GIULIANO, V. E. Application of statistical association techniques for the NASA document collection NASA-CR-1020 c08 N68c08 N68-17154 GLASER. P. E. Space technology transfer and developing nations NASA-CR-1222 c34 N68-37216 GLASSMAN, A. J. GLASSMAN, A. J. Use of similarity parameters for examination of geometry characteristics of high-expansion-ratio axial-flow turbines NASA-TN-D-4248 Analysis of fan-turbine efficiency Characteristics in terms of size and. c01 N68-10529 characteristics in terms of size and. stage number NASA-TM-X-1581 c28 N68-22725 GLAWE, G. E. Preliminary tests with mass flux probe in supersonic stream NASA-TM-X-1524 c14 N68-18834 A small combination sensing probe for measurement of temperature, pressure, and flow direction NASA-TN-D-4816 c14 N68-36021

GLENN, D. C. Friction torque of ball bearings in vacuum with seven polytetrafluoroethylene composition retainer materials NASA-TN-D-4355 c15 N68 GODLEWSKI, M. P. Experimental determination of neutron fluxes c15 N68-16468 in Plum Brook reactor HB-6 facility with use of sulfur pellets and gold foil NASA-TM-X-1497 c22 N c22 N68-15643 GOELZ, R. R. Combustion instability in steel and ablative rocket chambers NASA-TM-X-1511 c28 N68-15644 Stabilizing effects of several injector face baffle configurations on screech in a 20,000 pound-thrust hydrogen-oxygen rocket NASA-TN-D-4515 c28 N68-21679 GOETTELMAN, R. C. Implosively accelerated shock tube driver NASA-CR-950 c12 c12 N68-10646 GOETZ, R. C. Divergence of some all-movable control surfaces including drag loading NASA-TN-D-4793 c32 N68-35496 GOFORTH, T. T. Seismic effects of sonic booms NASA-CR-1137 c13 N68-35151 GOLDBERG, F. N. Numerical procedures for calculating real fluid properties of normal and parahydrogen NASA-TN-D-4341 c08 N68-15798 GOLDMAN, G. C. Electrical characteristics of a dc compact arc in argon from 1 to 10 atmospheres and from 600 to 1200 amperes NASA-TM-X-1596 c29 N68-25818 GOLDMAN, L. J. Computer program for design of two dimensional supersonic nozzle with sharp edged throat NASA-TM-X-1502 c01 N68-1 NNSH-IN-X-1502 CO1 N68-14 Analytical investigation of supersonic turbomachinery blading. 1 - Computer program for blading design NASA-TN-D-4421 CO8 N68-18 Analytical c01 N68-14747 c08 N68-18620 maphin=u=u=4421 COB Ni Analytical investigation of supersonic turbomachinery blading. 2 - Analysis of impulse turbine-blade sections NASA-TN-D-4422 COB No DOTENT COB No DOTENT COB No c03 N68-20276 GOLDSTEIN, C. M. Collisionless cylindrical diode NASA-TN-D-4516 c10 N68-21122 GOLDSTEIN, M. Boundary conditions for the diffusion solution of coupled conduction-radiation problems c33 N68-26759 NASA-TN-D-4618 GOLDSTEIN, M. E. Shape of a magnetically balanced arc NASA-TN-D-4736 c25 N68-30784 GOODMAN, F. O. A three-dimensional hard spheres theory of scattering of gas atoms from a solid surface NASA-CR-933 c12 N68-10499 GOODSON, K. W. Effect of ground proximity on the longitudinal, lateral, and control aerodynamic characteristics of a tilt-wing four-propeller V/STOL model NASA-TN-D-4237 c02 N68-11519 GORDON, W. A. Stabilization of dc arcs in static argon atmospheres for use in spectrochemical analysis NASA-TN-D-4236 c06 N68-11512 A servocontroller for programming sample vaporization in direct current arc spectrochemical analysis NASA-TN-D-4769 c06 N68-31948 GOREE, W. S. Cryogenic magnetometer development report, 1 Jul. 1964 - 7 Mar. 1967 NASA-CR-1073 Final c14 N68-26703 GORLAND, S. Control of contaminants in liquid-metal system NASA-TM-X-1432 c17 N68-11912

HAMMER, D. C.

GOTO. J. T. The buckling of thin-walled circular cylinders under axial compression and bending NASA-CR-1160 c32 N68-33226 GRACEY, W. Evaluation of a closed-circuit television display in landing operations with a helicopter COST c05 N68-16594 GRAFTON, S. B. Static and dynamic longitudinal stability derivatives of a powered 0.18-scale model of a fan-in-wing VTOL aircraft NASA-TN-D-4322 c02 N68-158 c02 N68-15894 Calculation of the dynamic longitudinal stability of a tilt-wing V/STOL aircraft and correlation with model flight tests NASA-TN-D-4344 c02 N68-15941 GRAHAM, R. E. Aerodynamic stability characteristics of the Apollo command module NASA-TN-D-4688 c01 N68-31445 NASA-IN-D-4668 C01 N68-314
GRANTIAN, W. D.
A piloted fixed-base simulator study of lowspeed flight characteristics of an arrow-wing
supersonic transport design
NASA-IN-D-4277 c05 N68-134 c05 N68-13609 GRAVES, E. B. Aerodynamic characteristics of several hypersonic boost-glide-type configurations at Mach numbers from 2.30 to 4.63 NASA-TM-X-1601 col N68-33 c01 N68-33836 NASA-TM-X-1501 col N68-33836 GRAVES, R. A., JR. Flight test analysis of Apollo heat shield material using the Pacemaker vehicle system NASA-TN-D-4713 c33 N68-30747 GRAY. V. H. Boiling heat transfer coefficients, interface behavior, and vapor quality in rotating boiler operating to 475 G*s NASA-TN-D-4136 c33 N68c33 N68-17566 GREEN, R. N. A semigraphical method for a deorbit trajectory design study NASA-TN-D-4801 c30 N68-36077 GREENBERG, J. M. Interstellar grains NASA-SP-140 c30 N68-11456 NASA-SP-140 c30 / GREENBERG, M. D. Inviscid flow field induced by a rotor in ground effect NASA-CR-1027 c01 / c01 N68-22475 GREVE, R. Inorganic separator for a high temperature silver-zinc battery NASA-CR-965 c03 N68-16321 GREYERBIEHL, J. A theoretical approach to the determination of magnetic torques by near field measurement 233 NGB#24 NASA-TN-D-4485 c23 N68-24146 c30 N68-17215 Guidance, flight mechanics and trajectory optimization. Volume 17 - Guidance system performance analysis NASA-CR-1016 c30 H Guidance, flight mechanics and trajectory optimization. Volume 5 - State c30 N68-21442 determination and/or estimation NASA-CR-1004 c30 GRIFFIN, W. S. A breadboard flueric-controlled pneumatic c30 N68-21685 stepping motor system NASA-TN-D-4495 c03 N68-21651 NASA-IN-D-4495 C03 N68 GRIMSLEY, J. D. Heat treatment for improved stress-corrosion resistance of 17-7 pH stainless steel NASA-IN-D-4673 c17 N68 c17 N68-29379 GROEBNER, W. Lie series for celestial mechanics, accelerators, satellite stabilization and optimization NASA-CR-1046 c19 N68-25841 GROSE, W. L. A digital computer program for calculating the

performance of single or multiple diaphragm shock tubes for arbitrary equilibrium real gas mixtures NASA-TN-D-4802 c11 N68-35466 GROSSMAN, L. N. Thermal conductivity of coated particle uranium dioxide tungsten cermets NASA-CR-1154 c2 c22 N68-32983 GRUBER, C. Optically induced free-carrier light modulator NASA-IN-D-4608 GRUMTFEST, I. J. The role of energy in deformation NASA-CR-1039 c23 N68-25868 c24 N68-21949 GRUNWALD, K. J. Flight investigation of performance characteristics during landing approach of a large powered-lift jet transport Arge powered-fift jet transport NASA-TN-D-4261 c02 N68 GURKLIS, J. A. Machining and grinding of ultrahigh-strength steels and stainless steel alloys NASA-SP-5084 c15 N68 c02 N68-11638 c15 N68-21241 GYORGAK, C. A. Extrusion of 1/2 and 3/8-inch-diameter thin-wall tungsten tubing in lengths near 10 feet NASA-TM-X-1638 c15 N68-32977

Н

HACKING, C. A. Study and applications of retrodirective and self adaptive electromagnetic-wave phase controls to a Mars probe NASA-CR-977 c21 N68-18484 HACKLER, C. T. Lunar module pilot control considerations NASA-TN-D-4131 c21 c21 N68-16836 HAFERD, A. M. Numerical procedures for calculating real fluid properties of normal and parahydrogen NASA-TN-D-4341 HAGEDORN, N. H. c08 N68-15798 Parametric mass analysis and comparison of two types of reactant cooling-and-storage units for a lunar-based hydrogen-oxygen regenerative fuel-cell system NASA-TN-D-4386 c03 N68-16631 HAGER, R. D. Use of wire lacing to reduce blade vibration in an axial-flow compressor rotor NASA-TM-X-1603 c32 N68-28238 HAKURA, Y. Polar cap absorptions and associated solar terrestrial events throughout the 19th solar cucle NASA-TN-D-4473 c29 N68-25880 HALL, A. M. Thermal and mechanical treatment for precipitation-hardening stainless steels NASA-SP-5089 c15 N68-20433 HALL, A. W. Flight investigation of performance characteristics during landing approach of a large powered-lift jet transport NASA-TN-D-4261 c02 N68-1 c02 N68-11638 HALL, G. R. Full-scale ground proximity investigation of a VTOL fighter model aircraft NASA-CR-1098 c02 N68-2 c02 N68-28233 ANDR-LA-1090 CO2 M HALLER, H. C. Analytical comparison of Rankine cycle space radiators constructed of central, double, and block-vapor-chamber fin-tube geometries geometries NASA-TN-D-4411 c33 HAMILL, T. D. Liquid drops - Numerical and asymptotic solutions of their shapes NASA-TN-D-4779 c12 c33 N68-16324 c12 N68-33165 HAMILTON, H. H. Effect of hinge-line bleed on heat transfer and pressure distribution over a wedge-flap combination at Mach 10.4 NASA-TN-D-4686 c01 N68-29955 HAMMER, D. C. Damping of a torsional oscillator in liquid

HAMMER, H. A.

PERSONAL AUTHOR INDEX

c01 N68-29405

helium 4 and 3 from 0.4 deg to 2.5 deg K NASA-TN-D-4381 c26 N68-17594 HAMMER, H. A. Midcourse-guidance procedure with single position fix obtained from onboard optical measurements NASA-TN-D-4246 c21 N68-11521 HAMPSHIRE, W. F., II A semigraphical method for a deorbit trajectory design study NASA-TN-D-4801 c30 N68-36077 AMAROCK, B. J. Incompressibly lubricated Rayleigh step journal bearing. 1 - Zero-order perturbation solution NASA-TN-D-4839 c15 N68-36098 HAND, R. B. Two-stage potassium test turbine. Volume 4 - Materials support of performance and endurance tests NASA-CR-925 c03 N68-16351 HANNUM, N. P. Stabilizing effects of several injector face baffle configurations on screech in a 20,000 pound-thrust hydrogen-oxygen rocket NASA-TN-D-4515 c28 N68-2 c28 N68-21679 Effect of thrust per element on combustion stability characteristics of hydrogen oxygen rocket engines NASA-TN-D-4851 c28 N68-36515 HANSON, M. P. Glass, boron, and graphite filament wound resin composites and liners for cryogenic pressure vessels NASA-TN-D-4412 c18 N68-16623 HANYOK, J. Monomolecular contamination of optical surfaces NASA-TN-D-4612 c14 N68-25375 HAPP, W. W. Coding schemes for run-length information based on Poisson distribution NASA-TN-D-4572 c07 N68-25852 HARDY, G. H. Saturn 5 manual backup guidance and control piloted simulation study NASA-TN-D-4481 c21 N68-19061 HARPER, T. P. Coating selection program - Theory NASA-CR-1041 c18 N68-22391 NASA-CK-1041 HARRINGTON, D. E. Performance of a collapsible plug nozzle having either two-position cylindrical or variable angle floating shrouds at Mach numbers from 0 to 2.0 COL NG NASA-TM-X-1657 c01 N68-36132 HARRIS, D. Properties of selected radioisotopes. bibliography, part 1 - Unclassified literature NASA-SP-7031 c06 N68-29959 HARRIS, R. L. Effects of pressure suits and backpack loads on man*s self-locomotion in earth and simulated lunar gravity NASA-TN-D-4464 c05 N68-20354 NASA-IN-J-4404 HARRISON, J. K. Calculations of non-diffuse infrared radiation from the lunar surface incident onto a unit element above the surface NASA-TM-X-1567 c29 N64 c29 N68-21731 HARRISON, S. R. A study of an electric field measuring instrument NASA-CR-970 c14 N68-25903 HART, F. D. Modal density of thin circular cylinders NASA-CR-897 c32 N68-11967 Noise reduction shape factors in the low Noise reduction shape factors in the low frequency range NASA-CR-1155 c32 N68 HARTH, G. H., III Mechanical properties and column behavior of thin wall beryllium tubing NASA-TN-D-4833 c17 N68 c32 N68-33266 c17 N68-37053 HARVEY, W. D. Experimental investigation of laminar-flow separation on a flat plate induced by deflected trailing-edge flap at Mach 19

```
NASA-TN-D-4671 c01 N68-2
HATCHER, D. M.
A quasi-omnidirectional slot array antenna for
        spacecraft use at microwave frequencies
NASA-TN-D-4362 c07
                                                                 c07 N68-18616
     The input admittance of a rectangular
        aperture antenna loaded with a dielectric
        plug
        NASA-TN-D-4430
                                                                  c07 N68-20333
HATCHER, N. M.
An automatic balancing system for use on
        frictionlessly supported attitude-controlled
test platforms
NASA-TN-D-4426 c09 N68-1
                                                                  c09 N68-19185
ANUSER, J. R.
A study of charge storage in silicon oxide
resulting from non-penetrating electron
        NASA-CR-1088
                                                                  c26 N68-26603
HAYES, C.
     Supersonic aerodynamic characteristics of a
        model of an air-to-ground missile
NASA-TM-X-1491
                                                                  c01 N68-16480
     Effects of simulated wing damage on the
aerodynamic characteristics of a swept-wing
airplane model
         NASA-TM-X-1550
                                                                  c01 N68-22002
HAYNES, G. A.
Effects of 22 MeV proton and 2.4 MeV
        electron radiation on boron and
aluminum-doped silicon solar cells
NASA-TN-D-4407
                                                                  c26 N68-19924
HAYS, R. B.
     Application of cell culture as a primary
toxicity screen of possible spacecraft
         contaminants
        NASA-TN-D-4251
                                                                  c04 N68-10122
NASA-TN-U-1600
HEALY, F. M.
Effects of reduced airspeed for landing
approach on flying qualities of a large jet
transport equipped with powered lift
NASA-TN-D-4804 co2 N68-;
TTTM A P. JR.
                                                                  c02 N68-37075
HEATH, A. R., JR.
The geometric properties of an expandable
whirling-membrane solar-energy concentrator
         NASA-TN-D-4532
                                                                  c03 N68-22258
HEATH, C. A.
Nuclear thermionic space power system concept
        employing heat pipes
NASA-TN-D-4299
                                                                  c22 N68-19146
HECHT, R.
Study of new methods to measure low pressure
NASA-CR-1120 c14 N68
                                                                  c14 N68-33022
 HEDGEPETH, J. M.
     Large low-frequency orbiting radio telescope
NASA-CR-1201 c31 N6
HEFFERNAN, P. J.
Waveform distortion in a maximum-likelihood
                                                                   c31 N68-37900
        Darlington detector for M-ary PFM signals
NASA-TN-D-4294 c07 N68-18542
 HEFFNER, P.
      Theoretical and practical resolution limits
for processing pulse frequency modulation
         telemetry
telemetry
NASA-TN-D-4180 c07
HEIDELBERG, L. J.
Overall performance in argon of a 6-inch
radial-bladed centrifugal compressor
                                                                  c07 N68-18247
         NASA-TM-X-1622
                                                                  c01 N68-30033
 HEIDMANN, M. F.
      Performance study of rotating gas jet
generator for strong traveling transverse
         acoustic modes
         NASA-TN-D-4380
                                                                  c12 N68-16998
NASA-IN-D-4300 C12

HEIM, R. J.

A generalized experimental investigation

of hot gas recirculation and ingestion

for jet VTOL aircraft

NASA-CR-1147 c01
                                                                   c01 N68-33043
 HELLWIG, H. W.
Mars landing mission mode comparison
NASA-TM-X-1629
                                                                   c30 N68-29988
HENDRICKS, H. D.
Experimental study of transmission and
backscatter of 0.075 to 1.0 MeV electrons by
aluminum and stainless steel
NASA-TN-D-4363 c24 N68-1
                                                                   c24 N68-17898
      Investigation of electron-radiation-induced
```

dielectric breakdowns in a typical capacitor meteoroid detector system NASA-TN-D-4738 c14 N68~33277 NADA-IN-D-4738 c14 N HENDRICKS, R. C. Mist-flow heat transfer using single-phase variable-property approach NASA-TN-D-4149 c33 N c33 N68-11636 HENDRICKS, S. J. The geomagnetic secular variation 1900–1965 NASA-TN-D-4527 c13 N64 c13 N68-21543 HENKEL, S. J., JR. Parts and materials application review for space systems NASA-SP-6505 c15 N68-10120 HENLEY, C. E., JR. The influence of fixture stress concentrations on ring accelerometers NASA-TN-D-4540 c14 N68-25830 HENNING, A. B. Flight test of a 15-foot-diameter /4.6-meter/ Flight test of a 15-foot-diameter /4.6-meter/ 120 deg conical spacecraft simulating parachute deployment in a Mars atmosphere NASA-TN-D-4266 c31 N68-11961 Performance of a 16.6-meter-diameter modified ringsail parachute in a simulated Martian environment NASA-TM-X-1500 c31 N68-14092 Unbiole ottitude determined in a simulated NASA-TM-X-1500 c31 N68-14092 Vehicle attitude determination with a single onboard camera NASA-TN-D-4359 c31 N68-19275 HENRY, C. J. Hydrodynamics of aircraft tire hydroplaning NASA-CR-1125 c12 N68-31593 HENRY, G. Procedures for estimating the effects of design and operational characteristics of jet aircraft on ground noise NASA-CR-1053 c02 N68-26930 HENRY, R. C. Wind-tunnel study to explore the use of slot spoilers to modulate the flap-induced lift of a wing NASA-TN-D-4664 c01 N68-28830 NASA-IN-D-4664 CO. HENRY, R. M. Wind velocity profiles measured by the smoke-trail method at Wallops Island, Virginia, 1963 and 1964 NASA-TN-D-4365 C2. c20 N68-17024 Wind data from the 250-foot /76.2-meter/ tower at Wallops Island, Virginia NASA-TN-D-4395 c20 N68-18246 Revised upper-air wind data for Wallops Island based on serially completed data for the years 1956 to 1964 NASA-TN-D-4570 c20 N68c20 N68-24028 HERMAN, J. R. Research on field-aligned propagation of HF radiowaves using Alouette 2 topside sounder data and digital ray-tracing techniques NASA-TN-D-4748 c07 N68c07 N68-31639 HERMANN, P. C. High performance structures NASA-CR-1038 c32 N68-23399 HERR, R. W. Experimental investigation of the use of soft side legs to improve touchdown stability of legged landing vehicles NASA-TN-D-4680 c31 N68c31 N68-29962 HERRING, H. J. A method of calculating compressible turbulent boundary layers NASA-CR-1144 c12 N68-35096 HERRON, C. R. Optimal computing forms for the two-body C and S series NASA-TN-D-4643 c19 N68-29407 HERSCH, M. Hydrogen-oxygen chemical reaction kinetics in rocket engine combustion NASA-TN-D-4250 c33 N68c33 N68-11642 Performance and stability characteristics of nitrogen tetroxide-hydrazine combustors c27 N68-35072 NASA-TN-D-4776 HESKETH, W. D. Effects of zinc concentration on output of zinc doped germanium detectors NASA-TN-D-4834 c26 N68-37055 HESTERMAN, V. W. Cryogenic magnetometer development Final

report, 1 Jul. 1964 - 7 Mar. 1967 NASA-CR-1073 c14 N68-26703 HETTEL, H. J. Correlation of transient spectra with performance in coaxial plasma guns NASA-TN-D-4385 c25 N68-17070 Enhancement of ion cyclotron waves in hydrogen helium mixtures NASA-TN-D-4271 c25 N68-18485 HEYDA, J. F. Plate-gap model of a porous solid and its application to impact by reduced density projectiles NASA-CR-1140 c32 N68-31912 HIBBARD, R. R. Theoretical temperatures of thin-film solar cells in earth orbit NASA-TN-D-4331 c33 N68 On the solubilities and rates of solution of c33 N68-14270 On the solubilities and rates of solution gases in liquid methane NASA-TN-D-4701 c27 M HICKAM, C. W., JR. Corrosion product of the tantalum interstitial oxygen potassium system at 1800 deg F /1255 deg K/ NASA-TN-D-4213 c17 M c27 N68-30077 c17 N68-11511 HICKEY, D. H. Large-scale wind-tunnel investigation of a model with an external jet-augmented flap NASA-TN-D-4278 c02 N6 c02 N68-11627 HICKS, R. M. Prediction of aircraft sonic boom characteristics from experimental near field results NASA-TM-X-1477 c02 N68-11772 HINKS, D. Frequency coded threshold logic unit for pattern recognition application NASA-CR-1035 c05 c05 N68-22448 HINTERKEUSER, E. G. Subjective response to synthesized flight noise signatures of several types of V/STOL aircraft NASA-CR-1118 c05 N68-33009 HINTON, D. E. Radiometric measurements of the earth*s infrared horizon from the X-15 in three spectral intervals NASA-TN-D-4654 c21 N68-28262 A celestial attitude measurement instrument for Project Scanner NASA-TN-D-4742 c21 N68-31938 Attitude determination of the spin-stabilized Project Scanner spacecraft NASA-TN-D-4740 c21 N68-31957 HIRSCH, R. Calculation of the turbulent boundary layer and of transition on a plane plate c12 N68-17563 NASA-TT-F-520 HO. B. Design of guidance and control systems for optimum utilization of information NASA-CR-997 c10 N68-23438 HODGKINS, R. L. Hydra 1 data display system NASA-TN-D-4554 c08 N68-25002 HOEINE, J. C. A study of turbofan-engine compressor noise suppression techniques NASA-CR-1056 c28 N68-26771 HOELKER, R. F. Numerical studies of transitions between the restricted problem of three bodies and the problem of two fixed centers and the Kepler problem NASA-TM-X-1465 c21 N68-11146 NASA-14-X-1465 HOENIE, A. F. Thermal and mechanical treatment for precipitation-hardening stainless steels NASA-SP-5089 c15 N68-20433 HOFFMAN, A. C. Development of a cobalt-tungsten ferromagnetic, high-temperature, structural alloy NASA-TN-D-4338 HOFFMAN, C. A. c17 N68-18145 Use of surface replication, extraction replication, and thin-film electron microscopy

I-137

in the study of dispersion-strengthened materials NASA-TN-D-4461 c17 N68-18999 HOFFMAN, E. E. Cb-1Zr sodium thermal convection loop NASA-CR-1097 c22 N68-35153 HOFFMAN, R. J. Combustion instability prediction using a nonlinear bipropellant vaporization model NASA-CR-920 c33 N68-15833 HOFFMAN, S. Forces and moments produced by air and helium jets exhausting parallel to a flat plate in a near vacuum NASA-TN-D-4408 c12 N68-19000 HDFMANN, L. G. New methods in adaptive flight control NASA-CR-1152 c21 N68-33904 HOGGE, J. E. Three ballistic camera data reduction methods applicable to reentry experiments NASA-TN-D-4260 c30 N68-11145 HOHL, F. 1L, F. Effects of axial gradients of velocity and magnetic field, electrode stagger, and ion slip on parameters in MHD accelerators NASA-TN-D-4239 c28 N68. c28 N68-10502 Gravitational experiments with a collisionless two-dimensional computer model NASA-TN-D-4646 c30 N68-28884 NASA-TN-D-4646 c30 NG Dynamics of a one-dimensional plasma sheath NASA-TN-D-4651 c25 NG Theory and results on collective and collisional effects for a one-dimensional self-gravitating system NASA-TR-R-289 c30 NG c25 N68-30031 c30 N68-32978 HOLESKI, D. E. Experimental performance evaluation of a 6.02-inch /15.29-cm/ radial-inflow turbine with an exit diffuser NASA-TM-X-1480 c03 N68-11920 Experimental performance of a 5-inch /13 cm/ axial-flow turbine over a range of Reynolds number NASA-TM-X-1679 c03 N68-37263 Experimental performance of a 5-inch single-stage axial-flow turbine designed for a Brayton cycle space power system NASA-TM-X-1666 c03 N68-37943 NASA-IN-A-1000 HOLLAND, J. A. A celestial attitude measurement instrument for Project Scanner NASA-TN-D-4742 c21 N6 c21 N68-31938 NASA-IN-D-4742
 C21 N08-5.
 HOLLOWAY, P. F.
 The orbital recovery problem. Part 1 - An analysis technique for rapid determination of return opportunities and lateral-range requirements for recall to recovery networks NASA-TR-R-259
 C21 N08-30 c21 N68-30126 HOLMS. A. G. Multiple decision procedures for ANDVA of two-level factorial fixed-effects replication-free experiments NASA-TN-D-4272 c19 N68-11639 HOLDWACH, J. Cb-12r sodium thermal convection loop C22 N68-35153 HONNOLD, V. R. Transistor design effects on radiation resistance NASA-CR-1167 c10 N68-33767 HOPKINS, A. S. Narrow band cross-correlation analysis of fluctuating pressures beneath a turbulent boundary layer NASA-CR-1066 c12 NG c12 N68-23482 NASA-UN 1995 HOPKINS, J. B. Characteristics of tunneling p-n junctions NASA-TN-D-4403 c09 N c09 N68-19062 NRDD IN J 110 HORDON, M. J. Mechanism of the atmospheric interaction with the fatigue of metals NASA-CR-1165 c17 N68-35200 NADATION - 1100 HORNE, W. B. Review of causes and alleviation of low tire traction on wet runways NASA-TN-D-4406 CO c02 N68-19620 HORONJEFF, R. D. The noisiness of tones plus noise

c05 N68-30602 NASA-CR-1117 HORVATH, J. J. Some meteorological observations of the Southern Hemisphere stratosphere and mesosphere c20 N68-25617 NASA-TN-D-4264 Temperature, pressure, density, and wind measurements in the stratosphere and mesosphere, 1966 NASA-TR-R-288 c20 c20 N68-33036 HOSENTHIEN, H. H. Development of a general formula expanding the higher-order derivatives of the function tanh z in powers of tanh z and A-numbers NASA-TN-D-4296 c19 N c19 N68-14077 HOTCHIN, J. The microbiological flora of the Gemini 9 spacecraft before and after flight spacecrait verors and the control of the hydrogen-oxygen c04 N68-11968 reaction NASA-TN-D-4685 c33 N68-30041 HOWARD, F. G. Single-thermocouple method for determining heat flux to a thermally thick wall NASA-TN-D-4737 c33 N68-33208 HOWE, R. M. Trajectory optimization by a direct descent process NASA-CR-1070 c30 N68-25902 HOWELL, D. T. Supersonic aerodynamics of large-angle cones NASA-TN-D-4719 c01 N68-31551 HOWELL, J. R. Boundary conditions for the diffusion solution of coupled conduction-radiation problems NASA-TN-D-4618 c33 N68-26759 Thermal radiation heat transfer. Volume 1 -The blackbody, electromagnetic theory, and material properties NASA-SP-164 c33 N68 c33 N68-28530 HOWELL, J. T. Visual simulation facility for evaluation of lunar surface roving vehicles NASA-TN-D-4276 c11 N68-15858 NASA-IN-D-4276 C11 HOWELL, R. H. Drag associated with separated flow over two-dimensional V-shaped notches under transonic and supersonic conditions NASA-CR-1132 c12 c12 N68-35252 HOWLETT, J. T. An analytical procedure for predicting the two-dimensional impact dynamics of spacecraft landing gear NASA-TN-D-4434 c31 N68-19085 HRACH, F. J. Uut of the ecliptic plane probe mission employing electric propulsion NASA-TN-D-4455 c24 c28 N68-19581 HRUBY. R. J. Tabulated communication characteristics of a steady-state model of interplanetary space NASA-SP-3042 c30 N68-10164 HSU, L.-C. Synthesis of ultrahigh molecular-weight poly/ethylene terrephthalate/ NASA-TN-D-4335 c06 N HSU, Y. Y. Mist-flow heat transfer using single-phase c06 N68-14093 variable-property approach NASA-TN-D-4149 Analysis of boiling on a fin c33 N68-11636 NASA-TN-D-4797 c33 N68-34088 HSU, Y.-W. J, Y.-W. Plane Stress analysis of an edge-stiffened rectangular plate, taking into account bending and shear stiffness of the stiffeners NASA-CR-978 c32 N68-19 c32 N68-19311 HU, P. Plasma boundary interactions - 2 NASA-CR-1072 c25 N68-25821 HUANG, H.-Y. Conical bodies of given length and volume having maximum lift—to—drag ratio at hypersonic speeds. Variational methods NASA-CR-1156 c01 N68-33451

JEX, H. R.

HUCK, F. O. A lighting strategy for Lunar Orbiter mission design NASA-TN-D-4501 c14 N68-21942 HUCKINS, E. K., III Performance of a 19.7 meter diameter disk gap band parachute in a simulated Martian environment NASA-TM-X-1499 c31 N68-13797 HUDSON, W. R. Low-temperature resistance minimum and magnetoresistance for dilute alloys of iron in copper NASA-TN-D-4626 c26 N68-28239 HUFF, R. G. Determination of convective heat-transfer coefficients on adiabatic walls using a sinusoidally forced fluid temperature NASA-TM-X-1594 c33 N68-24618 NASA-TN-X-1594 C33 N68-24(HUFFMAN, J. K. Heat transfer and pressure distributions on spherically blunted 25 deg half-angle come at Mach 8 and angles of attack up to 90 deg NASA-TN-D-4792 c01 N68-354 c01 N68-35497 HUGHES. J. E. Aerodynamic stability characteristics of the Apollo command module NASA-TN-D-4688 c01 N68-31445 NASA-IN-D-468 CUI N65-HUGHES, T. F. A quasi-steady state analysis of the dynamic behavior of a conic body moving in a nonuniform wake NASA-TN-D-4691 C31 N68c31 N68-30032 HUMENIK, F. M. Dilution-jet mixing study for gas-turbine combustors NASA-TN-D-4695 c01 N6 HUNCZAK, H. R. Preliminary tests of a single-axis ammoniac01 N68-30128 resistojet attitude control system NASA-TM-X-1677 c28 N68-36512 HUNT, J. L. Effects of several ramp-fairing, umbilical, and pad configurations on derodynamic heating to Apollo command module at Mach 8 NASA-TM-X-1640 c01 N68-35141 HUNTER, P. A. An analysis of VGH data from one type of four-engine turbojet transport airplane during commercial operations NASA-TN-D-4330 c02 | c02 N68-16522 Summary of VGH data collected on one type of twin-engine jet airplane during airline operations NASA-TN-D-4529 c02 N68-22291 NASA-IN-D-4565 C02 N HUNTER, W. W., JR. Investigation of temperature measurements in 300 deg to 1100 deg K low-density air using an electron beam probe NASA-TN-D-4500 c14 N c14 N68-24244 HURT, G. J., JR. Analysis of human response in combined control tasks NASA-TN-D-4356 c05 N68-18014 HURWITZ, M. G. Error probabilities for maximum likelihood detection of M-ary Poisson processes in Poisson noise NASA-TN-D-4721 c07 N68-36105 Mathematical determination of geometrical image aberrations in single and double mirror systems NASA-TN-D-4692 c23 N68-36460 MASA-IN-D-4692 c23 NOS-HYETT, B. J. Calculations of Chandrasekhar*s X and Y functions and their analogs for noncoherent isotropic scattering NASA-TN-D-4712 c19 N68-30804 1

IGOE. W. B.

Reduction of wind-tunnel-model vibration by means of a tuned damped vibration absorber installed in the model NASA-TM-X-1606 c32 N68-28806 INGRAM, A. G. Effects of low temperatures on the mechanical properties of structural metals

NASA-SP-5012/01/ c17 N68-31605 INYANITOV, I. N. Electricity of the free atmosphere NASA-TT-F-425 c13 N68-10079 INGEBO, R. D. Maximum drop diameters for the atomization of liquid jets injected concurrently into accelerating or decelerating gas streams NASA-TN-D-4640 c12 M c12 N68-28364 INMAN, R. M. Analysis of turbulent liquid-metal heat transfer in channels with heat sources in the fluid power-law velocity profile c33 N68-14042 NASA-TN-D-4336 INCUYE, M. Comparison of experimental and theoretical shock shapes and pressure distributions on flat-faced cylinders at Mach 10.5 c01 N68-15778 NASA-TN-D-4397

J

JACHIMOWSKI, C. J. Effect of carbon dioxide and water vapor on the induction period of the hydrogen-oxygen NASA-TN-D-4685 c33 N68-30041 JACK. J. R. Experimental measurements of thermal radiation properties by cyclic incident radiation NASA-TM-X-1618 c33 | c33 N68-31498 Thermal radiative and electrical properties of a cadmium sulfide solar cell at low solar of a cadmium suifide solar cell at low s intensities and temperatures NASA-TN-D-4818 c03 M JACKSON, C. T., JR. A piloted simulator study of takeoff performance and handling qualities of a double delta supersonic transport c03 N68-35467 NASA-TN-D-4396 JACOBS, W. R. c02 N68-17391 Hydrodynamics of aircraft tire hydroplaning NASA-CR-1125 c12 N68-31593 JAIN, D. C. Quantum mechanical study of molecules transition probabilities, Einstein A coefficients and oscillator strengths of some band systems of diatomic molecules NASA-CR-975 c24 N68-11037 NASA-CK-975 C24 JALINK, A., JR. Radiometric measurements of the earth*s infrared horizon from the X-15 in three spectral intervals NASA-TN-D-4654 c21 N68-28262 NASA-IN-D-4004 JANOS, J. J. Forces and moments produced by air and helium jets exhausting parallel to a flat plate in a near vacuum C12 N68-19 NASA-TN-D-4408 c12 N68-19000 JECH. R. W. The effect of interfiber distance and temperature on the critical aspect ratio in composites NASA-TN-D-4548 c17 N68-22338 JEFFERIES, K. S. Experimental investigation of reactor-loop transients during startup of a simulated SNAP-8 system NASA-TN-D-4546 c03 N68-22257 JENKINS, R. S. A piezoelectric transducer for measuring cardiac and gross motor activity of small organisms NASA-TN-D-4590 c05 N68-25060 JERKE, J. M. The geometric properties of an expandable whirling-membrane solar-energy concentrator NASA-TN-D-4532 c03 N68-22258 JERNELL, L. S. Aerodynamic characteristics of bodies of revolution at Mach numbers from 1.50 to 2.86 and angles of attack to 180 deg NASA-TM-X-1658 c01 N68-36193 JEX, H. R. An experimental investigation of compensatory and pursuit tracking displays with rate and acceleration control dynamics and a disturbance input c07 N68-28272 NASA-CR-1082

JHA, S.

PERSONAL AUTHOR INDEX

A study of fully manual and augmented manual control systems for the Saturn 5 booster using analytical pilot models NASA-CR-1079 c31 N68 c31 N68-28426 JHA. , S. Excited states of xenon 128 NASA-TN-D-4305 c24 N68-15328 JIUSTO, J. E. Investigation of warm fog properties and fog modification concepts NASA-CR-1071 c20 N68-25816 JOHNS, A. L. Cold flow investigation of a low angle turbojet plug nozzle with fixed throat and translating shroud at Mach numbers from 0 to 2.0 NASA-TM-X-1619 c28 N68-29953 JOHNSEN, I. A. M-1 injector development - Philosophy and implementation NASA-TN-D-4730 c28 N68 JOHNSON, B. V. Exploratory flow and containment experiments c28 N68-30604 pioratory flow and containment experiments in a directed-wall-jet vortex tube with radial outflow and moderate superimposed axial flows Fifth interim summary technical report, Sep. 15, 1965 - May 30, 1967 NASA-CR-992 c22 N68-171: c22 N68-17131 Containment experiments in vortex tubes with radial outflow and large superimposed axial flows NASA-CR-993 c22 N68-18243 Experimental study of multi-component coaxial-flow jets in short chambers NASA-CR-1190 c22 N68-3 c22 N68-36615 JOHNSON, C. B. Pressure and flow field study at Mach number 8 of flow separation on a flat plate with deflected trailing edge flap NASA-TN-D-4308 c12 N68-17376 JOHNSON, C. R. Heat treatment for improved stress-corrosion resistance of 17-7 pH stainless steel NASA-TN-D-4673 c17 N68 c17 N68-29379 JOHNSON, E. G. Teleoperators and human augmentation. An AEC-NASA technology survey NASA-SP-5047 c05 i c05 N68-18870 Midcourse-guidance procedure with single position fix obtained from onboard optical measurements NASA-TN-D-4246 c21 N68-11521 JOHNSON, R. C. Performance of a venturi meter with separable diffuser NASA-TM-X-1570 c14 N68-21384 JOHNSON, R. E. Effects of freezing on primary silver oxide zinc cells NASA-TM-X-1681 c03 N6 c03 N68-37265 JOHNSON, R. L. Wear rate and friction coefficient in liquid nitrogen and hydrogen of steel sliding on polymer laminates /various fabrics and polymers/ NASA-TN-D-4463 c15 N68-20325 Investigation of the use of the lunar surface layer to store energy for generating power during the lunar night NASA-TM-X-1560 c03 N68c03 N68-20363 Friction and wear in cryogenic liquids for composites of phenolic and of polytetrafluoroethylene of various particle izes and concentrations NASA-TN-D-4565 c15 N68-24142 Preliminary evaluation of greases to 316 deg C and solid lubricants to 816 deg C in ball bearings NASA-TN-D-4652 c15 N68-28766 Friction and wear under fretting conditions of materials for use as wire friction dampers of compressor blade vibration NASA-TN-D-4630 c15 N68-2 JOHNSON, W. A. Pilot dynamic response to sudden flight control system failures and implications for c15 N68-28871 design NASA-CR-1087 c05 N68-26690

A study of fully manual and augmented manual control systems for the Saturn 5 booster using analytical pilot models NASA-CR-1079 c31 N c31 N68-28426 JOHNSON, W. R. Analytical investigation of thermal degradation of high-performance multilayer insulation in the vicinity of a penetration NASA-TN-D-4778 c33 N68-3 c33 N68-33167 JOHNSTON, A. S. Excited states of xenon 128 NASA-TN-D-4305 c24 N68-15328 JOHNSTON, J. R. Effect of cover gas pressures on accelerated cavitation damage in sodium NASA-TN-D-4235 c17 N68-10104 JOHNSTON, P. J. Experimental stability and control results at Mach 19 of an entry vehicle designed for an intermediate lift-drag ratio NASA-TN-D-4337 c31 N68-16240 JOLKOVSKI, R. M. Space technology transfer and developing nations NASA-CR-1222 c34 N68-37216 JONES, F. C. An autocorrelation approach to the Brown Twiss interferometer NASA-TN-D-4480 c14 c14 N68-25518 JONES, G. E. Microwave spectroscopy of molecules -Bibliography, 1964-1966 NASA-CR-951 c23 N68-10674 JONES, J. E. The aperature admittance of a ground plane mounted waveguide illuminating a perfectly conducting sheet NASA-TN-D-4366 c07 N68-18123 JONES, J. R. Performance of a wind tunnel model of an aerodynamically positioned variable flap ejector at Mach numbers from 0 to 2.0 c28 N68-30599 NASA-TM-X-1639 Static performance of an auxiliary inlet ejector nozzle for supersonic-cruise aircraft NASA-TM-X-1653 c28 N68-35 c28 N68-35764 Application of statistical association techniques for the NASA document collection NASA-CR-1020 c08 N68-: c08 N68-17154 c01 N68-35141 NASA-IM-X-1640 Heat transfer and pressure distributions on spherically blunted 25 deg half-angle cone at Mach 8 and angles of attack up to 90 deg NASA-TN-D-4792 CO1 N68-350 c01 N68-35497 JOPPA, R. G. The effect of the converging flow field of a tandem test section on longitudinal stability measurements c11 N68-36 NASA-CR-1198 c11 N68-36522 JOSLYN, A. W. Boiling heat transfer coefficients, interface behavior, and vapor quality in rotating boiler operating to 475 G*s C33 N68-NASA-TN-D-4136 c33 N68-17566 JOYNER, U. T. Effects of pavement texture on wet-runway braking performance NASA-TN-D-4323 c02 N68-14903 JUDD. J. H. Free-flight aerodynamic characteristics of a slender cone between Mach numbers of 7 and 8 NASA-TN-D-4245 col N68-10380 JULIAN, G. M. Excited states of xenon 128 NASA-TN-D-4305 c24 N68-15328 JULIANO, C. V. Discrimination of increases in the brightness of a flashing beacon NASA-CR-1220 c05 N68-3 JULIUS, A. L., JR. Calculations of solar plasma interaction with magnetic field of current loop and two parallel infinite lines of current c05 N68-37819 NASA-TN-D-4304 c29 N68-19188

K

KAATTARI, G. E. A method for predicting shock shapes and pressure distributions for a wide variety of blunt bodies at zero angle of attack c01 N68-21941 NASA-TN-D-4539 KAHN. D. Ny D. Attenuation and dispersion of longitudinal waves in viscous, partly ionized gases NA≪A-TM-X-1458 c07 N68-18703 KALAFUS, R. M. Electromagnetism in moving, conducting media NASA-CR-1025 c23 N68 c23 N68-21444 KALIKSTEIN, K. Application of dust for space structures NASA-CR-1136 c32 c32 N68-32976 KALIL, F. Optical and microwave communications - A comparison NASA-TN-D-3984 c07 N68-22019 KAMPER, R. A. Superconduction thin films NASA-CR-1189 c26 N68-35178 KAMPOS, B. Guidance, flight mechanics and trajectory optimization. Volume 9 - General perturbations theory NASA-CR-1008 c30 N68-20450 KANTARGES, G. T. The shock expansion tube and its application as a sonic boom simulator NASA-CR-1055 c11 N68-24966 KARP, I. M. MCFLARE, a Monte Carlo code to simulate solar flare events and estimate probable doses encountered on interplanetary missions NASA-TN-D-4311 c29 N68-16008 KARP, S. M-ary Poisson detection and optical communications NASA-TN-D-4623 c07 N68-29528 The design of a Pulse Position Modulated /PPM/ optical communication system NASA-TN-D-4814 c07 c07 N68-35174 Error probabilities for maximum likelihood detection of M-ary Poisson processes in Poisson noise NASA-TN-D-4721 c07 N68-36105 KARRAS, T. J. Theoretical and practical resolution limits for processing pulse frequency modulation telemetry NASA-TN-D-4180 c07 N68-18247 Dual detection system for AIMP PFM data processing NASA-TN-D-4561 c08 N68-24310 KASCAK, A. F. Feasibility of supporting liquid fuel on a solid wall in a radiating liquid-core nuclear rocket concept NASA-TN-D-4413 c27 N Effect of turbulent mixing on average fuel c27 N68-17093 temperatures in a gas-core nuclear rocket engine NASA-TN-D-4882 c22 N68-37927 KASHIWAGI, Y. Time-optimal rendezvous for elliptic orbits NASA-CR-1036 c30 N64 c30 N68-22202 KASKEL, A. L. Inviscid flow field induced by a rotor in ground effect NASA-CR-1027 coll c01 N68-22475 KASPER. H. J. Analytical and experimental investigation of outflow residuals in interconnected spherical tanks NASA-TN-D-4828 c12 N68-35104 KATCHEN, L. B. Temperature, pressure, density, and wind measurements in the stratosphere and mesosphere, 1966 NASA-TR-R-288 c20 N68-33036 KATSANIS, T. Computer program for calculating velocities and streamlines on a blade-to-blade stream surface of a turbomachine NASA-TN-D-4525 c01 N68-21374

KAYKATY, G. N. Analysis of the maximum performance of a paraboloidal solar collection system for space power NASA-TN-D-4415 c03 N68-18998 Analysis and selection of design conditions for a radioisotope Brayton-cycle space powerplant NASA-TN-D-4600 c03 N68-KEATING, J. C. Attitude determination of the spin-stabilized c03 N68-25829 Project Scanner spacecraft NASA-TN-D-4740 c21 N68-31957 KEITH, R. E. Adhesive bonding of stainless steels including precipitation-hardening stainless steels NASA-SP-5085 c15 N68-2 c15 N68-20056 KELLEY, G. F. Optimum maneuvers of hypervelocity vehicles NASA-CR-1078 c02 N68-25817 KELLY, D. H. Research study of a fundus tracker for experiments in stabilized vision NASA-CR-1121 c c05 N68-35109 KELLY, H. N. Free-flight and wind-tunnel studies of deployment of a dynamically and elastically scaled inflatable parawing model NASA-TN-D-4724 c02 N68-33879 KELLY, J. R. Flight investigation to determine the effect of longitudinal characteristics on low-speed instrument operation NASA-TN-D-4624 NASA-TN-D-4624 CO2 N68-CO2 c02 N68-19184 c02 N68-28153 KEMPER, J. T. Equilibrium normal-shock and stagnation-point properties of helium for incident-shock Mach numbers from 1 to 30 NASA-TN-D-4754 cl2 N68-3 c12 N68-35117 A digital computer program for calculating the performance of single or multiple diaphragm shock tubes for arbitrary equilibrium real gas mixtures NASA-TN-D-4802 c11 N68-35466 KENDALL, J. S. Containment experiments in vortex tubes with radial outflow and large superimposed axial flows NASA-CR-993 c22 N68-18243 Experimental investigation of containment in constant-temperature radial-inflow vortexes NASA-CR-1029 c12 N68-22200 ABA-CR-1025 Cr KENDALL, R. M. An analysis of the coupled chemically reacting boundary layer and charring ablator, part 1 Summary report NASA-CR-1060 cr c33 N68-25244 An analysis of the coupled chemically reacting boundary layer and charring ablator. Part 3 - Nonsimilar solution of the multicomponent laminar boundary layer by an integral matrix method NASA-CR-1062 c33 N68-26641 An analysis of the coupled chemically reacting boundary layer and charring ablator. Part 4 -A unified approximation for mixture transport properties for multicomponent boundary-layer applications NASA-CR-1063 c33 N68-26815 An analysis of the coupled chemically reacting boundary layer and charring ablator. Part 5 – A general approach to the thermochemical solution of mixed equilibrium-nonequilibrium, homogeneous or heterogeneous systems Nach-CD-1064 NASA-CR-1064 c KENG, E. Y. H. Investigation of radiant heat transfer c33 N68-26816 to particle-seeded gases for application to nuclear rocket engine design NASA-CR-953 c22 N68-10561 NABA-CA-500 KENIMER, R. L. Analysis of a star-field mapping technique for use in determining the attitude of a spin-stablized spacecraft C21 N NASA-TN-D-4637 c21 N68-28418

KENNEDY, J. S.

KENNEDY, J. S. An evaluation of sea surface temperature as neasured by the Nimbus 1 high resolution infrared radiometer NASA-TN-D-4078 c20 No c20 N68-10222 REANEN, T. W. Research and development of a vortex valve for flow modulation of a 16-percent aluminized 5500 deg F propellant gas NASA-CR-1091 c28 N68-23 c28 N68-28112 KERR, D. R. Investigation of refractory dielectrics for integrated circuits NASA-CR-995 c18 N64 c18 N68-18849 KERWIN, P. T. Analysis and selection of design conditions for a radioisotope Brayton-cycle space powerplant NASA-TN-D-4600 c03 N68-25829 KESTER, F. L. A study of aircraft fire hazards related to natural electrical phenomena Final report, Jun. 1966 - Jul. 1967 NASA-CR-1076 c02 N68-26691 KETNER, D. N. A high enthalpy plasma generator for entry heating simulation NASA-TN-D-4583 c11 N c11 N68-24560 KIM. O. K. The dielectric clad axial slot antenna c07 N68-26621 NASA-CR-1057 KIMZEY, J. H. Flammable and toxic materials in the oxygen atmosphere of manned spacecraft NASA-TN-D-3415 c05 N68-24756 KING, R. B. Polymer-film coating of magnesium for paraboloidal mirrors NASA-TN-D-4734 c18 N68-30597 KIRK, J. V. Large-scale wind-tunnel investigation of a model with an external jet-augmented flap NASA-TN-D-4278 KITTLE, J. W. c02 N68-11627 Dynamic stability of space vehicles. Volume 6 - Full scale dynamic testing for mode determination NASA-CR-940 c32 N68-11054 KLAHR, C. N. Application of dust for space structures NASA-CR-1136 c32 c32 N68-32976 KLANN, J. L. Analysis and selection of design conditions for a radicisotope Brayton-cycle space powerplant NASA-TN-D-4600 c03 N68-25829 KLANN. P. G. Comparison of absolute calculated and measured gamma and neutron doses in tungsten-water moderated critical assembly NASA-TN-D-4223 c22 N68-10291 KLASSEN, H. A. Performance in air of 4 inch /10.16-cm/ mean-diameter single stage axial-flow turbine for Reynolds numbers from 4,900 to 188,000 NASA-TN-D-4383 Cold-air investigation of effects of partial admission on performance of 3.75-inch mean-diameter single stage axial-flow turbine NASA-TN-D-4700 c03 N68-30241 Use of an electronic visualization technique in the study of gas journal bearing behavion NASA-TM-X-1609 c14 N68-35105 KLEINMAN, D. L. The human as an optimal controller and information processor NASA-CR-1151 c c05 N68-33304 KLIMA, S. J. Fatigue of liquid rocket engine metals at cryogenic temperatures to minus 452 deg F /4 deg K/ NASA-TN-D-4274 c17 N68-11637 Ultrasonic detection and measurement of fatigue cracks in notched specimens NASA-TN-D-4782 c32 N68-35071 KLINE, J. F. Scale model study of flow patterns in the inlet manifold of the fuel pump drive turbine for the M-1 hydrogen-oxygen rocket engine

PERSONAL AUTHOR INDEX

c12 N68-15639

NASA-TM-X-1513 Cold-air performance evaluation of scale model oxidizer pump-drive turbine for the M-1 hydrogen-oxygen rocket engine. 3 -Performance of first stage with inlet-feedpipe-manifold assembly NASA-TN-D-4392 c28 N68-1 Cold-air performance evaluation of scale model c28 N68-16413 oxidizer pump-drive turbine for the M-1 hydrogen-oxygen rocket engine. 4 -Performance of first stage with modified inlet feedpipe-manifold assembly NASA-TN-D-4393 c28 N68-18188 KLOPP, W. D. Ductility mechanisms and superplasticity in chromium alloys NASA-TN-D-4346 c14 N68-13973 Superplasticity in tungsten-rhenium alloys NASA-TN-D-4728 c17 N68-30605 KNAPP, H. Lie series for celestial mechanics, accelerators, satellite stabilization and optimization NASA-CR-1046 c19 N68-25841 KNIGHTON, M. H. Visual simulation facility for evaluation of lunar surface roving vehicles NASA-TN-D-4276 c11 N68-15858 KNOP, C. M. A quasi-omnidirectional slot array antenna for spacecraft use at microwave frequencies NASA-TN-D-4362 c07 c07 N68-18616 The dielectric clad axial slot antenna NASA-CR-1057 c c07 N68-26621 KNOTTS, E. F. Guidance, flight mechanics and trajectory optimization. Volume 14 - Entry guidance equations NASA-CR-1013 c30 N68-19985 KOBBEN, L. The use of the electron probe microanalyzer in materials research and development NASA-TN-D-4526 KOCMOND, W. C. Investigation of warm fog properties and fog c15 N68-28249 modification concepts NASA-CR-1071 c20 N68-25816 KUCZELA, L. J. Study of spaceborne multiprocessing, phase 2. Volume 1 - Summary c08 N68-31499 NASA-CR-1158 Study of spaceborne multiprocessing - Pha Volume 2 - Technical description Final Phase 2 report NASA-CR-1159 c08 N68~35560 KOENIG, D. G. Aerodynamic characteristics of a large-scale model with unswept wing and augmented jet flap NASA-TN-D-4610 c01 N68-259 c01 N68-25919 KOFSKEY. M. G. Performance evaluation of a two stage axial-flow turbine for two values of tip clearance NASA-TN-D-4388 c03 N68-14639 Aerodynamic evaluation of two-stage axial flow turbine designed for Brayton-cycle space power system NASA-TN-D-4382 c03 N68-16469 NASA-IN-D-4382 cub Experimental performance evaluation of an 8.5 inch /21.59 cm/ mean-diameter axial flow turbine at Reynolds numbers from 18,000 to 177,000 NASA-TN-D-4432 c03 c03 N68-18501 Aerodynamic performance of a 4.59-inch modified radial-inflow turbine for a single-shaft Brayton cycle space power system NASA-TM-X-1615 c03 N68~28870 KOLAR, M. J. High power kinetics of a two dimensional circulating liquid metal fuel reactor NASA-TN-D-4840 c2 c22 N68-36055 KORST, H. H. Drag associated with separated flow over two-dimensional V-shaped notches under transonic and supersonic conditions NASA-CR-1132 c12 N68-35252 KOVALEVSKY, L. Shell analysis manual

-

NASA-CR-912 c32 N68-24802 KOZIOL, J. S., JR. On electromagnetic switching properties of a bi-stable fluidic element with non-destructive memory NASA-TM-X-1613 c09 N68-30501 KRAPE, R. P. Applications study of electroadhesive devices NASA-CR-1211 c10 N68-37906 KRAUSE, L. N. Preliminary tests with mass flux probe in supersonic stream NASA-TM-X-1524 c14 N68-18834 Performance of a venturi meter with separable diffuser NASA-TH-X-1570 c14 N68-21384 A small combination sensing probe for measurement of temperature, pressure, and flow direction NASA-TN-D-4816 c14 N68-36021 KRAWEC, R. Enhancement of ion cyclotron waves in hydrogen helium mixtures NASA-TN-D-4271 c25 N68-18485 General operating characteristics of a back streaming direct-current plasma generator NASA-TN-D-4604 c25 NG c25 N68-25877 KREINS, E. R. A satellite view of Typhoon Marie 1966 development NASA-TN-D-4757 c20 N68-37869 KREJSA, E. A. Model for frequency response of a forced flow, hollow, single tube boiler NASA-TM-X-1528 cl2 N68-1 c12 N68-19340 KROHN, C. A. Practical reliability. Volume 4 -Prediction NASA-CR-1129 c15 N68-31979 KRUEGER, V. Criteria for selection of wire insulations for use in space applications NASA-TN-D-4553 c18 N68-2 c18 N68-28264 KRUGER, B. Effects of correlated noise with applications to Apollo tracking problems NASA-TN-D-4121 c10 N68-16749 KRUSE, R. L. Transition and flow reattachment behind an Apollo-like body at Mach numbers to 9 NASA-TN-D-4645 c01 N68-28220 KRUSTINS, J. A precision spacecraft radiometer for hectometer wavelengths NASA-TN-D-4634 c14 N68-28327 KRYTER, K. D. A preliminary study of the awakening and startle effects of simulated sonic booms NASA-CR-1193 c04 N c04 N68-33005 KUCHTA, B. J. Dynamic stability of space vehicles. Volume 12 - Re-entry vehicle landing ability and Volume control NASA-CR-946 c31 N68-24945 KUERS, G. The interpretation of daytime measurements by the Nimbus 1 and 2 high resolution infrared radiometers NASA-TN-D-4552 c14 N68-25862 KUESER, P. E. Properties of magnetic materials for use in high-temperature space power systems NASA-SP-3043 c17 c17 N68-17624 KULINSKI, E. S. A critical evaluation of the status and trends in high speed fluid film lubrication NASA-CR-1058 c15 N68-2 c15 N68-22810 KUMMER, W. H. Study of advanced antenna techniques for rendezvous radar NASA-CR-764 c07 c07 N68-28135 KUNZ. H. R. Vapor chamber fin studies. Operating characteristics of fin models NASA-CR-1139 c33 N68-33203 KUNZELMAN, R. C. Study and applications of retrodirective and self adaptive electromagnetic-wave phase controls to a Mars probe

LAMPKIN, B. A.

c21 N68-18484

KURKOWSKI, R. L. Saturn 5 manual backup guidance and control piloted simulation study NASA-TN-D-4481 c21 N68-19061 L LA BUDDE, C. D. Quantum mechanical study of molecules -Eigenvalues and eigenvectors of real symmetric matrices NASA-CR-983 c24 N68-11903 LABUS, T. L. Liquid reorientation in spheres by means of low-G accelerations NASA-TM-X-1659 c12 N68-35114 LACOVIC, R. F. Experimental investigation of vapor ingestion in the Centaur liquid hydrogen tank NASA-TM-X-1482 c12 N68-1: Capillary rise in the annular region of concentric cylinders during coast periods of Atlas Centaur flights c12 N68-2: NASA-TM-X-1558 c12 N68-2: c12 N68-19225 c12 N68-23353 Management of cryogenic propellants in a full scale orbiting space vehicle NASA-TN-D-4571 c28 N68c28 N68-25099 NASA-IN-U-4071 LAHSER, H. F. Visual simulation facility for evaluation of lunar surface roving vehicles NASA-TN-D-4276 cll N68 c11 N68-15858 LAHTI. G. P. MCFLARE, a Monte Carlo code to simulate solar flare events and estimate probable doses encountered on interplanetary missions c29 N68-16008 NASA-TN-D-4311 Preliminary considerations for fast-spectrum, liquid-metal cooled nuclear reactor program for space-power applications NASA-TN-D-4315 c22 N68-18197 Fission neutron attenuation in lithium-6, natural lithium hydride, and tungsten NASA-TN-D-4684 c24 c24 N68-30001 Comparison of small water-graphite nuclear rocket stages with chemical upper stages for unmanned missions NASA-TN-D-4827 c22 LAKSHMIKANTHAM, C. Structural design synthesis approach to c22 N68-35073 filamentary composites NASA-CR-964 c32 N68-11191 Minimum weight design aspects of stiffened cylinders under compression NASA-CR-963 c32 N68-11282 LALLI, V. R. Electrical stress analysis of a microthruster power conditioner NASA-TM-X-1686 c09 N68-37944 LAMAR, J. E. A theoretical study of the effect of pivot location on the aerodynamic-center movement of variable-sweep wings in incompressible flow NASA-TN-D-4635 c01 N68-28817 modified Multhopp approach for predicting A modified Multhopp approach for predicting lifting pressures and camber shape for composite planforms in subsonic flow NASA-TN-D-4427 coll N68-A modified multihopp approach for predicting lifting pressures and camber shape for composite planforms in subsonic flow NASA-TN-D-4427, SUP. coll N68-MB. Ma c01 N68-28868 c01 N68-31515 LAMB, M. Aerodynamic characteristics in pitch of a modified half ring wing body combination and a swept wing body combination at Mach 2.16 to 3.70 NASA-TM-X-1551 col Net c01 N68-21940 LAMBERTI, J. M. Design and preliminary operation of the Lewis magnetohydrodynamic generator facility NASA-TN-D-4867 c11 N68-37259

NASA-CR-977

Shaping of precipitation-hardening stainless steels by casting and powder-metallurgy NASA-SP-5086 c15 N68-19307

KURA. J. G.

LAMPKIN, B. A. Navigator performance using a hand-held

sextant to measure the angle between a moving flashing light and a simulated star NASA-TN-D-4174 c21 N68-13558 A hand-held sextant qualified for space flight NASA-TN-D-4585 c21 N68-24512 LAMPKIN, E. C. The effect of some telescope factors on variability of performance in sextant sighting NASA-TN-D-4781 c21 N68-330 c21 N68-33006 The effects of irradiation and star magnitude on sextant sighting performance on sextant signting performance NASA-TN-D-4780 c21 LANCASHIRE, R. B. Study of plasma diagnostics using laser interferometry with emphasis on its application to cesium plasmas c21 N68-33456 NASA-TM-X-1652 c16 N68-35593 LANCASTER, E. R. Optimal computing forms for the two-body C and S series NASA-TN-D-4643 c19 N68-29407 LAND, N. S. Experimental study of aeroelastic instability of overexpanded rocket nozzle extensions NASA-TN-D-4471 c32 N68-3 c32 N68-21099 LANDRUM, E. J. Effect of shape changes on the aerodynamic characteristics of a twisted and cambered arrow wing at Mach number 2.03 NASA-TN-D-4796 c01 N6 c01 N68-35665 LANE, D. H. Properties of magnetic materials for use in high-temperature space power systems NASA-SP-3043 c17 c17 N68-17624 LANTZ. E. Small high-temperature nuclear reactors for space power NASA-TN-D-4371 c22 N68-15792 NASA-IN-D-4371 Preliminary considerations for fast-spectrum, liquid-metal cooled nuclear reactor program for space-power applications NASA-IN-D-4315 Nuclear thermionic space power system concept c22 N68-18197 Nuclear thermionic space power system concept employing heat pipes NASA-TN-D-4299 c22 N68-Reactivity control of fast-spectrum reactors by reversible hydriding of yttrium zones NASA-TN-D-4615 c22 N68c22 N68-19146 c22 N68-24559 LANZO, C. D. A coaxial-flow-stabilized arc NASA-TN-D-4517 c25 N68-20296 Measurement of the transmissivity of a carbon-particle-seeded nitrogen jet NASA-TN-D-4722 c2 c23 N68-30596 LARK, R. F. Cryogenic positive expulsion bladders NASA-TM-X-1555 c18 N68-20329 ARMIE, F. M. A simple laboratory method for reduction of rhythm and rate in large-scale monitoring of electrocardiogram CO5 N68-32 NASA-TN-D-4751 c05 N68-32100 LARSON, R. Design of guidance and control systems for optimum utilization of information NASA-CR-997 c10 N68-23438 LASAGNA, P. L. Preliminary measured and predicted XB-70 engine noise NASA-TM-X-1565 c02 N68-21834 LASSITER, W. S. Striking characteristics of the magnetron ionization gage in helium from 1.9 times 10 to the minus 7 torr to 7 times 10 to the minus 10 torr NASA-TN-D-4681 c14 N68-29951 LATHEM, W. C. Divergent-flow contact-ionization electrostatic thrustor for satellite attitude control and station keeping NASA-TN-D-4420 c28 N68-20187 LAVAN, Z. Analytical investigation of incompressible turbulent swirling flow in pipes NASA-CR-1169 c12 N68-36343 LAVI. R. Full-scale ground proximity investigation of a VTOL fighter model aircraft NASA-CR-1098 c02 N68-2 c02 N68-28233

LAWRENCE, J. Characteristics of a variable spaced planar thermionic converter with a tungsten emitter and a niobium collector NASA-CR-1033 c03 N68-23476 LAWRENCE, T. R. Survey of CO sub 2 laser development for space applications NASA-TN-D-4794 c16 N68-35175 LE DOUX, F. N. Clean-room facilities for Explorer 35 spacecraft NASA-TN-D-4577 c11 N68-28311 LEA, W. A. Some arguments favoring non-conventional types of computers NASA-TM-X-1544 c08 N68-19336 J. G. K. Phase and group refractive indices from the collisionless magnetoionic theory NASA-TM-X-1553 cl3 NG. LEE. c13 N68-21904 LEE. R. Procedures for estimating the effects of design and operational characteristics of jet aesign and operational characteristics of aircraft on ground noise NASA-CR-1053 c02 i LELAND, T. J. W. Effects of pavement texture on wet-runway braking performance NASA-TN-D-4323 c02 i c02 N68-26930 c02 N68-14903 LENHERR, F. K. Analysis of geometry and design point performance of axial flow turbines. 1 -Development of the analysis method and the loss coefficient correlation NASA-CR-1181 c28 N68-35101 LEDNARD, R. F. Scattering of 42-MeV /6.7-pJ/ alpha particles from even isotopes of cadmium NASA-TN-D-4256 c24 i c24 N68-11074 Gamma ray angular correlations following inelastic scattering of 42-MeV alpha particles from magnesium 24 NASA-TN-D-4683 c24 N68-29375 LESCO, D. J. Flight evaluation of an electrostatic accelerometer for measurement of low-level orbital accelerations NASA-TM-X-1488 c14 N68-13974 Analog computer simulation of a dc arc emission spectrometer control system to define requirements for optimum control NASA-TN-D-4770 c08 N68-32055 LESSOFF, H. Low drive temperature stable memory cores NASA-TN-D-4573 c09 c09 N68-24388 LEVERTON, J. W. Helicopter noise - A blade slap. Part 1 -Review and theoretical study NASA-CR-1221 co2 N c02 N68-37932 LEVIN, A. D. An analytical investigation of the aerodynamic and performance characteristics of an unpowered rotor entry vehicle NASA-TN-D-4537 c31 N68-21758 LEVINE, S. H. A study of an electric field measuring instrument NASA-CR-970 c14 N68-25903 LEVINSKY, E. S. Nonlinear lift and pressure distribution of slender conical bodies with strakes at low speeds NASA-CR-1202 c01 N68-37255 LEVY, A. J. An annular lithium-drifted germanium detector for studying nuclear reaction gamma-ray NASA-CR-1138 c14 l c14 N68-35152 NASA-UK-1130 LEWIS, G. W. Use of wire lacing to reduce blade vibration in an axial-flow compressor rotor NASA-TM-X-1603 LIBBEY, C. E. c32 N68-28238 Wind-tunnel investigation of the static aerodynamic characteristics of a multilobe gliding parachute NASA-TN-D-4672 c01 N68 c01 N68-28447 LIBOVE, C. Plane stress analysis of an edge-stiffened

I-144

LUMB, D. R.

rectangular plate, taking into account bending and shear stiffness of the stiffeners NASA-CR-978 c32 N68-19 c32 N68-19311 NASA-CR-970 C. LICHTENSTEIN, J. H. Analytical investigation of effects of physical and aerodynamic parameters on dynamic behavior of Project Fire reentry vehicle NASA-TM-X-1589 c31 N68-26645 LIEBERT, C. H. Theoretical temperatures of thin-film solar cells in earth orbit NASA-TN-D-4331 c33 N68-14270 Spectral emissivity of highly doped silicon NASA-TN-D-4303 c26 NG c26 N68-21708 LIEBLEIN, S. Analytical comparison of Rankine cycle space radiators constructed of central. double, and block-vapor-chamber fin-tube geometries NASA-TN-D-4411 c33 N68-16324 Analysis of radiator characteristics of a single-loop 100-kilowatt Brayton space power system using a pure gas and a gas-solid suspension NASA-TN-D-4659 c03 N68-28280 LINCOLN, R. S. Discrimination of increases in the brightness of a flashing beacon NASA-CR-1220 c05 N68-37819 LING, C. K. Additional studies of quasi-optimum feedback control techniques NASA-CR-1099 c10 N68-28307 LISAGOR, W. B. Equipment and procedures for glass-bead peening titanium-alloy tanks NASA-TN-D-4288 cl c15 N68-12890 Stress-corrosion cracking of Ti-6Al-4V titanium alloy in nitrogen tetroxide NASA-TN-D-4289 c17 N68-12891 NASA-TN-D-4289 c17 N68-12 LITCHFORD, G. B. Analysis of cumulative errors associated with category 2 and 3 operations with requirements for additional research NASA-CR-1188 C02 LIYELPETER, YA. YA. Motion of conducting bodies in a magnetic c02 N68-35595 field NASA-TT-F-460 c25 N68-16286 LOATS, H. L., JR. A study of the performance of an astronaut during ingress and egress maneuvers through airlocks and passageways NASA-CR-971 c05 N68-2 LOCKWODD, V. E. Measurements of ground effect on a low-aspectc05 N68-20339 ratio ogee-wing airplane model and calculations of landing-flare trajectories NASA-TN-D-4329 c02 N68-14090 NRON-IN & LONA LOMAX, H. On the construction of highly stable, explicit, numerical methods for integrating coupled ordinary differential equations with parasitic eigenvalues NASA-TN-D-4547 Clable implicit and explicit numerical methods c19 N68-21978 Stable implicit and explicit numerical methods for integrating quasi-linear differential equations with parasitic-stiff and parasitic-saddle eigenvalues NASA-TN-D-4703 c19 N68-29275 LOOMIS, J. S. Low-temperature resistance minimum and magnetoresistance for dilute alloys of iron in copper NASA-TN-D-4626 c26 N68-28239 LORENZ, P. The microbiological flora of the Gemini 9 spacecraft before and after flight NASA-CR-972 c04 c04 N68-11968 LORENZO, C. F. Computer program for symbolic reduction of block diagrams using FORMAC NASA-TN-D-4617 c08 N c08 N68-24967 NASA-IN-D-401/ Practical stability criterion and its application to digital simulation NASA-TN-D-4203 Experimental longitudinal dynamics of an empty Stub D Atlas vehicle c08 N68-26640

NASA-TM-X-1682 c31 N68-37942 NHON-11. LOSER, J. B. Advanced valve technology, a survey NASA-SP-5019 ID c15 N68-10402 NASA-SP-5019 c15 N68-104 LOUTHAN, M. R., JR. Role of hydrogen chloride in hot salt stress corrosion cracking of titanium aluminum alloys NASA-CR-1133 c17 N68-330 c17 N68-33019 LOVING, D. L. Subsonic longitudinal aerodynamic measurements on a transport model in two slotted tunnels differing in size NASA-TM-X-1660 c(NASA-TM-X-1660 c(LOWDERMILK, W. H. Mechanism and kinetics of corrosion of selected iron and cobalt alloys in refluxing mercury NASA-TN-D-4450 c) c01 N68-35617 c17 N68-21654 LOWE, A. Procedures for estimating the effects of design and operational characteristics of jet aircraft on ground noise NASA-CR-1053 co2 N68-26 c02 N68-26930 NASA-UN-1000 LOWES, F. B. Navigation and guidance analysis of a Mars probe launched from a manned flyby spacecraft NASA-TN-D-4512 C21 N68-21 c21 N68-21754 Navigation and guidance systems performance for three typical manned interplanetary missions NASA-TN-D-4629 c21 N68-28236 LOWMAN, P. D., JR. Geologic applications of orbital photography NASA-TN-D-4155 cl3 N68 c13 N68-11714 LUBOMSKI, J. F. Structural feasibility study of pressurized tanks for liquid-methane fueled supersonic aircraft NASA-TN-D-4295 c32 N68-12370 LUDWIG, G. H. Space sciences data processing NASA-TN-D-4508 c08 N68-The role of the experimenter associated with multi-experiment scientific satellites c08 N68-22510 NASA-TN-D-4731 c34 N68-33682 LUDWIG, L. P. Friction and wear in cryogenic liquids for composites of phenolic and of polytetrafluoroethylene of various particle sizes and concentrations NASA-TN-D-4565 C15 N68-2 c15 N68-24142 LUEDERS, H. G. Experimental investigation of advanced concepts to increase turbine blade loading. 2 - Performance evaluation of plain rotor blade NASA-CR-1172 LUKAS, J. S. c28 N68-32987 A preliminary study of the awakening and startle effects of simulated sonic booms NASA-CR-1193 c04 N c04 N68-33005 LUKENS, D. R. Dynamic stability of space vehicles. Volume 3 ~ Torsional vibration modes NASA-CR-937 c32 N68-10568 Dynamic stability of space vehicles. Volum 4 - Full scale testing for flight centrol Volume parameters NASA-CR-938 c32 N68-10574 Dynamic stability of space vehicles. Vol 6 - Full scale dynamic testing for mode Volume determination NASA-CR-940 c32 N68-11054 Dynamic stability of space vehicles. Volume 5 - Impedance testing for flight control parameters NASA-CR-939 c32 N68-11485 Dynamic stability of space vehicles. Volume 13 - Aerodynamic model tests for control parameter determination NASA-CR-947 c32 N68-23452 LUKIN, L. Relative roles of gravitational and inertial work in the energy cost of human locomotion co5 N68c05 N68-21859 LUMB, D. R. Performance of several convolutional and block codes with threshold decoding

LUNDSTROM, R. R.

PERSONAL AUTHOR INDEX

NASA-TN-D-4402 c07 N68-18178 LUNDSTROM, R. R. Flight test of a 15-foot-diameter /4.6-meter/ 120 deg conical spacecraft simulating parachute deployment in a Mars atmosphere NASA-TN-D-4266 c31 N68-11961 Performance of a 16.6-meter-diameter cross parachute in a simulated Martian environment NASA-TM-X-1543 c31 N68-21833 LUOMA, A. A. Subsonic longitudinal aerodynamic measurements on a transport model in two slotted tunnels differing in size NASA-TM-X-1660 LURE. A. I. c01 N68-35617 Analytical mechanics. Stability of motion. Celestial ballistics NASA-TT-F-503 c23 N68-37792 LYKOV, A. V. Heat and mass transfer. Volume 1 -Convective heat exchange in a homogeneous medium NASA-TT-F-431 c33 N68-11721 NASA-IT-1-401 LYNCH, J. H. Calculations to support operation of the Plum Brook reactor NASA-TM-X-1496 c22 c22 N68-16056 Gamma heating in thin heavy-element absorbers NASA-TN-X-1680 c22 N68c22 N68-37260 LYNCH, M. P. Bimetal sensor for averaging temperature measurement of nonuniform temperature profiles NASA-TN-D-4242 c14 N68-15936

M

MAAG, W. L. A 4500 deg R /2500 deg K/ flowing-gas facility NASA-TM-X-1506 c11 N68-14115 Analytical investigation of electrically heated wire mesh for flowing gas heaters NASA-TN-D-4595 c33 N c33 N68-25312 MAC KAY, J. S. Low variable thrust interplanetary trajectory data NASA-TN-D-4431 c30 N68-21228 MAC QUEEN, R. M. Infrared observations of the outer solar corona NASA-CR-969 c30 N68-20353 MACHELL, R. M. Summary of Gemini extravehicular activity NASA-SP-149 c30 N68-15891 MACK, R. J. K, R. J. Aerodynamic characteristics of a parasol-wing-body combination utilizing favorable lift interference at Mach numbers from 3.00 to 4.63 NASA-TN-D-4855 c01 N68-3 c01 N68-37854 MASA-IN-10-4855 MACOSKO, R. P. Performance of a multiple single-pass counterflow NaK-cooled mercury Rankine cycle condenser NASA-TM-X-1548 MADDALON, D. V. Proceure distributions and consumption c33 N68-20340 Pressure distributions and aerodynamic characteristics of 90 deg and 15 deg blunted cones in nitrogen and helium at Mach 20 NASA-TN-D-4314 c01 N68-17896 MADDEN, R. B. Computing program for axial distribution of aerodynamic normal-force characteristics for axisymmetric multistage launch vehicles NASA-TN-D-4342 c31 N68-18615 MADSON, L. P. Digital readout and control system for a 64-inch /1.63-m/ scattering chamber NASA-TN-D-4324 c14 N68-14018 MAEDA, K. Temporal variations of mesospheric oxygen and ozone during auroral events NASA-TN-D-3993 c13 N68-10369 MAGEE, J. L. Calculation of capture cross sections for ion polar molecule collisions involving methyl cyanide NASA-TM-X-1586 c24 N68-23893 MAGLIERI, D. J. A summary of results on sonic-boom pressure signature variations associated with atmospheric conditions NASA-TN-D-4588 c02 N68-24662 MAHADEVAN, P. Evaluation of the effects of space environment exposure on index of refraction and extinction coefficients of Apollo window materials NASA-CR-1019 c31 N68-20467 MAIDANIK, G. Panel loss factors due to gas-pumping at structural joints NASA-CR-954 c32 N68-11489 NASA-CK⁻⁹⁵⁴C³² No³⁵ Radiation and coupling between two collinear open ended waveguides NASA-TK-D-4556C⁰⁹ N68 MALCOLM, G. N. c09 N68-28668 A computer program for systematically analyzing free-flight data to determine the aerodynamics of axisymmetric bodies NASA-TN-D-4766 c01 N68-33081 MALIK, P. V. Project Gemini - A technical summary NASA-CR-1106 c31 N68-25577 MALIKOV, G. F. Computations of elastic tensometric elements NASA-TT-F-513 MALONE, J. H. c32 N68-15796 Cryogenic temperature measurement using platinum resistance thermometers NASA-TN-D-4499 cl c14 N68-20324 NASA-IN-D-4499 C14 NO MANGAD, M. Guidance, flight mechanics and trajectory optimization. Volume 4 - The calculus of variations and modern applications NASA-CR-1003 C30 NG c30 N68-15193 NASA-CR-1003 c3 MANNING, C. R., JR. Equipment and procedures for glass-bead peening titanium-alloy tanks NASA-TN-D-4288 Stress-corrosion cracking of Ti-6A1-4V titanium alloy in nitrogen tetroxide NASA-TN-D-4289 c1 c15 N68-12890 c17 N68-12891 NASA-IN-J-4005 MANNING, J. C. Measurements of winds and temperatures at altitudes up to 65 kilometers in the Southern Hemisphere NASA-TN-D-4429 c20 N68-19084 MANNING, L. A. Analysis of launch windows from circular orbits for representative Mars missions NASA-TM-X-1651 c30 c30 N68-33371 MARGASON, R. J. Aerodynamic characteristics of a five jet VTOL configuration in the transition speed range NASA-TN-D-4812 c01 N68-36081 MARGUERON, C. Space technology transfer and developing nations NASA-CR-1222 c34 N68-37216 MARINI, J. W. On the decrease of the radar cross section of the Apollo command module due to reentry plasma effects NASA-TN-D-4784 c07 N c07 N68-35140 MARKUSEN, A. The microbiological flora of the Gemini 9 spacecraft before and after flight NASA-CR-972 c04 c04 N68-11968 MARR, J. W. Leakage testing handbook NASA-CR-952 c15 N68-20389 MARSH, A. H. A study of turbofan-engine compressor noise suppression techniques NASA-CR-1056 c28 N6 c28 N68-26771 MARSH, K. R. Additional studies on the feasibility of V/STOL concepts for short-haul transport aircraft NASA-CR-670/01/ c02 N68-11174 MARSIK, S. J. Radiation-induced reduction of divalent copper salts in solutions NASA-TN-D-4451 c00 c06 N68-19434

MC INTYRE, J. E.

MARTIN, A. W. Propulsion system dynamic simulation theory and equations NASA-CR-928 cl1 N68-19273 MARTIN, D. C. Welding of precipitation-hardening stainless 910019 NASA-SP-5087 c15 N68-21429 Method of brazing aluminum to stainless steel for high-stress-fatigue applications NASA-SP-5040 c15 N68-22778 MARTIN, E. D. Inviscid hypersonic flow over a blunt body with high rates of mass and heat transfer NASA-TN-D-4252 col NG c01 N68-17555 NRDR-IN-D-4252 CO1 N68-: Results of including a boundary shock wave in the calculation of the flight parameters of a large high-speed meteor NASA-TN-D-4325 Cl2 N68-: c12 N68-18997 MARTIN, H. L. Effects of low temperatures on the mechanical properties of structural metals NASA-SP-5012/01/ c17 N68-31605 MARTIN, J. A. Study and applications of retrodirective and self adaptive electromagnetic-wave phase controls to a Mars probe NASA-CR-977 c21 N68-18484 MASH-Un-Sr. MARTIN, R. C. Adhesive bonding of stainless steels including precipitation-hardening stainless steels NASA-SP-5085 c15 N68-2 c15 N68-20056 MARTO, P. J. MARTO, P. J. Boiling heat transfer coefficients, interface behavior, and vapor quality in rotating boiler operating to 475 G*s NASA-TN-D-4136 c33 N68c33 N68-17566 MARVIN, J. G. Comparison of convective stagnation heat transfer in air, CO2-N2, and CO2-Ar gas mixture NASA-TN-D-4255 c33 N68-11811 Comparison of experimental and theoretical shock shapes and pressure distributions on flat-faced cylinders at Mach 10.5 NASA-TN-D-4397 c01 N68-15778 MASCITTI, V. R. A simplified equilibrium hydrocarbon-air combustion gas model for use in air-breathing engine cycle computer programs NASA-TN-D-4747 c28 N68-35 c28 N68-35115 MASCY, A. C. A FORTRAN program for computation of mass in earth orbit required for interplanetary missions NASA-TM-X-1541 c30 N68-19330 MASICA, W. J. Effects of liquid depth on lateral sloshing under weightless conditions NASA-TN-D-4458 cl2 N6 Liquid reorientation in spheres by means of c12 N68-24758 Iow-G accelerations NASA-TM-X-1659 c12 N68-35114 MASLQUSKI, E. A. Qutgassing of water vapor from concrete surfaces in vacuum environment NASA-TM-X-1536 c11 N68-19207 MASSER, C. C. Photographic study of a bromine jet in a coaxial airstream NASA-TN-D-4660 c12 c12 N68-28370 MASSEY, G. A. Study of vibration measurement by laser methods NASA-CR-985 c16 N68-14070 MATHENY, N. W. Preliminary flight evaluation of the stability and control derivatives and dynamic characteristics of the unaugmented XB-70-1 airplane including comparisons with predictions NASA-TN-D-4578 c02 N68-24498 MATTSON, W. F. A 4500 deg R /2500 deg K/ flowing-gas facility NASA-TM-X-1506 c11 N68-14115 Analytical investigation of electrically heated wire mesh for flowing gas heaters NASA-TN-D-4595 c33 N68-25312

MAYER, J. T. Summary of radiation effects on thermionic insulator materials c22 N68-17095 NASA-TN-D-4414 MAYO, W. Analysis of uranyl fluoride solution reactors containing voided tubes NASA-TN-D-4270 c22 N68-15197 Small high-temperature nuclear reactors for space power NASA-TN-D-4371 c22 N68-15792 Reactivity control of fast-spectrum reactors by reversible hydriding of yttrium zones by reversions neutrony of a c22 NG NASA-TN-D-4615 c22 NG Neutronic effects on moderator insertion in c22 N68-24559 fast-spectrum reactors NASA-TM-X-1614 c22 N68-29950 Non-in-A-1014 C22 N68-2: Neutronic calculations of fuel and poison drum control of refractory-metal, fast-spectrum, space power reactors NASA-TN-D-4709 C22 N68-30 c22 N68-30750 MC ALEESE, J. D. Method for determining normal modes and frequencies of a launch vehicle utilizing its component normal modes c32 N68-22275 NASA-TN-D-4550 NASA-IN-D-4523 NO BRIDE, B. J. Partition functions and thermodynamic properties to high temperatures for H sub 3 and H sub 2 ions NASA-TN-D-4523 c33 N68-21732 MC CABE, J. T. Research and development of high-performance axial-flow turbomachinery. Volume 3 -Design of backup gas bearings NASA-CR-802 c03 N68-24597 MC CARTY, J. L. Response characteristics of impacting Response characteristics of impacting penetrometers appropriate to lunar and planetary missions NASA-TN-D-4454 c32 N68-Experimental study of vertical impacts of an LM-type landing gear assembly under simulated lunar gravity NASA-TN-D-4711 c32 N68c32 N68-20364 c32 N68-30505 MC CLOUD, J. L., III An investigation of full-scale helicopter rotors at high advance ratios and advancing tip Mach numbers NASA-TN-D-4632 c01 N68-28268 Radiant-interchange configuration factors for spherical and conical surfaces to spheres NASA-TN-D-4457 c33 N68-20 c33 N68-20331 MC DONALD, G. E. Very high burnup vapor transport fuel pin concept for long life nuclear reactors NASA-TN-D-4860 c22 c22 N68-37209 NC DONALD, J. A. Seismic effects of sonic booms NASA-CR-1137 c13 N68-35151 NASA-CK-1137 C13 MC ELMAN, J. A. Flutter of buckled, simply supported, rectangular panels at supersonic speeds NASA-TN-D-4357 c32 c32 N68-17651 R GEHEE, J. R. Investigation of a compartmented-gas-bag landing system having multiple impact capabilities NASA-TN-D-4710 c32 c32 N68-31602 MC GUNIGAL, T. E. A digital voltage-controlled oscillator for phase lock loops NASA-TN-D-4521 c09 N68-24389 MC INTIRE, H. O. Shaping of precipitation-hardening stainless steels by casting and powder-metallurgy NASA-SP-5086 c15 N68-19307 MC INTOSH, R. E. A study of the possible uses of plasma for millimeter wave generation NASA-TN-D-4309 c25 N c25 N68-18614 NASA-TN-D-4309 c25 MC INTYRE, J. E. Guidance, flight mechanics and trajectory optimization. Volume 13 - Numerical optimization methods NASA-CR-1012 c30 NG Guidance, flight mechanics and trajectory optimization. Volume 7 - The Pontryagin c30 N68-19315

maximum principle NASA-CR-1006 c30 N68-20084 Guidance, flight mechanics and trajectory optimization. Volume 10 - Dynamic programming NASA-CR-1009 c30 N68-21077 NASA-CR-1009 c30 N68-21077 MC INTYRE, R. D. Tensile properties of tantalum and tungsten 10-fiber bundles at 1000 deg F /812 K/ NASA-TN-D-4725 c17 N68-30504 KAY, J. M. Landing loads and accelerations of the XB-70-1 airplane NASA-TN-D-4836 c c02 N68-36073 MC KEE, T. B. Preliminary infrared horizon profiles from Project Scanner NASA-TM-X-1483 c21 N68-11949 Infrared horizon profiles for summer conditions from Project Scanner NASA-TN-D-4741 c21 N68-33450 MC KINZIE, D. J., JR. Calculations of solar plasma interaction with magnetic field of current loop and two parallel infinite lines of current NASA-TN-D-4304 c29 N68-19188 MC LAFFERTY, G. H. Studies of specific nuclear light bulb and open-cycle vortex stabilized gaseous nuclear rocket engines NASA-CR-1030 c22 N68-22038 HC LAIN, A. G. Experimental and theoretical investigation of the ablative performance of five phenolic-nylon-based materials NASA-TN-D-4374 c18 N68-19710 MC LAIN, L. J. Flow-field investigations on the X-15 airplane and model up to hypersonic speeds Airplane and model up to hypersonic speeds NASA-TN-D-4813 col N68-35173 MC LAUGHLIN, M. D. Simulation studies of the supersonic transport in the present day air traffic control system NASA-TN-D-4638 co2 N68-29372 MASA-IN-D-4638 CU2 N68-2 MC LEMORE, H. C. Hot-gas ingestion investigation of large-scale jet VTOL fighter-type models NASA-TN-D-4609 CO2 N68-2 c02 N68-28277 MC LEOD, N. J. Preliminary measured and predicted XB-70 engine noise NASA-TM-X-1565 c02 N68-21834 MC MILLAN, A. R. Experimental investigations of simulated meteoroid damage to various spacecraft structures NASA-CR-915 c31 N68-14638 MC MILLIN, L. M. A satellite view of Typhoon Marie 1966 development NASA-TN-D-4757 c20 N68-37869 MC NEELY, J. T. Mars landing mission mode comparison NASA-TM-X-1629 c30 N68-29988 MC NEILL, R. B. Differential systems NASA-CR-1164 MC QUAIN, R. H. Space applications 1966 NASA-SP-156 c19 N68-33426 c31 N68-16015 MBA-BF-156 CSI N68 MC RUER, D. T. A study of fully manual and augmented manual control systems for the Saturn 5 booster using analytical pilot models NASA-CR-1079 c31 N c31 N68-28426 MC WITHEY, R. R. A three-dimensional analysis of the effects A three-dimensional analysis of the effect of heat generation in plates NASA-TN-D-4326 c33 N MEDLIN, J. W., JR. Thermal design verification testing of the c33 N68-18122 anchored interplanetary monitoring platform **1)** NASA-TN-D-4112 c33 N68-10299 MEDWID, D. W. Viewing devices for observing flow conditions in hot mercury systems NASA-TM-X-1578 c11 N68-22737

PERSONAL AUTHOR INDEX

MEEROV, M. V. Multivariable control systems NASA-TT-F-435 c10 N68-37293 MEIER, J. J. The dielectric clad axial slot antenna CO7 N68-26621 NASA-CR-1057 MEIER, L. Design of guidance and control systems for optimum utilization of information NASA-CR-997 NASA-CR-997 c10 NG MEISSNER, C. W., JR. An annotated bibliography of computer-aided circuit analysis and design NASA-SP-7023 c10 NG c10 N68-23438 c10 N68-19882 MASH-SF-1000 MELEASON, E. T. Wind tunnel investigation of techniques for reducing cowl drag of an axisymmetric external-compression inlet at Mach 2.49 NASA-TM-X-1516 col N68-18189 Water condensation effects of heated vitiated air on flow in a large supersonic wind tunnel NASA-TM-X-1636 MELLOR, G. L. A method of calculating compressible turbulent boundary layers NASA-CR-1144 c11 N68-30598 c12 N68-35096 MENDELSON, A. Elastoplastic analysis of circular cylindrical inclusion in uniformly stressed infinite homogeneous matrix NASA-TN-D-4350 c32 N68-15769 Elastic-plastic torsion problem for strain-hardening materials NASA-TN-D-4391 c32 N68-17045 MENDENHALL, M. R. Investigation of methods for predicting the aerodynamic characteristics of two-lobed parawings NASA-CR-1166 c01 N68-33765 MASA-CR-1100 MENDEZ, J. C. Guidance, flight mechanics and trajectory optimization. Volume 6 - The N-body problem and special perturbation techniques NASA-CR-1005 C30 N68c30 N68-15741 MENDOZA, J. P. Prediction of aircraft sonic boom characteristics from experimental near field results NASA-TM-X-1477 c02 N68-11772 MENG, P. R. Change in inducer net positive suction head requirement with flow coefficient in low temperature hydrogen /27.9 deg to 36.6 deg R/ NASA-TN-D-4423 c28 N68-18221 MENSING, A. E. Containment experiments in vortex tubes with radial outflow and large superimposed axial flows NASA-CR-993 c22 N68-18243 MERCY, K. R. Environmental test contribution to spacecraft reliability NASA-TN-D-4181 c31 N68-10192 MERRICK, R. B. On board calculations of a two impulse abort to a preselected landing site NASA-TN-D-4599 c21 N68 c21 N68-25103 MERRICK, V. K. A technique for passive attitude control of solar oriented interplanetary spacecraft NASA-TN-D-4641 c21 N6 c21 N68-28361 MICHELS, C. J. Correlation of transient spectra with performance in coaxial plasma guns NASA-TN-D-4385 c25 N68-17070 Coaxial plasma gun research at Lewis Research Center NASA-TM-X-1600 c25 NG MICHELS, T. E. Planck functions and integrals - Methods of c25 N68-28154 computation NASA-TN-D-4446 c19 N68-18455 MIDDEN, R. E. Description and initial calibration of the Langley 20-inch hypersonic arc heated tunnel NASA-TN-D-4653 cll N68-2 MIDDLEHURST, B. M. Chronological catalog of reported lunar c11 N68-28947 events

MONTEALEGRE, A.

NASA-TR-R-277 c30 N68-28192 MHONTIATE C., MIHALOEW, J. R. Feasibility study of a tungsten water moderated nuclear rocket. 7 - System dynamics and control analysis NASA-TM-X-1426 NASA-TM-X-1426 MIXKELSON, D. C. Wind tunnel investigation of airframe installation effects on underwing engine nacelles at Mach numbers from 0.56 to 1.46 NASA-TM-X-1683 CO2 N68c22 N68-18252 c02 N68-37941 MTL. M. L. Helicopters - Calculation and design. Volume 2 - Vibrations and dynamic stability NASA-TT-F-519 co2 N68c02 N68-23456 MILLARD, J. P. An uncertainty analysis for satellite calorimetric measurements NASA-TN-D-4354 c14 N68-16529 MILLER, B. A. Analysis of several methane-fueled engine cycles for Mach 3.0 flight NASA-TN-D-4699 c28 | c28 N68-29378 MILLER, B. J. Guidance, flight mechanics and trajectory optimization. Volume 2 - Observation theory and sensors NASA-CR-1001 c30 N68-19676 MILLER, C. D. Simultaneous correction of velocity and mass bias in photography of meteors NASA-TR-R-280 c30 N68-15484 MILLER, C. G., III Pressure distributions and aerodynamic characteristics of 90 deg and 15 deg blunted cones in nitrogen and helium at Mach 20 NASA-TN-D-4314 CO1 N68-17 c01 N68-17896 Experimental base pressures on 9 deg spherically blunted cones at Mach numbers from 10.5 to 20 NASA-TN-D-4800 c01 N68-35668 MILLER, D. K. Modal density of thin circular cylinders c32 N68-11967 NASA-CR-897 MILLER, E. F. MILLER, E. F.
Modified vibration transducer calibration system which directly yields a plot of sensitivity versus frequency NASA-TN-D-4760 cl4 M
MILLER, G. K., JR.
A manual navigation method for evaluating transfer orbits for lunar landings NASA-TN-D-4756 c21 M c14 N68-31958 c21 N68-33271 MILLER, J. M. MILLER, J. H. Study of propellant valve leakage in a vacuum Final summary report NASA-CR-1047 c27 N68-2 MILLER, J. V. Potential use of high frequency induction heating for high temperature liquid metal heat transfer testing NASA-IM-X-1510 c33 N68-2 Prolimingry considerations for frequency c27 N68-21893 c33 N68-16300 Preliminary considerations for fast-spectrum, liquid-metal cooled nuclear reactor program for space-power applications NASA-TN-D-4315 c22 N68-18197 Characteristics of a space-power nuclear reactor with considerations for venting or containing gaseous fission products NASA-TM-X-1631 c22 N68 c22 N68-30516 MILLER, M. J. Detailed performance of a radial-bladed centrifugal pump impeller in water NASA-TN-D-4613 c12 N68-26651 Visual observations of flow through a radial-bladed centrifugal impeller NASA-TN-D-4282 c12 N68-28842 MASA-IN-D-4282 C12 N68-MILLER, P. C. Effects of low temperatures on the mechanical properties of structural metals NASA-SP-5012/01/ C17 N68c17 N68-31605 NASA-SP-5012/01/ c1 NILLER, R. W. Wind velocity profiles measured by the smoke-trail method at Wallops Island, Virginia, 1963 and 1964 NASA-TN-D-4365 c2 c20 N68-17024 MILLER, W. Self-synchronizing bi-orthogonal coded PCM telemetry system

NASA-TR-R-292 MILLER. W. E. c07 N68-36333 Experimental study of transmission and backscatter of 0.075 to 1.0 MeV electrons by aluminum and stainless steel NASA-TN-D-4363 c24 N68-17898 MILLUNZI, A. C. Hot isostatic compaction of tungsten-uranium dioxide fuels with high-volume fraction of uranium dioxide NASA-TM-X-1563 c22 N68 c22 N68-21705 MILNER, J. L. Free vibration of a rotating beam-connected space station NASA-TN-D-4753 c32 N68-33225 NINER, W. E. The equations of motion for optimized propelled flight expressed in Delaunay and the the texperiment of the Poincare variables and modifications of these variables NASA-TN-D-4478 c30 N68-24371 MITCHELL, G. A. An experimental investigation of the restart area ratio of a Mach 3.0 axisymmetric mixed compression inlet NASA-TM-X-1547 c01 N68-21703 Performance of centerbody vortex generators in an axisymmetric mixed-compression inlet at Mach numbers from 2.0 to 3.0 NASA-TN-D-4675 c01 N68-28795 NASA-TN-D-4675 col N68 Effect of model forebody shape on perforated tunnel wall interference NASA-TM-X-1656 col N68 Blockage effects of cone-cylinder bodies on c01 N68-36133 perforated wind tunnel wall interference NASA-TM-X-1655 coll c01 N68-36134 MITCHELL, J. C. Influence of structure and material research on advanced launch systems* weight, performance, and cost Summary report, May 25, 1965 - Jun. 30, 1967 NASA-CR-974 c31 N68 c31 N68-11520 MIGHELL, R. E. Preliminary study of advanced life-support technology for a Mars surface module c05 N NASA-CR-1083 c05 N68-28319 MIXSON, J. S. Experimental modes of vibration of 14 deg conical-frustum shells with free ends NASA-TN-D-4428 c3 c32 N68-20954 MODICA, A. P. Study of optical radiation in the wavelength regions of 0.4216 mu, 0.4278 mu, 0.4835 mu, and 0.5165 mu behind normal shock waves in a simulated Martian atmosphere NASA-TM-X-1634 cl2 N68c12 N68-32982 NASA-TH-X-1634
 C12 N68-3296
 MOELLER, C. E.
 NASA contributions to development of special-purpose thermocouples. A survey NASA-SP-5050
 C14 N68-3562
 MOFFITT, T. P.
 Effect of a variable stator area on performance of a single-stage turbine suitable for air cooling. 2 - Stator detailed losses with 130 percent design area
 NASA-TM-X-1635
 C03 N68-3050 c14 N68-35620 c03 N68-30506 Effect of variable stator area on performance of a single-stage turbine suitable for air cooling. 3 – Turbine performance with 130-percent design stator area NASA-TM-X-1663 c03 N68-35536 MONROE, D. E. KNCE, D. E. Cold-air investigation of a turbine for high-temperature-engine application. 3 - Overall stage performance NASA-TN-D-4389 c01 N68-1. c01 N68-15743 MONTA, W. J. Drag due to two-dimensional surface roughness in a turbulent boundary layer at Mach 3 with and without heat transfer and without heat transfer NASA-TN-D-4746 cl2 Nd MUNTEALEGRE, A. Evaluation of turbulence correlations in a coaxial flow of dissimilar fluids NASA-CR-961 cl2 Nd c12 N68-33054 c12 N68-12892 Measurement of turbulent correlations in a coaxial flow of dissimilar fluids NASA-CR-960 cl2 No c12 N68-13612

MONTEITH, L. K.

MONTEITH, L. K. A study of charge storage in silicon oxide resulting from non-penetrating electron irradiation NASA-CR-1088 c26 N68-26603 An investigation of thin film oxygen partial pressure sensors NASA-CR-1182 c14 N68-35149 MONTOYA, E. J. Wind-tunnel investigation of the flow field beneath the fuselage of the X-15 airplane at Mach numbers from 4 to 8 NASA-TM-X-1469 MOORE, E. T., JR. Explosive hypervelocity launchers NASA-CR-982 c02 N68-11147 c11 N68-15777 MOORE, P. Chronological catalog of reported lunar events NASA-TR-R-277 c30 N68-28192 MOORE, R. A. Modeling the human operator with finite-state machines NASA-CR-1112 c05 N68-28847 MOORE, R. D. Effects of wall pressure distribution and liquid temperature on incipient cavitation of Freon-114 and water in venturi flow NASA-TN-D-4340 c12 N68-14641 NACH-IN-D-4340 Venturi scaling studies on thermodynamic effects of developed cavitation of Freon-114 NASA-TN-D-4387 c12 N68-15329 NASA-TN-D-4387 MOORE, R. H., JR. Static longitudinal aerodynamic characteristics of several configurations used in the development of the Little Joe 2-Apollo test vehicle at Mach numbers from 0.056 to 4.65 NASA-TN-D-4439 c31 N68-22953 Experimental verification of scale factors for parawing opening characteristics NASA-TN-D-4665 c02 N68-3: c02 N68-31956 MORAKIS, J. C. Statistical tests for signal detection NASA-TR-R-273 c10 N68-11789 MORAN, F. J. A technique for passive attitude control of solar oriented interplanetary spacecraft NASA-TN-D-4641 c21 N6 c21 N68-28361 MORELLI, J. P. Aerodynamic characteristics of a large-scale model with unswept wing and augmented jet flap NASA-TN-D-4610 col N68-25919 MORGAN. C. J. Effect of chamber pressure, flow per element, and contraction ratio on acoustic-mode instability in hydrogen-oxygen rockets NASA-TN-D-4733 c33 N68-30518 MORGAN, J. L. Design and preliminary operation of the Lewis magnetohydrodynamic generator facility NASA-TN-D-4867 cll N68-3 c11 N68-37259 MOROZ, V. I. Physics of planets NASA-TT-F-515 c30 N68-21802 MORRIS, G. J. Turbojet-engine noise studies to evaluate effects of inlet-guide-vane-rotor spacing NASA-TN-D-4690 c28 N68-30040 MORRIS, J. F. RIS, J. F. Computer programs for plane collisionless sheaths between field-modified emitter and thermally ionized plasma exemplified by cesium NASA-TM-X-1562 c08 N68-21499 Pairs of emitter and collector sheaths for cesium thermionic diodes NASA-TN-D-4419 c25 N68-21623 Effects of arrival rates of absorbate ions and atoms on surface coverage, hence work functions, of emitting electrodes NASA-TN-D-4369 c25 N68-25630 Some interactions of polycrystalline tungsten electrodes with cesium plasmas NASA-TN-D-4745 c25 N68-30593 Emitter and collector sheaths for cesium thermionic diodes with polycrystalline tungsten electrodes NASA-TN-D-4744 c25 N68-31640 Collisionless sheaths between field-modified

PERSONAL AUTHOR INDEX

emitters and thermally ionized plasmas exemplified by cesium NASA-TN-D-4376 c25 N68-33021 NASA-IN-D-4076 C23 M MORRIS, O. A. Aerodynamic characteristics in pitch of a modified half ring wing body combination and a swept wing body combination at Mach 2.16 to 3.70 NASA-TM-X-1551 c01 N c01 N68-21940 Aerodynamic characteristics of a parasol-wing-body combination utilizing favorable lift interference at Mach numbers from 3.00 to 4.63 NASA-TN-D-4855 c01 N68-37854 MORRIS, R. D. Radiation damage in thick copper and gold specimens produced by low-energy protons NASA-TN-D-4452 c26 N68-21219 MORRIS, W. D. Experimental pressure distributions on a blunt lifting-entry body at Mach 3.71 NASA-TN-D-4494 c01 N68-2 c01 N68-21681 MORRISETTE, E. L. Effect of two-dimensional multiple sine-wave protrusions of the pressure and heat-transfer distributions for a flat plate at Mach 6 NASA-TN-D-4437 col N68-19 c01 N68-19063 MORTENSEN, R. E. Mathematical problems of modeling stochastic nonlinear dynamic systems NASA-CR-1168 c19 N68-35472 NASH-CA-1100 CIP NOC MOSELEY, W. C., JR. Aerodynamic stability characteristics of the Apollo Launch Escape Vehicle /LEV/ with canard surfaces deployed c01 N68-11640 NASA-TN-D-4280 Aerodynamic stability characteristics of the Apollo command module NASA-TN-D-4688 c01 N68-31445 NASA-TN-D-4688 c01 N68-31 MOSHER, E. J. A theoretical approach to the determination of magnetic torques by near field measurement NASA-TN-D-4485 c23 N68-24 c23 N68-24146 NASA-IN-J-4400 MOSKALENKO, YU. YE. Problems of space biology. Volume 5 -Dynamics of the cerebral blood volume under normal conditions and gravitational stresses c04 N68-15477 NASA-TT-F-492 MOYER, C. B. An analysis of the coupled chemically reacting boundary layer and charring ablator, part 1 Summary report NASA-CR-1060 c: c33 N68-25244 An analysis of the coupled chemically reacting Finite difference solution for the in-depth response of charring materials considering surface chemical and energy balances NASA-CR-1061 c33 N68-266 c33 N68-26692 MROZ, T. S. Polymer-film coating of magnesium for paraboloidal mirrors NASA-TN-D-4734 c18 N68-30597 MIGH IN STATE MUELLER, L. A. Effect of finned-tube assembly techniques on the heat-transfer characteristics of a space radiator NASA-TM-X-1557 c33 N68-21704 Viewing devices for observing flow conditions in hot mercury systems NASA-TM-X-1578 c11 N68-22737 MUENCH, B. Directional distribution in the reflection of the effect on heat trans heat radiation and its effect on heat transfer NASA-TT-F-497 c33 N68-21536 MUHLSTEIN, L., JR. An experimental study of the influence of the turbulent boundary layer on panel flutter NASA-TN-D-4486 c32 N68-18721 MULLEN, L. O. Superconduction thin films NASA-CR-1189 c26 N68-MULLER, A. F. Flow-induced vibrations of a flat plate suspended in a narrow channel Final report c26 N68-35178 NASA-CR-1186 c12 N68-35086 MULLER, R. Self-synchronizing bi-orthogonal coded PCM

telemetry system NASA-TR-R-292 c07 N68-36333 NROA-IN-N-WURROW, H. N. Flight test of a 40-foot-nominal-diameter nghi test of a 40-root-nominal-diameter modified ringsail parachute deployed at a Mach number of 1.64 and a dynamic pressure of 9.1 pounds per square foot NASA-TM-X-1484 c31 N68-119 c31 N68-11919 MURTAGH, T. B. Navigation and guidance analysis of a Mars probe launched from a manned flyby spacecraft NASA-TN-D-4512 c21 N68-21754 Navigation and guidance systems performance for three typical manned interplanetary missions NASA-TN-D-4629 c21 N68-28236 MUSEN, P. Investigations in Hansen*s planetary theory NASA-TN-D-4169 c30 N68-11369 On the Poincare-von Zeipel and Brown-Shook methods of the elimination of the short period terms from a Hamiltonian NASA-TN-D-4399 c19 N68-17532 In some possible simplifications and changes in Hansen*s lunar theory NASA-TN-D-4562 c30 N68-26642 MYERS, I. T. Effects of cable and circuit parameters on the precision calibration of a charge amplifier

ampiller NASA-TN-D-4300 c09 N68-16530

Ν

NACHTIGALL, A. J.	
Fatigue of liquid rocket engine meta	ls at
cryogenic temperatures to minus 45	
/4 deg K/	5 409 1
NASA-TN-D-4274	c17 N68-11637
	CI/ NO0-1103/
NAGEL, M. R.	
Problems and programs on the use of	
submillimeter waves in space	
NASA-SP-182	c07 N68-35522
NAGY, J. A.	
The influence of fixture stress conc	entrations
on ring accelerometers	
NASA-TN-D-4540	c14 N68-25830
NAGY. L. A.	C14 NGC 20000
	A.L
Design and preliminary operation of	
Lewis magnetohydrodynamic generato	
NASA-TN-D-4867	cli N68-37259
NAKANISHI, S.	
Experimental investigation of mercur	ч
propellant feed isolators for Kauf	
thrusters	
NASA-TM-X-1579	c28 N68-23477
NASHICK, G. H.	C20 N00-204/7
	_
Vapor chamber fin studies. Operatin	g
characteristics of fin models	
NASA-CR-1139	c33 N68-33203
NAUMANN, É. C.	
On the prediction of the vibratory b	ehavior
of free-free truncated conical she	
NASA-TN-D-4772	c32 N68-33057
An experimental and analytical vibra	
nu experimental and analytical vivra	cion study
of thin cylindrical shells with an	d without
longitudinal stiffeners	
NASA-TN-D-4705	c32 N68-33738
NAYFEH, A. H.	
Non-linear orbit determination metho	ds
NASA-CR-1040	c30 N68-21864
NEALY, J. E.	
A digital computer program for calcu	lating the
performance of single or multiple	alaphragm
shock tubes for arbitrary equilibr	ium real gas
mixtures	
NASA-TN-D-4802	cll N68-35466
NELSON, T. M.	
Feasibility study of optimum on-off	attitude
control system for spacecraft	
NASA-TN-D-4519	c31 N68-21260
	COI 800-21200
NEU, J. T.	
Evaluation of the effects of space e	NVIFONMENT
exposure on index of refraction an	
coefficients of Apollo window mate	
NASA-CR-1019	c31 N68-20467
NEUMAN, F.	
Performance of several convolutional	and block
codes with threshold decoding	
anna s ann anna ann a bhairte	

I-151

c07 N68-18178 NASA-TN-D-4402 Use of an electroluminescent display in manual tracking and in a reading task NASA-TN-D-4841 c05 N68-36457 NASA-IN-D-4841 CUS N68-364 NEWMAN, J. C., JR. Prediction of fatigue-crack-propagation behavior in panels with simulated rivet forces NASA-TN-D-4702 C32 N68-320 NEWSOM, W. A., JR. Wind-tunnel investigation of a deflectedc32 N68-32074 slipstream cruise-fan V/STOL aircraft wing NASA-TN-D-4262 c01 N68-11036 NASA-IN-D-4252 CUI NEWTON, J. K. Digital program for dynamics of non-rigid gravity gradient satellites NASA-CR-1119 C30 H c30 N68-32744 NICHOLS, H. E. Two-stage potassium test turbine. Volume 2 -Mechanical design and development NASA-CR-923 c03 N68-17075 NICHOLS, L. D. Design and preliminary operation of the Lewis magnetohydrodynamic generator facility NASA-TN-D-4867 c11 N68-37259 NICHOLS, L. L. Measurement of the B 10/n, alpha/Li 7, Li 7* relative cross sections in the keV region NASA-TN-D-4783 c24 N68-33763 NASA-IM-2-4765 C24 NG6-55 NIEBERDING, W. C. Sensitivity of quartz, piezoelectric pressure transducers as a function of temperature from 20 deg to 477 deg K NASA-TM-X-1479 c14 N68-11 c14 N68-11867 Modified vibration transducer calibration system which directly yields a plot of sensitivity versus frequency NASA-TN-D-4760 cl4 c14 N68-31958 NIEDRA, J. M. Length of winding on a torus in two ideal models NASA-TM-X-1674 c03 N68-37217 NIELSEN, J. N. Investigation of methods for predicting the aerodynamic characteristics of two-lobed parawings NASA-CR-1166 c01 N68-33765 NIENDORF, L. R. Self evacuated multilayer insulation of lightweight prefabricated panels for cryogenic storage tanks NASA-TN-D-4375 c33 N68-18046 NIES, G. E. Self evacuated multilayer insulation of lightweight prefabricated panels for cryogenic storage tanks NASA-TN-D-4375 c33 c33 N68-18046 NIME, E. J. Low variable thrust interplanetary trajectory data NASA-TN-D-4431 c30 N68-21228 NOEL, W. M. Space technology transfer and developing nations NASA-CR-1222 c34 N68-37216 NORGREN, C. T. Dilution-jet mixing study for gas-turbine combustors NASA-TN-D-4695 c01 N68-30128 NORWOOD, J., JR. The preheating of plasma in a megajoule theta-pinch experiment NASA-TN-D-4708 c25 N68-33372 NUSBAUM, W. J. Performance evaluation of a two stage axial-flow turbine for two values of tip clearance NASA-TN-D-4388 c03 N68-14639 Aerodynamic evaluation of two-stage axial flow turbine designed for Brayton-cycle space power system NASA-TN-D-4382 c03 N68-16469 NASA-IN-D-4302 CU3 Experimental performance evaluation of an 8.5 inch /21.59 cm/ mean-diameter axial flow turbine at Reynolds numbers from 18,000 to 177,000 NASA-TN-D-4432 c03 N68-18501 NUSSLE, R. C. An experimental investigation of the effect

NYSMITH, C. R.

of gravity on a forced circulation pattern for the effects of atmospheric attenuation,

in spherical tanks NASA-TN-D-4409 Liquid inflow to initially empty, hemispherical ended cylinders during weightlessness NASA-TN-D-4628 NYSMITH, C. R. Penetration resistance of double sheet structures at velocities to 8.8 km/sec NASA-TN-D-4568 C32 N68-25104

0

OBERTO, R. J. Analysis of performance characteristics in ground effect of a large scale V/STOL multi-fan-in-wing transport model NASA-CR-1180 c28 N68-35594 OBRIEN, K. Protection against space radiation NASA-SP-169 c29 N68-26128 **DERTEL**, G. K. The preheating of plasma in a megajoule theta-pinch experiment NASA-TN-D-4708 c25 N68-33372 OGELMAN, H. B. Experimental tests of the supernovae origin of cosmic rays NASA-TN-D-4732 c29 N68-33370 OHARE, B. J. Flight investigation of the effects of Apollo heat-shield singularities on ablator performance NASA-TN-D-4791 c33 N68-35116 CHASHI, H. Analytical and experimental study of dynamic characteristics of turbopumps NASA-TN-D-4298 c0 c01 N68-21950 OLOFSON, C. T. Machining and grinding of ultrahigh-strength steels and stainless steel alloys NASA-SP-5084 c15 N68 c15 N68-21241 OLSON. M. D. Nonlinear flutter of a circular cylindrical shell in supersonic flow NASA-TN-D-4265 c32 N68-12864 CLSTAD, W. B. Equilibrium normal-shock and stagnation-point properties of helium for incident-shock Mach numbers from 1 to 30 NASA-TN-D-4754 C12 N68-35 c12 N68-35117 ONDREJCIN, R. S. Role of hydrogen chloride in hot salt stress corrosion cracking of titanium aluminum alloys NASA-CR-1133 c17 N68-33019 ONEAL, R. L. The Explorer 23 micrometeoroid satellite. Description and results for the period November 6, 1964, through November 5, 1965 NASA-TN-D-4284 c31 N68-28198 OPARIN, A. I. The orgin and initial development of life NASA-TT-F-488 c04 N68-24272 ORR, C., JR. Investigation of radiant heat transfer to particle-seeded gases for application to nuclear rocket engine design NASA-CR-953 c22 N68-10561 OSBORN, W. M. Operation of a liquid fluorine pump in cavitating flow at an inducer tip speed of 188 feet per second /57.3 m/sec/ NASA-TM-X-1573 cl5 N68-282 c15 N68-28241 OSGOOD, D. R. Hydra 1 data display system NASA-TN-D-4554 c08 N68-25002 NADA-IN-2 OSTRACH, S. A critical evaluation of the status and trends in high speed fluid film lubrication NASA-CR-1058 cl5 N68-2 tation effects on melting ablation c15 N68-22810 NASA-TN-D-4614 c33 N68-26650 NH3A-IN-D-301 OSWALD, R. G. Microwave spectroscopy of molecules -Bibliography, 1964-1966 NASA-CR-951 c23 N68-10674 OVERBECK, J. W. Correction of balloon X-ray astronomy data

PERSONAL AUTHOR INDEX

K X-ray escape, and energy resolution NASA-CR-1045 cl3 c13 N68-23436 P PACKE, D. R. Analysis of pressure-drop function in Rankine space power boilers with discussion of flow maldistribution implications NASA-TN-D-4498 PADDEN. J. B. c33 N68-20066 Oxidation resistant materials for transpiration cooled gas turbine blades. 1 -Sheet specimen screening tests NASA-CR-930 c17 N68-17591 Oxidation resistant materials for transpiration cooled gas turbine blades, 2 - Wire specimen tests NASA-CR-1184 c17 N68-35098 PADDOCK, G. B. Dynamic stability of space vehicles. Volume 1 - Lateral vibration modes NASA-CR-935 c32 N68 c32 N68-10231 PAGE. V. R. Large-scale wind-tunnel tests of a deflected slipstream STOL model with wings of various aspect ratios NASA-TN-D-4448 c02 N68-18771 Wing surface pressure data from large-scale wind-tunnel tests of a propeller-driven STOL model NASA-TM-X-1527 c02 N68-19065 Large-scale wind-tunnel investigation of an airplane model with a tilt wing of aspect ratio 8.4, and four propellers, in the presence of a ground plane NASA-TN-D-4493 col N6 c01 N68-20370 PALITZ, M. Wind-tunnel investigation of the flow field beneath the fuselage of the X-15 airplane at Mach numbers from 4 to 8 NASA-TM-X-1469 Flow-field investigations on the X-15 c02 N68-11147 NASA-TN-D-4813 c01 N68 c01 N68-35173 PALLADIN, A. V. Biochemistry of the nervous system c04 N68-13432 NASA-TT-F-439 NASA-TT-F-439 c04 N6 PALLMANN, A. J. Radiative heating and cooling functions for the lower Martian atmosphere under the condition of Local Thermodynamic Equilibrium /LTE/ NASA-CR-1044 c30 N68-22860 PALMER, R. R. Guidance, flight mechanics and trajectory optimization. Volume 8 - Boost guidance equations NASA-CR-1007 c30 N68-20449 Guidance, flight mechanics and trajectory optimization. Volume 5 - State determination and/or estimation NASA-CR-1004 c30 N68-21685 PAG. H.-P. Magnetohydrodynamic flows over a rotating disk NASA-CR-989 c25 N68-14078 PAPELL, S. S. Minimum film-boiling heat flux in vertical flow of liquid nitrogen NASA-TN-D-4307 c33 N c33 N68-16683 On the influence of nonuniform magnetic fields on ferromagnetic colloidal sols NASA-TN-D-4676 c06 N68-30044 PARK. S. K. Gravitational experiments with a collisionless two-dimensional computer model NASA-TN-D-4646 c30 N68-28884 PARKER, H. MOS field-effect-transistor technology NASA-CR-1113 c08 N68-35193 PARKER, J. A. The effects of molecular structure on the thermochemical properties of phenolics and related polymers NASA-TR-R-276 c33 N68-11038 PARKER, J. F., JR. Effect of heat stress and prolonged activity

on perceptual-motor performance NASA-CR-1153 c05 N68-31480 PARKER, R. J. Reduced pressure environment effects on rolling element fatigue life with super refined mineral oil lubricant NASA-TN-D-4348 c15 N68-15010 Residual stress and subsurface hardness changes induced during rolling contact NASA-TN-D-4456 c15 N68-20199 Effect of ball-race conformity on spinning friction NASA-TN-D-4669 PATCH. R. W. c15 N68-28258 Partition functions and thermodynamic properties to high temperatures for H sub 3 and H sub 2 ions NASA-TN-D-4523 c3 PATTERSON, J. C., JR. A wind tunnel investigation of jet-wake c33 N68-21732 effect of a high-bypass engine on wing-nacelle interference drag of a subsonic transport NASA-TN-D-4693 c01 N68-30595 PAULSON, W. A. Comparison of absolute calculated and measured gamma and neutron doses in tungsten-water moderated critical assembly NASA-TN-D-4223 c22 N68-10291 Postshutdown cooling requirements of tungsten water-moderated nuclear rocket NASA-TM-X-1568 c22 c22 N68-21111 PAVLI, A. J. Experimental evaluation of several advanced ablative materials as nozzle sections of a storable-propellant rocket engine NASA-TM-X-1559 c28 N68c28 N68-19708 PAVLOVIC, D. M. Properties of magnetic materials for use in high-temperature space power systems NASA-SP-3043 c17 N68-17624 PEARS, C. D. An investigation of the mechanisms of heat transfer in low-density phenolic-nylon chars NASA-CR-966 c18 N68-11978 PEARSONS, K. S. The noisiness of tones plus noise NASA-CR-1117 c05 N68-30602 PEDERSON, P. D., JR. Microbiological exploration of the stratosphere. Development and flights of the Mark 2 and 3 sampling systems NASA-CR-1101 c04 N68-28247 PEELE, E. L. A theoretical and experimental investigation of the three-dimensional vibration characteristics of a scaled model of an asymmetrical launch vehicle NASA-TN-D-4707 c32 c32 N68-32051 PEGG, R. J. An investigation of the helicopter height velocity diagram showing effects of density altitude and gross weight NASA-TN-D-4536 c02 N68-3 c02 N68-22033 PELLEGRINO, J. A. Computer driven electroluminescent vertical scale indicator NASA-CR-919 c05 N68-1 PELOUCH, J. J., JR. Scale 1/14.2 investigation of submerged nozzle c05 N68-10648 for SL-3 260-inch solid rocket NASA-TM-X-1546 c28 N68-20186 NASA-IM-X-1940 C28 N PENDERGRAFT, 0. C., JR. Transonic aerodynamic characteristics of powered models of several Apollo launch-escape vehicle configurations NASA-TN-D-4843 c31 N68-37074 PENZES, L. E. Dynamic stability of space vehicles. Volume 15 - Shell dynamics with special applications to control problems NASA-CR-949 c32 N68-23453 PEREL, D. H. An evaluation of the thermally radiant environs of a man on the lunar surface NASA-TN-D-4243 c30 c30 N68-11630 PERKINS, P. J. Self evacuated multilayer insulation of lightweight prefabricated panels for cryogenic storage tanks

NASA-TN-D-4375 c33 N68-18046 PERLMUTTER, M. Rarefied-gas couette flow and heat transfer between parallel plates by model sampling NASA-TN-D-4579 cl2 N6 c12 N68-24129 NR5A-IN-D-4579 PERZ, D. A. Experimental evaluation of a voltage regulator-exciter for a 15 kilovolt-ampere Brayton cycle alternator NASA-IN-D-4697 Performance characteristics of 15 kVA homopolar inductor alternator for 400 Hz c03 N68-29960 Brayton-cycle space-power system NASA-TN-D-4698 c03 N68-30002 PESCHON, J. Design of guidance and control systems for optimum utilization of information NASA-CR-997 c10 N68-23438 NASA-CM-997 C10 PETERSON, D. A. Experimental evaluation of 7.82-inch /19.8-cm/ diameter throat inserts in a storable-propellant rocket engine NASA-TM-X-1463 c28 c28 N68-22272 NASA-TM-X-1463 c28 N66 PETERSON, J. P. Plastic buckling of plates and shells under biaxial loading NASA-TN-D-4706 c32 N66 PETRASEK, D. W. Refractory metal fiber nickel base alloy composites for use at high temperatures NASA-TN-D-4787 c17 N66 PEFEFFR. R. c32 N68-31946 c17 N68-33684 PFEFFER, R. Analysis of radiator characteristics of a single-loop 100-kilowatt Brayton space power system using a pure gas and a gas-solid suspension NASA-TN-D-4659 c03 N68-28280 NASA-IN-D-4659 CU3 NG6-2644
 PHILBIN, E. J.
 Evaluation of the effects of space environment exposure on index of refraction and extinction coefficients of Apollo window materials NASA-CR-1019 C31 N68-2044 c31 N68-20467 PHILIPP, W. H. Radiation-induced reduction of divalent copper salts in solutions NASA-TN-D-4451 c06 N68-19434 PHILLIPS, B. Experimental investigation of acoustic liners to suppress screech in storable propellant rocket motors NASA-TN-D-4442 c28 N68-Experimental investigation of an acoustic liner with variable cavity depth NASA-TN-D-4492 c33 N68-Effects of high-wave amplitude and mean flow on a Helmholtz resonator NASA-TN-X-1582 c12 N68-UTTCC t2 N68c28 N68-18249 c33 N68-21680 c12 N68-23423 PHILLIPS, W. P. Measurements of ground effect on a low-aspectratio ogee-wing airplane model and calculations of landing-flare trajectories NASA-TN-D-4329 c02 N68-14090 PIERCE, W. S. Crack growth in 2014-T6 aluminum tensile and tank specimens cyclically loaded at cryogenic temperatures NASA-TN-D-4541 c17 N68-21768 PINCKNEY, S. Z. Static-temperature distribution in à flat plate compressible turbulent boundary layer with heat transfer NASA-TN-D-4611 c33 N68-25917 PITTS, D. E. A computer program for calculating model planetary atmospheres NASA-TN-D-4292 c30 c30 N68-15793 PITTS, S. W. A FORTRAN program for computation of mass in earth orbit required for interplanetary missions NASA-TM-X-1541 c30 N68-19330 NASA-IA-A-I341
 Counter Nasa-IA-A-I341
 PLATT, M.
 Analysis of geometry and design point performance of axial flow turbines. 1 – Development of the analysis method and the loss coefficient correlation NASA-CR-1181
 C28 N68c28 N68-35101

NASA-CR-1181 c28 N68-3510 Analysis of geometry and design point performance of axial flow turbines.

PLATT, M.

PLUMER, J. A.

PERSONAL AUTHOR INDEX

Part 2 - Computer program NASA-CR-1187 c28 N68-36617 PLUMER, J. A. A study of aircraft fire hazards related to natural electrical phenomena Final report, Jun. 1966 - Jul. 1967 NASA-CR-1076 c02 N68-26691 POLHAMUS, E. C. Application of the leading-edge-suction analogy of vortex lift to the drag due to lift of sharp-edge delta wings NASA-TN-D-4739 c01 N68-31990 POPPA, H. Method and results of studying vapor deposition nucleation processes by in situ electron microscopy NASA-TN-D-4506 c06 N68-21430 PORTER, T. R. Fatigue-crack-propagation and fracturetoughness characteristics of 7079 aluminum-alloy sheets and plates in three aged conditions NASA-CR-996 c32 N68-15476 NAGA-UN 350 POSCHENRIEDER, W. P. Improvement and optimization of a mass spectrometer employing a photoionization source NASA-CR-1018 c14 N68-17329 POTTER, A. E., JR. Effect of green light on spectral response of cuprous sulfide-cadium sulfide photovoltaic cells NASA-TN-D-4333 c03 N68-14082 POUQUET, J. Remote detection of terrain features from Nimbus 1 high resolution infrared radiometer nighttime measurements NASA-TN-D-4603 c13 N68-POVINELLI, F. P. Displacement of disintegrating liquid jets in c13 N68-28872 crossflow NASA-TN-D-4334 c33 N68-15942 POWELL, A. H. Development of electrical switchgear for space nuclear electrical systems NASA-CR-1026 c03 N68-29460 POWELL, C. A., JR. Tables of energy and angular distributions of thick target bremsstrahlung in metals NASA-TN-D-4755 c2 POWERS, B. G. c24 N68-35535 A review of transport handling-qualities criteria in terms of preliminary XB-70 flight experience NASA-TM-X-1584 c02 N68-23901 PREDVODITELEV, A. S. Studies in physical gas dynamics NASA-TT-F-505 c12 N68-16839 NASA-II-F-500 PREISSER, J. S. Flight test of a 40-foot-nominal-diameter modified ringsail parachute deployed at a Mach number of 1.64 and a dynamic pressure of 9.1 pounds per square foot NASA-TM-X-1484 c31 N68-11919 Flight test of a 30 foot nominal diameter cross parachute deployed at a Mach number of 1.57 and a dynamic pressure of 9.7 pounds per square foot NASA-TM-X-1542 c31 N68-21778 NASA-IN-X-1542 Flight test of a 40-foot nominal diameter disk gap band parachute deployed at a Mach number of 1.91 and a dynamic pressure of 11.6 pounds per square foot NASA-IN-X-1575 c02 N68-242 c02 N68-24245 Flight test of a 40-foot-nominal-diameter disk-gap-band parachute deployed at a Mach number of 2.72 and a dynamic pressure of 9.7 pounds per square foot NASA-TM-X-1623 c31 N68-29993 PREYSS, A. E. A theory and model of human learning behavior in a manual control task NASA-CR-1124 c05 N68-31911 NMON-INCLAIL PRICE, D. B. Derivation of approximate equations for solving the planar rendezvous problem NASA-IN-D-4670 c3 c30 N68-28841 PRICE, H. E. A descriptive model for determining optimal

human performance in systems. Volume 3 -An approach for determining the optimal role of man and allocation of functions in an aerospace system NASA-CR-878 c05 N68-19165 PRIDE, R. A. Effects of longtime environmental exposure on mechanical properties of sheet materials for a supersonic transport NASA-TN-D-4318 c17 N68-17897 NNSH-IN-D-4510 PRITCHARD, E. B. The orbital recovery problem. Part 1 - An analysis technique for rapid determination of return opportunities and lateral-range requirements for recall to recovery networks in the opportunities and lateral-range NASA-TR-R-259 c21 N68-30126 PROK, G. M. Enhancement of ion cyclotron waves in hydrogen helium mixtures NASA-TN-D-4271 c25 NG PRUST, H. W., JR. Cold-air investigation of a turbine for high-temperature engine application. 2 -Detailed analytical and experimental investigation of stator performance c25 N68-18485 investigation of stator performance NASA-TN-D-4418 c28 N68-16632 NHOH-IN-U-4410 C28 N68-166 Effect of a variable stator area on performance of a single-stage turbine suitable for air cooling. 2 - Stator detailed losses with 130 percent design area NASA-TM-X-1635 C03 N68-3056 c03 N68-30506 PRZYBYSZEWSKI, J. S. Deposition of sputtered molybdenum disulfide films and friction characteristics of such films in vacuum NASA-TN-D-4269 c review of lubrication of sliding and c17 N68-11644 rolling element electrical contacts in vacuum NASA-TN-D-4476 c15 N68-21979 Stress-strain behavior of cold-welded copper-copper microjunctions in vacuum as determined from electrical resistance measurements NASA-TN-D-4743 c17 N68-31517 PURDUM, D. L. Computer assisted instruction. Feasibility c08 N68-13897 model of an asymmetrical launch vehicle NASA-TN-D-4707 c32 c32 N68-32051 NASA-IN-D-4707 PUTRE, H. A. Feasibility of supporting liquid fuel on a solid wall in a radiating liquid-core nuclear rocket concept NASA-TN-D-4413 c27 N c27 N68-17093 NASA-TN-U-4410 PYRON, C. H., JR. An investigation of the mechanisms of heat transfer in low-density phenolic-nylon chars c18 N68-11978 Q QUAN. V.

Analytical predictions of delivered specific impulse NASA-CR-1123 C27 N68-32793 QUITTER, J. P. Critical electrical aspects of alternating-current power source for Centaur space vehicle NASA-TH-X-1569 Electromagnetic compatibility verification for the Centaur and Surveyor space vehicles NASA-TH-X-1673 C31 N68-36971

R

RAFFO, P. L. Yielding and fracture in tungsten and tungsten-rhenium alloys NASA-TN-D-4567 cl7 N68-24477 RAINEY, A. G. Effects of flexibility on lift and pitchingmoment characteristics of a series of low-

RINDAL, R. A.

aspect-ratio wing-body combinations at transonic speeds NASA-TN-D-4655 c01 N68-37065 RASATIN-14055 CUI NOO RALSION, H. J. Relative roles of gravitational and inertial work in the energy cost of human locomotion NASA-CR-1042 c05 N68c05 N68-21859 RAMASASTRY, J. Research on field-aligned propagation of HF radiowaves using Alouette 2 topside sounder data and digital ray-tracing techniques NASA-TN-D-4748 c07 N68-3 c07 N68-31639 RAMBO, G. E. Investigation of electron-radiation-induced dielectric breakdowns in a typical capacitor meteoroid detector system NASA-TN-D-4738 c14 N68-3 c14 N68-33277 RANDALL, N. D. Adhesive bonding of stainless steels including precipitation-hardening stainless steels NASA-SP-5085 c15 N68-2 c15 N68-20056 RANDLE, R. J. The effect of some telescope factors on variability of performance in sextant sighting NASA-TN-D-4781 c21 N68-330 c21 N68-33006 The effects of irradiation and star magnitude on sextant sighting performance NASA-TN-D-4780 c21 N68-33456 RASCHKE, E. The radiation balance of the earth-atmosphere system from radiation measurements of the Nimbus 2 meteorological satellite NASA-TN-D-4589 c13 N68-28222 RAY. E. J. Effect of large sideslip angles on stability characteristics of a T-tail transport configuration NASA-TM-X-1665 c01 N68-36112 RE, R. J. Subsonic longitudinal aerodynamic measurements on a transport model in two slotted tunnels differing size NASA-TM-X-1660 c01 N68-35617 REDD. B. Aerodynamic stability characteristics of the Apollo Launch Escape Vehicle /LEV/ with canard surfaces deployed NASA-TN-D-4280 c01 N68-11640 REED, R. E., JR. Determination of stresses in elastic solids using three stress functions and three equations NASA-TN-D-4253 c19 N68-10355 Remarks on imperfections of axially loaded cylinders NASA-TM-X-1552 c32 N68-21767 REED, T. E. Dynamic stability of space vehicles. Volume 6 - Full scale dynamic testing for mode determination NASA-CR-940 c32 N68-11054 Dynamic stability of space vehicles. Volume 8 - Atmospheric disturbances that affect flight control analysis NASA-CR-942 c32 N68-11089 REETZ, A., JR. Protection against space radiation NASA-SP-169 c29 N68-26128 NRSA-DF-109 C29 N68-REGETZ, J. D., JR. Feasibility study of optimum on-off attitude control system for spacecraft NASA-TN-D-4519 C31 N68-REICHARD, D. W. Beduced preserve contenent off attic31 N68-21260 Reduced pressure environment effects on rolling element fatigue life with super refined mineral oil lubricant NASA-TN-D-4348 c15 N68-15010 Residual stress and subsurface hardness changes induced during rolling contact NASA-TN-D-4456 c15 N68-20199 REILLY, H. J. Calculations to support operation of the Plum Brook reactor NASA-TM-X-1496 c22 N68-16056 Gamma heating in thin heavy-element absorbers c22 N68-37260 NASA-TM-X-1680 EILLY, R. E. Effect of heat stress and prolonged activity

on perceptual-motor performance NASA-CR-1153 c05 N68-31480 NASA-CR-1153 c05 N68-3 REINMANN, J. J. Power transfer to ion cyclotron waves in a two ion species plasma NASA-TM-X-1481 c25 N68-1 c25 N68-11404 REISS, J. R. Electromagnetic compatibility verification for the Centaur and Surveyor space vehicles NASA-TM-X-1673 c31 N68-36971 NASA-INTA-IOTO RENSELAER, D. J. Analysis of performance characteristics in ground effect of a large scale V/STOL multi-fan-in-wing transport model c28 No NASA-CR-1180 c28 N68-35594 RASA-CR-1100 C20 NOO REPIC, E. M. Study of technology requirements for atmosphere braking to orbit about Mars and Venus. Volume 1 ~ Summary, January -October 1967 NASA-CR-1131 c30 N68-34086 RESHOTKO, M. Flow and wall-temperature sensitivity in parallel passages for large inlet to exit density ratios in subsonic flow NASA-TN-D-4649 c33 NG c33 N68-28371 REYNOLDS, T. W. Adsorption-desorption behavior of homogeneous and heterogeneous metal surfaces c24 N68-34175 NASA-TN-D-4789 REZNIK, J. F. SNAP-8 simulator loop mechanical design NASA-TM-X-1515 cl c11 N68-18460 RICE, J. H. Calculation of capture cross sections for ion polar molecule collisions involving methyl cyanide NASA-TM-X-1586 -24 N68-23893 RICE, R. R. Cryogenic storage systems for earth-orbital and Mars-flyby missions NASA-TN-D-4619 c03 N6 c03 N68-28420 RICHARDS, W. E. Optically induced free-carrier light modulator NASA-TN-D-4608 c23 N68-2: c23 N68-25868 RICHARDSON, C. S. Effect of speed brakes on the supersonic Trect of speed brakes on the supersonic aerodynamic characteristics of a variable sweep tactical fighter model at Mach numbers from 1.60 to 2.50 NASA-TN-D-4773 c02 N68-33 c02 N68-33669 Effects of variations in nose and windshield geometry on supersonic aerodynamic characteristics of a variable-sweep tactical fighter model NASA-TM-X-1664 c02 N68-37066 RICHARDSON, P. D. Use of a transcendental approximation in transient conduction analysis NASA-CR-955 c19 N68-11109 RIDDLE, D. W. An experimental study of the influence of the turbulent boundary layer on panel flutter NASA-TN-D-4486 c32 N68c32 N68-18721 RIGDON, W. S. Radiative and convective heating during atmospheric entry NASA-CR-1170 c33 N68-35248 RILEY, D. R. A simulator study of pilot control of remote orbital docking of large attitude-stabilized components NASA-TN-D-4263 c31 N68-11476 RIND. E. High energy proton damage in silicon surface barrier detectors NASA-TN-D-4528 c26 N68-24660 RINDAL, R. A. An analysis of the coupled chemically reacting boundary layer and charring ablator, part 1 Summary report NASA-CR-1060 c c33 N68-25244 An analysis of the coupled chemically reacting boundary layer and charring ablator. Part 2 -Finite difference solution for the in-depth response of charring materials considering surface chemical and energy balances NACA-256 c33 N68~26692 NASA-CR-1061 An analysis of the coupled chemically reacting

I-155

RINGLAND, R. F.

PERSONAL AUTHOR INDEX

boundary layer and charring ablator. Part 4 -A unified approximation for mixture transport properties for multicomponent boundary-layer applications NASA-CR-1063 c33 N68-26815 NBAR-CK-1053 CO3 NOB-208 An analysis of the coupled chemically reacting boundary layer and charring ablator. Part 6 -An approach for characterizing charring ablator response with in-depth coking reactions NASA-CR-1065 c33 N68-26817 RINGLAND, R. F. Dynamic stability of space vehicles. Volume 10 - Exit stability NASA-CR-944 c32 N68-18825 RISH, F. L. Shell analysis manual NASA-CR-912 RITTER, R. C. c32 N68-24802 An annular lithium-drifted germanium detector for studying nuclear reaction gamma-rays NASA-CR-1138 c14 N c14 N68-35152 ROARK, T. P. Interstellar grains NASA-SP-140 c30 N68-11456 NASA-57-140 C30 ROBERTSON, J. B. Photometry of an iron artificial meteor reentering at 11 kilometers per second NASA-TN-D-4312 C30 c30 N68-16750 ROBERTSON, R. L. Guidance, flight mechanics and trajectory optimization. Volume 16 - Mission constraints and trajectory interfaces NASA-CR-1015 c30 N68-20468 ROBERTSON, W. G. The effects of lunar gravity on metabolic rates NASA-CR-1102 c05 N68-28833 ROBINSON, L. A. Study and applications of retrodirective and self adaptive electromagnetic-wave phase controls to a Mars probe NASA-CR-977 c21 N68-18484 ROBINSON, R. C. Fluctuating pressures on the afterbodies of five blunt atmosphere entry vehicles NASA-TN-D-4591 c32 N68-24508 Dynamic response of a family of axisymmetric hammerhead models to unsteady aerodynamic loading NASA-TN-D-4504 c01 N68-25916 RNDA IN 5 100 ROCHING, A. P. Analytical investigation of incompressible turbulent swirling flow in pipes cl2 N NASA-CR-1169 c12 N68-36343 RODGERS, D. L. Development and flight testing of a fluidic control system NASA-CR-913 c02 N68-10047 ROELKE, R. J. Turbojet and turbofan cycle considerations and engine configurations for application in lightweight aircraft NASA-TM-X-1624 c28 ROGALLO, V. L. A piezoelectric transducer for measuring c28 N68-31476 cardiac and gross motor activity of small organisms NASA-TN-D-4590 c05 N68-25060 RDGERS, R. C. Study of underexpanded exhaust jets of an X-15 airplane model and attached ramjet engine simulator at Mach 6.86 NASA-TM-X-1571 c28 N68-24614 NASA-IN-X-15/1 C20 NG ROHAL, R. G. Nuclear design data for experiments to be conducted in Horizontal Through Hole 1 of the Plum Brook Reactor NASA-TM-X-1509 c22 NG c22 N68-15855 ROHATGI, V. Plasma boundary interactions - 2 NASA-CR-1072 c25 N68-25821 ROHLIK, H. E. Analytical determination of radial inflow Analytical determination of radial inflow turbine design geometry for maximum efficiency NASA-TN-D-4384 c03 N68-159 ROLLBUHLER, R. J. Experimental investigation of reaction control, storable bipropellant thrustors c03 N68-15943

NASA-TN-D-4416 c28 N68-20064 ROM, F. E. Very high burnup vapor transport fuel pin concept for long life nuclear reactors NASA-TN-D-4860 c22 c22 N68-37209 ROMAN, J. A useful modification of the Wright spirometer NASA-TN-D-4234 c14 N68-10057 FM handling and analog-to-digital conversion of biomedical data from a 1,000-flight study NASA-TN-D-4488 c05 N68-21537 Recording and signal-conditioning techniques and equipment used in a 1,000-flight biomedical study NASA-TN-D-4487 c05 N68-21538 A simple laboratory method for reduction of rhythm and rate in large-scale monitoring of electrocardiogram NASA-TN-D-4751 c05 N68-32100 ROSA, A. Inorganic separator for a high temperature silver-zinc battery NASA-CR-965 c03 N68-16321 ROSEN, A. Explicit upper bounds for error propagation in the n-body field NASA-TN-D-4511 c30 N68-32094 ROSEN, J. S. The Runge-Kutta equations by quadrature methods NASA-TR-R-275 c19 N68-10121 The computation of the partial volumes of the components in solution NASA-TN-D-4199 c06 N68-11621 Lattice structures in solutions NASA-TN-D-4297 Multi-step Runge-Kutta methods c06 N68-18219 NASA-TN-D-4400 c19 N68-21100 NASA-IN-J-4900 ROSENBAUM, B. N. MCFLARE, a Monte Carlo code to simulate solar flare events and estimate probable doses encountered on interplanetary missions 220 N58-160 NASA-TN-D-4311 c29 N68-16008 ROSENBAUM, J. L. Computer driven electroluminescent vertical scale indicator NASA-CR-919 c05 N68-10648 ROSENBLUM, L. Mechanism and kinetics of corrosion of selected iron and cobalt alloys in refluxing mercury NASA-TN-D-4450 c17 N68-21654 ROSENTHAL, A. Venture into space - Early years of Goddard Space Flight Center NASA-SP-4301 cll N6 c11 N68-30317 ROSS, E. C. MOS field-effect-transistor technology NASA-CR-1113 cd c08 N68-35193 ROSSBACH, R. J. Two-stage potassium test turbine. Volume 2 - Fluid dynamic design and performance NASA-CR-922 c03 N68-16439 ROSSETTI, S. Analysis of radiator characteristics of a single-loop 100-kilowatt Brayton space power system using a pure gas and a gas-solid suspension NASA-TN-D-4659 c03 N68-28280 ROTH, J. R. In, J. K. Periodic, small-amplitude solutions to the spatially uniform plasma continuity equations NASA-TN-D-4472 c25 N68-22887 Analysis of integrated charged particle energy spectra from gridded electrostatic analyzers NASA-TN-D-4718 c25 N68-30093 ROUZER, L. E. Microwave pump requirements for field operational broadband rutile traveling-wave masers NASA-TN-D-4764 c16 N68-33635 ROY, R. Frequency coded threshold logic unit for pattern recognition application NASA-CR-1035 c05 N68-22448

PERSONAL AUTHOR INDEX

ROYAL, T. M. An investigation of thin film oxygen partial pressure sensors NASA-CR-1182 c14 N68-35149 NASA-CR-1182 c14 N68-3514 ROYSTER, D. M. Coatings and surface treatments for longtime protection of Ti-8A1-1Mo-1V alloy sheet from hot salt stress corrosion NASA-TN-D-4319 c17 N68-1737 Effects of longtime environmental exposure on mechanical properties of sheet materials for a supersonic transport NASA-TN-D-4318 c17 N68-1785 Hot salt stress corrosion creating and its c17 N68-17377 c17 N68-17897 Hot salt stress corrosion cracking and its effect on tensile properties of Ti-8Al-1Mo-1V titanium-alloy sheet NASA-TN-D-4674 c17 N68-30000 ROZENMAN, T. Stability of shear flow with density gradient and viscosity NASA-CR-958 c12 N68-15530 NASA-CK-958 cl2 N68 RUBENSTEIN, L. S. Effects of composition and heat treatment on high-temperature strength of arc-melted tungsten hafnium carbon alloys NASA-TN-D-4379 c17 N68-17317 RUCH, R. Parametric analysis of radioisotope cascaded thermoelectric generators NASA-TM-X-1501 c22 N68-14585 NASA-IN-X-ISUI C22 NGO-14565 RUDDUCK, R. C. The reflection coefficient of a TEM mode parallel-plate waveguide illuminating a conducting sheet - The large wedge angle case NASA-CR-1174 c07 N68-35172 RUEDELE, R. W. Successful restart of a cryogenic upper-stage vehicle after coasting in earth orbit NASA-TM-X-1649 c31 N68c31 N68-33683 RUGGERI, R. S. Effects of wall pressure distribution and liquid temperature on incipient cavitation of Freon-114 and water in venturi flow NASA-TN-D-4340 cl2 N68-14 c12 N68-14641 NASA-IN-D-4340 CI2 NO-2. Venturi scaling studies on thermodynamic effects of developed cavitation of Freon-114 NASA-TN-D-4387 c12 N68-15329 NHSA-IN-J-307 RUGGIERO, R. J. Guidance, flight mechanics and trajectory optimization. Volume 5 - State determination and/or estimation NASA-CR-1004 c30 N68-21685 RUHLIN, C. L. Subsonic and transonic flutter and flow investigations of the T-tail of a large multiget cargo airplane NASA-TN-D-4316 c02 c02 N68-17055 NASA-IN-D-4316 CU2 NG-RUMMLER, D. R. Mechanical properties and column behavior of thin wall beryllium tubing NASA-TN-D-4833 C17 N68c17 N68-37053 NASA-TN-U-4000 RUSTGI, O. P. Study on a technique for detecting photons in the 100-1000 angstrom wavelength region Final report, 15 Apr. 1965 - 15 Oct. 1967 Content of the technique c24 N68-NASA-CR-1096 c24 N68-28250 RYAN, P. E. A generalized experimental investigation of hot gas recirculation and ingestion for jet VTOL aircraft NASA-CR-1147 c01 c01 N68-33043

S

 SAGERMAN, G. D.
 Comparison of small water-graphite nuclear rocket stages with chemical upper stages for unmanned missions NASA-TN-D-4827
 C22 N68-35073
 SAHNI, R. C.
 Quantum mechanical study of molecules transition probabilities, Einstein A coefficients and oscillator strengths of some band systems of diatomic molecules NASA-CR-975
 C24 N68-11037
 Quantum mechanical study of molecules -Eigenvalues and eigenvectors of real symmetric matrices NASA-CR-983
 C24 N68-11903 SAWYER, J. W.

SALMI, R. J. Scale 1/14.2 investigation of submerged nozzle for SL-3 260-inch solid rocket c28 N68-2 NASA-TM-X-1546 c28 N68-2 Effect of thrust per element on combustion stability characteristics of hydrogen oxygen c28 N68-20186 rocket engines NASA-TN-D-4851 c28 N68-36515 NASA-TM-J-4001 SALTERS, L. B., JR. Studies of flow distortion in the tailpipes of hydrogen peroxide gas generators used for jet engine simulation NASA-TM-X-1671 cl2 N68-33 c12 N68-37067 NASA-IN-X-16/1 C12 NO SALZMAN, J. A. Effects of liquid depth on lateral sloshing under weightless conditions NASA-TN-D-4458 c12 NG c12 N68-24758 SAMADDAR, S. N. Electromagnetic properties of a circular aperture in a dielectric-covered or uncovered ground plane NASA-TN-D-4752 c07 N68-35537 NASA-TN-D-4752 c07 N68-33 SAMSON, J. A. R. Studies of photoabsorption by atomic hydrogen, oxygen, and nitrogen NASA-CR-998 c24 N68-13 SANATOR, R. J. Effect on bluntness on hypersonic two-dimensional inlet type flows NASA-CR-1145 c01 N68-33 CANPECRD M C c24 N68-18118 c01 N68-35523 SANDFORD, M. C. Subsonic and transonic flutter and flow investigations of the T-tail of a large multijet cargo airplane NASA-TN-D-4316 c02 c02 N68-17055 SANDROCK, G. D. Development of a cobalt-tungsten ferromagnetic, high-temperature, structural alloy NASA-TN-D-4338 c17 N68-18145 Some observations concerning the oxidation of the cobalt-base superalloy L-605 /HS-25/ NASA-TN-D-4715 c17 N68c17 N68-29954 SANGER, N. L. Noncavitating performance of two-area-ratio water jet pumps having throat lengths of 7.25 diameters c15 N68-17564 NASA-TN-D-4445 Cavitating performance of two low-area-ratio water jet pumps having throat lengths of 7.25 diameters NASA-TN-D-4592 c03 N68-24461 Noncavitating and cavitating performance of two low-area-ratio water jet pumps with throat lengths of 5.66 diameters NASA-TN-D-4759 cl2 c12 N68-31960 NASA-TN-D-4709 SANTARPIA, D. E. A digital voltage-controlled oscillator for phase lock loops NASA-TN-D-4521 c09 N6 c09 N68-24389 SARAFI, Z. W. Ultrasonic attenuation in superconducting tantalum NASA-TN-D-4806 c26 N68-35356 SATO, R. N. A useful modification of the Wright spirometer NASA-TN-D-4234 c14 N68-10057 SAVAGE, H. F. Radiation damage in thick copper and gold specimens produced by low-energy protons NASA-TN-D-4452 c26 N68-21219 SAVIN, G. N. Rib-reinforced plates and shells NASA-TT-F-427 c32 N68-10407 SAVINO, J. M. Transient solidification of a flowing liquid on a cold plate including heat capacities of frozen layer and plate NASA-TN-D-4353 c33 N68-15742 SAWYER, J. C. Generation of long time creep data of refractory alloys at elevated temperatures NASA-CR-1115 c17 N68-29992 SAWYER, J. W. Comparison of the Mach 3.0 aerodynamic characteristics of tension string, tension shell, and 120 deg conical shapes

SAWYER, R. H.

NASA-TN-D-4360 c01 N68-18720 NASA-IN-U-3000 SAWYER, R. H. Simulation studies of the supersonic transport in the present day air traffic control system 1000-10-04638 c02 N68-29372 BAZONOV, V. N. Magnetobrems /synchrotron/ emission and reabsorption NASA-TT-F-521 c25 N68-16700 NASA-TI--7321 SCAL2DT3, L. L. Practical stability criterion and its application to digital simulation NASA-TN-D-4203 Load relief autopilot analysis to minimize launch vehicle peak thrust vector deflection result another c08 N68-26640 requirements NASA-TN-D-4786 c21 N68-33756 SCHALLA, R. L. Effect of green light on spectral response of cuprous sulfide-cadium sulfide photovoltaic cells NASA-TN-D-4333 c03 N68-14082 SCHETT, A. Lie series for celestial mechanics, accelerators, satellite stabilization and NASA-CR-1046 c19 N68-25841 NASA-CR-1046 c19 N68-SCHEUERMANN, C. M. Mechanism and kinetics of corrosion of selected iron and cobalt alloys in refluxing mercury NASA-TN-D-4450 c17 N68-SCHIFFMAN, B. M. Micrówave technique development for advanced radio astronomy and radiometry missions NASA-CR-979 c09 N68-SCHITPD. M. c17 N68-21654 c09 N68-13617 NASA-CR-979 CU9 Nos SCHILDER, M. Additional studies of quasi-optimum feedback control techniques NASA-CR-1099 c10 N68 c10 N68-28307 SCHILLING, B. L. Approximation of the spanwise distribution of wind-tunnel-boundary interference on lift of wings in rectangular perforated-wall test sections NASA-TR-R-285 c01 N68-24617 NASA-TK-K-285 CUI N68-SCHMADEBECK, R. L. A numerical least-square method for resolving complex pulse height spectra NASA-SP-3044 C24 N68c24 N68-29520 SCHMID, P. E. Lunar far-side communication satellites NASA-TN-D-4509 c31 N68-25358 SCHNIDT, J. F. Laminarization of a turbulent boundary layer as observed from heat-transfer and boundary layer measurements in conical nozzles NASA-TN-D-4788 c12 N68-33642 NASA-IN-Jun-2700 SCHOENBERG, A. A. Analysis of pressure-drop function in Rankine space power boilers with discussion of flow maldistribution implications c33 N68-NASA-TN-D-4498 c33 N68-20066 SCHDENSTER, J. A. Experimental investigation of the longitudinal vibration of a representative launch vehicle with simulated propellants NASA-TN-D-4502 c32 N68-2 c32 N68-21869 SCHOESSOW, G. J. Graphite triple point and solidus-liquidus interface experimentally determined up to 1000 atmospheres NASA-CR-1148 c22 N68-29390 NASA-CR-1148 SCHUERCH, H. U. Large low-frequency orbiting radio telescope NASA-CR-1201

NASA-CR-1201 c31 N68-37900 SCHUETT, R. Dynamic stability of space vehicles. Volume 3 - Torsional vibration modes NASA-CR-937 c32 N68-10568 SCHUL2-JANDER, B. Theory of the investigation of the atmosphere of binary stars by analogy between gas dynamics and shallow-water flows NASA-TN-D-4520 c30 N68-25385 SCHUM, H. J.

Cold-air investigation of a turbine for high-temperature engine application. 2 -

PERSONAL AUTHOR INDEX

Detailed analytical and experimental Investigation of stator performance NASA-TN-D-4418 c28 N68-16632 NASA-TN-D-4418 C28 N68-Effect of variable stator area on performance of a single-stage turbine suitable for air cooling. 1 - Stator overall performance with 130-percent design area NASA-TM-X-1632 c01 N68c01 N68-29994 Effect of variable stator area on performance of a single-stage turbine suitable for air cooling. 3 - Turbine performance with 130-percent design stator area NASA-TM-X-1663 c03 N68-35536 SCHWARTZ, I. R. Second conference on sonic boom research CO2 N68-34907 NASA-SP-180 SCHWARTZ, M. D. Guidance, flight mechanics and trajectory optimization. Volume 4 - The calculus of variations and modern applications c30 N68-15193 NASA-CR-1003 SCHMARTZ, S. Radiative equilibrium in an atmosphere with constant Einstein absorption coefficient NASA-TN-D-4479 c13 N c13 N68-22861 NASA-IN-D-4479 cl3 NGG-2200 SCIBBE, H. W. Friction torque of ball bearings in vacuum with seven polytetrafluoroethylene composition retainer materials NASA-TN-D-4355 cl5 N68-1640 c15 N68-16468 Cooling studies with 40-millimeter-bore ball bearings using low flow rates of 60 deg R /33 deg K/ hydrogen gas NASA-TN-D-4616 c15 N68 c15 N68-24456 SCIULLI, J. A. A logarithmic encoder for binary word compression NASA-TN-D-4290 c08 N68-18179 NASA-IN-D-4290 COB NOB-18. SCULLIN, V. J. Analytical investigation of supersonic turbomachinery blading. 1 - Computer program for blading design NASA-TN-0-4421 SECHLER, E. E. The buckling of thin-walled circular c08 N68-18620 cylinders under axial compression and bending NASA-CR-1160 c32 N68-33226 SECUNDE, R. R. Evaluation of alternating-current line-voltage regulators in auxiliary electric power systems NASA-TN-D-4627 c03 N68-28101 SEEBASS, A. R. Sonic boom research NASA-SP-147 c02 N68-21413 SEIDENSTEIN, S. Discrimination of increases in the brightness of a flashing beacon NASA-CR-1220 c05 N68-37819 SEKAS, N. J. Local heat transfer for water in entrance regions of tubes with tapered flow areas and nonuniform heat fluxes NASA-TM-X-1554 c33 N68-20338 ranon-10-A-1004 Tests of a single tube-in-shell water-boiling heat exchanger with a helical-wire insert and several inlet flow-stabilizing devices NASA-TN-D-4767 C33 N68-3 c33 N68-32099 SENHEL, J. W., JR. Two-stage potassium test turbine. Volume 4 - Materials support of performance and endurance tests NASA-CR-925 c03 N68-16351 NASA-CR-925 C03 N68 SERAFINI, T. T. Effect of film processing on cryogenic properties of poly/ethylene terephthalate/ NASA-TN-D-4762 c18 N68 c18 N68-33034 SEWALL, J. L. An experimental and analytical vibration study of thin cylindrical shells with and without longitudinal stiffeners NASA-TN-D-4705 c32 N68-33738 SHAHROKHI, F. Mie-scattering function NASA-CR-1022 c24 N68-21227 BHAKER, F. J. Nethod of calculating the normal modes and frequencies of a branched Timoshenko beam NASA-TN-D-4560 c02 NG c02 N68-22886

PERSONAL AUTHOR INDEX

SINCLAIR, J. H.

SHAKROKHI, F. Radiation heat transfer in absorbing, scattering, and emitting medium NASA-CR-1023 c33 N68-22318 SHAMSHINS, D. Effect on bluntness on hypersonic two-dimensional inlet type flows NASA-CR-1145 c c01 N68-35523 SHAPIRO, H. Monomolecular contamination of optical surfaces NASA-TN-D-4612 c14 N68-25375 SHAPIRO, W. Research and development of high-performance axial-flow turbomachinery. Volume 3 -Design of backup gas bearings NASA-CR-802 c03 N68-24597 SHEPARD, C. E. A high enthalpy plasma generator for entry heating simulation NASA-TN-D-4583 cll N c11 N68-24560 SHEPHERD, L. J. Relative annoyance and loudness judgements of various simulated sonic boom waveforms NASA-CR-1192 c04 c04 N68-35103 SHERMAN, W. L. Relativistic models of the universe with pressure equal to zero and time-dependent uniformity NASA-TR-R-282 SHERRY, M. E. c30 N68-20192 Application of statistical association techniques for the NASA document collection NASA-CR-1020 c08 N68c08 N68-17154 NASA-CR-1020 cd SHIFRIN, K. S. Scattering of light in a turbid medium NASA-TT-F-477 cd SHIGEMOTO, F. H. Investigation of air-flow velocity by laser backscatter NASA-TN-D-4453 cd c13 N68-22462 c20 N68-20375 SHINDO, S. The effect of the converging flow field of a tandem test section on longitudinal stability measurements converging flow field of a tandem test section on longitudinal stability measurements converging flow field of a tandem test section on longitudinal stability measurements converging flow field of a tandem test section on longitudinal stability NASA-CR-1198 cl1 N68 SHNEYDERMAN, A. L. Computations of elastic tensometric elements c11 N68-36522 NASA-TT-F-513 c32 N68-15796 SHOFNER, F. M. Application of negative feedback to reduction of glow discharge noise NASA-CR-1173 c16 N68-35099 SHOOK, D. F. Ages of D/d,n/He sup 3 and T/d,n/He sup 4 neutrons in water and tungsten-water mixtures NASA-TN-D-4581 c22 N68-25058 NASA-IN-D-4581 C22 Not SHOUMAN, A. R. Nonlinear heat transfer and temperature distribution through fins and electric filaments of arbitrary geometry with temperature-dependent properties and heat generation NASA-TN-D-4257 c33 N68-14052 SHOWMAN, R. D. Simple processors of star tracker commands for stabilizing an inertially oriented satellite NASA-TN-D-4490 c21 N68-SHREWSBURY, G. D. Effect of boattail juncture shape on pressure c21 N68-19236 drag coefficients of isolated afterbodies NASA-TM-X-1517 c01 N6 c01 N68-19237 Effect of a simulated wing on the pressure-drag coefficients of various 15 deg boattails at Mach numbers from 0.56 to 1.00 NASA-TM-X-1662 c01 N68-35672 Static performance of an auxiliary inlet ejector nozzle for supersonic-cruise aircraft NASA-TM-X-1653 c28 N68-35 c28 N68-35764 SHROUT, B. L. Effect of shape changes on the aerodynamic characteristics of a twisted and cambered arrow wing at Mach number 2.03 NASA-TN-D-4796 c01 N68-35665 SHULEMOVICH, A. M. Computations of elastic tensometric elements NASA-TT-F-513 c32 N68 c32 N68-15796

SICKLE, J. W. Wind-tunnel study to explore the use of slot spoilers to modulate the flap-induced lift of a wing NASA-TN-D-4664 c01 N68-28830 SIDDON, T. E. The shock expansion tube and its application as a sonic boom simulator NASA-CR-1055 c11 N68-24966 SIEGEL, B. L. Design and operation of a high-temperature tungsten-mesh gas heater NASA-TM-X-1466 c22 N68-10134 A 4500 deg R /2500 deg K/ flowing-gas facility NASA-TM-X-1506 c11 N68-14115 Heat-transfer correlation for gas flow across heated banks of wire meshes or tubes NASA-TN-D-4514 c33 N68-20374 SIEGEL, R. Transient solidification of a flowing liquid on a cold plate including heat capacities of frozen layer and plate NASA-TN-D-4353 c33 N68-1 c33 N68-15742 Thermal radiation heat transfer. Volume 1 -The blackbody, electromagnetic theory, and material properties NASA-SP-164 c33 N68 c33 N68-28530 Conformal mapping for steady two-dimensional solidification on a cold surface in flowing liquid NASA-TN-D-4771 c33 N68-32073 SIGMAN, D. R. Power transfer to ion cyclotron waves in a two ion species plasma NASA-TM-X-1481 c25 N68-1 c25 N68-11404 SIGNORELLI, R. A. The effect of interfiber distance and temperature on the critical aspect ratio in composites NASA-TN-D-4548 c17 Refractory metal fiber nickel base alloy composites for use at high temperatures c17 N68-22338 NASA-TN-D-4787 c17 N68-33684 NASA-TN-D-4787 c17 N68 SIKORA, P. F. Hot isostatic compaction of tungsten-uranium dioxide fuels with high-volume fraction of uranium dioxide NASA-TM-X-1563 c22 N68-21705 SILSBY, N. S. Simulation studies of the supersonic transport in the present day air traffic control system NASA-TN-D-4638 c02 N68-29372 SIMMONS, J. A. Study of propellant valve leakage in a vacuum Final summary report NASA-CR-1047 c27 N68-21893 SIMON, F. F. Minimum film-boiling heat flux in vertical flow of liquid nitrogen NASA-TN-D-4307 c33 N68-16683 NASA-IN-D 400. SIMON, W. E. Transient thermodynamic analysis of a fuel-cell system NASA-TN-D-4601 c03 N68-25304 SIMONEAU, R. J. Minimum film-boiling heat flux in vertical flow of liquid nitrogen NASA-TN-D-4307 c33 N c33 N68-16683 SIMONS, M. A study of charge storage in silicon oxide resulting from non-penetrating electron irradiation NASA-CR-1088 c26 N68-26603 SINCLAIR, A. R. Comparison of experimental and theoretical shock shapes and pressure distributions on flat-faced cylinders at Mach 10.5 NASA-TN-D-4397 c01 N68-15778 NASA-IN-D 405. SINCLAIR, D. H. Cryogenic temperature measurement using platinum resistance thermometers NASA-IN-D-4499 cl c14 N68-20324 NASA-IN-D-4499 C14 NOO-SINCLAIR, J. H. Compatibility of several iron-base, cobalt-base, and nickel-base alloys with refluxing potassium at 1800 deg F NASA-TM-X-1617 c17 N68c17 N68-30065

SINGH, J. J.

SINGH, J. J. High energy proton damage in silicon surface barrier detectors NASA-TN-D-4528 c26 N68-24660 SIVITER, J. H., JR. Flight investigation of a capacitance-type meteoroid detector using an inflatable paraglider NASA-TN-D-4530 c14 N68-22290 SLABY, J. G. A 4500 deg R /2500 deg K/ flowing-gas facility NASA-TM-X-1506 c11 N68-14115 SLINEY, H. E. Preliminary evaluation of greases to 316 deg C and solid lubricants to 816 deg C in ball bearings NASA-TN-D-4652 c15 N68-28766 SLUKHAI, I. A. Russian rocketry, a historical survey NASA-TT-F-426 SLUNDER, C. J. Thermal and mechanical treatment for a31 N68-22262 precipitation-hardening stainless steels NASA-SP-5089 SMELTZER, D. B. Investigation of a large-scale mixed c15 N68-20433 Investigation of a large-scale mixed compression axisymmetric inlet system capable of high performance at Mach numbers 0.6 to 3.0 NASA-TM-X-1507 c28 N68-170 Investigation of a nearly isentropic mixed compression axisymmetric inlet system at Mach numbers 0.6 to 3.2 NASA-TN-D-4557 c28 N68-230 c28 N68-17028 c28 N68-23354 SMITH, C. C., JR. Hot-gas ingestion investigation of large-scale jet VTOL fighter-type models NASA-TN-D-4609 c02 N68-28277 NASA-IN-D-4609 c0 SMITH, D. W. Navigator performance studies for space navigation using the NASA CV-990 research aircraft NASA-TN-D-4449 c21 N68-21123 A hand-held sextant qualified for space flight NASA-TN-D-4585 c21 N68-24512 SMITH, F. Z. Pyrotechnic shaped charge separation systems for aerospace vehicles NASA-TM-X-1607 c31 N68-28869 SMITH. G. L. Theoretical error analysis of a Doppler range-rate and phase-modulated range tracking system NASA-TN-D-4267 c10 N68-11513 SMITH, H. E. Lunar module pilot control considerations NASA-TN-D-4131 c21 N68-16836 NASA-TN-D-4131 c21 N68-1 SMITH, J. W. An analysis of the limit-cycle and structural-resonance characteristics of the X-15 stability augmentation system NASA-TN-D-4287 c02 N68-1 c02 N68-11545 SMITH, L. J. Sound measurements on a full-scale jet-engine inlet-noise-suppressor cowling NASA-TN-D-4639 c02 N6 c02 N68-29887 SMITH, O. E. Scalar and component wind correlations between altitude levels for Cape Kennedy, Florida, and Santa Monica, California c13 N68-20278 NASA-TN-D-3815 SMITH, R. C. An analytical investigation of the aerodynamic and performance characteristics of an unpowered rotor entry vehicle NASA-TN-D-4537 c31 N68-21758 SNITH, R. E., JR. Vehicle attitude determination with a single onboard camera NASA-TN-D-4359 c31 N68-19275 SMITH, R. L. Dynamic pressure limits for flat plates as related to nuclear fuel elements NASA-TN-D-4417 cl2 N c12 N68-16227 SMITH, S. H. Fatigue-crack-propagation and fracturetoughness characteristics of 7079 aluminum-

PERSONAL AUTHOR INDEX

alloy sheets and plates in three aged conditions NASA-CR-996 c32 N68-15476 SMITH, W. S. Temperature, pressure, density, and wind measurements in the stratosphere and mesosphere, 1966 NASA-TR-R-288 c20 N68-33036 SHITH, W. W. Use of a transcendental approximation in transient conduction analysis NASA-CR-955 c19 N68-11109 MITHRICK, J. J. Effects of cable and circuit parameters on the precision calibration of a charge amplifier NASA-TN-D-4300 c09 N c09 N68-16530 SMOLSKII, B. M. Heat and mass transfer. Volume 1 -Convective heat exchange in a homogeneous medium NASA-TT-F-431 c33 N68-11721 An investigation of the mechanisms of heat transfer in low-density phenolic-nylon chars NASA-CR-966 c18 N68-11978 SNEEGAS, E. C. Advanced valve technology, a survey NASA-SP-5019 c15 N68-10402 SNYDER, C. T. A piloted simulator study of takeoff performance and handling qualities of a double delta supersonic transport action of the supersonic transport NASA-TN-D-4396 c02 N68-17391 Analog study of the longitudinal response of a swept-wing transport airplane to wind shear and sustained gusts during landing approach NASA-TN-D-4477 c01 N68-19180 SNYDER, W. J. A summary of rotor-hub bending moments encountered by a high performance hingeless-rotor helicopter during nap-of-the-earth maneuvers NASA-TN-D-4574 c02 N68-24499 SOBEL, L. H. Buckling of shells of revolution with various wall constructions. Volume 3 - User*s manual for BOSOR NASA-CR-1051 c32 N68~23355 Buckling of shells of revolution with various wall constructions. Volume 2 - Basic equations and method of solution NASA-CR-1050 c32 N68-23451 Buckling of shells of revolution with various wall constructions. Volume 1 - Numerical results NASA-CR-1049 c32 N68-24481 SODERMAN, P. T. Wing surface pressure data from large-scale wind-tunnel tests of a propeller-driven STOL model NASA-TM-X-1527 c02 N68-19065 NASA-IN-A-192, SOEDER, R. H. Performance of a multiple single-pass counterflow NaK-cooled mercury Rankine cycle condenser NASA-TM-X-1548 c33 N68-20340 SOFFER, L. Activation of sodium, lithium, and potassium in compact fast reactors and its effect on shielding NASA-TM-X-1512 c22 N68-20355 Analysis and selection of design conditions for a radioisotope Brayton-cycle space powerplant NASA-TN-D-4600 c03 N68-25829 NASA-TN-D-4600 c03 N68-SOKOLOWSKI, D. E. Screech suppression techniques for rocket combustors using earth-storable propellants NASA-TN-X-1595 c28 N68c28 N68-26644 SOKOLSKII, V. N. Russian solid-fuel rockets c28 N68-11829 NASA-TT-F-415 SOLTIS, R. F. Detailed performance of a radial-bladed centrifugal pump impeller in water NASA-TN-D-4613 c12 N68-26651 Visual observations of flow through a radial-bladed centrifugal impeller

PERSONAL AUTHOR INDEX

STAFFANSON, F. L.

NASA-TN-D-4282 c12 N68-28842 SOMERLOCK, C. R. A precision spacecraft radiometer for hectometer wavelengths NASA-TN-D-4634 c14 N68-28327 NNSA-IN-B-1007 SOMES, A. H. Tabulated communication characteristics of a steady-state model of interplanetary space NASA-SP-3042 c30 N68-10164 NASA-ST-3042 C30 SOMMER, R. W. Evaluation of a closed-circuit television display in landing operations with a helicopter NASA-TN-D-4313 c05 N68-16594 Flight investigation to determine the effect of longitudinal characteristics on low-speed instrument operation NASA-TN-D-4364 c02 N68-19184 Effects of reduced airspeed for landing approach on flying qualities of a large jet transport equipped with powered lift NASA-TN-D-4804 c02 N68-37075 SORENSEN, N. E. Investigation of a large-scale mixed compression axisymmetric inlet system capable of high performance at Mach numbers 0.6 to 3.0 NASA-TM-X-1507 c2 c28 N68-17028 Investigation of a nearly isentropic mixed compression axisymmetric inlet system at Mach numbers 0.6 to 3.2 NASA-TN-D-4557 c28 N68-23 SORRELLS, R. B., III Evaluation of boundary layer and wake survey data reduction techniques in compressible c28 N68-23354 flows c12 N68-19709 NASA-TN-D-4401 SOUDERS, S. W. A semigraphical method for a deorbit trajectory design study NASA-TN-D-4801 c30 N68-36077 NASA-TN-D-4801 c30 N68-3 SOURIS, G. A. Project Gemini - A technical summary NASA-CR-1106 c31 N68-2 SOUTH, J. C., JR. Calculation of axisymmetric supersonic flow past blunt bodies with sonic corners, including a program description and listing NASA-TN-D-4563 c01 N68-2 SOVEY. J. S. c31 N68-25577 c01 N68-25093 SOVEY, J. S. Performance tests of a 1/2-millipound /2.2 mN/ ammonia resistojet thrustor system NASA-TN-D-4249 c28 N68-10562 Preliminary tests of a single-axis ammonia-resistojet attitude control system NASA-TM-X-1677 c28 NG SPACKMAN, D. J. Injection start of a Brayton cycle c28 N68-36512 turbocompressor operating on gas bearings in a closed loop NASA-TM-X-1590 c03 N68-24757 Use of an electronic visualization technique in the study of gas journal bearing behavior in the study of gas journal bearing content NASA-TM-X-1609 cl4 N68-SPADY, A. A., JR. Effects of pressure suits and backpack loads on man*s self-locomotion in earth and simulated lunar gravity c14 N68-35105 NASA-TN-D-4464 c05 N68-20354 SPAGNUOLO, A. C. Design and performance of two vacuum chambers and solar simulators for solar-cell research NASA-TM-X-1503 cll N68-1 c11 N68-16695 NASA-TM-X-1503 cii t Outgassing of water vapor from concrete surfaces in vacuum environment NASA-TM-X-1536 cii 1 Evaluation of tantalum to stainless steel transition joints NASA-TM-X-1540 ci5 1 Avguager A C c11 N68-19207 c15 N68-21898 SPAKUSKI, A. E. A 23.4 square-foot /2.17-SQ-M/ cadmium sulfide thin-film solar cell array NASA-TM-X-1519 c03 N68-20432 SPALVINS, T. Deposition of sputtered molybdenum disulfide Films and friction characteristics of such films in vacuum NASA-TN-D-4269 c17 N68 c17 N68-11644

SPANGLER, S. B. Investigation of methods for predicting the aerodynamic characteristics of two-lobed parawings parawings NASA-CR-1166 c0 SPARROW, G. W. Derivation of approximate equations for solving the planar rendezvous problem NASA-TN-D-4670 c3 c01 N68-33765 c30 N68-28841 SPEAR J S. Visual simulation facility for evaluation of lunar surface roving vehicles NASA-TN-D-4276 c11 N68-15858 SPENCER, A. R. Oxidation resistant materials for transpiration cooled gas turbine blades. 1 -Sheet specimen screening tests NASA-CR-930 c17 N68-17 c17 N68-17591 Oxidation resistant materials for transpiration cooled gas turbine blades. 2 - Wire specimen tests NASA-CR-1184 c17 i SPENCER, B., JR. Hypersonic aerodynamic characteristics of c17 N68-35098 low-wave-drag elliptical-body-tail combinations as affected by changes in stabilizer configuration NASA-TM-X-1620 c01 N68-29952 SPEWOCK, M. Properties of magnetic materials for use in high-temperature space power systems NASA-SP-3043 c17 c17 N68-17624 SPISZ, E. W. Experimental measurements of thermal radiation properties by cyclic incident radiation NASA-TM-X-1618 c33 N68-33 c33 N68-31498 Thermal radiative and electrical properties of a cadmium sulfide solar cell at low solar intensities and temperatures NASA-TN-D-4818 c03 N68-35467 SPRAGUE, E. L. Transient chilldown of a single thick-walled tube by liquid and gaseous hydrogen c33 N68-10368 NASA-TN-D-4238 Analytical investigation of thermal degradation of high-performance multilayer insulation in the vicinity of a penetration NASA-TN-D-4778 c33 N68c33 N68-33167 SPREEMANN, K. P. Wind-tunnel investigation of lateral aerodynamic characteristics of a powered four-duct-propeller VTOL model in transition NASA-TN-D-4343 c02 N68-1 c02 N68-17023 SPREITER, J. R. External aerodynamics of the magnetosphere NASA-TN-D-4482 c29 N c29 N68-25181 NASA-IN-D-4402 C25 NG-SPUCKLER, C. M. Experimental investigation of nucleate boiling bubble dynamics in normal and zero gravities NASA-IN-D-4301 C33 N68c33 N68-15330 SPURLOCK, J. M. Study of propellant valve leakage in a vacuum Final summary report NASA-CR-1047 c27 N68-21893 SPURLOCK, O. F. A trajectory code for maximizing the payload of multistage launch vehicles NASA-TN-D-4729 c30 N68 c30 N68-31989 STABE, R. G. Scale model study of flow patterns in the inlet manifold of the fuel pump drive turbine for the M-1 hydrogen-oxygen rocket engine NASA-TM-X-1513 c12 N68-150 c12 N68-15639 Cold-air performance evaluation of scale model oxidizer pump-drive turbine for the M-1 hydrogen-oxygen rocket engine. 3 -Performance of first stage with inlet-feedpipe-manifold assembly NASA-TN-D-4392 c28 N6 c28 N68-16413 Cold-air performance evaluation of scale model oxidizer pump-drive turbine for the M-1 hydrogen-oxygen rocket engine. 4 -Performance of first stage with modified inlet feedpipe-manifold assembly NASA-TN-D-4393 c28 No c28 N68-18188 STAFFANSON, F.L. Entry length for the rocket meteorological radiation shield

STAGGS, J. F.

PERSONAL AUTHOR INDEX

NASA-CR-1200 c14 N68-36530 STAGGS, J. F. Divergent-flow contact-ionization electrostatic thrustor for satellite attitude control and station keeping NASA-TN-D-4420 c28 N68-20187 STALEY, J. A. Dynamic stability of space vehicles. Volume 2 - Determination of longitudinal vibration modes NASA-CR-936 c32 STANKIEWICZ, N. Thermodynamic study of plasmas using the c32 N68-10280 principle of maximum entropy NASA-TN-D-4621 c25 N68-25920 STARK, W. W. Full-scale ground proximity investigation of a VTOL fighter model aircraft NASA-CR-1098 c02 N68-28233 STATON, L. D. Dynamics of a one-dimensional plasma sheath NASA-TN-D-4651 STAYLOR, W. F. Aerodynamic characteristics of a modified c25 N68-30031 cone - Conical-frustum entry configuration at Mach 6.0 NASA-TN-D-4598 c31 N68-24964 STEFFEN, F. W. Performance of a wind tunnel model of an aerodynamically positioned variable flap ejector at Mach numbers from 0 to 2.0 NASA-TM-X-1639 c28 N c28 N68-30599 NHJA-IM-X-1539 C28 Comparison of experimental and predicted heat transfer characteristics for a cylindrical ejector NASA-TM-X-1641 c33 c33 N68-32988 STEFFENS, L. E. Description and flight performance results of the Wasp sounding rocket NASA-TM-X-1518 c31 N68-17094 STEIGERWALD, E. A. Generation of long time creep data of refractory alloys at elevated temperatures NASA-CR-1115 c17 N68-29992 NMON-ON III STEIN, B. A. Coatings and surface treatments for longtime protection of Ti-8Al-1Mo-1V alloy sheet from hot salt stress corrosion C17 N68c17 N68-17377 Effects of longtime environmental exposure on mechanical properties of sheet materials for a supersonic transport NASA-TN-D-4318 c17 N68-178 c17 N68-17897 STEKETEE, F. D. Dynamic stability of space vehicles. Volume 11 - Entry disturbance and control NASA-CR-945 c32 N6 c32 N68-11133 STEPHENS, J. R. Ductility mechanisms and superplasticity in chromium alloys NASA-TN-D-4346 c14 N68-13973 STEPKA, F. S. Considerations of turbine cooling systems for Mach 3 flight NASA-TN-D-4491 c33 N68c33 N68-19187 STERNFELD, H., JR. Subjective response to synthesized flight noise signatures of several types of V/STOL aircraft NASA-CR-1118 c05 N68-33009 STEVENS, N. J. Thermal investigation of an ion engine microthrustor NASA-TM-X-1473 c28 N68-10496 STEWART, W. L. Use of similarity parameters for examination of geometry characteristics of high-expansion-ratio axial-flow turbines NASA-TN-D-4248 c Analysis of fan-turbine efficiency characteristics in terms of size and c01 N68-10529 stage number NASA-TM-X-1581 c28 N68-22725 Turbojet and turbofan cycle considerations and engine configurations for application in lightweight aircraft NASA-TM-X-1624 c28 N68-31476 STEWART, W. M. Scattering of 42-MeV /6.7-pJ/ alpha

particles from even isotopes of cadmium NASA-TN-D-4256 c24 l c24 N68-11074 Gamma ray angular correlations following inelastic scattering of 42-MeV alpha particles from magnesium 24 c24 N68-29375 NASA-TN-D-4683 STIEFVATER, O. L. A study of trace contaminant identification by microwave double resonance spectroscopy NASA-CR-967 c24 N68-11634 STOCHL, R. J. Temperature and liquid-level sensor for liquid-hydrogen pressurization and expulsion studies NASA-TN-D-4339 c14 N68-15893 STOFAN, A. J. Experimental investigation of vapor ingestion in the Centaur liquid hydrogen tank NASA-TM-X-1482 c12 N68-19225 Management of cryogenic propellants in a full scale orbiting space vehicle NASA-TN-D-4571 c28 N68c28 N68-25099 Centaur launch vehicle propellant utilization system NASA-TN-D-4848 c28 N68-36 STONE, D. R. Effects of lee-surface volume addition on longitudinal aerodynamics of a high-lift-drag-ratio wing-body configuration c28 N68-36507 at Mach 6.0 NASA-TN-D-4361 c01 N68-17880 STONE, J. R. Local heat transfer for water in entrance regions of tubes with tapered flow areas and nonuniform heat fluxes NASA-TN-X-1554 c33 N68-Tests of a single tube-in-shell water-boiling heat exchanger with a helical-wire insert and several inlet flow-stabilizing devices NASA-TN-D-4767 c33 N68c33 N68-20338 c33 N68-32099 STORTI, G. M. Investigation of electron-radiation-induced dielectric breakdowns in a typical capacitor meteoroid detector system NASA-TN-D-4738 c14 N68-33277 Experimental investigation and analysis of dielectric breakdowns induced by electron irradiation in polymer films NASA-TN-D-4810 c24 N68-36070 STRACK, W. C. Some numerical comparisons of three-body trajectories with patched two body trajectories for low thrust rockets NASA-TN-D-4559 c30 N68-22289 STROHECKER, D. E. Deformation processing of precipitation-hardening stainless steels NASA-SP-5088 c17 c17 N68-21917 STROUB, R. H. An investigation of full-scale helicopter rotors at high advance ratios and advancing tip Mach numbers NASA-TN-D-4812 col NGi STROUD, C. W. A study of the reaction-plane approximation in ablation analyses NASA-TN-D-4817 c33 NGi c01 N68-28268 c33 N68-36072 STROUD, W. J. Stresses caused by an in plane line load used to rotate a thin-walled spherical satellite NASA-TN-D-4425 c31 N68c31 N68-20198 STRUTZ, L. W. Preliminary flight evaluation of the stability and control derivatives and dynamic characteristics of the unaugmented XB-70-1 airplane including comparisons with predictions NASA-TN-D-4578 c02 N68-24498 STUART, F. R. The buckling of thin-walled circular cylinders under axial compression and bending NASA-CR-1160 c32 N68-33226 STUBBS, S. M. Water pressure and accelerations during landing of a dynamic model of the Apollo spacecraft with a deployed-heat-shield impact-attenuation system NASA-TN-D-4275 c31 N68-18822

PERSONAL AUTHOR INDEX

TAYLOR, G. R.

STUMPFF, K. A fast method of orbit computation NASA-TN-D-4470 c30 N68-20356 On the application of spinors to the problems of celestial mechanics NASA-TN-D-4447 c3 On the application of Lie-series to the problems of celestial mechanics NASA-TN-D-4460 c3 c30 N68-22885 c30 N68-26643 STYER, E. F. Studies of cost effective structures design for future space systems - Summary Final report, 17 Oct. 1966 - 17 Oct. 1967 NASA-CR-1068 c34 N6 c34 N68-26813 SUIT, W. T. A simulator study of pilot control of remote orbital docking of large attitude-stabilized components NASA-TN-D-4263 c31 N68-11476 SULLIVAN, D. B. Superconduction thin films NASA-CR-1189 c26 N68-35178 SULLIVAN, G. M. Simple processors of star tracker commands for stabilizing an inertially oriented satellite NASA-TN-D-4490 c21 N68-1: c21 N68-19236 SULLIVAN, R. E. Reactivity insertions in compact reactor cores due to fuel movement NASA-TM-X-1587 c22 N68-23894 SULLIVAN, T. L. Texture strengthening and fracture toughness of titanium alloy sheet at room and cryogenic temperatures NASA-TN-D-4444 c17 N68-22884 SUMMERS, A. L. External aerodynamics of the magnetosphere NASA-TN-D-4482 c29 N68-25181 SUMP, W. D. Tatigue-crack-propagation and fracture-toughness characteristics of 7079 aluminumalloy sheets and plates in three aged conditions NASA-CR-996 c32 N68-15476 NASA-CK-990 SUTHERLAND, W. W. Relative annoyance and loudness judgements of various simulated sonic boom waveforms 004 N68-35103 SUTTON. K. Experimental and theoretical investigation of the ablative performance of five phenolic-nylon-based materials NASA-TN-D-4374 c18 N68-19710 Description and operating parameters of a Mach 2 nozzle system for the Langley 11-inch ceramic-heated tunnel NASA-TN-D-4750 c11 N68-33190 SWARTZ, P. C. Temperature, pressure, density, and wind measurements in the stratosphere and mesosphere, 1966 NASA-TR-R-288 c20 c20 N68-33036 NASA-IK-K-200 SWENSON, B. L. Analysis of launch windows from circular orbits for representative Mars missions NASA-IK-X-1651 c30 / c30 N68-33371 SWETT, C. C. Enhancement of ion cyclotron waves in hydrogen helium mixtures NASA-TN-D-4271 c25 N68-18485 SWIFT, C. T. The aperature admittance of a ground plane mounted waveguide illuminating a perfectly conducting sheet NASA-TN-D-4366 c07 N68 c07 N68-18123 The input admittance of a rectangular aperture antenna loaded with a dielectric plug NASA-TN-D-4430 c07 N68-20333 Electromagnetic properties of a circular aperture in a dielectric-covered or uncovered ground plane NASA-TN-D-4752 c07 N68-35537 SWIGERT, P. Computer program for symbolic reduction of block diagrams using FORMAC NASA-TN-D-4617 c08 N68-24967 PLOT3D - A package of FORTRAN subprograms to draw three-dimensional surfaces

NASA-TM-X-1598 c19 N68-28240 NASA-IN-A 1995 SWIKERT, N. A. Friction and wear under fretting conditions of materials for use as wire friction dampers of compressor blade vibration 1990 - 19900 - 1990 - 19900 - 19900 - 19900 - 19900 - 19900 - 19900 - 19900 - 19900 - 19900 - 19900 - 19 c15 N68-28871 SYKES, N. P. Stresses caused by an in plane line load used to rotate a thin-walled spherical satellite NASA-TN-D-4425 c31 N68c31 N68-20198 SYMONS, E. P. Liquid inflow to initially empty, hemispherical ended cylinders during weightlessness NASA-TN-D-4628 c12 N68-25866 Liquid vapor interface configurations in toroidal tanks during weightlessness NASA-TN-D-4819 cl. SYROVATSKII, S. I. Magnetobrems /synchrotron/ emission and c12 N68-35823 reabsorption NASA-TT-F-521 c25 N68-SZABO, S. V., JR. Management of cryogenic propellants in a full scale orbiting space vehicle NASA-TN-D-4571 c28 N68c25 N68-16700 c28 N68-25099 Successful restart of a cryogenic upper-stage vehicle after coasting in earth orbit NASA-TM-X-1649 c3 c31 N68-33683 Centaur launch vehicle propellant utilization system NASA-TN-D-4848 c28 N68-36507 SZANCA, E. M. Cold-air investigation of a turbine for high-temperature-engine application. 3 - Overall stage performance NASA-TN-D-4389 col N68-1 Effect of variable stator area on performance c01 N68-15743 of a single-stage turbine suitable for air cooling. 1 - Stator overall performance with 130-percent design area NASA-TM-X-1632 c01 N68-29994 NB3A-16-X-1632 COL NGG-Effect of variable stator area on performance of a single stage turbine suitable for air cooling. 4 - Stator overall performance with 70 percent design area NASA-TM-X-1675 C28 N68c28 N68-37264 SZUCH, J. R. Experimental verification of a double dead time model describing chugging in liquid bipropellant rocket engines NASA-TN-D-4564 c33 N68-25102 Т TABACHNICK, B. J. A descriptive model for determining optimal human performance in systems. Volume 3 - An approach for determining the optimal role of man and allocation of functions in an aerospace system NASA-CR-878 c05 N68-19165 TAILLON, N. V. A method for the surface installation and fairing of static-pressure orifices on a large supersonic-cruise airplane NASA-TM-X-1530 c01 TAMBURRO, M. B. Guidance, flight mechanics and trajectory optimization. Volume 3 - The two-body c01 N68-19341 problem NASA-CR-1002 Guidance, flight mechanics and trajectory optimization. Volume 1 - Coordinate c30 N68-14089 systems and time measure NASA-CR-1000 c30 N6 Guidance, flight mechanics and trajectory optimization. Volume 14 - Entry guidance c30 N68-16103 equations NASA-CR-1013 c30 N68-19985 TASHJIAN, H. Tabulated communication characteristics of a steady-state model of interplanetary space NASA-SP-3042 c30 N68c30 N68-10164 TAYLOR, G. R. Review of causes and alleviation of low tire traction on wet runways NASA-TN-D-4406 c02 N68-19620 TAYLOR, H. E.

TAYLOR, H. E. Aspect determination in lunar shadow on Explorer 35 NASA-TN-D-4544 c30 N68-24486 TAYLOR, J. J. Mars landing mission mode comparison NASA-TM-X-1629 c30 N68-29988 TAYLOR, L. W., JR. An analysis of the limit-cycle and structural-resonance characteristics of the X-15 stability augmentation system NASA-TN-D-4287 c02 N68-1 c02 N68-11545 ARSH-IN-D-4207 CU2 NOS-1. TAYLOR, M. F. Correlation of local heat transfer coefficients for single phase turbulent flow of hydrogen in tubes with temperature ratios to 23 NASA-TN-D-4332 c33 N68-14240 Photographic study of a bromine jet in a coaxial airstream NASA-TN-D-4660 c12 c12 N68-28370 TAYLOR, T. Self-synchronizing bi-orthogonal coded PCM telemetry system NASA-TR-R-292 c07 N68-36333 TAYLOR, W. C. The effects of a plasma in the near-zone field of an antenna, 2 NASA-CR-1149 c07 c07 N68-33042 TEICHMAN, L. A. The fabrication and testing of Pageos 1 NASA-TN-D-4596 c31 N68-25820 TEPER, G. L. A study of fully manual and augmented manual control systems for the Saturn 5 booster using analytical pilot models NASA-CR-1079 c31 N c31 N68-28426 TERBEEK, H. G. Cryogenic temperature measurement using platinum resistance thermometers NASA-TN-D-4499 cl. c14 N68-20324 TEREN, F. Analytical calculation of partial derivatives relating lunar and planetary midcourse correction requirements to guidance system injection errors NASA-TN-D-4518 c30 N68-20368 stability analysis and minimum thrust vector control requirements of booster vehicles during atmospheric flight NASA-TN-D-4593 c21 N68-24409 Thrust-vector control requirements for large launch vehicles with solid-propellant first stages NASA-TN-D-4662 c31 N68-28690 A trajectory code for maximizing the payload of multistage launch vehicles NASA-TN-D-4729 c30 N68 c30 N68-31989 Load relief autopilot analysis to minimize launch vehicle peak thrust vector deflection requirements NASA-TN-D-4786 c21 N68-33756 THALLER, L. H. Discharge characteristics of some copper oxide-magnesium thermal cells NASA-TN-D-4306 c03 N68-20344 Effect of amount of electrolyte, drain rate and electrode geometry on performance of copper oxide-magnesium thermal cells NASA-TN-D-4790 c03 N68-34234 THAU, F. E. Additional studies of quasi-optimum feedback control techniques NASA-CR-1099 c10 N68-28307 THEON, J. S. Some meteorological observations of the Southern Hemisphere stratosphere and mesosphere NASA-TN-D-4264 c20 N68-25617 Temperature, pressure, density, and wind measurements in the stratosphere and mesosphere, 1966 NASA-TR-R-288 c20 c20 N68-33036 THIBODEAU, J. R., III Use of planetary oblateness for parking-orbit alinement NASA-TN-D-4657 c30 N68-28408 THINGER, B. E. Gamma flux and heat deposition in Plum Brook

PERSONAL AUTHOR INDEX

reactor - Comparison of calculation and experiment NASA-TM-X-1539 c22 N68-22022 THOLLOT, P. A. Experimental investigation of reactor-loop transients during startup of a simulated SNAP-8 system NASA-TN-D-4546 c03 N68-22257 THOMAS, L. G. Visual simulation facility for evaluation of lunar surface roving vehicles NASA-TN-D-4276 c11 N68-15858 THOMAS, N. Radiative and convective heating during atmospheric entry NASA-CR-1170 c33 N68-35248 THOMAS, R. D. Automated data collection system applied to Hall effect and resistivity measurements NASA-TM-X-1464 c03 N c03 N68-10103 NASA-IM-X-1464 C03 NG Spectral emissivity of highly doped silicon NASA-TN-D-4303 c26 NG THOMPSON, W. M., JR. A theoretical and experimental investigation of the three-dimensional vibration characteristics of a scaled c26 N68-21708 model of an asymmetrical launch vehicle NASA-TN-D-4707 c32 c32 N68-32051 NASA-TN-D-4707 c32 N68-THOMSON, R. G. Ballistic limit of aluminum plates determined by an exploding foil gun technique NASA-TN-D-4259 c32 N68c32 N68-11355 Plastic behavior of circular plates under transverse impulse loadings of Gaussian distribution NASA-TR-R-279 c32 N68-14640 THORPE, M. L. Induction plasma heating - System performance, hydrogen operation and gas core reactor simulator development c25 N68-29888 NASA-CR-1143 TIBBS, D. F. Evaluation of a closed-circuit television display in landing operations with a helicopter NASA-TN-D-4313 c05 N6 TINLING, B. E. A technique for passive attitude control of solar oriented interplanetary spacecraft NASA-TN-D-4641 c21 N6 c05 N68-16594 c21 N68-28361 TITRAN, R. H. Creep of tantalum T-222 alloy in ultrahigh vacuum for times up to 10,000 hours c17 N68-24111 NASA-TN-D-4605 TODD, C. A. Computer program for calculating isothermal, turbulent jet mixing of two gases NASA-TN-D-4378 c12 N68-18146 TOLSON, R. H. A new method of testing small samples for goodness of fit to normal populations NASA-TN-D-4405 c19 c19 N68-19144 TOMAZIC, W. A. M-1 injector development - Philosophy and implementation NASA-TN-D-4730 c28 N68-30604 TOWNSEND, G. E. Guidance, flight mechanics and trajectory optimization. Volume 3 - The two-body problem NASA-CR-1002 c30 N68-14089 Guidance, flight mechanics and trajectory optimization. Volume 1 - Coordinate systems and time measure NASA-CR-1000 c30 c30 N68-16103 Guidance, flight mechanics and trajectory optimization. Volume 11 - Guidance equations for orbital operations NASA-CR-1010 c30 N Guidance, flight mechanics and trajectory optimization. Volume 8 - Boost guidance c30 N68-17215 equations NASA-CR-1007 c30 N68-20449 optimization. Volume 5 - State determination and/or estimation NASA-CR-1004 c30 N68-21685 TRAVERS. A. Experimental investigation of flow patterns in

radial-outflow vortexes using a rotating-peripheral-wall water vortex tube NASA-CR-991 c22 N68 NASA-CR-991 c22 N68-16478 Experimental investigation of radial-inflow vortexes in jet-injection and rotating peripheral-wall water vortex tubes NASA-CR-1028 TREBILCOCK, W. R. Optimal computing forms for the two-body C and S series NASA-TN-D-4643 C19 c19 N68-29407 TROMBKA, J. I. A numerical least-square method for resolving complex pulse height spectra NASA-SP-3044 c24 N68c24 N68-29520 TROUT, O. F., JR. An investigation of leakage of large-diameter O-ring seals on spacecraft air-lock hatches NASA-TN-D-4394 c31 N68c31 N68-17498 TROUTMAN, S. J. Automatic control of water cooling in space suits NASA-CR-1085 c05 N68-26701 TSAL, L. L. The reflection coefficient of a TEM mode parallel-plate waveguide illuminating a conducting sheet - The large wedge angle case NASA-CR-1174 c07 N68-35172 TSAKONAS, S. Hydrodynamics of aircraft tire hydroplaning NASA-CR-1125 c12 N6 c12 N68-31593 TSCHUKCD, H. F. A. Mathematical determination of geometrical image aberrations in single and double mirror austema NASA-TN-D-4692 c23 N68-36460 TUQUILA, W. J. Experimental study of aeroelastic instability of overexpanded rocket nozzle extensions NASA-TN-D-4471 c32 N68-21099 TURNER, R. E. A matrix method for studying motions of spacecraft consisting of interconnected rigid bodies NASA-TN-D-4749 c32 N68-33092 TURNER, T. R. A moving-belt ground plane for wind-tunnel ground simulation and results for two jet-flap configurations NASA-TN-D-4228 c01 N68-10060 Wind-tunnel investigation of a 3/8-scale automobile model over a moving-belt ground plane NASA-TN-D-4229 c01 N68-10093 TURNEY, R. L. Dynamic stability of space vehicles. Volume 6 - Full scale dynamic testing for mode determination NASA-CR-940 c32 N68-11054 TYSL, E. R. Overall performance in argon of a 6-inch radial-bladed centrifugal compressor NASA-TM-X-1622 c01 N68-30033

Y

UGUCCINI, O. W. An integrating sphere spectroradiometer for solar simulator measurements NASA-TN-D-4822 cl4 N68-35534 UNGAR, E. E. Panel loss factors due to gas-pumping at structural joints NASA-CR-954 c32 N68-11489

Y

- VAGI, J. J.
 Welding of precipitation-hardening stainless steels
 NASA-SP-5087
 C15 N68-21429
 VAHL, W. A.
 Calibration of 30 deg included-angle cone for
- VAHL, V. A. Calibration of 30 deg included-angle cone for determining local flow conditions in Mach number range of 1.51 to 3.51 NASA-TN-D-4679 c14 N68-30127 Flow field properties near an arrow wing-body
 - Flow field properties near an arrow wing-body model at Mach numbers of 1.60, 2.36, and 2.96 NASA-TN-D-4809 col N68-37238

VALERINO, A. S. SNAP-8 simulator loop mechanical design NASA-TM-X-1515 cl c11 N68-18460 VALGORA, M. E. Performance characteristics of 15 kVA homopolar inductor alternator for 400 Hz Brayton-cycle space-power system c03 N68-30002 NASA-TN-D-4698 NASA-TN-D-4698 c03 N68-301 VAN DOEREN, R. E. Input admittance and reflection coefficient of a circular aperture in a ground plane covered by a homogeneous dielectric or plasma slab NASA-CR-1177 c25 N68-35 VAN HOUTEN, J. J. The shock expansion tube and its application c25 N68-35171 as a sonic boom simulator NASA-CR-1055 c11 N68-24966 Investigation of the calibration of microphones for sonic boom measurement NASA-CR-1075 c14 c14 N68-25316 VAN LEYNSEELE, F. J. Evaluation of lateral-directional handling qualities of piloted reentry vehicles utilizing a fixed base simulation NASA-TN-D-4410 c31 N c31 N68-19226 VANCO, M. R. Computer program for design of two dimensional supersonic nozzle with sharp edged throat c01 N68-14747 NASA-TM-X-1502 VARY, A. A radiator concept based on capillary retention of liquid NASA-TN-D-4370 c03 N68-28310 VELEZ, C. E. General Lagrangian interpolation formulas NASA-TN-D-4424 c19 N68-22809 Local-error control and its effects on the optimization of orbital integration NASA-TN-D-4542 c30 N c30 N68-25867 VENDELL, E. W. Boundary corrections for a three-coil conductivity/velocity plasma probe NASA-TN-D-4538 VERETTE, R. M. Shell analysis manual c25 N68-21691 NASA-CR-912 c32 N68-24802 VERMA, G. R. Quantum mechanical study of molecules -Eigenvalues and eigenvectors of real symmetric matrices c24 N68-11903 NASA-CR-983 VERMILLION, C. H. Constructing inexpensive automatic picture-transmission ground stations NASA-SP-5079 c c07 N68-19624 VICK, A. R. VICK, A. H. An experimental study of flame propagation in supersonic premixed flows of hydrogen and air NASA-TN-D-4631 c33 N68-28100
 VILLASENOR, A. J. Digital spectral analysis NASA-TN-D-4510 c08 N68-25268
 VINCENT, D. W. Experimental investigation of acoustic liners to suppress screech in storable propellant to suppress screech in storable propellant rocket motors NASA-TN-D-4442 c28 N68-18249 Screech suppression techniques for rocket combustors using earth-storable propellants NASA-TN-X-1595 VINCENT, J. S. A search for unbound helium 3 levels with c28 N68-26644 isobaric spin 1/2 NASA-TN-D-4377 c24 N68-15638 VINCENT, T. L. Multisegmented optimal trajectories NASA-CR-1103 c30 N68-25895 VINH, N. X. Optimum maneuvers of hypervelocity vehicles NASA-CR-1078 c02 N68-25817 VIN2, F. L. Visual simulation facility for evaluation of lunar surface roving vehicles NASA-TN-D-4276 c11 N68-15858 VODOPIA, S. N. Study of advanced antenna techniques for rendezvous radar NASA-CR-764 c07 N68-28135

VOGT, W. G.

PERSONAL AUTHOR INDEX

VOGT, W. G. Lyapunov stability for partial differential equations. Part 1 - Lyapunov stability theory and the stability of solutions to partial differential equations. Part 2 -Contraction groups and equivalent norms NASA-CR-1100 c19 c19 N68-27457 VOLKIN, H. C. Coupled-channels method for rearrangement collisions NASA-TN-D-4633 c24 N68-28265 Iterated commutators and functions of operators NASA-TN-J-405, VOLPICELLI, R. J. A study of trace contaminant identification by microwave double resonance spectroscopy c24 N68-11634 NASA-TN-D-4857 c19 N68-36525 VONBUN, F. C. Determining the spin axis of a spinning satellite NASA-TN-D-4483 c30 N68-21182 A Hummingbird for the L sub 2 lunar libration point NASA-TN-D-4468 c30 N68-21733 Space trajectories and errors in time, frequency, and tracking station location NASA-TN-D-4507 c30 N c30 N68-25271 NASA-IN-D-4507 c30 N VORREITER, J. W. A high enthalpy plasma generator for entry heating simulation NASA-IN-D-4583 c11 N c11 N68-24560 VRANCIK, J. E. Semiconductor switches for aerospace alternating-current power applications NASA-TM-X-1495 c09 c09 N68-15649 Evaluation of alternating-current line-voltage regulators in auxiliary electric power systems NASA-TN-D-4627 c03 N68-28101 Prediction of windage power loss in alternators NASA-TN-D-4849 c03 N68-37162 VYAS, R. K. Membrane analysis of scalloped shells NASA-TN-D-4687 c32 N68-28832

W

WAGNER, J. M. Use of wire lacing to reduce blade vibration in an axial-flow compressor rotor NASA-TM-X-1603 c32 N68-28238 WALBERG, G. D. Experimental and theoretical investigation of the ablative performance of five phenolic-nylon-based materials NASA-TN-D-4374 c18 N68-19710 WALLACE, S. A. Relativistic models of the universe with pressure equal to zero and time-dependent uniformity NASA-TR-R-282 c30 N68-20192 WALLMARK, J. T. MOS field-effect-transistor technology NASA-CR-1113 c08 N68-35193 WALSH. E. J. Research on field-aligned propagation of HF radiowaves using Alouette 2 topside sounder data and digital ray-tracing techniques NASA-TN-D-4748 c07 N68c07 N68-31639 WALSH, T. M. Factors affecting the design and use of a photographic sextant for space navigation NASA-TN-D-4285 c21 N6 c21 N68-11902 Analysis of a star-field mapping technique for use in determining the attitude of a spin-stablized spacecraft NASA-TN-D-4637 c21 N68-28418 MADA-IN-D-403/ A celestial attitude measurement instrument for Project Scanner NASA-TN-D-4742 Attitude determination of the spin-stabilized Project Scanner spacecraft c21 N68-31938 NASA-TN-D-4740 c21 N68-31957 And In D 1140 constraints on optical qualities of a spacecraft window NASA-TN-D-4845 ci c23 N68-36470 WALTON, T. E., JR. Flight investigation of the effects of Apollo

heat-shield singularities on ablator performance NASA-TN-D-4791 c33 N68-35116 WANHAINEN, J. P. Cooled baffle development for M-1 engine using a subscale rocket engine NASA-TM-X-1267 c28 N68-18216 Experimental investigation of acoustic liners to suppress screech in storable propellant rocket motors NASA-TN-D-4442 c28 N68-18249 Effect of chamber pressure, flow per element, and contraction ratio on acoustic-mode instability in hydrogen-oxygen rockets NASA-TN-D-4733 c33 c33 N68-30518 Effect of thrust per element on combustion stability characteristics of hydrogen oxygen rocket engines NASA-TN-D-4851 c28 N68-36515 WARD, J. J. Parametric analysis of radioisotope cascaded thermoelectric generators NASA-TM-X-1501 Parametric analysis of radioisotope c22 N68-14585 thermoelectric generators NASA-TM-X-1453 c03 N68-14630 WARE, G. M. Wind-tunnel investigation of the static aerodynamic characteristics of a multilobe gliding parachute NASA-TN-D-4672 c01 N68-28447 WARNECK, P. Improvement and optimization of a mass spectrometer employing a photoionization source NASA-CR-1018 c14 N68-17329 WARNECKE, G. A satellite view of Typhoon Marie 1966 development NASA-TN-D-4757 c20 N68-37869 NASA-IN-D-4/37 C. WARNER, D. N., JR. Effects of edge constraints on optical qualities of a spacecraft window NASA-IN-D-4845 c. c23 N68-36470 NASA-IN-D-4645 C25 WARNER, R. E. A search for unbound helium 3 levels with isobaric spin 1/2 NASA-TN-D-4377 c24 N68-15638 WARSHAY, M. Effects of boundary layer buildup in shock tubes upon chemical rate measurements NASA-TN-D-4795 cl2 N WASKO, R. A. c12 N68-34089 Performance of annular plug and expansion-deflection nozzles including external flow effects at transonic Mach numbers NASA-TN-D-4462 c01 N68-20330 NASA-IN-U-4452 col No Performance of a collapsible plug nozzle having either two-position cylindrical or variable angle floating shrouds at Mach numbers from 0 to 2.0 NUMBERS ITOM O to 2.0 NASA-TM-X-1657 c WASSERBAUER, C. A. Aerodynamic performance of a 4.59-inch modified radial-inflow turbing for a c01 N68-36132 single-shaft Brayton cycle space power system NASA-TM-X-1615 c03 N68-28870 NASA-1M-X-1615 C03 N68-288 WASSERBAUER, J. F. Experimental investigation of the dynamic response of a supersonic inlet to external and internal disturbances NASA-TM-X-1648 c01 N68-33374 WASSUM, D. L. Preliminary study of drag reduction for coasting missiles at Mach numbers from 1.57 to 4.63 NASA-TM-X-1537 c01 N68-19206 WATERS, J. Optical absorption in fused silica during TRIGA reactor pulse irradiation NASA-CR-1031 c22 N68-21124 Optical absorption and fluorescence in fused silica during TRIGA pulse irradiation NASA-CR-1191 c22 N68 c22 N68-35826 WATERS, W. J. Application of directional solidification to a NASA nickel-base alloy /TAZ-88/

PERSONAL AUTHOR INDEX

NASA-TN-D-4390 c17 N68-15637 NASA-IN-U-4555 WATLINGTON, R. A. Some laboratory techniques of wave analysis with application to the Apollo program NASA-TM-X-1599 c08 N68-30240 WATSON, R. D. Pressure distributions and aerodynamic characteristics of 90 deg and 15 deg blunted cones in nitrogen and helium at Mach 20 NASA-TN-D-4314 c01 N68-17896 WATT. J. J. Transient chilldown of a single thick-walled tube by liquid and gaseous hydrogen NASA-TN-D-4238 c33 N68-10368 WATTS, J. W. An analysis of energetic space radiation and dose rates NASA-TN-D-4404 c29 N68 c29 N68-16837 WEAVER, W. L. Revised upper-air wind data for Wallops Island based on serially completed data for the years 1956 to 1964 NASA-TN-D-4570 c20 N68-24028 WEBB, L. D. Characteristics and use of X-15 air-data sensors NASA-TN-D-4597 c14 N68-25317 WEBB, P. The principle of the space activity suit NASA-CR-973 c05 N68-11510 Automatic control of water cooling in space auite NASA-CR-1085 c05 N68-26701 WEBELER, R. W. H. Damping of a torsional oscillator in liquid helium 4 and 3 from 0.4 deg to 2.5 deg K NASA-TN-D-4381 c26 N68-17594 WEBER, K. E. Stress corrosion of titanium alloys under simulated supersonic flight conditions NASA-CR-981 cl7 N68-11522 WEBER, R. J. The boiloff problem with methane fuel in supersonic aircraft NASA-TM-X-1604 c27 N68-28155 WEETON, J. W. Refractory metal fiber nickel base alloy composites for use at high temperatures NASA-TN-D-4787 c17 c17 N68-33684 WEI, M. H. Y. Nonlinear lift and pressure distribution of slender conical bodies with strakes at low speeds NASA-CR-1202 c01 N68-37255 WEIBERG, J. A. Large-scale wind-tunnel tests of an airplane model with two propellers and rotating cylinder flaps NASA-TN-D-4489 c01 N68-19189 WEIGEL, C. Overall performance in argon of a 6-inch radial-bladed centrifugal compressor NASA-TM-X-1622 col c01 N68-30033 WEILL, J. Lie series for celestial mechanics accelerators, satellite stabilization and optimization NASA-CR-1046 c19 N68-25841 WEINBERG, J. L. The zodiacal light and the interplanetary medium NASA-SP-150 c30 N68-27475 WEINSTEIN, H. Evaluation of turbulence correlations in a coaxial flow of dissimilar fluids NASA-CR-961 cl2 N c12 N68-12892 Measurement of turbulent correlations in a coaxial flow of dissimilar fluids NASA-CR-960 c12 No c12 N68-13612 Analytical investigation of the mixing of two parallel streams of dissimilar fluids NASA-CR-956 cl2 N68c12 N68-13619 Stability of shear flow with density gradient and viscosity NASA-CR-958 c12 N68-15530 Experimental investigation of the mixing of two parallel streams of dissimilar fluids NASA-CR-957 c12 N68-15571 Experimental investigation of turbulence in

the mixing region between coaxial streams NASA-CR-959 cl2 N6 c12 N68-16897 WEINSTOCK, H. Design of a precision tilt and vibration isolation system NASA-TR-R-281 c14 c14 N68-19642 R, D. H. Pilot dynamic response to sudden flight WEIR. control system failures and implications for design c05 N68-26690 NASA-CR-1087 WEIRICH, R. L. Calibration of 30 deg included-angle cone for determining local flow conditions in Mach number range of 1.51 to 3.51 NASA-TN-D-4679 c14 N68-30127 Flow field properties near an arrow wing-body model at Mach numbers of 1.60, 2.36, and 2.96 NASA-TN-D-4809 col N68-37238 WEISS, E. H. A fast method of orbit computation NASA-TN-D-4470 c30 N68-20356 WELLS, W. R. Correlation study of lunar radii obtained from photographic and lunar gravitational field data NASA-TN-D-4636 c30 N68-28409 WELT, S. Additional studies of quasi-optimum feedback control techniques NASA-CR-1099 c10 N68 c10 N68-28307 WELTHER, B. L. Chronological catalog of reported lunar events NASA-TR-R-277 c30 N68-28192 WENGER, N. C. Analysis of electromagnetic waves on a dielectric rod immersed in a plasma including a discussion of diagnostic applications c25 N68-37237 NASA-TN-D-4866 WENZEL, A. B. Target pressure and damage data from impacts by explosively propelled projectiles NASA-TM-X-1597 c32 N68 c32 N68-25819 WENZEL, G. E. An integrated-circuit direct-coupled amplifier for spacecraft use NASA-TN-D-4584 c07 N68-24845 WENZEL, L. M. Experimental verification of a double dead time model describing chugging in liquid bipropellant rocket engines NASA-TN-D-4564 c33 N68-25102 WESLING, G. C. Two-stage potassium test turbine. Volume 2 - Fluid dynamic design and performance NASA-CR-922 c03 N68-16439 WESTFALL, R. M. Small high-temperature nuclear reactors for space power NASA-TN-D-4371 c22 N68-15792 Applications of Monte Carlo analysis to tungsten resonance absorption NASA-TN-D-4545 c22 N68-21924 Neutronic calculations of fuel and poison drum control of refractory-metal, fast-spectrum, space power reactors NASA-TN-D-4709 c22 N68-30750 WHIPPLE, D. L. Experimental investigation of the dynamic response of a supersonic inlet to external and internal disturbances NASA-TM-X-1648 c01 N68-33374 WHITE, J. A. A study of the effect of measurement errors upon a range controller for an entry vehicle NASA-TN-D-4317 c21 N68-1 c21 N68-14732 WHITE, J. S. Landing site dispersions of an uncontrolled lander on Mars NASA-TN-D-4587 c30 N68-24557 WHITE, M. D. WHITE, M. D.
 Proposed analytical model for the final stages of landing a transport airplane NASA-TN-D-4438
 CO2 N68-WHITLOCK, C. H.
 Performance of a 16.6-meter-diameter modified ringsail parachute in a simulated c02 N68-21112

Martian environment NASA-TM-X-1500 c31 N68-14092 Dynamic stability of a 4.6-meter-diameter 120 deg conical spacecraft at Mach numbers from 0.78 to 0.48 in a simulated Martian environment NASA-TN-D-4558 c31 N68-22301 WHITLOW, J. B., JR. Airplane size and staging effects on SST cruise sonic boom NASA-TN-D-4677 c02 N68-28831 WHITMAN, R. I. Preliminary infrared horizon profiles from Project Scanner NASA-TM-X-1483 c21 N68-11949 Infrared horizon profiles for summer conditions from Project Scanner NASA-TN-D-4741 c21 N68-33450 WHITMARSH, C. L., JR. Reactivity effects caused by radial power Rattering in a small, fast-spectrum reactor NASA-TN-D-4459 c22 N68-1 c22 N68-19925 Method for calculating allowable creep stress in linearly increasing stress environment NASA-TN-D-4352 c22 N6 c22 N68-26764 WHITNEY, W. J.
 Cold-air investigation of a turbine for high-temperature-engine application. 3 - Overall stage performance NASA-TN-D-4389 c01 N68-15743 Comparative study of mixed and isolated flow methods for cooled-turbine performance analyses NASA-TM-X-1572 c01 N68-21692 WHITTDUCK, M. M. Guidance, flight mechanics and trajectory optimization. Volume 6 - The N-body problem and special perturbation techniques NASA-CR-1005 c30 N68c30 N68-15741 WILCOX, P. R. A least squares method for the reduction of free-oscillation data NASA-TN-D-4503 c19 N68-25869 Dynamic response of a family of axisymmetric hammerhead models to unsteady aerodynamic loading NASA-TN-D-4504 c01 N68-25916 WILDT, R. Radiative equilibrium in an atmosphere with constant Einstein absorption coefficient NASA-TN-D-4479 c13 N68-22861 WILKINSON, M. C. Study of radiation hazards to man on extended missions NASA-CR-1037 c29 N68-22849 NASA-CK-1037 C29 N6B-22849 WILLIAMS, J. L. Line-of-sight velocity as an indicator of pericynthion altitude of selenocentric orbits NASA-TM-X-1508 c30 N68-19622 VILLIANS, J. R. Investigation of tethered station keeping C31 N68-11641 NASA-TN-D-4258 c31 l Correlation study of lunar radii obtained from photographic and lunar gravitational field data NASA-TN-D-4636 c30 N68-28409 WILLIAMS, R. M., JR. Electrical performance of a rhenium-niobium cylindrical thermionic converter NASA-TN-D-4533 c03 Thermal performance of a rhenium niobium cylindrical thermionic converter c03 N68-21766 NASA-TN-D-4582 c03 N68-WILLIS, E. A., JR. Optimal finite-thrust transfer between planet c03 N68-25059 approach and departure asymptotes with specified intermediate orbit NASA-TN-D-4534 c28 c28 N68-22096 WILLIS, N. C., JR. Analysis of three-fluid, crossflow heat exchangers NASA-TR-R-284 c33 N68-23513 NASA-TR-R-284 c33 N68 WILSON, J. W. Analysis and mechanization of three and four gimbal systems NASA-TN-D-4689 c11 N68 c11 N68-29957 WILSON, R. H., JR. Numerical analysis - Abstracts of presentations

PERSONAL AUTHOR INDEX

NASA-SP-170 c19 N68-33245 NASA-OF-115 WILSON, R. J. Landing loads and accelerations of the XB-70-1 airplane NASA-TN-D-4836 cf c02 N68-36073 WILSON, V. C. Characteristics of a variable spaced planar thermionic converter with a tungsten emitter and a niobium collector NASA-CR-1033 c03 N68-23476 WINKLER, E. L. The effects of molecular structure on the thermochemical properties of phenolics and related polymers NASA-TR-R-276 c33 N68-11038 WINSTON, N. M. An investigation of extremely flexible lifting rotors NASA-TN-D-4465 c01 N68-19954 A hovering investigation of an extremely flexible lifting rotor NASA-TN-D-4820 c01 N68-36334 WINTER, J. M. Experimental evaluation of 7.82-inch Appertmental evaluation of 7.82-inch /19.8-cm/ diameter throat inserts in a storable-propellant rocket engine NASA-TM-X-1463 c28 WINTUCKY, W. T. c28 N68-22272 Instrumentation of a SNAP-8 simulator facility NASA-TM-X-1525 c14 N68-19001 WINZIG, C. H. Injection start of a Brayton cycle turbocompressor operating on gas bearings in a closed loop NASA-TM-X-1590 c03 N68 WISANDER, D. W. Wear rate and friction coefficient in liquid nitrogen and hydrogen of steel sliding on polymer laminates /various fabrics and rolymers c03 N68-24757 polymers/ NASA-TN-D-4463 c15 N68-20325 Friction and wear in cryogenic liquids for composites of phenolic and of polytetrafluoroethylene of various particle sizes and concentrations NASA-TN-D-4565 c15 N68-24142 NASA-IN-D-4065 CIS M WISEMAN, G. G. Investigation of electrocaloric effects in ferroelectric substances Final report, 1 Mar. 1964 - 1 Jul. 1967 NASA-CR-1080 c26 Notes NASA-CR-108 c26 N68-25972 WISSMANN, J. W. Dynamic stability of space vehicles. Structural dynamics model testing NASA-CR-1195 c32 N68-35632 NASA-UN-11950 C32 NGG-WITCOFSKI, R. D. Experimental stability and control results at Mach 19 of an entry vehicle designed for an intermediate lift-drag ratio NASA-TN-D-4337 c31 NG8c31 N68-16240 NASA-TN-D-4337 WITTE, W. G. Flight test analysis of Apollo heat shield material using the Pacemaker vehicle system NASA-TN-D-4713 Flight investigation of the effects of Apollo heat-shield singularities on ablator Defermine performance NASA-TN-D-4791 c33 N68-35116 WITZKE, W. R. Superplasticity in tungsten-rhenium alloys NASA-TN-D-4728 c17 N68-30605 WOHL, M. L. Determination of intersection of particle flight path with surface of helical tubular void region NASA-TN-D-4435 c22 N68-18541 WOLF, J. S. Some observations concerning the oxidation of the cobalt-base superalloy L-605 /HS-25/ NASA-TN-D-4715 c17 N68-29954 WOLF, P. Nie-scattering function NASA-CR-1022 Radiation heat transfer in absorbing. c24 N68-21227 Hadiation heat transfer in absorbing, scattering, and emitting medium NASA-CR-1023 C33 N68-2 WOLOWICZ, C. H. Preliminary flight evaluation of the stability c33 N68-22318

and control derivatives and dynamic characteristics of the unaugmented XB-70-1 airplane including comparisons with predictions NASA-TN-D-4578 WONG, R. Y. c02 N68-24498 Performance in air of 4 inch /10.16-cm/ mean-diameter single stage axial-flow turbine for Reynolds numbers from 4,900 to 188,000 NASA-TN-D-4383 c03 N68-1 Injection start of a Brayton cycle turbocompressor operating on gas bearings in c03 N68-16228 a closed loop NASA-TM-X-1590 c03 N68-24757 Use of an electronic visualization technique in the study of gas journal bearing behavior NASA-TM-X-1609 c14 N68-3 c14 N68-35105 WOOD, J. C. SNAP-8 simulator loop mechanical design NASA-TM-X-1515 cll N68-18460 WOODWARD, H. T. Study of optical radiation in the wavelength regions of 0.4216 mu, 0.4278 mu, 0.4835 mu, and 0.5165 mu behind normal shock waves in a simulated Martian atmosphere NASA-TM-X-1634 c12 N68-32982 WOOLF, H. M. On the computation of solar elevation angles and the determination of sunrise and sunset times NASA-TM-X-1646 c13 N68-35179 WORTMAN, J. J. Semiconductor piezojunction transducers NASA-CR-1089 c2 c26 N68-26627 An investigation of thin film oxygen partial pressure sensors NASA-CR-1182 c14 N68-35149 WORTZ, E. C. The effects of lunar gravity on metabolic rates NASA-CR-1102 c05 N68-28833 WRIGHT, D. L. Modified vibration transducer calibration system which directly yields a plot of system which directly yields a plot of sensitivity versus frequency, NASA-TN-D-4760 cl4 N68-31958 Analysis of electromagnetic waves on a dielectric rod immersed in a plasma including a discussion of diagnostic applications NASA-TN-D-4866 c25 N68-37237 WRIGHT, J. J. An analysis of energetic space radiation and dose rates NASA-TN-D-4404 c29 N68-16837 WRIGHT, M. A. Mechanism of the atmospheric interaction with the fatigue of metals NASA-CR-1165 c17 N68-35200 WRIGHT, R. H. Approximation of the spanwise distribution of wind-tunnel-boundary interference on lift of wings in rectangular perforated-wall test sections NASA-TR-R-285 c01 N68-24617 Wind-tunnel-boundary interference on V/STOL models NASA-TR-R-286 cl1 N68-31592 WRIGHT, R. D. Combustion instability prediction using a nonlinear bipropellant vaporization model NASA-CR-920 c33 NG c33 N68-15833 WRIGHTS, G. N. Conis, G. N. Effect of 10 sup 20 neutron per square centimeter irradiation on embrittlement of polycrystalline tungsten NASA-TN-D-4661 c17 N68-28818 NASA-IN-U-4001 C17 N WU, D. C. F. The TEM radiation pattern of a thin-walled parallel-plate waveguide analyzed by a surface integration technique NASA-CR-1052 C07 N c07 N68-22746 WUERKER, R. F. Particle acceleration by evaporation pressure NASA-CR-927 c16 N68-10467 WYDE, S. S. Vapor chamber fin studies. Operating characteristics of fin models NASA-CR-1139 c33 N68-33203

Y

YACOBUCCI, H. G. Preliminary study of a thermionic reactor core composed of short-length externally fueled diodes NASA-TN-D-4805 c22 N68-34087 NASA-IN-U-4805 ZAGELOWICH, J. Self-synchronizing bi-orthogonal coded PCM telemetry system NASA-TR-R-292 c07 N68-36333 NASA-IN-N-GS YAGER, T. J. Effects of pavement texture on wet-runway braking performance NASA-TN-D-4323 c02 NASA-TN-D-4323 c02 NASA-TN-D-4323c02 lReview of causes and alleviation of low
tire traction on wet runways
NASA-TN-D-4406c02 lYATES, E. C., JR.
Subsonic and transonic flutter and flow
investigations of the T-tail of a large
multijet cargo airplane
NASA-TN-D-4316c02 lYEH, F. C.YeH, F. C.c02 l c02 N68-14903 c02 N68-19620 c02 N68-17055 YEH, F. C. Management of cryogenic propellants in a full scale orbiting space vehicle NASA-TN-D-4571 c28 N68c28 N68-25099 YOUNG, E. D. Transient behavior of arterial systems in response to flow pulses NASA-CR-990 c04 N68-12494 YOUNG, L. Microwave technique development for advanced radio astronomy and radiometry missions NASA-CR-979 c09 c09 N68-13617 An automatic balancing system for use on frictionlessly supported attitude-controlled test platforms NASA-TN-D-4426 c09 N68 YOUNG, S. G. Effect of cover gas pressures on accelerated cavitation damage in sodium NASA-TN-D-4235 c17 N68 c09 N68-19185 c17 N68-10104 Cavitation damage of stainless steel, nickel, and an aluminum alloy in water for ASTM round robin tests NASA-TM-X-1670 c17 N68-36076 YOUNGER, C. L. Effect of 10 sup 20 neutron per square centimeter irradiation on embrittlement of polycrystalline tungsten NASA-TN-D-4661 c17 N68-28818 YUSKA, J. A. Description and flight performance results of the Wasp sounding rocket NASA-TM-X-1518 c31 N68-17094

Ζ

ZALOVCIK, J. A. Effect of thrust and altitude in steep approaches on ground track noise NASA-TN-D-4241 c c01 N68-11253 ZAPLATYNSKY, I. Determination of electric potential across the oxide scale during oxidation of tantalum, niobium, and magnesium NASA-TN-D-4240 c17 N68-10 c17 N68-10498 ZARETSKY, E. V. Reduced pressure environment effects on rolling element fatigue life with super refined mineral oil lubricant NASA-TN-D-4348 c15 c15 N68-15010 Residual stress and subsurface hardness changes induced during rolling contact NASA-TN-D-4456 c15 c15 N68-20199 Effect of ball-race conformity on spinning friction NASA-TN-D-4669 c15 N68-28258 Fatigue life of 120 mm bore ball bearings at 600 deg F with fluorocarbon, polyphenyl ether, and synthetic paraffinic base lubricants NASA-TN-D-4850 c15 N68~36075 ZAWACKI, T. S. Experimental investigation of turbulence in the mixing region between coaxial streams

ZIERING, S.

NASA-CR-959c12 N68-16897ZIERING, S.Plasma boundary interactions - 2
NASA-CR-1072c25 N68-25821ZIMMERMAN, W. F.Two-stage potassium test turbine.
Volume 4.- Materials support of performance
and endurance tests
NASA-CR-925c03 N68-16351ZIOCK, K.An annular lithium-drifted germanium detector
for studying nuclear reaction gamma-rays
NASA-CR-1138c14 N68-35152ZOBY, E. V.Charts for equilibrium isentropic expansion of
air behind shocks up to 50000 feet per second
/15.24 kilometers per second/
NASA-TN-D-4247c33 N68-11144Approximate relations for laminar
heat-transfer and shear-stress functions in
equilibrium dissociated air
NASA-TN-D-4484c33 N68-20065Empirical stagnation-point heat-transfer
relation in several gas mixtures at high
enthalpy levels
NASA-TN-D-4799c33 N68-35468

NASA SCIENTIFIC AND TECHNICAL REPORTS FOR 1968

A Selected Listing

Typical Corporate Source Index Listing

ABERDEEN PROVI The depende as determ BRL-1286	NG GROUND, nce of yiel ined from b	a stress or	tion tests	176
TITLE	REPORT NUMBER	SUBJECT CATEGORY NUMBER	NASA ACCESSION NUMBER	

Listings in this index are arranged alphabetically by corporate source. The title of the document provides the user with a brief description of the subject matter. The report number helps to indicate the type of document cited (e.g., NASA report, translation, NASA contractor report). The subject category number indicates the subject category in the abstract section in which the citation is located. The NASA accession number denotes the number by which the citation is identified within the subject category. The titles are arranged under each personal author in ascending accession number order.

Α

AEROSPACE PRODUCTS RESEARCH CORP., SANTA MENDSPACE PRODUCTS RESERVON CORF., SANTA MONICA, CALIF. Computer driven electroluminescent vertical scale indicator NASA-CR-919 c05 N66 AEROTHERM CORP., PALO ALTO, CALIF. An analysis of the coupled chemically accting boundary layor and chemically c05 N68-10648 reacting boundary layer and charring ablator. Part 3 - Nonsimilar solution of the multicomponent laminar boundary layer by an integral matrix method NASA-CR-1062 c33 N68-26641 analysis of the coupled chemically reacting An Finite difference solution for the in-depth response of charring materials considering surface chemical and energy balances NASA-CR-1061 c33 N68-26692 AIR VEHICLE CORP., LA JOLLA, CALIF. Nonlinear lift and pressure distribution of slender conical bodies with strakes at low speeds NASA-CR-1202 c01 N68-37255 AIRESEARCH MFG. CD., LOS ANGELES, CALIF. Recuperator for solar Brayton cycle system NASA-CR-1150 c03 N68-33062 ALLIED RESEARCH ASSOCIATES, INC., CONCORD, MASS. Structural design synthesis approach to filamentary composites NASA-CR-964 c32 N68-11191 Minimum weight design aspects of stiffened cylinders under compression NASA-CR-963 c32 N68-11282 ANDREW CORP., CHICAGO, ILL. The dielectric clad axial slot antenna NASA-CR-1057 c07 N68-26621 APPLIED PHYSICS LAB., JOHNS HOPKINS UNIV., SILVER SPRING, MD. Extended duration, recoverable primate satellite NASA-CR-926 NRINC RESEARCH CORP., ANNAPOLIS, MD. Microelectronic device data handbook. c05 N68-15306 Volume 1 - Text NASA-CR-1110 c09 N68-29525 Microelectronic device data handbook. Volume 2 - Manufacturer and specific device information NASA-CR-1111 c c09 N68-29526

ARIZONA UNIV., TUCSON. Multisegmented optimal trajectories NASA-CR-1103 c30 N68-25895 Chronological catalog of reported lunar events NASA-TR-R-277 c30 N68-28192 ASTRO RESEARCH CORP., SANTA BARBARA, CALIF. An evaluation of boron-polymer film layer composites for high-performance structure NASA-CR-1114 Large low-frequency orbiting radio c18 N68-35100 telescope NASA-CR-1201 c31 N68-37900 ATLANTIC RESEARCH CORP., ALEXANDRIA, VA. Study of propellant valve leakage in a vacuum Final summary report NASA-CR-1047 c27 N68-21893 AUTONETICS, ANAHEIM, CALIF. Study of spaceborne multiprocessing - Pha Volume 2 - Technical description Final - Phase 2 report NASA-CR-1159 c08 N68 AVCO CORP., WILMINGTON, MASS. Investigation of the dynamic characteristics of a V antenna for the RAE satellite, c08 N68-35560 phase A Final report

c08 N68-18144

В

NASA-CR-962

BELL AEROSYSTEMS CO., BUFFALO, N. Y. A generalized experimental investigation of hot gas recirculation and ingestion for jet VTOL aircraft NASA-CR-1147 c01 c01 N68-33043 NASA-CK-1147 c0 BENDIX CORP., ANN ARBOR, MICH. Study of mineral stability in the lunar environment Final report NASA-CR-1034 c1 c13 N68-25579 BENDIX CORP., DAVENPORT, IOWA. Development of a liquid shroud cryogenic supercritical pressure storage system c03 N68-22842 NASA-CR-1048 BENDIX CORP., DETROIT, MICH. Oxidation resistant materials for transpiration cooled gas turbine blades. 1 -Sheet specimen screening tests NASA-CR-930 c17 N68-17591 BENDIX CORP., MADISON HEIGHTS, MICH. Oxidation resistant materials for transpiration cooled gas turbine blades. 2 - Wire specimen tests NASA-CR-1184 c17 N68-35098 NASH-UK-1184 CI7 NOC'S BENDIX CORP., SOUTHFIELD, MICH. Research and development of a vortex valve for flow modulation of a 16-percent aluminized 5500 deg F propellant gas NASA-CR-1091 c28 N68c28 N68-28112 NASA-CR-1091 C28 Noo-BIOTECHNOLOGY, INC., ARLINGTON, VA. Effect of heat stress and prolonged activity on perceptual-motor performance NASA-CR-1153 C05 N68-BOEING C0., MORTON, PA. Supplement to feasibility of V/STOL concepts for short-haul transport aircraft NASA-CR-743/1/ C02 N68c05 N68-31480 NASA-CR-743/1 c02 N68-35177 BOEING CO., PHILADELPHIA, PA. Subjective response to synthesized flight noise signatures of several types of V/STOL aircraft NASA-CR-1118 c05 N68-33009 BOEING CO., RENTON, WASH. Study of aircraft in short haul transportation systems NASA-CR-986 c02 N68-13517

Fatigue-crack-propagation and fracture-touchness characteristics of 7079 aluminumalloy sheets and plates in three aged conditions NASA-CR-996 c32 N68-15476 BOEING CO., SEATTLE, WASH. Lunar Orbiter 3 - Photography NASA-CR-984 c30 N68-15725 Study of radiation hazards to man on extended missions NASA-CR-1037 c29 N68-22849 Ultraviolet-proton radiation effects on solar concentrator reflective surfaces Final report, Jun. 1965 - Aug. 1967 NASA-CR-1024 c17 N68c17 N68-23560 Lunar Orbiter 3 - Photographic mission summary NASA-CR-1069 c31 N68-24738 Studies of cost effective structures design for future space systems - Summary Final report, 17 Oct. 1966 - 17 Oct. 1967 NASA-CR-1068 c34 N6 c34 N68-26813 Lunar Orbiter 4 - Photographic mission summary, volume 1 NASA-CR-1054 c c31 N68-26814 NASA-CK-1054 Lunar Orbiter 5 - Photography Final report NASA-CR-1094 c31 N68-28202 Lunar Orbiter 4. Photography NASA-CR-1093 c30 N68-28275 Lunar Orbiter 5. Photographic mission summary NASA-CR-1095 c31 N68-28891 Lunar Orbiter 4. Extended-mission spacecraft operations and subsystem performance NASA-CR-1092 c31 N68-28997 Lunar Orbiter 3 - Extended-mission spacecraft operations and subsystem erformance NASA-CR-1109 c31 N68-29995 Lunar Orbiter 5. Extended-mission spacecraft operations and subsystem performance NASA-CR-1142 Lunar Orbiter 2 - Extended mission spacecraft operations and subsystem c31 N68-30631 erformance NASA-CR-1141 c31 N68-31477 Maintainability of manned spacecraft for long-duration flights. Volume 1 - Summary report NASA-CR-1108 c31 N68-33008 BOLT, BERANEK, AND NEWMAN, INC., CAMBRIDGE, MASS. Panel loss factors due to gas-pumping at structural joints NASA-CR-954 c32 N68-11489 The human as an optimal controller and information processor NASA-CR-1151 c c05 N68-33304

COD NOG-33304 BOLT, BERANEK, AND NEWMAN, INC., VAN NUYS, CALIF. The noisiness of tones plus noise NASA-CR-1117 BROWN UNIV., PROVIDENCE, R. I. Use of a transcendental approximation in

transient conduction analysis NASA-CR-955

CALIFORNIA INST. OF TECH., PASADENA. The buckling of thin-walled circular cylinders under axial compression and bending NASA-CR-1160 c32 N68-33226 Almost sure stability of long cylindrical shells with random imperfections NASA-CR-1161 c32 N68-33419 Buckling of conical shells under axial compression NASA-CR-1162 c32 N68-35198 Experimental investigation of the effect of general imperfections on the buckling of cylindrical shells NASA-CR-1163 c32 N68-35199 CALIFORNIA UNIV., SAN FRANCISCO. Relative roles of gravitational and inertial work in the energy cost of human locomotion

CORPORATE SOURCE INDEX

NASA-CR-1042 c05 N68-2. CASE INST. OF TECH., CLEVELAND, OHIO. A critical evaluation of the status and trends in high speed fluid film lubrication NASA-CR-1058 c15 N68-2: c05 N68-21859 c15 N68-22810 CATHOLIC UNIV. OF AMERICA, WASHINGTON, D. Magnetohydrodynamic flows over a rotating disk NASA-CR-989 c25 N68-14078 CHRYSLER CORP., HUNTSVILLE, ALA. Design handbook umbilical locking mechanism development program NASA-CR-1021 c15 N68-23356 CHRYSLER CORP., NEW ORLEANS, LA. Applications study of electroadhesive devices NASA-CR-1211 c10 N68-37906 COLORADO UNIV., BOULDER. Optimum maneuvers of hypervelocity vehicles NASA-CR-1078 c02 N68-25817 CONSULTANTS IN ENGINEERING SCIENCE /CONESCO/, WATERTOWN, MASS. Procedures for estimating the effects of design and operational characteristics of jet aircraft on ground noise NASA-CR-1053 c02 N68-26 CORNELL AERONAUTICAL LAB., INC., BUFFALD, c02 N68-26930 Y. Investigation of warm fog properties and fog modification concepts NASA-CR-1071 c20 N68-25816 D DECISION SCIENCE, INC., SAN DIEGO, CALIF. Modeling the human operator with finite-state machines NASA-CR-1112 c05 N68-28847 DOUGLAS AIRCRAFT CO., INC., NEWPORT BEACH, CALIF. Inorganic separator for a high temperature silver-zinc battery NNON-UK-900 Research on the utilization of pattern recognition techniques to identify and classify objects in video data Final report NASA-CR-999 c10 N68-1 NASA-CR-965 c03 N68-16321 c10 N68-19229 DOUGLAS AIRCRAFT CO., INC., SANTA MONICA, CALTE. Narrow band cross-correlation analysis of fluctuating pressures beneath a turbulent boundary layer NASA-CR-1066 c12 N68-23482 Ultrahigh vacuum adhesion related to the lunar surface NASA-CR-1090 c30 N68-28373 NASA-CR-1090 c30 Planetary flight handbook. Part 6 - Mars stopover missions using Venus swingbys NASA-SP-35, PT. 6 c30 Radiative and convective heating during c30 N68-30098 atmospheric entry NASA-CR-1170 c3 DU PONT DE NEMOURS /E. I./ AND CO., AIKEN, c33 N68-35248 s. c. Role of hydrogen chloride in hot salt stress corrosion cracking of titanium aluminum alloys NASA-CR-1133 c17 DUDLEY OBSERVATORY, ALBANY, N. Y. The microbiological flora of the Gemini 9 c17 N68-33019 spacecraft before and after flight NASA-CR-972 c04 N68-11968 DYNAMIC SCIENCE CORP., MONROVIA, CALIF. A geometrically nonlinear analysis of arbitrarily loaded shells of revolution NASA-CR-909 c32 1 c32 N68-14584 Combustion instability prediction using a nonlinear bipropellant vaporization model NASA-CR-920 c33 N68-15833 A study of aircraft fire hazards related to natural electrical phenomena Final report, Jun. 1966 - Jul. 1967 NASA-CR-1076 c02 N68c02 N68-26691 Ε

ENVIRONMENTAL RESEARCH ASSOCIATES,

RANDALLSTOWN, MD. A study of the performance of an astronaut during ingress and egress maneuvers through airlocks and passageways

c19 N68-11109

NASA-CR-971 c05 N68-20339 ESSO RESEARCH AND ENGINEERING CO., LINDEN, N. J. Study of methods for chemical synthesis of edible fatty acids and lipids Final technical report NASA-CR-1105 c04 N68-28278 Study of methods for chemical synthesis of edible fatty acids and lipids - Final summary NASA-CR-1104

c04 N68-28829

F

FLORIDA UNIV., GAINESVILLE. Graphite triple point and solidus-liquidus interface experimentally determined up to 1000 atmospheres NASA-CR-1148 c22 N68-29390 FUNDAMENTAL METHODS ASSOCIATES, INC., NEW YORK.

Application of dust for space structures NASA-CR-1136 c32 N68-32976

G

- GARRETT CORP., LOS ANGELES, CALIF. The effects of lunar gravity on metabolic rates NASA-CR-1102 c05 N68-28833 GCA TECHNOLOGY DIV., GCA CORP., BEDFORD, MASS. Improvement and optimization of a mass spectrometer employing a photoionization source NASA-CR-1018 c14 N68-17329 GENERAL DYNAMICS CORP., SAN DIEGO, CALIF. Dynamic stability of space vehicles. Volume 1 - Lateral vibration modes NASA-CR-935 c32 N68-10231 Dynamic stability of space vehicles. Volume 9 - The effect of liftoff dynamics on launch vehicle stability and control c32 N68-10233 NASA-CR-943 Dynamic stability of space vehicles. Volume 2 - Determination of longitudinal vibration modes c32 N68-10280 NASA-CR-936 Dynamic stability of space vehicles. Volume 3 - Torsional vibration modes NASA-CR-937 c32 N68-10568 NASA-CK-957 Dynamic stability of space vehicles. Volum 4 - Full scale testing for flight control Volume parameters NASA-CR-938 c32 N68-10574 Dynamic stability of space vehicles. Volume 6 - Full scale dynamic testing for mode determination NASA-CR-940 c32 N68-11054 NDON-GR-340 C32 N Dynamic stability of space vehicles. Volume 8 - Atmospheric disturbances that affect flight control analysis NASA-CR-942 c32 N68-11089 C32 NG Dynamic stability of space vehicles. Volume 11 - Entry disturbance and control NASA-CR-945 c32 NG Anon-OK-945 C32 N68-11133 Dynamic stability of space vehicles. Volume 5 - Impedance testing for flight control parameters c32 N68-11485 NASA-CR-939 Dynamic stability of space vehicles. Volume 7 - The dynamics of liquids in fixed and moving containers NASA-CR-941 c32 N68-18769 NASA-CR-941 Dynamic stability of space vehicles. Volume 10 - Exit stability NASA-CR-944 c32 N68-18825 Evaluation of the effects of space environment exposure on index of refraction and extinction coefficients of Apollo window materials c31 N68-20467 NASA-CR-1019 Dynamic stability of space vehicles. Volu 13 - Aerodynamic model tests for control Volume parameter determination NASA-CR-947 c32 N68-23452 Dynamic stability of space vehicles. Volume 15 - Shell dynamics with special applications to control problems
 - c32 N68-23453 NASA-CR-949 Dynamic stability of space vehicles. Volume

14 - Testing for booster propellant sloshing parameters NASA-CR-948 c32 N68-23454 Dynamics stability of space vehicles. Volum 12 - Re-entry vehicle landing ability and Volume control NASA-CR-946 c31 N68-24945 Dynamic stability of space vehicles. Structural dynamics model testing NASA-CR-1195 c32 N68-35632 GENERAL ELECTRIC CO., CINCINNATI, OHIO. Design of two electromagnetic pumps NASA-CR-911 c15 N68-10503 Two-stage potassium test turbine. Volume 4 - Materials support of performance and endurance tests NASA-CR-925 c03 N68-16351 Two-stage potassium test turbine. Volume 2 - Fluid dynamic design and erformance c03 N68-16439 NASA-CR-922 Two-stage potassium test turbine. Volume 2 -Mechanical design and development c03 N68-17075 NASA-CR-923 NASA-CR-923 Two-stage potassium test turbine. Volum Test facilities NASA-CR-924, V. 3 c03 Development of electrical switchgear for Volume 3 c03 N68-18044 space nuclear electrical systems NASA-CR-1026 c03 N68-29460 Cb-1Zr sodium thermal convection loop NASA-CR-1097 c22 N68-35153 GENERAL ELECTRIC CO., KING OF PRUSSIA, PA. Plate-gap model of a porous solid and its application to impact by reduced density projectiles NASA-CR-1140 GENERAL ELECTRIC CO., PHILADELPHIA, PA. The role of energy in deformation NASA-CR-1039 c32 N68-31912 c24 N68-21949 NASA-CR-1039 c24 N68-Coating selection program - Theory NASA-CR-1041 c18 N68-GENERAL ELECTRIC CO., PITTSFIELD, MASS. A study of aircraft fire hazards related to natural electrical phenomena Final report, Jun. 1966 - Jul. 1967 NASA-CR-1076 c02 N68-GENERAL ELECTRIC CO., PLEASANTON, CALIF. Thermal conductivity of coated particle uranium dioxide tungsten cermets NASA-CR-1154 c22 N68-GENERAL ELECTRIC CO., SCHENECTADY, N. Y. Development of high-temperature vapor-filled c18 N68-22391 c02 N68-26691 c22 N68-32983 Development of high-temperature vapor-filled thyratrons and rectifiers c09 N68-15892 NASA-CR-994 Leakage testing handbook NASA-CR-952 c15 N68-20389 Characteristics of a variable spaced planar thermionic converter with a tungsten emitter and a niobium collector And a history corrector NASA-CR-1033 c03 N68-GENERAL MOTORS CORP., INDIANAPOLIS, IND. Experimental investigation of advanced concepts to increase turbine blade loading. 2 - Performance evaluation of plain rotor c03 N68-23476 blade NASA-CR-1172 c28 N68-32987 GENERAL MOTORS CORP., SANTA BARBARA, CALIF. Experimental investigations of simulated meteoroid damage to various spacecraft structures Structures c31 N68 NASA-CR-915 c31 N68 GENERAL PRECISION, INC., LITTLE FALLS, N. J. Additional studies of quasi-optimum feedback control techniques NASA-CR-1099 c10 N68 c31 N68-14638 c10 N68-28307 GENERAL TECHNICAL SERVICES, INC., UPPER DARBY, PA. Transient behavior of arterial systems in response to flow pulses NASA-CR-990 c04 N68-12494 GEOPHYSICS CORP. OF AMERICA, BEDFORD, MASS. Studies of photoabsorption by atomic hydrogen, oxygen, and nitrogen NASA-CR-998 c24 NG GEORGIA INST. OF TECH., ATLANTA. Investigation of radiant heat transfer to particle-seeded gases for application c24 N68-18118 to nuclear rocket engine design

I-173

NASA-CR-953

N. Y.

-----Η HARTMAN-HUYCK SYSTEMS CO., HUNTINGTON STATION,

c22 N68-10561

A cathode ray tube suitable for viewing under high ambient NASA-CR-1185 c09 N68-33224 HELIODYNE CORP., VAN NUYS, CALIF. Non-linear orbit determination methods NAN-CR-1040 c30 NG HONEYWELL, INC., MINNEAPOLIS, MINN. Development and flight testing of a fluidic c30 N68-21864 control system NASA-CR-913 NMBH-CK-913 CO2 N68-10047 HUGHES AIRCRAFT CO., CULVER CITY, CALIF. Study of advanced antenna techniques for rendezvous radar rendezvous radar NASA-CR-764 c07 N68-28135 HUGHES AIRCRAFT CO., FULLERTON, CALIF. Transistor design effects on radiation resistance NASA-CR-1167 c10 N68-33767 HUMPHREYS CORP., CONCORD, N. H. Induction plasma heating - System performance, hydrogen operation and gas core reactor simulator development NASA-CR-1143 c25 c25 N68-29888

ł

IIT RESEARCH INST., CHICAGO, ILL. Evaluation of turbulence correlations in a coaxial flow of dissimilar fluids NASA-CR-961 cl2 N c12 N68-12892 Measurement of turbulent correlations in a coaxial flow of dissimilar fluids NASA-CR-960 c12 N c12 N68-13612 Analytical investigation of the mixing of two parallel streams of dissimilar fluids NASA-CR-956 c12 N68-13619 Stability of shear flow with density gradient and viscosity NASA-CR-958 c12 N68-15530 Experimental investigation of the mixing of two parallel streams of dissimilar fluids NASA-CR-957 c12 N68-15571 Experimental investigation of turbulence in the mixing region between coaxial streams NASA-CR-959 cl2 NG c12 N68-16897 High performance structures NASA-CR-1038 c32 N68-23399 Preliminary study of advanced life-support technology for a Mars surface module c05 N68-28319 NASA-CR-1083 Analytical investigation of incompressible turbulent swirling flow in pipes NASA-CR-1169 c12 N68-36343 NASA-CK-1169 C12 ILLINOIS UNIV., URBANA. Drag associated with separated flow over two-dimensional V-shaped notches under transonic and supersonic conditions NASA-CR-1132 INNSBRUCK UNIV. /AUSTRIA/. Lie series for celestial mechanics, c12 N68-35252 accelerators, satellite stabilization and optimization NASA-CR-1046 INTERNATIONAL BUSINESS MACHINES CORP., CAMBRIDGE, MASS. c19 N68-25841 Investigation of refractory dielectrics for integrated circuits NASA-CR-995 c18 N68-18849 ISRAEL PROGRAM FOR SCIENTIFIC TRANSLATIONS, ISKAEL PRUGRAM FOR SCIENTIFIC TRANSLA LTD., JERUSALEM. Electricity of the free atmosphere NASA-TT-F-425 Rib-reinforced plates and shells NASA-TT-F-427 c13 N68-10079 c32 N68-10407 Heat and mass transfer. Volume 1 -Convective heat exchange in a homogeneous medium NASA-TT-F-431 c33 N68-11721 Russian solid-fuel rockets NASA-TT-F-415 c28 N68-11829 Biochemistry of the nervous system NASA-TT-F-439 c04 N68-13432 Measurement of pulse distortion in digital

CORPORATE SOURCE INDEX

information transmission c07 N68-17542 NASA-TT-F-434 Multivariable control systems NASA-TT-F-435 cl0 N6i Analytical mechanics. Stability of motion. Celestial ballistics NASA-TT-F-503 c23 N6i ITEK CORP., PALO ALTO, CALIF. An analysis of the coupled chemically c10 N68-37293 c23 N68-37792 reacting boundary layer and charring ablator, part 1 Summary report NASA-CR-1060 c c33 N68-25244 An analysis of the coupled chemically reacting boundary layer and charring ablator. Part 3 - Nonsimilar solution of the multicomponent laminar boundary layer by an integral matrix method NHDA-CK-1062 An analysis of the coupled chemically reacting boundary layer and charring ablator. Part 2 -Finite difference solution for the in-depth response of charring materials considering surface chemical and energy balances NASA-CR-1061 C33 N68-2669 c33 N68-26641 c33 N68-26692 An analysis of the coupled chemically reacting boundary layer and charring ablator. Part 4 -A unified approximation for mixture transport properties for multicomponent boundary-layer applications NASA-CR-1063 c33 N68-26815 An analysis of the coupled chemically reacting boundary layer and charring ablator. Part 5 -A general approach to the thermochemical solution of mixed equilibrium-nonequilibrium, homogeneous or heterogeneous systems homogeneous or neterogeneous systems NASA-CR-1064 An analysis of the coupled chemically reacting boundary layer and charring ablator. Part 6 -An approach for characterizing charring c33 N68-26816 ablator response with in-depth coking reactions NASA-CR-1065 c33 N68-26817

JET PROPULSION LAB., CALIF. INST. OF TECH., PASADENA.

- Mariner-Mars 1964 Final project report NASA-SP-139 c3 c31 N68-18743 Leakage testing handbook NASA-CR-952 c15 N68-20389
- JOHNS HOPKINS UNIV., BALTINORE, MD. Infrared observations of the outer solar corona
 - NASA-CR-969 c30 N68-20353

Κ

KANSAS UNIV., LAWRENCE. Investigation of electrocaloric effects in ferroelectric substances Final report, 1 Mar. 1964 - 1 Jul. 1967 NASA-CR-1080 c26 N68-25972

L

LAFAYETTE CLINIC, DETROIT, MICH. System and process development for selection of high stress tolerance personnel NASA-CR-1122 c05 N68 LEHIGH UNIV., BETHLEHEM, PA. Fatigue crack propagation in cylindrical c05 N68-35102 shells c32 N68-37840 NASA-CR-1197 LING-TEMCO-VOUGHT, INC., ANAHEIM, CALIF. The shock expansion tube and its application as a sonic boom simulator NASA-CR-1055 c11 N68-24966 LING-TEMCO-VOUGHT, INC., DALLAS, TEX. Investigation of the calibration of microphones for sonic boom measurement c14 N68-25316 NASA-CR-1075 Investigation of electron interaction in matter Final report, 9 Feb. 1967 - 9 Feb. 1968 NASA-CR-1194 c24 N68-37708 LITCHFORD SYSTEMS, NORTHPORT, N. Y. Analysis of cumulative errors associated with category 2 and 3 operations with requirements

I-174

for additional research NASA-CR-1188 c02 N68-LITTLE /ARTHUR D./, INC., CAMBRIDGE, MASS. The application of high temperature radiative c02 N68-35595 thermal conductivity of minerals and rocks to a model of lunar volcanism NASA-CR-916 c13 N68-10283 Application of statistical association techniques for the NASA document collection NASA-CR-1020 c08 N68-17154 Space technology transfer and developing nations nations NASA-CR-1222 C34 N68-37 LITTON SYSTEMS, INC., MINNEAPOLIS, MINN. Microbiological exploration of the stratosphere. Development and flights of the Mark 2 and 3 sampling systems "ACA-CP-1101 C04 N68-28 c34 N68-37216 NASA-CR-1101 c04 N68-28247 LOCKHEED AIRCRAFT CORP., SUNNYVALE, CALIF. Buckling of shells of revolution with various wall constructions. Volume 3 - User*s manual for BOSOR NASA-CR-1051 c32 N68-23355 wall constructions. Volume 2 - Basic equations and method of solution NASA-CR-1050 c32 N68-23451 Buckling of shells of revolution with various wall constructions. Volume 1 - Numerical results NASA-CR-1049 c32 N68-24481 LOCKHEED ELECTRONICS CO., HOUSTON, TEX. Analysis of Luna 9 photography NASA-CR-980 c14 N68-16838 LOCKHEED MISSILES AND SPACE CO., PALO ALTO, CALIF. Design and construction of an engineering model solid cryogen refrigerator for infrared detector cooling at 50 deg K NASA-CR-988 C23 LOCKHEED MISSILES AND SPACE CO., SUNNYVALE, c23 N68-13115 CALIF. Discrimination of increases in the brightness of a flashing beacon NASA-CR-1220 c05 N68-37819 LOCKHEED-CALIFORNIA CD., BURBANK. Stress corrosion of titanium alloys under simulated supersonic flight conditions NASA-CR-981 c17 N68-11522 NASA-CK-901 LOUISIANA STATE UNIV., BATON ROUGE. A study of sensitization in types 301 and 304L stainless steels using Moessbauer spectroscopy NASA-CR-1077 c17 NG LOVELACE FOUNDATION FOR MEDICAL EDUCATION AND RESEARCH, ALBUQUERQUE, N. MEX. The intangibles of habitability during long c17 N68-25318 duration space missions Auration space missions NASA-CR-1084 C30 N LTV AEROSPACE CORP., DALLAS, TEX. Additional studies on the feasibility of V/STOL concepts for short-haul transport aircraft NASA-CR-670/01/ C02 No c30 N68-26702 c02 N68-11174 M

- MARTIN CO., BALTIMORE, MD. Parts and materials application review for space systems NASA-SP-6505 c15 N6 MARTIN CO., ORLANDO, FLA. Propagation of millimeter and submillimeter c15 N68-10120
- Waves
- NASA-CR-863 c07 N68-27063 MASSACHUSETTS INST. OF TECH., CAMBRIDGE. A three-dimensional hard spheres theory
- of scattering of gas atoms from a solid
- surface NASA-CR-933 c12 N68-10499
- Correction of balloon X-ray astronomy data for the effects of atmospheric attenuation, K X-ray escape, and energy resolution
- MASA-CR-1045 A theory and model of human learning behavior in a manual control task NASA-CR-1124 CO5 N68-31911 MATERIALS RESEARCH CORP., ORANGEBURG, N. Y. An aluminum nitride melting technique

- NASA-CR-1171 c17 N68-33335 MCDONNELL-DOUGLAS CO., LONG BEACH, CALIF. A study of turbofan-engine compressor noise suppression techniques NASA-CR-1056 MCDONNELL-DOUGLAS CO., ST. LOUIS, MO. Project Gemini - A technical summary c28 N68-26771 Project Gemini - A technical summary NASA-CR-1106 c31 MECHANICAL TECHNOLOGY, INC., LATHAN, N. Y. Research and development of high performance axial-flow turbomachinery. Volume 2 - Design of gas bearings c31 N68-25577 NASA-CR-801 c15 N68-25042 NASA-CR-801 c15 N68 MELPAR, INC., FALLS CHURCH, VA. Thin-Film Personal Communications and Telemetry System /TFPCTS/ NASA-CR-914 c09 N68 MICHIGAN UNIV., ANN ARBOR. Electromagnetism in moving, conducting media NASA-CR-1025 c23 N68 C09 N68-10420 c23 N68-21444 Trajectory optimization by a direct descent process NASA-CR-1070 c30 N68-25902 MIDWEST RESEARCH INST., KANSAS CITY, MO. Advanced valve technology, a survey NASA-SP-5019 c15 N68-10402 MISSISSIPPI STATE UNIV., STATE COLLEGE.
 - Microwave spectroscopy of molecules -Bibliography, 1964-1966 NASA-CR-951 c23 N68-10674

N

NATIONAL AERONAUTICS AND SPACE ADMINISTRATION. AMES RESEARCH CENTER, MOFFETT FIELD, CALIF. Tabulated communication characteristics of a steady-state model of interplanetary space steady-state model of interplanetary space NASA-SP-3042 c30 N68-10164 Determination of stresses in elastic solids using three stress functions and three equations NASA-TN-D-4253 c19 N68-10355 The effects of molecular structure on the thermochemical properties of phenolics and related polymers NASA-TR-R-276 c33 N68-11038 Theoretical error analysis of a Doppler range-rate and phase-modulated range tracking svstem NASA-TN-D-4267 c10 N68-11513 Large-scale wind-tunnel investigation of a model with an external jet-augmented flap NASA-TN-D-4278 c02 N6 c02 N68-11627 characteristics from experimental near field results NASA-TM-X-1477 c02 Comparison of convective stagnation heat transfer in air, CO2-N2, and CO2-Ar gas c02 N68-11772 mixtures NASA-TN-D-4255 c33 N68-11811 Factors affecting the design and use of a photographic sextant for space navigation NASA-TN-D-4285 c21 N6 c21 N68-11902 Ballistic-range tests of a drag-ring configuration at Mach numbers around 2 NASA-TN-D-4291 c01 c01 N68-11936 NASA-TN-D-4291 col N68-115 Navigator performance using a hand-held sextant to measure the angle between a moving flashing light and a simulated star NASA-TN-D-4174 c21 N68-135 Comparison of experimental and theoretical shock shapes and pressure distributions on flat-faced cylinders at Mach 10.5 NASA-TN-D-4397 c01 N68-155 An uncertainty analysis for satellite c21 N68-13558 c01 N68-15778 An uncertainty analysis for satellite calorimetric measurements NASA-TN-D-4354 c14 N68-16529 NASA-IN-D-4034 Investigation of a large-scale mixed compression axisymmetric inlet system capable of high performance at Mach numbers 0.6 to 3.0 NASA-IM-X-1507 c28 piloted simulator study of takeoff performance and hereiter performance and handling qualities of a double delta supersonic transport NASA-TN-D-4396 c02 N68-17391

Inviscid hypersonic flow over a blunt body with high rates of mass and heat transfer

c01 N68-17555 NASA-TN-D-4252 NASA-IN-D-4232 CUI NOS-1 Performance of several convolutional and block codes with threshold decoding NASA-TN-D-4402 CO7 N68-14 c07 N68-18178 An experimental study of the influence of the turbulent boundary layer on panel flutter NASA-TN-D-4486 c32 NG c32 N68-18721 Large-scale wind-tunnel tests of a deflected slipstream STOL model with wings of various aspect ratios NASA-TN-D-4448 c02 N68-18771 A critical evaluation of the use of ultrasonic absorption for determing high-temperature gas properties NASA-TN-D-4433 c24 N68-18949 NASA-IN-D-4433 c24 N68-. Results of including a boundary shock wave in the calculation of the flight parameters of a large high-speed meteor NASA-IN-D-4325 c12 N68c12 N68-18997 Saturn 5 manual backup guidance and control piloted simulation study NASA-TN-D-4481 c21 N68-19061 Lunar beacons - A preliminary look at their position estimation and their use in lunar orbit estimation NASA-TM-X-1529 c30 N68-19064 Wing surface pressure data from large-scale wind-tunnel tests of a propeller-driven STOL model NASA-TM-X-1527 c02 N68-19065 Analog study of the longitudinal response of a swept-wing transport airplane to wind shear and sustained gusts during landing approach NASA-TN-D-4477 c01 N68-NASA-TN-D-4477 cOl N68-19180 Large-scale wind-tunnel tests of an airplane model with two propellers and rotating cylinder flaps NASA-TN-D-4489 c01 N68-19189 Simple processors of star tracker commands for stabilizing an inertially oriented satellite NASA-TN-D-4490 c21 N68-19236 A FORTAN program for computation of mass in earth orbit required for interplanetary missions NASA-TM-X-1541 c30 N68-19330 Large-scale wind-tunnel investigation of an airplane model with a tilt wing of aspect ratio 8.4, and four propellers, in the presence of a ground plane NASA-TN-D-4493 col N6 c01 N68-20370 Investigation of air-flow velocity by laser backscatter NASA-TN-D-4453 c20 N68-20375 Proposed analytical model for the final stages of landing a transport airplane NASA-TN-D-4438 c02 N68-21112 Navigator performance studies for space navigation using the NASA CV-990 research aircraft RHOM-IN-U-4449 c21 N68-21123 Radiation damage in thick copper and gold specimens produced by low-energy protons protons NASA-TN-D-4452 c26 N68-21219 The penetration of porous projectiles in aluminum and plastic targets NASA-TN-D-4505 c32 N68-21293 Method and results of studying vapor deposition nucleation processes by in situ electron microscopy NASA-TN-D-4506 Boundary corrections for a three-coil conductivity/velocity plasma probe c06 N68-21430 NASA-TN-D-4538 c25 N68-21691 An analytical investigation of the aerodynamic and performance characteristics of an unpowered rotor entry vehicle NASA-TN-D-4537 c31 N68-217 c31 N68-21758 Remarks on imperfections of axially loaded cylinders NASA-TM-X-1552 c32 N68-21767 Phase and group refractive indices from the collisionless magnetoionic theory NASA-TM-X-1553 c13 N68-21904 A method for predicting shock shapes and pressure distributions for a wide variety of blunt bodies at zero angle of attack c01 N68-21941 NASA-TN-D-4539 On the construction of highly stable,

CORPORATE SOURCE INDEX

explicit, numerical methods for integrating coupled ordinary differential equations with parasitic eigenvalues NASA-TN-D-4547 c19 N68c19 N68-21978 Investigation of a nearly isentropic mixed compression axisymmetric inlet system at Mach numbers 0.6 to 3.2 NASA-TN-D-4557 c28 N68-23354
 whom Tim - P-907
 c28 No

 Tables of Fe I line intensities.
 volume 1 - Temperatures from 1000 deg to 6500 deg K.

 Volume 2 - Temperatures between 6500 deg and 20,000 deg K
 c25 No
 c25 N68-24161 Fluctuating pressures on the afterbodies of five blunt atmosphere entry vehicles NASA-TN-D-4591 c c32 N68-24508 hand-held sextant qualified for space flight NASA-TN-D-4585 c21 N68-2 c21 N68-24512 Landing site dispersions of an uncontrolled lander on Mars NASA-TN-D-4587 c30 N68-24557 high enthalpy plasma generator for entry heating simulation NASA-TN-D-4583 cll N c11 N68-24560 plezoelectric transducer for measuring cardiac and gross motor activity of small organisms NASA-TN-D-4590 c05 N68-25060 On board calculations of a two impulse abort to a preselected landing site NASA-TN-D-4599 c21 N68-25103 Penetration resistance of double sheet structures at velocities to 8.8 km/sec NASA-TN-D-4568 c32 c32 N68-25104 External aerodynamics of the magnetosphere NASA-TN-D-4482 C29 NG A least squares method for the reduction of free-oscillation data c29 N68-25181 NASA-TN-D-4503 c19 N68-25869 Dynamic response of a family of axisymmetric hammerhead models to unsteady aerodynamic loading NASA-TN-D-4504 c01 N68-25916 NASA-TN-D-4504 Aerodynamic characteristics of a large-scale model with unswept wing and augmented jet flap NASA-TN-D-4610 c01 N68-25919 Transition and flow reattachment behind an Apollo-like body at Mach numbers to 9 NASSA-TN-D-665 NASA-TN-D-4645 c01 N68-28220 An investigation of full-scale helicopter rotors at high advance ratios and advancing tip Mach numbers NASA-TN-D-4632 c01 N68-28268 On the use of algebraic methods in the analysis and design of model-following control systems NASA-TN-D-4663 c19 N68-28281 A technique for passive attitude control of solar oriented interplanetary spacecraft NASA-TN-D-4641 c21 N68 c21 N68-28361 Membrane analysis of scalloped shells NASA-TN-D-4687 c32 N68-28832 NASA-IN-J-4007 C32 N68-2 Stable implicit and explicit numerical methods for integrating quasi-linear differential equations with parasitic-stiff and parasitic-saddle eigenvalues NASA-TN-D-4703 C19 N68-2 c19 N68-29275 Calculations of Chandrasekhar*s X and Y functions and their analogs for noncoherent isotropic scattering NASA-TN-D-4712 c19 N68-30804 NABA-IN-D-4/12 Study of optical radiation in the wavelength regions of 0.4216 mu, 0.4278 mu, 0.4835 mu, and 0.5165 mu behind normal shock waves in a simulated Martian atmosphere NASA-TM-X-1634 c12 N68-32982 The effect of some telescope factors on variability of performance in sextant sighting NASA-TN-D-4781 c21 N68-330 c21 N68-33006 A method for computing luminous efficiencies from meteor data NASA-TN-D-4803 c30 N68-33 Finite amplitude waves in fluid-filled elastic tubes - Wave distortion, shock waves, and Korotkoff sounds c12 N68-33 c30 N68-33055 c12 N68-33056 A computer program for systematically analyzing free-flight data to determine the aerodynamics of axisymmetric bodies

I-176

NASA-TN-D-4766 c01 N68-33081 Analysis of launch windows from circular orbits for representative Mars missions NASA-TM-X-1651 c30 c30 N68-33371 The effects of irradiation and star magnitude on sextant sighting performance NASA-TN-D-4780 c21 N68-33456 Entries from earth orbit that simulate acceleration stresses of manned planetary missions NASA-TN-D-4847 c31 N68-36056 Use of an electroluminescent display in manual Use of an electroluminescent display in tracking and in a reading task NASA-TN-D-4841 c(Effects of edge constraints on optical qualities of a spacecraft window NASA-TN-D-4845 c2 c05 N68-36457 c23 N68-36470 The influence of gaseous environment on the self-adhesion of metals NASA-TN-D-4868 c17 N60 c17 N68-36970 Wind tunnel investigation of the low speed high lift aerodynamics of a one-fifth scale variable sweep supersonic transport NASA-TN-D-4844 c01 N68c01 N68-37365 NASA-IN-D-4044 NATIONAL AERONAUTICS AND SPACE ADMINISTRATION. ELECTRONICS RESEARCH CENTER, CAMBRIDGE, MASS. Numerical studies of transitions between the restricted problem of three bodies and the problem of two fixed centers and the Kepler problem NASA-TM-X-1465 c21 N A study of the possible uses of plasma for millimeter wave generation NASA-TN-D-4309 c25 N c21 N68-11146 c25 N68-18614 Attenuation and dispersion of longitudinal waves in viscous, partly ionized gases NASA-TM-X-1458 c07 N68-18703 MASA-TM-X-1458 C07 M68-1 Characteristics of tunneling p-n junctions NASA-TN-D-4403 c09 N68-1 Some arguments favoring non-conventional types of computers c09 N68-19062 NASA-TM-X-1544 C08 Design of a precision tilt and vibration isolation system NASA-TR-R-281 C14 c08 N68-19336 c14 N68-19642 Many-body theory of a rapidly varying inhomogeneous electron gas NASA-TR-R-283 c26 N68-24273 The equations of motion for optimized propelled flight expressed in Delaunay and Poincare variables and modifications of these variables NASA-TN-D-4478 c30 N68-24371 Low drive temperature stable memory cores NASA-TN-D-4573 c09 c09 N68-24388 Coding schemes for run-length information based on Poisson distribution NASA-TN-D-4572 c07 N68 Radiation and coupling between two collinear c07 N68-25852 open ended waveguides NASA-TN-D-4656 c09 N68-28668 M-ary Poisson detection and optical communications NASA-TN-D-4623 c07 N68-29528 Dn electromagnetic switching properties of a bi-stable fluidic element with non-destructive memory NASA-TM-X-1613 c09 N68-30501

 NASA-TM-X-1613
 C09 N68-3

 Research on field-aligned propagation of HF
 radiowaves using Alouette 2 topside sounder

 data and digital ray-tracing techniques
 NASA-TN-D-4748
 C07 N68-3

 The design of a Pulse Position Modulated
 /PPM/ optical communication system
 NASA-TN-D-4814
 C07 N68-3

 Survey of CO sub 2 laser development for space applications
 NASA-TN-D-4794
 C16 N68-3

 c07 N68-31639 c07 N68-35174 c16 N68-35175 Problems and programs on the use of submillimeter waves in space NASA-SP-182 c07 N68-35522 Error probabilities for maximum likelihood detection of M-ary Poisson processes in Poisson noise NASA-TN-D-4721 c07 N68-36105 Mathematical determination of geometrical image aberrations in single and double mirror NASA-TN-D-4692 c23 N68-36460

NATIONAL AERONAUTICS AND SPACE ADMINISTRATION. FLIGHT RESEARCH CENTER, EDWARDS, CALIF. A useful modification of the Wright spirometer NASA-TN-D-4234 c14 N68-10057 Wind-tunnel investigation of the flow field beneath the fuselage of the X-15 airplane at Mach numbers from 4 to 8 NASA-TM-X-1469 c02 N68-1 An analysis of the limit-cycle and structural-resonance characteristics of the X-15 c02 N68-11147 stability augmentation system NASA-TN-D-4287 c02 N68-11545 Evaluation of lateral-directional handling qualities of piloted reentry vehicles utilizing a fixed base simulation NASA-TN-D-4410 c31 N c31 N68-19226 method for the surface installation and fairing of static-pressure orifices on a large supersonic-cruise airplane NASA-TM-X-1530 c01 N68-19341 FM handling and analog-to-digital conversion of biomedical data from a 1,000-flight study NASA-TN-D-4488 c05 N68-21537 Recording and signal-conditioning techniques and equipment used in a 1,000-flight biomedical study COS N68-21538 Preliminary measured and predicted XB-70 engine noise NASA-TM-X-1565 c02 A review of transport handling-qualities criteria in terms of preliminary XB-70 c02 N68-21834 flight experience NASA-TM-X-1584 c02 N68-23901 Preliminary flight evaluation of the stability and control derivatives and dynamic characteristics of the unaugmented XB-70-1 airplane including comparisons with predictions NASA-TN-D-4578 c02 N68-24498 Characteristics and use of X-15 air-data sensors NASA-TN-D-4597 c14 N68-25317 Wind-tunnel calibration of a 40 deg conical pressure probe at Mach numbers from 3.5 to 7.4 NASA-TN-D-4678 c12 N68-28801 X-15 analog and digital inertial systems flight experience NASA-TN-D-4642 c08 N68-29404 simple laboratory method for reduction of rhythm and rate in large~scale monitoring of electrocardiogram ASA-TN-D-4768 NASA-TN-D-4768 (1) Atmospheric conditions associated with turbulence encountered by the XB-70 airplane above 40,000 feet altitude NASA-TN-D-4768 (1) c05 N68-32100 c13 N68-33416 Flow-field investigations on the X-15 airplane and model up to hypersonic speeds NASA-TN-D-4813 c01 N68-35173 NASA-IN-D-4013 COI NO. Landing loads and accelerations of the XB-70-1 airplane CO2 NG. NASA-TN-D-4836 CO2 NG NATIONAL AERONAUTICS AND SPACE ADMINISTRATION. GODDARD INST. FOR SPACE STUDIES, NEW YORK. Radiative equilibrium in an atmosphere with Rediative equilibrium in an atmosphere with c02 N68-36073 constant Einstein absorption coefficient NASA-TM-D-4479 cl3 N68-NATIONAL AERONAUTICS AND SPACE ADMINISTRATION. GODDARD SPACE FLIGHT CENTER, GREENBELT, MD. Environmental test contribution to spacecraft c13 N68-22861 reliability NASA-TN-D-4181 c31 N68-10192 An evaluation of sea surface temperature as measured by the Nimbus 1 high resolution infrared radiometer NASA-TN-D-4078 c20 N68-10222 Thermal design verification testing of the anchored interplanetary monitoring platform **D** NASA-TN-D-4112 c33 N68-10299 Optical alignment of silicon crystals NASA-TN-D-4187 c23 N68-10354 Temporal variations of mesospheric oxygen and ozone during auroral events c13 N68-10369 NASA-TN-D-3993 The applications technology satellite image

CORPORATE SOURCE INDEX

dissector camera experiment NASA-TN-D-4186 c14 N68-10647 Investigations in Hansen*s planetary theory c30 N68-11369 NASA-TN-D-4169 Geologic applications of orbital photography NASA-TN-D-4155 cl Statistical tests for signal detection NASA-TR-R-273 cl c13 N68-11714 c10 N68-11789 Effects of correlated noise with applications to Apollo tracking problems NASA-TN-D-4121 c10 N68-16749 methods of the elimination of the short period terms from a Hamiltonian NASA-TN-D-4399 c19 N68-17532 A logarithmic encoder for binary word compression NASA-TN-D-4290 c08 N68-18179 NASH-IN-9-4230 Theoretical and practical resolution limits for processing pulse frequency modulation telemetry NASA-TN-D-4180 c07 N68-18247 Planck functions and integrals - Methods of computation NASA-TN-D-4446 c19 N68-18455 Waveform distortion in a maximum-likelihood Darlington detector for M-ary PFM signals NASA-TN-D-4294 c07 N68-18542 fast method of orbit computation NASA-TN-D-4470 A c30 N68-20356 The operation of an electron paramagnetic resonance spectrometer NASA-TN-D-4469 c14 N68-21169 Determining the spin axis of a spinning satellite NASA-TN-D-4483 c30 N68-21182 The geomagnetic secular variation 1900-1965 NASA-TN-D-4527 c13 N6 c13 N68-21543 Hummingbird for the L sub 2 lunar libration point NASA-TN-D-4468 c30 N68-21733 Optical and microwave communications - A comparison NASA-TN-D-3984 c07 N68-22019 Space sciences data processing NASA-TN-D-4508 c08 N68-22510 General Lagrangian interpolation formulas NASA-TN-D-4424 c19 N68-22809 On the application of spinors to the problems of celestial mechanics NASA-TN-D-4447 c30 N68-22885 theoretical approach to the determination of magnetic torques by near field measurement NASA-TN-D-4485 c23 N68-24 c23 N68-24146 Dual detection system for AIMP PFM data processing NASA-TN-D-4561 c08 N68-24310 A digital voltage-controlled oscillator for phase lock loops NASA-TN-D-4521 c09 N6 c09 N68-24389 Aspect determination in lunar shadow on Explorer 35 NASA-TN-D-4544 c30 N68-24486 Star tracker calibration NASA-TN-D-4594 c21 N68-24555 Digital spectral analysis NASA-TN-D-4510 c08 N68-25268 Space trajectories and errors in time, frequency, and tracking station location NASA-TN-D-4507 c30 N c30 N68-25271 Lunar far-side communication satellites NASA-TN-D-4509 c31 N68-25358 Monomolecular contamination of optical surfaces NASA-TN-D-4612 c14 N68-25375 Theory of the investigation of the atmosphere of binary stars by analogy between gas dynamics and shallow-water flows NASA-TN-D-4520 c30 N68-25385 An autocorrelation approach to the Brown Twiss interferometer NASA-TN-D-4480 c14 N68-25518 Some meteorological observations of the Southern Hemisphere stratosphere and mesosphere NASA-TN-D-4264 c20 N68-25617 The influence of fixture stress concentrations on ring accelerometers NASA-TN-D-4540 c14 N68-25830 The interpretation of daytime measurements by the Nimbus 1 and 2 high resolution infrared radiometers NASA-TN-D-4552 c14 N68-25862 Local-error control and its effects on the optimization of orbital integration c30 N68-25867 NASA-TN-D-4542 Optically induced free-carrier light modulator NASA-TN-D-4608 c23 N68-2 Polar cap absorptions and associated solar terrestrial events throughout the 19th solar c23 N68-25868 cvcle NASA-TN-D-4473 c29 N68-25880 On some possible simplifications and changes in Hansen*s lunar theory NASA-TN-D-4562 c30 N68 c30 N68-26642 On the application of Lie-series to the problems of celestial mechanics NASA-TN-D-4460 c30 N68-26643 The radiation balance of the earth-atmosphere system from radiation measurements of the Nimbus 2 meteorological satellite c13 N68-28222 NASA-TN-D-4589 The use of the electron probe microanalyzer in materials research and development NASA-TN-D-4526 c15 N68-28249 On the perturbations of small-eccentricity satellites NASA-TN-D-4531 c30 N68-28251 Criteria for selection of wire insulations for use in space applications NASA-TN-D-4553 c18 N68-28264 Clean-room facilities for Explorer 35 spacecraft c11 N68-28311 NASA-TN-D-4577 precision spacecraft radiometer for hectometer wavelengths NASA-TN-D-4634 c14 N68-28327 Remote detection of terrain features from Nimbus 1 high resolution infrared radiometer nighttime measurements NASA-TN-D-4603 c13 N68-28872 Heat treatment for improved stress-corrosion resistance of 17-7 pH stainless steel NASA-TN-D-4673 c17 N68c17 N68-29379 Optimal computing forms for the two-body C and S series NASA-TN-D-4643 c19 N68-29407 Cold wall thermal vacuum, thermal design check for fully insulated experiment packages c11 N68-29478 NASA-TN-D-4644 numerical least-square method for resolving complex pulse height spectra NASA-SP-3044 c24 N68-29520 Properties of selected radioisotopes. bibliography, part 1 - Unclassified literature NASA-SP-7031 c06 N68-29959 NASA-TN-D-4696 NASA-TN-D-4696 The dynamic characteristics of satellites c19 N68-30594 having long elastic members NASA-TN-D-4576 c31 N68-31978 Explicit upper bounds for error propagation in the n-body field NASA-TN-D-4511 c30 N68-32094 Temperature, pressure, density, and wind measurements in the stratosphere and mesosphere, 1966 NASA-TR-R-288 c20 c20 N68-33036 Electron spin resonance of lithium-diffused silicon NASA-TR-R-290 c26 N68-33228 Experimental tests of the supernovae origin of cosmic rays NASA-TN-D-4732 c29 N68-33370 Microwave pump requirements for field operational broadband rutile traveling-wave nasers NASA-TN-D-4764 c16 N68-33635 The role of the experimenter associated with multi-experiment scientific satellites NASA-TN-D-4731 c34 N68-33682 the decrease of the radar cross section of the Apollo command module due to reentry plasma effects NASA-TN-D-4784 c07 N68-35140

Self-synchronizing bi-orthogonal coded PCM

NATIONAL AERONAUTICS AND SPACE ADMINISTRATION.

telemetry system c07 N68-36333 NASA-TR-R-292 A satellite view of Typhoon Marie 1966 development NASA-TN-D-4757 c20 N68-37869 NATIONAL AERONAUTICS AND SPACE ADMINISTRATION. LANGLEY RESEARCH CENTER, LANGLEY STATION, VA. Wind-tunnel investigation of a 3/8-scale automobile model over a moving-belt ground plane NASA-TN-D-4229 c01 N68-10093 Application of cell culture as a primary toxicity screen of possible spacecraft contaminants NASA-TN-D-4251 c04 N68-10122 Free-flight aerodynamic characteristics of a slender cone between Mach numbers of 7 and 8 NASA-TN-D-4245 c01 N68-10380 Effects of axial gradients of velocity and magnetic field, electrode stagger, and ion slip on parameters in MHD accelerators NASA-TN-D-4239 c28 N68-10502 Wind-tunnel investigation of a deflected-slipstream cruise-fan V/STOL aircraft wing NASA-TN-D-4262 c01 N68-11036 NASA-IN-0-4202 Charts for equilibrium isentropic expansion of air behind shocks up to 50000 feet per second /15.24 kilometers per second/ NASA-TN-D-4247 c33 N68-11144 Three ballistic camera data reduction methods applicable to reentry experiments NASA-TN-D-4260 c30 N68-Effect of thrust and altitude in steep c30 N68-11145 Effect of thrust and altitude in steep approaches on ground track noise NASA-TN-D-4241 col N68-J Ballistic limit of aluminum plates determined by an exploding foil gun technique NASA-TN-D-4259 c32 N68-J A general method for designing circular array c01 N68-11253 c32 N68-11355 antennas to obtain quasi-omnidirectional patterns NASA-TN-D-4254 c07 N68-11475 A simulator study of pilot control of remote orbital docking of large attitude-stabilized components NASA-TN-D-4263 c31 N68-11476 Products of some generalized functions NASA-TN-D-4244 c c19 N68-11494 Effect of ground proximity on the longitudinal, lateral, and control aerodynamic characteristics of a tilt-wing four-propeller V/STOL model NASA-TN-D-4237 c02 N68-11519 Midcourse-guidance procedure with single position fix obtained from onboard optical . measurements MASA-TN-D-4246 c21 N68-1 Flight investigation of performance characteristics during landing approach of a large powered-lift jet transport NASA-TN-D-4261 c02 N68-1 c21 N68-11521 c02 N68-11638 Investigation of tethered station keeping c31 N68-11641 NASA-TN-D-4258 Flight test of a 40-foot-nominal-diameter Mach number of 1.64 and a dynamic pressure of 9.1 pounds per square foot NASA-TM-X-1484 c31 N68-11 c31 N68-11919 Preliminary infrared horizon profiles from Project Scanner NASA-TM-X-1483 c21 N c21 N68-11949 MASA-IN-X-1483 Experimental pressure distributions and aerodynamic characteristics of a low-fineness-ratio cylinder at a Mach number of 10.5 and angles of attack from 0 deg to 90 deg NASA-TM-X-1487 Flight test of a 15-foot-diameter /4.6-meter/ 120 deg conical spacecraft simulating parachute deployment in a Mars atmosphere NASA-TN-D-4266 c31 N68-11961 Nonlinear flutter of a circular cylindrical shell in supersonic flow NASA-TN-D-4265 c32 N68-12864 Equipment and procedures for glass-bead peening titanium-alloy tanks NASA-TN-D-4288 cl c15 N68-12890 Stress-corrosion cracking of Ti-6A1-4V titanium alloy in nitrogen tetroxide NASA-TN-D-4289 c17 N68-12891

A piloted fixed-base simulator study of lowspeed flight characteristics of an arrow-wing supersonic transport design NASA-TN-D-4277 c05 N68-J Performance of a 19.7 meter diameter disk gap band parachute in a simulated Martian c05 N68-13609 environment c31 N68-13797 NASA-TM-X-1499 Measurements of ground effect on a low-aspect-ratio ogee-wing airplane model and calculations of landing-flare trajectories NASA-TN-D-4329 c02 N68-14090 Influence of discrete ring stiffeners and prebuckling deformations on the buckling of eccentrically stiffened orthotropic cylinders NASA-TN-D-4283 c32 N68-14 c32 N68-14091 Performance of a 16.6-meter-diameter modified ringsail parachute in a simulated Martian environment NASA-TM-X-1500 c31 N68 c31 N68-14092 Plastic behavior of circular plates under transverse impulse loadings of Gaussian distribution NASA-TR-R-279 c32 N68-14640 c32 N68-1 A study of the effect of measurement errors upon a range controller for an entry vehicle NASA-TN-D-4317 c21 N68-1 c21 N68-14732 Effects of pavement texture on wet-runway braking performance NASA-TN-D-4323 c02 N68-14903 Static and dynamic longitudinal stability derivatives of a powered 0.18-scale model of a fan-in-wing VTOL aircraft NASA-TN-D-4322 c02 N68-158 c02 N68-15894 Calculation of the dynamic longitudinal stability of a tilt-wing V/STOL aircraft and correlation with model flight tests NASA-TN-D-4344 c02 N68-15941 NASA-TN-D-4344 CU2 NG8-Experimental stability and control results at Mach 19 of an entry vehicle designed for an intermediate lift-drag ratio NASA-TN-D-4337 c31 N68c31 N68-16240 Wind tunnel investigation of three proposed launch vehicles at Mach numbers from 2.30 to 4.63 NASA-TN-X-1498 c01 N6 Supersonic aerodynamic characteristics of a model of an air-to-ground missile c01 N68-16299 model of an air-to-ground missile NASA-TM-X-1491 c01 M An analysis of VGH data from one type of four-engine turbojet transport airplane during commercial operations NASA-TN-D-4330 c02 M Evaluation of a closed-circuit television display in landing operations with a helicopter NASA-TN-D-4313 c05 M c01 N68-16480 c02 N68-16522 NASA-TN-D-4313 c05 N68-16594 Photometry of an iron artificial meteor reentering at 11 kilometers per second c30 N68-16750 NASA-TN-D-4312 NASA-TN-D-4312 c30 N68-1 Wind-tunnel investigation of lateral aerodynamic characteristics of a powered four-duct-propeller VTOL model in transition NASA-TN-D-4343 c02 N68-1 c02 N68-17023 Wind velocity profiles measured by the smoke-trail method at Wallops Island, Virginia, 1963 and 1964 NASA-TN-D-4365 c20 Subsonic and transonic flutter and flow c20 N68-17024 investigations of the T-tail of a large multijet cargo airplane NASA-TN-D-4316 c02 N68-17055 Accuracy study of finite difference methods NASA-TN-D-4372 c32 N6 c32 N68-17068 NBSA-IN-D-4372 C32 NBS-Bounds for the eigenvalues of a matrix NASA-IN-D-4373 c19 N68-1 Pressure and flow field study at Mach number 8 of flow separation on a flat plate with deflected trailing edge flap NASA-IN-D-4308 c12 N68-1 Continue and surface transmosts for c19 N68-17334 c12 N68-17376 Coatings and surface treatments for longtime protection of Ti-8Al-1Mo-1V alloy sheet from hot salt stress corrosion NASA-TN-D-4319 c17 N68-17377 An investigation of leakage of large-diameter O-ring seals on spacecraft air-lock hatches NASA-TN-D-4394 c31 N68-17 Residual static strength and slow crack growth behavior of duplex-annealed Ti-8A1~1No-1V c31 N68-17498

sheet NASA-TN-D-4358 c32 N68-17588 Flutter of buckled, simply supported, rectangular panels at supersonic speeds NASA-TN-D-4357 c32 c32 N68-17651 MB3A-IN-U-4357 C32 N68-1 Effects of lee-surface volume addition on longitudinal aerodynamics of a high-lift-drag-ratio wing-body configuration at Mach 6.0 NASA-TN-D-4361 c01 N68-17880 characteristics of 90 deg and 15 deg blunted cones in nitrogen and helium at Mach 20 cones in nitrogen and nelium at Mach 20 NASA-TN-D-4314 coll N68-178 Effects of longtime environmental exposure on mechanical properties of sheet materials for a supersonic transport NASA-TN-D-4318 cl7 N68-178 c01 N68-17896 c17 N68-17897 Experimental study of transmission and backscatter of 0.075 to 1.0 MeV electrons by aluminum and stainless steel NASA-TN-D-4363 c24 N68-17898 A real-gas study of low-density wedge-induced laminar separation on a highly cooled blunt flat plate at M infinity equals 12 NASA-TN-D-4320 col N68c01 N68-17899 Analysis of human response in combined control tasks NASA-TN-D-4356 c05 N68-18014 three-dimensional analysis of the effects of heat generation in plates NASA-TN-D-4326 c33 N68-18122 The aperature admittance of a ground plane The aperature admittance of a ground plane mounted waveguide illuminating a perfectly conducting sheet NASA-TN-D-4366 c07 N68-16 Wind data from the 250-foot /76.2-meter/ tower at Wallops Island, Virginia NASA-TN-D-4395 c20 N68-16 Low-subsonic flight and force investigation of c07 N68-18123 c20 N68-18246 a supersonic transport model with a double-delta wing NASA-TN-D-4179 c02 N68-18250 Pressure and heat transfer on blunt curved plates with concave and convex surfaces in hypersonic flow NASA-TN-D-4367 c12 N68-18253 Computing program for axial distribution of aerodynamic normal-force characteristics for axisymmetric multistage launch vehicles NASA-TN-D-4342 c31 N68-1 c31 N68-18615 quasi-omnidirectional slot array antenna for spacecraft use at microwave frequencies NASA-TN-D-4362 c07 c07 N68-18616 NBSA-IN-D-4362 COV N66-Comparison of the Mach 3.0 aerodynamic characteristics of tension string, tension shell, and 120 deg conical shapes NASA-IN-D-4360 col N68-Light-Induced Modulation of Absorption c01 N68-18720 /LIMA/ in cadmium sulfide NASA-TN-D-4466 c26 N68-18772 Water pressure and accelerations during landing of a dynamic model of the Apollo spacecraft with a deployed-heat-shield impact-attenuation system NASA-TN-D-4275 c31 N68-18822 Forces and moments produced by air and helium jets exhausting parallel to a flat plate in a near vacuum NASA-TN-D-4408 c12 N68-19000 Effect of two-dimensional multiple sine-wave protrusions of the pressure and heat-transfer distributions for a flat plate at Mach 6 NASA-TN-D-4437 c01 N68-19063 MASA-1W-14-37 Measurements of winds and temperatures at altitudes up to 65 kilometers in the Southern Hemisphere NASA-TN-D-4429 c20 N68-19084 An analytical procedure for predicting the two-dimensional impact dynamics of spacecraft landing gear NASA-TN-D-4434 c31 N68-19085 NASA-IN-D-4434 C31 NG Flutter of corrugation stiffened panels at MACH 3 and comparison with theory NASA-TN-D-4321 C32 NG A new method of testing small samples for goodness of fit to normal populations NASA-TN-D-4405 C19 NG c32 N68-19143

- c19 N68-19144
- Flight investigation to determine the effect

CORPORATE SOURCE INDEX

of longitudinal characteristics on low-speed instrument operation NASA-TN-D-4364 c02 N68-19184 An automatic balancing system for use on frictionlessly supported attitude-controlled test platforms NASA-TN-D-4426 c09 N68-19185 Preliminary study of drag reduction for coasting missiles at Mach numbers from 1.57 to 4.63 NASA-TM-X-1537 c01 c01 N68-19206 Vehicle attitude determination with a single onboard camera NASA-TN-D-4359 c31 N68-19275 Review of causes and alleviation of low tire traction on wet runways NASA-TM-2406 c02 N68-19620 Line-of-sight velocity as an indicator of pericynthion altitude of selenocentric orbits NASA-TM-X-1508 c30 N68-19622 Evaluation of boundary layer and wake survey data reduction techniques in compressible flows NASA-TN-D-4401 c12 N68-19709 Experimental and theoretical investigation of the ablative performance of five phenolic-nylon-based materials NASA-TN-D-4374 c18 N6 An annotated bibliography of computer-aided c18 N68-19710 circuit analysis and design NASA-SP-7023 c10 N68-19882 Effects of 22 MeV proton and 2.4 MeV electron radiation on boron and aluminum-doped silicon solar cells NASA-TN-D-4407 c26 N68-19924 An investigation of extremely flexible lifting rotors NASA-TN-D-4465 c01 N68-19954 Approximate relations for laminar heat-transfer and shear-stress functions in equilibrium dissociated air NASA-TN-D-4484 c33 Relativistic models of the universe with c33 N68-20065 pressure equal to zero and time-dependent uniformity NASA-TR-R-282 c30 N68-20192 Stresses caused by an in plane line load used to rotate a thin-walled spherical satellite NASA-TN-D-4425 c31 N68c31 N68-20198 The input admittance of a rectangular aperture antenna loaded with a dielectric plug NASA-TN-D-4430 c07 N68-20333 Effects of pressure suits and backpack loads on man*s self-locomotion in earth and simulated lunar gravity NASA-TN-D-4464 c05 N68 c05 N68-20354 Response characteristics of impacting penetrometers appropriate to lunar and planetary missions NASA-TN-D-4454 c32 c32 N68-20364 Experimental modes of vibration of 14 deg conical-frustum shells with free ends NASA-TN-D-4428 c32 N68-20954 Experimental study of aeroelastic instability of overexpanded rocket nozzle extensions NASA-TN-D-4471 c32 N68-21099 NASA-TN-D-4471 C32 N6 Simulator study of pilot control over the lunar module during ascent from the lunar surface by using visual guidance cues NASA-TM-X-1549 C21 N6 c21 N68-21366 Interference effects of canard controls on the longitudinal aerodynamic characteristics of a winged body at Mach 10 NASA-TN-D-4436 c01 N68-21 Experimental pressure distributions on a blunt c01 N68-21579 lifting-entry body at Mach 3.71 NASA-TN-D-4494 c01 N68-21681 Flight test of a 30 foot nominal diameter cross parachute deployed at a Mach number of 1.57 and a dynamic pressure of 9.7 pounds per square foot NASA-TM-X-1542 c31 N68-21778

- Performance of a 16.6-meter-diameter cross parachute in a simulated Martian environment NASA-TM-X-1543 c31 N68-2 c31 N68-21833
- Experimental investigation of the longitudinal vibration of a representative launch vehicle with simulated propellants

NASA-TN-D-4502 c32 N68-21869 A lighting strategy for Lunar Orbiter mission design NASA-TN-D-4501 c14 N68-21942 Effects of simulated wing damage on the aerodynamic characteristics of a swept-wing airplane model NASA-TM-X-1550 c01 N68-22002

 NASA-TM-X-1550
 c01 N68-22

 An investigation of the helicopter height
 velocity diagram showing effects of density

 altitude and gross weight
 NASA-TN-D-4536
 c02 N68-22

 Effects of shock impingement and other factors
 on leading-edge heat transfer
 NASA-TN-D-4543

 NASA-TN-D-4543
 c33 N68-22

 c02 N68-22033 c33 N68-22118 The geometric properties of an expandable whirling-membrane solar-energy concentrator NASA-TN-D-4532 c03 N68c03 N68-22258 Flight investigation of a capacitance-type meteoroid detector using an inflatable paraglider NASA-TN-D-4530 c14 N68-Summary of VGH data collected on one type of twin-engine jet airplane during airline c14 N68-22290 operations NASA-TN-D-4529 c02 N68-22291 Dynamic stability of a 4.6-meter-diameter 120 deg conical spacecraft at Mach numbers from 0.78 to 0.48 in a simulated Martian environment NASA-TN-D-4558 c31 N68-22301 Capacitor-type meteoroid-penetration sensors -Description and test results NASA-TN-D-4524 c14 N68-22883 Application of maximum likelihood techniques to the design of optimum star trackers NASA-TN-D-4549 c21 c21 N68-23377 NB3A-IN-D-4349 Revised upper-air wind data for Wallops Island based on serially completed data for the years 1956 to 1964 NASA-TN-D-4570 c20 N68-24028 Investigation of temperature measurements in 300 deg to 1100 deg K low-density air using an electron beam probe NASA-TN-D-4500 c14 N c14 N68-24244 Flight test of a 40-foot nominal diameter Flight test of a 40-foot nominal diameter disk gap band parachute deployed at a Mach number of 1.91 and a dynamic pressure of 11.6 pounds per square foot NASA-TM-X-1575 c02 N68-2424 Suppression of temperature rise in lossy diodes inside resonant cavities by application of pressurized liquid nitrogen NASA-TN-D-4556 c09 N68-2434 c02 N68-24245 c09 N68-24387 Trends in repeated loads on transport airplanes NASA-TN-D-4586 c02 N68-24476 A summary of rotor-hub bending moments encountered by a high performance hingeless-rotor helicopter during nap-of-the-earth maneuvers NASA-TN-D-4574 c02 N68-24499 Study of underexpanded exhaust jets of an X-15 airplane model and attached ramjet engine simulator at Mach 6.86

NASA-TM-X-1571 c28 N68-2 Approximation of the spanwise distribution of wind-tunnel-boundary interference on lift of wings in rectangular perforated-wall test c28 N68-24614 sections

- NASA-TR-R-285 c01 N68-24617 High energy proton damage in silicon surface barrier detectors NASA-TN-D-4528 c26 N68
- c26 N68-24660 A summary of results on sonic-boom pressure signature variations associated with atmospheric conditions NASA-TN-D-4588
- c02 N68-24662 Aerodynamic characteristics of a modified cone - Conical-frustum entry configuration at Mach 6.0
- c31 N68-24964 NASA-TN-D-4598 Calculation of axisymmetric supersonic flow past blunt bodies with sonic corners, including a program description and listing NASA-TN-D-4563 col N68-
- nnan-IN-U-4563 c01 N68-25093 Investigation of the effect of wheel braking on side-force canability of
- on side-force capability of a pneumatic tire NASA-TN-D-4602 c02 N68-2 c02 N68-25313 aark s dag bada

The fabrication and testing of Pageos 1 NASA-TN-D-4596 c31 N68-25820 Evaluation of a full-scale lunar-gravity simulator by comparison of landing-impact tests of a full-scale and a 1/6-scale model NASA-TN-D-4474 c11 N68-25853 Static-temperature distribution in a flat plate compressible turbulent boundary layer with heat transfer NASA-TN-D-4611 c33 N68-25917 An omnidirectional flush-mounted microwave antenna with a simple feed for use on spacecraft NASA-TN-D-4555 c07 N68-25918 Analytical investigation of effects of physical and aerodynamic parameters on dynamic behavior of Project Fire reentry vehicle NASA-TM-X-1589 c31 N68-26645 An experimental study of flame propagation in supersonic premixed flows of hydrogen and air NASA-TN-D-4631 c33 N68-28100 NASA-TIN-D-4631 Study of the optimum values of several parameters affecting longitudinal handling qualities of VTOL aircraft NASA-TN-D-4624 c02 N68-28153 The Explorer 23 micrometeoroid satellite. Description and results for the period November 6, 1964, through November 5, 1965 NASA-TN-D-4284 c31 N68-28198 Radiometric measurements of the earth*s infrared horizon from the X-15 in three spectral intervals NASA-TN-D-4654 c21 c21 N68-28262 Hot-gas ingestion investigation of large-scale jet VTOL fighter-type models NASA-TN-D-4609 c02 N68-28277 Local afterbody heat transfer to a blunt two-dimensional configuration at Mach 8 NASA-TN-D-4443 c12 | c12 N68-28282 Correlation study of lunar radii obtained from photographic and lunar gravitational field data NASA-TN-D-4636 c30 N Analysis of a star-field mapping technique for use in determining the attitude of a c30 N68-28409 spin-stablized spacecraft NASA-TN-D-4637 c2 Wind-tunnel investigation of the static c21 N68-28418 Wind-tunnel investigation of the static aerodynamic characteristics of a multilobe gliding parachute NASA-TN-D-4672 col N68 Reduction of wind-tunnel-model vibration by means of a tuned damped vibration absorber installed in the model NASA-TM-X-1606 c32 N68 c01 N68-28447 c32 N68-28806 theoretical study of the effect of pivot location on the aerodynamic-center movement of variable-sweep wings in incompressible flow NASA-TN-D-4635 c01 N68-28817 Wind-tunnel study to explore the use of slot spoilers to modulate the flap-induced lift of a wing NASA-TN-D-4664 c01 N68-28830 Derivation of approximate equations for solving the planar rendezvous problem NASA-TN-D-4670 c3 c30 N68-28841 NASA-IN-D-4670 A modified Multhopp approach for predicting lifting pressures and camber shape for composite planforms in subsonic flow NASA-TN-D-4427 Gravitational experiments with a collisionless c01 N68-28868 two-dimensional computer model NASA-TN-D-4646 c30 N68-28884 Description and initial calibration of the Langley 20-inch hypersonic arc heated tunnel NASA-TN-D-4653 cll N68-28947 Simulation studies of the supersonic transport In the present day air traffic control system NASA-TN-D-4638 c02 N68-29372

NASA-TN-D-4638 c02 N68-29372 Experimental investigation of laminar-flow separation on a flat plate induced by deflected trailing-edge flap at Mach 19 NASA-TN-D-4671 c01 N68-29405 Noise reduction by means of inlet-guide-vane choking in an axial-flow compressor NASA-TN-D-4682 c02 N68-29406 Photographic photographic entry of artificial metoors

Photographic photometry of artificial meteors

NASA-TN-D-4667 c14 N68-29418 Striking characteristics of the magnetron ionization gage in helium from 1.9 times 10 to the minus 7 torr to 7 times 10 to the minus 10 torr NASA-TN-D-4681 c14 N68-29951 NADATIN-U-4681 C14 H Hypersonic aerodynamic characteristics of low-wave-drag elliptical-body-tail combinations as affected by changes in stabilizer configuration NASA-TM-X-1620 c01 H c01 N68-29952 Effect of hinge-line bleed on heat transfer and pressure distribution over a wedge-flap combination at Mach 10.4 NASA-TN-D-4686 c01 N68-29955 Analysis and mechanization of three and four gimbal systems NASA-TN-D-4689 c11 N68-29957 Experimental investigation of the use of soft side legs to improve touchdown stability of side legs to improve touchdown statifity of legged landing vehicles NASA-TN-D-4680 c31 N68-2: Flight test of a 40-foot-nominal-diameter disk-gap-band parachute deployed at a Mach number of 2.72 and a dynamic pressure of 9.7 c31 N68-29962 pounds per square foot NASA-TM-X-1623 c31 N68-29993 Hot salt stress corrosion cracking and its effect on tensile properties of Ti-8Al-1Mo-1V titanium-alloy sheet NASA-TN-D-4674 c17 N68-30000 Aron-IN-U-4074 c17 Aerodynamic characteristics of two blunt, half-cone wedge entry configurations at Mach numbers from 2.30 to 4.63 NASA-TM-X-1621 c01 c01 N68-30030 NADA-IN-A-1021 Dynamics of a one-dimensional plasma sheath NASA-TN-D-4651 c25 N64 c25 N68-30031 nhon-in-1-4001 Turbojet-engine noise studies to evaluate effects of inlet-guide-vane-rotor spacing NASA-TN-D-4690 c28 N68-30040 Effect of carbon dioxide and water vapor on the induction period of the hydrogen-oxygen reaction NASA-TN-D-4685 c33 N68-30041 NBAR-IN-U-4665 C33 N66-3 The orbital recovery problem. Part 1 - An analysis technique for rapid determination of return opportunities and lateral-range requirements for recall to recovery networks NASA-TR-R-259 C21 N68-3 NASA-TR-R-259 c21 N68-30126 Calibration of 30 deg included-angle cone for determining local flor and the determining local flow conditions in Mach number range of 1.51 to 3.51 NASA-TN-D-4679 c14 Luminous efficiencies of three nickel artificial meteors between 9.8 and 11.4 c14 N68-30127 kilometers per second NASA-TN-D-4666 c30 N68-30244 Experimental study of vertical impacts of an LM-type landing gear assembly under simulated lunar gravity NASA-TN-D-4711 c32 N68-30505 A wind tunnel investigation of jet-wake effect of a high-bypass engine on wing-nacelle interference drag of a subsonic transport NASA-TN-D-4693 col N68-305 c01 N68-30595 Flight test analysis of Apollo heat shield material using the Pacemaker vehicle system NASA-TN-D-4713 c33 N68-Design of bodies to produce specified sonic-boom signature sonic-boom signatures NASA-TN-D-4704 c01 N68-31484 Α modified multihopp approach for predicting lifting pressures and camber shape for composite planforms in subsonic flow NASA-TN-D-4427, SUP. co1 NASA-TN-D-4427, SUP. Supersonic aerodynamics of large-angle cones c01 N68-31551 Test sections for small theoretical wind-tunnel-boundary interference on V/STOL models NASA-TR-R-286 c11 N68-31592 Investigation of a compartmented-gas-bag landing system having multiple impact capabilities NASA-TN-D-4710 c32 N68-31602 A celestial attitude measurement instrument for Project Scanner NASA-TN-D-4742 c21 N68-31938

Plastic buckling of plates and shells under

CORPORATE SOURCE INDEX

biaxial loading NASA-TN-D-4706 c32 N68-3 Attitude determination of the spin-stabilized c32 N68-31946 Project Scanner spacecraft NASA-TN-D-4740 c21 N68-31957 simplified method for calculating laminar à. heat transfer over bodies at an angle of attack NASA-TN-D-4720 c33 N68-31959 Application of the leading-edge-suction analogy of vortex lift to the drag due to lift of sharp-edge delta wings NASA-TN-D-4739 theoretical and experimental c01 N68-31990 investigation of the three-dimensional vibration characteristics of a scaled model of an asymmetrical launch vehicle NASA-TN-D-4707 c32 N68-320 Prediction of fatigue-crack-propagation behavior in panels with simulated rivet forces NASA-TN-D-4702 c32 N68-320 Theory and results on collective and collisional effects for a one-dimensional self-gravitating system NASA-TR-R-289 c30 N68-329 Drag due to the state of t c32 N68-32051 c32 N68-32074 c30 N68-32978 Drag due to two-dimensional surface roughness in a turbulent boundary layer at Mach 3 with and without heat transfer ANASA-TN-D-4746 c12 A matrix method for studying motions of spacecraft consisting of interconnected c12 N68-33054 rigid bodies NASA-TN-D-4749 c32 N68-33092 Description and operating parameters of Mach 2 nozzle system for the Langley 11-inch ceramic-heated tunnel NASA-TN-D-4750 c11 N68-33190 Single-thermocouple method for determining heat flux to a thermally thick wall NASA-TN-D-4737 c33 N68-33208 A manual navigation method for evaluating transfer orbits for lunar landings NASA-TN-D-4756 c21 l c21 N68-33271 The preheating of plasma in a megajoule theta-pinch experiment NASA-TN-D-4708 c25 N68-33372 Infrared horizon profiles for summer conditions from Project Scanner NASA-TN-D-4741 c21 N68-33450 Effect of speed brakes on the supersonic aerodynamic characteristics of a variable sweep tactical fighter model at Mach numbers from 1.60 to 2.50 NASA-TN-D-4773 c02 N68-3 c02 N68-33669 An experimental and analytical vibration study of thin cylindrical shells with and without longitudinal stiffeners NASA-TN-D-4705 c32 N68c32 N68-33738 Aerodynamic characteristics of several hypersonic boost-glide-type configurations at Mach numbers from 2.30 to 4.63 NASA-TM-X-1601 c01 N68-33836 Free-flight and wind-tunnel studies of deployment of a dynamically and elastically scaled inflatable parawing model NASA-TN-D-4724 c02 N68-33879 simplified equilibrium hydrocarbon-air a simplified equilibrium nyarocaroon-air combustion gas model for use in air-breathing engine cycle computer programs
 NASA-TN-D-4747
 Flight investigation of the effects of Apollo heat-shield singularities on ablator c28 N68-35115 performance NASA-TN-D-4791 c33 N68-35116 Equilibrium normal-shock and stagnation-point properties of helium for incident-shock Mach numbers from 1 to 30 NASA-TN-D-4754 c12 N68-35 Effects of several ramp-fairing, umbilical, and pad configurations on aerodynamic heating c12 N68-35117 to Apollo command module at Mach 8 NASA-TM-X-1640 c01 N68-35141 digital computer program for calculating the performance of single or multiple diaphragm shock tubes for arbitrary equilibrium real gas mixtures NASA-TN-D-4802 c11 N68-35466

Empirical stagnation-point heat-transfer relation in several gas mixtures at high

NATIONAL AERONAUTICS AND SPACE ADMINISTRATION.

- enthalpy levels NASA-TN-D-4799 c33 N68-35468 Surfaces including drag loading NASA-TN-D-4793 c32 N68-35496 NASA-IN-D-4793 Heat transfer and pressure distributions on spherically blunted 25 deg half-angle cone at Mach 8 and angles of attack up to 90 deg NASA-TN-D-4792 Higher-order-mode effects on the aperture admittance of a rectangular waveguide covered with dielectric and plasma slabs NASA-TN-D-4774 c07 N68-35524 Tables of energy and angular distributions of thick target bremsstrahlung in metals NASA-TN-D-4755 c24 N68-5 c24 N68-35535 Electromagnetic properties of a circular aperture in a dielectric-covered or uncovered ground plane NASA-TN-D-4752 c07 N68-35537 Subsonic longitudinal aerodynamic measurements on a transport model in two slotted tunnels differing in size c01 N68-35617 NASA-TM-X-1660 NASA-IN-X-1000 Effect of shape changes on the aerodynamic characteristics of a twisted and cambered arrow wing at Mach number 2.03 NASA-TN-D-4796 c01 N68-35665 NASA-IN-D-4796 Experimental base pressures on 9 deg spherically blunted cones at Mach numbers from 10.5 to 20 NASA-TN-D-4800 Experimental investigation and analysis of dielectric breakdowns induced by electron is polytoper filmers filmers c01 N68-35668 irradiation in polymer films NASA-TN-D-4810 c24 N68-36070 Detailed description and results of a method for computing mean and fluctuating quantities in turbulent boundary layers NASA-TN-D-4815 c12 N6 A study of the reaction-plane approximation in ablation analyses NASA-TN-D-4817 c33 N6 c12 N68-36071 A semigraphical method for a deorbit tratectory doctor of the second sec trajectory design study NASA-TN-D-4801 c30 N68-36077 Aerodynamic characteristics of a five jet VTOL configuration in the transition speed range NASA-TN-D-4812 c01 N68-36081 An exploratory study of parallel stage separation of reusable launch vehicles NASA-TN-D-4765 c31 c31 N68-36106 NB3A-IN-0-4705 Effect of large sideslip angles on stability characteristics of a T-tail transport configuration NASA-TM-X-1665 c01 N68-36112 Aerodynamic characteristics of bodies of revolution at Mach numbers from 1.50 to 2.86 and angles of attack to 180 deg NASA-TM-X-1658 col N68-3 c01 N68-36193 A hovering investigation of an extremely flexible lifting rotor NASA-TN-D-4820 c01 N68-36334
- Low-density, leading-edge bluntness, and ablation effects on wedge-induced laminar boundary layer separation at moderate enthalpies in hypersonic flow NASA-TN-D-4829 c12 N68-36458
- Simplified technique for determining pericynthion altitude of lunar orbits NASA-TN-D-4811 c3 c30 N68-36459
- synthesis of human response in closed-loop tracking tasks NASA-TN-D-4842 c05 N68 c05 N68-36461
- Effects of nose shape and fin geometry on static stability of a high-fineness-ratio sounding rocket NASA-TM-X-1661 c01 N68-36509
- Proton-produced defects in n-type silicon c26 N68-37051
- NASA-TN-D-4830 c26 N68-37 Mechanical properties and column behavior of thin wall beryllium tubing NASA-TN-D-4833 c17 N68-37 Effect on base drag of recessing the bases of conical afterbodies at subsonic and transonic encode c17 N68-37053
- speeds NASA-TN-D-4821 c01 N68-37054

- Effects of zinc concentration on output of zinc doped germanium detectors NASA-TN-D-4834 c26 N68-37055
- Effects of flexibility on lift and pitchingmoment characteristics of a series of lowaspect-ratio wing-body combinations at c01 N68-37065
- aspect-ratio Wing-oody combinations at transonic speeds NASA-TN-D-4655 col N68-3 Effects of variations in nose and windshield geometry on supersonic aerodynamic characteristics of a variable-sweep tactical
- cnaracteristics of a variable-sweep tactical fighter model NASA-TM-X-1664 c02 N68-3' Studies of flow distortion in the tailpipes of hydrogen peroxide gas generators used for jet engine simulation NASA-TM-X-1671 c12 N68-3' c02 N68-37066
- c12 N68-37067 A combined Newton-Raphson and gradient
- parameter correction technique for solution of optimal-control problems NASA-TR-R-293 c19 N68c19 N68-37073
- NASA-TR-R-293 c19 N68-Transonic aerodynamic characteristics of powered models of several Apollo launch-escape vehicle configurations NASA-TN-D-4843 c31 N68-Effects of reduced airspeed for landing approach on flying qualities of a large jet transport equipped with powered lift NASA-TN-D-4804 c02 N68-Elev field presenting near an arout wingerbody c31 N68-37074
- c02 N68-37075 model at Mach numbers of 1.60, 2.36, and 2.96
- NASA-TN-D-4809 c01 N68-37238 Acrodynamic characteristics of a parasol-wing-body combination utilizing favorable lift interference at Mach numbers from 3.00 to 4.63 NASA-TN-D-4855 COI N68-
- c01 N68-37854
- NASA-TN-D-4855 NATIONAL AERONAUTICS AND SPACE ADMINISTRATION. LEWIS RESEARCH CENTER, CLEVELAND, OHIO. Electron microscopy technique for determination of dispersoid distribution in powder blends c17 N68-10051
 - NASA-TM-X-1468 c17 N68-1005 A moving-belt ground plane for wind-tunnel ground simulation and results for two jet-flap configurations NASA-TN-D-4228 c01 N68-10060
 - Automated data collection system applied to NASA-TM-X-1464 c03 N
 - c03 N68-10103 Effect of cover gas pressures on accelerated cavitation damage in sodium NASA-TN-D-4235 c17 N68
 - c17 N68-10104 Shielding requirements for the NASA Plum
 - Brook HB-6 beamhole radiation effects facility NASA-TM-X-1461 c22 N68-10133
 - Design and operation of a high-temperature tungsten-mesh gas heater c22 N68-10134
 - NASA-TM-X-1466 Comparison of absolute calculated and measured gamma and neutron doses in tungsten-water moderated critical assembly NASA-TN-D-4223 c22 N68-10
 - c22 N68-10291 Transient chilldown of a single thick-walled tube by liquid and gaseous hydrogen NASA-TN-D-4238 c33 N68-10368
 - Thermal Investigation of an ion engine microthrustor
 - NASA-TM-X-1473 c28 N68-10496 Application of liquid-layer solid-sample spark technique to spectrochemical spark
 - source NASA-TM-X-1429 c06 N68-10497
 - Determination of electric potential across the oxide scale during oxidation of tantalum, niobium, and magnesium NASA-TN-D-4240
 - c17 N68-10498 NASA-IN-D-4240 CI/ NGG-10496 Use of similarity parameters for examination of geometry characteristics of high-expansion-ratio axial-flow turbines NASA-TN-D-4248 CO1 N68-10529 Performance tests of a 1/2-millipound /2.2 mN/ ammonia resistojet thrustor sustem
 - system NASA-TN-D-4249 c28 N68-10562
 - Scattering of 42-MeV /6.7-pJ/ alpha particles from even isotopes of cadmium NASA-TN-D-4256 c24 |
 - c24 N68-11074

Power transfer to ion cyclotron waves in a two ion species plasma NASA-TM-X-1481 c25 N68-11404 Weak locally homogeneous turbulence and heat transfer with combined two-dimensional shear and normal strain NASA-TN-D-4273 c33 N68-11491
 mpon-in-u-u-42/3
 c33 l

 Corrosion product of the tantalum interstitial oxygen potassium system at 1800 deg F /1255 deg K/ NASA-TN-D-4213
 c17 l
 c17 N68-11511 Stabilization of dc arcs in static argon atmospheres for use in spectrochemical analysis NASA-TN-D-4236 c06 N68-11512 Mist-flow heat transfer using single-phase variable-property approach NASA-TN-D-4149 c33 N68-11636 Fatigue of liquid rocket engine metals at cryogenic temperatures to minus 452 deg F /4 deg K/ NASA-TN-D-4274 c17 N68-11637 Multiple decision procedures for ANDVA of two-level factorial fixed-effects replicationfree experiments NASA-TN-D-4272 c19 N68-11639 Hydrogen-oxygen chemical reaction kinetics in rocket engine combustion NASA-TN-D-4250 c33 N68-11642 Non-Th-D-4269 c17 N68 c17 N68-11644 Effect of gravity on self-pressurization of spherical liquid-hydrogen tankage NASA-TN-D-4286 c27 N66 c27 N68-11645 Sensitivity of quartz, piezoelectric pressure transducers as a function of temperature from 20 deg to 477 deg K NASA-TM-X-1479 c14 N68-11 c14 N68-11867 Control of contaminants in liquid-metal systems NASA-TM-X-1432 c17 N68-11912 Experimental performance evaluation of a 6.02-inch /15.29-cm/ radial-inflow turbine with an exit diffuser NASA-TM-X-1480 c03 N68-11920 Structural feasibility study of pressurized tanks for liquid-methane fueled supersonic aircraft NASA-TN-D-4295 c32 N68-12370 Ductility mechanisms and superplasticity in chromium alloys NASA-TN-D-4346 c14 N68-13973 Flight evaluation of an electrostatic accelerometer for measurement of low-level orbital accelerations NASA-TM-X-1488 c14 N68-13974 NASA-IM-X-1488 C14 Cardiac R-wave detector NASA-TM-X-1489 C05 Digital readout and control system for a 64-inch /1.63-m/ scattering chamber NASA-TN-D-4324 c14 c05 N68-13999 c14 N68-14018 Analysis of turbulent liquid-metal heat transfer in channels with heat sources in the fluid power-law velocity profile NASA-TN-D-4336 c33 N68-14 c33 N68-14042 Effect of green light on spectral response of cuprous sulfide-cadium sulfide photovoltaic NASA-TN-D-4333 c03 N68-14082 Synthesis of ultrahigh molecular-weight poly/ethylene terrephthalate/ NASA-TN-D-4335 c06 N68-14093 4500 deg R /2500 deg K/ flowing-gas facility NASA-TM-X-1506 c11 N68-14115 correlation of local heat transfer coefficients for single phase turbulent flow of hydrogen in tubes with temperature ratios to 23 NASA-TN-D-4332 c33 N68-14240 Theoretical temperatures of thin-film solar cells in earth orbit NASA-TN-D-4331 c33 N68-14270 Parametric analysis of radioisotope cascaded thermoelectric generators NASA-TM-X-1501 c22 N68-14585 Parametric analysis of radioisotope

CORPORATE SOURCE INDEX

thermoelectric generators NASA-TM-X-1453 c03 N68-14630 Performance evaluation of a two stage axial-flow turbine for two values of tip clearance NASA-TN-D-4388 c03 N68-14639 Effects of wall pressure distribution and liquid temperature on incipient cavitation of Freon-114 and water in venturi flow NASA-TN-D-4340 c12 N68-1 Computer program for design of two dimensional c12 N68-14641 supersonic nozzle with sharp edged throat c01 N68-14747 NASA-TM-X-1502 Technique for recovery of alkali-metal reaction products NASA-TN-D-4310 c c17 N68-14888 Establishing allowable temperature gradients for tungsten-uranium dioxide fuel elements using experimental cyclic strain data NASA-TN-D-4279 c2 c22 N68-14986 Reduced pressure environment effects on rolling element fatigue life with super refined mineral oil lubricant NASA-TN-D-4348 c15 N68-15010 Analysis of uranyl fluoride solution reactors containing voided tubes NASA-TN-D-4270 c22 N68c22 N68-15197 Excited states of xenon 128 NASA-TN-D-4305 c24 N68-15328 Venturi scaling studies on thermodynamic effects of developed cavitation of Freon-114 NASA-TN-D-4387 c12 N68-15329 Experimental investigation of nucleate boiling bubble dynamics in normal and zero gravities NASA-TN-D-4301 c33 N68-15330 Simultaneous correction of velocity and mass bias in photography of meteors NASA-TR-R-280 c30 N68-15484 Application of directional solidification to a NASA nickel-base alloy /TAZ-8B/ NASA-TN-D-4390 c17 N68-15637 search for unbound helium 3 levels with isobaric spin 1/2 NASA-TN-D-4377 c24 N68-15638 Scale model study of flow patterns in the inlet manifold of the fuel pump drive turbine for the M-1 hydrogen-oxygen rocket engine NASA-TM-X-1513 c12 N68-15639 Experimental determination of neutron fluxes in Plum Brook reactor HB-6 facility with use of sulfur pellets and gold foil NASA-TM-X-1497 c22 N68-15643 Combustion instability in steel and ablative rocket chambers NASA-TM-X-1511 c28 N68-15644 Semiconductor switches for aerospace alternating-current power applications NASA-TM-X-1495 c09 c09 N68-15649 Transient solidification of a flowing liquid on a cold plate including heat capacities of frozen layer and plate NASA-TN-D-4353 c33 N68-15742 Cold-air investigation of a turbine for high-temperature-engine application. 3 - Overall stage performance NASA-TN-D-4389 c01 N68-15743 Electrical properties of xenon-filled thermionic diodes in radiation field of a nuclear reactor NASA-TN-D-4368 c25 N68-15747 Elastoplastic analysis of circular cylindrical inclusion in uniformly stressed infinite homogeneous matrix NASA-TN-D-4350 c32 N68-15769 Small high-temperature nuclear reactors for space power NASA-TN-D-4371 c22 N68-15792 Numerical procedures for calculating real fluid properties of normal and parahydrogen NASA-TN-D-4341 c08 N68-NASA-TN-D-4341 Nuclear design data for experiments to be conducted in Horizontal Through Hole 1 of the Plum Brook Reactor NASA-TM-X-1509 c22 N68-15855 Temperature and liquid-level sensor for liquid-hydrogen pressurization and expulsion studies NASA-TN-D-4339 c14 N68-15893

- Bimetal sensor for averaging temperature measurement of nonuniform temperature profiles NASA-TN-D-4242 c14 N68-15936 Displacement of disintegrating liquid jets in crossflow
- NASA-TN-D-4334 c33 N68-15942 Analytical determination of radial inflow turbine design geometry for maximum efficiency NASA-TN-D-4384 c03 N68-15943
- MCFLARE, a Monte Carlo code to simulate solar flare events and estimate probable doses encountered on interplanetary missions
- NASA-TN-D-4311 c29 N68-16008 Calculations to support operation of the Plum Brook reactor NASA-TM-X-1496 c22 N68-16056 Dynamic pressure limits for flat plates as related to nuclear fuel elements NASA-TN-D-4417
- related to ALL NASA-TN-D-4417 Performance in air of 4 inch /10.16-cm/ mean-diameter single stage axial-flow turbine for Reynolds numbers from 4,900 to 188,000 c03 N68-16228
- NB3A-IN-J-4383 CU3 No Potential use of high frequency induction heating for high temperature liquid metal heat transfer testing NASA-TM-X-1510 c33 N68-16300
- Analytical comparison of Rankine cycle space radiators constructed of central double, and block-vapor-chamber fin-tube geometries
- NASA-TN-D-4411 c33 N68-16324 Cold-air performance evaluation of scale model oxidizer pump-drive turbine for the M-1 hydrogen-oxygen rocket engine. Performance of first stage with inlet-feedpipe-manifold assembly NASA-TN-D-4392 3 c28 N68-16413
- Friction torque of ball bearings in vacuum with seven polytetrafluoroethylene composition retainer materials NASA-TN-D-4355 c15 N68-16468
- Aerodynamic evaluation of two-stage axial flow turbine designed for Brayton-cycle space
- power system NASA-TN-D-4382 c03 No Effects of cable and circuit parameters on c03 N68-16469 the precision calibration of a charge amplifier NASA-TN-D-4300
- c09 N68-16530 Glass, boron, and graphite filament wound resin composites and liners for cryogenic pressure vessels
- NASA-TN-D-4412 c18 N68-16623 Parametric mass analysis and comparison of two types of reactant cooling-and-storage units for a lunar-based hydrogen-oxygen regenerative fuel-cell system
- NASA-TN-D-4386 c03 N68-16631 Cold-air investigation of a turbine for high-temperature engine application. Detailed analytical and experimental 2 -
- investigation of stator performance NASA-TN-D-4418 c28 N Minimum film-boiling heat flux in vertical c28 N68-16632 flow of liquid nitrogen NASA-TN-D-4307
- c33 N68-16683 Design and performance of two vacuum chambers and solar simulators for solar-cell research NASA-TM-X-1503 cl1 N68-1
- c11 N68-16695 performance study of rotating gas jet generator for strong traveling transverse coustic modes
- NASA-TN-D-4380 c12 N68-16998 Experimental determination of gamma exposure
- rate in Plum Brook HB-6 facility NASA-TM-X-1490 c22 N68-17022 Elastic-plastic torsion problem for strain-hardening materials
- NASA-TN-D-4391 c32 N68-17045 Correlation of transient spectra with
- performance in coaxial plasma guns NASA-TN-D-4385 c25 N68-17070
- Feasibility of supporting liquid fuel on a solid wall in a radiating liquid-core nuclear rocket concept NASA-TN-D-4413 c27 N c27 N68-17093
- Description and flight performance results of the Wasp sounding rocket

NATIONAL AERONAUTICS AND SPACE ADMINISTRATION. CONT

c31 N68-17094 NASA-TM-X-1518 Summary of radiation effects on thermionic insulator materials c22 N68-17095 NASA-TN-D-4414 Reduction of apparent-power requirement of phase-controlled parasitically loaded urboalternator by multiple parasitic loads c03 N68-17110 NASA-TN-D-4302 Effects of composition and heat treatment on high-temperature strength of arc-melted tungsten hafnium carbon alloys NASA-TN-D-4379 c17 N68-17317 Noncavitating performance of two-area-ratio water jet pumps having throat lengths of 7.25 diameters c15 N68-17564 NASA-TN-D-4445

 NASA-TN-D-4445
 c15 N68-17564

 Boiling heat transfer coefficients, interface

 behavior, and vapor quality in rotating

 boiler operating to 475 G*s

 NASA-TN-D-4136
 c33 N68-17566

 Damping of a torsional oscillator in liquid

 helium 4 and 3 from 0.4 deg to 2.5 deg K

 NASA-TN-D-4381
 c26 N68-17594

 Self evacuated multilayer insulation of lightweight prefabricated panels for cryogenic storage tanks NASA-TN-D-4375 c33 N68-18046 Development of a cobalt-tungsten ferromagnetic, high-temperature, structural alloy NASA-TN-D-4338 c17 N68-18145 Computer program for calculating isothermal, turbulent jet mixing of two gases NASA-TN-D-4378 cl2 N68 c12 N68-18146 NASA-TN-D-4378 c12 N68-11 Cold-air performance evaluation of scale model oxidizer pump-drive turbine for the M-1 hydrogen-oxygen rocket engine. 4 -Performance of first stage with modified inlet feedpipe-manifold assembly NASA-TN-D-4393 c28 N68-11 Wind tunnel investigation of techniques for reducing cowl drag of an axisymmetric external-compression inlet at Mach 2.49 NASA-TM-X-1516 c01 N68-11 Pressure-rise characteristics for a liquid c28 N68-18188 c01 N68-18189 Pressure-rise characteristics for a liquid hydrogen dewar for homogeneous, normal gravity quiescent, and zero gravity tests NASA-TM-X-1134 c33 N68-181 c33 N68-18196 Preliminary considerations for fast-spectrum, liquid-metal cooled nuclear reactor program for space-power applications NASA-TN-D-4315 c22 N68-18197 Cooled baffle development for M-1 engine using a subscale rocket engine NASA-TM-X-1267 c28 N68-18216 Change in inducer net positive suction head requirement with flow coefficient in low temperature hydrogen /27.9 deg to 36.6 deg R/ NASA-TN-D-4423 c28 N68-Experimental investigation of acoustic liners to suppress screech in storable propellant c28 N68-18221 rocket motors NASA-TN-D-4442 c28 N68-18249 Feasibility study of a tungsten water moderated nuclear rocket. 7 - System dynamics and control analysis NASA-TM-X-1426 c2; c22 N68-18252 Operational amplifiers for use in nuclear spectroscopy · · · · · NASA-TN-D-4349 c24 SNAP-8 simulator loop mechanical design NASA-TM-X-1515 c11 c24 N68-18254 c11 N68-18460 Enhancement of ion cyclotron waves in hydrogen helium mixtures NASA-TN-D-4271 c25 N68-18485 Experimental performance evaluation of an 8.5 inch /21.59 cm/ mean-diameter axial flow turbine at Reynolds numbers from 18,000 to 177,000 NASA-TN-D-4432 c03 c03 N68-18501 Determination of intersection of particle flight path with surface of helical tubular void region NASA-TM-D-4435 c22 N68-14 Oxide deformation and fiber reinforcement in a tungsten metal oxide composite NASA-TN-D-4475 c17 N68-14 c22 N68-18541

- c17 N68-18610 Analytical investigation of supersonic turbomachinery blading. 1 - Computer program

for blading design NASA-TN-D-4421 c08 N68-18620 NRGR-IN-J-4421 CO8 N68 Dynamic characteristics of parasitic loading speed controller for 10 kilowatt Brayton cycle turboalternator NASA-TM-X-1456 CO3 N68 c03 N68-18702 Preliminary tests with mass flux probe in supersonic stream NASA-TM-X-1524 c14 N68-18834 Analysis of the maximum performance of a paraboloidal solar collection system for space power NASA-TN-D-4415 c03 N68-18998 Use of surface replication, extraction replication, and thin-film electron microscopy in the study of dispersion-strengthened materials NASA-TN-D-4461 c17 N68-18999 Instrumentation of a SNAP-8 simulator facility NASA-TM-X-1525 c14 N68-19001 Nuclear thermionic space power system concept employing heat pipes NASA-TN-D-4299 c22 N68-19146 Considerations of turbine cooling systems for Mach 3 flight MAGA 5 light NASA-TN-D-4301 Calculations of solar plasma interaction with magnetic field of current loop and two parallel infinite lines of current NASA-TN-D-4304 c29 N68-1 c33 N68-19187 c29 N68-19188 Outgassing of water vapor from concrete surfaces in vacuum environment NASA-TM-X-1536 c1 c11 N68-19207 Experimental investigation of vapor ingestion in the Centaur liquid hydrogen tank NASA-TM-X-1482 cl2 N68c12 N68-19225 Effect of boattail juncture shape on pressure drag coefficients of isolated afterbodies NASA-TM-X-1517 c01 N68-19237 Similarity solution for turbulent mixing between a jet and a faster moving coaxial stream NASA-TN-D-4441 c12 N68-19246 Model for frequency response of a forced flow, hollow, single tube boiler NASA-TM-X-1528 c12 N68-19340 Effect of surface roughness on the 0.66-micron normal spectral emittance of vapor-deposited rhenium from 1500 deg K to 2100 deg K NASA-TM-X-1514 c17 N68-19347 Radiation-induced reduction of divalent copper salts in solutions c06 N68-19434 NASA-TN-D-4451 NAGA-IN-D-4401 Out of the ecliptic plane probe mission employing electric propulsion NASA-TN-D-4455 Experimental evaluation of several advanced ablative materials as nozzle sections of a c28 N68-19581 storable-propellant rocket engine NASA-TM-X-1559 c28 N68-19708 Reactivity effects caused by radial power flattening in a small, fast-spectrum reactor NASA-TN-D-4459 c22 N68-1 c22 N68-19925 Experimental investigation of reaction control, storable bipropellant thrustors NASA-TN-D-4416 c28 N c28 N68-20064 Analysis of pressure-drop function in Rankine space power boilers with discussion of flow maldistribution implications NASA-TN-D-4498 c33 N68-20066 Scale 1/14.2 investigation of submerged nozzle for SL-3 260-inch solid rocket NASA-TM-X-1546 c28 N68-20186 Divergent-flow contact-ionization electrostatic thrustor for satellite attitude control and station keeping NASA-TN-D-4420 c28 N68-20 c28 N68-20187 Residual stress and subsurface hardness changes induced during rolling contact NASA-TN-D-4456 c15 N68-20199 Analytical investigation of supersonic turbomachinery blading. 2 - Analysis of impulse turbine-blade sections NASA-TN-D-4422 c03 N c03 N68-20276 Electron-beam, crystallization of silicon, germanium, and cadmium sulfide NASA-TN-D-4522 c26 N68-20295 A coaxial-flow-stabilized arc

CORPORATE SOURCE INDEX

NASA-TN-D-4517 c25 N68-20296 Cryogenic temperature measurement using platinum resistance thermometers NASA-TN-D-4499 cl c14 N68-20324 Wear rate and friction coefficient in liquid nitrogen and hydrogen of steel sliding on polymer laminates /various fabrics and polymers/ NASA-TN-D-4463 c15 N68-20325 Cryogenic positive expulsion bladders NASA-TM-X-1555 c18 N68-20329 Performance of annular plug and expansion-deflection nozzles including external flow effects at transonic Mach numbers NASA-TN-D-4462 c01 N68-20330 Radiant-interchange configuration factors for spherical and conical surfaces to spheres NASA-TN-D-4457 c33 N68-20331 NB3A-IN-U-4437 Local heat transfer for water in entrance regions of tubes with tapered flow areas and nonuniform heat fluxes NASA-TM-X-1554 c33 N68-20338 Performance of a multiple single-pass counterflow NaK-cooled mercury Rankine cycle condenser NASA-TM-X-1548 c33 N68-20340 Discharge characteristics of some copper oxide-magnesium thermal cells NASA-TN-D-4306 c03 N68-20344 An experimental investigation of the effect of gravity on a forced circulation pattern in spherical tanks NASA-TN-D-4409 c12 N68 c12 N68-20352 Activation of sodium, lithium, and potassium in compact fast reactors and its effect on shielding NASA-TM-X-1512 c22 N68-20355 Investigation of the use of the lunar surface layer to store energy for generating power during the lunar night NASA-TM-X-1560 c03 N68-20363 Analytical calculation of partial derivatives relating lunar and planetary midcourse correction requirements to guidance system injection errors NASA-TN-D-4518 c30 N68-20368 Heat-transfer correlation for gas flow across heated banks of wire meshes or tubes NASA-TN-D-4514 c: c33 N68-20374 A 23.4 square-foot /2.17-SQ-M/ cadmium sulfide thin-film solar cell array NASA-TM-X-1519 c03 N68-20432 Postshutdown cooling requirements of tungsten water-moderated nuclear rocket NASA-TM-X-1568 c22 c22 N68-21111 Collisionless cylindrical diode NASA-TN-D-4516 c10 N68-21122 c15 N68-21226 Low variable thrust interplanetary trajectory data NASA-TN-D-4431 c30 N68-21228 NASA-IN-D-4401 C30 Noo Feasibility study of optimum on-off attitude control system for spacecraft NASA-TN-D-4519 C31 N68 Computer code for calculating temperature c31 N68-21260 profiles in a propellant tank NASA-TM-X-1556 c27 N68-21267 An experimental study of liquid flow into a baffled spherical tank during weightlessness NASA-TM-X-1526 c12 N68-213 c12 N68-21365 Computer program for calculating velocities and streamlines on a blade-to-blade stream surface of a turbomachine NASA-TN-D-4525 c01 N68 c01 N68-21374 Performance of a venturi meter with separable diffuser NASA-TM-X-1570 c14 N68-21384 Electron microscope technique suggested to reveal microstructures of dispersion-strengthened materials NASA-TM-X-1561 c17 N68-21431 Computer programs for plane collisionless

sheaths between field-modified emitter and thermally ionized plasma exemplified by cesium NASA-TH-X-1562 co8 N68-21499

- Critical electrical aspects of alternating-current power source for Centaur space vehicle NASA-TM-X-1569 c03 N68-21562 Pairs of emitter and collector sheaths for cesium thermionic diodes NASA-TN-D-4419 c25 N68-21623 A breadboard flueric-controlled pneumatic stepping motor system NASA-TN-D-4495 c03 N68-21651 Mechanism and kinetics of corrosion of selected iron and cobalt alloys in refluxing mercury
- refluxing mercury NASA-TN-D-4450 c17 N68-21654 Stabilizing effects of several injector face baffle configurations on screech in a 20,000 pound-thrust hydrogen-oxygen rocket
- baffle configurations on screech in a 20,000 pound-thrust hydrogen-oxygen rocket NASA-TN-D-4515 c28 N68-21679 Experimental investigation of an acoustic liner with variable cavity depth
- NASA-TN-D-4492 c33 N68-21680 Comparative study of mixed and isolated flow methods for cooled-turbine performance analyses NASA-TM-X-1572 c01 N68-21692
- NASA-TM-X-1572 c01 N68-21692 An experimental investigation of the restart area ratio of a Mach 3.0 axisymmetric mixed compression inlet
- NASA-TM-X-1547 col N68-21703 Effect of finned-tube assembly techniques on the heat-transfer characteristics of a space radiator
- NASA-TM-X-1557 c33 N68-21704 Hot isostatic compaction of tungsten-uranium dioxide fuels with high-volume fraction of uranium dioxide
- NASA-TM-X-1563 c22 N68-21705 Spectral emissivity of highly doped silicon NASA-TN-D-4303 c26 N68-21708
- Viscosity of gas mixtures NASA-TN-D-4496 c12 N68-21724 Partition functions and thermodynamic
- properties to high temperatures for H sub 3 and H sub 2 ions NASA-TN-D-4523 c33 N68-21732
- Electrical performance of a rhenium-niobium cylindrical thermionic converter NASA-TN-D-4533 c03 N68-21766
- NASA-IN-D-4555 C05 NOS-21766 Crack growth in 2014-T6 aluminum tensile and tank specimens cyclically loaded at cryogenic temperatures NASA-TN-D-4541 c17 N68-21768
- MAGN-IN-D-4541 C1/ NGO-21/08 Design and performance of flueric analog to pulse frequency converter NASA-IN-D-4497 C03 N68-21835
- NASA-TN-D-4497 c03 N68-21835 Evaluation of tantalum to stainless steel transition joints NASA-TM-X-1540 c15 N68-21898
- NASA-TM-X-1540 c15 N68-21898 Applications of Monte Carlo analysis to tungsten resonance absorption
- NASA-TN-D-4545 c22 N68-21924 Aerodynamic characteristics in pitch of a modified half ring wing body combination and a swept wing body combination at Mach 2.16 to 3.70 NASA-TM-X-1551 c01 N68-21940
- NASA-TM-X-1551 coll N68-21940 Experiments on stability of herringbone grooved gas-lubricated journal bearings to high compressibility numbers
- NASA-TN-D-4440 c15 N68-21965 A review of lubrication of sliding and rolling element electrical contacts in vacuum
- NASA-TN-D-4476 c15 N68-21979 Gamma flux and heat deposition in Plum Brook reactor - Comparison of calculation and experiment
- experiment NASA-TM-X-1539 c22 N68-22022 Optimal finite-thrust transfer between planet approach and departure asymptotes with specified intermediate orbit NASA-TN-D-4534 c28 N68-22096
- Experimental investigation of reactor-loop transients during startup of a simulated SNAP-8 system
- NASA-TN-D-4546 c03 N68-22257 An explanation of anomalous non-Hookean deformation of ionic single crystals
- NASA-TN-D-4513 c26 N68-22271

NATIONAL AERONAUTICS AND SPACE ADMINISTRATION. CONT

Experimental evaluation of 7.82-inch /19.8-cm/ diameter throat inserts in a storable-propellant rocket engine NASA-TM-X-1463 c28 c28 N68-22272 Method for determining normal modes and frequencies of a launch vehicle utilizing its component normal modes NASA-TN-D-4550 c32 N68-22275 Some numerical comparisons of three-body trajectories with patched two body trajectories for low thrust rockets NASA-TN-D-4559 c30 N68-22289 The effect of interfiber distance and temperature on the critical aspect ratio in composites c17 N68-22338 NASA-TN-D-4548 Analysis of fan-turbine efficiency characteristics in terms of size and stage number NASA-TM-X-1581 c28 N68-22725 Viewing devices for observing flow conditions in hot mercury systems NASA-TM-X-1578 cll N68c11 N68-22737 Wind tunnel investigation of fluctuating pressures on a 1/10-scale Centaur model at transonic speeds NASA-TM-X-1574 c31 c31 N68-22742 NASA-IN-2-1574 C31 No8 Texture strengthening and fracture toughness of titanium alloy sheet at room and cryogenic temperatures NASA-IN-D-4444 c17 N68 c17 N68-22884 Method of calculating the normal modes and frequencies of a branched Timoshenko beam NASA-TN-D-4560 c02 NG c02 N68-22886 Periodic, small-amplitude solutions to the spatially uniform plasma continuity equations NASA-TN-D-4472 c25 N68-22 c25 N68-22887 Capillary rise in the annular region of concentric cylinders during coast periods of Atlas Centaur flights NASA-TM-X-1558 c12 N68-23353 Effects of high-wave amplitude and mean flow on a Helmholtz resonator NASA-TM-X-1582 c12 N68-23423 Experimental investigation of mercury propellant feed isolators for Kaufman thrusters NASA-TM-X-1579 c28 N68-23477 Calculation of capture cross sections for ion polar molecule collisions involving nethyl cyanide NASA-TM-X-1586 c24 N68-2: Reactivity insertions in compact reactor cores due to fuel movement NASA-TM-X-1587 c22 N68-2: c24 N68-23893 c22 N68-23894 Tankage systems for a methane-fueled supersonic transport NASA-TM-X-1591 c02 N68-23895 The release of hydrogen on ball milling chromium in water NASA-TN-D-4569 c15 N68-23900 Creep of tantalum T-222 alloy in ultrahigh vacuum for times up to 10,000 hours NASA-TN-D-4605 c17 N68-24111 CI/ N6 Rarefied-gas couette flow and heat transfer between parallel plates by model sampling NASA-TN-D-4579 cl2 N6 c12 N68-24129 A computer program for reversion of the cumulative binomial probability distribution NASA-TM-X-1592 c19 N68-24141 Friction and wear in cryogenic liquids for composites of phenolic and of polytetrafluoroethylene of various particle sizes and concentrations NASA-TN-D-4565 c15 N68c15 N68-24142 Atlas-Centaur flight performance for Surveyor mission A NASA-TN-D-4580 c31 N68-24338 Stability analysis and minimum thrust vector control requirements of booster vehicles during atmospheric flight NASA-TN-D-4593 c21 N68-24409 NASA-IN-D-4393 C21 N68 Cooling studies with 40-millimeter-bore ball bearings using low flow rates of 60 deg R /33 deg K/ hydrogen gas NASA-TN-D-4616 c15 N68

NASA-TN-D-4616 c15 N68-24456 Cavitating performance of two low-area-ratio water jet pumps having throat lengths of 7.25 diameters

NASA-TN-D-4592 c03 N68-24461 Yielding and fracture in tungsten and tungsten-rhenium alloys c17 N68-24477 NASA-TN-D-4567 Ionic conductivity of solid mixtures NASA-TN-D-4606 c26 N68-24510 Electrical and mechanical properties of a superior high-temperature cobalt-iron magnetic material NASA-TN-0-4551 c17 N68-24558 Reactivity control of fast-spectrum reactors by reversible hydriding of yttrium zones NASA-TN-D-4615 c22 N68 c22 N68-24559 Determination of convective heat-transfer coefficients on adiabatic walls using a sinusoidally forced fluid temperature NASA-TM-X-1594 c33 N68-24618 Inelastic scattering form factors using projected Hartree-Fock wave functions NASA-TN-D-4566 c24 N68-24661 Injection start of a Brayton cycle turbocompressor operating on gas bearings in a closed loop NASA-TM-X-1590 c03 N68-24757 Effects of liquid depth on lateral sloshing under weightless conditions NASA-TN-D-4458 c12 N68-24758 Mixing and reaction studies of hydrazine and nitrogen tetroxide using photographic and spectral techniques NASA-TN-D-4467 c33 N68-24965 NASA-IN-D-4467 Computer program for symbolic reduction of block diagrams using FORMAC NASA-TN-D-4617 Ages of D/d₉/He sup 3 and T/d₉n/He sup 4 neutrons in water and tungsten-water mixtures NASA-TN-D COLOR c08 N68-24967 NASA-TN-D-4581 c22 N68-25058 Thermal performance of a rhenium niobium cylindrical thermionic converter NASA-TN-D-4582 c03 N68-25059 Management of cryogenic propellants in a full scale orbiting space vehicle NASA-TN-D-4571 c28 N68-25099 Experimental verification of a double dead time model describing chugging in liquid bipropellant rocket engines NASA-TN-D-4564 c33 N68-25102 Vapor pressure of potassium to 2170 deg K NASA-TN-D-4535 c33 N68-25122 Analytical investigation of electrically heated wire mesh for flowing gas heaters NASA-TN-D-4595 c33 N68-25312 Critical-speed analysis of flexibly mounted rigid rotors NASA-TN-D-4607 c32 N68-25421 Effects of arrival rates of absorbate ions and atoms on surface coverage, hence work functions, of emitting electrodes NASA-TN-D-4369 c25 N68-25630 Electrical characteristics of a dc compact arc in argon from 1 to 10 atmospheres and from 600 to 1200 amperes NASA-TM-X-1596 c29 N68-25818 Target pressure and damage data from impacts by explosively propelled projectiles NASA-TM-X-1597 c32 N68 NASA-TM-X-1597 c32 N68-25819 Analysis and selection of design conditions for a radioisotope Brayton-cycle space powerplant NASA-TN-D-4600 c03 N68-25829 Liquid inflow to initially empty, hemispherical ended cylinders during weightlessness NASA-TN-D-4628 c12 N68-25866 General operating characteristics of a back streaming direct-current plasma generator NASA-TN-D-4604 c25 NG c25 N68-25877 Thermodynamic study of plasmas using the principle of maximum entropy NASA-TN-D-4621 c25 c25 N68-25920 Practical stability criterion and its application to digital simulation NASA-TN-D-4203 c08 N68-26640 Screech suppression techniques for rocket combustors using earth-storable propellants NASA-TM-X-1595 c28 N68-26644 Body rotation effects on melting ablation c33 N68-26650 NASA-TN-D-4614 Detailed performance of a radial-bladed

CORPORATE SOURCE INDEX

centrifugal pump impeller in water NASA-TN-D-4613 c12 N68-26651 Effects of nuclear radiation on a highreliability silicon power diode I-change in 1-5 design characteristics NASA-TN-D-4620 c09 N68c09 N68-26662 Boundary conditions for the diffusion solution of coupled conduction-radiation problems NASA-TN-D-4618 c33 N68-26759 Method for calculating allowable creep stress in linearly increasing stress environment NASA-TN-D-4352 c22 N6 c22 N68-26764 Evaluation of alternating-current line-voltage regulators in auxiliary electric power systems NASA-TN-D-4627 c03 N68-28101 Coaxial plasma gun research at Lewis Research Center NASA-TM-X-1600 c25 N68-28154 The boiloff problem with methane fuel in supersonic aircraft NASA-TM-X-1604 c27 N68-28155 Centaur/Surveyor nose fairing aerodynamic heating investigation NASA-TM-X-1605 c33 c33 N68-28156 Use of wire lacing to reduce blade vibration in an axial-flow compressor rotor NASA-TM-X-1603 c32 N68-28238 Low-temperature resistance minimum and magnetoresistance for dilute alloys of iron in copper NASA-TN-D-4626 c26 N68-28239 PLOT3D - A package of FORTRAN subprograms to draw three-dimensional surfaces NASA-TM-X-1598 c19 c19 N68-28240 Deration of a liquid fluorine pump in cavitating flow at an inducer tip speed of 188 feet per second /57.3 m/sec/ NASA-TM-X-1573 c15 N68-28241 Effect of ball-race conformity on spinning friction NASA-TN-D-4669 c15 N68-28258 An explanation of Fitzgerald*s audiofrequency resonances and sound beams NASA-TN-D-4625 c23 N68-28259 Effect of crystal transformation and atomic ordering on friction and wear of two cobaltbase alloys in vacuum NASA-TN-D-4668 c15 N68-28260 Coupled-channels method for rearrangement collisions c24 N68-28265 NASA-TN-D-4633 Analysis of radiator characteristics of a single-loop 100-kilowatt Brayton space power system using a pure gas and a gas-solid suspension NASA-TN-D-4659 c03 N68-28280 Axial power tailoring to obtain constant fuel-centerline temperature in a nuclear reactor NASA-TN-D-4658 c22 N68-28304 A radiator concept based on capillary retention of liquid NASA-TN-D-4370 c03 N68-28310 Study of vibration induced stresses in design of fuel-element support assembly for tungsten water-moderated nuclear reactor NASA-TM-X-1608 c32 N c32 N68-28330 MASA-IN-A-1000 C32 NOO-Maximum drop diameters for the atomization of liquid jets injected concurrently into accelerating or decelerating gas streams NASA-TN-D-4640 c12 N68c12 N68-28364 Compilation of thermophysical properties of liquid lithium NASA-TN-D-4650 c17 N68-28365 NASA THE FOOL Photographic study of a bromine jet in a coaxial airstream NASA-TN-D-4660 cl2 Flow and wall-temperature sensitivity in c12 N68-28370 parallel passages for large inlet to exit density ratios in subsonic flow NASA-TN-D-4649 c33 NG c33 N68-28371 Thermal radiation heat transfer. Volume 1 -The blackbody, electromagnetic theory, and material properties NASA-SP-164 c33 N68-28530 Thrust-vector control requirements for large launch vehicles with solid-propellant first stages

NASA-TN-D-4662 c31 N68-28690 Preliminary evaluation of greases to 316 deg C and solid lubricants to 816 deg C in ball bearings NASA-TN-D-4652 c15 N68-28766 Performance of centerbody vortex generators in an axisymmetric mixed-compression inlet at Mach numbers from 2.0 to 3.0 NASA-TN-D-4675 coll for c c01 N68-28795 c17 N68-28818 Airplane size and staging effects on SST cruise sonic boom NASA-TN-D-4677 c02 N68-28831 NASA-TN-D-4677 c02 N68-Visual observations of flow through a radial-bladed centrifugal impeller NASA-TN-D-4282 c12 N68-Pyrotechnic shaped charge separation systems for aerospace vehicles NASA-TM-X-1607 c31 N68-Aerodynamic performance of a 4.59-inch modified radial-inflow turbine for a sindle-shaft Bravton cucle space power c12 N68-28842 c31 N68-28869 single-shaft Brayton cycle space power system NASA-TM-X-1615 c03 N68-28870 Friction and wear under fretting conditions of materials for use as wire friction dampers of compressor blade vibration NASA-TN-D-4630 c15 N68-28871 Gamma ray angular correlations following inelastic scattering of 42-MeV alpha particles from magnesium 24 NASA-TN-D-4683 c24 N68-29375 Analysis of several methane-fueled engine cycles for Mach 3.0 flight NASA-TN-D-4699 c28 N68-29378 Sound measurements on a full-scale jet-engine inlet-noise-suppressor cowling NASA-TN-D-4639 c02 N68-29887 Influence of surface active agents on friction, deformation, and fracture of lithium fluoride NASA-TN-D-4716 c15 N68-29918 Neutronic effects on moderator insertion in fast-spectrum reactors NASA-TM-X-1614 c22 N68-29950 Cold flow investigation of a low angle turbojet plug nozzle with fixed throat and translating shroud at Mach numbers from 0 to 2.0 NASA-TM-X-1619 c28 N68-29953 Some observations concerning the oxidation of the cobalt-base superalloy L-605 /HS-25/ NASA-TN-D-4715 c17 N68-29954 Experimental evaluation of a voltage regulator-exciter for a 15 kilovolt-ampere Brayton cycle alternator NASA-TN-D-4697 c03 N68-29960 High temperature creep-rupture properties of a tungsten-uranium dioxide cermet produced from coated particles NASA-TM-M-1000 produced from coated particles NASA-TM-X-1625 c17 N68-29987 Effect of variable stator area on performance of a single-stage turbine suitable for air cooling. 1 - Stator overall performance with 130-percent design area NASA-TM-X-1632 c01 N68-29994 Fission neutron attenuation in lithium-6, natural lithium hydride, and tungsten NASA-TN-D-4684 c2 c24 N68-30001 Performance characteristics of 15 kVA homopolar inductor alternator for 400 Hz Brayton-cycle space-power system NASA-TN-D-4698 c03 Overall performance in argon of a 6-inch radial-bladed centrifugal compressor c03 N68-30002 NASA-TM-X-1622 col N68-3 On the influence of nonuniform magnetic fields c01 N68-30033 on ferromagnetic colloidal sols NNON-IN-V-40/6 C06 N68 A numerical procedure for calculating stress and deformation near a slit in a three-dimensional elastic-plastic solid NASA-TN-D-4717 C32 N68 Compatibility NASA-TN-D-4676 c06 N68-30044 c32 N68-30045 Compatibility of several iron-base, cobalt-base, and nickel-base alloys with refluxing potassium at 1800 deg F

NATIONAL AERONAUTICS AND SPACE ADMINISTRATION. CONT

NASA-TM-X-1617

c17 N68-30065

- Chromium and nickel powders made by reduction of their oxides with magnesium, lithium, or sodium vapors NASA-TN-D-4714 c17 N68-30066 NASA-IN-U-4/14 C17 No-Cn the solubilities and rates of solution of gases in liquid methane C27 N68-Analysis of integrated charged particle energy spectra from gridded electrostatic c27 N68-30077 analyzers NASA-TN-D-4718 c25 N68-30093 Dilution-jet mixing study for gas-turbine combustors NASA-TN-D-4695 c01 N68-30128 Cold-air investigation of effects of partial admission on performance of 3.75-inch mean-diameter single stage axial-flow turbine NASA-TN-D-4700 c03 N68-30241 Tensile properties of tantalum and tungsten 10-fiber bundles at 1000 deg F /812 K/ NASA-TN-D-4725 c17 N68-30504 Effect of a variable stator area on performance of a single-stage turbine suitable for air cooling. 2 - Stator detailed losses with 130 percent design area NASA-TM-X-1635 c03 N68-30506 Characteristics of a space-power nuclear reactor with considerations for venting or containing qaseous fission products NASA-TN-D-4700 c03 N68-30241 containing gaseous fission products NASA-TM-X-1631 c22 N68-30516 NASA-IM-X-1631 Effect of chamber pressure, flow per element, and contraction ratio on acoustic-mode instability in hydrogen-oxygen rockets NASA-TN-D-4733 C33 N68-NASA-TN-D-4733 Low-energy electron diffraction study of oxygen adsorption on molybdenum /111/ surface NACA-TN-D-4735 c06 N68-30582 c33 N68-30518 NASA-TN-D-4735 c06 N68-Some interactions of polycrystalline tungsten electrodes with cesium plasmas NASA-TN-D-4745 c25 N68-30593 Measurement of the transmissivity of a carbon-particle-seeded nitrogen jet Polymer-film coating of magnesium for paraboloidal minant paraboloidal mirrors NASA-TN-D-4734 c18 N68-30597 Water condensation effects of heated vitiated air on flow in a large supersonic wind tunnel NASA-TM-X-1636 cll N68-30 c11 N68-30598 NASA-IM-X-1636 Cli N Performance of a wind tunnel model of an aerodynamically positioned variable flap ejector at Mach numbers from 0 to 2.0 NASA-TM-X-1639 C28 N c28 N68-30599 M-1 injector development - Philosophy and implementation implementation NASA-TN-D-4730 c28 N68-3 Superplasticity in tungsten-rhenium alloys NASA-TN-D-4728 c17 N68-3 Neutronic calculations of fuel and poison drum control of refractory-metal, fast-spectrum, space power reactors NASA-TN-D-4709 c22 N68-3 c28 N68-30604 c17 N68-30605 c22 N68-30750 Preliminary analysis of a titanium alloy honeycomb solar absorber having blackened walls NASA-TN-D-4727 c03 N68-30751 Shape of a magnetically balanced arc NASA-TN-D-4736 c25 N68-30784 Turbojet and turbofan cycle considerations and engine configurations for application in lightweight aircraft NASA-TM-X-1624 c28 N6 c28 N68-31476 Experimental measurements of thermal radiation properties by cyclic incident radiation NASA-TM-X-1618 c33 N68-3: wnon-im-X-1618 c33 N68-31498 Stress-strain behavior of cold-welded copper-copper microjunctions in vacuum as determined from electrical resistance measurements measurements NASA-TN-D-4743 c17 Emitter and collector sheaths for cesium thermionic diodes with polycrystalline c17 N68-31517 tungsten electrodes NASA-TN-D-4744 c25 N68-31640 A servocontroller for programming sample vaporization in direct current arc spectrochemical analysis
 - NASA-TN-D-4769 c06 N68-31948

Modified vibration transducer calibration system which directly yields a plot of sensitivity versus frequency NASA-TN-D-4760 c14 | c14 N68-31958 Noncavitating and cavitating performance of two low-area-ratio water jet pumps with throat lengths of 5.66 diameters NASA-TN-D-4759 c12 N68-31960 An efficient method for computation of character tables of finite groups NASA-TN-D-4763 c19 N68-31961 A trajectory code for maximizing the payload of multistage launch vehicles NASA-TN-D-4729 c30 N68-31989 Analog computer simulation of a dc arc emission spectrometer control system to define requirements for optimum control NASA-TN-D-4770 c08 N68-32055 Anomalous diffusion in a plasma formed from the exhaust beam of an electron-bombardment ion thruster NASA-TN-D-4758 c25 N68-32072 Conformal mapping for steady two-dimensional solidification on a cold surface in flowing liquid NASA-TN-D-4771 c33 N68-32073 Tests of a single tube-in-shell water-boiling heat exchanger with a helical-wire insert and several inlet flow-stabilizing devices NASA-TN-D-4767 c33 N68-32099 Electron-bombardment filament designs for heating cylindrical thermionic converters NASA-TM-X-1630 c Extrusion of 1/2 and 3/8-inch-diameter thin-wall tungsten tubing in lengths c22 N68-32968 near 10 feet NASA-TM-X-1638 c15 N68-32977 Comparison of experimental and predicted heat transfer characteristics for a cylindrical ejector NASA-TM-X-1641 c33 N68-32988 Collisionless sheaths between field-modified emitters and thermally ionized plasmas exemplified by cesium NASA-TN-D-4376 c25 N68 c25_N68-33021 Effect of film processing on cryogenic properties of poly/ethylene terephthalate/ NASA-TN-D-4762 c18 N68 c18 N68-33034 Liquid drops - Numerical and asymptotic solutions of their shapes NASA-TN~D-4779 cl; c12 N68-33165 Analytical investigation of thermal degradation of high-performance multilayer insulation in the vicinity of a penetration NASA-TN-D-4778 c33 N68-33167 Effect of residual stress on fracture strength of AISI 301 stainless-steel and Ti-5A1-2.5Sn ELI titanium cracked thin wall cylinders NASA-TN-D-4777 c32 Influence of chemisorbed films of various c32 N68-33191 gases on adhesion and friction of tungsten in vacuum NASA-TN-D-4694 c15 N68-33227 Investigation of electron-radiation-induced dielectric breakdowns in a typical capacitor meteoroid detector system NASA-TN-D-4738 c14 N68-33277 Influence of chemisorbed films on adhesion and friction of clean iron c17 N68-33278 NASA-TN-D-4775 Atlas-Centaur flight performance for Surveyor mission B NASA-TM-X-1616 c31 N68-33332 Experimental investigation of the dynamic response of a supersonic inlet to external and internal disturbances NASA-TM-X-1648 c01 N68-33374 Laminarization of a turbulent boundary layer as observed from heat-transfer and boundary layer measurements in conical nozzles NASA-TN-D-4788 cl2 N68-Successful restart of a cryogenic upper-stage c12 N68-33642 vehicle after coasting in earth orbit NASA-TM-X-1649 c3 NASA-TM-X-1649 c31 N68-33683 Refractory metal fiber nickel base alloy composites for use at high temperatures NASA-TN-D-4787 c17 c17 N68-33684 Load relief autopilot analysis to minimize

CORPORATE SOURCE INDEX

launch vehicle peak thrust vector deflection requirements NASA-TN-D-4786 c21 NG Measurement of the B 10/n, alpha/Li 7, Li 7* relative cross sections in the keV c21 N68-33756 region c24 N68-33763 NASA-TN-D-4783 Preliminary study of a thermionic reactor core composed of short-length externally fueled diodes c22 N68-34087 NASA-TN-D-4805 Analysis of boiling on a fin NASA-TN-D-4797 c33 N68-34088 Effects of boundary layer buildup in shock tubes upon chemical rate measurements c12 N68-34089 NASA-TN-D-4795 Adsorption-desorption behavior of homogeneous and heterogeneous metal surfaces NASA-TN-D-4789 c24 N68-34175 Effect of amount of electrolyte, drain rate and electrode geometry on performance of copper oxide-magnesium thermal cells NASA-TN-D-4790 c03 NG c03 N68-34234 Ultrasonic detection and measurement of fatigue cracks in notched specimens NASA-TN-D-4782 c32 N68-35071 Performance and stability characteristics of nitrogen tetroxide-hydrazine combustors NASA-TN-D-4776 c27 c27 N68-35072 Comparison of small water-graphite nuclear rocket stages with chemical upper stages for unmanned missions NASA-TN-D-4827 c22 N68-35073 Analytical and experimental investigation of outflow residuals in interconnected spherical tanks NASA-TN-D-4828 c12 N68-35104 Use of an electronic visualization technique in the study of gas journal bearing behavior NASA-TM-X-1609 c14 N68-35105 Liquid reorientation in spheres by means of low-G accelerations NASA-TM-X-1659 c12 N68-35114 Ultrasonic attenuation in superconducting tantalum NASA-TN-D-4806 c26 N68-35356 Performance evaluation of Atlas-Centaur restart capability in earth orbit NASA-TM-X-1647 c31 N6 Thermal radiative and electrical properties c31 N68-35357 of a cadmium sulfide solar cell at low solar intensities and temperatures NASA-TN-D-4818 c03 N68-35467 An integrating sphere spectroradiometer for solar simulator measurements NASA-TN-D-4822 c14 N68-35534 NASA-TM-J24022 Effect of variable stator area on performance of a single-stage turbine suitable for air cooling. 3 - Turbine performance with 130-percent design stator area NASA-TM-X-1663 CO3 N68c03 N68-35536 Study of plasma diagnostics using laser interferometry with emphasis on its application to cesium plasmas c16 N68-35593 NASA-TM-X-1652 Effect of a simulated wing on the pressure-drag coefficients of various 15 deg boattails at Mach numbers from 0.56 to 1.00 NASA-TM-X-1662 c01 N68-35672 Static performance of an auxiliary inlet ejector nozzle for supersonic-cruise aircraft NASA-TM-X-1653 c28 N68-35 c28 N68-35764 Liquid vapor interface configurations in toroidal tanks during weightlessness NASA-TN-D-4819 c12 N68-35823 A small combination sensing probe for measurement of temperature, pressure, and flow direction NASA-TN-D-4816 c14 N68-36021 High power kinetics of a two dimensional circulating liquid metal fuel reactor NASA-TN-D-4840 c22 c22 N68-36055 Comparative study of fuselage tanks for liquid methane fueled supersonic aircraft NASA-TN-D-4837 c02 N68-36074 600 deg F with fluorocarbon, polyphenyl ether, and synthetic paraffinic base

lubricants c15 N68-36075 NASA-TN-D-4850 Cavitation damage of stainless steel, nickel, and an aluminum alloy in water for ASTM round robin tests NASA-TM-X-1670 c17 N68-36076 Incompressibly lubricated Rayleigh step journal bearing. 1 - Zero-order perturbation solution NASA-TN-D-4839 c15 N68-36098 NASA-TM-X-1657 Performance of a collapsible plug nozzle having either two-position cylindrical or variable angle floating shrouds at Mach numbers from 0 to 2.0 NASA-TM-X-1657 col NG c01 N68-36132 Effect of model forebody shape on perforated tunnel wall interference NASA-TM-X-1656 c01 N68-36133 Blockage effects of cone-cylinder bodies on perforated wind tunnel wall interference NASA-TM-X-1655 c01 N6 c01 N68-36134 Centaur launch vehicle propellant utilization system NASA-TN-D-4848 c28 N68-36507 NAA-TM-24-040 C20 NOO-D Preliminary tests of a single-axis ammonia-resistojet attitude control system NASA-TM-X-1677 C28 N68-3 Effect of thrust per element on combustion stability characteristics of hydrogen oxygen c28 N68-36512 rocket engines NASA-TN-D-4851 c28 N68-36515 Iterated commutators and functions of operators NASA-TN-D-4857 c19 N68-36525 Electromagnetic compatibility verification for the Centaur and Surveyor space vehicles NASA-TM-X-1673 c31 N68c31 N68-36971 Prediction of windage power loss in alternators NASA-TN-D-4849 c03 N68-37162 Very high burnup vapor transport fuel pin concept for long life nuclear reactors NASA-TN-D-4860 c22 N68-37209 Critical speed analysis of rigid rotors on flexible foundations NASA-TN-D-4858 c15 N68-37214 Length of winding on a torus in two ideal models NASA-TM-X-1674 c03 N68-37217 Analysis of electromagnetic waves on a a dislectric rod immersed in a plasma including a discussion of diagnostic applications NASA-TN-D-4866 c25 N68-37237 The role of chemical reactions in the mechanism of comminution of ductile metals into ultrafine powders by grinding NASA-TN-D-4862 c15 N68-37239 The excitation spectrum for a Bose gas with repulsive and attractive interactions NASA-TN-D-4838 c24 N64 c24 N68-37240 Design and preliminary operation of the Lewis magnetohydrodynamic generator facility NASA-TN-D-4867 cll N68-3 c11 N68-37259 Gamma heating in thin heavy-element absorbers NASA-TM-X-1680 c22 N68-Experimental performance of a 5-inch /13 cm/ axial-flow turbine over a range of Reynolds c22 N68-37260 number c03 N68-37263 NASA-TM-X-1679 Effect of variable stator area on performance of a single stage turbine suitable for air cooling, 4 - Stator overall performance with 70 percent design area NASA-TM-X-1675 c28 N68 c28 N68-37264 Effects of freezing on primary silver oxide zinc cells NASA-TM-X-1681 c03 N68-37265 Effect of turbulent mixing on average fuel temperatures in a gas-core nuclear rocket engine NASA-TN-D-4882 c22 N68-37927 NASH-IN-J-4062 Comparison between cemented and soldered cover glass for silicon solar cells NASA-TM-X-1687 Wind tunnel investigation of airframe c03 N68-37935 installation effects on underwing engine nacelles at Mach numbers from 0.56 to 1.46 NASA-TM-X-1683 c02 N68-37941 Experimental longitudinal dynamics of an

empty Stub D Atlas vehicle NASA-TM-X-1682 c31 N68-37942 Experimental performance of a 5-inch single-stage axial-flow turbine designed for a Brayton cycle space power system NASA-TM-X-1666 c03 N68-Electrical stress analysis of a microthruster c03 N68-37943 power conditioner NASA-TM-X-1686 c09 N68-37944 NASA-TM-X-1686 c09 N6 NATIONAL AERONAUTICS AND SPACE ADMINISTRATION. MANNED SPACECRAFT CENTER, HOUSTON, TEX. An evaluation of the thermally radiant environs of a man on the lunar surface NASA-TN-D-4243 Aerodynamic stability characteristics of the Apollo Launch Escape Vehicle /LEV/ with Apolio Launch Escape venicle /LEv/ with canard surfaces deployed NASA-TN-D-4280 col N6 general analytical method for artificial-satellite lifetime determination NASA-TN-D-4281 c30 N6 c01 N68-11640 c30 N68-11754 Gemini summary conference NASA-SP-138 c30 N68-14941 A computer program for calculating model planetary atmospheres NASA-TN-D-4292 c30 N68-15793 Summary of Gemini extravehicular activity NASA-SP-149 c30 c30 N68-15891 Subcritical cryogenic storage development and flight test NASA-TN-D-4293 c23 N68-15950 Lunar module pilot control considerations NASA-TN-D-4131 c21 c21 N68-16836 Review of NASA-MSC electroencephalogram and electrocardiogram electrode systems including application techniques NASA-TN-D-4398 c04 N68-21383 Navigation and guidance analysis of a Mars probe launched from a manned flyby spacecraft NASA-TN-D-4512 c21 N68-21 c21 N68-21754 Chemically induced ignition in aircraft and spacecraft electrical circuitry by glycol/water solutions NASA-TN-D-4327 c31 N68-22213 Static longitudinal aerodynamic characteristics of several configurations used in the development of the Little Joe 2-Apollo test vehicle at Mach numbers from 0.056 to 4.65 NASA-TN-D-4439 c3 Analysis of three-fluid, crossflow heat c31 N68-22953 exchangers NASA-TR-R-284 c33 N68-23513 The distribution and properties of a weighted sum of chi squares NASA-TN-D-4575 c19 N68-24565 Flammable and toxic materials in the oxygen atmosphere of manned spacecraft NASA-TN-D-3415 c05 N68-24756 An integrated-circuit direct-coupled amplifier for spacecraft use NASA-TN-D-4584 c07 N68-24845 Hydra 1 data display system NASA-TN-D-4554 c08 N68-25002 Transient thermodynamic analysis of a fuel-cell system NASA-TN-D-4601 c03 N68-25304 Navigation and guidance systems performance for three typical manned interplanetary missions NASA-TN-D-4629 c21 N68-28236 Use of planetary oblateness for parking-orbit alinement NASA-TN-D-4657 c30 N68-28408 Cryogenic storage systems for earth-orbital and Mars-flyby missions NASA-TN-D-4619 c03 N68-28420 Mars landing mission mode comparison NASA-TM-X-1629 c30 N68-29988 quasi-steady state analysis of the dynamic behavior of a conic body moving in a nonuniform wake NASA-TN-D-4691 c31 N68-30032

NACH-IN-D-4631 Some laboratory techniques of wave analysis with application to the Apollo program NASA-TM-X-1599 CO8 N68-30240 Aerodynamic stability characteristics of the Apollo command module NASA-TN-D-4688 CO1 N68-31445

I-191

Experimental verification of scale factors for parawing opening characteristics NASA-TN-D-4665 c02 N68-31956 NASA-TN-D-4665 c02 NG First U.S. manned six-pass orbital mission /Mercury-Atlas 8, spacecraft 16/ NASA-TN-D-4807 c31 NG NATIONAL AERONAUTICS AND SPACE ADMINISTRATION. MANNED SPACECRAFT CENTER, LANGLEY STATION, VA. On the prediction of the vibratory behavior of free-free truncated conical shells NASA-TN-D-4772 c32 NG NATIONAL AERONAUTICS AND SPACE ADMINISTRATION. c31 N68-35022 c32 N68-33057 NATIONAL AERONAUTICS AND SPACE ADMINISTRATION. MARSHALL SPACE FLIGHT CENTER, HUNTSVILLE, ALA. The Runge-Kutta equations by quadrature methods NASA-TR-R-275 c19 N68-10121 The computation of the partial volumes of the components in solution NASA-TN-D-4199 c06 N68-11621 Nonlinear heat transfer and temperature distribution through fins and electric filaments of arbitrary geometry with temperature-dependent properties and heat generation NASA-TN-D-4257 c33 N68-14052 Development of a general formula expanding the higher-order derivatives of the function tanh z in powers of tanh z and A-numbers NASA-TN-D-4296 c19 M c19 N68-14077 Automation in Saturn 1 first stage checkout NASA-TN-D-4328 c31 N68-15570 Visual simulation facility for evaluation of lunar surface roving vehicles NASA-TN-D-4276 cll N68-An analysis of energetic space radiation and c11 N68-15858 dose rates NASA-TN-D-4404 c29 N68-16837 Lattice structures in solutions NASA-TN-D-4297 c06 N68-18219 Shaping of precipitation-hardening stainless steels by casting and powder-metallurgy NASA-SP-5086 c15 N68-19307 Surface treatments for precipitation-hardening stainless steels NASA-SP-5090 c15 N68-19343 Adhesive bonding of stainless steels including precipitation-hardening stainless steels NASA-SP-5085 c15 N68-20056 NASA-SP-5085 Scalar and component wind correlations between altitude levels for Cape Kennedy, Florida, and Santa Monica, California NASA-TN-D-3815 C13 N6 c13 N68-20278 Thermal and mechanical treatment for precipitation-hardening stainless steels c15 N68-20433 NASA-SP-5089 Multi-step Runge-Kutta methods NASA-TN-D-4400 c19 N68-21100 Machining and grinding of ultrahigh-strength steels and stainless steel alloys NASA-SP-5084 c15 N68c15 N68-21241 Welding of precipitation-hardening stainless NASA-SP-5087 c15 N68-21429 Calculations of non-diffuse infrared radiation from the lunar surface incident onto a unit element above the surface NASA-TM-X-1567 c29 N6 c29 N68-21731 Deformation processing of precipitationhardening stainless steels NASA-SP-5088 c17 N68-21917 Analytical and experimental study of dynamic characteristics of turbopumps NASA-TN-D-4298 c0 c01 N68-21950 Motion of an artificial satellite under combined influence of planar and Keplerian force fields NASA-TN-D-4622 c30 N68-28113 Flat conductor cable technology NASA-SP-5043 c09 N68-28879 Free vibration of a rotating beam-connected space station NASA-TN-D-4753 c3: Classical fifth-, sixth-, seventh-, and c32 N68-33225 eighth-order Runge-Kutta formulas with stepsize control NASA-TR-R-287 c19 N68-36753

CORPORATE SOURCE INDEX

NATIONAL AERONAUTICS AND SPACE ADMINISTRATION, WASHINGTON, D. C. NASA Thesaurus - Subject terms for indexing NASA Inesaurus - Subject terms for indexing scientific and technical information. Volume 1 - Alphabetical listing A-L NASA-SP-7030, V. 1 c34 N68-11 NASA Thesaurus - Subject terms for indexing scientific and technical information. Volume 2 - Alphabetical c34 N68-11307 Induction volume information. volume listing M-Z NASA-SP-7030, V. 2 C34 Noc --NASA Thesaurus - Subject terms for indexing scientific and technical information. Volume 3 - Appendixes Vasa-SP-7030, V. 3 C34 N68-113 C30 N68-114 c34 N68-11308 c34 N68-11309 c30 N68-11456 Aerospace Medicine and Biology - A continuing bibliography with indexes NASA-SP-7011/43/ c c04 N68-14671 Aerospace Medicine and Biology - A continuing bibliography with indexes NASA-SP-7011/42/ c Scientific satellites c04 N68-14725 NASA-SP-133 c31 N68-14965 Problems of space biology. Volume 5 -Dynamics of the cerebral blood volume under normal conditions and gravitational stresses NASA-TT-F-492 c04 N68-15477 Significant achievements in space science 1966 NASA-SP-155 Aerospace Medicine and Biology - A continuing bibliography with indexes c30 N68-15748 NASA-SP-7011/44/ c0 Third annual NASA University Conference c04 N68-15899 on Manual Control NASA-SP-144 Space applications 1966 c05 N68-15901 NASA-SP-156 c31 N68-16015 Motion of conducting bodies in a magnetic field NASA-TT-F-460 c25 N68-16286 Aerospace medicine and biology Continuing bibliography with indexes, during December 1967 NASA-SP-7011/45/ c04 N68-16517 Magnetobrems /synchrotron/ emission and reabsorption NASA-TT-F-521 c25 N68-16700 Studies in physical gas dynamics NASA-TT-F-505 c12 N68-16839 Calculation of the turbulent boundary layer and of transition on a plane plate NASA-TT-F-520 c12 N6 c12 N68-17563 Surveyor 5 Preliminary report NASA-SP-163 c31 N68-17844 Teleoperators and human augmentation. An AEC-NASA technology survey NASA-SP-5047 c05 N68-18870 Potential applications of satellite geodetic techniques to geosciences NASA-SP-158 c13 N68-18902 Constructing inexpensive automatic picture-transmission ground stations NASA-SP-5079 c07 N68-19624 Aerospace medicine and biology - A continuing bibliography with indexes NASA-SP-7011/47/ c04 N68-20026 Aerospace medicine and biology - A continuing bibliography with indexes NASA-SP-7011/48/ c04 N68c04 N68-20027 An introduction to the assurance of human performance in space systems NASA-SP-6506 c05 N68-20357 Sonic boom research NASA-SP-147 c02 N68-21413 Surveyor 6. A preliminary report NASA-SP-166 c31 N68-21443 NASA-SP-160 Col No6-21443 Directional distribution in the reflection of heat radiation and its effect on heat transfer NASA-TT-F-497 c33 N68-21536 Physics of planets NASA-TT-F-515 c30 N68-21802 Management. A continuing literature survey, with indexes 1962 - 1967 with indexes, 1962 - 1967 NASA-SP-7500 c34 N68-21828 Aerospace medicine and biology - A cumulative index NASA-SP-7011/46/ c04 N68-22194

CORPORATE SOURCE INDEX

Russian rocketry, a historical survey NASA-TT-F-426 c31 N68-22262 Recent advances in display media NASA-SP-159 C09 N68 Method of brazing aluminum to stainless steel for high-stress-fatigue applications c09 N68-22302 NASA-SP-5040 c15 N68-22778 NASA-SF-2040 C15 NGG-Aerospace Medicine and Biology. A continuing bibliography with indexes NASA-SP-7011/49/ c04 N68-Helicopters - Calculation and design. Volume 2 - Vibrations and dynamic stability c04 N68-22882 volume 2 - vibrations and dynamic stability NASA-TT-F-519 co2 N68 Management - A continuing literature survey, with indexes, 1962-1967 NASA-SP-7500/02/ c34 N68 Cumulative index to NASA Tech Briefs, c02 N68-23456 c34 N68-24567 1963-1967 NASA-SP-5021/06/ c34 N68-: Aerospace medicine and biology - A continuing c34 N68-25221 bibliography with indexes NASA-SP-7011/50/ Protection against space radiation c04 N68-25844 c29 N68-26128 NASA-SP-169 Bioregenerative systems NASA-SP-165 c04 N68-26207 The zodiacal light and the interplanetary medium NASA-SP-150 c30 N68-27475 Aerospace Medicine and Biology - A continuing bibliography with indexes, May 1968 NASA-SP-7011/51/ c04 N68-28246 NASA-SP-7011/51/ c04 Communications satellites. A continuing bibliography with indexes NASA-SP-7004/04/ c31 NASA scientific and technical reports for 1967. A selected listing NASA-SP-7029 c34 The pole of the untituing c31 N68-28379 c34 N68-29039 The role of the vestibular organs in space exploration NASA-SP-152 c04 N68-29128 Lasers and masers A continuing bibliography with indexes, Apr. - Dec. 1967 NASA-SP-7009/03/ c16 N68 c16 N68-29438 High energy propellants - A continuing bibliography with indexes NASA-SP-7002/04/ c: c27 N68-30313 Venture into space - Early years of Goddard Space Flight Center NASA-SP-4301 c11 N68-30317 Planetary atmospheres Continuing bibliography with indexes, Jun. 1966 -Dec. 1967 NASA-SP-7017/02/ c30 N68-30601 NASA-SP-7017/02/ C30 NBS-Lubrication, corrosion and wear. A continuing bibliography with indexes NASA-SP-7020/02/ c15 N68-Effects of low temperatures on the mechanical properties of structural metals NASA-SP-5012/01/ c17 N68c15 N68-31522 c17 N68-31605 Visual information display systems. A survey c08 N68-32159 NASA-SP-5049 Lunar surface studies Continuing bibliography with indexes NASA-SP-7003/04/ c Aerospace Medicine and Biology A continuing bibliography with indexes NASA-SP-7011/52/ c c30 N68-32631 c04 N68-32707 Bibliographies on aerospace science A continuing bibliography with indexes NASA-SP-7006/03/ c34 c34 N68-32769 Aerospace electronic systems technology NASA-SP-154 c3 c30 N68-33169 Numerical analysis - Abstracts of presentations NASA-SP-170 c19 N68-33245 Surveyor 7 Preliminary report NASA-SP-173 c31 N68-33553 Exploring space with a camera NASA-SP-168 c30 N68-34870 Second conference on sonic boom research NASA-SP-180 c02 c02 N68-34907 Aerospace Medicine and Biology - A continuing bibliography with indexes NASA-SP-7011/53/ c c04 N68-35069 On the computation of solar elevation angles and the determination of sunrise and sunset

times

c13 N68-35179

NASA-TM-X-1646

A study of NASA University programs NASA-SP-185 c34 N68-35564 NASA contributions to development of special-purpose thermocouples. A survey NASA-SP-5050 c14 N c14 N68-35620 NASA space vehicle design criteria /environment/. Models of Mars atmosphere /1967/ NASA-SP-8010 c30 N68-37220 Aerospace medicine and biology - A continuing bibliography with indexes NASA-SP-7011/54/ c04 N68-3 NATIONAL BUREAU OF STANDARDS, BOULDER, COLO. Superconduction thin films NASA-CP-1190 -25 MCC c04 N68-38051 NASA-CR-1189 c26 N68-35178 NATIONAL METEOROLOGICAL CENTER, SUITLAND, MD. On the computation of solar elevation angles and the determination of sunrise and sunset times NASA-TM-X-1646 c: NATIONAL RESEARCH CORP., CAMBRIDGE, MASS. Study of density calibration in space c13 N68-35179 Final report, Jun. 29, 1966 - Jan. 16, 1967 NASA-CR-987 cl c14 N68-12669 Study of new methods to measure low pressur NASA-CR-1120 c14 N6 c14 N68-33022 NASA-CH-1120 NEW YORK UNIV., N. Y. Guantum mechanical study of molecules transition probabilities, Einstein A coefficients and oscillator strengths of some band systems of diatomic molecules NASA-CR-975 c24 N68-11037 Quantum mechanical study of molecules Eigenvalues and eigenvectors of real symmetric matrices Symmetric matrices NASA-CR-983 NIELSEN ENGINEERING AND RESEARCH, INC., PALO ALTO, CALIF. Investigation of methods for predicting the aerodynamic characteristics of two-lobed c24 N68-11903 aerodynamic characteristics of two-looed parawings NASA-CR-1166 c01 N68-NORTH AMERICAN AVIATION, INC., COLUMBUS, OHIO. Infrared radiometric stress instrumentation application range study NASA-CR-1067 c32 N68-NORTH AMERICAN AVIATION, INC., DOWNEY, CALIF. Influence of structure and material research on advanced launch systems* weight, nerformance. and cost Summary report, May c01 N68-33765 c32 N68-24971 Performance, and cost Summary report, May 25, 1965 - Jun. 30, 1967 NASA-CR-974 c31 N68 c31 N68-11520 Guidance, flight mechanics and trajectory optimization. Volume 3 - The two-body problem NASA-CR-1002 c30 N68-14089 optimization. Volume 4 - The calculus of variations and modern applications NASA-CR-1003 c30 N68-15193 NASA-CR-1003 C30 N68-Guidance, flight mechanics and trajectory optimization. Volume 6 - The N-body problem and special perturbation techniques NASA-CR-1005 C30 N68-Guidance, flight mechanics and trajectory optimization. Volume 1 - Coordinate systems and time measure NASA-CR-1000 C30 N68-Guidance, flight mechanics and trajectory c30 N68-15741 c30 N68-16103 Guidance, flight mechanics and trajectory optimization. Volume 11 - Guidance equations for orbital operations Guidance, flight mechanics and trajectory optimization. Volume 12 - Relative motion, guidance equations for terminal rendezvous NASA-CR-1011 c30 N68c30 N68-17215 c30 N68-19186 Guidance, flight mechanics and trajectory optimization. Volume 13 - Numerical optimization methods NASA-CR-1012 c30 N68-1 Guidance, flight mechanics and trajectory optimization. Volume 2 - Observation theory c30 N68-19315 and sensors NASA-CR-1001 c30 N68-19676 Ouidance, flight mechanics and trajectory optimization. Volume 14 - Entry guidance equations NÁSA-CR-1013 c30 N68-19985

NORTH AMERICAN AVIATION, INC., LOS ANGELES,

Guidance, flight mechanics and trajectory optimization. Volume 7 - The Pontryagin maximum principle NASA-CR-1006 c30 N Guidance, flight mechanics and trajectory optimization. Volume 8 - Boost guidance c30 N68-20084 equations NASA-CR-1007 c30 N68-20449 Guidance, flight mechanics and trajectory optimization. Volume 9 - General perturbations theory NASA-CR-1008 c30 | Guidance, flight mechanics and trajectory optimization. Volume 16 - Mission c30 N68-20450 constraints and trajectory interfaces NASA-CR-1015 c3 c30 N68-20468 Guidance, flight mechanics and trajectory optimization. Volume 10 - Dynamic programming NASA-CR-1009 c30 N68-21077 Guidance, flight mechanics and trajectory optimization. Volume 15 - Application of optimization techniques NASA-CR-1014 c30 N68-21231 Guidance, flight mechanics and trajectory optimization. Volume 17 - Guidance system performance analysis NASA-CR-1016 c30 N68-21442 Guidance, flight mechanics and trajectory optimization. Volume 5 - State determination and/or estimation NASA-CR-1004 c30 N68-21685 Earthquake prediction from laser surveying NASA-SP-5042 c13 N68-23706 Shell analysis manual NASA-CR-912 c32 N68-24802 NORTH AMERICAN AVIATION, INC., LOS ANGELES, CALIF. Propulsion system dynamic simulation theory and equations NASA-CR-928 c11 N68-19273 NORTH AMERICAN ROCKWELL CORP., ANAHEIM, CALIF. NURIN AMERICAN ROCKWELL CORP., ANAMEIM, CALIF. Study of spaceborne multiprocessing, phase 2. Volume 1 - Summary NASA-CR-1158 c08 N68-NORTH AMERICAN ROCKWELL CORP., DOWNEY, CALIF. Influence of structure and material research on advanced launch systems weight, performance, and cost. Phase 3 - Design synthesis of recoverable launch vehicle structures c08 N68-31499 structures NASA-CR-1116 c32 N68-28335 Study of technology requirements for atmosphere braking to orbit about Mars and Venus. Volume 1 - Summary, January -October 1967 NASA-CR-1131 c30 N68 c30 N68-34086 NORTH AMERICAN ROCKWELL CORP., LOS ANGELES, CALIF. Analysis of performance characteristics in ground effect of a large scale V/STOL multi-fan-in-wing transport model NASA-CR-1180 c28 N c28 N68-35594 NORTH CAROLINA STATE COLL., RALEIGH. Modal density of thin circular cylinders NASA-CR-897 c32 c32 N68-11967 Noise reduction shape factors in the low frequency range NASA-CR-1155 c32 NORTHERN RESEARCH AND ENGINEERING CORP., c32 N68-33266 CAMBRIDGE, MASS. Analysis of geometry and design point performance of axial flow turbines. 1 -Development of the analysis method and the loss coefficient correlation NASA-CR-1181 c28 N68-35101 NASA-CK-1181 Analysis of geometry and design point performance of axial flow turbines, Part 2 - Computer program NASA-CR-1187 c28 N68-36617 NORTHROP CORP., HAWTHORNE, CALIF. A study of an electric field measuring instrument NASA-CR-970 c14 N68-25903 Genetic states of simulated lunar rocks NASA-CR-1081 c30 N68-26689 Full-scale ground proximity investigation of a VTOL fighter model aircraft NASA-CR-1098 c02 N68-28 c02 N68-28233

CORPORATE SOURCE INDEX

Study on a technique for detecting photons in the 100-1000 angstrom wavelength region Final report, 15 Apr. 1965 - 15 Oct. 1967 NASA-CR-1096 c24 N68-28250 NORTON RESEARCH CORP., CAMBRIDGE, MASS. Mechanism of the atmospheric interaction with the fatigue of metals NASA-CR-1165 c17 N68-35200

0

OHIO STATE UNIV., COLUMBUS.	
The TEM radiation pattern of a thin-walled	
parallel-plate waveguide analyzed by a	
surface integration technique	
NASA-CR-1052 c07 N68	-22746
Input admittance and reflection coefficient	of
a circular aperture in a ground plane cove	red
by a homogeneous dielectric or plasma slat	J
NASA-CR-1177 c25 N68	-35171
The reflection coefficient of a TEM mode	
parallel-plate waveguide illuminating a	
conducting sheet - The large wedge angle o	ase
NASA-CR-1174 c07 N68	-35172

Ρ

PENNSYLVANIA STATE UNIV., UNIVERSITY PA	₹K•	
Differential systems		
NASA-CR-1164	c19	N68-33426
PHILCO CORP., HOUSTON, TEX.		
Computer assisted instruction. Feas	[61]]	ty
study		
NASA-CR-917		N68-13897
PHYSICS INTERNATIONAL CO., SAN LEANDRO,	CALI	(F.
Explosive hypervelocity launchers		
NASA-CR-982	c11	N68-15777
PITTSBURGH UNIV., PA.		
Lyapunov stability for partial diffe		
equations. Part 1 - Lyapunov stab		
theory and the stability of solution		
partial differential equations. Partial		
Contraction groups and equivalent		
NASA-CR-1100		N68-27457
PLANNING RESEARCH CORP., WASHINGTON, D.		
Introduction to the derivation of mi		
requirements profiles for system e		
NASA-SP-6503		N68-15683
PRATT AND WHITNEY AIRCRAFT, EAST HARTFO	RD.,	
Research and development of high-per	forma	ince
axial-flow turbomachinery. Volume		
Design of turbine-compressor		
NASA-CR-800	c03	N68-24596
Research and development of high		
performance axial-flow turbomaching	ery.	
Volume 2 - Désign of gas bearings		
NASA-CR-801	c15	N68-25042
Vapor chamber fin studies. Operatin	g	
characteristics of fin models		
NASA-CR-1139	c33	N68-33203
PRATT AND WHITNEY AIRCRAFT, PHILADELPHI	A, P/	۹.
Research and development of high-per		ance
axial-flow turbomachinery. Volume	3 -	
Design of backup gas bearings		
NASA-CR-802	c03	N68-24597
PRINCETON UNIV., N. J.		
A method of calculating compressible		
turbulent boundary layers		
NASA-CR-1144	c12	N68-35096

R

 RADIO CORP. OF AMERICA, PRINCETON, N. J.

 MOS field-effect-transistor technology

 NASA-CR-1113
 c08 N68-35193

 RENSSELAER POLYTECHNIC INST., TROY, N. Y.

 Frequency coded threshold logic unit for pattern recognition application

 NASA-CR-1035
 c05 N68-22448

 RESEARCH SYSTEMS, INC., LEXINGTON, MASS.

 A study of trace contaminant identification by microwave double resonance spectroscopy

 NASA-CR-967
 c24 N68-11634

 RESEARCH TRIANGLE INST., DURHAM, N. C.

 A study of charge storage in silicon oxide resulting from non-penetrating electron irradiation

 NASA-CR-1088
 c26 N68_26603

CORPORATE SOURCE INDEX

Semiconductor piezojunc	tion transducers
NASA-CR-1089	c26 N68-26627
Practical reliability.	Volume 1 - Parameter
variations analysis	Toruno 2 Toruno tor
NASA-CR-1126	c15 N68-31478
Practical reliability.	Volume 4 -
Prediction	
NASA-CR-1129	c15 N68-31979
Practical reliability.	Volume 5 - Parts
NASA-CR-1130	c15 N68-31980
Practical reliability.	Volume 2 -
Computation	
NASA-CR-1127	c15 N68-32760
Practical reliability.	
NASA-CR-1128	c15 N68-32779
An investigation of this	n film oxygen partial
pressure sensors	
NASA-CR-1182	c14 N68-35149
RICE UNIV., HOUSTON, TEX.	011 100 00140
	• • • • • • • • • • • • • • • • • • •
Conical bodies of given	
having maximum lift-t	o-drag ratio at
hypersonic speeds. V	ariational methods
NASA-CR-1156	c01 N68-33451

S

SANDIA CORP., ALBUQUERQUE, N. MEX. Contamination control principles
NASA-SP-5045 c11 N68-10384 Santa Barbara Research Center, Goleta, Calif.
Dual radiometer assembly for Project Scanner
NASA-CR-1086 c14 N68-28965 SCIENTIFIC TRANSLATION SERVICE, LA CANADA,
CALIF.
Computations of elastic tensometric elements NASA-TT-F-513 c32 N68-15796
Scattering of light in a turbid medium
NASA-TT-F-477 c13 N68-22462 The orgin and initial development of life
NASA-TT-F-488 c04 N68-24272
SERENDIPITY ASSOCIATES, CHATSWORTH, CALIF. A descriptive model for determining optimal
human performance in systems, volume 4 Final
summary report NASA-CR-879
A descriptive model for determining optimal
human performance in systems, volume 1 NASA-CR~876
A descriptive model for determining optimal
human performance in systems. Volume 2 – Part A – System development activities
concerned with putting man in an aerospace
system. Part B – Development of man- machine systems – Some concepts and
guidelines
NASA-CR-877, V. 2 c05 N68-15120
A descriptive model for determining optimal human performance in systems. Volume 3 -
An approach for determining the optimal role
of man and allocation of functions in an aerospace system
NASA-CR-878 c05 N68-19165
SOUTHAMPTON UNIV. /ENGLAND/. The response of a simply supported plate to
transient forces. Part 2 - The effect of
N-waves at oblique incidence NASA-CR-1176 c32 N68-33168
The response of a simply supported plate to
transient forces. Part 1 - The effect of N-waves at normal incidence
NASA-CR-1175 c32 N68-33737
Helicopter noise – A blade slap. Part 1 – Review and theoretical study
NASA-CR-1221 c02 N68-37932
SOUTHERN RESEARCH INST., BIRMINGHAM, ALA. An investigation of the mechanisms of heat
transfer in low-density phenolic-nylon chars
NASA-CR-966 c18 N68-11978 SOUTHWEST RESEARCH INST., SAN ANTONIO, TEX.
Flow-induced vibrations of a flat plate suspended in a narrow channel Final report
suspended in a narrow channel Final report NASA-CR-1186 c12 N68-35086
SPACE SCIENCES, INC., WALTHAM, MASS.
Plasma boundary interactions - 2 NASA-CR-1072 c25 N68-25821
ST. LOUIS UNIV., MO.
Subsolar-meridian mean annual distributions for Martian troposphere below 50 kilometers
NASA-CR-1043 c30 N68-19192

I-195

c30 N68-22860 C30 STANFORD RESEARCH INST., MENLO PARK, CALIF. Implosively accelerated shock tube driver NASA-CR-950 c12 c12 N68-10646 Ricrowave technique development for advanced radio astronomy and radiometry missions NASA-CR-979 c09 N68-13617 NACH-CR-975 Study and applications of retrodirective and self adaptive electromagnetic-wave phase controls to a Mars probe NASA-CR-977 c21 c21 N68-18484 NASA-CR-977 C21 N Design of guidance and control systems for optimum utilization of information NASA-CR-997 C10 N c10 N68-23438 Cryogenic magnetometer development report, 1 Jul. 1964 - 7 Mar. 1967 NASA-CR-1073 Final c14 N68-26703 preliminary study of the awakening and startle effects of simulated sonic booms NASA-CR-1193 c04 N c04 N68-33005 The effects of a plasma in the near-zone field of an antenna, 2 NASA-CR-1149 c07 N68-33042 Relative annoyance and loudness judgements of various simulated sonic boom waveforms NASA-CR-1192 c04 N68c04 N68-35103 Research study of a fundus tracker for experiments in stabilized vision NASA-CR-1121 CO5 NG STEVENS INST. OF TECH., HOBOKEN, N. J. A laboratory scale model technique for investigating pneumatic tire hydroplaning c05 N68-35109 NASA-CR-1074 c11 N68-23357 Hydrodynamics of aircraft tire hydroplaning NASA-CR-1125 cl: Sylvania electric products. Inc.. Mountain c12 N68-31593 VIEW, CALIF. VIEW, CALIF.
 Study of vibration measurement by laser methods
 NASA-CR-985
 c16 N68-144
 SYRACUSE UNIV. RESEARCH INST., N. Y.
 Plane stress analysis of an edge-stiffened rectangular plate, taking into account bending and shear stiffness of the stiffeners NASA-CR-978
 C32 N68-193
 SYSTEMS TECHNOLOGY, INC., HAWTHORNE, CALIF.
 Pilot dynamic response to sudden flight control system failures and implications for design c16 N68-14070 c32 N68-19311 design NASA-CR-1087 c05 N68-26690 An experimental investigation of compensatory and pursuit tracking displays with rate and acceleration control dynamics and a disturbance input NASA-CR-1082 c07 N68 A study of fully manual and augmented manual c07 N68-28272 control systems for the Saturn 5 booster using analytical pilot models NASA-CR-1079 c31 Ni SYSTEMS TECHNOLOGY, INC., PRINCETON, N. J. New methods in adaptive flight control c31 N68-28426 NASA-CR-1152 c21 N68-33904 T -

TECHTRAN CORP., GLEN BURNTE, MD.	
A descriptive model for determining optimal	
human performance in systems, volume 1	
NASA-CR-876 c05 N68	-14262
TELEDYNE INDUSTRIES, INC., GARLAND, TEX.	
Seismic effects of sonic booms	
NASA-CR-1137 c13 N68	-35151
TENNESSEE UNIV., TULLAHOMA.	
Mie-scattering function	
NASA-CR-1022 c24 N68	-21227
Radiation heat transfer in absorbing,	
scattering, and emitting medium	
NASA-CR-1023 c33 N68	-22318
Application of negative feedback to	
reduction of glow discharge noise	
NASA-CR-1173 c16 N68	-35099
THERM ADVANCED RESEARCH, INC., ITHACA, N. Y.	
Inviscid flow field induced by a rotor in	
ground effect	
NASA-CR-1027 c01 N68	-22475

TRACOR, INC., ROCKVILLE, MD.

TRACOR, INC., ROCKVILLE, MD.
An analytical study of the measured wall pressure field under supersonic turbulent boundary layers
NASA-CR-888
CLEVELAND, OHIO.
Generation of long time creep data of refractory alloys at elevated temperatures
NASA-CR-1115
C17 N68-29992
TRW SYSTEMS GROUP, REDONDO BEACH, CALIF.
Mathematical problems of modeling stochastic nonlinear dynamic systems
NASA-CR-1168
C19 N68-35472
TRW SYSTEMS, CLEVELAND, OHIO.
Analytical predictions of delivered specific impulse
NASA-CR-1123
C27 N68-32793
TRW SYSTEMS, REDONDO BEACH, CALIF.
Particle acceleration by evaporation pressure NASA-CR-927
C16 N68-10467

U

UNITED AIRCRAFT CORP., EAST HARTFORD, CONN. Experimental investigation of flow patterns in radial-outflow vortexes using a rotating-peripheral-wall water vortex tube NASA-CR-991 c22 N68-16478 Exploratory flow and containment experiments in a directed-wall-jet vortex tube with radial outflow and moderate superimposed axial flows Fifth interim summary technical report, Sep. 15, 1965 - May 30, 1967 NASA-CR-992 c22 N68-17 c22 N68-17131 Containment experiments in vortex tubes with radial outflow and large superimposed axial flows NASA-CR-993 c22 N68-18243 Optical absorption in fused silica during TRIGA reactor pulse irradiation NASA-CR-1031 c22 N68-21124 Studies of specific nuclear light bulb and open-cycle vortex stabilized gaseous nuclear rocket engines NASA-CR-1030 c22 N68-22038 Experimental investigation of radial-inflow vortexes in jet-injection and rotating peripheral-wall water vortex tubes NASA-CR-1028 c22 N68-22088 Experimental investigation of containment in constant-temperature radial-inflow vortexes c12 N68-22200 NASA-CR-1029 Optical absorption in transparent materials following high-temperature reactor irradiation NASA-CR-1032 c22 N68-23481 Optical absorption and fluorescence in fused silica during TRIGA pulse irradiation NASA-CR-1191 c22 N68-35826 Experimental study of multi-component coaxial-flow jets in short chambers NASA-CR-1190 c22 N68-36615 NASA-CK-1190 c22 N68-36615 UNITED AIRCRAFT CORP., FARMINGTON, CONN. A study of the critical computational problems associated with strandown factor associated with strapdown inertial navigation systems NASA-CR-968 c21 NG UTAH UNIV., SALT LAKE CITY. Entry length for the rocket meteorological radiation shield NASA-CR-1200 c14 NG c21 N68-21652 c14 N68-36530

V

VIRGINIA POLYTECHNIC INST., BLACKSBURG. Time-optimal rendezvous for elliptic orbits NASA-CR-1036 VIRGINIA UNIV., CHARLOTTESVILLE. An annular lithium-drifted germanium detector for studying nuclear reaction gamma-rays NASA-CR-1138 c14 N68-35152

W

WASHINGTON UNIV., SEATTLE. The effect of the converging flow field of a tandem test section on longitudinal stability measurements NASA-CR-1198 c11 N68-36522

CORPORATE SOURCE INDEX

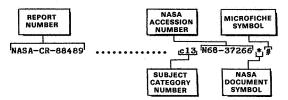
WEBB ASSOCIATES, YELLOW SPRINGS, OHIO.The principle of the space activity suitNASA-CR-973c05 N68-11510Automatic control of water cooling in spacesuitsc05 N68-26701WESTINGHOUSE ELECTRIC CORP., BALTIMORE, MD.Digital program for dynamics of non-rigidgravity gradient satellitesNASA-CR-119c30 N68-32744WESTINGHOUSE ELECTRIC CORP., LIMA, OHIO.Properties of magnetic materials for usein high-temperature space power systemsNASA-SP-3043c17 N68-17624WISCONSIN UNIV., MADISON.Ultraviolet dayglow and stellar brightnessmeasurement from the X-15 aircraftNASA-CR-1017c30 N68-19590WOLF RESEARCH AND DEVELOPMENT CORP.,WEST CONCORD, MASS.Data display programmingNASA-CR-107c08 N68-37254

REPORT/ACCESSION NUMBER INDEX

NASA SCIENTIFIC AND TECHNICAL REPORTS FOR 1968

A Selected Listing

Typical Report/Accession Number Index Listing



Listings in this index are arranged alphanumerically by report number. The subject category number indicates the subject category in the abstract section in which the citation is located. The NASA accession number denotes the number by which the citation is identified within the subject category. An asterisk (*) indicates that the item is a NASA report. A pound sign (#) indicates that the item is available on microfiche.

•	
ARA-327-5	c32 N68-11282*#
ARA-327-6	c32 N68-11191*#
ARC-R-276	c18 N68-35100*#
ARC-R-282	c31 N68-37900*#
ARC-R-202	COT NO0-01004#
ASTM-STP-431	c15 N68-21226*#
BSR-2022	17 100 00000
BSR-2022	c13 N68-25579*#
C6-1476.22/33, V. 1	c08 N68-31499*#
C6-1476.22/33. V. 2	c08 N68-35560*#
00-14/0.22/JJg V. C	COO WOO-33300+#
CAL-RM-1788-P-17	c20 N68-25816*#
D2-100752-4. V. 4	c31 N68-31477*#
D2-100753-2, V. 2	c30 N68-15725*#
P2-100753-4, V. 3	c31 N68-29995*#
D2-100754-1, V. 1	c31 N68-26814*#
D2-100754-2. V. 2	c30 N68-28275*#
D2-100754-4, V. 4	c31 N68-28997*#
D2-100755-1, V. 1	c31 N68-28891*#
D2-100755-2, V. 2	c31 N68-28202*#
D2-100755-4, V. 4	c31 N68-30631*#
D2-113204-1	c31 N68-33008*#
D2-114116-1	c34 N68-26813*#
D8-0375, V. 3	c02 N68-35177*#
D8-0375, V. 3 D8-0907A	c02 N68-35177*#
D8-0375, V. 3	c02 N68-35177*#
D8-0375, V. 3 D8-0907A	c02 N68-35177*# c05 N68-33009*#
D8-0375, V. 3 D8-0907A DAC-60874	c02 N68-35177*# c05 N68-33009*# c12 N68-23482*#
D8-0375, V. 3 D8-0907A	c02 N68-35177*# c05 N68-33009*#
D8-0375, V. 3 D8-0907A DAC-60074 DCC65SD526	c02 N68-35177*# c05 N68-33009*# c12 N68-23482*#
D8-0375, V. 3 D8-0907A DAC-60074 DCC65SD526	c02 N68-35177*# c05 N68-33009*# c12 N68-23482*# c18 N68-22391*#
D8-0375, V. 3 D8-0907A DAC-60874 D0C658D526	c02 N68-35177*# c05 N68-33009*# c12 N68-23482*#
D8-0375, V. 3 D8-0907A DAC-60874 DOC65SD526 DP/NASA/-1130	c02 N68-35177*# c05 N68-33009*# c12 N68-23482*# c18 N68-22391*# c17 N68-33019*#
D8-0375, V. 3 D8-0907A DAC-60874 D0C65SD526 DP/NASA/-1130 E-4213	c02 N68-35177*# c05 N68-33009*# c12 N68-23482*# c18 N68-22391*# c17 N68-33019*# c01 N68-30128*#
D8-0375, V. 3 D8-0907A DAC-60874 DOC65SD526 DP/NASA/-1130 E-4213 E-4324	c02 N68-35177*# c05 N68-33009*# c12 N68-23482*# c18 N68-22391*# c17 N68-33019*#
D8-0375, V. 3 D8-0907A DAC-60874 D0C65SD526 DP/NASA/-1130 E-4213	c02 N68-35177*# c05 N68-33009*# c12 N68-23482*# c18 N68-22391*# c17 N68-33019*# c01 N68-30128*# c27 N68-30077*#
D8-0375, V. 3 D8-0907A DAC-60874 DOC65SD526 DP/NASA/-1130 E-4213 E-4324 E-4324 E-4337	c02 N68-35177*# c05 N68-33009*# c12 N68-23482*# c18 N68-22391*# c17 N68-33019*# c01 N68-30128*# c27 N68-30077*# c17 N68-30065*#
D8-0375, V. 3 D8-0907A DAC-60874 DGC65SD526 DP/NASA/-1130 E-4213 E-4324 E-4324 E-4337 E-4386	C02 N68-35177*# C05 N68-33009*# C12 N68-23482*# C18 N68-22391*# C17 N68-33019*# C01 N68-30128*# C27 N68-30077*# C17 N68-30065*# C17 N68-30066*#
D8-0375, V. 3 D8-0907A DAC-60874 DOC65SD526 DP/NASA/-1130 E-4213 E-4324 E-4324 E-4337	c02 N68-35177*# c05 N68-33009*# c12 N68-23482*# c18 N68-22391*# c17 N68-33019*# c01 N68-30128*# c27 N68-30077*# c17 N68-30065*#
D8-0375, V. 3 D8-0907A DAC-60874 DOC65SD526 DP/NASA/-1130 E-4213 E-4324 E-4337 E-4386 E-4386 E-4407	C02 N68-35177*# C05 N68-33009*# C12 N68-23482*# C18 N68-22391*# C17 N68-33019*# C01 N68-30128*# C27 N68-30077*# C17 N68-30065*# C17 N68-30066*#
D8-0375, V. 3 D8-0907A DAC-60874 DOC65SD526 DP/NASA/-1130 E-4213 E-4324 E-4337 E-4386 E-4386 E-4407	C02 N68-35177*# C05 N68-33009*# C12 N68-23482*# C18 N68-22391*# C17 N68-33019*# C01 N68-30128*# C27 N68-30077*# C17 N68-30065*# C17 N68-30066*#
D8-0375, V. 3 D8-0907A DAC-60874 DGC65SD526 DP/NASA/-1130 E-4213 E-4324 E-4324 E-4337 E-4386	c02 N68-35177*# c05 N68-33009*# c12 N68-23482*# c18 N68-22391*# c17 N68-33019*# c01 N68-30128*# c27 N68-30077*# c17 N68-30065*# c17 N68-30066*# c03 N68-30241*#
D8-0375, V. 3 D8-0907A DAC-60874 DOC65SD526 DP/NASA/-1130 E-4213 E-4324 E-4337 E-4386 E-4407 EDR-4909, V. 2	c02 N68-35177*# c05 N68-33009*# c12 N68-23482*# c18 N68-22391*# c17 N68-33019*# c01 N68-30128*# c27 N68-30065*# c17 N68-30065*# c17 N68-30066*# c13 N68-30241*# c28 N68-32987*#
D8-0375, V. 3 D8-0907A DAC-60874 DOC65SD526 DP/NASA/-1130 E-4213 E-4324 E-4337 E-4386 E-4407 EDR-4909, V. 2 F-910091-10	c02 N68-35177*# c05 N68-33009*# c12 N68-23482*# c18 N68-22391*# c17 N68-33019*# c01 N68-30128*# c27 N68-30065*# c17 N68-30065*# c03 N68-30241*# c28 N68-32987*# c22 N68-16478*#
D8-0375, V. 3 D8-0907A DAC-60874 DGC65SD526 DP/NASA/-1130 E-4213 E-4324 E-4324 E-4337 E-4386 E-4407 EDR-4909, V. 2 F-910091-10 F-910091-11	c02 N68-35177*# c05 N68-33009*# c12 N68-23482*# c18 N68-22391*# c17 N68-33019*# c01 N68-30128*# c27 N68-30065*# c17 N68-30065*# c17 N68-30066*# c13 N68-30241*# c28 N68-32987*#
D8-0375, V. 3 D8-0907A DAC-60874 DOC65SD526 DP/NASA/-1130 E-4213 E-4324 E-4337 E-4386 E-4407 EDR-4909, V. 2 F-910091-10	c02 N68-35177*# c05 N68-33009*# c12 N68-23482*# c18 N68-22391*# c17 N68-33019*# c01 N68-30128*# c27 N68-30128*# c17 N68-30065*# c17 N68-30065*# c03 N68-30241*# c28 N68-32987*# c22 N68-16478*#
D8-0375, V. 3 D8-0907A DAC-60074 D0C65SD526 DP/NASA/-1130 E-4213 E-4324 E-4337 E-4337 E-436 E-4407 EDR-4909, V. 2 F-910091-10 F-910091-11 F-910091-12	C02 N68-35177*# C05 N68-33009*# C12 N68-23482*# C18 N68-22391*# C17 N68-3019*# C01 N68-30128*# C27 N68-30065*# C17 N68-30065*# C17 N68-30066*# C13 N68-30241*# C28 N68-32987*# C22 N68-16478*# C22 N68-18243*#
D8-0375, V. 3 D8-0907A DAC-60874 D0C65SD526 DP/NASA/-1130 E-4213 E-4324 E-4337 E-4337 E-4386 E-4407 EDR-4909, V. 2 F-910091-10 F-910091-11 F-910091-12 F-910091-14	c02 N68-35177*# c05 N68-33009*# c12 N68-23482*# c18 N68-22391*# c17 N68-33019*# c01 N68-30128*# c27 N68-30077*# c17 N68-30065*# c17 N68-30066*# c03 N68-32987*# c28 N68-32987*# c22 N68-16478*# c22 N68-17131*# c22 N68-17131*# c22 N68-22088*#
D8-0375, V. 3 D8-0907A DAC-60874 D0C65SD526 DP/NASA/-1130 E-4213 E-4324 E-4337 E-4337 E-436 E-4407 EDR-4909, V. 2 F-910091-10 F-910091-11 F-910091-14 F-910091-14 F-910091-15 F-910091-15	C02 N68-35177*# C05 N68-33009*# C12 N68-23482*# C18 N68-2391*# C17 N68-33019*# C01 N68-300128*# C01 N68-30065*# C17 N68-30066*# C17 N68-30066*# C17 N68-30241*# C28 N68-32987*# C22 N68-16478*# C22 N68-16478*# C22 N68-1243*# C22 N68-1243*# C22 N68-22200*#
D8-0375, V. 3 D8-0907A DAC-60874 D0C65SD526 DP/NASA/-1130 E-4213 E-4324 E-4337 E-4337 E-4386 E-4407 EDR-4909, V. 2 F-910091-10 F-910091-11 F-910091-12 F-910091-14	c02 N68-35177*# c05 N68-33009*# c12 N68-23482*# c18 N68-22391*# c17 N68-33019*# c01 N68-30128*# c27 N68-30077*# c17 N68-30065*# c17 N68-30066*# c03 N68-32987*# c28 N68-32987*# c22 N68-16478*# c22 N68-17131*# c22 N68-17131*# c22 N68-22088*#
D8-0375, V. 3 D8-0907A DAC-60874 D0C65SD526 DP/NASA/-1130 E-4213 E-4324 E-4337 E-4337 E-436 E-4407 EDR-4909, V. 2 F-910091-10 F-910091-11 F-910091-14 F-910091-14 F-910091-15 F-910091-15	C02 N68-35177*# C05 N68-33009*# C12 N68-23482*# C18 N68-2391*# C17 N68-33019*# C01 N68-300128*# C01 N68-30065*# C17 N68-30066*# C17 N68-30066*# C17 N68-30241*# C28 N68-32987*# C22 N68-16478*# C22 N68-16478*# C22 N68-1243*# C22 N68-1243*# C22 N68-22200*#

F-910485-2	c22	N68-23481*#
G-910091-16 G-910485-3		N68-36615*# N68-35826*#
GCA-TR-67-2-N		N68-18118*# N68-17329*#
GD/C-BTD-67-023, V. 11 GD/C-BTD-67-029	c32 c32	N68-11133*# N68-18825*#
GD/C-BTD-67-031 GD/C-BTD-67-045	c32 c32	N68-10233*# N68-11485*#
GD/C-BTD-67-049 GD/C-BTD-67-053	c32 c32	N68-10574*# N68-10280*#
GD/C-BTD-67-056 GD/C-BTD-67-057, V. 8	c32 c32	N68-18769*# N68-11089*#
GD/C-BTD-67-089, V. 14	c32	N68-23454*#
GD/C-BTD-67-112, V. 13 GD/C-BTD-67-120	c32 c32	N68-23452*# N68-23453*#
• • • • • • • • • • • • •	002	100 20400.#
GDC-DBE67-001	c31	N68-20467*#
GDC-DDF65-001 GDC-DDF65-003, V. 3		N68-10231*# N68-10568*#
L-5774		N68-30244*#
LAC-4-17-67-1, V. 2	c.32	N68-23451*#
LEC/HASD-671-40-019	c14	N68-16838 * #
LR-20922	c04	N68-35103*#
ME-1065-678	c32	N68-19311*#
NA-67-384	c11	N68-19273*#
NASA-CR-670/01/	c02	N68-11174*#
NASA-CR-743/1/	c02	N68-35177*#
NASA-CR-764	c07 c03	N68-28135*# N68-24596*#
NASA-CR-801	c15	N68-25042*#
NASA-CR-802	c03	N68-24597*#
NASA-CR-863	c07 c05	N68-27063*#
NASA-CR-876 NASA-CR-877, V. 2	c05	N68-14262*# N68-15120*#
NASA-CR-878	c05	N68-19165*#
NASA-CR-879	c05	N68-10381*#
NASA-CR-888 NASA-CR-897	c12 c32	N68-22087*# N68-11967*#
NASA-CR-909	c32	N68-14584*#
NASA-CR-911	c15	N68-10503*#
NASA-CR-912	c32	N68-24802*#
NASA-CR-913NASA-CR-914	c02 c09	N68-10047*# N68-10420*#
NASA-CR-915	c31	N68-14638*#
NASA-CR-916	c13	N68-10283*#
NASA-CR-917	c08	N68-13897*#
NASA-CR-920	c05 c33	N68-10648*# N68-15833*#
NASA-CR-922	c03	N68-16439*#
NASA-CR-923	c03	N68-17075*#
NASA-CR-924, V. 3		N68-18044*#
NASA-CR-925	c03	N68-16351*#
	c03 c05	N68-16351*# N68-15306*#
NASA-CR-925 NASA-CR-926 NASA-CR-927 NASA-CR-928	c03 c05 c16 c11	N68-16351*# N68-15306*# N68-10467*# N68-19273*#
NASA-CR-925 NASA-CR-926 NASA-CR-927 NASA-CR-927 NASA-CR-928 NASA-CR-930	c03 c05 c16 c11 c17	N68-16351*# N68-15306*# N68-10467*# N68-19273*# N68-17591*#
NASA-CR-925 NASA-CR-926 NASA-CR-927 NASA-CR-928 NASA-CR-930 NASA-CR-933	c03 c05 c16 c11 c17 c12	N68-16351*# N68-15306*# N68-10467*# N68-19273*# N68-17591*# N68-10499*#
NASA-CR-925 NASA-CR-926 NASA-CR-927 NASA-CR-927 NASA-CR-928 NASA-CR-930	c03 c05 c16 c11 c17 c12 c32	N68-16351*# N68-15306*# N68-10467*# N68-19273*# N68-17591*#
NASA-CR-925 NASA-CR-926 NASA-CR-926 NASA-CR-927 NASA-CR-928 NASA-CR-930 NASA-CR-933 NASA-CR-935 NASA-CR-935 NASA-CR-937	c03 c05 c16 c11 c17 c12 c32 c32 c32	N68-16351*# N68-15306*# N68-19273*# N68-19273*# N68-1929*# N68-10499*# N68-10231*# N68-10280*# N68-10568*#
NASA-CR-925 NASA-CR-926 NASA-CR-926 NASA-CR-928 NASA-CR-930 NASA-CR-933 NASA-CR-935 NASA-CR-936	c03 c05 c16 c11 c17 c12 c32 c32	N68-16351*# N68-15306*# N68-10467*# N68-19273*# N68-19273*# N68-10231*# N68-10231*# N68-10280*# N68-10568*# N68-10574*#

NASA-CR-940		c32 N68-11054*#	NASA-CR-1029		c12 N68-22200*#
NASA-CR-941		c32 N68-18769*#	NASA-CR-1030		c22 N68-22038*#
NASA-CR-942	*********	c32 N68-11089*#	NASA-CR-1031		c22 N68-21124*# c22 N68-23481*#
NASA-CR-943 NASA-CR-944		c32 N68-10233*# c32 N68-18825*#	NASA-CR-1032 NASA-CR-1033		c22 N68-23481*# c03 N68-23476*#
NASA-CR-945		c32 N68-11133*#	NASA-CR-1034		c13 N68-25579*#
NASA-CR-946	• • • • • • • • • • • • • • • • • • • •	c31 N68-24945*#	NASA-CR-1035		c05 N68-22448*#
NASA-CR-947 NASA-CR-948		c32 N68-23452*# c32 N68-23454*#	NASA-CR-1036 NASA-CR-1037		c30 N68-22202*# c29 N68-22849*#
NASA-CR-940		c32 N68-23454*# c32 N68-23453*#	NASA-CR-1037		c32 N68-23399*#
NASA-CR-950		c12 N68-10646*#	NASA-CR-1039		c24 N68-21949*#
NASA-CR-951	• • • • • • • • • • • • • • • • • • • •	c23 N68-10674*#	NASA-CR-1040	******	c30 N68-21864*# c18 N68-22391*#
NASA-CR-952 NASA-CR-953		c15 N68-20389*# c22 N68-10561*#	NASA-CR-1041 NASA-CR-1042		c18 N68-22391*# c05 N68-21859*#
NASA-CR-954		c32 N68-11489*#	NASA-CR-1043		c30 N68-19192*#
NASA-CR-955		c19 N68-11109*#	NASA-CR-1044		c30 N68-22860*#
NASA-CR-956 NASA-CR-957		c12 N68-13619*# c12 N68-15571*#	NASA-CR-1045 NASA-CR-1046		c13 N68-23436*# c19 N68-25841*#
NASA-CR-958		c12 N68-15530*#	NASA-CR-1047		c27 N68-21893*#
NASA-CR-959		c12 N68-16897*#	NASA-CR-1048	******	c03 N68-22842*#
NASA-CR-960	••••••	c12 N68-13612*#	NASA-CR-1049		c32 N68-24481*# c32 N68-23451*#
NASA-CR-961 NASA-CR-962		c12 N68-12892*# c08 N68-18144*#	NASA-CR-1050 NASA-CR-1051		c32 N68-23355*#
NASA-CR-963		c32 N68-11282*#	NASA-CR-1052		c07 N68-22746*#
NASA-CR-964		c32 N68-11191*#	NASA-CR-1053		c02 N68-26930*#
NASA-CR-965 NASA-CR-966		c03 N68-16321*# c18 N68-11978*#	NASA-CR-1054 NASA-CR-1055	* * * * * * * * * * * * * * * * * * * *	c31 N68-26814*# c11 N68-24966*#
NASA-CR-967		c24 N68-11634*#	NASA-CR-1056		c28 N68-26771*#
NASA-CR-968		c21 N68-21652*#	NASA-CR-1057	•••••	c07 N68-26621*#
NASA-CR-969		c30 N68-20353*#	NASA-CR-1058		c15 N68-22810*# c33 N68-25244*#
NASA-CR-970 NASA-CR-971		c14 N68-25903*# c05 N68-20339*#	NASA-CR-1060 NASA-CR-1061		c33 N68-26692*#
NASA-CR-972		c04 N68-11968*#	NASA-CR-1062		c33 N68-26641*#
NASA-CR-973		c05 N68-11510*#	NASA-CR-1063		c33 N68-26815*#
NASA-CR-974 NASA-CR-975		c31 N68-11520*# c24 N68-11037*#	NASA-CR-1064 NASA-CR-1065		c33 N68-26816*# c33 N68-26817*#
NASA-CR-977		c21 N68-18484*#	NASA-CR-1066		c12 N68-23482*#
NASA-CR-978	•••••	c32 N68-19311*#	NASA-CR-1067		c32 N68-24971*#
NASA-CR-979		c09 N68-13617*#	NASA-CR-1068		c34 N68-26813*# c31 N68-24738*#
NASA-CR-980 NASA-CR-981	• • • • • • • • • • • • • • • • • • • •	c14 N68-16838*# c17 N68-11522*#	NASA-CR-1069 NASA-CR-1070		c30 N68-25902*#
NASA-CR-982		c11 N68-15777*#	NASA-CR-1071		c20 N68-25816*#
NASA-CR-983		c24 N68-11903*#	NASA-CR-1072		c25 N68-25821*#
NASA-CR-984 NASA-CR-985		c30 N68-15725*# c16 N68-14070*#	NASA-CR-1073 NASA-CR-1074		c14 N68-26703*# c11 N68-23357*#
NASA-CR-986		c02 N68-13517*#	NASA-CR-1075		c14 N68-25316*#
NASA-CR-987	••••	c14 N68-12669*#	NASA-CR-1076		c02 N68-26691*#
NASA-CR-988 NASA-CR-989	••••••	c23 N68-13115*# c25 N68-14078*#	NASA-CR-1077 NASA-CR-1078		c17 N68-25318*# c02 N68-25817*#
NASA-CR-999		c04 N68-12494*#	NASA-CR-1079		c31 N68-28426*#
NASA-CR-991		c22 N68-16478*#	NASA-CR-1080		c26 N68-25972*#
NASA-CR-992	*****	$c_{22} N68 - 17131 * #$	NASA-CR-1081 NASA-CR-1082	********************	c30 N68-26689*# c07 N68-28272*#
NASA-CR-993 NASA-CR-994		c22 N68-18243*# c09 N68-15892*#	NASA-CR-1082		c05 N68-28319*#
NASA-CR-995		c18 N68-18849*#	NASA-CR-1084		c30 N68-26702*#
NASA-CR-996	•••••••••••••••••••••••••	c32 N68-15476*#	NASA-CR-1085		c05 N68-26701*#
NASA-CR-997 Nasa-CR-998		c10 N68-23438*# c24 N68-18118*#	NASA-CR-1086 NASA-CR-1087		c14 N68-28965*# c05 N68-26690*#
NASA-CR-999		c10 N68-19229*#	NASA-CR-1088		c26 N68-26603*#
NASA-CR-1000		c30 N68-16103*#	NASA-CR-1089		c26 N68-26627*#
NASA-CR-1001 NASA-CR-1002		c30 N68-19676*# c30 N68-14089*#	NASA-CR-1090 NASA-CR-1091		c30 N68-28373*# c28 N68-28112*#
NASA-CR-1002 NASA-CR-1003		c30 N68-15193*#	NASA-CR-1092		c31 N68-28997*#
NASA-CR-1004		c30 N68-21685*#	NASA-CR-1093		c30 N68-28275*#
NASA-CR-1005		c30 N68-15741*#	NASA-CR-1094 NASA-CR-1095		c31 N68-28202*# c31 N68-28891*#
NASA-CR-1006 NASA-CR-1007		c30 N68-20084*# c30 N68-20449*#	NASA-CR-1095		c24 N68-28250*#
NASA-CR-1008		c30 N68-20450*#	NASA-CR-1097		c22 N68-35153*#
NASA-CR-1009		c30 N68-21077*#	NASA-CR-1098		c02 N68-28233*#
NASA-CR-1010 NASA-CR-1011		c30 N68-17215*# c30 N68-19186*#	NASA-CR-1099 NASA-CR-1100		c10 N68-28307*# c19 N68-27457*#
NASA-CR-1012		c30 N68-19315*#	NASA-CR-1101		c04 N68-28247*#
NASA-CR-1013	•••••	c30 N68-19985*#	NASA-CR-1102		c05 N68-28833*#
NASA-CR-1014 NASA-CR-1015		c30 N68-21231*# c30 N68-20468*#	NASA-CR-1103 NASA-CR-1104		c30 N68-25895*# c04 N68-28829*#
NASA-CR-1013		c30 N68-21442*#	NASA-CR-1104	********	c04 N68-28278*#
NASA-CR-1017		c30 N68-19590*#	NASA-CR-1106		c31 N68-25577*#
NASA-CR-1018		c14 N68-17329*#	NASA-CR-1107		c08 N68-37254*# c31 N68-33008*#
NASA-CR-1019 NASA-CR-1020		c31 N68-20467*# c08 N68-17154*#	NASA-CR-1108 NASA-CR-1109		c31 N68-33008*# c31 N68-29995*#
NASA-CR-1021		c15 N68-23356*#	NASA-CR-1110		c09 N68-29525*#
NASA-CR-1022		c24 N68-21227*#	NASA-CR-1111		c09 N68-29526*#
NASA-CR-1023 NASA-CR-1024		c33 N68-22318*# c17 N68-23560*#	NASA-CR-1112 NASA-CR-1113		c05 N68-28847*# c08 N68-35193*#
NASA-CR-1025		c23 N68-21444*#	NASA-CR-1114		c18 N68-35100*#
NASA-CR-1026		c03 N68-29460*#	NASA-CR-1115		c17 N68-29992*#
NASA-CR-1027 NASA-CR-1028		c01 N68-22475*# c22 N68-22088*#	NASA-CR-1116 NASA-CR-1117		c32 N68-28335*# c05 N68-30602*#
				······································	

NASA-CR-1118	NASA-SP-148
NASA-CR-1119 c30 N68-32744*	NASA-SP-149
NASA-CR-1120 c14 N68-33022*	
NASA-CR-1121 c05 N68-35109*	
NASA-CR-1122 c05 N68-35102*	NASA-SP-154 c30 N68-33169*#
NASA-CR-1123 c27 N68-32793*	
NASA-CR-1125	
NASA-CR-1126 c15 N68-31478*	
NASA-CR-1127 c15 N68-32760*	
NASA-CR-1128 c15 N68-32779*	
NASA-CR-1129 c15 N68-31979*	NASA-SP-165
NASA-CR-1130	¥ NASA-SP-166 c31 N68-21443*#
NASA-CR-1131 c30 N68-34086*	NASA-SP-168
NASA-CR-1132	NASA-SP-169 c29 N68-26128*#
NASA-CR-1133	NASA-SP-170
NASA-CR-1136 c32 N68-32976*	NASA-SP-173
NASA-CR-1137 cl3 N68-35151*	
NASA-CR-1138	
NASA-CR-1139 c33 N68-33203*	
NASA-CR-1140	
NASA-CR-1141	
NASA-CR-1144	
NASA-CR-1145	
NASA-CR-1147 c01 N68-33043*	
NASA-CR-1148 c22 N68-29390*	
NASA-CR-1149 c07 N68-33042*	
NASA-CR-1150 c03 N68-33062*	
NASA-CR-1151 c05 N68-33304*	
NASA-CR-1152	¥ NASA-SP-5045
NASA-CR-1153	¥ NASA-SP-5047 c05 N68-18870*#
NASA-CR-1154	NASA-SP-5049
NASA-CR-1155	# NASA-SP-5050
NASA-CR-1156	
NASA-CR-1158 c08 N68-31499*	
NASA-CR-1159	
NASA-CR-1160 c32 N68-33226*	
NASA-CR-1161	
NASA-CR-1162	
NASA-CR-1165 c17 N68-35200*	
NASA-CR-1166	
NASA-CR-1167 c10 N68-33767*	
NASA-CR-1168 c19 N68-35472*	
NASA-CR-1169 c12 N68-36343*	
NASA-CR-1170 c33 N68-35248*	
NASA-CR-1171	
NASA-CR-1172 c28 N68-32987*	
NASA-CR-1173 c16 N68-35099*	
NASA-CR-1174 c07 N68-35172*	
NASA-CR-1175 c32 N68-33737*	
NASA-CR-1176 c32 N68-33168*	
NASA-CR-1177	# NASA-SP-7011/46/ c04 N68-22194*#
NASA-CR-1180 c28 N68-35594*	
NASA-CR-1181	
NASA-CR-1182	# NASA-SP-7011/49/ c04 N68-22882*#
NASA-CR-1184	
NASA-CR-1185 c09 N68-33224*	# NASA-SP-7011/51/ c04 N68-28246*#
NASA-CR-1186	
NASA-CR-1187 c28 N68-36617*	
NASA-CR-1188 c02 N68-35595*	
NASA-CR-1189	
NASA-CR-1190 c22 N68-36615*	
NASA-CR-1191 c22 N68-35826*	
NASA-CR-1192	
NASA-CR-1192	
NASA-CR-1197	
NASA-CR-1198 cl1 N68-36522*	
NASA-CR-1200	
NASA-CR-1201	
NASA-CR-1202 c01 N68-37255*	
NASA-CR-1211 c10 N68-37906*	
NASA-CR-1220 c05 N68-37819*	
NASA-CR-1221 c02 N68-37932*	
NASA-CR-1222	
	NASA-TM-X-1432 c17 N68-11912*#
NASA-SP-35, PT. 6	
NASA-SP-133	
NASA-SP-138	
NASA-SP-139	# NASA-TM-X-1461 c22 N68-10133*#
NASA-SP-139	# NASA-TM-X-1461 c22 N68-10133*# # NASA-TM-X-1463 c28 N68-22272*#
NASA-SP-139	# NASA-TM-X-1461 c22 N68-10133*# # NASA-TM-X-1463 c28 N68-22272*# # NASA-TM-X-1464 c03 N68-10103*#
NASA-SP-139	# NASA-TM-X-1461 c22 N68-10133*# # NASA-TM-X-1463 c28 N68-22272*# # NASA-TM-X-1464 c03 N68-10103*#

NASA-TM-X-1466	****************	c22 N68-10134*#	NASA-TM-X-1587		c22	N68-23894*#
NASA-TM-X-1468		c17 N68-10051*#	NASA-TM-X-1589		c31	N68-26645*#
NASA-TM-X-1469	*****************	c02 N68-11147*#	NASA-TM-X-1590			N68-24757*#
NASA-TM-X-1473		c28 N68-10496*#	NASA-TM-X-1591			N68-23895*#
NASA-TM-X-1477	* * * * * * * * * * * * * * * * * * * *	c02 N68-11772*#	NASA-TM-X-1592			N68-24141*#
NASA-TM-X-1479	*****************	c14 N68-11867*#	NASA-TM-X-1594	*****************		N68-24618*#
NASA-TM-X-1480	****************	c03 N68-11920*#	NASA-TM-X-1595			N68-26644*#
NASA-TM-X-1481	*****************	c25 N68-11404*#	NASA-TM-X-1596	*********		N68-25818*#
NASA-TM-X-1482		c12 N68-19225*#	NASA-TM-X-1597			N68-25819*#
NASA-TM-X-1483	***************	c21 N68-11949*#	NASA-TM-X-1598		c19	N68-28240*#
NASA-TM-X-1484	******************	c31 N68-11919*#	NASA-TM-X-1599			N68-30240*#
NASA-TM-X-1487	••••	c01 N68-11958*#	NASA-TM-X-1600	******		
NASA-TM-X-1488 NASA-TM-X-1489	*******	c14 N68-13974*#	NASA-TM-X-1601 NASA-TM-X-1603		c01	N68-33836*#
NASA-TM-X-1409		c05 N68-13999*# c22 N68-17022*#	NASA-TM-X-1604	********	c32 c27	N68-28238*# N68-28155*#
NASA-TM-X-1490		c01 N68-16480*#	NASA-TM-X-1605	* * * * * * * * * * * * * * * * * * * *	c33	N68-28156*#
NASA-TM-X-1495		c09 N68-15649*#	NASA-TM-X-1606			N68-28806*#
NASA-TM-X-1496		c22 N68-16056*#	NASA-TM-X-1607			N68-28869*#
NASA-TM-X-1497		c22 N68-15643*#	NASA-TM-X-1608		c32	N68-28330*#
NASA-TM-X-1498		c01 N68-16299*#	NASA-TM-X-1609			N68-35105*#
NASA-TM-X-1499		c31 N68-13797*#	NASA-TM-X-1613			N68-30501*#
NASA-TM-X-1500		c31 N68-14092*#	NASA-TM-X-1614		c22	N68-29950*#
NASA-TM-X-1501		c22 N68-14585*#	NASA-TM-X-1615		c03	N68-28870*#
NASA-TM-X-1502		c01 N68-14747*#	NASA-TM-X-1616		c31	N68-33332*#
NASA-TM-X-1503	***************	c11 N68-16695*#	NASA-TM-X-1617		c17	N68-30065*#
NASA-TM-X-1506		c11 N68-14115*#	NASA-TM-X-1618		c33	N68-31498*#
NASA-TM-X-1507		c28 N68-17028*#	NASA-TM-X-1619	*****		N68-29953*#
NASA-TM-X-1508		c30 N68-19622*#	NASA-TM-X-1620			N68-29952*#
NASA-TM-X-1509	••••	c22 N68-15855*#	NASA-TM-X-1621		c01	N68-30030*#
NASA-TM-X-1510	**********	c33 N68-16300*#	NASA-TM-X-1622	•••••		N68-30033*#
NASA-TM-X-1511		c28 N68-15644*#	NASA-TM-X-1623	*********		N68-29993*#
NASA-TM-X-1512	• • • • • • • • • • • • • • • • • • • •	c22 N68-20355*#	NASA-TM-X-1624		c28	N68-31476*#
NASA-TM-X-1513 NASA-TM-X-1514		c12 N68-15639*# c17 N68-19347*#	NASA-TM-X-1625	• • • • • • • • • • • • • • • • • • • •	c17 c30	N68-29987*#
NASA-TM-X-1514 NASA-TM-X-1515	*****		NASA-TM-X-1629			N68-29988*#
NASA-TM-X-1515 NASA-TM-X-1516	********************	c11 N68-18460*# c01 N68-18189*#	NASA-TM-X-1630 NASA-TM-X-1631	••••••	c22	N68-32968*#
NASA-TM-X-1517	******	c01 N68-19237*#	NASA-TM-X-1632	*********************		N68-30516*# N68-29994*#
NASA-TM-X-1518		c31 N68-17094*#	NASA-TM-X-1634		c12	N68-32982*#
NASA-TM-X-1519		c03 N68-20432*#	NASA-TM-X-1635			N68-30506*#
NASA-TM-X-1524		c14 N68-18834*#	NASA-TM-X-1636			N68-30598*#
NASA-TM-X-1525		c14 N68-19001*#	NASA-TM-X-1638		c15	N68-32977*#
NASA-TM-X-1526		c12 N68-21365*#	NASA-TM-X-1639			N68-30599*#
NASA-TM-X-1527		c02 N68-19065*#	NASA-TM-X-1640			N68-35141*#
NASA-TM-X-1528		c12 N68-19340*#	NASA-TM-X-1641		c33	N68-32988*#
NASA-TM-X-1529		c30 N68-19064*#	NASA-TM-X-1646		c13	N68-35179*#
NASA-TM-X-1530	•••••	c01 N68-19341*#	NASA-TM-X-1647		c31	N68-35357*#
NASA-TM-X-1536		c11 N68-19207*#	NASA-TM-X-1648	• • • • • • • • • • • • • • • • • • • •		N68-33374*#
NASA-TM-X-1537		c01 N68-19206*#	NASA-TM-X-1649	***************	c31	N68-33683*#
NASA-TM-X-1539		c22 N68-22022*#	NASA-TM-X-1651		c30	N68-33371*#
NASA-TM-X-1540	•••••	c15 N68-21898*#	NASA-TM-X-1652		c16	N68-35593*#
NASA-TM-X-1541 NASA-TM-X-1542		c30 N68-19330*#	NASA-TM-X-1653	***************	c28	N68-35764*#
NASA-TM-X-1542 NASA-TM-X-1543		c31 N68-21778*# c31 N68-21833*#	NASA-TM-X-1655 NASA-TM-X-1656		c01 c01	N68-36134*# N68-36133*#
NASA-TM-X-1544		c08 N68-19336*#	NASA-TM-X-1657		c01	N68-36132*#
NASA-TM-X-1546		c28 N68-20186*#	NASA-TM-X-1658		c01	N68-36193*#
NASA-TM-X-1547		c01 N68-21703*#	NASA-TM-X-1659			N68-35114*#
NASA-TM-X-1548		c33 N68-20340*#	NASA-TM-X-1660		c01	N68-35617*#
NASA-TM-X-1549		c21 N68-21366*#	NASA-TM-X-1661		c01	N68-36509*#
NASA-TM-X-1550		c01 N68-22002*#	NASA-TM-X-1662		c01	N68-35672*#
NASA-TM-X-1551		c01 N68-21940*#	NASA-TM-X-1663		c03	N68-35536*#
NASA-TM-X-1552		c32 N68-21767*#	NASA-TM-X-1664		c02	N68-37066*#
NASA-TM-X-1553	• • • • • • • • • • • • • • • • • • • •	c13 N68-21904*#	NASA-TM-X-1665		c01	N68-36112*#
NASA-TM-X-1554	• • • • • • • • • • • • • • • • • • • •	c33 N68-20338*#	NASA-TM-X-1666		c03	N68-37943*#
NASA-TM-X-1555	********	c18 N68-20329*#	NASA-TM-X-1670			N68-36076*#
NASA-TM-X-1556	******	c27 N68-21267*#	NASA-TM-X-1671			N68-37067*#
NASA-TM-X-1557		c33 N68-21704*#	NASA-TM-X-1673			N68-36971*#
NASA-TM-X-1558 NASA-TM-X-1559	•••••	c12 N68-23353*#	NASA-TM-X-1674	•••••		N68-37217*#
NASA-TM-X-1559 NASA-TM-X-1560	****************	c28 N68-19708*# c03 N68-20363*#	NASA-TM-X-1675	••••••		N68-37264*#
NASA-TM-X-1560 NASA-TM-X-1561	*********	cl7 N68-21431*#	NASA-TM-X-1677 NASA-TM-X-1679			N68-36512*# N68-37263*#
NASA-TM-X-1561	*******************	c08 N68-21499*#	NASA-TM-X-1680	*****		N68-37260*#
NASA-TM-X-1563		c22 N68-21705*#	NASA-TM-X-1681			N68-37265*#
NASA-TM-X-1565		c02 N68-21834*#	NASA-TM-X-1682			N68-37942*#
NASA-TM-X-1567		c29 N68-21731*#	NASA-TM-X-1683			N68-37941*#
NASA-TM-X-1568	*****	c22 N68-21111*#	NASA-TM-X-1686			N68-37944*#
NASA-TM-X-1569	*******	c03 N68-21562*#	NASA-TM-X-1687			N68-37935*#
NASA-TM-X-1570		c14 N68-21384*#	NASA-TM-X-55798			N68-25271*#
NASA-TM-X-1571	•••••	c28 N68-24614*#				
NASA-TM-X-1572		c01 N68-21692*#	NASA-TN-D-3415			N68-24756*#
NASA-TM-X-1573		c15 N68-23241*#	NASA-TN-D-3815			N68-20278*#
NASA-TM-X-1574		c31 N68-22742*#	NASA-TN-D-3984			N68-22019*#
NASA-TM-X-1575		c02 N68-24245*#	NASA-TN-D-3993			N68-10369*#
NASA-TM-X-1578	•••••	c11 N68-22737*#	NASA-TN-D-4078	•••••		N68-10222*#
NASA-TM-X-1579 NASA-TM-X-1581	•••••	c28 N68-23477*#	NASA-TN-D-4112			N68-10299*#
NASA-IM-X-1581 NASA-TM-X-1582	*****************	c28 N68-22725*# c12 N6d-23423*#	NASA-TN-D-4121 NASA-TN-D-4131			N68-16749*# N68-16836*#
NASA-TM-X-1582 NASA-TM-X-1584	•••••	c12 N68-23901*#	NASA-TN-D-4131			N68-17566*#
NASA-TM-X-1586	*****************	A second seco	NASA-TN-D-4149	****************		N68-11636*#
		22 20000 · #	1			

NUMBER	

NASA-TN-D-4155		c13 N68-11714*#	NASA-TN-D-4309		c25 N68-18614*#
NASA-TN-D-4169	******	c30 N68-11369*#	NASA-TN-D-4310		c17 N68-14888*#
NASA-TN-D-4174	********	c21 N68-13558*#	NASA-TN-D-4311		c29 N68-16008*#
NASA-TN-D-4179 NASA-TN-D-4180	•••••••	c02 N68-18250*#	NASA-TN-D-4312	********	c30 N68-16750*#
NASA-TN-D-4181	*****************	c07 N68-18247*# c31 N68-10192*#	NASA-TN-D-4313 NASA-TN-D-4314	********	c05 N68-16594*# c01 N68-17896*#
NASA-TN-D-4186		c14 N68-10647*#	NASA-TN-D-4315		c22 N68-18197*#
NASA-TN-D-4187	•••••	c23 N68-10354*#	NASA-TN-D-4316		c02 N68-17055*#
NASA-TN-D-4199 NASA-TN-D-4203		c06 N68-11621*#	NASA-TN-D-4317		c21 N68-14732*#
NASA-TN-D-4203	*******************	c08 N68-26640*# c17 N68-11511*#	NASA-TN-D-4318 NASA-TN-D-4319	* * * * * * * * * * * * * * * * * * * *	c17 N68-17897*# c17 N68-17377*#
NASA-TN-D-4223	*****	c22 N68-10291*#	NASA-TN-D-4320		c01 N68-17899*#
NASA-TN-D-4228		c01 N68-10060*#	NASA-TN-D-4321	***************	c32 N68-19143*#
NASA-TN-D-4229	*****	c01 N68-10093*#	NASA-TN-D-4322	******	c02 N68-15894*#
NASA-TN-D-4234 NASA-TN-D-4235		c14 N68-10057*# c17 N68-10104*#	NASA-TN-D-4323 NASA-TN-D-4324	***************	c02 N68-14903* c14 N68-14018*#
NASA-TN-D-4236		c06 N68-11512*#	NASA-TN-D-4325		c12 N68-18997*#
NASA-TN-D-4237	******	c02 N68-11519*#	NASA-TN-D-4326		c33 N68-18122*#
NASA-TN-D-4238	**************	c33 N68-10368*#	NASA-TN-D-4327	* * * * * * * * * * * * * * * * * * * *	c31 N68-22213*#
NASA-TN-D-4239 NASA-TN-D-4240	****************	c28 N68-10502*# c17 N68-10498*#	NASA-TN-D-4328 NASA-TN-D-4329	•••••	c31 N68-15570*# c02 N68-14090*
NASA-TN-D-4241	***************	c01 N68-11253*#	NASA-TN-D-4330		c02 N68-16522*#
NASA-TN-D-4242	••••••	c14 N68-15936*#	NASA-TN-D-4331	•••••	c33 N68-14270*#
NASA-TN-D-4243	*******	c30 N68-11630*#	NASA-TN-D-4332		c33 N68-14240*#
NASA-TN-D-4244 NASA-TN-D-4245	*******************	c19 N68-11494*# c01 N68-10380*#	NASA-TN-D-4333 NASA-TN-D-4334	*****************	c03 N68-14082*# c33 N68-15942*#
NASA-TN-D-4246		c21 N68-11521*#	NASA-TN-D-4335	•••••••	c06 N68-14093*#
NASA-TN-D-4247		c33 N68-11144*#	NASA-TN-D-4336		c33 N68-14042*#
NASA-TN-D-4248	********	c01 N68-10529*#	NASA-TN-D-4337	• • • • • • • • • • • • • • • • • • • •	c31 N68-16240*#
NASA-TN-D-4249 NASA-TN-D-4250	•••••	c28 N68-10562*# c33 N68-11642*#	NASA-TN-D-4338 NASA-TN-D-4339	*****	c17 N68-18145*# c14 N68-15893*#
NASA-TN-D-4250 NASA-TN-D-4251	*****************	c33 N68-11642*# c04 N68-10122*#	NASA-TN-D-4340	******************	c14 N68-15893*# c12 N68-14641*#
NASA-TN-D-4252		c01 N68-17555*#	NASA-TN-D-4341		c08 N68-15798*#
NASA-TN-D-4253	***************	c19 N68-10355*#	NASA-TN-D-4342	***************	c31 N68-18615*#
NASA-TN-D-4254 NASA-TN-D-4255	***************	c07 N68-11475*#	NASA-TN-D-4343	****************	c02 N68-17023*#
NASA-TN-D-4256	*********************	c33 N68-11811*# c24 N68-11074*#	NASA-TN-D-4344 NASA-TN-D-4346	••••••	c02 N68-15941*# c14 N68-13973*#
NASA-TN-D-4257	******	c33 N68-14052*#	NASA-TN-D-4347	* * * * * * * * * * * * * * * * * * * *	c15 N68-21226*#
NASA-TN-D-4258	•••••	c31 N68-11641*#	NASA-TN-D-4348	*****	c15 N68-15010*#
NASA-TN-D-4259 NASA-TN-D-4260		c32 N68-11355*# c30 N68-11145*#	NASA-TN-D-4349		c24 N68-18254*#
NASA-TN-D-4260 NASA-TN-D-4261	**********************	c30 N68-11145*# c02 N68-11638*#	NASA-TN-D-4350 NASA-TN-D-4352	******************	c32 N68-15769*# c22 N68-26764*#
NASA-TN-D-4262		c01 N68-11036*#	NASA-TN-D-4353		c33 N68-15742*#
NASA-TN-D-4263	••••••	c31 N68-11476*#	NASA-TN-D-4354		c14 N68-16529*#
NASA-TN-D-4264 NASA-TN-D-4265	***************	c20 N68-25617*#	NASA-TN-D-4355	•••••	c15 N68-16468*#
NASA-TN-D-4266	****************	c32 N68-12864*# c31 N68-11961*#	NASA-TN-D-4356 NASA-TN-D-4357		c05 N68-18014*# c32 N68-17651*#
NASA-TN-D-4267		c10 N68-11513*#	NASA-TN-D-4358	**************	c32 N68-17588*#
NASA-TN-D-4269	•••••	c17 N68-11644*#	NASA-TN-D-4359		c31 N68-19275*#
NASA-TN-D-4270 NASA-TN-D-4271	••••••	c22 N68-15197*# c25 N68-18485*#	NASA-TN-D-4360 NASA-TN-D-4361		c01 N68-18720*# c01 N68-17880*#
NASA-TN-D-4271 NASA-TN-D-4272	********************	c19 N68-11639*#	NASA-TN-D-4362		c01 N68-17880*# c07 N68-18616*#
NASA-TN-D-4273	*********	c33 N68-11491*#	NASA-TN-D-4363		c24 N68-17898*#
NASA-TN-D-4274	* * * * * * * * * * * * * * * * * * * *	c17 N68-11637*#	NASA-TN-D-4364		c02 N68-19184*#
NASA-TN-D-4275 NASA-TN-D-4276	••••••	c31 N68-18822*# c11 N68-15858*#	NASA-TN-D-4365 NASA-TN-D-4366	***************	c20 N68-17024*# c07 N68-18123*#
NASA-TN-D-4277	•••••	c05 N68-13609*#	NASA-TN-D-4367		c12 N68-18253*#
NASA-TN-D-4278	• • • • • • • • • • • • • • • • • • • •	c02 N68-11627*#	NASA-TN-D-4368		c25 N68-15747*#
NASA-TN-D-4279	•••••	c22 N68-14986*#	NASA-TN-D-4369	••••••	c25 N68-25630*#
NASA-TN-D-4280 NASA-TN-D-4281	********************	c01 N68-11640* c30 N68-11754*#	NASA-TN-D-4370 NASA-TN-D-4371		c03 N68-28310*# c22 N68-15792*#
NASA-TN-D-4282		c12 N68-28842*#	NASA-TN-D-4372		c32 N68-17068*#
NASA-TN-D-4283	•••••	c32 N68-14091*#	NASA-TN-D-4373		c19 N68-17334*#
NASA-TN-D-4284	••••••	c31 N68-28198*#	NASA-TN-D-4374	• • • • • • • • • • • • • • • • • • • •	c18 N68-19710*#
NASA-TN-D-4285 NASA-TN-D-4286	******************	c21 N68-11902*# c27 N68-11645*#	NASA-TN-D-4375 NASA-TN-D-4376	******************	c33 N68-18046*# c25 N68-33021*#
NASA-TN-D-4287	******************	c02 N68-11545*#	NASA-TN-D-4377	******************	c24 N68-15638*#
NASA-TN-D-4288	****************	c15 N68-12890*#	NASA-TN-D-4378		c12 N68-18146*#
NASA-TN-D-4289	• • • • • • • • • • • • • • • • • • • •	c17 N68-12891*#	NASA-TN-D-4379	•••••	c17 N68-17317*#
NASA-TN-D-4290 NASA-TN-D-4291	********	c08 N68-18179*# c01 N68-11936*#	NASA-TN-D-4380		c12 N68-16998*# c26 N68-17594*#
NASA-TN-D-4292	****************	c30 N68-15793*#	NASA-TN-D-4381 NASA-TN-D-4382	***************************************	c03 N68-16469*#
NASA-TN-D-4293	•••••	c23 N68-15950*#	NASA-TN-D-4383		c03 N68-16228*#
NASA-TN-D-4294	. • • • • • • • • • • • • • • • • • • •	c07 N68-18542*#	NASA-TN-D-4384		c03 N68-15943*#
NASA-TN-D-4295 NASA-TN-D-4296	*****	c32 N68-12370*# c19 N68-14077*#	NASA-TN-D-4385		c25 N68-17070*#
NASA-TN-D-4297	•••••	c19 N68-14077*# c06 N68-18219*#	NASA-TN-D-4386 NASA-TN-D-4387	* * * * * * * * * * * * * * * * * * * *	c03 N68-16631*# c12 N68-15329*#
NASA-TN-D-4298		c01 N68-21950*#	NASA-TN-D-4388		c03 N68-14639*#
NASA-TN-D-4299	•••••	c22 N68-19146*#	NASA-TN-D-4389	•••••	c01 N68-15743*#
NASA-TN-D-4300 NASA-TN-D-4301	*************	c09 N68-16530*#	NASA-TN-D-4390	•••••	c17 N68-15637*#
NASA-TN-D-4302	•••••	c33 N68-15330*# c03 N68-17110*#	NASA-TN-D-4391 NASA-TN-D-4392	*******************	c32 N68-17045*# c28 N68-16413*#
NASA-TN-D-4303	•••••	c26 N68-21708*#	NASA-TN-D-4393		c28 N68-18188*#
NASA-TN-D-4304	•••••	c29 N68-19188*#	NASA-TN-D-4394	••••••	c31 N68-17498*#
NASA-TN-D-4305 NASA-TN-D-4306	******************	c24 N68-15328*# c03 N68-20344*#	NASA-TN-D-4395 NASA-TN-D-4396	*******************	c20 N68-18246*# c02 N68-17391*#
NASA-TN-D-4307	******************	c33 N68-16683*#	NASA-TN-D-4397	*******	c01 N68-15778*#
NASA-TN-D-4308	•••••	c12 N68-17376*#	NASA-TN-D-4398	*******	c04 N68-21383*#

NASA-TN-D-4399	••••	c19 N68-17532*#	NASA-TN-D-4486		c32 N68-18721*#
NASA-TN-D-4400	*****************	c19 N68-21100*#	NASA-TN-D-4487		c05 N68-21538*#
NASA-TN-D-4401	•••••	c12 N68-19709*#	NASA-TN-D-4488		c05 N68-21537*#
NASA-TN-D-4402	*******	c07 N68-18178*#	NASA-TN-D-4489		c01 N68-19189*#
NASA-TN-D-4403	• • • • • • • • • • • • • • • • • • • •	c09 N68-19062*#	NASA-TN-D-4490		c21 N68-19236*#
NASA-TN-D-4404	****************	c29 N68-16837*#	NASA-TN-D-4491		c33 N68-19187*#
NASA-TN-D-4405		c19 N68-19144*#	NASA-TN-D-4492		c33 N68-21680*#
NASA-TN-D-4406	* * * * * * * * * * * * * * * * * * * *	c02 N68-19620*#	NASA-TN-D-4493		c01 N68-20370*#
NASA-TN-D-4407	•••••	c26 N68-19924*#	NASA-TN-D-4494		c01 N68-21681*#
NASA-TN-D-4408		c12 N68-19000*#	NASA-TN-D-4495		c03 N68-21651*#
NASA-TN-D-4409	******	c12 N68-20352*#	NASA-TN-D-4496	****************	c12 N68-21724*#
NASA-TN-D-4410		c31 N68-19226*#	NASA-TN-D-4497		c03 N68-21835*#
NASA-TN-D-4411		c33 N68-16324*#	NASA-TN-D-4498		c33 N68-20066*#
NASA-TN-D-4412		c18 N68-16623*#	NASA-TN-D-4499	******	c14 N68-20324*#
NASA-TN-D-4413		c27 N68-17093*#	NASA-TN-D-4500		c14 N68-24244*#
NASA-TN-D-4414	• • • • • • • • • • • • • • • • • • • •	c22 N68-17095*#	NASA-TN-D-4501		c14 N68-21942*#
NASA-TN-D-4415	**************	c03 N68-18998*#	NASA-TN-D-4502	*****************	c32 N68-21869*#
NASA-TN-D-4416		c28 N68-20064*#	NASA-TN-D-4503		c19 N68-25869*#
NASA-TN-D-4417		c12 N68-16227*#	NASA-TN-D-4504		c01 N68-25916*#
NASA-TN-D-4418		c28 N68-16632*#	NASA-TN-D-4505		c32 N68-21293*#
NASA-TN-D-4419	****************	c25 N68-21623*#	NASA-TN-D-4506		c06 N68-21430*#
NASA-TN-D-4420		c28 N68-20187*#	NASA-TN-D-4507		c30 N68-25271*#
NASA-TN-D-4421	*********	c08 N68-18620*#	NASA-TN-D-4508	*******	c08 N68-22510*#
NASA-TN-D-4422	•••••	c03 N68-20276*#	NASA-TN-D-4509		c31 N68-25358*#
NASA-TN-D-4423	*****	c28 N68-18221*#	NASA-TN-D-4510		c08 N68~25268*#
NASA-TN-D-4424	• • • • • • • • • • • • • • • • • • • •	c19 N68-22809*#	NASA-TN-D-4511		c30 N68-32094*#
NASA-TN-D-4425	••••	c31 N68-20198*#	NASA-TN-D-4512	• • • • • • • • • • • • • • • • • • • •	c21 N68-21754*#
NASA-TN-D-4426	•••••	c09 N68-19185*#	NASA-TN-D-4513	• • • • • • • • • • • • • • • • • • • •	c26 N68-22271*#
NASA-TN-D-4427		c01 N68-28868*#	NASA-TN-D-4514	*********	c33 N68-20374*#
NASA-TN-D-4427		c01 N68-31515*#	NASA-TN-D-4515	••••••	c28 N68-21679*#
NASA-TN-D-4428	•••••	c32 N68-20954*#	NASA-TN-D-4516	• • • • • • • • • • • • • • • • • • • •	c10 N68-21122*#
NASA-TN-D-4429 NASA-TN-D-4430	****************	c20 N68-19084*# c07 N68-20333*#	NASA-TN-D-4517 NASA-TN-D-4518	••••	c25 N68-20296*# c30 N68-20368*#
	•••••			*****	
NASA-TN-D-4431	•••••	c30 N68-21228*#	NASA-TN-D-4519 NASA-TN-D-4520		c31 N68-21260*# c30 N68-25385*#
NASA-TN-D-4432	• • • • • • • • • • • • • • • • • • • •	c03 N68-18501*#	NASA-TN-D-4520		c09 N68-24389*#
NASA-TN-D-4433	••••••	c24 N68-18949*#	NASA-TN-D-4522		c26 N68-20295*#
NASA-TN-D-4434 NASA-TN-D-4435	•••••	c31 N68-19085*# c22 N68-18541*#	NASA-TN-D-4522 NASA-TN-D-4523		c33 N68-21732*#
NASA-TN-D-4435			NASA-IN-D-4525		c14 N68-22883*#
NASA-TN-D-4430	*****************		NASA-TN-D-4525		c01 N68-21374*#
NASA-TN-D-4438	• • • • • • • • • • • • • • • • • • • •	c01 N68-19063*# c02 N68-21112*#	NASA-TN-D-4526		c15 N68-28249*#
NASA-TN-D-4439		c31 N68-22953*#	NASA-TN-D-4527		c13 N68-21543*#
NASA-TN-D-4440		c15 N68-21965*#	NASA-TN-D-4528		c26 N68-24660*#
NASA-TN-D-4441		c12 N68-19246*#	NASA-TN-D-4529		c02 N68-22291*#
NASA-TN-D-4442		c28 N68-18249*#	NASA-TN-D-4530		c14 N68-22290*#
NASA-TN-D-4443		c12 N68-28282*#	NASA-TN-D-4531		c30 N68-28251*#
NASA-TN-D-4444		c17 N68-22884*#	NASA-TN-D-4532		c03 N68-22258*#
NASA-TN-D-4445		c15 N68-17564*#	NASA-TN-D-4533		c03 N68-21766*#
NASA-TN-D-4446		c19 N68-18455*#	NASA-TN-D-4534		c28 N68-22096*#
NASA-TN-D-4447		c30 N68-22885*#	NASA-TN-D-4535		c33 N68-25122*#
NASA-TN-D-4448		c02 N68-18771*#	NASA-TN-D-4536		c02 N68-22033*#
NASA-TN-D-4449	*****	c21 N68-21123*#	NASA-TN-D-4537		c31 N68-21758*#
NASA-TN-D-4450		c17 N68-21654*#	NASA-TN-D-4538		c25 N68-21691*#
NASA-TN-D-4451		c06 N68-19434*#	NASA-TN-D-4539		c01 N68-21941*#
NASA-TN-D-4452		c26 N68-21219*#	NASA-TN-D-4540		c14 N68-25830*#
NASA-TN-D-4453		c20 N68-20375*#	NASA-TN-D-4541		c17 N68-21768*#
NASA-TN-D-4454		c32 N68-20364*#	NASA-TN-D-4542		c30 N68-25867*#
NASA-TN-D-4455		c28 N68-19581*#	NASA-TN-D-4543		c33 N68-22118*#
NASA-TN-D-4456		c15 N68-20199*#	NASA-TN-D-4544		c30 N68-24486*#
NASA-TN-D-4457		c33 N68-20331*#	NASA-TN-D-4545		c22 N68-21924*#
NASA-TN-D-4458		c12 N68-24758*#	NASA-TN-D-4546		c03 N68-22257*#
NASA-TN-D-4459		c22 N68-19925*#	NASA-TN-D-4547		c19 N68-21978*#
NASA-TN-D-4460	• • • • • • • • • • • • • • • • • • • •	c30 N68-26643*#	NASA-TN-D-4548		c17 N68-22338*#
NASA-TN-D-4461		c17 N68-18999*#	NASA-TN-D-4549		c21 N68-23377*#
NASA-TN-D-4462	• • • • • • • • • • • • • • • • • • • •	c01 N68-20330*#	NASA-TN-D-4550		c32 N68-22275*#
NASA-TN-D-4463		c15 N68-20325*#	NASA-TN-D-4551	••••	c17 N68-24558*#
NASA-TN-D-4464		c05 N68-20354*#	NASA-TN-D-4552		c14 N68-25862*#
NASA-TN-D-4465		c01 N68-19954*#	NASA-TN-D-4553		c18 N68-28264*#
NASA-TN-D-4466	***************	c26 N68-18772*#	NASA-TN-D-4554		c08 N68-25002*#
NASA-TN-D-4467	• • • • • • • • • • • • • • • • • • • •	c33 N68-24965*#	NASA-TN-D-4555		c07 N68-25918*#
NASA-TN-D-4468	• • • • • • • • • • • • • • • • • • • •	c30 N68-21733*#	NASA-TN-D-4556		c09 N68-24387*#
NASA-TN-D-4469	********	c14 N68-21169*#	NASA-TN-D-4557		c28 N68-23354*#
NASA-TN-D-4470	•••••	c30 N68-20356*#	NASA-TN-D-4558		c31 N68-22301*#
NASA-TN-D-4471	•••••	c32 N68-21099*#	NASA-TN-D-4559	•••••	c30 N68-22289*#
NASA-TN-D-4472		c25 N68-22887*#	NASA-TN-D-4560		c02 N68-22886*#
NASA-TN-D-4473	•••••	c29 N68-25880*# c11 N68-25853*#	NASA-TN-D-4561		c08 N68-24310*# c30 N68-26642*#
NASA-TN-D-4474 NASA-TN-D-4475		cli N68-25853*# cl7 N68-18610*#	NASA-TN-D-4562 NASA-TN-D-4563		c01 N68-25093*#
NASA-TN-D-4475	•••••	c17 N68-21979*#	NASA-TN-D-4564		c33 N68-25102*#
NASA-TN-D-4476	• • • • • • • • • • • • • • • • • • • •	c01 N68-19180*#	NASA-TN-D-4565		c15 N68-24142*#
NASA-TN-D-4477	• • • • • • • • • • • • • • • • • • • •	c30 N68-24371*#	NASA-TN-D-4566		c24 N68-24661*#
NASA-TN-D-4478	******************	c13 N68-22861*#	NASA-TN-D-4567		c17 N68-24477*#
NASA-TN-D-4480		c14 N68-25518*#	NASA-TN-D-4568		c32 N68-25104*#
NASA-TN-D-4481		c21 N68-19061*#	NASA-TN-D-4569		c15 N68-23900*#
NASA-TN-D-4482		c29 N68-25181*#	NASA-TN-D-4570		c20 N68-24028*#
NASA-TN-D-4483		c30 N68-21182*#	NASA-TN-D-4571		c28 N68-25099*#
NASA-TN-D-4484		c33 N68-20065*#	NASA-TN-D-4572		c07 N68-25852*#
NASA-TN-D-4485		c23 N68-24146*#	NASA-TN-D-4573		c09 N68-24388*#

NASA-TN-D-4574		c02 N68-24499*#	NASA-TN-D-4664		c01 N68-28830*#
NASA-TN-D-4575	•••••	c19 N68-24565*#		• • • • • • • • • • • • • • • • • • • •	c02 N68-31956*#
NASA-TN-D-4576 NASA-TN-D-4577		c31 N68-31978*# c11 N68-28311*#		* • • • • • • • • • • • • • • • • • • •	c30 N68-30244*# c14 N68-29418*#
NASA-TN-D-4578	* * * * * * * * * * * * * * * * * * * *	c02 N68-24498*#		*	c15 N68-28260*#
NASA-TN-D-4579		c12 N68-24129*#			c15 N68-28258*#
NASA-TN-D-4580		c31 N68-24338*#			c30 N68-28841*#
NASA-TN-D-4581 NASA-TN-D-4582		c22 N68-25058*# c03 N68-25059*#	and and the second second		c01 N68-29405*# c01 N68-28447*#
NASA-TN-D-4583		c11 N68-24560*#	see also income to a second		c17 N68-29379*#
NASA-TN-D-4584		c07 N68-24845*#			c17 N68-30000*#
NASA-TN-D-4585		c21 N68-24512*#			c01 N68-28795*#
NASA-TN-D-4586 NASA-TN-D-4587	*********************	c02 N68-24476*# c30 N68-24557*#	NASA-TN-D-4676 NASA-TN-D-4677	*********************	c06 N68-30044*# c02 N68-28831*#
NASA-TN-D-4588		c02 N68-24662*#		********	c12 N68-28801*#
NASA-TN-D-4589		c13 N68-28222*#	NASA-TN-D-4679	•••••	c14 N68-30127*#
NASA-TN-D-4590		c05 N68-25060*#	and the second	***************	c31 N68-29962*#
NASA-TN-D-4591 NASA-TN-D-4592	• • • • • • • • • • • • • • • • • • • •	c32 N68-24508*# c03 N68-24461*#	NASA-TN-D-4681 NASA-TN-D-4682		c14 N68-29951*# c02 N68-29406*#
NASA-TN-D-4593	*****	c21 N68-24409*#			c24 N68-29375*#
NASA-TN-D-4594		c21 N68-24555*#			c24 N68-30001*#
NASA-TN-D-4595	********	c33 N68-25312*#	NASA-TN-D-4685	••••••	c33 N68-30041*#
NASA-TN-D-4596 NASA-TN-D-4597	*****************	c31 N68-25820*# c14 N68-25317*#	NASA-TN-D-4686 NASA-TN-D-4687		c01 N68-29955*# c32 N68-28832*#
NASA-TN-D-4598		c31 N68-24964*#	NASA-TN-D-4688		c01 N68-31445*#
NASA-TN-D-4599		c21 N68-25103*#	NASA-TN-D-4689	•••••	c11 N68-29957*#
NASA-TN-D-4600	*********	c03 N68-25829*# c03 N68-25304*#	NASA-TN-D-4690		c28 N68-30040*# c31 N68-30032*#
NASA-TN-D-4601 NASA-TN-D-4602	******	c02 N68-25313*#	NASA-TN-D-4691 NASA-TN-D-4692	******************	c23 N68-36460*#
NASA-TN-D-4603		c13 N68-28872*#	NASA-TN-D-4693		c01 N68-30595*#
NASA-TN-D-4604		c25 N68-25877*#	NASA-TN-D-4694		c15 N68-33227*#
NASA-TN-D-4605		c17 N68-24111*# c26 N68-24510*#	NASA-TN-D-4695	•••••	c01 N68-30128*# c19 N68-30594*#
NASA-TN-D-4606 NASA-TN-D-4607		c32 N68-25421*#	NASA-TN-D-4696 NASA-TN-D-4697	*******************	c03 N68-29960*#
NASA-TN-D-4608		c23 N68-25868*#	NASA-TN-D-4698		c03 N68-30002*#
NASA-TN-D-4609		c02 N68-28277*#	NASA-TN-D-4699		c28 N68-29378*#
NASA-TN-D-4610 NASA-TN-D-4611		c01 N68-25919*# c33 N68-25917*#	NASA-TN-D-4700 NASA-TN-D-4701		c03 N68-30241*# c27 N68-30077*#
NASA-TN-D-4612		c14 N68-25375*#	NASA-TN-D-4702		c32 N68-32074*#
NASA-TN-D-4613		c12 N68-26651*#	NASA-TN-D-4703		c19 N68-29275*#
NASA-TN-D-4614		c33 N68-26650*#	NASA-TN-D-4704	• • • • • • • • • • • • • • • • • • • •	c01 N68-31484*#
NASA-TN-D-4615 NASA-TN-D-4616		c22 N68-24559*# c15 N68-24456*#	NASA-TN-D-4705 NASA-TN-D-4706	******************	c32 N68-33738*# c32 N68-31946*#
NASA-TN-D-4617		c08 N68-24967*#	NASA-TN-D-4707		c32 N68-32051*#
NASA-TN-D-4618		c33 N68-26759*#	NASA-TN-D-4708		c25 N68-33372*#
NASA-TN-D-4619		c03 N68-28420*#	NASA-TN-D-4709	*****	c22 N68-30750*#
NASA-TN-D-4620 NASA-TN-D-4621	· · · · · · · · · · · · · · · · · · ·	c09 N68-26662*# c25 N68-25920*#	NASA-TN-D-4710 NASA-TN-D-4711		c32 N68-31602*# c32 N68-30505*#
NASA-TN-D-4622		c30 N68-28113*#	NASA-TN-D-4712		c19 N68-30804*#
NASA-TN-D-4623		c07 N68-29528*#	NASA-TN-D-4713	*****	c33 N68-30747*#
NASA-TN-D-4624		c02 N68-28153*#	NASA-TN-D-4714	******	c17 N68-30066*# c17 N68-29954*#
NASA-TN-D-4625 NASA-TN-D-4626		c23 N68-28259*# c26 N68-28239*#	NASA-TN-D-4715 NASA-TN-D-4716	**********************	c15 N68-29918*#
NASA-TN-D-4627		c03 N68-28101*#	NASA-TN-D-4717		c32 N68-30045*#
NASA-TN-D-4628		c12 N68-25866*#	NASA-TN-D-4718		c25 N68-30093*#
NASA-TN-D-4629	****************	c21 N68-28236*#	NASA-TN-D-4719 NASA-TN-D-4720	***************	c01 N68-31551*# c33 N68-31959*#
NASA-TN-D-4630 NASA-TN-D-4631		c15 N68-28871*# c33 N68-28100*#	NASA-TN-D-4721		c07 N68-36105*#
NASA-TN-D-4632		c01 N68-28268*#	NASA-TN-D-4722		c23 N68-30596*#
NASA-TN-D-4633		c24 N68-28265*#	NASA-TN-D-4724		c02 N68-33879*#
NASA-TN-D-4634 NASA-TN-D-4635		c14 N68-28327*# c01 N68-28817*#	NASA-TN-D-4725 NASA-TN-D-4727		c17 N68-30504*# c03 N68-30751*#
NASA-TN-D-4636		c30 N68-28409*#	NASA-TN-D-4728		c17 N68-30605*#
NASA-TN-D-4637		c21 N68-28418*#	NASA-TN-D-4729		c30 N68-31989*#
NASA-TN-D-4638		c02 N68-29372*#	NASA-TN-D-4730		c28 N68-30604*#
NASA-TN-D-4639 NASA-TN-D-4640		c02 N68-29887*# c12 N68-28364*#	NASA-TN-D-4731 NASA-TN-D-4732		c34 N68-33682*# c29 N68-33370*#
NASA-TN-D-4641		c21 N68-28361*#	NASA-TN-D-4733		c33 N68-30518*#
NASA-TN-D-4642		c08 N68-29404*#	NASA-TN-D-4734		c18 N68-30597*#
NASA-TN-D-4643		c19 N68-29407*#	NASA-TN-D-4735		c06 N68-30582*#
NASA-TN-D-4644 NASA-TN-D-4645		c11 N68-29478*# c01 N68-28220*#	NASA-TN-D-4736 NASA-TN-D-4737		c25 N68-30784*# c33 N68-33208*#
NASA-TN-D-4646		c30 N68-28884*#	NASA-TN-D-4738		c14 N68-33277*#
NASA-TN-D-4649		c33 N68-28371*#	NASA-TN-D-4739		c01 N68-31990*#
NASA-TN-D-4650		c17 N68-28365*#	NASA-TN-D-4740		c21 N68-31957*#
NASA-TN-D-4651 NASA-TN-D-4652		c25 N68-30031*# c15 N68-28766*#	NASA-TN-D-4741 NASA-TN-D-4742		c21 N68-33450*# c21 N68-31938*#
NASA-TN-D-4653	********************	c11 N68-28947*#	NASA-TN-D-4742 NASA-TN-D-4743		c17 N68-31517*#
NASA-TN-D-4654	****************	c21 N68-28262*#	NASA-TN-D-4744		c25 N68-31640*#
NASA-TN-D-4655		c01 N68-37065*#	NASA-TN-D-4745		c25 N68-30593*#
NASA-TN-D-4656 NASA-TN-D-4657		c09 N68-28668*# c30 N68-28408*#	NASA-TN-D-4746 NASA-TN-D-4747		c12 N68-33054*# c28 N68-35115*#
NASA-TN-D-4658		c22 N68-28304*#	NASA-TN-D-4747 NASA-TN-D-4748		c07 N68-31639*#
NASA-TN-D-4659		c03 N68-28280*#	NASA-TN-D-4749		c32 N68-33092*#
NASA-TN-D-4660	• • • • • • • • • • • • • • • • • • • •	c12 N68-28370*#	NASA-TN-D-4750		c11 N68-33190*#
NASA-TN-D-4661 NASA-TN-D-4662		c17 N68-28818*# c31 N68-28690*#	NASA-TN-D-4751 NASA-TN-D-4752		c05 N68-32100*# c07 N68-35537*#
NASA-TN-D-4663		c19 N68-28281*#	NASA-TN-D-4753		c32 N68-33225*#

NASA-TN-D-4754		c12	N68-35117*#	NASA-TN-D-4857
NASA-TN-D-4755		c24	N68-35535*#	NASA-TN-D-4858
NASA-TN-D-4756		c21	N68-33271*#	NASA-TN-D-4860
NASA-TN-D-4757			N68-37869*#	NASA-TN-D-4862
NASA-TN-D-4758	********		N68-32072*#	NASA-TN-D-4866
NASA-TN-D-4759	***************		N68-31960*#	NASA-TN-D-4867
NASA-TN-D-4760			N68-31958*#	NASA-TN-D-4868
NASA-TN-D-4762 NASA-TN-D-4763	•••••		N68-33034*# N68-31961*#	NASA-TN-D-4882
NASA-TN-D-4764	*********		N68-33635*#	NASA-TR-R-259
NASA-TN-D-4765			N68-36106*#	NASA-TR-R-273
NASA-TN-D-4766	*****		N68-33081*#	NASA-TR-R-275 c19 N68-10121*#
NASA-TN-D-4767		c33	N68-32099*#	NASA-TR-R-276
NASA-TN-D-4768		c13	N68-33416*#	NASA-TR-R-277
NASA-TN-D-4769	******	c06	N68-31948*#	NASA-TR-R-279
NASA-TN-D-4770		c08	N68-32055*#	NASA-TR-R-280
NASA-TN-D-4771	• • • • • • • • • • • • • • • • • • • •		N68-32073*#	NASA-TR-R-281
NASA-TN-D-4772			N68-33057*#	NASA-TR-R-282
NASA-TN-D-4773			N68-33669*#	NASA-TR-R-283
NASA-TN-D-4774	******		N68-35524*#	
NASA-TN-D-4775 NASA-TN-D-4776			N68-33278*# N68-35072*#	NASA-TR-R-285
NASA-TN-D-4777	*****************		N68-33191*#	NASA-TR-R-286
NASA-TN-D-4778			N68-33167*#	NASA-TR-R-288
NASA-TN-D-4779			N68-33165*#	NASA-TR-R-289
NASA-TN-D-4780			N68-33456*#	NASA-TR-R-290
NASA-TN-D-4781	***********		N68-33006*#	NASA-TR-R-292
NASA-TN-D-4782		c32	N68-35071*#	NASA-TR-R-293
NASA-TN-D-4783	*********		N68-33763*#	· · · ·
NASA-TN-D-4784	*******		N68-35140*#	NASA-TT-F-415
NASA-TN-D-4786	******			NASA-TT-F-425
NASA-TN-D-4787	******	c17	N68-33684*#	NASA-TT-F-426
NASA-TN-D-4788 NASA-TN-D-4789			N68-33642*# N68-34175*#	NASA-TT-F-427
NASA-TN-D-4790	****************	c24	N68-34234*#	NASA-TT-F-431
NASA-TN-D-4791	****************	c33	N68-35116*#	NASA-TT-F-435
NASA-TN-D-4792		c01	N68-35497*#	NASA-TT-F-439
NASA-TN-D-4793		c32	N68-35496*#	NASA-TT-F-460
NASA-TN-D-4794		c16	N68-35175*#	NASA-TT-F-477
NASA-TN-D-4795	*************	c12	N68-34089*#	NASA-TT-F-488
NASA-TN-D-4796		c01	N68-35665*#	NASA-TT-F-492
NASA-TN-D-4797	•••••		N68-34088*#	NASA-TT-F-497
NASA-TN-D-4799	*********		N68-35468*#	NASA-TT-F-503
NASA-TN-D-4800	*************	c01	N68-35668*#	NASA-TT-F-505
NASA-TN-D-4801 NASA-TN-D-4802	••••••		N68-36077*#	NASA-TT-F-513
NASA-TN-D-4803	•••••		N68-35466*# N68-33056*#	NASA-TT-F-515
NASA-TN-D-4804			N68-37075*#	NASA-TT-F-520
NASA-TN-D-4805			N68-34087*#	NASA-TT-F-521
NASA-TN-D-4806		c26		
NASA-TN-D-4807		c31	N68-35022*#	NBS-9708
NASA-TN-D-4808	•••••	c30	N68-33055*#	
NASA-TN-D-4809			N68-37238*#	NCL-67-39
NASA-TN-D-4810			N68-36070*#	NCL-67-44R
NASA-TN-D-4811	*******		N68-36459*#	
NASA-TN-D-4812 NASA-TN-D-4813	*******	c01		NOR-67-221
NASA-TN-D-4814	*******************	c01	N68-35174*#	NRC-LR-486
NASA-TN-D-4815			N68-36071*#	NUC-TU-100 1111111111111111111111111111111111
NASA-TN-D-4816	*****		N68-36021*#	OR-8549
NASA-TN-D-4817			N68-36072*#	
NASA-TN-D-4818	****************		N68-35467*#	PHD-TR-307
NASA-TN-D-4819			N68-35823*#	· ·
NASA-TN-D-4820	•••••		N68-36334*#	PIFR-051
NASA-TN-D-4821	****************		N68-37054*#	
NASA-TN-D-4822 NASA-TN-D-4827			N68-35534*#	PWA-3154
NASA-TN-D-4828			N68-35073*# N68-35104*#	R67SD3012c03 N68-29460*#
NASA-TN-D-4829	******		N68-36458*#	R67SD3012
NASA-TN-D-4830			N68-37051*#	
NASA-TN-D-4833			N68-37053*#	RAD-TR-65-28
NASA-TN-D-4834			N68-37055*#	
NASA-TN-D-4836	••••••		N68-36073*#	REPT0-71000/8R-2 c24 N68-37708*#
NASA-TN-D-4837	**********		N68-36074*#	REPT4-17-67-1 c32 N68-24481*#
NASA-TN-D-4838			N68-37240*#	REPT4-17-67-4
NASA-TN-D-4839			N68-36098*#	REPT36
NASA-TN-D-4840 NASA-TN-D-4841			N68-36055*#	REPT66-7, PT. 1
NASA-TN-D-4842	******************		N68-36457*# N68-36461*#	REPT66-7, PT. 2 c33 N68-26692*# REPT66-7, PT. 3 c33 N68-26641*#
NASA-TN-D-4843	******************		N68-37074*#	REPT66-7, PT. 3
NASA-TN-D-4844			N68-37365*#	REPT66-7, PT. 5
NASA-TN-D-4845			N68-36470*#	REPT66-7, PT. 6
NASA-TN-D-4847			N68-36056*#	REPT67-2174 c05 N68-28833*#
NASA-TN-D-4848		c28	N68-36507*#	REPT101
NASA-TN-D-4849	•••••		N68-37162*#	REPT548-01-7-803, V. 1 c09 N68-29525*#
NASA-TN-D-4850			N68-36075*#	REPT548-01-7-803, V. 2 c09 N68-29526*#
NASA-TN-D-4851			N68-36515*#	REPT1223 cl1 N68-23357*#
NASA-TN-D-4855	*******	CUI	N68-37854*#	REPT1238 c12 N68-31593*#

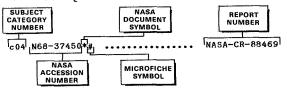
REPT1475	c32 N68-11489*#
REPT1520	c05 N68-30602*#
REPT1571	c05 N68-33304*#
REPT1691-23 REPT3734A-67	c07 N68-22746*#
REPT3734A-67	c03 N68-22842*#
RFPT4227	c28 N68-28112*#
REPT4227 REPT7322-3-T	c23 N68-21444*#
REPT20175-FR2	c02 N68-10047*#
RSIC-491	c15 N68-19307*#
RSIC-495	c17 N68-21917*#
RSIC-501	c15 N68-21241*#
RSIC-595	c15 N68-19343*#
RSIC-598	c15 N68-21429*#
RSIC-599	c15 N68-20056*#
RSIC-600	c15 N68-20433*#
	CIO NOO 20400-#
S-67-1014	c15 N68-20389*#
S-157	c08 N68-30240*#
SCR-328-1	c21 N68-21652*#
SD-67-994-1	c30 N68-34086*#
SD-67-1204-1	c32 N68-28335*#
SID-65-1200-1	c30 N68-16103*#
SID-65-1200-2, V. 2	c30 N68-19676*#
SID-65-1200-3	c30 N68-14089*#
SID-65-1200-4	c30 N68-15193*#
SID-65-1200-5	c30 N68-21685*#
SID-65-1200-6	c30 N68-15741*#
SID-65-1200-7, V. 7	c30 N68-20084*#
SID-65-1200-8	c30 N68-20449*#
SID-66-1678-1	c30 N68-20450*#
SID-66-1678-2, V. 10	c30 N68-21077*#
SID-66-1678-2, V. 10 SID-66-1678-3, V. 11	
SID-66-1678-3, V. 11	c30 N68-17215*#
SID-66-1678-4	c30 N68-19186*#
SID-66-1678-5	c30 N68-19315*#
SID-66-1678-6, V. 14	c30 N68-19985*#
SID-66-1678-7	c30 N68-21231*#
SID-66-1678-8, V. 16	c30 N68-20468*#
SID-66-1678-9	c30 N68-21442*#
SID-67-542-1	c31 N68-11520*#
	COI NOO IIOZO B
SM-48461-F	c03 N68-16321*#
SM-48464-F	c10 N68-19229*#
SN-9000	c02 N68-26691*#
TR-0-71200/TTR-112	c14 N68-25316*#
TR-0-71200/TTR-125	c11 N68-24966*#
TR-66-67	c31 N68-14638*#
TR-152-1	c31 N68-28426*#
TV-TAG-T	
TD-165-1	
TR-165-1	c05 N68-26690*#
TR-165-1 TR-170-1	c05 N68-26690*# c07 N68-28272*#
TR-165-1	c05 N68-26690*#
TR-165-1 TR-170-1 TR-3172	c05 N68-26690*# c07 N68-28272*# c04 N68-28247*#
TR-165-1 TR-170-1	c05 N68-26690*# c07 N68-28272*#
TR-165-1 TR-170-1 TR-3172	c05 N68-26690*# c07 N68-28272*# c04 N68-28247*#
TR-165-1 TR-170-1 TR-3172 TRACOR-67-070-U	c05 N68-26690*# c07 N68-28272*# c04 N68-28247*#
TR-165-1 TR-170-1 TR-3172 TRACOR-67-070-U TRW-02874-6008-R000	c05 N68-26690*# c07 N68-28272*# c04 N68-28247*# c12 N68-22087*# c27 N68-32793*#
TR-165-1 TR-170-1 TR-3172 TRACOR-67-070-U	c05 N68-26690*# c07 N68-28272*# c04 N68-28247*# c12 N68-22087*#
TR-165-1 TR-170-1 TR-3172 TRACOR-67-070-U TRW-02874-6008-R000 TRW-04848-6001-R0-000	c05 N68-26690*# c07 N68-28272*# c04 N68-28247*# c12 N68-22087*# c27 N68-32793*# c16 N68-10467*#
TR-165-1 TR-170-1 TR-3172 TRACOR-67-070-U TRW-02874-6008-R000	c05 N68-26690*# c07 N68-28272*# c04 N68-28247*# c12 N68-22087*# c27 N68-32793*#
TR-165-1 TR-170-1 TR-3172 TRACOR-67-070-U TRW-02874-6008-R000 TRW-04848-6001-R0-000 TRW-ER-7203	c05 N68-26690*# c07 N68-28272*# c04 N68-28247*# c12 N68-22087*# c27 N68-32793*# c16 N68-10467*# c17 N68-29992*#
TR-165-1 TR-170-1 TR-3172 TRACOR-67-070-U TRW-02874-6008-R000 TRW-04848-6001-R0-000 TRW-ER-7203 TT-66-51152	c05 N68-26690*# c07 N68-28272*# c04 N68-28247*# c12 N68-22087*# c27 N68-32793*# c16 N68-10467*# c17 N68-29992*# c28 N68-11829*#
TR-165-1 TR-170-1 TR-3172 TRACOR-67-070-U TRW-02874-6008-R000 TRW-04848-6001-R0-000 TRW-ER-7203 TT-66-51152 TT-67-51363	c05 N68-26690*# c07 N68-28272*# c04 N68-28247*# c12 N68-22087*# c27 N68-32793*# c16 N68-10467*# c17 N68-29992*# c28 N68-11829*# c31 N68-2262*#
TR-165-1 TR-170-1 TR-3172 TRACOR-67-070-U TRW-02874-6008-R000 TRW-04848-6001-R0-000 TRW-ER-7203 TT-66-51152 TT-67-51363 TT-67-51364	c05 N68-26690*# c07 N68-28272*# c04 N68-28247*# c12 N68-22087*# c16 N68-32793*# c16 N68-10467*# c17 N68-29992*# c28 N68-11829*# c31 N68-2262*# c32 N68-10407*#
TR-165-1 TR-170-1 TR-3172 TRACOR-67-070-U TRW-02874-6008-R000 TRW-04848-6001-R0-000 TRW-ER-7203 TT-66-51152 TT-67-51363	c05 N68-26690*# c07 N68-28272*# c04 N68-28274*# c12 N68-22087*# c27 N68-32793*# c16 N68-10467*# c17 N68-29992*# c28 N68-11829*# c31 N68-22262*# c32 N68-10407*# c33 N68-1121*#
TR-165-1 TR-170-1 TR-3172 TRACOR-67-070-U TRW-02874-6008-R000 TRW-02874-6008-R000 TRW-04848-6001-R0-000 TRW-ER-7203 TT-66-51152 TT-67-51363 TT-67-51367	c05 N68-26690*# c07 N68-28272*# c04 N68-28274*# c12 N68-22087*# c27 N68-32793*# c16 N68-10467*# c17 N68-29992*# c28 N68-11829*# c31 N68-22262*# c32 N68-10407*# c33 N68-1121*#
TR-165-1	c05 N68-26690*# c07 N68-28272*# c04 N68-28247*# c12 N68-22087*# c12 N68-32793*# c16 N68-10467*# c17 N68-29992*# c28 N68-11829*# c31 N68-2262*# c32 N68-10407*# c33 N68-11721*# c33 N68-11721*#
TR-165-1 TR-170-1 TR-3172 TRACOR-67-070-U TRW-02874-6008-R000 TRW-04848-6001-R0-000 TRW-ER-7203 TT-66-51152 TT-67-51363 TT-67-51370 TT-67-51370	c05 N68-26690*# c07 N68-28272*# c04 N68-28247*# c12 N68-22087*# c16 N68-32793*# c16 N68-10467*# c17 N68-29992*# c18 N68-11829*# c31 N68-2262*# c32 N68-11721*# c33 N68-11721*# c07 N68-37293*#
TR-165-1 TR-170-1 TR-3172 TRACOR-67-070-U TRW-02874-6008-R000 TRW-02874-6008-R000 TRW-04848-6001-R0-000 TRW-ER-7203 TT-66-51152 TT-67-51363 TT-67-51364 TT-67-51370 TT-67-51371 TT-67-51371	c05 N68-26690*# c07 N68-28272*# c04 N68-28247*# c12 N68-22087*# c16 N68-32793*# c16 N68-10467*# c17 N68-29992*# c31 N68-2262*# c31 N68-2262*# c32 N68-11721*# c33 N68-11721*# c10 N68-37293*# c13 N68-10079*#
TR-165-1 TR-170-1 TR-3172 TRACOR-67-070-U TRW-02874-6008-R000 TRW-04848-6001-R0-000 TRW-ER-7203 TT-66-51152 TT-67-51363 TT-67-51370 TT-67-51371 TT-67-51374	c05 N68-26690*# c07 N68-28272*# c04 N68-28274*# c12 N68-28277*# c12 N68-22087*# c16 N68-10467*# c17 N68-29992*# c31 N68-29992*# c31 N68-22262*# c32 N68-11829*# c33 N68-11721*# c07 N68-17542*# c10 N68-37293*# c13 N68-10079*# c13 N68-13432*#
TR-165-1 TR-170-1 TR-3172 TRACOR-67-070-U TRW-02874-6008-R000 TRW-02874-6008-R000 TRW-04848-6001-R0-000 TRW-ER-7203 TT-66-51152 TT-67-51363 TT-67-51364 TT-67-51370 TT-67-51371 TT-67-51371	c05 N68-26690*# c07 N68-28272*# c04 N68-28247*# c12 N68-22087*# c16 N68-32793*# c16 N68-10467*# c17 N68-29992*# c31 N68-2262*# c31 N68-2262*# c32 N68-11721*# c33 N68-11721*# c10 N68-37293*# c13 N68-10079*#

ACCESSION / REPORT NUMBER INDEX

NASA SCIENTIFIC AND TECHNICAL REPORTS FOR 1968

Typical Accession/Report Number

Index Listin,



Listings in this index are arranged numerically by NASA accession number. The subject category number indicates the subject category in the abstract section in which the citation is located. The NASA accession number denotes the number by which the citation is identified within the subject category. An asterisk (*) indicates that the item is a NASA report. A pound sign (#) indicates that the item is available on microfiche. The report numbers are the identification numbers that have been assigned to the item by the issuing body or other agency.

c02 N68-10047*#	NASA-CR-913
	REPT 20175-FR2
c17 N68-10051*#	NASA-TM-X-1468
c14 N68-10057*#	NASA-TN-D-4234
c01 N68-10060*#	NASA-TN-D-4228
c13 N68-10079*#	••••••••••••••••••••••••••••••••••••••
"	TT-67-51374
c01 N68-10093*#	NASA-TN-D-4229
c03 N68-10103*#	NASA-TM-X-1464
c17 N68-10104*#	NASA-TN-D-4235
c15 N68-10120*#	NASA-SP-6505
c19 N68-10121*#	NASA-TR-R-275
c04 N68-10122*#	NASA-IN-D-4251
c22 N68-10122*#	NASA-TM-X-1461
c22 N68-10134*#	••••••••••••••••••••••••••••••••••••••
c30 N68-10164*#	NASA-SP-3042
c31 N68-10192*#	••••••••••••••••••••••••••••••••••••••
c20 N68-10222*#	NASA-TN-D-4078
c32 N68-10231*#	GDC-DDF65-001
	NASA-CR-935
c32 N68-10233*#	•••••• GD/C-BTD-67-031
	NASA-CR-943
c32 N68-10280*#	•••••• GD/C-BTD-67-053
	NASA-CR-936
c13 N68-10283*#	•••••• NASA-CR-916
c22 N68-10291*#	••••••••••••••••••••••••••••••••••••••
c33 N68-10299*#	••••••••••••••••••••••••••••••••••••••
c23 N68-10354*#	••••••••••••••••••••••••••••••••••••••
c19 N68-10355*#	••••••••••••••••••••••••••••••••••••••
c33 N68-10368*#	••••••••••••••••••••••••••••••••••••••
c13 N68-10369*#	••••••••••••••••••••••••••••••••••••••
c01 N68-10380*#	••••••••••••••••••••••••••••••••••••••
c05 N68-10381*#	••••••••••••••••••••••••••••••••••••••
c11 N68-10384*#	NASA-SP-5045
c15 N68-10402*#	NASA-SP-5019
c32 N68-10407*#	••••••••••••••••••••••••••••••••••••••
	TT-67-51364
c09 N68-10420*#	NASA-CR-914
c16 N68-10467*#	NASA-CR-927
CIO NGO 10401-%	TRW-04848-6001-R0-000
c28 N68-10496*#	
c06 N68-10497*#	NASA-TM-X-1475
c17 N68-10498*#	NASA-IM-X-1425
c12 N68-10499*#	NASA-IN-D-4240
c12 N68-10499*# c28 N68-10502*#	NASA-CR-933
c15 N68-10503*#	••••••••••••••••••••••••••••••••••••••
c01 N68-10529*#	••••••••••••••••••••••••••••••••••••••
c22 N68-10561*#	••••••••••••••••••••••••••••••••••••••
c28 N68-10562*#	••••••••••••••••••••••••••••••••••••••
c32 N68-10568*#	GDC-DDF65-003, V. 3

TO MAD ADDADA	
c32 N68-10568*#	NASA-CR-937
c32 N68-10574*#	GD/C-BTD-67-049
·	NASA-CR-938
c12 N68-10646*#	NASA-CR-950
c14 N68-10647*#	NASA-TN-D-4186
c05 N68-10648*#	NASA-CR-919
c23 N68-10674*#	NASA-CR-951
c01 N68-11036*#	••••••••••••••••••••••••••••••••••••••
c24 N68-11037*#	NASA-CR-975
c33 N68-11038*#	NASA-TR-R-276
c32 N68-11054*#	NASA-CR-940
c24 N68-11074*#	NASA-TN-D-4256 GD/C-BTD-67-057, V. 8
c32 N68-11089*#	GD/C-BID-67-057, V. 8
10 840 11100+-	NASA-CR-942
c19 N68-11109*#	CD (C-PTD-C7.027 H 11
c32 N68-11133*#	GD/C-BTD-67-023, V. 11 NASA-CR-945
c33 N68-11144*#	NASA-CR-940
c30 N68-11145*#	NASA-TN-D-4260
c21 N68-11146*#	NASA-TM-X-1465
c02 N68-11147*#	NASA-TM-X-1469
c02 N68-11174*#	NASA-CR-670/01/
c32 N68-11191*#	ARA-327-6
	NASA-CR-964
c01 N68-11253*#	
c32 N68-11282*#	ARA-327-5
	NASA-CR-963
c34 N68-11307≠#	••••••••••••••••••••••••••••••••••••••
c34 N68-11308*#	NASA-SP-7030, V. 2
c34 N68-11309*#	••••••••••••••••••••••••••••••••••••••
c32 N68-11355*#	••••••••••••••••••••••••••••••••••••••
c30 N68-11369*#	NASA-TN-D-4169
c25 N68-11404*#	••••••••••••••••••••••••••••••••••••••
c30 N68-11456*#	NASA-SP-140
c07 N68-11475*#	NASA-TN-D-4254
c31 N68-11476*#	NASA-TN-D-4263
c32 N68-11485*#	GD/C-BTD-67-045
-90 NC0 11480**	NASA-CR-939
c32 N68-11489*#	NASA-CR-954 REPT-1475
c33 N68-11491*#	NASA-TN-D-4273
c33 N68-11491*# c19 N68-11494*#	**************************************
	NASA-TN-D-6266
	NASA-TN-D-4244
c05 N68-11510*#	NASA-CR-973
c05 N68-11510*# c17 N68-11511*#	NASA-CR-973 NASA-TN-D-4213
c05 N68-11510*# c17 N68-11511*# c06 N68-11512*#	NASA-CR-973 NASA-TN-D-4213 NASA-TN-D-4236
c05 N68-11510*# c17 N68-11511*# c06 N68-11512*# c10 N68-11513*#	NASA-CR-973 NASA-TN-D-4213 NASA-TN-D-4236 NASA-TN-D-4267
c05 N68-11510*# c17 N68-11511*# c06 N68-11512*# c10 N68-11513*# c02 N68-11519*#	NASA-CR-973 NASA-TN-D-4213 NASA-TN-D-4236
c05 N68-11510*# c17 N68-11511*# c06 N68-11512*# c10 N68-11513*# c02 N68-11519*#	NASA-CR-973 NASA-TN-D-4213 NASA-TN-D-4213 NASA-TN-D-4267 NASA-TN-D-4267 NASA-TN-D-4267
c05 N68-11510*# c17 N68-11511*# c06 N68-11512*# c10 N68-11513*# c02 N68-11513*# c31 N68-11520*#	NASA-CR-973 NASA-TN-D-4213 NASA-TN-D-4236 NASA-TN-D-4267 NASA-TN-D-4267 NASA-TN-D-4237 NASA-CR-974 SID-67-542-1
c05 N68-11510*# c17 N68-11511*# c06 N68-11512*# c10 N68-11513*# c02 N68-11513*# c31 N68-11520*#	NASA-CR-973 NASA-TN-D-4213 NASA-TN-D-4236 NASA-TN-D-4267 NASA-TN-D-4267 NASA-TN-D-4267 NASA-CR-974 SID-67-542-1
c05 N68-11510*# c17 N68-11511*# c06 N68-11512*# c10 N68-11513*# c02 N68-11513*# c31 N68-11520*# c21 N68-11521*#	NASA-CR-973 NASA-TN-D-4213 NASA-TN-D-4216 NASA-TN-D-4267 NASA-TN-D-4267 NASA-TN-D-4267 NASA-TN-D-4267 SID-67-542-1 NASA-CR-974 NASA-TN-D-4246
c05 N68-11510*# c17 N68-11511*# c06 N68-11512*# c10 N68-11513*# c02 N68-11513*# c31 N68-11520*# c21 N68-11521*# c17 N68-11522*#	NASA-CR-973 NASA-TN-D-4213 NASA-TN-D-4236 NASA-TN-D-4236 NASA-TN-D-4267 NASA-TN-D-4267 NASA-TN-D-4267 NASA-CR-974 SID-67-542-1 NASA-TN-D-4246 NASA-TN-D-4246 NASA-TN-D-4281 NASA-TN-D-4289 NASA-TN-D-4289
c05 N68-11510*# c17 N68-11511*# c06 N68-11512*# c02 N68-11513*# c02 N68-11513*# c31 N68-11520*# c21 N68-11521*# c17 N68-11522*# c02 N68-115451*# c06 N68-11621*# c08-11627*#	NASA-CR-973 NASA-TN-D-4213 NASA-TN-D-4216 NASA-TN-D-4267 NASA-TN-D-4267 NASA-TN-D-4267 NASA-TN-D-4267 NASA-TN-D-4267 SID-67-542-1 NASA-TN-D-4246 NASA-TN-D-4246 NASA-TN-D-4287 NASA-TN-D-4278
c05 N68-11510*# c17 N68-11511*# c06 N68-11512*# c02 N68-11513*# c02 N68-11519*# c31 N68-11521*# c21 N68-11521*# c17 N68-11522*# c02 N68-11621*# c02 N68-11627*# c03 N68-11627*# c30 N68-11630*#	NASA-CR-973 NASA-TN-D-4213 NASA-TN-D-4236 NASA-TN-D-4236 NASA-TN-D-4237 NASA-TN-D-4267 NASA-TN-D-4267 NASA-CR-974 SID-67-542-1 NASA-TN-D-4247 NASA-TN-D-4247 NASA-TN-D-4287 NASA-TN-D-4298 NASA-TN-D-4278 NASA-TN-D-4243
c05 N68-11510*# c17 N68-11511*# c06 N68-11512*# c10 N68-11513*# c02 N68-11513*# c31 N68-11520*# c21 N68-11521*# c17 N68-11522*# c02 N68-11545*# c02 N68-11642*# c03 N68-11630*# c30 N68-11634*#	NASA-CR-973 NASA-TN-D-4213 NASA-TN-D-4236 NASA-TN-D-4267 NASA-TN-D-4267 NASA-TN-D-4237 NASA-TN-D-4237 NASA-TN-D-4237 NASA-TN-D-4237 NASA-TN-D-4237 NASA-TN-D-4267 NASA-TN-D-4246 NASA-TN-D-4246 NASA-TN-D-4287 NASA-TN-D-4287 NASA-TN-D-4287 NASA-TN-D-4199 NASA-TN-D-4273 NASA-TN-D-4283 NASA-TN-D-4283 NASA-TN-D-4283 NASA-TN-D-4283 NASA-TN-D-4284 NASA-TN-D-4283 NASA-TN-D-4284 NASA-TN-D-4284 NASA-TN-D-4284 NASA-TN-D-4284 NASA-TN-D-4284 NASA-CR-967
c05 N68-11510*# c17 N68-11511*# c06 N68-11512*# c02 N68-11513*# c02 N68-11513*# c10 N68-11520*# c21 N68-11520*# c21 N68-11522*# c17 N68-11522*# c02 N68-11545*# c02 N68-11621*# c02 N68-11630*# c24 N68-11634*# c33 N68-11636*#	NASA-CR-973 NASA-TN-D-4213 NASA-TN-D-4236 NASA-TN-D-4267 NASA-TN-D-4267 NASA-TN-D-4267 NASA-TN-D-4267 NASA-TN-D-4267 NASA-TN-D-427 NASA-TN-D-4246 NASA-TN-D-4246 NASA-TN-D-4281 NASA-TN-D-428 NASA-TN-D-4278 NASA-TN-D-4278 NASA-TN-D-4278 NASA-TN-D-4278 NASA-TN-D-4278 NASA-TN-D-4278
<pre>c05 N68-11510*# c17 N68-11511*# c06 N68-11512*# c10 N68-11513*# c02 N68-11519*# c31 N68-11521*# c17 N68-11522*# c02 N68-11522*# c02 N68-11621*# c02 N68-11630*# c24 N68-11634*# c33 N68-11637*# c17 N68-11637*#</pre>	NASA-CR-973 NASA-TN-D-4213 NASA-TN-D-4236 NASA-TN-D-4236 NASA-TN-D-4237 NASA-TN-D-4267 NASA-TN-D-4267 NASA-TN-D-4267 NASA-TN-D-4267 NASA-TN-D-4243 NASA-TN-D-4287 NASA-TN-D-4287 NASA-TN-D-4287 NASA-TN-D-4278 NASA-TN-D-4243 NASA-TN-D-4243 NASA-TN-D-4243 NASA-TN-D-4243 NASA-TN-D-4243 NASA-TN-D-4243 NASA-TN-D-4243 NASA-TN-D-4243
<pre>c05 N68-11510*# c17 N68-11511*# c06 N68-11512*# c10 N68-11513*# c02 N68-11513*# c31 N68-11520*# c21 N68-11522*# c17 N68-11522*# c02 N68-11545*# c02 N68-11630*# c30 N68-11630*# c30 N68-11630*# c30 N68-11636*# c17 N68-11637*# c17 N68-11637*# c17 N68-11637*# c17 N68-11637*#</pre>	NASA-CR-973 NASA-TN-D-4213 NASA-TN-D-4236 NASA-TN-D-4267 NASA-TN-D-4267 NASA-TN-D-4237 NASA-TN-D-4237 NASA-TN-D-4237 NASA-TN-D-4237 NASA-TN-D-4267 NASA-TN-D-4246 NASA-TN-D-4246 NASA-TN-D-4246 NASA-TN-D-4287 NASA-TN-D-4287 NASA-TN-D-4287 NASA-TN-D-4287 NASA-TN-D-4287 NASA-TN-D-4287 NASA-TN-D-4287 NASA-TN-D-4287 NASA-TN-D-4284 NASA-TN-D-4243 NASA-TN-D-4243 NASA-TN-D-4243 NASA-TN-D-4243 NASA-TN-D-4243 NASA-TN-D-4243 NASA-TN-D-4243 NASA-TN-D-4261 NASA-TN-D-4261 NASA-TN-D-4261
<pre>c05 N68-11510*# c17 N68-11511*# c06 N68-11512*# c02 N68-11513*# c02 N68-11513*# c10 N68-11520*# c21 N68-11520*# c21 N68-11522*# c02 N68-11524*# c02 N68-11621*# c02 N68-11634*# c03 N68-11634*# c33 N68-11634*# c17 N68-11638*# c19 N68-11639*#</pre>	NASA-CR-973 NASA-TN-D-4213 NASA-TN-D-4236 NASA-TN-D-4236 NASA-TN-D-4267 NASA-TN-D-4267 NASA-TN-D-4267 NASA-TN-D-4267 NASA-TN-D-4267 NASA-TN-D-4267 NASA-TN-D-4267 NASA-TN-D-4267 NASA-TN-D-4268 NASA-TN-D-4287 NASA-TN-D-4278 NASA-TN-D-4278 NASA-TN-D-4278 NASA-TN-D-4278 NASA-TN-D-4274 NASA-TN-D-4247 NASA-TN-D-4274 NASA-TN-D-4274 NASA-TN-D-4274 NASA-TN-D-4274 NASA-TN-D-4274 NASA-TN-D-4274 NASA-TN-D-4274 NASA-TN-D-4274 NASA-TN-D-4274
<pre>c05 N68-11510*# c17 N68-11511*# c16 N68-11512*# c10 N68-11513*# c02 N68-11519*# c31 N68-11521*# c17 N68-11522*# c17 N68-11522*# c02 N68-11522*# c02 N68-11632*# c04 N68-11630*# c34 N68-11636*# c34 N68-11636*# c37 N68-11636*# c17 N68-11638*# c19 N68-11639*# c01 N68-11639*# c01 N68-11639*# c01 N68-11640*</pre>	NASA-CR-973 NASA-TN-D-4213 NASA-TN-D-4236 NASA-TN-D-4267 NASA-TN-D-4268 NASA-TN-D-4287 NASA-TN-D-4278 NASA-TN-D-4278 NASA-TN-D-4274 NASA-TN-D-4274 NASA-TN-D-4268 NASA-TN-D-4274 NASA-TN-D-4278 NASA-TN-D-4287 NASA-TN-D-4288 NASA-TN-D-4288 <tr< td=""></tr<>
<pre>c05 N68-11510*# c17 N68-11511*# c06 N68-11512*# c10 N68-11513*# c02 N68-11513*# c11 N68-11520*# c11 N68-11522*# c12 N68-11545*# c02 N68-11641*# c12 N68-11630*# c24 N68-11630*# c12 N68-11637*# c12 N68-11637*# c12 N68-11637*# c12 N68-11637*# c13 N68-11637*# c13 N68-11641*#</pre>	NASA-CR-973 NASA-TN-D-4213 NASA-TN-D-4236 NASA-TN-D-4267 NASA-TN-D-4267 NASA-TN-D-4237 NASA-TN-D-4237 NASA-TN-D-4237 NASA-TN-D-4237 NASA-TN-D-4267 NASA-TN-D-4267 NASA-TN-D-4248 NASA-TN-D-4287 NASA-TN-D-4287 NASA-TN-D-4287 NASA-TN-D-4287 NASA-TN-D-4287 NASA-TN-D-4243 NASA-TN-D-4243 NASA-TN-D-4243 NASA-TN-D-4243 NASA-TN-D-4243 NASA-TN-D-4243 NASA-TN-D-4243 NASA-TN-D-4243 NASA-TN-D-4274 NASA-TN-D-4272 NASA-TN-D-4272 NASA-TN-D-4272 NASA-TN-D-4273 NASA-TN-D-4274 NASA-TN-D-4280 NASA-TN-D-4280 NASA-TN-D-4280
<pre>c05 N68-11510*# c17 N68-11511*# c06 N68-11512*# c10 N68-11513*# c02 N68-11519*# c31 N68-11520*# c21 N68-11521*# c17 N68-11521*# c02 N68-11545*# c02 N68-11545*# c02 N68-11630*# c30 N68-11630*# c33 N68-11636*# c17 N68-11638*# c19 N68-11639*# c11 N68-11640*# c31 N68-11641*# c31 N68-11642*#</pre>	NASA-CR-973 NASA-TN-D-4213 NASA-TN-D-4236 NASA-TN-D-4267 NASA-TN-D-4267 NASA-TN-D-4237 NASA-TN-D-4267 NASA-TN-D-4237 NASA-TN-D-4267 NASA-TN-D-4267 NASA-TN-D-4267 NASA-TN-D-4267 NASA-TN-D-4268 NASA-TN-D-4287 NASA-TN-D-4287 NASA-TN-D-4287 NASA-TN-D-4272 NASA-TN-D-4261 NASA-TN-D-4261 NASA-TN-D-4272 NASA-TN-D-4272 NASA-TN-D-4258 NASA-TN-D-4258
<pre>c05 N68-11510*# c17 N68-11511*# c06 N68-11512*# c02 N68-11512*# c02 N68-11519*# c17 N68-11521*# c17 N68-11522*# c02 N68-11521*# c02 N68-11621*# c02 N68-11630*# c24 N68-11630*# c24 N68-11630*# c17 N68-11638*# c19 N68-11638*# c19 N68-11638*# c11 N68-11640* c31 N68-11644*# c33 N68-11644*#</pre>	NASA-CR-973 NASA-TN-D-4213 NASA-TN-D-4236 NASA-TN-D-4267 NASA-TN-D-4267 NASA-TN-D-4267 NASA-TN-D-4267 NASA-TN-D-4267 NASA-TN-D-4267 NASA-TN-D-4267 NASA-TN-D-4267 NASA-TN-D-4267 NASA-TN-D-4287 NASA-TN-D-4287 NASA-TN-D-4287 NASA-TN-D-4287 NASA-TN-D-4280 NASA-TN-D-4272 NASA-TN-D-4280 NASA-TN-D-4271 NASA-TN-D-4272 NASA-TN-D-4280
<pre>c05 N68-11510*# c17 N68-11511*# c10 N68-11512*# c10 N68-11512*# c12 N68-11520*# c21 N68-11520*# c17 N68-11522*# c17 N68-11545*# c02 N68-11621*# c02 N68-11630*# c30 N68-11634*# c33 N68-11637*# c17 N68-11637*# c19 N68-11637*# c19 N68-11637*# c19 N68-11637*# c11 N68-11643*# c11 N68-11644*# c31 N68-11644*# c31 N68-11644*# c31 N68-11644*# c31 N68-11644*# c37 N68-1</pre>	NASA-CR-973 NASA-TN-D-4213 NASA-TN-D-4236 NASA-TN-D-4267 NASA-TN-D-4267 NASA-TN-D-4267 NASA-TN-D-4267 NASA-TN-D-4267 NASA-TN-D-4267 NASA-TN-D-4267 NASA-TN-D-4267 NASA-TN-D-4261 NASA-TN-D-4274 NASA-TN-D-4287 NASA-TN-D-4287 NASA-TN-D-4287 NASA-TN-D-4284 NASA-TN-D-4243 NASA-TN-D-4243 NASA-TN-D-4243 NASA-TN-D-4243 NASA-TN-D-4243 NASA-TN-D-4243 NASA-TN-D-4243 NASA-TN-D-4274 NASA-TN-D-4276 NASA-TN-D-4286 NASA-TN-D-4280 NASA-TN-D-4280 NASA-TN-D-4280 NASA-TN-D-4280 NASA-TN-D-4286 NASA-TN-D-4286 NASA-TN-D-4286 NASA-TN-D-4286
<pre>c05 N68-11510*# c17 N68-11511*# c06 N68-11512*# c10 N68-11512*# c12 N68-11520*# c21 N68-11520*# c21 N68-11522*# c02 N68-11545*# c02 N68-11545*# c02 N68-11630*# c22 N68-11630*# c30 N68-11630*# c19 N68-11630*# c19 N68-11630*# c19 N68-11630*# c11 N68-11643*# c33 N68-11641*# c33 N68-11641*# c33 N68-11641*# c33 N68-11641*# c33 N68-11641*# c33 N68-11641*# c17 N68-1174*# c17</pre>	NASA-CR-973 NASA-TN-D-4213 NASA-TN-D-4236 NASA-TN-D-4267 NASA-TN-D-4267 NASA-TN-D-4267 NASA-TN-D-4267 NASA-TN-D-4267 NASA-TN-D-4267 NASA-TN-D-4267 NASA-TN-D-4267 NASA-TN-D-4267 NASA-TN-D-4276 NASA-TN-D-4287 NASA-TN-D-4278 NASA-TN-D-4278 NASA-TN-D-4278 NASA-TN-D-4278 NASA-TN-D-4274 NASA-TN-D-4274 NASA-TN-D-4274 NASA-TN-D-4274 NASA-TN-D-4274 NASA-TN-D-4274 NASA-TN-D-4274 NASA-TN-D-4274 NASA-TN-D-4275 NASA-TN-D-4286 NASA-TN-D-4250 NASA-TN-D-4250 NASA-TN-D-4268 NASA-TN-D-4286 NASA-TN-D-4286 NASA-TN-D-4155
<pre>c05 N68-11510*# c17 N68-11511*# c10 N68-11512*# c10 N68-11512*# c12 N68-11520*# c21 N68-11520*# c17 N68-11522*# c17 N68-11545*# c02 N68-11621*# c02 N68-11630*# c30 N68-11634*# c33 N68-11637*# c17 N68-11637*# c19 N68-11637*# c19 N68-11637*# c19 N68-11637*# c11 N68-11643*# c11 N68-11644*# c31 N68-11644*# c31 N68-11644*# c31 N68-11644*# c31 N68-11644*# c37 N68-1</pre>	NASA-CR-973 NASA-TN-D-4213 NASA-TN-D-4236 NASA-TN-D-4236 NASA-TN-D-4267 NASA-TN-D-4267 NASA-TN-D-4267 NASA-TN-D-4267 NASA-TN-D-4267 NASA-TN-D-4267 NASA-TN-D-4267 NASA-TN-D-4267 NASA-TN-D-4274 NASA-TN-D-4287 NASA-TN-D-4287 NASA-TN-D-4278 NASA-TN-D-4278 NASA-TN-D-4274 NASA-TN-D-4274 NASA-TN-D-4274 NASA-TN-D-4274 NASA-TN-D-4274 NASA-TN-D-4274 NASA-TN-D-4274 NASA-TN-D-4274 NASA-TN-D-4274 NASA-TN-D-4275 NASA-TN-D-4280 NASA-TN-D-4280 NASA-TN-D-4280 NASA-TN-D-4280 NASA-TN-D-4260 NASA-TN-D-4260 NASA-TN-D-4260 NASA-TN-D-4265 NASA-TN-D-4265 NASA-TN-D-4265 NASA-TN-D-4265 NASA-TN-D-4265 NASA-TN-D-4265
<pre>c05 N68-11510*# c17 N68-11511*# c06 N68-11512*# c02 N68-11512*# c02 N68-11520*# c17 N68-11522*# c17 N68-11522*# c02 N68-11545*# c02 N68-11621*# c02 N68-11630*# c24 N68-11630*# c24 N68-11630*# c17 N68-11630*# c17 N68-11638*# c19 N68-11639*# c19 N68-11649* c31 N68-11640* c31 N68-11640* c31 N68-11640* c31 N68-11640*# c33 N68-11642*# c17 N68-11644*# c33 N68-11644*# c33 N68-11645*# c13 N68-11645*# c13 N68-11645*# c13 N68-1174*# c33 N68-1174*# c33 N68-11721*#</pre>	NASA-CR-973 NASA-TN-D-4213 NASA-TN-D-4236 NASA-TN-D-4267 NASA-TN-D-4267 NASA-TN-D-4267 NASA-TN-D-4267 NASA-TN-D-4267 NASA-TN-D-4267 NASA-TN-D-4267 NASA-TN-D-4267 NASA-TN-D-4287 NASA-TN-D-4287 NASA-TN-D-4287 NASA-TN-D-4199 NASA-TN-D-4243 NASA-TN-D-4286 NASA-TN-D-4274 NASA-TN-D-4274 NASA-TN-D-4274 NASA-TN-D-4274 NASA-TN-D-4274 NASA-TN-D-4274 NASA-TN-D-4274 NASA-TN-D-4274 NASA-TN-D-4276 NASA-TN-D-4276 NASA-TN-D-4276 NASA-TN-D-4286 NASA-TN-D-4286 NASA-TN-D-4286 NASA-TN-D-4286 NASA-TN-D-4286 NASA-TN-D-4286 NASA-TN-D-4286 NASA-TN-D-4355 NASA-TN-D-4365
<pre>c05 N68-11510*# c17 N68-11511*# c06 N68-11512*# c10 N68-11512*# c12 N68-11520*# c21 N68-11520*# c21 N68-11522*# c17 N68-11522*# c02 N68-11545*# c02 N68-11630*# c20 N68-11630*# c30 N68-11630*# c17 N68-11630*# c19 N68-11630*# c19 N68-11630*# c19 N68-11643*# c11 N68-11641*# c33 N68-11642*# c17 N68-11642*# c17 N68-11645*# c13 N68-11645*# c13 N68-11645*# c13 N68-1174*# c33 N68-11721*# c30 N68-11754*# c30 N68-11754*#</pre>	NASA-CR-973 NASA-TN-D-4213 NASA-TN-D-4236 NASA-TN-D-4267 NASA-TN-D-4267 NASA-TN-D-4237 NASA-TN-D-4237 NASA-TN-D-4267 NASA-TN-D-4237 NASA-TN-D-4267 NASA-TN-D-4267 NASA-TN-D-4287 NASA-TN-D-4287 NASA-TN-D-4287 NASA-TN-D-4287 NASA-TN-D-4287 NASA-TN-D-4243 NASA-TN-D-4243 NASA-TN-D-4243 NASA-TN-D-4287 NASA-TN-D-4243 NASA-TN-D-4243 NASA-TN-D-4243 NASA-TN-D-4243 NASA-TN-D-4274 NASA-TN-D-4272 NASA-TN-D-4272 NASA-TN-D-4272 NASA-TN-D-4272 NASA-TN-D-4276 NASA-TN-D-4258 NASA-TN-D-4258 NASA-TN-D-4258 NASA-TN-D-4286 NASA-TN-D-4286 NASA-TN-D-4286 NASA-TN-D-4286 NASA-TN-D-4286 NASA-TN-D-4286 NASA-TN-D-4286 <tr< td=""></tr<>
<pre>c05 N68-11510*# c17 N68-11511*# c16 N68-11512*# c10 N68-11513*# c12 N68-11513*# c17 N68-11521*# c17 N68-11522*# c17 N68-11522*# c17 N68-11522*# c02 N68-11632*# c02 N68-11630*# c30 N68-11636*# c31 N68-11636*# c17 N68-11636*# c19 N68-11636*# c19 N68-11636*# c11 N68-11640* c31 N68-11642*# c13 N68-11644*# c27 N68-11644*# c13 N68-11644*# c13 N68-11644*# c33 N68-11724*# c30 N68-11724*# c30 N68-11725*#</pre>	NASA-CR-973 NASA-TN-D-4213 NASA-TN-D-4236 NASA-TN-D-4236 NASA-TN-D-4267 NASA-TN-D-4267 NASA-TN-D-4267 NASA-TN-D-4267 NASA-TN-D-4267 NASA-TN-D-4267 NASA-TN-D-4267 NASA-TN-D-4267 NASA-TN-D-4271 NASA-TN-D-4267 NASA-TN-D-4287 NASA-TN-D-4287 NASA-TN-D-4278 NASA-TN-D-4278 NASA-TN-D-4274 NASA-TN-D-4275 NASA-TN-D-4276 NASA-TN-D-4276 NASA-TN-D-4276 NASA-TN-D-4281 NASA-TN-D-4281
<pre>c05 N68-11510*# c17 N68-11511*# c10 N68-11512*# c10 N68-11512*# c12 N68-11520*# c21 N68-11522*# c17 N68-11522*# c17 N68-11522*# c02 N68-11631*# c02 N68-11631*# c24 N68-11630*# c31 N68-11636*# c17 N68-11636*# c19 N68-11630*# c19 N68-11630*# c11 N68-11640* c31 N68-11640* c31 N68-11640*# c31 N68-11640*# c31 N68-11640*# c31 N68-11640*# c31 N68-11645*# c13 N68-1174*# c33 N68-1174*# c30 N68-11774*# c30 N68-11774*# c30 N68-11774*# c02 N68-11774*# c02 N68-11774*# c03 N68-11774*# c04 N68-11774*# c04 N68-11774*# c05 N68-11774*# c05 N68-11774*# c06 N68-11774*# c06 N68-11774*# c06 N68-11774*# c07 N68-1174*# c07 N68-11</pre>	NASA-CR-973 NASA-TN-D-4213 NASA-TN-D-4236 NASA-TN-D-4267 NASA-TN-D-4267 NASA-TN-D-4267 NASA-TN-D-4267 NASA-TN-D-4267 NASA-TN-D-4267 NASA-CR-974 SID-67-542-1 NASA-TN-D-4287 NASA-TN-D-4287 NASA-TN-D-4287 NASA-TN-D-4287 NASA-TN-D-4199 NASA-TN-D-4274 NASA-TN-D-4280 NASA-TN-D-4280 NASA-TN-D-4280 NASA-TN-D-4280 NASA-TN-D-4281 NASA-TN-D-4286 NASA-TN-D-4286 NASA-TN-D-4286 NASA-TN-D-4286 NASA-TN-D-4286 NASA-TN-D-4288
<pre>c05 N68-11510*# c17 N68-11511*# c16 N68-11512*# c10 N68-11513*# c12 N68-11513*# c17 N68-11521*# c17 N68-11522*# c17 N68-11522*# c17 N68-11522*# c02 N68-11632*# c02 N68-11630*# c30 N68-11636*# c31 N68-11636*# c17 N68-11636*# c19 N68-11636*# c19 N68-11636*# c11 N68-11640* c31 N68-11642*# c13 N68-11644*# c27 N68-11644*# c13 N68-11644*# c13 N68-11644*# c33 N68-11724*# c30 N68-11724*# c30 N68-11725*#</pre>	NASA-CR-973 NASA-TN-D-4213 NASA-TN-D-4236 NASA-TN-D-4267 NASA-TN-D-4267 NASA-TN-D-4267 NASA-TN-D-4267 NASA-TN-D-4267 NASA-TN-D-4267 NASA-TN-D-4267 NASA-TN-D-4267 NASA-TN-D-4267 NASA-TN-D-4287 NASA-TN-D-4287 NASA-TN-D-4287 NASA-TN-D-4287 NASA-TN-D-4287 NASA-TN-D-4287 NASA-TN-D-4287 NASA-TN-D-4287 NASA-TN-D-4280 NASA-TN-D-4274 NASA-TN-D-4280 NASA-TN-D-4280 NASA-TN-D-4280 NASA-TN-D-4281 NASA-TN-D-4285 NASA-TN-D-4286 NASA-TN-D-4281 NASA-TN-D-4285 NASA-TN-D
<pre>c05 N68-11510*# c17 N68-11511*# c10 N68-11512*# c10 N68-11512*# c10 N68-11522*# c31 N68-11522*# c31 N68-11522*# c17 N68-11522*# c02 N68-11622*# c02 N68-11627*# c02 N68-11637*# c03 N68-11637*# c17 N68-11637*# c17 N68-11637*# c19 N68-11637*# c19 N68-11637*# c11 N68-11640*# c31 N68-11640*# c31 N68-11642*# c17 N68-11642*# c17 N68-11642*# c17 N68-11642*# c13 N68-11642*# c13 N68-11642*# c13 N68-11642*# c13 N68-11642*# c13 N68-11642*# c13 N68-11714*# c33 N68-11714*# c33 N68-1172*# c30 N68-1172*# c30 N68-11728*# c30 N68-1172*# c33 N68-1178*# c33 N68-118*# c33 N68-118*# c33 N68-118*# c33 N68-118*# c33 N68-118*# c33 N68-118*# c33 N68</pre>	NASA-CR-973 NASA-TN-D-4213 NASA-TN-D-4236 NASA-TN-D-4237 NASA-TN-D-4237 NASA-TN-D-4237 NASA-TN-D-4237 NASA-TN-D-4237 NASA-TN-D-4237 SID-67-542-1 NASA-TN-D-4237 NASA-TN-D-4237 NASA-TN-D-4237 NASA-TN-D-4287 NASA-TN-D-4287 NASA-TN-D-4287 NASA-TN-D-4278 NASA-TN-D-4278 NASA-TN-D-4278 NASA-TN-D-4278 NASA-TN-D-4274 NASA-TN-D-4280 NASA-TN-D-4280 NASA-TN-D-4280 NASA-TN-D-4280 NASA-TN-D-4281 NASA-TN-D-4281 NASA-TN-D-4281 NASA-TN-D-4281 NASA-TN-D-4281 NASA-TN-D-4281 NASA-TN-D-4

A Selected Listing

c22 N68-15643*#	••••••••••••••••••••••••••••••••••••••
c28 N68-15644*#	NASA-TM-X-1511
c09 N68-15649*#	NASA-TM-X-1495
c30 N68-15683*#	NASA-SP-6503
c30 N68-15725*#	D2-100753-2, V. 2
	NASA-CR-984
c30 N68-15741*#	NASA-CR-1005
	SID-65-1200-6
c33 N68-15742*#	NASA-TN-D-4353
c01 N68-15743*#	
c25 N68-15747*#	
c30 N68-15748*#	NASA-SP-155
c32 N68-15769*#	NASA-TN-D-4350
c11 N68-15777*#	NASA-CR-982
	PIFR-051
c01 N68-15778*#	NASA-TN-D-4397
c22 N68-15792*#	NASA-TN-D-4371
c30 N68-15793*#	NASA-TN-D-4292
c32 N68-15796*#	NASA-TT-F-513
c08 N68-15798*#	••••••••••••••••••••••••••••••••••••••
c33 N68-15833*#	NASA-CR-920
c22 N68-15855*#	NASA-TM-X-1509
c11 N68-15858*#	NASA-TN-D-4276
c30 N68-15891*#	NASA-SP-149
c09 N68-15892*#	NASA-CR-994
c14 N68-15893*#	NASA-TN-D-4339
c02 N68-15894*#	NASA-TN-D-4322
c04 N68-15899*#	NASA-SP-7011/44/
c05 N68-15901*#	NASA-SP-144
c14 N68-15936*#	NASA-TN-D-4242
c02 N68-15941*#	••••••••••••••••••••••••••••••••••••••
c33 N68-15942*#	••••••••••••••••••••••••••••••••••••••
c03 N68-15943*#	NASA-TN-D-4384
c23 N68-15950*#	NASA-TN-D-4293
c29 N68-16008*#	NASA-TN-D-4311
c31 N68-16015*#	NASA-SP-156
c22 N68-16056*#	NASA-TM-X-1496
c30 N68-16103*#	NASA-CR-1000
	SID-65-1200-1
c12 N68-16227*#	NASA-TN-D-4417
c03 N68-16228*#	NASA-TN-D-4383
c31 N68-16240*#	NASA-TN-D-4337
c25 N68-16286*#	NASA-TT-F-460
c01 N68-16299*#	NASA-TM-X-1498
c33 N68-16300*#	NASA-TM-X-1510
c03 N68-16321*#	NASA-CR-965
	SM-48461-F
c33 N68-16324*#	SM-48461-F NASA-TN-D-4411
c33 N68-16324*# c03 N68-16351*#	NASA-TN-D-4411
c03 N68-16351*#	NASA-TN-D-4411 NASA-CR-925
c03 N68-16351*# c28 N68-16413*#	NASA-TN-D-4411 NASA-CR-925 NASA-TN-D-4392
c03 N68-16351*# c28 N68-16413*# c03 N68-16439*#	NASA-TN-D-4411 NASA-CR-925 NASA-TN-D-4392 NASA-CR-922
c03 N68-16351*# c28 N68-16413*# c03 N68-16439*# c15 N68-16468*#	NASA-TN-D-4411 NASA-CR-925 NASA-TN-D-4392 NASA-TN-D-4352 NASA-TN-D-4355
c03 N68-16351*# c28 N68-16413*# c03 N68-16439*# c15 N68-16468*# c03 N68-16468*#	NASA-TN-D-4411 NASA-CR-925 NASA-TN-D-4392 NASA-TN-D-4392 NASA-TN-D-4355 NASA-TN-D-4382
c03 N68-16351*# c28 N68-16413*# c03 N68-16439*# c15 N68-16468*#	NASA-TN-D-4411 NASA-CR-925 NASA-TN-D-4392 NASA-TN-D-4352 NASA-TN-D-4355 NASA-TN-D-4355 NASA-TN-D-4362 NASA-TN-D-4362 NASA-TN-D-4362 NASA-TN-D-4362
c03 N68-16351*# c28 N68-16413*# c03 N68-16439*# c15 N68-16469*# c03 N68-16469*# c22 N68-16478*#	NASA-TN-D-4411 NASA-CR-925 NASA-CR-922 NASA-CR-922 NASA-TN-D-4355 NASA-TN-D-4355 NASA-TN-D-4355 NASA-TN-D-4362 F-910091-10 NASA-CR-991
c03 N68-16351*# c28 N68-16413*# c03 N68-16439*# c15 N68-16469*# c03 N68-16469*# c22 N68-16478*#	NASA-TN-D-4411 NASA-CR-925 NASA-TN-D-4392 NASA-TN-D-4392 NASA-TN-D-4392 NASA-TN-D-4355 NASA-TN-D-4382 F-910091-10 NASA-CR-991 NASA-TM-Z-1491
c03 N68-16351*# c28 N68-16413*# c03 N68-16439*# c15 N68-16468*# c03 N68-16468*# c22 N68-16478*# c01 N68-16480*# c04 N68-16517*#	NASA-TN-D-4411 NASA-TN-D-4312 NASA-CR-925 NASA-CR-922 NASA-CR-922 NASA-TN-D-4355 NASA-TN-D-4355 NASA-TN-D-4352 NASA-TN-D-4352 NASA-TN-D-4352 NASA-CR-910091-10 NASA-CR-991 NASA-TN-X-1491 NASA-SP-7011/45/
c03 N68-16351*# c28 N68-16413*# c03 N68-16439*# c15 N68-16468*# c03 N68-16469*# c22 N68-16478*# c01 N68-16480*# c04 N68-16517*# c02 N68-16522*#	NASA-TN-D-4411 NASA-TN-D-4311 NASA-CR-925 NASA-CR-925 NASA-CR-925 NASA-TN-D-4355 NASA-TN-D-4355 NASA-TN-D-4365 NASA-CR-921 NASA-TN-D-4355 NASA-TN-D-4355 NASA-TN-D-4355 NASA-TN-D-4351 NASA-TN-D-4353 NASA-TN-D-4353
c03 N68-16351*# c28 N68-16413*# c15 N68-16439*# c15 N68-16469*# c22 N68-16469*# c22 N68-16478*# c01 N68-16480*# c04 N68-16517*# c02 N68-16522*#	NASA-TN-D-4411 NASA-TN-D-4312 NASA-CR-925 NASA-CR-922 NASA-CR-922 NASA-TN-D-4355 NASA-TN-D-4355 NASA-TN-D-4352 NASA-TN-D-4352 NASA-TN-D-4352 NASA-CR-910091-10 NASA-CR-991 NASA-TN-X-1491 NASA-SP-7011/45/
c03 N68-16351*# c28 N68-16413*# c03 N68-16439*# c15 N68-16468*# c03 N68-16468*# c22 N68-16468*# c22 N68-16478*# c01 N68-16517*# c02 N68-16522*# c14 N68-16529*#	NASA-TN-D-4411 NASA-CR-925 NASA-CR-325 NASA-CR-322 NASA-CR-322 NASA-CR-322 NASA-TN-D-4355 NASA-TN-D-4355 NASA-CR-921 NASA-TN-D-4355 NASA-TN-D-4350 NASA-CR-991 NASA-CR-991 NASA-TM-X-1491 NASA-SP-7011/45/ NASA-TN-D-4354
c03 N68-16351+# c28 N68-16413*# c03 N68-16439*# c15 N68-16469*# c22 N68-16469*# c22 N68-16469*# c01 N68-16480*# c04 N68-16517*# c02 N68-16522*# c14 N68-16529*# c19 N68-16530*#	NASA-TN-D-4411 NASA-TN-D-4312 NASA-CR-925 NASA-CR-922 NASA-TN-D-4352 NASA-TN-D-4352 NASA-TN-D-4352 NASA-TN-D-4362 NASA-TN-D-4362 NASA-TN-D-4362 NASA-TN-D-4362 NASA-TM-TN-1491 NASA-TM-X-1491 NASA-SP-7011/45/ NASA-TN-D-4330 NASA-TN-D-4360
c03 N68-16351*# c28 N68-16413*# c03 N68-16439*# c15 N68-16469*# c03 N68-16469*# c22 N68-16478*# c01 N68-16480*# c04 N68-16517*# c02 N68-16522*# c14 N68-16529*# c09 N68-16594*#	NASA-TN-D-4411 NASA-TN-D-4312 NASA-CR-925 NASA-CR-922 NASA-TN-D-4352 NASA-TN-D-4355 NASA-TN-D-4355 NASA-TN-D-4355 NASA-TN-D-4355 NASA-TN-D-4362 NASA-TN-D-4362 NASA-TM-Z-101 NASA-TM-X-1491 NASA-TN-D-4330 NASA-TN-D-4330 NASA-TN-D-4360 NASA-TN-D-4313
c03 N68-16351*# c28 N68-16413*# c03 N68-16439*# c15 N68-16469*# c22 N68-16469*# c22 N68-16469*# c01 N68-16478*# c01 N68-16517*# c02 N68-16522*# c14 N68-16522*# c09 N68-16530*# c05 N68-16533*#	NASA-TN-D-4411 NASA-CR-925 NASA-CR-925 NASA-CR-922 NASA-CR-922 NASA-TN-D-4352 NASA-TN-D-4355 NASA-TN-D-4382 NASA-TN-D-4382 NASA-SP-7011/45/ NASA-SP-7011/45/ NASA-TN-D-4354 NASA-TN-D-4354 NASA-TN-D-4312 NASA-T
c03 N68-16351*# c28 N68-16413*# c03 N68-16439*# c15 N68-16469*# c22 N68-16469*# c22 N68-16478*# c04 N68-16478*# c04 N68-16517*# c02 N68-16522*# c14 N68-16529*# c05 N68-16524*# c05 N68-16632*# c03 N68-16631*# c28 N68-16632*#	NASA-TN-D-4411 NASA-TN-D-4312 NASA-CR-925 NASA-CR-922 NASA-TN-D-4352 NASA-TN-D-4355 NASA-TN-D-4355 NASA-TN-D-4352 NASA-TN-D-4352 NASA-TN-D-4352 NASA-TN-D-4362 NASA-TN-X-1491 NASA-TN-D-4330 NASA-TN-D-4330 NASA-TN-D-4330 NASA-TN-D-4330 NASA-TN-D-4330 NASA-TN-D-4330 NASA-TN-D-43430 NASA-TN-D-43430 NASA-TN-D-43430 NASA-TN-D-43430 NASA-TN-D-43430 NASA-TN-D-44313 NASA-TN-D-44348 NASA-TN-D-4418
c03 N68-16351*# c28 N68-16413*# c03 N68-16439*# c15 N68-16463*# c22 N68-16463*# c22 N68-16478*# c04 N68-16478*# c04 N68-16517*# c02 N68-16522*# c14 N68-16529*# c05 N68-1653*# c05 N68-16634*# c03 N68-16631*# c28 N68-16632*#	NASA-TN-D-4411 NASA-TN-D-4312 NASA-CR-925 NASA-CR-922 NASA-TN-D-4352 NASA-TN-D-4352 NASA-TN-D-4352 NASA-TN-D-4352 NASA-TN-D-4352 NASA-TN-D-4352 NASA-TN-D-4362 NASA-TN-X-1491 NASA-TN-D-4330 NASA-TN-D-4330 NASA-TN-D-4330 NASA-TN-D-4330 NASA-TN-D-4330 NASA-TN-D-4330 NASA-TN-D-4330 NASA-TN-D-4360 NASA-TN-D-4313 NASA-TN-D-44316 NASA-TN-D-4418
<pre>c03 N68-16351*# c28 N68-16413*# c03 N68-16439*# c15 N68-16469*# c22 N68-16469*# c22 N68-16478*# c01 N68-16478*# c04 N68-16512*# c02 N68-16522*# c14 N68-16522*# c09 N68-16530*# c05 N68-16594*# c18 N68-16623*# c03 N68-16631*# c23 N68-16632*#</pre>	NASA-TN-D-4411 NASA-CR-925 NASA-CR-925 NASA-CR-925 NASA-CR-925 NASA-CR-925 NASA-CR-925 NASA-TN-D-4355 NASA-TN-D-4355 NASA-TN-D-4362 NASA-TN-D-4363 NASA-CR-991 NASA-CR-991 NASA-TN-X-1491 NASA-TN-D-4330 NASA-TN-D-4364 NASA-TN-D-4313 NASA-TN-D-4313 NASA-TN-D-4312 NASA-TN-D-4313
<pre>c03 N68-16351*# c28 N68-16413*# c03 N68-16439*# c15 N68-16463*# c22 N68-16469*# c22 N68-16469*# c04 N68-16480*# c04 N68-16517*# c02 N68-16522*# c14 N68-16529*# c05 N68-16524*# c18 N68-16631*# c03 N68-16631*# c03 N68-16632*# c13 N68-16695*# c11 N68-16695*# c15 N68-16700*#</pre>	NASA-TN-D-4411 NASA-TN-D-4312 NASA-CR-925 NASA-CR-922 NASA-TN-D-4352 NASA-TN-D-4352 NASA-TN-D-4352 NASA-TN-D-4352 NASA-TN-D-4352 NASA-TN-D-4362 NASA-TN-D-4362 NASA-TN-D-4362 NASA-TN-D-4362 NASA-TN-D-4330 NASA-TN-D-4333 NASA-TN-D-4336 NASA-TN-D-4386 NASA-TN-D-4318 NASA-TN-D-4318 NASA-TN-D-4318 NASA-TN-D-4318 NASA-TN-D-4318 NASA-TN-D-4318 NASA-TN-D-4318
<pre>c03 N68-16351*# c28 N68-16413*# c03 N68-16439*# c15 N68-16469*# c22 N68-16469*# c22 N68-16478*# c04 N68-16478*# c04 N68-16512*# c05 N68-16522*# c14 N68-16522*# c14 N68-16529*# c05 N68-16530*# c05 N68-16534*# c18 N68-16632*# c33 N68-16632*# c33 N68-16632*# c11 N68-16695*# c11 N68-16695*# c10 N68-1670*# c10 N68-1670*#</pre>	NASA-TN-D-4411 NASA-TN-D-4312 NASA-CR-925 NASA-CR-922 NASA-TN-D-4352 NASA-TN-D-4352 NASA-TN-D-4352 NASA-TN-D-4352 NASA-TN-D-4352 NASA-TN-D-4362 NASA-TN-D-4362 NASA-TN-D-4362 NASA-TN-D-4362 NASA-TN-D-4330 NASA-TN-D-4333 NASA-TN-D-4336 NASA-TN-D-4386 NASA-TN-D-4318 NASA-TN-D-4318 NASA-TN-D-4318 NASA-TN-D-4318 NASA-TN-D-4318 NASA-TN-D-4318 NASA-TN-D-4318
c03 N68-16351+# c28 N68-16413*# c03 N68-16463*# c03 N68-16468*# c03 N68-16469*# c22 N68-16469*# c01 N68-16467*# c01 N68-16522*# c02 N68-16522*# c02 N68-16522*# c03 N68-16530*# c03 N68-16633*# c03 N68-16633*# c18 N68-16623*# c18 N68-16623*# c13 N68-16633*# c13 N68-16633*# c13 N68-16635*# c25 N68-16700*# c10 N68-16750*#	NASA-TN-D-4411 NASA-TN-D-4312 NASA-CR-925 NASA-CR-922 NASA-TN-D-4352 NASA-TN-D-4355 NASA-TN-D-4362 NASA-TN-D-4362 NASA-TN-D-4362 NASA-TN-D-4362 NASA-TN-D-4364 NASA-TN-D-4364 NASA-TN-D-4364 NASA-TN-D-4354 NASA-TN-D-4354 NASA-TN-D-4354 NASA-TN-D-4354 NASA-TN-D-4354 NASA-TN-D-4364 NASA-TN-D-4366 NASA-TN-D-4312 NASA-TN-D-4312
<pre>c03 N68-16351*# c28 N68-16413*# c03 N68-16439*# c15 N68-16463*# c22 N68-16468*# c22 N68-16468*# c04 N68-16480*# c04 N68-16517*# c02 N68-16522*# c14 N68-16529*# c05 N68-16529*# c05 N68-1653*# c05 N68-16631*# c03 N68-16631*# c13 N68-16632*# c13 N68-16635*# c11 N68-16655*# c11 N68-16700*# c10 N68-16750*# c21 N68-16750*# c21 N68-16750*#</pre>	NASA-TN-D-4411 NASA-CR-925 NASA-TN-D-4392 NASA-TN-D-4352 NASA-TN-D-4352 NASA-TN-D-4352 NASA-TN-D-4352 NASA-TN-D-4352 NASA-TN-D-4352 NASA-TN-D-4362 NASA-TN-D-4362 NASA-TN-D-4362 NASA-TN-D-4313 NASA-TN-D-4300 NASA-TN-D-4300 NASA-TN-D-4300 NASA-TN-D-4313 NASA-TN-D-4313 NASA-TN-D-4316 NASA-TN-D-4316 NASA-TN-D-4317 NASA-TN-D-4318 NASA-TN-D-4312 NASA-TN-D-4312 NASA-TN-D-4312 NASA-TN-D-4312
<pre>c03 N68-16351*# c28 N68-16413*# c03 N68-16439*# c15 N68-16463*# c22 N68-16468*# c22 N68-16468*# c04 N68-16480*# c04 N68-16517*# c02 N68-16522*# c14 N68-16529*# c05 N68-16529*# c05 N68-1653*# c05 N68-16631*# c03 N68-16631*# c13 N68-16632*# c13 N68-16635*# c11 N68-16655*# c11 N68-16700*# c10 N68-16750*# c21 N68-16750*# c21 N68-16750*#</pre>	NASA-TN-D-4411 NASA-CR-925 NASA-TN-D-4392 NASA-TN-D-4352 NASA-TN-D-4352 NASA-TN-D-4352 NASA-TN-D-4352 NASA-TN-D-4362 NASA-TN-D-4362 NASA-TN-D-4362 NASA-TN-D-4362 NASA-TN-D-4362 NASA-TN-D-4362 NASA-TN-D-4362 NASA-TN-D-4330 NASA-TN-D-4313 NASA-TN-D-4418 NASA-TN-D-4312 NASA-TN-D-4312 NASA-TN-D-4312 NASA-TN-D-4312
<pre>c03 N68-16351*# c28 N68-16413*# c03 N68-16439*# c15 N68-16469*# c22 N68-16469*# c22 N68-16478*# c04 N68-16478*# c04 N68-16512*# c05 N68-16522*# c14 N68-16522*# c14 N68-16529*# c05 N68-16530*# c05 N68-16631*# c18 N68-16632*# c33 N68-16632*# c11 N68-16635*# c11 N68-16655*# c10 N68-1670*# c28 N68-1670*# c21 N68-16836*# c21 N68-16836*# c21 N68-16836*#</pre>	NASA-TN-D-4411 NASA-CR-925 NASA-TN-D-4392 NASA-CR-922 NASA-TN-D-4355 NASA-TN-D-4355 NASA-TN-D-4352 NASA-TN-D-4362 NASA-TN-D-4362 NASA-TN-D-4362 NASA-TN-D-4362 NASA-TN-D-4362 NASA-TN-D-4362 NASA-TN-D-4362 NASA-TN-D-4362 NASA-TN-D-4330 NASA-TN-D-4330 NASA-TN-D-4330 NASA-TN-D-4330 NASA-TN-D-4330 NASA-TN-D-4330 NASA-TN-D-4330 NASA-TN-D-4330 NASA-TN-D-4330 NASA-TN-D-4313 NASA-TN-D-4307 NASA-TN-D-4307 NASA-TN-D-4312 NASA-TN-D-4131 NASA-TN-D-4131 NASA-TN-D-4131 NASA-TN-D-4131 NASA-TN-D-4404
<pre>c03 N68-16351*# c28 N68-16413*# c03 N68-16439*# c15 N68-16469*# c22 N68-16469*# c22 N68-16478*# c04 N68-16478*# c04 N68-16512*# c05 N68-16522*# c14 N68-16522*# c14 N68-16529*# c05 N68-16530*# c05 N68-16631*# c18 N68-16632*# c33 N68-16632*# c11 N68-16635*# c11 N68-16655*# c10 N68-1670*# c28 N68-1670*# c21 N68-16836*# c21 N68-16836*# c21 N68-16836*#</pre>	NASA-TN-D-4411 NASA-TN-D-4392 NASA-TN-D-4392 NASA-TN-D-4352 NASA-TN-D-4352 NASA-TN-D-4352 NASA-TN-D-4382 NASA-TN-D-4382 NASA-TN-D-4382 NASA-TN-D-4382 NASA-TN-D-4382 NASA-TN-D-4382 NASA-TN-D-4382 NASA-TN-D-4384 NASA-TN-D-4384 NASA-TN-D-4354 NASA-TN-D-4354 NASA-TN-D-4354 NASA-TN-D-4354 NASA-TN-D-4366 NASA-TN-D-4386 NASA-TN-D-4386 NASA-TN-D-4386 NASA-TN-D-4312 NASA-TN-D-4312 NASA-TN-D-4312 NASA-TN-D-4312 NASA-TN-D-4312 NASA-TN-D-4312 NASA-TN-D-4312 NASA-TN-D-4312 NASA-TN-D-4312 NASA-TN-D-4304
<pre>c03 N68-16351*# c28 N68-16413*# c03 N68-16439*# c15 N68-16469*# c22 N68-16469*# c22 N68-16469*# c04 N68-16480*# c04 N68-16517*# c02 N68-16522*# c14 N68-16529*# c05 N68-16529*# c05 N68-16534*# c05 N68-16631*# c03 N68-16631*# c13 N68-16631*# c11 N68-16695*# c11 N68-16695*# c10 N68-16750*# c10 N68-16750*# c21 N68-16836*# c29 N68-16837*# c14 N68-16838*#</pre>	NASA-TN-D-4411 NASA-TN-D-4392 NASA-TN-D-4392 NASA-TN-D-4352 NASA-TN-D-4352 NASA-TN-D-4352 NASA-TN-D-4352 NASA-TN-D-4352 NASA-TN-D-4362 NASA-TN-D-4362 NASA-TN-D-4362 NASA-TN-D-4362 NASA-TN-D-4313 NASA-TN-D-4300 NASA-TN-D-4300 NASA-TN-D-4300 NASA-TN-D-4300 NASA-TN-D-4313 NASA-TN-D-4313 NASA-TN-D-4316 NASA-TN-D-4316 NASA-TN-D-4316 NASA-TN-D-4312 NASA-TN-D-4312 NASA-TN-D-4312 NASA-TN-D-4312 NASA-TN-D-4313 NASA-TN-D-4312 NASA-TN-D-4312 NASA-TN-D-4312 NASA-TN-D-4312 NASA-TN-D-4312 NASA-TN-D-4312 NASA-TN-D-4312 NASA-TN-D-4300 NASA-TN-D-4300 NASA-TN-D-4300 NASA-TN-D-4312 NASA-TN-D-4300 NASA-TN-D-4300 NASA-TN-D-4300 NASA-T
<pre>c03 N68-16351*# c28 N68-16413*# c03 N68-16439*# c15 N68-16469*# c22 N68-16469*# c22 N68-16478*# c04 N68-16478*# c04 N68-16512*# c04 N68-16522*# c14 N68-16522*# c14 N68-16529*# c05 N68-16530*# c05 N68-16631*# c18 N68-16632*# c18 N68-16632*# c18 N68-16632*# c19 N68-16655*# c11 N68-16655*# c11 N68-16670*# c28 N68-1670*# c29 N68-1670*# c21 N68-16836*# c21 N68-16838*# c12 N68-16839*#</pre>	NASA-TN-D-4411 NASA-TN-D-4392 NASA-TN-D-4392 NASA-TN-D-4352 NASA-TN-D-4352 NASA-TN-D-4352 NASA-TN-D-4352 NASA-TN-D-4352 NASA-TN-D-4352 NASA-TN-D-4362 NASA-TN-D-4362 NASA-TN-D-4362 NASA-TN-D-4310 NASA-TN-D-4330 NASA-TN-D-4330 NASA-TN-D-4330 NASA-TN-D-4330 NASA-TN-D-4330 NASA-TN-D-4330 NASA-TN-D-4330 NASA-TN-D-4330 NASA-TN-D-4330 NASA-TN-D-4313 NASA-TN-D-4312 NASA-TN-D-4300 NASA-TN-D-4300
<pre>c03 N68-16351*# c28 N68-16413*# c03 N68-16439*# c15 N68-16468*# c02 N68-16468*# c22 N68-16478*# c04 N68-16517*# c04 N68-16517*# c02 N68-16522*# c14 N68-16530*# c05 N68-16530*# c05 N68-16632*# c03 N68-16632*# c13 N68-16632*# c13 N68-16635*# c11 N68-16695*# c11 N68-16695*# c10 N68-16750*# c10 N68-16750*# c29 N68-16836*# c21 N68-16837*# c12 N68-16839*# c12 N68-16839*# c12 N68-16837*#</pre>	NASA-TN-D-4411 NASA-CR-925 NASA-TN-D-4392 NASA-CR-925 NASA-TN-D-4352 NASA-TN-D-4355 NASA-TN-D-4362 NASA-TN-D-4382 NASA-TN-D-4382 NASA-TN-D-4382 NASA-TN-D-4382 NASA-TN-D-4382 NASA-TN-D-4382 NASA-TN-D-4382 NASA-TN-D-4384 NASA-TN-D-4384 NASA-TN-D-4354 NASA-TN-D-4354 NASA-TN-D-4350 NASA-TN-D-4300 NASA-TN-D-4310 NASA-TN-D-4312 NASA-TN-D-4306 NASA-TN-D-4307 NASA-TN-D-4312 NASA-TN-D-43040 NASA-TN-D-4305 NASA-TN-D-4305 NASA-TN-D-4306 NASA-TN-D-4307 NASA-TN-D-4308 NASA-TN-D-4
<pre>c03 N68-16351*# c28 N68-16413*# c03 N68-16439*# c15 N68-16463*# c22 N68-16468*# c03 N68-16469*# c22 N68-16478*# c04 N68-16517*# c02 N68-16522*# c14 N68-16529*# c05 N68-16529*# c05 N68-16524*# c18 N68-16631*# c03 N68-16631*# c18 N68-16632*# c18 N68-16632*# c18 N68-16635*# c19 N68-16700*# c10 N68-16700*# c10 N68-16750*# c21 N68-16836*# c21 N68-16838*# c12 N68-16839*# c12 N68-16897*# c12 N68-16897*#</pre>	NASA-TN-D-4411 NASA-TN-D-4392 NASA-TN-D-4392 NASA-TN-D-4352 NASA-TN-D-4352 NASA-TN-D-4352 NASA-TN-D-4352 NASA-TN-D-4352 NASA-TN-D-4352 NASA-TN-D-4362 NASA-TN-D-4362 NASA-TN-D-4362 NASA-TN-D-4310 NASA-TN-D-4330 NASA-TN-D-4330 NASA-TN-D-4330 NASA-TN-D-4330 NASA-TN-D-4330 NASA-TN-D-4330 NASA-TN-D-4330 NASA-TN-D-4330 NASA-TN-D-4330 NASA-TN-D-4313 NASA-TN-D-4418 NASA-TN-D-4312 NASA-TN-D-4312 NASA-TN-D-4312 NASA-TN-D-4312 NASA-TN-D-4312 NASA-TN-D-4312 NASA-TN-D-4312 NASA-TN-D-4313 NASA-TN-D-4312 NASA-TN-D-4312 NASA-TN-D-4300 NASA-TN-D-4300 NASA-TN-D-4300
c03 N68-16351*# c28 N68-16435*# c03 N68-16435*# c03 N68-164635*# c03 N68-16469*# c22 N68-16478*# c04 N68-16517*# c02 N68-16522*# c14 N68-16522*# c14 N68-16522*# c14 N68-16523*# c05 N68-16534*# c03 N68-16632*# c03 N68-16632*# c18 N68-16632*# c18 N68-16632*# c28 N68-16632*# c19 N68-16670*# c29 N68-16705*# c10 N68-16705*# c10 N68-1670*# c21 N68-16836*# c21 N68-16838*# c12 N68-16838*# c12 N68-16839*# c12 N68-16897*# c12 N68-16998*# c22 N68-16998*# c22 N68-17022*#	NASA-TN-D-4411 NASA-TN-D-4392 NASA-TN-D-4392 NASA-TN-D-4355 NASA-TN-D-4355 NASA-TN-D-4352 NASA-TN-D-4352 NASA-TN-D-4382 NASA-TN-D-4352 NASA-TN-D-4362 NASA-TN-D-4382 NASA-TN-D-4382 NASA-TN-D-4382 NASA-TN-D-4330 NASA-TN-D-4313 NASA-TN-D-44316 NASA-TN-D-4317 NASA-TN-D-4318 NASA-TN-D-4311 NASA-TN-D-4312 NASA-TN-D-4313 NASA-TN-D-4313 NASA-TN-D-44141 NASA-TN-D-4418 NASA-TN-D-4313 NASA-TN-D-4313 NASA-TN-D-44131 NASA-TN-D-44131 NASA-TN-D-44131 NASA-TN-D-44131 NASA-TN-D-44131 NASA-TN-D-4436 <td< td=""></td<>
c03 N68-16351+# c28 N68-16413+# c03 N68-16468+# c03 N68-16468+# c03 N68-16469+# c22 N68-16468+# c04 N68-16478+# c04 N68-16512+# c04 N68-16522+# c14 N68-16522+# c15 N68-16530+# c05 N68-16530+# c05 N68-16530+# c03 N68-16631+# c03 N68-16631+# c18 N68-16633+# c19 N68-16635+# c20 N68-16749+# c10 N68-16749+# c10 N68-16749+# c10 N68-16749+# c10 N68-16836+# c21 N68-16837+# c12 N68-16837+# c12 N68-16837+# c12 N68-16839+# c12 N68-16898+# c12 N68-16998+# c12 N68-16998+# c12 N68-16998+# c22 N68-17022+# c02 N68-17022+#	NASA-TN-D-4411 NASA-TN-D-4392 NASA-CR-925 NASA-TN-D-4352 NASA-TN-D-4352 NASA-TN-D-4352 NASA-TN-D-4382 NASA-TN-D-4382 NASA-TN-D-4382 NASA-TN-D-4382 NASA-TN-D-4382 NASA-TN-D-4382 NASA-TN-D-4382 NASA-TN-D-4382 NASA-TN-D-4382 NASA-TN-D-4384 NASA-TN-D-4354 NASA-TN-D-4354 NASA-TN-D-4364 NASA-TN-D-4386 NASA-TN-D-4386 NASA-TN-D-4386 NASA-TN-D-4386 NASA-TN-D-4386 NASA-TN-D-4386 NASA-TN-D-4386 NASA-TN-D-4386 NASA-TN-D-4386 NASA-TN-D-4387 NASA-TN-D-4388 NASA-TN-D
<pre>c03 N68-16351*# c28 N68-16413*# c03 N68-16439*# c15 N68-16463*# c03 N68-16463*# c22 N68-16468*# c04 N68-16478*# c04 N68-16517*# c02 N68-16522*# c14 N68-16529*# c05 N68-16529*# c05 N68-16524*# c18 N68-16632*# c33 N68-16631*# c33 N68-16631*# c18 N68-16632*# c33 N68-16655*# c19 N68-16670*# c10 N68-1670*# c10 N68-1675*# c21 N68-16836*# c29 N68-16838*# c12 N68-16838*# c14 N68-168</pre>	NASA-TN-D-4411 NASA-TN-D-4392 NASA-CR-925 NASA-TN-D-4352 NASA-TN-D-4352 NASA-TN-D-4352 NASA-TN-D-4352 NASA-TN-D-4352 NASA-TN-D-4362 NASA-TN-D-4362 NASA-TN-D-4362 NASA-TN-D-4362 NASA-TN-D-4362 NASA-TN-D-4354 NASA-TN-D-4354 NASA-TN-D-4355 NASA-TN-D-4356 NASA-TN-D-4356 NASA-TN-D-4356 NASA-TN-D-4356 NASA-TN-D-4354 NASA-TN-D-4356 NASA-TN-D-4356 NASA-TN-D-4312 NASA-TN-D-4312 NASA-TN-D-4312 NASA-TN-D-4313 NASA-TN-D-4313 NASA-TN-D-4312 NASA-TN-D-4313 NASA-TN-D-4313 NASA-TN-D-4313 NASA-TN-D-4312 NASA-TN-D-4313 NASA-TN-D-4313 NASA-TN-D-4313 NASA-TN-D-43143 NASA-TN-D-4380 NASA-TN-D-4380 NASA-TN-D-4380 NASA-TN-D-4380 NASA-TN-
<pre>c03 N68-16351*# c28 N68-16435*# c03 N68-16439*# c15 N68-16469*# c03 N68-16469*# c22 N68-16469*# c04 N68-16517*# c02 N68-16522*# c14 N68-16522*# c14 N68-16529*# c05 N68-16534*# c05 N68-16632*# c03 N68-16632*# c03 N68-16632*# c28 N68-16632*# c28 N68-16632*# c28 N68-16635*# c28 N68-16670*# c11 N68-16870*# c10 N68-1670*# c10 N68-1670*# c10 N68-16838*# c14 N68-16838*# c12 N68-16839*# c12 N68-16839*# c12 N68-16839*# c12 N68-16839*# c12 N68-16839*# c12 N68-1698*# c12 N68-1698*# c12 N68-17022*# c20 N68-17022*# c20 N68-17028*#</pre>	NASA-TN-D-4411 NASA-TN-D-4392 NASA-CR-925 NASA-TN-D-4352 NASA-TN-D-4352 NASA-TN-D-4352 NASA-TN-D-4352 NASA-TN-D-4352 NASA-TN-D-4352 NASA-TN-D-4362 NASA-TN-D-4362 NASA-TN-D-4362 NASA-TN-D-4362 NASA-TN-D-4330 NASA-TN-D-4331 NASA-TN-D-4331 NASA-TN-D-4313 NASA-TN-D-4312 NASA-TN-D-4312 NASA-TN-D-4313 NASA-TN-D-4313 NASA-TN-D-4313 NASA-TN-D-4313 NASA-TN-D-4340 LEC/HASD-671-40-019 NASA-TN-D-4380 NASA-TN-D-4380 NASA-TN-D-4380 NASA-TN-D-4380 NASA
<pre>c03 N68-16351*# c28 N68-16413*# c03 N68-16463*# c03 N68-16468*# c03 N68-16468*# c22 N68-16468*# c04 N68-16478*# c04 N68-16517*# c02 N68-16512*# c05 N68-16522*# c14 N68-16529*# c05 N68-16539*# c05 N68-16539*# c03 N68-16631*# c03 N68-16631*# c18 N68-16635*# c18 N68-16635*# c19 N68-16635*# c10 N68-1670*# c10 N68-1670*# c10 N68-16730*# c11 N68-16836*# c12 N68-16837*# c12 N68-16837*# c12 N68-16837*# c12 N68-16837*# c12 N68-16837*# c12 N68-16837*# c12 N68-16938*# c12 N68-16938*# c12 N68-16938*# c12 N68-16938*# c12 N68-16938*# c12 N68-17023*# c20 N68-17028*# c32 N68-17028*# c32 N68-17028*# c32 N68-17028*#</pre>	NASA-TN-D-4411 NASA-TN-D-4392 NASA-CR-925 NASA-TN-D-4352 NASA-TN-D-4352 NASA-TN-D-4352 NASA-TN-D-4352 NASA-TN-D-4382 NASA-TN-D-4382 NASA-TN-D-4382 NASA-TN-D-4382 NASA-TN-D-4382 NASA-TN-D-4382 NASA-TN-D-4382 NASA-TN-D-4382 NASA-TN-D-4384 NASA-TN-D-4354 NASA-TN-D-4354 NASA-TN-D-4354 NASA-TN-D-4300 NASA-TN-D-4301 NASA-TN-D-4302 NASA-TN-D-4312 NASA-TN-D-4312 NASA-TN-D-4312 NASA-TN-D-4312 NASA-TN-D-4312 NASA-TN-D-4312 NASA-TN-D-4312 NASA-TN-D-4312 NASA-TN-D-4312 NASA-TN-D-4313 NASA-TN-D-4314 NASA-TN-D-4312 NASA-TN-D-4313 NASA-TN-D-4314 NASA-TN-D-4313 NASA-TN-D-4343 NASA-TN-D-4343 NASA-TN-X-1490 NASA-TN-X-1490 NASA-TN-D
<pre>c03 N68-16351*# c28 N68-16413*# c03 N68-16439*# c15 N68-16463*# c03 N68-16463*# c22 N68-16468*# c04 N68-16478*# c04 N68-16517*# c02 N68-16522*# c14 N68-16529*# c05 N68-16529*# c05 N68-16524*# c18 N68-16632*# c33 N68-16631*# c33 N68-16631*# c33 N68-16632*# c33 N68-16635*# c11 N68-16635*# c25 N68-1670*# c10 N68-1675*# c21 N68-16836*# c21 N68-16838*# c12 N68-16837*# c12 N68-17022*# c22 N68-17022*# c20 N68-17028*# c22 N68-17028*# c32 N68-17045*# c32 N68-17055*#</pre>	NASA-TN-D-4411 NASA-CR-925 NASA-CR-925 NASA-TN-D-4352 NASA-TN-D-4352 NASA-TN-D-4352 NASA-TN-D-4352 NASA-TN-D-4352 NASA-TN-D-4362 NASA-TN-D-4362 NASA-TN-D-4362 NASA-TN-D-4362 NASA-TN-D-4362 NASA-TN-D-4362 NASA-TN-D-4364 NASA-TN-D-4354 NASA-TN-D-4350 NASA-TN-D-4350 NASA-TN-D-4350 NASA-TN-D-4350 NASA-TN-D-4350 NASA-TN-D-4350 NASA-TN-D-4350 NASA-TN-D-4350 NASA-TN-D-4350 NASA-TN-D-4366 NASA-TN-D-4312 NASA-TN-D-4312 NASA-TN-D-4312 NASA-TN-D-4312 NASA-TN-D-4313 NASA-TN-D-4312 NASA-TN-D-4312 NASA-TN-D-4312 NASA-TN-D-4365 NASA-TN-D-4380 NASA-TN-D-4380 NASA-TN-D-4365 NASA-TN-D-4365 NASA-TN-D-4365 NASA-TN-D-4365
<pre>c03 N68-16351*# c28 N68-16435*# c03 N68-16435*# c03 N68-164635*# c03 N68-16468*# c03 N68-16468*# c03 N68-16468*# c04 N68-16517*# c02 N68-16522*# c14 N68-16522*# c05 N68-16534*# c05 N68-16534*# c05 N68-16632*# c03 N68-16632*# c03 N68-16632*# c28 N68-16632*# c28 N68-16635*# c11 N68-16635*# c25 N68-16700*# c10 N68-1670*# c29 N68-16836*# c29 N68-16836*# c12 N68-16838*# c12 N68-16838*# c12 N68-16838*# c12 N68-16838*# c12 N68-16838*# c12 N68-16838*# c12 N68-16838*# c12 N68-16838*# c12 N68-16838*# c12 N68-1698*# c22 N68-17023*# c20 N68-17028*# c28 N68-17028*# c32 N68-17055*# c32 N68-17065*# c32 N68-17065*#</pre>	NASA-TN-D-4411 NASA-TN-D-4392 NASA-TN-D-4392 NASA-TN-D-4352 NASA-TN-D-4352 NASA-TN-D-4352 NASA-TN-D-4362 NASA-TN-D-4362 NASA-TN-D-4362 NASA-TN-D-4362 NASA-TN-D-4362 NASA-TN-D-4362 NASA-TN-D-4362 NASA-TN-D-4362 NASA-TN-D-4363 NASA-TN-D-4330 NASA-TN-D-4331 NASA-TN-D-4313 NASA-TN-D-4312 NASA-TN-D-4312 NASA-TN-D-4312 NASA-TN-D-4312 NASA-TN-D-4380 NASA-T
 c03 N68-16351*# c28 N68-16413*# c03 N68-16439*# c15 N68-16469*# c22 N68-16469*# c22 N68-16469*# c22 N68-16478*# c01 N68-1640*# c02 N68-16512*# c02 N68-16522*# c14 N68-16522*# c14 N68-16529*# c05 N68-16530*# c05 N68-16631*# c18 N68-16632*# c33 N68-16632*# c33 N68-16632*# c18 N68-16632*# c28 N68-16632*# c10 N68-1670*# c10 N68-1670*# c10 N68-1670*# c12 N68-16836*# c12 N68-16837*# c12 N68-16837*# c12 N68-16839*# c12 N68-1698*# c22 N68-17022*# c02 N68-17028*# c28 N68-17028*# c32 N68-17055*# c32 N68-1706*# c32 N68-1706*# c32 N68-1706*# c32 N68-1706*# c32 N68-1706*# c32 N68-1706*# c32 N68-17070*# 	NASA-TN-D-4411 NASA-CR-925 NASA-CR-922 NASA-CR-922 NASA-TN-D-4352 NASA-TN-D-4352 NASA-TN-D-4352 NASA-TN-D-4382 NASA-TN-D-4382 NASA-TN-D-4382 NASA-TN-D-4382 NASA-TN-D-4382 NASA-TN-D-4382 NASA-TN-D-4382 NASA-TN-D-4382 NASA-TN-D-4384 NASA-TN-D-4354 NASA-TN-D-4354 NASA-TN-D-4354 NASA-TN-D-4300 NASA-TN-D-4301 NASA-TN-D-4302 NASA-TN-D-4312 NASA-TN-D-4313 NASA-TN-D-4312 NASA-TN-D-4312 NASA-TN-D-4312 NASA-TN-D-4312 NASA-TN-D-4312 NASA-TN-D-4312 NASA-TN-D-4312 NASA-TN-D-4313 NASA-TN-D-4313 NASA-TN-D-4313 NASA-TN-D-4343 NASA-TN-D-4343 NASA-TN-D-4343 NASA-TN-D-4343 NASA-TN-D-4343 NASA-TN-D-4355
<pre>c03 N68-16351*# c28 N68-16435*# c03 N68-16435*# c03 N68-164635*# c03 N68-16468*# c03 N68-16468*# c04 N68-16517*# c02 N68-16522*# c14 N68-16522*# c14 N68-16522*# c05 N68-16534*# c05 N68-16632*# c05 N68-16632*# c03 N68-16632*# c28 N68-16632*# c28 N68-16632*# c28 N68-16635*# c28 N68-16635*# c29 N68-16700*# c10 N68-1670*# c21 N68-16836*# c29 N68-16836*# c12 N68-16836*# c12 N68-16836*# c12 N68-16838*# c12 N68-16838*# c12 N68-16838*# c12 N68-16838*# c12 N68-16838*# c12 N68-16838*# c12 N68-16988*# c12 N68-17023*# c20 N68-17028*# c22 N68-17055*# c32 N68-17070*# c33 N68-17075*# c25 N68-17075*# c25 N68-17075*# c27 N68-17075*# c27 N68-17075*#</pre>	NASA-TN-D-4411 NASA-TN-D-4392 NASA-TN-D-4352 NASA-TN-D-4352 NASA-TN-D-4352 NASA-TN-D-4352 NASA-TN-D-4362 NASA-TN-D-4362 NASA-TN-D-4362 NASA-TN-D-4362 NASA-TN-D-4362 NASA-TN-D-4362 NASA-TN-D-4362 NASA-TN-D-4364 NASA-TN-D-4364 NASA-TN-D-4354 NASA-TN-D-4356 NASA-TN-D-4350 NASA-TN-D-4350 NASA-TN-D-4350 NASA-TN-D-4350 NASA-TN-D-4350 NASA-TN-D-4350 NASA-TN-D-4312 NASA-TN-D-4365 NASA-TN-D-4365 NASA-TN-D-4365 NASA-TN-D-4365 NASA-TN-D-4365 NASA-T
<pre>c03 N68-16351*# c28 N68-16413*# c03 N68-16439*# c15 N68-16469*# c22 N68-16469*# c22 N68-16469*# c22 N68-16480*# c04 N68-16517*# c02 N68-16522*# c14 N68-16517*# c09 N68-16529*# c09 N68-16529*# c05 N68-16632*# c03 N68-16631*# c03 N68-16631*# c11 N68-16635*# c10 N68-16635*# c10 N68-1670*# c10 N68-1670*# c10 N68-1675*# c21 N68-16838*# c12 N68-17022*# c20 N68-17024*# c20 N68-17028*# c32 N68-17045*# c32 N68-17068*# c32 N68-17075*# c33 N68-17075*# c33 N68-17075*#</pre>	NASA-TN-D-4411 NASA-CR-925 NASA-CR-922 NASA-CR-922 NASA-TN-D-4352 NASA-TN-D-4382 NASA-TN-D-4382 NASA-TN-D-4382 NASA-TN-2-4382 NASA-TN-D-4382 NASA-TN-D-4312 NASA-TN-D-4313 NASA-TN-D-4312 NASA-TN-D-4313 NASA-TN-D-4313 NASA-TN-D-43443 NASA-TN-D-43443 NASA-

c14 N68-11867*#	••••••••••••••••••••••••••••••••••••••
c21 N68-11902*#	••••••••••••••••••••••••••••••••••••••
c24 N68-11903*#	
c17 N68-11912*#	
c31 N68-11919*#	
c03 N68-11920*#	NASA-TM-X-1480
c01 N68-11936*#	NASA-TN-D-4291
c21 N68-11949*#	NASA-TM-X-1483
c01 N68-11958*#	
c31 N68-11961*#	NASA-TN-D-4266
c32 N68-11967*#	NASA-CR-897
c04 N68-11968*#	NASA-CR-972
c18 N68-11978*#	NASA-CR-966
c32 N68-12370*#	NASA-TN-D-4295
c04 N68-12494*#	
c14 N68-12669*#	NASA-CR-987
c32 N68-12864*#	NASA-TN-D-4265
CO2 NOU 12004-#	NRC-LR-486
c15 N68-12890*#	NASA-TN-D-4288
c17 N68-12891*#	
	NASA-CR-961
c23 N68-13115*#	NASA-CR-988
c04 N68-13432*#	NASA-TT-F-439
	TT-67-51375
c02 N68-13517*#	NASA-CR-986
c21 N68-13558*#	NASA-TN-D-4174
c05 N68-13609*#	••••••••••••••••••••••••••••••••••••••
c12 N68-13612*#	NASA-CR-960
c09 N68-13617*#	•••••• NASA-CR-979
c12 N68-13619*#	••••••••••••••••••••••••••••••••••••••
c31 N68-13797*#	••••••••••••••••••••••••••••••••••••••
c08 N68-13897*#	••••••••••••••••••••••••••••••••••••••
	PHO-TR-307
c14 N68-13973*#	••••••••••••••••••••••••••••••••••••••
c14 N68-13974*#	••••••••••••••••••••••••••••••••••••••
c05 N68-13999*#	••••••••••••••••••••••••••••••••••••••
c14 N68-14018*#	••••••••••••••••••••••••••••••••••••••
c33 N68-14042*#	••••••••••••••••••••••••••••••••••••••
c33 N68-14052*#	••••••••••••••••••••••••••••••••••••••
c16 N68-14070*#	
c19 N68-14077*#	NASA-TN-D-4296
c25 N68-14078*#	
c03 N68-14082*#	
c30 N68-14089*#	
c02 N68-14090*	SID-65-1200-3 NASA-TN-D-4329
c02 N68-14090* c32 N68-14091*#	••••••••••••••••••••••••••••••••••••••
c32 N68-14091*#	NASA-TN-D-4329 NASA-TN-D-4283
c32 N68-14091*# c31 N68-14092*#	NASA-TN-D-4329 NASA-TN-D-4283 NASA-TN-D-4283 NASA-TM-X-1500
c32 N68-14091*# c31 N68-14092*# c06 N68-14093*#	NASA-TN-D-4329 NASA-TN-D-4283 NASA-TN-D-4283 NASA-TN-X-1500 NASA-TN-D-4335
c32 N68-14091*# c31 N68-14092*# c06 N68-14093*# c11 N68-14115*#	NASA-TN-D-4329 NASA-TN-D-4283 NASA-TN-D-4283 NASA-TM-X-1500 NASA-TM-Z-1506
c32 N68-14091*# c31 N68-14092*# c06 N68-14093*# c11 N68-14115*# c33 N68-14240*#	NASA-TN-D-4329 NASA-TN-D-4283 NASA-TN-D-4283 NASA-TM-X-1500 NASA-TN-D-4335 NASA-TN-D-4335 NASA-TN-X-1506 NASA-TN-D-4332
c32 N68-14091*# c31 N68-14092*# c06 N68-14093*# c11 N68-14115*# c33 N68-14240*# c05 N68-14262*#	NASA-TN-D-4329 NASA-TN-D-4283 NASA-TN-D-4283 NASA-TN-D-4335 NASA-TN-D-4335 NASA-TM-X-1506 NASA-TM-X-1506 NASA-CR-876
c32 N68-14091*# c31 N68-14092*# c06 N68-14093*# c11 N68-14115*# c33 N68-14240*# c05 N68-14262*# c33 N68-14270*#	NASA-TN-D-4329 NASA-TN-D-4283 NASA-TN-D-4283 NASA-TN-D-4335 NASA-TN-D-4335 NASA-TN-D-4335 NASA-TN-D-4332 NASA-TN-D-4331
c32 N68-14091*# c31 N68-14092*# c06 N68-14093*# c11 N68-14115*# c33 N68-14240*# c05 N68-14262*# c33 N68-14270*# c33 N68-14270*# c32 N68-14584*#	NASA-TN-D-4329 NASA-TN-D-4283 NASA-TM-X-1500 NASA-TM-X-1500 NASA-TM-D-4335 NASA-TM-X-1506 NASA-TM-X-1506 NASA-TM-D-4332 NASA-CR-876 NASA-CR-909
c32 N68-14091*# c31 N68-14092*# c06 N68-14093*# c11 N68-14115*# c33 N68-14240*# c05 N68-14262*# c33 N68-14220*# c32 N68-14270*# c32 N68-14585*#	NASA-TM-D-4329 NASA-TM-D-4283 NASA-TN-D-4283 NASA-TM-X-1500 NASA-TM-X-1500 NASA-TM-Z-4335 NASA-TM-Z-4332 NASA-CR-876 NASA-CR-876 NASA-CR-909 NASA-TM-X-1501
c32 N68-14091*# c31 N68-14093*# c11 N68-14093*# c11 N68-14115*# c33 N68-14240*# c33 N68-14220*# c33 N68-142270*# c32 N68-14584*# c22 N68-14585*# c03 N68-14630*#	NASA-TN-D-4329 NASA-TN-D-4283 NASA-TN-X-1500 NASA-TN-D-4335 NASA-TM-X-1500 NASA-TM-X-1500 NASA-TM-X-1500 NASA-CR-876 NASA-CR-876 NASA-CR-909 NASA-TM-X-1501 NASA-TM-X-1501 NASA-TM-X-1453
c32 N68-14091*# c31 N68-14092*# c06 N68-14093*# c11 N68-14115*# c33 N68-14240*# c05 N68-14262*# c33 N68-14220*# c32 N68-14270*# c32 N68-14585*#	NASA-TN-D-4329 NASA-TN-D-4283 NASA-TN-D-4283 NASA-TN-D-4335 NASA-TM-X-1500 NASA-TN-D-4335 NASA-TN-D-4335 NASA-TN-D-4332 NASA-TN-D-4333 NASA-TN-D-4331 NASA-TN-D-4331 NASA-TN-D-4331 NASA-TN-X-1509 NASA-TM-X-1503 NASA-TM-X-1503 NASA-CR-909 NASA-CM-X-1501 NASA-CR-915
c32 N68-14091*# c31 N68-14092*# c06 N68-14093*# c11 N68-14115*# c33 N68-14240*# c33 N68-14262*# c33 N68-14262*# c32 N68-14584*# c22 N68-14585*# c31 N68-14630*# c31 N68-14638*#	NASA-TM-D-4329 NASA-TM-D-4283 NASA-TN-D-4283 NASA-TM-X-1500 NASA-TM-Z-1500 NASA-TM-D-4335 NASA-TM-D-4332 NASA-CR-876 NASA-CR-876 NASA-CR-909 NASA-TM-X-1501 NASA-TM-X-1501 NASA-TM-X-1453 NASA-TM-X-1453 TR-66-67
c32 N68-14091*# c31 N68-14093*# c11 N68-14093*# c11 N68-14115*# c33 N68-14240*# c33 N68-14220*# c32 N68-14262*# c32 N68-14584*# c22 N68-14585*# c31 N68-14638*# c31 N68-14638*# c03 N68-14639*#	NASA-TN-D-4329 NASA-TN-D-4283 NASA-TN-D-4283 NASA-TM-X-1500 NASA-TM-Z-1500 NASA-TM-D-4335 NASA-TM-D-4335 NASA-TM-D-4332 NASA-CR-876 NASA-CR-876 NASA-TM-D-4331 NASA-TM-D-4331 NASA-CR-876 NASA-TM-X-1501 NASA-TM-X-1453 NASA-TM-X-1453 NASA-TM-X-1453 NASA-TN-D-4388
c32 N68-14091*# c31 N68-14092*# c11 N68-14092*# c11 N68-14115*# c33 N68-14240*# c33 N68-14220*# c33 N68-14220*# c32 N68-14585*# c32 N68-14585*# c31 N68-14630*# c31 N68-14630*# c32 N68-14630*# c32 N68-14630*#	NASA-TN-D-4329 NASA-TN-D-4283 NASA-TN-2-1500 NASA-TN-2-1500 NASA-TN-2-4353 NASA-TN-D-4352 NASA-TN-D-4352 NASA-CR-876 NASA-CR-876 NASA-CR-876 NASA-CR-909 NASA-CR-909 NASA-TN-2-4331 NASA-TN-2-4383 NASA-TN-2-4388 NASA-TR-27915 TR-66-67 NASA-TR-279
c32 N68-14091*# c31 N68-14093*# c11 N68-14093*# c11 N68-14115*# c33 N68-14240*# c33 N68-14240*# c33 N68-14262*# c33 N68-14584*# c22 N68-14585*# c31 N68-14638*# c31 N68-14638*# c33 N68-14638*# c32 N68-14640*# c12 N68-14641*#	NASA-TM-D-4329 NASA-TM-D-4283 NASA-TM-24283 NASA-TM-24283 NASA-TM-24335 NASA-TM-24335 NASA-TM-24335 NASA-TM-24332 NASA-CR-876 NASA-CR-876 NASA-CR-909 NASA-TM-24331 NASA-TM-24351 NASA-TM-21453 TR-66-67 NASA-TM-24388 NASA-TM-24388 NASA-TM-24384
c32 N68-14091*# c31 N68-14092*# c06 N68-14093*# c11 N68-14015*# c33 N68-14240*# c33 N68-14240*# c32 N68-14262*# c33 N68-14270*# c32 N68-14636*# c31 N68-14638*# c03 N68-14639*# c32 N68-14649*# c12 N68-14641*# c12 N68-14671*#	NASA-TN-D-4329 NASA-TN-D-4283 NASA-TN-D-4283 NASA-TN-D-4335 NASA-TM-Z-1506 NASA-TM-Z-1506 NASA-TM-Z-1506 NASA-TM-Z-1506 NASA-TM-Z-1506 NASA-TM-Z-4331 NASA-CR-876 NASA-TM-D-4331 NASA-TM-D-4331 NASA-TM-D-4331 NASA-TM-Z-1501 NASA-TM-X-1453 NASA-TM-X-1430 NASA-TM-X-14340 NASA-SP-7011/43/
c32 N68-14091*# c31 N68-14092*# c11 N68-14092*# c11 N68-14115*# c33 N68-14240*# c33 N68-14240*# c33 N68-14220*# c32 N68-14584*# c32 N68-14584*# c31 N68-14630*# c31 N68-14630*# c32 N68-14639*# c32 N68-14643*# c12 N68-14641*# c04 N68-14725*#	NASA-TN-D-4329 NASA-TN-D-4283 NASA-TN-D-4283 NASA-TN-D-4283 NASA-TN-D-4353 NASA-TN-D-4335 NASA-TN-D-4332 NASA-TN-D-4332 NASA-TN-D-4331 NASA-CR-876 NASA-TN-D-4331 NASA-TN-D-4331 NASA-TN-D-4331 NASA-TN-D-4331 NASA-TN-D-4331 NASA-TN-20-4331 NASA-TM-X-1601 NASA-TM-X-161 NASA-TM-X-1453 NASA-TM-D-4388 NASA-TN-D-4388 NASA-TN-D-4380 NASA-TN-D-4340 NASA-SP-7011/42/
c32 N68-14091*# c31 N68-14093*# c11 N68-14093*# c11 N68-14240*# c33 N68-14240*# c33 N68-14240*# c32 N68-14262*# c32 N68-14584*# c33 N68-14538*# c31 N68-14638*# c31 N68-14638*# c32 N68-14643*# c32 N68-14640*# c32 N68-14640*# c32 N68-14671*# c04 N68-14725*# c21 N68-14725*#	NASA-TM-D-4329 NASA-TM-D-4283 NASA-TM-D-4283 NASA-TM-Z-1500 NASA-TM-D-4335 NASA-TM-D-4335 NASA-TM-D-4332 NASA-TM-D-4332 NASA-CR-876 NASA-CR-909 NASA-TM-2-4331 NASA-TM-D-4332 NASA-CR-909 NASA-TM-2-4331 NASA-TM-2-4335 NASA-TM-X-1501 NASA-TM-X-1501 NASA-TM-X-1501 NASA-TM-X-1501 NASA-TM-X-1501 NASA-TM-2-4338 NASA-TM-2-4331 NASA-TN-D-4340 NASA-TN-D-4340 NASA-TN-D-4340 NASA-TN-D-4340 NASA-SP-7011/43/ NASA-SP-7011/42/ NASA-TN-D-4317
c32 N68-14091*# c31 N68-14092*# c06 N68-14093*# c11 N68-14115*# c33 N68-14240*# c33 N68-14240*# c32 N68-14260*# c32 N68-14265*# c31 N68-14636*# c31 N68-14638*# c32 N68-14639*# c32 N68-14640*# c12 N68-14640*# c12 N68-14671*# c04 N68-14725*# c14 N68-14725*# c14 N68-14725*# c14 N68-14725*# c14 N68-14725*# c14 N68-14725*# c14 N68-14747*#	NASA-TM-D-4329 NASA-TN-D-4283 NASA-TN-D-4283 NASA-TM-Z-1500 NASA-TM-Z-1500 NASA-TM-Z-1500 NASA-TM-Z-1500 NASA-TM-Z-4335 NASA-TM-D-4331 NASA-TM-D-4331 NASA-TM-D-4331 NASA-TM-D-4331 NASA-TM-D-4331 NASA-TM-Z-1501 NASA-TM-X-1501 NASA-TM-X-1453 NASA-TM-X-1453 NASA-TM-Z-1453 NASA-TM-D-4388 NASA-TM-D-4388 NASA-TN-D-4380 NASA-SP-7011/43/ NASA-SP-7011/42/ NASA-TM-D-4317 NASA-TM-D-4317
c32 N68-14091*# c31 N68-14092*# c11 N68-14092*# c11 N68-14015*# c33 N68-14240*# c33 N68-14240*# c32 N68-14262*# c32 N68-14584*# c31 N68-14638*# c31 N68-14639*# c32 N68-14639*# c32 N68-14639*# c32 N68-14641*# c12 N68-14641*# c04 N68-146725*# c21 N68-14732*# c17 N68-1468*#	NASA-TN-D-4329 NASA-TN-D-4283 NASA-TN-D-4283 NASA-TN-D-4335 NASA-TM-Z-1500 NASA-TM-Z-1500 NASA-TM-Z-1500 NASA-TM-Z-1500 NASA-TM-Z-1500 NASA-TM-D-4332 NASA-CR-876 NASA-TM-D-4331 NASA-TM-Z-1501 NASA-TM-X-1501 NASA-TM-X-1653 NASA-TM-X-1453 NASA-TM-X-1453 NASA-TM-X-1453 NASA-TM-X-1453 NASA-TM-X-1453 NASA-TM-X-1453 NASA-TM-X-1453 NASA-TM-X-1453 NASA-TM-D-4388 NASA-TN-D-4388 NASA-TN-D-4388 NASA-TN-D-4380 NASA-SP-7011/43/ NASA-SP-7011/43/ NASA-SP-7011/42/ NASA-TN-D-4310
<pre>c32 N68-14091*# c31 N68-14093*# c31 N68-14093*# c11 N68-14240*# c33 N68-14240*# c33 N68-14262*# c33 N68-14262*# c33 N68-14584*# c33 N68-14563*# c31 N68-14653*# c31 N68-14638*# c32 N68-14638*# c32 N68-14638*# c32 N68-14637*# c34 N68-14671*# c44 N68-14671*# c21 N68-14725*# c31 N68-14747*# c31 N68-14747*# c31 N68-14747*# c31 N68-14888*# c32 N68-14888*# c31 N68-1493*</pre>	NASA-TM-D-4329 NASA-TM-D-4283 NASA-TM-24283 NASA-TM-24283 NASA-TM-24335 NASA-TM-24335 NASA-TM-24335 NASA-TM-24335 NASA-TM-24335 NASA-TM-24332 NASA-TM-D-4332 NASA-TM-D-4332 NASA-CR-876 NASA-TM-D-4331 NASA-TM-24332 NASA-TM-D-4332 NASA-TM-2431 NASA-TM-X-1501 NASA-TM-X-1501 NASA-TM-X-1501 NASA-TM-X-1501 NASA-TM-X-1501 NASA-TN-D-4338 NASA-TN-D-4310 NASA-TN-D-4310 NASA-TM-X-1502 NASA-TM-X-16323
c32 N68-14091*# c31 N68-14092*# c31 N68-14092*# c11 N68-140192*# c33 N68-14240*# c33 N68-14240*# c32 N68-14262*# c33 N68-14267*# c32 N68-14584*# c31 N68-14638*# c31 N68-14639*# c32 N68-14640*# c32 N68-14640*# c12 N68-14641*# c04 N68-14725*# c12 N68-14725*# c11 N68-14725*# c11 N68-14725*# c21 N68-14747*# c17 N68-14888*# c02 N68-14903*	NASA-TM-D-4329 NASA-TN-D-4283 NASA-TN-D-4283 NASA-TM-Z-1500 NASA-TM-Z-1500 NASA-TM-Z-1500 NASA-TM-Z-1500 NASA-TM-Z-4335 NASA-TM-Z-4332 NASA-TM-D-4331 NASA-TM-D-4331 NASA-TM-D-4331 NASA-TM-D-4331 NASA-TM-Z-1501 NASA-TM-X-1501 NASA-TM-X-1453 NASA-TM-X-1453 NASA-TM-Z-1453 NASA-TM-Z-1453 NASA-TM-Z-1453 NASA-TM-Z-1453 NASA-TM-Z-1453 NASA-TM-Z-1453 NASA-TM-Z-1453 NASA-TM-D-4316 NASA-SP-7011/43/ NASA-SP-7011/42/ NASA-TM-D-4317 NASA-TM-D-4317 NASA-TM-D-4317 NASA-TM-D-4317 NASA-TM-D-4317 NASA-TM-D-4317 NASA-TM-D-4317 NASA-TM-D-4317 NASA-TM-D-4313 NASA-TM-D-4313 NASA-TM-D-4313 NASA-TM-D-4323 NASA-TM-D-4323
c32 N68-14091*# c31 N68-14093*# c11 N68-14092*# c11 N68-14092*# c11 N68-14115*# c33 N68-14240*# c33 N68-14240*# c32 N68-14270*# c32 N68-14584*# c31 N68-14630*# c31 N68-14639*# c32 N68-14639*# c32 N68-14643*# c12 N68-14641*# c14 N68-14772*# c14 N68-14772*# c17 N68-14888*# c17 N68-14888*# c17 N68-14903* c30 N68-1491*# c31 N68-14941*# c31 N68-14941*#	NASA-TN-D-4329 NASA-TN-D-4283 NASA-TN-D-4283 NASA-TN-D-4335 NASA-TM-Z-1500 NASA-TM-Z-1500 NASA-TM-Z-1500 NASA-TM-D-4335 NASA-TM-D-4335 NASA-TM-D-4331 NASA-CR-876 NASA-TM-D-4331 NASA-TM-D-4331 NASA-TM-D-4331 NASA-TM-X-1501 NASA-TM-X-1501 NASA-TM-X-1453 NASA-TM-X-1453 NASA-TM-X-1453 NASA-TM-X-1453 NASA-TM-24388 NASA-TN-D-4388 NASA-TN-D-4388 NASA-TN-D-4388 NASA-TN-D-4388 NASA-TN-D-4310 NASA-SP-7011/42/ NASA-TN-D-4310 NASA-TN-D-4310 NASA-TN-D-4323 NASA-TN-D-4310 NASA-TN-D-4323 NASA-SP-138 NASA-SP-138
<pre>c32 N68-14091*# c31 N68-14093*# c31 N68-14093*# c11 N68-14115*# c33 N68-14240*# c33 N68-14240*# c33 N68-14262*# c33 N68-14584*# c33 N68-14530*# c31 N68-14638*# c31 N68-14638*# c31 N68-14638*# c32 N68-14640*# c32 N68-14671*# c04 N68-14671*# c04 N68-14671*# c11 N68-14747*# c11 N68-14747*# c11 N68-14747*# c11 N68-14747*# c31 N68-14941*# c31 N68-14965*# c31 N68-14965*# c32 N68-14968*# c32 N68-14968*# c32 N68-14968*# c32 N68-1496*# c32 N68-1490*# c32 N68-14908*# c32 N68-1490*# c32 N68-149</pre>	NASA-TM-D-4329 NASA-TM-D-4283 NASA-TM-2-1500 NASA-TM-2-1500 NASA-TM-D-4335 NASA-TM-D-4335 NASA-TM-D-4332 NASA-CR-876 NASA-CR-876 NASA-CR-909 NASA-CR-909 NASA-TM-2-4331 NASA-TM-2-4310 NASA-TM-2-438 NASA-TN-D-4388 NASA-TN-D-4380 NASA-TN-D-4310 NASA-TM-2-4310 NASA-TM-2-4310 NASA-TM-2-4310 NASA-TM-2-4310 NASA-TM-2-4310 NASA-TM-2-4310 NASA-TM-2-4310 NASA-TM-2-4310 NASA-TM-2-4310 NASA-TM-2-4310 NASA-TM-2-4310 NASA-TM-2-4310 NASA-TM-2-4310 NASA-TM-D-4323 NASA-TM-D-4323 NASA-TM-D-43279
c32 N68-14091*# c31 N68-14092*# c31 N68-14092*# c11 N68-140192*# c11 N68-14240*# c33 N68-14240*# c33 N68-14240*# c32 N68-14263*# c33 N68-14263*# c31 N68-14638*# c31 N68-14638*# c32 N68-14639*# c32 N68-14640*# c12 N68-14640*# c12 N68-14671*# c14 N68-14725*# c10 N68-14747*# c17 N68-14888*# c01 N68-14747*# c17 N68-14888*# c02 N68-14965*# c31 N68-1491*# c31 N68-14965*# c32 N68-14965*# c31 N68-15910*#	NASA-TM-D-4329 NASA-TM-D-4283 NASA-TM-Z-1500 NASA-TM-Z-1500 NASA-TM-Z-1500 NASA-TM-D-4335 NASA-TM-D-4335 NASA-TM-D-4332 NASA-TM-D-4332 NASA-TM-D-4331 NASA-TM-D-4332 NASA-TM-D-4331 NASA-TM-D-4332 NASA-TM-D-4332 NASA-TM-D-4331 NASA-TM-X-1501 NASA-TM-X-1501 NASA-TM-X-1453 NASA-TM-X-1453 NASA-TM-D-4388 NASA-TM-D-4388 NASA-TM-D-4388 NASA-TM-D-4388 NASA-TM-D-4388 NASA-TM-D-4317 NASA-TM-D-4323 NASA-TM-D-4323 NASA-TM-D-4323 NASA-TM-D-4323
<pre>c32 N68-14091*# c31 N68-14093*# c31 N68-14092*# c11 N68-14015*# c33 N68-14240*# c33 N68-14240*# c33 N68-14270*# c32 N68-14584*# c33 N68-14638*# c33 N68-14639*# c31 N68-14639*# c32 N68-14639*# c32 N68-14643*# c32 N68-14641*# c14 N68-14772*# c17 N68-14772*# c17 N68-14732*# c17 N68-14903* c30 N68-1491*# c31 N68-14965*# c31 N68-14965*# c32 N68-14965*# c32 N68-15010*# c35 N68-15010*# c35 N68-15010*#</pre>	NASA-TN-D-4329 NASA-TN-D-4283 NASA-TN-D-4283 NASA-TN-2.1500 NASA-TN-2.4350 NASA-TN-2.4350 NASA-TN-D-4332 NASA-TN-D-4332 NASA-TN-D-4331 NASA-TN-D-4331 NASA-TN-D-4331 NASA-TN-D-4332 NASA-TN-D-4331 NASA-TN-D-4332 NASA-TN-D-4331 NASA-TN-D-4331 NASA-TM-X-1601 NASA-TM-X-1613 NASA-TM-X-1613 NASA-TM-X-1613 NASA-TN-D-4310 NASA-TN-D-4388 NASA-TN-D-4300 NASA-TN-D-4310 NASA-SP-7011/42/ NASA-TN-D-4317 NASA-TN-D-4310 NASA-TN-D-4310 NASA-TN-D-4313 NASA-TN-D-4323 NASA-TN-D-4323 NASA-TN-D-4323 NASA-TN-D-4328 NASA-TN-D-4328 NASA-TN-D-4328 NASA-TN-D-4328 NASA-TN-D-4328 NASA-TN-D-4328 NASA-TN-D-4328 NASA-TN-D-4328
c32 N68-14091*# c31 N68-14092*# c31 N68-14092*# c11 N68-140192*# c11 N68-14240*# c33 N68-14240*# c33 N68-14240*# c32 N68-14263*# c33 N68-14263*# c31 N68-14638*# c31 N68-14638*# c32 N68-14639*# c32 N68-14640*# c12 N68-14640*# c12 N68-14671*# c14 N68-14725*# c10 N68-14747*# c17 N68-14888*# c01 N68-14747*# c17 N68-14888*# c02 N68-14965*# c31 N68-1491*# c31 N68-14965*# c32 N68-14965*# c31 N68-15910*#	NASA-TM-D-4329 NASA-TM-D-4283 NASA-TM-2483 NASA-TM-X-1500 NASA-TM-24335 NASA-TM-24335 NASA-TM-D-4335 NASA-TM-D-4335 NASA-TM-D-4332 NASA-TM-D-4332 NASA-TM-D-4332 NASA-TM-D-4332 NASA-TM-D-4332 NASA-TM-D-4332 NASA-TM-D-4332 NASA-TM-D-4332 NASA-TM-X-1501 NASA-TM-X-1501 NASA-TM-X-1501 NASA-TM-X-1453 TR-66-67 NASA-TM-D-4388 NASA-TN-D-4300 NASA-TN-D-4340 NASA-TN-D-4340 NASA-TN-D-4340 NASA-TN-D-4310 NASA-TM-D-4310 NASA-TM-D-4310 NASA-TM-D-4323
c32 N68-14091*# c31 N68-14092*# c31 N68-14092*# c11 N68-140192*# c11 N68-140192*# c33 N68-14240*# c35 N68-14262*# c33 N68-14260*# c31 N68-14263*# c31 N68-14638*# c31 N68-14639*# c32 N68-14639*# c32 N68-14639*# c32 N68-14640*# c4 N68-14671*# c12 N68-14671*# c14 N68-14725*# c10 N68-14747*# c17 N68-14888*# c02 N68-14965*# c30 N68-14965*# c31 N68-14965*# c31 N68-15120*# c30 N68-1512*# c30 N68-1512*# c30 N68-1512*# c30 N68-1512*# c30 N68-1512*# c30 N68-1512*#	NASA-TM-D-4329 NASA-TM-D-4283 NASA-TM-X-1500 NASA-TM-Z-1500 NASA-TM-D-4335 NASA-TM-D-4335 NASA-TM-D-4332 NASA-TM-D-4332 NASA-TM-D-4332 NASA-TM-D-4331 NASA-TM-D-4332 NASA-TM-D-4331 NASA-TM-D-4332 NASA-TM-D-4332 NASA-TM-D-4331 NASA-TM-D-4333 NASA-TM-X-1501 NASA-TM-X-1501 NASA-TM-X-1453 NASA-TM-D-4388 NASA-TM-D-4388 NASA-TM-D-4388 NASA-TM-D-4388 NASA-TM-D-4340 NASA-SP-7011/43/ NASA-TM-D-4317 NASA-TM-D-4317 NASA-TM-D-4317 NASA-TM-D-4318 NASA-TM-D-4317 NASA-TM-D-4318 NASA-TM-D-4317 NASA-TM-D-4318 NASA-TM-D-4323 NASA-TM-D-4317 NASA-TM-D-4318 NASA-TM-D-4323 NASA-TM-D-4323 NASA-TM-D-4323 NASA-TM-D-4323 NASA-TM-D-43248 NAS
c32 N68-14091*# c31 N68-14092*# c31 N68-14092*# c11 N68-14092*# c33 N68-14240*# c33 N68-14240*# c33 N68-14220*# c32 N68-14630*# c31 N68-14630*# c31 N68-14639*# c32 N68-14639*# c32 N68-14639*# c32 N68-14639*# c32 N68-14643*# c12 N68-14671*# c04 N68-14671*# c04 N68-14671*# c17 N68-14888*# c01 N68-14903* c31 N68-14947*# c17 N68-14888*# c02 N68-14903* c31 N68-14965*# c31 N68-14965*# c31 N68-14965*# c30 N68-15120*# c30 N68-15197*# c22 N68-15197*#	NASA-TM-D-4329 NASA-TN-D-4283 NASA-TN-D-4283 NASA-TM-X-1500 NASA-TM-Z-1500 NASA-TM-Z-1500 NASA-TM-D-4335 NASA-TM-D-4332 NASA-TM-D-4331 NASA-TM-D-4331 NASA-TM-D-4331 NASA-TM-D-4331 NASA-TM-D-4331 NASA-TM-D-4331 NASA-TM-X-1501 NASA-TM-X-1453 NASA-TM-X-1453 NASA-TM-D-4388 NASA-TM-D-4388 NASA-TM-D-4388 NASA-TM-D-4388 NASA-SP-7011/43/ NASA-SP-7011/42/ NASA-TM-D-4317 NASA-TM-D-4318 NASA-TM-D-4317 NASA-TM-D-4318 NASA-TM-D-4317 NASA-TM-D-4318 NASA-TM-D-4318 NA
<pre>c32 N68-14091*# c31 N68-14093*# c31 N68-14093*# c11 N68-14115*# c33 N68-14240*# c33 N68-14240*# c33 N68-14584*# c33 N68-14530*# c31 N68-14530*# c31 N68-14638*# c33 N68-14638*# c33 N68-14638*# c34 N68-14638*# c34 N68-14671*# c34 N68-14671*# c34 N68-14671*# c34 N68-14671*# c31 N68-14747*# c31 N68-14747*# c31 N68-14941*# c31 N68-14941*# c31 N68-14941*# c31 N68-14941*# c31 N68-14941*# c33 N68-14965*# c33 N68-15120*# c30 N68-15127*# c33 N68-15197*# c22 N68-15197*# c35 N68-15195*# c35 N68-1</pre>	NASA-TN-D-4329 NASA-TN-D-4283 NASA-TN-D-4283 NASA-TN-X-1500 NASA-TM-Z-1500 NASA-TM-D-4335 NASA-TN-D-4335 NASA-TN-D-4332 NASA-TN-D-4332 NASA-TN-D-4331 NASA-TN-D-4332 NASA-TN-D-4331 NASA-TN-D-4331 NASA-TN-D-4331 NASA-TM-X-1501 NASA-TM-X-1501 NASA-TM-X-1501 NASA-TN-D-4310 NASA-TN-D-4340 NASA-TN-D-4340 NASA-TN-D-4340 NASA-TN-D-4310 NASA-TN-D-4317 NASA-TN-D-4310 NASA-TN-D-4310 NASA-TN-D-4310 NASA-TN-D-4323 NASA-TN-D-4323 NASA-TN-D-4310 NASA-TN-D-4310 NASA-TN-D-4310 NASA-TN-D-4310 NASA-TN-D-4323 NASA-TN-D-4324 NASA-TN-D-4324 NASA-TN-D-4324 NASA-TN-D-4279 NASA-TN-D-4270 NASA-CR-877, V. 2 NASA-CR-877, V. 2
c32 N68-14091*# c31 N68-14092*# c31 N68-14092*# c11 N68-14092*# c11 N68-14092*# c33 N68-14240*# c33 N68-14240*# c32 N68-14262*# c33 N68-14262*# c31 N68-14638*# c31 N68-14638*# c31 N68-14639*# c32 N68-14639*# c32 N68-14640*# c12 N68-14640*# c12 N68-14671*# c12 N68-14725*# c10 N68-14725*# c11 N68-14725*# c11 N68-14725*# c11 N68-14725*# c11 N68-14747*# c17 N68-14888*# c30 N68-14965*# c30 N68-14965*# c30 N68-1510*# c30 N68-15193*# c30 N68-15197*# c05 N68-15306*# c24 N68-15328*#	NASA-TM-D-4329 NASA-TM-D-4283 NASA-TM-2-1500 NASA-TM-2-1500 NASA-TM-2-4335 NASA-TM-D-4332 NASA-TM-D-4332 NASA-CR-876 NASA-CR-909 NASA-TM-2-4331 NASA-TM-2-4331 NASA-TM-2-4331 NASA-TM-2-4315 TR-66-67 NASA-TM-D-4388 NASA-TM-D-4388 NASA-TM-D-4388 NASA-TM-D-4317 NASA-TM-D-4317 NASA-TM-D-4317 NASA-TM-D-4317 NASA-TM-D-4317 NASA-TM-D-4318 NASA-TM-D-4317 NASA-TM-D-4317 NASA-TM-D-4318 NASA-TM-D-4317 NASA-TM-D-4318 NASA-TM-D-4318 NASA-TM-D-4318 NASA-TM-D-4318 NASA-TM-D-4318 NASA-TM-D-4318 NASA-TM-D-4318 NASA-TM-D-4318 NASA-TM-D-4318 NASA-TM-D-4318 NASA-TM-D-4318 NASA-TM-D-4318 NASA-TM-D-4318 NASA-TM-D-4318 NASA-TM-D-4318 NASA-TM-D-4318 NASA-TM-D-4328 NASA-TM-D-4328 NASA-TM-D-4328 NASA-TM-D-4305
<pre>c32 N68-14091*# c31 N68-14092*# c31 N68-14092*# c11 N68-14015*# c33 N68-14240*# c33 N68-14240*# c32 N68-14620*# c33 N68-14630*# c31 N68-14630*# c31 N68-14630*# c31 N68-14630*# c32 N68-14630*# c32 N68-14640*# c12 N68-14671*# c14 N68-14672*# c14 N68-14672*# c17 N68-14641*# c17 N68-14672*# c17 N68-14640*# c12 N68-14640*# c12 N68-14640*# c12 N68-14640*# c13 N68-14903* c30 N68-14903* c30 N68-14940*# c31 N68-14965*# c31 N68-14965*# c30 N68-15120*# c30 N68-15193*# c22 N68-15197*# c24 N68-15306*# c24 N68-15328*# c12 N68-15328*# c12 N68-15328*# c12 N68-15328*# c12 N68-15328*#</pre>	NASA-TN-D-4329 NASA-TN-D-4283 NASA-TN-2.1500 NASA-TN-2.1500 NASA-TN-2.4335 NASA-TN-2.4335 NASA-TN-D-4332 NASA-TN-D-4331 NASA-TM-X-1601 NASA-TN-D-4310 NASA-TN-D-4317 NASA-TN-D-4310 NASA-TN-D-4317 NASA-TN-D-4317 NASA-TN-D-4317 NASA-TN-D-4310 NASA-TN-D-4317 NASA-TN-D-4310 NASA-TN-D-4317
<pre>c32 N68-14091*# c31 N68-14093*# c31 N68-14093*# c11 N68-14115*# c33 N68-14262*# c33 N68-14262*# c33 N68-14262*# c33 N68-14538*# c33 N68-14538*# c33 N68-14638*# c31 N68-14638*# c31 N68-14638*# c31 N68-14638*# c32 N68-14638*# c32 N68-14640*# c32 N68-14671*# c4 N68-14671*# c12 N68-14725*# c11 N68-14747*# c17 N68-14747*# c17 N68-14747*# c17 N68-14941*# c31 N68-14965*# c30 N68-15120*# c30 N68-15127*# c30 N68-15197*# c22 N68-15328*# c33 N68-15328*# c34 N68-1538*# c34 N68-1538*# c34 N68-15430*# c34 N68-1548</pre>	NASA-TN-D-4329 NASA-TN-D-4283 NASA-TN-2-1500 NASA-TM-2-1500 NASA-TM-D-4335 NASA-TM-D-4335 NASA-TM-D-4332 NASA-CR-876 NASA-CR-909 NASA-CR-909 NASA-CR-915 TR-66-67 NASA-TM-2-4310 NASA-TN-D-4382 NASA-TN-D-4310 NASA-TN-D-4310 NASA-TM-D-4310 NASA-TM-D-4313 NASA-TM-D-4310 NASA-TM-D-4323 NASA-TM-D-4323 NASA-TM-D-4323 NASA-TM-D-4323 NASA-TM-D-4323 NASA-TM-D-4323 NASA-TM-D-4323 NASA-TM-D-4323 NASA-TM-D-4323 NASA-TM-D-4323 NASA-TM-D-4323 NASA-TM-D-4323 NASA-TM-D-4323 NASA-TM-D-4323 NASA-TM-D-4326 NASA-TM-D-4360 NASA-CR-1003 SID-65-1200-4 NASA-CR-1003 NASA-TM-D-4301
<pre>c32 N68-14091*# c31 N68-14092*# c31 N68-14092*# c33 N68-14240*# c33 N68-14240*# c33 N68-14240*# c33 N68-14240*# c33 N68-14250*# c33 N68-14638*# c31 N68-14638*# c31 N68-14638*# c31 N68-14639*# c32 N68-14639*# c32 N68-14640*# c4 N68-14671*# c4 N68-14671*# c12 N68-14725*# c12 N68-14747*# c17 N68-14888*# c32 N68-14965*# c32 N68-15197*# c30 N68-15197*# c32 N68-1530*# c32 N68-1548*# c32 N68-1530*# c32 N68-1548*# c32 N68-154</pre>	NASA-TM-D-4329 NASA-TM-D-4283 NASA-TM-2-1500 NASA-TM-2-1500 NASA-TM-D-4335 NASA-TM-D-4332 NASA-CR-876 NASA-CR-876 NASA-CR-909 NASA-TM-2-4331 NASA-CR-915 TR-66-67 NASA-TM-2-1453 NASA-TM-2-1453 NASA-TM-2-4380 NASA-TM-D-4380 NASA-TM-D-4380 NASA-TM-D-4380 NASA-TM-D-4323 NASA-TM-D-4317 NASA-TM-D-4317 NASA-TM-D-4317 NASA-TM-D-4317 NASA-TM-D-4318 NASA-TM-D-4317 NASA-TM-D-4317 NASA-TM-D-4318 NASA-TM-D-4317 NASA-TM-D-4318 NASA-TM-D-4318 NASA-TM-D-4318 NASA-TM-D-4318 NASA-TM-D-4318 NASA-TM-D-4318 NASA-TM-D-4318 NASA-TM-D-4318 NASA-TM-D-4318 NASA-TM-D-4318 NASA-TM-D-4318 NASA-TM-D-4318 NASA-TM-D-4318 NASA-TM-D-4318 NASA-TM-D-4318 NASA-TM-D-4318 NASA-TM-D-4305 NASA-TM-D-4301
<pre>c32 N68-14091*# c31 N68-14092*# c31 N68-14092*# c11 N68-14015*# c33 N68-14240*# c33 N68-14240*# c32 N68-14630*# c33 N68-14630*# c31 N68-14630*# c31 N68-14630*# c31 N68-14639*# c32 N68-14630*# c32 N68-14639*# c32 N68-14641*# c12 N68-14671*# c14 N68-14725*# c14 N68-14725*# c17 N68-1488*# c02 N68-14903* c30 N68-1491*# c31 N68-14965*# c32 N68-14986*# c31 N68-14986*# c31 N68-14985*# c32 N68-15120*# c30 N68-15120*# c30 N68-15133*# c22 N68-15137*# c22 N68-1530*# c22 N68-1530*# c33 N68-1530*# c33 N68-1530*# c33 N68-1530*# c32 N68-1530*# c33 N68-1547*# c34 N6</pre>	NASA-TN-D-4329 NASA-TN-D-4283 NASA-TN-2-1500 NASA-TM-2-1500 NASA-TM-D-4335 NASA-TM-D-4335 NASA-TM-D-4332 NASA-CR-876 NASA-CR-909 NASA-CR-909 NASA-CR-915 TR-66-67 NASA-TM-2-4310 NASA-TN-D-4382 NASA-TN-D-4310 NASA-TN-D-4310 NASA-TM-D-4310 NASA-TM-D-4313 NASA-TM-D-4310 NASA-TM-D-4323 NASA-TM-D-4323 NASA-TM-D-4323 NASA-TM-D-4323 NASA-TM-D-4323 NASA-TM-D-4323 NASA-TM-D-4323 NASA-TM-D-4323 NASA-TM-D-4323 NASA-TM-D-4323 NASA-TM-D-4323 NASA-TM-D-4323 NASA-TM-D-4323 NASA-TM-D-4323 NASA-TM-D-4326 NASA-TM-D-4360 NASA-CR-1003 SID-65-1200-4 NASA-CR-1003 NASA-TM-D-4301
<pre>c32 N68-14091*# c31 N68-14093*# c31 N68-14092*# c33 N68-14093*# c11 N68-14115*# c33 N68-14262*# c33 N68-14262*# c33 N68-14538*# c33 N68-14538*# c33 N68-14638*# c31 N68-14638*# c31 N68-14638*# c31 N68-14638*# c32 N68-14640*# c32 N68-14640*# c12 N68-14671*# c14 N68-14671*# c14 N68-14671*# c14 N68-14671*# c17 N68-14747*# c17 N68-14747*# c17 N68-14747*# c17 N68-14941*# c31 N68-14965*# c30 N68-15120*# c30 N68-15197*# c32 N68-15328*# c32 N68-15328*# c32 N68-15328*# c33 N68-15328*# c33 N68-15328*# c33 N68-15328*# c34 N68-15328*# c34 N68-15328*# c32 N68-15328*# c32 N68-15328*# c32 N68-15328*# c33 N68-15478*# c33 N68-1547*# c33 N68-1547*# c33 N68-1547*#</pre>	NASA-TM-D-4329 NASA-TM-D-4283 NASA-TM-2-1500 NASA-TM-2-1500 NASA-TM-D-4335 NASA-TM-D-4332 NASA-CR-876 NASA-CR-876 NASA-CR-909 NASA-TM-2-4331 NASA-CR-915 TR-66-67 NASA-TM-2-1453 NASA-TM-2-1453 NASA-TM-2-4380 NASA-TM-D-4380 NASA-TM-D-4380 NASA-TM-D-4380 NASA-TM-D-4323 NASA-TM-D-4317 NASA-TM-D-4317 NASA-TM-D-4317 NASA-TM-D-4317 NASA-TM-D-4318 NASA-TM-D-4317 NASA-TM-D-4317 NASA-TM-D-4318 NASA-TM-D-4317 NASA-TM-D-4318 NASA-TM-D-4318 NASA-TM-D-4318 NASA-TM-D-4318 NASA-TM-D-4318 NASA-TM-D-4318 NASA-TM-D-4318 NASA-TM-D-4318 NASA-TM-D-4318 NASA-TM-D-4318 NASA-TM-D-4318 NASA-TM-D-4318 NASA-TM-D-4318 NASA-TM-D-4318 NASA-TM-D-4318 NASA-TM-D-4318 NASA-TM-D-4305 NASA-TM-D-4301
<pre>c32 N68-14091*# c31 N68-14092*# c31 N68-14092*# c11 N68-14015*# c33 N68-14240*# c33 N68-14240*# c32 N68-14630*# c33 N68-14630*# c31 N68-14630*# c31 N68-14630*# c31 N68-14639*# c32 N68-14630*# c32 N68-14639*# c32 N68-14641*# c12 N68-14671*# c14 N68-14725*# c14 N68-14725*# c17 N68-1488*# c02 N68-14903* c30 N68-1491*# c31 N68-14965*# c32 N68-14986*# c31 N68-14986*# c31 N68-14985*# c32 N68-15120*# c30 N68-15120*# c30 N68-15133*# c22 N68-15137*# c22 N68-1530*# c22 N68-1530*# c33 N68-1530*# c33 N68-1530*# c33 N68-1530*# c32 N68-1530*# c33 N68-1547*# c34 N6</pre>	NASA-TN-D-4329 NASA-TN-2-1500 NASA-TN-2-1500 NASA-TN-2-1500 NASA-TN-2-4335 NASA-TN-2-4332 NASA-TN-D-4332 NASA-TN-D-4332 NASA-TN-D-4331 NASA-TN-D-4331 NASA-TN-0-4331 NASA-TN-0-4331 NASA-TN-0-4331 NASA-TN-2-4310 NASA-TN-2-1501 NASA-TN-2-1501 NASA-TN-2-4300 NASA-TN-D-4300 NASA-TN-D-4300 NASA-TN-D-4310 NASA-TN-D-4310 NASA-TN-D-4310 NASA-TN-D-4310 NASA-TN-D-4310 NASA-TN-D-4310 NASA-TN-D-4320 NASA-TN-D-4300 NASA-TN-D-4301 NASA-TN-D-4301 NASA-TN-D-4301 NASA-TN-D-4301 NASA-TN-D-4301 NASA-TN-D-4301 NASA-TN-D-4301 NASA-TN-D-4301 NASA-TN-D-4301 NASA-TN-D-4301 NASA-TN-D-4301 NASA-TN-D-4301 NASA-TN-D-4301 NASA-TN-D-4301 NASA-TN-D-4301
<pre>c32 N68-14091*# c31 N68-14093*# c31 N68-14092*# c33 N68-14093*# c11 N68-14115*# c33 N68-14262*# c33 N68-14262*# c33 N68-14538*# c33 N68-14538*# c33 N68-14638*# c31 N68-14638*# c31 N68-14638*# c31 N68-14638*# c32 N68-14640*# c32 N68-14640*# c12 N68-14671*# c14 N68-14671*# c14 N68-14671*# c14 N68-14671*# c17 N68-14747*# c17 N68-14747*# c17 N68-14747*# c17 N68-14941*# c31 N68-14965*# c30 N68-15120*# c30 N68-15197*# c32 N68-15328*# c32 N68-15328*# c32 N68-15328*# c33 N68-15328*# c33 N68-15328*# c33 N68-15328*# c34 N68-15328*# c34 N68-15328*# c32 N68-15328*# c32 N68-15328*# c32 N68-15328*# c33 N68-15478*# c33 N68-1547*# c33 N68-1547*# c33 N68-1547*#</pre>	NASA-TN-D-4329 NASA-TN-D-4283 NASA-TN-2-1500 NASA-TN-2-1500 NASA-TN-2-4335 NASA-TN-D-4335 NASA-TN-D-4332 NASA-TN-D-4332 NASA-CR-876 NASA-CR-876 NASA-CR-909 NASA-TN-0-4331 NASA-TN-2-4331 NASA-TN-2-4310 NASA-TN-D-4387 NASA-TN-D-4310 NASA-TN-D-4310 NASA-TN-D-4310 NASA-TN-D-4310 NASA-TN-D-4310 NASA-TN-D-4310 NASA-TN-D-4310 NASA-TN-D-4323 NASA-TN-D-4323 NASA-TN-D-4323 NASA-TN-D-4323 NASA-TN-D-4323 NASA-TN-D-4323 NASA-TN-D-4323 NASA-TN-D-4328 NASA-TN-D-4328 NASA-TN-D-4328 NASA-TN-D-4328 NASA-TN-D-4328 NASA-TN-D-4328 NASA-TN-D-4328 NASA-TN-D-4328 NASA-TN-D-4328 NASA-TN-D-4328 NASA-TN-D-4328 NASA-TN-D-4328 NASA-TN-D-4328 NASA-TN-D-4328 NASA-TN-D-4387
<pre>c32 N68-14091*# c31 N68-14092*# c31 N68-14092*# c11 N68-140192*# c11 N68-14115*# c33 N68-14240*# c35 N68-14262*# c33 N68-14270*# c32 N68-14563*# c31 N68-14639*# c31 N68-14639*# c31 N68-14639*# c32 N68-14639*# c32 N68-14640*# c44 N68-14671*# c44 N68-14671*# c14 N68-14725*# c10 N68-14747*# c17 N68-14888*# c30 N68-14965*# c30 N68-15010*# c30 N68-15010*# c30 N68-1501*# c30 N68-1501*# c30 N68-1501*# c30 N68-1501*# c31 N68-1502*# c31 N68-1502*# c33 N68-1532*# c33 N68-1532*# c33 N68-1532*# c33 N68-1532*# c33 N68-1532*# c34 N68-1532*# c32 N68-1532*# c32 N68-1532*# c32 N68-15476*# c34 N68-15477*# c34 N68-15476*# c34 N68-15477*# c34 N68-15484# c34 N68-15477*# c34 N68-15484# c34 N68</pre>	NASA-TM-D-4329 MASA-TM-D-4283 MASA-TM-X-1500 NASA-TM-X-1500 NASA-TM-X-1500 NASA-TM-D-4335 NASA-TM-D-4335 NASA-TM-D-4332 NASA-TM-X-1501 NASA-TM-X-1501 NASA-TM-D-4388 NASA-TM-D-4388 NASA-TN-D-43840 NASA-TN-D-4340 NASA-TN-D-4340 NASA-TM-D-4317 NASA-TM-D-4317 NASA-TM-D-4317 NASA-TM-D-4317 NASA-TM-D-4318 NASA-TM-D-4318 NASA-TM-D-4318 NASA-TM-D-4323 NASA-TM-D-4318 NASA-TM-D-43279 NASA-TM-D-4328 NASA-TM-D-4318 NASA-TM-D-4318 NASA-TM-D-43279 NASA-TM-D-4318 NASA-TM-D-4317
<pre>c32 N68-14091*# c31 N68-14093*# c31 N68-14092*# c33 N68-14093*# c11 N68-14115*# c33 N68-14262*# c33 N68-14262*# c33 N68-14530*# c32 N68-14530*# c31 N68-14638*# c31 N68-14638*# c31 N68-14638*# c31 N68-14638*# c32 N68-14640*# c12 N68-14671*# c14 N68-14671*# c14 N68-14671*# c14 N68-14671*# c17 N68-14747*# c17 N68-14747*# c17 N68-14941*# c31 N68-14965*# c30 N68-15120*# c30 N68-15120*# c30 N68-15197*# c31 N68-15328*# c32 N68-15328*# c32 N68-15328*# c33 N68-15328*# c33 N68-15328*# c33 N68-15328*# c33 N68-15328*# c34 N68-1547*# c34 N68-1547*# c34 N68-1547*# c31 N68-1547*# c31 N68-1547*# c31 N68-1547*# c31 N68-1547*# c31 N68-15570*# c32 N68-15570*#</pre>	NASA-TN-D-4329 NASA-TN-2-1500 NASA-TN-2-1500 NASA-TN-2-1500 NASA-TN-2-4335 NASA-TN-D-4335 NASA-TN-D-4332 NASA-TN-D-4332 NASA-TN-0-4332 NASA-TN-0-4331 NASA-TN-0-4331 NASA-TN-2-4331 NASA-TN-2-4331 NASA-TN-2-4380 NASA-TN-D-4380 NASA-TN-D-4380 NASA-TN-D-4380 NASA-TN-D-4380 NASA-TN-D-4380 NASA-TN-D-4380 NASA-TN-D-4380 NASA-TN-D-4301 NASA-TN-D-4328 NASA-TN-D-4301 NASA-TN-D-4328 NASA-TN-D-4380 NASA-TN-D-4328 NASA-TN-D-4328 NASA-TN-D-4328 NASA-TN-D-4328 NASA-TN-D-4328 NASA-TN-D-4328 NASA-TN-D-4328 NASA-TN-D-4328 NASA-TN-D-4328 NASA-TN-D-4328 NASA-TN-D-4328
<pre>c32 N68-14091*# c31 N68-14092*# c31 N68-14092*# c11 N68-14092*# c11 N68-14240*# c33 N68-14240*# c33 N68-14240*# c33 N68-14270*# c32 N68-14563*# c33 N68-14630*# c31 N68-14630*# c31 N68-14639*# c32 N68-14639*# c32 N68-14640*# c32 N68-14640*# c12 N68-14671*# c14 N68-14725*# c14 N68-14725*# c17 N68-14888*# c30 N68-14965*# c30 N68-15120*# c30 N68-15120*# c30 N68-15127*# c31 N68-1532*# c33 N68-1532*# c33 N68-1532*# c33 N68-1532*# c33 N68-1532*# c34 N68-1532*# c34 N68-1532*# c35 N68-1532*# c35 N68-1532*# c36 N68-1532*# c37 N68-1557*# c31 N68-</pre>	NASA-TM-D-4329 NASA-TM-D-4283 NASA-TM-2-1500 NASA-TM-2-1500 NASA-TM-D-4335 NASA-TM-D-4332 NASA-TM-D-4332 NASA-CR-876 NASA-CR-909 NASA-TM-2-4331 NASA-TM-2-4331 NASA-TM-2-4331 NASA-TM-2-4331 NASA-TM-2-4388 NASA-TM-D-4388 NASA-TM-D-4388 NASA-TM-D-4388 NASA-TM-D-4388 NASA-TM-D-4317 NASA-TM-D-4317 NASA-TM-D-4317 NASA-TM-D-4317 NASA-TM-D-4318 NASA-TM-D-4328 NASA-TM-D-4328 NASA-TM-D-4328 NASA-TM-D-4328 NASA-TM-D-4328 NASA-TM-D-4328 NASA-TM-D-4328 NASA-TM-D-4328 NASA-TM-D-4328 NASA-TM-D-4328 NASA-TM-D-4390
<pre>c32 N68-14091*# c31 N68-14093*# c31 N68-14092*# c33 N68-14093*# c11 N68-14115*# c33 N68-14262*# c33 N68-14262*# c33 N68-14530*# c32 N68-14530*# c31 N68-14638*# c31 N68-14638*# c31 N68-14638*# c31 N68-14638*# c32 N68-14640*# c12 N68-14671*# c14 N68-14671*# c14 N68-14671*# c14 N68-14671*# c17 N68-14747*# c17 N68-14747*# c17 N68-14941*# c31 N68-14965*# c30 N68-15120*# c30 N68-15120*# c30 N68-15197*# c31 N68-15328*# c32 N68-15328*# c32 N68-15328*# c33 N68-15328*# c33 N68-15328*# c33 N68-15328*# c33 N68-15328*# c34 N68-1547*# c34 N68-1547*# c34 N68-1547*# c31 N68-1547*# c31 N68-1547*# c31 N68-1547*# c31 N68-1547*# c31 N68-15570*# c32 N68-15570*#</pre>	NASA-TN-D-4329 MASA-TN-D-4283 MASA-TN-D-4283 MASA-TN-X-1500 NASA-TN-X-1500 NASA-TN-X-1500 NASA-TN-X-1500 MASA-TN-D-4332 NASA-TN-D-4332 NASA-TN-D-4331 NASA-TN-D-4331 NASA-TN-D-4331 NASA-TN-D-4331 NASA-TN-D-4331 NASA-TN-D-4331 NASA-TN-D-4331 NASA-TM-X-1601 NASA-TN-D-4388 NASA-TN-D-4388 NASA-TN-D-4300 NASA-TN-D-4300 NASA-TN-D-4301 NASA-TN-D-4317

c03 N68-17110*#	c13 N68-18902*# NASA-SP-158
c22 N68-17131*# F-910091-11	c24 N68-18949*#
NASA-CR-992	c12 N68-18997*# NASA-TN-D-4325
c08 N68-17154*# NASA-CR-1020	c03 N68-18998*#
c30 N68-17215*# NASA-CR-1010	c17 N68-18999*#
SID-66-1678-3, V. 11 c17 N68-17317*#NASA-TN-D-4379	c12 N68-19000*#
c17 N68-17317*# NASA-TN-D-4379 c14 N68-17329*#	c14 N68-19001*# NASA-TM-X-1525 c21 N68-19061*# NASA-TN-D-4481
NASA-CR-1018	c09 N68-19062*#
c19 N68-17334*#	c01 N68-19063*# NASA-TN-D-4437
c12 N68-17376*# NASA-TN-D-4308	c30 N68-19064*# NASA-TM-X-1529
c17 N68-17377*#	c02 N68-19065*# NASA-TM-X-1527
c02 N68-17391*# NASA-TN-D-4396	c20 N68-19084*#
c31 N68-17498*#	c31 N68-19085*#
c19 N68-17532*#NASA-TN-D-4399 c07 N68-17542*#NASA-TT-F-434	c32 N68-19143*#
COV NOS-17542+#	c19 N68-19144*#
c01 N68-17555*#	c05 N68-19165*# NASA-CR-878
c12 N68-17563*# NASA-TT-F-520	c01 N68-19180*# NASA-TN-D-4477
c15 N68-17564*# NASA-TN-D-4445	c02 N68-19184*#
c33 N68-17566*# NASA-TN-D-4136	c09 N68-19185*# NASA-TN-D-4426
c32 N68-17588*# NASA-TN-D-4358	c30 N68-19186*# NASA-CR-1011
c17 N68-17591*# NASA-CR-930	SID-66-1678-4
c26 N68-17594*#	c33 N68-19187*# NASA-TN-D-4491
c17 N68-17624*#NASA-SP-3043 c32 N68-17651*#NASA-TN-D-4357	c29 N68-19188*#
c31 N68-17844*# NASA-SP-163 c01 N68-17880*#	c30 N68-19192*#
c01 N68-17896*# NASA-TN-D-4314	c11 N68-19207*# NASA-TM-X-1536
c17 N68-17897*#NASA-TN-D-4318	c12 N68-19225*# NASA-TM-X-1482
c24 N68-17898*# NASA-TN-D-4363	c31 N68-19226*#
c01 N68-17899*#	c10 N68-19229*# NASA-CR-999
c05 N68-18014*#	SM-48464-F
c03 N68-18044*# NASA-CR-924, V. 3	c21 N68-19236*#
c33 N68-18046*#	c01 N68-19237*#NASA-TM-X-1517 c12 N68-19246*#NASA-TN-D-4441
c24 N68-18118*#GCA-TR-67-2-N NASA-CR-998	c12 N68-19246*#
c33 N68-18122*# NASA-TN-D-4326	NASA-CR-928
c07 N68-18123*# NASA-TN-D-4366	c31 N68-19275*#
c08 N68-18144*# NASA-CR-962	c15 N68-19307*# NASA-SP-5086
RAD-TR-65-28	RSIC-491
c17 N68-18145*#	c32 N68-19311*# ME-1065-678
c12 N68-18146*#	NASA-CR-978
C07 N68-18178*#	c30 N68-19315*# NASA-CR-1012
c08 N68-18179*#	SID-66-1678-5 c30 N68-19330*#NASA-TM-X-1541
c01 N68-18189*#	c08 N68-19336*#
c33 N68-18196*# NASA-TM-X-1134	c12 N68-19340*# NASA-TM-X-1528
c22 N68-18197*# NASA-TN-D-4315	c01 N68-19341*# NASA-TM-X-1530
c28 N68-18216*# NASA-TM-X-1267	c15 N68-19343*# NASA-SP-5090
c06 N68-18219*# NASA-TN-D-4297	RSIC-595
c28 N68-18221*#	c17 N68-19347*# NASA-TM-X-1514
c22 N68-18243*# F-910091-12	c06 N68-19434*# NASA-TN-D-4451
NASA-CR-993 c20 N68-18246*#NASA-TN-D-4395	c28 N68-19581*#NASA-TN-D-4455 c30 N68-19590*#NASA-CR-1017
c07 N68-18247*#	c02 N68-19620*#
c28 N68-18249*# NASA-TN-D-4442	c30 N68-19622*# NASA-TM-X-1508
c02 N68-18250*# NASA-TN-D-4179	c07 N68-19624*# NASA-SP-5079
c22 N68-18252*# NASA-TM-X-1426	c14 N68-19642*# NASA-TR-R-281
c12 N68-18253*# NASA-TN-D-4367	c30 N68-19676*# NASA-CR-1001
c24 N68-18254*#	SID-65-1200-2, V. 2
c19 N68-18455*#	c28 N68-19708*#NASA-TM-X-1559 c12 N68-19709*#NASA-TN-D-4401
c11 N68-18460*#NASA-TM-X-1515 c21 N68-18484*#NASA-CR-977	c12 N68-19709*#NASA-TN-D-4401 c18 N68-19710*#NASA-TN-D-4374
c25 N68-18485*#	c10 N68-19710*#
c03 N68-18501*# NASA-TN-D-4432	c26 N68-19924*# NASA-TN-D-4407
c22 N68-18541*# NASA-TN-D-4435	c22 N68-19925*# NASA-TN-D-4459
c07 N68-18542*# NASA-TN-D-4294	c01 N68-19954*# NASA-TN-D-4465
c17 N68-18610*# NASA-TN-D-4475	c30 N68-19985*# NASA-CR-1013
c25 N68-18614*# NASA-TN-D-4309	SID-66-1678-6, V. 14
c31 N68-18615*#	c04 N68-20026*# NASA-SP-7011/47/
c07 N68-18616*#NASA-TN-D-4362 c08 N68-18620*#NASA-TN-D-4421	c04 N68-20027*#NASA-SP-7011/48/ c15 N68-20056*#NASA-SP-5085
c08 N68-18620*#NASA-TN-D-4421 c03 N68-18702*#NASA-TM-X-1456	c15 N68-20056*#
c07 N68-18703*# NASA-TM-X-1458	c28 N68-20064*# NASA-TN-D-4416
c01 N68-18720*# NASA-TN-D-4360	c33 N68-20065*# NASA-TN-D-4484
c32 N68-18721*# NASA-TN-D-4486	c33 N68-20066*# NASA-TN-D-4498
c31 N68-18743*# NASA-SP-139	c30 N68-20084*# NASA-CR-1006
c32 N68-18769*# GD/C-BTD-67-056	SID-65-1200-7, V. 7
NASA-CR-941	c28 N68-20186*# NASA-TM-X-1546
CO2 N68-18771*#	c28 N68-20187*# NASA-TN-D-4420
c26 N68-18772*#NASA-TN-D-4466 c31 N68-18822*#NASA-TN-D-4275	c30 N68-20192*# NASA-TR-R-282 c31 N68-20198*# NASA-TN-D-4425
c31 N68-18825*#	c31 N68-20198*#NASA-TN-D-4425 c15 N68-20199*#NASA-TN-D-4456
NASA-CR-944	c03 N68-20276*#
c14 N68-18834*# NASA-TM-X-1524	c13 N68-20278*# NASA-TN-D-3815
c18 N68-18849*# NASA-CR-995	c26 N68-20295*#
c05 N68-18870*# NASA-SP-5047	c25 N68-20296*# NASA-TN-D-4517

c33	N68-21680*#	NASA-TN-D-4492
c01	N68-21681*#	
c30	N68-21685*#	NASA-CR-1004
		SID-65-1200-5
c25	N68-21691*#	NASA-TN-D-4538
c01	N68-21692*#	NASA-TM-X-1572
c01	N68-21703*#	NASA-TM-X-1547
c33	N68-21704*#	NASA-TM-X-1557
c22	N68-21705*#	NASA-TM-X-1563
c26	N68-21708*#	
c12	N68-21724*#	NASA-TN-D-4496
c29	N68-21731*#	NASA-TM-X-1567
	N68-21732*#	NASA-TN-D-4523
c30	N68-21733*#	NASA-TN-D-4468
c21	N68-21754*#	NASA-TN-D-4512
c31	N68-21758*#	NASA-TN-D-4537
c03	N68-21766*#	NASA-TN-D-4533
c32	N68-21767*#	NASA-TN-X-1552
c17	N68-21768*#	NASA-TN-D-4541
c31	N68-21778*#	NASA-TM-X-1542
c30	N68-21802*#	NASA-TT-F-515
c34	N68-21828*#	NASA-11-1-010
c31	N68-21833*#	
c02	N68-21834*#	NASA-TM-X-1565
c03 c05	N68-21835*#	NASA-TN-D-4497
	N68-21859*# N68-21864*#	NASA-CR-1042
c30 c32		
c32	N68-21869*#	NASA-TN-D-4502 NASA-CR-1047
	N68-21893*#	
c15	N68-21898*#	NASA-TM-X-1540
c13	N68-21904*#	NASA-TM-X-1553
c17	N68-21917*#	NASA-SP-5088
		RSIC-495
	N68-21924*#	NASA-TN-D-4545
c01	N68-21940*#	NASA-TM-X-1551
c01	N68-21941*#	••••••••••••••••••••••••••••••••••••••
c14	N68-21942*#	NASA-TN-D-4501
	N68-21949*#	NASA-CR-1039
c01	N68-21950*#	••••••••••••••••••••••••••••••••••••••
c15	N68-21965*#	••••••••••••••••••••••••••••••••••••••
c19	N68-21978*#	••••••••••••••••••••••••••••••••••••••
c15	N68-21979*#	••••••••••••••••••••••••••••••••••••••
c01	N68-22002*#	NASA-TM-X-1550
c07	N68-22019*#	••••••••••••••••••••••••••••••••••••••
c22	N68-22022*#	NASA-TM-X-1539
c02	N68-22033*#	
c22		F-910093-37
	· · •	NASA-CR-1030
c12	N68-22087*#	NASA-CR-888
		TRACOR-67-070-U
c22	N68-22088*#	F-910091-14
		NASA-CR-1028
c28	N68-22096*#	••••••••••••••••••••••••••••••••••••••
c33	N68-22118*#	NASA-SP-148
		NASA-TN-D-4543
c04	N68-22194*#	NASA-SP-7011/46/
c12	N68-22200*#	F-910091-15
010	100 22200 #	NASA-CR-1029
c30	N68-22202*#	NASA-CR-1036
c31	N68-22213*#	NASA-TN-D-4327
c03	N68-22257*#	
c03	N68-22258*#	NASA-TN-D-4532
c31	N68-22262*#	NASA-TT-F-426
		TT-67-51363
c26	N68-22271*#	NASA-TN-D-4513
	N68-22272*#	NASA-TM-X-1463
	N68-22275*#	NASA-TN-D-4550
	N68-22289*#	NASA-TN-D-4559
	N68-22290*#	NASA-TN-D-4530
	N68-22291*#	NASA-TN-D-4530
c02		
		NASA-TN-D-4558
	N68-22302*# N68-22318*#	NASA-CR-1023
c33 c17	N68-22338*#	NASA-CR-1025
C 10	N68-22391*#	
- 05	NC0. 30440+-	NASA-CR-1041
	N68-22448*#	NASA-CR-1035
	N68-22462*#	NASA-TT-F-477
	N68-22475*#	NASA-CR-1027
	N68-22510*#	
	N68-22725*#	NASA-TM-X-1581
	N68-22737*#	NASA-TM-X-1578
c31		NASA-TM-X-1574
c.07	N68-22746*#	NASA-CR-1052
	Neo Jongor -	REPT1691-23
	N68-22778*#	NASA-SP-5040
	N68-22809*#	NASA-TN-D-4424
c15	N68-22810*#	••••••••••••••••••••••••••••••••••••••

c14 N68-20324*#	
	••••••••••••••••••••••••••••••••••••••
c15 N68-20325*#	NASA-TN-D-4463
c18 N68-20329*#	••••••••••••••••••••••••••••••••••••••
c01 N68-20330*#	NASA-TN-D-4462
c33 N68-20331*#	••••••••••••••••••••••••••••••••••••••
c07 N68-20333*#	••••••••••••••••••••••••••••••••••••••
c33 N68-20338*#	••••••••••••••••••••••••••••••••••••••
c05 N68-20339*#	••••••••••••••••••••••••••••••••••••••
c33 N68-20340*#	••••••••••••••••••••••••••••••••••••••
c03 N68-20344*#	••••••••••••••••••••••••••••••••••••••
c12 N68-20352*#	
c30 N68-20353*#	
c05 N68-20354*#	••••••••••••••••••••••••••••••••••••••
c22 N68-20355*#	••••••••••••••••••••••••••••••••••••••
c30 N68-20356*∦	••••••••••••••••••••••••••••••••••••••
c05 N68-20357*#	NASA-SP-6506
c03 N68-20363*#	NASA-TM-X-1560
c32 N68-20364*#	••••••••••••••••••••••••••••••••••••••
c30 N68-20368*#	••••••••••••••••••••••••••••••••••••••
c01 N68-20370*#	••••••••••••••••••••••••••••••••••••••
c33 N68-20374*#	
c20 N68-20375*#	NASA-TN-D-4453
c15 N68-20389*#	NASA-CR-952
	S-67-1014
c03 N68-20432*#	NASA-TM-X-1519
c15 N68-20433*#	NASA-SP-5089
	RSIC-600
c30 N68-20449*#	NASA-CR-1007
	SID-65-1200-8
c30 N68-20450*#	NASA-CR-1008
	SID-66-1678-1
- 21 NCO 004624#	
c31 N68-20467*#	GDC-DBE67-001
	NASA-CR-1019
c30 N68-20468*#	NASA-CR-1015
	SID-66-1678-8, V. 16
c32 N68-20954*#	NASA-TN-D-4428
c30 N68-21077*#	NASA-CR-1009
	SID-66-1678-2, V. 10
c32 N68-21099*#	
c19 N68-21100*#	
c22 N68-21111*#	
c02 N68-21112*#	NASA-TN-D-4438
c10 N68-21122*#	••••••••••••••••••••••••••••••••••••••
c21 N68-21123*#	NASA-TN-D-4449
c22 N68-21124*#	F-910485-1
"	NASA-CR-1031
-14 NCO 01100+#	
c14 N68-21169*#	••••••••••••••••••••••••••••••••••••••
c30 N68-21182*#	••••••••••••••••••••••••••••••••••••••
c26 N68-21219*#	
c15 N68-21226*#	ASTM-STP-431
ore nee crede "	
	NACA-TN-D-4347
	NASA-TN-D-4347
c24 N68-21227*#	NASA-CR-1022
c24 N68-21227*# c30 N68-21228*#	
	NASA-CR-1022
c30 N68-21228*#	NASA-CR-1022 NASA-TN-D-4431 NASA-TN-D-4431 NASA-CR-1014
c30 N68-21228*# c30 N68-21231*#	NASA-CR-1022 NASA-TN-D-4431 NASA-TN-0-4431 NASA-CR-1014 SID-66-1678-7
c30 N68-21228*#	NASA-CR-1022 NASA-TN-D-4431 NASA-CR-1014 SID-66-1678-7 NASA-SP-5084
c30 N68-21228*# c30 N68-21231*# c15 N68-21241*#	NASA-CR-1022 NASA-TN-D-4431 NASA-TN-D-4431 NASA-CR-1014 SID-66-1678-7 NASA-SP-5084 RSIC-501
c30 N68-21228*# c30 N68-21231*# c15 N68-21241*# c31 N68-21260*#	NASA-CR-1022 NASA-TN-D-4431 NASA-TN-1014 SID-66-1678-7 NASA-SP-5084 RSIC-501 NASA-TN-D-4519
c30 N68-21228*# c30 N68-21231*# c15 N68-21241*#	NASA-CR-1022 NASA-TN-D-4431 NASA-TN-D-4431 NASA-CR-1014 SID-66-1678-7 NASA-SP-5084 RSIC-501
c30 N68-21228*# c30 N68-21231*# c15 N68-21231*# c31 N68-21260*# c27 N68-21267*#	NASA-CR-1022 NASA-TN-D-4431 NASA-TN-0-4431 SID-66-1678-7 NASA-SP-5084 RSIC-501 NASA-TN-D-4519 NASA-TN-21556
c30 N68-21228*# c30 N68-21231*# c15 N68-21241*# c31 N68-21260*# c27 N68-21267*# c32 N68-21267*#	NASA-CR-1022 NASA-TN-D-4431 NASA-TN-1014 SID-66-1678-7 NASA-SP-5084 RSIC-501 NASA-TN-D-4519 NASA-TN-D-4519 NASA-TN-D-4505
c30 N68-21228*# c30 N68-21231*# c15 N68-21241*# c31 N68-21260*# c32 N68-21267*# c32 N68-21293*# c12 N68-21365*#	NASA-CR-1022 NASA-TN-D-4431 NASA-TN-0-4431 SID-66-1678-7 NASA-SP-5084 RSIC-501 NASA-TN-D-4519 NASA-TM-X-1556 NASA-TM-X-1556 NASA-TM-X-1526
c30 N68-21228*# c30 N68-21231*# c15 N68-21241*# c31 N68-21260*# c27 N68-21267*# c32 N68-21293*# c12 N68-21365*# c21 N68-21366*#	NASA-CR-1022 NASA-TN-D-4431 NASA-TN-D-4431 NASA-CR-1014 SID-66-1678-7 NASA-SP-5084 RSIC-501 NASA-TN-D-4519 NASA-TN-D-4505 NASA-TN-D-4505 NASA-TN-D-4505 NASA-TM-X-1556 NASA-TM-X-1526
c30 N68-21228*# c30 N68-21231*# c15 N68-21241*# c31 N68-21260*# c27 N68-21267*# c32 N68-21267*# c12 N68-21365*# c11 N68-21366*# c01 N68-21374*#	NASA-CR-1022 NASA-TN-D-4331 NASA-TN-D-4331 NASA-CR-1014 SID-66-1678-7 NASA-SP-5084 RSIC-501 NASA-TN-D-4519 NASA-TN-24505 NASA-TM-X-1556 NASA-TM-X-1556 NASA-TM-X-1549 NASA-TM-X-1549 NASA-TM-X-1549
c30 N68-21228*# c30 N68-21231*# c15 N68-21241*# c31 N68-21260*# c27 N68-21267*# c32 N68-21267*# c32 N68-21365*# c12 N68-21366*# c01 N68-21386*# c04 N68-21383*#	NASA-CR-1022 NASA-CR-1012 NASA-TN-D-4431 SID-66-1678-7 NASA-SP-5084 RSIC-501 NASA-TM-D-4519 NASA-TM-X-1556 NASA-TM-X-1526 NASA-TM-X-1526 NASA-TM-X-1549 NASA-TM-X-1549 NASA-TM-D-4398
c30 N68-21228*# c30 N68-21231*# c15 N68-21241*# c31 N68-21260*# c27 N68-21267*# c32 N68-21267*# c12 N68-21365*# c11 N68-21366*# c01 N68-21374*#	NASA-CR-1022 NASA-CR-1012 NASA-TN-D-4431 SID-66-1678-7 NASA-SP-5084 RSIC-501 NASA-TM-D-4519 NASA-TM-X-1556 NASA-TM-X-1526 NASA-TM-X-1526 NASA-TM-X-1549 NASA-TM-X-1549 NASA-TM-D-4398
c30 N68-21228*# c30 N68-21231*# c15 N68-21241*# c31 N68-21260*# c27 N68-21267*# c32 N68-21267*# c12 N68-21365*# c11 N68-21366*# c01 N68-21374*# c04 N68-21383*#	NASA-CR-1022 NASA-CR-1022 NASA-TN-D-4431 SID-66-1678-7 NASA-SP-5084 RSIC-501 NASA-TN-D-4519 NASA-TM-Z-1556 NASA-TM-Z-1556 NASA-TM-Z-1549 NASA-TM-Z-1549 NASA-TN-D-4525 NASA-TN-D-4525 NASA-TN-D-4525 NASA-TN-D-4525 NASA-TN-D-4525 NASA-TN-D-4525 NASA-TN-D-4525 NASA-TN-D-4525
c30 N68-21228*# c30 N68-21231*# c15 N68-21241*# c27 N68-21260*# c27 N68-21267*# c32 N68-21267*# c12 N68-21365*# c11 N68-21366*# c01 N68-21374*# c04 N68-21383*# c14 N68-21384*# c02 N68-21413*#	NASA-CR-1022 NASA-TN-D-4431 NASA-TN-D-4431 NASA-CR-1014 SID-66-1678-7 NASA-SP-5084 RSIC-501 NASA-TN-D-4519 NASA-TN-D-4505 NASA-TM-X-1556 NASA-TM-X-1526 NASA-TM-X-1549 NASA-TM-D-4525 NASA-TM-D-4525 NASA-TM-D-4398 NASA-TM-D-4398 NASA-TM-X-1570 NASA-SP-147
c30 N68-21228*# c30 N68-21231*# c15 N68-21241*# c31 N68-21260*# c27 N68-21267*# c32 N68-21267*# c12 N68-21365*# c11 N68-21366*# c01 N68-21374*# c04 N68-21383*#	NASA-CR-1022 NASA-CR-1012 NASA-TN-D-4431 SID-66-1678-7 NASA-SP-5084 RSIC-501 NASA-TN-D-4519 NASA-TN-D-4519 NASA-TN-21526 NASA-TN-21526 NASA-TN-21526 NASA-TN-21526 NASA-TN-D-4525 NASA-TN-D-4598 NASA-TN-D-4598 NASA-TN-D-4598 NASA-TM-2-1570 NASA-SP-5087
c30 N68-21228*# c30 N68-21231*# c15 N68-21241*# c27 N68-21260*# c27 N68-21267*# c32 N68-21267*# c12 N68-21365*# c11 N68-21366*# c01 N68-21374*# c04 N68-21383*# c14 N68-21384*# c02 N68-21413*# c15 N68-21429*#	NASA-CR-1022 NASA-CR-1022 NASA-TN-D-4431 SID-66-1678-7 NASA-SP-5084 RSIC-501 NASA-TN-D-4519 NASA-TM-X-1556 NASA-TM-X-1556 NASA-TM-X-1549 NASA-TM-X-1549 NASA-TM-X-1549 NASA-TM-X-1570 NASA-TM-X-1570 NASA-TM-X-1570 NASA-TM-X-1570 NASA-SP-147 NASA-SP-5087 RSIC-598
c30 N68-21228*# c30 N68-21231*# c15 N68-21241*# c27 N68-21260*# c27 N68-21267*# c32 N68-21267*# c12 N68-21365*# c11 N68-21365*# c10 N68-21365*# c14 N68-21383*# c14 N68-21384*# c15 N68-21429*# c06 N68-21430*#	NASA-CR-1022 NASA-TN-D-4431 NASA-TN-D-4431 SID-66-1678-7 NASA-SP-5084 RSIC-501 NASA-TN-D-4519 NASA-TN-D-4505 NASA-TM-X-1556 NASA-TM-X-1556 NASA-TM-X-1549 NASA-TM-X-1549 NASA-TM-X-1549 NASA-TM-24305 NASA-TM-24305 NASA-TM-24305 NASA-SP-147 NASA-SP-5087 RSIC-598 NASA-TN-D-4506
c30 N68-21228*# c30 N68-21231*# c15 N68-21241*# c27 N68-21260*# c27 N68-21267*# c32 N68-21267*# c12 N68-21365*# c11 N68-21366*# c01 N68-21374*# c04 N68-21383*# c14 N68-21384*# c02 N68-21413*# c15 N68-21429*#	NASA-CR-1022 NASA-TN-D-4431 NASA-TN-D-4431 SID-66-1678-7 NASA-SP-5084 RSIC-501 NASA-TN-D-4519 NASA-TN-D-4505 NASA-TM-X-1556 NASA-TM-X-1556 NASA-TM-X-1549 NASA-TM-X-1549 NASA-TM-X-1549 NASA-TM-24305 NASA-TM-24305 NASA-TM-24305 NASA-SP-147 NASA-SP-5087 RSIC-598 NASA-TN-D-4506
c30 N68-21228*# c30 N68-21231*# c15 N68-21241*# c27 N68-21260*# c27 N68-21267*# c32 N68-21267*# c12 N68-21365*# c11 N68-21365*# c10 N68-21365*# c14 N68-21383*# c14 N68-21384*# c15 N68-21429*# c06 N68-21430*#	NASA-CR-1022 NASA-CR-1022 NASA-TN-D-4431 SID-66-1678-7 NASA-SP-5084 RSIC-501 NASA-TN-D-4519 NASA-TN-D-4519 NASA-TN-21526 NASA-TN-21526 NASA-TN-21526 NASA-TN-24525 NASA-TN-D-4525 NASA-TN-D-4526 NASA-TN-D-4598 NASA-TN-21508 NASA-TN-25087 RSIC-598 NASA-TN-24506 NASA-TN-24506 NASA-TN-24506 NASA-TN-24506
c30 N68-21228*# c30 N68-21231*# c15 N68-21241*# c31 N68-21260*# c27 N68-21267*# c32 N68-21267*# c12 N68-21365*# c1 N68-21365*# c1 N68-21365*# c1 N68-213374*# c1 N68-213384*# c1 N68-21384*# c15 N68-21439*# c16 N68-21430*# c17 N68-21431*#	NASA-CR-1022 NASA-CR-1022 NASA-TN-D-4431 SID-66-1678-7 NASA-SP-5084 RSIC-501 NASA-TM-2-4519 NASA-TM-2-4505 NASA-TM-X-1556 NASA-TM-X-1549 NASA-TM-X-1549 NASA-TM-X-1549 NASA-TM-D-4525 NASA-TM-D-4525 NASA-TM-2-4506 NASA-TM-X-1570 NASA-SP-5087 RSIC-598 NASA-TM-2-4506 NASA-TM-2-4506 NASA-TM-2-4506 NASA-TM-2-4506
c30 N68-21228*# c30 N68-21231*# c15 N68-21241*# c27 N68-21260*# c27 N68-21267*# c32 N68-21267*# c12 N68-21365*# c14 N68-21366*# c14 N68-21383*# c15 N68-21413*# c15 N68-21429*# c06 N68-21431*# c17 N68-21431*# c30 N68-21442*#	NASA-CR-1022 NASA-TN-D-4431 NASA-TN-D-4431 SID-66-1678-7 NASA-SP-5084 RSIC-501 NASA-TN-D-4519 NASA-TN-D-4505 NASA-TM-X-1556 NASA-TM-X-1556 NASA-TM-X-1549 NASA-TM-X-1549 NASA-TM-X-1549 NASA-TM-X-1570 NASA-TM-X-1570 NASA-SP-104 RSIC-598 NASA-TM-X-1561 NASA-TM-X-1561 NASA-TM-X-1561 NASA-TM-X-1561 NASA-TM-X-1570 NASA-TM-X-1570 NASA-TM-X-1570 NASA-TM-X-1570 NASA-TM-X-1561 NASA-TM-X-1561 NASA-TM-X-1561 NASA-TM-X-1561 NASA-TM-X-1561
c30 N68-21228*# c30 N68-21231*# c15 N68-21241*# c27 N68-21260*# c27 N68-21267*# c32 N68-21267*# c12 N68-21365*# c11 N68-21365*# c10 N68-21374*# c14 N68-21383*# c15 N68-21413*# c15 N68-21430*# c17 N68-21431*# c31 N68-21443*# c31 N68-21443*#	NASA-CR-1022 NASA-CR-1012 NASA-CR-1014 SID-66-1678-7 NASA-SP-5084 RSIC-501 NASA-TM-D-4519 NASA-TM-2-1556 NASA-TM-2-1526 NASA-TM-2-1526 NASA-TM-2-1526 NASA-TM-2-1526 NASA-TM-2-1526 NASA-TM-2-1527 NASA-SP-147 NASA-SP-5087 RSIC-598 NASA-TM-2-1561 NASA-TM-2-1561 NASA-TM-2-1561 NASA-SP-166
c30 N68-21228*# c30 N68-21231*# c15 N68-21241*# c27 N68-21260*# c27 N68-21267*# c32 N68-21267*# c12 N68-21365*# c14 N68-21366*# c14 N68-21383*# c15 N68-21413*# c15 N68-21429*# c06 N68-21431*# c17 N68-21431*# c30 N68-21442*#	NASA-CR-1022 NASA-CR-1014 SID-66-1678-7 NASA-SP-5084 RSIC-501 NASA-TM-D-4519 NASA-TM-2+1556 NASA-TM-2+1556 NASA-TM-2+1526 NASA-TM-X-1549 NASA-TM-X-1549 NASA-TM-X-1549 NASA-TM-24505 NASA-TM-24505 NASA-TM-24505 NASA-TM-24506 NASA-TM-24506 NASA-TM-24506 NASA-SP-5087 RSIC-598 NASA-SP-5087 RSIC-598 NASA-TM-2+506 NASA-TM-2+506 NASA-CR-1016 SID-66-1678-9 NASA-CR-1025
c30 N68-21228*# c30 N68-21231*# c15 N68-21241*# c27 N68-21260*# c27 N68-21267*# c32 N68-21267*# c12 N68-21365*# c11 N68-21365*# c10 N68-21374*# c14 N68-21383*# c15 N68-21413*# c15 N68-21430*# c17 N68-21431*# c31 N68-21443*# c31 N68-21443*#	NASA-CR-1022 NASA-CR-1014 NASA-TN-D-4431 NASA-CR-1014 SID-66-1678-7 NASA-SP-5084 RSIC-501 NASA-TN-D-4519 NASA-TN-D-4505 NASA-TN-D-4505 NASA-TN-D-4505 NASA-TN-D-4505 NASA-TN-D-4505 NASA-TN-D-4525 NASA-TN-D-4525 NASA-TN-D-4598 NASA-TN-D-4598 NASA-TN-D-4598 NASA-SP-147 NASA-SP-5087 RSIC-598 NASA-TN-D-4506 NASA-TN-D-4506 NASA-TN-D-4506 NASA-TN-D-4506 NASA-TN-D-4506 NASA-TN-D-4506 NASA-TN-D-4506 NASA-TN-D-4506 NASA-TN-D-4506 NASA-TN-D-4506 NASA-TN-D-4506 NASA-TN-D-4506 NASA-TN-D-4506 NASA-TN-20-1025 REPT,-7322-3-T
c30 N68-21228*# c30 N68-21231*# c15 N68-21241*# c31 N68-21260*# c27 N68-21267*# c32 N68-21267*# c32 N68-21365*# c14 N68-21366*# c14 N68-21384*# c15 N68-21438*# c15 N68-21443*# c17 N68-21431*# c30 N68-21442*# c31 N68-21443*# c31 N68-21444*#	NASA-CR-1022 NASA-CR-1022 NASA-TN-D-4431 SID-66-1678-7 NASA-SP-5084 RSIC-501 NASA-TN-D-4519 NASA-TM-X-1556 NASA-TM-X-1556 NASA-TM-X-1549 NASA-TM-X-1549 NASA-TM-X-1549 NASA-TM-X-1549 NASA-TM-X-1570 NASA-TM-X-1570 NASA-TM-X-1570 NASA-SP-5087 RSIC-598 NASA-TM-D-4506 NASA-TM-X-1566 NASA-TM-X-1566 NASA-TM-D-4506 NASA-TM-D-4506 NASA-TM-X-1566 NASA-TM-D-4506 NASA-TM-X-1566 NASA-TM-X-1566 NASA-CR-1016 SID-66-1678-9 NASA-SP-1025 REPT7322-3-T
c30 N68-21228*# c30 N68-21231*# c15 N68-21241*# c27 N68-21260*# c27 N68-21267*# c32 N68-21267*# c12 N68-21365*# c12 N68-21365*# c186-21366*# c10 N68-21374*# c14 N68-21383*# c15 N68-21413*# c15 N68-21429*# c06 N68-21431*# c31 N68-21443*# c31 N68-21444*# c31 N68-21444*# c38 N68-2149*#	NASA-CR-1022 NASA-CR-1014 NASA-TN-D-4431 NASA-CR-1014 SID-66-1678-7 NASA-SP-5084 RSIC-501 NASA-TM-D-4519 NASA-TM-2-1526 NASA-TM-2-1526 NASA-TM-2-1526 NASA-TM-2-1526 NASA-TM-2-1527 NASA-TM-2-1508 NASA-TM-2-1508 NASA-TM-2-1561 NASA-SP-166 NASA-SP-166 NASA-TM-2-1562 NASA-TM-2-1562 NASA-TM-2-1562 NASA-TM-2-1562 NASA-TM-2-1562 NASA-TM-2-1562
c30 N68-21228*# c30 N68-21231*# c15 N68-21241*# c31 N68-21260*# c27 N68-21267*# c32 N68-21267*# c12 N68-21365*# c12 N68-21365*# c14 N68-21374*# c14 N68-21374*# c14 N68-21384*# c04 N68-21431*# c15 N68-21431*# c15 N68-21431*# c17 N68-21431*# c31 N68-21443*# c31 N68-21443*# c33 N68-21444*# c33 N68-21499*# c33 N68-21536*#	NASA-CR-1022 NASA-TN-D-4431 NASA-TN-D-4431 SID-66-1678-7 NASA-SP-5084 RSIC-501 NASA-TM-2-1556 NASA-TM-2-1556 NASA-TM-X-1526 NASA-TM-X-1549 NASA-TM-X-1549 NASA-TM-X-1549 NASA-TM-X-1549 NASA-TM-X-1549 NASA-TM-X-1570 NASA-TM-X-1570 NASA-TM-X-1570 NASA-SP-5087 RSIC-598 NASA-TM-X-1561 NASA-CR-1016 SID-66-1678-9 NASA-CR-1025 REPT7322-3-T NASA-TM-X-1561 NASA-TM-X-1562 NASA-CR-1025
c30 N68-21228*# c30 N68-21231*# c15 N68-21241*# c31 N68-21260*# c27 N68-21267*# c32 N68-21267*# c32 N68-21365*# c12 N68-21365*# c14 N68-21383*# c14 N68-21384*# c15 N68-21432*# c15 N68-21432*# c16 N68-21431*# c30 N68-21443*# c31 N68-21443*# c31 N68-21443*# c33 N68-21443*# c33 N68-21443*# c33 N68-21443*# c33 N68-21443*# c33 N68-21443*# c33 N68-21435*# c33 N68-21435*# c33 N68-21435*# c33 N68-21435*#	NASA-CR-1022 NASA-CR-1014 NASA-TN-D-4431 NASA-TN-D-4431 NASA-CR-1014 SID-66-1678-7 NASA-SP-5084 RSIC-501 NASA-TN-D-4519 NASA-TN-D-4519 NASA-TN-D-4505 NASA-TN-D-4505 NASA-TN-D-4505 NASA-TN-D-4505 NASA-TN-D-4598 NASA-TN-D-4598 NASA-TN-D-4598 NASA-TN-D-4598 NASA-TN-D-4506 NASA-SP-5087 RSIC-598 NASA-TN-D-4506 NASA-TN-D-4506 NASA-TN-D-4506 NASA-TN-D-4506 NASA-TN-D-4506 NASA-TN-D-4506 NASA-TN-D-4506 NASA-TN-D-4506 NASA-TN-D-4506 NASA-TN-D-4506 NASA-TN-D-4506 NASA-TN-2-4506 NASA-TN-2-4506 NASA-TN-2-4506 NASA-TN-2-4506 NASA-TN-2-4506 NASA-TN-2-4506 NASA-TN-2-4506 NASA-TN-2-4506 NASA-TN-2-4506 NASA-TN-2-4506 NASA-TN-2-4506 NASA-TN-2-4506 NASA-TN-2-4506 NASA-TN-2-4506 NASA-TN-2-44488
c30 N68-21228*# c30 N68-21231*# c15 N68-21241*# c27 N68-21260*# c27 N68-21267*# c32 N68-21267*# c32 N68-21365*# c188-21365*# c188-21365*# c188-21365*# c19 N68-21374*# c19 N68-21383*# c15 N68-21413*# c17 N68-21431*# c30 N68-21442*# c31 N68-21443*# c31 N68-21444*# c33 N68-21444*# c33 N68-21536*# c05 N68-21537*# c05 N68-21537*# c05 N68-21537*#	NASA-CR-1022 NASA-CR-1014 NASA-TN-D-4431 NASA-CR-1014 SID-66-1678-7 NASA-SP-5084 RSIC-501 NASA-TN-D-4519 NASA-TN-D-4519 NASA-TN-2-1526 NASA-TN-2-4525 NASA-TN-2-4525 NASA-TN-2-4525 NASA-TN-2-4525 NASA-TN-2-4526 NASA-TN-2-4506 NASA-SP-5087 RSIC-598 NASA-TN-2-4506 NASA-TN-2-1561 NASA-SP-166 NASA-SP-167 NASA-SP-166 NASA-TN-2-32-3-T NASA-TN-2-4488 NASA-TN-2-4488
c30 N68-21228*# c30 N68-21231*# c15 N68-21241*# c31 N68-21260*# c27 N68-21267*# c32 N68-21267*# c32 N68-21365*# c12 N68-21365*# c14 N68-21383*# c14 N68-21384*# c15 N68-21432*# c15 N68-21432*# c16 N68-21431*# c30 N68-21443*# c31 N68-21443*# c31 N68-21443*# c33 N68-21443*# c33 N68-21443*# c33 N68-21443*# c33 N68-21443*# c33 N68-21443*# c33 N68-21435*# c33 N68-21435*# c33 N68-21435*# c33 N68-21435*#	NASA-CR-1022 NASA-TN-D-4431 NASA-TN-D-4431 SID-66-1678-7 NASA-SP-5084 RSIC-501 NASA-TM-2-1556 NASA-TM-2-1556 NASA-TM-2-1526 NASA-TM-2-1526 NASA-TM-2-1529 NASA-TM-2-1529 NASA-TM-2-1529 NASA-TM-2-1508 NASA-TM-2-1508 NASA-TM-2-1508 NASA-TM-2-1508 NASA-TM-2-1508 NASA-TM-2-1508 NASA-CR-1016 SID-66-1678-9 NASA-CR-1025 REPT7322-3-T NASA-TM-2-1561 NASA-TM-2-168 NASA-TM-2-168 NASA-CR-1025 REPT7322-3-T NASA-TM-2-488 NASA-TN-D-4488 NASA-TN-D-4488 NASA-TN-D-4487
c30 N68-21228*# c30 N68-21231*# c15 N68-21241*# c27 N68-21260*# c27 N68-21267*# c32 N68-21267*# c32 N68-21365*# c188-21365*# c188-21365*# c188-21365*# c19 N68-21374*# c19 N68-21383*# c15 N68-21413*# c17 N68-21431*# c30 N68-21442*# c31 N68-21443*# c31 N68-21444*# c33 N68-21444*# c33 N68-21536*# c05 N68-21537*# c05 N68-21537*# c05 N68-21537*#	NASA-CR-1022 NASA-CR-1014 SID-66-1678-7 NASA-SP-5084 RSIC-501 NASA-TM-D-4519 NASA-TM-X-1556 NASA-TM-X-1556 NASA-TM-X-1526 NASA-TM-X-1549 NASA-TM-X-1549 NASA-TM-X-1549 NASA-TM-D-4528 NASA-TM-D-4398 NASA-TM-X-1570 NASA-SP-5087 RSIC-598 NASA-TM-X-1561 NASA-SP-5087 RSIC-598 NASA-TM-X-1561 NASA-SP-166 NASA-CR-1016 SID-66-1678-9 NASA-CR-1025 REPT7322-3-T NASA-TM-X-1562 NASA-TM-X-1562 NASA-TM-X-1562 NASA-TM-X-1562 NASA-TM-X-1562 NASA-TM-X-1562 NASA-TM-X-1562 NASA-TM-X-1562 NASA-TM-X-1562 NASA-TM-X-4487 NASA-TN-D-4487
c30 N68-21228*# c30 N68-21231*# c15 N68-21241*# c31 N68-21260*# c27 N68-21267*# c32 N68-21267*# c32 N68-21267*# c12 N68-21365*# c14 N68-21383*# c14 N68-21384*# c15 N68-21438*# c15 N68-21439*# c15 N68-21431*# c31 N68-21442*# c31 N68-21443*# c31 N68-21444*# c33 N68-21444*# c33 N68-21437*# c33 N68-21437*# c33 N68-21536*# c33 N68-21537*# c35 N68-21537*# c33 N68-21537*# c33 N68-21543*# c33 N68-21543*# c33 N68-21543*#	NASA-CR-1022 NASA-CR-1014 NASA-TN-D-4431 NASA-TN-D-4431 NASA-CR-1014 SID-66-1678-7 NASA-SP-5084 RSIC-501 NASA-TN-D-4519 NASA-TN-D-4519 NASA-TN-D-4505 NASA-TN-D-4505 NASA-TN-D-4505 NASA-TN-D-4525 NASA-TN-D-4525 NASA-TN-D-4526 NASA-TN-D-4596 NASA-TN-D-4506 NASA-TN-D-4506 NASA-TN-D-4506 NASA-TN-D-4506 NASA-TN-D-4506 NASA-TN-D-4506 NASA-TN-2-4506 NASA-TN-2-4506 NASA-TN-2-4506 NASA-TN-2-4506 NASA-TN-2-4506 NASA-TN-2-4506 NASA-TN-2-4506 NASA-TN-2-4506 NASA-TN-2-4506 NASA-TN-2-4506 NASA-TN-2-44506 NASA-TN-2-4488 NASA-TN-2-4488 NASA-TN-D-4487 NASA-TN-D-4487 NASA-TN-D-4487 NASA-TN-D-4487 NASA-TN-D-4527
c30 N68-21228*# c30 N68-21231*# c15 N68-21241*# c31 N68-21260*# c27 N68-21267*# c32 N68-21267*# c32 N68-21365*# c18 N68-21365*# c18 N68-21365*# c19 N68-21383*# c10 N68-21383*# c15 N68-21433*# c15 N68-21431*# c17 N68-21431*# c31 N68-21442*# c31 N68-21443*# c33 N68-21443*# c33 N68-21444*# c33 N68-21444*# c33 N68-21536*# c33 N68-21537*# c35 N68-21537*# c35 N68-21537*# c33 N68-21543*# c33 N68-21562*# c33 N68-21562*	NASA-CR-1022 NASA-TN-D-4431 NASA-TN-D-4431 NASA-CR-1014 SID-66-1678-7 NASA-SP-5084 RSIC-501 NASA-TN-D-4519 NASA-TN-D-4519 NASA-TN-2-1526 NASA-TN-2-1526 NASA-TN-2-4525 NASA-TN-2-4525 NASA-TN-2-4526 NASA-TN-2-4526 NASA-TN-2-1561 NASA-SP-5087 RSIC-598 NASA-TN-2-1561 NASA-SP-166 NASA-SP-166 NASA-TN-2-1562 NASA-TN-2-4488 NASA-TN-2-4485
c30 N68-21228*# c30 N68-21231*# c15 N68-21231*# c31 N68-21241*# c31 N68-21260*# c27 N68-21267*# c32 N68-21267*# c12 N68-21366*# c12 N68-21366*# c14 N68-213374*# c14 N68-213374*# c14 N68-213374*# c15 N68-21413*# c15 N68-21413*# c15 N68-21430*# c30 N68-21431*# c31 N68-21443*# c31 N68-21443*# c33 N68-21444*# c33 N68-21538*# c33 N68-21538*# c33 N68-21543*# c33 N68-21543*# c33 N68-21543*# c33 N68-21543*# c33 N68-21543*# c33 N68-21543*# c33 N68-21543*# c33 N68-21562*# c35 N68-21562*# c35 N68-21562*# c35 N68-21562*# c35 N68-21562*#	NASA-CR-1022 NASA-CR-1014 SID-66-1678-7 NASA-SP-5084 RSIC-501 NASA-TM-D-4519 NASA-TM-2-1556 NASA-TM-2-1556 NASA-TM-2-1526 NASA-TM-2-1526 NASA-TM-2-1526 NASA-TM-2-1526 NASA-TM-2-1526 NASA-TM-2-1527 NASA-TM-2-1528 NASA-TM-2-1508 NASA-TM-2-1508 NASA-TM-2-1561 NASA-SP-166 NASA-CR-1016 SID-66-1678-9 NASA-CR-1025 REPT7322-3-T NASA-TM-2-1562 NASA-TM-2-1562 NASA-TM-2-168 NASA-TM-2-1626 NASA-TM-2-168 NASA-TM-2-168 NASA-TM-2-4497 NASA-TM-2-4438
c30 N68-21228*# c30 N68-21231*# c15 N68-21241*# c31 N68-21260*# c27 N68-21267*# c32 N68-21267*# c32 N68-21267*# c12 N68-21365*# c14 N68-21365*# c14 N68-21338*# c14 N68-21384*# c15 N68-21429*# c15 N68-21429*# c17 N68-21431*# c17 N68-21431*# c30 N68-21442*# c31 N68-21442*# c31 N68-21444*# c33 N68-2156*# c05 N68-21538*# c13 N68-21538*# c13 N68-21538*# c13 N68-2152*# c13 N68-2152*# c13 N68-21562*# c13 N68-21562*# c13 N68-21579*# c13 N68-21579*** c13 N68-21579*** c13 N68-21579*** c13 N68-21579*	NASA-CR-1022 NASA-TN-D-4431 NASA-TN-D-4431 NASA-SP-5084 RSIC-501 NASA-TM-2+4519 NASA-TM-2+4519 NASA-TM-2+4505 NASA-TM-X-1556 NASA-TM-X-1526 NASA-TM-X-1549 NASA-TM-D-4525 NASA-TM-X-1570 NASA-TM-2+508 RSIC-598 NASA-TM-2+5087 RSIC-598 NASA-TM-2+5087 RSIC-598 NASA-TM-2+5087 RSIC-598 NASA-TM-2+506 NASA-TM-2+5087 RSIC-598 NASA-TM-2+5087 NASA-TM-2+5087 NASA-CR-1016 SID-66-1678-9 NASA-TM-2+648 NASA-TM-2+488 NASA-TM-D-4488 NASA-TM-D-4485 NASA-TM-D-4485 NASA-TM-2+4495
c30 N68-21228*# c30 N68-21231*# c15 N68-21231*# c31 N68-21241*# c31 N68-21260*# c27 N68-21267*# c32 N68-21267*# c12 N68-21366*# c12 N68-21366*# c14 N68-213374*# c14 N68-213374*# c14 N68-213374*# c15 N68-21413*# c15 N68-21413*# c15 N68-21430*# c30 N68-21431*# c31 N68-21443*# c31 N68-21443*# c33 N68-21444*# c33 N68-21538*# c33 N68-21538*# c33 N68-21543*# c33 N68-21543*# c33 N68-21543*# c33 N68-21543*# c33 N68-21543*# c33 N68-21543*# c33 N68-21543*# c33 N68-21562*# c35 N68-21562*# c35 N68-21562*# c35 N68-21562*# c35 N68-21562*#	NASA-CR-1022 NASA-TN-D-4431 NASA-TN-D-4431 NASA-CR-1014 SID-66-1678-7 NASA-SP-5084 RSIC-501 NASA-TN-D-4519 NASA-TN-D-4519 NASA-TN-2-1526 NASA-TN-2-1526 NASA-TN-2-4525 NASA-TN-2-4525 NASA-TN-2-4526 NASA-TN-2-4526 NASA-TN-2-4526 NASA-TN-2-4526 NASA-TN-2-4526 NASA-TN-2-4526 NASA-TN-2-4526 NASA-TN-2-4526 NASA-TN-2-4526 NASA-TN-2-4526 NASA-TN-2-4436
c30 N68-21228*# c30 N68-21231*# c15 N68-21241*# c31 N68-21260*# c27 N68-21267*# c32 N68-21267*# c32 N68-21267*# c12 N68-21365*# c14 N68-21365*# c14 N68-21338*# c14 N68-21384*# c15 N68-21429*# c15 N68-21429*# c17 N68-21431*# c17 N68-21431*# c30 N68-21442*# c31 N68-21442*# c31 N68-21444*# c33 N68-2156*# c05 N68-21538*# c13 N68-21538*# c13 N68-21538*# c13 N68-2152*# c13 N68-2152*# c13 N68-21562*# c13 N68-21562*# c13 N68-21579*# c13 N68-21579*** c13 N68-21579*** c13 N68-21579*** c13 N68-21579*	NASA-CR-1022 NASA-TN-D-4431 NASA-TN-D-4431 NASA-SP-5084 RSIC-501 NASA-TM-2+4519 NASA-TM-2+4519 NASA-TM-2+4505 NASA-TM-X-1556 NASA-TM-X-1526 NASA-TM-X-1549 NASA-TM-D-4525 NASA-TM-X-1570 NASA-TM-2+508 RSIC-598 NASA-TM-2+5087 RSIC-598 NASA-TM-2+5087 RSIC-598 NASA-TM-2+5087 RSIC-598 NASA-TM-2+506 NASA-TM-2+5087 RSIC-598 NASA-TM-2+5087 NASA-TM-2+5087 NASA-CR-1016 SID-66-1678-9 NASA-TM-2+648 NASA-TM-2+488 NASA-TM-D-4488 NASA-TM-D-4485 NASA-TM-D-4485 NASA-TM-2+4495
c30 N68-21228*# c30 N68-21231*# c15 N68-21241*# c31 N68-21260*# c27 N68-21267*# c32 N68-21267*# c32 N68-21267*# c12 N68-21365*# c14 N68-21365*# c14 N68-21338*# c14 N68-21384*# c15 N68-21429*# c15 N68-21429*# c17 N68-21431*# c17 N68-21431*# c30 N68-21442*# c31 N68-21442*# c31 N68-21444*# c33 N68-2156*# c05 N68-21538*# c13 N68-21538*# c13 N68-21538*# c13 N68-2152*# c13 N68-2152*# c13 N68-21562*# c13 N68-21562*# c13 N68-21579*# c13 N68-21579*** c13 N68-21579*** c13 N68-21579*** c13 N68-21579*	NASA-CR-1022 NASA-TN-D-4431 NASA-TN-D-4431 NASA-CR-1014 SID-66-1678-7 NASA-SP-5084 RSIC-501 NASA-TN-D-4519 NASA-TN-D-4519 NASA-TN-2-1526 NASA-TN-2-1526 NASA-TN-2-4525 NASA-TN-2-4525 NASA-TN-2-4526 NASA-TN-2-4526 NASA-TN-2-4526 NASA-TN-2-4526 NASA-TN-2-4526 NASA-TN-2-4526 NASA-TN-2-4526 NASA-TN-2-4526 NASA-TN-2-4526 NASA-TN-2-4526 NASA-TN-2-4436
c30 N68-21228*# c30 N68-21231*# c15 N68-21241*# c31 N68-21260*# c27 N68-21267*# c32 N68-21293*# c12 N68-21366*# c12 N68-21366*# c14 N68-21383*# c14 N68-21383*# c14 N68-21384*# c15 N68-21429*# c15 N68-21429*# c17 N68-21431*# c30 N68-21442*# c31 N68-21442*# c31 N68-21444*# c33 N68-21538*# c33 N68-21538*# c33 N68-21538*# c33 N68-21538*# c33 N68-21538*# c33 N68-2152*# c33 N68-2152*# c33 N68-21551*# c33 N68-21651*# c34 N68-21652*# c34 N68-21652*# c37 N68-21652*# c37 N68-21654*#	NASA-CR-1022 NASA-TN-D-4431 NASA-TN-D-4431 NASA-CR-1014 SID-66-1678-7 NASA-SP-5084 RSIC-501 NASA-TN-D-4519 NASA-TN-D-4519 NASA-TM-X-1526 NASA-TM-X-1526 NASA-TM-D-4398 NASA-TM-D-4398 NASA-TM-D-4398 NASA-TM-D-4398 NASA-TM-D-4398 NASA-TM-D-4398 NASA-TM-D-4398 NASA-TM-2-1561 SID-66-1678-9 NASA-TM-X-1561 NASA-TM-X-1562 NASA-TM-X-1562 NASA-TM-D-4488 NASA-TM-D-4438 NASA-TM-D-4439 NASA-TM-D-4439
c30 N68-21228*# c30 N68-21231*# c15 N68-21241*# c31 N68-21260*# c27 N68-21267*# c32 N68-21267*# c32 N68-21267*# c12 N68-21366*# c12 N68-21366*# c14 N68-213374*# c14 N68-213374*# c14 N68-21384*# c15 N68-21413*# c15 N68-21413*# c15 N68-21430*# c30 N68-21443*# c31 N68-21443*# c31 N68-21444*# c33 N68-21444*# c33 N68-21444*# c33 N68-2153*# c33 N68-2153*# c33 N68-2153*# c33 N68-21543*# c33 N68-21543*# c34 N68-21543*# c35 N68-21543*# c35 N68-21543*# c35 N68-21543*# c35 N68-21543*# c35 N68-21543*# c35 N68-21543*# c35 N68-21543*# c35 N68-21543*# c36 N68-21543*# c36 N68-21543*# c37 N68-21543*# c37 N68-21543*# c37 N68-21543*# c38 N68-21543*# c38 N68-21543*# c38 N68-21562*# c38 N68-21552*#	NASA-CR-1022 NASA-CR-1014 SID-66-1678-7 NASA-CR-1014 SID-66-1678-7 NASA-SP-5084 RSIC-501 NASA-TM-D-4519 NASA-TM-2-1556 NASA-TM-2-1526 NASA-TM-2-1526 NASA-TM-2-1526 NASA-TM-2-4398 NASA-TM-2-4398 NASA-TM-2-4398 NASA-TM-2-4398 NASA-TM-2-4398 NASA-SP-167 NASA-SP-166 NASA-CR-1016 SID-66-1678-9 NASA-CR-1025 REPT7322-3-T NASA-SP-166 NASA-TM-2-487 NASA-TM-2-488 NASA-TM-2-488 NASA-TM-2-488 NASA-TM-2-488 NASA-TM-2-488 NASA-TM-2-488 NASA-TM-2-488 NASA-TM-2-488 NASA-TM-2-488 NASA-TM-2-488 NASA-TM-2-488 NASA-TM-2-489

c03 N68-22842*#	NASA-CR-1048	c01 N68-24617*#	NASA-TR-R-285
	REPT3734A-67	c33 N68-24618*#	NASA-TM-X-1594
c29 N68-22849*#	NASA-CR-1037	c26 N68-24660*#	NASA-TN-D-4528
c30 N68-22860*#	••••••••••••••••••••••••••••••••••••••	c24 N68-24661*#	••••••••••••••••••••••••••••••••••••••
-17 100 00001+-	REPT101	c02 N68-24662*#	••••••••••••••••••••••••••••••••••••••
c13 N68-22861*# c04 N68-22882*#	•••••••NASA-TN-D-4479 ••••••NASA-SP-7011/49/	c31 N68-24738*# c05 N68-24756*#	NASA-CR-1069 NASA-TN-D-3415
c14 N68-22883*#	NASA-5P-7011/45/	c03 N68-24757*#	NASA-IN-D-0410
c17 N68-22884*#	••••••••••••••••••••••••••••••••••••••	c12 N68-24758*#	••••••••••••••••••••••••••••••••••••••
c30 N68-22885*#	••••••••••••••••••••••••••••••••••••••	c32 N68-24802*#	••••••••••••••••••••••••••••••••••••••
c02 N68-22886*#	NASA-TN-D-4560	c07 N68-24845*#	••••••••••••••••••••••••••••••••••••••
c25 N68-22887*#	••••••••••••••••••••••••••••••••••••••	c31 N68-24945*#	NASA-CR-946
c31 N68-22953*# c12 N68-23353*#	NASA-TN-D-4439 NASA-TM-X-1558	c31 N68-24964*# c33 N68-24965*#	NASA-TN-D-4598 NASA-TN-D-4467
c28 N68-23354*#	NASA-TN-D-4557	c11 N68-24966*#	NASA-IN-D-4407
c32 N68-23355*#	••••••••••••••••••••••••••••••••••••••		TR-0-71200/TTR-125
	REPT4-17-67-4	c08 N68-24967*#	NASA-TN-D-4617
c15 N68-23356*#	NASA-CR-1021	c32 N68-24971*#	NASA-CR-1067
c11 N68-23357*#	••••••••••••••••••••••••••••••••••••••	c08 N68-25002*# c15 N68-25042*#	NASA-TN-D-4554
c21 N68-23377*#	REPT1223 NASA-TN-D-4549	c22 N68-25058*#	••••••••••••••••••••••••••••••••••••••
c32 N68-23399*#	••••••••••••••••••••••••••••••••••••••	c03 N68-25059*#	NASA-TN-D-4582
c12 N68-23423*#	••••••••••••••••••••••••••••••••••••••	c05 N68-25060*#	••••••••••••••••••••••••••••••••••••••
c13 N68-23436*#	••••••••••••••••••••••••••••••••••••••	c01 N68-25093*#	••••••••••••••••••••••••••••••••••••••
c10 N68-23438*#	••••••••••••••••••••••••••••••••••••••	c28 N68-25099*#	••••••••••••••••••••••••••••••••••••••
c32 N68-23451*#	LAC-4-17-67-1, V. 2	c33 N68-25102*#	NASA-TN-D-4564
c32 N68-23452*#	NASA-CR-1050 GD/C-BTD-67-112, V. 13	c21 N68-25103*# c32 N68-25104*#	NASA-TN-D-4599 NASA-TN-D-4568
COL 100 10402.	NASA-CR-947	c33 N68-25122*#	NASA-TN-D-4535
c32 N68-23453*#	GD/C-BTD-67-120	c29 N68-25181*#	NASA-TN-D-4482
	NASA-CR-949	c34 N68-25221*#	NASA-SP-5021/06/
c32 N68-23454*#	GD/C-BTD-67-089, V. 14	c33 N68-25244*#	NASA-CR-1060
c02 N68-23456*#	NASA-CR-948	-00 NG0 050601	REPT66-7, PT. 1
c03 N68-23476*#	NASA-TT-F-519 NASA-CR-1033	c08 N68-25268*# c30 N68-25271*#	NASA-TN-D-4510 NASA-TM-X-55798
c28 N68-23477*#		COU NOU 20271.#	NASA-TN-D-4507
c22 N68-23481*#	F-910485-2	c03 N68-25304*#	••••••••••••••••••••••••••••••••••••••
	NASA-CR-1032	c33 N68-25312*#	••••••••••••••••••••••••••••••••••••••
c12 N68-23482*#	DAC-60874	c02 N68-25313*#	NASA-TN-D-4602
c33 N68-23513*#	NASA-CR-1066	c14 N68-25316*#	TB-0-71200 (TTB-112
c17 N68-23560*#	••••••••••••••••••••••••••••••••••••••	c14 N68-25317*#	TR-0-71200/TTR-112 NASA-TN-D-4597
c13 N68-23706*#	••••••••••••••••••••••••••••••••••••••	c17 N68-25318*#	
c24 N68-23893*#	••••••••••••••••••••••••••••••••••••••	c31 N68-25358*#	NASA-TN-D-4509
c22 N68-23894*#	••••••••••••••••••••••••••••••••••••••	c14 N68-25375*#	••••••••••••••••••••••••••••••••••••••
c02 N68-23895*#	NASA-TM-X-1591	c30 N68-25385*#	••••••••••••••••••••••••••••••••••••••
c15 N68-23900*# c02 N68-23901*#	NASA-TN-D-4569 NASA-TM-X-1584	c32 N68-25421*# c14 N68-25518*#	••••••••••••••••••••••••••••••••••••••
c20 N68-24028*#	••••••••••••••••••••••••••••••••••••••	c31 N68-25577*#	••••••••••••••••••••••••••••••••••••••
c17 N68-24111*#	••••••••••••••••••••••••••••••••••••••	c13 N68-25579*#	BSR-2022
c12 N68-24129*#	••••••••••••••••••••••••••••••••••••••		NASA-CR-1034
c19 N68-24141*#	••••••••••••••••••••••••••••••••••••••	c20 N68-25617*#	••••••••••••••••••••••••••••••••••••••
c15 N68-24142*#	NASA-TN-D-4565	c25 N68-25630*#	••••••••••••••••••••••••••••••••••••••
c23 N68-24146*# c25 N68-24161*#	•••••••D-4485 ••••••NASA-TN-D-4485 ••••••NASA-SP-3041	c20 N68-25816*#	••••••••••••••••••••••••••••••••••••••
c14 N68-24244*#	NASA-TN-D-4500	c02 N68-25817*#	NASA-CR-1078
c02 N68-24245*#	••••••••••••••••••••••••••••••••••••••	c29 N68-25818*#	••••••••••••••••••••••••••••••••••••••
c04 N68-24272*#	••••••••••••••••••••••••••••••••••••••	c32 N68-25819*#	••••••••••••••••••••••••••••••••••••••
c26 N68-24273*#	••••••••••••••••••••••••••••••••••••••	c31 N68-25820*#	••••••••••••••••••••••••••••••••••••••
c08 N68-24310*# c31 N68-24338*#	NASA-TN-D-4561	c25 N68-25821*#	••••••••••••••••••••••••••••••••••••••
c30 N68-24371*#	••••••D-4580 •••••D-4580 NASA-TN-D-4478	c03 N68-25829*# c14 N68-25830*#	NASA-TN-D-4600 NASA-TN-D-4540
c09 N68-24387*#	NASA IN D 4470	c19 N68-25841*#	NASA-TR-D-4540
c09 N68-24388*#	•••••••D-4573	c04 N68-25844*#	NASA-SP-7011/50/
c09 N68-24389*#	••••••••••••••••••••••••••••••••••••••	c07 N68-25852*#	•••••••NASA-TN-D-4572
c21 N68-24409*#	••••••••••••••••••••••••••••••••••••••	c11 N68-25853*#	••••••••••••••••••••••••••••••••••••••
c15 N68-24456*# c03 N68-24461*#	••••••D-4616 •••••D-4592	c14 N68-25862*# c12 N68-25866*#	••••••••••••••••••••••••••••••••••••••
c02 N68-24476*#	NASA-TN-D-4586	c30 N68-25867*#	••••••••••••••••••••••••••••••••••••••
c17 N68-24477*#	••••••••••••••••••••••••••••••••••••••	c23 N68-25868*#	••••••••••••••••••••••••••••••••••••••
c32 N68-24481*#	••••••••••••••••••••••••••••••••••••••	c19 N68-25869*#	••••••••••••••••••••••••••••••••••••••
	REPT4-17-67-1	c25 N68-25877*#	••••••••••••••••••••••••••••••••••••••
c30 N68-24486*# c02 N68-24498*#	••••••D-4544 •••••NASA-TN-D-4578	c29 N68-25880*# c30 N68-25895*#	••••••••••••••••••••••••••••••••••••••
c02 N68-24498*#	••••••D-4578 •••••D-4578 NASA-TN-D-4574	c30 N68-25902*#	NASA-CR-1103
c32 N68-24508*#	NASA-IN-D-4574	c14 N68-25902*#	NASA-CR-1070
c26 N68-24510*#	••••••••••••••••••••••••••••••••••••••		NCL-67-39
c21 N68-24512*#	••••••••••••••••••••••••••••••••••••••	c01 N68-25916*#	•••••••NASA-TN-D-4504
c21 N68-24555*#	NASA-TN-D-4594	c33 N68-25917*#	••••••••••••••••••••••••••••••••••••••
c30 N68-24557*#	NASA-TN-D-4587	c07 N68-25918*#	NASA-TN-D-4555
c17 N68-24558*# c22 N68-24559*#	••••••D-4551 •••••D-4615	c01 N68-25919*# c25 N68-25920*#	NASA-TN-D-4610 NASA-TN-D-4621
c11 N68-24560*#	NASA-IN-D-4613	c26 N68-25972*#	••••••••••••••••••••••••••••••••••••••
c19 N68-24565*#	••••••D-4575	c29 N68-26128*#	••••••••••••••••••••••••••••••••••••••
c34 N68-24567*#	NASA-SP-7500/02/	c04 N68-26207*#	•••••• NASA-SP-165
c03 N68-24596*#	NASA-CR-800	c26 N68-26603*#	NASA-CR-1088
c03 N68-24597*# c28 N68-24614*#	••••••••••••••••••••••••••••••••••••••	c07 N68-26621*# c26 N68-26627*#	••••••••••••••••••••••••••••••••••••••
200 H00-04014*#		1 000 100-2002/**	••••••••••••••••••••••••••••••••••••••

1	c05 N68-28319*#	NASA-CR-1083
1	c14 N68-28327*#	NASA-TN-D-4634
1	c32 N68-28330*#	NASA-TM-X-1608
1	c32 N68-28335*#	NASA-CR-1116
		SD-67-1204-1
1	c21 N68-28361*#	
	c12 N68-28364*#	
	c17 N68-28365*#	
	c12 N68-28370*#	••••••••••••••••••••••••••••••••••••••
ļ	c33 N68−28371*#	••••••••••••••••••••••••••••••••••••••
	c30 N68−28373*#	NASA-CR-1090
1	c31 N68-28379*#	NASA-SP-7004/04/
	c30 N68-28408*#	NASA-TN-D-4657
	c30 N68-28409*#	NASA-TN-D-4636
	c21 N68-28418*#	••••••••••••••••••••••••••••••••••••••
	c03 N68-28420*#	NASA-TN-D-4619
	c31 N68-28426*#	NASA-CR-1079
- 1		TR-152-1
	c01 N68-28447*#	NASA-TN-D-4672
		NASA-SP-164
	c09 N68-28668*#	NASA-TN-D-4656
-	c31 N68-28690*#	NASA-TN-D-4662
	c15 N68-28766*#	••••••••••••••••••••••••••••••••••••••
	c01 N68-28795*#	NASA-TN-D-4675
1	c12 N68-28801*#	
	c32 N68-28806*#	NASA-TM-X-1606
	c01 N68-28817*#	NASA-TN-D-4635
	c17 N68-28818*#	NASA-TN-D-4661
	c04 N68-28829*#	NASA-CR-1104
	c01 N68-28830*#	NASA-TN-D-4664
1	c02 N68-28831*#	NASA-TN-D-4677
	c32 N68-28832*#	
	c05 N68-28833*#	
		REPT67-2174
	c30 N68-28841*#	NASA-TN-D-4670
	c12 N68-28842*#	••••••••••••••••••••••••••••••••••••••
	c05 N68-28847*#	NASA-CR-1112
	c01 N68-28868*#	
	c31 N68-28869*#	
1	c03 N68-28870*#	NASA-TM-X-1615
-		
	c15 N68-28871*#	
	c13 N68-28872*#	NASA-TN~D-4603
	c09 N68-28879*#	NASA-SP-5043
-	c30 N68-28884*#	NASA-TN-D-4646
	c31 N68-28891*#	D2-100755-1, V. 1
		NASA-CR-1095
	c11 N68-28947*#	••••••••••••••••••••••••••••••••••••••
	c14 N68-28965*#	NASA-CR-1086
	c31 N68-28997*#	D2-100754-4, V. 4
		NASA-CR-1092
	c34 N68-29039*#	NASA-SP-7029
	c04 N68-29128*#	NASA-SP-152
- 8	c19 N68-29275*#	
	c02 N68-29372*#	NASA-TN-D-4638
	c24 N68-29375*#	••••••••••••••••••••••••••••••••••••••
	c28 N68-29378*#	NASA-TN-D-4699
	c17 N68-29379*#	NASA-TN-D-4673
	c22 N68-29390*#	NASA-CR-1148
1	c08 N68-29404*#	NASA-TN-D-4642
		NASA-TN-D-4671
1	c01 N68-29405*#	
	c02 N68-29406*#	NASA-TN-D-4682
	c19 N68-29407*#	••••••••••••••••••••••••••••••••••••••
	c14 N68-29418*#	••••••••••••••••••••••••••••••••••••••
	c16 N68-29438*#	NASA-SP-7009/03/
	c03 N68-29460*#	NASA-CR-1026
		R675D3012
	c11 N68-29478*#	NASA-TN-D-4644
	c24 N68-29520*#	
	c09 N68-29525*#	NASA-CR-1110
		REPT548-01-7-803, V. 1
	c09 N68-29526*#	••••••••••••••••••••••••••••••••••••••
		REPT548-01-7-803, V. 2
	c07 N68-29528*#	NASA-TN-D-4623
	c02 N68-29887*#	••••••••••••••••••••••••••••••••••••••
1	c25 N68-29888*#	NASA-CR-1143
-	c15 N68-29918*#	
	c22 N68-29950*#	NASA-TM-2-4710 NASA-TM-X-1614
	c14 N68-29951*#	NASA-TN-D-4681
	c01 N68-29952*#	NASA-TM-X-1620
	c28 N68-29953*#	NASA-TM-X-1619
	c17 N68-29954*#	••••••••••••••••••••••••••••••••••••••
	c01 N68-29955*#	••••••••••••••••••••••••••••••••••••••
	c11 N68-29957*#	
	c06 N68-29959*#	NASA-SP-7031
	c03 N68-29960*#	NASA-TN-D-4697
	c31 N68-29962*#	NASA-TN-D-4680
	c17 N68-29987*#	
		••••••••••••••••••••••••••••••••••••••
	c30 N68-29988*#	

c08 N68-26640*#	NASA-TN-D-4203
c33 N68-26641*#	NASA-CR-1062
	REPT66-7, PT. 3
c30 N68-26642*#	NASA-TN-D-4562
c30 N68-26643*#	••••••••••••••••••••••••••••••••••••••
c28 N68-26644*#	••••••••••••••••••••••••••••••••••••••
c31 N68-26645*#	••••••••••••••••••••••••••••••••••••••
c33 N68-26650*#	••••••••••••••••••••••••••••••••••••••
c12 N68-26651*#	••••••••••••••••••••••••••••••••••••••
c09 N68-26662*#	••••••••••••••••••••••••••••••••••••••
c30 N68-26689*#	NASA-CR-1081
	NCL-67-44R
c05 N68-26690*#	•••••• NASA-CR-1087
	TR-165-1
c02 N68-26691*∰	••••••••••••••••••••••••••••••••••••••
	SN-9000
c33 N68-26692*#	••••••••••••••••••••••••••••••••••••••
	REPT66-7, PT. 2
c05 N68-26701*#	NASA-CR-1085
c30 N68-26702*#	NASA-CR-1084
c14 N68-26703*#	NASA-CR-1073
c33 N68-26759*#	NASA-TN-D-4618 NASA-TN-D-4352
c22 N68-26764*# c28 N68-26771*#	NASA-CR-1056
c34 N68-26813*#	D2-114116-1
CU4 NOC 20010-#	NASA-CR-1068
c31 N68-26814*#	D2-100754-1, V. 1
	NASA-CR-1054
c33 N68-26815*#	NASA-CR-1034
	REDT66-7. DT. 4
c33 N68-26816*#	NASA-CR-1064
000 10010 #	REPT66-7, PT. 5
c33 N68-26817*#	NASA-CR-1065
	REPT66-7, PT. 6
c02 N68-26930*#	NASA-CR-1053
c07 N68-27063*#	NASA-CR-863
.	QR-8549
c19 N68-27457*#	NASA-CR-1100
c30 N68-27475*#	NASA-SP-150
c33 N68-28100*#	
c03 N68-28101*#	••••••••••••••••••••••••••••••••••••••
c28 N68-28112*#	
	REPT4227
c30 N68-28113*#	••••••••••••••••••••••••••••••••••••••
c07 N68-28135*#	••••••••••••••••••••••••••••••••••••••
c02 N68-28153*#	••••••••••••••••••••••••••••••••••••••
c25 N68-28154*#	••••••••••••••••••••••••••••••••••••••
c27 N68-28155*#	••••••••••••••••••••••••••••••••••••••
c33 N68-28156*#	NASA-TM-X-1605
c30 N68-28192*#	NASA-TR-R-277
c31 N68-28198*#	NASA-TN-D-4284
c31 N68-28202*#	D2-100755-2, V. 2 NASA-CR-1094
c01 N68-28220*#	NASA-CR-1094
c13 N68-28222*#	NASA-TN-D-4589
c02 N68-28233*#	NASA-CR-1098
002 NOO 20200.#	NOR-67-221
c21 N68-28236*#	
c32 N68-28238*#	NASA-TM-X-1603
c26 N68-28239*#	
c19 N68-28240*#	••••••••••••••••••••••••••••••••••••••
c15 N68-28241*#	
c04 N68-28246*#	NASA-SP-7011/51/
c04 N68-28247*#	
	TR-3172
c15 N68-28249*#	••••••••••••••••••••••••••••••••••••••
c24 N68-28250*#	••••••••••••••••••••••••••••••••••••••
c30 N68-28251*#	••••••••••••••••••••••••••••••••••••••
c15 N68-28258*#	
c23 N68-28259*#	NASA-TN-D-4625
c15 N68-28260*#	••••••••••••••••••••••••••••••••••••••
c21 N68-28262*#	NASA-TN-D-4654
c21 N68-28262*# c18 N68-28264*#	NASA-TN-D-4654 NASA-TN-D-4553
c21 N68-28262*# c18 N68-28264*# c24 N68-28265*#	NASA-TN-D-4654 NASA-TN-D-4553 NASA-TN-D-4553 NASA-TN-D-4633
c21 N68-28262*# c18 N68-28264*# c24 N68-28265*# c01 N68-28268*#	NASA-TN-D-4654 NASA-TN-D-4553 NASA-TN-D-4553 NASA-TN-D-4633 NASA-TN-D-4632
c21 N68-28262*# c18 N68-28264*# c24 N68-28265*#	NASA-TN-D-4654 NASA-TN-D-4553 NASA-TN-D-4533 NASA-TN-D-4632 NASA-TN-D-4632 NASA-CR-1082
c21 N68-28262*# c18 N68-28264*# c24 N68-28265*# c01 N68-28268*# c07 N68-28272*#	NASA-TN-D-4654 NASA-TN-D-4553 NASA-TN-D-4533 NASA-TN-D-4633 NASA-TN-D-4632 NASA-CR-1082 TR-170-1
c21 N68-28262*# c18 N68-28264*# c24 N68-28265*# c01 N68-28268*#	NASA-TN-D-4654 NASA-TN-D-4553 NASA-TN-D-4553 NASA-TN-D-4633 NASA-TN-D-4632 NASA-TN-D-4632 NASA-CR-1082 TR-170-1 D2-100754-2, V. 2
c21 N68-28262*# c18 N68-28264*# c24 N68-28265*# c01 N68-28268*# c07 N68-28272*# c30 N68-28275*#	NASA-TN-D-4654 NASA-TN-D-4553 NASA-TN-D-4533 NASA-TN-D-4633 NASA-TN-D-4632 NASA-CR-1082 TR-170-1 D2-100754-2, V. 2 NASA-CR-1093
c21 N68-28262*# c18 N68-28264*# c24 N68-28265*# c01 N68-28268*# c07 N68-28278*# c30 N68-28275*# c30 N68-28275*#	NASA-TN-D-4654 NASA-TN-D-4553 NASA-TN-D-4553 NASA-TN-D-4632 NASA-CR-1082 TR-170-1 D2-100754-2, V.2 NASA-CR-1093 NASA-CR-1093 NASA-TN-D-4609
c21 N68-28262*# c18 N68-28265*# c24 N68-28265*# c01 N68-28268*# c07 N68-28272*# c30 N68-28275*# c02 N68-28277*# c04 N68-28277*#	NASA-TN-D-4654 NASA-TN-D-4553 NASA-TN-D-4533 NASA-TN-D-4633 NASA-TN-D-4632 NASA-CR-1082 TR-170-1 D2-100754-2, V. 2 NASA-CR-1093 NASA-CR-1093 NASA-CR-1105
c21 N68-28262*# c18 N68-28264*# c24 N68-28265*# c01 N68-28265*# c07 N68-28265*# c30 N68-28272*# c30 N68-28275*# c02 N68-282277*# c04 N68-282278## c03 N68-28280*#	NASA-TN-D-4654 NASA-TN-D-4553 NASA-TN-D-4533 NASA-TN-D-4633 NASA-TN-D-4632 NASA-CR-1082 TR-170-1 D2-100754-2, V. 2 NASA-CR-1093 NASA-CR-1093 NASA-CR-1093 NASA-CR-1105 NASA-TN-D-4659
c21 N68-28262*# c18 N68-28264*# c24 N68-28264*# c01 N68-28268*# c07 N68-28268*# c30 N68-28275*# c30 N68-28275*# c02 N68-28277*# c04 N68-28277*# c03 N68-28280*# c19 N68-28281*#	NASA-TN-D-4654 NASA-TN-D-4553 NASA-TN-D-4533 NASA-TN-D-4633 NASA-TN-D-4632 NASA-CR-1082 TR-170-1 D2-100754-2, V. 2 NASA-CR-1093 NASA-CR-1093 NASA-CR-1093 NASA-TN-D-4609 NASA-TN-D-4659 NASA-TN-D-4653
c21 N68-28262*# c18 N68-28265*# c24 N68-28265*# c01 N68-28268*# c07 N68-28272*# c30 N68-28275*# c02 N68-28275*# c04 N68-28277*# c03 N68-28280*# c19 N68-28281*# c12 N68-28282*#	NASA-TN-D-4654 NASA-TN-D-4553 NASA-TN-D-4533 NASA-TN-D-4633 NASA-TN-D-4632 NASA-CR-1082 TR-170-1 D2-100754-2, V. 2 NASA-CR-1093 NASA-CR-1093 NASA-CR-1095 NASA-TN-D-4609 NASA-TN-D-4659 NASA-TN-D-4659
c21 N68-28262*# c18 N68-28264*# c24 N68-28264*# c01 N68-28268*# c07 N68-28268*# c30 N68-28275*# c30 N68-28275*# c02 N68-28277*# c04 N68-28277*# c03 N68-28280*# c19 N68-28281*#	NASA-TN-D-4654 NASA-TN-D-4553 NASA-TN-D-4533 NASA-TN-D-4633 NASA-TN-D-4632 TR-170-1 D2-100754-2, V. 2 NASA-CR-1093 NASA-TN-D-4609 NASA-TN-D-4609 NASA-TN-D-4663 NASA-TN-D-4663 NASA-TN-D-4663
c21 N68-28262*# c18 N68-28264*# c24 N68-28265*# c01 N68-28268*# c07 N68-28272*# c30 N68-28275*# c02 N68-28277*# c04 N68-28278*# c03 N68-28280*# c19 N68-28281*# c12 N68-28282*# c22 N68-28304*#	NASA-TN-D-4654 NASA-TN-D-4553 NASA-TN-D-4533 NASA-TN-D-4633 NASA-TN-D-4632 NASA-TN-D-4632 TR-170-1 D2-100754-2, V. 2 NASA-CR-1093 NASA-CR-1093 NASA-CR-1093 NASA-TN-D-4659 NASA-TN-D-4659 NASA-TN-D-4653 NASA-TN-D-4658
c21 N68-28262*# c18 N68-28264*# c24 N68-28265*# c01 N68-28265*# c07 N68-28275*# c30 N68-28275*# c02 N68-28275*# c04 N68-282878*# c03 N68-28280*# c19 N68-28280*# c19 N68-28282*# c22 N68-28282*# c10 N68-28307*#	NASA-TN-D-4654 NASA-TN-D-4553 NASA-TN-D-4533 NASA-TN-D-4632 NASA-TN-D-4632 NASA-CR-1082 TR-170-1 D2-100754-2, V. 2 NASA-TN-D-4692 NASA-CR-1093 NASA-CR-1093 NASA-TN-D-4699 NASA-TN-D-4659 NASA-TN-D-4659 NASA-TN-D-4653 NASA-TN-D-4643 NASA-TN-D-4643 NASA-TN-D-4658 NASA-TN-D-4658 NASA-CR-1099

c17 N68-29992*# NASA-CR-1115	c06 N68-31948*#
TRW-ER-7203	c02 N68-31956*#
c31 N68-29993*# NASA-TM-X-1623	c21 N68-31957*#
c01 N68-29994*#	c14 N68-31958*#
c31 N68-29995*# D2-100753-4, V. 3	c33 N68-31959*#
NASA-CR-1109	c12 N68-31960*#
c17 N68-30000*# NASA-TN-D-4674	c19 N68-31961*#
c24 N68-30001*#	c31 N68-31978*#
c03 N68-30002*#	c15 N68-31979*# NASA-CR-1129
c01 N68-30030*# NASA-TM-X-1621	c15 N68-31980*# NASA-CR-1130
c25 N68-30031*# NASA-TN-D-4651	c30 N68-31989*#
c31 N68-30032*# NASA-TN-D-4691	c01 N68-31990*# NASA-TN-D-4739
c01 N68-30033*# NASA-TM-X-1622	c32 N68-32051*# NASA-TN-D-4707
c28 N68-30040*# NASA-TN-D-4690	c08 N68-32055*# NASA-TN-D-4770
c33 N68-30041*# NASA-TN-D-4685	c25 N68-32072*# NASA-TN-D-4758
c06 N68-30044*#	c33 N68-32073*# NASA-TN-D-4771
c32 N68-30045*# NASA-TN-D-4717	c32 N68-32074*# NASA-TN-D-4702
c17 N68-30065*# E-4337	c30 N68-32094*# NASA-TN-D-4511
NASA-TM-X-1617	c33 N68-32099*#
c17 N68-30066*# E-4386	c05 N68-32100*# NASA-TN-D-4751
NASA-TN-D-4714	c08 N68-32159*# NASA-SP-5049
c27 N68-30077*# E-4324	c30 N68-32631*# NASA-SP-7003/04/
NASA-TN-D-4701	c04 N68-32707*# NASA-SP-7011/52/
c25 N68-30093*#	c30 N68-32744*# NASA-CR-1119
c30 N68-30098*# NASA-SP-35, PT. 6	c15 N68-32760*#
c21 N68-30126*# NASA-TR-R-259	c34 N68-32769*# NASA-SP-7006/03/
c14 N68-30127*# NASA-TN-D-4679	c15 N68-32779*# NASA-CR-1128
c01 N68-30128*# E-4213	c27 N68-32793*# NASA-CR-1123
NASA-TN-D-4695	TRW-02874-6008-R000
c08 N68-30240*# NASA-TM-X-1599	c22 N68-32968*#
S-157	c32 N68-32976*# NASA-CR-1136
c03 N68-30241*# E-4407	c15 N68-32977*#
NASA-TN-D-4700	c30 N68-32978*#
c30 N68-30244*# L-5774	c12 N68-32982*#NASA-TM-X-1634
NASA-TN-D-4666	c22 N68-32983*# NASA-CR-1154
c27 N68-30313*# NASA-SP-7002/04/	c28 N68-32987*# EDR-4909, V. 2
c11 N68-30317*# NASA-SP-4301	NASA-CR-1172
c09 N68-30501*# NASA-TM-X-1613	c33 N68-32988*#
c17 N68-30504*# NASA-TN-D-4725	c04 N68-33005*# NASA-CR-1193
c32 N68-30505*# NASA-TN-D-4711	c21 N68-33006*#
c03 N68-30506*# NASA-TM-X-1635	c31 N68-33008*# D2-113204-1
c22 N6B-30516*# NASA-TM-X-1631	NASA-CR-1108
c33 N68-30518*#	c05 N68-33009*# D8-0907A
C06 N68-30582*#	NASA-CR-1118
c25 N68-30593*#	c17 N68-33019*# DP/NASA/-1130
c19 N68-30594*#NASA-TN-D-4696 c01 N68-30595*#NASA-TN-D-4693	NASA-CR-1133
	c25 N68-33021*#
i de la companya de l	
c18 N68-30597*#NASA-TN-D-4734 c11 N68-30598*#NASA-TM-X-1636	c18 N68-33034*#
c28 N68-30599*#	c07 N68-33042*#
c30 N68-30601*# NASA-SP-7017/02/	c01 N68-33043*#
c05 N68-30602*# NASA-CR-1117	c12 N68-33054*#
REPT1520	c30 N68-33055*#
c28 N68-30604*# NASA-TN-D-4730	c12 N68-33056*#
c17 N68-30605*# NASA-TN-D-4728	c32 N68-33057*#
c31 N68-30631*# D2-100755-4, V. 4	c03 N68-33062*# NASA-CR-1150
NASA-CR-1142	c01 N68-33081*# NASA-TN-D-4766
c33 N68-30747*# NASA-TN-D-4713	c32 N68-33092*#
c22 N68-30750*#	c12 N68-33165*#
c03 N68-30751*# NASA-TN-D-4727	c33 N68-33167*# NASA-TN-D-4778
c25 N68-30784*# NASA-TN-D-4736	c32 N68-33168*# NASA-CR-1176
c19 N68-30804*#	c30 N68-33169*# NASA-SP-154
c01 N68-31445*#	c11 N68-33190*#
c28 N68-31476*#	c32 N68-33191*#
c31 N68-31477*# D2-100752-4, V. 4	c33 N68-33203*# NASA-CR-1139
NASA-CR-1141	PWA-3154
c15 N68-31478*# NASA-CR-1126	c33 N68-33208*#
c05 N68-31480*# NASA-CR-1153	c09 N68-33224*# NASA-CR-1185
c01 N68-31484*# NASA-TN-D-4704	c32 N68-33225*# NASA-TN-D-4753
c33 N68-31498*# NASA-TM-X-1618	c32 N68-33226*# NASA-CR-1160
c08 N68-31499*# C6-1476.22/33, V. 1	c15 N68-33227*#
NASA-CR-1158	c26 N68-33228*# NASA-TR-R-290
c01 N68-31515*# NASA-TN-D-4427, SUP.	c19 N68-33245*# NASA-SP-170
c17 N68-31517*# NASA-TN-D-4743	c32 N68-33266*#
c15 N68-31522*# NASA-SP-7020/02/	c21 N68-33271*#
c01 N68-31551*#	c14 N68-33277*#
	c17 N68-33278*#
	c05 N68-33304*#
REPT1238 c32 N68-31602*#NASA-TN-D-4710	REPT1571 c31 N68-33332*#
c17 N68-31605*#	
c07 N68-31639*#	
c25 N68-31640*g	c29 N68-33370*#
c05 N68-31911*#	c25 N68-33372*#
c32 N68-31912*#	c01 N68-33374*#
c21 N68-31938*#	c13 N68-33416*#
c32 N68-31946*#	c32 N68-33419*# NASA-CR-1161

.

c03 N68-35536*#	••••••••••••••••••••••••••••••••••••••
c07 N68-35537*#	
c08 N68-35560*#	C6-1476.22/33, V. 2
	NASA-CR-1159
c34 N68-35564*#	NASA-SP-185
c16 N68-35593*#	NASA-TM-X-1652
c28 N68-35594*#	
c02 N68-35595*#	NASA-CR-1188
c01 N68-35617*#	NASA-TM-X-1660
c14 N68-35620*#	NASA-SP-5050
c32 N68-35632*#	NASA-CR-1195
c01 N68-35665*#	
c01 N68-35668*#	
c01 N68-35672*#	NASA-TM-X-1662
c28 N68-35764*#	NASA-TM-X-1653
c12 N68-35823*#	••••••••••••••••••••••••••••••••••••••
c22 N68-35826*#	G-910485-3
	NASA-CR-1191
c14 N68-36021*#	••••••••••••••••••••••••••••••••••••••
c22 N68-36055*#	••••••••••••••••••••••••••••••••••••••
c31 N68-36056*#	NASA-TN-D-4847
c24 N68-36070*#	NASA-TN-D-4810
c12 N68-36071*#	••••••••••••••••••••••••••••••••••••••
c33 N68-36072*#	NASA-TN-D-4817
c02 N68-36073*#	NASA-TN-D-4836
c02 N68-36074*#	NASA-TN-D-4837
c15 N68-36075*#	••••••••••••••••••••••••••••••••••••••
c17 N68-36076*#	NASA-TM-X-1670
c30 N68-36077*#	NASA-TN-D-4801
c01 N68-36081*#	NASA-TN-D-4812
c15 N68-36098*#	NASA-TN-D-4839
c07 N68-36105*#	NASA-TN-D-4721 NASA-TN-D-4765
c31 N68-36106*#	
c01 N68~36112*#	
c01 N68-36132*# c01 N68-36133*#	
c01 N68-36134*# c01 N68-36193*#	
c07 N68-36333*#	NASA-TM-X-1658 NASA-TR-R-292
c01 N68-36334*#	NASA-TN-D-4820
c12 N68-36343*#	NASA-CR-1169
c05 N68-36457*#	NASA-TN-D-4841
c12 N68-36458*#	NASA-TN-D-4829
c30 N68-36459*#	
c23 N68-36460*#	
c05 N68-36461*#	
c23 N68-36470*#	••••••••••••••••••••••••••••••••••••••
c28 N68-36507*#	
c01 N68-36509*#	NASA-TM-X-1661
c28 N68-36512*#	NASA-TM-X-1677
c28 N68-36515*#	••••••••••••••••••••••••••••••••••••••
c11 N68-36522*#	NASA-CR-1198
c19 N68-36525*#	••••••••••••••••••••••••••••••••••••••
c14 N68-36530*#	NASA-CR-1200
c22 N68-36615*#	
	NASA-CR-1190
c28 N68-36617*#	NASA-CR-1187
c19 N68-36753*#	NASA-TR-R-287 NASA-TN-D-4858
c17 N68-36970*# c31 N68-36971*#	
c31 N68-36971*# c26 N68-37051*#	••••••••••••••••••••••••••••••••••••••
c17 N68-37053*#	NASA-TN-D-4833
c01 N68-37054*#	
c26 N68-37055*#	NASA-TN-D-4834
c01 N68-37065*#	••••••••••••••••••••••••••••••••••••••
c02 N68-37066*#	••••••••••••••••••••••••••••••••••••••
c12 N68-37067*#	
c19 N68-37073*#	
c31.N68-37074*#	NASA-TN-D-4843
c02 N68-37075*#	
c03 N68-37162*#	••••••••••••••••••••••••••••••••••••••
c22 N68-37209*#	••••••••••••••••••••••••••••••••••••••
c15 N68-37214*#	••••••••••••••••••••••••••••••••••••••
c34 N68-37216*#	NASA-CR-1222
c03 N68-37217*#	NASA-TM-X-1674
c30 N68-37220*#	
	NASA-SP-8010
c25 N68-37237*#	••••••••••••••••••••••••••••••••••••••
c25 N68-37237*# c01 N68-37238*#	NASA-TN-D-4866 NASA-TN-D-4809
c25 N68-37237*# c01 N68-37238*# c15 N68-37239*#	NASA-TN-D-4866 NASA-TN-D-4809 NASA-TN-D-4802 NASA-TN-D-4862
c25 N68-37237*# c01 N68-37238*# c15 N68-37239*# c24 N68-37240*#	NASA-TN-D-4866 NASA-TN-D-4809 NASA-TN-D-4869 NASA-TN-D-4868
c25 N68-37237*# c01 N68-37238*# c15 N68-37239*# c24 N68-37239*# c08 N68-37254*#	NASA-TN-D-4866 NASA-TN-D-4809 NASA-TN-D-4809 NASA-TN-D-4868 NASA-TN-D-4838 NASA-CR-1107
c25 N68-37237*# c01 N68-37238*# c15 N68-37239*# c24 N68-37240*# c08 N68-37254*# c01 N68-37255*#	NASA-TN-D-4866 NASA-TN-D-4809 NASA-TN-D-4809 NASA-TN-D-4862 NASA-TN-D-4838 NASA-CR-1107 NASA-CR-1202
c25 N68-37237*# c01 N68-37238*# c15 N68-37239*# c24 N68-37240*# c08 N68-37254*# c01 N68-37255*# c11 N68-37259*#	NASA-TN-D-4866 NASA-TN-D-4809 NASA-TN-D-4802 NASA-TN-D-4862 NASA-TN-D-4838 NASA-CR-1107 NASA-CR-1202 NASA-TN-D-4867
c25 N68-37237*# c01 N68-37238*# c15 N68-37239*# c24 N68-37240*# c08 N68-37254*# c01 N68-37255*# c11 N68-37259*# c22 N68-37260*#	NASA-TN-D-4866 NASA-TN-D-4809 NASA-TN-D-4809 NASA-TN-D-4838 NASA-TN-D-4838 NASA-CR-1107 NASA-CR-1202 NASA-CR-1202 NASA-TN-D-4867 NASA-TM-Z-1680
c25 N68-37237*# c01 N68-37238*# c15 N68-37239*# c24 N68-37240*# c08 N68-37254*# c01 N68-37255*# c11 N68-37259*# c22 N68-37260*# c03 N68-37263*#	NASA-TN-D-4866 NASA-TN-D-4809 NASA-TN-D-4809 NASA-TN-D-4838 NASA-TN-D-4838 NASA-CR-1107 NASA-CR-1202 NASA-TN-D-4868 NASA-CR-1202 NASA-TN-D-4868 NASA-CR-1602 NASA-TN-D-4868 NASA-CR-1602 NASA-TN-CR-1680 NASA-TM-X-1679
c25 N68-37237*# c01 N68-37238*# c15 N68-37240*# c24 N68-37240*# c01 N68-37254*# c11 N68-37255*# c11 N68-37259*# c22 N68-37260*# c03 N68-37263*# c28 N68-37264*#	NASA-TN-D-4866 NASA-TN-D-4809 NASA-TN-D-4802 NASA-TN-D-4838 NASA-CR-1107 NASA-CR-1202 NASA-CR-1202 NASA-CR-1202 NASA-TN-D-4867 NASA-TM-X-1679 NASA-TM-X-1675
c25 N68-37237*# c01 N68-37238*# c15 N68-37239*# c24 N68-37240*# c08 N68-37254*# c01 N68-37255*# c11 N68-37259*# c22 N68-37260*# c03 N68-37263*#	NASA-TN-D-4866 NASA-TN-D-4809 NASA-TN-D-4809 NASA-TN-D-4838 NASA-CR-1107 NASA-CR-1202 NASA-TN-D-4868 NASA-CR-1202 NASA-TN-D-4868 NASA-CR-1602 NASA-CR-1660 NASA-TM-X-1679

c19 N68-33426*#	••••••••••••••••••••••••••••••••••••••
c21 N68-33450*#	••••••••••••••••••••••••••••••••••••••
c01 N68-33451*#	••••••••••••••••••••••••••••••••••••••
•	REPT36
c21 N68-33456*#	NASA-TN-D-4780
c31 N68-33553*#	NASA-SP-173
c16 N68-33635*#	NASA-TN-D-4764
c12 N68-33642*#	NASA-IN-D-4788
c02 N68-33669*#	
c34 N68-33682*#	NASA-TN-D-4731
c31 N68-33683*#	••••••••••••••••••••••••••••••••••••••
c17 N68-33684*#	••••••••••••••••••••••••••••••••••••••
c32 N68-33737*#	•••••• NASA-CR-1175
c32 N68-33738*#	••••••NASA-TN-D-4705
c21 N68-33756*#	••••••••••••••••••••••••••••••••••••••
c24 N68-33763*#	••••••••••••••••••••••••••••••••••••••
c01 N68-33765*#	NASA-CR-1166
c10 N68-33767*#	NASA-CR-1167
c01 N68-33836*#	
c02 N68-33879*#	••••••••••••••••••••••••••••••••••••••
c21 N68-33904*#	••••••••••••••••••••••••••••••••••••••
c30 N68-34086*#	••••••••••••••••••••••••••••••••••••••
	SD-67-994-1
c22 N68-34087*#	NASA-TN-D-4805
c33 N68-34088*#	NASA-TN-D-4797
c12 N68-34089*#	NASA-TN-D-4795
c24 N68-34175*#	NASA-TN-D-4795
c03 N68-34234*#	
c30 N68-34870*	NASA-SP-168
c02 N68-34907*#	NASA-SP-180
c31 N68-35022*#	NASA-TN-D-4807
c04 N68-35069*#	NASA-SP-7011/53/
c32 N68-35071*#	••••••••••••••••••••••••••••••••••••••
c27 N68-35072*#	••••••••••••••••••••••••••••••••••••••
c22 N68-35073*#	••••••••••••••••••••••••••••••••••••••
c12 N68-35086*#	••••••••••••••••••••••••••••••••••••••
c12 N68-35096*#	•••••• NASA-CR-1144
c17 N68-35098*#	•••••• NASA-CR-1184
c16 N68-35099*#	••••••••••••••••••••••••••••••••••••••
c18 N68-35100*#	ARC-R-276
	NASA-CR-1114
c28 N68-35101*#	••••••••••••••••••••••••••••••••••••••
c05 N68-35102*#	••••••••••••••••••••••••••••••••••••••
c04 N68-35103*#	LR-20922
	NASA-CR-1192
c12 N68-35104*#	••••••••••••••••••••••••••••••••••••••
c14 N68-35105*#	••••••••••••••••••••••••••••••••••••••
c05 N68−35109*#	••••••••••••••••••••••••••••••••••••••
c12 N68-35114*#	••••••••••••••••••••••••••••••••••••••
c28 N68-35115*#	••••••••••••••••••••••••••••••••••••••
c33 N68-35116*#	••••••••••••••••••••••••••••••••••••••
c12 N68-35117*#	••••••••••••••••••••••••••••••••••••••
c07 N68-35140*#	••••••••••••••••••••••••••••••••••••••
c01 N68-35141*#	••••••••••••••••••••••••••••••••••••••
c14 N68-35149*#	
c13 N68-35151*#	NASA-CR-1137
c14 N68-35152*#	NASA-CR-1138
c22 N68-35153*#	NASA-CR-1097
	R67SD3014
c25 N68-35171*#	NASA-CR-1177
c07 N68-35172*#	NASA-CR-1174
c01 N68-35173*#	••••••••••••••••••••••••••••••••••••••
c07 N68-35174*#	
c16 N68-35175*#	
	NASA-TN-D-4794
c02 N68-35177*#	NASA-TN-D-4794 D8-0375, V. 3
c02 N68-35177*#	D8-0375, V. 3
	D8-0375, V. 3 NASA-CR-743/1/
c02 N68-35177*# c26 N68-35178*#	D8-0375, V. 3 NASA-CR-743/1/ NASA-CR-1189
c26 N68-35178*#	D8-0375, V. 3 NASA-CR-743/1/ .NASA-CR-1189 NBS-9708
c26 N68-35178*# c13 N68-35179*#	D8-0375, V. 3 NASA-CR-743/1/ NASA-CR-743/1/ NASA-CR-1189 NBS-9708 NASA-TM-X-1646
c26 N68-35178*# c13 N68-35179*# c08 N68-35193*#	D8-0375, V. 3 NASA-CR-743/1/ NASA-CR-743/1/ NASA-CR-1189 NBS-9708 NASA-TM-X-1646 NASA-CR-1113
c26 N68-35178*# c13 N68-35179*# c08 N68-35193*# c32 N68-35198*#	D8-0375, V. 3 NASA-CR-743/1/ NASA-CR-1189 NBS-9708 NASA-TM-X-1646 NASA-CR-1113 NASA-CR-1113
c26 N68-35178*# c13 N68-35179*# c08 N68-35193*# c32 N68-35198*# c32 N68-35199*#	D8-0375, V. 3 NASA-CR-743/1/ NASA-CR-1189 NBS-9708 NASA-TM-X-1646 NASA-CR-1113 NASA-CR-1162 NASA-CR-1162
c26 N68-35178*# c13 N68-35179*# c08 N68-35193*# c32 N68-35198*# c32 N68-35198*# c32 N68-35199*# c17 N68-35200*#	D8-0375, V. 3 NASA-CR-743/1/ NASA-CR-7189 NBS-9708 NASA-TM-X-1646 NASA-CR-1113 NASA-CR-1163 NASA-CR-1163 NASA-CR-1165
c26 N68-35178*# c13 N68-35179*# c08 N68-35193*# c32 N68-35198*# c32 N68-35199*# c17 N68-35200*# c33 N68-35248*#	D8-0375, V. 3 NASA-CR-743/1/ NASA-CR-1189 NBS-9708 NASA-TM-X-1646 NASA-CR-1113 NASA-CR-1163 NASA-CR-1163 NASA-CR-1165 NASA-CR-1170
c26 N68-35178*# c13 N68-35179*# c08 N68-35193*# c32 N68-35198*# c32 N68-35198*# c17 N68-35200*# c33 N68-35248*# c12 N68-35252*#	DB-0375, V. 3 NASA-CR-743/1/ NASA-CR-1189 NBS-9708 NASA-TM-X-1646 NASA-TM-X-1646 NASA-CR-1113 NASA-CR-1162 NASA-CR-1163 NASA-CR-1163 NASA-CR-1170 NASA-CR-1170
c26 N68-35178*# c13 N68-35179*# c08 N68-35193*# c32 N68-35199*# c17 N68-35200*# c17 N68-35248*# c12 N68-35252*# c26 N68-35356*#	D8-0375, V. 3 NASA-CR-743/1/ NASA-CR-1189 NBS-9708 NASA-CR-1189 NASA-CR-1189 NASA-CR-1164 NASA-CR-1162 NASA-CR-1162 NASA-CR-1165 NASA-CR-1165 NASA-CR-1170 NASA-CR-1172 NASA-CR-1132 NASA-CR-1132
c26 N68-35178*# c13 N68-35179*# c08 N68-35193*# c32 N68-35193*# c17 N68-35200*# c17 N68-35200*# c12 N68-352248*# c12 N68-35252*# c26 N68-35357*#	DB-0375, V. 3 NASA-CR-743/1/ NASA-CR-1189 NBS-9708 NASA-TM-X-1646 NASA-CR-1113 NASA-CR-1163 NASA-CR-1163 NASA-CR-1165 NASA-CR-1165 NASA-CR-1170 NASA-CR-1170 NASA-CR-1170 NASA-CR-1170 NASA-CR-1170 NASA-CR-1170 NASA-CR-1170 NASA-TM-D-4806 NASA-TM-X-1647
c26 N68-35178*# c13 N68-35179*# c08 N68-35193*# c32 N68-35198*# c32 N68-35199*# c17 N68-35200*# c13 N68-35248*# c12 N68-35252*# c26 N68-35356*# c31 N68-3536*# c31 N68-3546*#	DB-0375, V. 3 NASA-CR-743/1/ NASA-CR-1189 NBS-9708 NASA-TM-X-1646 NASA-CR-1113 NASA-CR-1162 NASA-CR-1162 NASA-CR-1163 NASA-CR-1165 NASA-CR-1170 NASA-CR-1170 NASA-CR-1132 NASA-CR-1132 NASA-CR-1132 NASA-CR-1132 NASA-CR-1132 NASA-CR-1132 NASA-CR-1132 NASA-CR-1132 NASA-CR-1132 NASA-CR-1132 NASA-CR-1132 NASA-CR-1132 NASA-CR-1132 NASA-CR-1132 NASA-CR-1132
c26 N68-35178*# c13 N68-35193*# c32 N68-35193*# c32 N68-35193*# c17 N68-35200*# c17 N68-35248*# c12 N68-35248*# c26 N68-35252*# c26 N68-35356*# c31 N68-35356*# c11 N68-35466*# c03 N68-35467*#	DB-0375, V. 3 NASA-CR-743/1/ NASA-CR-1189 NBS-9708 NASA-TM-X-1646 NASA-CR-1113 NASA-CR-1113 NASA-CR-1163 NASA-CR-1165 NASA-CR-1165 NASA-CR-1172 NASA-CR-1172 NASA-CR-1132 NASA-CR-1132 NASA-CR-1132 NASA-CR-1143 NASA-CR-1142 NASA-CR-1143 NASA-CR-1143 NASA-CR-1143 NASA-CR-1143 NASA-CR-1143 NASA-CR-1143 NASA-CR-1143 NASA-CR-1143 NASA-CR-1143 NASA-CR-1143 NASA-CR-1143 NASA-CR-1143 NASA-CR-1142 NASA-CR-1143 NASA-CR-1142 NASA-CR-1143 NASA-CR-1144 NASA
c26 N68-35178*# c13 N68-35179*# c08 N68-35193*# c32 N68-35198*# c17 N68-35200*# c17 N68-35248*# c12 N68-35252*# c26 N68-35356*# c21 N68-35356*# c11 N68-35466*# c33 N68-35467*# c33 N68-35468*#	DB-0375, V. 3 NASA-CR-743/1/ NASA-CR-1189 NBS-9708 NASA-TM-X-1646 NASA-CR-1113 NASA-CR-1163 NASA-CR-1163 NASA-CR-1165 NASA-CR-1165 NASA-CR-1165 NASA-CR-1170 NASA-CR-1170 NASA-CR-1170 NASA-CR-1132 NASA-TN-D-4806 NASA-TN-D-4808 NASA-TN-D-4818 NASA-TN-D-4818
c26 N68-35178*# c13 N68-35179*# c08 N68-35193*# c32 N68-35198*# c32 N68-35199*# c17 N68-35200*# c13 N68-3520*# c12 N68-35252*# c26 N68-35356*# c31 N68-35467*# c11 N68-35467*# c33 N68-35467*# c33 N68-35467*# c39 N68-35472*#	DB-0375, V. 3 NASA-CR-743/1/ NASA-CR-1189 NBS-9708 NASA-TM-X-1646 NASA-CR-1113 NASA-CR-1162 NASA-CR-1162 NASA-CR-1165 NASA-CR-1170 NASA-CR-1170 NASA-CR-1170 NASA-CR-1132 NASA-CR-1132 NASA-CR-11647 NASA-TN-D-4802 NASA-TN-D-4802 NASA-TN-D-4818 NASA-TN-D-4818 NASA-CR-11647 NASA-TN-D-4818 NASA-TN-D-4818 NASA-CR-11647
c26 N68-35178*# c13 N68-35179*# c08 N68-35193*# c32 N68-35193*# c17 N68-35200*# c17 N68-35248*# c12 N68-35248*# c26 N68-35252*# c26 N68-35256*# c31 N68-35456*# c11 N68-35466*# c13 N68-35467*# c33 N68-35468*# c32 N68-35496*#	DB-0375, V. 3 NASA-CR-743/1/ NASA-CR-743/1/ NASA-CR-1189 NBS-9708 NASA-TM-X-1646 NASA-CR-1113 NASA-CR-1113 NASA-CR-1163 NASA-CR-1165 NASA-CR-1165 NASA-CR-1172 NASA-CR-1165 NASA-CR-1172 NASA-CR-1132 NASA-CR-1165 NASA-TM-D-4806 NASA-TM-D-4818 NASA-TM-D-4818 NASA-TM-D-4799 NASA-TM-D-4795
c26 N68-35178*# c13 N68-35179*# c08 N68-35193*# c32 N68-35198*# c17 N68-35200*# c17 N68-35200*# c12 N68-352248*# c12 N68-35252*# c26 N68-35355*# c31 N68-35357*# c11 N68-35357*# c33 N68-35466*# c33 N68-35466*# c33 N68-35468*# c19 N68-35496*# c10 N68-35497*#	DB-0375, V. 3 NASA-CR-743/1/ NASA-CR-1189 NBS-9708 NASA-TM-X-1646 NASA-CR-1113 NASA-CR-1113 NASA-CR-1162 NASA-CR-1162 NASA-CR-1165 NASA-CR-1165 NASA-CR-1165 NASA-CR-1165 NASA-CR-1170 NASA-CR-1170 NASA-TN-D-4806 NASA-TN-D-4806 NASA-TN-D-4808 NASA-TN-D-4808 NASA-TN-D-4808 NASA-TN-D-4808 NASA-TN-D-4808 NASA-TN-D-4808 NASA-TN-D-4808 NASA-TN-D-4808 NASA-TN-D-4808 NASA-TN-D-4799 NASA-TN-D-4793 NASA-TN-D-4793
c26 N68-35178*# c13 N68-35179*# c08 N68-35193*# c32 N68-35193*# c32 N68-35198*# c33 N68-35200*# c17 N68-3520*# c18-35262*# c26 N68-35356*# c11 N68-35466*# c13 N68-35467*# c33 N68-35467*# c33 N68-35467*# c32 N68-35496*# c19 N68-35497*# c07 N68-35422*#	DB-0375, V. 3 NASA-CR-743/1/ NASA-CR-1189 NBS-9708 NASA-CR-1189 NASA-CR-1162 NASA-CR-1163 NASA-CR-1163 NASA-CR-1165 NASA-CR-1170 NASA-CR-1170 NASA-CR-1170 NASA-CR-1132 NASA-CR-1132 NASA-CR-1132 NASA-CR-11647 NASA-TN-D-4802 NASA-TN-D-4810 NASA-TN-D-4810 NASA-TN-D-4799 NASA-CR-1168 NASA-CR-1168 NASA-CR-1168 NASA-CR-1168 NASA-CR-1168 NASA-CR-1168 NASA-CR-1168 NASA-CR-1168 NASA-CR-1168 NASA-CR-1168 NASA-CR-1168 NASA-CR-1168
c26 N68-35178*# c13 N68-35179*# c08 N68-35193*# c32 N68-35193*# c32 N68-35193*# c17 N68-35200*# c17 N68-35248*# c12 N68-3526*# c18 N68-35252*# c26 N69-353557*# c11 N68-3556*# c11 N68-35467*# c33 N68-35467*# c33 N68-35467*# c32 N68-35496*# c10 N68-35522*# c01 N68-35522*# c01 N68-35522*#	DB-0375, V. 3 NASA-CR-743/1/ NASA-CR-1189 NBS-9708 NASA-CR-1180 NASA-CR-1180 NASA-CR-1113 NASA-CR-1113 NASA-CR-1163 NASA-CR-1163 NASA-CR-1163 NASA-CR-1163 NASA-CR-1163 NASA-CR-1163 NASA-CR-1163 NASA-CR-1164 NASA-CR-1165 NASA-CR-1164 NASA-TM-D-4806 NASA-TM-D-4806 NASA-TM-D-4807 NASA-TM-D-4808 NASA-TM-D-4808 NASA-TM-D-4808 NASA-TM-D-4808 NASA-TM-D-4793 NASA-TN-D-4793 NASA-TN-D-4793 NASA-TN-D-4793 NASA-TN-D-4793 NASA-TN-D-4793 NASA-SP-182 NASA-CR-1145
c26 N68-35178*# c13 N68-35179*# c08 N68-35193*# c32 N68-35193*# c17 N68-35200*# c17 N68-35248*# c18 N68-3526*# c26 N68-35356*# c21 N68-35356*# c31 N68-35466*# c11 N68-35466*# c33 N68-35466*# c19 N68-3546*# c19 N68-3546*# c10 N68-35497*# c01 N68-35522*# c01 N68-35522*# c01 N68-35524*#	DB-0375, V. 3 NASA-CR-743/1/ NASA-CR-1189 NBS-9708 NASA-TM-X-1646 NASA-CR-1113 NASA-CR-1113 NASA-CR-1163 NASA-CR-1163 NASA-CR-1165 NASA-CR-1165 NASA-CR-1165 NASA-CR-1165 NASA-CR-1170 NASA-CR-1167 NASA-TN-D-4806 NASA-TN-D-4806 NASA-TN-D-4806 NASA-TN-D-4806 NASA-TN-D-4806 NASA-TN-D-4806 NASA-TN-D-4806 NASA-TN-D-4806 NASA-TN-D-4806 NASA-TN-D-4806 NASA-TN-D-4806 NASA-TN-D-4806 NASA-TN-D-4806 NASA-TN-D-4806 NASA-TN-D-4806 NASA-TN-D-4806 NASA-TN-D-4792 NASA-CR-1145 NASA-CR-1145
c26 N68-35178*# c13 N68-35179*# c08 N68-35193*# c32 N68-35198*# c32 N68-35198*# c32 N68-35200*# c17 N68-35200*# c18-35262*# c18-35356*# c11 N68-35356*# c11 N68-35356*# c11 N68-35466*# c19 N68-35466*# c19 N68-35496*# c19 N68-35496*# c01 N68-35522*# c01 N68-35522*# c01 N68-35522*# c01 N68-35522*# c01 N68-35522*# c01 N68-35522*# c01 N68-35522*# c01 N68-35522*# c01 N68-35522*#	DB-0375, V. 3 NASA-CR-743/1/ NASA-CR-1189 NBS-9708 NASA-CR-1189 NASA-CR-1189 NASA-CR-1163 NASA-CR-1163 NASA-CR-1165 NASA-CR-1165 NASA-CR-1170 NASA-CR-1170 NASA-CR-1170 NASA-CR-1170 NASA-CR-1170 NASA-CR-1170 NASA-TN-D-4802 NASA-TN-D-4802 NASA-TN-D-4799 NASA-TN-D-4792 NASA-TN-D-4792 NASA-TN-D-4792 NASA-TN-D-4792 NASA-TN-D-4792 NASA-TN-D-4792 NASA-TN-D-4792 NASA-TN-D-4792 NASA-TN-D-4792 NASA-TN-D-4792 NASA-TN-D-4792 NASA-TN-D-4792 NASA-TN-D-4792 NASA-TN-D-4792 NASA-TN-D-4792 NASA-TN-D-4792 NASA-TN-D-4792 NASA-TN-D-4794
c26 N68-35178*# c13 N68-35179*# c08 N68-35193*# c32 N68-35193*# c17 N68-35200*# c17 N68-35248*# c18 N68-3526*# c26 N68-35356*# c21 N68-35356*# c31 N68-35466*# c11 N68-35466*# c33 N68-35466*# c19 N68-3546*# c19 N68-3546*# c10 N68-35497*# c01 N68-35522*# c01 N68-35522*# c01 N68-35524*#	DB-0375, V. 3 NASA-CR-743/1/ NASA-CR-1189 NBS-9708 NASA-TM-X-1646 NASA-CR-1113 NASA-CR-1113 NASA-CR-1163 NASA-CR-1163 NASA-CR-1165 NASA-CR-1165 NASA-CR-1165 NASA-CR-1165 NASA-CR-1170 NASA-CR-1167 NASA-TN-D-4806 NASA-TN-D-4806 NASA-TN-D-4806 NASA-TN-D-4806 NASA-TN-D-4806 NASA-TN-D-4806 NASA-TN-D-4806 NASA-TN-D-4806 NASA-TN-D-4806 NASA-TN-D-4806 NASA-TN-D-4806 NASA-TN-D-4806 NASA-TN-D-4806 NASA-TN-D-4806 NASA-TN-D-4806 NASA-TN-D-4806 NASA-TN-D-4792 NASA-CR-1145 NASA-CR-1145

c10 N68-37293*#	•••••• TT-67-51371
c01 N68-37365*#	••••••••••••••••••••••••••••••••••••••
c24 N68-37708*#	•••••• NASA-CR-1194
	REPT0-71000/8R-2
c23 N68-37792*#	NASA-TT-F-503
· · · · •	TT-68-50305
- 05 NC0 33010+ "	
c05 N68-37819*#	•••••• NASA-CR-1220
c32 N68-37840*#	••••••••••••••••••••••••••••••••••••••
c01 N68-37854*#	••••••••••••••••••••••••••••••••••••••
c20 N68-37869*#	NASA-TN-D-4757
c31 N68-37900*#	•••••• ARC-R-282
	NASA-CR-1201
c10 N68-37906*#	••••••••••••••••••••••••••••••••••••••
c22 N68-37927*#	••••••••••••••••••••••••••••••••••••••
c02 N68-37932*#	••••••••••••••••••••••••••••••••••••••
c03 N68-37935*#	••••••••••••••••••••••••••••••••••••••
c02 N68-37941*#	••••••••••••••••••••••••••••••••••••••
c31 N68-37942*#	NASA-TM-X-1682
c03 N68-37943*#	••••••••••••••••••••••••••••••••••••••
c09 N68-37944*#	••••••••••••••••••••••••••••••••••••••
c04 N68-38051*#	••••••••••••••••••••••••••••••••••••••

Collections of NASA Documents

NASA is depositing its technical documents and bibliographic tools in eleven Federal Regional Technical Report Centers. Each center, located in one of the organizations listed below is prepared to furnish the general public such services as personal reference, interlibrary loans, photocopy service, and assistance in obtaining retention copies of NASA documents.

California: University of California,	Missouri: Linda Hall Library, Kansas City
Berkeley	New York: Columbia University, New York
Colorado: University of Colorado,	Pennsylvania: Carnegie Library of
Boulder	Pittsburgh
District of Columbia: Library of Congress	Texas: Southern Methodist University,
Georgia: Georgia Institute of Technology,	Dallas
Atlanta	Washington: University of Washington,
Illinois: The John Crerar Library, Chicago	Seattle
Massachusetts: Massachusetts Institute	
of Technology, Cambridge	

NASA publications are currently being forwarded to the public libraries in the cities listed below: `

California: Los Angeles and San Diego Colorado: Denver Connecticut: Hartford Massachusetts: Boston Michigan: Detroit Minnesota: St. Paul and Minneapolis Missouri: Kansas City and St. Louis New Jersey: Trenton New York: Brooklyn, Buffalo, Rochester and New York
Ohio: Cleveland, Cincinnati, Dayton, Toledo and Akron
Oklahoma: Oklahoma City
Tennessee: Memphis
Texas: Fort Worth and Dallas
Washington: Seattle
Wisconsin: Milwaukee

In addition, NASA regularly sends its publications to the Enoch Pratt Free Library located in Baltimore, Maryland and the Wilmington Institute Free Library, Wilmington, Delaware.

An extensive collection of NASA and NASA-sponsored scientific and technical publications available to the public for reference purposes is maintained at the Technical Information Service, American Institute of Aeronautics and Astronautics, 750 Third Avenue, New York, New York 10017.

NATIONAL AFRONAUTICS AND SPACE ADMINISTRATION WASHINGTON, D. C. 20546 OFFICIAL BUSINESS

FIRST CLASS MAIL



POSTAGE AND FEES PAID NATIONAL AERONAUTICS AND SPACE ADMINISTRATION

POSTMASTER: If Undeliverable (Section 158 Postal Manual) Do Not Return

"The aeronautical and space activities of the United States shall be conducted so as to contribute . . . to the expansion of human knowledge of phenomena in the atmosphere and space. The Administration shall provide for the widest practicable and appropriate dissemination of informiation concerning its activities and the results thereof."

-NATIONAL AERONAUTICS AND SPACE ACT OF 1958

NASA SCIENTIFIC AND TECHNICAL PUBLICATIONS

TECHNICAL REPORTS: Scientific and technical information considered important, complete, and a lasting contribution to existing knowledge.

TECHNICAL NOTES: Information less broad in scope but nevertheless of importance as a contribution to existing knowledge.

TECHNICAL MEMORANDUMS:

Information receiving limited distribution because of preliminary data, security classification, or other reasons.

CONTRACTOR REPORTS: Scientific and technical information generated under a NASA contract or grant and considered an important contribution to existing knowledge. TECHNICAL TRANSLATIONS: Information published in a foreign language considered to merit NASA distribution in English.

SPECIAL PUBLICATIONS: Information derived from or of value to NASA activities. Publications include conference proceedings, monographs, data compilations, handbooks, sourcebooks, and special bibliographies.

TECHNOLOGY UTILIZATION

PUBLICATIONS: Information on technology used by NASA that may be of particular interest in commercial and other non-aerospace applications. Publications include Tech Briefs, Technology Utilization Reports and Notes, and Technology Surveys.

Details on the availability of these publications may be obtained from:

SCIENTIFIC AND TECHNICAL INFORMATION DIVISION NATIONAL AERONAUTICS AND SPACE ADMINISTRATION Washington, D.C. 20546